Extended Polycyclic Aromatic Hydrocarbons based on Diarenoperylenes

Xuan Yang

杨宣

Dissertation

Heidelberg

2020

Inaugural-Dissertation

Zur Erlangung der Doktorwürde der

Naturwissenschaftlichen-Mathematischen Gesamtfakultät

der Ruprecht-Karls-Universität Heidelberg

vorgelegt von

Xuan Yang, M. Sc.

aus Tianjin, Volksrepublik China

Juni 2020

Tag der mündlichen Prüfung: 26.06.2020

Extended Polycyclic Aromatic Hydrocarbons based on Diarenoperylenes

Gutacher: Prof. Dr. Michael Mastalerz

Prof. Dr. Milan Kivala

Abstract

This thesis deals with the synthesis and investigation of larger polycyclic aromatic hydrocarbons (PAHs) obtained via π-extension of 2,10-di-*tert*-butyldibenzoperylene. Four types of π-extensions based on dibenzoperylene were achieved:

1. Bay region extension (Chapter 3.1): Nine *cata*-condensed (hetero)annulated coronenes were synthesized by a three-step approach via selective bromination of diarenoperylenes as the key-step. The influence of introducing different heteroatoms (nitrogen and sulfur) on the molecular structures as well as the photophysical and electrochemical properties were investigated.

2. *L*-region extension (Chapter 3.2.2): Two-fold cyclopentannulation at the *L*-regions and regioselective triflyloxylations have been achieved in a single step based on a dibenzoperylene. Larger contorted PAHs were obtained based on the bistriflate. The structures of the obtained contorted PAHs were studied by NMR techniques and single crystal X-ray diffraction analyses.

3. Extension at both bay and *L*-regions (Chapter 3.2.3): Contorted PAHs with two embedded azulene units were synthesized. The influences of the curvature on the aromaticity and the conjugation were investigated by theoretical calculations.

4. Linear extension (Chapter 3.3): Triptycene end-capped perylene oligomers with up to thirteen linearly fused benzene rings were obtained. The influence of the conjugation length on the molecular photophysical properties were studied. Regioselective brominations were achieved on these perylene oligomers and one PAH molecule with two coronene units was obtained.

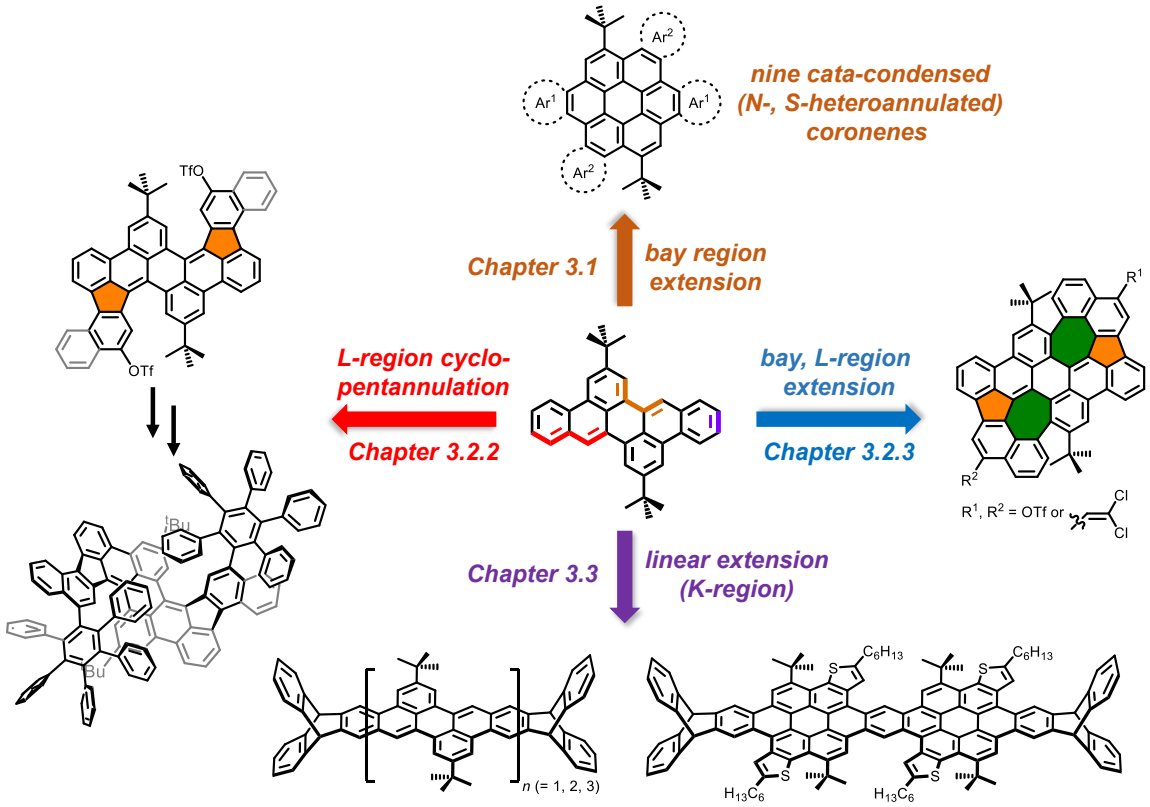

Kurzzusammenfassung

In dieser Arbeit werden die Synthese und Analyse großer polyzyklischer aromatischer Kohlenwasserstoffe (PAKs), die über π-Erweiterung des 2,10-Di-*tert*-butyldibenzoperylen erhalten wurden, behandelt. Vier verschiedene π-Erweiterungen des Dibenzoperylenes wurden erreicht:

1. Erweiterung der *Bay*-Region (Kapitel 3.1): Durch eine dreistufige Synthese, bei der die selektive Bromierung der Diarenoperylene den Schlüsselschritt darstellt, konnten neun *cata*-kondensierte, (hetero)annelierte Coronene dargestellt werden. Der Einfluss von verschiedenen Heteroatomen (Stickstoff und Schwefel) auf die molekularen Strukturen, die photophysikalischen und elektrochemischen Eigenschaften werden ebenfalls diskutiert.

2. Erweiterung der *L*-Region (Kapitel 3.2.2) durch eine zweifache Cyclopentannulierung und eine regioselektive Triflyloxylierung in einem Schritt am Dibenzoperylen. Größere PAKs konnten ausgehend von dem synthetisch wertvollen Bistriflat aufgebaut werden. Die Strukturen der erhaltenen größeren verzerrten PAKs wurden durch NMR-Techniken und Einkristall-Röntgenbeugungsanalyse untersucht.

3. Erweiterung von *Bay*- und *L*-Region (Kapitel 3.2.3): Es wurden verzerrte PAKs mit zwei eingebetteten Azuleneinheiten synthetisiert. Die Einflüsse der Krümmung auf Aromatizität und Konjugation wurden durch theoretische Berechnungen untersucht.

4. Lineare Erweiterung (Kapitel 3.3): Es gelang Perylen-Oligomere mit Triptycen-Endgruppen und bis zu 13 linear verbundenen Benzolringen zu erhalten. Der Einfluss der Länge des konjugierten Systems auf die photophysikalischen Eigenschaften wurde untersucht. Eine regioselektive Bromierung wurde ebenfalls erreicht, durch die PAKs mit zwei Coronen-Einheiten erhalten wurden.

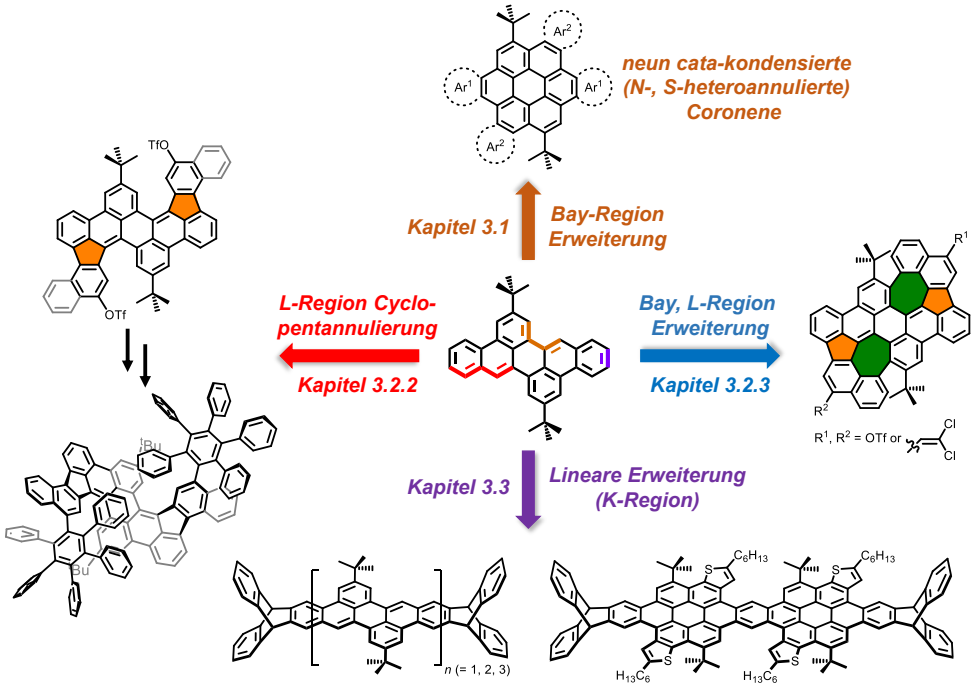

Publications

Die vorliegende Arbeit wurde von Oktober 2016 bis Januar 2020 in dem Arbeitskreis von Herrn Prof. Dr. Michael Mastalerz an der Ruprecht-Karls-Universität Heidelberg angefertigt.

Teile dieser Arbeit wurden bereit veröffentlicht:

Xuan Yang, Frank Rominger, Michael Mastalerz, *Angew. Chem. Int. Ed.* **2019**, *58*, 17577-17582; *Angew. Chem.* **2019**, *131*, 17741-17746: **"Contorted Polycyclic Aromatic Hydrocarbons with Two Embedded Azulene Units"**.

Xuan Yang, Marvin Hoffmann, Frank Rominger, Tobias Kirschbaum, Andreas Dreuw, Michael Mastalerz, *Angew. Chem. Int. Ed.* **2019**, *58*, 10650-10654; *Angew. Chem.* **2019**, *131*, 10760-10764: **"Functionalized Contorted Polycyclic Aromatic Hydrocarbons by a One-Step Cyclopentannulation and Regioselective Triflyloxylation"**.

Xuan Yang, Frank Rominger, Michael Mastalerz, *Org. Lett.* **2018**, *20*, 7270-7273: **"Cata-Condensed Heteroannulated Coronenes via Selective Bromination of Diarenoperylenes as Key-Step"**.

Poster:

Xuan Yang, Marvin Hofmann, Frank Rominger, Tobias Kirschbaum, Andreas Dreuw, Michael Mastalerz, *Conjugated Oligomers and Polymers (KOPO)*, **2019**, Physikzentrum Bad Honnef, Germany (May 8-11, 2019): **"One-Pot Cyclopentannulation and Triflation of a Naphthalene-Extended Diarenoperylene"**.

Xuan Yang, Frank Rominger, Michael Mastalerz, *CURO-π³*, **2018**, Oxford, UK (September 5-7, 2018): **"Facile Synthetic Route to a Series of Extended Coronenes via a Regio-Selective Bromination based on Diarenoperylenes"**.

Xuan Yang, Frank Rominger, Michael Mastalerz, *Conjugated Oligomers and Polymers (KOPO)*, **2017**, Physikzentrum Bad Honnef, Germany (August 27-30, 2017): **"Selective Functionalization of Diarenoperylenes towards Extended Polycyclic Aromatic Hydrocarbons"**.

Table of Contents

1. Introduction

1.1 Polycyclic Aromatic Hydrocarbons

Since its first isolation in 2004, when Geim and co-workers reported a micromechanical cleavage approach for the exfoliation of highly oriented pyrolyzed graphite by repeated peeling, graphene, a two-dimensional (2D) atomical monolayer composed of a hexagonal network of sp^2 hybridized carbon atoms, has been intensively investigated.[1] Because of its unique physical and chemical properties, such as single-atom thickness, high charge-carrier mobility ($> 2\times10^5$ $cm^2\cdot V^{-1}\cdot s^{-1}$),[2] high tensile strength ($> 1.9\times10^7$ psi)[3] and high thermal conductivity (> 5300 $W\cdot m^{-1}\cdot K^{-1}$),[4] graphene can be broadly applied in electronics,[2, 5] optical sensing,[6] catalysis,[7] energy storage[8] and conversion,[9] DNA sequencing[10] and water purification.[11]

Nevertheless, the lack of band gap makes graphene highly conductive, thus unsuitable for optoelectronic (semiconductive) devices.[12] For example, the current cannot be switched off between source and drain electrodes when graphene is used as an active component in field-effect transistors (FETs), although a high charge-carrier mobility was achieved ($> 2\times10^5$ $cm^2\cdot V^{-1}\cdot s^{-1}$ at room temperature[2]).[13] As the physical properties of extended π-systems highly depend on size, shapes and edge structures,[14] decreasing the scale of the hypothetically infinite graphene to the nanoscale, which allows the sp^2 hybridized carbon framework exhibiting a finite band gap due to quantum confinement, is necessary for applications in organic electronics.[15] Another necessity of decreasing the scale of graphene comes from the extrapolation from finite to infinite structures in the theoretical analyses of extended π-systems. Commonly, building up a homologous series of monodisperse oligomers and then making the convergence of their properties to predict the corresponding polymers is a general approach to this problem.[16] Thus, research based on nanoscale graphene or graphene cutouts with even smaller scale is of significance to build up the interconnection between these materials.

Theoretically, cutting a graphene monolayer into fragments gives nanographenes, in which at least one dimension is between 1 and 100 nm. Depending on the size and shape, nanographene can be further divided into graphene nanoribbons (GNRs, 1-100 nm width, length/ratios >10)[13] and polycyclic aromatic hydrocarbons (PAHs).[17] The relationship of graphene, GNRs and PAHs is illustrated in Figure 1.1. PAH is a common name given to an aromatic hydrocarbon which contains more than two unsubstituted fused benzene rings.[15a, 17a] It can be treated as graphene at the molecular scale and has attracted attention from synthetic chemistry, supramolecular chemistry and material sciences.[15e, 16a, 18] PAHs serve as ideal model compounds to investigate the role of edge structures, peripheral functionalizations, defined structural defects such as non-hexagonal rings and holes or heteroatom incorporation on the properties of π-extended systems.[16a]

Furthermore, based on the elementary subunits of the PAHs, π-extended molecules with a variety of substitutions can be used in various roles, such as organic dyes,[19] organic semiconductors[18b, 20] and objects for biological research.[21] Molecular structures of a few representative subunits of PAHs, including naphthalene, anthracene, phenanthrene, pentacene, triphenylene, pyrene, perylene and coronene, are shown in Figure 1.2a.

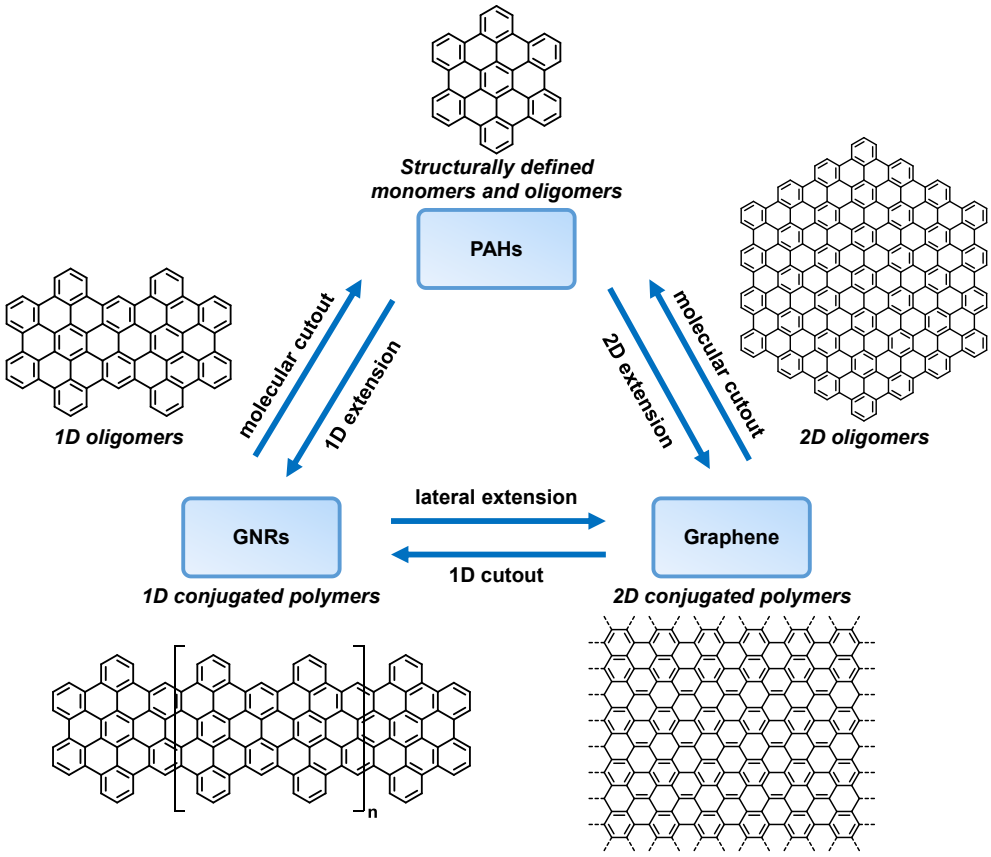

Figure 1.1 Illustration of the relationship between polycyclic aromatic hydrocarbons (PAHs), graphene nanoribbons (GNRs) and graphene.[16a]

There are two widely applied approaches to obtain nanographenes, the "top-down" as well as the "bottom-up" approach, as illustrated in Figure 1.2b and c. The "top-down" method starts from high-level carbon sources, such as fullerenes, graphene and carbon nanotubes (CNTs). For instance, the cage of fullerenes (C_{60}) could be opened to produce oxidized graphene fragments after treatment by strong acids and chemical oxidants, which exhibit strong luminescence properties in aqueous solution under photoexcitation.[22] A mixture of nanographenes with different sizes and shapes could also be obtained from CNTs by fragmentation of double-walled CNTs with a mixture of concentrated H_2SO_4 and HNO_3[23] or by unzipping CNTs via solution-based oxidative treatment.[24] Etching polymethylmethacrylate (PMMA) mask protected pristine graphene or multiwalled CNTs with an electron beam or an argon plasma could also produce nanographenes with different shapes.[15c, 25] Although it was reported that nanographenes obtained via the "top-down" approach exhibit valuable applications, such as in polymer solar cells with enhanced power

conversion efficiencies or behaving as an oxidization catalyst in the conversion from benzyl alcohol to benzaldehyde,[15b, 22a, 23, 26] it should be noted that such procedures are commonly accomplished by high-cost physical methods with harsh reaction conditions, such as plasma etching,[25] helium ion beam lithography[27] or high-power microwave irradiated exfoliation.[28] More importantly, the obtained structures are not atomically precise and undefined structural defects could be expected.[13]

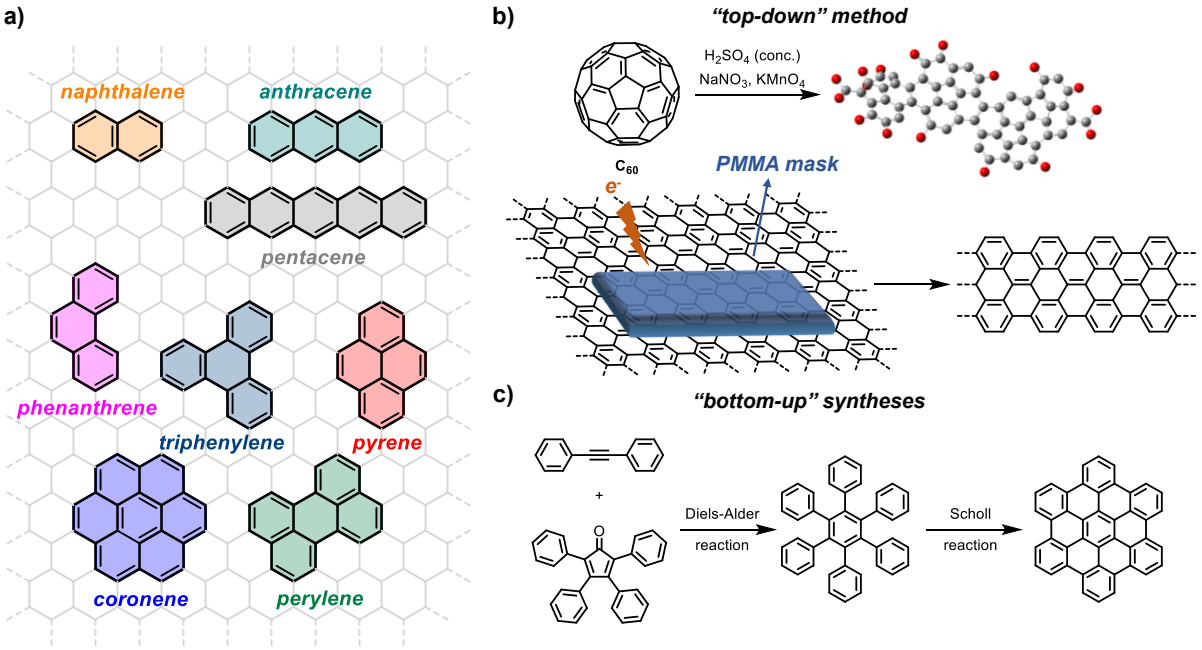

Figure 1.2 Typical six-membered-ring subunits of PAHs as cut-outs of graphene (a). Illustration of representative "top-down" (b) and "bottom-up" (c) methods for the fabrication of nanographenes. "Top-down" methods include cage-opening of fullerene (C_{60}) under acidic conditions (b, top) and cutting of graphene sheets by lithography using an argon plasma (b, bottom). "Bottom-up" method includes organic synthesis of PAHs (*peri*-HBC) by subsequent Diels-Alder reaction of 1,2-diphenylethyne with tetraphenylcyclopentadienone and cyclodehydrogenation of hexaphenylbenzene (c). The molecular structure shown in (b, top) is only for schematic illustration, which was not completely defined in Ref. [22b]. Colors for atoms: grey = carbon, red = oxygen. Hydrogen atoms in (b, top) are omitted for clarity. PMMA: polymethylmethacrylate.

In order to establish reliable structure-property relationships and to engineer reproducible electronical and optical properties of such π-systems for nanoelectronic applications, it is necessary to develop methods to obtain atomically defined nanographenes via low-cost procedures.[29] In this context, "bottom-up" syntheses have been applied to obtain nanoscale π-extended systems. A variety of PAHs has been synthesized, ranging from the representative hexa-*peri*-hexabenzocoronene (*peri*-HBC) to a large nanographene propeller with 258 sp^2 hybridized carbon atoms by fusing seven *peri*-HBC units.[18a, 30] A series of facile synthetic strategies towards π-extended PAHs were developed and the obtained structurally defined molecules serve as model compounds to investigate structure-property relationships of π-extended materials.[29] These achievements undoubtedly show the significance of organic synthesis in material sciences.

Some representative and several recently developed synthetic strategies towards PAHs will be briefly summarized in Section 1.2. Some PAHs with curved structures will be shown in Section

1.3. Finally, one of the most representative subunits of PAHs, perylene, along with *cata*-condensed diarenoperylenes, which serve as the starting points of this thesis, will be discussed in Section 1.4.

1.2 Synthetic Strategies for PAHs

1.2.1 π-Extension of Smaller PAHs

Although various synthetic methods have been reported for the syntheses of PAHs, these approaches can be overall classified into two groups, one of which is to make π-extension directly on existing PAHs units. A representative example is the Diels-Alder reaction at the bay regions of PAHs, which exhibit a diene-like character and thus can react with various dienophiles such as arynes, alkenes, alkynes and quinones to produce π-extended PAHs.[31] The synthesis of coronene **5** reported by Clar and co-workers in 1957 serves as a representative example (Scheme 1.1a).[32] In this route, π-extension at the two bay regions of perylene **1** was achieved by two times of Diels-Alder reaction with maleic anhydride in refluxing chloranil as solvent and subsequent decarboxylation in the presence of soda-lime in vacuum. Bromomaleic anhydride was used as the reactant in the second step of Diels-Alder reaction with 1,12-benzoperylene **3** to ensure a smooth progress of the reaction. The overall yield of these four steps was reported to be 25%. Scott and co-workers reported that nitroethylene serves as an effective reagent to make π-extension at the bay regions of PAHs. In this case 1,12-benzoperylene **3** was produced by Diels-Alder cycloaddition of perylene **1** with nitroethylene in 1,2-dichlorobenzene (*o*-DCB) at 175 °C in 58% yield.[33]

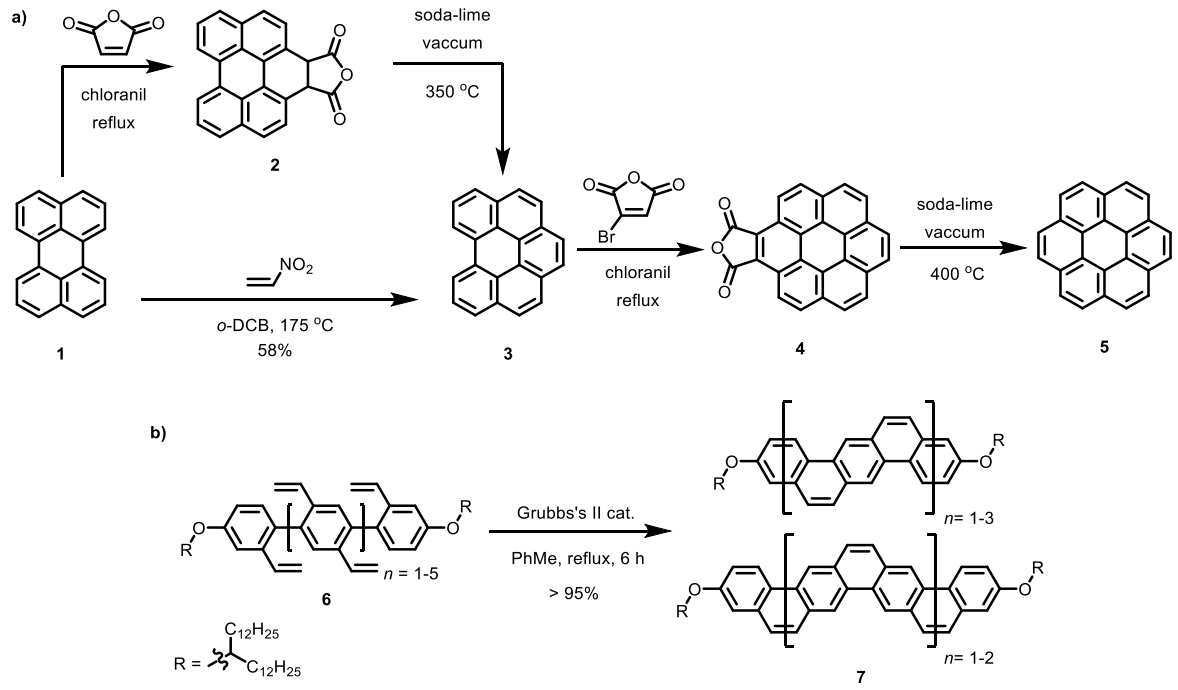

Scheme 1.1 PAHs obtained by bay region π-extension by Diels-Alder cycloaddition (a) and by ring-closing olefin metathesis (b).[32-34] *o*-DCB: 1,2-dichlorobenzene. Grubbs's II catalyst: (1,3-bis(2,4,6-trimethylphenyl)-2-imidazolidinylidene)dichloro(phenylmethylene)(tricyclohexylphosphine)ruthenium.

Intramolecular ring-closing olefin metathesis (RCM) serves as another way to make π-extension at the bay region.[35] The approach was combined with iterative Suzuki-Miyaura cross-coupling reactions by Fang and co-workers to synthesize a series of 1D extended ladder-type oligomers and the final RCM steps gave high yields of > 95% in all five cases (Scheme 1.1b).[34, 36]

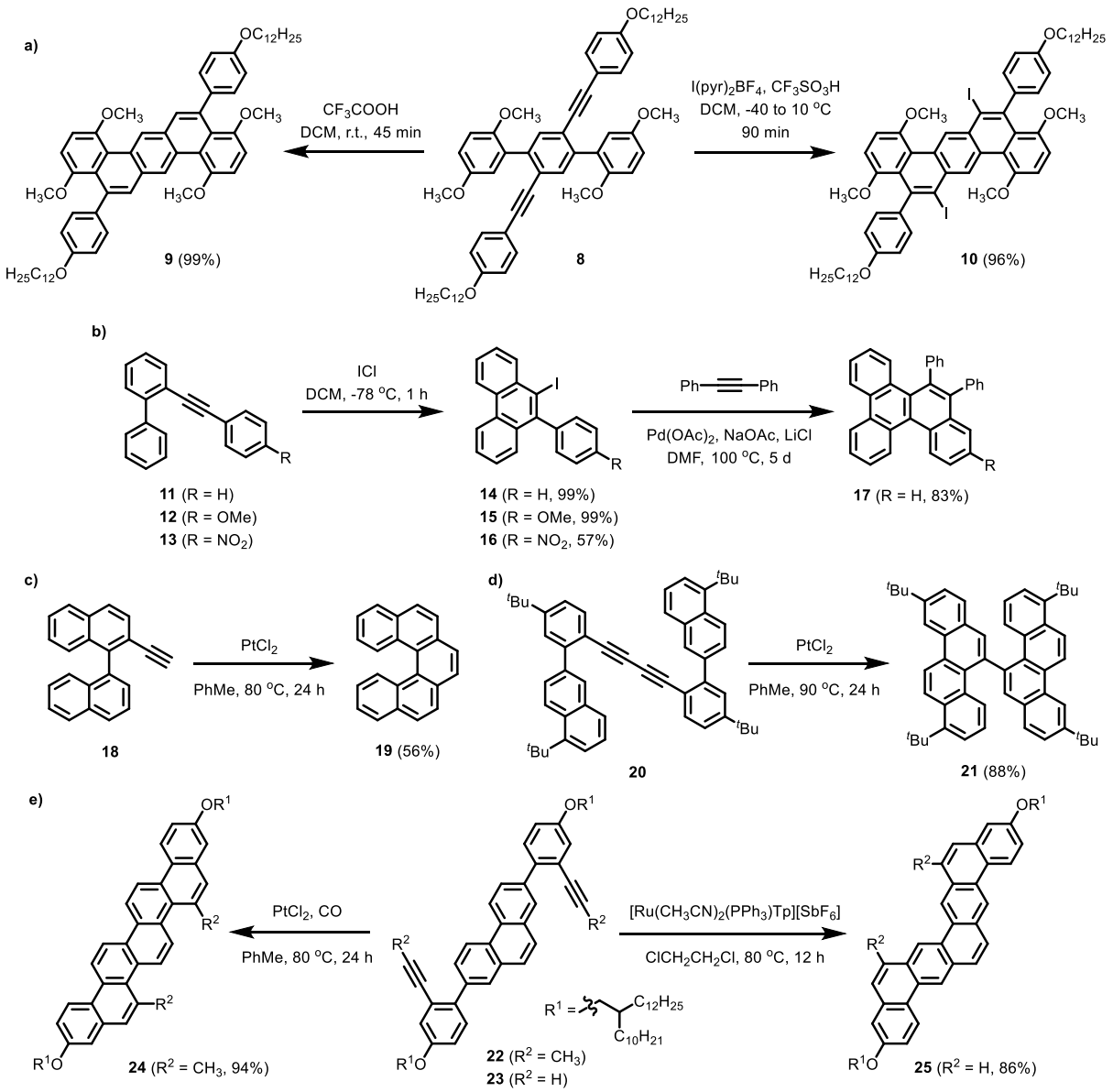

Scheme 1.2 PAHs obtained by cyclohexannulation of alkyne-containing aromatic compounds.[37] pyr: pyridine. Tp: tris(1-pyrazolyl)borate.

The third type of bay-region extension is the intramolecular cyclohexannulation of alkyne-containing aromatic compounds. Swager and co-workers reported the electrophilic cyclization of acetylenic arenes induced by strong electrophiles such as trifluoroacetic acid (TFA) or $I(pyr)_2BF_4$ (Scheme 1.2a).[37a, 38] Acetylenic arene **8** could be double cyclized using TFA to give compound **9** in quantitative yield (99%), while cyclized compound **10** with two iodo groups could be obtained in 96% yield when $I(pyr)_2BF_4$ was used. However, the presence of a *para*-alkoxy group on the

phenylethynyl moiety is crucial to the success of the cyclization. To overcome this drawback, ICl-induced iodocyclization was applied by Larock and co-workers to prepare a series of phenanthrene derivatives (Scheme 1.2b).[37b, 39] The reaction was tolerated even with electron-withdrawing groups (-NO_2) attached at the *para*-position of the phenylethynyl group (compound **13**) and the iodo group on compound **14** could be used for further palladium-catalyzed alkyne annulation. Metal catalysts with high electron affinities for π-systems, such as Pt^{II}, Au^{I} and Ru^{II} could also be applied to trigger such electrophilic annulations.[40] For instance, as reported by Fürstner and co-workers, dibenzo[*c*,*g*]phenanthrene (**19**) could be obtained by $PtCl_2$-induced annulation from an alkyne precursor in 65% yield.[37c] This approach was also employed by Liu and co-workers[37d] (**21**, Scheme 1.2d) and Müllen and co-workers[41] as the key-step in their constructions of PAHs. Liu and co-workers reported the regiocontrolled synthesis of ethene-bridged *para*-phenylene oligomers (**24** and **25**, Scheme 1.2e), which was achieved by using Pt^{II} or Ru^{II} catalyst .[37e] The annulation took place at the more hindered carbon of the central phenanthrene to give product **24** when $PtCl_2$ was used, whereas aromatization catalyzed by Ru^{II} complex proceeded through cyclizations of the less-hindered positions of the central aromatic arrays to the adjacent terminal alkynes. The different regioselectivity could be explained by the steric hinderance introduced by the bulky Ru^{II} complex.[40]

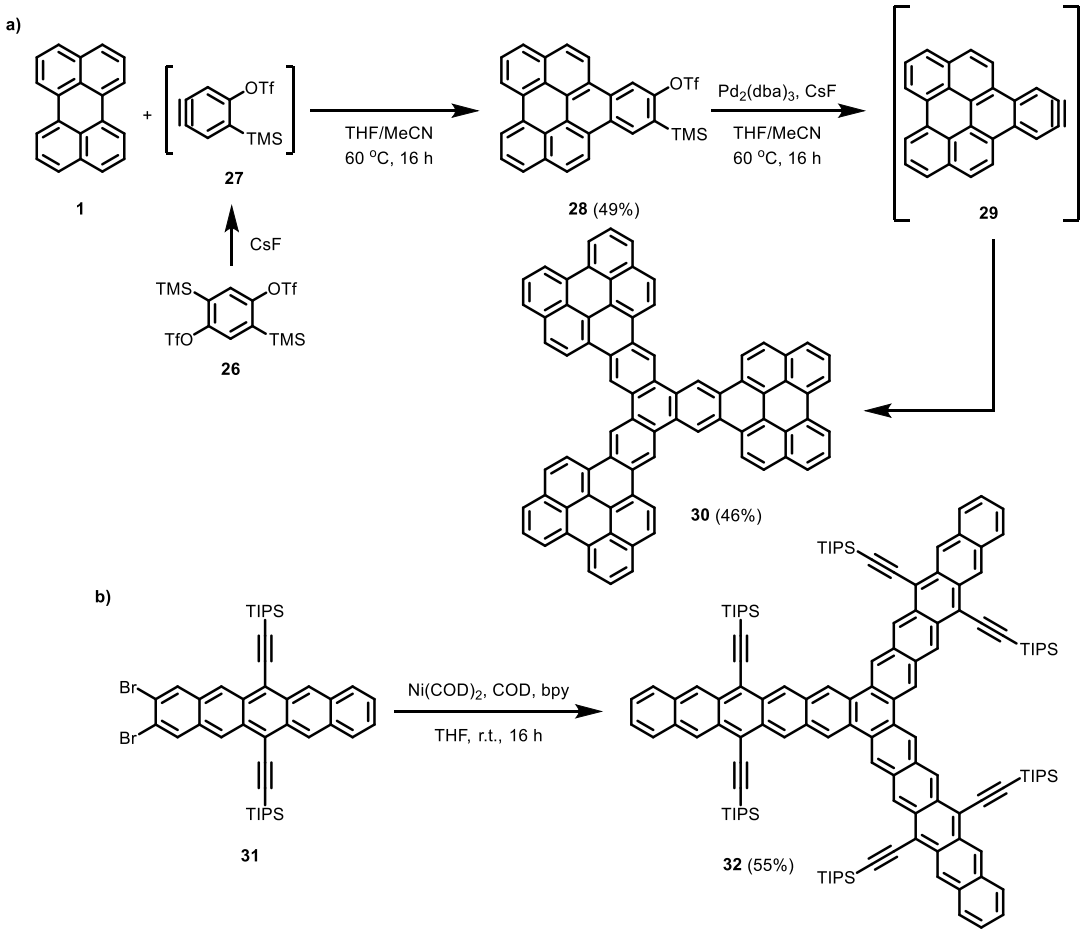

Scheme 1.3 PAHs obtained by cyclotrimerization.[42] TMS: trimethylsilyl. dba: dibenzylideneacetone. COD: 1,5-cyclooctadiene. bpy: 2,2'-bipyridine. TIPS: triisopropylsilyl.

Besides the π-extensions at the bay-regions, transition metal catalyzed cyclotrimerization of arynes to synthesize C_3-symmetric PAHs serve as another strategy to directly make π-extension based on small PAH precursors. Since 1998, Peña and co-workers have reported the syntheses of various triphenylene derivatives such as starphenes and cloverphenes via a [2+2+2] cycloaddition of benzyne derivatives.[43] For instance, triflate **28** was prepared by the Diels-Alder cycloaddition of perylene **1** with benzyne intermediate **27** generated from **26**, which could be used as the precursor of benzyne **29** in the following Pd^0-catalyzed cycloaddition to produce three-fold symmetric PAH **30** (Scheme 1.3a).[42a] **30** could be obtained by one-pot reaction between perylene **1** and bisbenzyne precursor **26** without the need to isolate aryne precursor **28** although no overall yield was reported. The strategy of cyclotrimerization was also used by Bunz and co-workers to synthesize hexadecastarphene **32** using *o*-dibromoarene **31** through Ni^0-catalyzed Yamamoto coupling without tedious preparation of aryne precursors (Scheme 1.3b).[42b, 44]

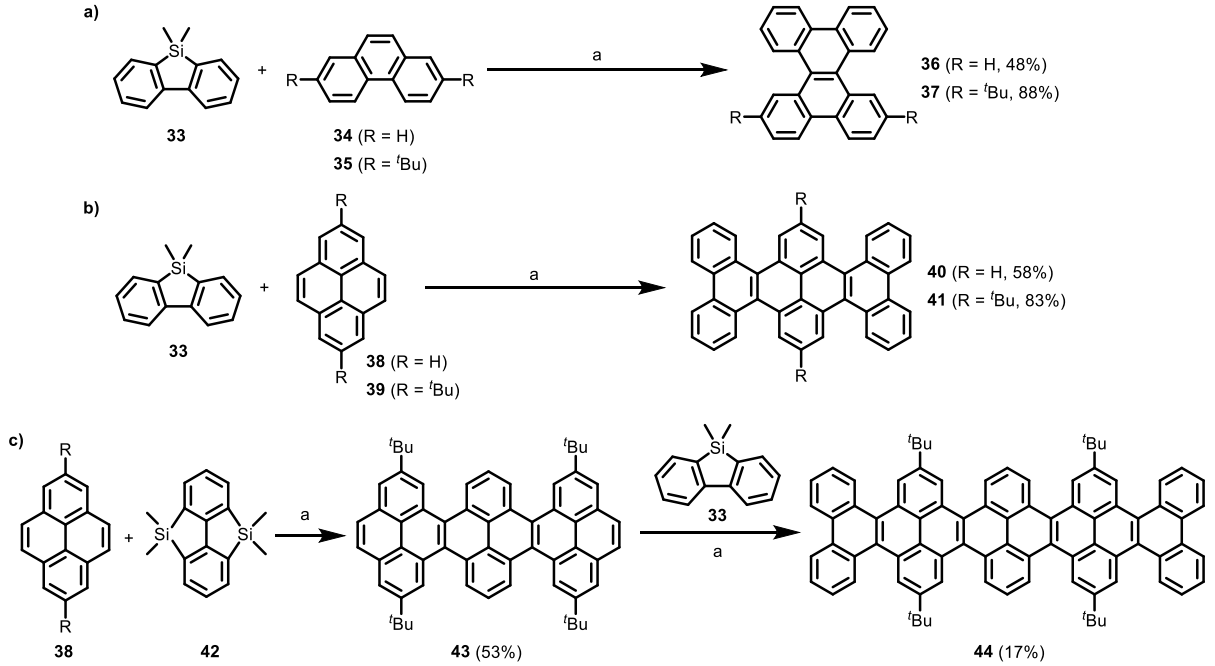

Scheme 1.4 *K*-region extension by C-H arylation reactions developed by Itami and co-workers.[45] [a] $Pd(CH_3CN)_2(SbF_6)_2$, *o*-chloranil, $ClCH_2CH_2Cl$, 80 °C, 2-8 h.

K-regions of PAHs can be extended by C-H arylation reaction in a single step, which was developed by Itami and co-workers.[46] This strategy was achieved by $Pd(CH_3CN)_2(SbF_6)_2$-catalyzed arylation using dibenzo[*b*,*d*]silole derivatives or other silicon-bridged arenes as the key reactants in the presence of *o*-chloranil. For instance, dibenzosilole derivative **33** was used to extend the *K*-region of phenanthrene (Scheme 1.4a).[45] This strategy is also suitable to achieve two-fold annulation based on pyrene (Scheme 1.4b).[45] By using the two-fold functionalized substrate **42**, linear oligomer **44** with three pyrene subunits was obtained after two consecutive C-H arylation reactions (Scheme 1.4c).[45]

1.2.2 Two-Step Strategy: Precursor Formation followed by a Ring-Closing Step

Besides extending π-systems based on existing PAH frameworks, another more widely used synthetic strategy for extended PAHs comprises two key steps: the formation of precursors and a ring-closing step.[16a, 18a, 47] As shown in Scheme 1.5, the synthesis of (hexa-*tert*-butyl) *peri*-HBC **51** serves as one of the most representative examples. The precursor hexaphenylbenzene **49** or hexa-*tert*-butylhexaphenylbenzene **50** could be obtained by cobalt-mediated [2+2+2] cyclotrimerization of diphenylacetylene **45**,[48] by Suzuki-Miyaura cross-coupling reaction between 1,4-diiodo-2,3,5,6-tetraphenylbenzene **46** and phenylboronic acid **47**[49] or by a Diels-Alder reaction of diphenylacetylene **45** with tetraphenylcyclopentadienone **48**.[50] The synthesis of (hexa-*tert*-butyl) *peri*-HBC **51** was accomplished by a ring-closing step, which was usually achieved by intramolecular cyclodehydrogenation of hexaphenylbenzene **50** in the presence of oxidants (*eg*. $FeCl_3$).[18a, 47a, 51]

This two-step strategy is also effective to construct more complex π-systems in recent publications. For instance, Murakami, in 2018 Itami and co-workers reported a synthetic route for substituted triphenylenes through the Pd-catalyzed annulative dimerization of monochlorinated oligo-*para*-phenylenes (Scheme 1.6).[52] The obtained (oligo)phenylene units were oriented parallel to each other in the corresponding products. Two of these triphenylene derivatives were fully cyclized after intramolecular cyclodehydrogenation to give the small graphene nanoribbon segments **54** and **57**, both in yields of > 70%.

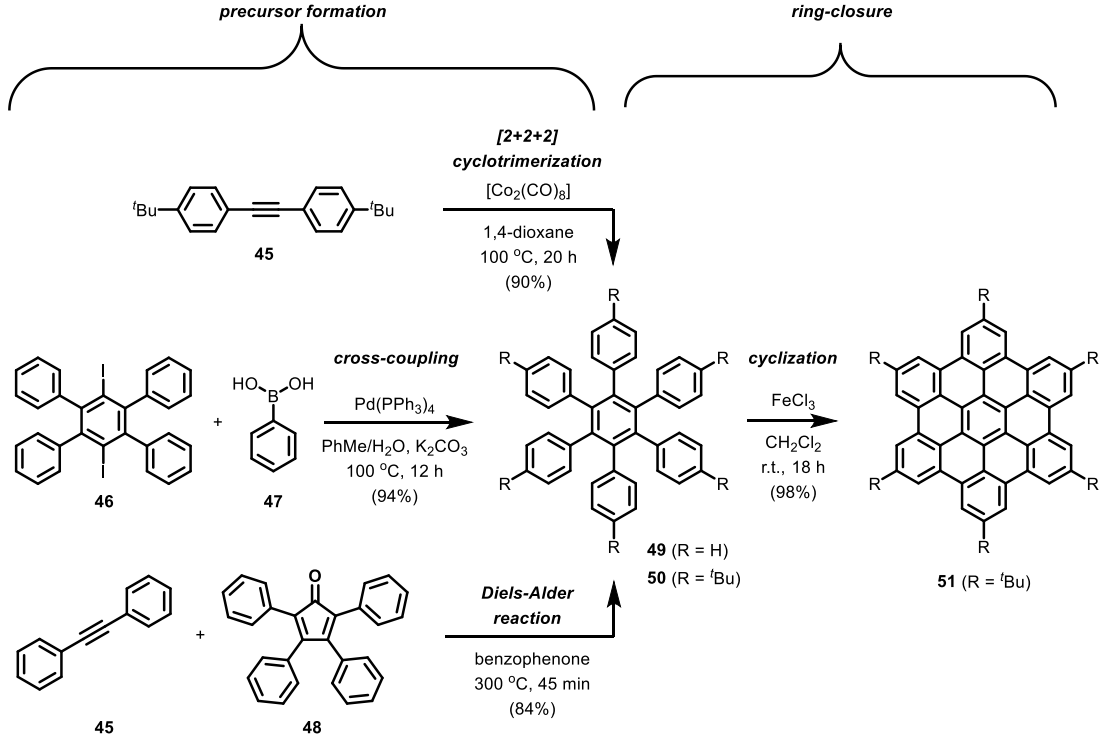

Scheme 1.5 Illustration of the two-stage strategy to obtain PAHs by taking the synthesis of *peri*-HBC as an example.[16a, 18a]

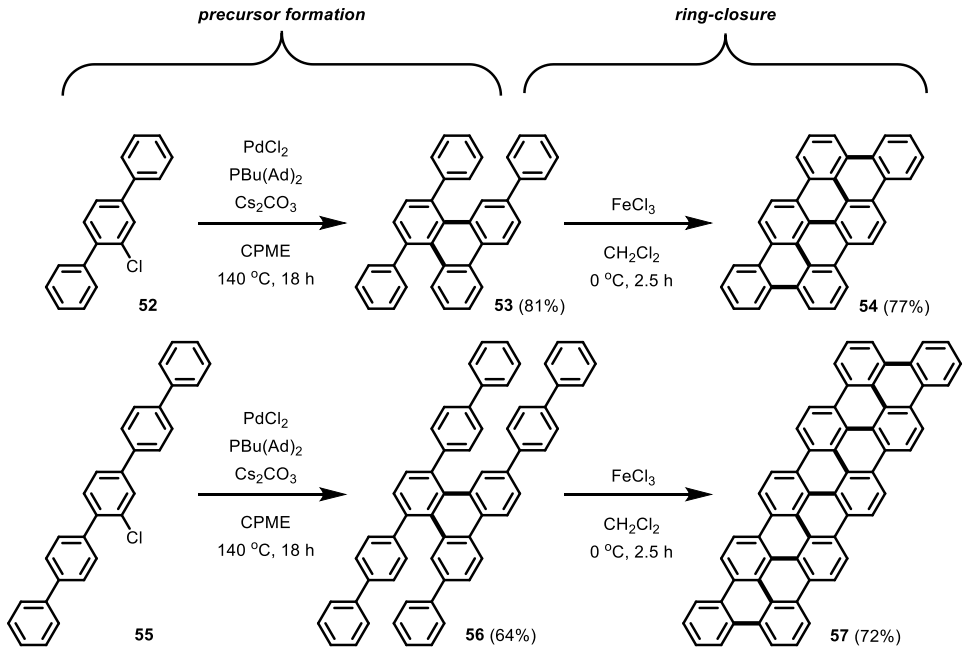

Scheme 1.6 The two-stage strategy illustrated by the synthetic route of graphene nanoribbon segments **54** and **57** reported by Itami and co-workers as an example.[52] C-C bonds highlighted in bold indicate the new C-C bonds formed during the annulative dimerization and cyclodehydrogenation. Ad: 1-adamantyl. CPME: cyclopentyl methyl ether.

Although various methods are available to prepare the precursor from small π-moieties, the key factors here are the ring-closing reactions to furnish the final PAHs. As the two most important ways to perform ring-closing steps, oxidative cyclodehydrogenation (often called Scholl reaction) and cyclization under photoirradiation undoubtedly play indispensable roles in the syntheses of PAHs. Both reactions will be discussed more detailed in the following chapters. Note that within the scope of this thesis, the main part discussed is intramolecular aromatic coupling reactions.

1.2.2.1 Oxidative Cyclodehydrogenation (Scholl Reaction)

Oxidative cyclodehydrogenation or oxidative coupling, which is often simply named "Scholl reaction", has not lost any attraction to organic chemists in the past decades, despite the development of many modern C-H activation procedures, such as annulative π-extension reported by Itami and co-workers.[46, 53] Up till now it is still a powerful synthetic tool to construct large π-systems by multiple biaryl bond formations in a single step without the necessity of prior installation of functional groups, such as halides, boronic acids/esters.[54]

The development of the Scholl reaction can be dated back to more than a century ago. In 1910, Scholl and Mansfeld reported that π-extended quinone **59** can be obtained from **58** in the presence of excess amount of neat anhydrous $AlCl_3$ at 140-145°C for 45 minutes while no yield was reported (Scheme 1.7a).[55] In following studies, perylene **1** was synthesized from 1,1'-binaphthalene **60** or directly from naphthalene **61** via intermolecular oxidative coupling (Scheme 1.7b).[56] Based on this approach, various π-systems were obtained by similar procedures.[57]

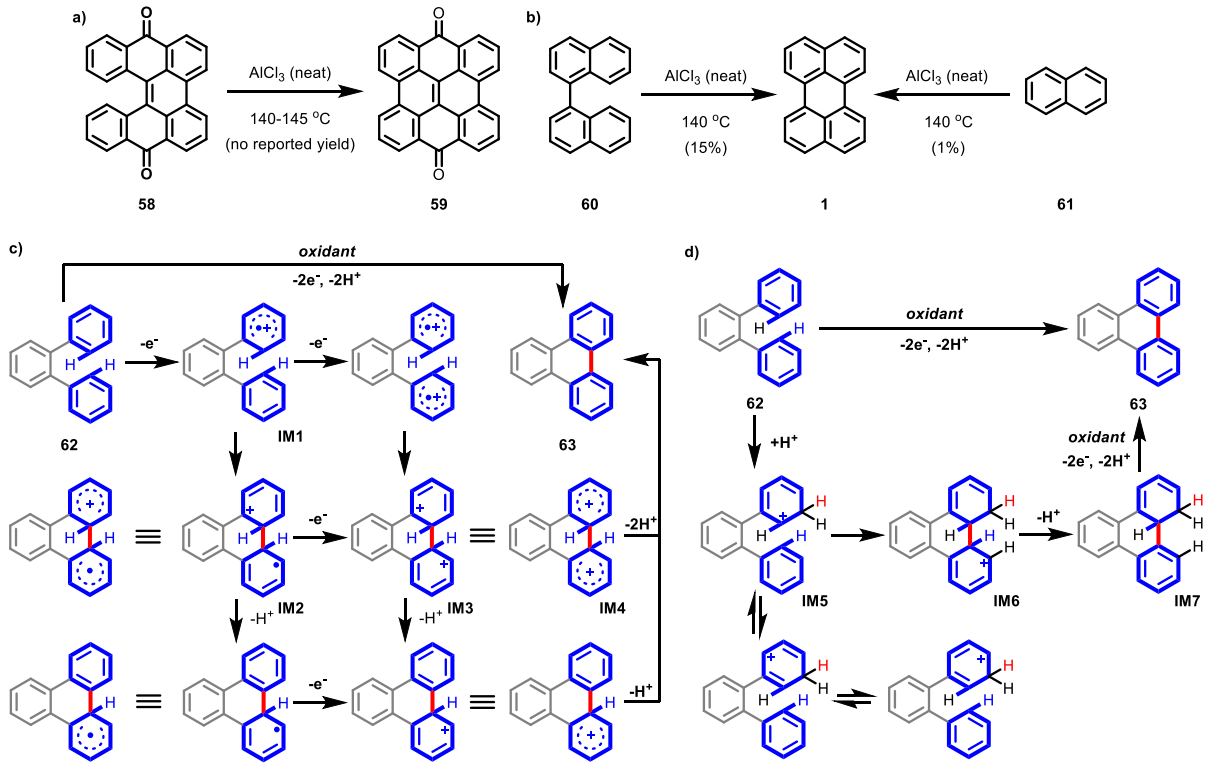

Scheme 1.7 Examples of intramolecular cyclodehydrogenation reactions reported by Scholl and co-workers (a and b). Radical cation (electron transfer, c) and arenium cation (proton transfer, d) mechanism for the Scholl reaction taking the formation of triphenylene **63** as an example.[55-56, 58]

The oxidative cyclodehydrogenation can be performed with a variety of oxidants and acids, such as $FeCl_3$,[59] $MoCl_5$,[60] 2,3-dichloro-5,6-dicyano-1,4-benzoquinone (DDQ)/Brønsted acids (methanesulfonic acid, trifluoromethanesulfonic acid, *etc.*)[61] and Lewis acids ($AlCl_3$, $Cu(OTf)_2$, $Sc(OTf)_3$, *etc.*),[62] and phenyliodine bis(trifluoroacetate) (PIFA)/$BF_3{\cdot}Et_2O$.[63] The Scholl reaction can be best described as proceeding through either a radical cation pathway [58, 61, 64] or an arenium cation pathway.[65] In a typical radical cation process (Scheme 1.7c), precursor **62** was firstly one-electron oxidized in the presence of oxidant to produce radical cation **IM1**, followed by the formation of one C-C bond to form the distonic radical cation **IM2**. After removal of a second electron and the following loss of two protons, triphenylene **63** is obtained. A typical arenium cation process (Scheme 1.7d) starts with the protonation of one benzenoid ring on **62** at a carbon atom in *meta*-position of the electron-releasing group. The formed arenium ion intermediate **IM5** can be stabilized by delocalization of the positive charge over the phenyl ring. Then an intramolecular Friedel-Crafts-type electrophilic attack of the formed arenium ion ring to the adjacent benzenoid ring takes place and one new C-C bond is formed, followed by a rapid proton loss to give a nonaromatic cyclohexadiene intermediate **IM7**. The final triphenylene **63** is formed after rearomatization by removing two electrons and two protons in the presence of oxidant.

The two mechanisms can explain reaction outcomes under different conditions, especially when considering the cyclization of aromatic hydrocarbons in the presence of oxidizing or non-

oxidizing Lewis acids.[54a] However, attention should be paid to the fact that there are still controversies about the two mechanisms till now and the specific mechanism of a Scholl-type reaction is not easy to determine in most cases. Most of the Lewis acids used are also milder or stronger oxidants and the chemical reactivities of paramagnetic cation radicals and diamagnetic arenium ions are quite similar in a given Scholl-type reaction.[58] For example, the arenium ion mechanism was supported by a series of computational results reported by King and co-workers.[63, 66] When investigating the cyclodehydrogenation to form unsubstituted *peri*-HBC, they found that the arenium ion mechanism is favored in comparison to radical cation pathway, as the energy of transition states in arenium ion pathway is relatively lower both in vacuum and solution. These findings are consistent with the Scholl reactions proceeding in acidic media, such as anhydrous HF[67] and $PhSO_3H$,[65c] which do not promote radical cation formation. However, Rathore and co-workers claimed that the radical cation mechanism is favored during a Scholl-type reaction after investigating various cyclodehydrogenation processes in the presence of many oxidants and comparing the redox potentials of a series of Scholl precursors and the corresponding cyclized products measured by cyclic voltammetry (CV).[58] They found that precursors with oxidation potentials lower than 1.7 V vs. saturated calomel electrodes (SCE), which can be readily oxidized to radical cations using DDQ/H^+ or $FeCl_3$ as oxidants, could undergo cyclodehydrogenation reactions in the presence of DDQ/H^+ or $FeCl_3$, whereas precursors with oxidation potentials higher than 1.7 V vs. SCE do not. The necessity to use powerful oxidants (DDQ/H^+ or $FeCl_3$) does not support the arenium cation mechanism, in which the dihydro intermediate **IM7** could be easily rearomatized even by I_2 or O_2. The fact that bubbling the reaction mixture with N_2 or argon gas to remove gaseous HCl in the cases using $FeCl_3$ also contradicts the deduction by King and co-workers that Scholl reactions could be self-promoted by the production of acid in each C-C bond formation.[66a]

However, the uncertainty in the mechanism of the Scholl reaction does not compromise its practicability in syntheses of π-extended molecules. One important example is *peri*-HBC and its derivatives. As reported by Clar and co-workers, heating tetrabenzoperopyrene at more than 480 °C produces *peri*-HBC although the yield was not reported.[68] Later, Halleux *et al*. reported that *peri*-HBC can be obtained in about 3% yield by treating hexaphenylbenzene **49** in molten $AlCl_3$/NaCl for 2.5 hours.[51] It was not until Müllen and co-workers used the $CuCl_2/AlCl_3$ or $FeCl_3$-promoted oxidation of hexaphenylbenzenes that *peri*-HBC derivatives could be obtained in high yields (> 90%).[18a] Especially the conditions where $FeCl_3$ is dissolved in CH_3NO_2 prior to its addition to a diluted solution of the precursors in CH_2Cl_2 provide the best yields for the broadest scope of *peri*-HBCs, which opened the door to the syntheses of large PAHs.[48f, 50f, 69]

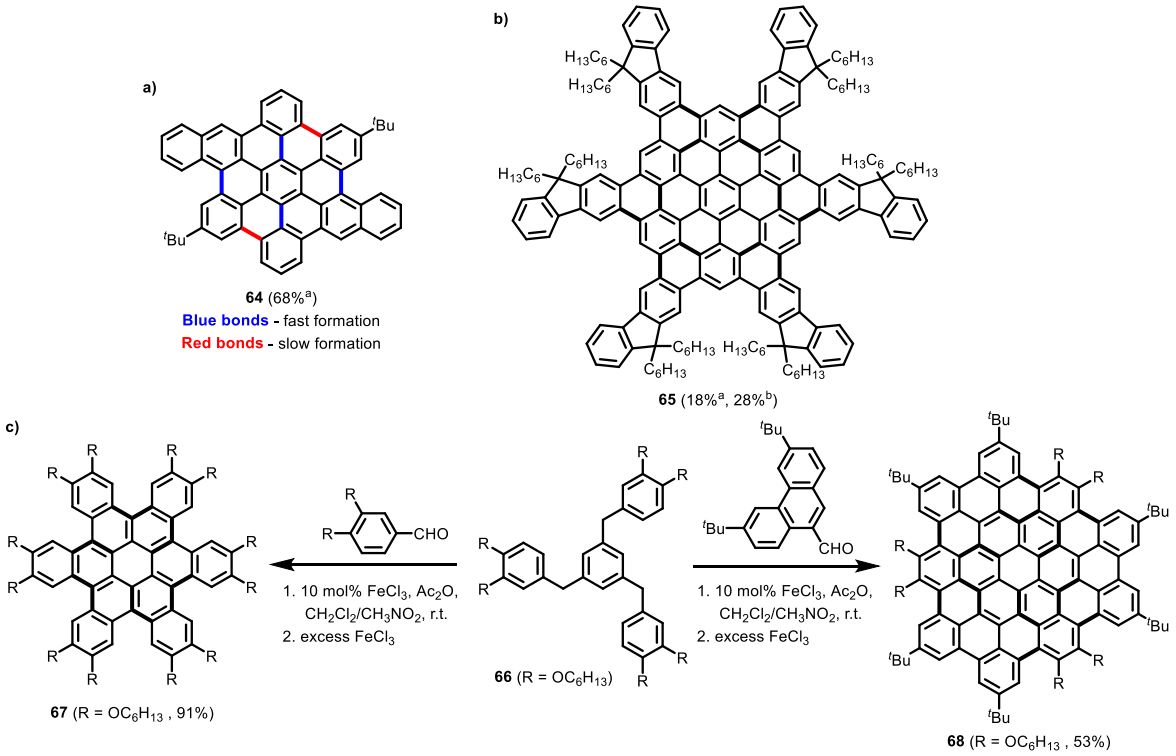

Scheme 1.8 Selected examples of PAHs obtained by Scholl reaction.[70] The C-C bonds formed during Scholl-type reactions are highlighted in bold. [a]$FeCl_3$, CH_3NO_2, CH_2Cl_2, r.t.; [b]DDQ, CH_3SO_3H, CH_2Cl_2, 0 °C.

In addition to the *peri*-HBC, some representative PAHs obtained by Scholl reactions are shown in Scheme 1.8.[70] When synthesizing PAH **64**, Dichtel and co-workers found that the formation rates of C-C bonds at different positions during the Scholl reaction were different.[70a] A partially cyclized intermediate was isolated after the rapid formation of first four bonds. The final fully fused HBC derivative **64** could be obtained after longer reaction time in 68% yield. Another interesting example is shown in Scheme 1.8b. Rathore and co-workers reported the synthesis of six-fold fluorene fused *peri*-HBC **65** performing a twelve-fold Scholl cyclization as the final step.[70b] Using DDQ/CH_3SO_3H the reaction could give a higher yield of 28% than that using $FeCl_3/CH_3NO_2$ (18%). Twelve hexyl chains effectively restrict the intermolecular aggregation, which makes this giant PAH well soluble in common organic solvents. Wei and co-workers reported a facile method to synthesize a series of π-extended derivatives of hexa-*cata*-hexabenzocoronenes (*cata*-HBC) with a three-fold symmetry by reacting 1,3,5-tribenzylbenzene derivative **66** with aromatic aldehydes in the presence of $FeCl_3$ and acetic anhydride as oxidant/Lewis acid and a dehydrating agent, respectively, in a CH_2Cl_2/CH_3NO_2 mixture. The extended coronene **68** with 72 sp^2 hybridized carbon atoms in the aromatic central core was obtained in a one-pot reaction in 53% yield, which was a combination of Friedel-Crafts hydroarylation, intramolecular alkylation, dehydrogenative aromatization and intramolecular cyclodehydrogenation.[70c, 71] Unfortunately, no mechanistic studies were performed to further investigate this one-pot tandem reaction.

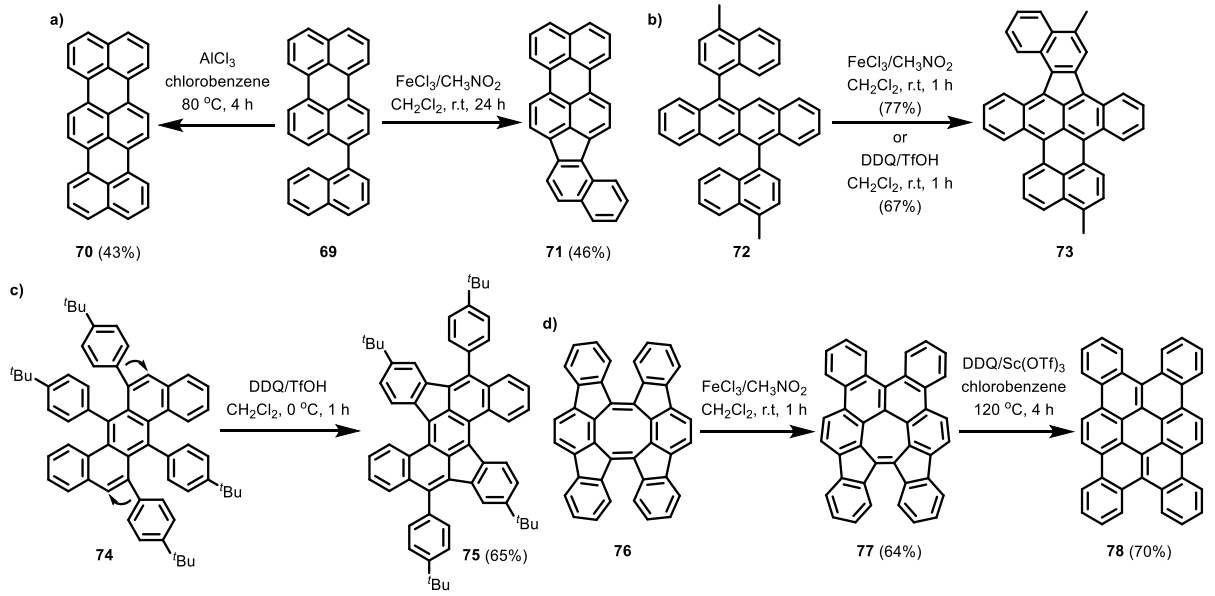

Scheme 1.9 Selected examples of reactions involving different cyclization pathways (a),[72] unsymmetric cyclization (b),[73] 1,2-shift of aryl groups (c)[74] and skeletal rearrangement (d)[75] under Scholl conditions.

It is worth emphasizing that potential unexpected outcomes are included in Scholl reactions. In some cases, the obtained product does not adopt the structures as expected.[16a, 47b, 54a, 54b] The application scopes of above mentioned synthetic methods are limited by several factors in a few cases, such as incomplete cyclization,[76] possible different pathways of cyclization or even unsymmetric cyclization,[72-73] undesired chlorination,[62, 77] unexpected 1,2-aryl shifts[74, 78] and unexpected structural rearrangements.[75, 79] For instance, Müllen and co-workers reported that the cyclization product varies when using different reaction conditions in the Scholl reaction of 3-(1-naphthyl)perylene **69** (Scheme 1.9a).[72] While terrylene **70** was formed in the presence of $AlCl_3$ in chlorobenzene, the cyclopentannulation to compound **71** was favored when $FeCl_3/CH_3NO_2$ was used. This phenomenon could be rationalized by the assumption that the Scholl reaction may proceed by different mechanisms in the presence of oxidizing and non-oxidizing Lewis acids.[54a] Murata and co-workers reported that the Scholl reaction of 5,11-dinaphthyltetracene **72** gave an unsymmetric two-fold cyclized product **73** with one five-membered and one six-membered ring formed, which exhibits a twisted backbone and an absorption band up to 950 nm was found (Scheme 1.9b).[73] DFT calculations indicate that the unsymmetric cyclization proceeds via unprecedented dicationic intermediates, which is different from the above discussed arenium ion or radical cation mechanism. The two-fold cyclization was proposed to be performed stepwise. The formation of the five-membered ring is kinetically favored in the first step and the hexagonal ring is prone to be formed in the second step due to the structural constraint after the cyclopentannulation. The two-fold cyclopentannulation of 6,7,13,14-tetraarylbenzo[*k*]tetraphene **74** with unexpected regioselective 1,2-migration of aryl groups during the Scholl reaction was reported by Feng and co-workers (Scheme 1.9c).[74] Based on DFT calculations, this 1,2-migration was proposed to occur

prior to the Scholl cyclization and both the arenium ion as well as the radical cation pathway show rationality in explaining the 1,2-shift of aryl groups, although the rearrangement of aryl groups was previously reported to proceed through arenium ion intermediates.[79d] Tobe and co-workers reported that the molecular backbone of cyclooctatetraene derivative **76** could be transformed to a seven-membered ring containing PAH **77** in the presence of $FeCl_3/CH_3NO_2$, which could be further rearranged to tetrabenzocoronene **78** via a skeletal isomerization (Scheme 1.9d).[75] DFT calculations indicate that the rearrangement could be ascribed to acid-catalyzed isomerization of 9,9'-bifluorenylidene into dibenzo[*g*,*p*]chrysene moieties. Therefore, attention should be paid when designing the synthetic routes of PAHs using Scholl reactions as the ring-closing step. Unconventional synthetic methods are still necessary to be developed, in order to compensate the Scholl reactions for the ring-closing step to obtain PAHs, which are difficult to access by Scholl reactions.

1.2.2.2 Photocyclization

As an effective way to perform aryl-aryl ring closure, the cyclization of stilbene and related compounds by photochemistry serves as an alternative method to the Scholl reaction for the ring-closing step in the synthetic procedures of PAHs.[80] Under UV irradiation, stilbene **79** undergoes an electrocyclic rearrangement forming dihydrophenanthrene, followed by an aromatization to give phenanthrene **34** in the presence of oxidants such as I_2 or O_2 (Scheme 1.10a). Nuckolls and co-workers obtained a series of hexa-*cata*-hexabenzocoronenes (*cata*-HBC, **84-86**) via the photocyclization of stilbene-type precursors **81-83** in the ring-closing step in high yields (> 80%, Scheme 1.10b).[81]

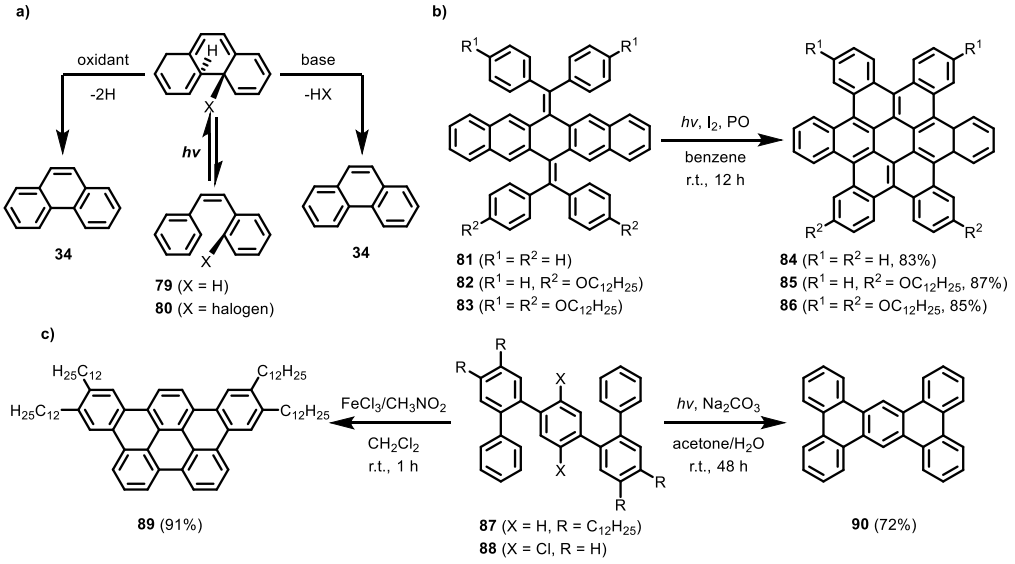

Scheme 1.10 a) Two pathways towards phenanthrene **34** via oxidation or photocyclodehydrohalogenation.[80a] b) Synthesis of *cata*-HBCs using photocyclization in the ring-closing step.[81a] c) Different results of cyclization of oligophenylene precursor **87** or **88** via Scholl reaction or photocyclodehydrohalogenation.[82] PO: propylene oxide.

The photocyclization can also be performed by photocyclodehydrohalogenation, which proceeds through an elimination pathway in absence of oxidants (Scheme 1.10a). In this case, functional groups such as halogens are necessary to be presented at the *ortho*-position of one phenyl ring, thus achieving high regioselectivity in the ring-closing step. This method was proposed by Hata and co-workers in 1970s.[83] Hartley and co-workers used this approach to synthesize dibenzo[*fg*,*op*] naphthacenes and tetrabenzanthanthrenes[78b, 84] while Bach and co-workers employed it to prepare phenanthro[9,10-*c*]thiophenes.[85] Morin and co-workers reported the synthesis of tribenzo[*f*,*k*,*m*]tetraphene **90** (Scheme 1.10c) from the chlorinated precursor **88** by cyclodehydrochlorination (CDHC) in 72% yield using chlorine atoms as directing groups,[82a, 86] whereas PAH **89** with another π-backbone could be obtained under oxidative condition (Scholl reaction) efficiently in 91% yield from non-halogenated precursor **87** as reported by Müllen and co-workers.[82b]

1.3 PAHs with Contorted Structures

Besides the synthetic strategies towards PAHs, the structures of π-backbones of PAHs should also be considered. In comparison to planar PAHs, contorted or curved PAHs are more attractive synthetic targets, as they represent cutouts of fullerenes, carbon-nanotubes or other 3D aromatic allotropes such as the Mackay crystals.[87] There are different strategies to introduce curvature into π-systems. Among them the most two widely used methods are implementing steric congestion at their periphery such as introducing cove or fjord regions (Figure 1.3), and embedding non-hexagonal rings, such as five-, seven-, or eight-membered rings into the fused aromatic framework. Both approaches will be discussed in this section, respectively. Note that in the second method, introducing non-hexagonal rings into the π-backbones of PAHs does not necessarily produce non-planar structures in some specific fusing patterns.[88] As this thesis does not deal with the 3D π-systems, such as carbon nanorings or nanobelts,[89] they are not involved in this chapter.

1.3.1 Contortion by the Creation of Cove and Fjord Regions

Typical edge topologies of PAHs are illustrated in Figure 1.3.[16a] These regions correspond to the concave armchair edge (bay region), convex armchair region (*K*-region) and zigzag edge (*L*-region) according to the nomenclature of graphene.[17a, 90] Cove and fjord regions are structural features inducing non-planarity of PAHs due to the steric hinderance.[29]

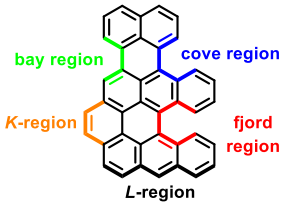

Figure 1.3 Schematic illustration of typical peripheral structures of PAHs.[16a, 17a, 90]

For PAHs with cove regions, one of the most representative examples is *cata*-HBC **84** (Figure 1.4a) and its derivatives. Parent *cata*-HBC **84** was first synthesized by Clar and Stephen in 1965 after seven steps starting from 2-(2,5-dimethylbenzyl)benzoic acid.[91] A revised synthetic route to **84** and its derivatives comes from the photocyclization of stilbene-type precursors in the ring-closing step, as discussed in Section 1.2.2.2. Their intermolecular packing behaviors and applications in electronic devices were systematically investigated by Nuckolls and co-workers,[81, 92] and Müllen and co-workers.[93] As shown by X-ray diffraction analysis of a single crystal (Figure 1.4b),[94] the parent *cata*-HBC **84** adopts a conformation where the exterior benzo-groups fold alternately above or below the π-plane, creating two concave surfaces. The six *cata*-condensed benzenoid rings deviate from the ring located in the center of coronene by 23.3°-27.5°. High charge-carrier mobility of > 1 $cm^2 \cdot V^{-1} \cdot s^{-1}$ in alkoxy substituted *cata*-HBC based organic field-effect transistors (OFETs) was achieved.[95]

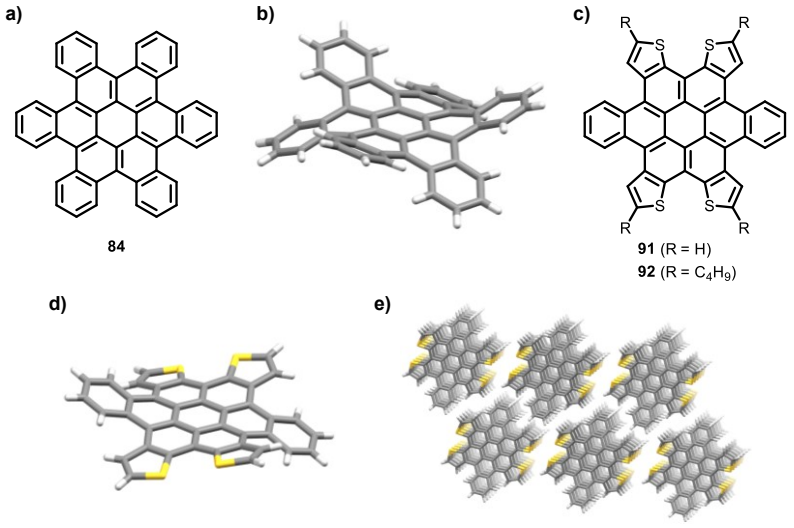

Figure 1.4 Molecular structure (a) and side-view of single crystal structure (b, CCDC 1426976) of *cata*-HBC **84**. Molecular structure (c) of thiophene substituted *cata*-HBC **91** and **92**. Side view (d, CCDC 817721) and columnar packing motif (e) of crystal structure of **91**.

When four peripheral benzenoid rings of *cata*-HBC **84** were replaced by thiophene rings, PAH **91** without alkyl chains shows similar alternate up-down conformation in the crystal structure (Figure 1.4d).[81b] The overall π-plane of **91** is more flattened than *cata*-HBC **84** because of the reduced steric interactions between the five-membered thiophene rings at the periphery. **91** forms a columnar packing motif where atoms of one of the molecules in a stack almost completely eclipse with the next nearest neighbors (Figure 1.4e). This packing mode was ascribed to the molecular corrugation of **91** and intermolecular sulfur-sulfur interactions. PAH **92** with substituted butyl chains on the thiophene rings shows both the alternative up-down and up-down-down-up-down-down (butterfly) conformations in crystal structures due to the interactions with solvent molecules. The incorporation of thiophene units gives a more flexible structure in comparison to the parent

cata-HBC **84**. The conformation of PAH **92** in solid state could be further controlled by growth of co-crystals from solution with electron acceptors, such as tetracyano-*p*-quinodimethane (TCNQ) and fullerene (C_{60}). It adopts the butterfly conformation when the electron acceptor is small enough to be completely enveloped in the case of co-crystals with TCNQ. The conformation of **92** could be transformed to the up-down type when the electron acceptor (C_{60}) is relatively large, which serves as a π-backbone with adjustable supramolecular structure.[81b]

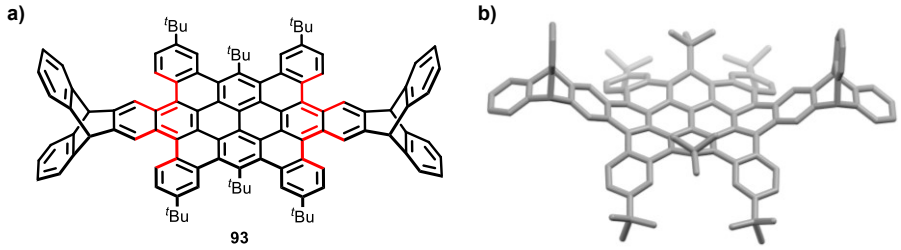

Figure 1.5 Molecular structure (a) and single crystal structure (b, CCDC: 1497325) of PAH **93**.[96] Cove regions are highlighted in red in (a).

Mastalerz and co-workers reported the synthesis of a large contorted hexabenzoovalene derivative (**93**) (Figure 1.5) with two peripheral triptycene units, which was obtained by a Scholl reaction using an $FeCl_3$/DDQ mixture in 90% yield in the final ring-closing step.[96-97] As a result of the large steric hindrance from four cove regions and the presence of two central bulky *tert*-butyl groups, the whole system is highly contorted in a U-shaped conformation, which is stable in solution even at 150 °C. This conformation could be converted to an undulated S-shape conformer in the solid state after regioselective removal of the two central *tert*-butyl groups under acidic conditions. The red-emitting photoluminescent property of **93** in solution remains in thin-films with ionic matrices and its application in organic electronics has been proved.[98] Light-emitting electrochemical cells based on hexabenzoovalene **93** exhibit irradiances of around 220 $\mu W \cdot cm^{-2}$ with an external quantum efficiency of 0.78% and stabilities over 220 h. The variations of the electroluminescence band shapes are dependent on the relative intensity of the applied electric field.

Besides the cove regions, introducing fjord regions comprising five carbon atoms is another effective approach to make curved PAHs. Helicenes with at least five fused benzene rings are one of the most representative examples for PAHs with fjord regions.[99] The racemization free energy of [5]helicene (**94**, Figure 1.6a) was estimated to be $\Delta G^{\ddagger}$ = 24.1 $kcal \cdot mol^{-1}$ at 300 K.[99c] The $\Delta G^{\ddagger}$ values are getting higher with increasing of n, which reach a plateau at around 42 $kcal \cdot mol^{-1}$ when n = 7. Therefore, the interconverting energy barriers are high enough to form stable enantiomers in [n]helicenes ($n \geq 5$) at room temperature.

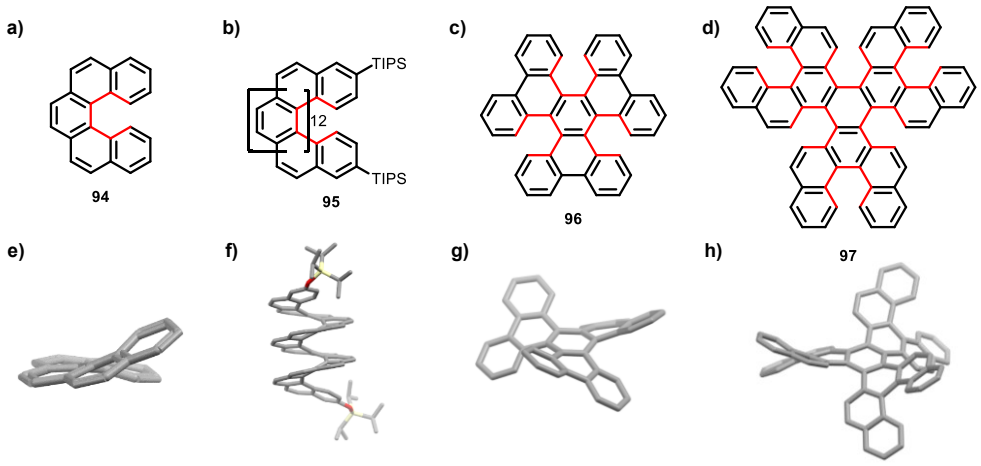

Figure 1.6 Structural formulae (a-d) and corresponding crystal structures (e-h, CCDC 1137287, 1051159, 114449, 1814742) of selected examples of helicenes.[100] Hydrogen atoms are omitted in the crystal structures for clarity. Fjord regions are highlighted in red. TIPS: triisopropylsilyl.

The two terminal benzenoid rings in [5]helicene **94** overlap only partially with each other due to steric repulsion (Figure 1.6a and e).[100a, 101] With increasing of number of fused rings, the overall molecular structure undergoes a helical twist and the final thermodynamically most favored conformation results from the optimization of the energy cost of the induced torsional strain against the energy benefit of the minimized steric interaction (*eg*. [16]helicene **95**).[99e, 100b] Another representative example of PAHs with fjord regions is PAH **96**, which comprises three fjord regions and serves as the smallest propeller derived from benzene.[100c] It adopts a D_3 symmetric helical conformation, in which three biphenyl subunits are twisted out of the central ring by 30° on average, due to the steric repulsion caused by the three fjord regions (Figure 1.6c and g). This propeller could be further extended to construct hexapole helicene **97**.[102] Due to the presence of six fjord regions, there are ten pairs of possible diastereomers in PAH **97**. **97** was obtained by Pd^0-catalyzed [2+2+2] cycloaddition of benzyne precursor as a racemic mixture in C_2 symmetric patterns, which is the second most stable racemic mixture among these possible isomers.[102b] The most thermodynamically stable racemic mixture (Figure 1.6h, one isomer from the racemic mixture) with D_3 symmetry could be obtained from the second most stable racemic mixture by treatment in toluene at 100 °C for three hours. The twisting angle of one of the three benzene rings surrounding the central ring was found to be 35.7° in the second most stable racemic mixture as determined by single crystal X-ray diffraction analysis, which is higher than those of the corresponding triple helicenes[103] due to the additional repulsion from the outer moieties in **97**. Because of the unique chirality and optoelectronic properties, these helicene-type PAHs showed potential to be applied in circular dichroism,[104], nonlinear optics[105] and have been applied as model compounds to investigate the chiral-induced spin selectivity effect.[106]

1.3.2 Contortion by Embedding Non-Hexagonal Rings

Introducing non-hexagonal rings, such as four-, five-, seven- or eight-membered rings, into the planar graphene nanosheets is another effective strategy to create curved PAHs.[107] Figure 1.7 illustrates how the introduction of non-hexagonal rings affects the conformation of π-planes of PAHs, using the [*n*]circulenes as model compounds, which feature a central *n*-sided polygon fully surrounded by fused six-membered benzene rings.[108] With different values of *n*, four types of [*n*]circulenes can be obtained: positively curved (*n* = 4-5), planar (*n* = 6), negatively curved (*n* = 7-16) and helical (*n* > 16).[109] Here the definition of curvature for polyaromatic systems (positive, zero or negative) is according to the corresponding Gaussian curvatures as discussed by Mayor and co-workers.[109] For [*n*]circulenes with *n* = 3-5, the distortion forces the planar structure to form a bowl-shaped topology. [6]Circulene equals coronene, which is a strain-free structure and thus planar. The values of the internal angles of polygons in [7-16]circulenes are larger than 120°, which induce ring strain that forces the planar pattern to form a saddle-like structure. When the number of fused benzene rings further increases (> 16), circulenes start to form unique helical structures according to calculations.[108, 110]

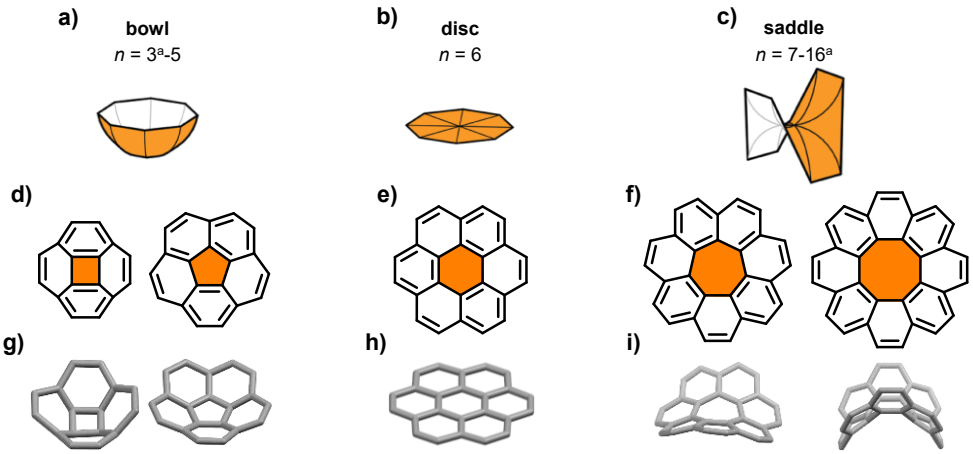

Figure 1.7 a-c) Schematic illustration of surfaces with positive (a), zero (b) and negative (c) Gaussian curvatures. d-f) Molecular structures of [*n*]circulenes (*n* = 4-8). g-i) Side views of X-ray single crystal structures of [*n*]circulenes (*n* = 4-8, CCDC 747755, 1129824, 1129883, 1122357, 938414). In the cases of [4]- and [8]circulene, the parent structures have not been made and the substituents of their known derivatives are omitted for clarity. [a][*n*]Circulenes with *n* = 3 and *n* > 8 have not been synthesized. Schematic illustration of surfaces are reproduced from Ref.[109] with permission from The Royal Society of Chemistry 2017.

Within the scope of this thesis, [5]circulenes (corannulene) and its derivatives, which are the most studied cases among the three possible positively curved [*n*]circulenes,[17b, 111] will not be discussed in detail. On the other hand, research interest in introduction of heptagons or octagons into 2D π-systems to induce negative curvatures has been growing over decades,[112] as both theoretical[113] and experimental[114] studies indicate the potential differences of the electronic and optical properties of π-systems with negative curvatures from the basic planar systems.

From the viewpoint of synthesis, the seven-membered rings in large PAHs were incorporated either by using seven-membered ring-containing small substrates,[115] or by forming the heptagonal rings via intramolecular Friedel-Crafts acylation,[116] oxidative cyclodehydrogenation,[79c, 117] ring expansion of cyclohexanone,[118] or intramolecular cyclotrimerization of alkynes.[119] Since 2012, Miao and co-workers have reported a series of negatively curved PAHs.[115-116, 118, 120] One of the most representative compounds is PAH **98** (Figures 1.8a and e), which was obtained by ring expansion of tetra-*tert*-butylbisanthenequinone with trimethylsilyldiazomethane and a final ten-fold Scholl cyclization as two key steps.[118] PAH **98** shows a saddle-like structure and the naphthalene moiety in the center is severely out-of-plane deformated with a dihedral angle of 77.2°, which is larger than the deformation of the naphthalene moiety in fullerene (42.5°).[121] Another representative example is shown in Figures 1.8b and f. An oxidative ring closure leading to the formation of five seven-membered rings around a corannulene central core by a Scholl reaction gave the large saddle-shaped PAH **99** in 40% yield, as reported by Itami, Scott and co-workers.[117e] As determined by single crystal X-ray diffraction analysis, the whole molecule shows a negative curvature. The presence of five helical hexa[7]circulene[122] moieties makes this grossly warped nanographene a chiral molecule with two enantiomers, in which the energy barrier of racemization is 18.9 kcal·mol^{-1} as predicted by DFT calculations, suggesting a rapid interconversion of different isomers at room temperature.

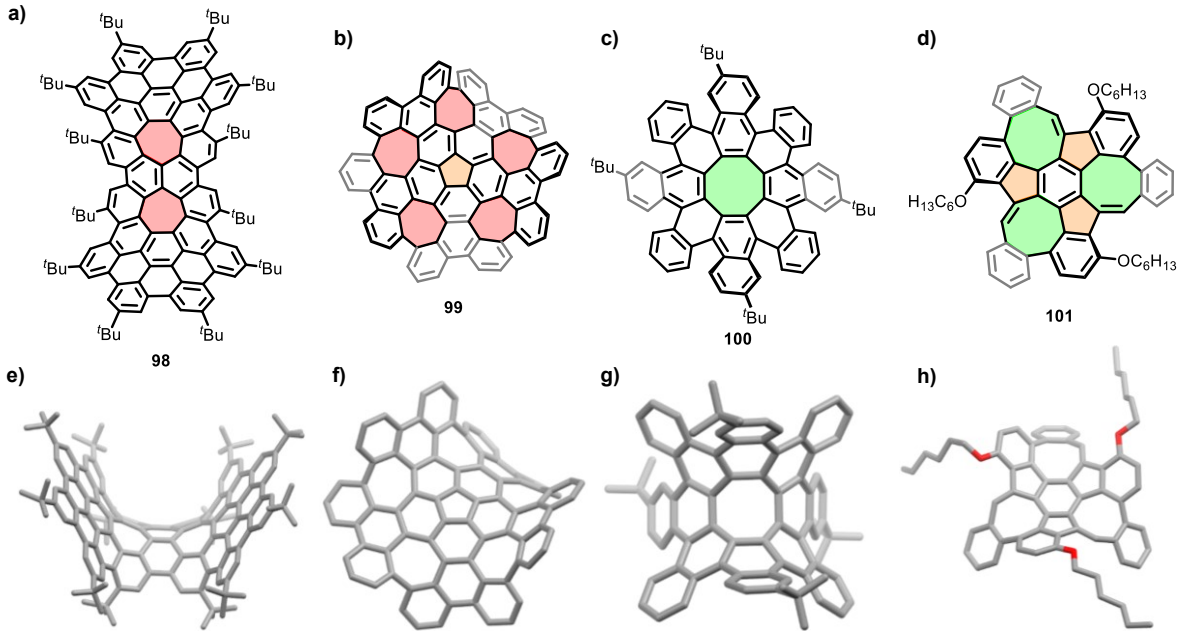

Figure 1.8 Structural formulae (a-d) and corresponding crystal structures (e-h, CCDC 1584279, 919707, 1922249, 1954750) of selected contorted PAHs embedded with non-hexagonal rings.[117e, 118, 120f, 123] The embedded five-, seven- and eight-membered rings are highlighted in orange, red and green, respectively. Hydrogen atoms are omitted in the crystal structures for clarity.

Similar to the construction of seven-membered rings in PAHs, the introduction of eight-membered rings in PAHs can be achieved by oxidative cyclodehydrogenation,[120c, 124] Diels-Alder

cycloaddition[125], [4+4] cyclodimerization[126], or by reactions based on octagonal ring-containing substrates.[127] Miao and co-workers reported the synthesis and the crystal structure of octabenzo-[8]circulene **100**, which exhibits a saddle-shaped π-backbone with D_2 symmetry (Figures 1.8c and g).[120f] Due to the presence of the four *tert*-butyl groups at the periphery, two racemic enantiomers were observed in the crystal structure of PAH **100**. The energy barrier between the two enantiomers was predicted to be only 9.2 kcal·mol^{-1} by DFT calculations, suggesting a flexible conformation of **100** with a high interconversion rate at room temperature (1.1×10^6 Hz at 25 °C). Recently, Mastalerz and co-workers reported the contorted PAH **101** with three embedded five-membered and three eight-membered rings, which is negatively curved in a shape of a monkey saddle (Figures 1.8d and h).[123] Three octagonal rings were formed via a base-mediated three-fold condensation of a truxene-based trisaldehyde precursor in 58% yield.[128] Owing to the inherent chirality, the inversion barrier was estimated to be 102-104 kJ·mol^{-1} by DFT calculations, which is high enough to handle the chiral HPLC-separated enantiopure monkey saddle PAH at room temperature without racemization. This conformational stability serves as one necessary prerequisite to be able to construct a fully conjugated sp^2 hybridized carbon atoms based cage containing four of the monkey saddle PAHs.[123]

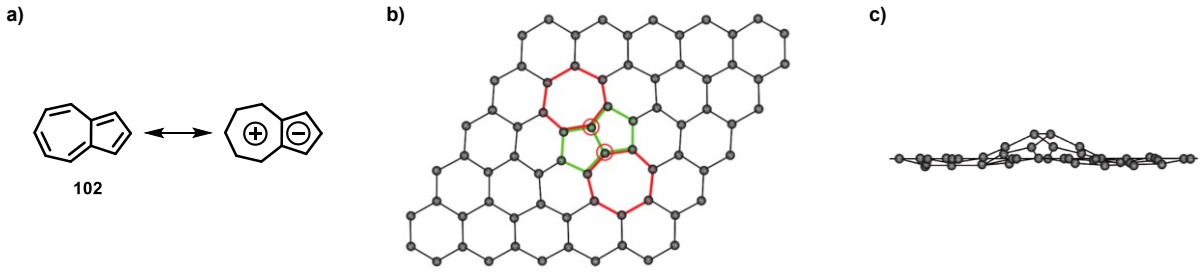

Figure 1.9 a) Molecular structure of azulene **102** and its polarized resonance structures. b-c) DFT-optimized structural model of inverse Stone-Wales defect. b) and c) are reprinted with permission from Ref.[107] Copyright (2011) American Chemical Society.

When a pentagonal aromatic ring shares two carbon atoms with another heptagonal aromatic ring, a nonbenzenoid and nonalternant aromatic hydrocarbon subunit, which is named "azulene",[129] is formed. Azulene **102** (bicyclo[5.3.0]decapentaene, Figure 1.9a) is an aromatic bicyclic isomer of naphthalene **61**. Due to the non-mirror-related HOMO-LUMO geometry reducing the repulsive interaction between the two unpaired electrons, azulene **56** exhibits a small energy gap between the ground state (S_0) and the first excited state (S_1), which makes the $S_0 \rightarrow S_1$ transition of azulene observable as a weak absorption in the visible light region and makes azulene appear a unique bright blue color.[110] Azulene and its derivatives have a wide application in material sciences,[130] including electrochromic materials,[131] molecular switches,[132] near-infrared (NIR) resonance materials,[133] nonlinear optical materials[134] and molecular devices.[135]

The azulene scaffold was also found as a defect in graphenes.[107] It can be viewed as a subunit of a specific defect composed of two joined pentagons placed between two heptagons (inverse Stone-Wales defect, Figure 1.9b), which can be one of the reconstruction modes of the graphene lattice from double-vacancy defects.[136] DFT-optimized structural mode of inverse Stone-Wales defect containing graphene lattice (Figure 1.9b and c) shows a contorted conformation. As the structural defects in the graphene lattice have a large influence on its mechanical, thermal, electronic and magnetic properties,[107, 137] PAHs with intentionally introduced defects, such as azulene units, serve as important model compounds to evaluate the structure-property relationship of such π-extended materials.[16a]

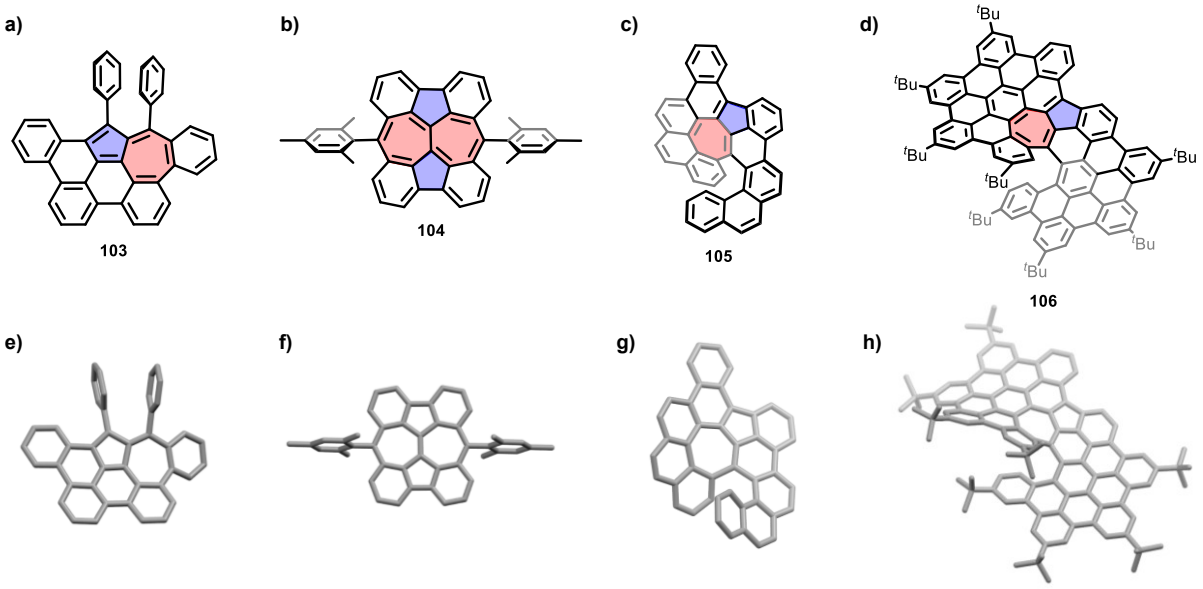

Figure 1.10 Structural formulae (a-d) and corresponding crystal structures (e-h, CCDC 1380411, 1906918, 1966144, 1949090) of some recently reported azulene-embedded PAHs.[88, 138] Hydrogen atoms are omitted in the crystal structures for clarity. The embedded five- and seven-membered rings are highlighted in blue and red, respectively.

Synthesis and property investigations of azulene embedded PAHs are of interest in recent years. But there were only a few successful approaches published, due to the difficulties in synthesis and potential instability resulting from the biradical triplet ground state character of such subunits.[139] Azulene embedded PAHs could be obtained from precursor monolayers on surfaces,[140] whereas only a few cases of soluble azulene-based PAHs have been synthesized in solution on a larger scale.[88, 133, 138, 141] Konishi and co-workers reported the azulene-based PAH **103** with additional six fused benzene rings (Figure 1.10a).[138a] Its X-ray single crystal structure shows a slightly warped saddle-like conformation (Figure 1.10e). PAH **104** with two fused azulene units and two additional *peri*-fused hexagonal rings was later reported by the same group (Figure 1.10b and f).[88] Very recently, Liu, Feng and co-workers reported three π-extended azulene-embedded helical PAHs via ICl-promoted cyclopentannulation of arylalkynes and subsequent Scholl reactions.[138b] Two of them (**105** and **106**) are shown in Figures 1.10c and d, respectively.

Different from azulene containing molecule **102**, the embedded azulene units in PAHs **105** and **106** are highly twisted due to the steric crowdedness of the π-extended helical structures and the azulene unit in **105** possesses a large twisting degree of 16.1° between the five- and seven-membered rings.

1.4 Perylene and *cata*-Condensed Diarenoperylenes

As this thesis deals with the PAHs based on *cata*-condensed diarenoperylenes, it is necessary to have a short discussion about perylene and the corresponding diarenoperylenes, after briefly summarizing the synthetic strategies and structures of PAHs. Perylene **1** is an important model compound and many of the properties of oligorylenes can be explained by examining the properties of this PAH subunit.[142] As discussed in Chapter 1.2.2.1, perylene was the first reported aromatic hydrocarbon synthesized via an oxidative cyclodehydrogenation by Scholl and co-workers in 1910, while this compound in industrial scale is prepared from acenaphthene via perylene-3,4,9,10-tetracarboxylic dianhydride (PTCDA) as the key and low-cost intermediate.[143]

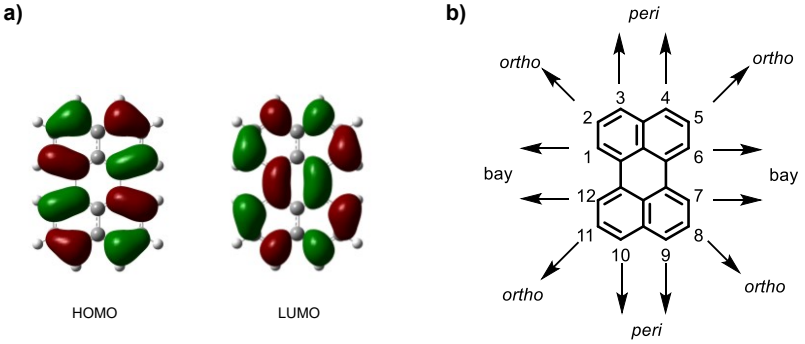

Figure 1.11 a) DFT calculated frontier molecular orbitals of perylene at the B3LYP/6-311+G** level. b) Atom numbering system of perylene.[144]

A relatively small energy gap between the ground (S_0) and first excited (S_1) state was found in perylene when comparing to hydrocarbons of similar molecular weight.[145] DFT calculations reveal that the HOMO of perylene has an antibonding interaction along the bonds connecting two naphthalene units, whereas the LUMO has a bonding interaction along these bonds (Figure 1.11a). This causes a destabilization of the HOMO compared to the LUMO, which effectively decreases the HOMO-LUMO gap to 2.6 eV.[146] As a result a strong absorption in the UV/Vis region with a molar extinction coefficient of $\varepsilon = 3.4 \times 10^4$ $M^{-1} \cdot cm^{-1}$ at 440 nm (in toluene) was observed for perylene, which consists of four vibrational subbands with a 1400 cm^{-1} interval and could be assigned to the HOMO→LUMO transition.[144, 147] The corresponding fluorescent emission maximum from S_1 of perylene is at 444 nm (in toluene) with a quantum yield near unity (98%).[145, 147c, 148]

As an important subunit, perylene can be chemically decorated or extended in many ways, such as π-extension at the bay regions,[32-33, 42a] direct functionalization at 2,5,8,11-positions[149] or

substitution and extension at the *peri* positions to produce oligorylenes[150] (atom numberings see Figure 1.11b) and perylene mono- (PMIs) or diimides (PDIs), which own important applications in material sciences, notably in the area of organic electronics.[151]

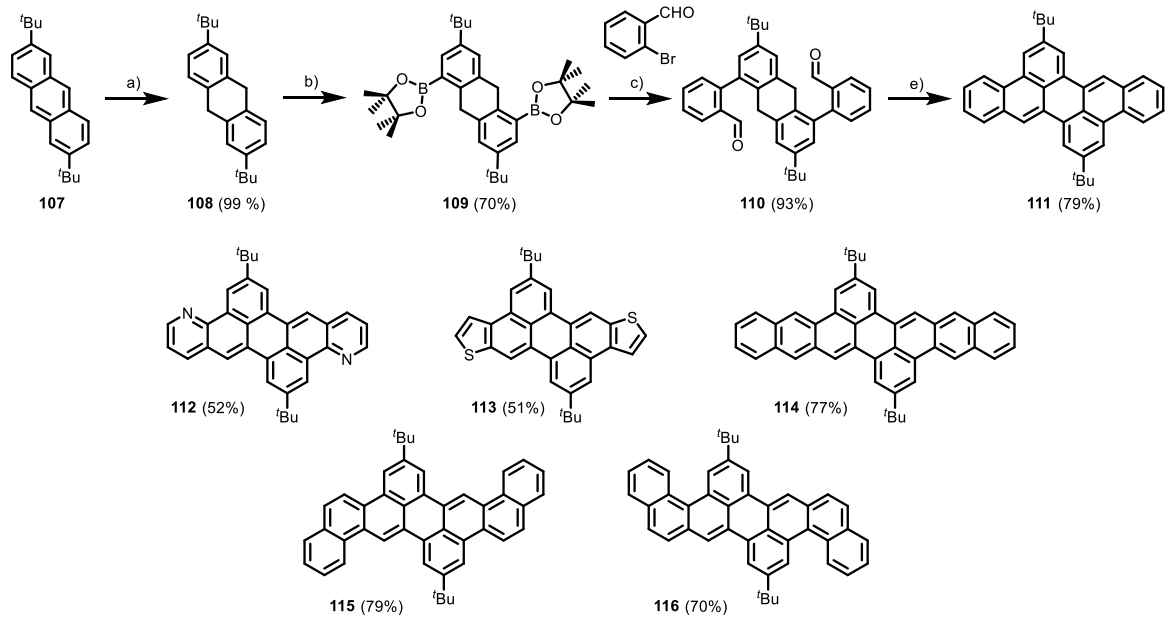

Scheme 1.11 Synthetic route of bis-*tert*-butyl dibenzoperylene **111** and diarenoperylenes **112-116** obtained by this approach.[128b] Yields given in parentheses for diarenoperylenes **112-116** are the combined yields for the two-step reaction from diboronic ester **109**. a) Na, *t*-BuOH, THF, r.t., 6 h; b) $[Ir(COD)OMe]_2$, 3,4,7,8-tetramethyl-9,10-phenanthroline, bis(pinacolato)diboron, THF, 85 °C, 48 h; c) $Pd_2(dba)_3$, *t*-Bu_3PHBF_4, K_2CO_3, THF/H_2O, 80 °C, 16 h; d) *t*-BuOK, THF, 60 °C, 16 h.

Fusing two benzene rings to the 2,3- and 8,9-positions of perylene **1** gives *cata*-condensed dibenzoperylene (dibenzo[*fg*,*qr*]pentacene). In 2016, Mastalerz and co-workers reported a facile route to various arene- and heteroarene-fused diarenoperylenes (Scheme 1.11).[128b] Birch reduction of 2,7-di-*tert*-butylanthracene **107** gave dihydroanthracene **108** in quantitative yield, which was efficiently functionalized by regioselective two-fold borylation via C-H activation with an iridium catalyst to give **109** in 70% yield. After palladium-catalyzed Suzuki-Miyaura cross-coupling reaction with bromobenzaldehyde and subsequent intramolecular condensation in the presence of an organic base, the *cata*-condensed dibenzoperylene **111** was obtained. The overall yield of this four-step approach is over 50%. Simply changing the aromatic bromoaldehyde reactants in the cross-coupling reaction allows the introduction of heterocyclic aromatic rings, such as in dipyridino perylene **112** and dithieno perylene **113**, as well as the syntheses of the larger linear and angular *cata*-condensed compounds **114-116**, with over 50% combined yields for the cross-coupling reactions and condensations in all cases. Note that Clar and co-workers reported the synthesis of unsubstituted dibenzoperylene with the same π-framework of **111** in 1932 by $AlCl_3$-mediated intermolecular coupling reaction of 9-bromophenanthrene with a yield of around 5% after recrystallization.[152] The structure of this PAH was further confirmed by X-ray crystallographic

analysis in 1959 as reported by Lipscomb and co-workers.[153] The synthesis of unsubstituted dinaphthoperylene with the same backbone of **114** was also reported by Clar and co-workers in 1966 by an Elbs reaction of perylene-3,9-diylbis(*o*-tolylmethanone).[154]

Except PAH **116**, which shows a twisted π-plane due to the presence of two fjord regions, all diarenoperylenes possess planar structures. In the cases of **111**, **115** and **116**, herringbone-type packing motifs were observed (Figure 1.12). The shortest distance between two adjacent parallel arranged π-planes is 3.32 Å for PAH **111** and 3.22 Å for PAH **115**. No π-stacking was found in the packing motif of the twisted molecule **116**. PAHs **112**, **113** and **114** are packing in a brickwork-type fashion. The nitrogen-containing PAH **112** shows a closer contact of parallel arranged π-planes with a shortest distance of 3.24 Å than those of the thiophene-fused compound **113** ($d_{\pi\text{-}\pi}$ = 3.48 Å) and dibenzoheptacene **114** ($d_{\pi\text{-}\pi}$ = 3.31 Å). Based on the π-stacking, these compounds have potential to be applied in organic electronics. Angular-shaped compound **115** gives a field-effect hole mobility of 0.12 $cm^2 \cdot V^{-1} \cdot s^{-1}$ in thin-film transistors (TFTs), which is the highest among this series and still owns potential to be improved by fabricating single-crystal field-effect transistors.

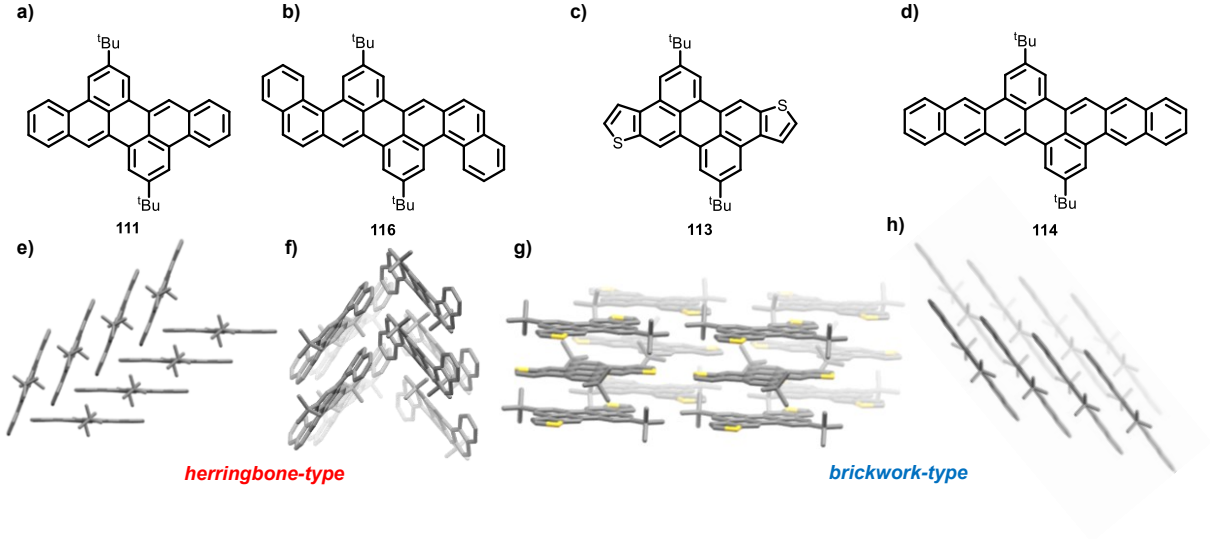

Figure 1.12 Molecular structures (a-d) and packing motifs in the crystalline states (e-h) of diarenoperylenes **111** (a and e), **116** (b and f), **113** (c and g) and **114** (d and h). CCDC: 1482799, 1482805, 1482803, 1482801.[128b] Hydrogen atoms are omitted in the crystal structures for clarity.

2. Objectives

Considering the facile synthetic approach, pronounced π-stacking in the solid states and the potentials to further improve the device performances in organic electronics of the (hetero)diarenoperylenes discussed in chapter 1.4, the researches of this thesis start from these compounds. The aim of this thesis is the synthesis and investigation of structure-property relationships of PAHs based on these diarenoperylenes.

The first issue to deal with is whether the regioselective functionalization could be achieved in practice based on these (hetero)diarenoperylenes. Interesting bond length distributions in the X-ray single crystal structures of the dibenzoperylene **111** and its analogs were observed. The two C-C bonds at the [*a*] and [*k*] edges (highlighted in red in Scheme 2.1), were found to be signicantly shorter in bond lengths than other ones on the π-frameworks thus supposed to be more olefinic. If the regioselective functionalization could be done as expected, a series of *cata*-condensed coronenes would be obtained after two steps. It would be also possible to synthesize different heteroannulated coronenes by changing the reactants during the synthesis, which serve as the model compounds to investigate the impact of various heteroannulations on the properties of this π-system.

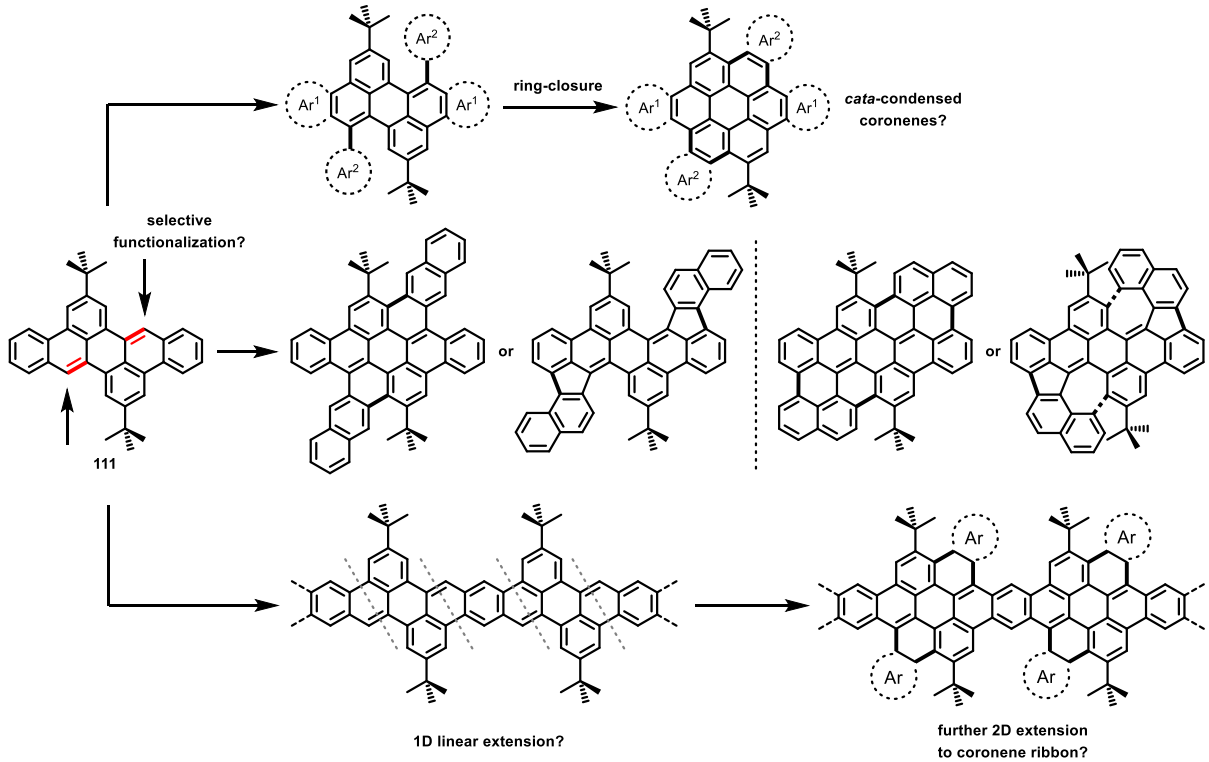

Scheme 2.1 Proposed routes for π-extension based on diarenoperylenes. New C-C bonds formed during the reactions are highlighted in bold.

Furthermore, this π-system could be further extended by substitution with two naphthyl moieties. In this scenario, different possibilities exist in the ring-closing steps of the two naphthyl

substituted compounds. It is of significance to investigate whether the following ring-closing step proceeds through the six-membered ring formation to give further extended coronenes, or through cyclopentannulation at the *L*-regions. Structures and properties of the final PAHs in both cases should be investigated.

Using double functionalized building blocks in the synthetic route of dibenzoperylene offers the possibility to achieve 1D linear π-extension to construct a series of perylene oligomers, which serve as model compounds to investigate the influence of conjugation length on the molecular optophysical properties. Furthermore, it is of significance to investigate whether the regioselective functionalization could be achieved on these 1D oligomers. The regioselectively functionalized 1D oligomers would give the opportunities to synthesize coronene ribbons.

3. Results and Discussion

3.1 Synthesis, Structures and Properties of a Variety of *cata*-Condensed Heteroannulated Coronenes Obtained by a Three-Step Route

3.1.1 Introduction

As a classical subunit of polycyclic aromatic hydrocarbons (PAHs), coronene and its π- extended derivatives have been investigated over decades, due to their good properties of charge transport (μ_h > 1 $cm^2 \cdot V^{-1} \cdot s^{-1}$),[95] light absorption, and promising application in organic electronics.[18a, 81, 92, 93b] Hexabenzocoronenes (HBCs) including *peri*-HBC and *cata*-HBC serve as the most representative extension type of coronene. Fine-tuning chemical and physical properties of this small molecular cut-out of graphene can be achieved by incorporating heteroatoms, such as nitrogen,[155] sulfur[156] and oxygen[157] into the coronene-based π-systems.

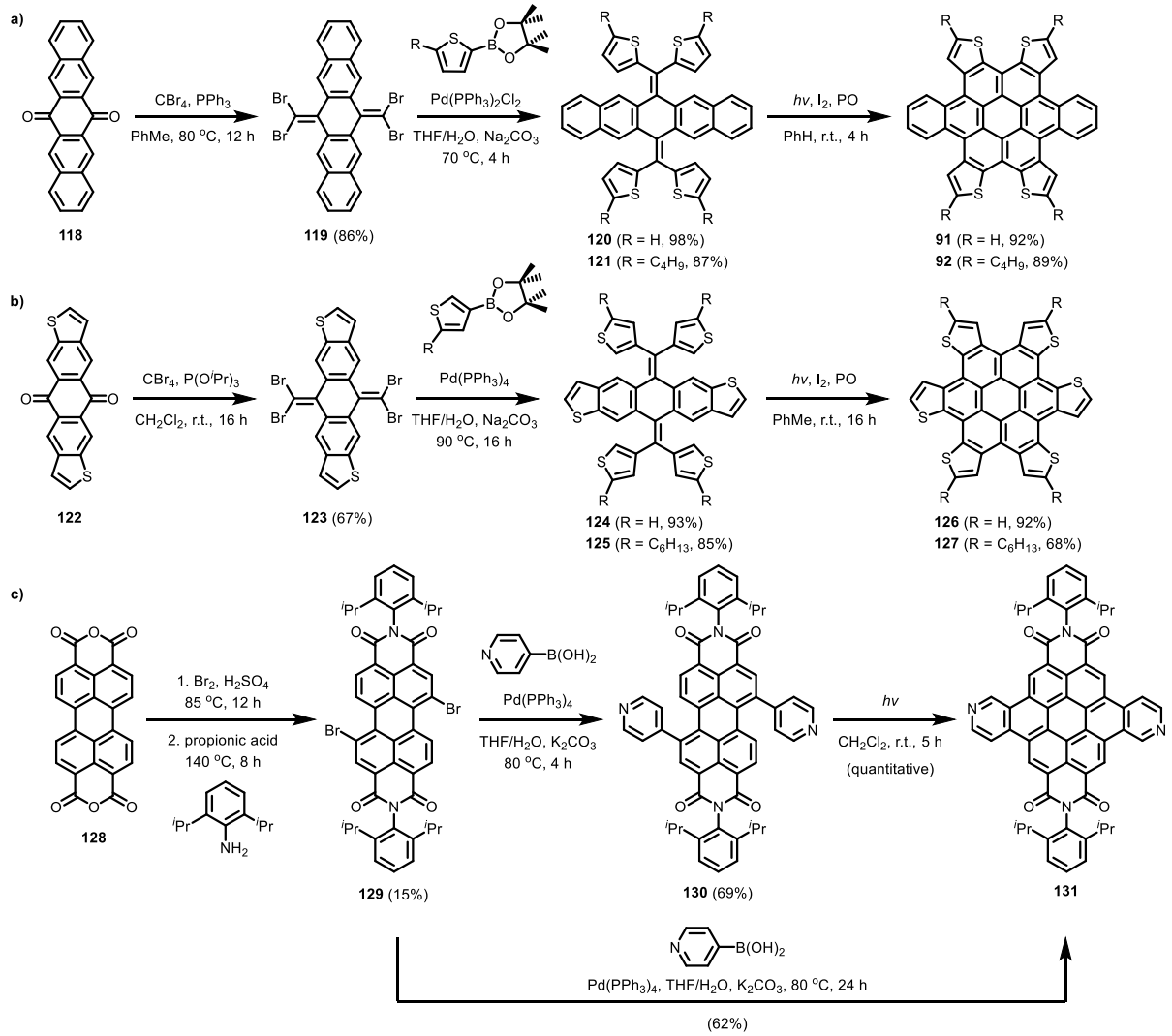

Scheme 3.1.1 Reported synthetic routes of tetra-,[81b] hexathiophene-fused[93a] and pyridine-fused coronenes.[158] PO: propylene oxide.

For instance, the sulfur-containing coronenes could be obtained by embedding thienyl units into the system. From the corresponding anthraquinone or pentacene diketones, tetra-[81b] and hexathiophene-fused[93a] coronenes have been obtained (Scheme 3.1.1). In the cases of dibenzotetrathienocoronene **91** and hexathienocoronene **127**, columnar packing motifs were observed in the crystal structures, which were proven to be beneficial to enhance charge transport properties by charge migration along the columnar structures because of extensive interactions between the π-orbitals of adjacent aromatic cores with delocalized electrons.[159]

As discussed above, in most cases of the reported synthetic routes of the extended coronenes, multi-fold biaryl formation mostly via transition-metal-catalyzed cross-coupling serves as the key step. Thus only highly symmetric products can be obtained. Meanwhile, nitrogen-containing heteroannulated *cata*-condensed coronenes are even more rarely reported than the thiophene-fused ones. Only a few cases have been reported.[158, 160] For example, perylene diimide **131** with two pyridine units fused at the bay regions could be obtained by the combination of Suzuki-Miyaura cross-coupling reaction based on dibrominated perylene diimide **129** and subsequent sunlight-promoted cyclization, or by one-pot cross-coupling reaction with longer refluxing time and exposure to sunlight (Scheme 3.1.1c).[158]

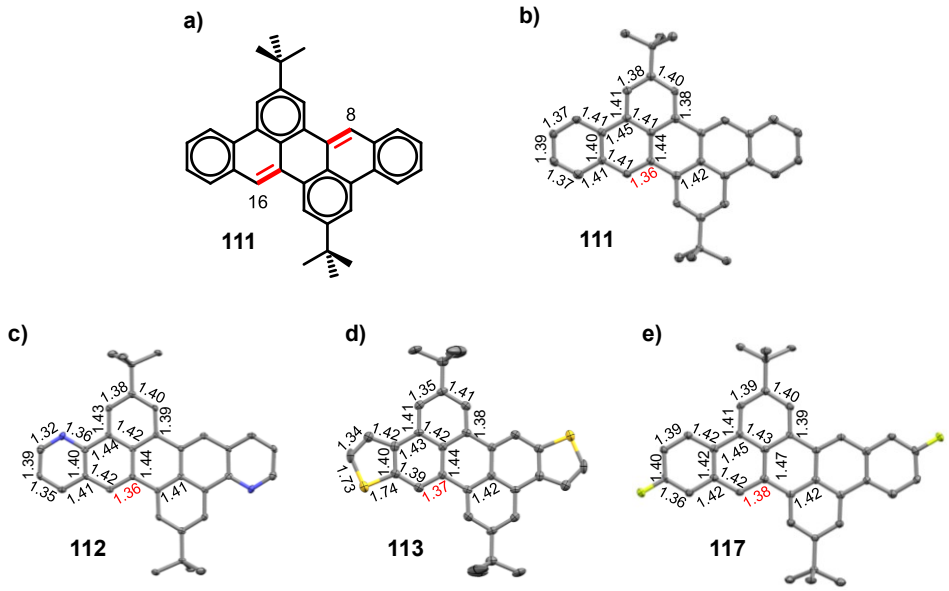

Figure 3.1.1 (a) Depicted scaffold model of dibenzoperylene **111** according to Clar's sextet rule. The most olefinic bonds are highlighted in red. (b-e) X-ray crystal structures of dibenzoperylene **111** (b), dipydinoperylene **112** (c), dithienoperylene **113** (d) and difluorodibenzoperylene **117** (e).[128b] CCDC: 1482799 (**111**), 1482800 (**112**), 1482803 (**113**), 1482802 (**117**). ORTEP plots are at the 50% probability. Hydrogen atoms are omitted for clarity. Bond lengths are given in Å. Colors for heteroatoms: blue = nitrogen, yellow = sulfur, green = fluorine.

The researches in this thesis are based on 2,10-di-*tert*-butyldibenzoperylene **111** and its derivatives reported by Mastalerz and co-workers (Figure 3.1.1a).[128b] High-quality X-ray crystal structures were obtained for all diarenoperylenes, which allow a detailed analysis in the solid state to get further insights to bond characters. A unique distribution of C-C bond lengths could be

observed when analyzing the bond length alternation of dibenzoperylene **111**. This π-system can be properly described as a π-scaffold with a maximum of four benzenoid sextets according to Clar's rule (Figure 3.1.1a),[161] which indicates that two bonds, the [*a*] and [*k*] edges (highlighted in red), are of a more olefinic character. This is supported by the result that the observed lengths of both two C-C bonds, both of which are 1.36 Å, are the shortest in the whole system. It is supposed that the 8 and 16 positions in compound **111** should be most prone to being attacked by an electrophile. Similar distribution patterns of the C-C bond lengths were observed in the dipyridino- (**112**) and difluoro- (**117**) compounds, in which the lengths of the C-C bonds at the same positions were found to be 1.36 Å and 1.38 Å, respectively (Figure 3.1.1c and e). The two shortest C-C bonds in the sulfur-containing compound **113** are the ones between positions 2 and 3 of the fused thiophene rings, with a length of 1.34 Å for both bonds (Figure 3.1.1d). If these two bonds were overlooked, the two bonds at the [*a*] and [*k*] edges, which exhibit a length of 1.37 Å in both cases, also show more olefinic characters than other C-C bonds in the π-framework.[128b] Thus similar reactivity is supposed to be exhibited in all these diarenoperylenes.

3.1.2 Regioselective Bromination of Diarenoperylenes

The bond length analyses led to the attempted electrophilic bromination based on these diarenoperylenes, which started with dibenzoperylene **111** (Scheme 3.2.1). Compound **111** was dissolved in CH_2Cl_2 and different equivalents of bromine (Br_2) diluted in CH_2Cl_2 were added dropwise to the substrate solution at room temperature. The mixture was stirred for four hours at room temperature, during which the reaction was monitored by TLC analysis.

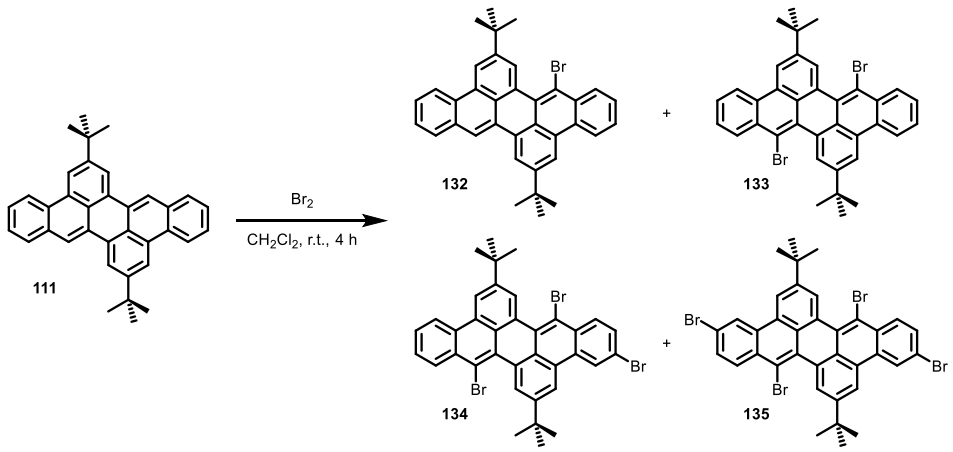

Scheme 3.1.2 Bromination of dibenzoperylene **111** with bromine.

Table 3.1.1 Results of bromination of **111** with bromine.

Entry	Br_2 [equiv.]	Substrate conc. [mM]	Products (isolated yields)
1	2.5	6.5	**133** (66%) + **134** (21%)
2	4.0	6.5	A mixture of **133**, **134** and **135**. **135** (7%) isolated.
3	2.5	23.7	**132** (20%) + **133** (32%) + **134** (19%)

Up to four products could be isolated after reaction by silica gel column chromatography. The products isolated are shown in Scheme 3.1.2 and the corresponding isolated yields are summarized in Table 3.1.1. The reaction result is dependent to the amount of bromine and the concentration of **111** in CH_2Cl_2. When 2.5 equiv. of bromine have been used, dibromide **133** was isolated in 66% yield along with 21% of tribromide **134** (entry 1), whereas the yield of **133** decreased to 32% with more monobromide **132** (20%) isolated when the substrate was more concentrated (entry 3). When more bromine (4 equiv.) was used, bromide with up to four-fold bromination was detected and isolated (entry 2).

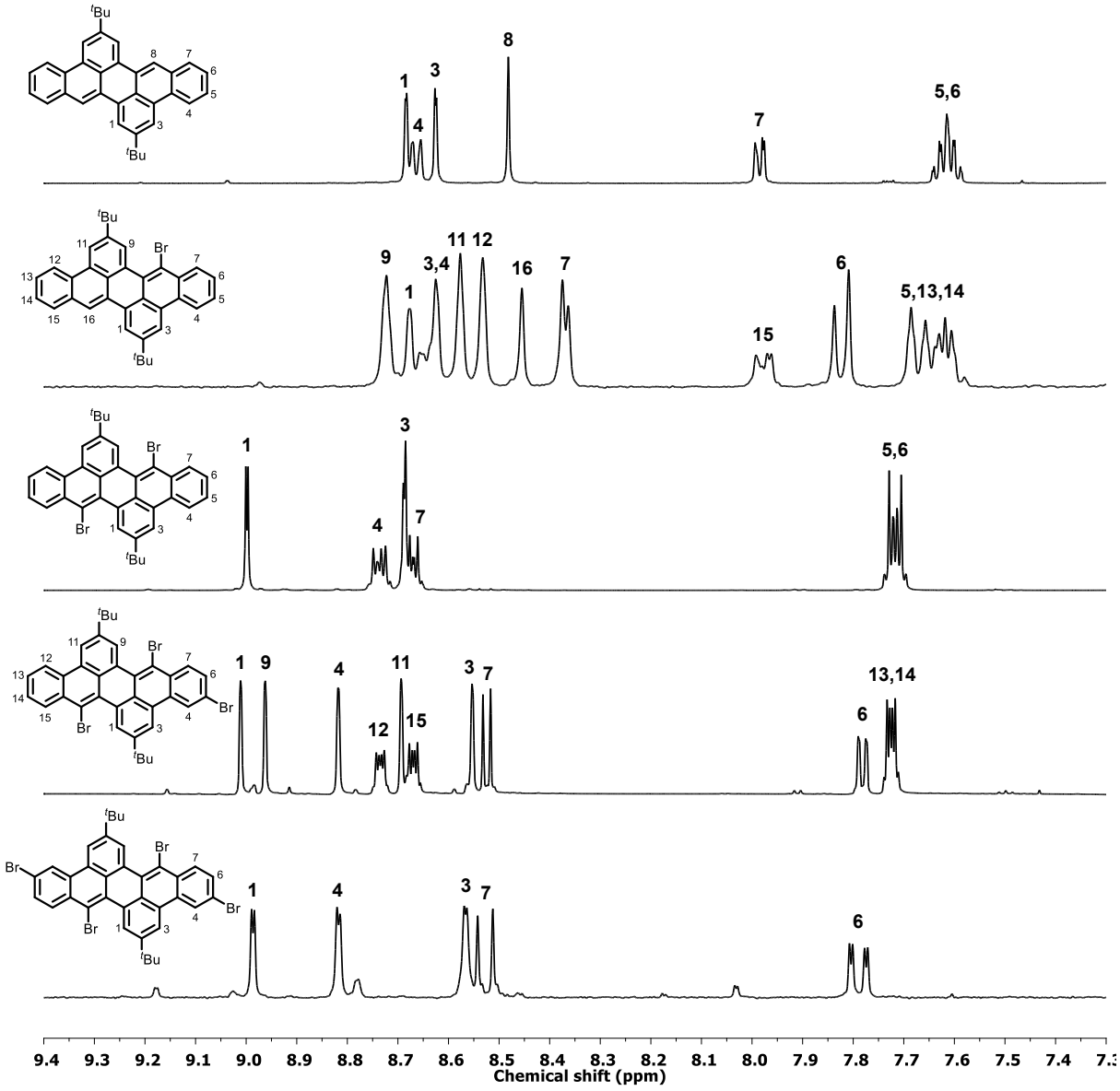

Figure 3.1.2 ^{1}H NMR spectra (300 MHz, $CDCl_3$) of substrate **111** and bromides **132**-**135**. Depicted are only the aromatic regions.

The molecular structures of all bromides were characterized by MALDI-TOF MS and ^{1}H NMR spectra (Figure 3.1.2). The signals of m/*z* = 544.172, 622.112, 699.976, 779.888 found in

the MALDI-TOF mass spectra of **132** ([M]$^+$ calcd. for $C_{36}H_{31}Br$, 544.159), **133** ([M]$^+$ calcd. for $C_{36}H_{30}Br_2$, 622.070), **134** ([M]$^+$ calcd. for $C_{36}H_{29}Br_3$, 699.980) and **135** ([M]$^+$ calcd. for $C_{36}H_{28}Br_4$, 779.889), respectively, along with the broadened isotopic distribution patterns due to the introduction of bromine atoms fit the simulated patterns, indicating multi-fold bromination took place during the reactions. Information about the positions of bromine atoms in these bromides could be found in the ^{1}H NMR spectra (Figure 3.1.2). Compared with the ^{1}H NMR spectrum of substrate **111**, the singlet at 8.48 ppm at position 8 vanishes in the spectra of dibromide, tribromide and tetrabromide. No singlet could be observed in the spectra of dibromide and tetrabromide. Furthermore, the doublet at 8.68 ppm with a small coupling constant of J = 1.3 Hz, which could be assigned to the proton at position 1 in substrate **111**, down-field shifts to 9.00 ppm after bromination. Similar phenomenons were also observed in the spectra of tribromide **134** (9.01 ppm for position 1 and 8.96 ppm for position 9) and tetrabromide (8.98 ppm for position 1). Only bromination at positions 8 and 16 could make the bromine atoms close enough in distance to positions 1 and 9, to cause significant influences on the chemical shifts of both positions. These evidences suggest that the bromination occurs at positions 8 and 16 as expected.

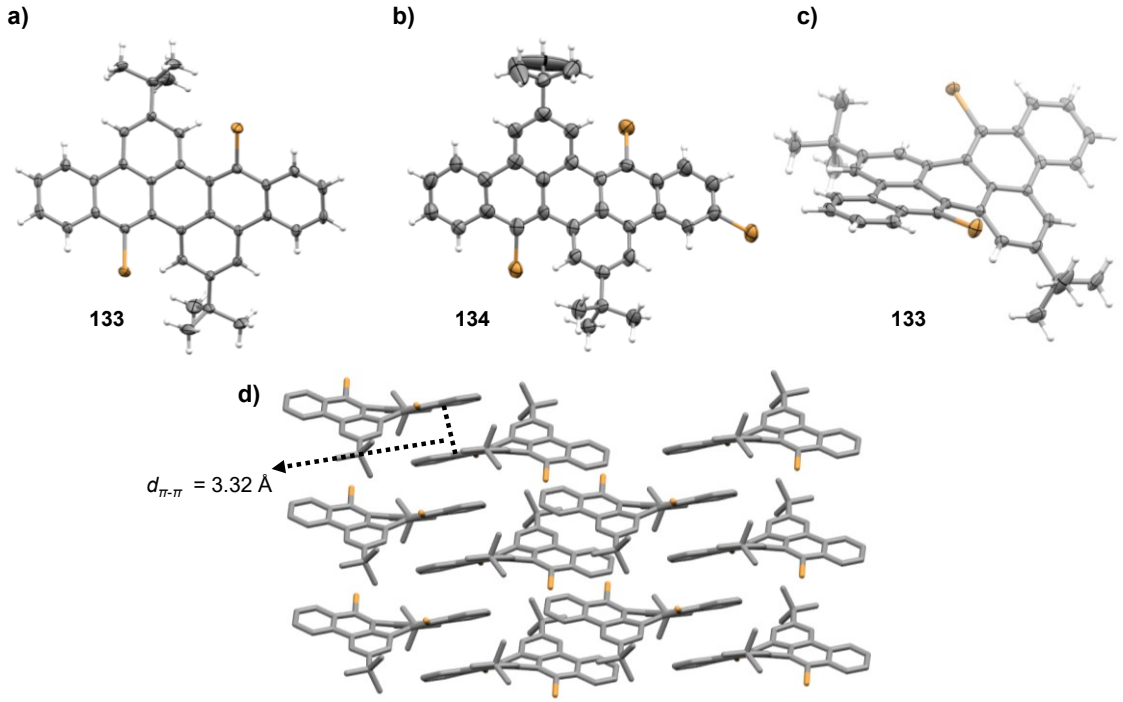

Figure 3.1.3 X-ray crystal structures of dibromide **133** (a), tribromide **134** (b), a side-view of **133** (c) and packing motif of dibromide **133** (d). ORTEP plots in a-c are at 50% probability. Enclathrated solvent molecules and hydrogen atoms in d are omitted for clarity. Colors for heteroatoms: orange = bromine.

The molecular structures of dibromide **133** and tribromide **134** were further confirmed by growing single crystals suitable for X-ray diffraction analysis (Figure 3.1.3). The crystals were obtained by diffusing methanol vapor into the solutions of compound **133** or **134** in CH_2Cl_2. The bromine atoms are distributed as depicted in Scheme 3.1.1 and the position of the third bromine

atom in tribromide **134** could be assigned to position 5. The molecular geometry of dibromide **133** (Figure 3.1.3c) is not planar any more in comparison to that of dibenzoperylene **111**,[128b] because of the steric repulsion between the attached bromine atoms and hydrogen atoms at positions 1 and 9. **133** crystallizes in the monoclinic space group *C*2/c. A herringbone-type packing motif similar to that of substrate **111** in the solid state was not observed for dibromide **133**. A close contact between two benzene rings at the *cata*-positions of the perylene subunits with a shortest distance of $d_{\pi\text{-}\pi}$ = 3.32 Å was observed due to π-π interaction.

These results indicate that the bromination occurs at the positions 8 and 16, which are in accordance with the assumption that the 8- and 16-positions in compound **111** should be most prone to being attacked by electrophiles. The yields are no more than 66% when bromine was used as the bromination reagent and the selectivity is also limited as overbromination was observed.

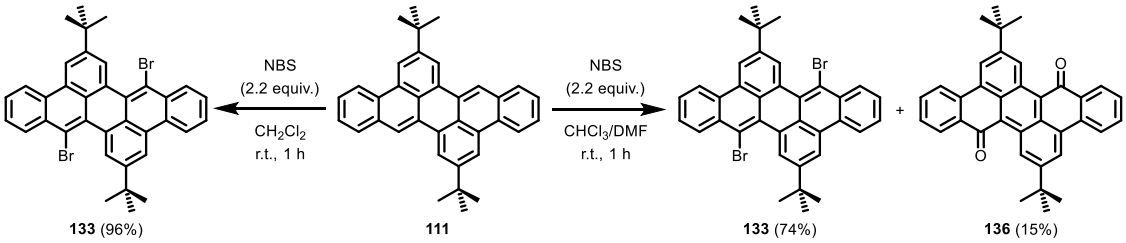

Scheme 3.1.3 Products of treating dibenzoperylene **111** with NBS in different solvents. Isolated yields are given in parentheses.

In order to further improve the yield, *N*-bromosuccinimide (NBS) was used instead for this transformation. As shown in Scheme 3.1.3, treating **111** with 2.2 equiv. of NBS in CH_2Cl_2 at room temperature for one hour gave dibromide **133** in a nearly quantitative yield of 96%. Besides the yield, the selectivity was also increased in comparison to the use of bromine, as no overbromination was observed when more NBS (4 equiv.) was added. Changing the solvent to a mixture of $CHCl_3$ and DMF gave a decreased yield of 74%, due to the fact, that an oxidation was observed during the process (Scheme 3.1.3). Diketone **136** was isolated in 15% yield as a side product. The reason of the formation of diketone during the reaction is not clear. The residual water in DMF, which may serve as a competing reactant during the substitution may account for this phenomenon.

The structure of diketone **136** was confirmed by ^{1}H NMR spectrum (Figure 3.1.4) and X-ray single crystal analysis (Figure 3.1.5). The signal at 8.68 ppm of proton at position 1 in the ^{1}H NMR spectrum of substrate **111** significantly down-field shifts to 10.01 ppm in that of diketone **136** due to the presence of the electron withdrawing oxygen atoms. The steric repulsion between the inserted oxygen atoms and protons at position 1 causes the central benzene ring of perylene moiety slightly deformed and thus the π-plane of **136** slightly twisted in comparison to **111**. A herringbone-type stacking was observed in the packing of **136**. A closer intermolecular contact was found in diketone

136 when compared with **111**, as the average distance between two parallel arranged π-planes is $d_{\pi\text{-}\pi}$ = 3.23 Å in **136**, smaller than that of $d_{\pi\text{-}\pi}$ = 3.40 Å in **111**.[128b]

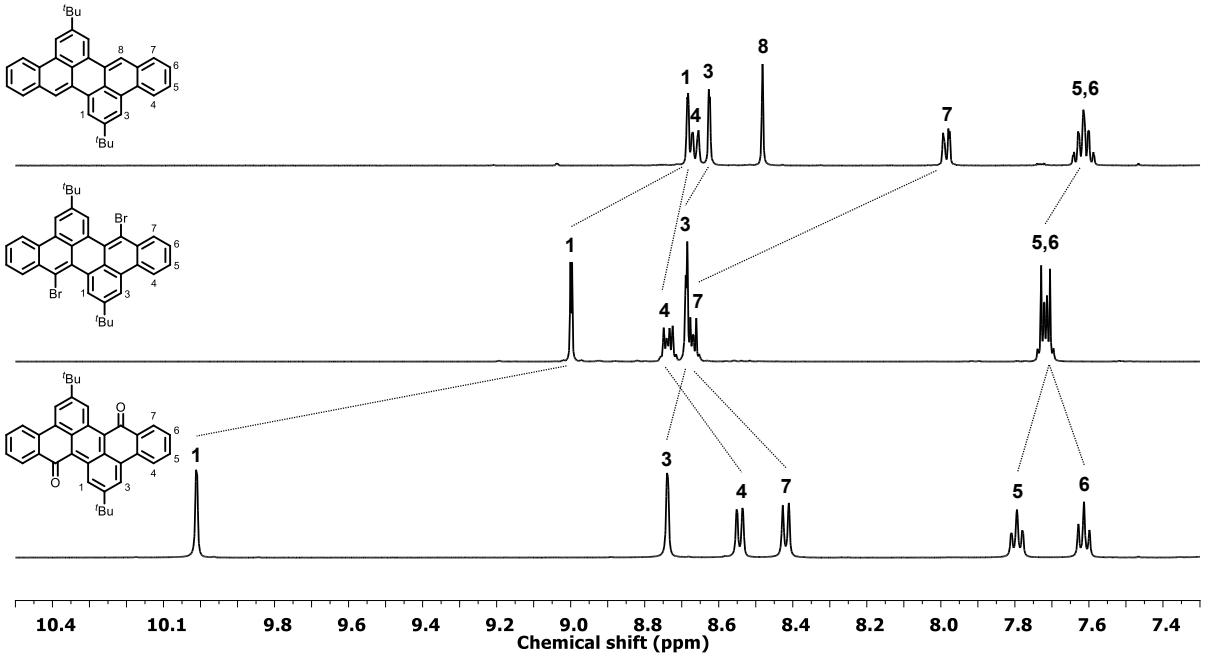

Figure 3.1.4 ^{1}H NMR spectra (500 MHz, $CDCl_3$) of substrate **111**, dibromides **133** and diketone **136**. Depicted are only the aromatic regions.

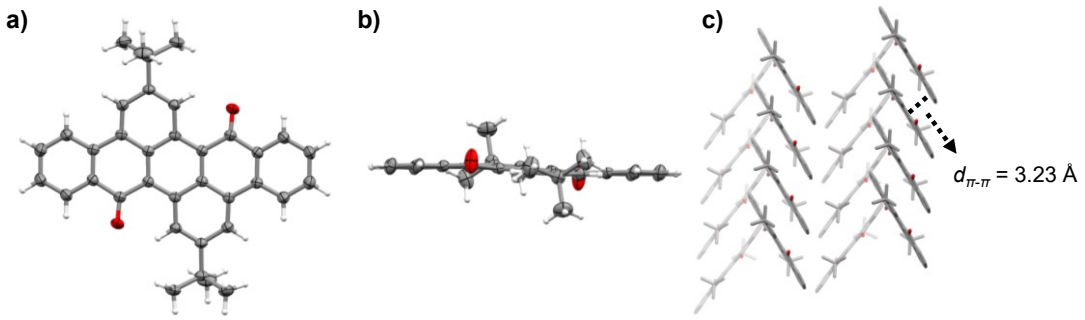

Figure 3.1.5 Front view (a) and side view (b) of X-ray crystal structure of diketone **136** (a). Packing motif of diketone **136** (c). ORTEP plots in a and b are at 50% probability. Enclathrated solvent molecules and hydrogen atoms in d are omitted for clarity. Colors for heteroatom: red = oxygen.

Based on the optimized reaction conditions, brominations were further performed based on other diarenoperylenes (Scheme 3.1.4). Based on the dipyridino- (**112**) and difluoro- (**117**) compounds, bromination with NBS (2.2 equiv.) under the same conditions gave the desired dibromides in 97% yields in both cases. However, in the case of thiophene-fused perylene **113**, the regioselectivity of two-fold bromination decreases. As the two α-positions of the thiophene rings were easily brominated at the same time, tetrabromide **139** was isolated as the main product in 21% yield even with only 2.2 equiv. of NBS. The yield of this tetrabromide could be increased to 91% by using 4.4 equiv. of NBS. In order to realize a selective two-fold bromination, the two α-positions of thiophene rings were blocked by bulky *tert*-butyl groups in compound **141**. Tetra-*tert*-

butyldithienoperylene **141** was obtained either by direct Friedel-Crafts *tert*-butylation of **113** using *tert*-butyl chloride in the presence of $AlCl_3$ in 48% yield, or by a subsequent two-step reaction including the cross-coupling reaction of diboronic ester **109** with 3-bromo-5-(*tert*-butyl)thiophene-2-carbaldehyde and then an intramolecular condensation in the presence of *t*-BuOK in an overall yield of 53%. Based on **141**, two-fold regioselective bromination was achieved in 85% yield.

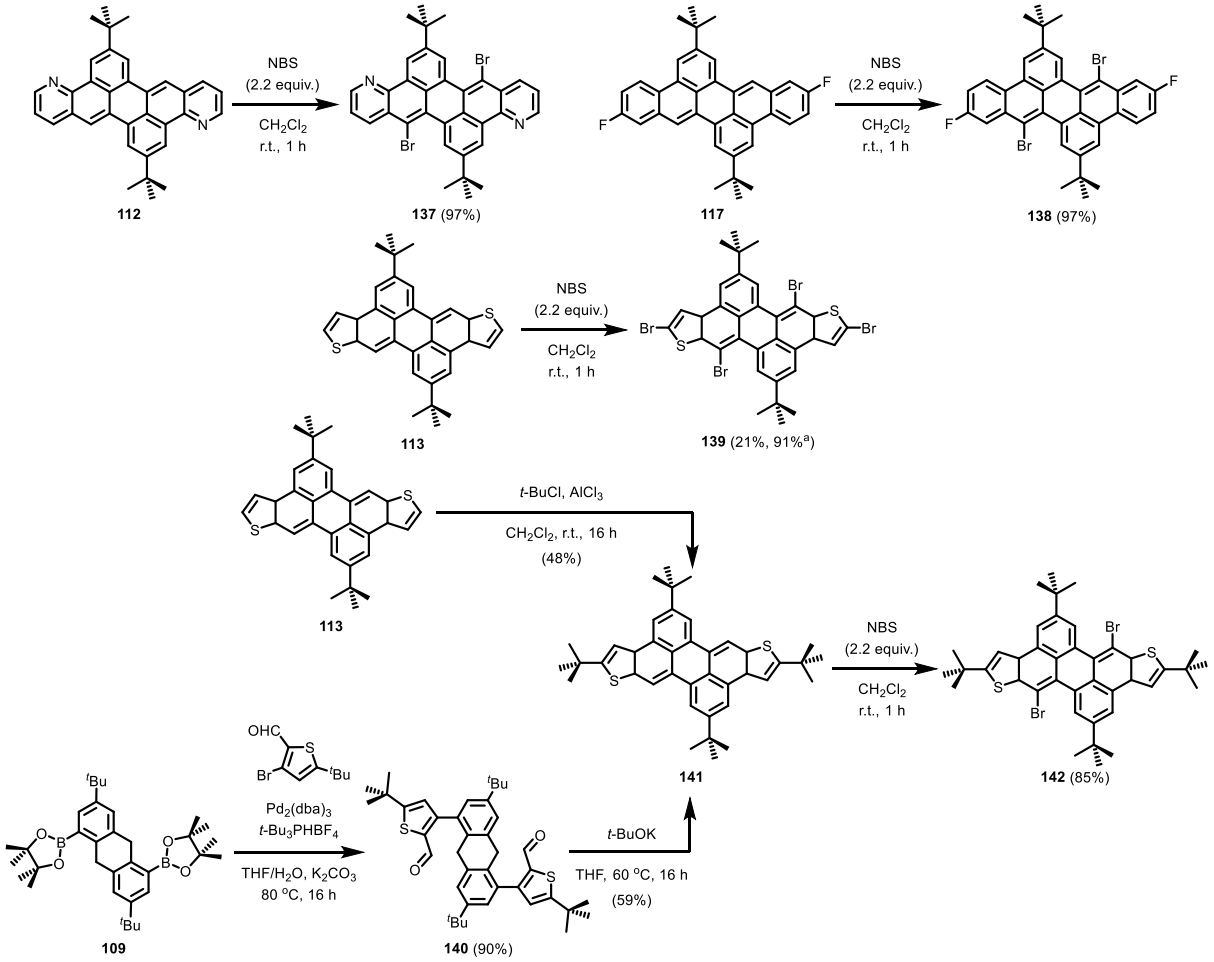

Scheme 3.1.4 Synthesis of tetra-*tert*-butyldithienoperylene **141** and bromination of diarenoperylenes **112**, **113**, **117** and **141** with NBS. [a]4.4 equiv. of NBS. Isolated yields are given in parentheses.

All obtained bromides were fully characterized. The molecular structures of the dibromides **137** and **142** were further confirmed by single crystal X-ray diffraction analysis (Figure 3.1.6). Both compounds crystallize in the triclinic space group $P\ \bar{1}$. Similar to dibromide **133**, dipyridino- and dithienoperylenes exhibit twisted π-planes in both cases after the substitutions with bromine atoms. There are π-π interactions between two pyridinobenzene units of two adjacent molecules and the closest distance is with $d_{\pi\text{-}\pi}$ = 3.70 Å, larger than that between two dipyridinoperylene **112** molecules ($d_{\pi\text{-}\pi}$ = 3.14 Å). No intermolecular π-π interactions were observed in the packing motif of compound **142** containing four bulky *tert*-butyl groups and two bromine atoms. The closest contact between one π-plane and an adjacent *tert*-butyl group on one thiophene ring is $d_{t\text{-Bu-H}\cdots\pi}$ = 2.75 Å.

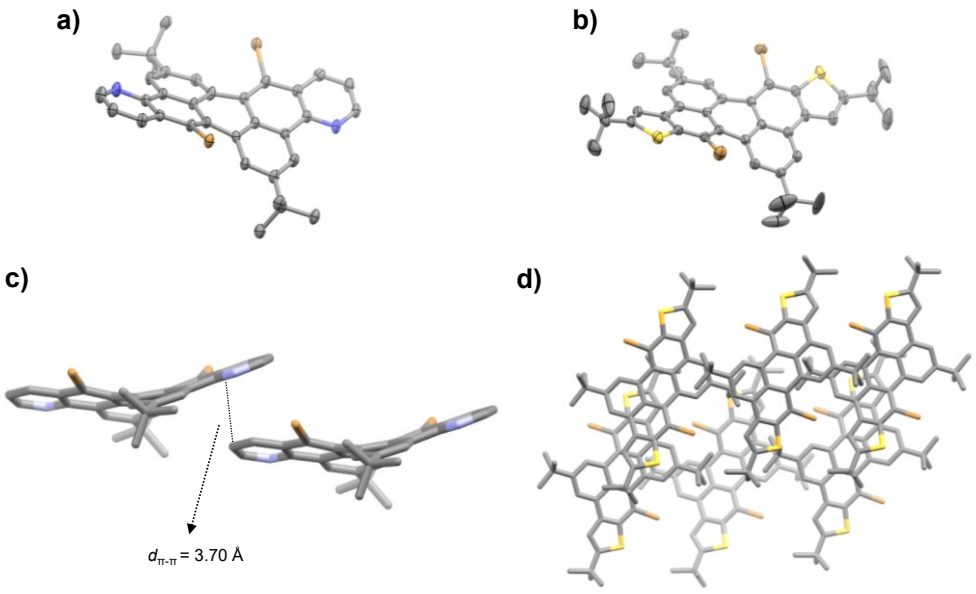

Figure 3.1.6 X-ray single crystal structures of **137** (a and c) and **142** (b and d). ORTEP plots in a and b are at 50% probability. Enclathrated solvent molecules and hydrogen atoms are omitted for clarity. Colors for heteroatoms: orange = bromine, blue = nitrogen, yellow = sulfur.

3.1.3 Cross-Coupling Reactions based on Dibromides

Aryl halides are synthetically valuable in transition metal-catalyzed cross-coupling reactions.[162] Based on the obtained dibromides **133**, **137**, **138** and **142**, two-fold palladium-catalyzed Suzuki-Miyaura cross-coupling reactions with (substituted) phenyl, pyridino or thienyl boronic acid (pinacol ester) were performed under Fu conditions.[163] The obtained products and corresponding isolated yields are shown in Scheme 3.1.5. In the cases of reactions between dibromides and phenyl or thienyl boronic acid (or pinacol ester), the yields of the two-fold products were all > 80%. Exceptions are the reactions of (3-(hexyloxy)phenyl)boronic acid pinacol ester with dibromides **133** and **142**. The isolated yields were 50% and 36%, respectively. No conversion was observed in the reaction of dibromide **133** with unsubstituted pyridin-3-ylboronic acid. An electron donating group (-OMe) at the *para*-position of the -$B(OH)_2$ group on pyridin-3-ylboronic acid is necessary for the cross-coupling reaction and the yield of reaction between (6-methoxypyridin-3-yl)boronic acid and **133** was 89%. Dibromides **133** and **137** could also be used in the palladium-catalyzed Sonogashira-Hagihara cross-coupling reactions with phenyl acetylene and the corresponding products **161** and **162** have been isolated in 88% and 95% yields, respectively.

Single crystals of the products **149**, **152**, **154**, **156**, and **161** were obtained by diffusing methanol vapor into the solutions of these compounds in CH_2Cl_2 or THF and have been suitable for X-ray diffraction analysis (Figure 3.1.7, Figure 3.1.8 and Figure 3.1.9).

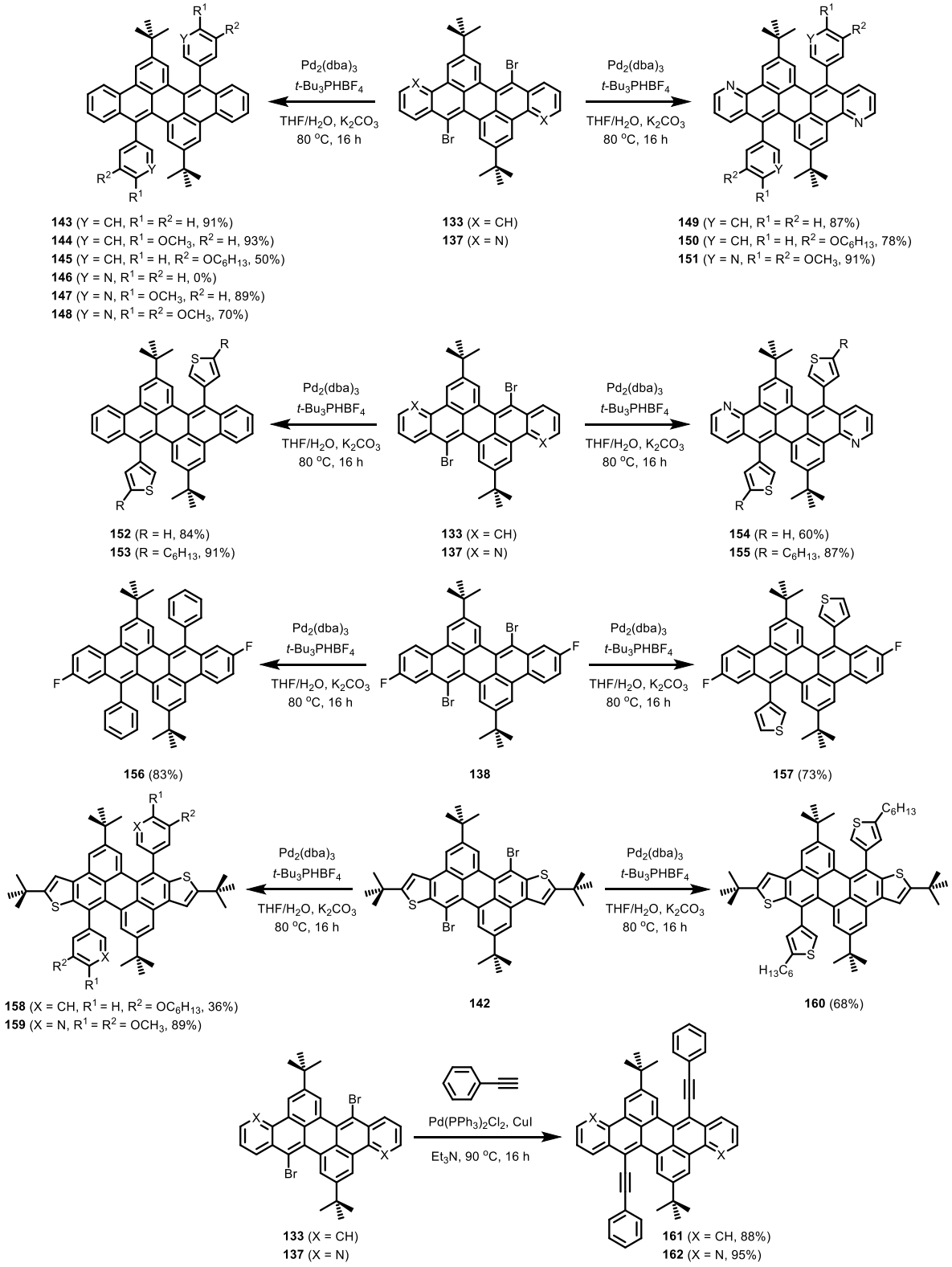

Scheme 3.1.5 Two-fold cross-coupling reactions based on dibromides **133**, **137**, **138** and **142**. Phenyl boronic acid, (4-methoxyphenyl)boronic acid, (3-(hexyloxy)phenyl)boronic acid pinacol ester, pyridin-3-ylboronic acid, (6-methoxypyridin-3-yl)boronic acid, (5,6-dimethoxypyridin-3-yl)boronic acid pinacol ester, thiophen-3-ylboronic acid or (5-hexylthiophen-3-yl)boronic acid pinacol ester were used in the corresponding Suzuki-Miyaura cross-coupling reactions. The reactions were catalyzed by 10 mol% [Pd]. The isolated yields are given in parentheses.

As shown in Figure 3.1.7, thiophene substituted compound **152** crystallizes in the triclinic space group $P\ \bar{1}$. The two benzene rings (colored in blue) fused on the *K*-regions of the central perylene moiety deviate to the same side of the molecular π-backbone and the angle between these two benzene rings is 51.2°. By analysing the detailed C-C bond lengths of this cross-coupling product in the solid state, it was found that the two bonds on the [*a*] and [*k*] edges of the dibenzoperylene framework have lengths of 1.38 Å, which are slightly longer than those at the same positions on the unsubstituted dibenzoperylene **111** (1.36 Å) but still shorter than other C-C bonds in the hexagonal rings where both edges are located and those in the central ring of the perylene moiety. Hence the two C-C bonds still exhibit more olefinic characters. No intermolecular π-π interaction was observed in the packing of compound **152**. The shortest distance between one π-backbone and thiophene ring on an adjacent molecule is $d_{\text{Ar-H}\cdots\pi}$ = 2.61 Å. Difluoro compound **156** crystallizes in the monoclinic space group *C*2/c. The angle between the two blue-marked benzene rings is 45.4°. There was also no intermolecular π-π interaction observed as the adjacent two π-planes are not parallel in space. A close contact was found between fluorine-attached benzene ring and another perylene moiety with a shortest distance of $d_{\pi\text{-}\pi}$ = 3.24 Å.

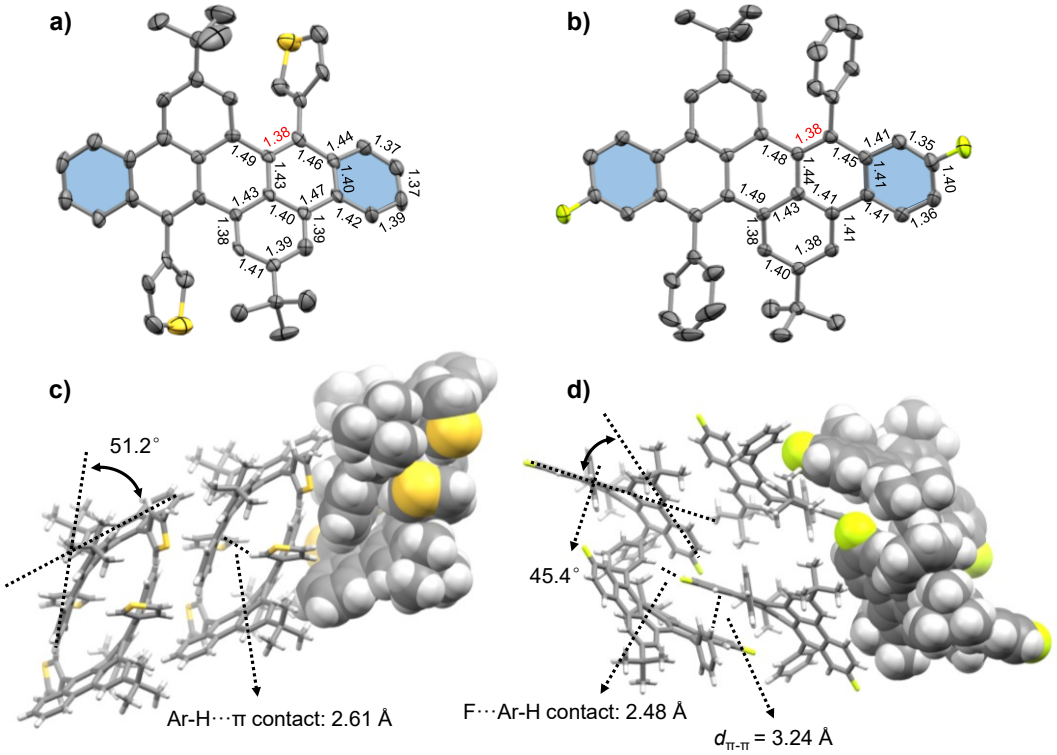

Figure 3.1.7 X-ray crystal structures of **152** (a and c) and **156** (b and d). ORTEP plots in a and b are at 50% probability. Hydrogen atoms (in a and b) and enclathrated solvent molecules are omitted for clarity. Bond lengths are given in Å. Colors for heteroatoms: yellow = sulfur, green = fluorine.

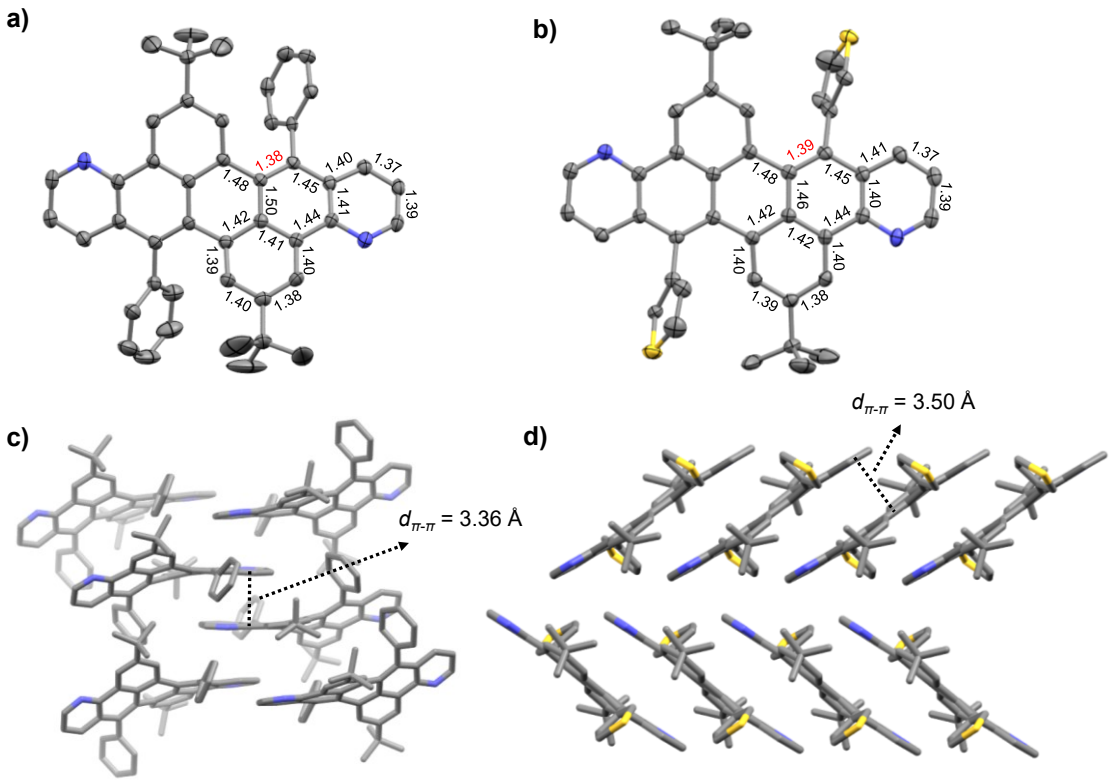

Figure 3.1.8 X-ray crystal structures of two pyridine-fused compounds **149** (a and c) and **154** (b and d). ORTEP plots in a and b are at 50% probability. Hydrogen atoms and enclathrated solvent molecules are omitted for clarity. C-C bond lengths are given in Å. Colors for heteroatoms: yellow = sulfur, blue = nitrogen.

Phenyl substituted pyridine-fused perylene **149** crystallizes in the monoclinic space group $P2_1/c$ (Figure 3.1.8a). The substitution with two phenyl rings also causes contortion of the molecular π-framework. The angle between the two planes where two pyridine rings are located is 43.2°. The two bonds on the [*a*] and [*k*] edges of the dipyridinoperylene framework have lengths of 1.38 Å, which are shorted than the other C-C bonds in the framework. In each unit cell, two parallelly arranged pyridine rings were observed on the two adjacent molecules and the distance is $d_{\pi-\pi}$ = 3.36 Å. Thiophene-substituted compound **154** also crystallizes in the monoclinic space group $P2_1/c$ (Figure 3.1.8b) with a similar distribution of C-C bond lengths. However, in comparison to the structure of unsubstituted dipyridinoperylene **112**,[128b] the dipyridinoperylene backbone of compound **154** is still planar after the attachment of two thiophene rings, which is different from the structures of other cross-coupling products discussed above. It is worth mentioning that the arrangement type of molecules varies from brickwork-type for parent dipyridinoperylene **112** to herringbone-type after substituted with thiophene rings for compound **154**. The distance between two adjacent π-planes is $d_{\pi-\pi}$ = 3.50 Å.

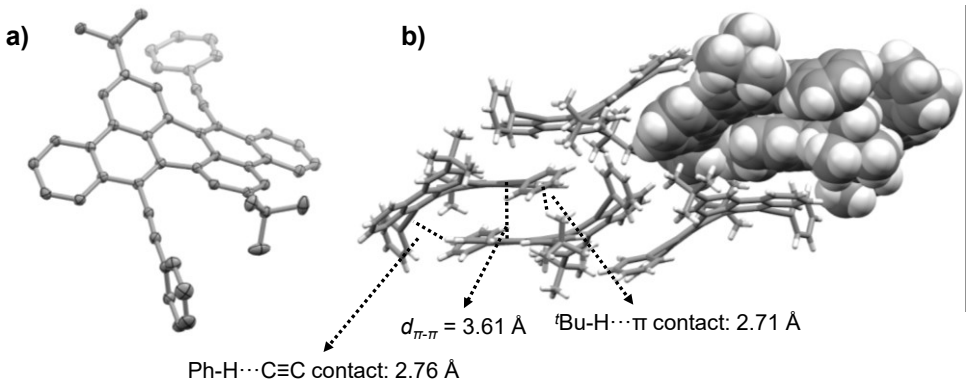

Figure 3.1.9 X-ray crystal structure of **161**. ORTEP plot in a is at 50% probability. Hydrogen atoms in a and enclathrated solvent molecules in a and b are omitted for clarity.

Phenylethynyl substituted dibenzoperylene **161** crystallizes in a monoclinic space group $P2_1/n$ (Figure 3.1.9). A twisted molecular structure was observed in **161** and the angle between two peripheral benzene rings fused to the central perylene moiety is 40.3° based on the crystallographic data. The distance of π-stacking between two parallel arranged π-planes is 3.61 Å.

3.1.4 Cyclization of Cross-Coupling Products to *cata*-Condensed Heteroannulated Coronenes

According to the proposed synthetic route, *cata*-condensed heteroannulated coronenes could be obtained after the cyclodehydrogenation between the attached aromatic rings and the central perylene backbone. Cyclizations were first performed on compound **152** by oxidative cyclodehydrogenation under Rathore conditions.[58] Treating **152** in a CH_2Cl_2 solution with 3 equiv. of 2,3-dichloro-5,6-dicyano-1,4-benzoquinone (DDQ) and trifluoromethanesulfonic acid (TfOH) gave the desired two-fold cyclized product **163** as yellow solid in 90% yield.

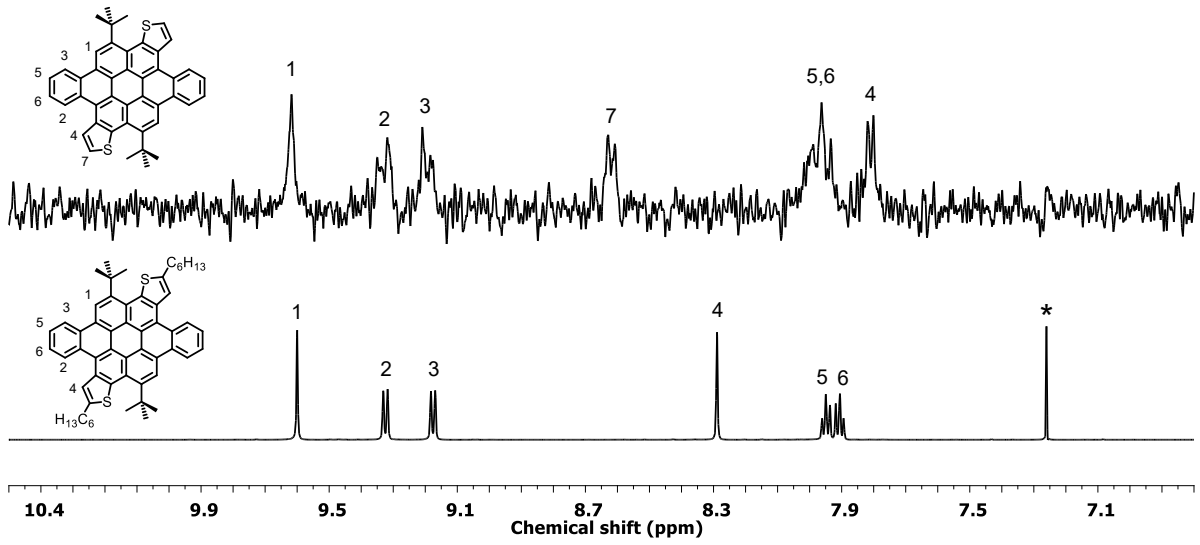

Figure 3.1.10 ^{1}H NMR spectra of **163** (300 MHz, $Cl_2CDCDCl_2$, 298 K) and **164** (300 MHz, $CDCl_3$, 298 K). Depicted are only the aromatic regions. *$CHCl_3$.

Unfortunately, the product shows poor solubilities in common organic solvents (less than 0.5 mg·mL^{-1}), such as CH_2Cl_2, $CHCl_3$, THF and toluene. Compared with the hexyl chain decorated coronene **164**, which has been synthesized and will be discussed in the following part, the ^{1}H NMR spectrum of **163** in $CDCl_3$ or 1,1,2,2-tetrachloroethane-d_2 (TCE- d_2) is much more poorly resolved than that of **164** in $CDCl_3$ at room temperature (Figure 3.1.10). Only broad signals with low signal to noise ratio were observed in the aromatic region of the ^{1}H NMR spectrum of **163**. Considering the potential difficulties in the purification and characterization for compounds with low solubility, substrates **145**, **150**, **153**, **155**, **158** and **160** substituted with hexyl or hexyloxyl chains were selected in the next cyclization reactions. For the substrates substituted with pyridine rings, compounds **148**, **151** and **159** were chosen.

Besides the oxidative cyclodehydrogenation (Scholl reaction), a photochemical cyclization is another approach in the ring-closing step of synthesizing PAHs, as discussed in chapter 1.2.2.2.[80a] Photocyclization (Mallory reaction) is often accomplished by photoirradiation in the presence of an oxidant such as I_2. Excess amount of propylene oxide is often required to consume the HI formed during the reaction.[80a, 164]

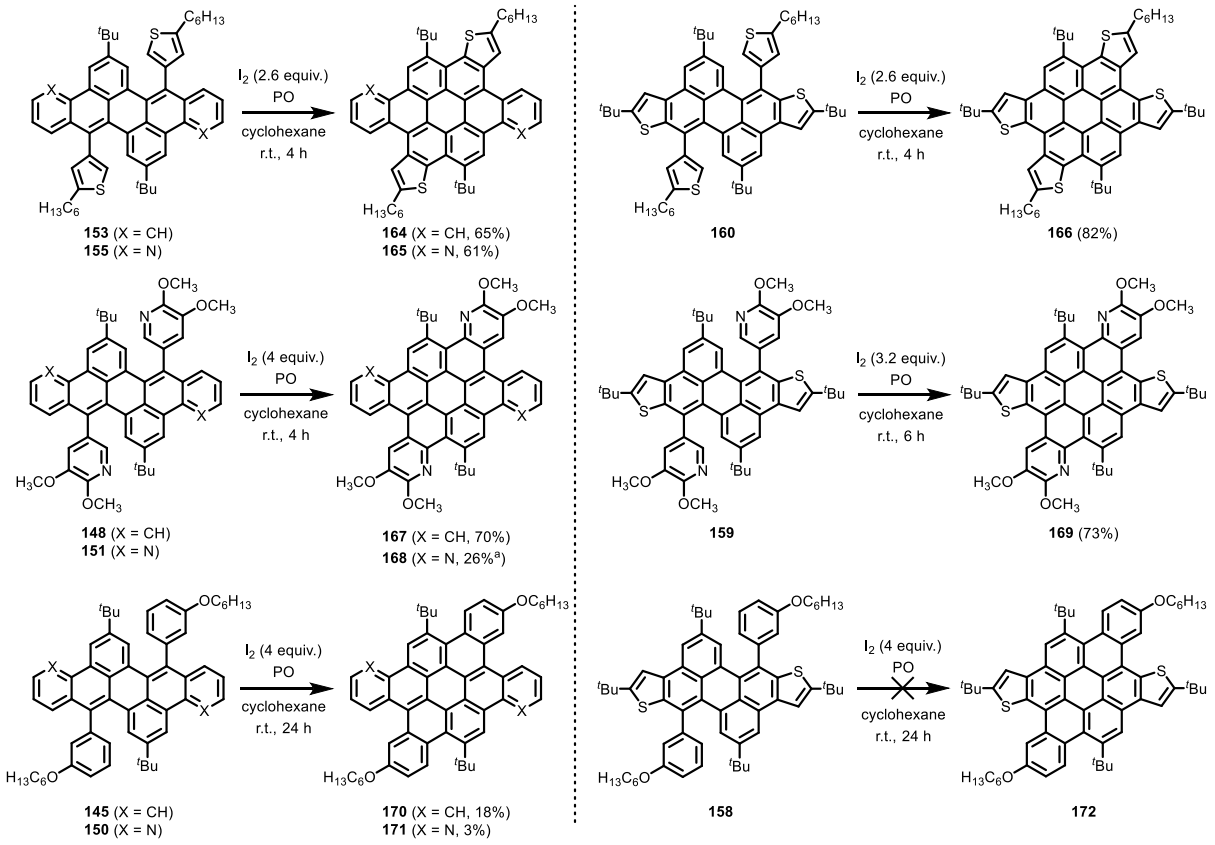

Scheme 3.1.6 *Cata*-condensed coronenes **164**-**172** synthesized by photocyclization. Isolated yields are given in parentheses. PO: propylene oxide. [a]Irradiation for 16 h.

An overview of the designed *cata*-condensed coronenes and the results of the photocyclization are shown in Scheme 3.1.6. For the three substrates substituted with

5-hexylthiophen-3-yl groups (**153**, **155** and **160**), photocyclizations gave the two-fold cyclized products in yields of > 60%. The highest yield of 82% in this series was achieved in the formation of tetrathiophene-fused coronene **166**. The photoreactions were also achieved in the cases of two 5,6-dimethoxypyridin-3-yl substituted substrates **148** and **159**, with the isolated yields of the products of 70% and 73%, respectively. A lower yield of 26% was obtained in the formation of tetrapyridinocoronene **168** after irradiation overnight, which could be ascribed to the low solubility of substrate **151** in cyclohexane (< 0.5 μM). The aggregated substrate particles could only be partially consumed during the reaction. Alternatively toluene was used to increase the solubility of the substrate **151**, followed by running the reaction under irradiation in the presence of I_2/PO. A lower yield of < 5% was obtained after irradiation overnight, as the double cyclized product **168** generated during the reaction formed an opaque thin layer on the inner wall of the photoreactor, which blocked the light source and actually stopped the reaction. Relatively poor yields were also obtained in the cases of three 3-(hexyloxy)phenyl substituted substrates **145**, **150** and **158**. Irradiating compound **145** in the presence of I_2/PO for 16 hours gave product **170** in an isolated yield of 18%. The yield further decreases to 3% in the formation of dipyridinocoronene **171** and there was no conversion in the case of **158**.

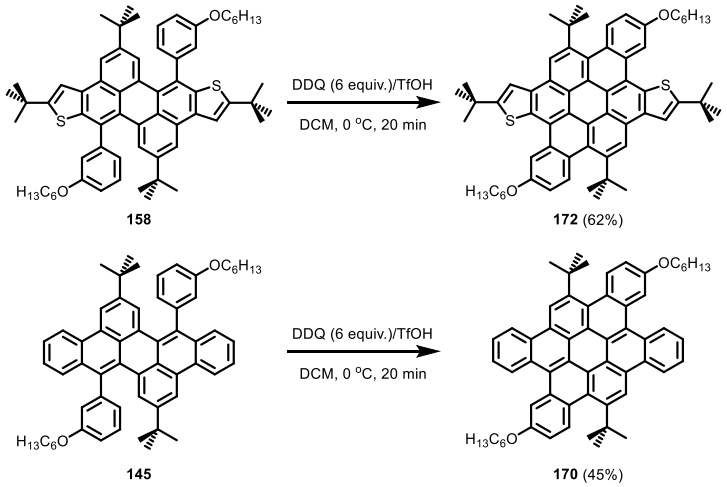

Scheme 3.1.7 Synthesis of extended coronenes **170** and **172** by Scholl reactions.

In order to obtain the last coronene **172**, a Scholl reaction was performed. Treating substrate **158** with 6 equiv. of DDQ in CH_2Cl_2/TfOH gave the two-fold cyclized product **172** in 62% yield. The yield of synthesizing coronene **170** was increased to 45% under the same conditions, higher than that obtained by photocyclization (18%). Part of the product was lost as phenol species due to cleavage of the C-O bonds under acidic conditions, which explained the moderate yields.[165] Similar phenomena were reported by Kumar and co-workers when performing the oxidative cyclotrimerization of *o*-dialkoxybenzenes in the presence of $FeCl_3/CH_3NO_2$.[166] Traces of monohydroxypentaalkoxytriphenylene were isolated as a side product in the absence of other acid

additives, whereas the yield of this compound could be increased up to 20% with 0.3% of Brønsted acids, such as TFA, H_2SO_4 and HCl.[166a] Scholl conditions with DDQ/TfOH are not suitable for the pyridine-containing substrate **150**. One possible reason is that the cyclization cannot proceed via radical cation or arenium cation intermediate formed at the desired positions, with the interference of the arenium cation formed by protonation of the pyridine units under acidic conditions (Scheme 3.1.8). Gryko and co-workers found that oxidative cyclodehydrogenation based on imidazo-[1,2-*a*]pyridine derivative does not work in the presence of $FeCl_3/CH_3NO_2$ or DDQ/CH_3SO_3H, although the detailed reason was not investigated.[167]

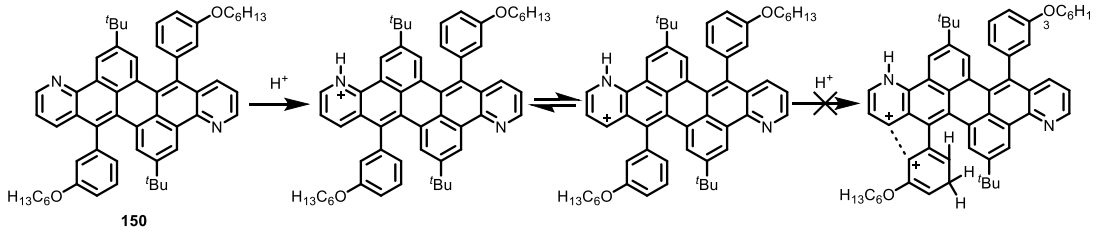

Scheme 3.1.8 The proposed reason of the result that cyclization did not work based on pyridine-containing substrate **150** in the presence of DDQ/TfOH. Protonation first occurs at the pyridine units. The arenium cation intermediate could not be produced or the formed arenium cation could not attack the *tert*-butyl group attached benzene ring, with the interference of the formed pyridine arenium cation.

All nine *cata*-condensed coronene compounds were fully characterized by NMR, mass spectra, FT-IR, elemental analysis, UV/Vis absorption, fluorescence emission spectra and electrochemical cyclovoltammetry. Their molecular geometries were optimized by DFT methods and the structures of seven molecules were further analyzed by single crystal X-ray diffraction. The detailed results are presented in the following chapters.

3.1.5 Single Crystal X-ray Structures of *cata*-Condensed Coronenes

High-quality single crystals of coronenes **164-166**, **169-172** suitable for X-ray diffraction analysis were obtained by diffusing methanol vapor into the solutions of these compounds in $CHCl_3$ or CH_2Cl_2. Due to the low solubility, crystals of the two dimethoxypyridine-fused coronenes **167** and **168** were not obtained by solvent vapor diffusion or by recrystallization from hot solutions in common organic solvents such as $CHCl_3$ or *o*-DCB. The crystal structures of three hexylthiophene-fused coronenes **164-166** were shown in Figure 3.1.11. **164** crystallizes in the triclinic space group $P\ \bar{1}$ with two additional $CHCl_3$ molecules in the asymmetric unit. Due to the two generated cove regions, the coronene is contorted with angles of 16.0° between the *cata*-annulated ring (highlighted in blue) and the central benzene ring (highlighted in red) and 22.7° between the thiophene ring (highlighted in orange) and the central ring (Figure 3.1.11a and d). The coronene molecules are arranged in an offset coplanar fashion, with a shortest distance of d = 3.40 Å. The offset is too large for an efficient π-stacking, as no overlap was observed between two adjacent π-backbones.

Pyridine-fused coronene **165** crystallizes in the monoclinic space group $P2_1/c$ and shows a slightly higher contortion of the thiophene moieties (26.0°) and a smaller one (12.5°) of the pyridine units relative to the center. The molecules are also linearly coplanar arranged, while the pyridine moieties show a π-stacking with a distance of $d_{\pi\text{-}\pi}$ = 3.37 Å. Coronene **166** fused with four thiophene rings crystallizes in the trigonal space group $R\ \bar{3}$. This molecule shows the relative planar π-plane among these three compounds. The deviation from planarity is 4.6° between the *tert*-butyl substituted thiophene ring and the central ring and 21.2° between the hexyl-substituted thiophene ring and the central ring. Intermolecular contacts between the *tert*-butyl group and π-plane have been observed with the shortest distance of d = 2.76 Å, where there is no π-stacking between the molecules in the crystalline state.

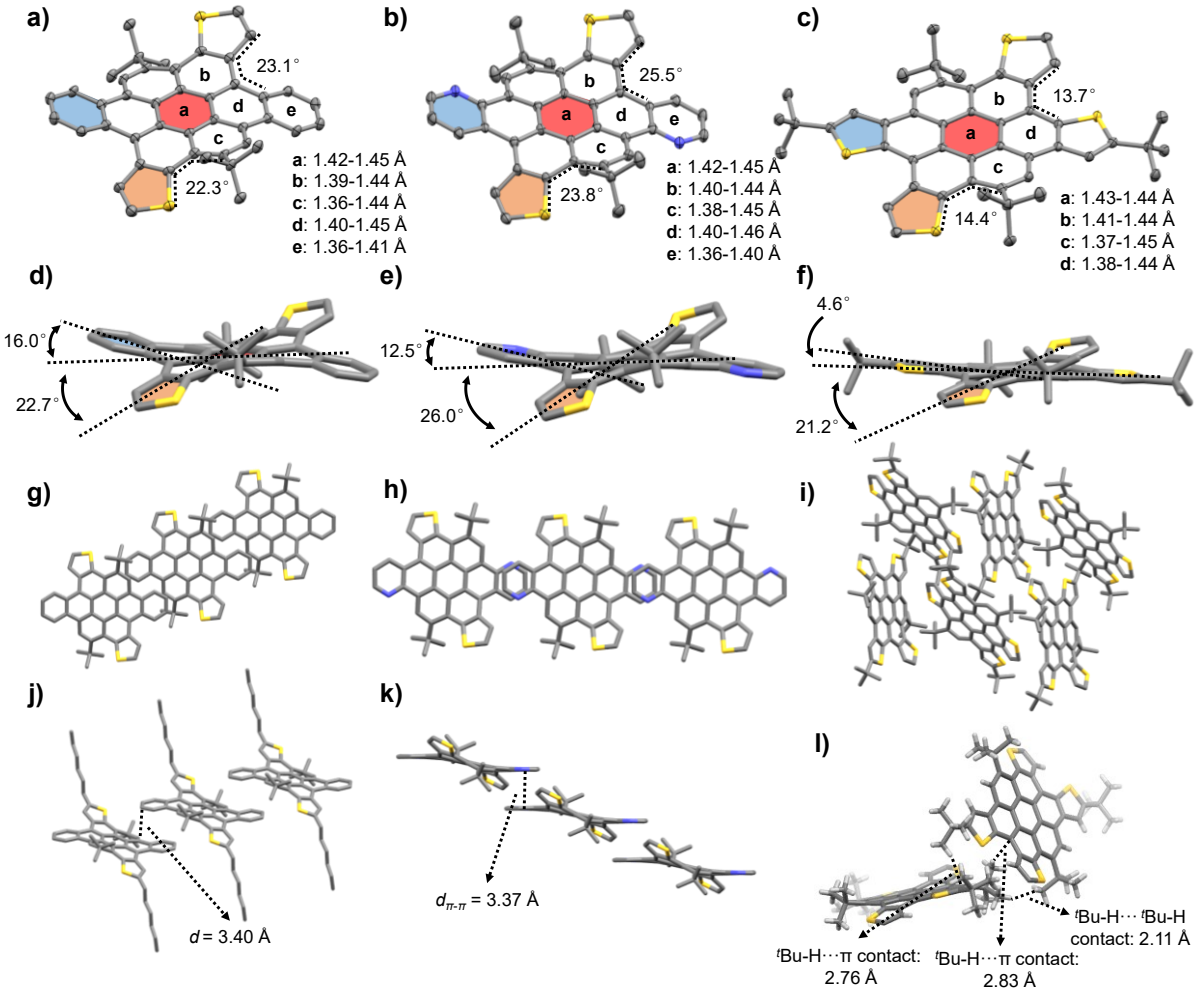

Figure 3.1.11 X-ray crystal structures of thiophene-fused coronenes **164** (a, d, g and f), **165** (b, e, h and k) and **166** (c, f, i and l). ORTEP plots in a-c are at the 50% probability. Bond lengths shown are only C-C bonds. Enclathrated solvent molecules, hydrogen atoms as well as the hexyl chains (except in j) are omitted for clarity. Colors for heteroatoms: blue = nitrogen, yellow = sulfur.

As shown in Figure 3.1.12, coronenes **170** and **171** show similar crystalline motifs, both crystallizing in the triclinic space group $P\ \bar{1}$. Both coronenes are arranged in offset coplanar fashions without π-stacking. Attention should be paid to the fact that in both molecules, besides the

two cove regions, steric repulsion between the fused hexoxyphenyl rings and the bulky *tert*-butyl groups contort both coronenes more than the thiophene-fused ones **164-166**. The dihedral angles of the four carbon atom in the *tert*-butyl groups attached bay regions are 27.2°-28.0° for both molecules, larger than those thiophene-fused compounds **164-166** at the same positions (14.4°-26.0°). The angle between the hexyloxy group attached benzene ring (highlighted in orange) and the central ring (highlighted in red) is 28.2° for **170** and 28.4° for **171**, both larger than their thiophene-fused congeners **164-165** (21.2°-26.0°). Both thiophene and pyridine-fused coronene **169**, which crystallizes in a monoclinic space group $P2_1/n$, shows less twisted π-plane than that of **170** or **171**. The angle between the dimethoxypyridine ring (highlighted in orange) and the central ring (highlighted in red) is 23.8°. The molecule resides on an inversion center with one additional disordered $CHCl_3$ molecule in the asymmetric unit. Four molecular dimers in offset coplanar motif surround one molecule in the center, which is perpendicular to these dimers.

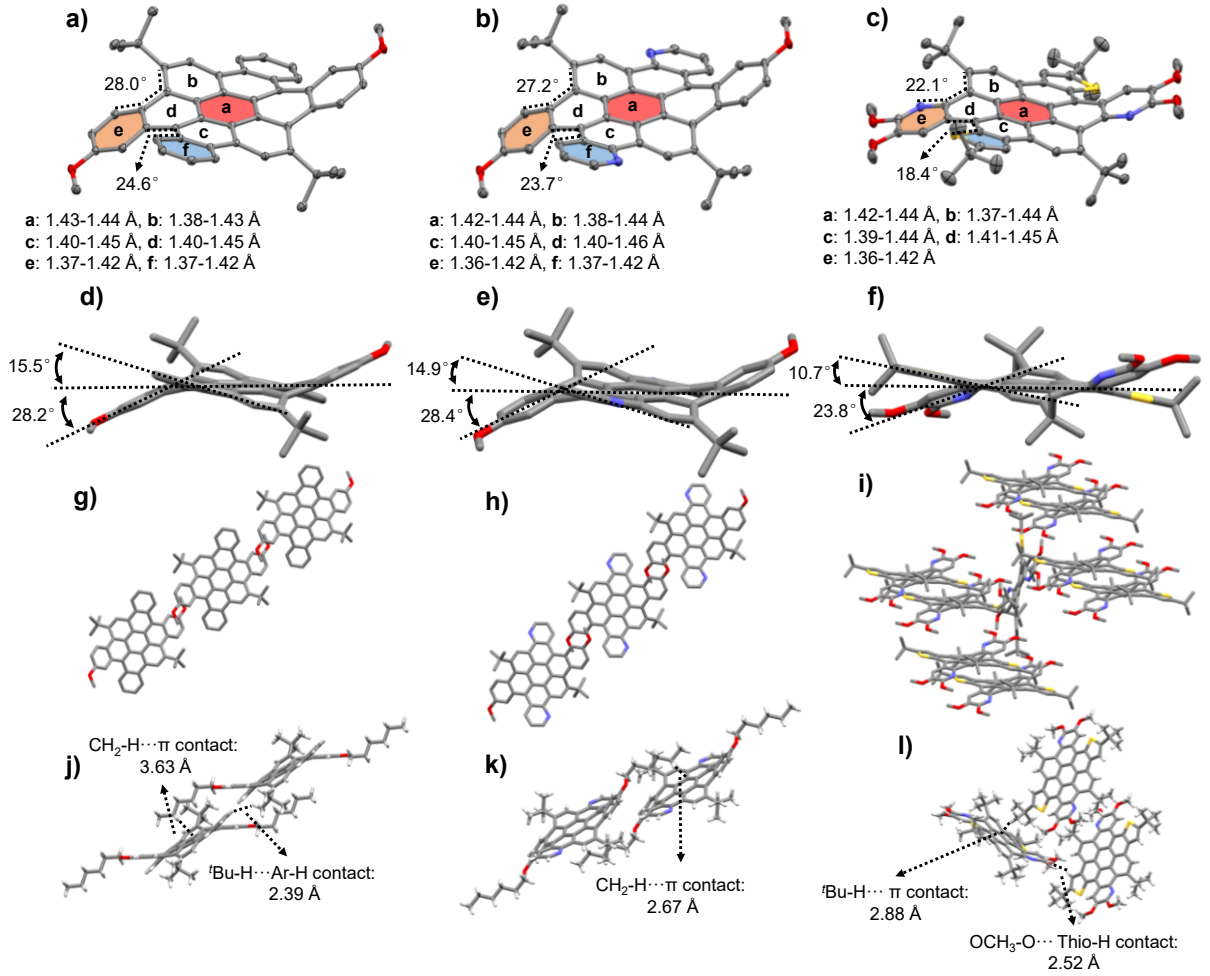

Figure 3.1.12 X-ray crystal structures of coronenes **170** (a, d, g and j), **171** (b, e, h and k) and **169** (c, f, i and l). ORTEP plots in a-c are at the 50% probability. Bond lengths shown are only C-C bonds. Enclathrated solvent molecules, hydrogen atoms (except in j-l) are omitted for clarity. The hexyloxy chains in a, b, d and e are replaced by methoxy groups. Colors for heteroatoms: blue = nitrogen, yellow = sulfur, red = oxygen.

As shown in Figure 3.1.13, dibenzodithienocoronene **172** crystallizes in an orthorhombic space group *Fdd*2 without inversion symmetry. The molecular contortion of **172** is different from the other coronenes discussed above. In this case, as two fused hexyloxybenzene rings bend towards the same side while two fused thiophene rings bend towards the opposite side of the molecular π-backbone, the molecule exhibits a negative curvature.[168] The average angle between the hexyloxy attached benzene rings (highlighted in orange) and the central ring (highlighted in red) is 31.1°, larger than those of other coronenes discussed above. The bending deformation of two hexyloxy attached benzene rings is 56.4° as indicated in Figure 3.1.13b. A linearly coplanar arrangement was observed between two adjacent molecules. The shortest distance between one hexyloxy attached benzene ring and one thiophene ring is $d_{\pi\text{-}\pi}$ = 3.25 Å. Due to the negative curvature, **172** is a racemic crystal containing two enantiomers, with two chiral biaryl axes formed during cyclization. Two molecules with the same stereochemistry ((*M*,*M*) or (*P*,*P*)) form one π-dimer in the crystal lattice (two isomers highlighted in green and light blue in Figure 3.1.13c, respectively).

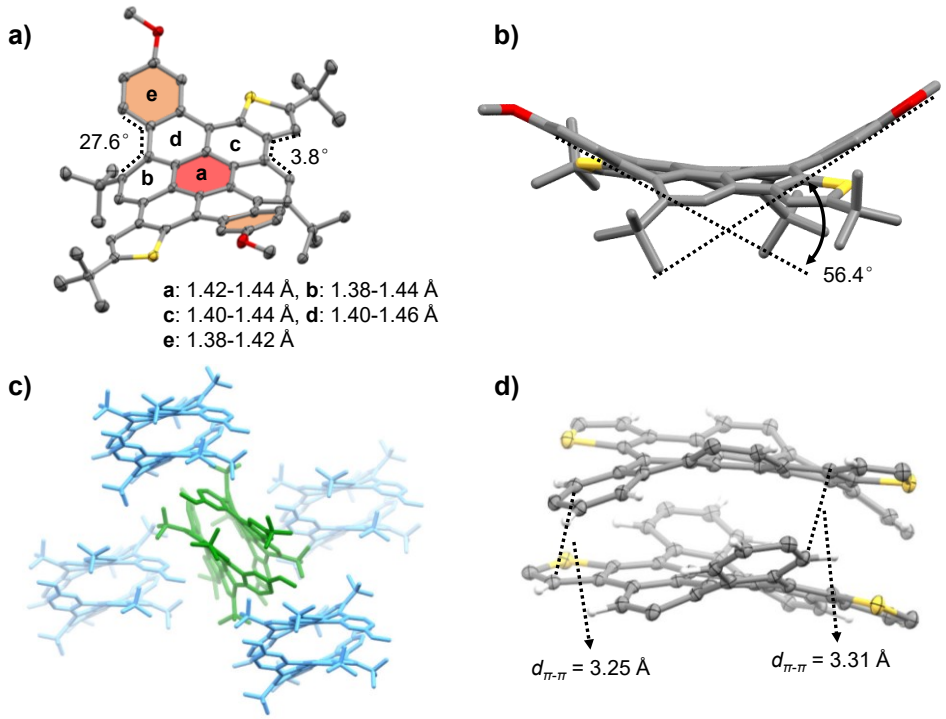

Figure 3.1.13 Front view (a) and side view (b) of X-ray crystal structures of coronene **172**. (c) Packing motif of **172**. (d) A close view of the packing motif of a molecular dimer including two (*P*,*P*)-enantiomers. ORTEP plots in a and d are at the 50% probability. Enclathrated solvent molecules, hydrogen atoms (in a-c), the hexyloxy chains and the *tert*-butyl groups (in d) are omitted for clarity. The two enantiomers in c are highlighted in green for (*M*,*M*) isomer and light blue for (*P*,*P*) isomer. Colors for heteroatoms: yellow = sulfur, red = oxygen.

The racemic mixture of coronene **172** observed in its crystal structure has been proved by applying temperature-dependent ^{1}H NMR analysis (Figure 3.1.14). At low temperatures, two signals of the -OCH_2 moieties on the hexyloxy chains coalesce at around -70 °C. The transition energy barrier estimated from a van't Hoff isotherm is only 41.5 kJ·mol^{-1} (9.92 kcal·mol^{-1}),

suggesting a flexible molecular π-backbone with two rapid interconverting isomers in solution at room temperature. The parameters calculated for temperature-dependent ^{1}H NMR spectra of **172** are shown as follows:

$$k_c = \frac{\pi}{\sqrt{2}} \times \Delta v \text{ if } \frac{\Delta v}{J_{AB}} >> 10$$

$$\text{Eyring: } k = \frac{k_B \times T_C}{h} \times K^{\dagger} \qquad \text{Van't Hoff isotherm: } \Delta G^{\dagger} = -RT \ln K^{\dagger}$$

v: shift in Hz, J_{AB}: coupling constant, k: rate constant, T_C: coalescence temperature

$\Delta v = v_A - v_B = 1302.23 - 1261.58 = 40.6$ Hz, $T_C = -70$ °C = 203 K

$$k_c = \frac{\pi}{\sqrt{2}} \times \Delta v = 90.2\ Hz$$

$$\Delta G^{\dagger} = RT_C \ln \frac{k_B \times T_C}{h \times k_C} = 8.314 \times 203 \times \ln \frac{1.38 \times 10^{-23} \times 203}{6.63 \times 10^{-34} \times 90.2} = 41.5\ kJ \cdot mol^{-1}$$

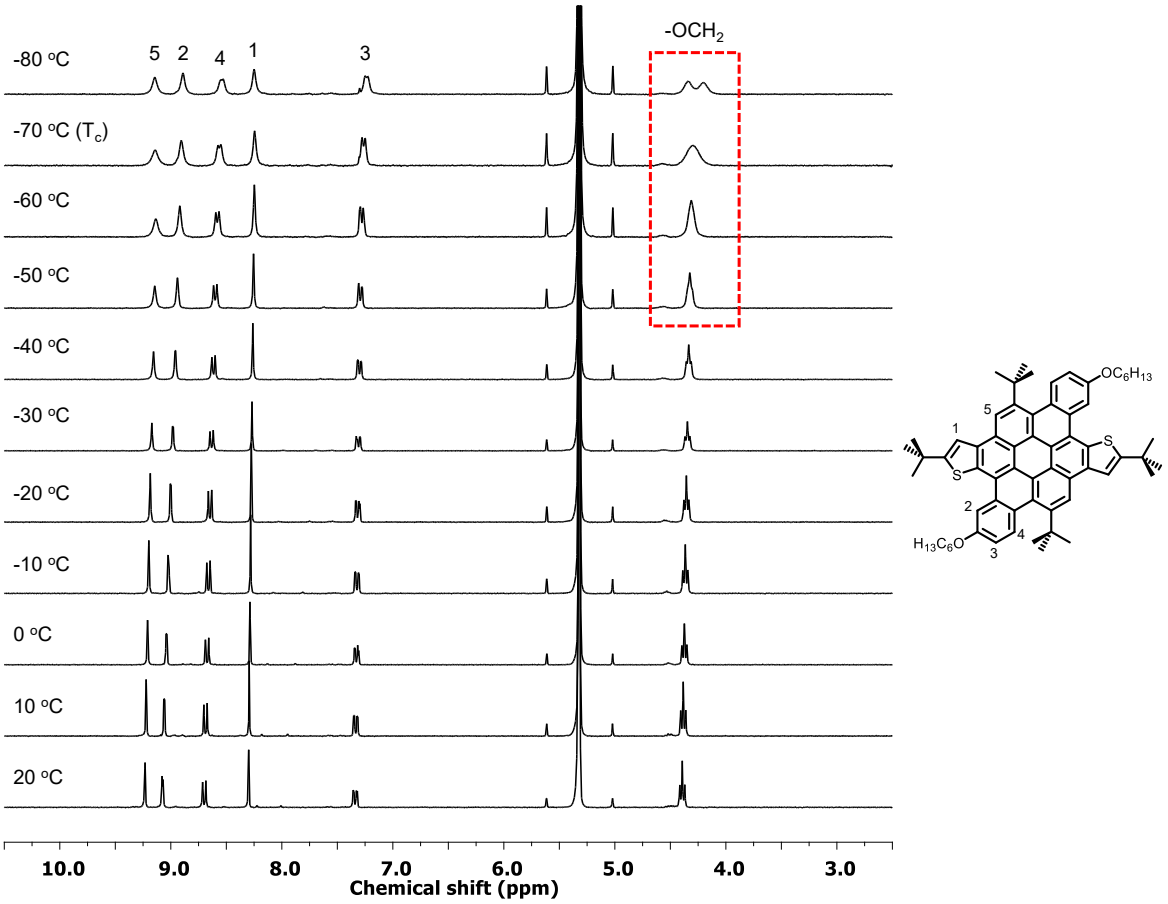

Figure 3.1.14 ^{1}H NMR spectra (300 MHz, CD_2Cl_2) of coronene **172** at different temperatures.

3.1.6 DFT Calculations

In order to investigate the influence of different heteroatoms on the electronic properties of this series of *cata*-condensed coronenes, geometry optimizations based on density functional theory (DFT) at the B3LYP/6-311G* level were carried out using *Spartan* 14.[169] The calculated frontier molecular orbitals (FMOs) are depicted in Figures 3.1.15-17.

Coronene **170** shows E_{HOMO}= -5.09 eV and E_{LUMO}= -2.09 eV. Substituting the two hexyloxy attached benzene rings with dimethoxypyridine or hexylthiophene rings stabilizes the HOMO levels slightly by 0.03-0.04 eV and destabilizes the LUMO levels by 0.11-0.15 eV.

For the coronenes **171**, **168** and **165**, which were synthesized from dipyridinoperylene **112**, both FMOs get stabilized because of the electron-withdrawing nature of pyridyl units. The HOMOs are stabilized by 0.13-0.14 eV and the LUMOs are 0.10-0.16 eV lower, in comparison to those of coronenes **170**, **167** and **164**. Substitutions of the hexyloxy attached benzene rings by pyridine or thiophene rings causes similar influences on FMOs to those of coronenes **170**, **167** and **164**. The HOMOs get slightly stabilized by 0.04 eV while the LUMOs get destabilized by 0.07-0.09 eV.

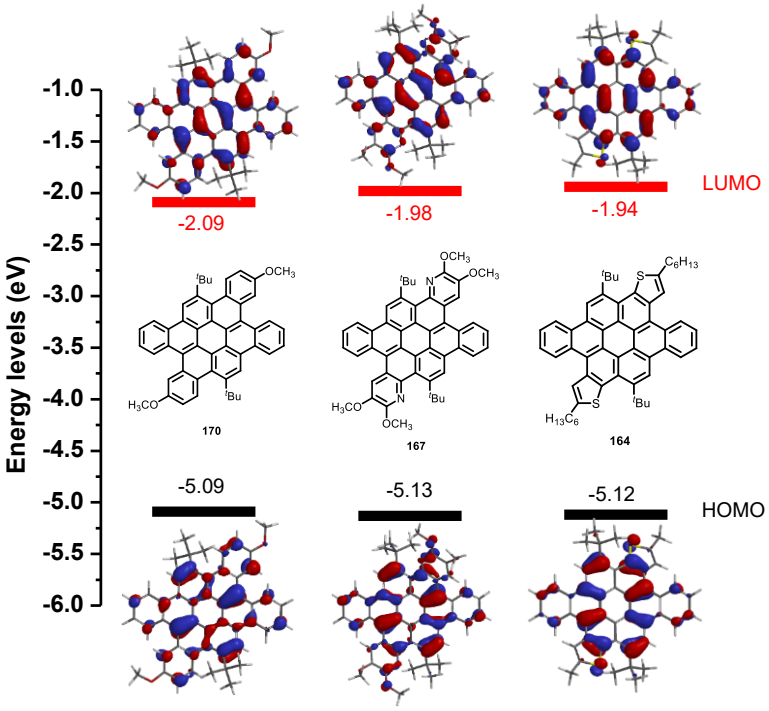

Figure 3.1.15 Frontier molecular orbital levels of three coronenes **170**, **167** and **164** synthesized from dibenzoperylene **111** based on DFT at the B3LYP/6-311G* level.

The FMOs of *tert*-butyl thiophene *cata*-annulated coronene **169** remains the same level compared with **167**, whereas tetrathiophene-fused coronene **166** gives the highest LUMO level of -1.75 eV among this series. Negatively curved coronene **172** shows the highest HOMO level of -4.93 eV and the smallest HOMO-LUMO gap of 3.01 eV among the nine coronenes. The calculated high HOMO level and small bandgap of **172** is in consistence with the measured UV/Vis

absorption spectra and electrochemical characterization (chapter 3.1.7). To sum up, the FMOs of this *cata*-condensed coronene series highly depend on the aromatic units fused at the [3,4] and [9,10] *K*-regions of the central coronene core, whereas annulation with pyridine or thiophene rings at the [5,6] and [11,12] *K*-regions of the central coronene core results in slightly stabilized HOMOs and destabilized LUMOs.

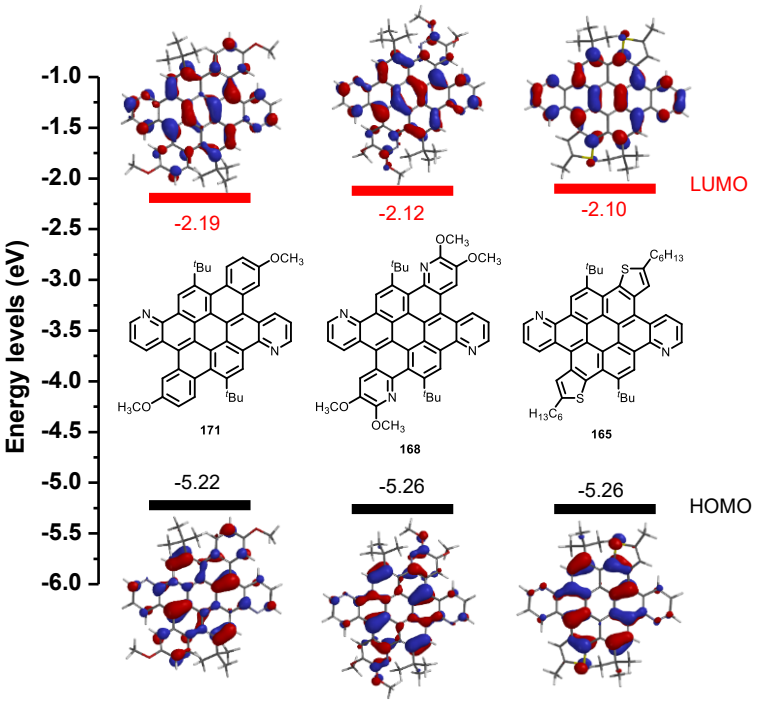

Figure 3.1.16 Frontier molecular orbital levels of three coronenes **171**, **168** and **165** synthesized from dipyridinoperylene **112** based on DFT at the B3LYP/6-311G* level.

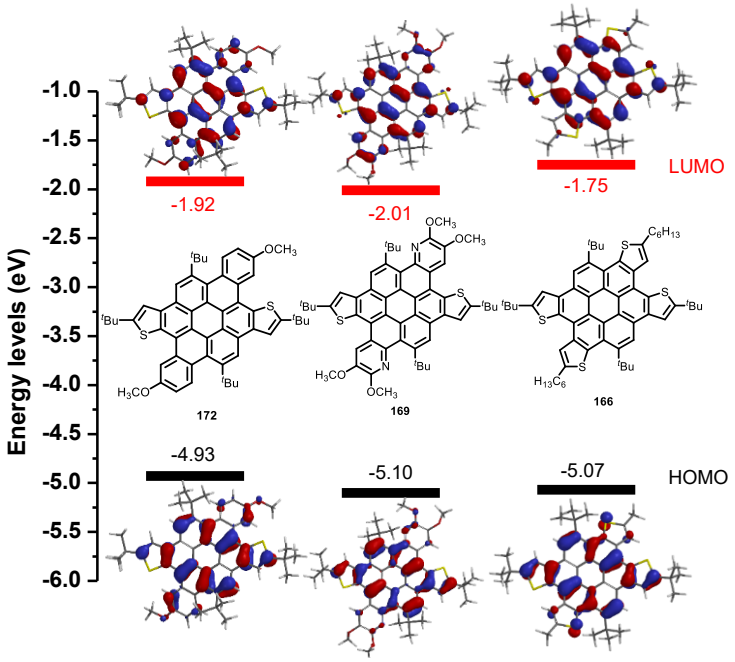

Figure 3.1.17 Frontier molecular orbital levels of three coronenes **172**, **169** and **166** synthesized from dithienoperylene **140** based on DFT at the B3LYP/6-311G* level.

3.1.7 Spectroscopic and Electrochemical Properties

All coronenes as well as the uncyclized precursors were investigated by photophysical and electrochemical measurements (Figure 3.1.18 and Table 3.1.2). All spectroscopic measurements were performed in CH_2Cl_2 at room temperature. As proposed by Clar, the *β*- and *p*-bands are used for the interpretation of the absorption bands of PAHs.[170] *β*-band refers to a lower-wavelength absorption that results from absorption of light oriented along the long axis of the molecule, while a higher-wavelength *p*-band refers to short-axis absorption. Well-resolved *β*- and *p*-band (π-π* transitions) absorptions were observed in UV/Vis spectra of all compounds. For the non-cyclized precursors (Figure 3.1.11a and b), the *p*-band absorption maxima of compounds **145**, **148** and **153**, which were synthesized from dibenzoperylene **111**, are in the range of λ = 431-435 nm. Absorption peaks with similar positions were observed in the *p*-band absorption of precursors *cata*-annulated with pyridine (**150**, **151** and **155**) compared with the benzo-compounds (**145**, **148** and **153**), whereas in cases of more electron-rich thiophene-fused precursors (**158**-**160**), *p*-band absorption maxima significantly red-shift to λ = 474-478 nm. A similar phenomenon was also found in the corresponding fluorescent emission spectra. The benzene-fused compounds **145**, **148**, **153** and pyridine-fused compounds **150**, **151** and **155** show similar emission maxima at λ = 472-481 nm, whereas the emission maxima of thiophene-fused compounds **158**-**160** are bathochromically shifted to λ = 529-533 nm.

After cyclization, all fused coronenes show sharp *β*-band absorptions in the range of λ = 350-370 nm with significantly increased extinction coefficients. The three coronenes **164**-**166** fused with hexylthiophene rings exhibit the highest extinction coefficients ($\varepsilon > 1.60 \times 10^5$ M^{-1} cm^{-1}). Tetrabenzocoronene **170** without heteroatoms shows two *β*-band absorption peaks a λ = 355 nm and λ = 373 nm, along with one shoulder peak at λ = 344 nm.

Two *p*-band absorption peaks at λ = 422 nm and λ = 447 nm were observed for **170**, with a high extinction coefficient of $\varepsilon = 3.68 \times 10^4$ M^{-1} cm^{-1} at λ = 447 nm. Note that **170** shows the most bathochromic shift in *p*-band absorption, in comparison to other eight heteroannulated coronenes in this series and the highest corresponding extinction coefficient for the *p*-band absorption also comes from tetrabenzocoronene **170**. In the cases of two coronenes fused with two pyridine rings as well as two thiophene rings (**165** and **169**), the *β*-band absorptions get sharper and show only one maximum at λ = 364 nm and 368 nm, respectively. The corresponding extinction coefficients increase in comparison to tetrabenzocoronene **170**. Tetrapyridinocoronene **168** shows moderate absorptions for both the *β*- and *p*-bands. Coronene **166** with four thiophene units shows a sharp *β*-band absorption peak at λ = 363 nm with the highest extinction coefficient of $\varepsilon = 1.75 \times 10^5$ $M^{-1}\cdot cm^{-1}$ among this coronene series, which is slightly lower than that of hexathienocoronene ($\varepsilon = 2.48 \times 10^5$ $M^{-1}\cdot cm^{-1}$ at λ = 370 nm).[93a] Pyridine-fused coronenes (**167**-

169, **171**, except **165**) and negatively curved coronene **172** show increased absorbance in α-band[170c] (n-π* transition) at around λ = 480 nm than other coronenes in this series, of which **172** shows the most bathochromic shift (peak at λ = 484 nm). Emission spectra with similar patterns were found in this series. One main emission peak at λ = 476-486 nm and one secondary peak at 509-524 nm were observed in all cases. Negatively curved coronene **172** shows slightly more bathochromic shifted emission peaks at λ = 491 nm and λ = 524 nm than other coronenes of this series. In comparison to those uncyclized precursors and diarenoperylenes before bromination,[128b] the fluorescence quantum yields of all coronenes decrease, whereas nitrogen-containing coronenes **167**, **168** and **171** show moderate quantum yields of 22%-35%.

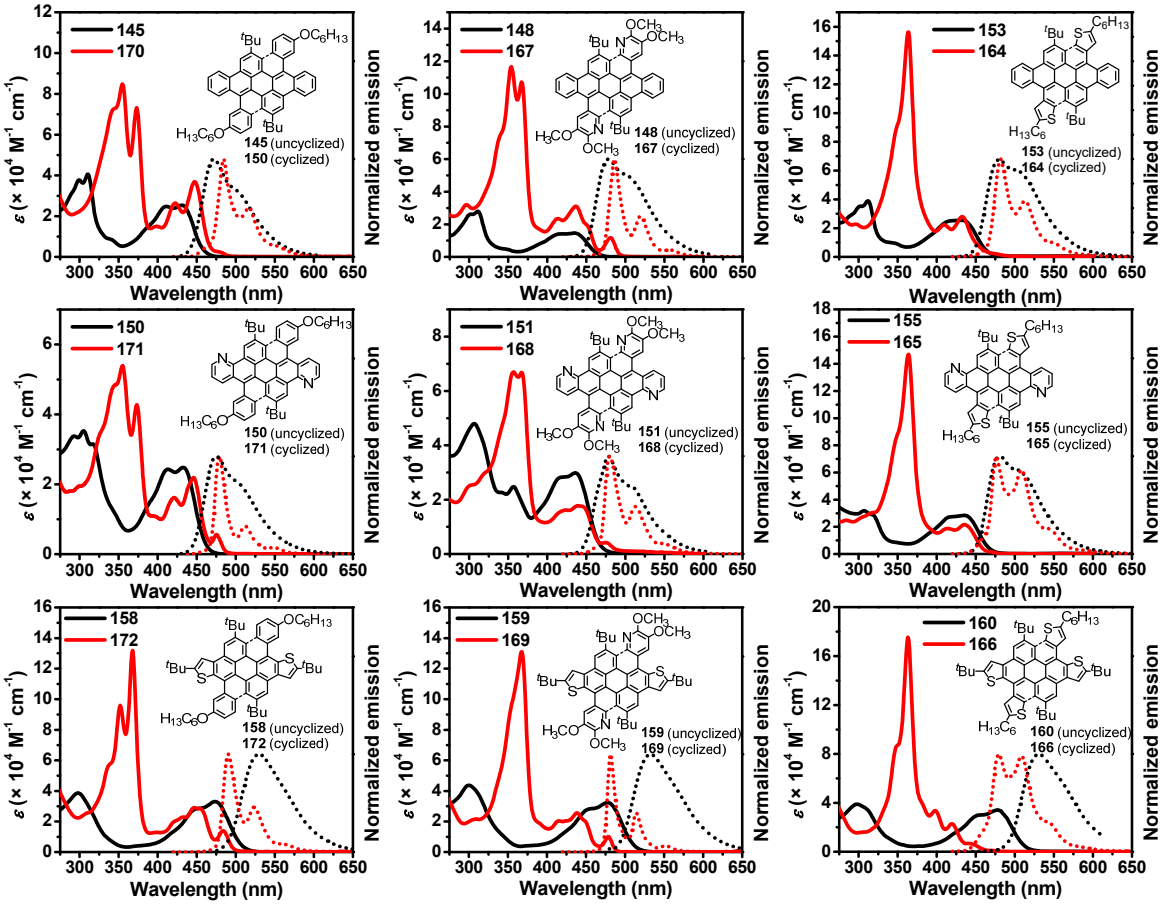

Figure 3.1.18 Absorption (solid line) and normalized emission (dot line) spectra of uncyclized precursors (black line) and *cata*-annulated coronenes (red line) measured in CH_2Cl_2 (molar concentration = 4-26 μM) at room temperature.

The ionization potentials (IPs) and electron affinities (EAs) of all uncyclized precursors and fused coronenes were investigated by cyclovoltammetry measurements. The results (Table 3.1.2) were estimated from the onsets of first oxidation wave and reduction wave, respectively. Cyclization does not affect much on the IPs and EAs. As expected, the IPs of pyridine-fused coronenes (**171**, **168**, **165** and **167**) are about 0.2 eV lower than tetrabenzocoronene **170**, in which tetrapyridinocoronene **168** shows the lowest values at IP = -5.4 eV and EA = -3.3 eV. In cases of

164, **172** and **166**, fusing with thiophene rings slightly increases the IPs, when compared with tetrabenzocoronene **170**. This trend has also been confirmed by DFT calculations, indicating the impact of electron donating/withdrawing heteroatoms on the electronic structures of these π-systems.

Table 3.1.2 Summary of the photophysical and electrochemical characterization of *cata*- condensed coronenes **164**-**172** and their corresponding uncyclized precursors.

Compd	λ_{abs} [nm][a]	E_g^{opt} [eV][a,b]	λ_{em} (λ_{ex}) [nm][a]	$\tilde{\nu}$ [cm^{-1}] [a,c]	Φ [%][a,d]	IP^{CV} [eV][e]	EA^{CV} [eV][f]	E_g^{CV} [eV]	E_{HOMO} [eV][g]	E_{LUMO} [eV][g]
145	299, 311, 341, 411, 431	2.7	472, 502 (311)	2015	53.5±1.3	-5.2	-2.5	2.7	-5.1	-2.0
148	302, 311, 647, 416, 435	2.7	478, 501 (311)	2068	58.4±0.6	-5.3	-2.6	2.7	-5.2	-2.1
153	302, 312, 416, 432	2.7	479, 502 (416)	2271	14.1±1	-5.2	-2.5	2.7	-5.1	-2.0
150	293, 305, 317, 414, 433	2.7	475, 500 (414)	2042	55.3±0.7	-5.4	-2.6	2.8	-5.2	-2.1
151	306, 341, 357, 418, 436	2.7	478, 506 (341)	2015	54.4±2.0	-5.3	-2.6	2.7	-5.3	-2.2
155	307, 317, 421, 435	2.7	481, 502 (421)	2198	12.4±0.4	-5.3	-2.7	2.7	-5.2	-2.1
158	298, 452, 474	2.4	529 (452)	2193	76.3±2.3	-5.0	-2.6	2.4	-4.8	-1.9
159	300, 376, 456, 478	2.4	533 (478)	2156	77.5±1.0	-5.1	-2.6	2.5	-4.9	-2.0
160	298, 454, 478	2.4	531 (310)	2088	37.7±0.1	-5.0	-2.6	2.4	-4.8	-1.9
170	355, 373, 399, 422, 447	2.7	485, 517 (373)	1753	15.0±0.4	-5.2	-2.6	2.6	-5.1	-2.1
167	354, 367, 414, 436, 481	2.5	486, 519 (367)	2360	35.0±0.4	-5.3	-3.0	2.3	-5.1	-2.0
164	296, 349, 363, 409, 433	2.7	482, 512 (363)	2348	2.5±0.1	-5.2	-2.5	2.7	-5.1	-1.9
171	355, 373, 421, 446, 475	2.5	479, 512 (355)	1545	21.9±0.6	-5.4	-2.6	2.8	-5.2	-2.2
168	357, 367, 424, 439, 475	2.5	480, 513 (367)	1946	23.1±1.2	-5.4	-3.3	2.1	-5.3	-2.1
165	284, 350, 364, 413, 436	2.7	476, 509 (364)	1927	2.7±0.1	-5.3	-2.6	2.7	-5.3	-2.1
172	352, 368, 447, 454, 484	2.5	491, 524 (368)	2005	17.5±0.5	-5.0	-2.6	2.4	-4.9	-1.9
169	368, 415, 438, 479	2.5	482, 515 (368)	2084	16.4±0.8	-5.2	-2.5	2.6	-5.1	-2.0
166	350, 363, 398, 419, 442	2.7	480, 509 (363)	1791	6.8±0.1	-5.1	-2.5[h]	n.d.	-5.1	-1.8

[a] Measured in CH_2Cl_2 at room temperature. [b] Estimated from absorption onset. [c] Stock's shift. [d] Fluorescence quantum yield. [e] Ionization potential. [f] Electron affinity. IPs and EAs were estimated by cyclic voltammetry in 0.1 M nBu$_4$NClO$_4$ in CH_2Cl_2 at room temperature. The scan speed was 100 mV/s and ferrocene/ferrocenium (Fc/Fc^+) was used as internal reference. IP^{CV} = -(E_{onset}^{ox} + 4.8 eV). EA^{CV} = -(E_{onset}^{red} + 4.8 eV). [g] Calculated by density functional theory (DFT) using Spartan 14 at B3LYP/6-311G* level. [h] EA^{CV} = IP^{CV} + E_g^{opt}.

3.1.8 Conclusions

In conclusion, a three-step synthetic route to (tetrakis)-heteroannulated coronenes was developed, based on 2,10-*tert*-butyldiarenoperylenes via a regioselective bromination as key-step. In comparison to prior existing synthetic approaches to heteroannulated coronenes,[81, 93, 171] this one allows the construction of less symmetric compounds and in principle the access to a large variety of constitutional or positional isomers. Seven of the nine obtained *cata*-annulated coronenes were characterized by single crystal X-ray diffraction analysis. Contorted molecular π-backbones were observed in all seven cases and one of them exhibits negative curvature. As the aromatic boronic acid or ester could be changed to other aromatic reactants such as naphthyl boronic acid or anthracyl boronic acid, the two-fold brominated diarenoperylenes show potential to be used in cross-coupling reactions to synthesize a large variety of further π-extended aromatics.

3.2 Functionalized Contorted Polycyclic Aromatic Hydrocarbons by a Cyclopentannulation and Regioselective Triflyloxylation in One-Step

3.2.1 Introduction

As discussed in chapter 1.2.2.1, the oxidative cyclodehydrogenation (Scholl reaction) serves as a powerful tool to synthesize PAHs in the ring-closing stage by multiple biarylic C-C bond formations in one step without the necessity of prior installation of reactive functional groups.[54a, 54b] In most cases, multiple six-membered benzene rings are formed in the presence of oxidants and acids via radical cation or arenium cation mechanism in Scholl reactions.[54a, 54b] In comparison to those cases where six-membered rings are formed, Scholl-type reactions with the formation of five-,[72-74, 77-78, 172] seven-[75, 79c, 117e, 173] or eight-membered[120c, 123-124] rings were less reported.

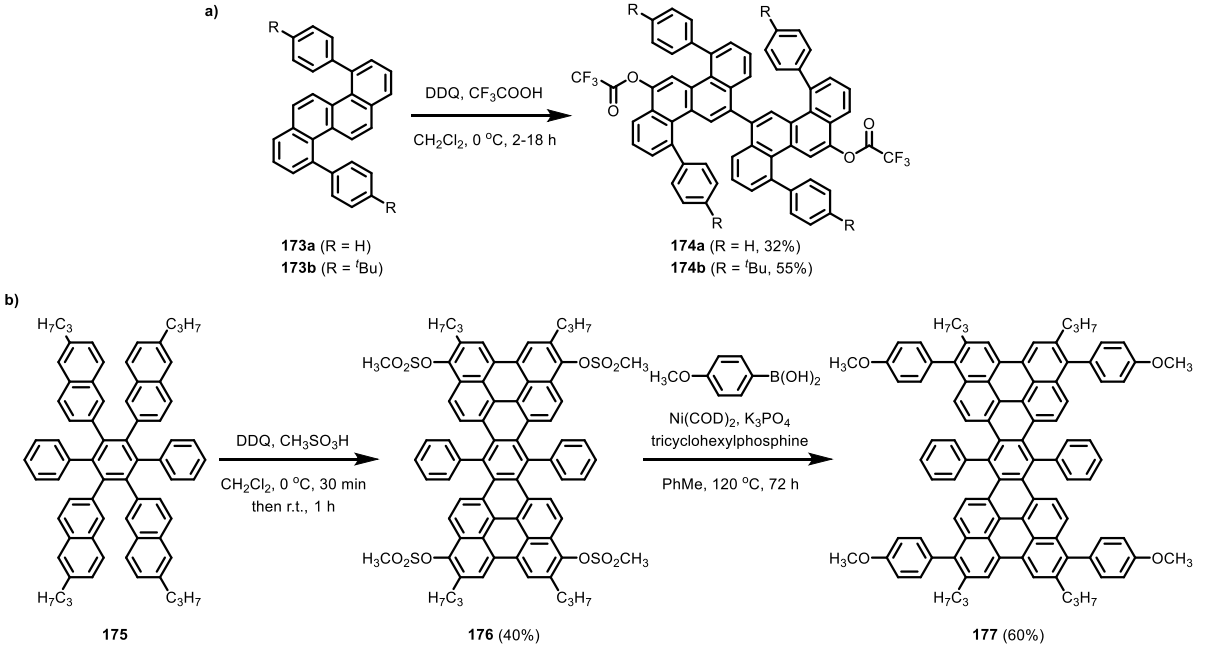

Scheme 3.2.1 Reported regioselective oxylations during Scholl-type reactions.[174]

Although large PAHs can be selectively post-functionalized after the ring-closing step of the synthetic routes in a few cases,[97, 175] selective functionalization during Scholl reactions was seldom reported. Oxylation has been reported as a competing reaction to the cyclization under Scholl conditions.[174a, 176] But regioselective oxylations during oxidative cyclodehydrogenation were only reported in a few publications. For example, Quayle and co-workers reported that the intermolecular oxidative coupling products obtained by treating diphenylchrysene **173a** and **173b** with DDQ/TFA were found to be substituted by two trifluoroacetate groups (Scheme 3.2.1a).[174a] Miao and co-workers observed a four-fold mesyloxylation during the Scholl cyclization of PAH

175 in the presence of DDQ and excess methanesulfonic acid. The methanesulfonate groups could serve as functional groups for the subsequent cross-coupling reactions (Scheme 3.2.1b).[174b]

In this chapter, Scholl cyclizations of two isomeric naphthalene-substituted dibenzoperylenes are discussed. Treating one of them under Scholl conditions gives contorted PAHs containing two five-membered rings, while performing a Scholl reaction with the other isomer under similar conditions produces contorted PAHs with two azulene units embedded. In both cases, regioselective two-fold triflyloxylation was observed during the Scholl reaction and the obtained bistriflates could be used for further reactions.

3.2.2 Contorted PAHs with two Embedded Five-membered Rings

3.2.2.1 Scholl Cyclization of Diphenyl Dibenzoperylene 143

During the investigation of Scholl reactions of phenyl-substituted dibenzoperylenes to *cata*-condensed coronenes, it was found that different from alkoxyphenyl substituted dibenzoperylene **145**, performing the reaction using phenyl-substituted substrate **143** under Scholl conditions does not give coronene **178** via the formation of two six-membered rings (Scheme 3.2.2). A well-resolved ^{1}H NMR spectrum of the isolated double cyclized product was obtained in $Cl_2CDCDCl_2$ (Figure 3.2.1a, bottom). Nine signals with nearly the same integrals were found in the aromatic region of the ^{1}H NMR spectrum of PAH **179**, indicating two new C-C bonds formed in the obtained product. This is in accordance with the information observed in the MALDI-TOF mass spectrum (Figure 3.2.1c). The double cyclized product was confirmed by the monoisotopic signal of m/*z* = 612.281 (calcd. for $[M]^+$, $C_{48}H_{36}$, 612.282) and a matching isotopic distribution pattern with the simulated one. In comparison to the ^{1}H NMR spectrum of tetrabenzocoronene **170**, the singlet in the low field at δ = 9.41 ppm for H-1 in PAH **170** was not observed for PAH **179**. By the help of the 2D NMR techniques (^{1}H-^{1}H COSY spectrum, Figure 3.2.1b), it was found that every signal in the aromatic region is coupled with other signals. If the double cyclized product was fused coronene **178** with two hexagonal rings formed, one singlet for the two red-marked protons (Scheme 3.2.2) at symmetric positions would be expected. By further analyzing the ^{1}H-^{1}H COSY NMR spectrum, it was found that the two signals for H-1 and H-9, respectively, are coupled with each other, suggesting that these two protons are at one benzene ring. The same results were also observed in protons 2-4 and protons 5-8. Thus the NMR results indicate that the cyclized product could not adopt the structure of fused coronene **178** but the two-fold five-membered ring-cyclized product **179** (Scheme 3.2.2). The cyclopentannulation occurs at the *L*-regions (zigzag edge) of the *cata*-condensed dibenzoperylene π-framework. When treating **143** with 12 equiv. of $FeCl_3$ in CH_2Cl_2/CH_3NO_2 mixture, incomplete conversion was observed even after refluxing the mixture overnight and the isolated yield of double cyclized product **179** was only 20%. The yield was

improved to 65% by using DDQ (6 equiv.)/TfOH. Photocyclization with I_2 (10 equiv.)/propylene oxide under UV irradiation overnight was also tried based on diphenyl dibenzoperylene **143** while no conversion was observed.

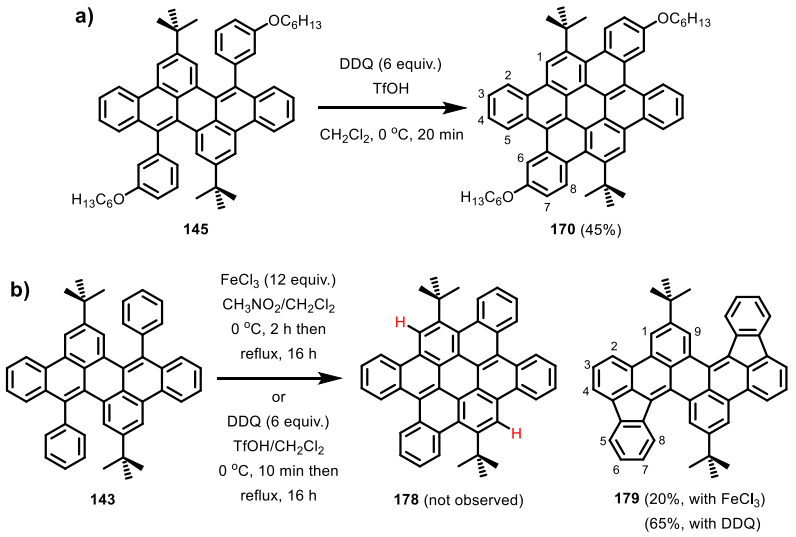

Scheme 3.2.2 Cyclization of substrate **145** and **143** under Scholl conditions.

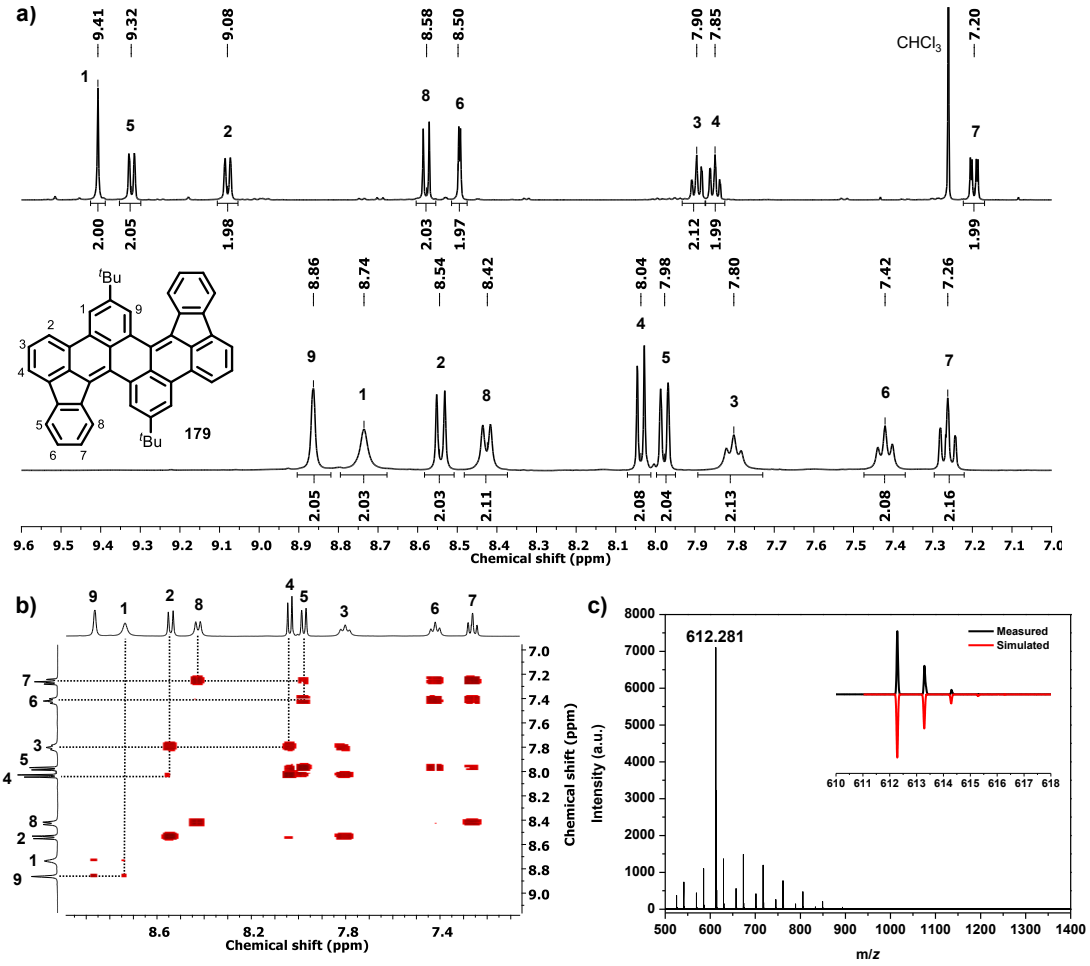

Figure 3.2.1 a) ^{1}H NMR spectra of PAHs **170** (600 MHz, $CDCl_3$, 298 K, top) and **179** (400 MHz, $Cl_2CDCDCl_2$, 298 K, bottom). Depicted are only the aromatic regions. Peak assignments of PAH **170** are according to the numbering of the molecular structure in Scheme 3.2.2. b) ^{1}H-^{1}H COSY NMR spectrum of PAH **179** (400 MHz, $Cl_2CDCDCl_2$, 298 K). c) MALDI-TOF MS (DCTB, calibrated with PEG600, reflective positive mode) of PAH **179**.

The molecular structure of the five-membered ring-containing PAH **179** was unambiguously confirmed by single-crystal X-ray diffraction (Figure 3.2.2). Different from dibenzoperylene **111** which exhibits a planar π-plane,[128b] cyclopentannulated product **179** adopts a twisted π-backbone. The angle between the two blue-marked benzene rings (Figure 3.2.2a) is 47.8°. PAH **179** crystallizes in the monoclinic space group $P2_1/n$. A parallel arrangement between two adjacent fluoranthene moieties was observed with an average distance of $d_{\pi\text{-}\pi}$ = 3.56 Å.

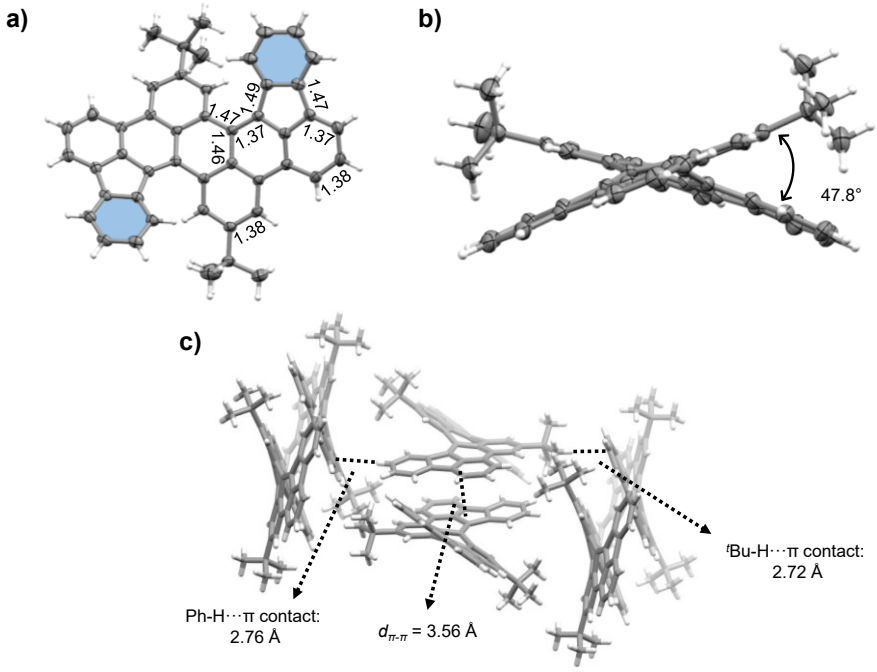

Figure 3.2.2 Front view (a) and side view (b) of single crystal X-ray structure of PAH **179**. (c) Packing motif of PAH **179**. ORTEP plots in a and b are at the 50% probability. Enclathrated solvent molecules are omitted for clarity. C-C bonds in a with lengths of > 1.46 Å or < 1.38 Å are given in Å.

3.2.2.2 Scholl Cyclization of Dinaphthyl Dibenzoperylene 180

In order to further extend this system, dibenzoperylene dibromide **133** was reacted with 2- naphthylboronic acid in palladium-catalyzed Suzuki-Miyaura cross-coupling reaction to give naphthyl-substituted dibenzoperylene **180** in 86% yield (Scheme 3.2.3), as a mixture of atropisomers due to the rotation of the two formed C-C bonds. When **180** was treated with 10 equiv. of $FeCl_3$ in a CH_2Cl_2/CH_3NO_2 mixture, again a two-fold cyclopentannulation took place, giving the product **181** as an orange-red solid in 76% yield. PAH **181** could also be obtained by a Scholl reaction in the presence of DDQ (2.2 equiv.)/TfOH/CH_2Cl_2 in a yield of 63%. By the MALDI HRMS (Figure 3.2.3c), the two-fold cyclization was confirmed by a monoisotopic signal of m/z = 712.3114 (calcd. for $[M]^+$, $C_{56}H_{40}$, 712.3130) and a fitting isotopic distribution pattern to the calculated one.

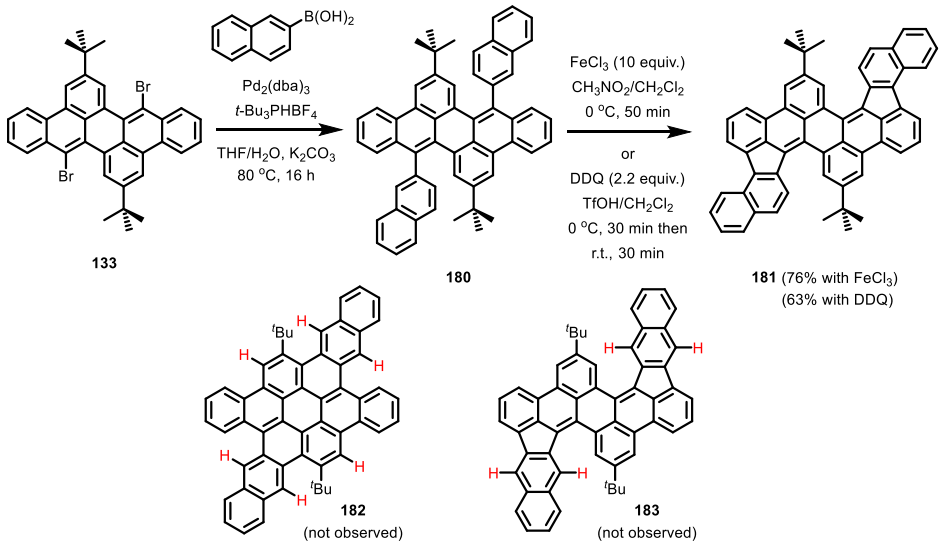

Scheme 3.2.3 Synthesis of double cyclopentannulated PAH **181**.

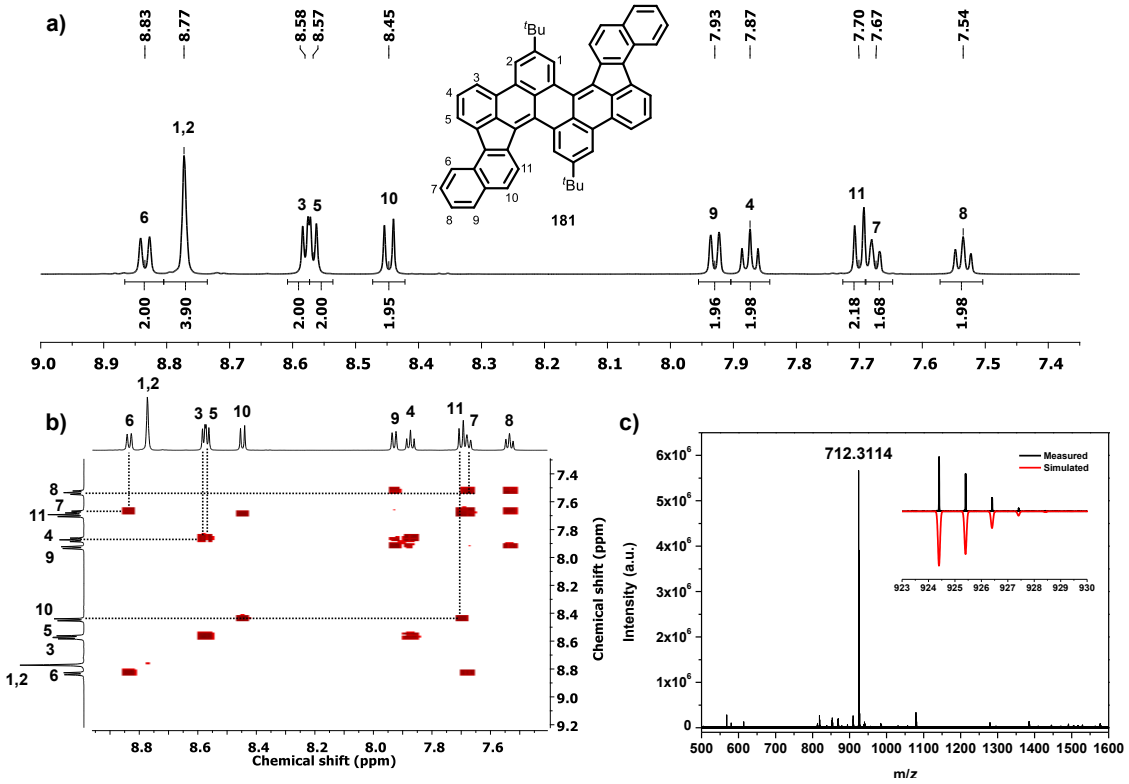

Figure 3.2.3 a) ^{1}H NMR spectrum of PAH **181** (600 MHz, $Cl_2CDCDCl_2$, 298 K). Depicted is only the aromatic region. b) ^{1}H-^{1}H COSY NMR spectrum of PAH **181** (600 MHz, $Cl_2CDCDCl_2$, 298 K). c) MALDI HRMS (DCTB, linear positive mode) of PAH **181**.

The molecular structure of the obtained PAH **181** was confirmed by ^{1}H NMR (Figure 3.2.3a) and 2D ^{1}H-^{1}H COSY NMR spectroscopy (Figure 3.2.3b). The singlet at δ = 8.77 ppm with an integral of four is an overlap of the signals for protons 1 and 2 at the *ortho*-positions of the *tert*-butyl groups. Except this singlet, no singlet was observed in the aromatic region of the ^{1}H NMR spectrum. As indicated by ^{1}H-^{1}H COSY NMR spectroscopy, protons 3-5, 6-9 and 10-11 are on the same aromatic rings, respectively, which in only possible for the structure of **181** being the one

depicted in Scheme 3.2.3. The product should not adopt the structure of the extended heptacene **182**, as three singlets from the red-marked protons would be expected in the aromatic region of the ^{1}H NMR spectrum. Benzofluoranthene-type structure **183** is also not possible as the four red-marked protons would give two singlets in the aromatic region of the ^{1}H NMR spectrum, which were not observed in experiments.

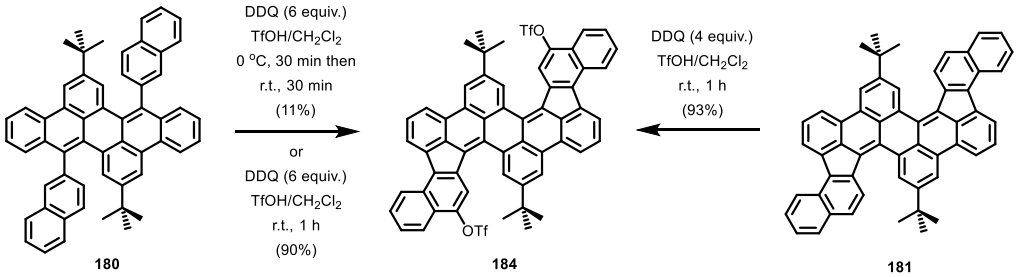

Scheme 3.2.4 Synthesis of bistriflate **184**.

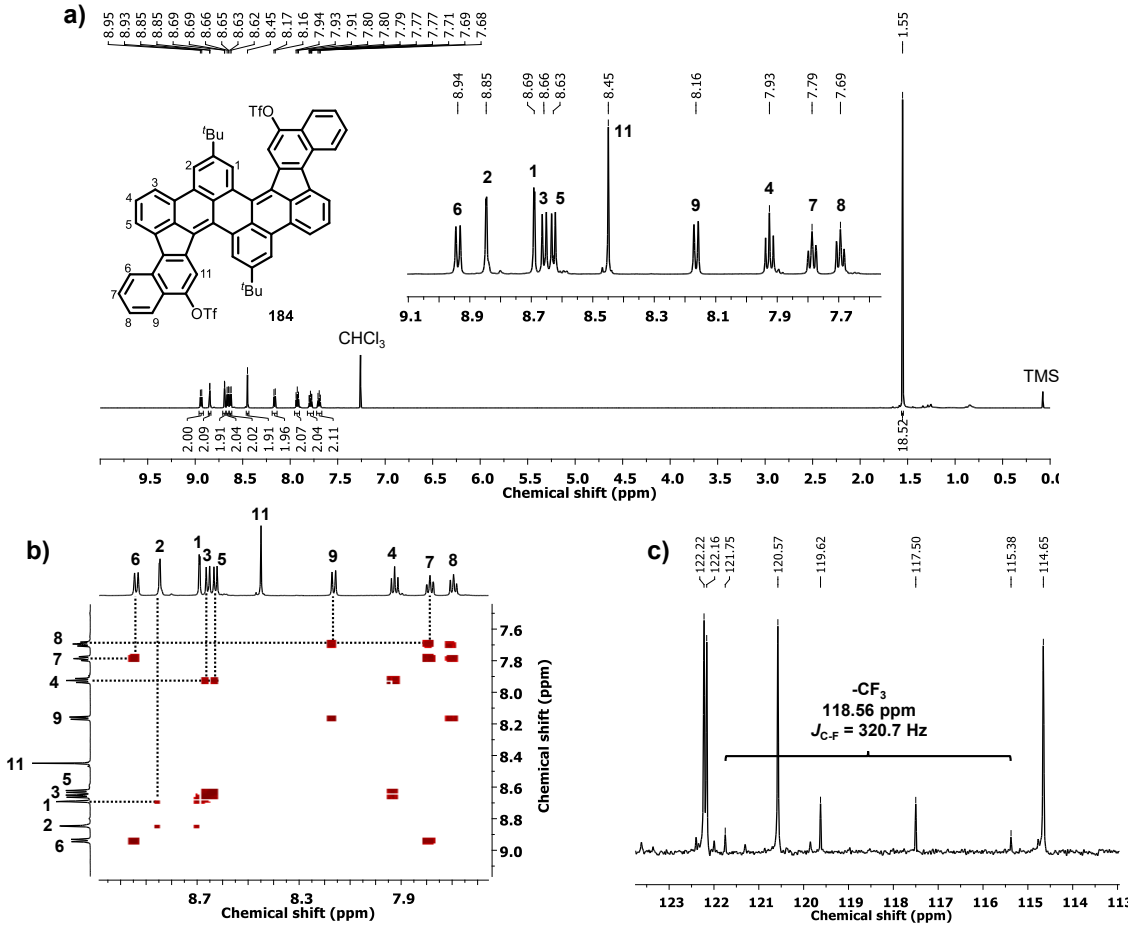

Figure 3.2.4 a) ^{1}H NMR spectrum of bistriflate **184** (600 MHz, $CDCl_3$, 298 K). b) ^{1}H-^{1}H COSY NMR spectrum of bistriflate **184** (600 MHz, $CDCl_3$, 298 K). c) A zoom-in region of the ^{13}C NMR spectrum (151 MHz, $CDCl_3$, 298 K) of bistriflate **184** showing the quartet of -CF_3 groups.

However, when naphthyl-substituted dibenzoperylene **180** was treated with 6 equiv. of DDQ in a TfOH/CH_2Cl_2 mixture at 0 °C, then warmed up to room temperature within 30 minutes, a two-fold regioselective triflyloxylation occurred in addition to the two-fold cyclopentannulation,

giving bistriflate **184** in 11% yield. The isolated yield of bistriflate **184** was increased to 90% when the reaction was allowed to be performed directly at room temperature for one hour (Scheme 3.2.4). Bistriflated **184** could also be obtained from double cyclized compound **181** in the presence of DDQ (4 equiv.)/TfOH/CH_2Cl_2 in 93% yield. This result indicates that the triflyloxylation during the Scholl-type reaction occurs after the Scholl cyclization.

The depicted molecular structure of bistriflate **184** in Scheme 3.2.4 is supported by NMR results (Figure 3.2.4). There are eleven signals in the aromatic region of the ^{1}H NMR spectrum, suggesting the presence of two new substituents on the π-framework. The fused singlet at δ = 8.77 ppm for protons 1 and 2 in the spectrum of PAH **181** (Figure 3.2.3a) splits into two doublets with small coupling constants of J = 1.5-1.7 Hz at δ = 8.69 ppm and δ = 8.85 ppm, respectively, in the spectrum of bistriflate **184** (Figure 3.2.4a). Supported by the information from ^{1}H-^{1}H COSY NMR spectrum (Figure 3.2.4b), only one singlet at 8.45 ppm was observed in the aromatic region of the spectrum of bistriflate **184**, suggesting that the substitutions should be at position 10 or 11 (numbering see Scheme 3.2.4). A characteristic quartet at δ = 118.56 ppm with a coupling constant of $J_{C\text{-}F}$ = 320.7 Hz in the corresponding ^{13}C NMR spectrum (Figure 3.2.4c) indicates the presence of trifluoromethyl group.

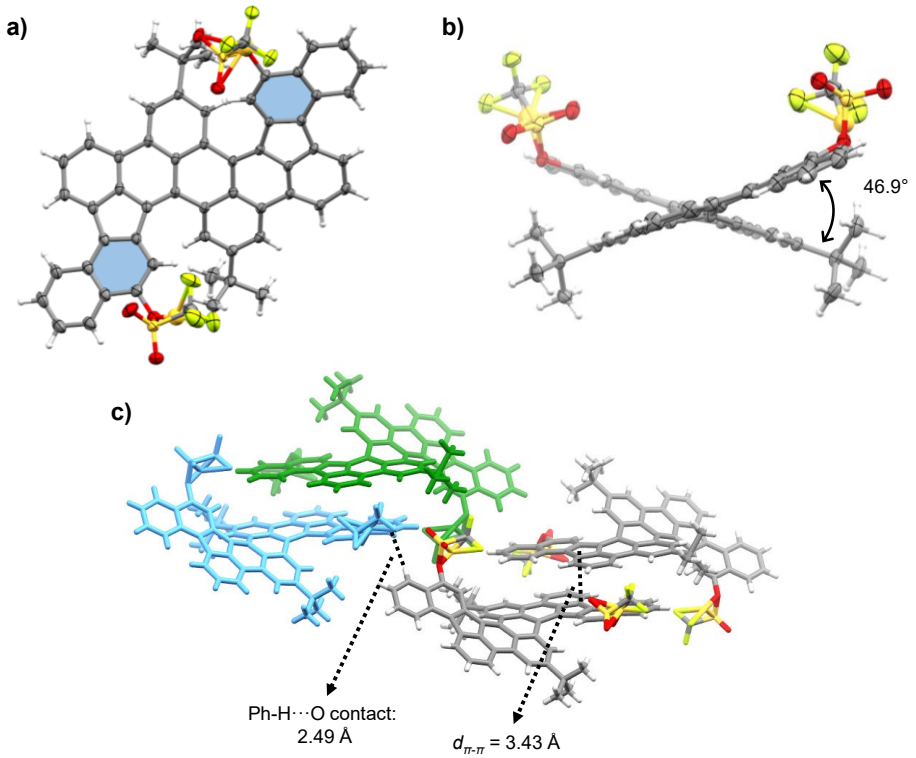

Figure 3.2.5 Front view (a) and side view (b) of single crystal X-ray structure of bistriflate **184**. (c) Packing motif of bistriflate **184**. Highlighted are the two enantiomers in different colors. (*M*,*M*): green and (*P*,*P*): light-blue. ORTEP plots in a and b are at the 50% probability. Enclathrated solvent molecules are omitted for clarity. Colors for heteroatoms: red = oxygen, yellow = sulfur, green = fluorine.

Diffusing methanol vapor into a solution of the bistriflate **184** in $CHCl_3$ gave high quality single crystals of **184**, which allows to clearly define its molecular structure by single crystal X-ray diffraction analysis (Figure 3.2.5). As indicated by the single crystal structure, the two-fold triflyoxylation occurs regioselectively at position 10. Bistriflate **184** crystallizes in the triclinic space group $P\ \bar{1}$. Similar to PAH **179** (Figure 3.2.2), a twisted π-backbone was observed in bistriflate **184** and the angle between the two blue-marked benzene rings (Figure 3.2.5a) is 46.9°, which is slightly smaller than that of PAH **179** (47.8°). Parallel arrangement between two adjacent benzo[*j*]fluoranthene moieties was also observed in bistriflate **184**. The average distance of $d_{\pi\text{-}\pi}$ = 3.43 Å is shorter than that of PAH **179** (3.56 Å). It should be noted that bistriflate **184** crystallizes as a mixture of two racemic (*M*,*M*)- and (*P*,*P*)-enantiomers with a ratio of 1:1 in each unit cell due to the conformational contortion.

3.2.2.3 Further Extension based on Bistriflate 184

Aryl triflates (trifluoromethanesulfonates) as pseudo-halides represent efficient partners for various cross-coupling reactions with organoboron reagents.[162a, 177] In order to demonstrate the synthetic value of the obtained bistriflate, **184** was used in Suzuki-Miyaura cross-coupling reactions with 4-*tert*-butylphenylboronic acid or 4-anisyl boronic acid, giving the corresponding two-fold cross-coupling products **185** or **186** in isolated yield of 65% or 72%, respectively (Scheme 3.2.5). Suzuki-Miyaura cross-coupling reaction based on bistriflate **184** was also performed with dihexyloxynaphthalene monoboronic ester **187**. The products **189** was isolated in 43% yield, as a mixture of atropisomers due to the rotation of the formed C-C bonds.

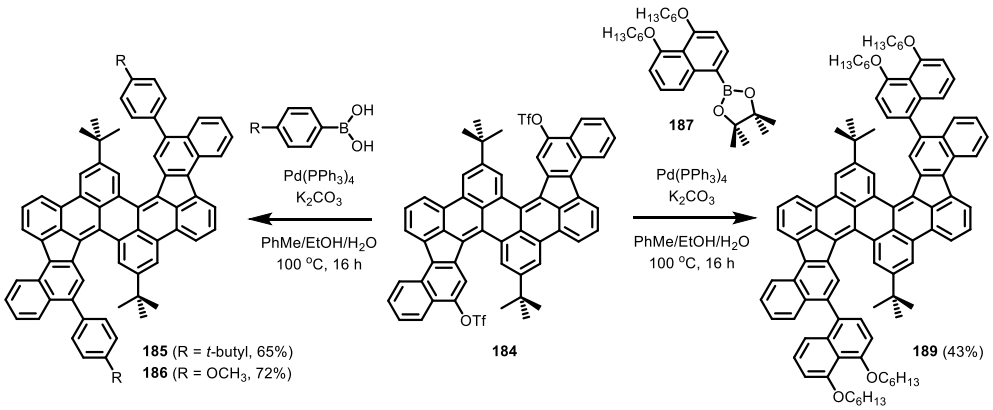

Scheme 3.2.5 Suzuki-Miyaura cross-copupling reactions based on bistriflate **184**.

PAHs **189** serve as a precursor for subsequent Scholl-type reactions. Treating **189** with 6 equiv. of $FeCl_3$ in CH_2Cl_2/CH_3NO_2 gave double cyclized product **191** as a dark-red solid in 93% yield. MALDI HRMS (Figure 3.2.6c) with a monoisotopic signal of m/*z* = 1361.7341 (calcd. for $[M]^+$, $C_{100}H_{96}O_4$, 1361.7342) as well as a fitting isotopic distribution pattern to the calculated one suggests that the product is two-fold cyclized.

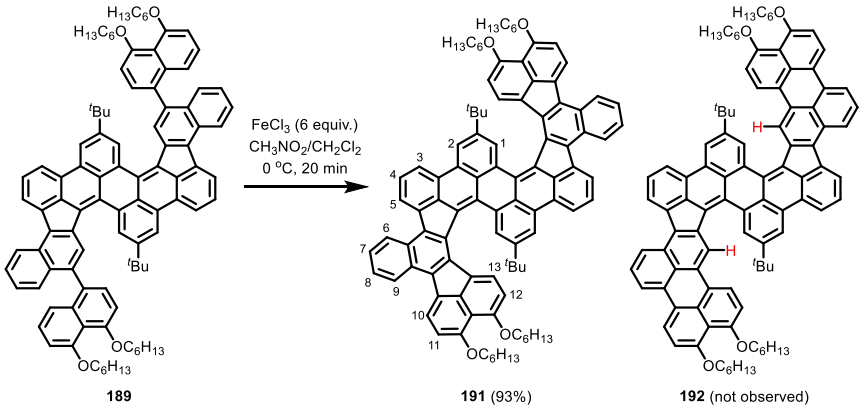

Scheme 3.2.6 Scholl cyclization of PAH **189**.

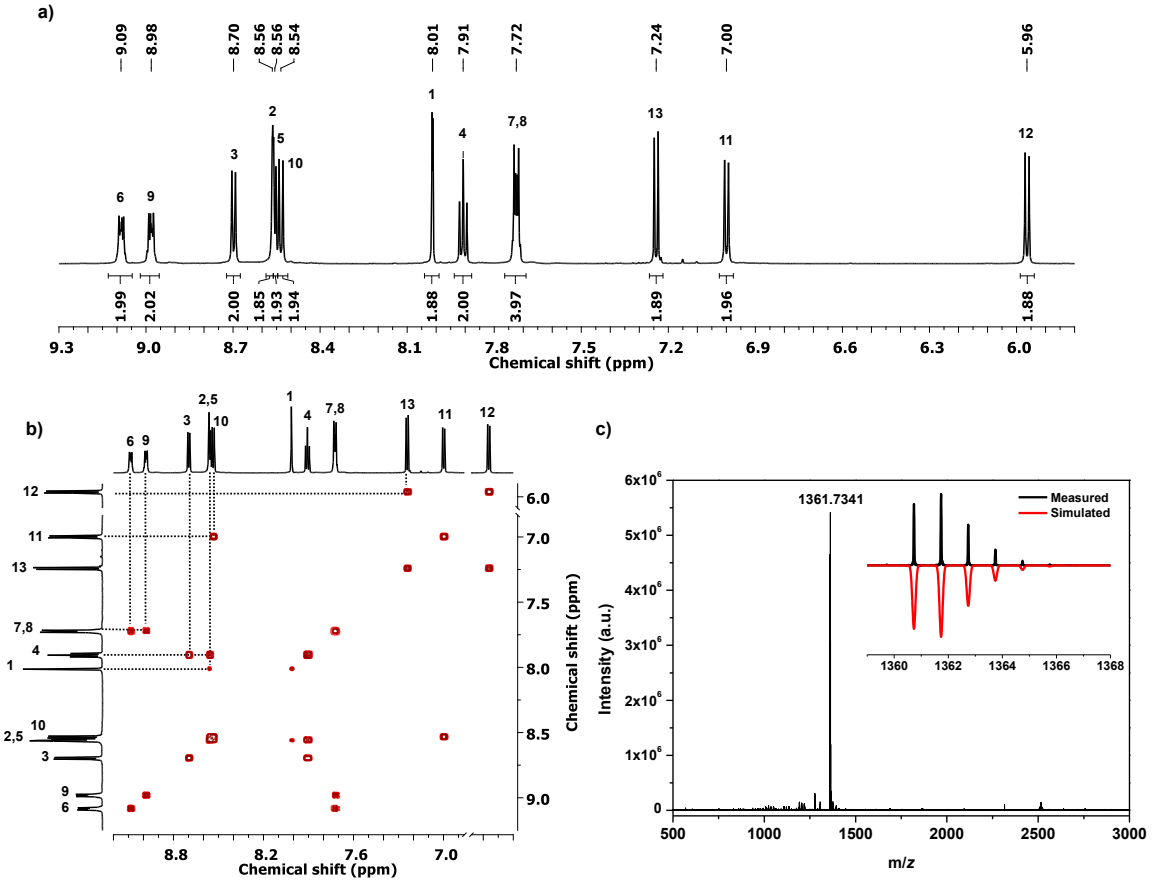

Figure 3.2.6 a) ^{1}H NMR spectrum of PAH **191** (600 MHz, CD_2Cl_2, 298 K). Depicted is only the aromatic region. Peak assignments are according to the numbering of molecular structure in Scheme 3.2.6. b) ^{1}H-^{1}H COSY NMR spectrum of PAH **191** (600 MHz, CD_2Cl_2, 298 K). c) MALDI HRMS (DCTB, linear positive mode) of PAH **191**.

By analyzing the 1D and 2D NMR spectra (Figure 3.2.6), the product does not form two new perylene moieties as depicted in structure **192** in Scheme 3.2.6. There is no singlet in the aromatic region of the ^{1}H NMR spectrum (Figure 3.2.6a). If it would have been the product with the six-membered rings, a singlet for the red-marked protons on the perylene moieties would be expected (Scheme 3.2.6). Thus the proposed formation of five-membered rings (structure **192**) is

preferred. This assumption is supported by the 2D ^{1}H-^{1}H COSY NMR spectrum (Figure 3.2.6b). Protons 1-2, 3-5, 6-9, 10-11 and 12-13 should be located on the same benzene ring, respectively.

As shown in the ^{1}H NMR spectrum of PAH **192** (Figure 3.2.6a), one highly upfield-shifted doublet was observed at δ = 5.96 ppm with a coupling constant of J = 8.2 Hz, which could be assigned to proton 12 or 13. As single crystals of PAH **192** suitable for X-ray diffraction analysis have not been obtained, geometry optimization and calculations of chemical shifts for protons were performed by DFT methods at the B3LYP/6-31+G* level in order to solve this problem (Figure 3.2.7). According the DFT optimized model, the helical arrangement of the π-plane is responsible for finding H-12 in the anisotropy cone of the *tert*-butyl attached benzene rings (ring a in Figure 3.2.7). In comparison to H-12, the position of H-13 is less favored for the anisotropic effect. This is in accordance with the calculated ^{1}H NMR shifts (Figure 3.2.7b). The predicted NMR shift for H-12 (5.47 ppm) is significantly lower than that for H-13 (7.43 ppm). Therefore, the upfield-shifted doublet at 5.96 ppm in the ^{1}H NMR spectrum of PAH **192** could be assigned to H-12.

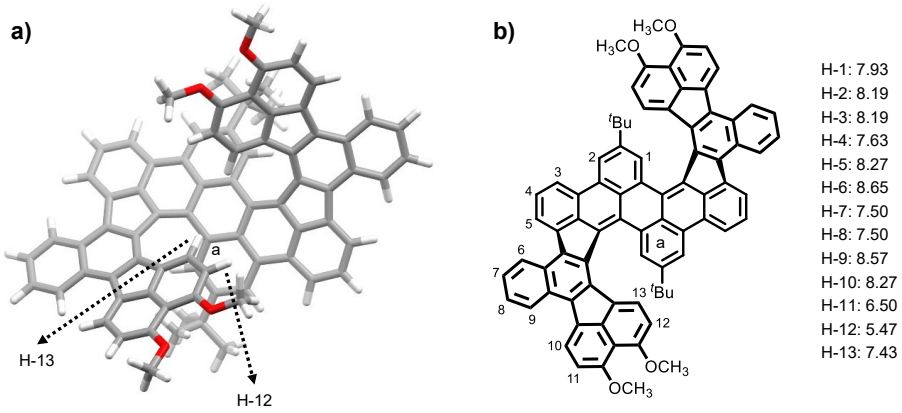

Figure 3.2.7 a) Optimized molecular model of PAH **191**. b) Numbering of protons on the π-framework of PAH **191** and the calculated ^{1}H NMR shifts. The calculations are based on DFT at the B3LYP/6-31+G* level with the GIAO method. The solvent chloroform was simulated using the polarized continuum model (PCM). The hexyloxy chains were replaced by methoxy groups for simplification. The NMR shifts are given in ppm relative to tetramethylsilane in chloroform.

As discussed in chapter 3.2.2.2, bistriflate **184** is a mixture of two racemic (*M*,*M*)- and (*P*,*P*)-enantiomers in the crystalline state. As a derivative of molecule **184**, PAH **191** was supposed to exhibit similar chirality as **184**. Only one set of peaks was observed in the ^{1}H NMR spectrum of **191**, which indicates **191** must be either nonracemic as (*M*,*P*)-helicene or racemic in a mixture of (*M*,*M*)/(*P*,*P*)-helicenes. Analytic HPLC equipped with a chiral AD-H column using an eluent of *n*-hexane:isopropanol (v/v = 95/5) at room temperature was performed to analyze the chirality of PAH **191**. Two baseline separated peaks with a ratio of nearly 1:1 were observed in the chiral HPLC spectrum (Figure 3.2.8), which serves as one evidence for the assumption that PAH **191** is a mixture of two racemic enantiomers in *n*-hexane solution at room temperature.

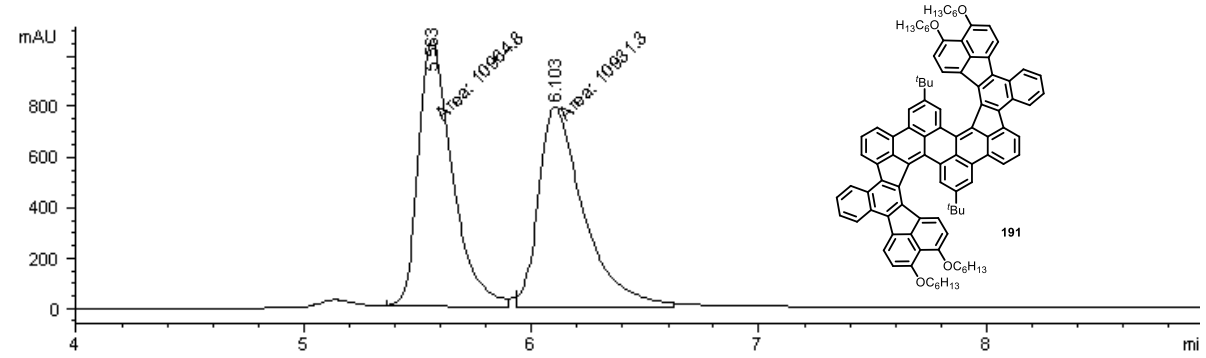

Figure 3.2.8 Analytical chiral HPLC chromatogram of PAH **191**. The chromatogram was obtained at room temperature using an analytical column packed with amylose tris(3,5-dimethylphenylcarbamate) (AD-H) coated on 5 µm silica gel with an eluent of *n*-hexane:isopropanol (95:5) at a flow rate of 0.7 mL/min.

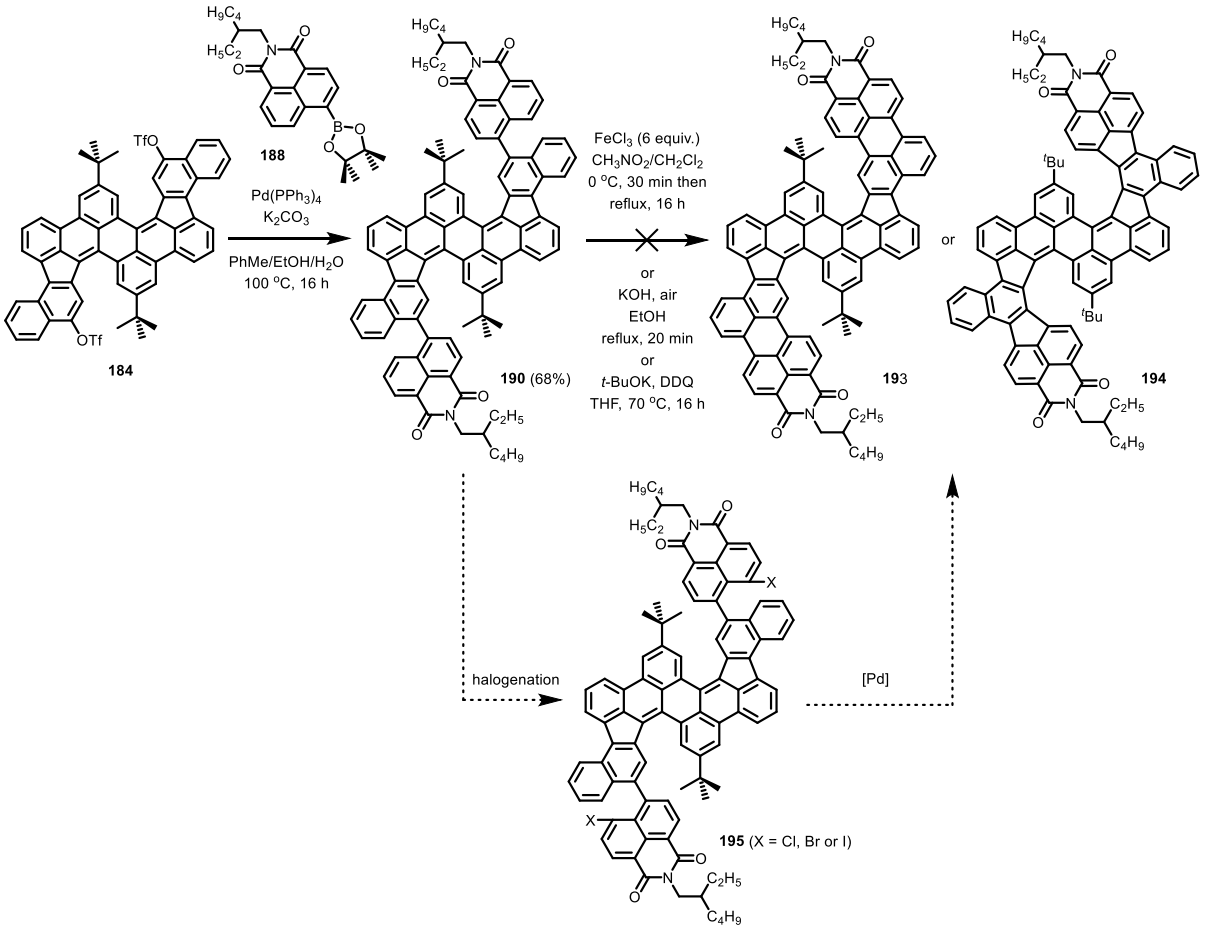

Scheme 3.2.7 Synthesis and cyclization of PAH **190**.

Suzuki-Miyaura cross-coupling reaction of bistriflate **184** with naphthalene monoimide-based monoboronic ester **188** gave the two-fold product **190** in 68% yield. PAH **193** with two newly formed perylene moieties or PAH **194** with four pentagonal rings could be formed by doubly cyclizing naphthalene monoimide substituted PAH **190**. However, attempts to cyclize PAH **190** by oxidative cyclodehydrogenation failed (Scheme 3.2.7). Treating **190** with 6 equiv. of $FeCl_3$ in CH_2Cl_2/CH_3NO_2 converted all the substrate to something undefined with $R_f = 0$ on the TLC plate using pure $CHCl_3$ as eluent. No conversion was observed when treating PAH **190** in a KOH melt

under ambient conditions.[178] Other reaction conditions have not been investigated deeply to cyclize this compound up to now. One possible route to make the cyclization is to functionalize the monoimide substituted naphthalene units by halogenation, followed by performing the ring-closing step by palladium-catalyzed intramolecular C-H arylation in the presence of a base.[83a, 179]

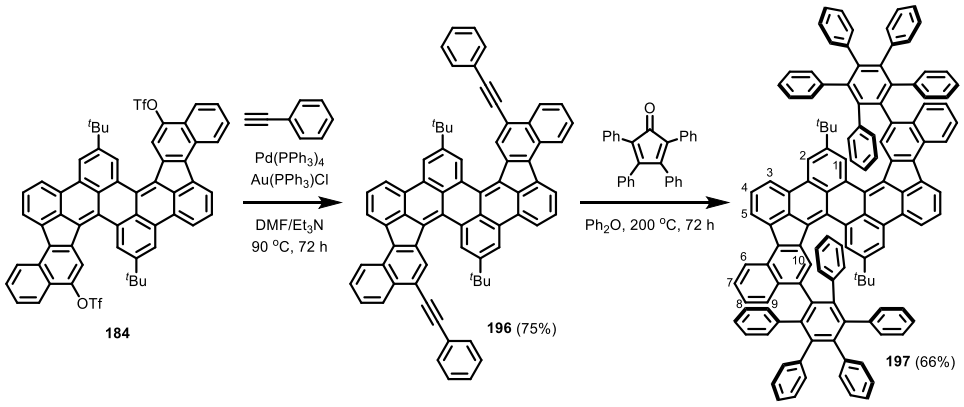

Scheme 3.2.8 Synthesis of PAH **197**.

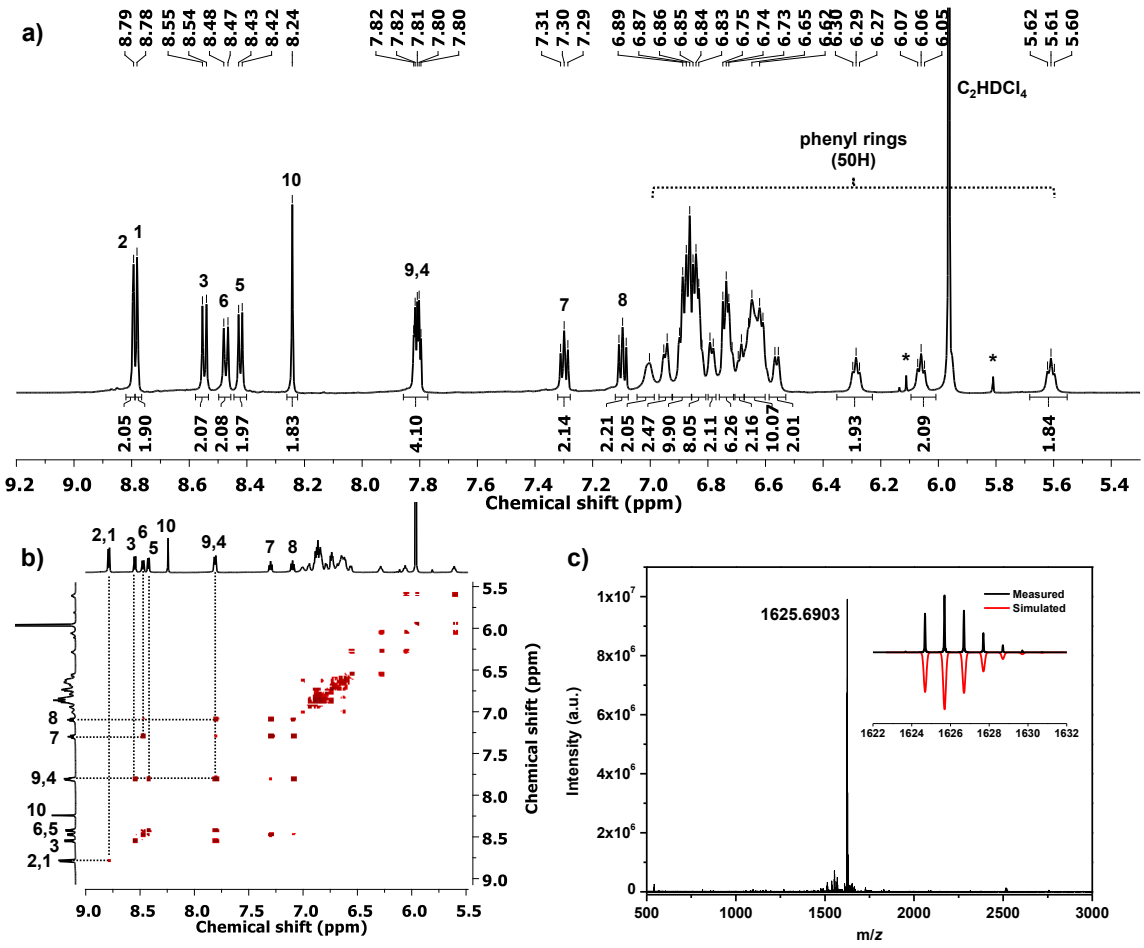

Figure 3.2.9 a) ^{1}H NMR spectrum of PAH **197** (600 MHz, $Cl_2CDCDCl_2$, 298 K). Depicted is only the aromatic region. Peak assignments are according to the numbering of molecular structure in Scheme 3.2.8. *Satellite peaks of $Cl_2CHCHCl_2$ solvent peak. b) ^{1}H-^{1}H COSY NMR spectrum of PAH **197** (600 MHz, $Cl_2CDCDCl_2$, 298 K). c) MALDI HRMS (DCTB, linear positive mode) of PAH **197**.

Palladium-catalyzed Sonogashira-Hagihara cross-coupling reaction with phenylacetylene was also performed based on bistriflate **184**, which gives bis(phenylethynyl)-substituted product **196** in 75% yield in the presence of a double-catalyst system (Pd^0/Au^I) (Scheme 3.2.8).[180] The obtained intermediate **196** was further reacted with tetraphenylcyclopentadienone in a Diels-Alder reaction followed by CO-extrusion, to give Diels-Alder product **197** in 66% yield.[30b, 181] MALDI HRMS (Figure 3.2.9b) with a monoisotopic signal of m/*z* = 1625.6903 (calcd. for $[M]^+$, $C_{128}H_{88}$, 1625.6919) and a fitting isotopic distribution pattern to the simulated one serve as evidences for the formation of the Diels-Alder product. A well-resolved ^1H NMR spectrum of PAH **197** was obtained in $Cl_2CDCDCl_2$ at room temperature (Figure 3.2.9a). Assisted by the information of ^1H-^1H correlation given by 2D COSY spectroscopy (Figure 3.2.9b), H-1 to H-10 on the π-framework of the dibenzoperylene could be assigned properly. The signals ranging from 6.89 ppm to 5.60 ppm with a total integral of 50 could be assigned to the protons of the ten phenyl groups.

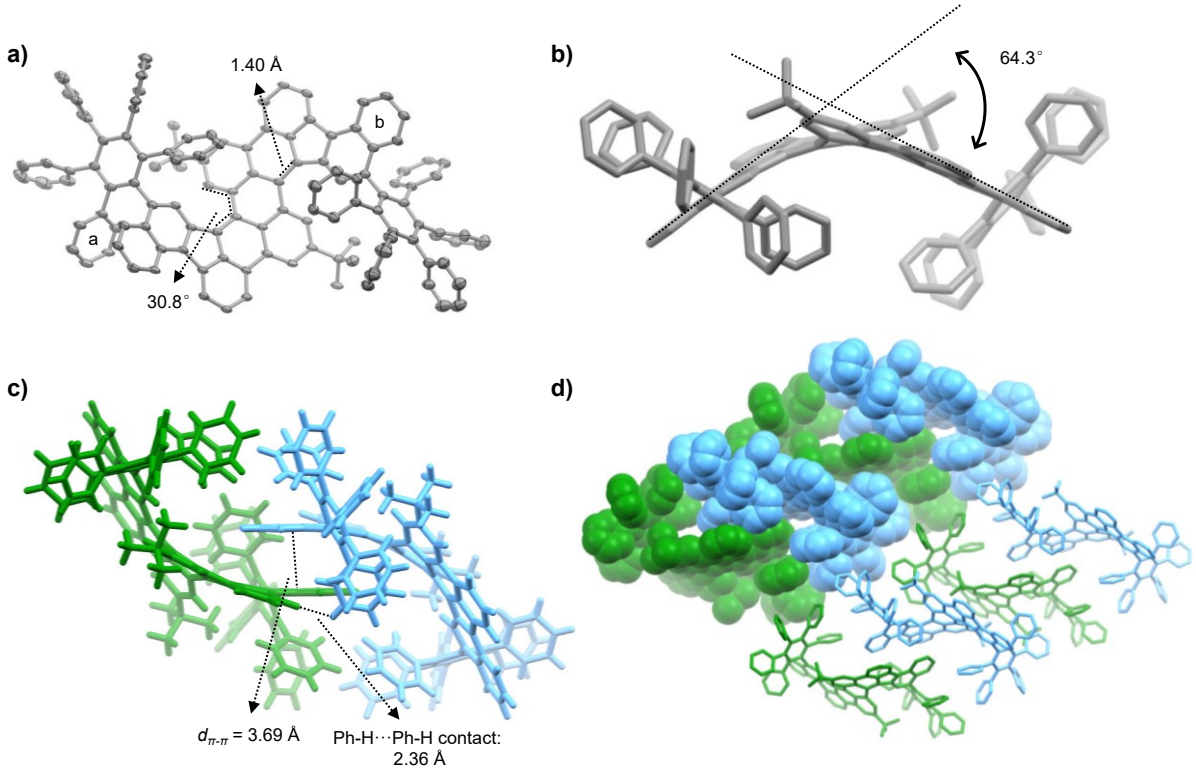

Figure 3.2.10 X-ray crystal structure of PAH **197**. a) and b) Structure of (*P*,*P*)-enatiomer from two different perspectives. c) A close view of a dimer of two enantiomers. d) Packing motif. The two enantiomers are highlighted in different colors. (*M*,*M*): green and (*P*,*P*): blue. Hydrogen atoms as well as enclathrated solvent molecules have been omitted for clarity. The view in (a) is an ORTEP plot with thermal ellipsoids set at 30% probability.

Single crystals of PAH **197** suitable for X-ray diffraction analysis were obtained by diffusing methanol vapor into a solution of **197** in $CHCl_3$ (Figure 3.2.10). PAH **197** crystallizes in the triclinic space group $P\bar{1}$. Similar to those of the two benzene rings fused compound **179** (Figure 3.2.2) and bistriflate **184** (Figure 3.2.5), the central dibenzoperylene moiety of PAH **197** exhibits a twisted π-backbone. When the two peripheral benzene rings a and b (Figure 3.2.10a) were

considered, the angle between the two planes where both rings are located is 64.3° (Figure 3.2.10b). Due to the conformational contortion, the C-C bonds at the [*a*] and [*k*] edges of the dibenzoperylene π-framework exhibit bond lengths of 1.40 Å in both cases, which are longer than the C-C bonds at the same positions of dibenzoperylene **111** (1.36 Å),[128b] benzene-fused compound **179** (1.38 Å) and bistriflate **184** (1.38 Å). PAH **197** owns a chiral C_2-symmetry with two helical twists and a racemic mixture of the (*M*,*M*)- and (*P*,*P*)-enantiomers with a ratio of 1:1 was observed in each unit cell. Parallel arrangement could be found between two adjacent benzo[*j*]fluoranthene moieties with an average distance of $d_{\pi\text{-}\pi}$ = 3.69 Å (Figure 3.2.10c). This result suggests that the contortion motif of cyclopentannulated bistriflate **184** remains after the following two step reactions to PAH **197**. There was no interconversion from (*M*,*M*)/(*P*,*P*)-helicenes to (*M*,*P*)-helicene, even during the Diels-Alder reaction at 200 °C.

3.2.2.4 Spectroscopic and Electrochemical Properties

Both the substituted dibenzoperylene substrates and the cyclopentannluated products were characterized by UV/Vis and fluorescence spectroscopy (Figure 3.2.11) as well as cyclic voltammetry. Frontier molecular orbitals (FMOs) were calculated by DFT at the B3LYP/6-311G* level of theory and the results are summarized in Table 3.2.1.

As shown in Figure 3.2.11a, both substrates **143** and **180** give very similar absorption spectra with maximum absorption peaks at 432 and 433 nm, respectively, for the π-π* transitions (*p*-band), both of which are similar to that of dibenzoperylene **111** (λ = 434 nm).[128b] This result suggests that the substituents of phenyl or naphthyl groups do not have a significant influence on the optical properties of the dibenzoperylene derivatives. Double cyclopentannulated PAHs **178** and **181** show remarkable bathochromic shifts for this absorption (Figure 3.2.11b), in comparison to the corresponding uncyclized precursors **143** and **180**. Dibenzo-PAH **178** exhibits a maximum absorption peak at λ = 499 nm, while this absorption for naphthalene extended PAH **181** is further red-shifted to λ = 518 nm with an increased extinction coefficient of $\varepsilon = 7.0 \times 10^4$ $M^{-1}\cdot cm^{-1}$. Bathochromic shifts were also observed in the corresponding fluorescent emission spectra of both five-membered ring-containing PAHs compared with the uncyclized precursors. Substrates **143** and **180** show emission maxima at λ = 472 nm and 481 nm, respectively, with fluorescence quantum yields of Φ = 51%-54%, which are lower than that of dibenzoperylene **111** (Φ = 68%).[128b] Dibenzo PAH **178** shows an emission maximum of λ = 525 nm with a bathochromic shift of 53 nm and increased quantum yield of Φ = 67% in comparison to precursor **143**. The emission maximum for the naphthalene extended PAH **181** is further red-shifted to λ = 547 nm while the corresponding quantum yield is significantly decreased to Φ = 3.9%. As estimated by cyclic voltammetry, cyclopentannulation decreases the electron affinities by 0.6-0.7 eV and ionization potentials by

0.2 eV for these four PAHs. Thus the electrochemical band gaps are lowered by 0.4-0.5 eV, which are in accordance with the measured optical band gaps and DFT calculated HOMO-LUMO gaps.

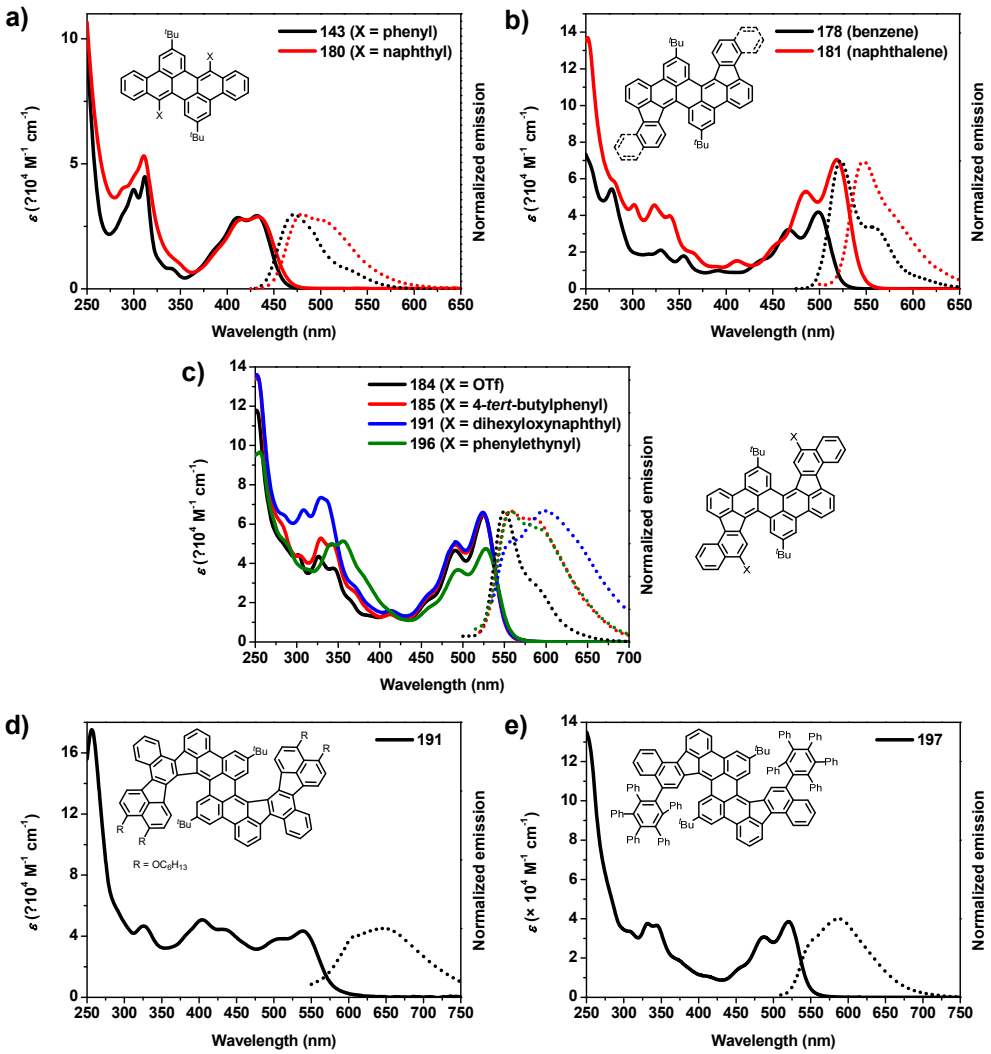

Figure 3.2.11 Absorption (solid line) and normalized emission (dot line) spectra of uncyclized precursors **143** and **180** (a), cyclopentannulated PAHs (b-e) and measured in $CHCl_3$ (molar concentration = 8-19 µM) at room temperature.

Substitutions with electron withdrawing groups (triflyloxy groups) or aromatic moieties (substituted phenyls, dihexyloxynaphthyls or phenylethynyls) at 12,24-positions of PAH **181** causes slightly a bathochromic shift (6-10 nm) in the absorption maximum for *p*-band. Fluorescence emission maxima at λ = 551-561 nm with low quantum yields of Φ = 3%-13% were observed in these substituted PAHs. Double helical PAH **191** containing four pentagonal rings shows a broad absorption band from λ = 360 nm to λ = 470 nm and a *p*-band absorption maximum at λ = 539 nm along with an optical band gap of 2.1 eV, which also exhibits the most bathochromic emission peak at λ = 646 nm among this series of PAHs with a moderate quantum yield of 25%. The broad absorption band from λ = 360 nm to λ = 470 nm for PAH **191** is supported by the time dependent DFT (TDDFT) predicted UV/Vis spectrum (Figure 3.2.12). Two relatively strong absorption

oscillators were observed in the TDDFT predicted UV/Vis absorption spectrum at 396 nm and 471 nm, which could be assigned to the transitions of HOMO-4 to LUMO+2, HOMO-6 to LUMO and HOMO-1 to LUMO+1. The low electrochemical bandgap of E_g = 2.0 eV for PAH **191** estimated by electrochemistry is consistent with its small optical bandgap (E_g = 2.1 eV).

Table 3.2.1 Summary of the photophysical and electrochemical characterization of precursors **143**, **180** and cyclopentannulated PAHs.

Compd	$\lambda_{max}^{p\text{-}band}$ [nm][a]	E_g^{opt} [eV][a,b]	λ_{em} (λ_{ex}) [nm][a]	$\tilde{\nu}$ [cm^{-1}][c]	Φ [%][a,d]	IP^{CV} [eV][e]	EA^{CV} [eV][f]	E_g^{CV} [eV]	E_{HOMO} [eV][g]	E_{LUMO} [eV][g]
143	432	2.7	472, 524 (412)	1962	53.9±0.7	-5.1	-2.4	2.7	-5.1	-2.0
178	499	2.4	525, 552 (467)	992	67.0±1.9	-5.3	-3.0	2.3	-5.3	-2.6
180	433	2.7	481, 504 (417)	2305	51.4±0.4	-5.1	-2.4	2.7	-5.2	-2.0
181	518	2.3	547 (485)	1023	3.9±0.1	-5.3	-3.1	2.2	-5.3	-2.7
184	525	2.2	551, 585 (491)	899	8.3±0.4	-5.2	-3.1	2.1	-5.5	-2.9
185	524	2.3	558, 585 (491)	1163	5.5±0.6	-5.4	-3.2	2.2	-5.3	-2.6
189	524	2.2	561, 598 (491)	2362	13.4±0.1	-5.2	-3.0	2.2	-5.3	-2.7
191	539	2.1	608, 646 (510)	3073	24.7±1.0	-5.2	-3.2	2.0	-5.3	-2.7
196	528	2.2	557, 589 (494)	986	3.3±0.1	-5.4	-3.2	2.2	-5.3	-2.8
197	520	2.3	557, 587 (487)	2195	3.6±0.5	-5.4	-3.1	2.3	-5.2	-2.6

[a] Measured in $CHCl_3$ at room temperature. [b] Estimated from absorption onset. [c] Stock's shift. [d] Fluorescence quantum yield. [e] Ionization potential. [f] Electron affinity. IPs and EAs were estimated by cyclic voltammetry in 0.1 M *n*-Bu_4NClO_4 in CH_2Cl_2 or *o*-DCB at room temperature. The scan speed was 100 mV·s^{-1} and ferrocene/ferrocenium (Fc/Fc^+) was used as internal reference. IP^{CV} = -(E_{onset}^{ox} + 4.8 eV). EA^{CV} = -(E_{onset}^{red} + 4.8 eV). [g] Calculated by DFT using Spartan 14 at the B3LYP/6-311G* level.

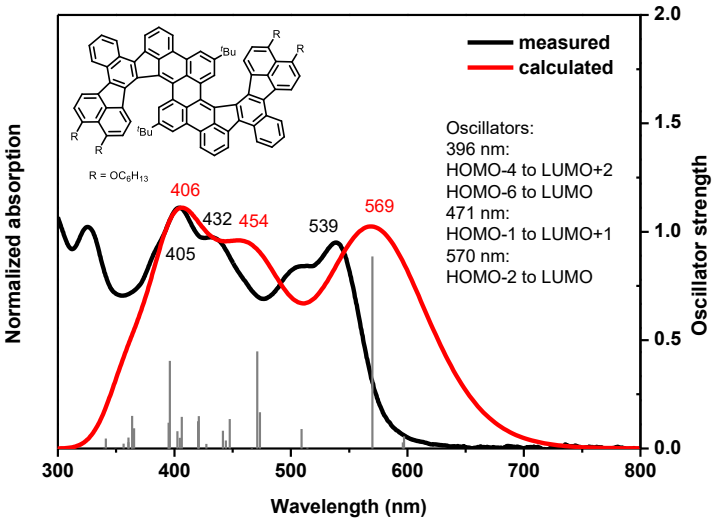

Figure 3.2.12 Comparison of UV/Vis absorption spectrum measured in $CHCl_3$ (black) and calculated UV/Vis absorption spectrum (red) based on TDDFT at the B3LYP/6-311G** (PCM-$CHCl_3$) level of PAH **191**. Peak positions are given in nm. The hexyloxy chains were replaced by methoxy groups during the calculation.

3.2.3 Contorted PAHs with two Embedded Azulene Units

3.2.3.1 Scholl Cyclization of Dinaphthyl Dibenzoperylene 198

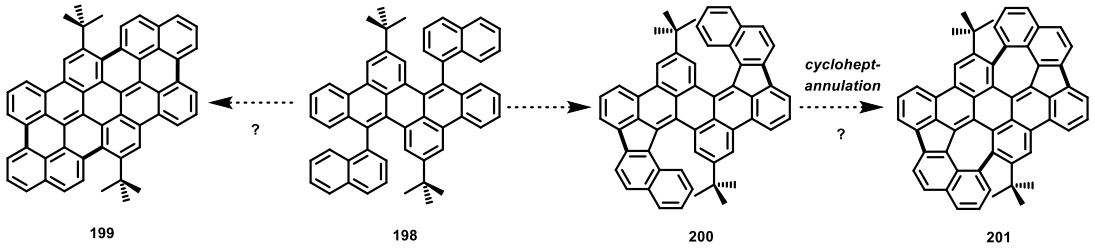

Scheme 3.2.9 Possible products of the cyclodehydrogenation of dinaphthyl dibenzoperylene **198**. Newly formed C-C bonds are highlighted in bold.

As presented in Chapter 3.2.2, Scholl-type oxidations of diphenyl dibenzoperylene **143** and dinaphthyl dibenzoperylene **180** in the presence of $FeCl_3/CH_3NO_2$ or DDQ/TfOH in CH_2Cl_2 gave the cyclopentannulated products **178** and **181**, respectively. Following this idea, PAH **198** (Scheme 3.2.9) was designed, which serves as a constitutional isomer of dinaphthyl dibenzoperylene **180**. Cyclodehydrogenation of compound **198** could hypothetically give PAH **199** by the formation of four new C-C bonds as well as four new hexagonal rings. It is also possible that two five-membered rings as well as two additional seven-membered rings would be generated in the structure of PAH **201** during the cyclodehydrogenation.

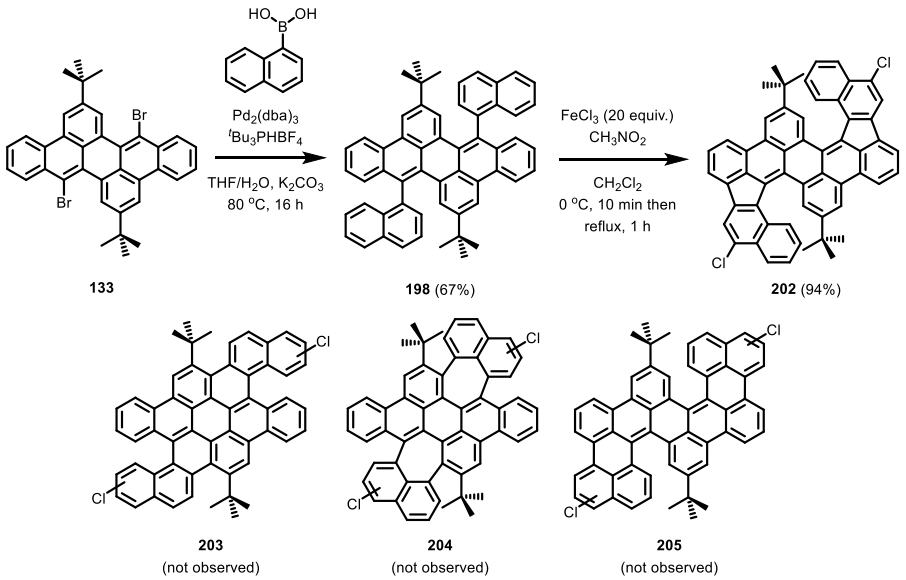

Scheme 3.2.10 Synthesis of naphthyl-substituted dibenzoperylene **198** and oxidative cyclodehydrogenation of **198** in the presence of $FeCl_3/CH_3NO_2$.

Based on dibromide **133**, dinaphthyl dibenzoperylene **198** was obtained by Suzuki-Miyaura cross-coupling reaction with 1-naphthylboronic acid under Fu conditions[163] in 67% yield (Scheme 3.2.10). Oxidative cyclodehydrogenation of PAH **198** was first performed in the presence of $FeCl_3/CH_3NO_2$ in CH_2Cl_2. After treating PAH **198** with 20 equiv. of $FeCl_3$ in a mixture of

CH_3NO_2/CH_2Cl_2 under refluxing conditions for one hour, the substrate was fully consumed and the product was collected as a dark purple solid in 94% yield. MALDI-TOF MS (Figure 3.2.13c) giving a monoisotopic signal of m/*z* = 780.285 (calcd. for $[M]^+$, $C_{56}H_{38}Cl_2$, 780.235) and a fitting isotopic distribution pattern to the calculated one suggests that a two-fold chlorination occurs in addition to the formation of two new C-C bonds in the obtained product.

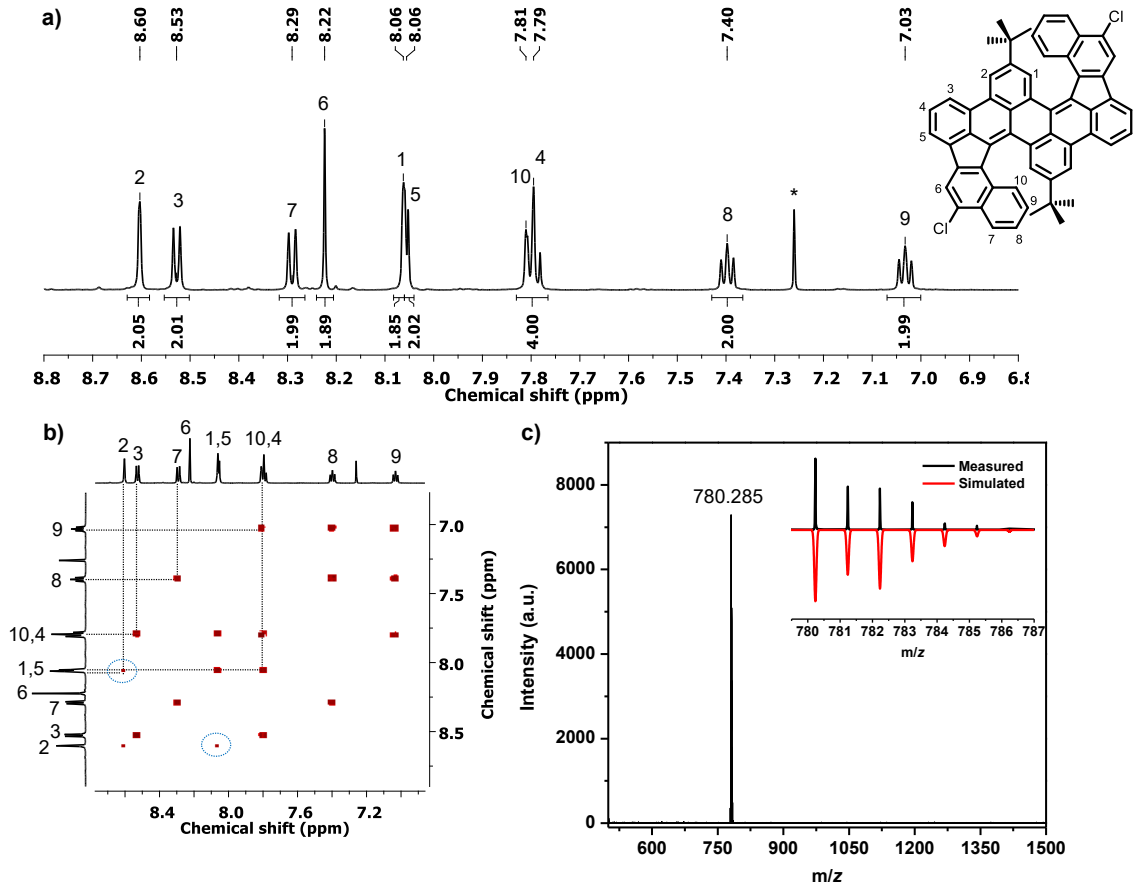

Figure 3.2.13 a) ^{1}H NMR spectrum of dichloride **202** (600 MHz, $Cl_2CDCDCl_2$, 298 K). Depicted is only the aromatic region. *Residual $CHCl_3$. b) ^{1}H-^{1}H COSY NMR spectrum of PAH **202** (600 MHz, $Cl_2CDCDCl_2$, 298 K). c) MALDI-TOF MS (DCTB, reflective positive mode) of PAH **202**.

More information about the molecular structure of the product could be obtained by NMR techniques. Nine signals with comparable integrals were observed in the aromatic region of the ^{1}H NMR spectrum of this dichloride (Figure 3.2.13a). The two singlets at 8.60 ppm and 8.06 ppm exhibit correlation in the corresponding 2D ^{1}H-^{1}H COSY NMR spectrum (marked in blue circles in Figure 3.2.13b), suggesting that both singlets should be doublet with small coupling constants (around 1.5 Hz). These two signals could be assigned to the two *ortho*-positions (H-1 and H-2) of the *tert*-butyl groups. Thus in determining the structure of the obtained product, structures of **203** and **204** (Scheme 3.2.10) could be excluded, in which the one of the two *ortho*-positions of the *tert*-butyl groups are blocked due to the formation of C-C bonds. The presence of the singlet at 8.22 ppm in the ^{1}H NMR spectrum, which shows no correlation with other signals in the aromatic region,

could help to exclude the possibility of structure **205** (Scheme 3.2.10), in which no singlet is expected even after two-fold chlorination. If there was no rearrangement during the reaction, the only one possibility for structure of the product is PAH **202** (Scheme 3.2.10). By analyzing the ^{1}H-^{1}H COSY NMR spectrum, protons 3-5 and 7-10 should be on the same benzene ring, respectively, which are in accordance with structure **202**.

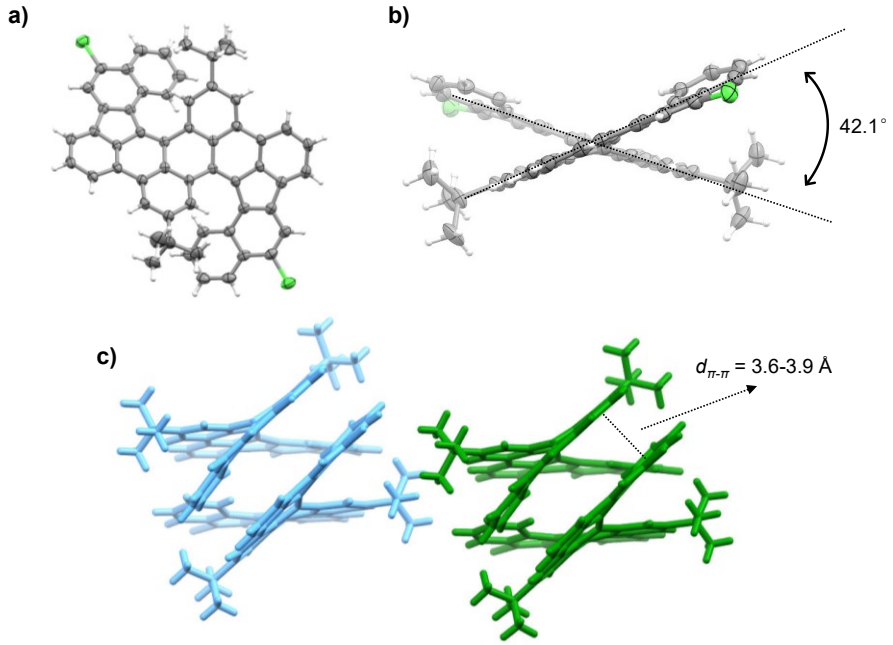

Figure 3.2.14 Single crystal X-ray structure of PAH **202**. a) and b) Structure of (*M*,*M*)-enantiomer from two different perspectives. c) Packing motif. The two enantiomers are highlighted in different colors. (*M*,*M*): blue and (*P*,*P*): green. Enclathrated solvent molecules have been omitted for clarity. ORTEP plots in a and b are at the 30% probability. Color for heteroatoms: green = chlorine.

One problem is the determination of the positions of the two chlorine atoms, which could also be possible to be placed at position 6 (Figure 3.2.13a). Crystal structure of PAH **202** as defined by X-ray diffraction analysis, which was obtained by analyzing the single crystals grown by diffusing methanol vapor into a solution of **202** in *o*-DCB, serves as a direct evidence for the molecular structure of this dichloride (Figure 3.2.14). The chlorination occurs in *para*-positions of the prior existing C-C biaryl bonds, which is in contrast to the positions of triflyloxylation observed for the dinaphthyl dibenzoperylene **180** discussed in chapter 3.2.2. PAH **202** crystallizes in the monoclinic space group *P*2/*c*. Similar to the pentagonal ring-containing PAHs in chapter 3.2.2, dichloride **202** adopts a twisted π-backbone. The angle between the two planes where the two chlorine atoms attached benzene rings are located is 42.1°. Furthermore, dichloride **202** crystallizes as a racemic mixture of two double helicene enantiomers (*M*,*M*) and (*P*,*P*), which is in accordance with the analytical chiral HPLC result (Figure 3.2.15). Each enantiomer forms a dimer where the aromatic helical units of adjacent molecules are arranged in a coplanar fashion by π stacking

($d_{\pi\text{-}\pi}$ = 3.6-3.9 Å). Limited by the relatively low resolution of the crystallographic data, accurate determination of bond lengths and angles are not possible.

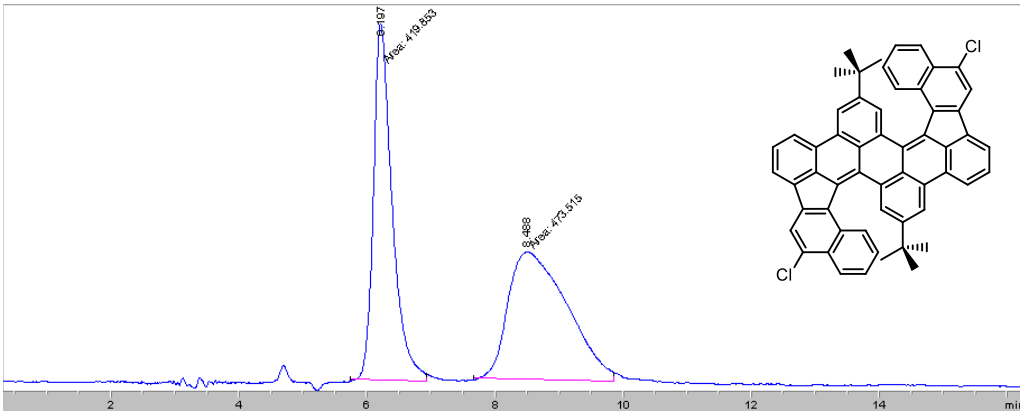

Figure 3.2.15 Analytical chiral HPLC chromatogram of PAH **202**. The chromatogram was obtained at room temperature using an analytical column packed with amylose tris(3,5-dimethylphenylcarbamate) (AD-H) coated on 5 µm silica gel with an eluent of *n*-hexane:isopropanol (99:1) at a flow rate of 0.7 mL/min.

Oxidative cyclodehydrogenation of PAH **198** in the presence of $FeCl_3/CH_3NO_2$ in CH_2Cl_2 gave two-fold cyclopentannulated dichlorinated PAH **202** in 94% yield. No conversion was observed when PAH **202** was treated again with $FeCl_3/CH_3NO_2$, indicating no additional C-C bonds were formed under these conditions. In order to test the possibility of further cycloheptannulation, where two new C-C bonds are formed between position 1 and 10 (Figure 3.2.13a), Scholl reaction based on PAH **198** was performed under Rathore conditions in the presence of DDQ/TfOH.

Treating PAH **198** with DDQ (8 equiv.) in a $TfOH/CH_2Cl_2$ mixture causes a full conversion of the substrate and three dark-blue spots were observed with R_f = 0.25-0.35 by performing the TLC analysis using an eluent of petroleum ether/chloroform/ethyl acetate (v/v/v = 30:2:1). This three species were isolated by silica gel column chromatography and characterized by NMR and MS techniques (Figure 3.2.16 and Figure 3.2.17). The ^{1}H NMR spectra of the first eluted (R_f = 0.35, PAH **208**) and the last eluted (R_f = 0.25, PAH **206**) fractions give nine (Figure 3.2.16c) and eight (Figure 3.2.16a) signals, respectively, with comparable integrals in the aromatic regions. One possibility is that the last eluted fraction (PAH **206**) could be one compound after four-fold cyclodehydrogenation as well as two-fold substitution at the periphery. The ^{13}C NMR spectrum of this fraction (R_f = 0.25) gives a quartet at δ = 118.89 ppm with a coupling constant of $J_{C\text{-}F}$ = 320.6 Hz (Figure 3.2.17c), which is a characteristic peak for the -CF_3 unit on triflyloxy group and quite similar to that of bistriflate **184** (Figure 3.2.4c). This suggests the presence of triflyloxy groups in PAH **206**. By analyzing the 2D ^{1}H-^{1}H COSY NMR spectrum of PAH **206** (Figure 3.2.17a), it was found that signals for H-1 and H-5 are two singlets without correlations with other protons in the aromatic region. Protons 2-4 and 6-8 should be on the same aromatic ring, respectively. One signal for the

correlation between H-8 and the *tert*-butyl group was observed in the ^{1}H-^{1}H ROESY NMR spectrum of PAH **206** (Figure 3.2.17b).

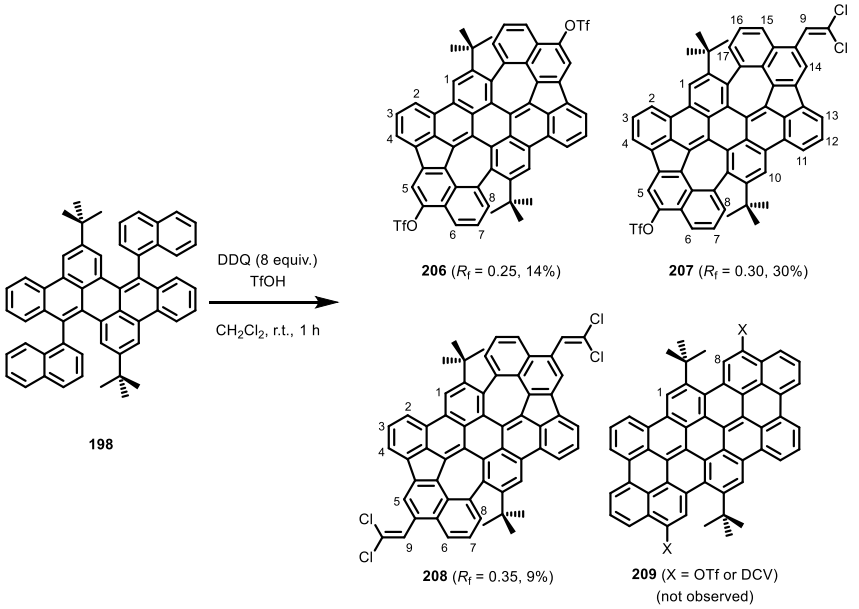

Scheme 3.2.11 Oxidative cyclodehydrogenation of **198** in the presence of DDQ/TfOH. DCV: dichlorovinylidene.

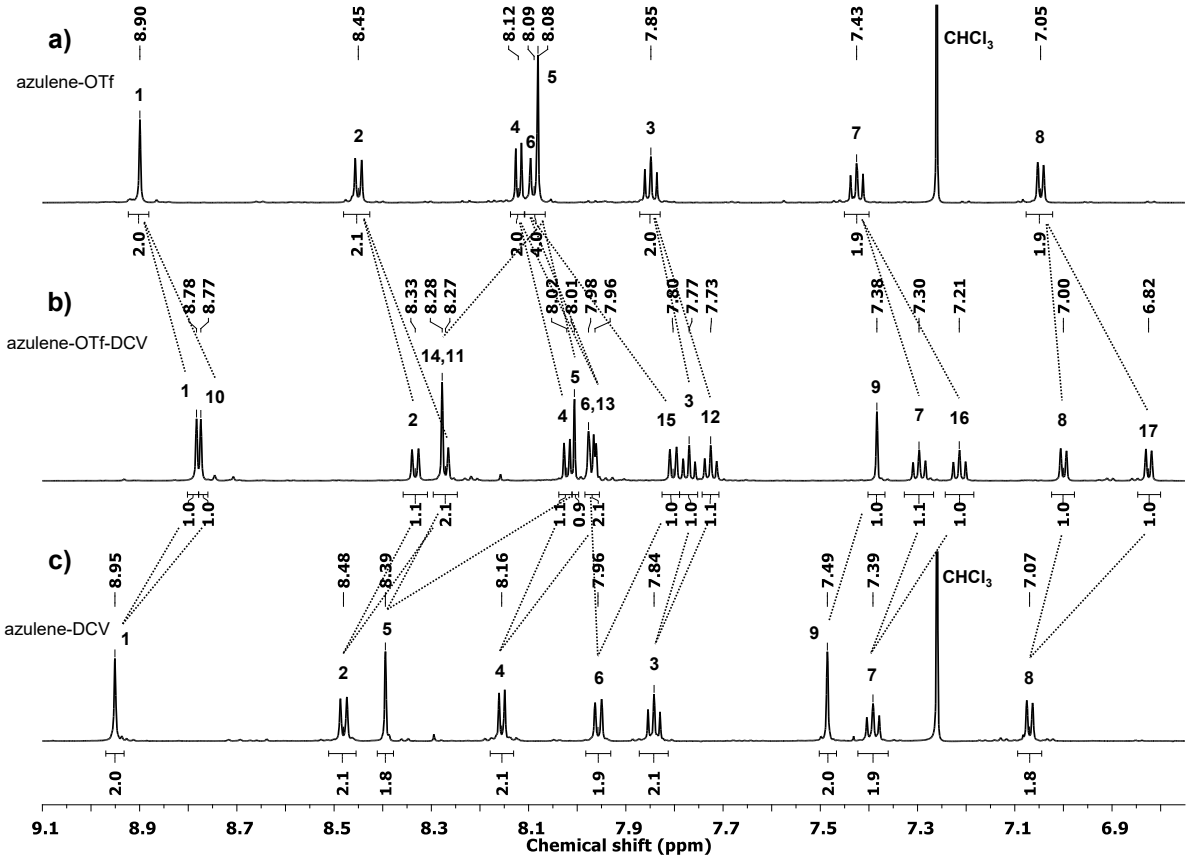

Figure 3.2.16 ^{1}H NMR spectra of PAHs **206** (600 MHz, $CDCl_3$, 298 K, a, azulene-OTf), **207** (600 MHz, CD_2Cl_2, 298 K, b, azulene-OTf-DCV) and **208** (600 MHz, $CDCl_3$, 298 K, c, azulene-DCV). Depicted are only the aromatic regions. Peak assignments are according to the numbering of molecular structure in Scheme 3.2.11.

Based on the information presented above, a π-framework with two embedded azulene units and two triflyloxy-group substitutions could be drawn as the structure of PAH **206** in Scheme 3.2.11. The isomeric structure of **209**, which would also own two protons as singlets (H-1 and H-8) in the ^{1}H NMR spectrum and the correlation of one aromatic proton (H-8) with the *tert*-butyl group, is not reasonable as the signal for H-8 is not a singlet in the experimentally measured ^{1}H NMR spectrum (Figure 3.2.16a).

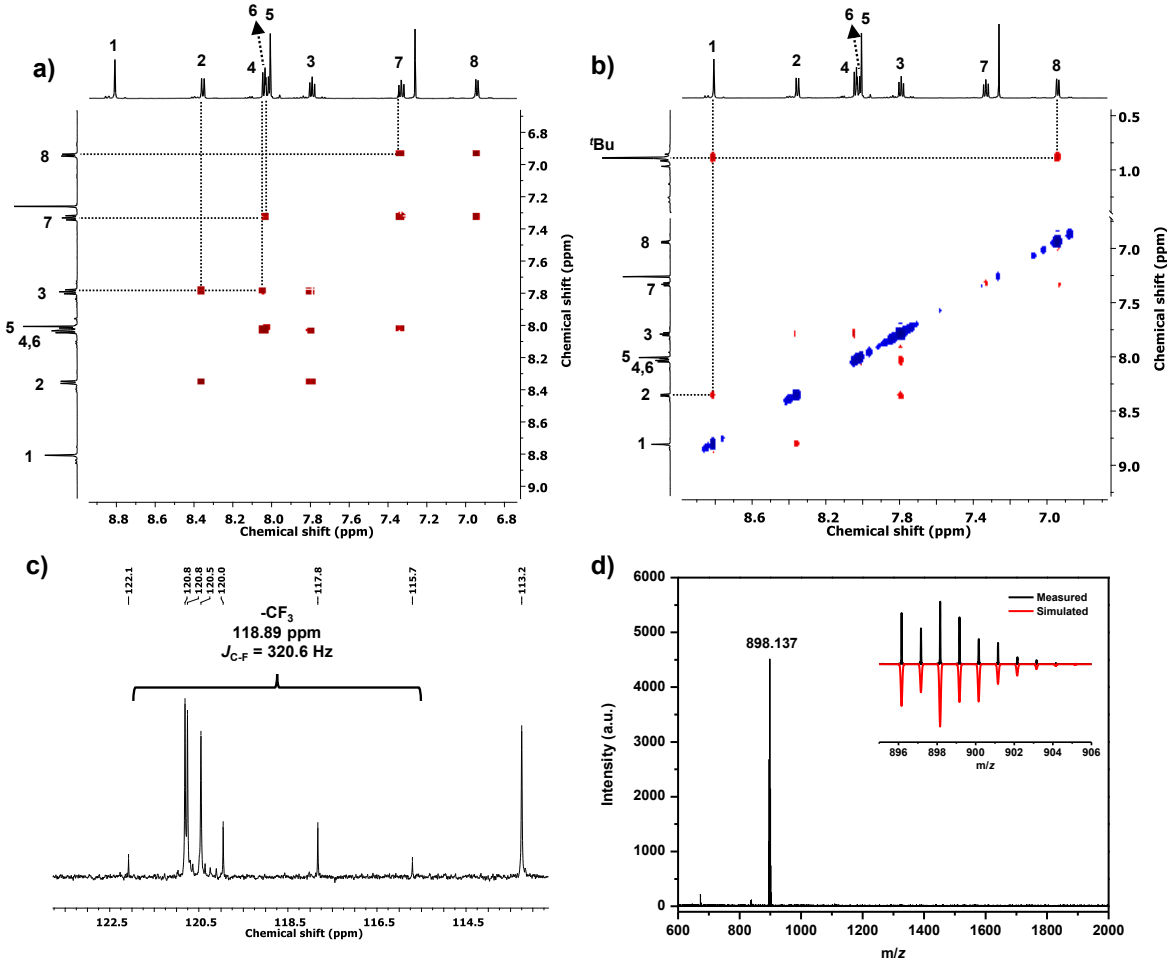

Figure 3.2.17 a) ^{1}H-^{1}H COSY NMR spectrum of PAH **206** (600 MHz, $CDCl_3$, 298 K). b) ^{1}H-^{1}H ROESY NMR spectrum of PAH **206** (600 MHz, $CDCl_3$, 298 K). Peak assignments are according to the numbering of molecular structure in Scheme 3.2.11. c) A zoom-in region of ^{13}C NMR spectrum of PAH **206** (600 MHz, $CDCl_3$, 298 K) showing the quartet of -CF_3 groups. d) MALDI-TOF spectrum (DCTB, reflective positive mode) of PAH **208**.

The ^{1}H NMR spectrum of the first eluted fraction (R_f = 0.35, PAH **208**) shows a very similar pattern (Figure 3.2.16c) with that of PAH **206**, except a relatively larger down-field shift of the singlet for H-5 (from 8.08 ppm for **206** to 8.39 ppm for **208**) than other signals and the presence of one additional singlet at 7.49 ppm. It is possible that this compound (PAH **208**) owns the same π-framework with PAH **206**. It is supposed that this double azulene-embedded π-framework is substituted with two dichlorovinylidene (DCV) units to give a structure of PAH **208** in Scheme 3.2.11. The proton on the DCV unit could account for the presence of the additional singlet at

7.49 ppm (for H-9). MALDI-TOF spectrum (Figure 3.2.17d) with a monoisotopic signal of m/*z* = 898.137 (calcd. for $[M]^+$, $C_{60}H_{36}Cl_4$, 898.155) and a fitting isotopic distribution pattern to the calculated one serves as one evidence for the attachment of two DCV units.

The ^{1}H NMR spectrum of the second eluted fraction (R_f = 0.30, PAH **207**) shows 17 signals with comparable integrals in the aromatic region, suggesting one possibility for substitutions at unsymmetric positions of the π-framework. Using the molecular structure of PAH **207** in Scheme 3.2.11, all signals in the ^{1}H NMR spectrum could be assigned properly.

With the preliminary determinations of molecular structures for these isolated products, the yield of each component could be calculated (Scheme 3.2.11). Treating **198** with 8 equiv. of DDQ in a mixture TfOH/CH_2Cl_2 with a substrate concentration of c = 1.67 mmol·L^{-1} could produce PAHs **206**, **207** and **208** in 14%, 30% and 9% yield, respectively. Doubling the concentration of substrate **198** and slightly increasing the amount of DDQ from 8 to 10 equiv., could shift the yields towards the desired bistriflate **206** from 14% to 25% and significantly reduce the amount of the DCV-containing PAHs **207** and **208** from overall 39% to 13%.

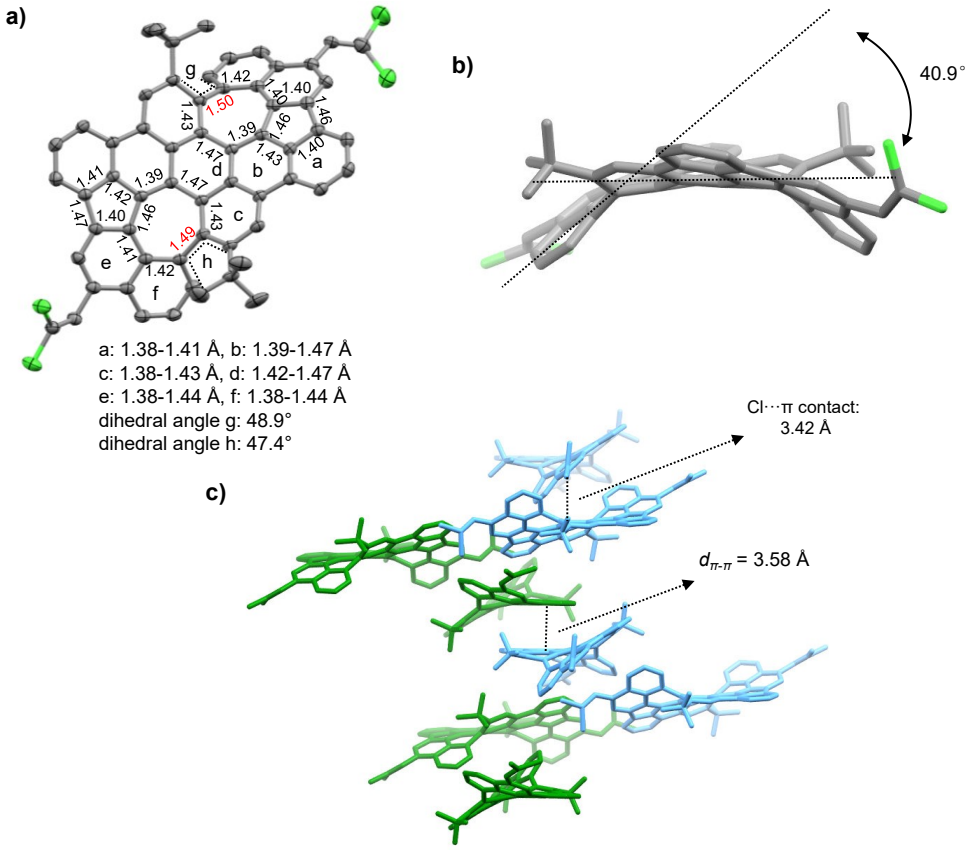

Figure 3.2.18 Single crystal X-ray structure of PAH **208**. a-b) Single enantiomer (*M*,*M*)-**208** from different perspectives. c) Packing motif in one unit cell. The two C-C bonds with the longest lengths in the π-framework are highlighted in red. The two enantiomers are highlighted in blue for (*P*,*P*)- and green for (*M*,*M*)-enantiomer. Hydrogen atoms as well as enclathrated solvent molecules have been omitted for clarity. The view in (a) is an ORTEP plot with thermal ellipsoids set at 50% probability. Bond lengths in (a) are given in Å. Color for heteroatoms: green = chlorine.

Single crystals of double DCV substituted PAH **208** suitable for X-ray diffraction analysis were obtained by diffusing methanol vapor into a solution of **208** in chloroform (Figure 3.2.18), which serve as one direct evidence for the proposed structure of PAH **208** in Scheme 3.2.11. Two azulene moieties are surrounded by eleven six-membered rings in this π-framework. PAH **208** crystallizes in a monoclinic *C*2/c space group. Due to the presence of the two azulene units and the steric repulsion between the DCV-attached naphthalene moieties and the bulky *tert*-butyl groups after cycloheptannulation, the π-framework of PAH **208** is contorted in a negative curvature.[109, 168] The angle between the peripheral benzene ring (f) and the central benzene ring (d) is 40.9° (Figure 3.2.18b). The two C-C bonds formed during cycloheptannulation exhibit longer lengths of 1.49-1.50 Å in comparison to other bonds in the π-framework. With the exception of one bond to the five-membered ring, which is between 1.37 and 1.39 Å, and the bond shared with the substituted six-membered rings, the remaining five C-C bonds are significantly longer (between 1.42 and 1.50 Å), which is in contrast to pure azulene, where all bond lengths, with exception of the shared one with the cyclopentadienyl ring (1.49 Å), are between 1.37 and 1.42 Å.[182] Thus less aromaticity is expected in the two embedded azulene units than unsubstituted azulene. PAH **208** crystallizes in a mixture of two racemic (*P*,*P*)- and (*M*,*M*)-enantiomers. Parallel arrangement between the azulene-fused naphthalene units (rings a and b in Figure 3.2.18a) of the two (*P*,*P*)- and (*M*,*M*)-enantiomers in the center of each unit cell was observed and the average π distance is $d_{\pi\text{-}\pi}$ = 3.58 Å.

In this Scholl-type reaction, the triflyloxylation is competing with the attachment of DCV units. As the DCV-attached PAHs **207** and **208** were isolated in overall yields of 13%-39%, such high number of DCV units could not come from the 1,1,2,2-tetrachloroethane impurities in the CH_2Cl_2 solvent. Thus it is more reasonable to assume that the CH_2Cl_2 solvent is involved in the formation of the DCV-bearing PAHs. Moreover, isolated monotriflate **207** or bistriflate **208** was treated with DDQ/TfOH in CH_2Cl_2 but no conversion was observed, suggesting the triflyloxy groups could not be converted to DCV units under these conditions. Oxidative cyclo-dehydrogenation of precursor **198** in the presence of DDQ/TfOH was also performed in other anhydrous solvents, such as 1,2-dichloroethane, 1,1,2,2-tetrachloroethane, chloroform, dibromomethane, benzene, chlorobenzene, *o*-DCB and nitrobenzene. However, no azulene species were observed in each case.

Based on these reaction results, it was supposed that the substitution of DCV unit and triflyloxylation are independent of each other. A possible mechanism is shown in Scheme 3.2.12. The considered naphthalene moiety **A** is oxidized by DDQ to give radical cation species, which could be transformed into two different types **B** and **E**. Similar to the mechanism of trifluoroacetoxylation reported by Little *et al*,[174a] radical cation **B** is attacked by nucleophile

trifluoromethanesulfonate, followed by the elimination of one electron and one proton to give one-fold triflated PAH **D**.

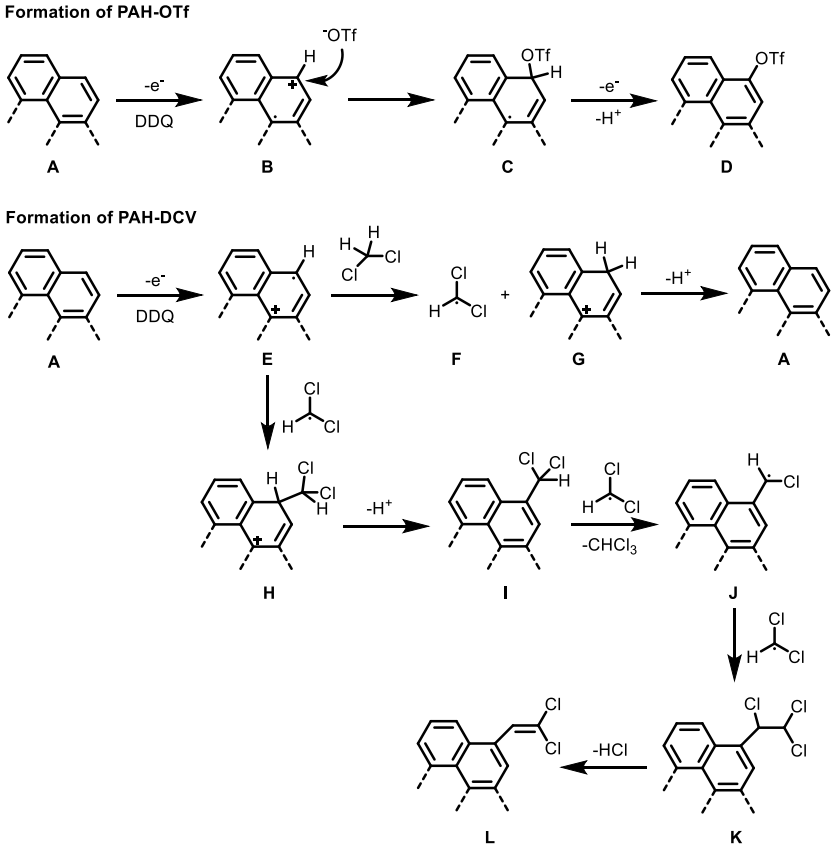

Scheme 3.2.12 A proposed mechanism for the formations of TfO- and DCV-bearing PAHs.

The formation of DCV-bearing PAHs, however, is not easy to be explained by nucleophilic or electronphilic substitution. Thus a route involving free radicals was proposed. Radical cation **E** is reacted with the DCM molecule to produce the DCM radical **F**. The generated hydrogenated cation **G** could be recovered to the substrate **A** after deprotonation. The recombination between **E** and DCM radical **F** gives the adduct cation **H**. The dichloromethyl substituted intermediate **I** is produced after deprotonation, which is reacted with another DCM radical **F** to give radical **J** after the elimination of one chloroform molecule. **J** is recombined again with DCM radical **F** to produce the adduct **K**. The DCV substituted PAH **L** is generated after the elimination of HCl. It has to be conceded that this assumption is only hypothetical as no DCV-substitution under similar conditions was reported. Furthermore, the formation of the DCM radical promoted by an aromatic hydrocarbon radical cation is open to question. It was demonstrated that DCM radical **F** can be generated via photolysis of DCM.[183] But this reason can be excluded here in this reaction as the isolated yields of DCV-bearing PAHs did not change when the reaction was performed in dark.

3.2.3.2 Cross-Coupling Reactions based on Bistriflate 206 and Curvature Modulation by Detachment of *tert*-Butyl Groups

The triflyloxy groups of PAH **206** can again serve as functional groups for palladium-catalyzed cross-coupling reactions. Suzuki-Miyaura cross-coupling of bistriflate **206** with 4-*tert*-butyl phenyl boronic acid or mesityl boronic acid gave two new azulene-bearing PAHs **210** or **211** in 79% or 93% yield, respectively (Scheme 3.2.13). Both compounds are still good soluble in common organic solvents such as CH_2Cl_2 or $CHCl_3$, so that they could be fully characterized in solution. Furthermore, the success of both cross-coupling reactions serve as evidences for the determination of the structure of bistriflate **206**.

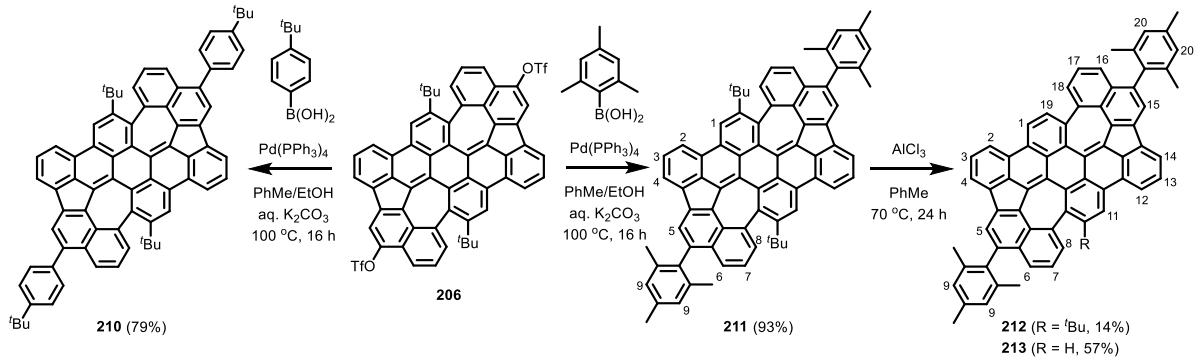

Scheme 3.2.13 Suzuki-Miyaura cross-coupling reactions based on bistriflate **206** and detachment of *tert*-butyl groups of PAH **211**.

Steric repulsion between the DCV-attached naphthalene moieties and the bulky *tert*-butyl groups could be observed in the crystal structure of PAH **208**, making the dihedral angles of the bay regions where the two *tert*-butyl groups are attached are 47.7°-48.9° (Figure 3.2.18a). It could be expected that the PAH π-framework of bistriflate **206**, which owns the same π-framework with PAH **208**, would remain in PAH **211** after cross-coupling reaction and the curvature could be modified if the bulky *tert*-butyl groups were detached. Therefore, PAH **211** was treated with anhydrous $AlCl_3$ to remove the *tert*-butyl groups via retro-Friedel-Crafts alkylation in the presence of stoichiometric Lewis acid.[184] One-fold de-*tert*-butylated PAH **212** and double de-*tert*-butylated PAH **213** were isolated by silica gel column chromatography in 14% and 57% yield, respectively, after treating PAH **211** with 3 equiv. of $AlCl_3$ in hot toluene (Scheme 3.2.13). All three PAHs were characterized by ^{1}H NMR spectroscopy (Figure 3.2.19). The singlet at δ = 9.03 ppm for H-1 on PAH **211** is up-field shifted to δ = 7.98 ppm on PAH **213** after two-fold de-*tert*-butylation at the *ortho*-positions of H-1.

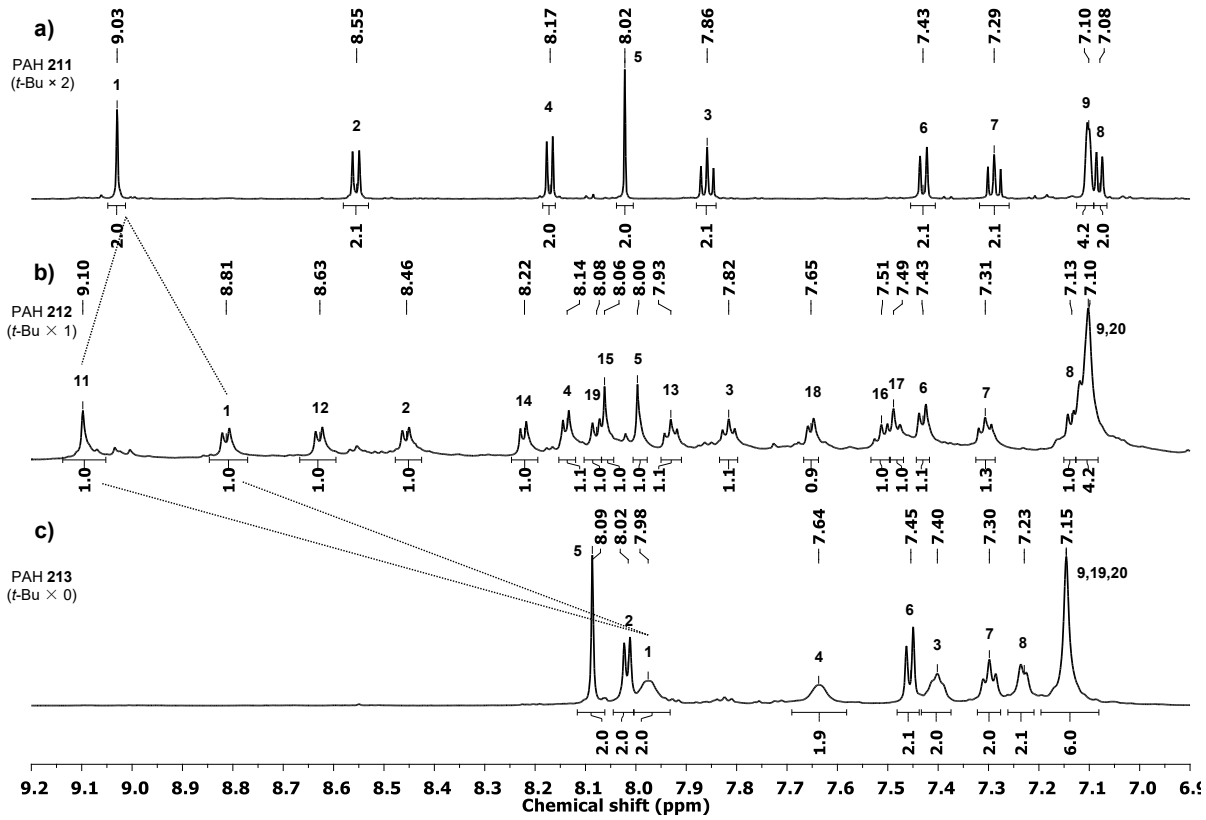

Figure 3.2.19 ^{1}H NMR spectra of PAHs **211** (600 MHz, CD_2Cl_2, 298 K, a), **212** (600 MHz, CD_2Cl_2, 298 K, b) and **213** (600 MHz, CD_2Cl_2, 298 K, c). Depicted are only the aromatic regions. Peak assignments are according to the numbering of molecular structure in Scheme 3.2.13.

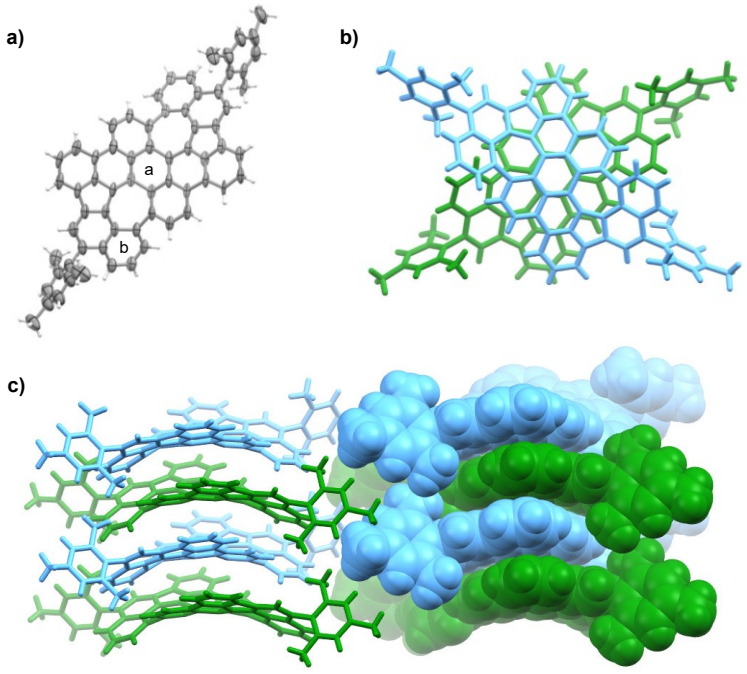

Figure 3.2.20 Single crystal X-ray structure of PAH **213**. a) Molecular structure of single enantiomer (*M*,*M*)-**213**. b) A dimer of two racemic enantiomers. c) Packing motif. The two enantiomers are highlighted in blue for (*P*,*P*)-**213** and green for (*M*,*M*)-**213**. The view in (a) is an ORTEP plot with thermal ellipsoids set at 20% probability. Enclathrated solvent molecules have been omitted for clarity.

Single crystals of doubly de-*tert*-butylated PAH **213** suitable for X-ray diffraction analysis were obtained by diffusing *n*-hexane vapor into a solution of **213** in chlorobenzene (Figure 3.2.20). This result serves as another evidence for the molecular structure of azulene bistriflate **206**. In comparison to that of DCV-bearing PAH **208** (Figure 3.2.18), PAH **213** exhibits a more planar π-backbone due to the removal of the two bulky *tert*-butyl groups at the bay regions. The angle between the peripheral benzene ring b and the central one a (marked in Figure 3.2.20a) is around 31.2°, smaller than that of PAH **208** (40.9°). However, the crystallographic data quality is not sufficient to discuss the bond lengths and angles in more detail due to the low resolution. PAH **208** crystallizes in the space group P_c as a racemic mixture of two negatively curved enantiomers. A dimerized packing motif involving two racemic enantiomers was observed. The distance between two enantiomers in each π-dimer is $d_{\pi\text{-}\pi}$ = 3.7-3.9 Å.

3.2.3.3 Spectroscopic and Electrochemical Properties

The uncyclized precursor **198**, helical dichloride **202** and the azulene PAHs **206-208**, **210-213** were investigated by UV/Vis absorption and emission spectroscopy as well as cyclovoltammetry (CV). Frontier molecular orbitals and their corresponding energy levels have been calculated by DFT methods using *Spartan 14* package.[169]

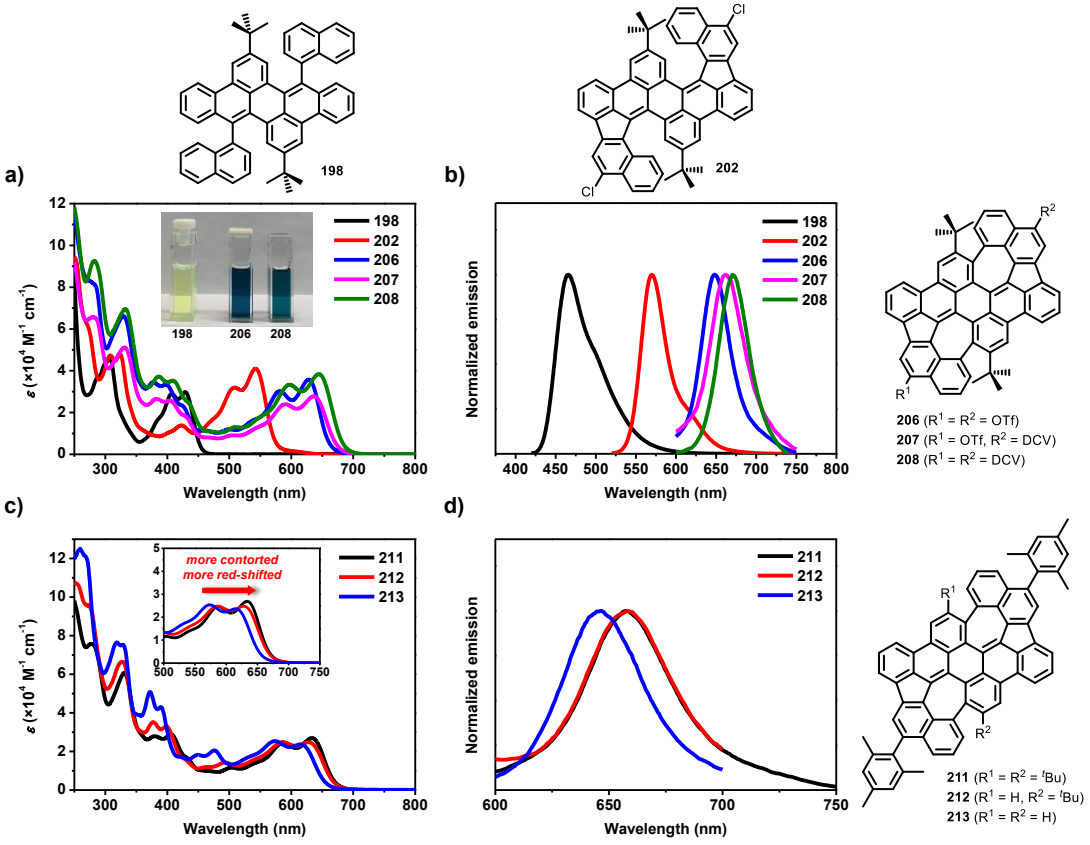

Figure 3.2.21 Absorption (a, c) and emission (b, d) spectra measured in $CHCl_3$ at room temperature (c = 12-25 µmol·L^{-1}). Inserted in (a) is an optical image of PAHs **198**, **206** and **208** in chloroform (c = 12 µmol·L^{-1}) under ambient conditions.

Absorption and emission spectra are shown in Figure 3.2.21. The detailed data is summarized in Table 3.2.2. Cyclization has a big impact on the spectroscopic and electrochemical properties of PAHs within this series. In comparison to the precursor **198**, which exhibits an absorption maximum at λ = 429 nm for the most bathochromically shifted peak (S_0-S_1 transitions), helical dichloride **202** shows bathochromic shift after double cyclopentannulation, giving an absorption maximum at λ = 542 nm, which is similar to that five-membered ring containing PAHs discussed in Chapter 3.2.2.

After the formation of azulene moieties in the π-backbone, a further bathochromical shift in the UV/Vis spectra was observed in all azulene PAHs. The most bathochromically shifted peak in the UV/Vis spectrum of PAH **206** with two OTf groups is found at λ = 628 nm and shifts with the degree of substitution with DCV groups to λ = 636 nm (PAH **207**) and finally to λ = 644 nm (PAH **208**), which could be simply explained by expansion of the π-system by the olefinic double bond of each DCV unit. The differences in the measured absorption spectra are supported by the TDDFT calculated UV/Vis spectra (Figure 3.2.22). These absorption maxima at the longest wavelengths are comparable to those of close-shell PAHs embedded with azulene units in the literatures, which are in the range of λ = 536-692 nm.[138, 141b, 141c] Similar with the changes in the UV/Vis spectra, the fluorescence emission is shifted as well from λ = 648 nm for PAH **206** through λ = 662 nm for PAH **207** to λ = 671 nm for PAH **208**. The azulene PAHs exhibit emission in the NIR regime with fluorescence quantum yields between Φ = 18%-26%.

Table 3.2.2 Summary of the photophysical and electrochemical characterization of PAHs **198**, **202**, **206-208** and **211-213**.

PAHs	λ_{max} [nm][a,b]	E_g^{opt} [eV][a,c]	λ_{em} (λ_{ex}) [nm][a,d]	$\tilde{\nu}$ [cm^{-1}][e]	Φ [%][f]	$E_{1/2}^{ox}$ [V]	IP^{CV} [eV][g]	$E_{1/2}^{red}$ [V]	EA^{CV} [eV][h]	E_g^{CV} [eV]	E_{HOMO} [eV][i]	E_{LUMO} [eV][i]
198	429	2.7	466 (407)	1851	57±1	0.64	-5.3	-	-2.6	2.8	-5.2	-2.0
202	542	2.2	570 (509)	906	16±0	0.71 1.02	-5.4	-1.57 -1.71	-3.3	2.1	-5.4	-2.9
206	628	1.9	648 (280)	491	20±1	0.42 0.84	-5.1	-	-3.3	1.8	-5.3	-3.1
207	636	1.8	662 (280)	617	26±1	0.25 0.70	-5.0	-	-3.2	1.8	-5.3	-3.0
208	644	1.8	671 (282)	625	24±1	0.32 0.74	-5.0	-1.64 -1.79	-3.3	1.7	-5.2	-3.0
211	633	1.8	658 (277)	600	25±1	0.21 0.66	-5.0	-1.78 -2.02	-3.1	1.9	-5.0	-2.7
212	628	1.8	658 (272)	726	22±1	0.20 0.62	-5.0	-1.79 -2.09	-3.1	1.9	-5.0	-2.7
213	615	1.9	646 (272)	780	18±1	0.40 0.82	-5.0	-1.66 -1.93	-3.2	1.8	-5.1	-2.7

[a] Measured in $CHCl_3$ at room temperature. [b] Absorption maximum at the longest wavelength. [c] Estimated from absorption onset. [d] Emission maximum. [e] Stock's shift. [f] Fluorescence quantum yield. [g] Ionization potential. [h] Electron affinity. $E_{1/2}^{ox}$, $E_{1/2}^{red}$, IPs and EAs were measured by cyclic voltammetry in 0.1 M *n*-Bu_4NClO_4 in CH_2Cl_2 at room temperature. The scan speed was 100 mV·s^{-1} and ferrocene/ferrocenium (Fc/Fc^+) was used as internal reference. IP^{CV} = -(E_{onset}^{ox} + 4.8 eV). EA^{CV} = -(E_{onset}^{red} + 4.8 eV). [i] Calculated by DFT using Spartan 14 at B3LYP/6-311G* level.

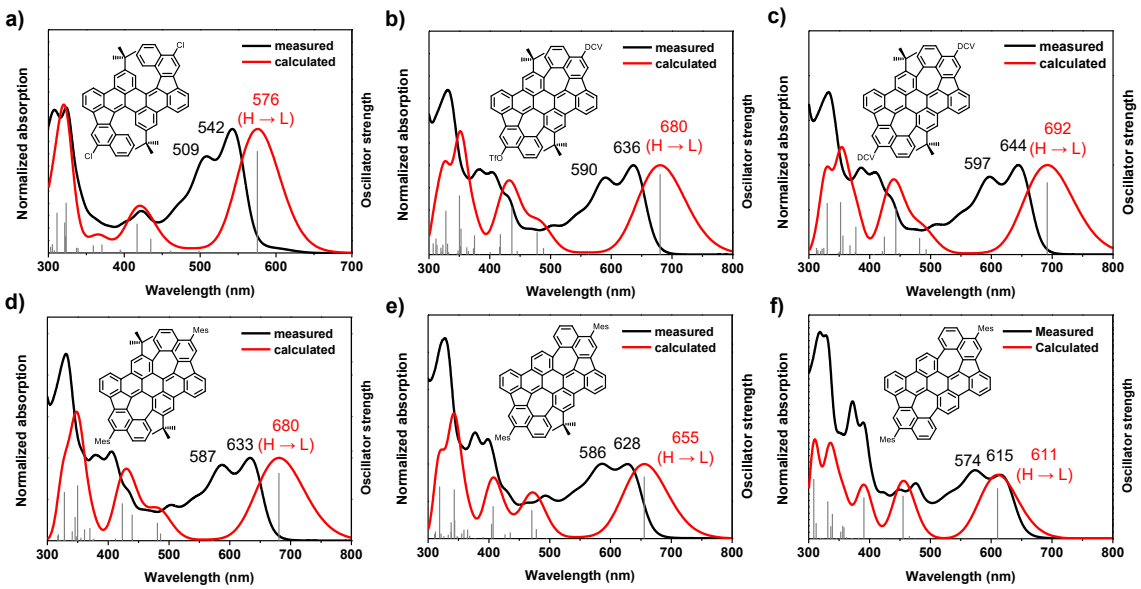

Figure 3.2.22 Comparisons of UV/Vis absorption spectrum measured in $CHCl_3$ (black) and calculated UV/Vis absorption spectrum (red) based on TDDFT at the B3LYP/6-311G* (PCM-$CHCl_3$) level. Peak positions are given in nm. H: HOMO. L: LUMO. DCV: dichlorovinylidene. Mes: mesityl.

The formations of azulene units in the π-backbones increase the ionization potentials by 0.3-0.4 eV in comparison to the uncyclized precursor **198** or helical dichloride **202** (Table 3.2.2). Cyclopentannulation or further cycloheptannulation decreases the electron affinities by 0.5-0.7 eV in comparison to the uncyclized precursor **198**. Thus the bandgaps estimated by electrochemical measurements decrease from 2.8 eV for precursor **198**, 2.1 eV for the helical dichloride **202**, to 1.7-1.9 eV for azulene PAHs. This is in accordance with the DFT calculated FMOs.

A combination of PAHs **211-213** serves as a good model to investigate the influences of differently curved π-planes on molecular properties. As shown by single crystal X-ray structure as well as DFT optimized molecular structures, PAHs with the bulky *tert*-butyl groups at the bay regions exhibit more contorted structures. PAH **211** attached with two *tert*-butyl groups shows the longest wavelength absorption at λ = 633 nm (S_0-S_1 transition from HOMO to LUMO), which shifts to λ = 628 nm for PAH **212** with one *tert*-butyl group and to λ = 615 nm for PAH **213** without *tert*-butyl groups.

3.2.3.4 Discussion of Aromaticity by Theoretical Calculations

Nuclear independent chemical shifts NICS(0) were calculated for DFT optimized structures of PAHs **211-213** (Figure 3.2.23), in order to estimate the aromaticity of the embedded azulene units and compare the difference of aromaticity for the same π-framework but with different curvatures. The pentagonal rings exhibits NICS(0) values of 0.9-2.2, while the values are increased to 6.1-6.6 for the heptagonal rings. This result suggests that the embedded azulene units in this π-framework exhibits antiaromatic character, which is in accordance with the results of the bond

length distribution in the single crystal X-ray structure of DCV-bearing PAH **208** (Figure 3.2.18a) and other reported PAHs with embedded azulene units.[88, 140d, 141b] Relatively high aromatic characters (more negative NICS(0) values) are found in the four peripheral six-membered rings of this π-framework in all three molecules, which are highlighted in grey in Figure 3.2.23. The most contorted PAH **211** with two *tert*-butyl groups has Σ_{NICS}= -42.5, whereas PAH **212** is slightly more aromatic (Σ_{NICS}= -44.5). The most negative sum of NICS(0) values is found for double de-*tert*-butylated PAH **213** with Σ_{NICS}= -47.5, suggesting that the more contorted the system, the less aromatic it is. This result is in agreement with the UV/Vis absorption spectra (Figure 3.2.21c).

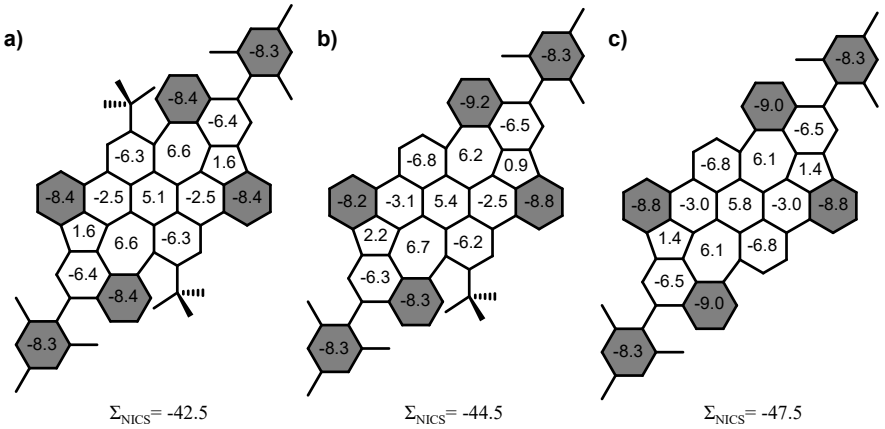

Figure 3.2.23 DFT calculated NICS(0) values of PAH **211** (a), **212** (b) and **213** (c) at the B3LYP/6-31G* level. Grey-colored rings show clear benzenoid character. The values at bottom are the sum of the NICS(0) values of π-backbone.

Calculations of anisotropy of the induced current density (ACID)[185] have been performed based on the DFT optimized structures of two *tert*-butyl groups attached azulene PAH **211** and double de-*tert*-butylated PAH **213** at the HF/6-31+G* level, in order to further investigate the aromaticity of the azulene-embedded π-frameworks. The corresponding plots are shown in Figure 3.2.24, in which the magnetic field points out of the paper plane in both cases. Both PAHs exhibit similar patterns of ring currents. Diamagnetic ring currents, which are highlighted with clockwise red arrows, were found in the eight six-membered rings a, e, f, g, i, k, l and o, indicating the local aromaticity in these rings. This ring current distribution is consistent with the calculated NICS(0) value in these rings, which are in the range of -6.3 to -9.0. The eight rings are located at the periphery of the molecular π-framework, thus clockwise ring currents delocalized along the outer rims of both molecules could be observed. It could be expected that both PAHs exhibit global aromaticity. Relatively weak paratropic ring current were observed in the inside rims of the two six-membered rings a and o, which is similar to an isolated benzene ring.[186] In rings b and n, the ring currents are not uniform, thus both rings are more or less nonaromatic. The calculated NICS(0) values of -2.5 to -3.0 in these rings, which are less negative than the rings shown above, support the nonaromaticity.

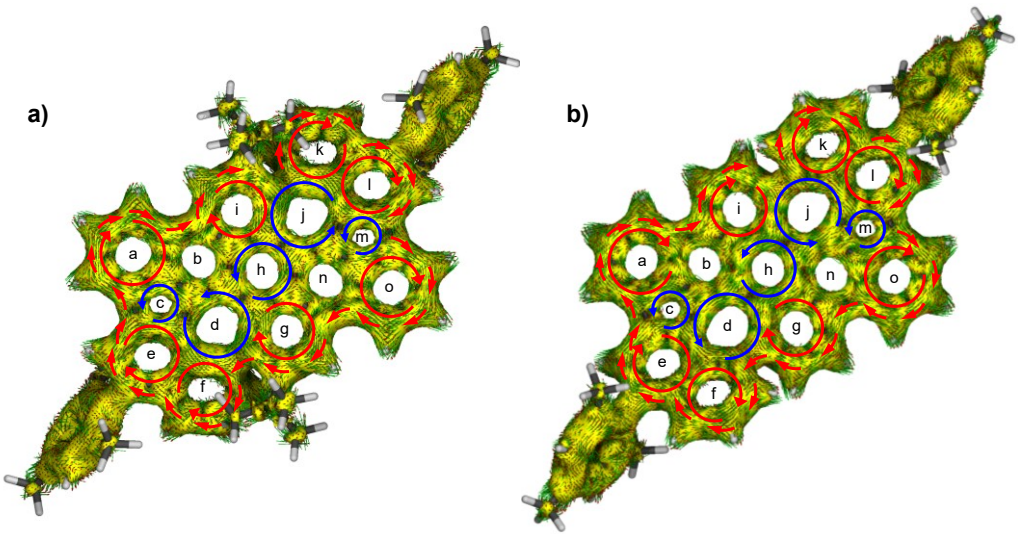

Figure 3.2.24 Calculated ACID plots for PAHs **211** (a) and **213** (b) at the HF/6-31+G* level. The isosurface value is 0.05 and the magnetic field points out of the paper plane. The diamagnetic (clockwise) and paramagnetic (counterclockwise) ring currents are highlighted by red and blue arrows, respectively.

In the two embedded azulene units (rings c, d, j, m) and the central six-membered ring h, paramagnetic (counterclockwise) ring currents were observed, suggesting the azulene moieties and ring h exhibit weak local antiaromaticities. This is in consistence with the calculated NICS(0) values, which are all positive (1.6-6.6, Figure 3.2.23), and is similar to those of other reported azulene embedded PAHs.[138, 141b, 141c]

3.2.3.5 Chiral Resolution

As discussed for the single crystal structures of PAHs **202**, **208** and **213**, two racemic enantiomers were observed in all three cases. For helical dichloride **202**, azulene PAHs **206** and **211**, two peaks with comparable integrals have been observed by chiral HPLC at room temperature (Figure 3.2.15 for helical dichloride **202** and Figure 3.2.26 for **206** and **211**).

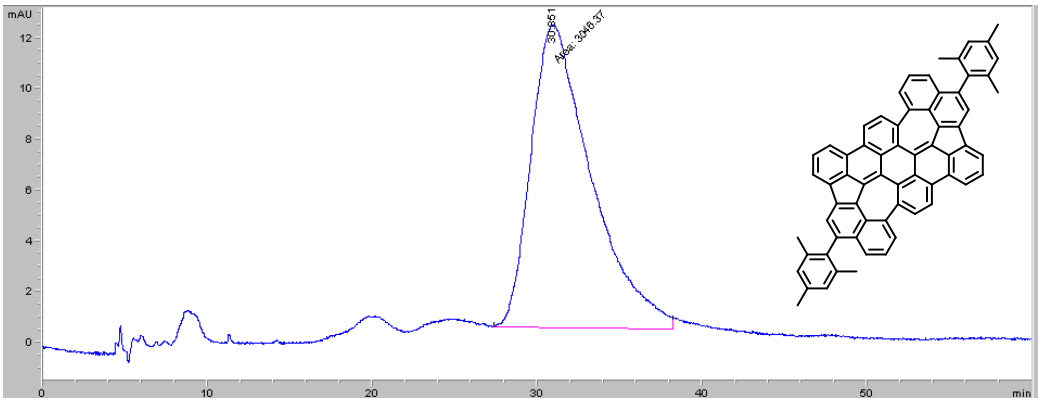

Figure 3.2.25 Analytical chiral HPLC chromatogram of PAH **213**. The chromatogram was obtained at room temperature using an analytical column packed with amylose tris(3,5-dimethylphenylcarbamate) (AD-H) coated on 5 µm silica gel with an eluent of *n*-hexane:isopropanol (90:10) at a flow rate of 0.7 mL/min.

Only one broad peak was observed in the case of de-*tert*-butylated PAH **213** (Figure 3.2.25), suggesting a rapid interconversion of the two enantiomers to each other at room temperature. This is supported by the energy scan of different conformations of PAH **213** by DFT calculation at the B3LYP/6-311G* level of theory. The predicted energy barrier between the optimized structures of two racemic enantiomers of PAH **213** is 22.5 kcal·mol^{-1}, which is significantly lower than the value (31.2 kcal·mol^{-1}) of PAH **211** with two *tert*-butyl groups attached calculated at the same level.

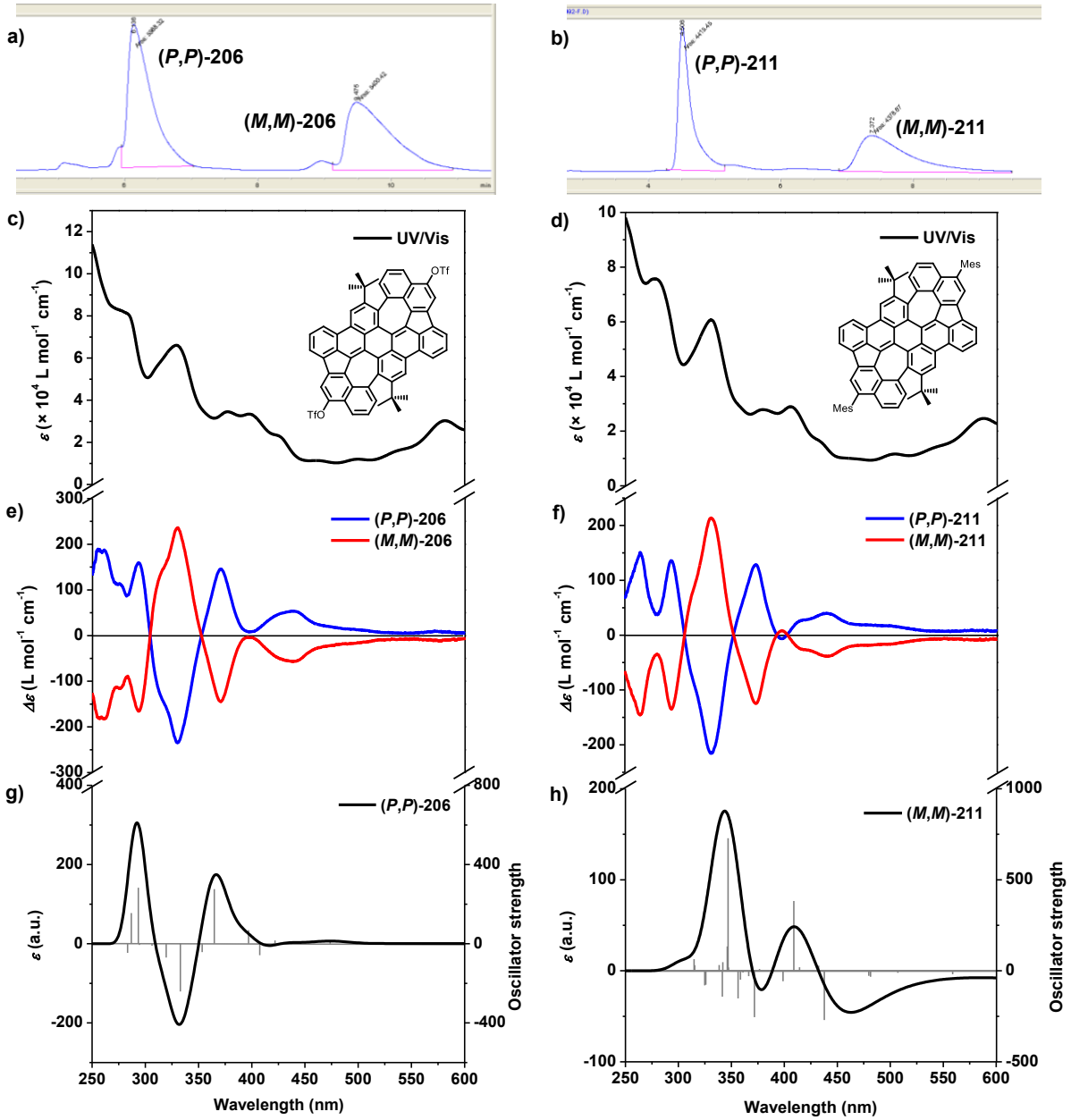

Figure 3.2.26 a-b) Semi-preparative chiral HPLC chromatograms of PAHs **206** and **211**. The column was a Chiralpak IE^{TM} column based on amylose *tris* (3,5-dichlorophenylcarbamate) using *n*-heptane/*i*-propanol (v/v = 95/5 for **206** and v/v = 99/1 for **211**) as eluent with a flow rate of 20 mL·min^{-1}. c-d) UV/Vis absorption spectra of PAHs **206** and **211** in racemic mixtures measured in chloroform at room temperature (c = 12-15 µmol·L^{-1}) e-f) CD spectra of the separated enantiomers of PAHs **206** and **211** measured in chloroform at room temperature (c = 12-15 µmol·L^{-1}) g-h) TDDFT calculated ECD spectra (cam-B3LYP/6-311G*, PCM-$CHCl_3$, σ = 0.5 eV) for (*P*,*P*)-**206** and (*M*,*M*)-**211**.

For PAHs **206** and **211**, which are soluble enough in the solvent mixture of *n*-heptane and *i*-propanol, semi-preparative chiral HPLC equipped with a Chiralpak IE^{TM} column based on amylose *tris* (3,5-dichlorophenylcarbamate) using *n*-heptane/*i*-propanol as eluent was applied to separate these enantiomers. Due to the low solubilities of dichloride **202** and DCV-bearing PAH **208** in *n*-heptane (< 0.5 mg·mL^{-1}), separations of both molecules were not performed.

The measured circular dichroism (CD) spectra of the separated enantiomers clearly shows that the two isolated fractions are mirror images with opposite Cotton effects (Figure 3.2.26).[187] Due to the same PAH backbone, both PAHs **206** and **211** show similar CD spectra. The most intense band arises at 329 nm ($|\Delta\varepsilon|$ = 234 L·mol^{-1}·cm^{-1}, g_{abs} = 3.54 × 10^{-3}) for PAH **206** and 331 nm ($|\Delta\varepsilon|$ = 214 L·mol^{-1}·cm^{-1}, g_{abs} = 3.52 × 10^{-3}) for PAH **211**,[188] which corresponds to the absorption maxima for the β-bands. The chirality of these four enantiomers was assigned by comparison of the experimentally measured CD spectra with the TDDFT simulated ECD spectra (Figure 3.2.26g and h) of (*P*,*P*)-**206** and (*M*,*M*)-**211**. Thus the first eluted fractions from chiral HPLC correspond to the (*P*,*P*)-enantiomers for both PAHs.

3.2.4 Conclusions

Based on two isomeric naphthyl-substituted dibenzoperylenes **180** and **198**, two types of larger contorted and soluble PAHs have been synthesized by cyclopentannulation (and cycloheptannulation) in one step, respectively. In both cases, unprecedented highly regioselective bistriflyloxylations were observed during the oxidative cyclodehydrogenation reactions under Scholl-type conditions, using DDQ as an oxidant in combination with triflic acid. The obtained key π-backbones were characterized by single crystal X-ray diffraction analysis.

In the first case, the results of the reactions indicate that the oxylation occurs after the cyclopentannulation. Double helicene **191** and oligophenyl PAH **197** were synthesized by transition metal catalyzed cross-coupling reactions based on bistriflate **184**. In comparison to the uncyclized precursor **180**, PAHs after cyclopentannulation exhibit obvious bathochromic shifts in the UV/Vis absorption and fluorescence emission spectra.

In the second case, contorted PAHs with two embedded azulene units were obtained by oxidative cyclodehydrogenation of compound **198**, during which the substitutions of dichlorovinylene groups were competing with the regioselective triflyloxylation. The triflyloxy groups were transformed to aryl units by palladium catalyzed cross-coupling reactions. With the attachment of solubilizing mesityl groups, the relationship between aromaticity and the degree of curvature of these PAHs was investigated by simply stepwise removing the *tert*-butyl groups in the bay regions. With the recovery of the molecular planarity, the molecular aromaticity increases. All azulene embedded PAHs show a distinct emission close to the near-infrared (NIR) region between

650 and 670 nm with relatively high quantum yields of 20%-30%, suggesting that these PAHs own potential applications in biological areas by decorating with other functional groups to interact the specific sites in the organisms for biological imaging or probes.[189] The chiral resolution and successful enantioseparation of PAHs **206** and **211** indicates that this azulene embedded π-backbone with the attachment of two *tert*-butyl groups could serve as a building block for the synthesis of larger chiral curved PAHs.

3.3 Linear Type Perylene Oligomers and Coronene Oligomers

3.3.1 Introduction

Linearly extended fused polycyclic π-systems are interesting compounds in respect not only to organic electronics,[190] but also to get a deeper insight into aromaticity and stability of large π-systems.[191] However, the synthesis of high level acenes has challenged chemists. Non-substituted higher homologues of the linearly fused [n]acenes with n ≥ 6 are prone of photo-oxidation or photo-dimerization via formal [4+4] cycloadditions, which can be ascribed to the existence of open-shell singlet diradical ground states in large oligoacenes.[192] Various methods were developed to improve the stability of acene species.[18b, 193] Introducing electron-withdrawing groups, such as nitrogen atoms, or pyrene units to take advantage of its cross-conjugated character, into π-scaffolds, serve as classic approaches. Based on this strategy, syntheses of various azaacenes (*N*-heteroacenes) have been reported.[18b, 20, 194] For example, pyrene-fused *N*-heteroacenes with length up to 30 conjugated linearly fused rings have been obtained by iterative condensations and deprotections between diamine **214** and pyrenetetraone **215** (Scheme 3.3.1a).[195] The similar π-scaffolds could also be applied to the construction of 3D systems using similar iterative strategy (Scheme 3.3.1b).[196]

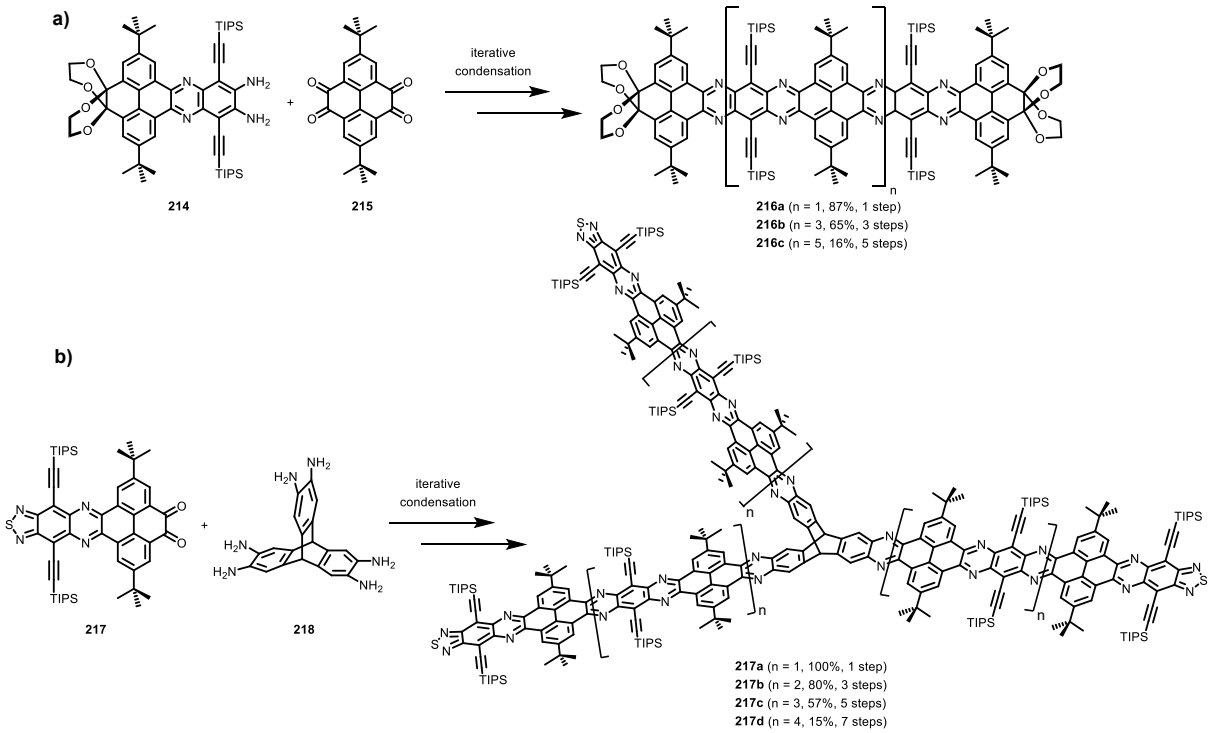

Scheme 3.3.1 Examples of syntheses pyrene-fused *N*-heteroacenes. TIPS: triisopropylsilyl.[195-196]

In comparison to the widely reported *N*-heteroacenes, linearly extended acene species containing only C and H atoms are rare. Different from *N*-heteroacenes which can be obtained by acid-catalyzed condensation between aromatic diamines with *ortho*-quinones[197] or by palladium-

catalyzed coupling reactions of diamines with activated halides,[160, 198] synthesizing and stabilizing oligoacenes is more challenging. For instance, unsubstituted heptacene, octacene and nonacene were generated in polymer or noble gas matrices from α-bridged diketones (Scheme 3.3.2a),[199] or by thermal cleavage of diheptacenes.[200] Nonacene and decacene can be obtained in small scale from partially saturated precursors on Au(111) surface by heating at high temperature or by scanning tunneling microscope (STM) tip-induced reactions (Scheme 3.3.2b).[201] Construction via 2D extension has been demonstrated as another strategy to synthesize stable larger acenes in solution.[202] Zhang and co-workers reported a pyrene-fused stable nonatwistacene obtained by a retro-Diels-Alder process involving the thermal elimination of lactam bridges (Scheme 3.3.2c).[202c] This system could be further extended to a dodecatwistacene by a similar synthetic procedure and contains twelve conjugated linearly fused rings (Scheme 3.3.2d).[202d]

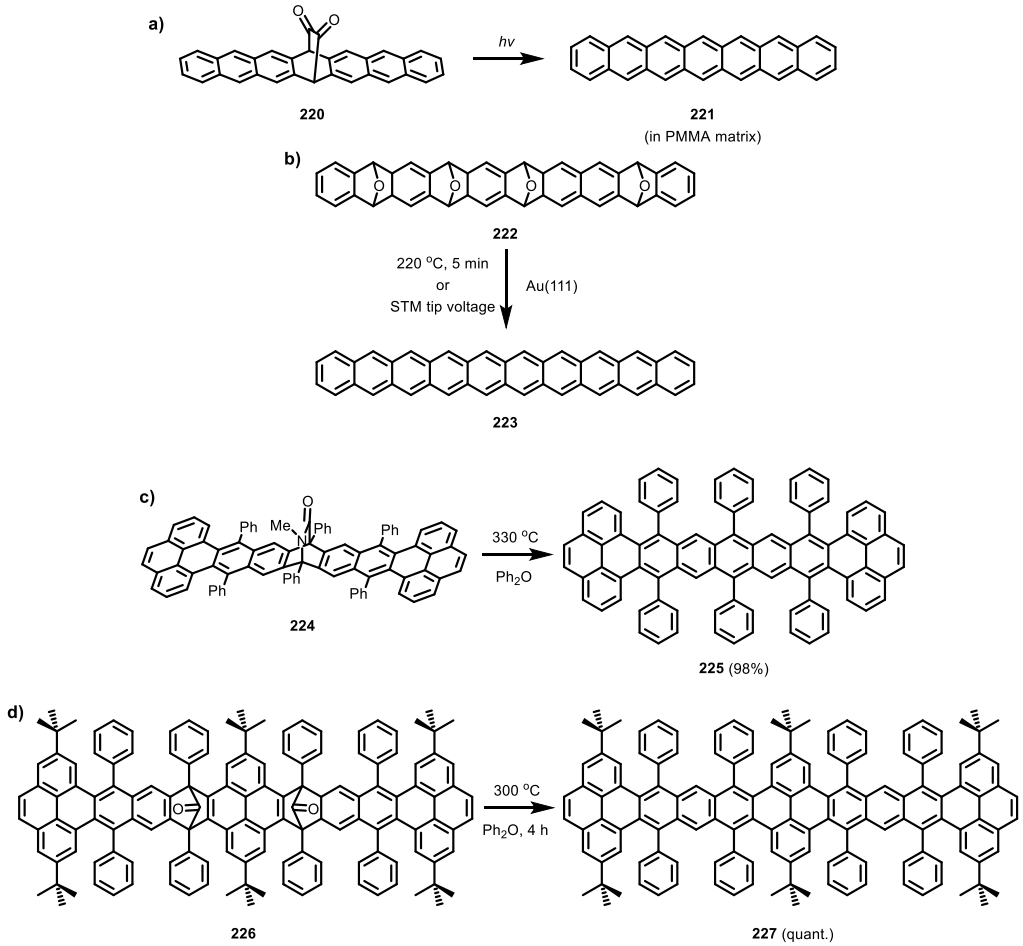

Scheme 3.3.2 Examples of syntheses of oligoacenes.[199a, 201a, 202c, 202d]

As discussed in Chapter 1.4, a series of stable diarenoperylenes could be obtained by intramolecular condensation reactions of two aldehyde groups with two methylene groups on the dihydroanthracene backbone in the presence of strong base (*eg*. *t*-BuOK).[128b] This approach is also suitable to construct larger π-systems based on truxene from similar aldehyde precursors.[123, 128a] Furthermore, high stability was observed in these diarenoperylene molecules as four sextets can be

drawn on these π-backbones according to Clar's rule.[161] These results suggest that this diarenoperylene system owns potential to be further linearly extended to oligoacenes. The molecular design is illustrated in Scheme 3.3.3a. An oligoacene with nine conjugated linear-fused rings can be obtained by linearly fusing two dibenzoperylene units with one benzenoid ring shared. A high stability should be expected as seven Clar's sextets can be drawn on this longer π-backbone. Based on this strategy, oligoacenes of more than 13 rings along the π-backbone with high stability is possible to be obtained. It should be noted that this π-scaffold was chosen by Risko and co-workers as a model structure to investigate the electronic band structures and to predict physical properties such as band gaps and charge carrier mobilities of polyacenes with different edge topologies by theoretical calculations (Scheme 3.3.3b).[203]

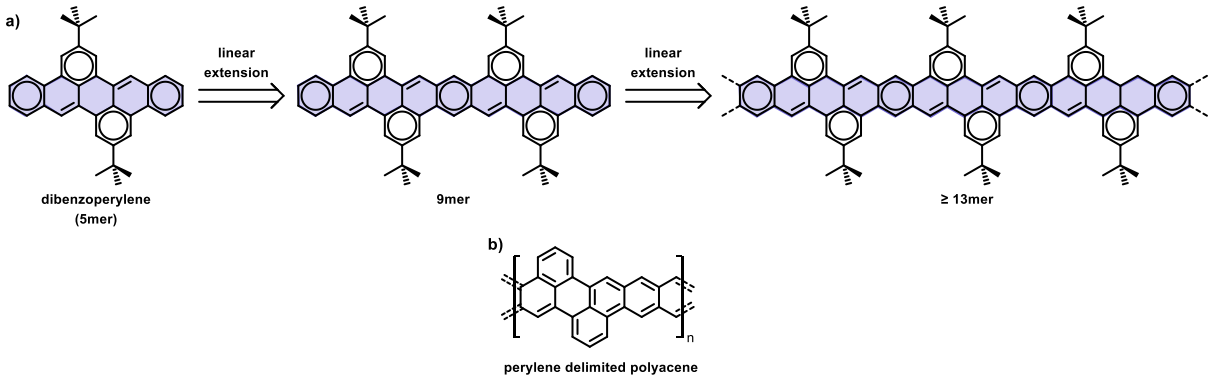

Scheme 3.3.3 (a) Structures of the designed perylene oligomers. The sextets are drawn as circles. 5mer, 9 mer or 13mer is named after the number of linearly fused benzene rings (highlighted in blue) in the molecular π-framework. (b) The model structure of perylene delimited polyacence investigated by Risko and co-workers.[203]

3.3.2 Target Molecules and Synthesis of PO-5

The π-framework of the target linearly extended perylene oligomers is presented in Scheme 3.3.3. One factor to be considered is the solubility of these oligoacenes, which determines whether the designed oligomers can be fully characterized in solution. Dibenzoperylene **111** exhibits good solubilities in common organic solvents. However, the solubility of dibenzoheptacene **114** (Scheme 1.11) with two more *cata*-condensed benzene rings decreases significantly and is less than 1 mg·mL^{-1} in 1,1,2,2-tetrachloroethane or *o*-DCB at room temperature.[128b] The poor solubility made the purification and characterization difficult. Thus, it could be supposed that the solubilities of the target longer perylene oligomers (9mer and 13mer in Scheme 3.3.3) might be low. In order to deal with this issue, chemical modifications should be made. Triptycene has been proven to be an ideal structural unit in large π-systems to weaken intermolecular packing and thus increase the solubility.[96, 197d, 204] Based on this strategy, triptycene was introduced into this oligoacene systems as end groups and four triptycene end-capped perylene oligomers PO-5 (**228**), PO-9 (**229**), PO-13 (**230**) and PO-17 (**231**) were designed (Scheme 3.3.4a), in which the number after PO stands for the number of linearly fused benzene rings in the π-backbones.

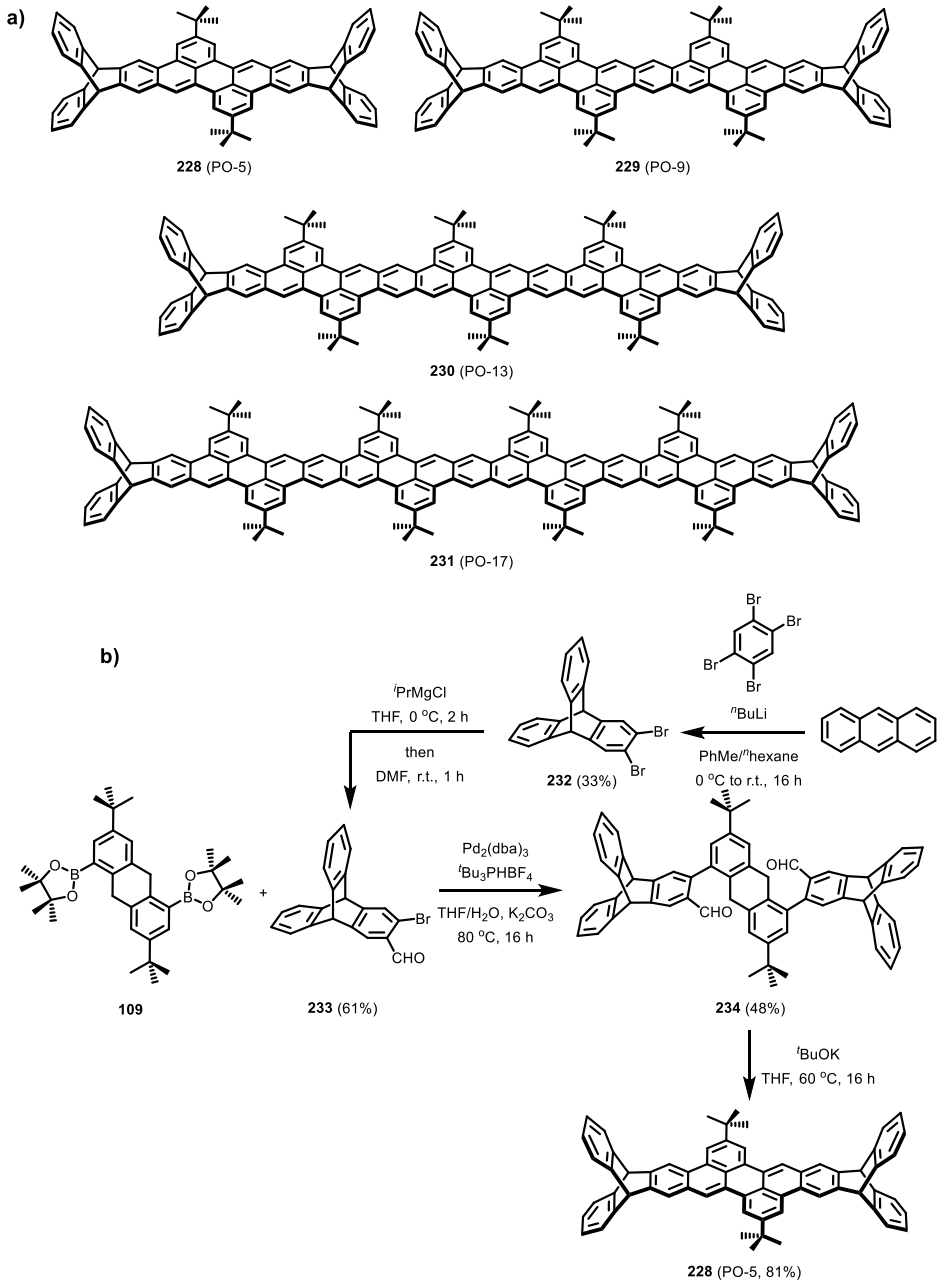

Scheme 3.3.4 a) Molecular structures of target perylene oligomers (**228**-**231**). b) Synthesis of PO-5 (**228**).

The synthetic route to PO-5 (**228**) is shown in Scheme 3.3.4b. Diels-Alder reaction of anthracene with dibromobenzyne, which was produced from 1,2,4,5-tetrabromobenzene in the presence of *n*-BuLi, gave 2,3-dibromotriptycene **232** in 33% yield.[205] Bromotriptycylaldehyde **232** could be obtained in 61% yield via metal-halogen exchange of **232** promoted by *i*-PrMgCl followed by quenching with anhydrous DMF. Two-fold Suzuki-Miyaura cross-coupling reaction between reduced anthracene diboronic ester **109** and bromotriptycylaldehyde **232** under Fu conditions[163] gave dialdehyde **234** in 48% yield. Intramolecular condensation of dialdehyde **234** in the presence of *t*-BuOK gave the triptycene end-capped PAH PO-5 (**228**) in 81% yield.

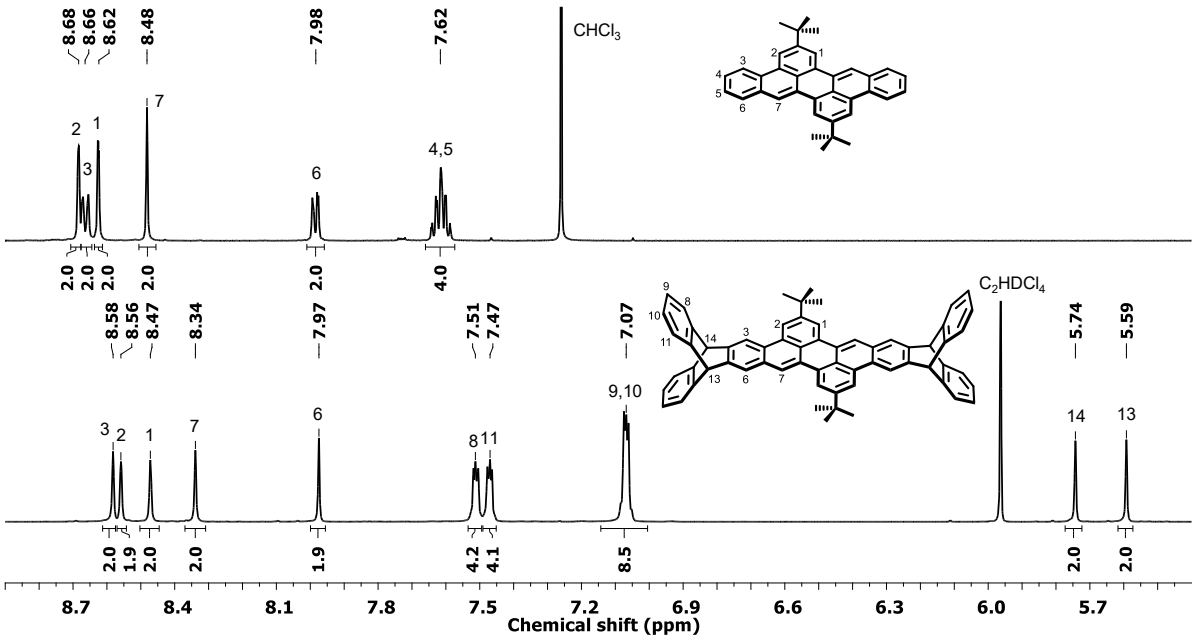

Figure 3.3.1 ^{1}H NMR spectra of dibenzoperylene **111**[128b] (top, 600 MHz, $CDCl_3$, 298 K) and PO-5 (**228**, bottom, 600 MHz, $Cl_2CDCDCl_2$, 298 K). Only aromatic regions are shown.

The molecular structure of PO-5 (**228**) was confirmed by ^{1}H NMR spectroscopy (Figure 3.3.1). In comparison to the spectrum of dibenzoperylene **111** without triptycene end caps, signals for protons on the central π-framework of PO-5 (**228**) exhibit similar chemical shifts. The signals of the protons for H-1 and H-2 at the two *ortho*-positions of the *tert*-butyl groups up-field shift by 0.10-0.15 ppm, while the singlet at δ = 8.48 ppm for H-7 in **111** up-field shifts to 8.34 ppm in **228**. The signals for the bridgeheads (H-13, 14) of the triptycene units were observed as two singlets at δ = 5.74 ppm and δ = 5.59 ppm. The two signals for bridgeheads observed and the split of the multiplet at δ = 7.53-7.45 ppm indicate different chemical environments of two bridgehead protons and different chemical environments of H-8 and H-11 on one triptycene unit.

3.3.3 Synthesis of PO-9

3.3.2.1 Route A

As shown in Scheme 3.3.5, compound **232** without the triptycene end caps was chosen as a model compound to develop the synthetic route of PO-9 (**229**). In order to obtain perylene oligomer **232**, synthesizing the aromatic tetraaldehyde precursor **233** is critical. Tetraaldehyde **233** could be broken down to three subunits, one equiv. of 2,5-dibromoterephthalaldehyde **235** along with two equiv. of dihydroanthracene diboronic ester **109** and two equiv. of 2-bromobenzaldehyde **234** as end cap. A simple idea to synthesize compound **233** is to perform the palladium-catalyzed Suzuki-Miyaura cross-coupling reaction using a mixture of these three components and to obtain **233** in one pot. The reaction was performed under Fu conditions and the products with corresponding isolated yields are shown in Scheme 3.3.5. The mixture obtained after the reaction was isolated by

silica gel column chromatography. Reacting these three compounds in a molar ratio of 2:2:1 gave one-fold coupled product **236** in 15% yield and two-fold coupled product **110** in 24% yield. Besides both side products, the desired tetraaldehyde precursor **237** was isolated in a low yield of 3%. The relatively lower solubility and different reactivity of the 2,5-dibromoterephthalaldehyde **235** in comparison to 2-bromobenzaldehyde **234** may lead to the result that the reaction of **235** was not comparable to that of 2-bromobenzaldehyde in this irreversible process of C-C bond formation, which could explain the low yield of the desired product.

This result indicates that this one-pot approach is not feasible to construct longer extended oligomers. In addition to the low yield (3%) of the tetraaldehyde precursor **237**, large amounts of the starting materials would be lost as unrecyclable side products. Thus another synthetic route had to be explored.

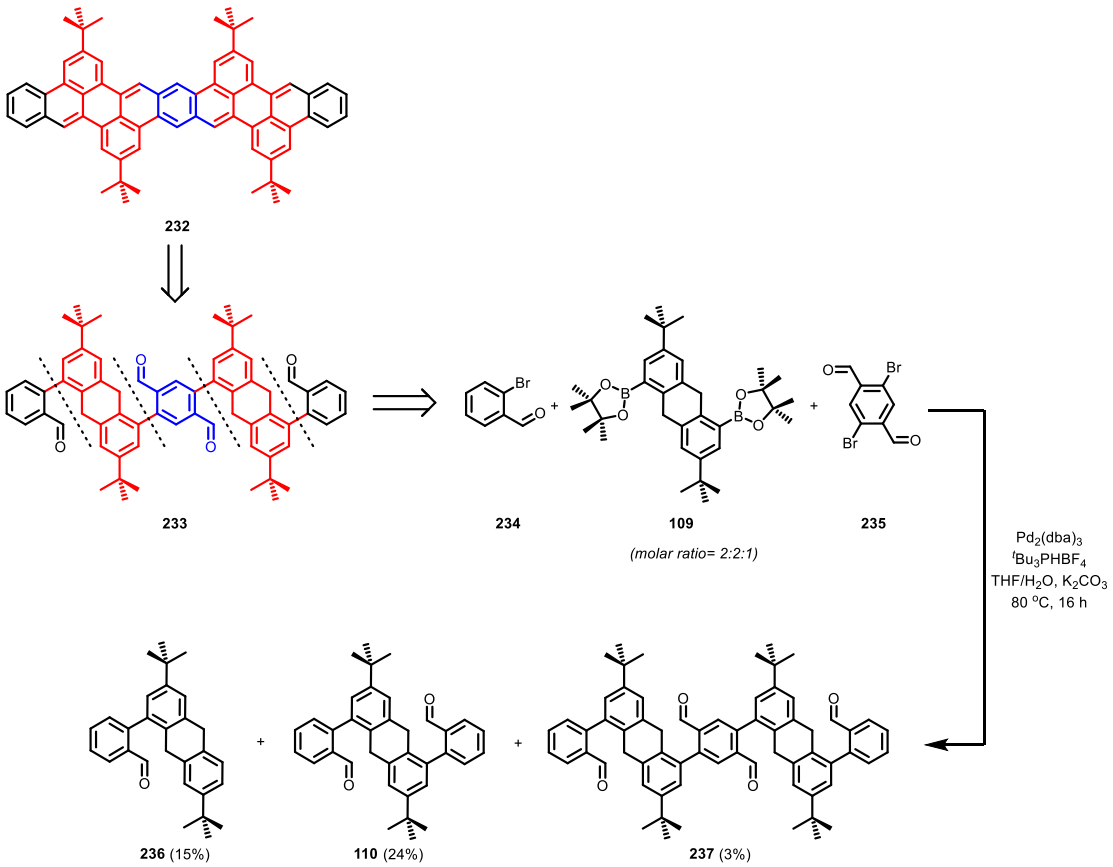

Scheme 3.3.5 Synthesis of the tetraaldehyde precursor **232** for perylene oligomer **232** by one-step reaction.

3.3.2.2 Route B

One reasonable route to the aromatic aldehyde precursor is to apply step-by-step reactions with precise control of the products in each step. As shown in Scheme 3.3.6, the two aromatic boronic esters **241** and **242** were proposed to serve as the possible intermediates. They should react with bromotriptycylaldehyde **233** to obtain corresponding aldehyde precursor **243** or **244**, respectively, which could be converted to PO-9 (**229**) by intramolecular condensation.

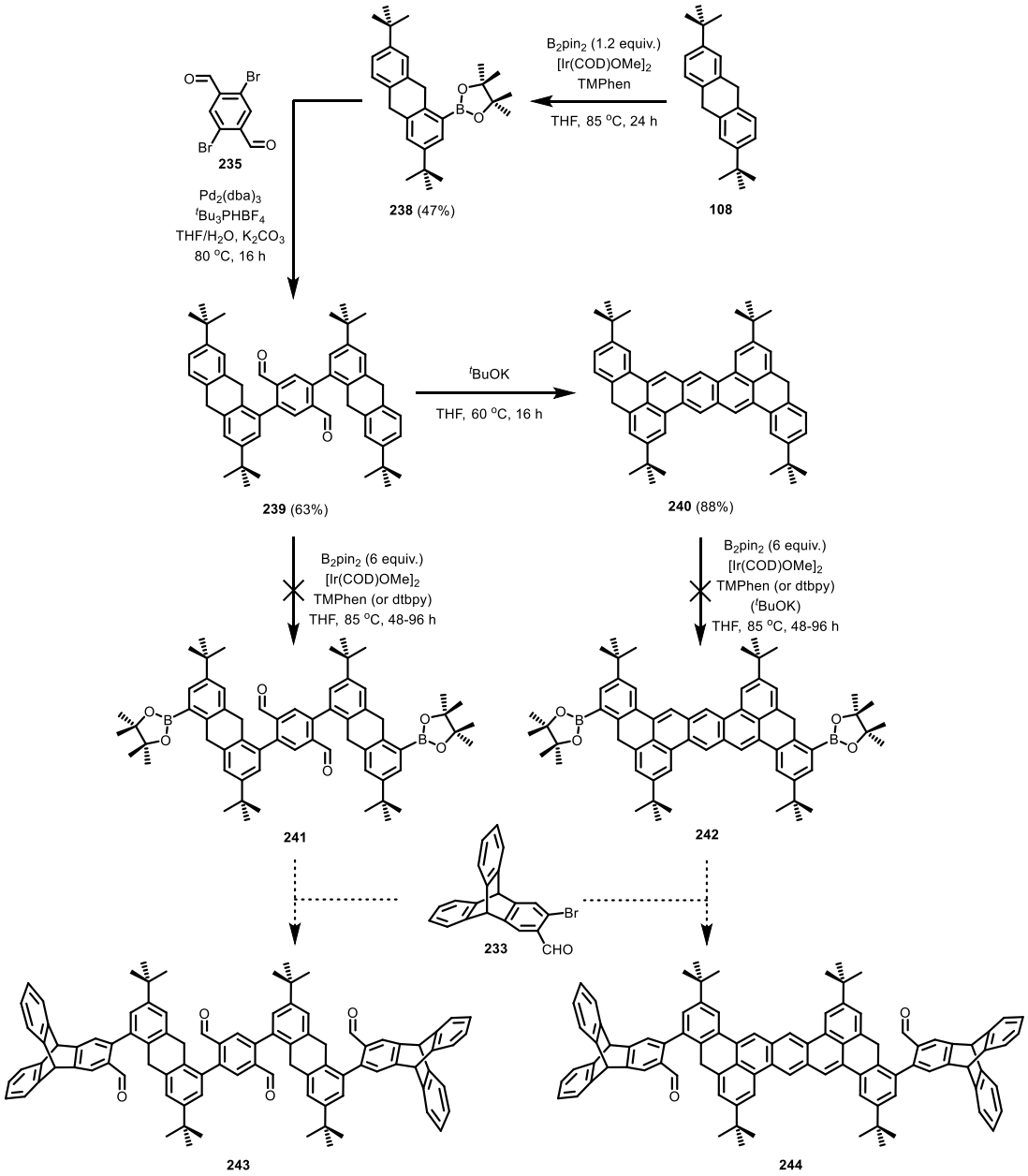

Scheme 3.3.6 Synthesis of the tetraaldehyde precursor **243** or dialdehyde precursor **244** for PO-9 (**229**) by direct two-fold borylation via C-H activation of reduced anthracene derivative **239** or **240** as the key step.

In order to obtain diboronic ester **241** or **242**, dihydroanthracene monoboronic ester **238**, which could be isolated in 47% yield by iridium-catalyzed borylation of 2,6-di-*tert*-butyl-9,10-dihydroanthracene **108** using a decreased amount (1.2 equiv.) of B_2pin_2, was reacted with 2,5-dibromoterephthalaldehyde **235** to give two-fold coupling product **239** in 63% yield. **239** could be further converted to condensated product **240** in 88% yield. Unfortunately, the iridium-catalyzed borylation, which proceeds regioselectively and efficiently on the parent dihydroanthracene **108**,[128b] did not work in both cases of longer compounds **239** and **240**. A condition screening was performed by using different ligands (dtbpy or TMPhen), adding additional bases (*eg*. *t*-BuOK) and running the reaction for different time (48-96 h), whereas no conversion was observed in each case.

The unreacted substrates were recollected after precipitation from CH_2Cl_2/methanol in > 90% yields in all cases. Another method still has to be explored.

3.3.2.3 Route C

Although intermediate **241** was not obtained by direct borylation via C-H activation by *Route B*, it is still valuable during the synthetic procedures of tetraaldehyde **243**, as diboronic ester **241** could be further broken down to two subunits **109** and **235** (Scheme 3.3.7). Reacting of two bifunctional substrates may produce oligomers or polymers in the cross-coupling reactions, which is controversy to the idea of precisely controlling the product in each step. However, the oligomerization or polymerization could be suppressed by applying one of the two bifunctional substrates in excess amount, which is already proven to be effective in synthesizing ladder-type benzo[k]tetraphene-derived oligomers.[34]

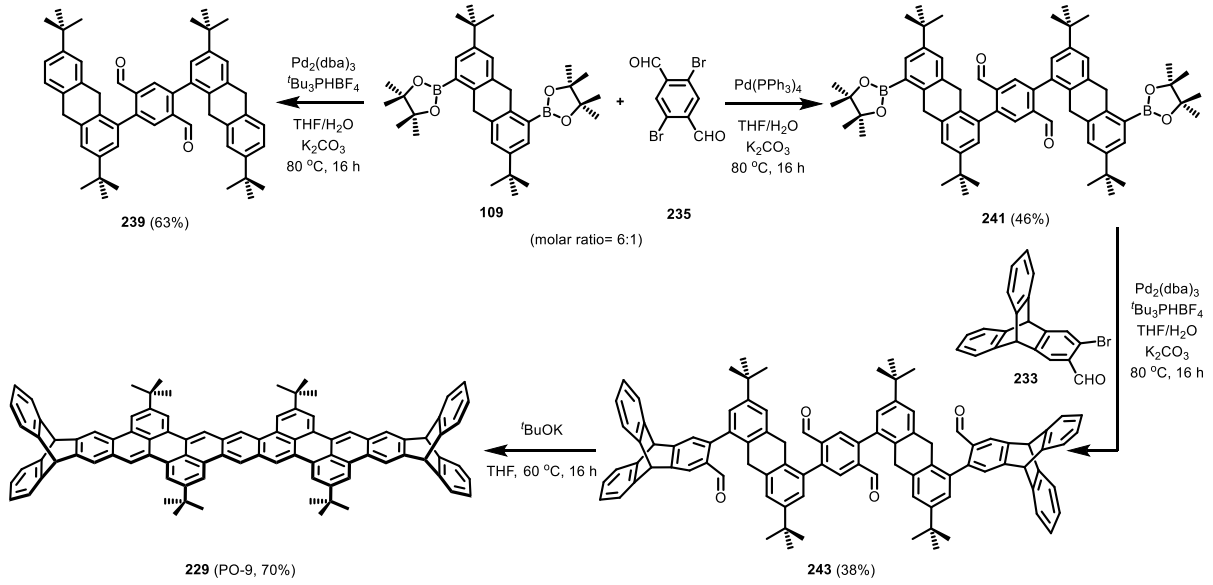

Scheme 3.3.7 Synthesis of PO-9 (**229**) via diboronic ester intermediate **241**. The palladium catalyst load is 10 mol% in all cases.

Following this idea, a Suzuki-Miyaura cross-coupling reaction between diboronic ester **109** and 2,5-dibromoterephthalaldehyde **235** in a molar ratio of 6:1 was performed (Scheme 3.3.7). The reaction was first performed in the presence of $Pd_2(dba)_3$/*t*-Bu_3PHBF_4. However, the reaction did not work as the isolated double coupled product was found to be deborylated,[206] giving compound **239** in 63% yield. By using $Pd(PPh_3)_4$ as a catalyst with the same loading (10 mol%) as $Pd_2(dba)_3$, the intermediate **241** was isolated after cross-coupling reaction in 46% yield. Diboronic ester **241** could be isolated from the residual diboronic ester **109** by flash silica gel column chromatography.

The success of this reaction offers the opportunities to construct the linearly π-extended perylene oligomers. Reacting diboronic ester **241** with bromotriptycylaldehyde **233** in Suzuki-Miyaura cross-coupling reaction under Fu conditions gave the tetraaldehyde **243** in 38% yield,

which could be converted to triptycene end-capped perylene oligomer PO-9 (**229**) as an orange-red solid in 70% yield. PO-9 (**229**) exhibits good solubilities (> 5 mg·mL^{-1}) in common organic solvents, such as CH_2Cl_2, $CHCl_3$ or chlorobenzene.

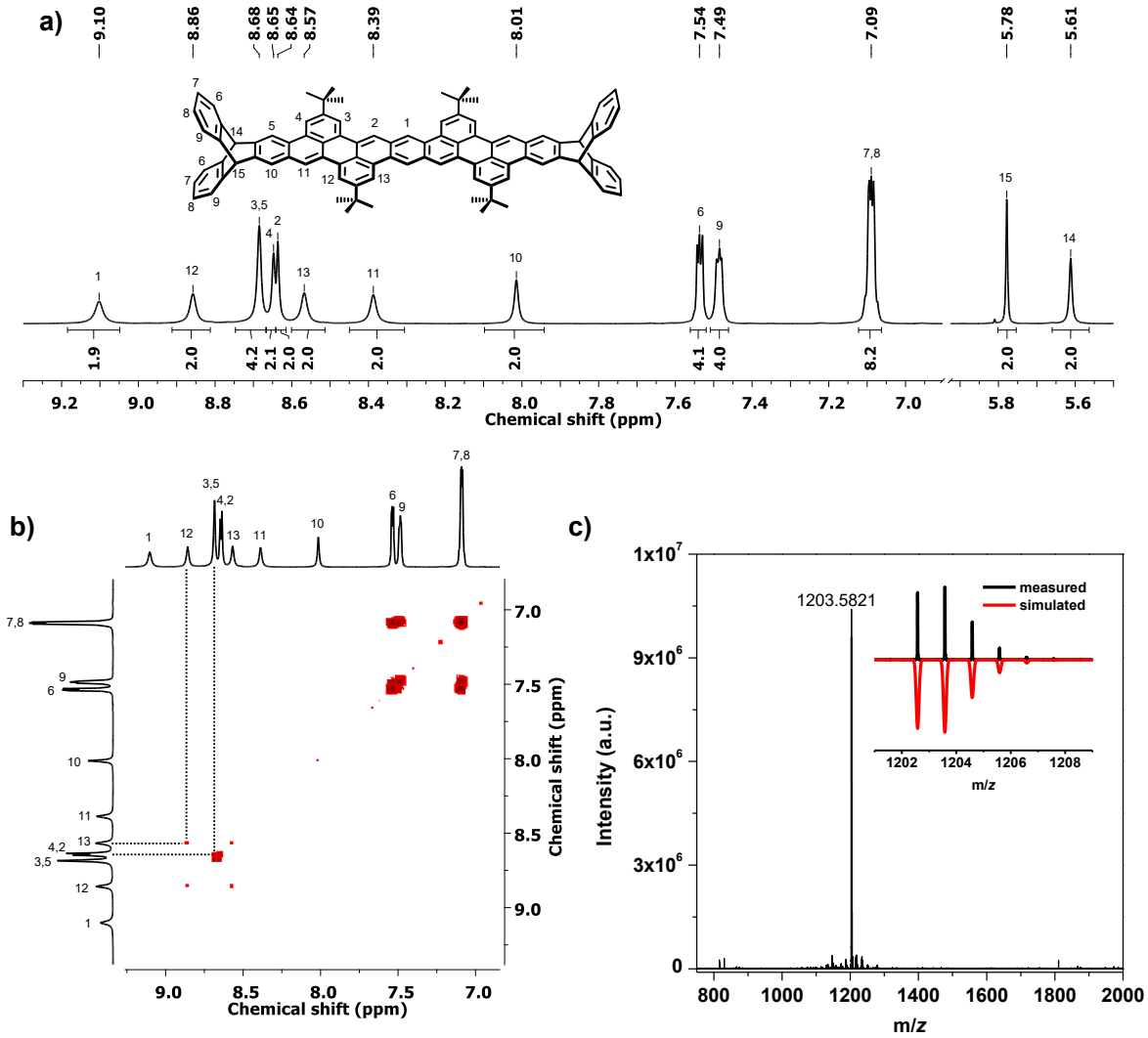

Figure 3.3.2 a) ^{1}H NMR spectrum (600 MHz, $Cl_2CDCDCl_2$, 298 K) of PO-9 (**229**). Depicted is only the aromatic region. For full spectrum, see Figure 7.138. b) ^{1}H-^{1}H COSY NMR spectrum (600 MHz, $Cl_2CDCDCl_2$, 298 K) of PO-9 (**229**). c) MALDI HRMS (DCTB, linear positive mode) of PO-9 (**229**).

High resolution mass spectrum (MALDI) (Figure 3.3.2c) with a monoisotopic signal of m/*z* = 1203.5821 (calcd. for $[M]^+$, $C_{94}H_{74}$, 1203.5824) and the fitting isotopic distribution pattern to the simulated one indicate the formation of this triptycene end capped perylene dimer π-framework. A well-resolved ^{1}H NMR spectrum of PO-9 (**229**) was obtained in TCE-d_2 at room temperature (Figure 3.3.2a). H-3, 4, 12 and 13 at the *ortho*-positions of the *tert*-butyl groups could be identified by the correlations shown by the 2D ^{1}H-^{1}H COSY NMR spectrum (Figure 3.3.2b). The most down-field shifted singlet at 9.10 ppm of this π-framework could be assigned to the proton on the central benzenoid ring connecting two perylene units (H-1).

Single crystals of PO-9 (**229**) suitable for X-ray diffraction analysis have been obtained by diffusing *n*-hexane vapor into a solution of **229** in CH_2Cl_2, which confirms the molecular structure of this perylene oligomer (Figure 3.3.3). PO-9 (**229**) crystallizes in the triclinic space group $P\ \bar{1}$ and adopts a planar π-backbone, which is similar to parent dibenzoperylene **111**.[128b] The length of the central nonacene π-framework is 2.21 nm.

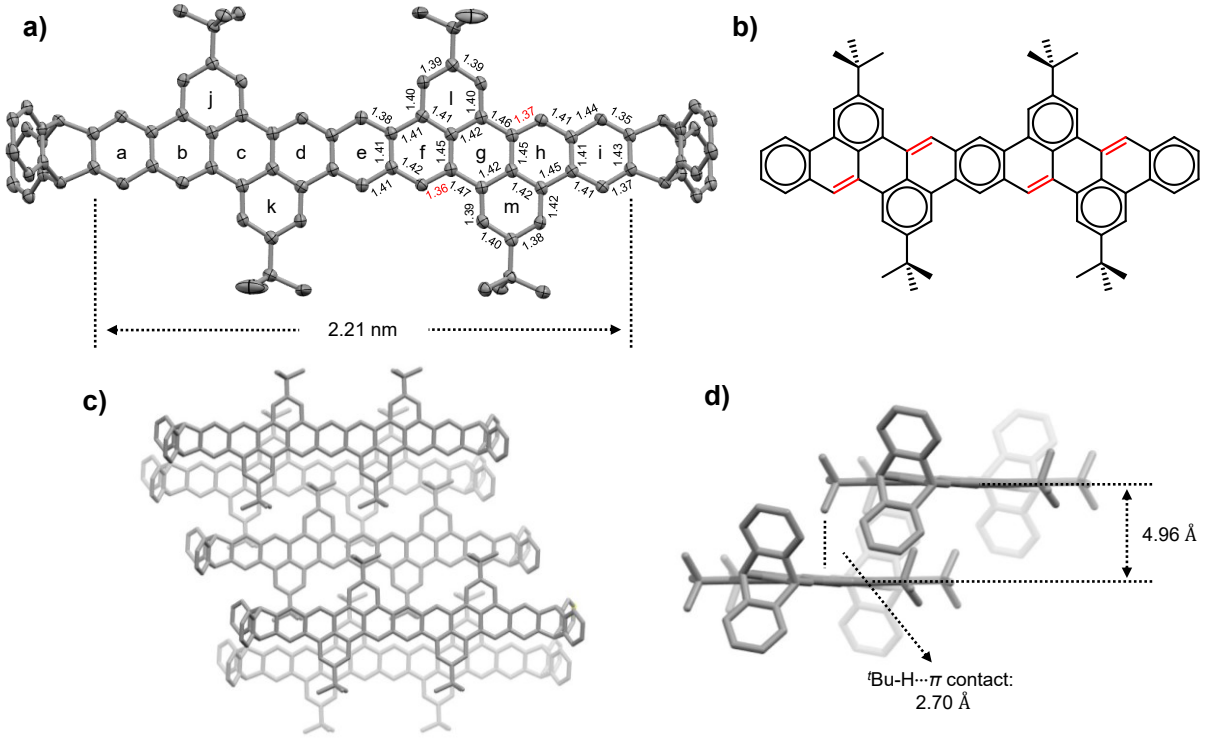

Figure 3.3.3 Single crystal X-ray structure of PO-9 (**229**). (a) An ORTEP plot with thermal ellipsoids set at 50% probability. C-C bond lengths are given in Å. (b) A depicted model of PO-9 (**229**) according to Clar's sextet rule. Isolated C-C double bonds are highlighted in red. (c) Packing motif. (d) A close view of two molecules in one unit cell. Hydrogen atoms as well as enclathrated solvent molecules have been omitted for clarity.

The crystallographic data quality is high enough to analyze the C-C bond lengths in detail. The C-C bonds of the central benzenoid ring (e) connecting two perylene units are in the range of 1.38-1.41 Å. The average C-C bond lengths of this six-membered ring is smaller than other rings of this π-framework. Slightly longer C-C bond lengths (1.39-1.42 Å) could be observed on the four rings (j-m) substituted with *tert*-butyl groups and the two end rings (a and i) shared with triptycyl end groups. Exception is one bond of 1.44 Å on the periphery impacted by the triptycene end groups.[197d] The distribution of these rings on the molecular π-backbone is in accordance with the depicted model of PO-9 (**229**) according to Clar's sextet rule in Figure 3.3.3b.[161] Within the two perylene moieties, the C-C bonds linking two *peri*-positions of the naphthalene units are relatively long (1.45-1.47 Å), which is consistent with the crystal structure[147a] and calculated model[207] of unsubstituted perylene **1**. The lengths of the four C-C bonds at the [*a*] and [*k*] edges of the two perylene units are 1.36-1.37 Å, which are the shortest ones in this π-framework and thus show more olefinic character. Therefore, similar to dibenzoperylene **111**[128b] discussed in chapter 3.1.1,

regioselective functionalization by electrophilic attack would be expected on this longer π-backbone. The oligomer molecules are arranged in an offset coplanar fashion. The average distance between two molecular π-backbones in each unit cell is 4.96 Å (Figure 3.3.3d). No π-π interaction was observed in the packing motif.

3.3.4 Synthesis of PO-13

Using a similar synthetic route to the tetraaldehyde precursor **243** (Scheme 3.3.7) for PO-9 (**229**), a possible approach to synthesize hexaaldehyde **246**, which is the precursor of PO-13 (**230**), is presented in Scheme 3.3.8.

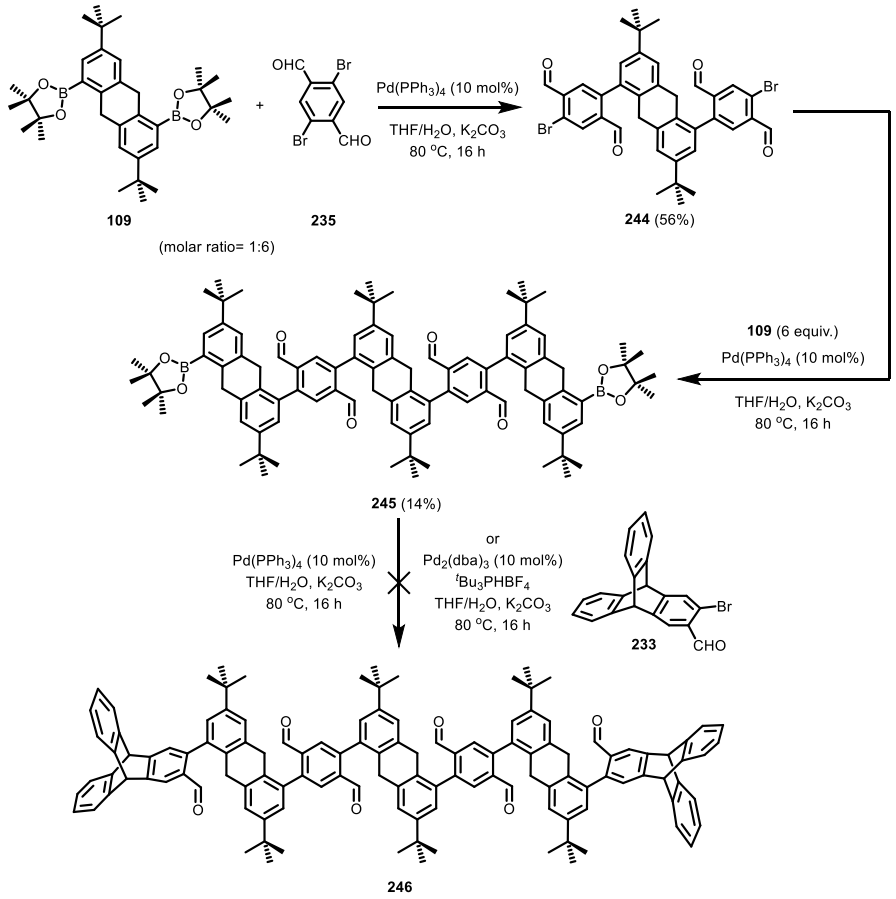

Scheme 3.3.8 Synthesis of the hexaaldehyde precursor **246** for PO-13 (**230**) via the diboronic ester intermediate **245**.

In this case, hexaaldehyde precursor **246** could be further broken down to bromotriptycylaldehyde **233** and diboronic ester intermediate **245** containing three dihydroanthracene moieties. By switching the molar ratio of **109** and **235** to 1:6 in the cross-coupling reaction, dibromide intermediate **244** was obtained in 56% yield. The diboronic ester **245** was then isolated after the reaction of **244** with six equiv. of **109** by flash silica gel column chromatography and recycling gel permeation chromatography (*r*-GPC) in 14% yield. Unfortunately, any attempt to synthesize hexaaldehyde precursor **246** in the following cross-coupling reaction between diboronic ester **245** and bromotriptycylaldehyde **233** failed. Only two

substrates (**245** and **233**) were recollected after refluxing the mixture overnight with vigorous stirring using $Pd_2(dba)_3$/*t*-Bu_3PHBF_4 or $Pd(PPh_3)_4$ as catalyst. The relative low solubility of **245** in THF may account for the failure. Therefore, this synthetic route should be optimized to ensure the solubility of the substates.

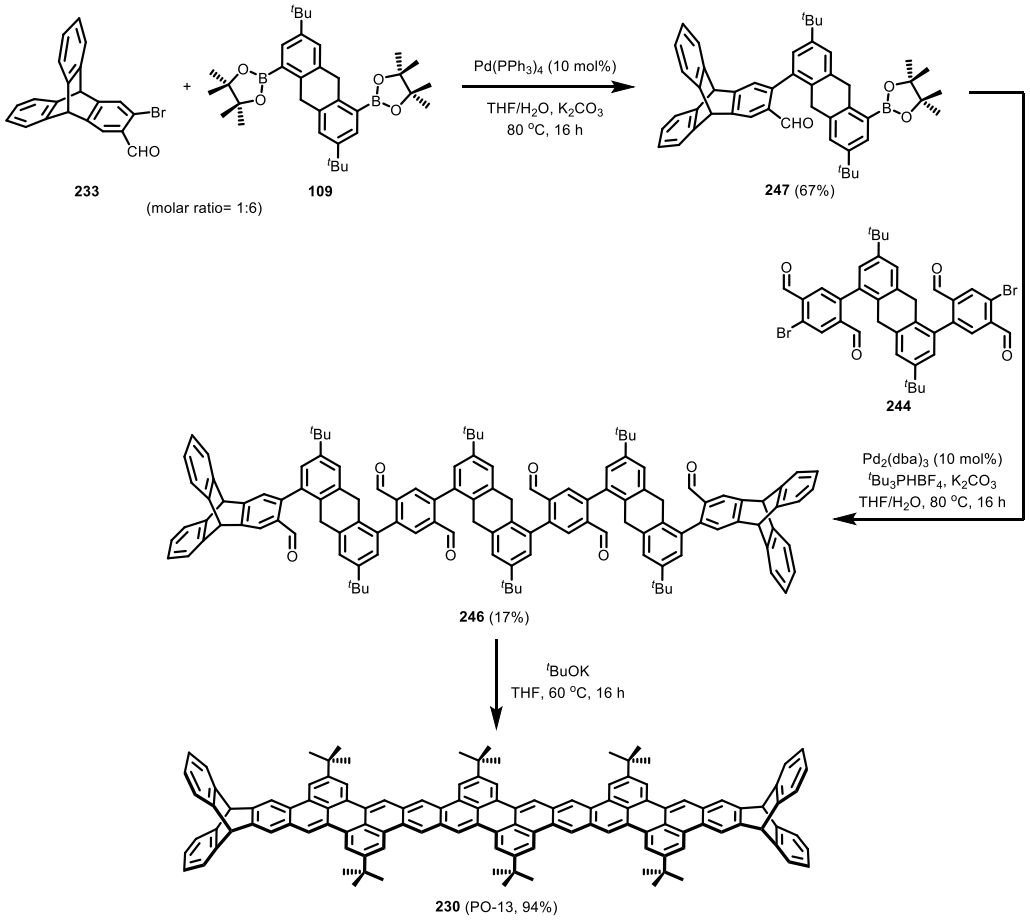

Scheme 3.3.9 Synthesis of PO-13 (**230**) via the hexaaldehyde precursor **246**.

The C-C bond formed during the two-fold cross coupling reaction to hexaaldehyde precursor **246** was reconsidered. The bond breaking positions were moved to the center by one dihydroanthracene unit, giving dibromide **244** and monoboronic ester intermediate **247** (Scheme 3.3.9). Monoboronic ester **247** was obtained by the cross-coupling reaction between bromotriptycylaldehyde **233** and diboronic ester **109** with a molar ratio of 1:6 in 67% yield. Reacting **247** with dibromide **244** in the following cross-coupling reaction under Fu conditions produced hexaaldehyde **246** in 17% yield. Flash silica gel column chromatography and *r*-GPC were necessary to completely purify **246** from the one-fold coupled byproduct. The structure of hexaaldehyde **246** was confirmed by ^{1}H NMR spectrum (Figure 3.3.4). With the increase of the number of dihydroanthracene and terephthalaldehyde units in the molecular framework, the signals for the aldehyde groups of the terephthalaldehyde units appear at 9.89-9.95 ppm on tetraaldehyde **243** and hexaaldehyde **246**. From dialdehyde **234** to hexaaldehyde **246**, signals for protons on the

dihydroanthracene and triptycene units are broadening, due to the increasing number of atropisomers caused by the rotations of C-C single bonds formed during the cross-coupling reactions. Treating hexaaldehyde **246** with *t*-BuOK in hot THF gave PO-13 (**230**) as a dark-red solid in a nearly quantitative yield of 94%. These results indicate that the appropriate combination of two intermediates in the cross-coupling reactions plays a big role in determining the results of these reactions.

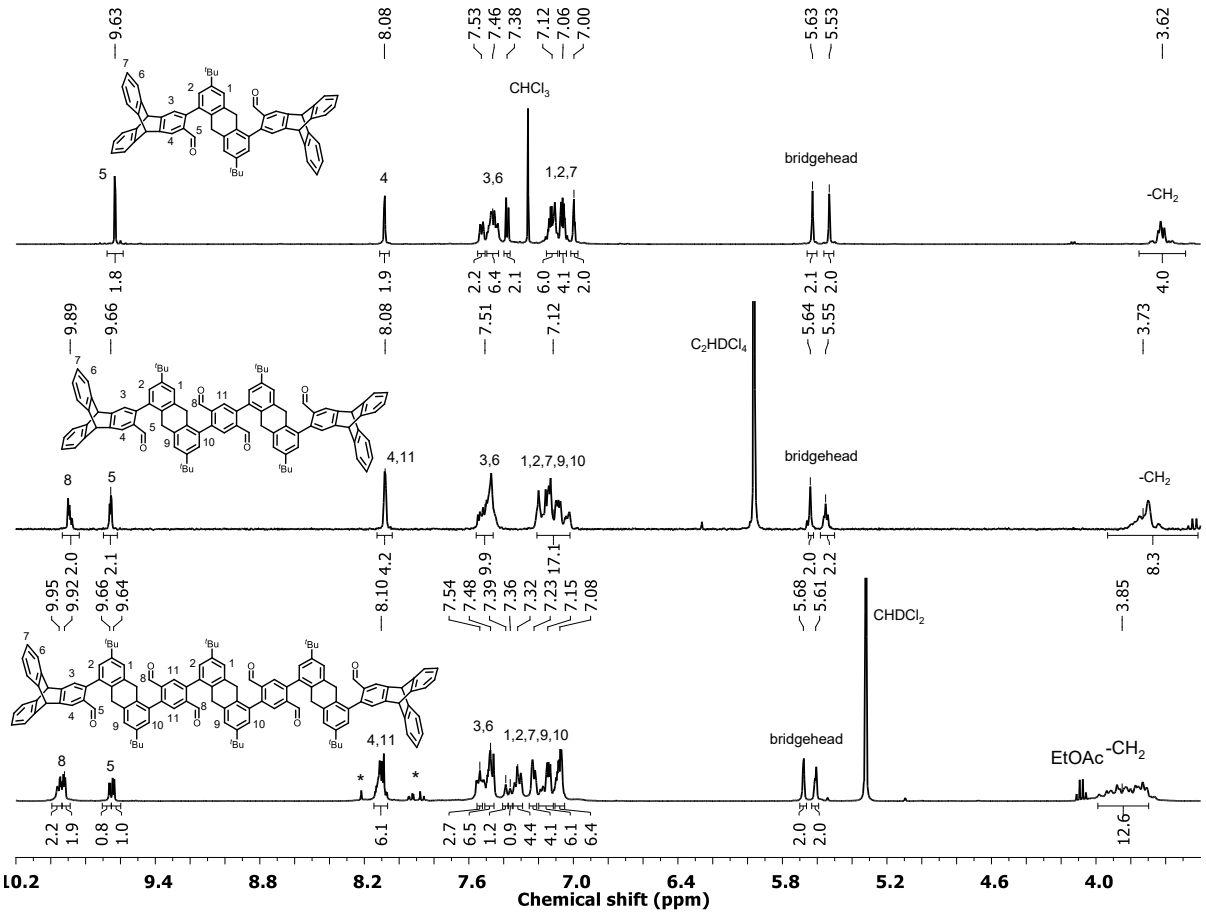

Figure 3.3.4 A comparison of ^{1}H NMR spectra of three aldehyde precursors. Top to bottom: dialdehyde **234** (400 MHz, $CDCl_3$, 298 K), tetraaldehyde **243** (400 MHz, $Cl_2CDCDCl_2$, 298 K) and hexaaldehyde **246** (400 MHz, CD_2Cl_2, 298 K). *Impurities.

The low yield of 17% in the reaction between dibromide **244** and monoboronic ester **247** limits the overall yield of PO-13 (**230**). One reason for the low yield is the relatively low stability of the six aldehyde groups during the reaction process, which may be disproportionated by Cannizzaro reactions in the presence of base (K_2CO_3).[208] Thus, another synthetic route with the protection of the aldehyde groups was performed (Scheme 3.3.10). The two aldehyde groups on dibromide **235** were reacted with ethylene glycol to form diacetal **248** in 66% yield, which was further reacted with diboronic ester **109** to produce protected intermediate **249**. The aldehyde group on compound **247** could be consumed by cyclization to give compound **250** in 80% yield. The obtained condensated monoboronic ester **250** was reacted with **249** to produce the protected

precursor **251** in 43% yield, which is higher than that (17%) of the reaction producing unprotected precursor **246** (Scheme 3.3.9). After deprotection and final condensation, PO-13 (**230**) was obtained. In comparison to that route using intermediates without the protection of the aldehyde groups (Scheme 3.3.9), the overall yield (29%) starting from compound **247** in this revised route is higher than that (16%) of the route shown in Scheme 3.3.9, although there were two more steps.

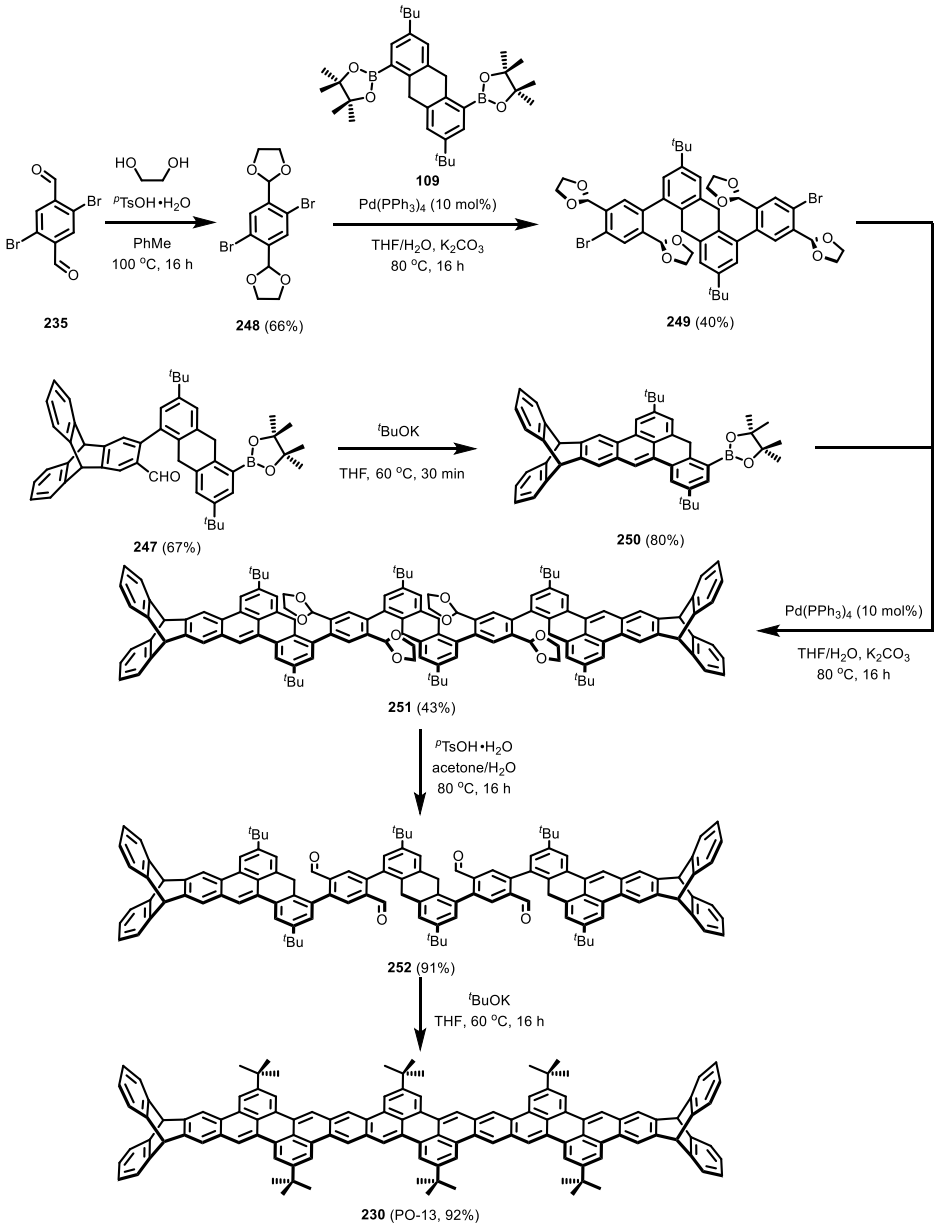

Scheme 3.3.10 Synthesis of PO-13 (**230**) via the protected intermediate **251**.

MALDI HRMS of PO-13 (**230**, Figure 3.3.5) with a monoisotopic signal of m/*z* = 1589.7857 (calcd. for $[M]^+$, $C_{124}H_{100}$, 1589.7858) and a fitting isotopic distribution pattern to the simulated one indicate the formation of this triptycene end capped π-framework with three perylene moieties.

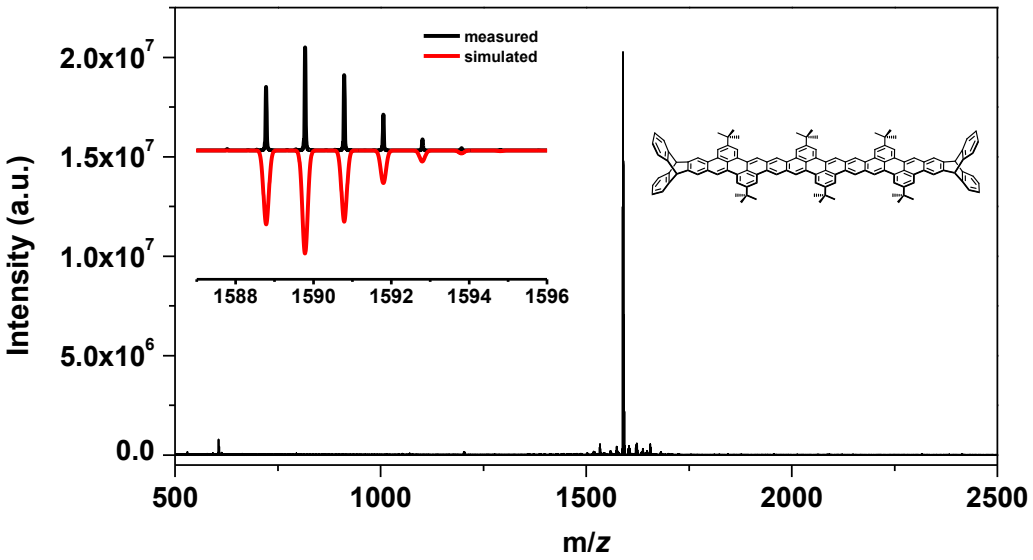

Figure 3.3.5 MALDI HRMS spectrum of PO-13 (**230**, DCTB, linear positive mode).

A ^{1}H NMR spectrum of PO-13 (**230**) recorded in $Cl_2CDCDCl_2$ at room temperature is shown in Figure 3.3.6b. Compared with that of the hexaaldehyde precursor **246** (Figure 3.3.6a) before intermolecular condensation, signals for the protons on the aldehyde groups (H-5, 8) disappear in the ^{1}H NMR spectrum of PO-13 (**230**), suggesting that all of the aldehyde groups were consumed during the reaction. The chemical shifts of the signals in the ^{1}H NMR spectrum of PO-13 (**230**) are quite similar to the signals in that of PO-9 (**229**, Figure 3.3.6c). One signal at δ = 9.18 ppm could correlate to the protons H-1, 14 on the benzene rings connecting two perylene units. Signals at δ = 7.50 and 7.08 ppm as well as two singlets at δ = 5.77 and 5.62 ppm for the bridgeheads indicate the presence of triptycene units. However, the ^{1}H NMR spectrum of PO-13 (**230**) is less resolved than that of the shorter oligomer PO-9 (**229**). If the integrals of the two signals for the two triptycene units were set to eight, the integrals of the other signals in the aromatic region are smaller than the expected values. For instance, the signal at δ = 9.18 ppm, which is expected to correlate to four protons (H-1, 14), only gives an integral of 0.8.

The ^{1}H NMR spectrum for PO-13 (**230**) was also measured in other deuterated solvents such as $CDCl_3$, THF-d_8, $Cl_2CDCDCl_2$ (containing 10 vol% CS_2) and aromatic solvents like benzene or *o*-DCB, but the results were all similar to that in $Cl_2CDCDCl_2$ shown in Figure 3.3.6b. ^{1}H NMR spectrum in $Cl_2CDCDCl_2$ at higher temperature (100 °C) was also measured but only gave a similar pattern with that recorded at room temperature. Measurements at low temperature (-30 °C) did not help to obtain a better resolved spectrum, suggesting that the poor resolution of the ^{1}H NMR spectrum for PO-13 is not caused by the open-shell biradical character, which was predicted to be present in polyacene species.[192] It is supposed that strong π-stacking exists between these perylene oligomer molecules, even after the introduction of triptycene end groups.

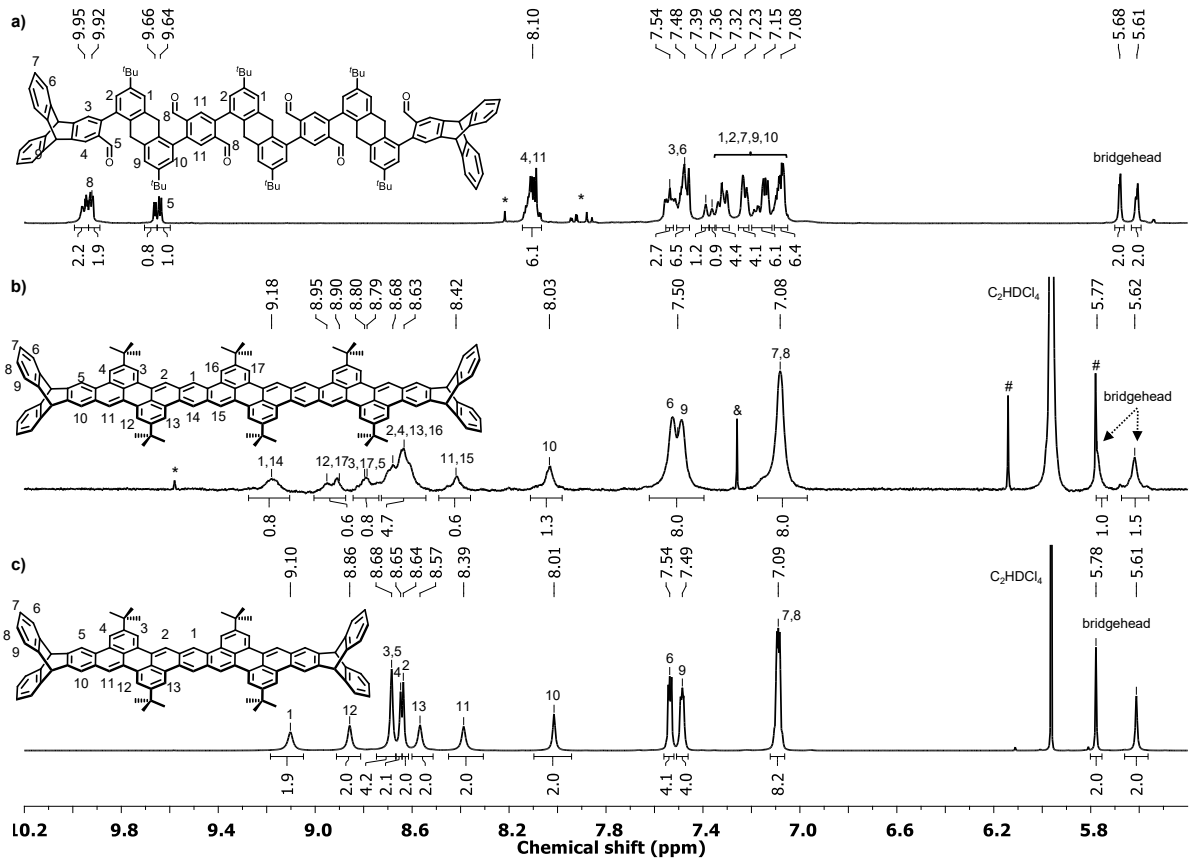

Figure 3.3.6 A comparison of ^{1}H NMR spectra of hexaaldehyde precursor **246** (a, 400 MHz, CD_2Cl_2, 298 K), PO-13 (**230**, b, 500 MHz, $Cl_2CDCDCl_2$, 298 K, c = 1.3 mmol·L^{-1}) and PO-9 (**229**, c, 600 MHz, $Cl_2CDCDCl_2$, 298 K, c = 11.0 mmol·L^{-1}). Only the aromatic regions are shown. *Impurities. #Satellite peaks of $Cl_2CHCHCl_2$ solvent. &Residual $CHCl_3$.

3.3.5 Attempts to Synthesize PO-17

Although a well-resolved ^{1}H NMR spectrum of perylene oligomer PO-13 (**143**) was not obtained, the fitting and clean MALDI HRMS indicates the successful synthesis of this oligomer. It is still worth to try a further linear extension to an oligomer containing four perylene units (PO-17, **231**).

The synthesis of PO-17 (**231**) starts with reacting monoboronic ester **247** with four equiv. of 2,5-dibromoterephthalaldehyde **235** giving monobromide **253** in 64% yield (Scheme 3.3.11). The reaction of diboronic ester **241** with triptycyl fragment **253** gave octaaldehyde **254** in 9 % isolated yield after purification by silica gel column chromatography and *r*-GPC. The molecular structure of octaaldehyde **254** was confirmed by ^{1}H NMR spectroscopy (Figure 3.3.7).

After treating octaaldehyde **254** with 30 equiv. of *t*-BuOK in dry THF at 60 °C overnight, an orange-red product was obtained after precipitation from methanol and washing with water and methanol. The obtained product was characterized by MALDI-TOF spectrum, which exhibits a complex result (Figure 3.3.8).

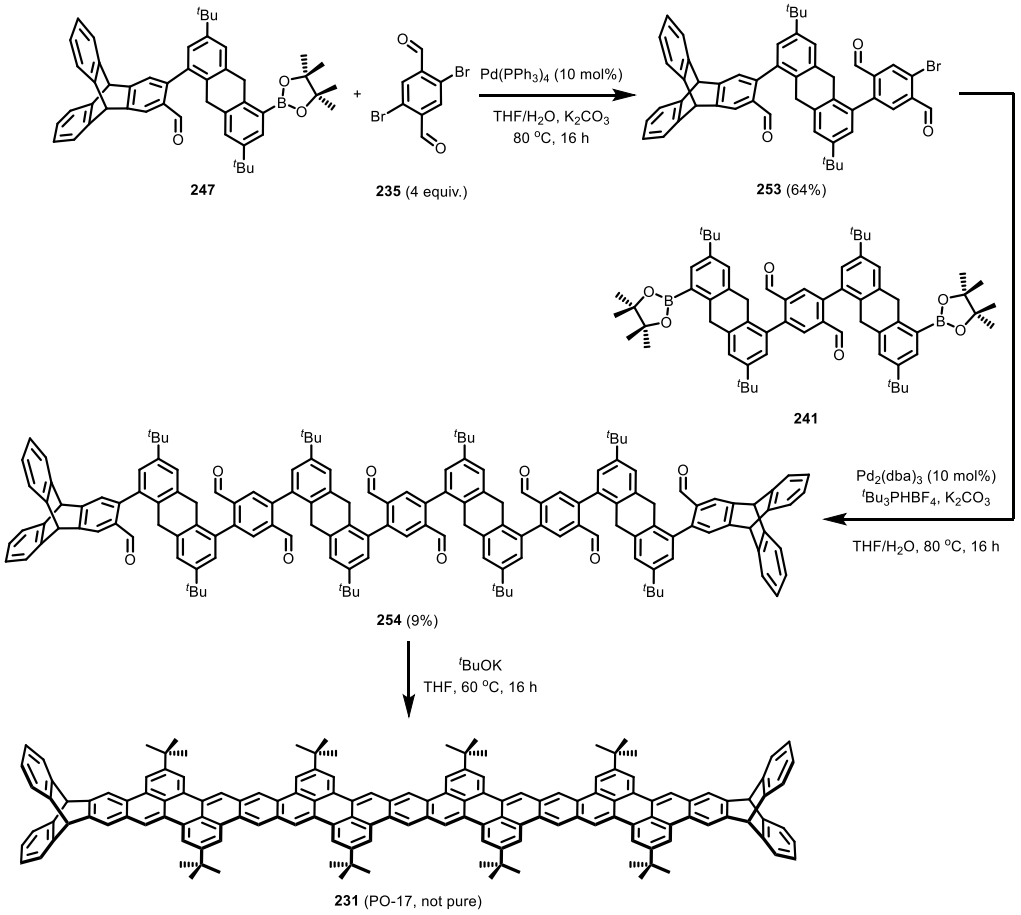

Scheme 3.3.11 Attempt to synthesize PO-17 (**231**) from octaaldehyde precursor **254**.

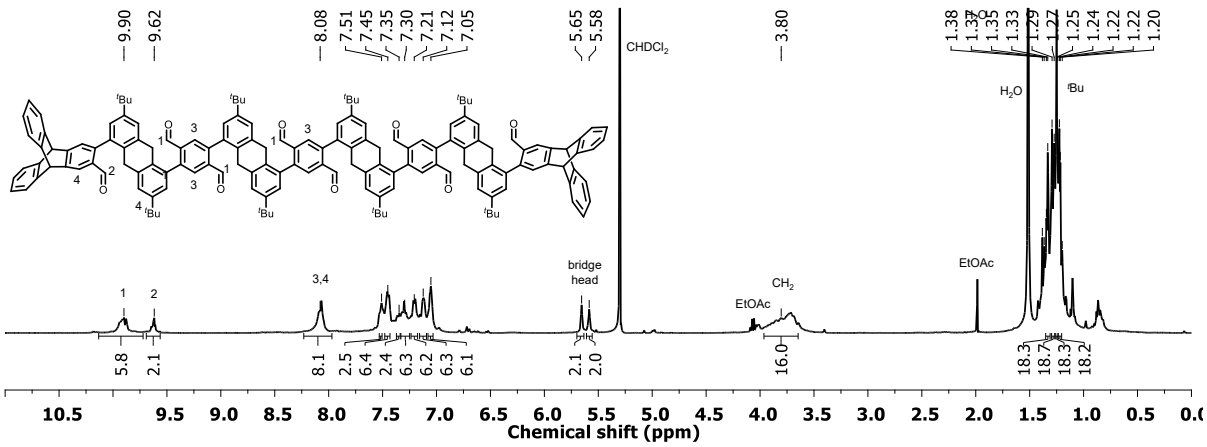

Figure 3.3.7 ^{1}H NMR spectrum (400 MHz, CD_2Cl_2, 298 K) of octaaldehyde **254**.

The monoisotopic signal of m/*z* = 1975.209 (calcd. for $[M]^+$, $C_{154}H_{126}$,1974.986) and a fitting isotopic distribution pattern to the calculated one (Figure 3.3.8) indicate that formation of the triptycene end capped perylene tetramer (PO-17, **231**). However, some other peaks for new species formed during the reaction were observed. As indicated in Figure 3.3.8, these signals suggest the uncomplete condensation (ring-closure), which could be ascribed to the formation of up to four carboxyl groups from the corresponding aldehyde groups. On the other hand, the signals for

hydroxy groups (-CH_2OH) were also observed. As shown in Figure 3.3.9, two new peaks at $\tilde{\nu}$ = 1692 cm^{-1} and 1060 cm^{-1} appear in the FT-IR spectrum of this sample in comparison to that of shorter oligomer PO-9 (**229**), which could be assigned to the C=O stretching of the aromatic carboxylic acids and C-O stretching of -CH_2OH groups, respectively.

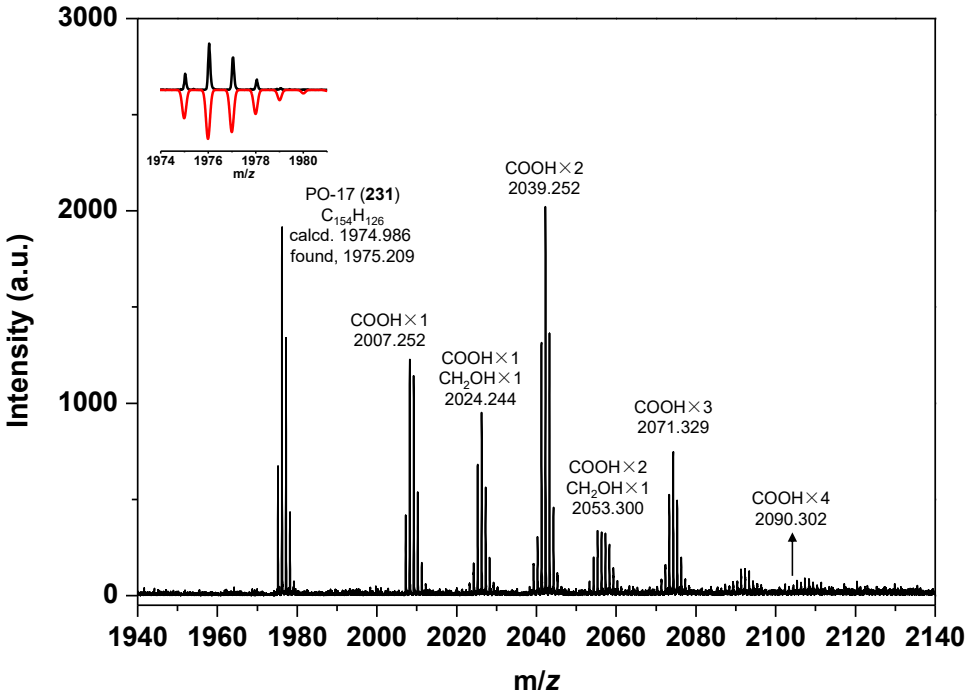

Figure 3.3.8 MALDI-TOF spectrum (DCTB, reflective positive mode) of mixture obtained after treating octaaldehyde **254** with *t*-BuOK in THF. Inserted figure besides the first signal is a comparison of the measured isotopic pattern of this signal (black) with the calculated one (red). COOH×1 means there is one aldehyde group in octaaldehyde **254** oxidized to carboxyl group during the reaction. The values given are the monoisotopic signals of each isotopic distribution pattern.

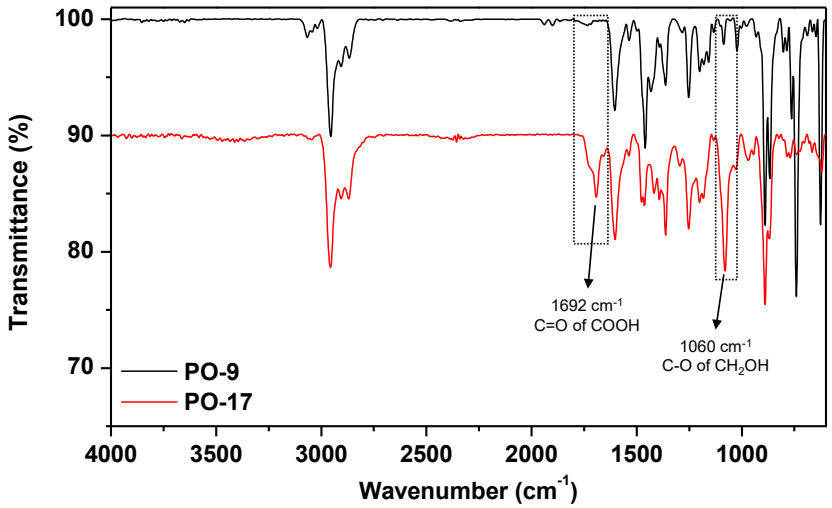

Figure 3.3.9 FT-IR spectra (ATR, neat) of PO-9 (**229**) and PO-17 (**231**, not pure).

Therefore, a Cannizzaro-type disproportionation of aldehyde groups in the presence of strong base (*t*-BuOK) occurred in this reaction.[208] In this case, the base-promoted

disproportionation is competing with the intramolecular condensation, possibly because the reaction rate of the condensation is not as high as those based on the lower level substrates for PO-5 and PO-9. Further purification, such as recrystallization, washing with different solvents and *r*-GPC, were tried, but no improvement was found by measuring MALDI-TOF mass spectra. Silica gel column chromatography is not suitable for this oligomer, as the crude product shows limited solubilities in common organic solvents and there was only one spot with $R_f = 0$ found on the TLC plate using common solvents as eluents, even with *o*-DCB or CS_2.

As the final perylene oligomer is difficult to be purified after the reaction, it is reasonable to find an appropriate condition, which could give the oligomer as pure product directly after workup and precipitation. Thus, condition optimization of the final condensation was performed, by using different bases (KOH, NaOH, Cs_2CO_3 or Et_3N), solvents (toluene, benzene, CH_2Cl_2 or 1,4-dioxane), substrate concentrations (0.1-10 $mmol \cdot L^{-1}$) and temperatures (60 °C or room temperature) of the reaction. But unfortunately, reactions under these conditions neither produced PO-17 nor improved the purity of PO-17.

3.3.6 2D Extension to Coronene Oligomers based on Perylene Oligomers

As discussed in Section 3.3.2.3, by analyzing the bond lengths of the single crystal structure of PO-9 (**229**) in detail, its π-scaffold can be best depicted as the one containing seven Clar sextets (Figure 3.3.3) and the four C-C bonds at the [*a*] and [*k*] edges of the two perylene units exhibit more olefinic character. Therefore, it is possible that this perylene oligomer can also be regioselectively brominated in a similar way with dibenzoperylene **111** (Scheme 3.1.3).

This assumption was experimentally confirmed. Treating PO-9 (**229**) with 4.5 equiv. of NBS in CH_2Cl_2 at room temperature for 1 hour gave the corresponding tetrabromide **256** in a nearly quantitative yield of 94% (Scheme 3.3.12). Triptycyl dibromide **255** was obtained from PO-5 (**228**) under similar conditions in 88% yield. The regioselective bromination was also achieved based on oligomer with three perylene units PO-13 (**230**). The hexabromide **257** was obtained in 85% yield. The molecular structures of the three bromides were confirmed by ^1H NMR spectroscopy (Figure 3.3.10) and MALDI-TOF spectrometry (Figure 3.3.11). Due to the multifold brominations, the isotopic distribution patterns in the mass spectra of both bromides get broadened, but still fit to the simulated ones. The results suggest that the reactivity of electrophilic substitution still remains in the long systems with the same π-scaffolds.

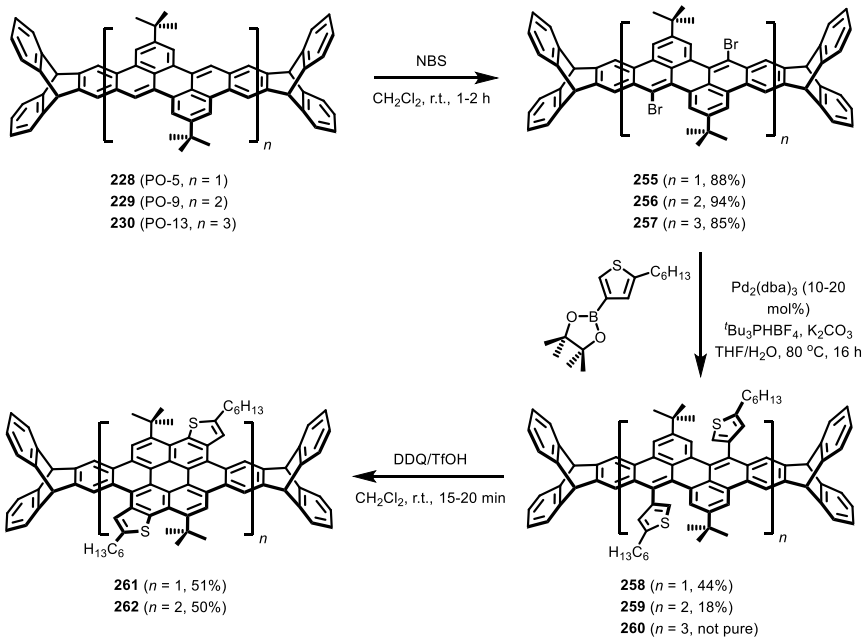

228 (PO-5, *n* = 1)
229 (PO-9, *n* = 2)
230 (PO-13, *n* = 3)

255 (*n* = 1, 88%)
256 (*n* = 2, 94%)
257 (*n* = 3, 85%)

261 (*n* = 1, 51%)
262 (*n* = 2, 50%)

258 (*n* = 1, 44%)
259 (*n* = 2, 18%)
260 (*n* = 3, not pure)

Scheme 3.3.12 2D extension of perylene oligomers (**228**-**230**) by regioselective bromination, Suzuki-Miyaura cross-coupling and Scholl cyclization.

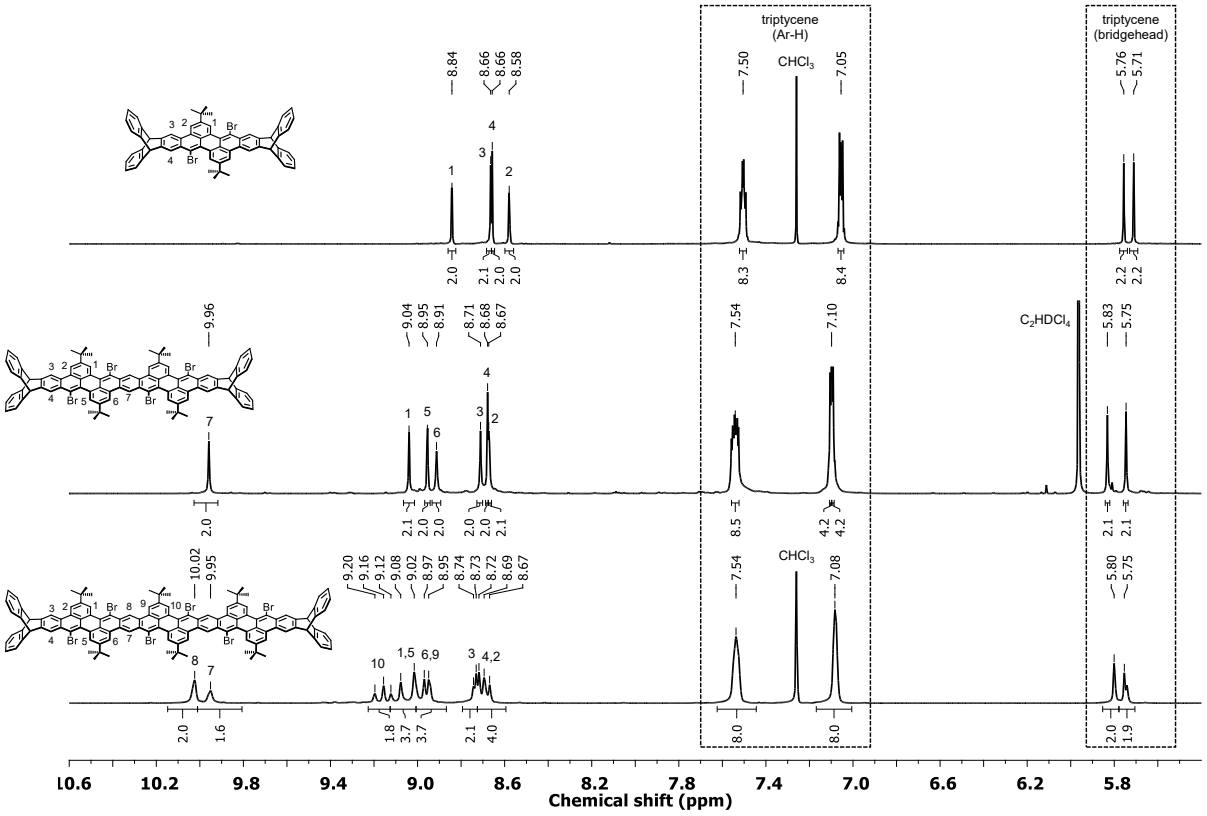

Figure 3.3.10 ^{1}H NMR spectra (600 MHz, 298 K) of dibromide **255** (in $CDCl_3$), tetrabromide **256** (in $Cl_2CDCDCl_2$) and hexabromide **257** (in $CDCl_3$). Only the aromatic regions are shown.

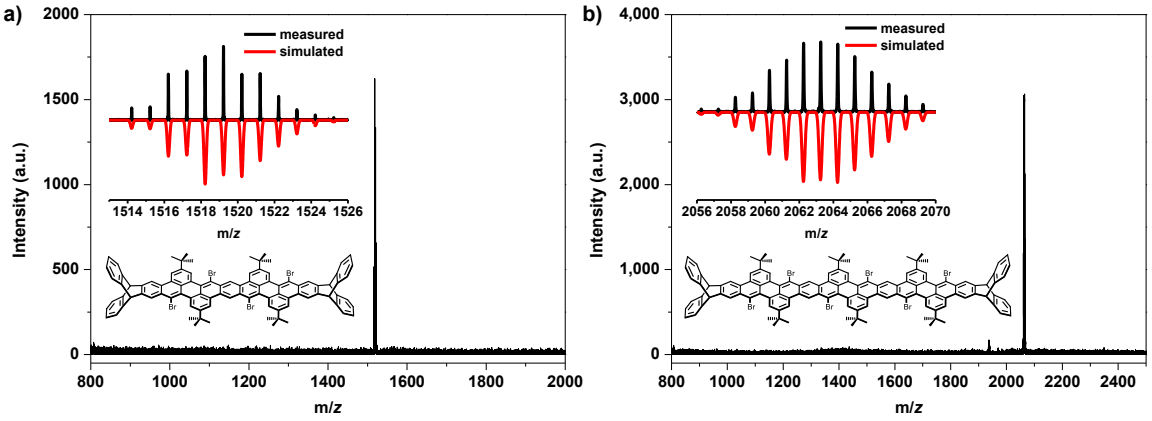

Figure 3.3.11 MALDI-TOF MS (DCTB, reflective positive mode) of tetrabromide **256** (a) and hexabromide **257** (b). Inserted figures are the isotopic distribution patterns of the MALDI HRMS (DCTB, linear positive mode) of the two compounds, in comparison to the corresponding calculated patterns.

These obtained bromides can be further extended by Suzuki-Miyaura cross-coupling reactions with 2-(5-hexylthiophen-3-yl)boronic acid pinacol ester (Scheme 3.3.12). The two-fold and four-fold cross-coupling products **258** and **259** were isolated in 44% and 18% yields, respectively, after performing reactions under Fu conditions by silica gel column chromatography. The reaction to produce six-fold product also works under similar conditions. The product obtained after the reaction and isolated by flash silica gel column chromatography is a mixture of four-fold, five-fold and six-fold products, as indicated by MALDI-TOF spectrometry (Figure 3.3.12), in which the four-fold and five-fold product were debrominated after reaction. Further purification of the desired product **260** was not achieved by silica gel column chromatography, *r*-HPLC (equipped with normal-phase silica gel column or nitrophenyl column), *r*-GPC or preparative TLC. The difference between two cross-coupling products is too small to be differentiated by available separation techniques.

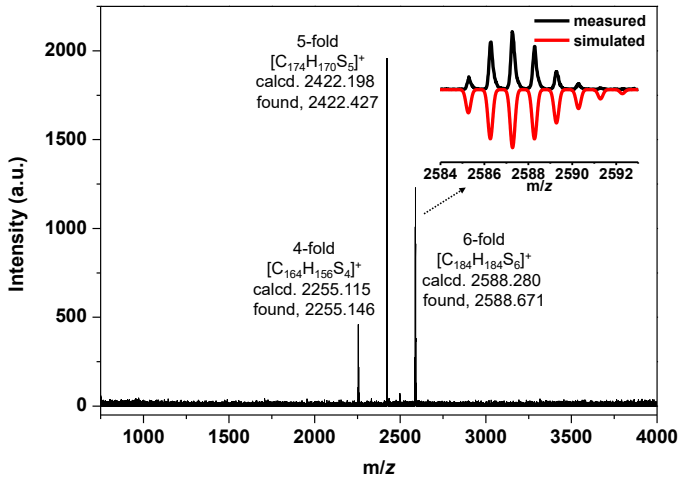

Figure 3.3.12 MALDI-TOF spectrum (DCTB, reflective positive mode) of the mixture obtained after the cross-coupling reaction based on hexabromide **257**.

The isolated pure cross-coupling products **258** and **259** serve as precursors for triptycene end-capped coronene oligomers **261** and **262**, respectively. PAHs containing one or two thiophene-annulated coronenes can be obtained by treating **258** or **259** with DDQ in CH_2Cl_2/TfOH in 51% or 50% yield, respectively (Scheme 3.3.12). MALDI-TOF spectra (Figure 3.3.14) with expected monoisotopic signals and fitted isotopic distribution pattern with the calculated ones indicate the formations of two triptycene end capped perylene monomer **261** and dimer **262**. Well-resolved ^{1}H NMR spectra were obtained in both cases (Figure 3.3.13). With the exception of three new signals for H-5, 6, 7 in coronene dimer **262**, elongation of the π-backbone from monomer to dimer does not affect the chemical shifts of the protons much. The protons on the central benzene ring connecting two perylene units on coronene dimer **262** exhibit a highly down-field shifted singlet at 11.07 ppm.

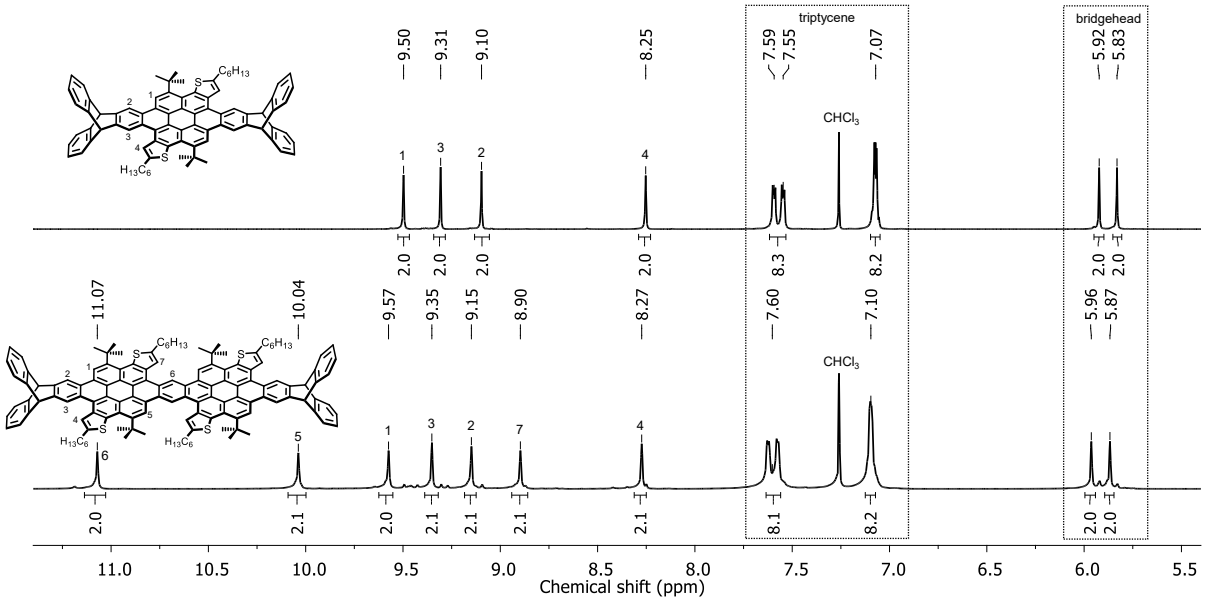

Figure 3.3.13 ^{1}H NMR spectra (600 MHz, 298 K, $CDCl_3$) of coronene oligomers **261** and **262**. Only the aromatic regions are shown.

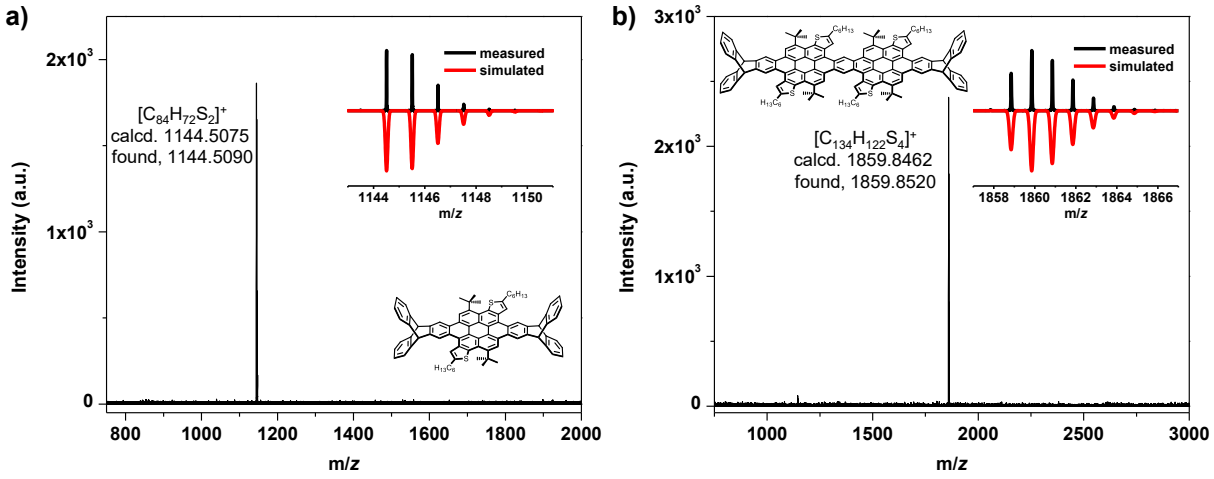

Figure 3.3.14 MALDI-TOF spectra (DCTB, reflective positive mode) of triptycene end capped coronene oligomers **261** and **262**.

3.3.7 Spectroscopic Properties

The three perylene oligomers (**228**-**230**) and two coronene oligomers **261** and **262** were investigated by absorption and emission spectroscopy. FMOs and their corresponding energy levels have been calculated by DFT methods using Gaussian 09 package.[209] The data are summarized in Table 3.3.1.

Well-resolved *β*-band and *p*-band (*π*-*π** transitions) absorptions were observed in all three POs (Figure 3.3.15a). For parent PO-5 (**228**), the absorption maximum at the longest wavelength (*p*-band) is at λ = 449 nm. With the linear extension of the *π*-backbone, a significant bathochromic shift in the *p*-band was observed. The *p*-band absorption of PO-9 (**229**) is red-shifted to λ = 510 nm and PO-13 (**230**) is further shifted to λ = 534 nm. The optical bandgap estimated from absorption onset is getting lower, from E_g = 2.7 eV for PO-5 to E_g = 2.2 eV for PO-13 (Table 3.3.1). The calculated UV/Vis spectra of these three perylene oligomers by TDDFT using the polarized continuum model (PCM) with $CHCl_3$ solvent support this trend (Figure 3.3.15c-e). The predicted absorption maxima at longest wavelengths, which could be assigned to HOMO to LUMO transitions in all cases, are λ = 464 nm for PO-5 (**141**), λ = 554 nm for PO-9 (**142**) and λ = 592 nm for PO-13 (**143**).

Table 3.3.1 Summary of the photophysical characterization of POs (**228**-**230**), coronene oligomers **261** and **262**.

Compd	λ_{max} **[nm]**[a,b]	E_g^{opt} **[eV]**[a,c]	λ_{em} (λ_{ex}) **[nm]**[a,d]	$\tilde{\nu}$ **[cm^{-1}]**[e]	Φ **[%]**[f]	τ **[ns]**[g]
PO-5 (**228**)	449	2.7	462, 494, 530 (422)	627	68±3	2.1
PO-9 (**229**)	510	2.4	523, 562, 610 (475)	487	86±1	1.5
PO-13 (**230**)	534	2.2	549, 591, 645 (499)	512	83±1	1.4
261	434	2.7	487, 516, 550 (371)	2508	7.3±0.1	1.4
262	495	2.4	514, 548 (422)	747	13±0.5	1.1

[a] Measured in $CHCl_3$ at room temperature (c = 2-13 μmol·L^{-1}). [b] Absorption maximum at the longest wavelength. [c] Estimated from absorption onset. [d] Emission maximum. [e] Stock's shift. [f] Fluorescence quantum yield. [g] Fluorescence lifetime.

Besides the bathochromic shifts, extinction coefficients increase significantly with the increase of the length of *π*-backbone. PO-13 gives the highest extinction coefficient of $\varepsilon = 1.66 \times 10^5$ M^{-1}·cm^{-1} at 534 nm. Similar bathochromic shifts were also observed in the fluorescence emission spectra of these perylene oligomers (Figure 3.3.15b). From PO-5 to PO-13, a large bathochromic shift of 87 nm was observed. The solutions of the three POs in chloroform under photoirradiation show obvious differences in colors, from light-blue for PO-5 to yellow-green for PO-9 then finally orange-yellow for PO-13. All three perylene oligomers exhibit high photoluminescent intensities. PO-5 shows similar fluorescence quantum yield of Φ = 68(±3)% to dibenzoperylene **111** without triptycene units.[128b] With the increase of the numbers of perylene

units on the π-framework, quantum yield of over 80% were observed in both PO-9 and PO-13. The energy levels of FMOs estimated by DFT calculations show a clear trend with the increase of molecular length (Figure 3.3.16). From PO-5 to PO-13, the HOMOs are gradually getting increased while LUMOs gradually decrease, leading to smaller bandgaps, which is consistent with the measured optical bandgaps (Table 3.3.1).

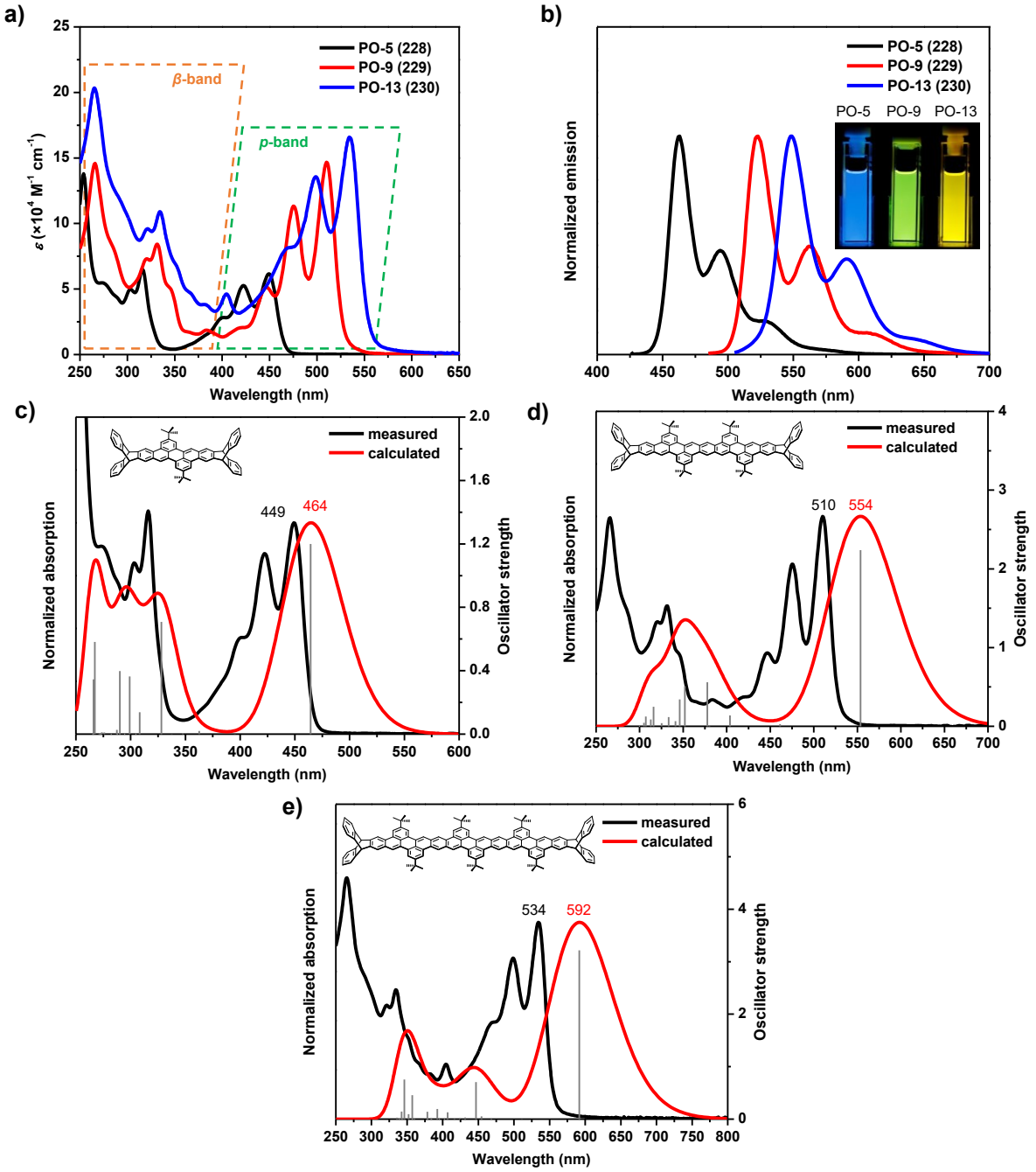

Figure 3.3.15 UV/Vis absorption (a) and fluorescence emission (b) spectra of POs (**228-230**) measured in chloroform at room temperature. Figure inserted in (b) is an optical image of POs (**228-230**) in chloroform (c = 5.0×10^{-6} M) under irradiation at 366 nm. c-e) Comparisons of UV/Vis absorption spectra measured in chloroform at room temperature (black) and calculated UV/Vis absorption spectra based on TDDFT at the B3LYP/6-311G* level with PCM-$CHCl_3$ (red) of POs (**228-230**). Positions for absorption maxima are given in nm.

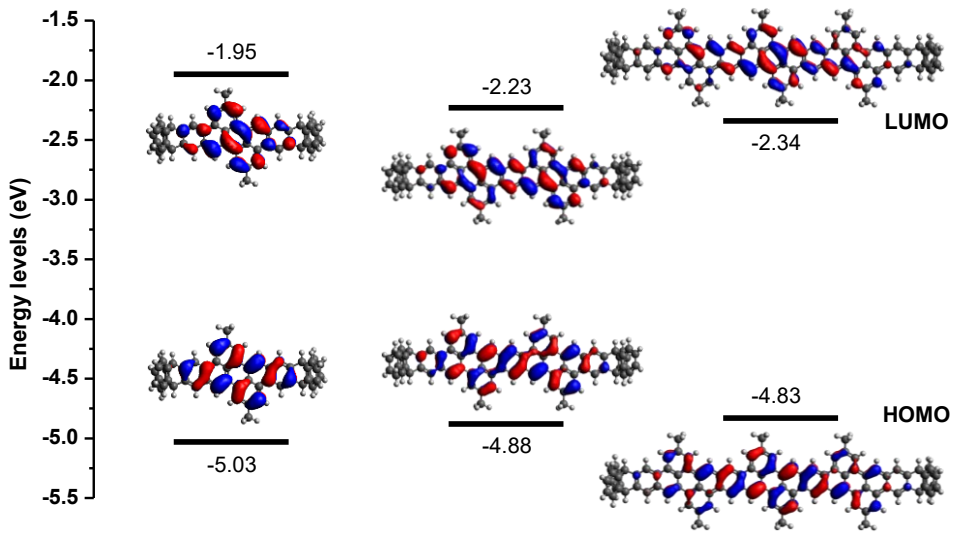

Figure 3.3.16 Frontier molecular orbitals and the corresponding energy levels of POs (**228**-**230**) calculated by DFT at the B3LYP/6-311G* level. The *tert*-butyl groups were replaced by methyl groups for simplification.

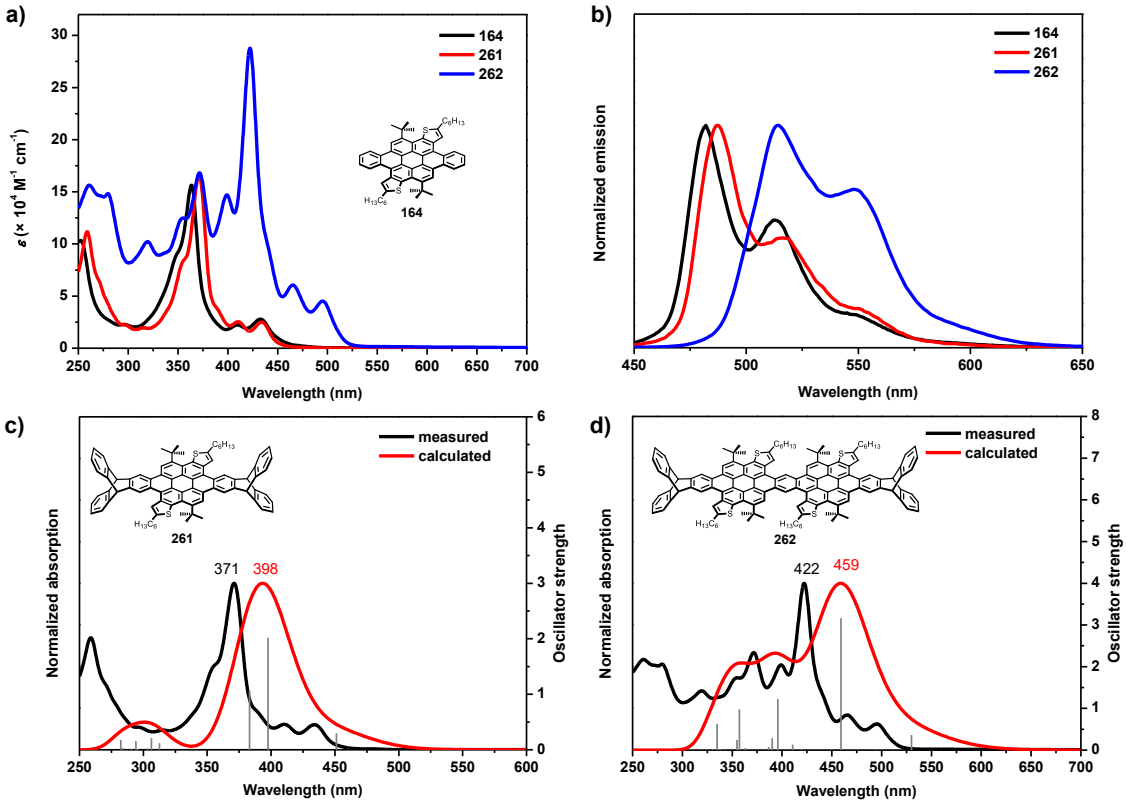

Figure 3.3.17 UV/Vis absorption (a) and fluorescence emission (b) spectra of thiophene-annulated coronene **164** without triptycene end caps and triptycene end capped coronene monomer **261** and dimer **262** measured in chloroform at room temperature. c-d) Comparisons of UV/Vis absorption spectra measured in chloroform at room temperature (black) and calculated UV/Vis absorption spectra based on TDDFT at the B3LYP/6-311G* level with PCM-$CHCl_3$ (red) of triptycene end capped coronene monomer **261** and dimer **262**. Positions for absorption maxima are given in nm.

For perylene oligomers after the formation of thiophene-annulated coronenes, *β*-band absorption with a sharp absorption maximum was found in both molecules (Figure 3.3.17a). In comparison to the thiophene-annulated coronene **164** without triptycene end caps (Chapter 3.1),

which gives a β-band absorption maximum at λ = 363 nm, the absorption of compound **261** exhibits a bathochromic shift of 8 nm to λ = 371 nm, due to the introduction of triptycene end caps. The p-band absorption maximum does not change from **164** to **261**. Dimerizing the thiophene annulated coronene units to form oligomer **262** makes the β-band absorption maximum red-shift to λ = 422 nm along with an increased maximum extinction coefficient of $\varepsilon = 2.88\times 10^5$ $M^{-1}\cdot cm^{-1}$, which is nearly 1.7 times of that of coronene monomer **261** ($\varepsilon = 1.66 \times 10^5$ $M^{-1}\cdot cm^{-1}$). The p-band absorption is bathochromically shifted from λ = 434 nm for **261** to λ = 495 nm for **262**. The decreased optical band gap from E_g = 2.7 eV for **261** to E_g = 2.4 eV for **262** estimated from the corresponding absorption onsets is supported by the energy levels of FMOs calculated by DFT methods (Figure 3.3.18).

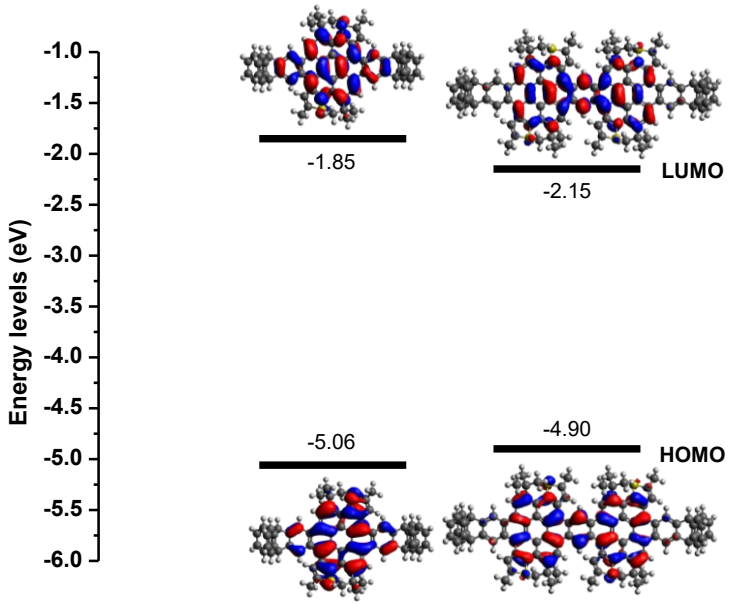

Figure 3.3.18 Frontier molecular orbitals and the corresponding energy levels of coronene monomer **261** and dimer **262** calculated by DFT at the B3LYP/6-311G* level. The hexyl chains were replaced by methyl groups for simplification.

Fluorescence emission spectra of the compounds in this series exhibit a similar trend with the UV/Vis absorption spectra. The maximum emission peak red-shifts from λ = 487 nm for monomer **261** to λ = 514 nm for dimer **262**. After the formation of thiophene annulated coronenes, the fluorescence quantum yields of oligomers **261** (Φ = 7.3±0.1%) and **262** (Φ = 13±0.5%) are smaller than those of the perylene oligomers **228-230** (Φ = 68%-86%), which is in the same trend with the *cata*-condensed coronenes in comparison to their uncyclized precursors shown in Chapter 3.1.

Perylene oligomers **228-230** sharing the same type π-framework but with different conjugation lengths serve as good models to investigate the effective conjugation length (ECL) of this PAH series. This was performed by fitting the UV/Vis absorption or fluorescence emission of POs to an exponential function (Equation 1).[210] In Equation 1, n refers to the number of linearly

fused benzene rings in the π-backbones. λ_1 belongs to parent compound. Here isolated benzene with absorption peak of 255 nm and emission peak of 287 nm was taken.[211] λ_n refers to the wavelength of absorption peak or emission peak of PAH with n linearly fused benzene rings. Absorption maximum at the longest wavelength and emission at the most intensive wavelength were chosen to the calculation. Estimation of ECL was made based on the assumption that the maximum conjugation is virtually reached for an n_{ECL}, which fulfills Equation 2.

$$\lambda_n = \lambda_\infty - (\lambda_\infty - \lambda_1)\, e^{-b(n-1)} \qquad \text{(Equation 1)}$$

$$\lambda_\infty - \lambda_{ECL} \leq 1\ nm \qquad \text{(Equation 2)}$$

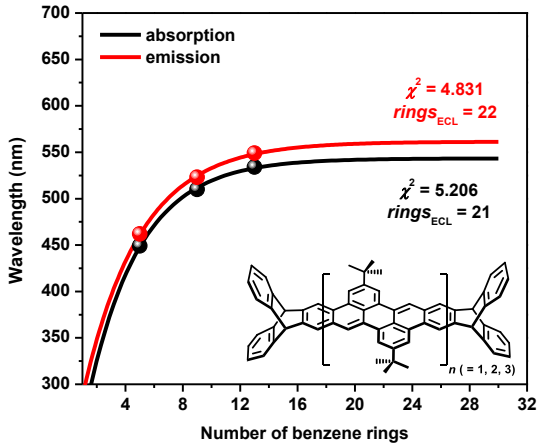

Figure 3.3.19 Exponential fits of POs (**228**-**230**) of the absorption maxima of the *p*-band (black) and the fluorescence emission maxima (red) vs. number of linearly fused benzene rings, respectively. χ^2: reduced chi-square.

Exponential function fitting results derivated from absorption or emission data gave similar rate of convergence (Figure 3.3.19). The number of linearly fused benzene rings which reaches the criteria of ECL defined by Equation 2 was estimated to be 21 from the absorption data or 22 from the emission data. The largest absorption maximum where the polyperylene can reach is about 543 nm and the corresponding emission maximum was estimated to be 561 nm. It is supposed that PO-13 (**230**), with the largest molecular length in this series, nearly reaches the ECL with the difference between its absorption peak and λ_{ECL} is only around 10 nm.

3.3.8 Discussion of Aromaticity

For the three perylene oligomers **228**-**230** and three coronene oligomers **261**-**263**, NICS(0) values were calculated based on DFT at the B3LYP/6-31G* level of theory to investigate the local aromaticity of these π-backbone (Figure 3.3.20). The four peripheral benzene rings on the π-backbone of PO-5 (**228**) give NICS(0) values of -7.8 to -8.8, suggesting relatively high aromaticity in these rings. The central ring connecting two naphthalene moieties inside the perylene unit gives a positive NICS(0) value of 6.1. Thus antiaromaticity is expected in this ring. This

distribution pattern of (anti)aromaticity on the π-framework is also observed in perylene dimer **229** and trimer **230** according to the calculated NICS(0) values. The rings connecting two perylene units exhibit the most negative values (-9.2 or -9.3) on the π-framework, suggesting the largest aromaticity would be located in these positions. This distribution pattern is consistent with the depicted π-scaffold model of this type of perylene oligomers shown in Figure 3.3.20d and is also consistent with the C-C bond length alternation of the single crystal structure of PO-9 (**229**) discussed in Figure 3.3.3.

Aromaticity of these perylene oligomers could be further analyzed by ACID plots calculated at the B3LYP/3-21G level (Figure 3.3.21). The benzene rings which exhibit uniform clockwise ring currents thus higher local aromaticity is located in those positions giving the most negative NICS(0) values in Figure 3.3.20. Therefore, local aromaticity predicted by the ACID plots is consistent with the calculated NICS(0) values. One different result from the prediction of NICS(0) values is that the rings connecting two naphthalene moieties, which are expected to be show local antiaromaticities suggested by NICS(0) values, do not exhibit uniform paratropic (counterclockwise) ring currents. The ring current on the π-frameworks of these perylene oligomers could be described like this. Diamagnetic ring currents are on the outer rims of the π-frameworks, whereas the continuous ring currents are broken by the rings shared by two naphthalene moieties of each perylene unit. The diamagnetic ring currents were found on the two phenanthrene units in PO-5, two phenanthrene units and one benzo[*k*]tetraphene unit in PO-9 and two phenanthrene units and two benzo[*k*]tetraphene units in PO-13. As the ring currents along the outer edges of these π-backbones are all diamagnetic, global aromaticity could be expected in these perylene oligomers.

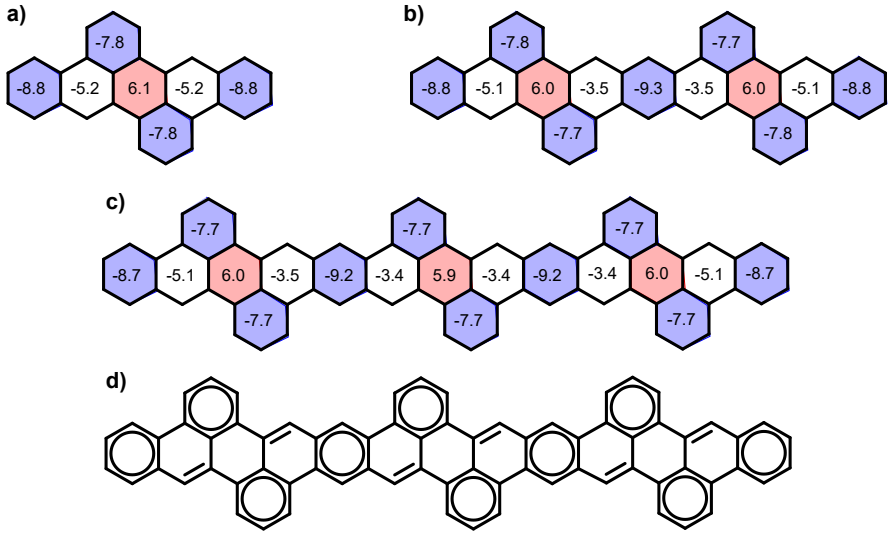

Figure 3.3.20 DFT calculated NICS(0) values of PO-5 (a), PO-9 (b), PO-13 (c) at the B3LYP/6-31G* level of theory. Rings highlighted with blue indicate high aromaticitiy, while rings highlighted in red indicate antiaromaticity. d) A depicted model of π-scaffold for the π-backbone of perylene oligomers according to Clar's sextet rule. The triptycene end caps are omitted for clarity.

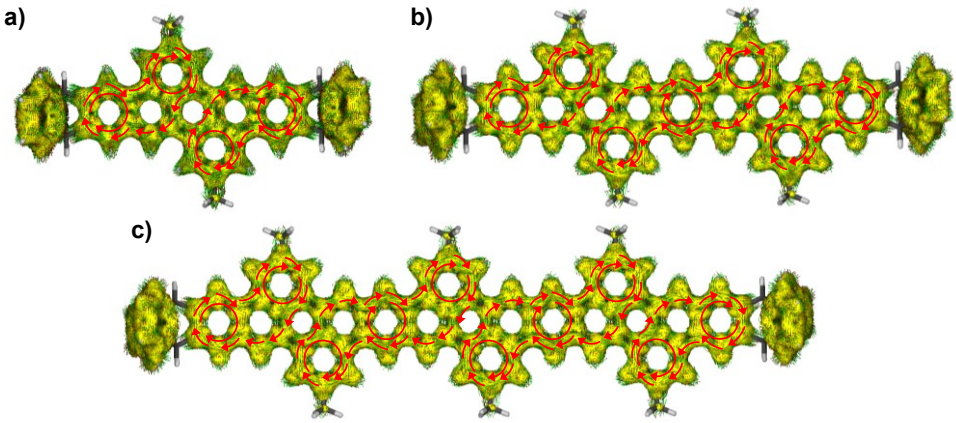

Figure 3.3.21 Calculated ACID plots for perylene oligomers **228** (a), **229** (b) and **230** (c) at the HF/3-21G level. The isosurface value is 0.05 and the magnetic field points out of the paper plane. The diamagnetic (clockwise) ring currents are highlighted by red arrows.

After the formation of thiophene-annulated coronenes, all the benzene rings on the peripheries of the molecular π-frameworks as well as the thiophene rings give quite negative NICS(0) values (-6.6 to -9.4), indicating local aromaticity (Figure 3.3.22). Similar to those perylene oligomers **228**-**230**, rings connecting two perylene units on these coronene oligomers exhibit the most negative NICS(0) values of -10.5, indicating relatively large local aromaticity.

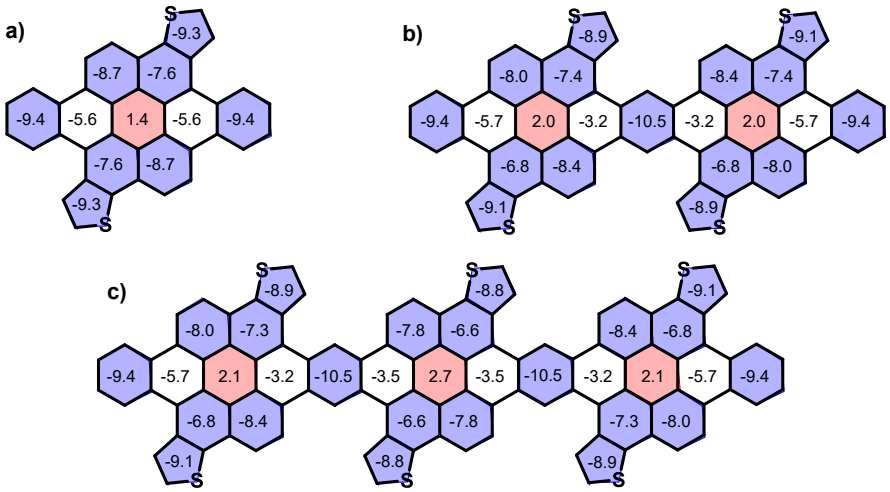

Figure 3.3.22 DFT calculated NICS(0) values of coronene monomer (a), dimer (b) and trimer (c) at the B3LYP/6-31G* level of theory. Rings highlighted with blue indicate high aromaticity, while rings highlighted in red indicate antiaromaticity. The triptycene end caps are omitted for clarity.

However, no rings exhibit uniform diamagnetic ring currents in the corresponding ACID plots (Figure 3.3.23). Uniform paratropic (counterclockwise) ring currents were observed in the rings connecting two coronene moieties. Thus these rings are expected to exhibit weak local antiaromaticity, which is consistent with the calculated NICS(0) values (1.4 to 2.7). Uniform diamagnetic ring currents were observed in the outer rims of these coronene oligomers, suggesting these π-frameworks exhibit global aromaticity.

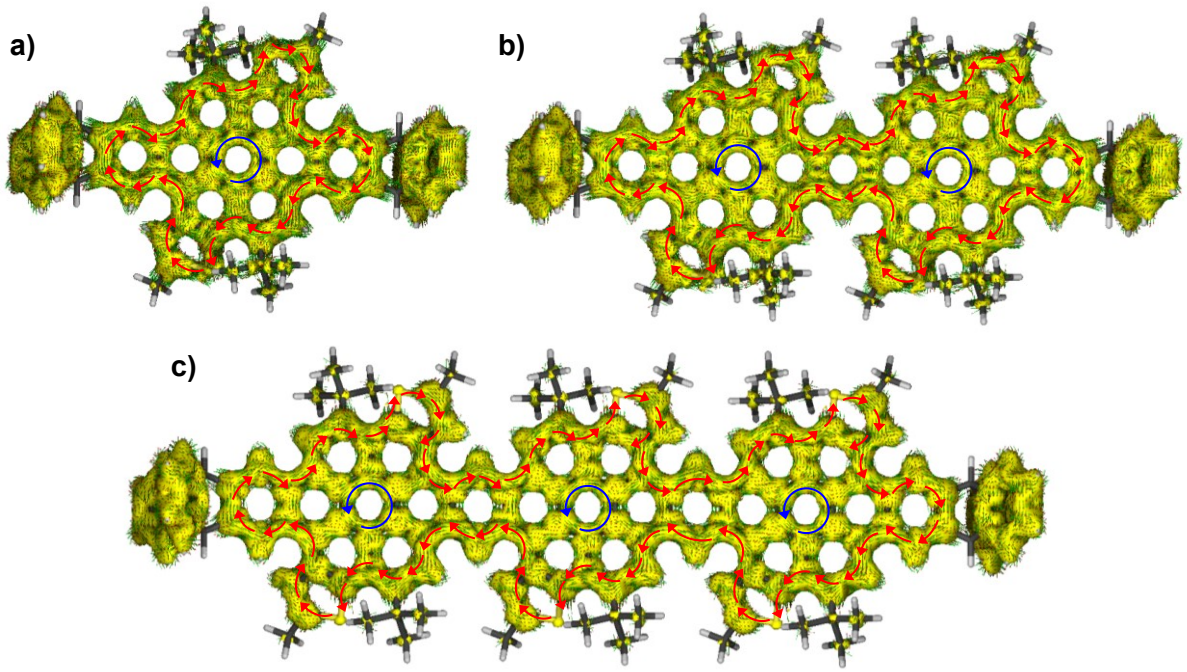

Figure 3.3.23 Calculated ACID plots for triptycene end capped thiophene annulated coronene monomer (a), dimer (b) and trimer (c) at the HF/3-21G level. The isosurface value is 0.05 and the magnetic field points out of the paper plane. The diamagnetic (clockwise) and paramagnetic (counterclockwise) ring currents are highlighted by red and blue arrows, respectively.

3.3.9 Conclusions

In this chapter, three triptycene end-capped 1D extended perylene oligomers with up to 13 linearly fused rings were successfully obtained via aldehyde precursors by step-by-step cross-coupling reactions and the final multi-fold intramolecular condensation in the presence of a strong base (*t*-BuOK). Single crystal structure analyses of PO-9 (**229**) indicate that this perylene oligomer adopts a planar conformation. The distinct C-C bond length distribution of **229** suggests that four bonds at [*a*] and [*k*] edges of the perylene units show more olefinic character. With the increase of the length of π-backbone, significant bathochromic shifts were observed in the UV/Vis absorption and fluorescent emission spectra of these three perylene oligomers. Exponential fitting suggests that the conjugation would be saturated when the number of linearly fused rings reaches 21 to 22.

Regioselective bromination was achieved based on all three perylene oligomers with high yields. After subsequent multi-fold Suzuki-Miyaura cross-coupling reactions and intramolecular cyclodehydrogenations under Scholl conditions, oligomers containing up to two thiophene-annulated coronenes were synthesized and isolated as pure compounds. In comparison to the corresponding perylene oligomers, significantly enhanced absorption in β-band were observed in the UV/Vis spectra of two coronene oligomers.

4. Summary and Outlook

This thesis presents the syntheses and characterizations of a series of larger PAHs by π-extension based on 2,10-di-*tert*-butyldibenzoperylene (**111**). The relationships between the molecular structures and the corresponding properties of these obtained PAHs were investigated.

Due to the presence of two isolated C-C double bonds at the [*a*] and [*k*] edges of 2,10-di-*tert*-butyldibenzoperylene (**111**), which are prone to be electrophilically attacked, regioselective two-fold bromination was achieved based on four diarenoperylenes in > 85% yields (Figure 4.1). Based on these dibromides, nineteen compounds were obtained after palladium-catalyzed two-fold cross-coupling reactions. Nine of them were applied in the following ring-closing step, either by photo-induced cyclization or by oxidative cyclodehydrogenation, to finally synthesize a series of *cata*-condensed (tetrakis)-heteroannulated coronenes (Figure 4.1), which can be interpreted as the π- extensions at the two bay regions of diarenoperylenes. In contrast to prior existing synthetic routes to heteroannulated coronenes, this approach allows the construction of less symmetric compounds. Seven *cata*-condensed coronenes were characterized by single crystal X-ray diffraction analysis. Contorted π-backbones were observed in all seven cases, due to the two generated cove regions. Six molecules adopt S-shaped contortion in the crystal structures, whereas dithiophene-fused coronene **172** shows a unique negative curvature. These brominated key intermediates show potential to be used in cross-coupling reactions with large number of reaction partners to synthesize various further π-extended aromatics with fine-tune photophysical and electrochemical properties.

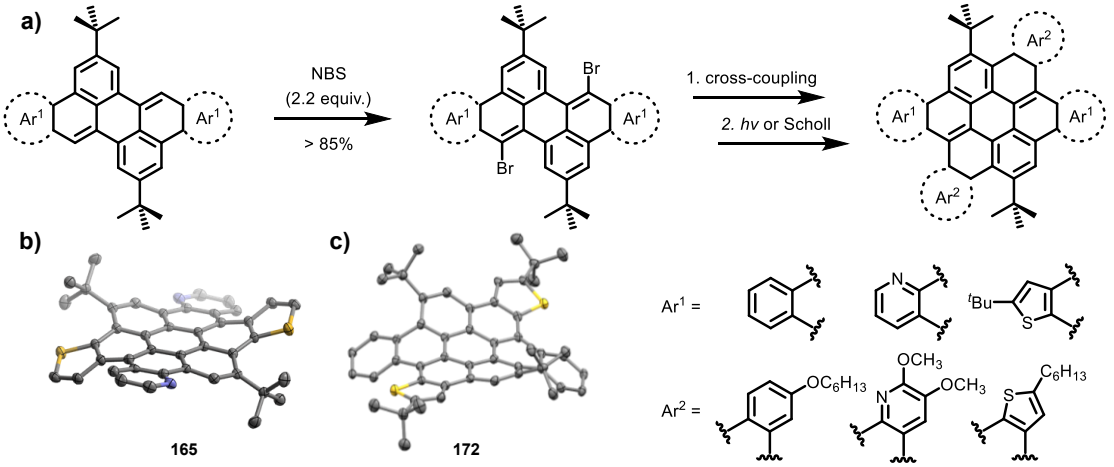

Figure 4.1 a) The three-step synthetic approach to *cata*-condensed (tetrakis)-heteroannulated coronenes. b) and c) Side-view of single crystal structures of coronene **165** (b, S-shaped) and **172** (c, negatively curved).

Different experimental results were observed when treating two naphthyl-substituted dibenzoperylenes **180** and **198** under Scholl-type conditions (Figure 4.2 and Figure 4.3). When **180** was treated with $FeCl_3/CH_3NO_2$ or DDQ (2.2 equiv.)/TfOH in CH_2Cl_2, double cyclized product **181** was obtained after cyclopentannulation in which two new C-C bonds were formed between the two

naphthyl groups and the *L*-regions of PAH **180** (Figure 4.2). When the amount of DDQ was increased to 6 equiv., an unprecedented highly regioselective bistriflyloxylation was observed, giving bistriflate **184** in 90% yield from **180** in one-pot. The obtained bistriflate **184** could be used in the following cross-coupling reactions to further extend this system. PAH **191** containing four five-membered rings and PAH **197** with highly twisted conformation were obtained, both in racemic mixtures of two enantiomers.

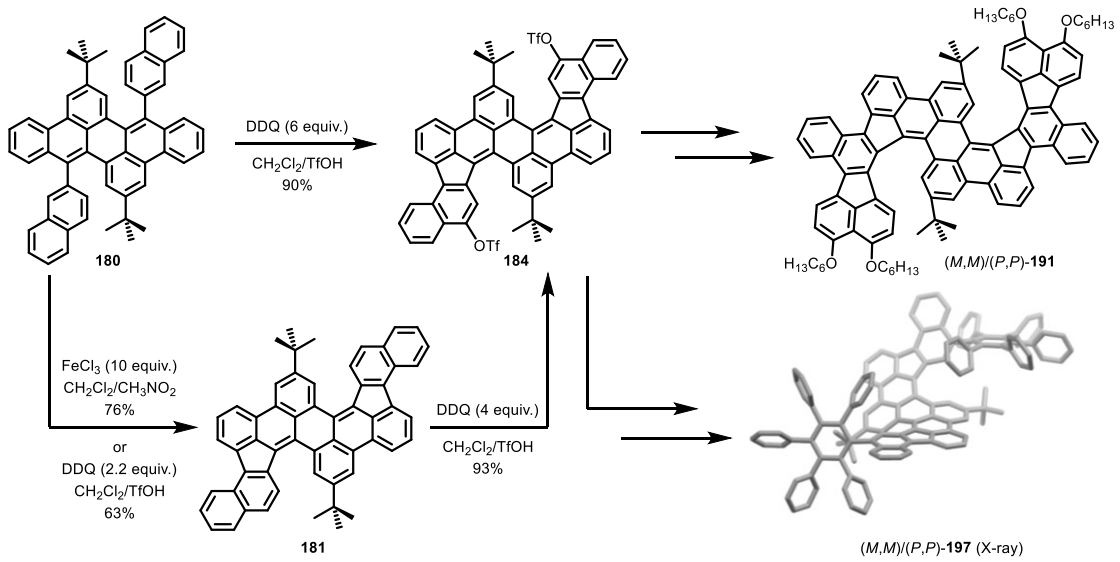

Figure 4.2 Cyclopentannulation and regioselective triflyloxylation based on PAH **180**.

Besides the two-fold cyclopentannulation, further two-fold cycloheptannulations were observed when naphthyl-substituted dibenzoperylene **198** was treated with DDQ (8 equiv.)/TfOH in CH_2Cl_2, giving PAHs with two azulene moieties embedded (Figure 4.3). Again a regioselective bistriflyloxylation was detected in this case, while this substitution was competing with the attachments of dichlorovinylene (DCV) groups. Based on this phenomenon, three azulene-embedded PAHs **206**-**208** were isolated by silica gel column chromatography. The azulene embedded π-backbone was confirmed by X-ray diffraction analysis of single crystal structure of DCV-attached PAH **208**. Due to the negative curvature, a contorted π-backbone with two racemic enantiomers was found. The triflyloxy groups on PAH **206** could be transformed to aryl units by palladium catalyzed cross-coupling reactions. Furthermore, with the attachment of solubilizing mesityl groups, the degree of contortion of the azulene embedded π-backbone could be fine-tuned by simply stepwise removing the *tert*-butyl groups in the bay regions. Azulene embedded PAH **213** with a more planar conformation exhibits more aromaticity while its UV/Vis absorption maxima for *p*-band hypochromatically shifted by 18 nm in comparison to that of contorted PAH **211**. The two racemic enantiomers of PAHs **206** and **211** were further isolated by semi-preparative chiral HPLC. Mirror symmetric CD spectra of two enantiomers were observed in both PAHs. Distinct emissions close to the near-infrared (NIR) regime between λ = 650 and 670 nm with relatively high

quantum yields of Φ = 20%-30% were observed in these azulene embedded PAHs, suggesting that these PAHs own potential applications in biological areas.

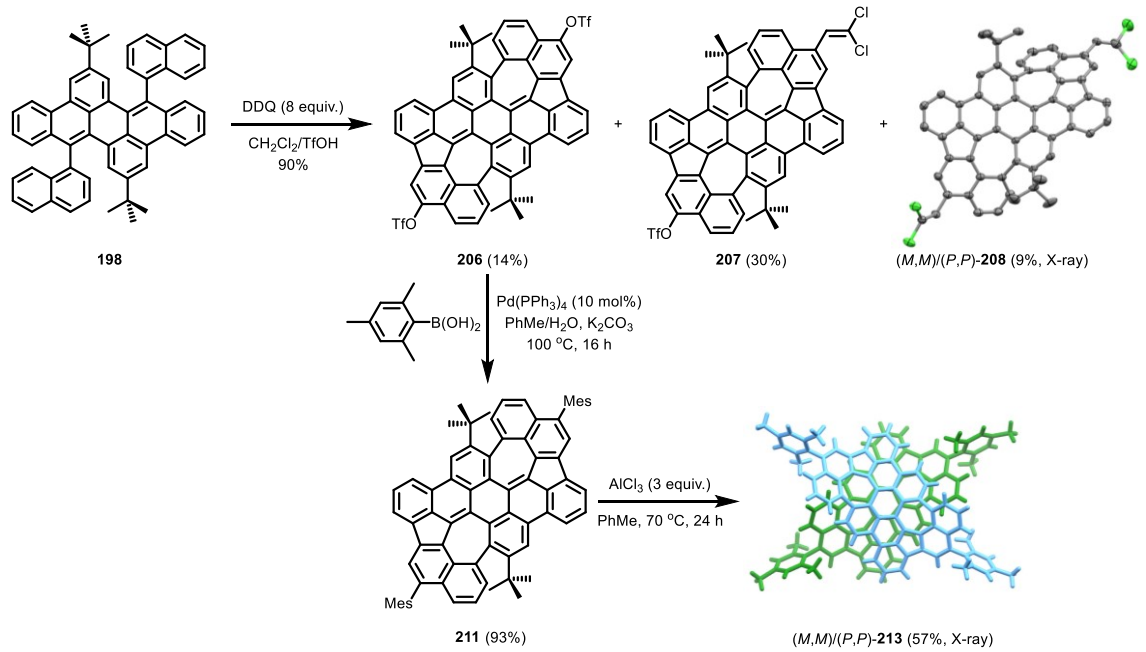

Figure 4.3 Formation of azulene embedded PAHs starting from PAH **198**.

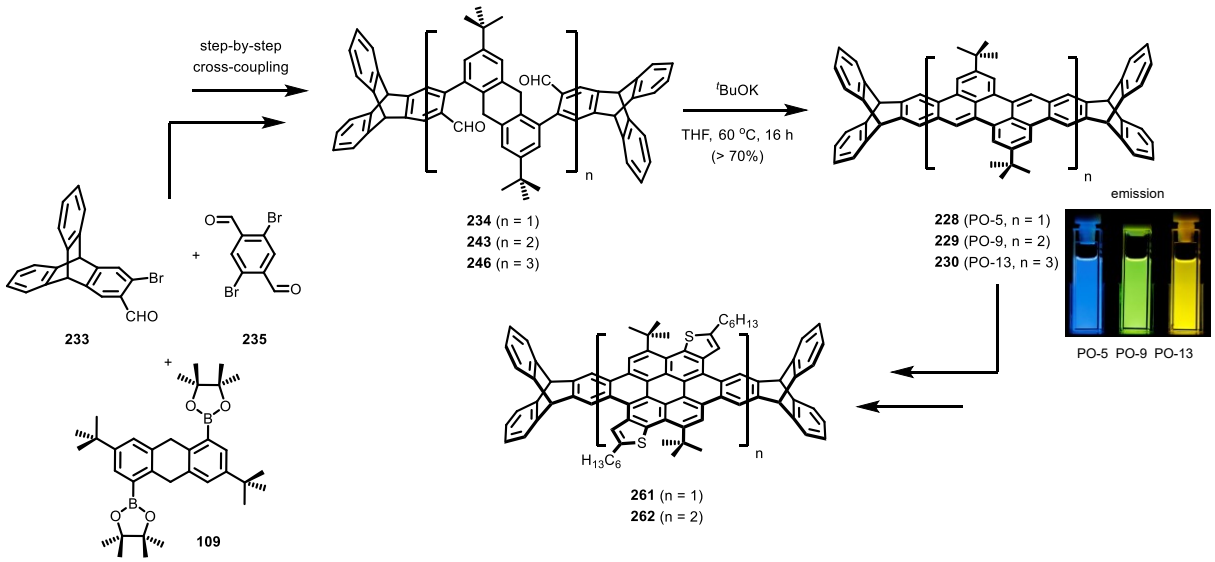

Figure 4.4 Syntheses of perylene oligomers **228**-**230** and thiophene-annulated coronene oligomers **261** and **262**.

Three triptycene end-capped perylene oligomers (**228**-**230**) with up to thirteen linearly fused benzene rings were obtained by iterative cross-coupling reactions and the final multi-fold intramolecular condensations (Figure 4.4). The molecular structure of PO-9 (**229**) was unambiguously characterized by single crystal X-ray diffraction, which exhibits a planar π-backbone with a length of 2.21 nm. Based on the analyses of C-C bond lengths and results of DFT calculations, this π-backbone of PO-9 (**229**) could be reasonably depicted as a π-scaffold containing seven Clar's sextet, which explains its high stability. Linear π-extension leads to

significant bathochromic shifts in the UV/Vis absorption and fluorescent emission spectra. Exponential fitting suggests that the conjugation can be saturated when the number of linearly fused rings reaches 21 - 22. These perylene oligomers were further extended by highly efficient multifold regioselective bromination. Oligomers containing one and two thiophene-annulated coronene moieties (**261** and **262**) were synthesized and isolated, after the Suzuki-Miyaura cross-coupling reactions and the subsequent Scholl cyclizations.

The results presented in this thesis would contribute to the rapid development of PAH-based chemistry and material sciences. As structurally well-defined graphene fragments, PAHs provide reliable structure-property correlations and proper control of the material performances. The development of the chemistry of PAHs has promoted the bottom-up synthesis of atomically precise GNRs and invention of emerging PAH- or GNR-based materials such as topological insulators. Hence, the researches regarding PAH-based materials are of significance and indispensable.

The main purpose of this thesis was to explore and optimize the synthetic approaches towards various PAHs, to perform basic characterizations and to establish the structure-property correlations from a chemical perspective. The applications of these molecules were not included. Facile fabricating approaches, unique molecular structures, exciting properties and final good applications are always demanding by organic chemists as well as physicists and material scientists. In the near future more potential applications of these PAHs in material sciences and biological areas should be explored, with the collaborations with researchers in these areas.

5. Experimental Section

5.1 General Remarks

Thin Layer Chromatography (TLC): For thin layer chromatography silica gel 60 F254 plates from Merck were used and examined under UV-light irradiation (254 nm and 365 nm).

Column Chromatography: Column chromatography[212] was performed using silica gel with particle sizes of 0.040-0.063 mm (Macherey-Nagel & Co. KG, Düren) using petroleum ether, ethyl acetate, dichloromethane, chloroform or their mixtures as eluents. For elaboration of the right eluent, thin layer chromatography was performed in a way that the fraction with the highest R_f value was $R_f < 0.4$ and this mixture was then used for the corresponding column chromatography.

Size Exclusion Chromatography (SEC): Polystyrene beads (200-400 mesh, Bio-Beads S-X1 from Bio-Rad Laboratories, Inc.) with a column of 150 cm length and 6 cm inner diameter using dichloromethane as eluent were used to perform size exclusion chromatography. Prior to usage the beads were washed six to ten times using alternating dichloromethane and methanol with swelling times greater than two hours.

Melting points (m.p.): Melting points (not corrected) were measured with a Büchi Melting Point B-545.

Infrared (IR) Spectroscopy: IR spectra were recorded neat on a Fourier transform spectrophotometer (Bruker Lumos) equipped with a ZnSe ATR crystal. The signal intensity was described as: s (strong), m (medium) and w (weak).

Nuclear Magnetic Resonance Spectroscopy (NMR): NMR spectra (^{1}H, ^{13}H, ^{19}F, 2D coupling experiments) were recorded in $CDCl_3$, CD_2Cl_2 or $Cl_2CDCDCl_2$ using Bruker Avance 300 (300 MHz) , Bruker Avance III 400 (400 MHz) , Bruker Avance 500 (500 MHz) or Bruker Avance III 600 (600 MHz) spectrometer at 298 K, unless otherwise mentioned. Chemical shifts (δ) are reported in parts per million (ppm) relative to traces of $CHCl_3$ (δ_H = 7.26 ppm, δ_C = 77.0 ppm), $CHDCl_2$ (δ_H = 5.32 ppm, δ_C = 54.0 ppm) or $Cl_2CHCDCl_2$ (δ_H = 5.963 ppm, δ_C = 73.78 ppm) in the corresponding deuterated solvent. Signals were assigned by 2D NMR experiments (^{1}H,^{1}H-COSY, ^{1}H,^{1}H-NOESY, ^{1}H,^{1}H-ROESY, ^{1}H,^{13}C-HSQC, ^{1}H,^{13}C-HMBC).

Mass Spectrometry (MS): High resolution mass spectrometry (HRMS) experiments were carried out on a Fourier Transform Ion Cyclotron Resonance (FT-ICR) mass spectrometer ApexQe hybrid 9.4 T (Bruker Daltonik GmbH, Bremen, Germany) equipped with a 9.4 T superconducting magnet and interfaced to an Apollo II MTP Dual ESI/MALDI source for DART, ESI and MALDI experiments. MALDI-TOF MS experiments were carried out on a Bruker AutoFlex Speed time-of-

flight with DCTB (*trans*-2-[3-(4-*tert*-butylphenyl)-2-methyl-2-propenylidene]malo-nonitrile) as matrix. Electron ionization (EI) mass spectra were recorded on a Varian 3800, on a JEOL JMS-700 or on a JEOL AccuTOF GCx spectrometer. Molecule fragments were given as a mass-to-charge proportion (*m/z*).

Elemental Analysis (EA): Elemental analysis was performed by the Microanalytical Laboratory of the University of Heidelberg using an Elementar Vario EL machine.

X-ray crystal structure analysis: Crystal structure analysis was accomplished on Bruker APEX II Quazar diffractometer with a molybdenum source ($\lambda_{MoK\alpha}$= 0.71073 Å) or a STOE Stadivari diffractometer with a copper source ($\lambda_{CuK\alpha}$ = 1.54178Å). Intensities were corrected for Lorentz and polarization effects, an empirical absorption correction was applied using SADABS[213] based on the Laue symmetry of the reciprocal space. The structures were solved by intrinsic phasing or by direct methods with dual-space recycling and refined by full-matrix least squares methods based on F_2 against all unique reflections.[214] All non-hydrogen atoms were given anisotropic displacement parameters. Hydrogen atoms were input at calculated positions and refined with a riding model. When found necessary, disordered groups and/or solvent molecules were subjected to suitable geometry and restraints and/or constraints.

UV-VIS and Fluorescence Spectroscopy: Absorption spectra were recorded on Jasco UV-VIS V-730 spectrophotometer. Fluorescence spectra were recorded on a Jasco FP-8300 spectrofluorometer.

Circular dichroism spectroscopy (CD spectroscopy): CD spectra were recorded with a Jasco J-1500 CD spectrometer.

Fluorescence Quantum Yields: Quantum yields Φ were obtained by the absolute method[215] using a PTI Quantum Master 40 with an Ulbricht integration sphere (LabSphere®, diameter:6", coated with Spectraflect®). Given Φ are average values of three independent measurements.

Fluorescence Lifetimes: Fluorescence lifetimes τ were determined using a Horiba Jobin Yvon Fluorocube with a pulsed light source.

Cyclic Voltammetry (CV): Electrochemical data were obtained in CH_2Cl_2 or *o*-DCB solution of 0.1 M *n*-Bu_4NClO_4, as indicated. Ferrocene was used as an internal standard. Cyclic voltammograms were obtained using a glassy carbon working electrode, a Pt counter electrode, and an Ag reference electrode.

Recycling Gel Permeation Chromatography (*r*GPC): Preparative GPC was performed on a Shimadzu LC-20AD recycling System using a PSS pre column (size: 50 x 20 mm) and PSS SDV column (size: 300 x 20 mm, porosity: 100 Å) with a flow-rate of 10-4-10 mL/min and a pressure

maximum of 200 bar. The columns were temperature regulated (40 °C) by a CTO-20AC air circulation oven. Detection of the sample were realized by a SPD-M20A photo diode array with a wavelength range of 190-800 nm.

Analytical Chiral High Performance Liquid Chromatography (analytical chiral HPLC): Chiral HPLC analysis was carried out using a Hewlett Packard HP 1100 with DAICEL Chiralpak AD-H column (25 cm × 0.46 cm, Amylose tris-(3,5-dimethylphenylcarbamate)) in combination with a DAICEL Chiralpak AD-H precolumn (1 cm × 0.4 cm).

Semi-preparative Chiral High Performance Liquid Chromatography (semi-preparative chiral HPLC): Semi-preparative chiral HPLC was performed on an Agilent 1200 series HPLC system using a Chiralpak® IE column from Daicel. Detection was accomplished at 254nm.

Theoretical Calculations: The geometry optimizations were performed based on Density Functional Theory (DFT)[216] calculations at B3LYP/6-311G* using Spartan 14 for compounds in Chapter 3.1 and 3.2, or using Gaussian 09 package[209] for compounds in Chapter 3.3. Frequency analysis was followed to assure that the optimized structures were stable states. Time-dependent DFT (TDDFT) calculation for the $S_0 \rightarrow S_n$ transitions using the same function and basis set were performed based on the optimized structures at ground states using Gaussian 09 package. Typically, the lowest 30 singlet roots of the nonhermitian eigenvalue equations were obtained to determine the vertical excitation energies and the solvent chloroform was simulated using the polarized continuum model (PCM) for calculated UV/Vis spectrum. NMR and nucleus-independent chemical shift (NICS) calculations were performed by employing the Gaussian 09 package with the GIAO method[217] and the Polarizable Continuum Model (PCM) to apply chloroform as solvent. Anisotropy of the induced current density (ACID) plots were calculated by Herges's method at the HF/6-31+G* level for the azulene PAHs in chapter 3.2.2 and the HF/3-21G level for perylene oligomers and coronene oligomers in chapter 3.3.

Software: Microsoft Word 2013 was used to write this thesis, chemical formulas were drawn using ChemDraw Professional 17.1.0.105 by Cambridgesoft and graphs were processed with OriginPro 8.5.0 by OriginLab Corp. IR and MS spectra were processed using ACD/Spectrus Processor (S40S41) by Advanced Chemistry Development, Inc. and plotted using OriginPro. NMR spectra were integrated and processed using MestReNova (v6.0.2-5475).

5.1.1 Solvents

The solvents were used from stock without further purification or drying unless otherwise noted. Dry solvents of THF (Honeywell ≥ 99.9%, inhibitor free), DCM (Honeywell ≥ 99.8%, stab. with 0.2% amylene), diethyl ether (Honeywell ≥ 99.8%, stab. with 0.2% BHT) and toluene (Honeywell

≥ 99.7%) were obtained from MBraun Solvent Purification Systems (MB SPS-800). Dry cyclohexane (Honeywell ≥ 99%) used in the photocyclization was distilled over CaH_2 before use.

Solvents	**Purities**	**Commercial source**
1,1,2,2-Tetrachloroethane-d_2	≥ 99.5%	Sigma-Aldrich
1,2-Dichlorobenzene	99%	Sigma-Aldrich
1,2-Dichlorobenzene-d_4	98%	Sigma-Aldrich
Acetone	≥ 99%	Honeywell
Chlorobenzene	99.8%	Sigma-Aldrich
Chloroform	> 99%	Sigma-Aldrich
Chloroform-*d*	99.8%	Sigma-Aldrich
Dichloromethane	n.d. (stab. with 0.2% ethanol)	VWR Chemicals
Dichloromethane-d_2	99.9%	Sigma-Aldrich
Diethyl ether	≥ 99.5%	Sigma-Aldrich
Ethanol	≥ 99.8%	Sigma-Aldrich
Ethyl acetate	≥ 99.5%	Honeywell
Methanol	≥ 99.8%	Honeywell
N,*N*-Dimethylformamide	≥ 99.8%	Sigma-Aldrich
n-Heptane	≥ 99%	Acros Organics
n-Hexane	98%	VWR Chemicals
n-Pentane	≥ 99%	Sigma-Aldrich
Petroleum ether (40-60 °C)		Honeywell
Tetrahydrofuran	≥ 99.9% (stab. with 250 ppm BHT)	Sigma-Aldrich
Toluene	≥ 99.7%	Sigma-Aldrich
Water	deionized	Uni-Heidelberg Institute

5.1.2 Chemicals and Reagents

All chemicals and reagents were used without further purification unless otherwise noted.

Chemicals	Purities	Commercial source
(±)-Propylene oxide	≥ 99%	Sigma-Aldrich
(1,5-Cyclooctadiene)(methoxy)iridium(I) dimer		Sigma-Aldrich
(4-(*tert*-Butyl)phenyl)boronic acid	97%	Acros Organics
[1,1′-Bis(diphenylphosphino)ferrocene]-dichloropalladium(II)	98%	Carbolution
1,2,4,5-Tetrabromobenzene	97%	Sigma-Aldrich
1-Naphthylboronic acid	98%	Carbolution
2,3-Dichloro-5,6-dicyano-1,4-benzoquinone	98%	Acros Organics
2,4,6-Trimethylphenylboronic acid	95%	Acros Organics
2,5-Dibromo-p-xylene	≥ 98%	Alfa Aesar
2-Methoxypyridine-5-boronic acid	95%	Alfa Aesar
2-Naphthylboronic acid	98%	Carbolution
3,4,7,8-Tetramethyl-1,10-phenanthroline	> 98%	Acros Organics
3-Thienylboronic acid	98%	Carbolution
4-Methoxylphenylboronic acid	97%	Carbolution
Acetic acid	> 99%	Honeywell
Acetic anhydride	99%	Grüssing GMBH
Aluminium chloride	99%	BASF
Ammonium chloride	≥ 99.5%	Honeywell
Anthracene	99%	Acros Organics
bis(pinacolato)diboron	99%	Carbolution
Bis(triphenylphosphine)palladium(II) dichloride	98%	Carbolution
Bromine	≥ 99.99%	Sigma-Aldrich
Celite 545		VWR Chemicals
Chromium(VI) oxide	99%	Alfa Aesar
Copper(I) iodide	≥ 99.5%	Sigma-Aldrich
Diphenylether	≥ 99%	Sigma-Aldrich
Ethylene glycol		VWR Chemicals
Hydrochloric acid	aq.36.5-38%	Sigma-Aldrich
Iodine	≥ 99.8%	Fluka
Iron(III) chloride (anhydrous)	98%	Alfa Aesar
Isopropylmagnesium chloride solution (2.0 M in THF)		Sigma-Aldrich
N-Bromosuccinimide	99%	Sigma-Aldrich
n-Butyllithium solution (2.5 M in hexane)		Acros Organics
Nitromethane	≥ 95%	Sigma-Aldrich
Phenylacetylene	97%	Carbolution

Phenylboronic acid	95%	Sigma-Aldrich
Potassium carbonate	99%	Grüssing GMBH
Potassium tert-butoxide	≥ 98%	Sigma-Aldrich
p-Toluenesulfonic acid	97%	abcr
Sodium bicarbonate	100%	Grüssing GMBH
Sodium chloride	≥ 99.8%	Sigma-Aldrich
Sodium metabisulfite	97%	Honeywell
Sodium sulfate	≥ 99%	Bernd Kraft
Sodium sulfite	97%	Grüssing GMBH
Sulfuric acid (conc.)	95-97%	Sigma-Aldrich
Tetrakis(triphenylphosphine)palladium(0)	99%	Sigma-Aldrich
Tetraphenylcyclopentadienone	99%	Acros Organics
Triethylamine	≥ 99.5%	Sigma-Aldrich
Trifluoromethanesulfonic acid	> 98.0%	TCI
Tris(dibenzylideneacetone)dipalladium(0)	97%	Acros Organics
Tri-*tert*-butylphosphonium tetrafluoroborate	97%	Sigma-Aldrich

5.1.3 General Procedures

General procedure (GP1) for the Suzuki-Miyaura cross coupling reactions between diarenoperylene dibromides and boronic acids (pinacol esters) in Chapter 3.1: In a screw-capped vial, perylene dibromide, boronic ester and K_2CO_3 were suspended in an argon-degassed solvent mixture of THF/water (v/v 4:1). A mixture of $Pd_2(dba)_3$ and *t*-Bu_3PHBF_4 was added under argon atmosphere and the mixture vigorously stirred at 80 °C overnight. After cooling down to room temperature, the mixture was diluted with dichloromethane (100 mL), washed with water (3 × 50 mL) and dried over Na_2SO_4. After removal of the solvent by rotary evaporation, the crude product was purified by silica gel chromatography and precipitation from dichloromethane/methanol to give the product (mixture of atropisomers) as yellow to dark-yellow solid.

General procedure (GP2) for the photocyclization in Chapter 3.1: The photoreactor equipped with a 150 W high-pressure quartz Hg vapor lamp was charged with the substrate and dry cyclohexane (300 mL) and purged with argon. Propylene oxide and iodine were added subsequently. The mixture was stirred at room temperature under the irradiation for several hours as indicated, during which an argon flow was constantly bubbled through the mixture. The reaction was monitored by TLC. The mixture was washed with 1M aq. $NaHSO_3$ (100 mL) and water (100 mL) and dried over anhydrous Na_2SO_4. After removal of the solvent by rotary evaporation, the crude product was purified by silica gel column chromatography. The product was obtained after precipitation (or recrystallization) and drying in vacuum to give the coronene as yellow to dark-red solid.

5.2 Syntheses

Dihydroanthracene diboronic ester **109**, diarenoperylenes **111**-**113** and **117** were synthesized via previously reported synthetic routes.[128b]

5.2.1 Compounds of Chapter 3.1

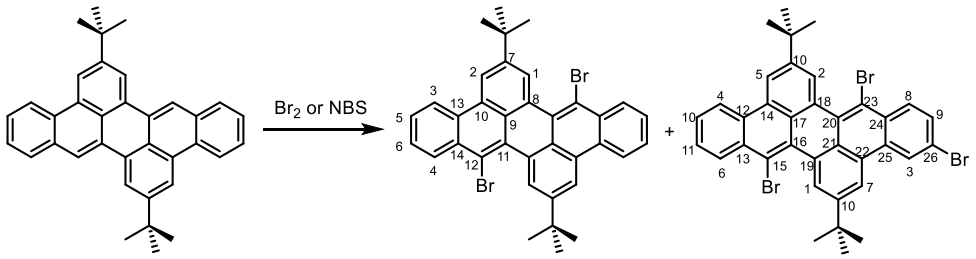

111 **133** **134**

Bromination with Br_2: To a solution of dibenzoperylene **111** (9 mg, 0.019 mmol) in dichloromethane (3 mL), a bromine solution (0.1 mL out of 0.25 mL Br_2 in 10 mL DCM, 0.05 mmol Br_2) was added dropwise. The mixture was stirred at room temperature for 4 hours. The reaction was quenched with saturated aqueous Na_2SO_3 (5 mL). The mixture was further diluted with water (10 mL) and extracted with dichloromethane (3 × 10 mL). The combined organic phase was washed with brine (30 mL) and dried over anhydrous Na_2SO_4. After removal of the solvent by rotary evaporation, the crude product was isolated by silica gel column chromatography (petroleum ether/dichloromethane 20:1) to give dibromide **133** as a yellow solid (8 mg, 66 %, R_f = 0.3) and tribromide **134** as a yellow solid (2.2 mg, 21 %, R_f = 0.35).

Bromination with NBS: Dibenzoperylene **111** (302 mg, 0.65 mmol) and NBS (255 mg, 1.43 mmol) were mixed in dry dichloromethane (30 mL). The mixture was stirred at room temperature for 1 hour. The mixture was diluted with dichloromethane (50 mL), washed with water (3 × 50 mL) and dried over anhydrous Na_2SO_4. After removal of the solvent by rotary evaporation, dibromide **133** was obtained after precipitation from dichloromethane/methanol (15 mL/ 50 mL) as a yellow solid (388 mg, 96 %).

8,16-dibromo-2,10-di-*tert*-butyldibenzo[*fg*,*qr*]pentacene (133)

m.p.: 277 °C (dec.). ^{1}H NMR (400 MHz, $CDCl_3$) δ (ppm) = 9.00 (d, J = 1.7 Hz, 2H, H-1), 8.76-8.71 (m, 2H, H-3), 8.70-8.65 (m, 4H, H-2, H-4), 7.74-7.69 (m, 4H, H-5, H-6), 1.56 (s, 18H). ^{13}C NMR (101 MHz, $CDCl_3$) δ (ppm) = 148.43 (C-7), 132.39 (C-14), 130.77 (C-13), 129.74 (C-11), 129.72 (C-9), 129.61 (C-4), 128.57 (C-1), 128.46 (C-8), 128.03 (C-12), 127.64 (C-6), 127.34 (C-5), 122.57 (C-3), 120.10 (C-10), 118.28 (C-2), 35.43, 31.33. FT-IR (ATR) $\tilde{\nu}$ (cm^{-1}) = 3073 (w), 2953 (m), 2904 (w), 2865 (w), 1927 (w), 1810 (w), 1679 (w), 1607 (m), 1562 (w), 1506 (w), 1477 (w), 1459 (w), 1417 (w), 1361 (m), 1334 (w), 1276 (w), 1250 (w), 1233 (m), 1201 (w), 1155 (w), 1114 (w), 1082 (w), 1047 (w), 1004 (m), 934 (w), 915 (m), 891 (m), 869 (m), 834 (m), 801 (w), 774 (m), 741 (s), 723 (m), 663 (w), 635 (m). UV/Vis (CH_2Cl_2): λ_{max} (nm) (log ε) = 311 (4.59), 339 (3.85), 410 (4.56), 431 (4.47). Fluorescence (CH_2Cl_2): λ_{em} (λ_{ex}) (nm) = 469, 509 (410). MALDI-TOF MS (DCTB)

(*m*/*z*): $[M]^+$ calcd. for $C_{36}H_{30}Br_2$, 622.069; found, 622.112. Elemental anal. calcd. for $C_{36}H_{30}Br_2 \cdot 0.5CH_3OH$: C 68.66, H 5.05; found: C 68.69, H 5.09.

5,8,16-tribromo-2,10-di-*tert*-butyldibenzo[*fg*,*qr*]pentacene (134)

m.p.: 254 °C (dec.). ^{1}H NMR (600 MHz, $CDCl_3$) δ (ppm) = 9.01 (s, 1H, H-1), 8.96 (s, 1H, H-2), 8.82 (s, 1H, H-3), 8.73 (dd, *J* = 6.2, 3.2 Hz, 1H, H-4), 8.69 (s, 1H, H-5), 8.67 (dd, *J* = 6.2, 3.4 Hz, 1H, H-6), 8.55 (s, 1H, H-7), 8.52 (d, *J* = 8.9 Hz, 1H, H-8), 7.78 (dd, *J* =8.9, 1.3 Hz, 1H, H-9), 7.74 - 7.71 (m, 2H, H-10, H-11), 1.56 (s, 9H, H-31), 1.55 (s, 9H, H-32). ^{13}C NMR (151 MHz, $CDCl_3$) δ (ppm) = 149.13 (C-28), 148.80 (C-27), 132.61 (C-13), 132.31 (C-25), 131.69 (C-8), 131.44 (C-19), 131.03 (C-12), 130.96 (C-9), 130.53 (C-20), 130.13 (C-18), 129.94 (C-6), 129.73 (C-16), 129.68 (C-15), 129.46 (C-1), 128.85 (C-2), 128.77 (C-21), 128.62 (C-23), 128.20 (C-17), 128.04 (C-11), 127.79 (C-10), 127.65 (C-22), 125.51 (C-3), 122.88 (C-4), 122.17 (C-24), 120.69 (C-14), 119.44 (C-26), 118.84 (C-5), 118.52 (C-7), 35.78, 35.73, 31.62. FT-IR (ATR) $\tilde{\nu}$ (cm^{-1}) = 3076 (w), 2958 (m), 2902 (w), 2865 (w), 1606 (w), 1552 (w), 1475 (w), 1462 (w), 1405 (w), 1361 (m), 1333 (w), 1270 (w), 1251 (w), 1231 (w), 1212 (w), 1166 (w), 1117 (w), 1097 (w), 1048 (w), 1007 (w), 917 (m), 902 (m), 869 (m), 837 (w), 810 (m), 775 (w), 749 (s), 665 (w), 638 (m). MALDI-TOF MS (DCTB, Kalib PEG600) (*m*/*z*): $[M]^+$ calcd. for $C_{36}H_{29}Br_3$, 699.979; found, 699.976. UV/Vis ($CHCl_3$): λ_{max} (nm) (log ε) = 302 (4.46), 313 (4.55), 341 (3.84), 413 (4.48), 435 (4.50).

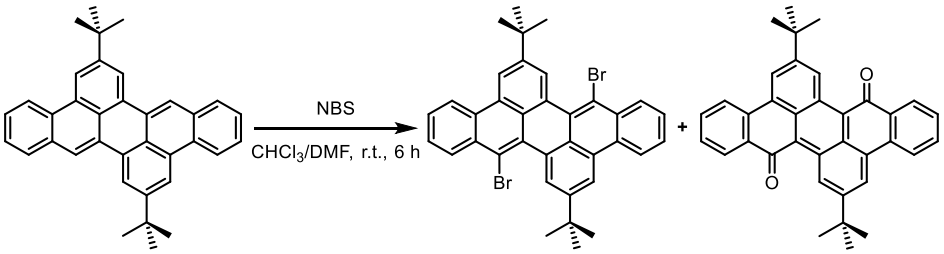

111 133 136

To a solution of dibenzoperylene **111** (9 mg, 0.02 mmol) in $CHCl_3$/DMF (0.5 mL/0.5 mL), NBS (7.8 mg, 0.044 mmol) was added in one portion. The mixture was diluted with DCM (40 mL), washed with water (3 × 30 mL) and dried over anhydrous Na_2SO_4. After removal of the solvent by rotary evaporation, the crude product was isolated by silica gel column chromatography (petroleum ether/dichloromethane 10:1) to give dibromide **133** as a yellow solid (9.2 mg, 74 %, R_f = 0.4) and diketone **136** as a dark purple solid (1.8 mg, 15 %, R_f = 0.15).

2,10-di-*tert*-butyldibenzo[*fg*,*qr*]pentacene-8,16-dione (136)

m.p.: 325 °C (dec.). ^{1}H NMR (500 MHz, $CDCl_3$) δ (ppm) = 10.01 (d, *J* = 1.67 Hz, 2H), 8.74 (d, *J* = 1.55 Hz, 2H), 8.55 (dd, *J* = 7.85, 1.01 Hz, 2H), 8.43 (d, *J* = 8.07 Hz, 2H), 7.81-7.78 (m, 2H), 7.63-7.60 (m, 2H), 1.63 (s, 18H). ^{13}C NMR (125 MHz, $CDCl_3$) δ (ppm) = 187.23, 151.75, 135.71, 133.03, 132.35, 131.90, 128.29, 128.06, 128.02, 127.63, 126.65, 125.56, 124.59, 122.63, 35.83, 31.13. FT-IR (ATR) $\tilde{\nu}$ (cm^{-1}) = 3149 (w), 3077 (w), 2950 (m), 2902 (w), 2864 (w), 1627 (s), 1594 (s), 1519 (w), 1483 (w), 1461 (w), 1414 (m), 1373 (m), 1357 (m), 1326 (w), 1307 (s), 1262 (m), 1226 (s), 1198 (m), 1160 (w), 1136 (w), 1099 (w), 1058 (m), 1034 (m), 952 (m), 918 (s), 881 (m), 807 (w),

792 (w), 771 (s), 738 (m), 722 (w), 704 (s), 626 (m). MALDI-TOF MS (DCTB) (*m*/*z*): $[M]^+$ calcd. for $C_{36}H_{30}O_2$, 494.225; found, 494.211. Elemental anal. cald. for $C_{36}H_{30}O_2$: C 87.42, H 6.11, found: C 87.34, H 6.40.

8,16-dibromo-2,10-di-*tert*-butylanthra[9,1-*gh*:10,5-*g'h'*]diquinoline (137)

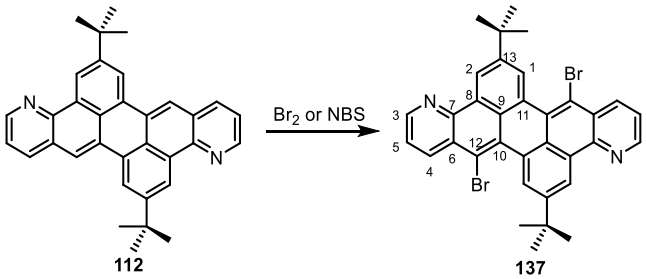

Bromination with Br_2: To a solution of dipyridine substrate **112** (7 mg, 0.015 mmol) in dichloromethane (3 mL), diluted bromine (0.1 mL out of 0.19 mL Br_2 in 10 mL DCM, 0.04 mmol Br_2) solution was added dropwise. The mixture was stirred at room temperature for 6 hours. The reaction was quenched with saturated aqueous Na_2SO_3 (5 mL). The mixture was further diluted with water (10 mL) and extracted with dichloromethane (3 × 10 mL). The combined organic phase was washed with brine (2 × 30 mL) and dried over anhydrous Na_2SO_4. After removal of the solvent by rotary evaporation, the product was obtained after silica gel column chromatography (petroleum ether/dichloromethane/ethyl acetate 20:3:1) as an orange solid (5 mg, 53 %).

Bromination with NBS: Dipyridine substrate (112 mg, 0.24 mmol) and NBS (94 mg, 0.53 mmol) was mixed in dry dichloromethane (11 mL). The mixture was stirred at room temperature for 1 hour. The mixture was diluted with dichloromethane (30 mL), washed with water (30 mL × 3) and dried over anhydrous Na_2SO_4. After removal of the solvent by rotary evaporation, the product was obtained after precipitation from dichloromethane/methanol (10 mL/20 mL) as an orange solid (146 mg, 97 %).

m.p.: 343 °C (dec.). ^{1}H NMR (400 MHz, $CDCl_3$) δ (ppm) = 9.41 (d, J = 1.9 Hz, 2H, H-2), 9.15 (d, J = 1.9 Hz, 2H, H-1), 8.99 (dd, J = 4.3, 1.4 Hz, 2H, H-3), 8.90 (dd, J = 8.4, 1.4 Hz, 2H, H-4), 7.64 (dd, J = 8.4, 4.3 Hz, 2H, H-5), 1.59 (s, 18H). ^{13}C NMR (101 MHz, $CDCl_3$) δ (ppm) = 149.34 (C-13), 149.05 (C-3), 146.32 (C-7), 136.98 (C-4), 130.20 (C-10), 129.91 (C-8), 129.86 (C-1), 129.36 (C-9), 128.65 (C-11), 127.75 (C-6), 122.71 (C-5), 121.12 (C-2), 117.74 (C-12), 35.56, 31.37. FT-IR (ATR) $\tilde{\nu}$ (cm^{-1}) = 3070 (w), 2954 (m), 2903 (w), 2864 (w), 1941 (w), 1608 (w), 1582 (w), 1556 (m), 1461 (w), 1443 (w), 1403 (m), 1389 (m), 1362 (m), 1320 (w), 1292 (w), 1264 (w), 1246 (m), 1204 (w), 1142 (w), 1095 (w), 1052 (w), 1011 (m), 913 (m), 893 (m), 839 (m), 814 (w), 783 (s), 758 (m), 725 (w), 678 (w), 661 (w), 639 (m). UV/Vis (CH_2Cl_2): λ_{max} (nm) (log ε) = 305 (4.51), 318 (4.49), 389 (4.27), 410 (4.50), 432 (4.52). Fluorescence (CH_2Cl_2): λ_{em} (λ_{ex}) (nm) = 465 (410). MALDI-TOF MS (DCTB) (*m*/*z*): $[M]^+$ calcd. for $C_{34}H_{28}N_2Br_2$, 624.059; found, 624.059. Elemental anal. calcd. for $C_{34}H_{28}Br_2N_2 \cdot 0.3H_2O$: C 64.84, H 4.58, N 4.45; found: C 64.85, H 4.64, N 4.16.

8,16-dibromo-2,10-di-*tert*-butyl-6,14-difluorodibenzo[*fg*,*qr*]pentacene (138)

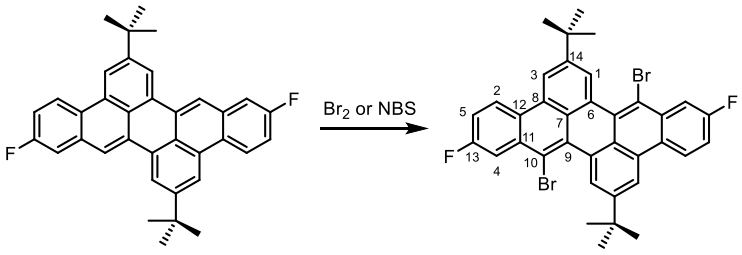

Bromination with Br_2: To a solution of difluorosubstrate (12.5 mg, 0.025 mmol) in dichloromethane (4 mL), diluted bromine (0.055 mmol) solution was added dropwise. The mixture was stirred at room temperature for 6 hours. The reaction was quenched with saturated aqueous Na_2SO_3 (3 mL). The mixture was further diluted with water (10 mL) and extracted with dichloromethane (3 × 10 mL). The combined organic phase was washed with brine (2 × 30 mL) and dried over anhydrous Na_2SO_4. After removal of the solvent by rotary evaporation, the product was obtained after silica gel column chromatography (petroleum ether/dichloromethane 40:1) as a yellow solid (10.8 mg, 65 %).

Bromination with NBS: Difluorosubstrate (64 mg, 0.128 mmol) and NBS (50 mg, 0.281 mmol) was mixed in dry dichloromethane (6 mL). The mixture was stirred at room temperature for 1 hour. The mixture was diluted with dichloromethane (30 mL), washed with water (30 mL × 3) and dried over anhydrous Na_2SO_4. After removal of the solvent by rotary evaporation, the product was obtained after precipitation from dichloromethane/methanol (5 mL/20 mL) as a yellow solid (82 mg, 97 %).

m.p.: 324 °C (dec.). ^{1}H NMR (600 MHz, $CDCl_3$) δ (ppm) = 8.97 (d, J = 1.6 Hz, 2H, H-1), 8.72 (dd, J = 9.1, 5.5 Hz, 2H, H-2), 8.60 (d, J = 1.3 Hz, 2H, H-3), 8.34 (dd, J = 11.2, 2.6 Hz, 2H, H-4), 7.45 (ddd, J = 9.5, 7.7, 2.6 Hz, 2H, H-5), 1.55 (s, 18H). ^{13}C NMR (151 MHz, $CDCl_3$) δ (ppm) = 162.39 (d, $J_{C,F}$ = 246.1 Hz, C-13), 149.18 (C-14), 134.52 (d, $J_{C,F}$ = 8.9 Hz, C-10), 131.12 (C-9), 129.85 (C-6), 128.70 (C-1), 128.52 (C-8), 127.78 (C-7), 127.52 (d, $J_{C,F}$ = 1.7 Hz, C-12), 125.40 (d, $J_{C,F}$ = 8.8 Hz, C-2), 119.12 (d, $J_{C,F}$ = 3.8 Hz, C-11), 118.66 (C-3), 116.52 (d, $J_{C,F}$ = 23.9 Hz, C-5), 114.81 (d, $J_{C,F}$ = 24.7 Hz, C-4), 35.75, 31.57. ^{19}F NMR (283 MHz, $CDCl_3$) δ (ppm) = -112.77. FT-IR (ATR) $\tilde{\nu}$ (cm-1) = 3092 (w), 2953 (m), 2903 (w), 2865 (w), 1609 (m), 1567 (w), 1511 (m), 1475 (m), 1421 (w), 1362 (w), 1340 (w), 1288 (w), 1275 (m), 1245 (w), 1231 (w), 1200 (w), 1178 (m), 1146 (w), 1111 (w), 1086 (w), 991 (m), 906 (w), 890 (w), 855 (s), 837 (w), 815 (s), 791 (m), 742 (w), 726 (w), 702 (w), 667 (w), 636 (m). MALDI-TOF MS (DCTB, Kalib PEG600) (*m*/*z*): $[M]^+$ calcd. for $C_{36}H_{28}F_2Br_2$, 658.050; found, 658.051.

5,7,12,14-tetrabromo-2,9-di-*tert*-butylperyleno[2,3-*b*:8,9-*b*']dithiophene (139)

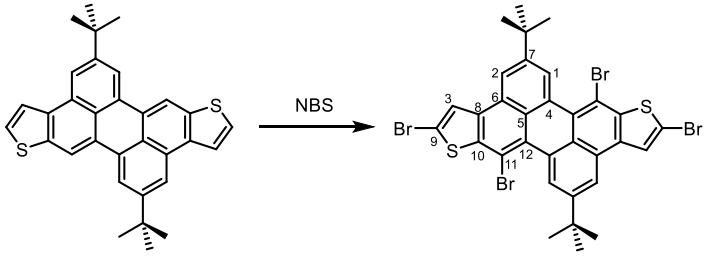

113 139

Dithienodibenzoperylene **113** (21 mg, 0.044 mmol) and NBS (35 mg, 0.194 mmol, 4.4 eq.) were dissolved in dichloromethane (2 mL) and stirred at room temperature for 1 hour. The mixture was diluted with dichloromethane (50 mL), washed with water (3 × 50 mL) and dried over anhydrous Na_2SO_4. After removal of the solvent by rotary evaporation, to give the product after precipitation from dichloromethane/methanol and dried in vacuum as a yellow solid (31 mg, 91 %).

m.p.: 357 °C (dec.). ^{1}H NMR (400 MHz, $CDCl_3$) δ (ppm) = 8.97 (d, J= 1.8 Hz, 2H, H-1), 8.10 (d, J= 1.8 Hz, 2H, H-2), 8.09 (s, 2H, H-3), 1.52 (s, 18H). ^{13}C NMR (101 MHz, $CDCl_3$) δ (ppm) = 149.26 (C-7), 144.46 (C-10), 135.27 (C-6), 129.26 (C-12), 127.46 (C-8), 127.10 (C-5), 126.74 (C-4), 126.51 (C-1), 126.09 (C-3), 118.82 (C-2), 116.44 (C-9), 110.26 (C-11), 35.33, 31.19. FT-IR (ATR) $\tilde{\nu}$ (cm^{-1}) = 2959 (w), 2864 (w), 1608 (w), 1538 (w), 1460 (m), 1392 (w), 1361 (w), 1337 (w), 1295 (w), 1265 (w), 1224 (w), 1201 (w), 1172 (w), 1105 (w), 1016 (w), 992 (w), 931 (m), 906 (w), 868 (m), 842 (w), 823 (s), 797 (w), 757 (w), 739 (w), 696 (w), 667 (w), 642 (w), 617 (w). UV/Vis (CH_2Cl_2): λ_{max} (nm) (log ε) = 291 (4.64), 336 (3.64), 347 (3.57), 370 (3.74), 389 (3.84), 416 (4.20), 439 (4.50), 466 (4.58). Fluorescence (CH_2Cl_2): λ_{em} (λ_{ex}) (nm) = 501, 522 (439). MALDI-TOF MS (DCTB) (*m*/*z*): $[M]^+$ calcd. for $C_{32}H_{24}S_2Br_4$, 791.801; found, 791.800. Elemental anal. calcd. for $C_{32}H_{24}Br_4S_2 \cdot 1.2H_2O$: C 47.22, H 3.27, found: C 47.21, H 3.34.

3,3'-(3,7-di-*tert*-butyl-9,10-dihydroanthracene-1,5-diyl)-bis(5-(*tert*-butyl)thiophene-2-carbaldehyde) (140)

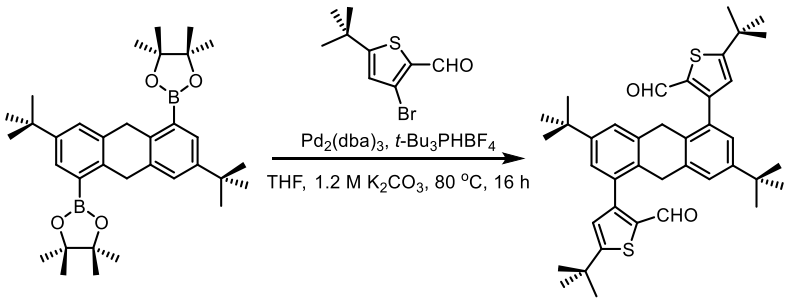

109 140

In a screw-capped vial, a mixture of diboronic pinacol ester **109** (1.96 g, 3.6 mmol), 3-bromo-5-(*tert*-butyl)thiophene-2-carbaldehyde (2.67 g, 10.8 mmol) and K_2CO_3 (994 mg, 7.2 mmol) were suspended in argon-degassed THF (24 mL) and water (6 mL). A mixture of $Pd_2(dba)_3$ (165 mg, 0.18 mmol) and *t*-Bu_3PHBF_4 (165 mg, 0.57 mmol) was added and the mixture stirred at 80 °C for 16 hours. After cooling down the reaction mixture to room temperature, it was diluted with dichloromethane (200 mL). The organic phase was washed with water (3 × 100 mL) and dried over anhydrous Na_2SO_4. After removal of the solvent by rotary evaporation, the crude product was

purified by silica gel column chromatography (petroleum ether/dichloromethane/ethyl acetate 40:10:1) to give the product **140** (mixture of atropisomers) as a colorless solid (2.02 g, 90%).

m.p.: 275 °C (dec.). ^{1}H NMR (400 MHz, CD_2Cl_2) δ (ppm) = 9.52 (s, 2H), 7.26 (d, J = 2.0 Hz, 2H), 7.19 (d, J = 2.0 Hz, 2H), 6.95 (s, 2H), 4.02-3.68 (m, 4H), 1.48 (s, 18H), 1.28 (s, 18H). ^{13}C NMR (101 MHz, $CDCl_3$) δ (ppm) = 184.32, 167.71, 151.88, 149.54, 138.12, 137.04, 133.26, 132.63, 127.29, 126.21, 125.55, 35.96, 35.07, 34.93, 32.47, 31.68. FT-IR (ATR) $\tilde{\nu}$ (cm^{-1}) = 2962 (m), 2903 (w), 2866 (w), 1660 (s), 1604 (w), 1574 (w), 1531 (w), 1477 (m), 1458 (m), 1441 (m), 1359 (m), 1295 (w), 1271 (w), 1248 (m), 1220 (m), 1158 (w), 1061 (w), 1023 (w), 931 (w), 885 (w), 869 (w), 842 (m), 819 (w), 686 (m), 655 (w). MALDI-TOF MS (DCTB) (*m*/*z*): $[M+Na]^+$ calcd. for $C_{40}H_{48}O_2S_2Na$, 647.299; found, 647.300. Elemental anal. calcd. for $C_{40}H_{48}O_2S_2$: C 76.88, H 7.74; found: C 76.71, H 8.04.

2,5,9,12-tetra-*tert*-butylperyleno[2,3-*b*:8,9-*b*']dithiophene (141)

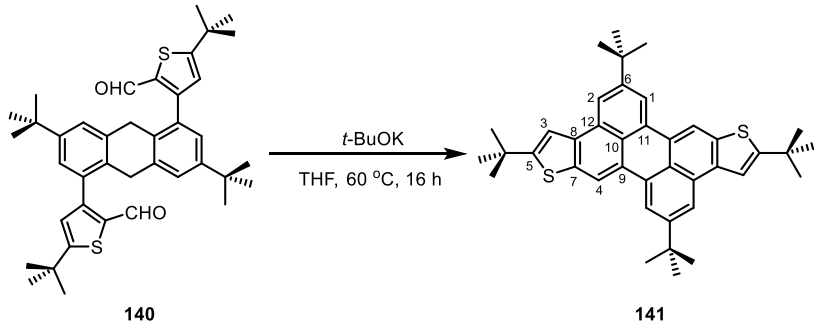

140 **141**

In a screw-capped vial, potassium *tert*-butoxide (168 mg, 1.5 mmol) was added to a suspension of atropisomeric mixture of dialdehyde **140** (150 mg, 0.24 mmol) in dry THF (6 mL) under argon atmosphere and stirred at 60 °C for 16 hours. After cooling down to room temperature, the reaction mixture was poured into 1M aq. HCl (50 mL) and extracted with dichloromethane (3 × 50 mL). The combined organic phase was washed with brine (2 × 50 mL) and dried over anhydrous Na_2SO_4. After removal of the solvent by rotary evaporation, the crude product was purified by silica gel column chromatography (petroleum ether/dichloromethane 20:1) to give the product **141** as a yellow solid (83 mg, 59 %).

m.p.: 373 °C (dec.). ^{1}H NMR (600 MHz, $CDCl_3$) δ (ppm) = 8.51 (s, 2H, H-4), 8.35 (d, J = 1.4 Hz, 2H, H-2), 8.10 (d, J = 1.4 Hz, 2H, H-1), 7.62 (s, 2H, H-3), 1.57 (s, 18H), 1.56 (s, 18H). ^{13}C NMR (151 MHz, $CDCl_3$) δ (ppm) = 158.38 (C-5), 149.17 (C-6), 137.17 (C-7), 135.72 (C-12), 131.55 (C-9), 130.03 (C-11), 127.64 (C-8), 124.53 (C-10), 118.82 (C-1), 117.58 (C-2), 116.18 (C-3), 113.86 (C-4), 35.20, 35.18, 32.43, 31.53. FT-IR (ATR) $\tilde{\nu}$ (cm^{-1}) = 3076 (w), 2956 (s), 2900 (m), 2865 (m), 1736 (w), 1606 (m), 1490 (m), 1458 (m), 1389 (w), 1361 (s), 1323 (w), 1294 (w), 1247 (s), 1221 (m), 1199 (m), 1175 (w), 1086 (w), 1049 (w), 1020 (w), 958 (m), 926 (w), 881 (w), 858 (s), 819 (s), 765 (w), 679 (m), 660 (w), 644 (w), 617 (w). UV/Vis (CH_2Cl_2): λ_{max} (nm) (log ε) = 280 (4.57), 291 (4.71), 333 (3.59), 351 (3.66), 368 (3.74), 397 (3.88), 420 (4.28), 443 (4.61), 471 (4.69). Fluorescence (CH_2Cl_2): λ_{em} (λ_{ex}) (nm) = 489, 522, 561 (443). MALDI-TOF MS (DCTB, Kalib PEG600) (*m*/*z*): $[M]^+$ calcd. for $C_{40}H_{44}S_2$, 588.288; found, 588.290. Elemental anal. calcd. for $C_{40}H_{44}S_2$: C 81.58, H 7.53; found: C 81.73, H 7.54.

7,14-dibromo-2,5,9,12-tetra-*tert*-butylperyleno[2,3-*b*:8,9-*b*']dithiophene (142)

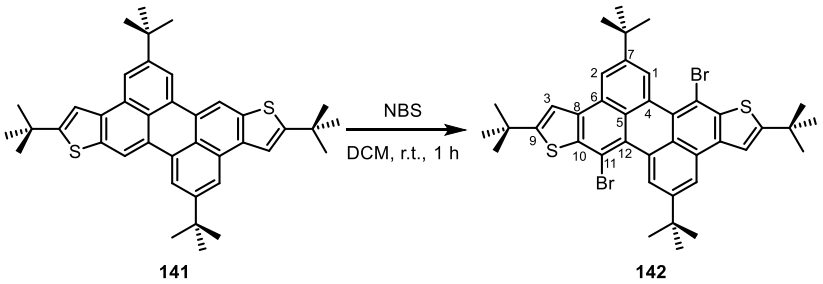

141 142

Dithienyl substrate **141** (59 mg, 0.1 mmol) and NBS (39 mg, 0.22 mmol, 2.2 equiv.) were dissolved in dichloromethane (4.5 mL) and stirred at room temperature for 1 hour. The mixture was diluted with dichloromethane (50 mL), washed with water (3 × 50 mL) and dried over anhydrous Na_2SO_4. After removal of the solvent by rotary evaporation, to give the product after silica gel column chromatography (petroleum ether/dichloromethane 50:1) and precipitation from dichloromethane/methanol and dried in vacuum as yellow solid (63 mg, 85 %).

m.p.: 371 °C (dec.). ^{1}H NMR (400 MHz, $CDCl_3$) δ (ppm) = 8.94 (s, 2H, H-1), 8.15 (s, 2H, H-2), 7.80 (s, 2H, H-3), 1.58 (s, 18H), 1.54 (s, 18H). ^{13}C NMR (101 MHz, $CDCl_3$) δ (ppm) = 159.72 (C-9), 148.55 (C-7), 141.57 (C-10), 135.35 (C-6), 129.69 (C-12), 127.74 (C-8), 127.58 (C-4), 125.97 (C-5), 125.88 (C-1), 118.34 (C-2), 117.06 (C-3), 111.52 (C-11), 35.35, 35.27, 32.36, 31.30. FT-IR (ATR) $\tilde{\nu}$ (cm^{-1}) = 2960 (s), 2902 (w), 2866 (w), 1608 (w), 1548 (w), 1501 (w), 1470 (m), 1431 (w), 1391 (w), 1362 (m), 1341 (m), 1308 (w), 1254 (m), 1232 (m), 1201 (m), 1141 (w), 1107 (w), 1049 (w), 1018 (w), 960 (m), 905 (w), 872 (w), 831 (s), 743 (w), 699 (w), 677 (w), 663 (m), 618 (w). UV/Vis (CH_2Cl_2): λ_{max} (nm) (log ε) = 293 (4.61), 336 (3.69), 370 (3.75), 389 (3.88), 416 (4.23), 440 (4.54), 466 (4.62). Fluorescence (CH_2Cl_2): λ_{em} (λ_{ex}) (nm) = 503, 521 (440). MALDI-TOF MS (DCTB) (*m*/*z*): $[M]^+$ calcd. for $C_{40}H_{42}S_2Br_2$, 746.107; found, 746.105. Elemental anal. calcd. for $C_{40}H_{42}Br_2S$: C 64.34, H 5.67; found: C 64.19, H 5.74.

2,10-di-*tert*-butyl-8,16-diphenyldibenzo[*fg*,*qr*]pentacene (143)

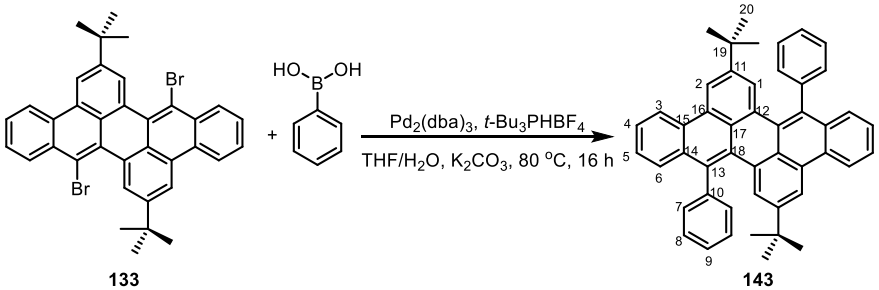

133 143

According to **GP1**, the dibromide **133** (50 mg, 0.08 mmol), phenylboronic acid (98 mg, 0.8 mmol), K_2CO_3 (28 mg, 0.2 mmol), $Pd_2(dba)_3$ (7.3 mg, 0.008 mmol) and *t*-Bu_3PHBF_4 (7.3 mg, 0.025 mmol) in THF/water (0.8 mL/0.2 mL) gave, after workup, silica gel column chromatography (petroleum ether/dichloromethane 10:1) and precipitation, **143** as a yellow solid (45 mg, 91 %).

m.p.: 344 °C (dec.). ^{1}H NMR (600 MHz, $CDCl_3$) δ (ppm) = 8.71 (d, *J* = 8.3 Hz, 2H, H-3), 8.49 (d, *J* = 1.4 Hz, 2H, H-2), 7.71 (d, *J* = 1.6 Hz, 2H, H-1), 7.65 (d, *J* = 8.3 Hz, 2H, H-4), 7.60 (t, *J* = 7.5 Hz, 2H, H-5), 7.50 (d, *J* = 2.4 Hz, 4H, H-7), 7.49 (s, 4H, H-8), 7.46-7.39 (m, 4H, H-6,9), 1.11 (s,

18H, H-20). ^{13}C NMR (151 MHz, $CDCl_3$) δ (ppm) = 148.08 (C-11), 141.84 (C-10), 134.63 (C-17), 133.28 (C-14), 132.02 (C-8), 131.01 (C-12), 130.23 (C-15), 129.26 (C-7), 128.97 (C-16), 128.92 (C-1), 127.86 (C-18), 127.74 (C-13), 127.69 (C-4), 127.26 (C-9), 126.23 (C-5), 126.19 (C-6), 122.31 (C-3), 116.90 (C-2), 34.72 (C-19), 31.13 (C-20). FT-IR (ATR) $\tilde{\nu}$ (cm^{-1}) = 3077 (w), 3058 (w), 2951 (m), 2952 (m), 2857 (m), 1956 (w), 1885 (w), 1818 (w), 1740 (w), 1603 (m), 1573 (w), 1515 (w), 1485 (m), 1461 (m), 1443 (m), 1420 (w), 1398 (w), 1378 (w), 1361 (m), 1318 (w), 1297 (w), 1273 (m), 1232 (w), 1201 (w), 1174 (w), 1149 (w), 1110 (w), 1074 (w), 1045 (w), 1030 (w), 1005 (w), 973 (w), 935 (w), 894 (m), 870 (m), 814 (w), 790 (w), 762 (s), 727 (m), 706 (m), 672 (w), 635 (s), 617 (w). UV/Vis ($CHCl_3$): λ_{max} (nm) (log ε) = 300 (4.60), 312 (4.65), 412 (4.45), 432 (4.47). Fluorescence ($CHCl_3$): λ_{em} (λ_{ex}) (nm) = 472, 524 (412). Φ = 53.9±0.7%. MALDI-TOF MS (DCTB) (*m*/*z*): $[M]^+$ calcd. for $C_{48}H_{40}$, 616.313; found, 616.312. Elemental anal. calcd. for $C_{48}H_{40}\cdot 0.2H_2O$: C 92.92, H 6.56, found: C 92.91, H 6.48.

2,10-di-*tert*-butyl-8,16-bis(4-methoxyphenyl)dibenzo[*fg*,*qr*]pentacene (144)

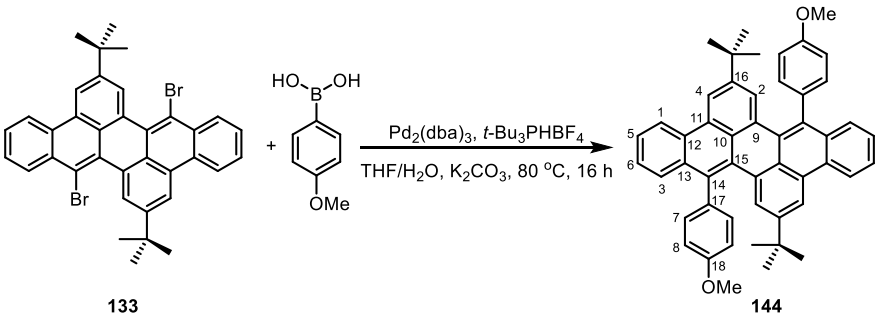

According to **GP1**, the dibromide **133** (22 mg, 0.035 mmol), 4-methoxylphenylboronic acid (53 mg, 0.35 mmol), K_2CO_3 (14 mg, 0.1 mmol), $Pd_2(dba)_3$ (3 mg, 0.0034 mmol) and *t*-Bu_3PHBF_4 (3 mg, 0.0112 mmol) in THF/water (0.35 mL/0.1 mL) gave, after workup, silica gel column chromatography (petroleum ether/dichloromethane 5:1) and precipitation, **144** as a yellow solid (22 mg, 93%).

m.p.: 303 °C (dec.). ^{1}H NMR (400 MHz, $CDCl_3$) δ (ppm) = 8.70 (d, *J* = 8.2 Hz, 2H, H-1), 8.48 (s, 2H, H-2), 7.74 (d, *J* = 8.2 Hz, 2H, H-3), 7.69 (d, *J* = 1.6 Hz, 2H, H-4), 7.60 (t, *J* = 7.4 Hz, 2H, H-5), 7.49 - 7.42 (m, 2H, H-6), 7.39 (d, *J* = 8.6 Hz, 4H, H-7), 7.04 (d, *J* = 8.7 Hz, 4H, H-8), 3.88 (s, 6H), 1.15 (s, 18H). ^{13}C NMR (101 MHz, $CDCl_3$) δ (ppm)= 159.01 (C-18), 147.95 (C-16), 134.26 (C-14), 133.93 (C-17), 133.53 (C-13), 133.09 (C-7), 131.25 (C-11), 130.35 (C-12), 128.94 (C-9), 128.72 (C-4), 128.05 (C-10), 127.95 (C-15), 127.73 (C-3), 126.17 (C-5, 6), 122.33 (C-1), 116.76 (C-2), 114.93 (C-8), 55.43, 34.75, 31.15. MALDI-TOF MS (DCTB) (*m*/*z*): $[M]^+$ calcd. for $C_{50}H_{44}O_2$, 676.334; found, 676.332. Elemental anal. calcd. for $C_{50}H_{44}O_2$: C 88.72, H 6.55, found: C 88.50, H 6.75.

2,10-di-*tert*-butyl-8,16-bis(3-(hexyloxy)phenyl)dibenzo[*fg*,*qr*]-pentacene (145)

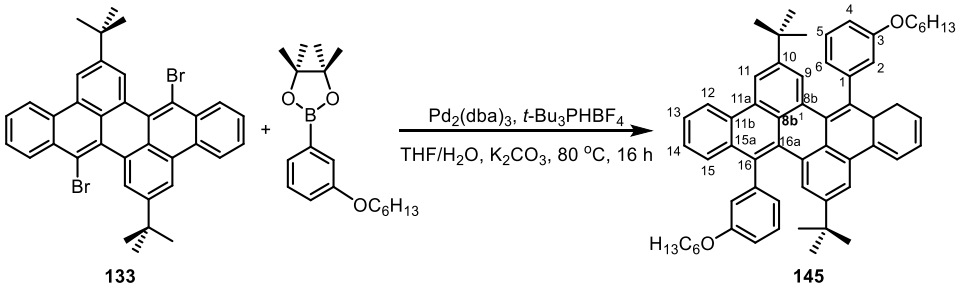

133 145

According to **GP1**, the dibromide **133** (436 mg, 0.7 mmol), (3-(hexyloxy)phenyl)boronic acid pinacol ester (852 mg, 2.8 mmol), K_2CO_3 (242 mg, 1.75 mmol), $Pd_2(dba)_3$ (32 mg, 0.035 mmol) and *t*-Bu_3PHBF_4 (32 mg, 0.11 mmol) in THF/water (7 mL/1.75 mL) gave, after workup, silica gel column chromatography (petroleum ether/dichloromethane 5:1) and washing with methanol (2 × 10 mL), **145** (mixture of atropisomers) as a bright yellow solid (290 mg, 50 %).

m.p.: 97 °C (dec.). ^{1}H NMR (600 MHz, $CDCl_3$) δ (ppm) = 8.71 (s, 1H, H-12), 8.69 (s, 1H, H-12), 8.50 (s, 2H, H-11), 7.83 (s, 1H, H-9), 7.83 (s, 1H, H-9), 7.70 (s, 1H, H-15), 7.69 (s, 1H, H-15), 7.60 (d, J = 7.3 Hz, 1H, H-13), 7.59 (s, J = 7.3 Hz, 1H, H-13), 7.45 (d, J = 7.6 Hz, 1H, H-14), 7.44 (d, J = 7.3 Hz, 1H, H-14), 7.43 - 7.40 (m, 1H, H-5), 7.40 - 7.38 (m, 1H, H-5), 7.07 (d, J = 7.4 Hz, 1H, H-6), 7.04 (d, J = 7.6 Hz, 1H, H-6), 7.02 (s, 1H, H-2), 6.98 (s, 1H, H-2), 6.96 (d, J = 2.1 Hz, 1H, H-4), 6.95 (d, J = 2.2 Hz, 1H, H-4), 3.95 - 3.84 (m, 4H, H-OCH_2), 1.74 - 1.66 (m, 4H, H-hex), 1.42 - 1.35 (m, 4H, H-hex), 1.30 - 1.24 (m, 8H, H-hex), 1.14 (s, 18H, H-*t*-Bu), 0.88 - 0.84 (m, 6H, H-hex). ^{13}C NMR (151 MHz, $CDCl_3$) δ (ppm) = 160.16 (C-3), 160.11 (C-3), 148.11 (C-10), 143.13 (C-1), 134.46 (C-16), 133.17 (C-15a), 131.01 (C-16a), 131.00 (C-16a), 130.24 (C-11b), 130.21 (C-5), 130.19 (C-5), 128.99 (C-11a), 128.62 (C-9), 127.82 (C-15), 127.69 (C-8b), 127.64 (C-8b^1), 126.20 (C-13), 126.16 (C-14), 124.27 (C-6), 124.11 (C-6), 122.25 (C-12), 117.66 (C-2), 117.50 (C-2), 116.97 (C-11), 113.91 (C-4), 113.90 (C-4), 68.02, 67.99, 34.78, 31.50, 31.49, 31.16, 29.13, 29.11, 22.56, 14.00. FT-IR (ATR) $\tilde{\nu}$ (cm^{-1}) = 3070 (w), 2954 (m), 2930 (m), 2864 (m), 2745 (w), 1924 (w), 1895 (w), 1837 (w), 1803 (w), 1768 (w), 1742 (w), 1598 (m), 1576 (m), 1515 (w), 1467 (m), 1428 (m), 1393 (w), 1363 (w), 1308 (w), 1282 (m), 1240 (m), 1187 (w), 1164 (w), 1145 (w), 1043 (m), 1029 (m), 962 (w), 930 (w), 872 (m), 815 (w), 783 (m), 762 (s), 733 (m), 706 (m), 641 (m), 611 (w). UV/Vis (CH_2Cl_2): λ_{max} (nm) (log ε) = 299 (4.58), 311 (4.61), 341 (3.93), 411 (4.39), 431 (4.40). Fluorescence (CH_2Cl_2): λ_{em} (λ_{ex}) (nm) = 472, 502 (311). Φ = 53.5±1.3%. τ = 2.45 ns. MALDI-TOF MS (DCTB) (*m*/*z*): $[M]^+$ calcd. for $C_{60}H_{64}O_2$, 816.490; found, 816.497. Elemental anal. calcd. for $C_{60}H_{64}O_2$: C 88.19, H 7.89, found: C 87.83, H 7.94.

5,5'-(2,10-di-*tert*-butyldibenzo[*fg*,*qr*]pentacene-8,16-diyl)bis(2-methoxypyridine) (147)

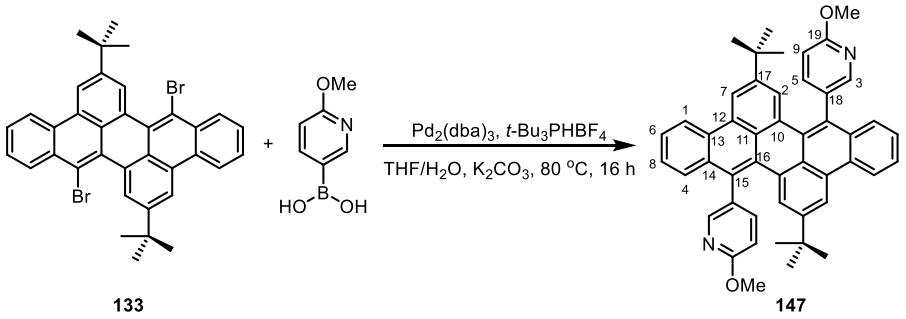

133 147

According to **GP1**, the dibromide **133** (22 mg, 0.035 mmol), 2-methoxypyridine-5-boronic acid (54 mg, 0.35 mmol), K_2CO_3 (14 mg, 0.1 mmol), $Pd_2(dba)_3$ (3.2 mg, 0.0035 mmol) and *t*-Bu_3PHBF_4 (3.2 mg, 0.011 mmol) in THF/water (0.35 mL/0.1 mL) gave, after workup, silica gel column chromatography (petroleum ether/dichloromethane 10:1) and precipitation, **147** (mixture of atropisomers) as a yellow solid (21 mg, 89%).

m.p.: 290 °C (dec.). ^{1}H NMR (600 MHz, $Cl_2CDCDCl_2$) δ (ppm) = 8.71 (d, J = 8.3 Hz, 2H, H-1), 8.48 (d, J = 1.1 Hz, 2H, H-2), 8.21 (d, J = 7.7 Hz, 2H, H-3), 7.74 (d, J = 8.3 Hz, 2H, H-4), 7.70 - 7.62 (m, 4H, H-5, 6), 7.54 (d, J = 2.9 Hz, 2H, H-7), 7.52 (t, J = 7.6 Hz, 2H, H-8), 6.92 (dd, J = 8.4, 3.7 Hz, 2H, H-9), 3.98 (br, 6H), 1.14 (s, 18H). ^{13}C NMR (151 MHz, $Cl_2CDCDCl_2$) δ (ppm) = 163.15 (C-19), 149.11 (C-3), 148.36 (C-17), 142.31 (C-5), 132.91 (C-14), 130.94 (C-10), 130.66 (C-13), 129.84 (C-15), 129.81 (C-18), 128.91 (C-7), 128.85 (C-12), 128.52 (C-16), 127.60 (C-11), 127.07 (C-4), 126.81 (C-8), 126.78 (C-6), 122.46 (C-1), 116.98 (C-2), 111.46 (C-9), 53.70, 34.59, 30.97. FT-IR (ATR) $\tilde{\nu}$ (cm^{-1}) = 2955 (w), 2903 (w), 2868 (w), 1602 (m), 1562 (w), 1516 (w), 1487 (s), 1418 (w), 1366 (m), 1301 (w), 1278 (s), 1246 (m), 1143 (w), 1124 (w), 1026 (m), 939 (w), 894 (w), 872 (w), 828 (m), 764 (s), 686 (w), 665 (w), 642 (w), 612 (w). MALDI-TOF MS (DCTB) (*m*/*z*): $[M]^+$ calcd. for $C_{48}H_{42}N_2O_2$, 678.325; found, 678.335. Elemental anal. calcd. for $C_{48}H_{42}N_2O_2$: C 84.92, H 6.24, N 4.13, found: C 84.63, H 6.24, N 3.86.

5,5'-(2,10-di-*tert*-butyldibenzo[*fg*,*qr*]pentacene-8,16-diyl)bis(2,3-dimethoxypyridine) (148)

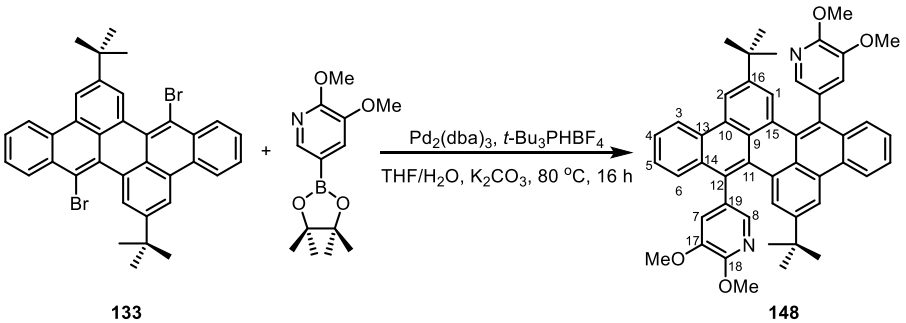

133 148

According to **GP1**, dibromide **133** (436 mg, 0.7 mmol), (5,6-dimethoxypyridin-3-yl)boronic acid pinacol ester (743 mg, 2.8 mmol), K_2CO_3 (242 mg, 1.75 mmol), $Pd_2(dba)_3$ (32 mg, 0.035 mmol) and *t*Bu_3PHBF_4 (32 mg, 0.11 mmol) in THF/water (7 mL/1.75 mL) gave, after workup, silica gel column chromatography (petroleum ether/dichloromethane /ethyl acetate 5:2:0.4) and precipitation from dichloromethane/methanol, **148** (mixture of atropisomers) as a bright yellow solid (363 mg, 70 %).

m.p.: 286 °C (dec.). ^{1}H NMR (600 MHz, $CDCl_3$) δ (ppm) = 8.73 (d, J = 8.2 Hz, 2H, H-3), 8.53 (s, 2H, H-2), 7.91 (d, J = 1.7 Hz, 1H, H-8), 7.82 (d, J = 1.7 Hz, 1H, H-8), 7.80 (d, J = 8.3 Hz, 1H, H-6), 7.78 (d, J = 8.2 Hz, 1H, H-6), 7.70 (d, J = 1.4 Hz, 1H, H-1), 7.68 (d, J = 1.4 Hz, 1H, H-1), 7.65 (t, J = 7.5 Hz, 2H, H-4), 7.56 - 7.48 (m, 2H, H-5), 7.16 (d, J = 1.6 Hz, 1H, H-7), 7.04 (d, J = 1.5 Hz, 1H, H-7), 4.12 (s, 3H), 4.11 (s, 3H), 3.78 (s, 3H), 3.70 (s, 3H), 1.17 (s, 18H). ^{13}C NMR (151 MHz, $CDCl_3$) δ (ppm) = 153.64 (C-18), 153.61 (C-18), 148.43 (C-16), 148.39 (C-16), 144.91 (C-17), 144.88 (C-17), 139.40 (C-8), 138.96 (C-8), 133.16 (C-14), 133.12 (C-14), 130.80 (C-19), 130.76 (C-19), 130.73 (C-12), 130.66 (C-12), 130.61 (C-11), 130.56 (C-11), 130.31 (C-13), 129.28 (C-10), 129.26 (C-10), 128.60 (C-15), 128.59 (C-15), 128.55 (C-1), 128.53 (C-1), 127.65 (C-9), 127.64 (C-9), 127.22 (C-6), 126.62 (C-4,5), 122.55 (C-3), 121.16 (C-7), 120.93 (C-7), 117.19 (C-2), 117.16 (C-2), 56.01, 55.91, 53.95, 34.78, 31.07, 31.05. FT-IR (ATR) $\tilde{\nu}$ (cm^{-1}) = 3061 (w), 2957 (w), 2865 (w), 1596 (w), 1569 (w), 1515 (w), 1484 (s), 1544 (m), 1395 (m), 1308 (w), 1253 (m), 1197 (m), 1174 (m), 1143 (m), 1080 (w), 1043 (w), 1017 (m), 952 (w), 927 (w), 894 (w), 871 (m), 817 (w), 789 (w), 765 (s), 708 (w), 682 (w), 637 (w). UV/Vis (CH_2Cl_2): λ_{max} (nm) (log ε) = 302 (4.42), 311 (4.45), 347 (3.68), 416 (4.15), 435 (4.17). Fluorescence (CH_2Cl_2): λ_{em} (λ_{ex}) (nm) = 478, 501 (311). Φ = 58.4±0.6%. τ = 2.86 ns. MALDI-TOF MS (DCTB, Kalib PEG 600) (m/z): [M]$^{+}$ calcd. for $C_{50}H_{46}N_2O_4$, 738.345; found, 738.342. Elemental anal. calcd. for $C_{50}H_{46}N_2O_4$: C 81.27, H 6.28, N 3.79, found: C 81.08, H 6.27, N 3.50.

2,10-di-*tert*-butyl-8,16-diphenylanthra[9,1-*gh*:10,5-*g'h'*]diquinoline (149)

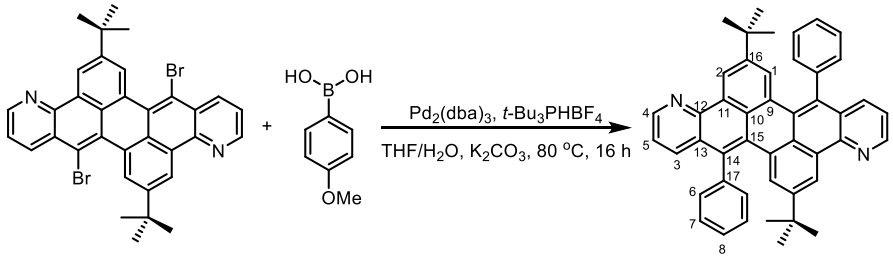

137 149

According to **GP1**, the dipyridinodibromide **137** (50 mg, 0.08 mmol), $Pd_2(dba)_3$ (7.3 mg, 0.008 mmol), *t*-Bu_3PHBF_4 (7.3 mg, 0.025 mmol), K_2CO_3 (28 mg, 0.2 mmol), THF (0.8 mL), water (0.2 mL) and phenylboronic acid (98 mg, 0.8 mmol) gave after workup, silica gel column chromatography (petroleum ether/dichloromethane/ethyl acetate 20:2:1) and precipitation, **149** as a yellow solid (43 mg, 87%).

m.p.: 350 °C (dec.). ^{1}H NMR (600 MHz, $Cl_2CDCDCl_2$) δ (ppm) = 9.19 (d, J = 1.9 Hz, 2H, H-1), 8.91 (dd, J = 4.2, 1.5 Hz, 2H, H-4), 7.92 (dd, J = 8.4, 1.4 Hz, 2H, H-3), 7.82 (d, J = 1.9 Hz, 2H, H-2), 7.55 - 7.50 (m, 4H, H-6), 7.47 - 7.42 (m, 6H, H-7, 8), 7.38 (dd, J = 8.4, 4.2 Hz, 2H, H-5), 1.10 (s, 18H). ^{13}C NMR (151 MHz, $Cl_2CDCDCl_2$) δ (ppm) = 148.86 (C-16), 148.24 (C-4), 145.86 (C-12), 140.26 (C-14), 134.80 (C-3), 133.39 (C-17), 131.49 (C-7), 130.39 (C-2), 130.08 (C-15), 129.88 (C-11), 129.60 (C-6), 129.03 (C-10), 128.05 (C-9), 127.89 (C-13), 127.73 (C-8), 121.55 (C-5), 119.42 (C-1), 34.65, 31.01. FT-IR (ATR) $\tilde{\nu}$ (cm^{-1}) = 3076 (w), 3053 (w), 3021 (w), 2950 (s), 2902 (w), 2864 (w), 1958 (w), 1885 (w), 1819 (w), 1605 (w), 1564 (m), 1503 (w), 1483 (w), 1461 (w), 1443 (w), 1404 (m), 1391 (m), 1361 (m), 1334 (w), 1301 (w), 1265 (w), 1230 (w), 1202 (w), 1181

(w), 1154 (w), 1113 (w), 1094 (w), 1073 (w), 1054 (w), 1029 (w), 1010 (w), 976 (w), 937 (w), 915 (w), 893 (s), 866 (w), 852 (w), 828 (w), 800 (w), 788 (s), 770 (s), 749 (w), 726 (s), 707 (s), 638 (s), 619 (w). MALDI-TOF MS (DCTB) (*m*/*z*): $[M]^+$ calcd. for $C_{46}H_{38}N_2$, 618.303; found, 618.268. Elemental anal. calcd. for $C_{46}H_{38}N_2$: C 89.28, H 6.19, N 4.53, found: C 88.90, H 6.20, N 4.23. UV/Vis ($CHCl_3$): λ_{max} (nm) (log ε) = 293 (4.55), 305 (4.55), 319 (4.44), 414 (4.48), 434 (4.49).

2,10-di-*tert*-butyl-8,16-bis(3-(hexyloxy)phenyl)anthra[9,1-*gh*:10,5-*g'h'*]diquinoline (150)

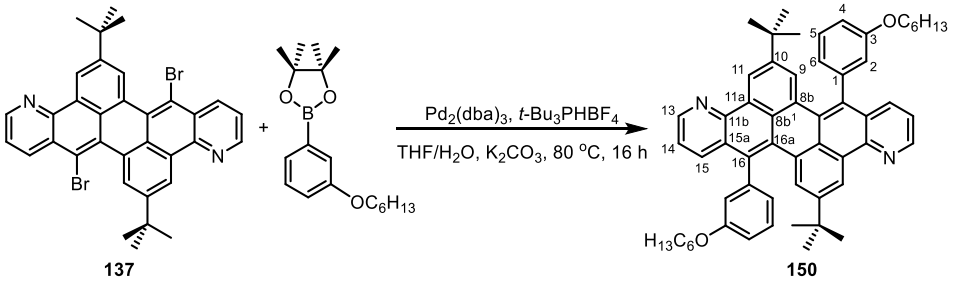

According to **GP1**, dibromide **137** (375 mg, 0.6 mmol), (3-(hexyloxy)phenyl)boronic acid pinacol ester (730 mg, 2.4 mmol), K_2CO_3 (207 mg, 1.5 mmol), $Pd_2(dba)_3$ (27 mg, 0.03 mmol) and tBu$_3$PHBF$_4$ (27 mg, 0.095 mmol) in THF/water (6 mL/1.5 mL) gave, after workup, silica gel column chromatography (petroleum ether/dichloromethane/ethyl acetate 25:5:1), **150** (mixture of atropisomers) as a yellow solid (384 mg, 78 %).

m.p.: 153 °C (dec.). ^{1}H NMR (500 MHz, CD_2Cl_2) δ (ppm) = 9.22 (s, 1H, H-11), 9.21 (s, 1H, H-11), 8.91 (d, J = 1.6 Hz, 1H, H-13), 8.90 (d, J = 1.6 Hz, 1H, H-13), 7.99 (dd, J = 6.0, 1.8 Hz, 2H, H-15), 7.98 (d, J = 1.8 Hz, 2H, H-9), 7.50 - 7.46 (m, 1H, H-5), 7.44 (d, J = 7.8 Hz, 1H, H-5), 7.41 (d, J = 4.2 Hz, 1H, H-14), 7.39 (d, J = 4.2 Hz, 1H, H-14), 7.07 (d, J = 7.5 Hz, 1H, H-6), 7.04 - 7.01 (m, 2H, H-6,2), 7.00 (d, J = 2.4 Hz, 1H, H-2), 6.99 - 6.98 (m, 1H, H-4), 6.97 - 6.96 (m, 1H, H-4), 3.96 - 3.87 (m, 4H, H-OCH$_2$), 1.74 - 1.66 (m, 4H, H-hex), 1.39 (m, 4H, H-hex), 1.29 - 1.25 (m, 8H, H-hex), 1.16 (s, 18H, H-*t*-Bu), 0.88 - 0.83 (m, 6H, H-hex). ^{13}C NMR (126 MHz, CD_2Cl_2) δ (ppm) = 161.07 (C-3), 161.02 (C-3), 149.44 (C-10), 148.79 (C-13), 146.64 (C-11b), 142.56 (C-1), 135.37 (C-15a), 134.03 (C-16), 131.24 (C-5), 131.17 (C-5), 130.97 (C-16a), 130.70 (C-15), 130.69 (C-15), 130.64 (C-9), 130.62 (C-9), 129.69 (C-8b), 128.54 (C-11a), 128.39 (C-8b), 124.34 (C-6), 124.14 (C-6), 122.05 (C-14), 120.00 (C-11), 118.12 (C-2), 117.95 (C-2), 114.58 (C-4), 68.68, 68.64, 35.35, 32.06, 32.05, 31.47, 29.69, 29.67, 26.21, 26.19, 23.13, 23.12, 14.33, 14.32. FT-IR (ATR) $\tilde{\nu}$ (cm^{-1}) = 3220 (w), 3066 (w), 3028 (w), 2955 (s), 2931 (m), 2865 (m), 1951 (w), 1654 (w), 1597 (m), 1573 (s), 1468 (m), 1392 (m), 1363 (w), 1334 (w), 1306 (m), 1284 (m), 1239 (m), 1222 (m), 1195 (w), 1171 (w), 1152 (w), 1095 (w), 1031 (w), 933 (w), 896 (m), 827 (w), 789 (s), 733 (m), 696 (m), 644 (w). UV/Vis (CH_2Cl_2): λ_{max} (nm) (log ε) = 293 (4.53), 305 (4.55), 317 (4.50), 414 (4.39), 433 (4.40). Fluorescence (CH_2Cl_2): λ_{em} (λ_{ex}) (nm) = 475, 500 (414). Φ = 55.3±0.7%. τ = 2.59 ns. MALDI-TOF MS (DCTB, Kalib PEG 600) (*m*/*z*): $[M]^+$ calcd. for $C_{58}H_{62}N_2O_2$, 818.481; found, 818.483. Elemental anal. calcd. for $C_{58}H_{62}N_2O_2 \cdot 0.5H_2O$: C 84.12, H 7.67, N 3.38, found: C 84.28, H 7.71, N 3.30.

2,10-di-*tert*-butyl-8,16-bis(5,6-dimethoxypyridin-3-yl)anthra[9,1-*gh*:10,5-*g'h'*]diquinoline (151)

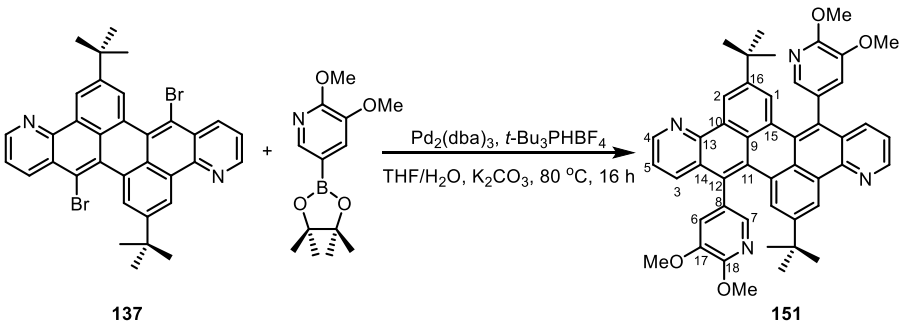

137 151

According to **GP1**, dibromide **137** (375 mg, 0.6 mmol), (5,6-dimethoxypyridin-3-yl)boronic acid pinacol ester (477 mg, 1.8 mmol), K_2CO_3 (207 mg, 1.7 mmol), $Pd_2(dba)_3$ (27 mg, 0.03 mmol) and tBu$_3$PHBF$_4$ (27 mg, 0.095 mmol) in THF/water (6 mL/1.5 mL) gave, after workup, silica gel column chromatography (petroleum ether/dichloromethane/ethyl acetate 10:5:3) and precipitation from dichloromethane/methanol, **151** (mixture of atropisomers) as a pale yellow solid (405 mg, 91 %).

m.p.: 374 °C (dec.). ^{1}H NMR (600 MHz, $Cl_2CDCDCl_2$) δ (ppm) = 9.24 (d, J = 1.6 Hz, 2H, H-2), 8.95 (dd, J = 4.0, 1.1 Hz, 2H, H-4), 8.02 (t, J = 7.5 Hz, 2H, H-3), 7.81 (d, J = 2.2 Hz, 1H, H-1), 7.81 (d, J = 2.2 Hz, 1H, H-1), 7.79 (d, J = 1.7 Hz, 1H, H-7), 7.78 (d, J = 1.7 Hz, 1H, H-7), 7.45 (dd, J = 8.1, 4.0 Hz, 2H, H-5), 7.09 (d, J = 1.7 Hz, 1H, H-6), 7.07 (d, J = 1.6 Hz, 1H, H-6), 4.06 (s, 3H), 4.05 (s, 3H), 3.75 (s, 3H), 3.72 (s, 3H), 1.17 (s, 18H). ^{13}C NMR (151 MHz, $Cl_2CDCDCl_2$) δ (ppm) = 153.80 (C-18), 153.77 (C-18), 149.06 (C-16), 148.56 (C-4), 145.99 (C-13), 144.95 (C-17), 138.92 (C-7), 138.72 (C-7), 134.27 (C-3), 130.51 (C-8), 129.88 (C-1), 129.72 (C-11), 129.70 (C-11), 129.52 (C-12), 129.49 (C-12), 129.19 (C-10), 129.16 (C-10), 128.96 (C-9), 128.93 (C-9), 128.78 (C-15), 127.83 (C-14), 127.80 (C-14), 121.81 (C-5), 120.43 (C-6), 120.36 (C-6), 119.79 (C-2), 56.01, 55.97, 53.97, 34.72, 30.98. FT-IR (ATR) $\tilde{\nu}$ (cm^{-1}) = 3021(w), 2948 (w), 2905 (w), 2866 (w), 1591 (w), 1568 (w), 1485 (s), 1460 (m), 1398 (s), 1296 (w), 1254 (s), 1201 (s), 1171 (m), 1146 (m), 1112 (w), 1038 (w), 1014 (m), 957 (w), 925 (w), 889 (w), 867 (w), 787 (m), 763 (m), 713 (w), 636 (m). UV/Vis (CH_2Cl_2): λ_{max} (nm) (log ε) = 306 (4.68), 341 (4.36), 357 (4.39), 418 (4.45), 421 (4.45), 436 (4.47). Fluorescence (CH_2Cl_2): λ_{em} (λ_{ex}) (nm) = 478, 506 (341). Φ = 54.4±2.0%. τ = 3.96 ns. MALDI-TOF MS (DCTB, Kalib PEG 600) (m/z): $[M]^+$ calcd. for $C_{48}H_{44}N_4O_4$, 740.336; found, 740.335. Elemental anal. calcd. for $C_{48}H_{44}N_4O_4$: C 77.81, H 5.99, N 7.56, found: C 77.74, H 6.11, N 7.32.

3,3'-(2,10-di-*tert*-butyldibenzo[*fg*,*qr*]pentacene-8,16-diyl)dithiophene (152)

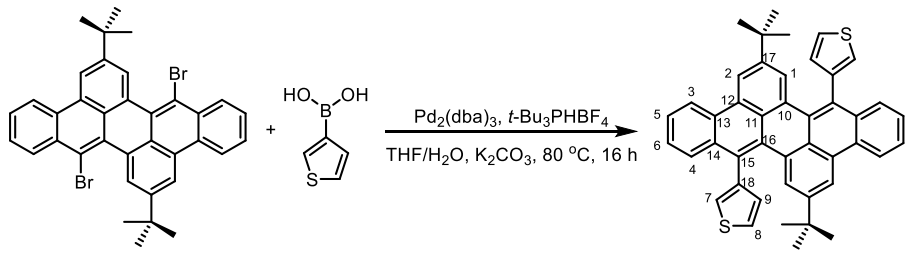

133 152

According to **GP1**, the dibromide **133** (50 mg, 0.08 mmol), $Pd_2(dba)_3$ (7.3 mg, 0.008 mmol), *t*- Bu_3PHBF_4 (7.3 mg, 0.025 mmol), K_2CO_3 (28 mg, 0.2 mmol), THF (0.8 mL), water (0.2 mL) and 3-thienylboronic acid (102 mg, 0.8 mmol) gave after workup, silica gel column chromatography (petroleum ether/dichloromethane 10:1) and precipitation, **152** as a yellow solid (42 mg, 84%).

m.p.: 340 °C (dec.). ^{1}H NMR (600 MHz, $Cl_2CDCDCl_2$) δ (ppm) = 8.69 (d, J = 8.3 Hz, 2H, H-3), 8.49 (s, 2H, H-1), 7.77 (d, J = 7.5 Hz, 2H, H-4), 7.72 (s, 2H, H-2), 7.63 (t, J = 7.5 Hz, 2H, H-6), 7.56 (br, 2H, H-7), 7.50 (t, J = 7.6 Hz, 2H, H-5), 7.24 (br, 4H, H-8, 9), 1.20 (s, 18H). ^{13}C NMR (151 MHz, $Cl_2CDCDCl_2$) δ (ppm) = 148.49 (C-17), 140.90 (C-18), 133.09 (C-14), 131.21 (C-15), 130.95 (C-9), 129.64 (C-13), 129.09 (C-8), 128.65 (C-12), 128.58 (C-10), 127.79 (C-2), 127.37 (C-11), 127.36 (C-4), 126.68 (C-5), 126.55 (C-6), 124.75 (C-7), 122.22 (C-3), 120.18 (C-16), 117.15 (C-1), 34.62, 31.16. FT-IR (ATR) $\tilde{\nu}$ (cm^{-1}) = 3116 (w), 3073 (w), 2951 (m), 2902 (w), 2865 (w), 1606 (w), 1572 (w), 1528 (w), 1508 (w), 1474 (w), 1462 (w), 1419 (w), 1410 (w), 1361 (w), 1277 (w), 1233 (w), 1200 (w), 1171 (w), 1141 (w), 1080 (w), 1045 (w), 935 (w), 921 (w), 888 (w), 869 (m), 841 (m), 813 (w), 784 (s), 752 (s), 730 (m), 710 (w), 692 (w), 666 (m), 635 (m). UV/Vis ($CHCl_3$): λ_{max} (nm) (log ε) = 302 (4.60), 313 (4.66), 418 (4.43), 428 (4.43). MALDI-TOF MS (DCTB) (*m*/*z*): $[M]^+$ calcd. for $C_{44}H_{36}S_2$, 628.225; found, 628.205. Elemental anal. calcd. for $C_{44}H_{36}S_2$: C 84.03, H 5.77, found: C 83.79, H 5.72.

4,4'-(2,10-di-*tert*-butyldibenzo[*fg*,*qr*]pentacene-8,16-diyl)bis(2-hexylthiophene) (153)

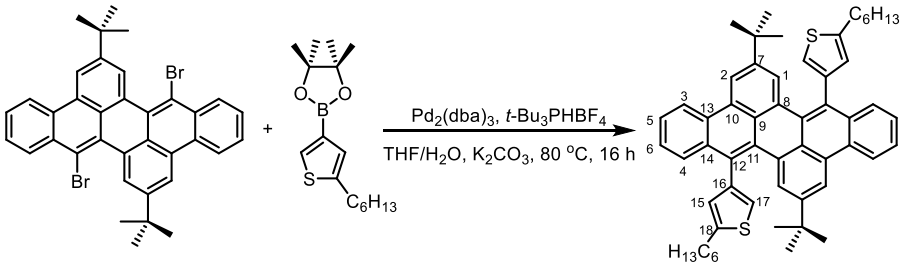

133 **153**

According to **GP1**, dibromide **133** (436 mg, 0.7 mmol), 2-(5-hexylthiophen-3-yl)-4,4,5,5-tetramethyl-1,3,2-dioxaborolane (824 mg, 2.8 mmol), K_2CO_3 (242 mg, 1.75 mmol), $Pd_2(dba)_3$ (64 mg, 0.07 mmol) and *t*-Bu_3PHBF_4 (64 mg, 0.22 mmol) in THF/water (7 mL/1.75 mL) gave, after workup, silica gel column chromatography (petroleum ether/dichloromethane 15:1) and precipitation, **153** as a pale yellow solid (510 mg, 91 %).

m.p.: 104 °C. ^{1}H NMR (400 MHz, $CDCl_3$) δ (ppm) = 8.70 (d, J = 8.1 Hz, 2H, H-3), 8.52 (d, J = 1.6 Hz, 2H, H-2), 7.91 (d, J = 1.4 Hz, 2H, H-1), 7.84 (d, J = 8.2 Hz, 2H, H-4), 7.66-7.56 (m, 2H, H-5), 7.49 (dd, J = 11.2, 4.0 Hz, 2H, H-6), 7.12-6.82 (m, 4H, H-15, 17), 2.88 (t, J = 7.7 Hz, 4H), 1.83-1.69 (m, 4H), 1.50-1.40 (m, 4H), 1.35 (dd, J = 8.9, 5.2 Hz, 8H), 1.26 (s, 18H), 0.91 (t, J = 7.0 Hz, 6H). ^{13}C NMR (101 MHz, $CDCl_3$) δ (ppm) = 148.29 (C-7), 146.86 (C-18), 140.86 (C-16), 133.48 (C-14), 131.30 (C-8), 130.19 (C-13), 129.63 (C-9), 128.97 (C-10), 128.61 (C-11), 128.30 (C-15), 127.74 (C-1), 127.61 (C-4), 127.54 (C-12), 126.30 (C-6), 126.22 (C-5), 122.29 (C-3), 122.15 (C-17), 117.10 (C-2), 34.83, 31.59, 31.50, 31.34, 30.22, 29.04, 22.61, 14.07. FT-IR (ATR) $\tilde{\nu}$ (cm^{-1}) = 3071 (w), 2954 (m), 2926 (m), 2855 (m), 1606 (w), 1572 (w), 1546 (w), 1513 (w), 1460 (m), 1420 (m), 1361 (m), 1274 (w), 1232 (w), 1200 (w), 1132 (w), 1076 (w), 1045 (w), 923 (w), 869 (m), 837

(m), 816 (w), 792 (w), 761 (s), 727 (m), 698 (m), 666 (m), 636 (m). UV/Vis (CH_2Cl_2): λ_{max} (nm) (log ε) = 302 (4.55), 312 (4.59), 345 (3.99), 416 (4.40), 432 (4.41). Fluorescence (CH_2Cl_2): λ_{em} (λ_{ex}) (nm) = 479, 502 (416). Φ = 14.1±1%. τ = 1.50 ns. MALDI-TOF MS (DCTB) (*m*/*z*): $[M]^+$ calcd. for $C_{56}H_{60}S_2$, 796.413; found, 796.421. Elemental anal. calcd. for $C_{56}H_{60}S_2$: C 84.34, H 7.59, found: C 84.09, H 7.55.

2,10-di-*tert*-butyl-8,16-di(thiophen-3-yl)anthra[9,1-*gh*:10,5-*g'h'*]diquinoline (154)

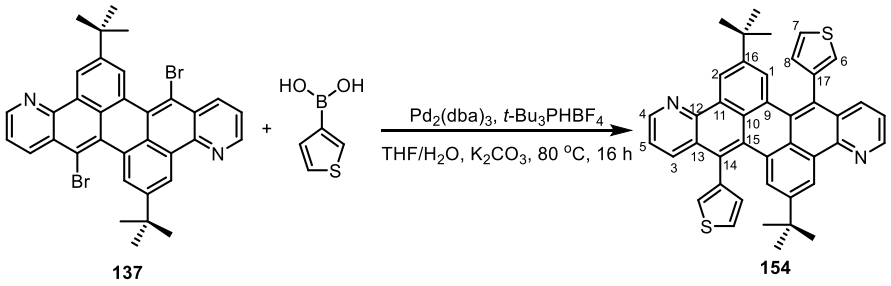

According to **GP1**, the dipyridinoperylene dibromide **137** (50 mg, 0.08 mmol), $Pd_2(dba)_3$ (7.3 mg, 0.008 mmol), *t*-Bu_3PHBF_4 (7.3 mg, 0.025 mmol), K_2CO_3 (28 mg, 0.2 mmol), THF (0.8 mL), water (0.2 mL) and 3-thienylboronic acid (102 mg, 0.8 mmol) gave after workup, silica gel column chromatography (petroleum ether/dichloromethane/ethyl acetate 20:2:1) and precipitation, **154** as a yellow solid (30 mg, 60%).

m.p.: >400 °C. ^{1}H NMR (600 MHz, $Cl_2CDCDCl_2$) δ (ppm) = 9.22 (d, *J* = 1.5 Hz, 2H, H-1), 8.92 (d, *J* = 3.9 Hz, 2H, H-4), 8.03 (d, *J* = 8.2 Hz, 2H, H-3), 7.88 (s, 2H, H-2), 7.64 - 7.54 (m, 2H, H-6), 7.43 (dd, *J* = 8.3, 4.2 Hz, 2H, H-5), 7.29 (s, 2H, H-7), 7.20 (s, 2H, H-8), 1.22 (s, 18H). ^{13}C NMR (151 MHz, $Cl_2CDCDCl_2$) δ (ppm) = 149.13 (C-16), 148.29 (C-4), 145.81 (C-12), 139.91 (C-17), 134.56 (C-3), 130.71 (C-8), 130.13 (C-15), 129.98 (C-11), 129.23 (C-2), 128.95 (C-10), 128.86 (C-9), 127.99 (C-13), 127.79 (C-14), 127.31 (C-6), 124.88 (C-7), 121.72 (C-5), 119.72 (C-1), 34.72, 31.15. FT-IR (ATR) $\tilde{\nu}$ (cm^{-1}) = 3085 (w), 2952 (m), 2902 (w), 2863 (w), 1606 (w), 1586 (w), 1568 (w), 1522 (w), 1474 (w), 1406 (m), 1361 (w), 1330 (w), 1308 (w), 1290 (w), 1267 (w), 1233 (w), 1207 (w), 1169 (w), 1145 (w), 1110 (w), 1096 (w), 1075 (w), 1054 (w), 1015 (w), 943 (w), 919 (w), 903 (w), 888 (w), 864 (w), 836 (m), 818 (w), 802 (w), 786 (s), 743 (w), 731 (m), 704 (w), 684 (m), 634 (s). UV/Vis ($CHCl_3$): λ_{max} (nm) (log ε)= 307 (4.48), 319 (4.40), 419 (4.40), 435 (4.41). MALDI-TOF MS (DCTB) (*m*/*z*): $[M]^+$ calcd. for $C_{42}H_{34}N_2S_2$, 630.216; found, 630.237. Elemental anal. calcd. for $C_{42}H_{34}N_2S_2$: C 79.96, H 5.43, N 4.44, found: C 79.99, H 5.26, N 4.63.

2,10-di-*tert*-butyl-8,16-bis(5-hexylthiophen-3-yl)anthra[9,1-*gh*:10,5-*g'h'*]diquinoline (155)

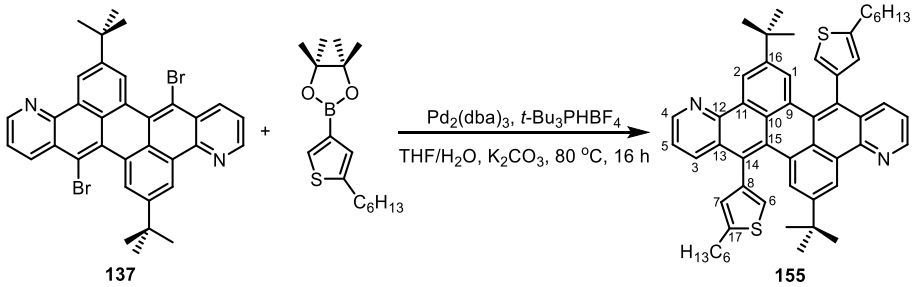

According to **GP1**, dibromide **137** (375 mg, 0.6 mmol), 2-(5-hexylthiophen-3-yl)-4,4,5,5-tetramethyl-1,3,2-dioxaborolane (706 mg, 2.4 mmol), K_2CO_3 (207 mg, 1.5 mmol), $Pd_2(dba)_3$ (55 mg, 0.06 mmol) and *t*-Bu_3PHBF_4 (55 mg, 0.19 mmol) in THF/water (6 mL/1.5 mL) gave, after workup, silica gel column chromatography (petroleum ether/dichloromethane/ethyl acetate 50:15:1) and precipitation, **155** as a yellow solid (415 mg, 87 %).

m.p.: 252 °C. ^{1}H NMR (600 MHz, $CDCl_3$) δ (ppm) = 9.25 (s, 2H, H-2), 8.93 (d, J = 3.1 Hz, 2H, H-4), 8.12 (d, J = 5.6 Hz, 2H, H-3), 8.06 (s, 2H, H-1), 7.43 (br, 2H, H-5), 7.05 (br, 2H, H-6), 6.87 (s, 2H, H-7), 2.87 (t, J = 7.7 Hz, 4H), 1.84 - 1.65 (m, 4H), 1.47 - 1.40 (m, 4H), 1.34 - 1.32 (m, 8H), 1.28 (s, 18H), 0.90 (t, J = 6.8 Hz, 6H). ^{13}C NMR (151 MHz, $CDCl_3$) δ (ppm) = 149.14 (C-16), 148.18 (C-4), 147.71 (C-17), 146.21 (C-12), 139.75 (C-8), 134.78 (C-3), 130.35 (C-15), 130.33 (C-11), 129.24 (C-1), 129.07 (C-10), 128.92 (C-14), 128.37 (C-9), 128.24 (C-13), 127.66 (C-7), 122.36 (C-6), 121.49 (C-5), 119.63 (C-2), 34.95, 31.55, 31.51, 31.31, 30.21, 29.04, 22.58, 14.07. FT-IR (ATR) $\tilde{\nu}$ (cm^{-1}) = 3065 (w), 2953 (m), 2927 (m), 2856 (m), 1607 (w), 1569 (w), 1544 (w), 1499 (w), 1460 (m), 1398 (m), 1360 (w), 1297 (w), 1264 (w), 1227 (w), 1202 (w), 1170 (w), 1128 (w), 1093 (w), 1022 (w), 924 (w), 895 (m), 855 (w), 836 (w), 784 (s), 765 (w), 753 (w), 732 (m), 709 (w), 680 (m), 639 (m). UV/Vis (CH_2Cl_2): λ_{max} (nm) (log ε) = 307 (4.50), 317 (4.46), 421 (4.44), 435 (4.45). Fluorescence (CH_2Cl_2): λ_{em} (λ_{ex}) (nm) = 481, 502 (421). Φ = 12.4±0.4%. τ = 2.07 ns. MALDI-TOF MS (DCTB) (*m*/*z*): $[M]^+$ calcd. for $C_{54}H_{58}N_2S_2$, 798.404; found, 798.366. Elemental anal. calcd. for $C_{54}H_{58}N_2S_2$: C 81.16, H 7.32, N 3.51, found: C 81.15, H 7.31, N 3.48.

2,10-di-*tert*-butyl-6,14-difluoro-8,16-diphenyldibenzo[*fg*,*qr*]pentacene (156)

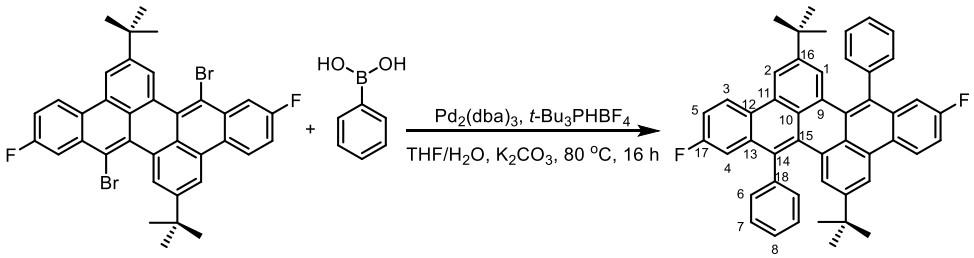

138 **156**

According to **GP1**, the difluorodibromide **138** (33 mg, 0.05 mmol), $Pd_2(dba)_3$ (4.6 mg, 0.005 mmol), *t*-Bu_3PHBF_4 (4.6 mg, 0.0158 mmol), K_2CO_3 (18 mg, 0.13 mmol), THF (0.5 mL), water (0.13 mL) and phenylboronic acid (61 mg, 0.5 mmol) gave after workup, silica gel column chromatography (petroleum ether/dichloromethane 15:1) and precipitation, **156** as a yellow solid (27 mg, 83%).

m.p.: 365 °C (dec.). ^{1}H NMR (400 MHz, $Cl_2CDCDCl_2$) δ (ppm) = 8.67 (dd, J = 9.2, 5.7 Hz, 2H, H-3), 8.39 (s, 2H, H-1), 7.69 (d, J = 1.3 Hz, 2H, H-2), 7.57 - 7.48 (m, 4H, H-6), 7.49 - 7.40 (m, 6H, H-7, 8), 7.35 (td, J = 8.3, 2.3 Hz, 2H, H-5), 7.28 (dd, J = 11.6, 2.5 Hz, 2H, H-4), 1.08 (s, 18H). ^{13}C NMR (101 MHz, $Cl_2CDCDCl_2$) δ (ppm) = 161.11 (d, $J_{C,F}$ = 244.6 Hz, C-17), 148.60 (C-16), 140.93 (C-18), 134.82 (d, $J_{C,F}$ = 8.0 Hz, C-13), 134.04 (d, $J_{C,F}$ =3.5 Hz, C-14), 131.57 (C-7), 130.65 (C-9), 129.55 (C-6), 128.86 (d, J = 9.1 Hz, C-2), 128.44 (C-11), 127.64 (C-8), 127.07 (C-10), 126.54 (C-12), 124.65 (d, $J_{C,F}$ = 8.6 Hz, C-3), 120.19 (C-15), 117.05 (C-1), 115.13 (d, $J_{C,F}$ = 23.8 Hz, C-5), 112.03 (d, $J_{C,F}$ = 22.7 Hz, C-4), 34.57, 30.96. ^{19}F NMR (283 MHz, $Cl_2CDCDCl_2$) δ (ppm) = - 113.56. FT-IR (ATR) $\tilde{\nu}$ (cm^{-1}) = 3084 (w), 3056 (w), 3019 (w), 2957 (m), 2906 (w), 2866 (w),

1952 (w), 1882 (w), 1812 (w), 1740 (w), 1613 (m), 1576 (w), 1519 (m), 1488 (m), 1477 (w), 1462 (w), 1440 (w), 1423 (m), 1397 (w), 1363 (w), 1297 (w), 1274 (w), 1234 (w), 1194 (m), 1175 (m), 1143 (w), 1102 (w), 1083 (w), 1029 (w), 992 (m), 921 (w), 894 (w), 869 (s), 816 (s), 778 (m), 765 (m), 746 (w), 732 (s), 704 (s), 674 (w), 650 (w), 635 (m). UV/Vis ($CHCl_3$): λ_{max} (nm) (log ε) = 300 (4.56), 311 (4.59), 412 (4.45), 433 (4.46). MALDI-TOF MS (DCTB) (*m*/*z*): $[M]^+$ calcd. for $C_{48}H_{38}F_2$, 652.294; found, 652.277. Elemental anal. calcd. for $C_{48}H_{38}F_2$: C 88.31, H 5.87, found: C 88.17, H 6.25.

3,3'-(2,10-di-*tert*-butyl-6,14-difluorodibenzo[*fg*,*qr*]pentacene-8,16-diyl)dithiophene (157)

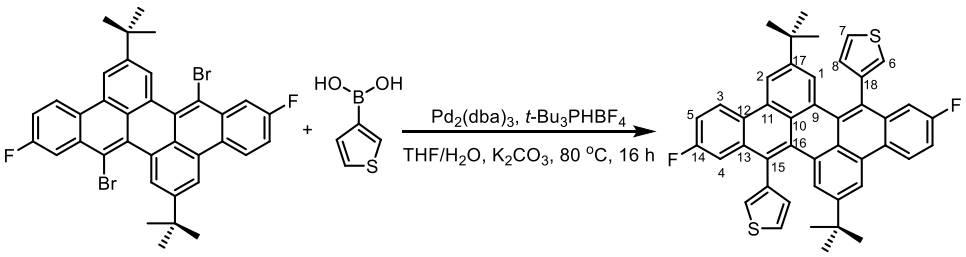

138 **157**

According to **GP1**, the difluorodibromide **138** (33 mg, 0.05 mmol), $Pd_2(dba)_3$ (4.6 mg, 0.005 mmol), *t*-Bu_3PHBF_4 (4.6 mg, 0.0158 mmol), K_2CO_3 (18 mg, 0.13 mmol), THF (0.5 mL), water (0.13 mL) and 3-thienylboronic acid (64 mg, 0.5 mmol) gave after workup, silica gel column chromatography (petroleum ether/dichloromethane 15:1) and precipitation, **157** as a yellow solid (24 mg, 73%).

m.p.: 374 °C (dec.). ^{1}H NMR (600 MHz, $Cl_2CDCDCl_2$) δ (ppm) = 8.67 (dd, J =9.1, 5.7 Hz, 2H, H-3), 8.42 (s, 2H, H-1), 7.73 (s, 2H, H-2), 7.59 (br, 2H, H-6), 7.41-7.36 (m, 4H, H-4, 5), 7.25 (br, 4H, 7, 8), 1.19 (s, 18H). ^{13}C NMR (151 MHz, $Cl_2CDCDCl_2$) δ (ppm) = 161.28 (d, $J_{C\text{-}F}$ = 244.8 Hz, C-14), 148.88 (C-17), 140.47 (C-18), 134.86 (d, $J_{C\text{-}F}$ = 8.2 Hz, C-13), 130.79 (d, $J_{C\text{-}F}$ = 13.3 Hz, C-15), 129.73 (C-9), 128.50 (d, J = 3.8 Hz, C-8), 128.46 (C-11), 127.77 (C-2), 127.20 (C-6), 126.91 (C-10), 126.43 (C-12), 124.87 (C-7), 124.71 (d, $J_{C,F}$ = 8.7 Hz, C-3), 120.18 (C-16), 117.32 (C-1), 115.24 (d, $J_{C,F}$ = 23.9 Hz, C-5), 111.74 (d, $J_{C,F}$ = 22.7 Hz, C-4), 34.64, 31.11. ^{19}F NMR (283 MHz, $Cl_2CDCDCl_2$) δ (ppm) = -113.42. FT-IR (ATR) $\tilde{\nu}$ (cm^{-1}) = 3119 (w), 3094 (w), 2955 (m), 2903 (w), 2863 (w), 1862 (w), 1729 (w), 1610 (m), 1580 (w), 1513 (m), 1476 (w), 1424 (m), 1399 (w), 1360 (w), 1292 (w), 1280 (w), 1237 (w), 1201 (w), 1173 (m), 1145 (w), 1102 (w), 1082 (w), 1020 (w), 993 (m), 930 (w), 894 (m), 867 (m), 841 (m), 824 (m), 814 (w), 796 (s), 780 (s), 738 (m), 720 (w), 699 (w), 661 (s), 636 (m), 609 (w). UV/Vis ($CHCl_3$): λ_{max} (nm) (log ε)= 312 (4.59), 419 (4.42), 431 (4.42). MALDI-TOF MS (DCTB) (*m*/*z*): $[M]^+$ calcd. for $C_{44}H_{34}F_2S_2$, 664.207; found, 664.247. Elemental anal. calcd. for $C_{44}H_{34}F_2S_2$: C 79.49, H 5.15, found: C 79.48, H 5.49.

2,5,9,12-tetra-*tert*-butyl-7,14-bis(3-(hexyloxy)phenyl)peryleno[2,3-*b*:8,9-*b*']dithiophene (158)

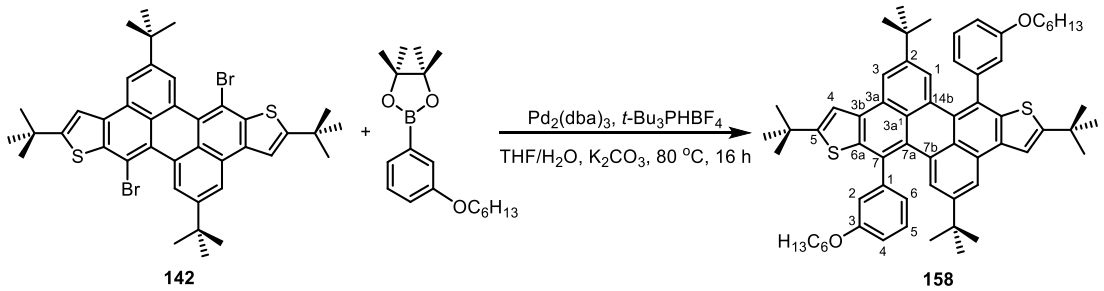

142 158

According to **GP1**, dibromide **142** (448 mg, 0.6 mmol), (3-(hexyloxy)phenyl)boronic acid pinacol ester (730 mg, 2.4 mmol), K_2CO_3 (221 mg, 1.6 mmol), $Pd_2(dba)_3$ (27 mg, 0.03 mmol) and *t*-Bu_3PHBF_4 (27 mg, 0.095 mmol) in THF/water (3 mL/0.8 mL) gave, after workup and silica gel column chromatography (petroleum ether/dichloromethane 6:1 to 4:1), **158** (mixture of atropisomers) as a yellow solid (204 mg, 36 %).

m.p.: 140 °C (dec.). ^{1}H NMR (600 MHz, $CDCl_3$) δ (ppm) = 7.96 (s, 2H, H-3), 7.74 (s, 2H, H-1), 7.66 (s, 2H, H-4), 7.46 (t, *J* = 7.9 Hz, 1H, H-phenyl-5), 7.41 (t, *J* = 7.9 Hz, 1H, H-phenyl-5), 7.29 (d, *J* = 7.4 Hz, 1H, H-phenyl-6), 7.18 (d, *J* = 7.5 Hz, 1H, H-phenyl-6), 7.14 (s, 1H, H-phenyl-2), 7.03 (s, 1H, H-phenyl-2), 6.95 (s, 1H, H-phenyl-4), 6.94 (s, 1H, H-phenyl-4), 3.96 - 3.90 (m, 2H, H-OCH_2), 3.89 - 3.82 (m, 2H, H-hex), 1.77 - 1.71 (m, 2H, H-hex), 1.71 - 1.66 (m, 2H, H-hex), 1.49 (s, 18H, H-*t*-Bu), 1.44 - 1.35 (m, 4H, H-hex), 1.32 - 1.25 (m, 8H, H-hex), 1.10 (s, 18H, H-*t*-Bu), 0.88 - 0.85 (m, 6H, H-hex). ^{13}C NMR (151 MHz, $CDCl_3$) δ (ppm) = 160.52 (C-phenyl-3), 160.46 (C-phenyl-3), 158.87 (C-5), 147.99 (C-2), 144.41 (C-phenyl-1), 144.40 (C-phenyl-1), 140.39 (C-6a), 135.30 (C-3a), 131.38 (C-7a), 131.36 (C-7a), 131.28 (C-7), 131.25 (C-7), 130.82 (C-phenyl-5), 130.76 (C-phenyl-5), 128.23 (C-14b), 127.64 (C-3a^1), 127.53 (C-1), 127.50 (C-1), 125.29 (C-3b), 125.29 (C-3b), 122.12 (C-phenyl-6), 122.04 (C-phenyl-6), 117.21 (C-3), 116.29 (C-4), 115.53 (C-phenyl-2), 115.31 (C-phenyl-2), 114.66 (C-phenyl-4), 114.56 (C-phenyl-4), 68.03, 67.95, 35.10, 34.50, 32.36, 31.52, 31.50, 30.96, 29.11, 29.09, 25.67, 25.65, 22.59, 22.57, 14.02, 14.01. FT-IR (ATR) $\tilde{\nu}$ (cm^{-1}) = 3066(w), 2956 (s), 2930 (m), 2864 (m), 1599 (s), 1577 (m), 1511 (w), 1465 (s), 1388 (w), 1361 (m), 1315 (w), 1279 (m), 1247 (s), 1223 (m), 1200 (s), 1154 (m), 1121 (w), 1044 (m), 1020 (m), 958 (m), 927 (w), 895 (w), 868 (m), 827 (m), 783 (m), 751 (m), 724 (w), 701 (m), 678 (m), 621 (w). UV/Vis (CH_2Cl_2): λ_{max} (nm) (log ε) = 298 (4.59), 452 (4.46), 474 (4.52). Fluorescence (CH_2Cl_2): λ_{em} (λ_{ex}) (nm) = 529 (452). Φ = 76.3±2.3%. τ = 4.00 ns. MALDI-TOF MS (DCTB) (*m*/*z*): $[M]^+$ calcd. for $C_{64}H_{76}O_2S_2$, 940.529; found, 940.526. Elemental anal. calcd. for $C_{64}H_{76}O_2S_2 \cdot 0.5H_2O$: C 80.88, H 8.17, found: C 80.88, H 8.18.

5,5'-(2,5,9,12-tetra-*tert*-butylperyleno[2,3-*b*:8,9-*b*']dithiophene-7,14-diyl)bis(2,3-dimethoxypyridine) (159)

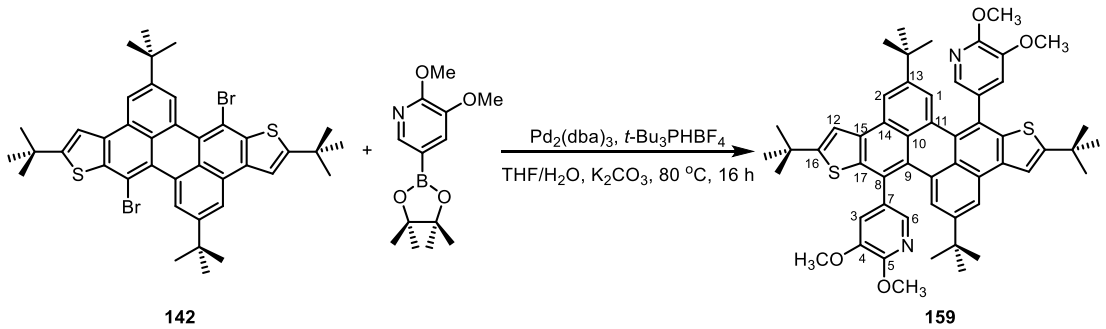

142 159

According to **GP1**, dibromide **142** (448 mg, 0.6 mmol), (5,6-dimethoxypyridin-3-yl)boronic acid pinacol ester (477 mg, 1.8 mmol), K_2CO_3 (221 mg, 1.6 mmol), $Pd_2(dba)_3$ (27 mg, 0.03 mmol) and *t*-Bu_3PHBF_4 (27 mg, 0.095 mmol) in THF/water (3 mL/0.8 mL) gave, after workup, silica gel column chromatography (petroleum ether/dichloromethane/ethyl acetate 30:5:1 to 30:5:2) and precipitation from dichloromethane/methanol, **159** (mixture of atropisomers) as a yellow solid (463 mg, 89 %).

m.p.: 356 °C (dec.). ^{1}H NMR (600 MHz, CD_2Cl_2) δ (ppm) = 8.17 (d, J = 1.6 Hz, 1H, H-6), 8.00 (s, 2H, H-2), 7.92 (d, J = 1.6 Hz, 1H, H-6), 7.71 (d, J = 1.3 Hz, 2H, H-1), 7.69 (s, 1H, H-12), 7.67 (s, 1H, H-12), 7.27 (d, J = 1.6 Hz, 1H, H-3), 6.98 (d, J = 1.6 Hz, 1H, H-3), 4.05 (s, 3H), 4.01 (s, 3H), 3.73 (s, 3H), 3.58 (s, 3H), 1.49 (s, 18H), 1.11 (s, 18H). ^{13}C NMR (151 MHz, CD_2Cl_2) δ (ppm) = 159.77 (C-13), 159.75 (C-13), 154.68 (C-5), 154.52 (C-5), 148.83 (C-16), 148.81 (C-16), 145.97 (C-4), 145.86 (C-4), 141.15 (C-9), 137.92 (C-6), 137.63 (C-6), 136.14 (C-10), 132.85 (C-8), 132.74 (C-8), 131.63 (C-17), 131.48 (C-17), 128.98 (C-14), 128.48 (C-11), 128.32 (C-11), 128.27 (C-7), 128.22 (C-7), 128.06 (C-12), 127.98 (C-12), 126.36 (C-15), 126.25 (C-15), 120.06 (C-3), 119.83 (C-3), 118.14 (C-2), 117.31 (C-1), 117.29 (C-1), 56.44, 56.25, 35.68, 35.04, 35.03, 32.65, 31.22, 31.18. FT-IR (ATR) $\tilde{\nu}$ (cm^{-1}) = 2957 (m), 2904 (w), 2866 (w), 1599 (w), 1567 (w), 1510 (w), 1489 (s), 1464 (m), 1399 (s), 1361 (w), 1317 (w), 1252 (s), 1198 (m), 1178 (m), 1154 (m), 1108 (w), 1046 (w), 1016 (m), 961 (w), 943 (w), 912 (w), 890 (w), 867 (m), 821 (m), 799 (w), 765 (m), 722 (w), 673 (w), 651 (w), 617 (w). UV/Vis (CH_2Cl_2): λ_{max} (nm) (log ε) = 300 (4.64), 376 (3.63), 456 (4.45), 478 (4.51). Fluorescence (CH_2Cl_2): λ_{em} (λ_{ex}) (nm) = 533 (478). Φ = 77.5±1.0%. τ = 4.51 ns. MALDI HRMS (DCTB) (*m*/*z*): $[M]^+$ calcd. for $C_{54}H_{58}N_2O_4S_2$, 862.3838; found, 862.3872. Elemental anal. calcd. for $C_{54}H_{58}N_2O_4S_2$: C 75.14, H 6.77, N 3.25, found: C 75.15, H 6.73, N 2.94.

2,5,9,12-tetra-*tert*-butyl-7,14-bis(5-hexylthiophen-3-yl)peryleno[2,3-*b*:8,9-*b*']dithiophene (160)

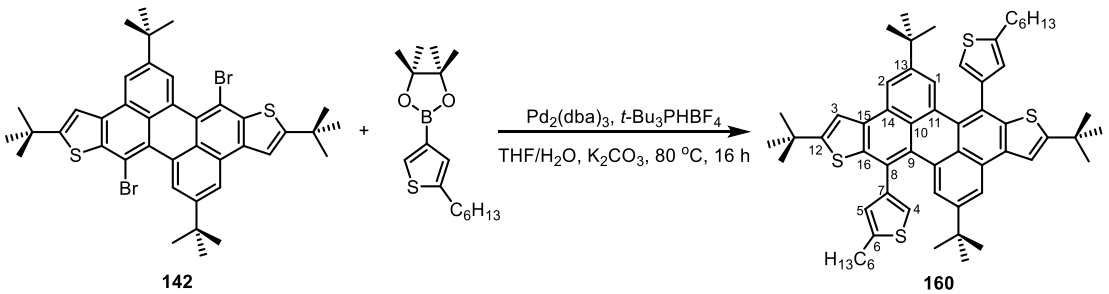

142 160

According to **GP1**, dibromide **142** (336 mg, 0.45 mmol), 2-(5-hexylthiophen-3-yl)-4,4,5,5-tetramethyl-1,3,2-dioxaborolane (794 mg, 2.7 mmol), K_2CO_3 (304 mg, 2.2 mmol), $Pd_2(dba)_3$ (21 mg, 0.023 mmol) and *t*-Bu_3PHBF_4 (21 mg, 0.073 mmol) in THF/water (4.5 mL/1.1 mL) gave, after workup, silica gel column chromatography (petroleum ether/dichloromethane 15:1 to 10:1) and precipitation, **160** as a yellow solid (282 mg, 68 %).

m.p.: 203 °C. ^{1}H NMR (500 MHz, $CDCl_3$) δ (ppm) = 7.98 (d, J = 1.6 Hz, 2H, H-2), 7.86 (d, J = 1.5 Hz, 2H, H-1), 7.66 (s, 2H, H-3), 7.47 (br, 2H, H-4), 6.71 (br, 2H, H-5), 2.77 (t, J = 7.0 Hz, 4H), 1.70 - 1.63 (m, 4H), 1.51 (s, 18H), 1.38 (br, 4H), 1.31 - 1.26 (m, 8H), 1.21 (s, 18H), 0.87 (t, J= 6.6 Hz, 6H). ^{13}C NMR (126 MHz, $CDCl_3$) δ (ppm) = 158.73 (C-12), 148.08 (C-13), 147.39 (C-6), 142.58 (C-7), 140.71 (C-16), 135.24 (C-14), 131.55 (C-9), 128.17 (C-11), 127.56 (C-10), 126.55 (C-1), 126.43 (C-8), 126.25 (C-15), 125.79 (C-5), 121.29 (C-4), 117.33 (C-2), 116.45 (C-3), 35.12, 34.57, 32.40, 31.55, 31.32, 31.11, 30.19, 29.01, 22.57, 14.05. FT-IR (ATR) $\tilde{\nu}$ (cm^{-1}) = 3085 (w), 2956 (s), 2927 (s), 2858 (m), 1606 (w), 1543 (w), 1509 (w), 1463 (m), 1388 (w), 1361 (m), 1251 (m), 1229 (m), 1202 (m), 1136 (w), 1087 (w), 1024 (w), 961 (w), 893 (w), 866 (m), 823 (m), 764 (w), 742 (m), 689 (w), 672 (w), 622 (w). UV/Vis (CH_2Cl_2): λ_{max} (nm) (log ε) = 298 (4.59), 454 (4.48), 478 (4.53). Fluorescence (CH_2Cl_2): λ_{em} (λ_{ex}) (nm) = 531 (310). Φ = 37.7±0.1%. τ = 2.86±0.01 ns. MALDI HRMS (DCTB) (*m*/*z*): $[M]^+$ calcd. for $C_{60}H_{72}S_4$, 920.4517; found, 920.4530. Elemental anal. cald. for $C_{60}H_{72}S_4$: C 78.21, H 7.88, found: C 78.50, H 7.84.

2,10-di-*tert*-butyl-8,16-bis(phenylethynyl)dibenzo[*fg*,*qr*]pentacene (161)

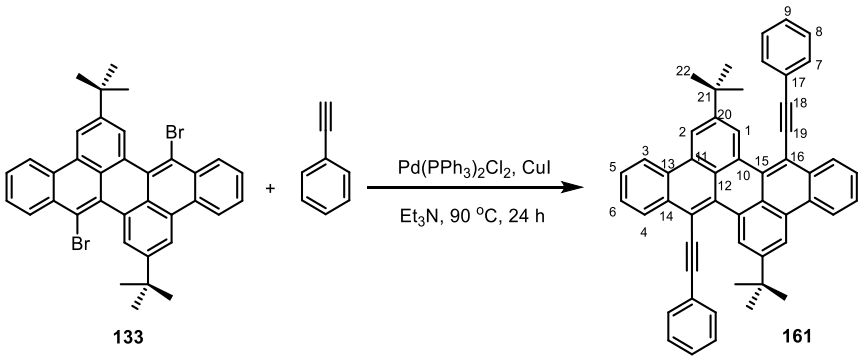

133 161

To a mixture of dibromide **133** (50 mg, 0.08 mmol), $Pd(PPh_3)Cl_2$ (5.6 mg, 0.008 mmol) and CuI (1.5 mg, 0.008 mmol) was added a solution of phenylacetylene (0.04 mL, 0.4 mmol) in argon degassed triethylamine (1 mL) under argon. The mixture was stirred at 90 °C in a screw-capped glassy vial for 24 hours. After cooling down to room temperature, the reaction was quenched by adding saturated aqueous NH_4Cl. The mixture was diluted with dichloromethane (50 mL), washed with brine (2 × 50 mL) and water (50 mL) and dried over anhydrous Na_2SO_4. After removal of the solvent by rotary evaporation, the product was obtained after silica gel column chromatography (petroleum ether/dichloromethane 6:1) and precipitation from dichloromethane/methanol as an orange solid (47 mg, 88%).

m.p.: 352 °C (dec.). ^{1}H NMR (600 MHz, $Cl_2CDCDCl_2$) δ (ppm) = 9.51 (d, J = 1.5 Hz, 2H, H-1), 8.77 - 8.74 (m, 4H, H-3, 4), 8.71 (d, J = 1.2 Hz, 2H, H-2), 7.73 (qd, J = 6.9, 3.6 Hz, 4H, H-5, 6), 7.64 (dd, J = 7.6, 1.6 Hz, 4H, H-7), 7.43 - 7.35 (m, 6H, H-8, 9), 1.45 (s, 18H). ^{13}C NMR (151 MHz,

$Cl_2CDCDCl_2$) δ (ppm) = 149.79 (C-20), 132.77 (C-14), 132.35 (C-15), 131.75 (C-7), 130.22 (C-10), 129.38 (C-13), 129.01 (C-6), 128.41 (C-9), 128.35 (C-8), 127.61 (C-11), 127.43 (C-4), 127.12 (C-5), 126.64 (C-1), 126.11 (C-12), 123.23 (C-17), 122.58 (C-3), 118.96 (C-2), 114.57 (C-16), 97.21 (C-18), 90.02 (C-19), 35.24 (C-21), 31.39 (C-22). FT-IR (ATR) $\tilde{\nu}$ (cm^{-1}) = 2955 (m), 1599 (m), 1566 (w), 1510 (w), 1484 (w), 1442 (w), 1417 (w), 1361 (w), 1272 (w), 1233 (w), 1165 (w), 1068 (w), 1024 (w), 906 (m), 874 (w), 812 (w), 786 (w), 754 (s), 689 (m), 637 (m). UV/Vis ($CHCl_3$): λ_{max} (nm) (log ε) = 329 (4.74), 367 (4.11), 452 (4.52), 477 (4.57). MALDI-TOF MS (DCTB, Kalib PEG600) (*m*/*z*): $[M]^+$ calcd. for $C_{52}H_{40}$, 664.312; found, 664.309. Elemental anal. cald. for $C_{52}H_{40}$: C 93.94, H 6.06, found: C 93.71, H 6.07.

2,10-di-*tert*-butyl-8,16-bis(phenylethynyl)anthra[9,1-*gh*:10,5-*g'h'*]diquinoline (162)

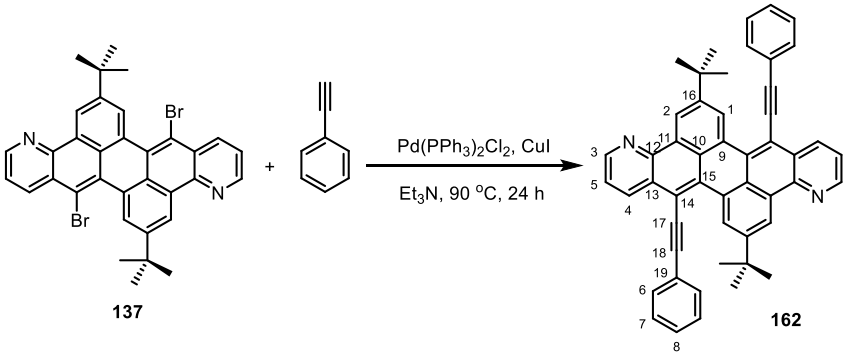

To a mixture of dipyridino dibromide **137** (50 mg, 0.08 mmol), $Pd(PPh_3)Cl_2$ (5.6 mg, 0.008 mmol) and CuI (1.5 mg, 0.008 mmol) was added a solution of phenylacetylene (0.04 mL, 0.4 mmol) in argon degassed triethylamine (1 mL) under argon. The mixture was stirred at 90 °C in a screw-capped glassy vial for 24 hours. After cooling down to room temperature, the reaction was quenched by adding saturated aq. NH_4Cl. The mixture was diluted with dichloromethane (50 mL), washed with brine (2 × 50 mL) and water (1 × 50 mL) and dried over anhydrous Na_2SO_4. After removal of the solvent by rotary evaporation, the product was obtained after silica gel column chromatography (petroleum ether/dichloromethane/ethyl acetate 20:4:1) and precipitation from chloroform/methanol as an orange solid (51 mg, 95%).

m.p.: >400 °C. ^{1}H NMR (600 MHz, $Cl_2CDCDCl_2$) δ (ppm) = 9.69 (d, *J* = 1.9 Hz, 2H, H-1), 9.44 (d, *J* = 1.9 Hz, 2H, H-2), 9.01 (dd, *J* = 4.2, 1.5 Hz, 2H, H-3), 8.96 (dd, *J* = 8.2, 1.5 Hz, 2H, H-4), 7.69 - 7.62 (m, 6H, H-5, 6), 7.44 - 7.37 (m, 6H, H-7, 8), 1.48 (s, 18H). ^{13}C NMR (151 MHz, $Cl_2CDCDCl_2$) δ (ppm) = 150.54 (C-16), 148.94 (C-3), 145.54 (C-12), 134.99 (C-4), 132.54 (C-15), 131.77 (C-6), 130.64 (C-13), 129.47 (C-11), 128.67 (C-8), 128.42 (C-7), 127.87 (C-1), 127.76 (C-9), 127.62 (C-10), 122.87 (C-19), 122.46 (C-5), 121.48 (C-2), 113.26 (C-14), 98.01 (C-18), 89.00 (C-17), 35.38, 31.43. FT-IR (ATR) $\tilde{\nu}$ (cm^{-1}) = 3066 (w), 3032 (w), 2958 (m), 2900 (w), 2863 (w), 1952 (w), 1925 (w), 1815 (w), 1795 (w), 1586 (w), 1567 (m), 1500 (w), 1484 (w), 1471 (w), 1456 (w), 1442 (w), 1406 (m), 1359 (w), 1333 (w), 1306 (w), 1282 (w), 1264 (w), 1238 (w), 1219 (m), 1201 (w), 1175 (w), 1152 (w), 1119 (w), 1070 (m), 1025 (w), 960 (w), 923 (w), 903 (w), 889 (m), 836 (w), 821 (w), 788 (s), 749 (s), 685 (s), 637 (s), 609 (w). MALDI-TOF MS (DCTB) (*m*/*z*): $[M]^+$ calcd. for $C_{50}H_{38}N_2$, 666.303; found, 666.279. Elemental anal. calcd. for $C_{50}H_{38}N_2 \cdot 0.5H_2O$: C 88.86, H 5.82, N 4.14, found: C 88.92, H 5.93, N 3.86.

9,18-di-*tert*-butyl-2,11-dihexyldibenzo[3,4:9,10]coroneno[1,2-*b*:7,8-*b*']dithiophene (164)

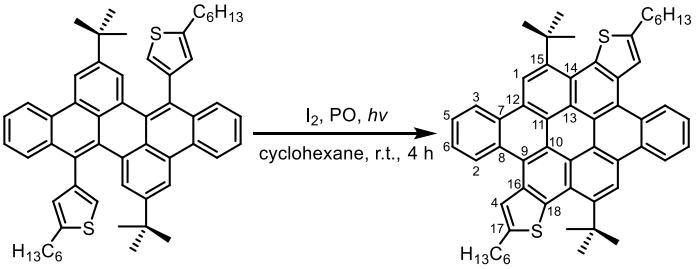

According to **GP2**, **153** (199 mg, 0.25 mmol), I_2 (165 mg, 0.65 mmol) and propylene oxide (7 mL) were used to setup the reaction. After irradiation for 4 hours, the mixture was washed with 1M aq. $NaHSO_3$ (100 mL) and water (100 mL) and dried over anhydrous Na_2SO_4. After removal of the solvent by rotary evaporation, the crude product was purified by silica gel column chromatography (petroleum ether/chloroform 10:1 to 5:1). The product was obtained after recrystallization from chloroform/methanol and dried in vacuum to give coronene **164** as a yellow solid (129 mg, 65 %). m.p.: 264 °C (dec.). ^{1}H NMR (600 MHz, $CDCl_3$) δ (ppm) = 9.60 (s, 2H, H-1), 9.32 (d, J = 8.0 Hz, 2H, H-2), 9.18 (d, J = 8.1 Hz, 2H, H-3), 8.29 (s, 2H, H-4), 7.95 (t, J = 7.3 Hz, 2H, H-5), 7.91 (t, J = 7.4 Hz, 2H, H-6), 3.13 (t, J = 7.6 Hz, 4H), 2.10 (s, 18H), 1.92 - 1.84 (m, 4H), 1.49 - 1.43 (m, 4H), 1.39 - 1.28 (m, 8H), 0.89 (t, J = 7.0 Hz, 6H). ^{13}C NMR (151 MHz, $CDCl_3$) δ (ppm) = 145.68 (C-17), 143.43 (C-15), 135.60 (C-18), 134.95 (C-16), 129.71 (C-7), 128.58 (C-8), 128.34 (C-2), 126.50 (C-5), 125.90 (C-6), 125.66 (C-14), 125.11 (C-10), 124.13 (C-13), 123.61 (C-3), 123.16 (C-4), 122.65 (C-9), 122.49 (C-1), 122.30 (C-11), 121.82 (C-12), 37.32, 33.91, 31.59, 31.52, 30.45, 28.89, 22.59, 14.08. FT-IR (ATR) $\tilde{\nu}$ (cm^{-1}) = 3066 (w), 2954 (m), 2924 (m), 2855 (m), 2722 (w), 1950 (w), 1924 (w), 1899 (w), 1752 (w), 1709 (w), 1609 (w), 1585 (w), 1548 (w), 1515 (w), 1452 (m), 1398 (m), 1365 (m), 1324 (w), 1289 (m), 1254 (w), 1187 (m), 1143 (w), 1122 (w), 1082 (w), 1036 (w), 957 (w), 922 (w), 894 (w), 876 (m), 842 (w), 820 (w), 789 (m), 754 (s), 719 (m), 696 (w), 679 (m), 658 (w), 637 (w). UV/Vis (CH_2Cl_2): λ_{max} (nm) (log ε) = 296 (4.36), 349 (4.96), 363 (5.19), 409 (4.35), 433 (4.45). Fluorescence (CH_2Cl_2): λ_{em} (λ_{ex}) (nm) = 482, 512, 550 (363). Φ = 2.5±0.1%. τ = 1.14 ns. MALDI-TOF MS (DCTB) (m/z): $[M]^+$ calcd. for $C_{56}H_{56}S_2$, 729.382; found, 792.373. Elemental anal. calcd. for $C_{56}H_{56}S_2$: C 84.80, H 7.12, S 8.08, found: C 84.56, H 7.42, S 8.04.

9,18-di-*tert*-butyl-2,11-dihexyldithieno[3',2':2,3;3'',2'':8,9]peryleno[1,12-*fgh*:7,6-*f'g'h'*]diquinoline (165)

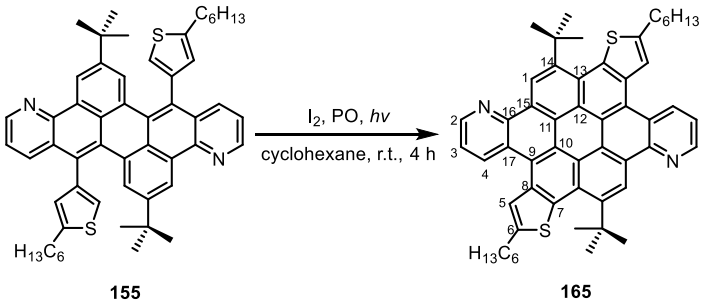

According to **GP2**, **155** (200 mg, 0.25 mmol), I_2 (165 mg, 0.65 mmol) and propylene oxide (7 mL) were used to setup the reaction. After irradiation for 4 hours, the mixture was washed with 1M aq. $NaHSO_3$ (100 mL) and water (100 mL) and dried over anhydrous Na_2SO_4. After removal of the solvent by rotary evaporation, the crude product was purified by silica gel column chromatography (petroleum ether/chloroform/ethyl acetate 50:10:1 to 50:20:1). The coronene **165** was obtained after precipitation from chloroform/methanol and drying in vacuum as a light-yellow solid (122 mg, 61 %).

m.p.: 336 °C (dec.). ^{1}H NMR (600 MHz, $Cl_2CDCDCl_2$) δ (ppm) = 10.42 (s, 2H, H-1), 9.61 (d, J = 8.1 Hz, 2H, H-2), 9.33 (d, J = 4.0 Hz, 2H, H-4), 8.16 (s, 2H, H-5), 7.86 (dd, J = 8.2, 4.1 Hz, 2H, H-3), 3.12 (t, J = 7.7 Hz, 4H), 2.10 (s, 18H), 1.91-1.83 (m, 4H), 1.46 (dt, J = 15.0, 7.3 Hz, 4H), 1.38-1.27 (m, 8H), 0.87 (t, J = 7.1 Hz, 6H). ^{13}C NMR (151 MHz, $CDCl_3$) δ (ppm) = 148.71 (C-4), 147.27 (C-6), 144.84 (C-16), 144.11 (C-14), 135.69 (C-8), 135.43 (C-2), 135.07 (C-7), 126.90 (C-13), 125.93 (C-10), 124.30 (C-1), 123.77 (C-11), 123.25 (C-12), 122.99 (C-9), 122.12 (C-5), 121.70 (C-15), 121.27 (C-17), 120.96 (C-3), 37.29, 33.83, 31.46, 31.43, 30.38, 28.86, 22.54, 14.12. FT-IR (ATR) $\tilde{\nu}$ (cm^{-1}) = 3079 (w), 2924 (s), 2854 (m), 1870 (w), 1807 (w), 1752 (w), 1680 (w), 1593 (w), 1570 (w), 1547 (w), 1501 (w), 1460 (m), 1432 (s), 1394 (m), 1365 (m), 1333 (w), 1299 (m), 1278 (m), 1241 (m), 1185 (m), 1141 (w), 1118 (w), 1092 (w), 1062 (w), 1037 (w), 1012 (w), 978 (w), 897 (m), 842 (w), 819 (w), 779 (s), 742 (m), 725 (m), 677 (m), 656 (w), 630 (w). UV/Vis (CH_2Cl_2): λ_{max} (nm) (log ε) = 284 (4.39), 350 (4.95), 364 (5.17), 413 (4.27), 436 (4.34). Fluorescence (CH_2Cl_2): λ_{em} (λ_{ex}) (nm) = 476, 509, 541 (364). Φ = 2.7±0.1%. τ = 1.10 ns. MALDI HRMS (DCTB) (*m*/*z*): $[M]^+$ calcd. for $C_{54}H_{54}N_2S_2$, 794.3728; found, 794.3741. Elemental anal. calcd. for $C_{54}H_{54}N_2S_2$: C 81.57, H 6.85, N 3.52, found: C 81.52, H 6.91, N 3.35.

5,8,13,16-tetra-*tert*-butyl-2,10-dihexylcoroneno[1,2-*b*:3,4-*b*':7,8-*b*'':9,10-*b*''']tetrathiophene (166)

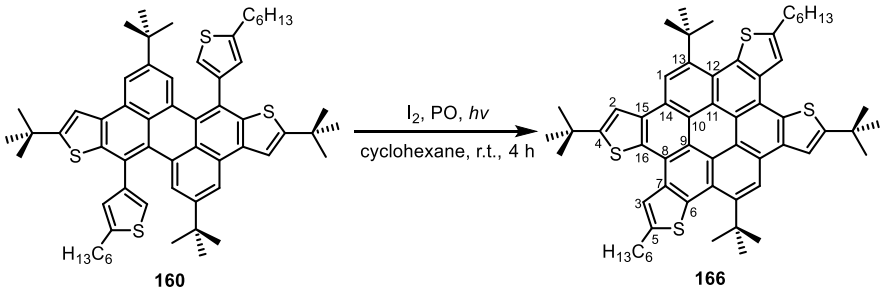

160 166

According to **GP2**, **160** (230 mg, 0.25 mmol), I_2 (165 mg, 0.65 mmol) and propylene oxide (7 mL) were used to setup the reaction. After irradiation for 4 hours, the mixture was washed with 1M aq. $NaHSO_3$ (100 mL × 1) and water (100 mL × 1) and dried over anhydrous Na_2SO_4. After removal of the solvent by rotary evaporation, the crude product was purified by silica gel column chromatography (petroleum ether/chloroform 10:1). The product **166** was obtained after precipitation from chloroform/methanol and drying in vacuum as a yellow solid (188 mg, 82 %).

m.p.: 272 °C (dec.). ^{1}H NMR (600 MHz, $CDCl_3$) δ (ppm) = 9.41 (s, 2H, H-1), 8.78 (s, 2H, H-3), 8.30 (s, 2H, H-2), 3.28 (t, J = 7.6 Hz, 4H), 2.10 (s, 18H), 2.01-1.96 (m, 4H), 1.78 (s, 18H), 1.61-1.55 (m, 4H), 1.47-1.37 (m, 8H), 0.94 (t, J = 7.2 Hz, 6H). ^{13}C NMR (151 MHz, $CDCl_3$) δ (ppm) =

158.10 (C-4), 145.65 (C-5), 142.64 (C-13), 135.91 (C-14), 134.90 (C-6), 133.59 (C-7), 132.32 (C-16), 124.58 (C-15), 123.51 (C-11), 122.82 (C-12), 122.56 (C-1), 121.31 (C-10), 120.89 (C-3), 120.46 (C-8), 120.17 (C-9), 116.61 (C-2), 37.15, 35.39, 34.12, 32.70, 31.76, 31.69, 30.70, 29.03, 22.68, 14.15. FT-IR (ATR) $\tilde{\nu}$ (cm^{-1}) = 2956 (m), 2919 (s), 2853 (m), 1602 (w), 1547 (w), 1517 (m), 1485 (w), 1460 (m), 1396 (w), 1363 (m), 1320 (m), 1293 (m), 1241 (s), 1192 (m), 1145 (m), 1111 (w), 1075 (w), 1043 (w), 1012 (w), 951 (m), 929 (m), 878 (m), 822 (s), 780 (m), 724 (m), 692 (m), 652 (w). UV/Vis (CH_2Cl_2): λ_{max} (nm) (log ε) = 350 (4.94), 363 (5.24), 398 (4.53), 419 (4.36), 442 (3.83). Fluorescence (CH_2Cl_2): λ_{em} (λ_{ex}) (nm) = 480, 509, 541 (363). Φ = 6.8±0.1%. τ = 2.33 ns. MALDI HRMS (DCTB) (*m*/*z*): $[M]^+$ calcd. for $C_{60}H_{68}S_4$, 916.4204; found, 916.4174. Elemental anal. calcd. for $C_{60}H_{68}S_4$: C 78.55, H 7.47, found: C 78.45, H 7.61.

10,20-di-*tert*-butyl-2,3,12,13-tetramethoxydibenzo[2,3:8,9]-peryleno[1,12-*fgh*:7,6-*f'g'h'*]diquinoline (167)

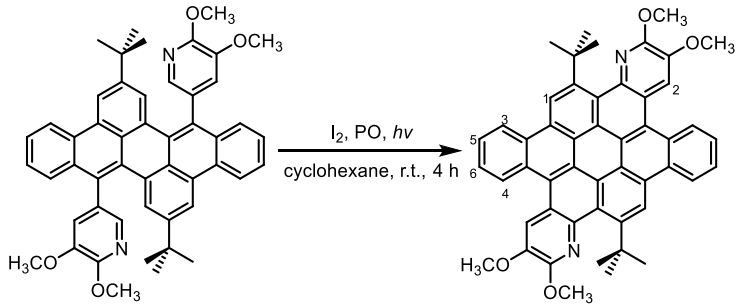

148 **167**

According to **GP2**, **148** (185 mg, 0.25 mmol)), I_2 (165 mg, 0.65 mmol) and propylene oxide (7 mL) were used to setup the reaction. After irradiation for 4 hours, the obtained suspension was filtered off. The filtrate was rinsed with *n*-hexane, methanol, ethanol and acetone. The filtrate was refluxed in chloroform (30 mL) for 30 minutes. After cooling down to room temperature, the mixture was filtered off and dried in vacuum to give **167** as light-yellow solid (128 mg, 70 %).

m.p.: > 400 °C. ^{1}H NMR (500 MHz, $Cl_2CDCDCl_2$) δ (ppm) = 9.49 (s, 2H, H-1), 9.15 (d, *J* = 8.1 Hz, 2H, H-3), 9.13 (d, *J* = 8.2 Hz, 2H, H-4), 8.69 (s, 2H, H-2), 7.94 (t, *J* = 7.0 Hz, 2H, H-5), 7.89 (t, *J* = 7.5 Hz, 2H, H-6), 4.36 (s, 6H), 4.06 (s, 6H), 1.98 (s, 18H, H-*t*-Bu). ^{13}C NMR was not available due to its low solubility. FT-IR (ATR) $\tilde{\nu}$ (cm^{-1}) = 3006 (w), 2983 (w), 2947 (w), 2861 (w), 1610 (w), 1530 (w), 1482 (s), 1407 (s), 1295 (w), 1265 (s), 1212 (s), 1195 (m), 1174 (m), 1134 (m), 1085 (w), 1101 (m), 887 (w), 838 (w), 815 (w), 789 (m), 767 (m), 722 (w), 682 (w), 626 (w). UV/Vis (CH_2Cl_2): λ_{max} (nm) (log ε) = 296 (4.51), 354 (5.07), 367 (5.03), 414 (4.37), 436 (4.49), 481 (4.07). Fluorescence (CH_2Cl_2): λ_{em} (λ_{ex}) (nm) = 486, 519, 557 (367). Φ = 35.0±0.4%. τ = 8.45 ns. MALDI-TOF MS (DCTB) (*m*/*z*): $[M]^+$ calcd. for $C_{50}H_{42}N_2O_4$, 734.314; found, 734.312. Elemental anal. calcd. for $C_{50}H_{42}N_2O_4 \cdot 0.2CHCl_3 \cdot 0.7H_2O$: C 78.17, H 5.70, N 3.63, found: C 78.12, H 5.83, N 3.21.

10,20-di-*tert*-butyl-2,3,12,13-tetramethoxydipyridino-[2',3':2,3;2'',3'':8,9]peryleno[1,12-*fgh*:7,6-*f'g'h'*]diquinoline (168)

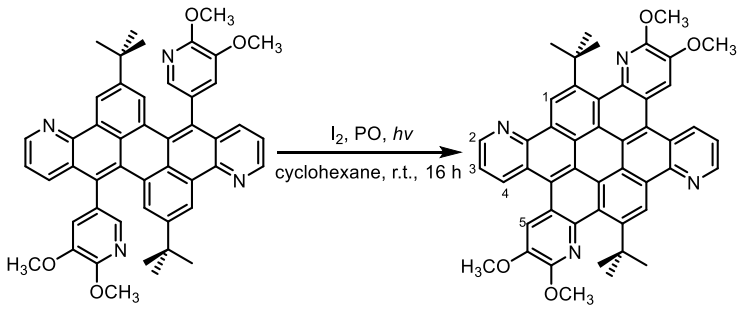

151 **168**

According to **GP2**, **151** (185 mg, 0.25 mmol), I_2 (254 mg, 1 mmol) and propylene oxide (10.5 mL) were used to setup the reaction. After irradiation for 16 hours, the obtained suspension was filtered off. The filtrate was refluxed in chloroform (10 mL) for 10 minutes. After cooling down to room temperature, the mixture was filtered off. The filtrate was rinsed with dichloromethane, ethanol and methanol, dried in vacuum to give **168** as a dark-red solid (48 mg, 26 %).

m.p.: 380 °C (dec.). ^{1}H NMR (300 MHz, $Cl_2CDCDCl_2$, 373 K) δ (ppm) = 10.44 (s, 2H, H-1), 9.57 (d, J = 8.2 Hz, 2H, H-2), 9.43 (br, 2H, H-4), 8.51 (s, 2H, H-5), 7.94 (dd, J = 7.7, 1.9 Hz, 2H, H-3), 4.42 (s, 6H, H-OMe), 4.11 (s, 6H, H-OMe), 2.09 (s, 18H, H-*t*-Bu). ^{13}C NMR was not available due to its low solubility. FT-IR (ATR) $\tilde{\nu}$ (cm^{-1}) = 3082 (w), 3009 (w), 2957 (w), 1606 (m), 1530 (w), 1483 (s), 1464 (s), 1400 (s), 1308 (w), 1269 (s), 1211 (s), 1180 (m), 1138 (m), 1092 (w), 1000 (m), 898 (w), 874 (w), 821 (w), 787 (m), 756 (w), 725 (w), 675 (w). UV/Vis (CH_2Cl_2): λ_{max} (nm) (log ε) = 301 (4.40), 321 (4.48), 357 (4.83), 367 (4.82), 424 (4.21), 439 (4.25), 475 (3.63). Fluorescence (CH_2Cl_2): λ_{em} (λ_{ex}) (nm) = 480, 513, 548 (367). Φ = 23.1±1.2%. τ = 8.70 ns. MALDI-TOF MS (DCTB, Kalib PEG600) (*m*/*z*): $[M]^+$ calcd. for $C_{48}H_{40}N_4O_4$, 736.304; found, 736.304. Elemental anal. calcd. for $C_{48}H_{40}N_4O_4 \cdot 3.6CHCl_3 \cdot 1.7H_2O$: C 51.77, H 3.96, N 4.68, found: C 51.62, H 3.99, N 4.73.

6,9,15,18-tetra-*tert*-butyl-2,3,11,12-tetramethoxydithieno-[2',3':2,3;2'',3'':8,9]peryleno[1,12-*fgh*:7,6-*f'g'h'*]diquinoline (169)

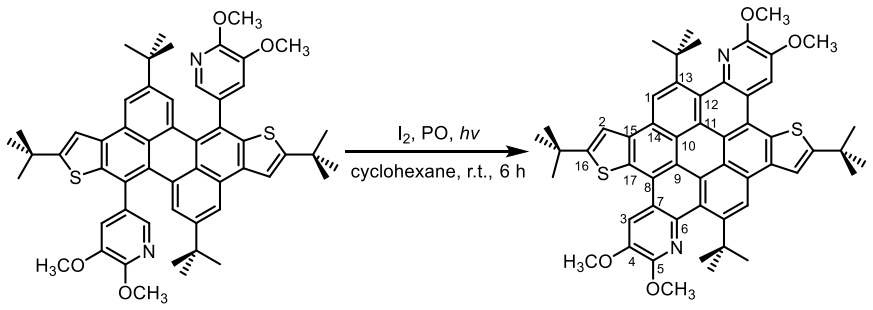

159 **169**

According to **GP2**, **159** (216 mg, 0.25 mmol), I_2 (203 mg, 0.8 mmol) and propylene oxide (7 mL) were used to setup the reaction. After irradiation for 6 hours, the product **169** was obtained after gel column chromatography (petroleum ether/ethyl acetate 10:1) and precipitation from chloroform/methanol as a dark-yellow solid (157 mg, 73 %).

m.p.: 378 °C (dec.). ^{1}H NMR (600 MHz, $CDCl_3$) δ (ppm) = 9.39 (s, 2H, H-3), 9.30 (s, 2H, H-1), 8.29 (s, 2H, H-2), 4.42 (s, 6H, H-OMe), 4.31 (s, 6H, H-OMe), 1.96 (s, 18H, H-*t*-Bu), 1.77 (s, 18H, H-*t*-Bu). ^{13}C NMR (151 MHz, $CDCl_3$) δ (ppm) = 157.76 (C-16), 151.01 (C-5), 146.75 (C-13), 143.20 (C-4), 138.37 (C-6), 136.31 (C-14), 132.05 (C-17), 126.15 (C-11), 125.24 (C-15), 123.81 (C-12), 123.36 (C-1), 121.49 (C-8), 120.59 (C-9), 120.20 (C-7), 120.11 (C-10), 116.99 (C-2), 113.14 (C-3), 56.22, 56.19, 39.02, 35.38, 33.90, 32.66. FT-IR (ATR) $\tilde{\nu}$ (cm^{-1}) = 2996 (w), 2954 (m), 2906 (w), 2863 (w), 1611 (w), 1591 (w), 1532 (w), 1510 (w), 1483 (s), 1399 (s), 1297 (w), 1267 (s), 1204 (s), 1134 (m), 1114 (m), 1061 (w), 1009 (m), 947 (w), 911 (w), 892 (w), 875 (w), 842 (m), 821 (m), 814 (m), 782 (m), 752 (w), 720 (w), 691 (w), 648 (w), 628 (w). UV/Vis (CH_2Cl_2): λ_{max} (nm) (log ε) = 309 (4.34), 355 (4.99), 368 (5.12), 415 (4.31), 438 (4.41), 479 (4.00). Fluorescence (CH_2Cl_2): λ_{em} (λ_{ex}) (nm) = 482, 515, 552 (368). Φ = 16.4±0.8%. τ = 5.22 ns. MALDI HRMS (DCTB) (*m*/*z*): $[M]^+$ calcd. for $C_{54}H_{54}N_2O_4S_2$, 858.3525; found, 858.3560. Elemental anal. calcd. for $C_{54}H_{54}N_2O_4S_2 \cdot 0.5H_2O$: C 74.71, H 6.39, N 3.23, found: C 74.67, H 6.36, N 2.99.

10,20-di-*tert*-butyl-3,13-bis(hexyloxy)tetrabenzo[*a*,*d*,*j*,*m*]coronene (170)

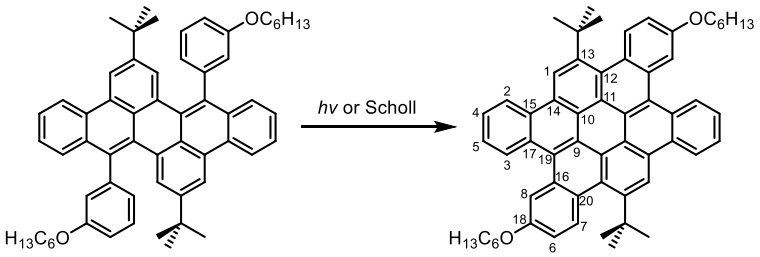

145 **170**

By photocyclization: According to **GP2**, **145** (188 mg, 0.23 mmol), I_2 (254 mg, 1.0 mmol) and propylene oxide (10.5 mL) were used to setup the reaction. After irradiation for 16 hours, the product **170** was obtained after gel column chromatography (petroleum ether/chloroform 3:1) as a yellow solid (34 mg, 18 %).

By Scholl cyclization: A Schlenk flask charged with **145** (65 mg, 0.08 mmol) was purged with argon. Dry dichloromethane (48 mL) was added to dissolve the substrate. The mixture was cooled down to 0 °C. DDQ (6 equiv., 109 mg, 0.48 mmol) was added in one portion under argon atmosphere. TfOH (1.6 mL) was then added dropwise under argon atmosphere at 0 °C over 5 minutes. The mixture was stirred at 0 °C for 20 minutes until TLC showed that the substrate was completely converted. The mixture was poured into saturated aqueous $NaHCO_3$ (30 mL). After stirring vigorously for 15 minutes, the mixture was extracted with dichloromethane (2 × 30 mL). The combined organic phase was washed with water (50 mL) and brine (50 mL), and dried over anhydrous Na_2SO_4. After removal of the solvent by rotary evaporation, the crude product was purified by silica gel column chromatography (petroleum ether/chloroform 3:1) and precipitation from chloroform/methanol to give the product as a yellow solid (29 mg, 45 %).

m.p.: 279 °C (dec.). ^{1}H NMR (600 MHz, $CDCl_3$) δ (ppm) = 9.41 (s, 2H, H-1), 9.32 (d, *J* = 8.0 Hz, 2H, H-3), 9.08 (d, *J* = 7.9 Hz, 2H, H-2), 8.58 (d, *J* = 8.9 Hz, 2H, H-7), 8.49 (d, *J* = 2.5 Hz, 2H, H-8), 7.93 - 7.87 (m, 2H, H-4), 7.87 - 7.82 (m, 2H, H-5), 7.20 (dd, *J* = 8.9, 2.5 Hz, 2H, H-6), 4.18 (t, *J* = 6.5 Hz, 4H, H-OMe), 1.92 - 1.87 (m, 4H, H-hex), 1.80 (s, 18H, H-*t*-Bu), 1.57 - 1.52 (m, 4H, H-

hex), 1.41 - 1.35 (m, 8H, H-hex), 0.93 (t, J = 7.0 Hz, 6H, H-hex). ^{13}C NMR (151 MHz, $CDCl_3$) δ (ppm) = 157.09 (C-18), 145.29 (C-13), 133.96 (C-7), 130.40 (C-15), 130.24 (C-16), 128.75 (C-12), 128.65 (C-3), 128.60 (C-17), 126.50 (C-14), 126.20 (C-4), 125.94 (C-20), 125.79 (C-5), 124.35 (C-1), 124.25 (C-19), 123.89 (C-2), 123.79 (C-9), 122.41 (C-11), 121.07 (C-10), 112.78 (C-6), 110.16 (C-8), 68.24, 38.58, 34.86, 31.67, 29.36, 25.85, 22.64, 14.07. FT-IR (ATR) $\tilde{\nu}$ (cm^{-1}) = 3076 (w), 3013 (w), 2955 (m), 2925 (m), 2861 (m), 1916 (w), 1608 (s), 1574 (w), 1539 (w), 1514 (w), 1447 (m), 1425 (m), 1391 (w), 1366 (w), 1348 (w), 1295 (w), 1232 (s), 1190 (m), 1111 (w), 1078 (m), 1048 (w), 1023 (m), 1001 (w), 983 (w), 930 (w), 877 (m), 849 (w), 828 (m), 791 (m), 758 (s), 727 (m), 675 (m), 628 (w). UV/Vis (CH_2Cl_2): λ_{max} (nm) (log ε) = 344 (4.86), 355 (4.93), 373 (4.86), 399 (4.18), 422 (4.42), 447 (4.57), 479 (3.38). Fluorescence (CH_2Cl_2): λ_{em} (λ_{ex}) (nm) = 485, 517, 554 (373). Φ = 15.0±0.4%. τ = 9.34 ns. MALDI-TOF MS (DCTB) (m/z): $[M]^+$ calcd. for $C_{60}H_{60}O_2$, 812.459; found, 812.462. Elemental anal. cald. for $C_{60}H_{60}O_2 \cdot H_2O$: C 86.71, H 7.52, found: C 86.89, H 7.64.

9,19-di-*tert*-butyl-6,16-bis(hexyloxy)dibenzo[2,3:8,9]peryleno[1,12-*fgh*:7,6-*f'g'h'*]diquinoline (171)

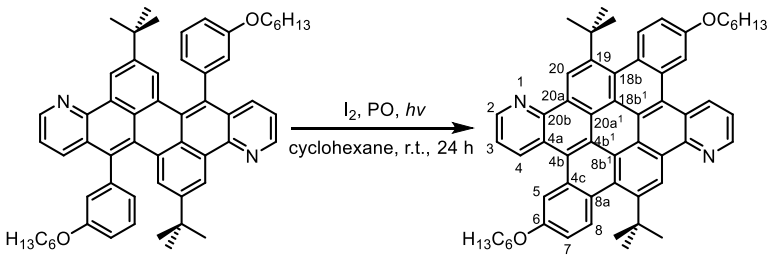

150 **171**

According to **GP2**, **150** (164 mg, 0.2 mmol), I_2 (203 mg, 0.8 mmol) and propylene oxide (7 mL) were used to setup the reaction. After irradiation for 24 hours, the product **171** was obtained after gel column chromatography (petroleum ether/chloroform/ethyl acetate 25:5:1) as a yellow solid (5 mg, 3 %).

m.p.: 267 °C (dec.). ^{1}H NMR (600 MHz, $CDCl_3$) δ (ppm) = 10.19 (s, 2H, H-20), 9.60 (dd, J = 8.3, 1.5 Hz, 2H, H-2), 9.27 (dd, J = 4.1, 1.5 Hz, 2H, H-4), 8.64 (d, J = 8.9 Hz, 2H, H-8), 8.30 (d, J = 2.5 Hz, 2H, H-5), 7.80 (dd, J = 8.2, 4.1 Hz, 2H, H-3), 7.22 (dd, J = 9.0, 2.5 Hz, 2H, H-7), 4.18 (t, J = 6.6 Hz, 4H, H-OCH_2), 1.93 - 1.87 (m, 4H, H-hex), 1.83 (s, 18H, H-*t*-Bu), 1.57 - 1.52 (m, 4H, H-hex), 1.41 - 1.35 (m, 8H, H-hex), 0.93 (t, J = 7.1 Hz, 6H, H-hex). ^{13}C NMR (151 MHz, $CDCl_3$) δ (ppm) = 157.56 (C-6), 148.35 (C-4), 146.06 (C-19), 146.03 (C-20b), 135.75 (C-2), 134.39 (C-8), 130.22 (C-4c), 129.85 (C-18b), 127.54 (C-20a), 126.22 (C-20), 126.02 (C-8a), 123.36 (C-4a), 123.32 (C-4b^1), 122.99 (C-4b), 122.98 (C-18b^1), 122.67 (C-20a^1), 120.63 (C-3), 112.43 (C-7), 110.25 (C-5), 68.31, 38.84, 34.88, 31.65, 29.35, 25.84, 22.63, 14.06. FT-IR (ATR) $\tilde{\nu}$ (cm^{-1}) = 3076 (w), 3007 (w), 2957 (m), 2924 (m), 2857 (m), 1609 (m), 1588 (m), 1566 (w), 1538 (w), 1506 (w), 1465 (m), 1452 (m), 1426 (m), 1399 (w), 1388 (w), 1365 (w), 1350 (w), 1333 (w), 1294 (w), 1262 (w), 1229 (m), 1205 (w), 1182 (w), 1167 (m), 1122 (w), 1114 (w), 1083 (w), 1071 (w), 1050 (w), 1027 (m), 1000 (w), 983 (w), 966 (w), 937 (w), 923 (w), 906 (w), 892 (w), 876 (w), 852 (w), 832 (m), 818 (m), 798 (s), 787 (s), 761 (w), 735 (w), 712 (w), 696 (w), 675 (m), 635 (w), 625 (w).

UV/Vis (CH_2Cl_2): λ_{max} (nm) (log ε) = 256 (4.78), 290 (4.26), 299 (4.29), 328 (4.55), 345 (4.68), 355 (4.73), 373 (4.63), 394 (4.04), 421 (4.21), 446 (4.34), 475 (3.75). Fluorescence (CH_2Cl_2): λ_{em} (λ_{ex}) (nm) = 479, 512, 548 (355). Φ = 21.9±0.6%. τ = 8.21 ns. MALDI-TOF MS (DCTB) (*m*/*z*): $[M]^+$ calcd. for $C_{58}H_{58}N_2O_2$, 814.449; found, 814.448. Elemental anal. calcd. for $C_{58}H_{58}N_2O_2 \cdot 0.3H_2O$: C 84.90, H 7.20, N 3.41, found: C 84.93, H 7.15, N 3.34.

2,8,11,17-tetra-*tert*-butyl-5,14-bis(hexyloxy)dibenzo[5,6:11,12]-coroneno[1,2-*b*:7,8-*b*']dithiophene (172)

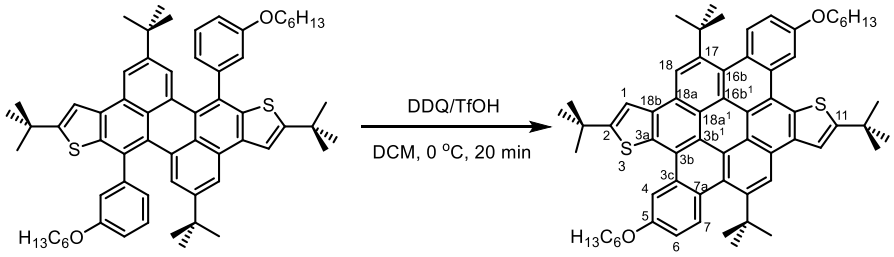

158 **172**

A Schlenk flask charged with **158** (38 mg, 0.04 mmol) was purged with argon. Dry dichloromethane (24 mL) was added to dissolve the substrate. The mixture was cooled down to 0 °C. DDQ (6 equiv., 54 mg, 0.24 mmol) was added in one portion under argon atmosphere. TfOH (0.8 mL) was then added dropwise under argon atmosphere at 0 °C over 5 minutes. The mixture was stirred at 0 °C for 20 minutes until TLC showed that the substrate was completely converted. The mixture was poured into saturated aqueous $NaHCO_3$ (30 mL). After stirring vigorously for 15 minutes, the mixture was extracted with dichloromethane (2 × 30 mL). The combined organic phase was washed with water (50 mL) and brine (50 mL), and dried over anhydrous Na_2SO_4. After removal of the solvent by rotary evaporation, the crude product was purified by silica gel column chromatography (petroleum ether/chloroform 4:1) and precipitation from chloroform/methanol to give the product as a dark yellow solid (23 mg, 62 %).

m.p.: 233 °C (dec.). ^{1}H NMR (600 MHz, $CDCl_3$) δ (ppm) = 9.16 (s, 2H, H-18), 9.07 (d, *J* = 2.5 Hz, 2H, H-4), 8.67 (d, *J* = 8.9 Hz, 2H, H-7), 8.22 (s, 2H, H-1), 7.32 (dd, *J* = 8.9, 2.5 Hz, 2H, H-6), 4.40 (t, *J* = 6.8 Hz, 4H, H-OCH_2), 2.08 - 1.99 (m, 4H, H-hex), 1.77 (s, 18H, H-*t*-Bu), 1.73 (s, 18H, H-*t*-Bu), 1.67 - 1.62 (m, 4H, H-hex), 1.49 - 1.40 (m, 8H, H-hex), 0.96 (t, *J* = 7.2 Hz, 6H, H-hex). ^{13}C NMR (151 MHz, $CDCl_3$) δ (ppm) = 157.65 (C-2), 157.58 (C-5), 144.68 (C-17), 136.09 (C-18a), 133.97 (C-7), 132.33 (C-3a), 129.02 (C-3c), 125.06 (C-18b), 124.81 (C-16b), 124.59 (C-7a), 124.43 (C-16b^1), 124.37 (C-18), 121.95 (C-3b), 121.38 (C-3b^1), 120.38 (C-18a^1), 116.53 (C-1), 113.44 (C-6), 106.56 (C-4), 68.53, 38.60, 35.33, 35.05, 32.67, 31.71, 29.30, 25.95, 22.72, 14.10. FT-IR (ATR) $\tilde{\nu}$ (cm^{-1}) = 2955 (m), 2928 (m), 2865 (m), 1611 (m), 1558 (w), 1541 (w), 1511 (w), 1479 (m), 1464 (m), 1366 (m), 1292 (w), 1206 (s), 1144 (w), 1124 (w), 1104 (w), 1050 (m), 1020 (w), 980 (w), 958 (w), 918 (w), 870 (w), 831 (m), 786 (w), 721 (w), 680 (w). UV/Vis (CH_2Cl_2): λ_{max} (nm) (log ε) = 339 (4.76), 352 (4.98), 368 (5.12), 397 (4.11), 433 (4.36), 447 (4.46), 454 (4.45), 484 (4.14). Fluorescence (CH_2Cl_2): λ_{em} (λ_{ex}) (nm) =491, 524, 562 (368). Φ = 17.5±0.5%. τ = 3.46 ns. MALDI-TOF MS (DCTB) (*m*/*z*): $[M]^+$ calcd. for $C_{64}H_{72}O_2S_2$, 936.497; found, 936.557. Elemental anal. calcd. for $C_{64}H_{72}O_2S_2 \cdot 0.5H_2O$: C 81.22, H 7.78, found: C 81.15, H 7.86.

5.2.2 Compounds of Chapter 3.2

9,19-di-*tert*-butyldibenzo[*hi*,*st*]diindeno[1,2,3-*de*:1',2',3'-*op*]pentacene (179)

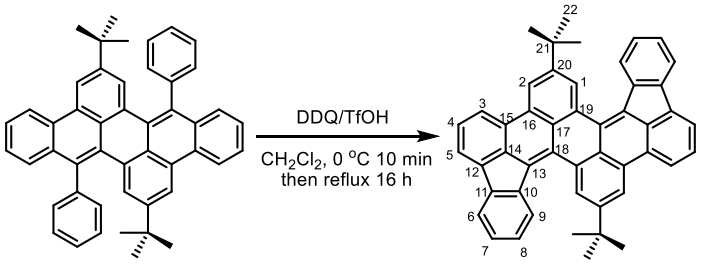

143 179

To a cooled solution (0 °C) of compound **143** (62 mg, 0.1 mmol) and 2,3-dichloro-5,6-dicyano-1,4-benzoquinone (DDQ, 136 mg, 0.6 mmol) in dry dichloromethane (60 mL) under argon atmosphere triflic acid (TfOH, 2 mL) was added dropwise. The mixture was then allowed to warm up and further refluxed overnight under argon atmosphere. After cooling down to room temperature, the mixture was poured into saturated aq. $NaHCO_3$ (100 mL). After stirring vigorously for 15 minutes, the mixture was extracted with dichloromethane (DCM, 3 × 50 mL). The combined organic phase was washed with aq. NH_4Cl (100 mL), water (100 mL) and dried over anhydrous Na_2SO_4. After removal of the solvent by rotary evaporation, the crude product was purified by silica gel column chromatography (petroleum ether/dichloromethane 10:1 to 1:1). The product was obtained after precipitation from tetrahydrofuran/methanol and drying in vacuum as an orange-red solid (40 mg, 65 %).

m.p.: 357 °C (dec.). ^{1}H NMR (400 MHz, $Cl_2CDCDCl_2$) δ (ppm) = 8.86 (s, 2H, H-1), 8.74 (s, 2H, H-2), 8.54 (d, J = 8.2 Hz, 2H, H-3), 8.43 (d, J = 7.8 Hz, 2H, H-9), 8.04 (d, J = 7.1 Hz, 2H, H-5), 7.98 (d, J = 7.4 Hz, 2H, H-6), 7.80 (t, J = 7.4 Hz, 2H, H-4), 7.42 (t, J = 7.3 Hz, 2H, H-7), 7.30-7.22 (m, 2H, H-8), 1.53 (s, 18H, H-22). ^{13}C NMR (101 MHz, $Cl_2CDCDCl_2$) δ (ppm) = 149.15 (C-20), 140.83 (C-11), 138.29 (C-10), 136.33 (C-15), 133.95 (C-14), 131.23 (C-13), 130.87 (C-18), 130.24 (C-19), 129.98 (C-17), 129.78 (C-16), 128.55 (C-1), 128.39 (C-7), 128.10 (C-4), 126.98 (C-8, 12), 123.84 (C-9), 121.34 (C-3), 121.17 (C-6), 119.64 (C-2), 119.42 (C-5), 35.37 (C-21), 31.29 (C-22). FT-IR (ATR) $\tilde{\nu}$ (cm^{-1}) = 3062 (w), 3014 (w), 2954 (w), 2904 (w), 2866 (w), 1952 (w), 1900 (w), 1840 (w), 1777 (w), 1756 (w), 1689 (w), 1601 (w), 1580 (w), 1510 (w), 1477 (w), 1461 (w), 1441 (m), 1408 (w), 1381 (w), 1361 (w), 1327 (w), 1310 (w), 1287 (w), 1270 (w), 1237 (w), 1220 (w), 1176 (w), 1159 (w), 1140 (w), 1113 (w), 1098 (w), 1064 (w), 1039 (w), 1027 (w), 1004 (w), 977 (w), 951 (w), 931 (w), 879 (m), 817 (w), 796 (w), 778 (m), 750 (s), 702 (m), 672 (w), 657 (m), 635 (w), 620 (w). UV/Vis ($CHCl_3$): λ_{max} (nm) (log ε) = 278 (4.74), 318 (4.28), 330 (4.32), 355 (4.25), 391 (4.00), 409 (3.95), 467 (4.51), 499 (4.62). Fluorescence ($CHCl_3$): λ_{em} (λ_{ex}) (nm) = 525, 552 (467). Φ = 67.0±1.9%. MALDI-TOF MS (DCTB, calibrated with PEG600) (m/z): $[M]^+$ calcd. for $C_{48}H_{36}$, 612.282; found, 612.281. Elemental anal. calcd. for $C_{48}H_{36}\cdot 0.4H_2O$: C 92.99, H 5.98, found: C 93.13, H 6.09.

2,10-di-*tert*-butyl-8,16-di(naphthalen-2-yl)dibenzo[*fg*,*qr*]pentacene (180)

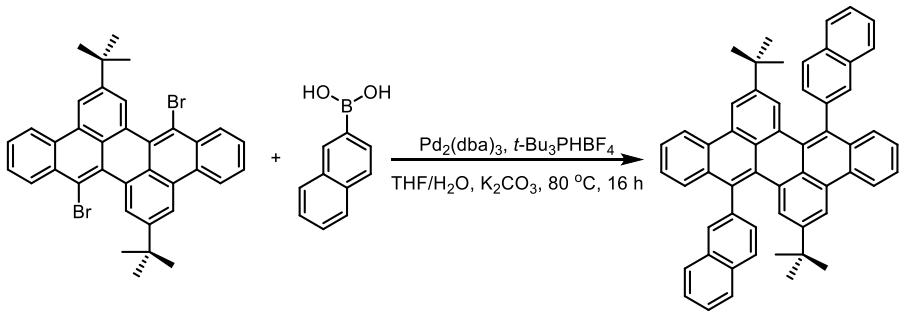

133 180

In a screw-capped vial, dibromide **133** (311 mg, 0.5 mmol), naphthalen-2-ylboronic acid (344 mg, 2 mmol) and K_2CO_3 (207 mg, 1.5 mmol) was suspended in argon-degassed THF/water (5.0 mL/1.3 mL) and a mixture of $Pd_2(dba)_3$ (23 mg, 0.025 mmol) and *t*-Bu_3PHBF_4 (23 mg, 0.079 mmol) was added under argon atmosphere. The mixture was stirred vigorously at 80 °C overnight. After cooling down to room temperature, the mixture was diluted with dichloromethane (100 mL), washed with water (3 × 50 mL) and dried over Na_2SO_4. After removal of the solvent by rotary evaporation, the crude product was purified by silica gel chromatography (petroleum ether/dichloromethane 8:1). The product was obtained after precipitation from dichloromethane/methanol and drying in vacuum as a yellow solid (309 mg, 86 %, mixture of atropisomers).

m.p.: 299 °C (dec.). ^{1}H NMR (600 MHz, $CDCl_3$) δ (ppm) = 8.71 (d, J = 4.0 Hz, 1H), 8.70 (d, J = 4.0 Hz, 1H), 8.45 (d, J = 1.5 Hz, 1H), 8.44 (d, J = 1.5 Hz, 1H), 8.06 (d, J = 8.3 Hz, 1H), 8.01 (s, 1H), 7.99 (d, J = 8.3 Hz, 1H), 7.92 (dd, J = 16.4, 7.5 Hz, 3H), 7.81 (d, J = 7.9 Hz, 1H), 7.73 (dd, J = 7.9, 2.9 Hz, 3H), 7.69 (d, J = 7.9 Hz, 1H), 7.66 (d, J = 1.7 Hz, 1H), 7.62 (d, J = 1.7 Hz, 1H), 7.61-7.58 (m, 2H), 7.56-7.49 (m, 3H), 7.49-7.45 (m, 1H), 7.42 (dd, J = 8.2, 7.0 Hz, 2H), 0.81 (s, 9H), 0.80 (s, 9H). ^{13}C NMR (151 MHz, $CDCl_3$) δ (ppm) = 148.16, 148.13, 139.19, 139.16, 134.50, 134.39, 134.24, 133.26, 132.78, 132.76, 130.95, 130.63, 130.55, 130.36, 130.31, 130.29, 130.02, 129.19, 129.11, 129.05, 129.04, 128.93, 128.72, 128.39, 128.27, 127.93, 127.88, 127.85, 127.79, 127.77, 127.76, 127.63, 127.62, 126.33, 126.28, 126.26, 126.16, 126.14, 126.04, 122.36, 122.35, 116.90, 116.89, 34.52, 34.50, 30.67, 30.65. FT-IR (ATR) $\tilde{\nu}$ (cm^{-1}) = 3055 (w), 3018 (w), 2956 (m), 2904 (w), 2867 (w), 1947 (w), 1919 (w), 1800 (w), 1628 (w), 1600 (m), 1572 (w), 1515 (w), 1502 (w), 1474 (w), 1462 (w), 1446 (w), 1420 (w), 1379 (w), 1362 (m), 1296 (w), 1271 (w), 1234 (w), 1202 (w), 1168 (w), 1144 (w), 1127 (w), 1078 (w), 1045 (w), 1020 (w), 950 (w), 930 (w), 902 (m), 872 (m), 856 (m), 819 (s), 790 (w), 758 (s), 744 (s), 699 (w), 669 (w), 638 (m), 607 (w). UV/Vis ($CHCl_3$): λ_{max} (nm) (log ε) = 291 (4.61), 311 (4.73), 417 (4.44), 433 (4.46). Fluorescence ($CHCl_3$): λ_{em} (λ_{ex}) (nm) = 481, 504 (417). Φ = 51.4±0.4%. MALDI-TOF MS (DCTB) (*m*/*z*): $[M]^+$ calcd. for $C_{56}H_{44}$, 716.344; found, 716.409. Elemental anal. calcd. for $C_{56}H_{44}\cdot 0.3H_2O$: C 93.11, H 6.22, found: C 93.13, H 6.57.

9,21-di-*tert*-butyldibenzo[*hi*,*st*]benzo[6,7]indeno[1,2,3-*de*]benzo[6,7]indeno[1,2,3-*op*]pentacene (181)

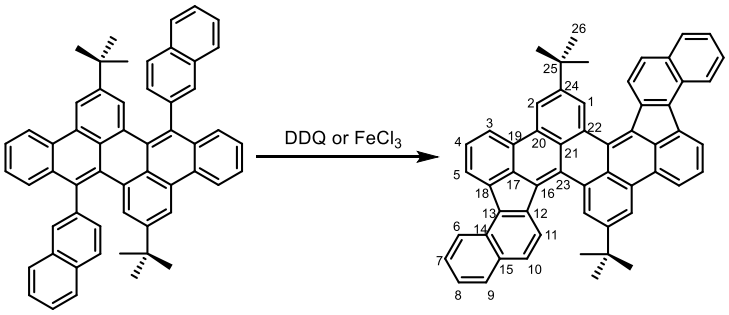

180 **181**

Using $FeCl_3/CH_3NO_2$: In a 250 mL Schlenk flask, a solution of **180** (86 mg, 0.12 mmol) in dry DCM (120 mL) was purged with argon for 15 min. A solution of $FeCl_3$ (195 mg, 1.2 mmol, 10 equiv.) in nitromethane (0.9 mL) was then added dropwise at 0 °C. The mixture was stirred at 0 °C for 50 minutes with a constant argon flow bubbling through the mixture. The reaction was quenched by adding methanol (2 mL), washed with aq. NH_4Cl (50 mL) and water (50 mL), dried over Na_2SO_4 and passed through a short pad of Celite®. After removal of the solvent by rotary evaporation, the product was obtained after recrystallization from chlorobenzene/*n*-heptane and drying in vacuum as an orange-red solid (65 mg, 76 %).

Using DDQ/TfOH: In a 50 mL Schlenk flask, a solution of **180** (29 mg, 0.04 mmol) in dry DCM (24 mL) was purged with argon for 15 min. DDQ (20 mg, 0.089 mmol, 2.2 equiv.) was added in one portion at 0 °C. TfOH (0.8 mL) was then added dropwise at 0 °C. The mixture was stirred at 0 °C for 30 minutes and then for another 30 minutes at room temperature. The reaction was quenched by pouring it into saturated aq. $NaHCO_3$ (30 mL). After stirring vigorously for 15 minutes, the mixture was extracted with dichloromethane (3 × 10 mL). The combined organic phase was washed with aq. NH_4Cl (50 mL), water (50 mL) and dried over anhydrous Na_2SO_4. After removal of the solvent by rotary evaporation, the product was obtained after recrystallization from chloroform/*n*-hexane and drying in vacuum as an orange-red solid (18 mg, 63 %).

m.p.: >400 °C (dec.). ^{1}H NMR (600 MHz, $Cl_2CDCDCl_2$) δ (ppm) = 8.83 (d, J = 8.5 Hz, 2H, H-6), 8.77 (s, 4H, H-1, 2), 8.58 (d, J = 5.0 Hz, 2H, H-3), 8.57 (d, J = 5.8 Hz, 2H, H-5), 8.45 (d, J = 8.6 Hz, 2H, H-10), 7.93 (d, J = 8.0 Hz, 2H, H-9), 7.87 (t, J = 7.6 Hz, 2H, H-4), 7.70 (d, J = 8.7 Hz, 2H, H-11), 7.70-7.65 (m, 2H, H-7), 7.54 (t, J = 7.4 Hz, 2H, H-8), 1.53 (s, 18H, H-26). ^{13}C NMR (151 MHz, $Cl_2CDCDCl_2$) δ (ppm) = 149.38 (C-24), 136.96 (C-18), 136.63 (C-16), 136.14 (C-13), 134.22 (C-15), 133.94 (C-17), 131.64 (C-12), 131.00 (C-22), 130.57 (C-23), 130.18 (C-20), 130.16 (C-21), 129.71 (C-14), 129.57 (C-1), 129.11 (C-9), 128.33 (C-4), 127.31 (C-11), 127.13 (C-7), 126.63 (C-19), 125.79 (C-8), 124.37 (C-6), 123.27 (C-3), 122.44 (C-10), 121.23 (C-5), 119.93 (C-2), 35.38 (C-25), 31.28 (C-26). FT-IR (ATR) $\tilde{\nu}$ (cm^{-1}) = 3075 (w), 3053 (w), 2963 (m), 2901 (w), 2864 (w), 1948 (w), 1921 (w), 1754 (w), 1582 (m), 1510 (w), 1477 (w), 1459 (m), 1441 (w), 1414 (m), 1394 (m), 1362 (w), 1312 (w), 1277 (w), 1238 (m), 1222 (w), 1180 (w), 1152 (w), 1106 (w), 1070 (w), 1023 (w), 1004 (w), 985 (w), 947 (w), 927 (w), 905 (w), 877 (m), 857 (w), 813 (s), 781 (w), 757 (m), 738 (s), 707 (m), 659 (m), 626 (w), 614 (w). UV/Vis ($CHCl_3$): λ_{max} (nm) (log ε) = 252 (5.14),

280 (4.77), 302 (4.66), 323 (4.66), 340 (4.60), 362 (4.30), 412 (4.18), 457 (4.41), 485 (4.72), 518 (4.85). Fluorescence ($CHCl_3$): λ_{em} (λ_{ex}) (nm) = 547 (485). Φ = 3.9±0.1%. MALDI HRMS (DCTB) (*m*/*z*): $[M]^+$ calcd. for $C_{56}H_{40}$, 712.3125; found, 712.3114. Elemental anal. calcd. for $C_{56}H_{40}\cdot 1.2H_2O$: C 91.57, H 5.82, found: C 91.61, H 6.00.

9,21-di-*tert*-butyldibenzo[*hi*,*st*]benzo[6,7]indeno[1,2,3-*de*]benzo[6,7]indeno[1,2,3-*op*]pentacene-12,24-diyl bis(trifluoromethanesulfonate) (184)

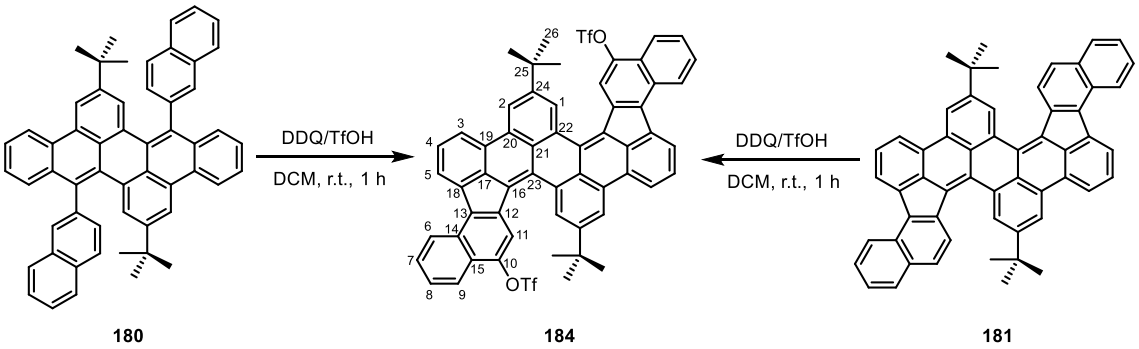

From **180**: In a 100 mL Schlenk flask, a solution of **180** (86 mg, 0.12 mmol) in dry dichloromethane (72 mL) was purged with argon for 15 min. DDQ (163 mg, 0.72 mmol, 6.0 equiv.) was added in one portion at room temperature. TfOH (3.6 mL) was then added dropwise. The mixture was stirred at room temperature for 1 hour. The reaction was quenched by pouring it into saturated aq. $NaHCO_3$ (70 mL). After stirring vigorously for 15 minutes, the mixture was extracted with dichloromethane (3 × 40 mL). The combined organic phase was washed with aq. NH_4Cl (100 mL), water (100 mL) and dried over anhydrous Na_2SO_4. After removal of the solvent by rotary evaporation, the product was obtained after silica gel column chromatography (petroleum ether/dichloromethane/ethyl acetate 50:5:1 to 30:3:1) as a dark-red solid (109 mg, 90 %).

From **181**: In a 50 mL Schlenk flask, a suspension of **181** (11 mg, 0.015 mmol) in dry dichloromethane (11 mL) was purged with argon for 15 min. DDQ (14 mg, 0.06 mmol, 4.0 equiv.) was added in one portion at room temperature. TfOH (0.5 mL) was then added dropwise. The mixture was stirred at room temperature for 1 hour. The reaction was quenched by pouring it into saturated aq. $NaHCO_3$ (30 mL). After stirring vigorously for 15 minutes, the mixture was extracted with dichloromethane (3 × 10 mL). The combined organic phase was washed with aq. NH_4Cl (50 mL), water (50 mL) and dried over anhydrous Na_2SO_4. After removal of the solvent by rotary evaporation, the product was obtained after silica gel column chromatography (petroleum ether/dichloromethane/ethyl acetate 50:5:1 to 30:3:1) as a dark-red solid (14 mg, 93 %).

m.p.: > 400 °C (dec.). ^{1}H NMR (600 MHz, $CDCl_3$) δ (ppm) = 8.94 (d, *J* = 8.5 Hz, 2H, H-6), 8.85 (d, *J* = 1.5 Hz, 2H, H-2), 8.69 (d, *J* = 1.7 Hz, 2H, H-1), 8.66 (d, *J* = 8.1 Hz, 2H, H-3), 8.63 (d, *J* = 7.4 Hz, 2H, H-5), 8.45 (s, 2H, H-11), 8.16 (d, *J* = 8.2 Hz, 2H, H-9), 7.93 (t, *J* = 7.7 Hz, 2H, H-4), 7.82-7.75 (m, 2H, H-7), 7.69 (t, *J* = 7.5 Hz, 2H, H-8), 1.55 (s, 18H, H-26). ^{13}C NMR (151 MHz, $CDCl_3$) δ (ppm) = 150.03 (C-24), 144.72 (C-10), 136.64 (C-13), 135.95 (C-18), 135.75 (C-12), 134.42 (C-17), 132.01 (C-23), 131.14 (C-14), 130.91 (C-20), 130.84 (C-16), 130.51 (C-22), 129.78 (C-21), 129.40 (C-1), 128.47 (C-4), 128.40 (C-7), 127.38 (C-8), 127.01 (C-19,15), 124.85 (C-6), 123.81 (C-5), 122.22 (C-9), 122.16 (C-3), 120.57 (C-2), 118.56 (q, $J_{C\text{-}F}$ = 320.7 Hz, -CF_3), 114.65

(C-11), 35.50 (C-25), 31.24 (C-26). FT-IR (ATR) $\tilde{\nu}$ (cm^{-1}) = 3076 (w), 2961 (w), 2908 (w),2871 (w), 1620 (w), 1584 (w), 1519 (w), 1478 (w), 1459 (w), 1423 (w), 1364 (w), 1315 (w), 1281 (w), 1243 (m), 1206 (s), 1184 (w), 1157 (w), 1139 (s), 1075 (w), 1031 (w), 1013 (m), 944 (w), 898 (m), 880 (w), 832 (m), 814 (s), 801 (w), 784 (w), 753 (s), 732 (m), 717 (m), 697 (w), 677 (w), 654 (w), 631 (w), 608 (w). UV/Vis ($CHCl_3$): λ_{max} (nm) (log ε) = 252 (5.07), 301 (4.65), 326 (4.64), 343 (4.57), 364 (4.33), 413 (4.20), 462 (4.35), 491 (4.67), 525 (4.81). Fluorescence ($CHCl_3$): λ_{em} (λ_{ex}) (nm) = 551, 585 (491). Φ = 8.3±0.4%. MALDI-TOF MS (DCTB) (*m*/*z*): $[M]^+$ calcd. for $C_{58}H_{38}F_6O_6S_2$, 1008.201; found, 1008.207. Elemental anal. calcd. for $C_{58}H_{38}F_6O_6S_2 \cdot H_2O$: C 67.83, H 3.93, found: C 67.77, H 4.01.

9,21-di-*tert*-butyl-12,24-bis(4-(*tert*-butyl)phenyl)dibenzo[*hi*,*st*]benzo[6,7]indeno[1,2,3-*de*]benzo[6,7]indeno[1,2,3-*op*]pentacene (185)

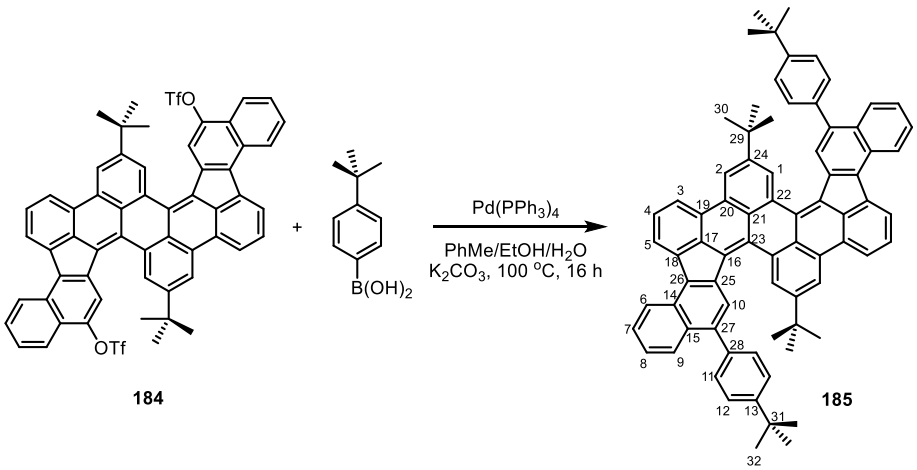

184 **185**

In a screw-capped vial, bistriflate **184** (30 mg, 0.03 mmol), (4-(*tert*-butyl)phenyl)boronic acid (22 mg, 0.12 mmol) were suspended in 2M aq. K_2CO_3 (0.07 mL, 0.14 mmol) and argon-degassed toluene/ethanol (0.22 mL/0.07 mL) and $Pd(PPh_3)_4$ (3.5 mg, 3 µmol) was added under argon atmosphere. The mixture was stirred vigorously at 100 °C overnight. After cooling down to room temperature, the mixture was diluted with dichloromethane (20 mL), washed with water (2 × 20 mL) and dried over Na_2SO_4. After removal of the solvent by rotary evaporation, the crude product was purified by silica gel column chromatography (petroleum ether/ethyl acetate 25:1). The product was obtained after precipitation from dichloromethane/methanol and drying in vacuum as a dark-red solid (19 mg, 65%).

m.p.: 381 °C (dec.). ^{1}H NMR (400 MHz, $CDCl_3$) δ (ppm) = 8.94 (d, *J* = 8.4 Hz, 2H, H-6), 8.78 (d, *J* = 1.8 Hz, 2H, H-1), 8.68 (d, *J* = 1.7 Hz, 2H, H-2), 8.60 (d, *J* = 7.4 Hz, 2H, H-3), 8.53 (d, *J* = 8.2 Hz, 2H, H-5), 8.41 (s, 2H, H-10), 8.07 (d, *J* = 8.0 Hz, 2H, H-9), 7.89-7.82 (m, 2H, H-4), 7.71-7.64 (m, 2H, H-7), 7.49-7.42 (m, 6H, H-8,12), 7.38 (br, 4H, H-11), 1.39 (s, 18H, H-32), 1.18 (s, 18H, H-30). ^{13}C NMR (101 MHz, $CDCl_3$) δ (ppm) = 150.08 (C-13), 149.30 (C-24), 139.80 (C-27), 138.14 (C-16), 137.40 (C-18), 136.40 (C-25), 135.66 (C-26), 134.53 (C-17), 132.69 (C-15), 131.90 (C-22), 131.41 (C-23), 130.84 (C-14), 130.72 (C-28), 130.42 (C-20), 130.02 (C-21), 129.74 (C-11), 128.92 (C-1), 128.18 (C-4), 127.59 (C-9), 126.91 (C-19), 126.83 (C-7), 125.56 (C-8), 125.05 (C-12), 124.75 (C-6), 123.74 (C-10), 123.10 (C-3), 120.97 (C-5), 120.43 (C-2), 35.09 (C-29), 34.58 (C-31),

31.42 (C-32), 31.06 (C-30). FT-IR (ATR) $\tilde{\nu}$ (cm^{-1}) = 3068 (w), 3030 (w), 2957 (m), 2903 (m), 2866 (m), 1910 (w), 1829 (w), 1797 (w), 1770 (w), 1597 (w), 1581 (m), 1546 (w), 1512 (w), 1475 (m), 1456 (m), 1414 (m), 1393 (m), 1379 (m), 1362 (m), 1311 (w), 1269 (w), 1239 (w), 1220 (w), 1202 (w), 1185 (w), 1145 (w), 1131 (w), 1115 (w), 1105 (w), 1014 (w), 957 (w), 925 (w), 901 (w), 879 (m), 837 (m), 814 (m), 802 (w), 763 (s), 718 (s), 686 (w), 659 (m), 642 (w), 625 (w). UV/Vis ($CHCl_3$): λ_{max} (nm) (log ε) = 252 (5.13), 280 (4.79), 303 (4.64), 329 (4.72), 343 (4.70), 366 (4.43), 413 (4.15), 463 (4.39), 491 (4.70), 524 (4.81). Fluorescence ($CHCl_3$): λ_{em} (λ_{ex}) (nm) = 558, 585 (491). Φ = 5.5±0.6%. MALDI HRMS (DCTB) (*m*/*z*): $[M]^+$ calcd. for $C_{76}H_{64}$, 976.5008; found, 976.5016. Elemental anal. calcd. for $C_{76}H_{64}\cdot 0.3H_2O$: C 92.89, H 6.63, found: C 92.84, H 6.70.

9,21-di-*tert*-butyl-12,24-bis(4-methoxyphenyl)dibenzo[*hi*,*st*]benzo[6,7]indeno[1,2,3-*de*]benzo[6,7]indeno[1,2,3-*op*]pentacene (186)

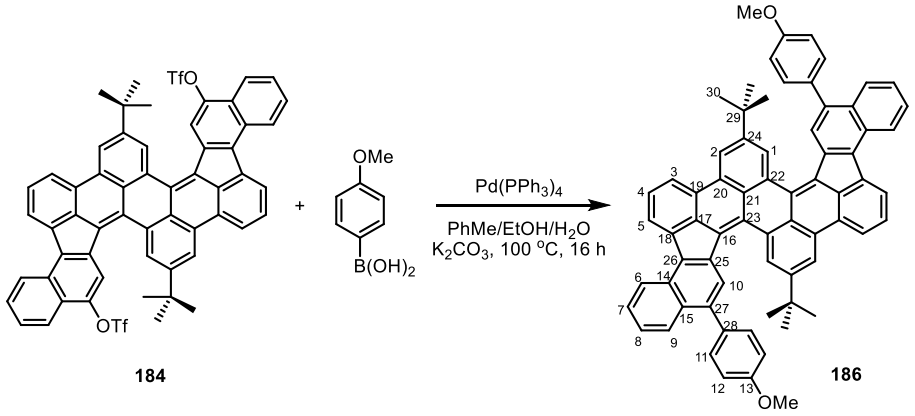

184 **186**

In a screw-capped vial, bistriflate **184** (20 mg, 0.02 mmol), (4-methoxyphenyl)boronic acid (12 mg, 0.08 mmol) was suspended in 2M aq. K_2CO_3 (0.05 mL, 0.1 mmol) and argon-degassed toluene/ethanol (0.15 mL/0.05 mL) and $Pd(PPh_3)_4$ (2.3 mg, 2 µmol) was added under argon atmosphere. The mixture was stirred vigorously at 100 °C overnight. After cooling down to room temperature, the mixture was diluted with dichloromethane (20 mL), washed with water (2 × 20 mL) and dried over Na_2SO_4. After removal of the solvent by rotary evaporation, the product was obtained after precipitation from dichloromethane/ethanol and drying in vacuum as a dark-red solid (13 mg, 72%).

m.p.: > 400 °C (dec.). ^{1}H NMR (600 MHz, $Cl_2CDCDCl_2$) δ (ppm) = 8.91 (d, *J* = 8.5 Hz, 2H, H-6), 8.75 (d, *J* = 1.4 Hz, 2H, H-1), 8.67 (d, *J* = 1.0 Hz, 2H, H-2), 8.60 (d, *J* = 7.5 Hz, 2H, H-3), 8.54 (d, *J* = 8.3 Hz, 2H, H-5), 8.37 (s, 2H, H-10), 7.99 (d, *J* = 8.4 Hz, 2H, H-9), 7.88 (t, *J* = 7.6 Hz, 2H, H-4), 7.70 - 7.66 (m, 2H, H-7), 7.46 (t, *J* = 7.5 Hz, 2H, H-8), 7.34 (br, 4H, H-11), 6.95 (d, *J* = 8.0 Hz, 4H, H-12), 3.84 (s, 6H, -OMe), 1.21 (s, 18H, H-30). ^{13}C NMR (151 MHz, $Cl_2CDCDCl_2$) δ (ppm) = 158.63 (C-13), 149.50 (C-24), 139.41 (C-27), 137.06 (C-19), 136.20 (C-25), 135.31 (C-26), 134.17 (C-17), 133.04 (C-28), 132.66 (C-15), 131.71 (C-16), 131.16 (C-20), 131.04 (C-11), 130.49 (C-23), 130.46 (C-14), 130.10 (C-22), 129.63 (C-21), 129.08 (C-1), 128.40 (C-4), 127.41 (C-9), 126.95 (C-7), 126.55 (C-18), 125.69 (C-8), 124.61 (C-6), 123.42 (C-10), 123.21 (C-3), 121.02 (C-5), 120.26 (C-2), 113.56 (C-12), 55.42 (-OMe), 34.96 (C-29), 30.93 (C-30). FT-IR (ATR) $\tilde{\nu}$ (cm^{-1}) = 3066 (w), 3036 (w), 2955 (m), 2904 (w), 2868 (w), 2834 (w), 2061 (w), 1915 (w), 1606 (m), 1581

(m), 1547 (w), 1512 (s), 1475 (w), 1456 (m), 1414 (m), 1393 (w), 1377 (w), 1362 (m), 1284 (m), 1244 (s), 1176 (m), 1144 (w), 1107 (w), 1035 (m), 1012 (w), 956 (w), 925 (w), 900 (w), 880 (m), 832 (m), 814 (m), 786 (w), 764 (s), 735 (w), 719 (m), 677 (w), 659 (w), 619 (w). HRMS-MALDI (DCTB) (*m*/*z*): $[M]^+$ calcd. for $C_{70}H_{52}O_2$, 924.3967; found, 924.4001. UV/Vis ($CHCl_3$): λ_{max} (nm) (log ε) = 252 (5.09), 281 (4.76), 303 (4.63), 330 (4.69), 343 (4.68), 367 (4.42), 412 (4.14), 460 (4.34), 490 (4.64), 523 (4.75). Fluorescence ($CHCl_3$): λ_{em} (λ_{ex}) (nm) = 554, 589 (490). Φ = 5.9±0.3%. MALDI HRMS (DCTB) (*m*/*z*): $[M]^+$ calcd. for $C_{70}H_{52}O_2$, 924.3967; found, 924.4001. Elemental anal. calcd. for $C_{70}H_{52}O_2 \cdot 0.5H_2O$: C 90.00, H 5.72, found: C 90.08, H 5.90.

12,24-bis(4,5-bis(hexyloxy)naphthalen-1-yl)-9,21-di-*tert*-butyldibenzo[*hi*,*st*]benzo[6,7]indeno[1,2,3-*de*]benzo[6,7]indeno[1,2,3-*op*]pentacene (189)

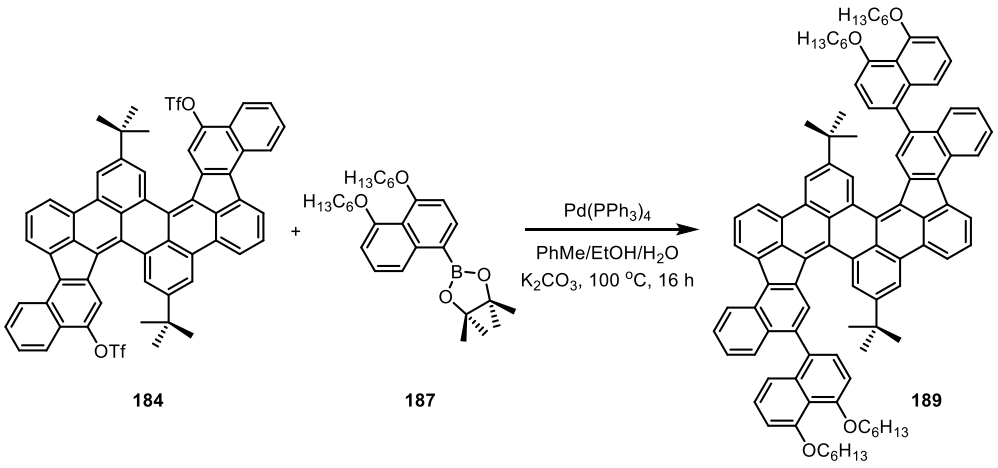

184 **187** **189**

In a screw-capped vial, bistriflate **184** (61 mg, 0.06 mmol), 2-(4,5-bis(hexyloxy)naphthalen-1-yl)-4,4,5,5-tetramethyl-1,3,2-dioxaborolane **187** (218 mg, 0.48 mmol) were suspended in 2M aq. K_2CO_3 (0.12 mL, 0.24 mmol) and argon-degassed toluene/ethanol (0.40 mL/0.12 mL) and $Pd(PPh_3)_4$ (7 mg, 6 µmol) was added under argon atmosphere. The mixture was stirred vigorously at 100 °C overnight. After cooling down to room temperature, the mixture was diluted with dichloromethane (50 mL), washed with water (2 × 40 mL) and dried over Na_2SO_4. After removal of the solvent by rotary evaporation, the crude product was purified by silica gel column chromatography (petroleum ether/ethyl acetate 20:1). The product (mixture of atropisomers) was obtained after precipitation from dichloromethane/methanol and drying in vacuum as a red solid (35 mg, 43%).

m.p.: 243 °C (dec.). ^{1}H NMR (600 MHz, CD_2Cl_2) δ (ppm) = 9.01 - 8.88 (m, 2H), 8.77 (s, 2H), 8.66 (s, 1H), 8.64 (s, 1H), 8.63 (s, 2H), 8.54 (s, 1H), 8.53 (s, 1H), 8.46 (d, *J* = 5.7 Hz, 1H), 8.39 (d, *J* = 12.5 Hz, 1H), 7.94-7.84 (m, 2H), 7.68-7.59 (m, 2H), 7.58-7.51 (m, 1H), 7.48 (t, *J* = 7.8 Hz, 1H), 7.37 (d, *J* = 7.7 Hz, 1H), 7.34-7.29 (m, 1H), 7.29-7.25 (m, 1H), 7.25-7.20 (m, 1H), 7.14 (d, *J* = 8.1 Hz, 1H), 7.08 (t, *J* = 7.3 Hz, 1H), 6.99 (d, *J* = 7.4 Hz, 1H), 6.89 (d, *J* = 7.3 Hz, 1H), 6.87-6.80 (m, 1H), 6.79-6.72 (m, 1H), 6.62 (d, *J* = 6.9 Hz, 1H), 6.62-6.51 (m, 1H), 4.24-4.07 (m, 4H), 4.06-3.90 (m, 4H), 2.02-1.83 (m, 8H), 1.67-1.53 (m, 8H), 1.50-1.38 (m, 16H), 1.37-1.26 (m, 9H), 1.01-0.89 (m, 21H). ^{13}C NMR (151 MHz, CD_2Cl_2) δ (ppm) = 157.62, 157.56, 157.31, 150.20, 150.04, 139.83, 139.46, 139.42, 137.83, 137.25, 137.22, 137.14, 136.98, 136.91, 136.87, 136.53, 136.50, 136.46,

136.33, 134.95, 134.51, 132.32, 131.95, 131.30, 131.26, 130.90, 130.84, 130.79, 130.41, 130.35, 130.32, 130.13, 129.72, 129.60, 128.79, 128.15, 127.53, 127.40, 126.79, 126.72, 126.15, 126.09, 125.13, 124.73, 124.58, 123.71, 121.67, 121.01, 120.70, 119.07, 118.43, 118.06, 107.48, 107.42, 107.14, 106.83, 106.58, 70.08, 69.85, 69.80, 35.76, 35.38, 32.40, 31.81, 31.16, 30.22, 30.15, 26.62, 23.33, 14.48. FT-IR (ATR) $\tilde{\nu}$ (cm^{-1}) = 3069 (w), 3045 (w), 2951 (w), 2928 (w),2856 (w),1914 (w), 1780 (w), 1759 (w), 1742 (w), 1716 (w), 1612 (w), 1599 (w), 1580 (s), 1546 (w), 1514 (w), 1474 (w), 1455 (w), 1428 (w), 1409 (w), 1367 (m), 1313 (w), 1276 (m), 1259 (m), 1235 (w), 1188 (w), 1164 (w), 1105 (w), 1068 (w), 1026 (w), 1010 (w), 983 (w), 923 (w), 902 (w), 889 (w), 879 (w), 826 (w), 813 (m), 781 (w), 766 (s), 753 (s), 720 (s), 701 (w), 684 (w), 659 (m), 628 (w), 616 (w), 595 (w), 583 (w), 567 (w), 561 (w). UV/Vis ($CHCl_3$): λ_{max} (nm) (log ε) = 252 (5.13), 284 (4.81), 309 (4.83), 329 (4.87), 336 (4.86), 368 (4.46), 413 (4.20), 462 (4.41), 491 (4.71), 524 (4.82). Fluorescence ($CHCl_3$): λ_{em} (λ_{ex}) (nm) = 561, 598 (491). Φ = 13.4±0.1%. MALDI HRMS (DCTB) (*m*/*z*): $[M]^+$ calcd. for $C_{100}H_{100}O_4$, 1365.7655; found, 1365.7659. Elemental anal. calcd. for $C_{100}H_{100}O_4$: C 87.93, H 7.38, found: C 87.87, H 7.51.

6,6'-(9,21-di-*tert*-butyldibenzo[hi,st]benzo[6,7]indeno[1,2,3-*de*]benzo[6,7]indeno[1,2,3-*op*]pentacene-12,24-diyl)bis(2-(2-ethylhexyl)-1*H*-benzo[*de*]isoquinoline-1,3(2*H*)-dione) (190)

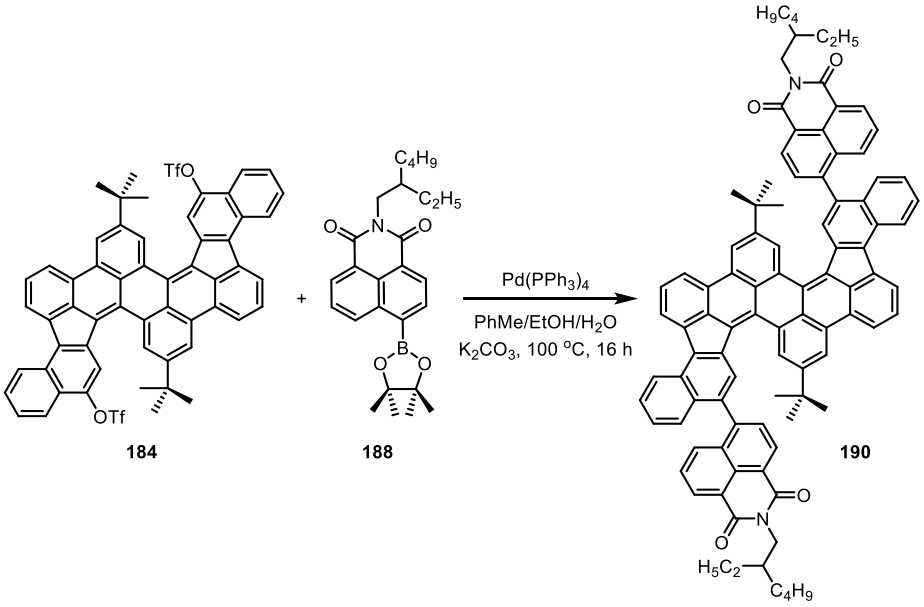

In a screw-capped vial, bistriflate **184** (61 mg, 0.06 mmol), 2-(2-ethylhexyl)-6-(4,4,5,5-tetramethyl-1,3,2-dioxaborolan-2-yl)-1*H*-benzo[*de*]isoquinoline-1,3(2*H*)-dione **188** (261 mg, 0.6 mmol) were suspended in 2M aq. K_2CO_3 (0.15 mL, 0.3 mmol) and argon-degassed toluene/ethanol (0.40 mL/0.15 mL) and $Pd(PPh_3)_4$ (7 mg, 6 µmol) was added under argon atmosphere. The mixture was stirred vigorously at 100 °C overnight. After cooling down to room temperature, the mixture was diluted with dichloromethane (50 mL), washed with water (2 × 40 mL) and dried over Na_2SO_4. After removal of the solvent by rotary evaporation, the crude product was purified by silica gel column chromatography (petroleum ether/dichloromethane/ethyl acetate 20:3:1 to 20:5:1). The product (mixture of atropisomers) was obtained after precipitation from dichloromethane/methanol and drying in vacuum as a red solid (54 mg, 68%).

m.p.: 252 °C (dec.). ^{1}H NMR (600 MHz, CD_2Cl_2) δ (ppm) = 9.15 - 8.87 (m, 1H), 8.80 - 8.45 (m, 11H), 8.44 - 8.25 (m, 3H), 8.25 - 8.05 (m, 1H), 8.03 - 7.94 (m, 1H), 7.94 - 7.86 (m, 3H), 7.80 - 7.56 (m, 4H), 7.56 - 7.45 (m, 1H), 7.44 - 6.83 (m, 5H), 4.18 - 4.02 (m, 4H), 2.03 - 1.89 (m, 2H), 1.43 - 1.31 (m, 16H), 1.28 (br, 5H), 1.13 (br, 4H), 1.00 - 0.91 (m, 12H), 0.79 - 0.71 (m, 9H). ^{13}C NMR (151 MHz, CD_2Cl_2) δ (ppm) = 165.01, 164.85, 164.80, 164.69, 164.65, 164.58, 164.39, 150.22, 150.08, 149.82, 149.78, 146.38, 146.25, 145.45, 145.18, 143.29, 137.48, 137.41, 137.34, 137.19, 137.14, 137.09, 136.59, 136.43, 136.40, 136.35, 136.32, 136.12, 136.03, 135.77, 135.57, 135.24, 134.80, 134.67, 133.98, 133.94, 133.41, 133.16, 132.75, 132.45, 132.24, 132.03, 131.92, 131.63, 131.53, 131.45, 131.34, 131.25, 131.14, 131.06, 130.97, 130.83, 130.75, 130.61, 130.29, 130.20, 130.16, 130.03, 129.74, 129.49, 129.47, 129.40, 129.33, 129.11, 128.96, 128.81, 128.56, 128.43, 127.98, 127.87, 127.82, 127.65, 127.51, 127.40, 127.25, 126.99, 126.94, 126.78, 126.66, 126.42, 125.41, 125.33, 124.48, 124.31, 124.21, 123.78, 123.72, 123.52, 123.42, 123.38, 123.12, 122.92, 122.69, 122.32, 122.21, 122.16, 120.88, 120.83, 85.14, 44.59, 44.52, 44.48, 38.52, 38.45, 38.39, 35.71, 35.56, 35.25, 35.20, 31.66, 31.44, 31.36, 31.31, 31.27, 31.00, 30.94, 29.34, 29.27, 25.29, 24.75, 24.72, 24.60, 23.66, 14.48, 14.41, 11.12, 11.01, 10.96. FT-IR (ATR) $\tilde{\nu}$ (cm^{-1}) = 3067 (w), 2956 (w), 2929 (w), 2862 (w), 1702 (m), 1661 (s), 1589 (m), 1511 (w), 1456 (w), 1414 (w), 1347 (m), 1232 (m), 1182 (w), 1143 (w), 1094 (w), 1067 (w), 1013 (w), 949 (w), 902 (w), 879 (w), 863 (w), 815 (w), 785 (m), 761 (s), 720 (m), 659 (w), 627 (w). MALDI HRMS (DCTB) (*m*/*z*): $[M]^+$ calcd. for $C_{96}H_{82}N_2O_4$, 1327.6307; found, 1327.6331. Elemental anal. calcd. for $C_{96}H_{82}N_2O_4 \cdot 0.5H_2O$: C 86.26, H 6.26, N 2.10, found: C 86.10, H 6.30, N 2.03.

12,28-di-*tert*-butyl-1,16,17,32-tetrakis(hexyloxy)dibenzo[*hi*,*st*]benzo[4,5]naphtho[1',8':6,7,8]-as-indaceno[3,2,1-*de*]benzo[4,5]naphtho[1',8':6,7,8]-as-indaceno[3,2,1-*op*]pentacene (191)

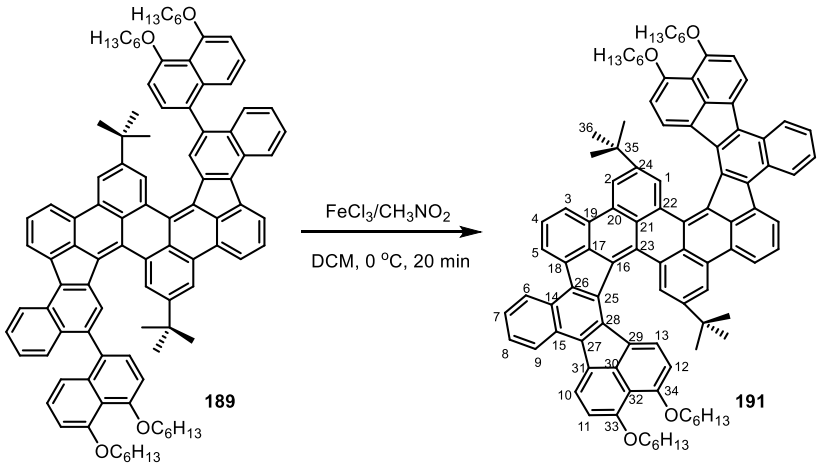

A Schlenk-flask charged with **189** (21 mg, 0.015mmol) was purged with argon. Dry dichloromethane (7.5 mL) was added to dissolve the substrate. A solution of $FeCl_3$ (25 mg, 0.15 mmol) in nitromethane (0.3 mL) was added dropwise to the mixture and stirred at room temperature for 20 minutes. Methanol (0.5 mL) was added. The mixture was diluted with dichloromethane (30 mL), washed with aq. NH_4Cl (20 mL) and water (20 mL) and dried over Na_2SO_4. After removal of the solvent by rotary evaporation, the crude product was purified by silica gel column chromatography (petroleum ether/chloroform/ethyl acetate 50:10:1). After washing

with 1 mL cold *n*-pentane and drying in vacuum, the product was obtained as a dark-red solid (19 mg, 93%).

m.p.: 345 °C (dec.). ^{1}H NMR (600 MHz, CD_2Cl_2) δ (ppm) = 9.14-9.05 (m, 2H, H-6), 9.02-8.95 (m, 2H, H-9), 8.70 (d, J = 7.5 Hz, 2H, H-3), 8.59-8.55 (m, 4H, H-2,5), 8.53 (d, J = 8.1 Hz, 2H, H-10), 8.01 (d, J = 1.8 Hz, 2H, H-1), 7.91 (t, J = 7.6 Hz, 2H, H-4), 7.76-7.69 (m, 4H, H-7,8), 7.24 (d, J = 8.1 Hz, 2H, H-13), 7.00 (d, J = 8.1 Hz, 2H, H-11), 5.96 (d, J = 8.2 Hz, 2H, H-12), 4.26-4.17 (m, 2H), 4.17-4.08 (m, 2H), 3.82-3.75 (m, 2H), 3.75-3.66 (m, 2H), 1.95-1.87 (m, 4H), 1.75-1.68 (m, 4H), 1.60-1.54 (m, 4H), 1.42-1.34 (m, 12H), 1.30-1.24 (m, 8H), 0.92 (t, J = 7.1 Hz, 6H), 0.86 (t, J = 7.0 Hz, 6H), 0.70 (s, 18H, H-36). ^{13}C NMR (151 MHz, CD_2Cl_2) δ (ppm) = 158.61 (C-33), 158.44 (C-34), 150.35 (C-24), 138.04 (C-18), 136.45 (C-26), 135.84 (C-30), 135.56 (C-17), 134.13 (C-27), 133.82 (C-25), 133.51 (C-16), 132.64 (C-22), 132.30 (C-23), 132.23 (C-28), 131.24 (C-15), 130.83 (C-14), 130.43 (C-1), 130.24 (C-20,21), 129.61 (C-31), 128.68 (C-13), 128.49 (C-4), 127.79 (C-29), 127.39 (C-19), 126.85 (C-8), 126.30 (C-7), 126.24 (C-10), 125.95 (C-6), 125.76 (C-9), 123.21 (C-3), 121.59 (C-5), 120.44 (C-2), 114.32 (C-32), 107.58 (C-11), 107.22 (C-12), 69.75, 69.63, 35.05, 32.30, 32.18, 30.68, 30.04, 29.62, 26.47, 26.31, 23.28, 23.22, 14.44, 14.41. FT-IR (ATR) $\tilde{\nu}$ (cm^{-1}) = 3104(w), 3068 (w), 2952 (w), 2927 (w), 2859 (w), 1595 (m), 1537 (w), 1500 (w), 1461 (w), 1437 (s), 1409 (w), 1388 (m), 1365 (w), 1329 (w), 1291 (w), 1270 (w), 1252 (m), 1233 (m), 1202 (w), 1178 (w), 1163 (w), 1110 (s), 1079 (w), 1049 (w), 1031 (w), 916 (w), 893 (w), 878 (w), 845 (w), 812 (m), 801 (m), 762 (m), 718 (m), 699 (m), 688 (w), 678 (w), 663 (w), 654 (w), 640 (w), 624 (w), 608 (w). UV/Vis ($CHCl_3$): λ_{max} (nm) (log ε) = 257 (5.24), 326 (4.67), 405 (4.70), 432 (4.65), 510 (4.58), 539 (4.64). Fluorescence ($CHCl_3$): λ_{em} (λ_{ex}) (nm) = 608, 646 (510). Φ = 24.7±1.0%. MALDI HRMS (DCTB) (*m*/*z*): $[M]^+$ calcd. for $C_{100}H_{96}O_4$, 1361.7342; found, 1361.7341. Elemental anal. calcd. for $C_{100}H_{96}O_4 \cdot 0.5H_2O$: C 87.62, H 7.13, found: C 87.60, H 6.99.

9,21-di-*tert*-butyl-12,24-bis(phenylethynyl)dibenzo[*hi*,*st*]benzo[6,7]indeno[1,2,3-*de*]benzo[6,7]indeno[1,2,3-*op*]pentacene (196)

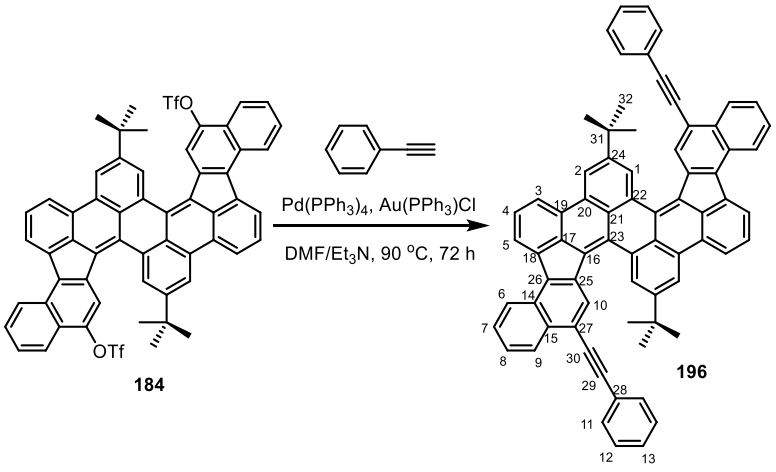

In a screw-capped vial, bistriflate **184** (101 mg, 0.1 mmol) and phenylacetylene (0.55 mL, 5 mmol) were suspended in argon-degassed DMF/Et_3N (0.6 mL/0.3 mL) and a mixture of $Pd(PPh_3)_4$ (29 mg, 0.025 mmol) and $Au(PPh_3)Cl$ (12 mg, 0.025 mmol) was added under argon atmosphere. The reaction mixture was stirred vigorously at 90 °C for 72 hours. After cooling down to room

temperature, the mixture was diluted with dichloromethane (100 mL), washed with aq. NH_4Cl (50 mL) and brine (2 × 50 mL) and dried over Na_2SO_4. After removal of the solvent by rotary evaporation, the crude product was purified by silica gel column chromatography (petroleum ether/chloroform/ethyl acetate 30:3:1 to pure chloroform) to give after precipitation from chloroform/methanol and drying in vacuum **196** as a dark-red solid (68 mg, 75%).

m.p.: 382 °C (dec.). ^{1}H NMR (400 MHz, $Cl_2CDCDCl_2$) δ (ppm) = 8.89 (d, J = 8.5 Hz, 2H, H-6), 8.86 (d, J = 1.7 Hz, 2H, H-1), 8.84 (d, J = 1.6 Hz, 2H, H-2), 8.81 (s, 2H, H-10), 8.63 (d, J = 5.6 Hz, 2H, H-3), 8.61 (d, J = 4.8 Hz, 2H, H-5), 8.54 (d, J = 8.2 Hz, 2H, H-9), 7.91 (t, J = 7.7 Hz, 2H, H-4), 7.77-7.71 (m, 2H, H-7), 7.66 (t, J = 7.5 Hz, 2H, H-8), 7.61-7.58 (m, 4H, H-11), 7.41-7.35 (m, 6H, H-12,13), 1.60 (s, 18H, H-32). ^{13}C NMR (101 MHz, $Cl_2CDCDCl_2$) δ (ppm) = 149.88 (C-24), 136.63 (C-19), 136.52 (C-26), 135.95 (C-25), 134.25 (C-17), 133.77 (C-15), 131.43 (C-11), 131.36 (C-21), 131.11 (C-16), 130.53 (C-23), 130.32 (C-20), 130.12 (C-14), 129.65 (C-22), 129.55 (C-1), 128.49 (C-4), 128.37 (C-12), 128.30 (C-13), 127.58 (C-7), 127.38 (C-9), 126.77 (C-18), 126.55 (C-8), 126.51 (C-10), 124.77 (C-6), 123.57 (C-5), 123.18 (C-28), 121.67 (C-3), 120.30 (C-2), 119.85 (C-27), 95.07 (C-29), 88.18 (C-30), 35.34 (C-31), 31.36 (C-32). FT-IR (ATR) $\tilde{\nu}$ (cm^{-1}) = 3061 (w), 3030 (w), 2957 (w), 2905 (w), 2867 (w), 2203 (w), 1940 (w), 1597 (w), 1579 (w), 1544 (w), 1505 (w), 1491 (w), 1477 (w), 1454 (w), 1443 (w), 1413 (w), 1385 (w), 1362 (w), 1311 (w), 1292 (w), 1276 (w), 1239 (w), 1221 (w), 1182 (w), 1154 (w), 1138 (w), 1070 (w), 1023 (w), 1007 (w), 947 (w), 924 (w), 912 (w), 900 (w), 875 (w), 845 (w), 826 (w), 813 (m), 806 (w), 785 (w), 776 (w), 752 (s), 715 (m), 691 (m), 675 (w), 659 (m), 631 (w), 622 (w), 603 (w), 593 (w), 559 (w). UV/Vis ($CHCl_3$): λ_{max} (nm) (log ε) = 256 (4.98), 288 (4.70), 313 (4.57), 342 (4.70), 356 (4.71), 466 (4.29), 494 (4.56), 528 (4.68). Fluorescence ($CHCl_3$): λ_{em} (λ_{ex}) (nm) = 557, 589 (494). Φ = 3.3±0.1%. MALDI HRMS (DCTB) (m/z): $[M]^+$ calcd. for $C_{72}H_{84}$, 912.3756; found, 912.3759. Elemental anal. calcd. for $C_{72}H_{48}\cdot 0.8H_2O$: C 93.23, H 5.39, found: C 93.29, H 5.62.

9,21-di-*tert*-butyl-12,24-bis(4',5',6'-triphenyl-[1,1':2',1''-terphenyl]-3'-yl)dibenzo[*hi*,*st*]benzo[6,7]indeno[1,2,3-*de*]benzo[6,7]indeno[1,2,3-*op*]pentacene (197)

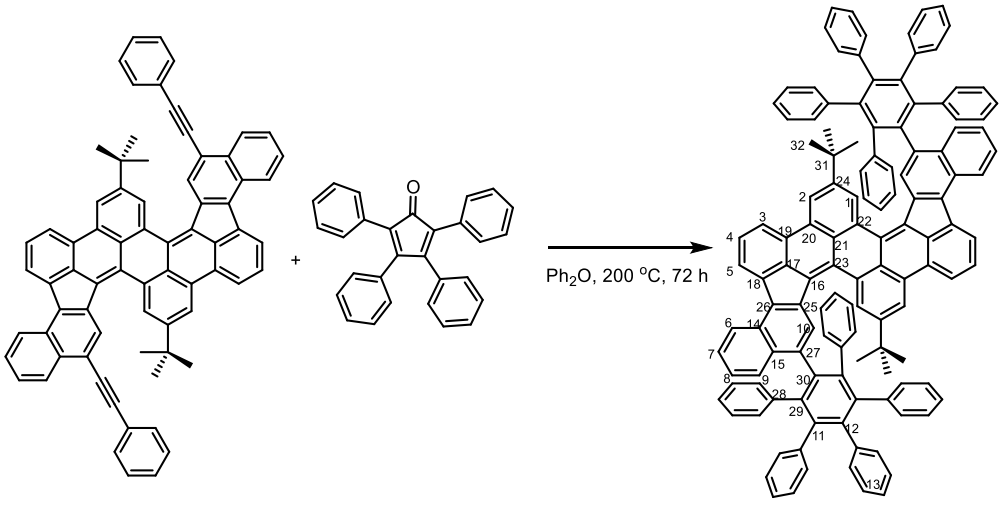

196 197

In a screw-capped vial, compound **196** (27 mg, 0.03 mmol) and tetraphenylcyclopentadienone (115 mg, 0.3 mmol) were suspended in argon-degassed diphenylether (0.8 mL). The mixture was stirred

at 200 °C for 72 h. After cooling down to room temperature, the mixture was suspended in methanol (20 mL) and then filtered off. The solid was purified by silica gel column chromatography (petroleum ether/chloroform/ethyl acetate 20:2:1 to pure chloroform), precipitation from chloroform/methanol and drying in vacuum **197** as a red solid (32 mg, 66%).

m.p.: >400 °C (dec.). ^{1}H NMR (600 MHz, $Cl_2CDCDCl_2$) δ (ppm) = 8.79 (s, 2H, H-2), 8.78 (s, 2H, H-1), 8.55 (d, J = 8.4 Hz, 2H, H-3), 8.47 (d, J = 8.7 Hz, 2H, H-6), 8.42 (d, J = 7.5 Hz, 2H, H-5), 8.24 (s, 2H, H-10), 7.86-7.77 (m, 4H, H-9,4), 7.30 (t, J = 7.6 Hz, 2H, H-7), 7.12-7.08 (m, 2H, H-8), 7.00 (br, 2H), 6.95 (d, J = 7.1 Hz, 2H), 6.92-6.86 (m, 10H), 6.86-6.81 (m, 8H), 6.79 (d, J = 6.9 Hz, 2H), 6.76-6.71 (m, 6H), 6.69 (d, J = 6.6 Hz, 2H), 6.67-6.60 (m, 10H), 6.56 (d, J = 7.2 Hz, 2H), 6.29 (t, J = 7.0 Hz, 2H), 6.06 (t, J = 7.1 Hz, 2H), 5.61 (t, J = 7.2 Hz, 2H), 1.58 (s, 18H). ^{13}C NMR (151 MHz, $Cl_2CDCDCl_2$) δ (ppm) = 148.49, 141.39, 140.67, 140.60, 140.55, 140.09, 140.07, 139.90, 138.36, 137.68, 137.35, 135.04, 134.33, 134.19, 132.88, 132.78, 132.76, 131.89, 131.27, 131.14, 131.08, 130.85, 130.42, 129.84, 129.37, 128.89, 128.45 (C-4), 127.94 (C-9), 127.88 (C-1), 127.01 (C-10), 126.61, 126.53, 126.44, 126.42, 126.37, 126.24, 125.89 (C-7), 125.81, 124.84, 124.78, 124.73, 124.44, 124.30 (C-8), 123.59 (C-6), 122.77 (C-5), 120.76 (C-3), 119.92 (C-2), 99.32, 35.03 (C-31), 31.38 (C-32). FT-IR (ATR) $\tilde{\nu}$ (cm^{-1}) = 3082 (w), 3057 (w), 3026 (w), 2960 (w), 2905 (w), 2867 (w), 1944 (w), 1599 (w), 1579 (w), 1547 (w), 1496 (w), 1477 (w), 1456 (w), 1442 (w), 1414 (w), 1395 (w), 1374 (w), 1361 (w), 1328 (w), 1312 (w), 1277 (w), 1240 (w), 1219 (w), 1203 (w), 1180 (w), 1154 (w), 1139 (w), 1072 (w), 1027 (w), 1013 (w), 1002 (w), 907 (w), 900 (w), 877 (w), 840 (w), 827 (w), 815 (w), 798 (w), 765 (m), 756 (m), 738 (w), 722 (m), 715 (w), 696 (s), 660 (w), 645 (w), 630 (w), 619 (w), 590 (w), 559 (w). UV/Vis ($CHCl_3$): λ_{max} (nm) (log ε) = 308 (4.53), 332 (4.57), 343 (4.56), 373 (4.28), 412 (4.03), 459 (4.20), 487 (4.49), 520 (4.59). Fluorescence ($CHCl_3$): λ_{em} (λ_{ex}) (nm) = 557, 587 (487). Φ = 3.6±0.5%. MALDI HRMS (DCTB) (m/z): $[M]^+$ calcd. for $C_{128}H_{88}$, 1625.6919; found, 1625.6903. Elemental anal. calcd. for $C_{128}H_{88}\cdot 0.5H_2O$: C 94.02, H 5.49, found: C 94.00, H 5.67.

2,10-Di-*tert*-butyl-8,16-di(naphthalen-1-yl)dibenzo[*fg*,*qr*]pentacene (198)

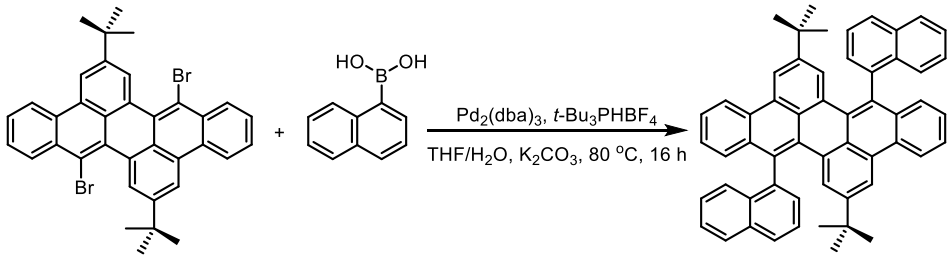

133 198

In a screw-capped vial a mixture of $Pd_2(dba)_3$ (68 mg, 0.075 mmol) and t-Bu_3PHBF_4 (68 mg, 0.237 mmol) was added to a suspension of dibromide **133** (468 mg, 0.75 mmol), naphthalen-1-ylboronic acid (1.03 g, 6.0 mmol) and K_2CO_3 (332 mg, 2.4 mmol) in argon-degassed THF/water (4.5 mL/1.2 mL). The mixture was stirred vigorously at 80 °C overnight under argon atmosphere. After cooling to room temperature, the mixture was diluted with dichloromethane (100 mL), washed with water (3 × 50 mL) and the organic layer dried over Na_2SO_4. After removal of the solvent by rotary evaporation, the crude product was purified by silica gel column chromatography (petroleum

ether/dichloromethane 10:1) to give after precipitation from dichloromethane/methanol and drying in vacuum the product **198** (mixture of atropisomers) as a yellow solid (362 mg, 67 %).

m.p.: 360 °C (dec.). ^{1}H NMR (600 MHz, $Cl_2CDCDCl_2$) δ (ppm) = 8.67 (d, J = 8.3 Hz, 1H), 8.63 (d, J = 8.3 Hz, 1H), 8.45 (d, J = 1.3 Hz, 1H), 8.40 (d, J = 1.3 Hz, 1H), 8.04 (d, J = 8.3 Hz, 1H), 7.97 (d, J = 8.2 Hz, 1H), 7.95 (d, J = 8.3 Hz, 2H), 7.74 (d, J = 1.6 Hz, 1H), 7.65 (d, J = 7.0 Hz, 1H), 7.62 (d, J = 7.1 Hz, 1H), 7.58 (d, J = 7.6 Hz, 2H), 7.57 - 7.52 (m, 3H), 7.48 (d, J = 1.6 Hz, 1H), 7.47 - 7.43 (m, 1H), 7.42 (d, J = 8.0 Hz, 1H), 7.41 - 7.38 (m, 1H), 7.29 (dd, J = 7.4, 6.9 Hz, 1H), 7.28 - 7.25 (m, 1H), 7.24 - 7.17 (m, 3H), 7.10 (d, J = 8.3 Hz, 1H), 0.77 (s, 10H), 0.68 (s, 8H). ^{13}C NMR (151 MHz, $Cl_2CDCDCl_2$) δ (ppm) = 148.60, 148.50, 139.60, 139.53, 134.51, 134.19, 133.94, 133.66, 133.15, 133.04, 132.73, 132.29, 130.88, 130.74, 129.80, 129.50, 129.32, 129.02, 128.96, 128.85, 128.80, 128.73, 128.36, 128.30, 128.05, 127.96, 127.92, 127.83, 127.43, 127.33, 127.19, 126.96, 126.93, 126.83, 126.70, 126.59, 126.44, 126.32, 126.30, 126.05, 125.94, 122.12, 122.09, 117.12, 117.03, 34.28, 34.23, 30.61, 30.49. FT-IR (ATR) $\tilde{\nu}$ (cm^{-1}) = 3061 (w), 3008 (w), 2960 (m), 2904 (w), 2866 (w), 1937 (w), 1823 (w), 1798 (w), 1703 (w), 1607 (w), 1573 (w), 1506 (w), 1475 (w), 1462 (w), 1446 (w), 1422 (w), 1395 (w), 1363 (m), 1318 (w), 1296 (w), 1273 (w), 1233 (w), 1215 (w), 1153 (w), 1123 (w), 1066 (w), 1038 (w), 1018 (w), 985 (w), 970 (w), 952 (w), 927 (w), 895 (m), 874 (m), 798 (w), 776 (s), 757 (s), 713 (s), 700 (w), 672 (w), 648 (m), 636 (m), 609 (w). UV/Vis ($CHCl_3$): λ_{max} (nm) (log ε) = 288 (4.57), 301 (4.64), 308 (4.66), 385 (4.22), 407 (4.46), 429 (4.47). Fluorescence ($CHCl_3$): λ_{em} (λ_{ex}) (nm) = 466 (407). Φ = 57.4±1.5%. MALDI HRMS (DCTB) (m/z): $[M]^+$ calcd. for $C_{56}H_{44}$, 716.3443; found, 716.3432. Elemental anal. calcd. for $C_{56}H_{44}$: C 93.81, H 6.19, found: C 93.81, H 6.26.

11,23-di-*tert*-butyl-5,17-dichlorodibenzo[*hi*,*st*]benzo[4,5]indeno[1,2,3-*de*]benzo[4,5]indeno[1,2,3-*op*]pentacene (202)

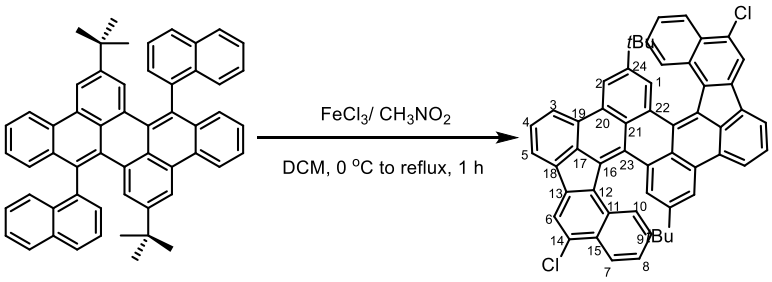

198 202

In a 250 mL Schlenk flask, a solution of **198** (115 mg, 0.16 mmol) in dry DCM (150 mL) was purged with argon for 15 min. A solution of $FeCl_3$ (519 mg, 3.2 mmol) in nitromethane (1.2 mL) was then added dropwise at 0 °C. The mixture was stirred at 0 °C for 5 minutes while continuing to bubble argon gas through the mixture. The mixture was then heated up to reflux for 1 hour. The reaction was quenched by adding methanol (5 mL). The mixture was washed with water (3 × 50 mL) and dried over Na_2SO_4. After removal of the solvent by rotary evaporation, the residue was refluxed in 10 mL *n*-heptane for 10 minutes. After cooling down to room temperature, the suspension was filtered off and the solid was washed with *n*-hexane (2 × 5 mL). The product **202** was obtained as a dark-purple solid (118 mg, 94 %) after drying in vacuum.

m.p.: >400 °C. ^{1}H NMR (600 MHz, $Cl_2CDCDCl_2$, 298 K) δ (ppm) = 8.60 (s, 2H, H-2), 8.53 (d, J = 8.1 Hz, 2H, H-3), 8.29 (d, J = 8.4 Hz, 2H, H-7), 8.22 (s, 2H, H-6), 8.06 (s, 2H, H-1), 8.06 (d, J = 4.3 Hz, 2H, H-5), 7.80 (dd, J = 12.4, 4.9 Hz, 4H, H-4, 10), 7.43 - 7.37 (m, 2H, H-8), 7.07 - 7.00 (m, 2H, H-9), 0.95 (s, 18H). ^{13}C NMR (151 MHz, $Cl_2CDCDCl_2$, 343 K) δ (ppm) = 149.54 (C-24), 140.34 (C-13), 135.78 (C-19), 134.63 (C-17), 133.76 (C-12), 133.07 (C-11), 132.36 (C-23), 131.66 (C-16), 131.20 (C-22), 131.15 (C-1), 130.54 (C-15), 130.17 (C-20), 129.72 (C-21), 129.49 (C-14), 128.38 (C-10), 127.88 (C-4), 126.91 (C-9), 126.70 (C-18), 126.01 (C-8), 125.52 (C-7), 122.26 (C-3), 120.27 (C-6), 120.09 (C-2), 120.04 (C-5), 34.72, 30.48. FT-IR (ATR) $\tilde{\nu}$ (cm^{-1}) = 3070 (w), 2961 (m), 2903 (w), 2867 (w), 1896 (w), 1779 (w), 1601 (w), 1575 (m), 1548 (w), 1514 (w), 1478 (w), 1460 (w), 1441 (w), 1414 (w), 1390 (m), 1360 (w), 1342 (w), 1305 (w), 1265 (w), 1244 (w), 1223 (w), 1198 (w), 1178 (w), 1146 (w), 1110 (w), 1030 (w), 949 (w), 933 (m), 878 (w), 867 (m), 823 (w), 810 (w), 784 (w), 757 (m), 742 (s), 707 (m), 675 (w), 658 (w), 638 (w), 620 (w). UV/Vis ($CHCl_3$): λ_{max} (nm) (log ε) = 270 (4.80), 308 (4.68), 324 (4.68), 423 (4.14), 509 (4.50), 542 (4.61). Fluorescence ($CHCl_3$): λ_{em} (λ_{ex}) (nm) = 570, 614 (509). Φ = 15.8±1.0%. MALDI HRMS (DCTB) (m/z): $[M]^+$ calcd. for $C_{56}H_{38}Cl_2$, 780.2350; found, 780.2351. Elemental anal. calcd. for $C_{56}H_{38}Cl_2 \cdot 0.5CHCl_3$: C 80.64, H 4.61, found: C 80.61, H 4.89.

Scholl cyclization of PAH 198 using DDQ/TfOH

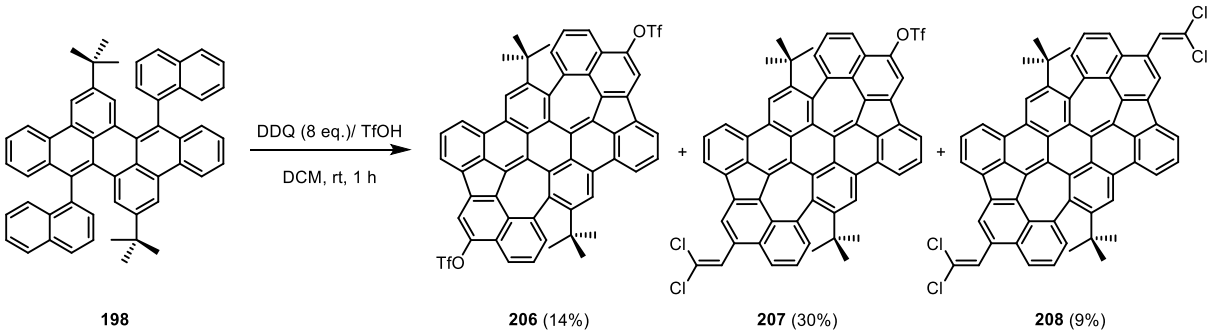

198 **206** (14%) **207** (30%) **208** (9%)

In a 100 mL Schlenk flask, a solution of PAH **198** (72 mg, 0.1 mmol) in dry DCM (60 mL) was purged with argon for 15 min. DDQ (182 mg, 0.8 mmol) was added in one portion at room temperature. First portion (1 mL) of TfOH was then added dropwise. After stirring at room temperature for 5 minutes, another portion (2 mL) of TfOH was added dropwise. The mixture was stirred at room temperature for 1 hour. The reaction was quenched by pouring into saturated aq. $NaHCO_3$ (100 mL). After stirring vigorously for 15 minutes, the mixture was extracted with dichloromethane (3 × 50 mL) and the organic layers combined. The organic phase was washed with aq. NH_4Cl (100 mL), water (100 mL) and dried over anhydrous Na_2SO_4. After removal of the solvent by rotary evaporation, the crude product mixture was separated by silica gel column chromatography (petroleum ether/chloroform/ethyl acetate 30:1:1 to 30:2:1). The three fractions were obtained after precipitation from dichloromethane/methanol and drying in vacuum, respectively, as dark-blue solid, with yields of product **206** (14 mg, 14%, third fraction, R_f = 0.25), product **207** (29 mg, 30%, second fraction, R_f = 0.30) and product **208** (8 mg, 9%, first fraction, R_f = 0.35).

Azulene-PAH 206

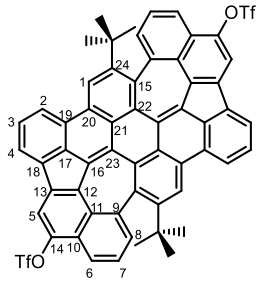

m.p.: > 400 °C. ^{1}H NMR (600 MHz, $CDCl_3$) δ (ppm) = 8.90 (s, 2H, H-1), 8.45 (d, J = 8.0 Hz, 2H, H-2), 8.12 (d, J = 7.0 Hz, 2H, H-4), 8.09 (d, J = 9.2 Hz, 4H, H-6,5), 7.87 - 7.83 (m, 2H, H-3), 7.45 - 7.40 (m, 2H, H-7), 7.05 (d, J = 7.0 Hz, 2H, H-8), 0.97 (s, 18H). ^{13}C NMR (151 MHz, $CDCl_3$) δ (ppm) = 153.91 (C-24), 143.81 (C-14), 135.72 (C-9), 135.06 (C-15), 135.04 (C-8), 134.94 (C-19), 134.70 (C-11), 134.09 (C-12), 133.71 (C-13), 133.21 (C-20), 131.49 (C-17), 130.65 (C-16), 130.34 (C-22), 129.80 (C-21), 128.08 (C-3), 126.16 (C-18), 125.66 (C-1), 125.48 (C-23), 125.00 (C-7), 124.71 (C-10), 120.81 (C-2), 120.75 (C-4), 120.45 (C-6), 118.89 (q, $J_{C\text{-}F}$ = 320.6 Hz, -CF_3), 113.25 (C-5), 38.90, 33.47. FT-IR (ATR) $\tilde{\nu}$ (cm^{-1}) = 3066 (w), 2963 (m), 2936 (w), 2911 (w), 2871 (w), 1928 (w), 1791 (w), 1744 (w), 1617 (w), 1585 (m), 1554 (w), 1478 (w), 1467 (w), 1424 (s), 1365 (w), 1347 (m), 1300 (w), 1244 (m), 1209 (s), 1136 (s), 1076 (w), 1057 (w), 1036 (w), 1001 (s), 973 (w), 947 (w), 927 (w), 892 (m), 862 (m), 840 (s), 821 (m), 806 (s), 780 (w), 757 (w), 714 (m), 690 (w), 670 (w), 658 (w), 636 (w), 608 (w). UV/Vis ($CHCl_3$): λ_{max} (nm) (log ε) = 280 (4.91), 329 (4.82), 377 (4.54), 397 (4.52), 424 (4.37), 460 (4.06), 500 (4.08), 546 (4.24), 582 (4.48), 628 (4.55). Fluorescence ($CHCl_3$): λ_{em} (λ_{ex}) (nm) = 648 (280). Φ = 19.8±1.0%. MALDI HRMS (DCTB) (*m*/*z*): $[M]^+$ calcd. for $C_{58}H_{34}F_6O_6S_2$, 1004.1701; found, 1004.1704. Elemental anal. calcd. for $C_{58}H_{34}F_6O_6S_2 \cdot 0.5H_2O$: C 68.70, H 3.48, found: C 68.68, H 3.52.

Azulene-PAH 207

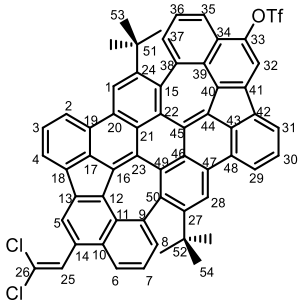

m.p.: > 400 °C. ^{1}H NMR (600 MHz, CD_2Cl_2) δ (ppm) = 8.78 (s, 1H, H-28), 8.77 (s, 1H, H-1), 8.33 (d, J = 8.0 Hz, 1H, H-29), 8.27 (d, J = 7.8 Hz, 2H, H-5,2), 8.02 (d, J = 7.0 Hz, 1H, H-31), 8.01 (s, 1H, H-32), 7.98 - 7.95 (m, 2H, H-35,4), 7.80 (d, J = 8.1 Hz, 1H, H-6), 7.77 (t, J = 7.4 Hz, 1H, H-30), 7.73 (t, J = 7.4 Hz, 1H, H-3), 7.38 (s, 1H, H-25), 7.30 (t, J = 7.7 Hz, 1H, H-36), 7.21 (t, J = 7.6 Hz, 1H, H-7), 7.00 (d, J = 7.1 Hz, 1H, H-37), 6.82 (d, J = 7.0 Hz, 1H, H-8), 0.89 (s, 9H, H-54), 0.88 (s, 9H, H-53). ^{13}C NMR (151 MHz, CD_2Cl_2) δ (ppm) = 154.43 (C-24), 154.15 (C-27), 144.30 (C-33), 136.73 (C-9), 136.51 (C-50), 136.33 (C-39), 136.17 (C-15), 135.71 (C-37), 135.62 (C-12), 135.42 (C-38), 135.29 (C-48), 135.11 (C-8), 135.07 (C-11), 135.03 (C-13), 134.67 (C-19), 134.62

(C-46), 134.04 (C-41), 133.99 (C-40), 133.62 (C-20), 132.37 (C-17), 131.95 (C-45), 131.86 (C-43), 131.10 (C-49), 130.64 (C-22), 130.40 (C-10), 130.24 (C-44), 130.20 (C-16), 130.18 (C-47), 128.51 (C-3), 128.43 (C-30), 128.31 (C-14), 128.06 (C-25), 126.72 (C-42), 126.50 (C-18), 126.41 (C-1), 126.14 (C-28), 126.01 (C-23), 125.83 (C-21), 125.61 (C-36), 125.20 (C-34), 124.73 (C-7), 124.02 (C-6), 123.74 (C-26), 122.22 (C-5), 121.35 (C-29), 121.12 (C-31), 120.91 (C-35), 120.88 (C-2), 120.76 (C-4), 119.48 (q, $J_{C\text{-}F}$ = 320.5 Hz, -CF_3), 113.76 (C-32), 39.38 (C-51), 39.36 (C-52), 33.80 (C-54), 33.76 (C-53). FT-IR (ATR) $\tilde{\nu}$ (cm^{-1}) = 3064 (w), 2962 (w), 2932 (w), 2908 (w), 2869 (w), 1924 (w), 1789 (w), 1584 (m), 1552 (w), 1477 (w), 1467 (w), 1425 (m), 1364 (w), 1349 (w), 1299 (w), 1244 (m), 1209 (s), 1138 (m), 1094 (w), 1067 (w), 1008 (m), 987 (w), 972 (w), 949 (w), 930 (w), 912 (m), 876 (m), 834 (m), 808 (m), 779 (w), 755 (s), 732 (w), 713 (w), 694 (w), 677 (w), 653 (w), 636 (w). UV/Vis ($CHCl_3$): λ_{max} (nm) (log ε) = 280 (4.82), 331 (4.71), 383 (4.42), 404 (4.41), 427 (4.27), 468 (3.90), 506 (3.96), 552 (4.14), 590 (4.38), 636 (4.44). Fluorescence ($CHCl_3$): λ_{em} (λ_{ex}) (nm) = 662 (280). Φ = 26.5±1.0%. MALDI HRMS (DCTB) (*m*/*z*): $[M]^+$ calcd. for $C_{59}H_{35}Cl_2F_3O_3S$, 950.1636; found, 950.1633. Elemental anal. calcd. for $C_{59}H_{35}Cl_2F_3O_3S$: C 74.45, H 3.71, found: C 74.61, H 4.14.

Azulene-PAH 208

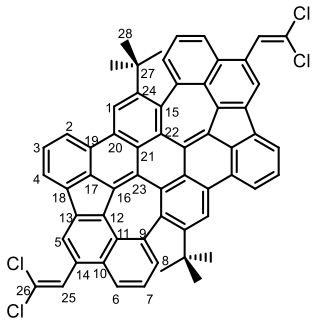

m.p.: > 400 °C. ^{1}H NMR (600 MHz, $CDCl_3$) δ (ppm) = 8.95 (s, 2H, H-1), 8.48 (d, *J* = 8.0 Hz, 2H, H-2), 8.39 (s, 2H, H-5), 8.15 (d, *J* = 7.0 Hz, 2H, H-4), 7.96 (d, *J* = 8.1 Hz, 2H, H-6), 7.84 (t, *J* = 7.5 Hz, 2H, H-3), 7.49 (s, 2H, H-25), 7.39 (t, *J* = 7.7 Hz, 2H, H-7), 7.07 (d, *J* = 7.1 Hz, 2H, H-8), 1.06 (s, 18H, H-28). ^{13}C NMR (151 MHz, $CDCl_3$) δ (ppm) = 153.52 (C-24), 136.45 (C-9), 135.95 (C-19,15), 135.15 (C-12), 134.92 (C-11), 134.40 (C-8), 134.15 (C-13), 133.59 (C-20), 131.83 (C-17), 130.29 (C-22), 129.96 (C-10), 129.68 (C-16), 127.96 (C-3), 127.73 (C-14), 127.41 (C-25,23), 126.33 (C-18), 125.68 (C-21), 125.49 (C-1), 124.01 (C-7), 123.68 (C-6), 123.49 (C-26), 121.84 (C-5), 120.33 (C-2,4), 38.87 (C-27), 33.67 (C-28). FT-IR (ATR) $\tilde{\nu}$ (cm^{-1}) = 3064 (w), 3011 (w), 2962 (w), 2929 (w), 2908 (w), 2869 (w), 1927 (w), 1735 (w), 1622 (w), 1586 (m), 1548 (w), 1478 (w), 1428 (m), 1399 (w), 1383 (w), 1364 (w), 1352 (w), 1334 (w), 1297 (w), 1281 (w), 1245 (w), 1223 (w), 1178 (w), 1151 (w), 1134 (w), 1080 (w), 1065 (w), 1013 (w), 971 (w), 919 (m), 906 (m), 893 (w), 879 (m), 857 (w), 844 (w), 809 (m), 798 (w), 776 (w), 755 (s), 734 (m), 712 (m), 695 (m), 669 (w), 650 (w), 624 (w). UV/Vis ($CHCl_3$): λ_{max} (nm) (log ε) = 282 (4.97), 332 (4.84), 386 (4.57), 409 (4.55), 431 (4.41), 472 (4.04), 511 (4.11), 557 (4.28), 597 (4.52), 644 (4.58). Fluorescence ($CHCl_3$): λ_{em} (λ_{ex}) (nm) = 671 (282). Φ = 23.6±1.0%. MALDI HRMS (DCTB) (*m*/*z*): $[M]^+$ calcd. for

$C_{60}H_{36}Cl_4$, 898.1548; found, 898.1580. Elemental anal. calcd. for $C_{60}H_{36}Cl_4 \cdot 0.5H_2O$: C 79.39, H 4.11, found: C 79.08, H 4.32.

Azulene-PAH 210

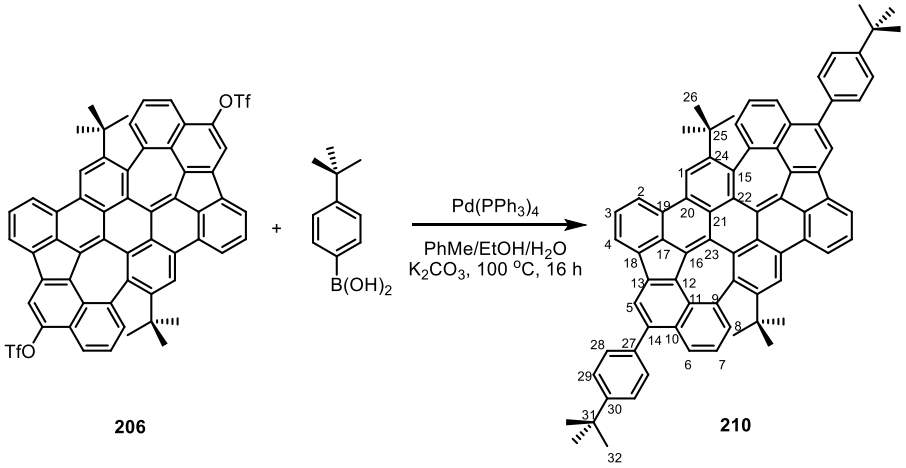

206 **210**

In a screw-capped vial, $Pd(PPh_3)_4$ (3.5 mg, 3 µmol) was added to a suspension of azulene bistriflate **206** (30 mg, 0.03 mmol), (4-(*tert*-butyl)phenyl)boronic acid (22 mg, 0.12 mmol) and 2M aq. K_2CO_3 (0.07 mL, 0.14 mmol) in argon-degassed toluene/ethanol (0.22 mL/0.07 mL). The mixture was stirred vigorously at 100 °C overnight under argon atmosphere. After cooling down to room temperature, the mixture was diluted with dichloromethane (20 mL), washed with water (2 × 20 mL) and dried over Na_2SO_4. After removal of the solvent by rotary evaporation, the crude product was purified by silica gel column chromatography (petroleum ether/ethyl acetate 30:1). After precipitation from dichloromethane/methanol and drying in vacuum azulene PAH **210** was obtained as a dark-green to dark-blue solid (23 mg, 79%).

m.p.: >400 °C. ^{1}H NMR (600 MHz, CD_2Cl_2) δ (ppm) = 8.97 (s, 2H, H-1), 8.48 (d, J = 8.1 Hz, 2H, H-2), 8.13 (s, 2H, H-5), 8.12 (d, J = 7.0 Hz, 2H, H-4), 8.02 (d, J = 8.2 Hz, 2H, H-6), 7.82 (t, J = 7.5 Hz, 2H, H-3), 7.65 - 7.60 (m, 8H, H-28,29), 7.24 (dd, J = 8.1, 7.2 Hz, 2H, H-7), 6.95 (d, J = 7.0 Hz, 2H, H-8), 1.46 (s, 18H, H-32), 1.09 (s, 18H, H-26). ^{13}C NMR (151 MHz, CD_2Cl_2) δ (ppm) = 154.04 (C-24), 151.20 (C-30), 138.67 (C-27), 138.36 (C-14), 136.96 (C-9), 136.89 (C-15), 136.84 (C-19), 136.32 (C-11), 135.19 (C-13), 134.95 (C-8), 134.66 (C-12), 134.38 (C-20), 132.52 (C-16), 132.43 (C-17), 131.16 (C-10), 130.52 (C-22), 130.32 (C-28), 130.06 (C-23), 128.45 (C-3), 126.90 (C-18), 126.46 (C-6), 126.33 (C-21), 126.26 (C-1), 126.02 (C-29), 124.26 (C-7), 122.20 (C-5), 120.82 (C-2), 120.78 (C-4), 39.35 (C-25), 35.16 (C-31), 33.97 (C-26), 31.77 (C-32). FT-IR (ATR) $\tilde{\nu}$ (cm^{-1}) = 3062 (w), 2957 (w), 2931 (w), 2902 (w), 2865 (w), 1912 (w), 1623 (w), 1586 (w), 1550 (w), 1511 (w), 1473 (w), 1462 (w), 1428 (m), 1386 (w), 1361 (w), 1299 (w), 1267 (w), 1244 (w), 1223 (w), 1200 (w), 1176 (w), 1149 (w), 1133 (w), 1117 (w), 1062 (w), 1019 (w), 954 (w), 933 (w), 909 (w), 887 (w), 836 (m), 809 (m), 777 (w), 755 (s), 732 (w), 713 (m), 698 (w), 671 (w), 652 (w), 644 (w), 629 (w), 608 (w). UV/Vis ($CHCl_3$): λ_{max} (nm) (log ε) = 281 (4.98), 332 (4.87), 380 (4.54), 409 (4.55), 432 (4.35), 470 (4.05), 506 (4.14), 557 (4.27), 594 (4.50), 641 (4.55). Fluorescence ($CHCl_3$): λ_{em} (λ_{ex}) (nm) = 667 (594). Φ = 28.4±1.0%. MALDI HRMS (DCTB) (m/z): $[M]^+$ calcd. for $C_{76}H_{60}$,

972.4695; found, 972.4723. Elemental anal. calcd. for $C_{76}H_{60}$: C 93.79, H 6.21, found: C 93.53, H 6.48.

Azulene-PAH 211

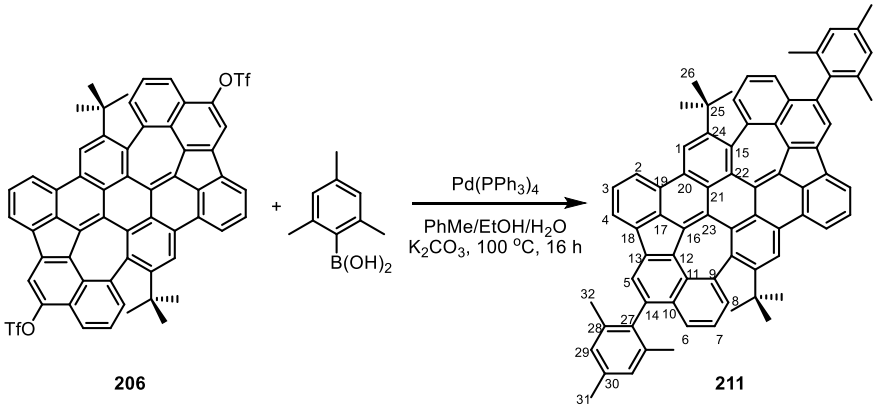

206 **211**

In a screw-capped vial, $Pd(PPh_3)_4$ (3.5 mg, 3 µmol) was added to a suspension of azulene bistriflate **206** (30 mg, 0.03 mmol), 2,4,6-trimethylphenylboronic acid (49 mg, 0.3 mmol) and 2M aq. K_2CO_3 (0.07 mL, 0.14 mmol) in argon-degassed toluene/ethanol (0.22 mL/0.07 mL). The mixture was stirred vigorously at 100 °C overnight under argon atmosphere. After cooling down to room temperature, the mixture was diluted with dichloromethane (20 mL), washed with water (2 × 20 mL) and the combined organic layer dried over Na_2SO_4. After removal of the solvent by rotary evaporation, the crude product was purified by silica gel column chromatography (petroleum ether/dichloromethane/ethyl acetate 15:1:0 to 40:2:1), to give azulene PAH **211** after precipitation from dichloromethane/methanol and drying in vacuum as a dark-blue solid (26 mg, 93%).

m.p.: >400 °C. ^{1}H NMR (600 MHz, CD_2Cl_2) δ (ppm) = 9.03 (s, 2H, H-1), 8.56 (d, J = 8.0 Hz, 2H, H-2), 8.17 (d, J = 7.0 Hz, 2H, H-4), 8.02 (s, 2H, H-5), 7.86 (t, J = 7.5 Hz, 2H, H-3), 7.43 (d, J = 8.2 Hz, 2H, H-6), 7.32 - 7.26 (m, 2H, H-7), 7.10 (d, J = 2.3 Hz, 4H, H-29), 7.08 (d, J = 7.0 Hz, 2H, H-8), 2.43 (s, 6H, H-31), 2.04 (s, 6H, H-32), 2.02 (s, 6H, H-32), 1.11 (s, 18H, H-26). ^{13}C NMR (151 MHz, CD_2Cl_2) δ (ppm) = 154.04 (C-24), 137.94 (C-28), 137.68 (C-30), 137.52 (C-28), 137.36 (C-27), 137.11 (C-19), 137.06 (C-14), 136.98 (C-9), 136.93 (C-15), 136.23 (C-11), 135.44 (C-13), 134.79 (C-8), 134.50 (C-20), 134.35 (C-12), 132.70 (C-16), 132.50 (C-17), 131.58 (C-10), 130.57 (C-22), 130.10 (C-23), 128.80 (C-21), 128.74 (C-29), 128.53 (C-3), 127.07 (C-18), 126.44 (C-21), 126.22 (C-1), 125.76 (C-6), 124.56 (C-7), 122.21 (C-5), 120.96 (C-4), 120.88 (C-2), 39.40 (C-25), 33.83 (C-26), 21.48 (C-31), 20.55 (C-32), 20.53 (C-32). FT-IR (ATR) $\tilde{\nu}$ (cm^{-1}) = 3060 (w), 3032 (w), 3000 (w), 2962 (m), 2917 (w), 2863 (w), 1921 (w), 1730 (w), 1611 (w), 1587 (m), 1554 (w), 1469 (w), 1460 (w), 1428 (w), 1397 (m), 1383 (w), 1363 (w), 1353 (w), 1338 (w), 1296 (w), 1272 (w), 1246 (w), 1224 (w), 1201 (w), 1173 (w), 1150 (w), 1133 (w), 1102 (w), 1066 (w), 1032 (w), 1014 (w), 969 (w), 940 (w), 922 (w), 915 (w), 887 (w), 850 (m), 827 (m), 811 (m), 797 (w), 779 (w), 757 (s), 735 (w), 715 (m), 702 (w), 685 (w), 670 (w), 657 (w), 637 (w), 607 (w). UV/Vis ($CHCl_3$): λ_{max} (nm) (log ε) = 277 (4.88), 331 (4.78), 379 (4.44), 406 (4.46), 430 (4.23), 468 (3.99), 504 (4.06), 550 (4.18), 587 (4.39), 633 (4.43). Fluorescence ($CHCl_3$): λ_{em} (λ_{ex}) (nm) = 658 (277). Φ = 25.4±0.9%. MALDI HRMS (DCTB) (m/z): $[M]^+$ calcd. for $C_{74}H_{56}$, 944.4382; found, 944.4398. Elemental anal. calcd. for $C_{74}H_{56}\cdot 0.5H_2O$: C 93.14, H 6.02, found: C 93.07, H 6.28.

De-*tert*-butylation of azulene-PAH 211

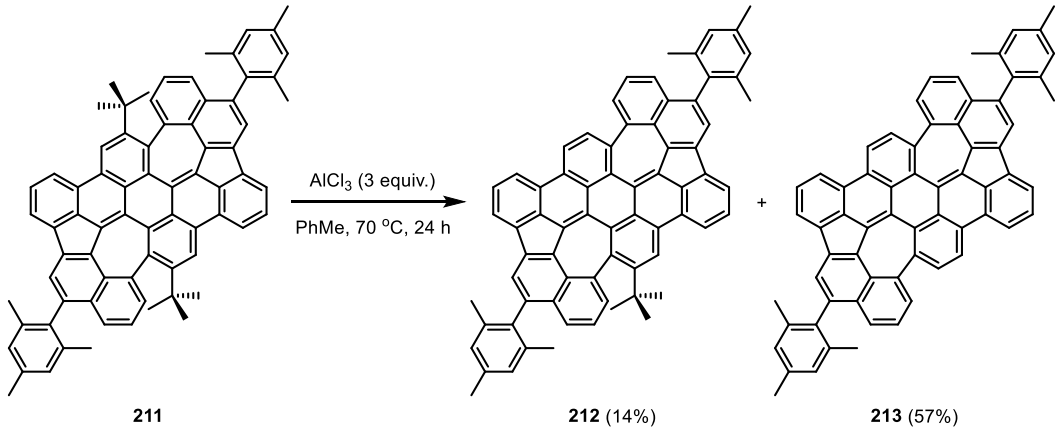

To a suspension of azulene-PAH **211** (15 mg, 0.016 mmol) in 0.5 mL dry toluene $AlCl_3$ (6.4 mg, 0.048 mmol) was added in one portion under argon atmosphere. The mixture was stirred at 70 °C for 24 hours in a screw-capped glassy vial. After cooling down to room temperature, the mixture was diluted with dichloromethane (30 mL), washed with 2M aq. HCl (30 mL), and the organic layer dried over Na_2SO_4 before filtering through a short pad of Celite®. After removal of the solvent by rotary evaporation, products **212** and **213** were separated by silica gel column chromatography (*n*-hexane /ethyl acetate 30:1 to 20:1 to collect **212**, then pure chloroform to collect **213**). The two fractions were obtained after precipitation from dichloromethane/methanol and drying in vacuum, respectively. Product **213** was obtained as a dark-blue to black solid (7.5 mg, 57%). Product **212** was obtained as a dark-blue solid (2 mg, 14%).

Azulene-PAH 212

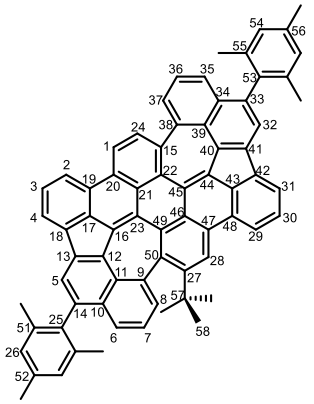

m.p.: >400 °C. ^{1}H NMR (600 MHz, CD_2Cl_2) δ (ppm) = 9.10 (s, 1H, H-28), 8.81 (d, J = 8.4 Hz, 1H, H-1), 8.63 (d, J = 8.0 Hz, 1H, H-29), 8.46 (d, J = 7.9 Hz, 1H, H-2), 8.22 (d, J = 7.0 Hz, 1H, H-31), 8.14 (d, J = 6.9 Hz, 1H, H-4), 8.08 (d, J = 8.5 Hz, 1H, H-24), 8.06 (s, 1H, H-32), 8.00 (s, 1H, H-5), 7.95 - 7.91 (m, 1H, H-30), 7.83 - 7.80 (m, 1H, H-3), 7.65 (d, J = 6.9 Hz, 1H, H-37), 7.53 - 7.50 (m, 1H, H-35), 7.48 (d, J = 7.5 Hz, 1H, H-36), 7.43 (d, J = 8.1 Hz, 1H, H-6), 7.33 - 7.29 (m, 1H, H-7), 7.14 (d, J = 7.0 Hz, 1H, H-8), 7.13 - 7.08 (m, 4H, H-26,54), 2.44 (s, 6H), 2.09 (s, 3H, H-Mes-CH_3), 2.04 (s, 3H, H-Mes-CH_3), 2.02 (s, 3H, H-Mes-CH_3), 1.98 (s, 3H, H-Mes-CH_3), 1.11 (s, 9H, H-58). ^{13}C NMR (151 MHz, CD_2Cl_2) δ (ppm) = 154.05 (C-27), 139.02 (C-33), 138.29 (C-51,55), 137.97 (C-52,56), 137.94 (C-15), 137.80 (C-52,56), 137.74 (C-38), 137.67 (C-51,55), 137.57 (C-53),

137.54 (C-14), 137.36 (C-11), 137.23 (C-25), 137.20 (C-50), 137.00 (C-19), 136.76 (C-9), 136.70 (C-48), 135.84 (C-13), 135.71 (C-24), 135.11 (C-39), 134.90 (C-41), 134.86 (C-12), 134.61 (C-8), 134.07 (C-40), 133.63 (C-20), 133.56 (C-47), 133.08 (C-44), 132.61 (C-17), 132.40 (C-37), 132.16 (C-16), 131.56 (C-43), 131.34 (C-22), 131.29 (C-10), 131.25 (C-34), 130.76 (C-23), 130.20 (C-45), 130.17 (C-49), 128.89 (C-3), 128.85 (C-26,54), 128.82 (C-26,54), 128.78 (C-30), 128.76 (C-26,54), 128.75 (C-26,54), 127.13 (C-42), 126.41 (C-18), 126.32 (C-46), 126.20 (C-28), 125.97 (C-35), 125.78 (C-1), 125.76 (C-6), 125.52 (C-36), 124.68 (C-7), 122.32 (C-5), 122.07 (C-32), 121.38 (C-4), 121.20 (C-2), 120.62 (C-29), 120.46 (C-31), 39.35 (C-57), 33.74 (C-58), 30.25 (C-Mes-CH_3), 21.48 (C-Mes-CH_3), 20.72 (C-Mes-CH_3), 20.56 (C-Mes-CH_3), 20.53 (C-Mes-CH_3), 20.45 (C-Mes-CH_3). FT-IR (ATR) $\tilde{\nu}$ (cm^{-1}) = 3064 (w), 2953 (w), 2921 (w), 2852 (w), 2731 (w), 1919 (w), 1626 (w), 1611 (w), 1587 (w), 1551 (w), 1458 (w), 1430 (m), 1405 (w), 1381 (w), 1363 (w), 1352 (w), 1303 (w), 1271 (w), 1239 (w), 1220 (w), 1203 (w), 1185 (w), 1172 (w), 1147 (w), 1130 (w), 1100 (w), 1032 (w), 1015 (w), 968 (w), 941 (w), 907 (w), 886 (w), 850 (m), 827 (w), 808 (m), 794 (w), 777 (w), 757 (s), 733 (w), 713 (w), 694 (w), 675 (w), 657 (w), 639 (w), 613 (w). UV/Vis ($CHCl_3$): λ_{max} (nm) (log ε) = 272 (4.98), 327 (4.82), 378 (4.55), 398 (4.52), 427 (4.21), 466 (4.08), 493 (4.15), 549 (4.23), 586 (4.39), 628 (4.39). Fluorescence ($CHCl_3$): λ_{em} (λ_{ex}) (nm) = 658 (272). Φ = 22.3±0.5%. MALDI HRMS (DCTB) (*m*/*z*): $[M]^+$ calcd. for $C_{70}H_{48}$, 888.3756; found, 888.3750. Elemental anal. calcd. for $C_{70}H_{48}\cdot 0.5H_2O$: C 93.61, H 5.50, found: C 93.70, H 5.62.

Azulene-PAH 213

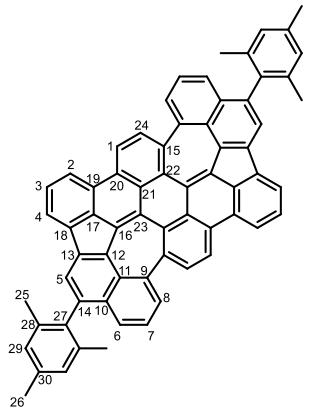

m.p.: >400 ºC. ^{1}H NMR (600 MHz, CD_2Cl_2, 298 K) δ (ppm) = 8.09 (s, 2H, H-5), 8.02 (d, *J* = 6.8 Hz, 2H, H-2), 7.98 (br, 2H, H-1), 7.64 (br, 2H, H-4), 7.46 (d, *J* = 8.1 Hz, 2H, H-6), 7.43 - 7.37 (m, 2H, H-3), 7.30 (t, *J* = 7.5 Hz, 2H, H-7), 7.23 (d, *J* = 6.4 Hz, 2H, H-8), 7.15 (br, 6H, H-24,29), 2.47 (s, 6H, H-26), 2.15 (br, 12H, H-25). ^{13}C NMR (151 MHz, CD_2Cl_2, 298 K) δ (ppm) = 138.16 (C-9), 137.30 (C-14), 137.24 (C-27), 136.90 (C-30), 136.82 (C-28), 136.41 (C-15), 135.67 (C-19), 135.06 (C-11), 134.95 (C-24), 134.02 (C-20), 133.51 (C-12), 132.66 (C-13), 131.33 (C-16), 130.98 (C-8), 130.91 (C-10), 130.32 (C-17), 130.10 (C-22), 129.44 (C-23), 128.47 (C-21), 128.38 (C-29), 127.55 (C-3), 125.14 (C-7), 124.93 (C-18), 124.77 (C-1), 124.44 (C-6), 121.15 (C-5), 119.97 (C-4), 119.55 (C-2), 21.29 (C-26), 20.36 (C-25). FT-IR (ATR) $\tilde{\nu}$ (cm^{-1}) = 3060 (w), 3032 (w), 2919 (w), 2919 (w), 2852 (w), 2731 (w), 1911 (w), 1783 (w), 1726 (w), 1633 (w), 1611 (w), 1594 (w), 1573 (w), 1549 (w), 1533 (w), 1475 (w), 1457 (w), 1431 (m), 1415 (w), 1377 (w), 1350 (w), 1304 (w), 1272 (w), 1257 (w), 1238 (w), 1220 (w), 1200 (w), 1178 (w), 1143 (w), 1127 (w), 1107 (w), 1065 (w), 1032

(w), 1013 (w), 958 (w), 941 (w), 893 (w), 849 (m), 827 (w), 800 (m), 778 (m), 752 (s), 729 (m), 716 (w), 684 (w), 643 (w), 628 (w). UV/Vis ($CHCl_3$): λ_{max} (nm) (log ε) = 260 (5.10), 319 (4.88), 328 (4.88), 353 (4.59), 372 (4.71), 390 (4.63), 423 (4.23), 449 (4.26), 476 (4.31), 540 (4.26), 574 (4.40), 615 (4.37). Fluorescence ($CHCl_3$): λ_{em} (λ_{ex}) (nm) = 646 (260). Φ = 17.9±0.2%. MALDI HRMS (DCTB) (*m*/*z*): $[M]^+$ calcd. for $C_{66}H_{40}$, 832.3130; found, 832.3149. Elemental anal. calcd. for $C_{66}H_{40}\cdot 0.5H_2O$: C 94.14, H 4.91, found: C 94.05 H 5.12.

5.2.3 Compounds of Chapter 3.3

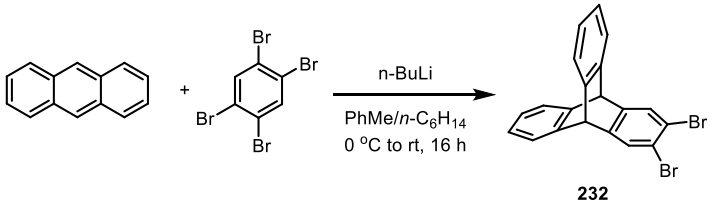

232

(*9r*,*10r*)-2,3-dibromo-9,10-dihydro-9,10-[1,2]benzenoanthracene (232)[205]

To a suspension of anthracene (5.0 g, 28 mmol) and 1,2,4,5-tetrabromobenzene (15.43g, 39.2 mmol) in dry toluene (125 mL) was added *n*-BuLi (2.5 M in hexane, 18 mL, 45 mmol, diluted in 63 mL dry hexane) slowly at 0 °C under argon atmosphere over 3 hours. The mixture was then gradually warmed up to room temperature and stirred overnight. The suspension was then filtered off and the filter cake was washed with dichloromethane (50 mL). The filtrate was concentrated under reduced pressure. The product was obtained after silica gel column chromatography (petroleum ether/dichloromethane 100:0 to 20:1) to give the product as colorless solid (3.88 g, 33 %).

^{1}H NMR (300 MHz, $CDCl_3$) δ (ppm) = 7.63 (s, 2H), 7.42 - 7.34 (m, 4H), 7.08 - 6.97 (m, 4H), 5.36 (s, 2H). The NMR data are in accordance to the literature data.[205]

(*9r*,*10r*)-3-bromo-9,10-dihydro-9,10-[1,2]benzenoanthracene-2-carbaldehyde (233)

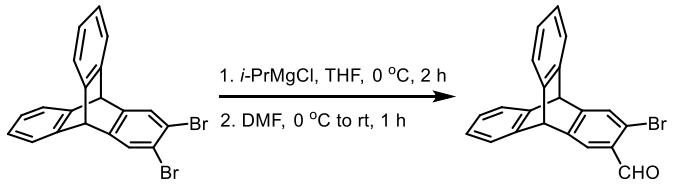

232 **233** (61%)

A 100 mL Schlenk-flask charged with **232** (2.97 g, 7.2 mmol) was purged with argon. Dry THF (48 mL) was added to dissolve the solid. The mixture was cooled down to 0 °C. *i*-PrMgCl (1.88 M in THF, 5.74 mL, 10.8 mmol) was then added dropwise over 10 minutes. The mixture was stirred at 0 °C for 2 hours. Dry DMF (1.8 mL) was then added dropwise and the mixture was then gradually warmed up to room temperature and stirred for 1 hour. Methanol (2 mL) was added to quench the reaction. The mixture was diluted with dichloromethane (50 mL), washed with water (50 mL), dried over anhydrous Na_2SO_4. After removal of the solvent by rotary evaporation, the crude product was purified by silica gel column chromatography (petroleum ether/dichloromethane/ethyl acetate 100:0:0 to 50:5:1 to 20:2:1) to give **233** as a colorless solid (1.58 g, 61 %).

m.p.: 258 °C (dec.). ^{1}H NMR (400 MHz, $CDCl_3$) δ (ppm) = 10.24 (s, 1H), 7.89 (s, 1H), 7.65 (s, 1H), 7.44 - 7.37 (m, 4H), 7.09 - 7.01 (m, 4H), 5.48 (s, 1H), 5.45 (s, 1H). ^{13}C NMR (101 MHz, $CDCl_3$) δ (ppm) = 191.57, 153.17, 145.50, 144.07, 143.15, 130.47, 128.88, 125.91, 125.74, 124.82, 124.02, 124.00, 123.96, 53.73, 53.34. FT-IR (ATR) $\tilde{\nu}$ (cm^{-1}) = 3069 (w), 3022 (w), 2969 (w), 2860 (w), 2754 (w), 1684 (s), 1612 (w), 1595 (m), 1561 (w), 1482 (w), 1457 (m), 1390 (m), 1319 (w), 1294 (w), 1244 (m), 1197 (m), 1157 (w), 1115 (w), 1023 (w), 975 (m), 940 (w), 914 (w), 896 (w), 877 (w), 859 (w), 833 (w), 801 (w), 739 (s), 697 (w), 626 (m). EI HRMS (*m*/*z*): $[M]^+$ calcd. for $C_{21}H_{13}BrO$, 362.0126; found, 362.0133. Elemental anal. calcd. for $C_{21}H_{13}BrO \cdot 0.1H_2O$: C 69.48, H 3.67, found: C 69.41, H 3.71.

3-(3,7-di-*tert*-butyl-5-((*9r*,*10r*)-3-formyl-9,10-dihydro-9,10-[1,2]benzenoanthracen-2-yl)-9,10-dihydroanthracen-1-yl)-9,10-dihydro-9,10-[1,2]benzenoanthracene-2-carbaldehyde (234)

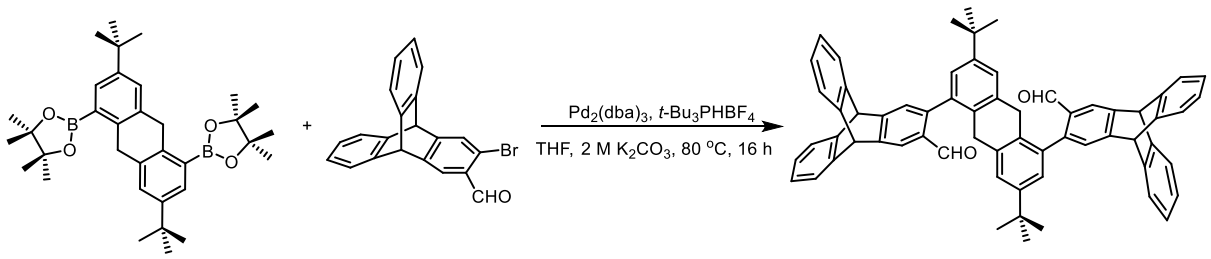

109 233 234

In a screw-capped glassy vial, a mixture of diboronic pinacol ester (**109**, 109 mg, 0.2 mmol) and triptycenyl bromoaldehyde (**233**, 188 mg, 0.52 mmol) was suspended in argon-degassed THF (1.3 mL). A argon-degassed aqueous solution of K_2CO_3 (2M, 0.4 mL) was then added. After stirred for 10 minutes at room temperature, a mixture of tris(dibenzylidene-acetone)dipalladium(0) ($Pd_2(dba)_3$, 18 mg, 0.02 mmol) and tri-*tert*-butylphosphonium tetrafluoroborate (*t*-Bu_3PHBF_4, 18 mg, 0.062 mmol) was added and the mixture was stirred at 80 °C for 16 hours. After cooling down to room temperature, the mixture was diluted with chloroform (50 mL). The organic layer was washed with sat. aq. NH_4Cl (3 × 50 mL) and dried over Na_2SO_4. After removal of the solvent by rotary evaporation, the crude product was purified by silica gel column chromatography (petroleum ether/chloroform/ethyl acetate 30:3:1 to 20:2:1) to give **234** as a colorless solid (mixture of atropisomers, 83 mg, 48 %).

m.p.: 326 °C (dec.). ^{1}H NMR (400 MHz, $CDCl_3$) δ (ppm) = 9.63 (s, 1H), 9.63 (s, 1H), 8.09 (s, 1H), 8.08 (s, 1H), 7.55 - 7.53 (m, 1H), 7.53 - 7.51 (m, 1H), 7.50 - 7.43 (m, 7H), 7.39 (s, 1H), 7.37 (s, 1H), 7.15 - 7.09 (m, 6H), 7.08 - 7.05 (m, 4H), 7.00 (t, J = 1.9 Hz, 2H), 5.63 (s, 2H), 5.53 (s, 2H), 3.71 - 3.54 (m, 4H), 1.21 (s, 18H). ^{13}C NMR (101 MHz, $CDCl_3$) δ (ppm) = 192.10, 192.01, 150.94, 150.78, 148.74, 144.79, 144.75, 144.73, 144.72, 144.67, 144.22, 144.13, 144.04, 136.68, 136.63, 135.42, 132.27, 132.25, 131.54, 131.48, 126.42, 126.35, 125.95, 125.84, 125.76, 125.74, 125.68, 125.64, 125.56, 125.54, 124.69, 124.13, 124.08, 124.02, 123.98, 123.96, 123.93, 123.89, 121.45, 121.36, 54.22, 54.20, 53.72, 34.42, 34.32, 31.34. FT-IR (ATR) $\tilde{\nu}$ (cm^{-1}) = 3066 (w), 3040 (w), 3020 (w), 2956 (m), 2904 (w), 2862 (w), 2750 (w), 1685 (s), 1602 (m), 1458 (m), 1393 (m), 1363 (w), 1334 (w), 1295 (w), 1248 (m), 1194 (m), 1156 (w), 1123 (w), 1102 (w), 1043 (w), 1021 (w), 964 (w), 875 (m), 828 (w), 796 (w), 783 (w), 740 (s), 688 (w), 670 (w), 628 (m). MALDI HRMS (DCTB)

(*m*/*z*): $[M+Na]^+$ calcd. for $C_{64}H_{52}O_2Na$, 875.3865; found, 875.3878. Elemental anal. calcd. for $C_{64}H_{52}O_2 \cdot 0.2CHCl_3$: C 87.93, H 6.00, found: C 87.97, H 5.89.

PO-5 (228)

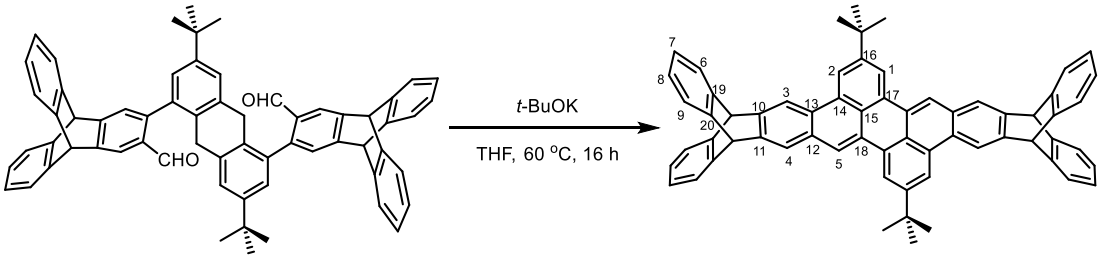

234 PO-5 (**228**)

To a solution of the dialdehyde **234** (60 mg, 0.07 mmol) in dry THF (3 mL) was added *t*-BuOK (47 mg, 0.42 mmol) under argon. The mixture was stirred at 60 °C for 16 hours in a screw-capped glassy vial. After cooling down to room temperature, the reaction was quenched by adding 2M aq. HCl (0.2 mL). After stirring for 10 minutes, most of the solvent was removed by rotary evaporation. The residue was suspended in methanol (3 mL). The suspension was then filtered off and the solid was washed with water (2 mL × 2) and methanol (2 mL × 2). The product was obtained after drying in vacuum as a dark-yellow solid (46 mg, 81 %).

m.p.: >400 °C. ^{1}H NMR (600 MHz, $Cl_2CDCDCl_2$) δ (ppm) = 8.58 (s, 2H, H-3), 8.56 (s, 2H, H-2), 8.47 (s, 2H, H-1), 8.34 (s, 2H, H-5), 7.97 (s, 2H, H-4), 7.53 - 7.49 (m, 4H, H-6), 7.49 - 7.45 (m, 4H, H-9), 7.14 - 7.00 (m, 9H, H-7,8), 5.74 (s, 2H, H-bridgehead), 5.59 (s, 2H, H-bridgehead), 1.59 (s, 18H). ^{13}C NMR (151 MHz, $Cl_2CDCDCl_2$) δ (ppm) = 149.28 (C-16), 144.55 (C-19), 144.53 (C-20), 143.20 (C-10), 143.08 (C-11), 130.63 (C-17), 130.41 (C-14), 130.22 (C-12), 129.02 (C-18), 127.58 (C-13), 125.48 (C-7,8), 125.43 (C-7,8), 125.17 (C-15), 123.92 (C-9), 123.88 (C-6), 123.19 (C-4), 119.82 (C-5), 119.07 (C-1), 118.61 (C-2), 117.17 (C-3), 53.82, 53.38, 35.21, 31.51. FT-IR (ATR) $\tilde{\nu}$ (cm^{-1}) = 3067 (w), 3041 (w), 3017 (w), 2957 (m), 2929 (w), 2865 (w), 1709 (w), 1605 (w), 1503 (w), 1458 (m), 1434 (w), 1415 (w), 1394 (w), 1375 (w), 1363 (w), 1272 (w), 1252 (w), 1201 (w), 1188 (w), 1157 (w), 1133 (w), 1105 (w), 1094 (w), 1064 (w), 1022 (w), 931 (w), 895 (m), 870 (m), 833 (w), 794 (w), 762 (m), 742 (s), 688 (w), 648 (w), 627 (s). UV/Vis ($CHCl_3$): λ_{max} (nm) (log ε) = 254 (5.14), 273 (4.74), 303 (4.70), 316 (4.81), 402 (4.45), 422 (4.72), 449 (4.79). Fluorescence ($CHCl_3$): λ_{em} (λ_{ex}) (nm) = 462, 494, 530 (422). Φ = 68±3%. τ = 2.1 ns. MALDI-TOF MS (DCTB, Kalib PEG600) (*m*/*z*): $[M]^+$ calcd. for $C_{64}H_{48}$, 816.375; found, 816.371. Elemental anal. calcd. for $C_{64}H_{48} \cdot 1.5H_2O$: C 91.07, H 6.09, found: 90.93, H 6.20.

2,5-dibromoterephthalaldehyde (235)[218]

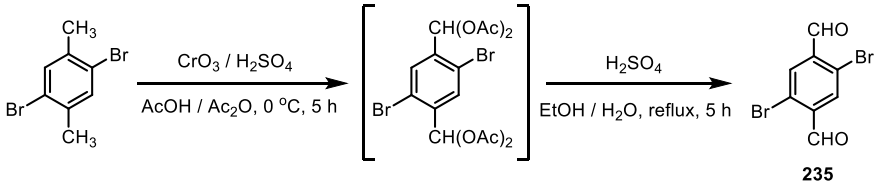

235

To a suspension of 1,4-dibromo-2,5-dimethylbenzene (8.0 g, 30 mmol) in a mixture of AcOH/Ac_2O (40 mL/80 mL) was added dropwise conc. H_2SO_4 (28 mL) over 10 minutes at 0 °C. The mixture

was stirred at 0 °C for 30 minutes. CrO_3 (12 g, 120 mmol) was then added in portions. The green suspension was stirred at 0 °C for 5 hours until TLC showed that the substrate was fully consumed. The dark-green mixture was poured into 300 mL ice-water. The suspension was filtered off and the filter cake was washed with water (4 × 30 mL) and cold methanol (2 × 20 mL) to give colorless solid. The colorless solid was refluxed in a mixture of ethanol/water (40 mL/40 mL) with conc. H_2SO_4 (4 mL) for 5 hours. The mixture was poured into 100 mL ice-water and filtered off. The filter cake was recrystallized from chloroform to give **235** as a light-yellow solid (3.37 g, 38 %).

^{1}H NMR (300 MHz, $CDCl_3$) δ (ppm) = 10.34 (s, 2H), 8.15 (s, 2H). The NMR data are in accordance to the literature data.[218]

2-(3,7-di-*tert*-butyl-9,10-dihydroanthracen-1-yl)-4,4,5,5-tetramethyl-1,3,2-dioxaborolane (238)

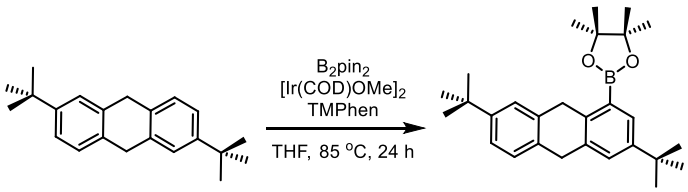

108 238

Inside a glovebox, bis(pinacolato)diboron (B_2pin_2, 38 mg, 0.15 mmol), (1,5-cyclooctadiene) (methoxy) iridium(I) dimer ($[Ir(COD)OMe]_2$, 14 mg, 0.0225 mmol) and 3,4,7,8-tetramethyl-9,10-phenanthroline (TMPhen, 11 mg, 0.045 mmol) were dissolved in dry THF (1.5 mL). The mixture was stirred vigorously for 10 minutes to obtain a dark green solution. The catalyst complex solution was then transferred into a small glassy vial containing dihydroanthracene (439 mg, 1.5 mmol) and B_2pin_2 (457 mg, 1.8 mmol). The vial was then screw-capped and the mixture was stirred at 85 °C for 24 hours. After cooling down to room temperature, the solvent was directly removed by rotary evaporation. The residue was suspended with 10 mL methanol. The suspension was filtered off. The solid was subject to silica gel column chromatography (petroleum ether/dichloromethane 5:1) to collect the monoboronic ester as a colorless solid (293 mg, 47 %).

m.p.: 195 °C. ^{1}H NMR (600 MHz, $CDCl_3$) δ (ppm) = 7.72 (d, J= 2.0 Hz, 1H), 7.39 (d, J = 1.7 Hz, 1H), 7.32 (s, 1H), 7.24 - 7.19 (m, 2H), 4.26 (s, 2H), 3.90 (s, 2H), 1.40 (s, 12H), 1.34 (s, 9H), 1.34 (s, 9H). ^{13}C NMR (151 MHz, $CDCl_3$) δ (ppm) = 148.81, 147.67, 140.67, 137.44, 136.44, 134.06, 130.51, 127.40, 126.55, 124.51, 122.73, 83.42, 36.60, 35.26, 34.38, 34.29, 31.52, 31.46, 24.93. FT-IR (ATR) $\tilde{\nu}$ (cm^{-1}) = 2960 (m), 2868 (w), 2809 (w), 1580 (w), 1502 (w), 1467 (m), 1405 (w), 1364 (s), 1322 (w), 1306 (m), 1286 (w), 1256 (s), 1208 (w), 1161 (m), 1136 (s), 1106 (w), 972 (w), 957 (w), 930 (w), 894 (w), 850 (m), 818 (m), 736 (m), 703 (w), 682 (w), 651 (w), 621 (w). DART MS (m/z): $[M+NH_4]^+$ calcd. for $C_{28}H_{43}O_2BN$, 436.3381; found, 436.3382. Elemental anal. calcd. for $C_{28}H_{39}BO_2$: C 80.37, H 9.40, found: C 80.33, H 9.66.

2,5-bis(3,7-di-*tert*-butyl-9,10-dihydroanthracen-1-yl)terephthalaldehyde (239)

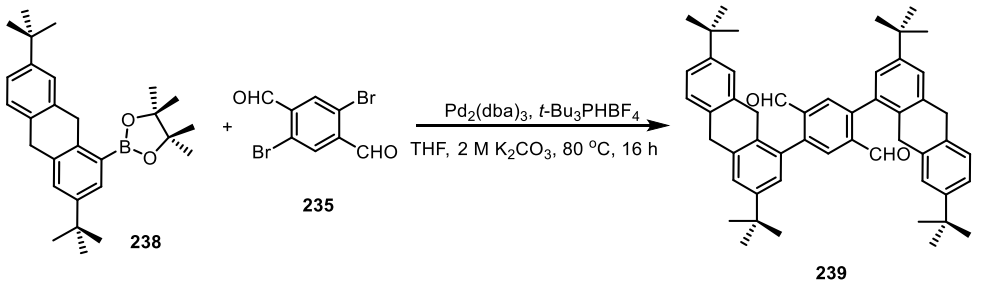

238 235 239

To a mixture of monoboronic ester (167 mg, 0.4 mmol) and 2,5-dibromoterephthalaldehyde (53 mg, 0.18 mmol) in argon-degassed THF (2 mL) and 2M aq. K_2CO_3 (0.5 mL) was added a mixture of $Pd_2(dba)_3$ (18 mg, 0.02 mmol) and tBu$_3$PHBF$_4$ (18 mg, 0.063 mmol) under argon atmosphere. The mixture was stirred vigorously at 80 °C for 16 hours in a screw-capped glassy vial. After cooling down to room temperature, the mixture was diluted with 70 mL dichloromethane, washed with brine (50 mL × 2) and dried over Na_2SO_4. After passing through a short pad of Celite® and removal of the solvent by rotary evaporation, the product was obtained after precipitation from dichloromethane/methanol as a colorless solid (mixture of atropisomers, 81 mg, 63%).

m.p.: 383 °C (dec.). ^{1}H NMR (600 MHz, CD_2Cl_2) δ (ppm) = 9.88 (s, 1H), 9.87 (s, 1H), 8.06 (s, 1H), 8.05 (s, 1H), 7.48 (s, 2H), 7.29 (d, J = 1.9 Hz, 1H), 7.28 - 7.24 (m, 2H), 7.24 - 7.21 (m, 2H), 7.21 - 7.17 (m, 2H), 7.13 (s, 1H), 4.02 (s, 2H), 4.01 (s, 2H), 3.88 - 3.78 (m, 1H), 3.73 (br, 2H), 3.64 (br, 1H), 1.37 (s, 10H), 1.34 (s, 8H), 1.27 (s, 8H), 1.24 (s, 10H). ^{13}C NMR (151 MHz, CD_2Cl_2) δ (ppm) = 192.43, 149.76, 149.72, 149.56, 145.03, 144.98, 138.29, 138.27, 137.66, 136.42, 136.35, 135.10, 135.06, 134.37, 134.36, 133.15, 133.00, 130.54, 130.51, 127.32, 127.26, 126.12, 125.98, 125.73, 125.68, 124.97, 123.82, 123.75, 36.94, 36.93, 34.99, 34.93, 34.85, 34.84, 34.65, 34.50, 31.75, 31.71, 31.70. FT-IR (ATR) $\tilde{\nu}$ (cm^{-1}) = 2960 (m), 2904 (w), 2864 (w), 2812 (w), 1688 (s), 1607 (w), 1571 (w), 1505 (w), 1475 (m), 1460 (m), 1423 (m), 1390 (m), 1361 (m), 1329 (w), 1267 (m), 1240 (w), 1202 (m), 1150 (m), 1103 (w), 953 (w), 917 (w), 900 (m), 872 (w), 840 (w), 815 (m), 774 (m), 754 (w), 732 (m), 711 (w), 697 (w), 656 (w), 624 (w). MALDI HRMS (DCTB) (m/z): $[M+Na]^+$ calcd. for $C_{52}H_{58}O_2Na$, 737.4335; found, 737.4335. Elemental anal. calcd. for $C_{52}H_{58}O_2$: C 87.35, H 8.18, found: C 87.09, H 8.43.

2,7,12,17-tetra-*tert*-butyl-4,14-dihydrotetrabenzo[*a*,*de*,*l*,*op*]pentacene (240)

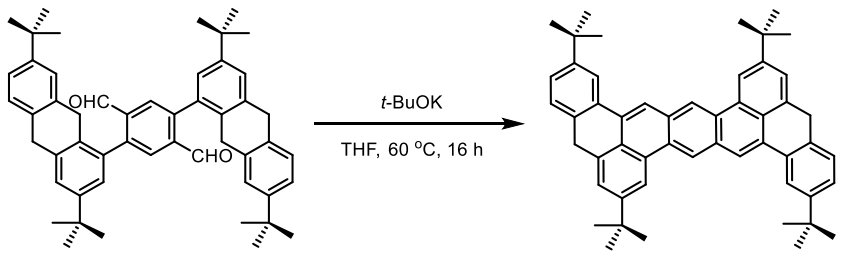

239 240

To a suspension of the dialdehyde (100 mg, 0.14 mmol) in dry THF (3.5 mL) was added t-BuOK (94 mg, 0.84 mmol) under argon atmosphere. The mixture was stirred at 60 °C for 16 hours in a screw-capped glassy vial. After cooling down to room temperature, the reaction was quenched by adding 2M aq. HCl (1 mL). The mixture was then suspended in methanol (10 mL), followed by

filtering off. The solid was rinsed with methanol (2 mL × 2), acetone (2 mL × 2) and ethanol (2 mL × 2). The product was obtained after drying in vacuum as a light-yellow solid (84 mg, 88%). m.p.: >400 °C. ^{1}H NMR (500 MHz, $Cl_2CDCDCl_2$) δ (ppm) = 9.10 (s, 2H), 8.74 (s, 2H), 8.44 (s, 2H), 8.26 (s, 2H), 7.63 (s, 2H), 7.40 (d, J = 7.8 Hz, 2H), 7.31 (d, J = 7.8 Hz, 2H), 4.56 (s, 4H), 1.56 (s, 18H), 1.47 (s, 18H). ^{13}C NMR spectrum is not available due to its low solubility. FT-IR (ATR) $\tilde{\nu}$ (cm^{-1}) = 2955 (s), 2902 (m), 2863 (m), 2800 (w), 1613 (m), 1570 (w), 1541 (w), 1498 (m), 1473 (m), 1419 (m), 1388 (w), 1360 (m), 1302 (w), 1261 (m), 1220 (w), 1200 (w), 1137 (w), 1093 (w), 1067 (w), 957 (w), 932 (w), 906 (w), 890 (s), 870 (m), 816 (s), 781 (w), 733 (w), 713 (w), 694 (w), 680 (w), 662 (w), 615 (s). MALDI HRMS (DCTB) (m/z): $[M]^+$ calcd. for $C_{52}H_{54}$, 678.4225; found, 678.4230. Elemental anal. calcd. for $C_{52}H_{54}\cdot 2.5CH_3OH$: C 86.23, H 8.50, found: C 85.94, H 8.75.

2,5-bis(3,7-di-*tert*-butyl-5-(4,4,5,5-tetramethyl-1,3,2-dioxaborolan-2-yl)-9,10-dihydroanthracen-1-yl)terephthalaldehyde (241)

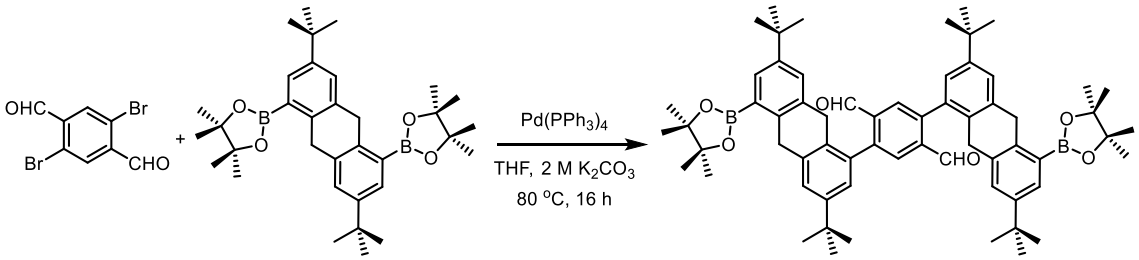

235 **109** **241**

In a screw-capped glassy vial, a mixture of **235** (275 mg, 0.94 mmol), **109** (3.05 g, 5.59 mmol) was suspended in argon-degassed THF (5.6 mL) and 2M aq. K_2CO_3 (1.4 mL). $Pd(PPh_3)_4$ (109 mg, 0.094 mmol) was then added. The mixture was stirred at 80 °C for 16 hours. After cooling down to room temperature, the mixture was diluted with chloroform (100 mL). The organic phase was washed with sat. aq. NH_4Cl (3 × 100 mL) and dried over anhydrous Na_2SO_4. After removal of the solvent by rotary evaporation, the crude product was purified by silica gel column chromatography (petroleum ether/dichloromethane/ethyl acetate 50:5:1 to 40:6:1) to give the product **241** as a colorless solid (mixture of atropisomers, 421 mg, 46 %).

m.p.: 380 °C (dec.). ^{1}H NMR (600 MHz, CD_2Cl_2) δ (ppm) = 9.87 (s, 1H), 9.87 (s, 1H), 8.07 (s, 1H), 8.06 (s, 1H), 7.68 (d, J = 2.1 Hz, 1H), 7.66 (d, J = 2.1 Hz, 1H), 7.48 (s, 2H), 7.28 (d, J = 1.9 Hz, 1H), 7.26 (d, J = 2.0 Hz, 1H), 7.20 (d, J = 2.0 Hz, 1H), 7.17 (d, J = 1.9 Hz, 1H), 4.41-4.37 (m, 2H), 4.33-4.28 (m, 2H), 3.81 (d, J = 17.3 Hz, 1H), 3.73 (d, J = 17.9 Hz, 2H), 3.65 (d, J = 17.3 Hz, 1H), 1.41 (s, 12H), 1.41 (s, 12H), 1.38 (s, 11H), 1.35 (s, 7H), 1.28 (s, 7H), 1.26 (s, 11H). ^{13}C NMR (151 MHz, CD_2Cl_2) δ (ppm) = 192.49, 149.47, 148.44, 148.41, 144.96, 144.91, 141.10, 141.06, 139.19, 139.17, 137.66, 136.48, 136.41, 134.67, 134.64, 133.34, 133.19, 131.19, 131.12, 130.57, 130.54, 128.00, 126.01, 125.87, 125.84, 125.80, 84.18, 84.17, 36.19, 35.13, 34.99, 34.97, 34.94, 34.76, 34.74, 31.78, 31.72, 31.68, 25.30. FT-IR (ATR) $\tilde{\nu}$ (cm^{-1}) = 2966 (m), 2907 (w), 2868 (w), 1692 (m), 1602 (w), 1584 (w), 1476 (w), 1461 (m), 1407 (w), 1366 (m), 1304 (m), 1274 (w), 1256 (m), 1202 (w), 1144 (s), 1111 (w), 977 (w), 965 (w), 915 (w), 898 (m), 854 (m), 836 (w), 797 (w), 756 (m), 740 (m), 706 (w), 681 (w), 658 (w), 630 (w), 607 (w). MALDI HRMS (DCTB) (m/z): $[M+Na]^+$

calcd. for $C_{64}H_{80}B_2O_6Na$, 989.6059; found, 989.6027. Elemental anal. calcd. for $C_{64}H_{80}B_2O_6 \cdot 0.5H_2O$: C 78.76, H 8.37, found: C 78.74, H 8.33.

2-(3,7-di-*tert*-butyl-5-((*9r*,*10r*)-3-formyl-9,10-dihydro-9,10-[1,2]benzenoanthracen-2-yl)-9,10-dihydroanthracen-1-yl)-5-(3,7-di-*tert*-butyl-5-(3-formyl-9,10-dihydro-9,10-[1,2]benzenoanthracen-2-yl)-9,10-dihydroanthracen-1-yl)terephthalaldehyde (243)

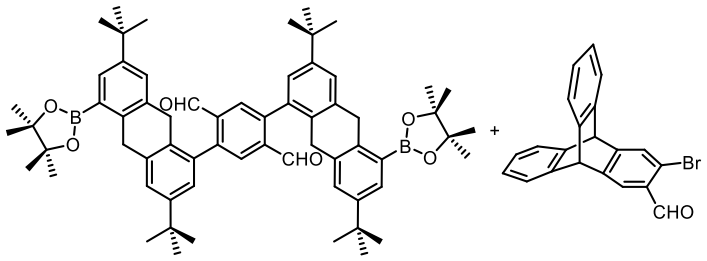

241 **233**

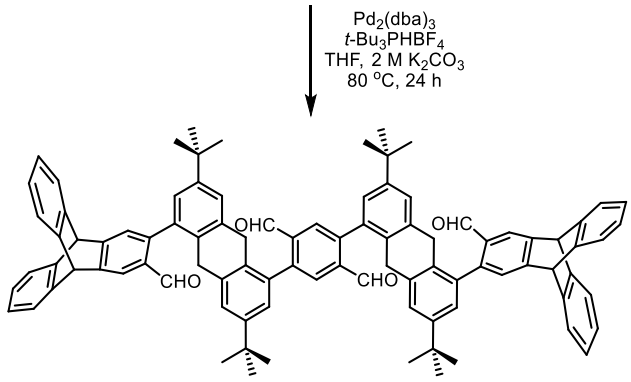

243

In a screw-capped glassy vial, a mixture of diboronic ester **241** (116 mg, 0.12 mmol) and **233** (96 mg, 0.26 mmol) was suspended in argon-degassed THF (0.8 mL) and 2M aq. K_2CO_3 (0.2 mL). A mixture of $Pd_2(dba)_3$ (11 mg, 0.012 mmol) and *t*-Bu_3PHBF_4 (11 mg, 0.038 mmol) was then added. The mixture was stirred at 80 °C for 16 hours. After cooling down to room temperature, the mixture was diluted with dichloromethane (50 mL). The organic phase was washed with sat. aq. NH_4Cl (3 × 50 mL) and dried over anhydrous Na_2SO_4. After removal of the solvent by rotary evaporation, the crude product was purified by silica gel column chromatography (petroleum ether/chloroform/ethyl acetate 20:7:1) to give the product **243** as a colorless solid (mixture of atropisomers, 58 mg, 38 %).

m.p.: 338 °C (dec.). ^{1}H NMR (600 MHz, $Cl_2CDCDCl_2$) δ (ppm) = 9.94 - 9.86 (m, 2H), 9.70 - 9.63 (m, 2H), 8.14 - 8.05 (m, 4H), 7.55 - 7.46 (m, 10H), 7.22 - 7.03 (m, 16H), 5.65 (s, 2H), 5.60 - 5.52 (m, 2H), 3.86 - 3.64 (m, 8H), 1.30 - 1.28 (m, 9H), 1.27 - 1.25 (m, 9H), 1.25 - 1.23 (m, 9H), 1.22 (s, 9H). ^{13}C NMR (151 MHz, $Cl_2CDCDCl_2$) δ (ppm) = 192.23, 192.20, 192.11, 192.04, 191.99, 150.73, 150.72, 150.69, 150.63, 149.15, 149.12, 149.09, 149.00, 148.71, 148.69, 148.65, 144.54, 144.37, 144.14, 144.11, 144.08, 144.04, 143.95, 143.93, 136.90, 136.85, 136.79, 136.75, 136.72, 136.69, 135.96, 135.84, 135.30, 135.21, 135.18, 135.14, 133.93, 133.89, 132.03, 132.00, 131.80, 131.21, 130.07, 130.02, 129.98, 129.93, 126.64, 126.29, 126.19, 126.16, 125.72, 125.60, 125.57, 125.49, 125.41, 124.62, 124.55, 124.52, 124.36, 124.17, 124.01, 123.92, 121.33, 121.29, 53.83, 53.28, 34.42, 34.31, 34.20, 34.16, 34.11, 31.27, 31.21, 31.19. FT-IR (ATR) $\tilde{\nu}$ (cm^{-1}) = 3066 (w), 2959 (m),

2906 (w), 2866 (w), 2751 (w), 1687 (s), 1603 (w), 1574 (w), 1477 (w), 1459 (m), 1420 (w), 1393 (m), 1363 (w), 1294 (w), 1247 (m), 1196 (m), 1152 (w), 1129 (w), 1102 (w), 1022 (w), 894 (m), 831 (w), 791 (w), 741 (s), 714 (w), 690 (w), 668 (w), 628 (m). MALDI HRMS (DCTB) (*m*/*z*): $[M+Na]^+$ calcd. for $C_{94}H_{82}O_4Na$, 1298.6144; found, 1298.6411. Elemental anal. calcd. for $C_{94}H_{82}O_4 \cdot 3H_2O$: C 84.91, H 6.67, found: 85.09, H 6.63.

PO-9 (229)

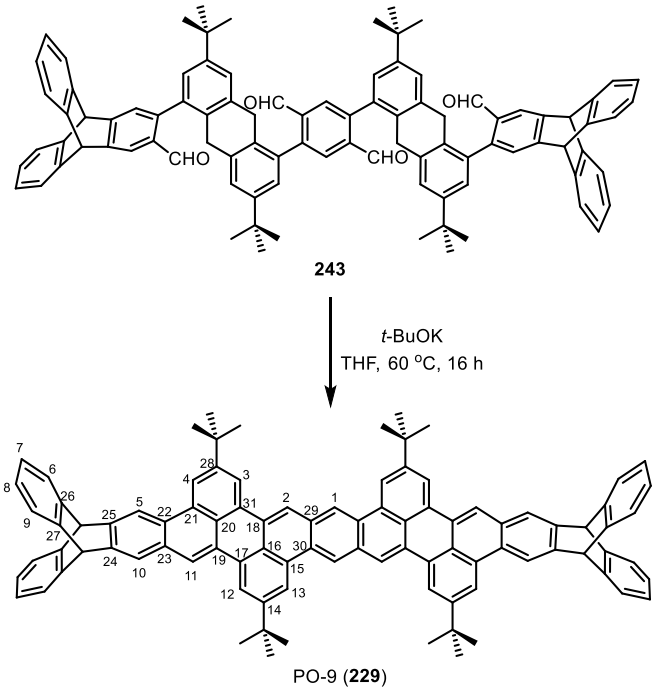

To a solution of the tetraldehyde **243** (41 mg, 0.032 mmol) in dry THF (2.5 mL) was added *t*-BuOK (50 mg, 0.448 mmol) under argon. The mixture was stirred at 60 °C for 16 hours in a screw-capped glassy vial. After cooling down to room temperature, the reaction was quenched by adding 2M aq. HCl (0.5 mL). After stirring for 10 minutes, the mixture was dropped into methanol (5 mL). The suspension was then filtered off and the solid was washed with water (2 mL × 2) and methanol (2 mL × 2). The product was obtained after drying in vacuum as an orange-red solid (27 mg, 70 %). m.p.: >400 °C. ^{1}H NMR (600 MHz, $Cl_2CDCDCl_2$) δ (ppm) = 9.10 (s, 2H, H-1), 8.86 (s, 2H, H-12), 8.68 (s, 4H, H-3, 5), 8.65 (s, 2H, H-4), 8.64 (s, 2H, H-2), 8.57 (s, 2H, H-13), 8.39 (s, 2H, H-11), 8.01 (s, 2H, H-10), 7.56 - 7.52 (m, 4H, H-6), 7.51 - 7.46 (m, 4H, H-9), 7.12 - 7.06 (m, 8H, H-7, 8), 5.78 (s, 2H, H-bridgehead), 5.61 (s, 2H, H-bridgehead), 1.68 (s, 36H). ^{13}C NMR (151 MHz, $Cl_2CDCDCl_2$) δ (ppm) = 149.82 (C-14), 149.38 (C-28), 144.52 (C-26,27), 143.30 (C-24), 143.27 (C-25), 131.29 (C-15), 130.62 (C-17,18), 130.35 (C-31), 130.23 (C-19), 129.37 (C-23), 129.31 (C-21), 128.79 (C-30), 127.65 (C-22), 125.51 (C-7), 125.48 (C-8), 125.15 (C-20), 125.08 (C-16), 123.94 (C-6), 123.93 (C-9), 123.29 (C-10), 122.42 (C-1), 120.77 (C-5), 120.09 (C-11), 119.69 (C-13), 119.45 (C-3), 119.26 (C-12), 118.93 (C-4), 117.18 (C-2), 53.85 (C-bridgehead), 53.40 (C-bridgehead), 35.33, 31.65. FT-IR (ATR) $\tilde{\nu}$ (cm^{-1}) = 3066 (w), 3044 (w), 3019 (w), 2955 (m), 2905 (w), 2867 (w), 1604 (m), 1536 (w), 1498 (w), 1460 (m), 1432 (w), 1392 (w), 1363 (w), 1283 (w), 1253 (w), 1201 (w), 1181 (w), 1158 (w), 1134 (w), 1086 (w), 1023 (w), 1002 (w), 932 (w), 890 (s),

868 (m), 803 (w), 786 (w), 763 (m), 741 (m), 688 (w), 664 (w), 648 (w), 626 (s). UV/Vis ($CHCl_3$): λ_{max} (nm) (log ε) = 266 (5.16), 320 (4.86), 331 (4.92), 384 (4.27), 447 (4.71), 475 (5.05), 510 (5.17). Fluorescence ($CHCl_3$): λ_{em} (λ_{ex}) (nm) = 523, 562, 610 (475). Φ= 86±1%. τ= 1.5 ns. MALDI HRMS (DCTB) (*m*/*z*): $[M]^+$ calcd. for $C_{94}H_{74}$, 1203.5824; found, 1203.5821. Elemental anal. calcd. for $C_{94}H_{74}\cdot H_2O$: C 92.42, H 6.27, found: C 92.13, H 6.51.

5,5'-(3,7-di-*tert*-butyl-9,10-dihydroanthracene-1,5-diyl)bis(2-bromoterephthalaldehyde) (244)

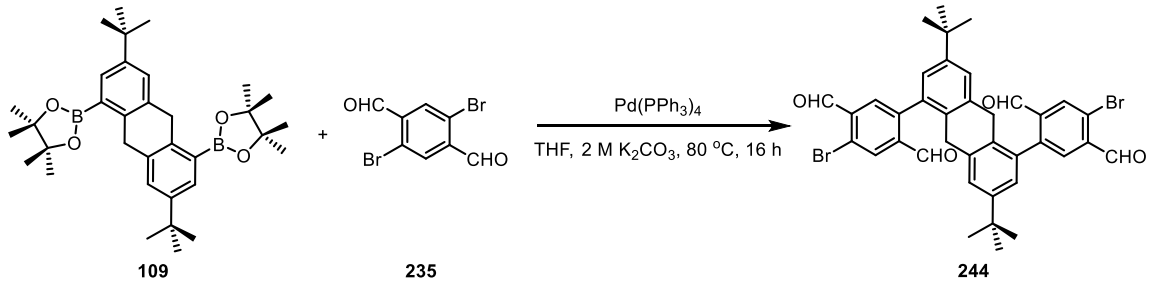

109 235 244

In a screw-capped glassy vial, a mixture of **109** (545 mg, 1 mmol), **235** (1.75 g, 6 mmol) was suspended in argon-degassed THF (8 mL) and 2M aq. K_2CO_3 (2 mL). $Pd(PPh_3)_4$ (116 mg, 0.1 mmol) was then added. The mixture was stirred at 80 °C for 16 hours. After cooling down to room temperature, the mixture was diluted with chloroform (100 mL). The organic phase was washed with water (3 × 100 mL) and dried over anhydrous Na_2SO_4. After removal of the solvent by rotary evaporation, the crude product was purified by silica gel column chromatography (petroleum ether/chloroform 1:1 to 1:2) to give the product **244** as a light-yellow solid (400 mg, 56 %).

m.p.: 353 °C (dec.). ^{1}H NMR (400 MHz, $CDCl_3$) δ (ppm) = 10.51 (d, J = 0.6 Hz, 2H), 9.77 (d, J = 5.1 Hz, 2H), 8.35 (s, 2H), 7.95 (s, 2H), 7.19 (d, J = 1.9 Hz, 2H), 7.08 (t, J = 2.3 Hz, 2H), 3.68 (m, 4H), 1.27 (s, 18H). ^{13}C NMR (101 MHz, $CDCl_3$) δ (ppm) = 191.19, 190.32, 190.29, 149.65, 149.61, 144.30, 144.28, 138.41, 138.37, 136.71, 136.68, 136.22, 136.20, 133.30, 133.29, 132.74, 132.73, 132.70, 131.92, 131.82, 125.75, 125.74, 125.61, 125.50, 34.51, 34.29, 31.29. FT-IR (ATR) $\tilde{\nu}$ (cm^{-1}) = 2961 (w), 2864 (w), 1691 (s), 1604 (w), 1476 (w), 1459 (w), 1419 (w), 1394 (w), 1372 (s), 1334 (w), 1305 (w), 1277 (w), 1251 (w), 1202 (w), 1179 (w), 1150 (s), 1107 (w), 1001 (m), 903 (w), 865 (m), 803 (m), 738 (m), 663 (w). MALDI HRMS (DCTB) (*m*/*z*): $[M+Na]^+$ calcd. for $C_{38}H_{34}O_4Br_2Na$, 737.0705; found, 737.0680. Elemental anal. calcd. for $C_{38}H_{34}BR_2O_4\cdot 0.5H_2O$: C 63.08, H 4.88, found: C 62.95, H 5.08.

(9r,10r)-3-(3,7-di-*tert*-butyl-5-(4,4,5,5-tetramethyl-1,3,2-dioxaborolan-2-yl)-9,10-dihydroanthracen-1-yl)-9,10-dihydro-9,10-[1,2]benzenoanthracene-2-carbaldehyde (247)

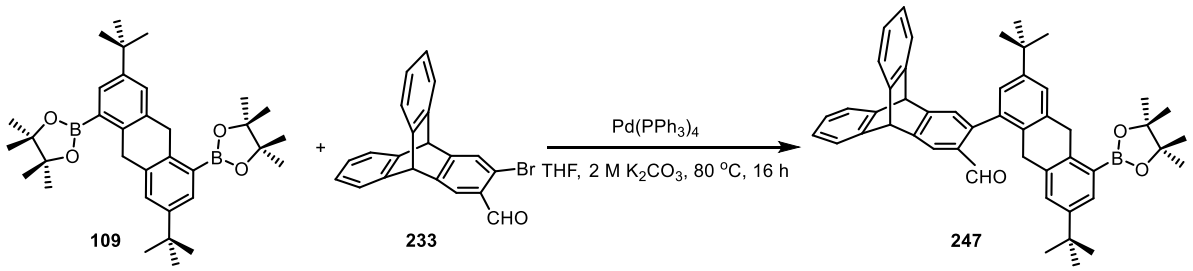

109 233 247

In a screw-capped glassy vial, a mixture of **233** (361 mg, 1 mmol) and **109** (3.27 g, 6 mmol) was suspended in argon-degassed THF (5 mL) and 2M aq. K_2CO_3 (1.3 mL). $Pd(PPh_3)_4$ (58 mg, 0.05

mmol) was then added. The mixture was stirred at 80 °C for 16 hours. After cooling down to room temperature, the mixture was diluted with dichloromethane (100 mL). The organic phase was washed with sat. aq. NH_4Cl (3 × 100 mL) and dried over anhydrous Na_2SO_4. After removal of the solvent by rotary evaporation, the crude product was purified by silica gel column chromatography (petroleum ether/dichloromethane/ethyl acetate 40:4:1 to 30:4:1) to give the product **247** as a colorless solid (470 mg, 67 %).

m.p.: 277 °C (dec.). ^{1}H NMR (600 MHz, $CDCl_3$) δ (ppm) = 9.61 (s, 1H), 8.08 (s, 1H), 7.71 (d, J = 2.2 Hz, 1H), 7.53 - 7.51 (m, 1H), 7.49 - 7.45 (m, 2H), 7.45 - 7.43 (m, 1H), 7.39 (s, 1H), 7.35 (d, J = 1.8 Hz, 1H), 7.14 (d, J = 1.8 Hz, 1H), 7.14 - 7.08 (m, 2H), 7.08 - 7.04 (m, 2H), 7.00 (d, J = 1.9 Hz, 1H), 5.62 (s, 1H), 5.53 (s, 1H), 4.40-4.37 (m, 1H), 4.26-4.23 (m, 1H), 3.64 - 3.51 (m, 2H), 1.41 (s, 12H), 1.30 (s, 9H), 1.26 (s, 9H). ^{13}C NMR (151 MHz, $CDCl_3$) δ (ppm) = 192.22, 150.70, 148.37, 147.85, 144.76, 144.67, 144.59, 144.43, 144.07, 144.02, 140.59, 138.27, 136.02, 135.05, 132.67, 131.49, 130.69, 127.57, 126.47, 125.72, 125.62, 125.51, 124.71, 124.11, 123.97, 123.94, 123.89, 121.31, 83.46, 54.16, 53.67, 35.72, 34.40, 34.38, 34.32, 31.43, 31.40, 24.94. FT-IR (ATR) $\tilde{\nu}$ (cm^{-1}) = 2964 (m), 2906 (w), 2867 (w), 1682 (m), 1602 (w), 1476 (m), 1460 (m), 1410 (w), 1388 (m), 1369 (s), 1308 (m), 1256 (m), 1197 (w), 1142 (s), 1107 (w), 1022 (w), 975 (w), 962 (w), 921 (w), 897 (m), 853 (m), 832 (w), 797 (w), 785 (w), 744 (s), 698 (w), 672 (w), 629 (m), 613 (w). MALDI HRMS (DCTB) (*m*/*z*): $[M+Na]^+$ calcd. for $C_{49}H_{51}BO_3Na$, 721.3838, found, 721.3825. Elemental anal. calcd. for $C_{49}H_{51}BO_3 \cdot 0.4H_2O$: C 83.37, H 7.40, found: C 83.47, H 7.42.

2-(3,7-di-*tert*-butyl-5-((*9r*,*10r*)-3-formyl-9,10-dihydro-9,10-[1,2]benzenoanthracen-2-yl)-9,10-dihydroanthracen-1-yl)-5-(3,7-di-*tert*-butyl-5-(4-(3,7-di-*tert*-butyl-5-(3-formyl-9,10-dihydro-9,10-[1,2]benzenoanthracen-2-yl)-9,10-dihydroanthracen-1-yl)-2,5-diformylphenyl)-9,10-dihydroanthracen-1-yl)terephthalaldehyde (246)

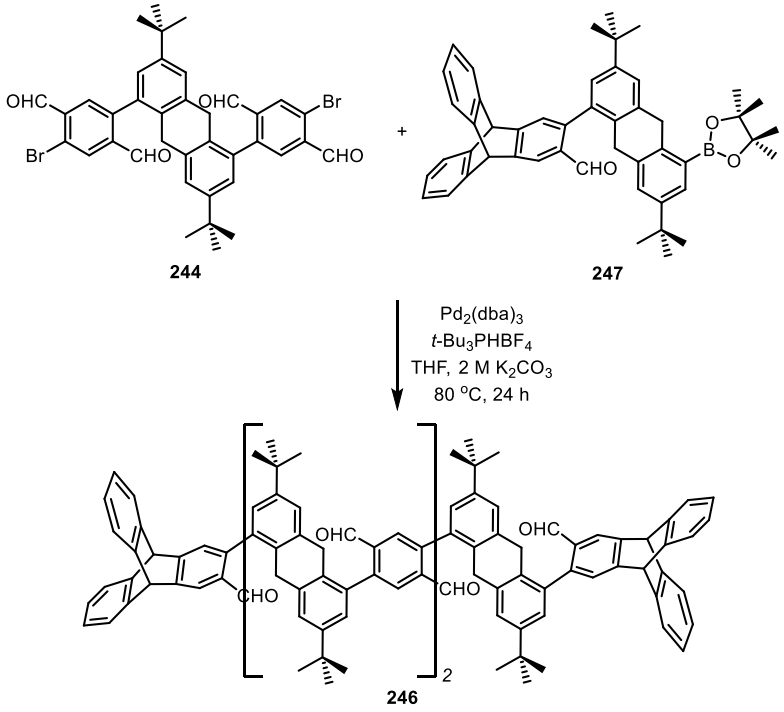

In a screw-capped glassy vial, a mixture of dibromide **244** (100 mg, 0.14 mmol) and **247** (235 mg, 0.34 mmol) was suspended in argon-degassed THF (1.4 mL) and 2M aq. K_2CO_3 (0.35 mL). A mixture of $Pd_2(dba)_3$ (13 mg, 0.014 mmol) and *t*-Bu_3PHBF_4 (13 mg, 0.044 mmol) was then added. The mixture was stirred at 80 °C for 16 hours. After cooling down to room temperature, the mixture was diluted with dichloromethane (50 mL). The organic phase was washed with sat. aq. NH_4Cl (3 × 50 mL) and dried over anhydrous Na_2SO_4. After removal of the solvent by rotary evaporation, the crude product was purified by silica gel column chromatography (petroleum ether/chloroform/ethyl acetate 30:6:1 to 20:2:1) to give the product **246** as a colorless to yellowish solid (mixture of atropisomers, 41 mg, 17 %).

m.p.: 342 °C (dec.). ^{1}H NMR (400 MHz, CD_2Cl_2) δ (ppm) = 9.97 - 9.92 (m, 2H), 9.92 - 9.87 (m, 2H), 9.64 (d, *J* = 3.0 Hz, 1H), 9.62 (d, *J* = 3.7 Hz, 1H), 8.13 - 8.05 (m, 6H), 7.53 - 7.50 (m, 2H), 7.49 - 7.44 (m, 6H), 7.37 (s, 1H), 7.34 (s, 1H), 7.33 - 7.27 (m, 4H), 7.23 - 7.19 (m, 4H), 7.18 - 7.10 (m, 6H), 7.09 - 7.03 (m, 6H), 5.66 (d, *J* = 1.9 Hz, 2H), 5.59 (d, *J* = 3.0 Hz, 2H), 3.97 - 3.68 (m, 12H), 1.38 - 1.32 (m, 18H), 1.30 - 1.27 (m, 19H), 1.26 - 1.22 (m, 18H). ^{13}C NMR (101 MHz, CD_2Cl_2) δ (ppm) = 192.50, 192.48, 192.43, 192.39, 192.28, 192.25, 151.52, 151.50, 151.48, 149.85, 149.83, 149.80, 149.75, 149.73, 149.70, 149.48, 149.45, 149.41, 145.60, 145.58, 145.53, 145.33, 144.81, 144.69, 137.81, 137.71, 137.51, 137.16, 137.07, 137.03, 137.02, 133.00, 132.91, 132.90, 132.83, 132.75, 132.74, 132.26, 132.24, 132.23, 130.74, 130.69, 130.67, 130.64, 128.80, 127.09, 127.04, 126.35, 126.31, 126.29, 126.15, 125.23, 124.80, 124.62, 124.50, 124.45, 121.88, 35.04, 34.99, 34.95, 34.91, 34.84, 31.79, 31.73, 31.67. (Signals of triptycene bridgeheads overlay with those of DCM solvent.) MALDI-TOF MS (DCTB) (*m*/*z*): $[M]^+$ calcd. for $C_{124}H_{112}O_6$, 1697.849; found, 1696.293.

2,2'-(2,5-dibromo-1,4-phenylene)bis(1,3-dioxolane) (248)

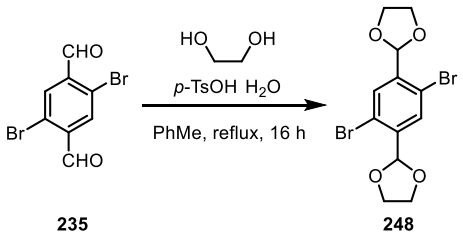

235 **248**

A mixture of **235** (993 mg, 3.4 mmol) and ethylene glycol (0.76 mL, 13.6 mmol) was suspended in toluene (20 mL). The mixture was refluxed overnight. After cooling down to room temperature, toluene was directly removed by rotary evaporation. The crude product was purified by silica gel column chromatography (petroleum ether/dichloromethane 1:1 to 1:2) to give the product **248** as a colorless solid (849 mg, 66 %).

m.p.: 186 °C. ^{1}H NMR (300 MHz, $CDCl_3$) δ (ppm) = 7.77 (s, 2H), 6.03 (s, 2H), 4.21 - 4.00 (m, 8H). ^{13}C NMR (75 MHz, $CDCl_3$) δ (ppm) = 139.15, 132.17, 121.74, 101.77, 65.53. FT-IR (ATR) $\tilde{\nu}$ (cm^{-1}) = 3099 (w), 2990 (w), 2951 (w), 2890 (m), 1982 (w), 1768 (w), 1486 (w), 1469 (w), 1377 (m), 1350 (m), 1333 (m), 1264 (w), 1227 (w), 1211 (w), 1178 (m), 1092 (m), 1051 (s), 1025 (s), 990 (m), 941 (s), 894 (m), 883 (m), 824 (m), 733 (w), 644 (w), 622 (w). EI MS (*m*/*z*): $[M]^+$ calcd. for $C_{12}H_{12}Br_2O_4$,

379.9, found, 379.0. Elemental anal. calcd. for $C_{12}H_{12}Br_2O_4$: C 37.93, H 3.18, found: C 37.89, H 3.31.

2,2',2'',2'''-((3,7-di-*tert*-butyl-9,10-dihydroanthracene-1,5-diyl)bis(5-bromobenzene-2,1,4-triyl))tetrakis(1,3-dioxolane) (249)

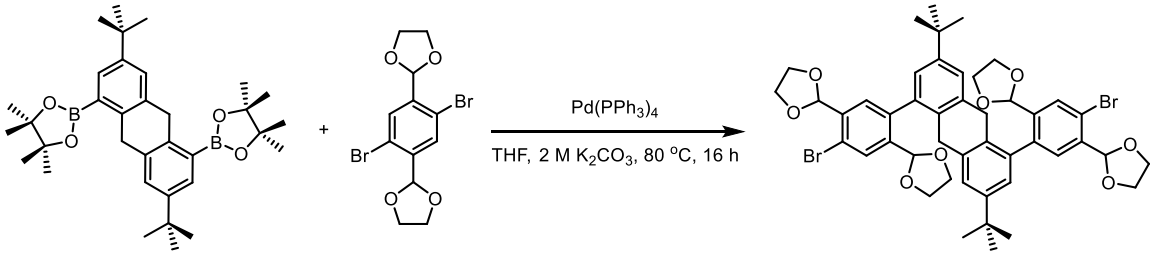

109 248 249

In a screw-capped glassy vial, a mixture of **109** (327 mg, 0.60 mmol) and **248** (1.37 g, 3.60 mmol) was suspended in argon-degassed THF (4.8 mL) and 2M aq. K_2CO_3 (1.2 mL). $Pd(PPh_3)_4$ (69 mg, 0.06 mmol) was then added. The mixture was stirred at 80 °C for 16 hours. After cooling down to room temperature, the mixture was diluted with chloroform (100 mL). The organic phase was washed with sat. aq. NH_4Cl (3 × 100 mL) and dried over anhydrous Na_2SO_4. After removal of the solvent by rotary evaporation, the crude product was purified by silica gel column chromatography (petroleum ether/chloroform 1:1 to 1:1.5) to give the product **249** as a colorless solid (mixture of atropisomers, 215 mg, 40 %).

m.p.: 336 °C (dec.). ^{1}H NMR (600 MHz, $CDCl_3$) δ (ppm) = 7.95 (s, 2H), 7.49 (s, 1H), 7.48 (s, 1H), 7.19 (s, 1H), 7.19 (s, 1H), 7.15 (d, J = 1.9 Hz, 1H), 7.13 (d, J = 1.9 Hz, 1H), 6.19 (s, 1H), 6.19 (s, 1H), 5.45 (s, 1H), 5.43 (s, 1H), 4.12 - 4.05 (m, 12H), 3.84 - 3.79 (m, 4H), 3.69 (s, 4H), 1.27 (s, 18H). ^{13}C NMR (151 MHz, $CDCl_3$) δ (ppm) = 148.22, 148.18, 140.64, 140.58, 138.33, 138.23, 137.11, 137.10, 136.80, 136.68, 136.00, 135.93, 132.13, 132.11, 131.46, 131.38, 129.84, 129.72, 125.44, 125.31, 124.41, 121.90, 121.85, 102.51, 102.49, 100.59, 100.51, 65.54, 65.47, 65.46, 65.39, 65.35, 65.34, 34.41, 34.21, 34.11, 31.36. FT-IR (ATR) $\tilde{\nu}$ (cm^{-1}) = 2958 (w), 2884 (w), 1605 (w), 1576 (w), 1476 (w), 1394 (w), 1376 (w), 1307 (w), 1254 (w), 1180 (m), 1076 (s), 1027 (w), 1000 (w), 967 (m), 943 (m), 897 (m), 826 (w), 742 (w), 696 (w), 655 (w). MALDI HRMS (DCTB) (*m*/*z*): $[M]^+$ calcd. for $C_{46}H_{50}Br_2O_8$, 888.1872; found, 888.1712. Elemental anal. calcd. for $C_{46}H_{50}Br_2O_8$: C 62.03, H 5.66, found: C 61.83, H 5.69.

2-((11r,16r)-2,7-di-*tert*-butyl-11,16-dihydro-4H-11,16-[1,2]benzenodibenzo[*a*,*de*]pentacen-5-yl)-4,4,5,5-tetramethyl-1,3,2-dioxaborolane (250)

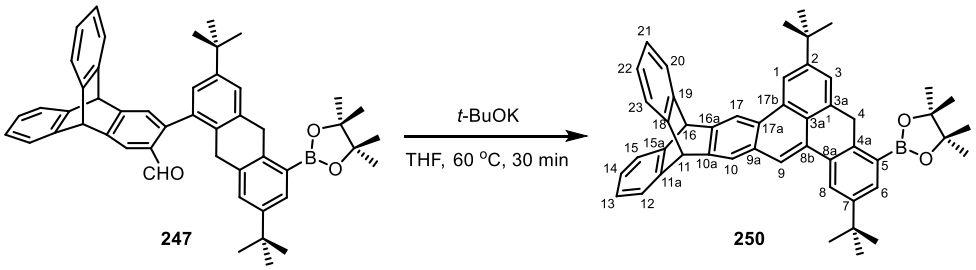

247 250

To a solution of **247** (49 mg, 0.07 mmol) in dry THF (2 mL) was added *t*-BuOK (16 mg, 0.14 mmol, 2 eq.) under argon atmosphere. The mixture was stirred at 60 °C for 30 minutes. The reaction was then quenched by adding 3 drops of 2M aq. HCl. The mixture was diluted with dichloromethane (50 mL). The organic phase was washed with water (3 × 30 mL) and dried over anhydrous Na_2SO_4. After removal of the solvent by rotary evaporation, the crude product was purified by silica gel column chromatography (petroleum ether/ethyl acetate 20:1 to 15:1) to give the product **250** as a light-pink solid (38 mg, 80 %).

m.p.: 301 °C (dec.). ^{1}H NMR (400 MHz, $CDCl_3$) δ (ppm)= 8.60 (s, 1H, H-17), 8.46 (s, 1H, H-1), 8.24 (d, J = 2.0 Hz, 1H, H-8), 8.10 (s, 1H, H-9), 7.93 (s, 1H, H-10), 7.86 (d, J = 2.1 Hz, 1H, H-6), 7.53 (d, J = 1.6 Hz, 1H, H-3), 7.51 - 7.43 (m, 4H, H-12, 15, 20, 23), 7.07 - 7.01 (m, 4H, H-13, 14, 21, 22), 5.69 (s, 1H, H-16), 5.59 (s, 1H, H-11), 4.79 (s, 2H, H-4), 1.53 (s, 9H), 1.45 (s, 9H), 1.42 (s, 12H). ^{13}C NMR (101 MHz, $CDCl_3$) δ (ppm) = 148.74 (C-18, 19, 15a, 11a), 148.15 (C-18, 19, 15a, 11a), 144.96 (C-2), 144.88 (C-7), 142.98 (C-10a), 142.67 (C-16a), 138.17 (C-4a), 134.15 (C-5), 132.98 (C-6), 131.52 (C-8a), 130.56 (C-9a), 130.20 (C-8b), 129.76 (C-3a), 128.12 (C-17a), 125.76 (C-3a^1), 125.39 (C-13, 14, 21, 22), 123.72 (C-3), 123.68 (C-12, 15, 20, 23), 123.13 (C-10), 123.10 (C-8), 118.00 (C-9), 117.18 (C-17), 115.89 (C-1), 83.55, 54.30 (C-16), 53.79 (C-11), 35.07, 34.66, 31.63, 31.48, 24.97. FT-IR (ATR) $\tilde{\nu}$ (cm^{-1}) = 2959 (m), 2907 (w), 2867 (w), 1610 (w), 1476 (m), 1461 (m), 1427 (w), 1411 (w), 1365 (m), 1343 (m), 1309 (m), 1258 (m), 1202 (w), 1140 (s), 1106 (w), 1025 (w), 996 (w), 964 (w), 940 (w), 889 (m), 852 (m), 830 (w), 785 (w), 746 (s), 705 (w), 680 (w), 628 (s). UV/Vis ($CHCl_3$): λ_{max} (nm) (log ε) = 268 (4.62), 274 (4.70), 291 (4.54), 322 (4.08), 345 (4.37), 361 (4.30), 379 (3.86). Fluorescence ($CHCl_3$): λ_{em} (λ_{ex}) (nm) = 382, 404, 428 (361). MALDI-TOF MS (DCTB, Kalib PEG600) (*m*/*z*): $[M]^+$ calcd. for $C_{49}H_{49}BO_2$, 680.383, found, 680.384. Elemental anal. calcd. for $C_{49}H_{49}BO_2 \cdot 0.4H_2O$: C 85.55, H 7.30, found: C 85.47, H 7.38.

Compound 251

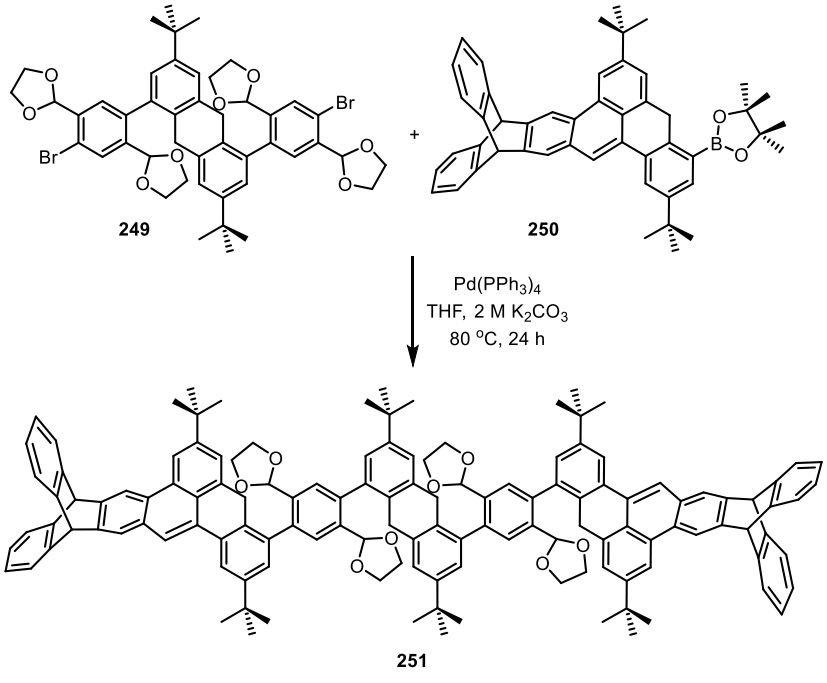

In a screw-capped glassy vial, a mixture of **249** (71 mg, 0.08 mmol) and **250** (218 mg, 0.32 mmol) was suspended in argon-degassed THF (0.8 mL) and 2M aq. K_2CO_3 (0.2 mL). $Pd(PPh_3)_4$ (9 mg, 0.008 mmol) was then added. The mixture was stirred at 80 °C for 16 hours. After cooling down to room temperature, the mixture was diluted with chloroform (50 mL). The organic phase was washed with sat. aq. NH_4Cl (3 × 40 mL) and dried over anhydrous Na_2SO_4. After removal of the solvent by rotary evaporation, the crude product was purified by silica gel column chromatography (petroleum ether/chloroform/ethyl acetate 30:6:1 to 20:10:1) to give the product **251** as a light-yellow solid (mixture of atropisomers, 64 mg, 43 %).

m.p.: >400 °C. ^{1}H NMR (600 MHz, $Cl_2CDCDCl_2$) δ (ppm) = 8.61 (s, 1H), 8.59 (s, 1H), 8.46 (s, 1H), 8.43 (s, 1H), 8.23 - 8.14 (m, 4H), 8.00 (s, 1H), 7.99 (s, 1H), 7.71 - 7.65 (m, 4H), 7.53 - 7.47 (m, 8H), 7.45 - 7.39 (m, 4H), 7.37 - 7.29 (m, 4H), 7.12 - 7.04 (m, 8H), 5.75 (s, 1H), 5.74 (s, 1H), 5.61 (s, 1H), 5.61 (s, 1H), 5.58 - 5.50 (m, 4H), 4.41 - 4.15 (m, 4H), 4.02 - 3.76 (m, 20H), 1.50 - 1.47 (m, 18H), 1.47 - 1.44 (m, 18H), 1.40 - 1.34 (m, 18H). ^{13}C NMR (151 MHz, $Cl_2CDCDCl_2$) δ (ppm) = 149.12, 149.02, 148.58, 148.56, 148.50, 148.47, 148.00, 147.91, 147.88, 147.75, 147.67, 144.67, 144.66, 144.62, 142.92, 142.87, 142.67, 142.66, 140.07, 139.95, 139.82, 138.49, 138.43, 137.08, 136.98, 136.92, 136.78, 136.70, 136.65, 136.61, 136.54, 136.48, 136.46, 136.39, 136.35, 136.27, 136.19, 136.15, 136.07, 136.00, 135.89, 135.83, 135.76, 135.73, 135.67, 135.62, 133.17, 133.08, 132.39, 131.99, 131.52, 131.41, 130.21, 130.16, 130.12, 129.88, 129.77, 129.60, 129.58, 129.01, 128.93, 128.87, 128.78, 128.73, 128.45, 128.34, 128.12, 128.05, 127.77, 127.74, 125.39, 124.23, 124.13, 123.86, 123.24, 119.64, 119.38, 118.11, 117.07, 115.97, 115.84, 101.43, 101.37, 101.32, 101.20, 101.13, 101.07, 101.03, 65.24, 65.17, 53.78, 53.39, 34.88, 34.83, 34.63, 34.61, 34.30, 34.26, 34.23, 31.41, 31.38, 31.32, 31.28. FT-IR (ATR) $\tilde{\nu}$ (cm^{-1}) = 2957 (m), 2873 (w), 1608 (w), 1574 (w), 1476 (m), 1461 (m), 1424 (w), 1393 (w), 1365 (m), 1260 (w), 1182 (m), 1141 (w), 1079 (s), 1028 (w), 967 (m), 944 (m), 893 (s), 790 (w), 744 (s), 700 (w), 668 (w), 628 (s). MALDI HRMS (DCTB) (*m*/*z*): $[M]^+$ calcd. for $C_{132}H_{124}O_8$, 1836.9251; found, 1836.9327. Elemental anal. calcd. for $C_{132}H_{124}O_8 \cdot 6.5H_2O$: C 81.08, H 7.06, found: C 81.08, H 6.73.

Compound 252

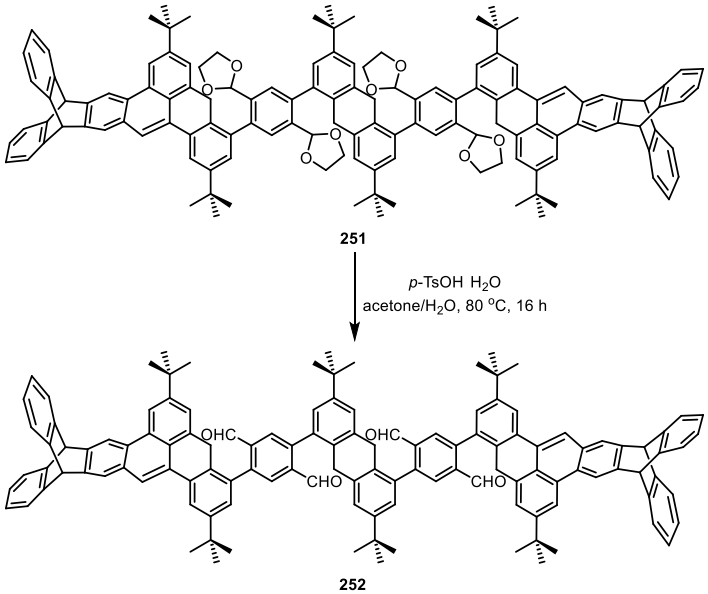

In a screw-capped glassy vial, compound **251** (46 mg, 0.025 mmol) was suspended in acetone/water (1.2 mL/0.3 mL). *p*-TsOH·H_2O (57 mg, 0.30 mmol) was then added. The mixture was stirred at 80 ºC for 16 hours. After cooling down to room temperature, the mixture was diluted with chloroform (50 mL). The organic phase was washed with sat. aq. NH_4Cl (3 × 40 mL) and dried over anhydrous Na_2SO_4. After removal of the solvent by rotary evaporation, the crude product was purified by flash silica gel column chromatography (petroleum ether/chloroform/ethyl acetate 20:5:1) to give the product **252** as a light-yellow solid (mixture of atropisomers, 38 mg, 91 %).

m.p.: >400 ºC. ^{1}H NMR (400 MHz, $Cl_2CDCDCl_2$) δ (ppm) = 10.06 - 9.97 (m, 2H), 9.97 - 9.92 (m, 2H), 8.61 (s, 1H), 8.60 (s, 1H), 8.48 (s, 1H), 8.45 (s, 1H), 8.28 (s, 2H), 8.23 (s, 1H), 8.22 (s, 1H), 8.19 - 8.10 (m, 4H), 8.02 (s, 1H), 8.01 (s, 1H), 7.54 - 7.46 (m, 8H), 7.40 - 7.30 (m, 4H), 7.30 - 7.23 (m, 4H), 7.13 - 7.04 (m, 8H), 5.75 (s, 1H), 5.74 (s, 1H), 5.62 (s, 1H), 5.62 (s, 1H), 4.40 - 3.77 (m, 8H), 1.50 (s, 9H), 1.48 (s, 9H), 1.46 (s, 9H), 1.45 - 1.42 (m, 9H), 1.38 - 1.32 (m, 18H). ^{13}C NMR (101 MHz, $Cl_2CDCDCl_2$) δ (ppm) = 192.16, 192.09, 192.02, 191.96, 149.57, 149.49, 149.16, 149.12, 144.57, 144.30, 144.19, 144.16, 143.16, 143.11, 143.05, 143.02, 137.07, 136.72, 135.68, 134.18, 134.15, 134.08, 134.04, 132.45, 132.37, 132.03, 131.98, 130.13, 130.01, 129.93, 129.68, 129.63, 129.47, 128.87, 127.90, 125.41, 125.21, 125.16, 123.85, 123.31, 118.79, 117.06, 116.37, 116.29, 53.84, 53.43, 34.82, 34.66, 34.30, 31.37, 31.29, 31.25. FT-IR (ATR) $\tilde{\nu}$ (cm^{-1}) = 3068 (w), 2958 (m), 2906 (w), 2867 (w), 2743 (w), 1691 (s), 1608 (w), 1574 (w), 1477 (m), 1460 (m), 1424 (w), 1392 (m), 1370 (m), 1277 (w), 1240 (w), 1200 (w), 1151 (m), 1023 (w), 893 (m), 817 (w), 787 (w), 743 (m), 700 (w), 628 (m). MALDI HRMS (DCTB) (*m*/*z*): $[M]^+$ calcd. for $C_{124}H_{108}O_4$, 1660.8247; found, 1660.8303. Elemental anal. calcd. for $C_{124}H_{108}O_4 \cdot 4H_2O$: C 85.88, H 6.74, found: C 85.75, H 6.80.

PO-13 (230)

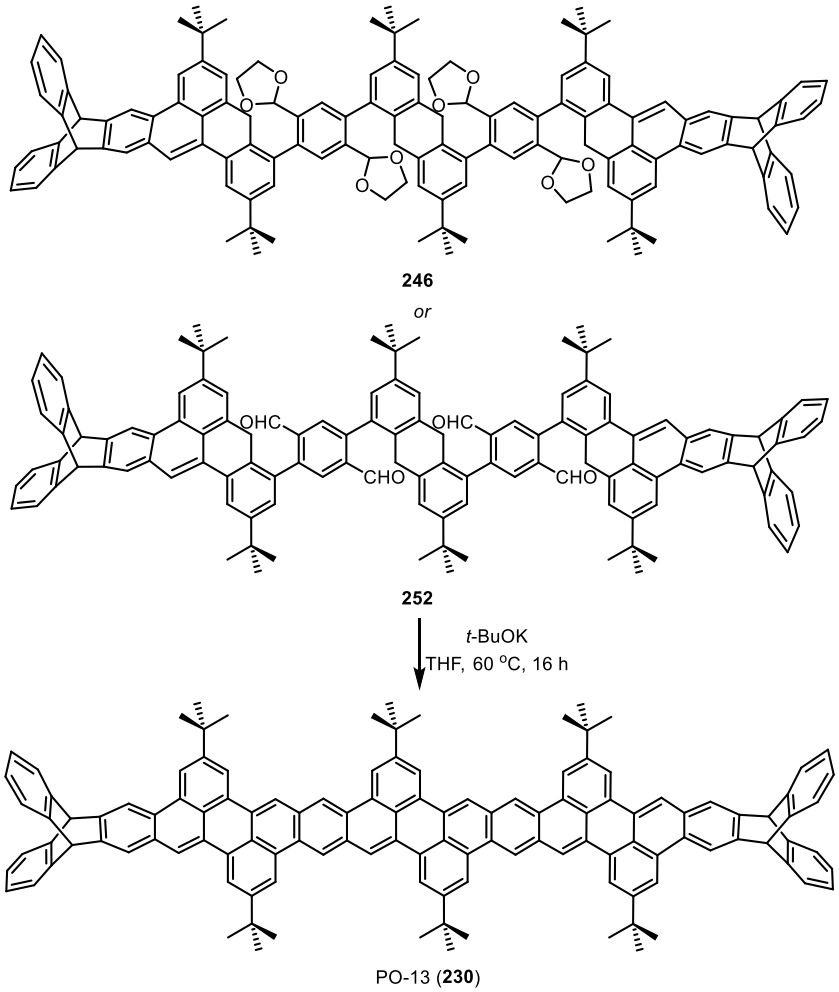

From 246: To a solution of compound **246** (17 mg, 0.01 mmol) in dry THF (1.5 mL) was added *t*-BuOK (22 mg, 0.2 mmol) under argon. The mixture was stirred at 60 °C for 16 hours in a screw-capped glassy vial. After cooling down to room temperature, the reaction was quenched by adding 2 drops of 2M aq. HCl. After stirring for ten minutes, the mixture was dropped into methanol (3 mL). The suspension was then filtered off and the solid was washed with water (2 × 2 mL) and methanol (2 × 2 mL). The product was obtained after drying in vacuum as a dark-red solid (15 mg, 94 %).

From 252: To a solution of compound **252** (13 mg, 7.82 µmol) in dry THF (1.3 mL) was added *t*-BuOK (12 mg, 0.11 mmol) under argon. The mixture was stirred at 60 °C for 16 hours in a screw-capped glassy vial. After cooling down to room temperature, the reaction was quenched by adding two drops of 2M aq. HCl. After stirring for 10 minutes, the mixture was dropped into methanol (3 mL). The suspension was then filtered off and the solid was washed with water (2 mL × 2) and methanol (2 mL × 2). The product was obtained after drying in vacuum as a dark-red solid (11 mg, 92 %).

m.p.: >400 °C. FT-IR (ATR) $\tilde{\nu}$ (cm^{-1}) = 3067 (w), 2956 (s), 2908 (w), 2868 (w), 1719 (w), 1687 (w), 1655 (w), 1603 (m), 1562 (w), 1540 (w), 1460 (m), 1434 (w), 1418 (w), 1393 (w), 1363 (m), 1291 (w), 1252 (m), 1201 (w), 1159 (w), 1086 (w), 1023 (w), 890 (s), 869 (s), 803 (w), 786 (w), 765 (w), 742 (s), 663 (w), 626 (s). UV/Vis ($CHCl_3$): λ_{max} (nm) (log ε) = 265 (5.31), 322 (4.98), 335

(5.04), 381 (4.58), 405 (4.66), 473 (4.91), 499 (5.13), 534 (5.22). Fluorescence ($CHCl_3$): λ_{em} (λ_{ex}) (nm) = 549, 591, 645 (499). Φ= 83±1%. τ= 1.4 ns. MALDI HRMS (DCTB) (*m*/*z*): $[M]^+$ calcd. for $C_{124}H_{100}$, 1589.7858; found, 1589.7857.

Compound 255

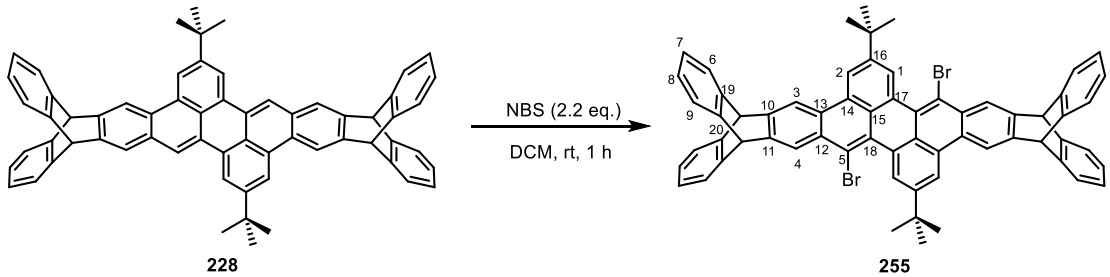

228 255

To a suspension of **228** (98 mg, 0.12 mmol) in dichloromethane (12 mL) was added *N*-bromosuccinimide (NBS, 47 mg, 0.264 mmol, 2.2 eq.) in one portion at room temperature. The mixture was stirred at room temperature for one hour. The reaction mixture was directly passed through a short pad of Celite®, followed by concentrated to ~2 mL by rotary evaporation. The residue was dropped into methanol (15 mL) to precipitate. The product was collected by filtration and rinse with methanol (2 mL) as a pale-yellow solid after drying in vacuum (103 mg, 88 %).

m.p.: >400 °C. ^{1}H NMR (600 MHz, $CDCl_3$) δ (ppm) = 8.84 (d, *J* = 1.4 Hz, 2H, H-1), 8.66 (s, 2H, H-3), 8.66 (s, 2H, H-4), 8.58 (d, *J* = 1.2 Hz, 2H, H-2), 7.52 - 7.49 (m, 8H, H-6,9), 7.07 - 7.04 (m, 8H, H-7,8), 5.76 (s, 2H, H-bridgehead), 5.71 (s, 2H, H-bridgehead), 1.53 (s, 18H). ^{13}C NMR (151 MHz, $CDCl_3$) δ (ppm) = 148.03 (C-16), 144.63 (C-19), 144.50 (C-20), 144.25 (C-10), 144.00 (C-11), 130.29 (C-14), 129.62 (C-18), 129.39 (C-12), 128.63 (C-13), 128.30 (C-17), 128.08 (C-1), 127.94 (C-15), 125.58 (C-7), 125.53 (C-8), 123.93 (C-4), 123.80 (C-6,9), 119.77 (C-5), 117.97 (C-2), 117.07 (C-3), 53.93 (C-bridgehead), 53.91 (C-bridgehead), 35.35, 31.31. FT-IR (ATR) $\tilde{\nu}$ (cm^{-1}) = 3067 (w), 3041 (w), 3020 (w), 2957 (m), 2906 (w), 2868 (w), 1941 (w), 1902 (w), 1786 (w), 1722 (w), 1675 (w), 1604 (w), 1561 (w), 1493 (w), 1475 (w), 1459 (m), 1430 (w), 1408 (w), 1363 (w), 1271 (w), 1253 (w), 1232 (w), 1203 (w), 1180 (w), 1157 (w), 1139 (w), 1108 (w), 1047 (w), 1023 (w), 1007 (w), 974 (w), 934 (w), 907 (w), 882 (m), 834 (w), 804 (w), 785 (w), 742 (s), 701 (w), 666 (w), 628 (m). UV/Vis ($CHCl_3$): λ_{max} (nm) (log ε) = 258 (4.95), 267 (4.86), 292 (4.48), 306 (4.59), 318 (4.67), 344 (3.90), 402 (4.30), 422 (4.50), 446 (4.54). Fluorescence ($CHCl_3$): λ_{em} (λ_{ex}) (nm) = 475 (318). Φ = 21±1%. τ = 0.79 ns. MALDI HRMS (DCTB) (*m*/*z*): $[M]^+$ calcd. for $C_{64}H_{46}Br_2$, 974.1956; found, 974.1955. Elemental anal. calcd. for $C_{64}H_{46}Br_2 \cdot 0.5H_2O$: C 78.13, H 4.82, found: C 78.09, H 4.93.

Compound 256

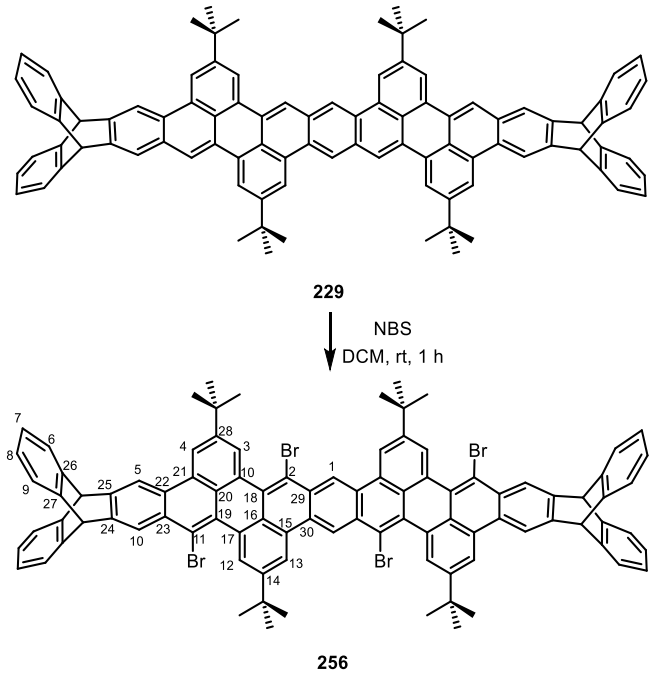

To a suspension of **229** (60 mg, 0.05 mmol) in dichloromethane (5 mL) was added NBS (40 mg, 0.0225 mmol, 4.5 equiv., dissolved in 3 mL dichloromethane) dropwise at room temperature. The mixture was stirred at room temperature for 1 hour. The reaction mixture was directly passed through a short pad of Celite®, followed by concentrated to ~3 mL by rotary evaporation. The residue was dropped into methanol (15 mL) to precipitate. The product was collected by filtration and rinse with methanol (2 mL) as a dark-orange solid after drying in vacuum (71 mg, 94 %).

m.p.: >400 °C. ^{1}H NMR (600 MHz, $Cl_2CDCDCl_2$) δ (ppm) = 9.96 (s, 2H, H-1), 9.04 (d, J = 0.9 Hz, 2H, H-3), 8.95 (d, J = 1.0 Hz, 2H, H-12), 8.91 (s, 2H, H-13), 8.71 (s, 2H, H-5), 8.68 (s, 2H, H-10), 8.67 (d, J = 1.1 Hz, 2H, H-4), 7.56 - 7.54 (m, 4H, H-6, 9), 7.54 - 7.52 (m, 4H, H-6, 9), 7.11 - 7.10 (m, 4H, H-7, 8), 7.10 - 7.09 (m, 4H, H-7, 8), 5.83 (s, 2H, H-bridgehead), 5.75 (s, 2H, H-bridgehead), 1.60 (s, 18H), 1.59 (s, 18H). ^{13}C NMR (151 MHz, $Cl_2CDCDCl_2$) δ (ppm) = 148.85 (C-14), 148.41 (C-28), 144.39 (C-24), 144.36 (C-25), 144.28 (C-26, 27), 131.06 (C-15), 130.60 (C-18), 129.97 (C-23), 129.72 (C-21), 129.57 (C-19), 129.18 (C-30), 129.10 (C-17), 128.64 (C-3), 128.57 (C-12), 128.36 (C-29), 128.02 (C-22), 127.77 (C-16), 127.72 (C-20), 125.55 (C-triptycene), 124.04 (C-triptycene), 123.99 (C-triptycene), 123.79 (C-10), 123.69 (C-1), 119.95 (C-11), 119.65 (C-2), 118.54 (C-13), 118.49 (C-4), 117.03 (C-5), 53.55 (C-bridgehead), 53.52 (C-bridgehead), 35.28, 35.21, 31.23, 31.15. FT-IR (ATR) $\tilde{\nu}$ (cm^{-1}) = 3068 (w), 2961 (m), 2906 (w), 2869 (w), 1719 (w), 1606 (w), 1520 (w), 1461 (m), 1431 (w), 1417 (w), 1364 (w), 1342 (w), 1270 (w), 1232 (w), 1201 (w), 1158 (w), 1097 (w), 1013 (w), 934 (w), 905 (w), 875 (m), 835 (m), 804 (w), 789 (w), 767 (w), 744 (s), 702 (w), 666 (w), 628 (m). UV/Vis ($CHCl_3$): λ_{max} (nm) (log ε) = 277 (5.16), 325 (4.84), 337 (4.87), 388 (4.41), 444 (4.69), 468 (4.93), 500 (4.99). Fluorescence ($CHCl_3$): λ_{em} (λ_{ex}) (nm) = 533 (337). Φ = 44±1%. τ = 0.86 ns. MALDI HRMS (DCTB) (m/z): $[M]^+$ calcd. for $C_{94}H_{70}Br_4$, 1518.2195; found, 1518.2184.

Compound 257

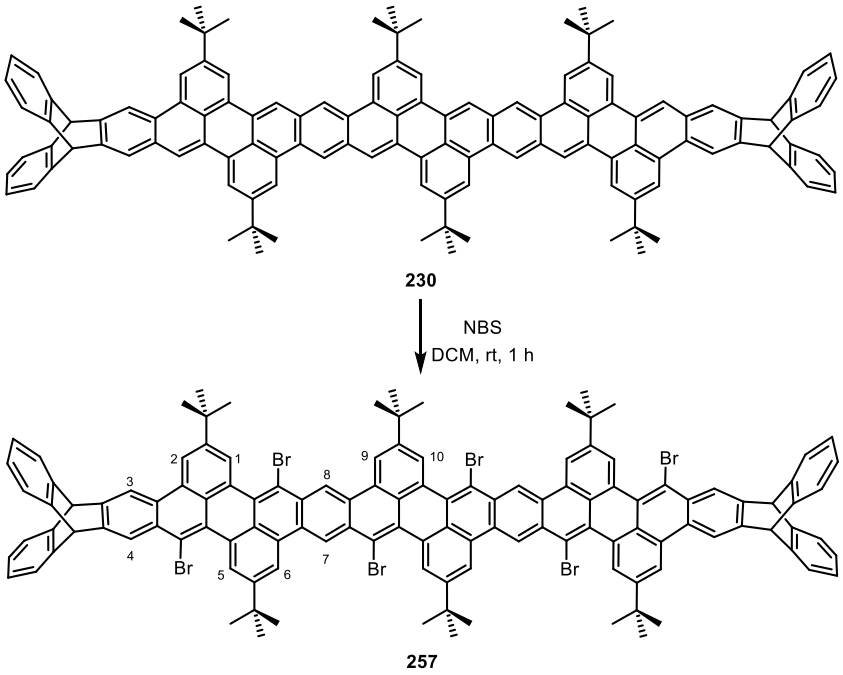

To a suspension of **230** (10 mg, 6.3 µmol) in dichloromethane (1 mL) was added NBS (8 mg, 44 µmol, 7 eq., dissolved in 0.7 mL dichloromethane) dropwise at room temperature. The mixture was stirred at room temperature for 2 hours. The mixture was then dropped into methanol (10 mL) to precipitate. The product was collected by filtration and rinse with methanol (2 mL) as a red solid after drying in vacuum (11 mg, 85 %).

m.p.: >400 °C. ^{1}H NMR (600 MHz, $CDCl_3$) δ (ppm) = 10.02 (br, 2H, H-8), 9.95 (br, 2H, H-7), 9.23 - 9.13 (m, 2H, H-10), 9.13 - 9.01 (m, 4H, H-1,5), 9.01 - 8.87 (m, 4H, H-6,9), 8.74 (d, J = 7.5 Hz, 2H, H-3), 8.73 - 8.59 (m, 4H, H-4,2), 7.54 (br, 8H, H-triptycene), 7.08 (br, 8H, H-triptycene), 5.80 (s, 2H), 5.75 (s, 2H), 1.68 - 1.54 (m, 54H). FT-IR (ATR) $\tilde{\nu}$ (cm^{-1}) = 3069 (w), 2957 (m), 2928 (m), 2866 (w), 1741 (w), 1605 (m), 1518 (w), 1460 (m), 1432 (m), 1415 (m), 1363 (m), 1340 (w), 1268 (m), 1230 (w), 1200 (m), 1157 (w), 1138 (w), 1099 (w), 1017 (m), 933 (w), 905 (w), 874 (s), 837 (m), 803 (w), 774 (w), 742 (s), 705 (w), 666 (w), 626 (m). UV/Vis ($CHCl_3$): λ_{max} (nm) (log ε) = 274 (5.08), 304 (4.90), 325 (4.82), 337 (4.86), 384 (4.42), 405 (4.48), 460 (4.73), 485 (4.98), 518 (5.08). Fluorescence ($CHCl_3$): λ_{em} (λ_{ex}) (nm) = 544 (337). Φ = 33±1%. τ = 0.34 ns. MALDI HRMS (DCTB) (m/z): $[M]^+$ calcd. for $C_{124}H_{94}Br_6$, 2064.2432; found, 2064.2551.

Compound 258

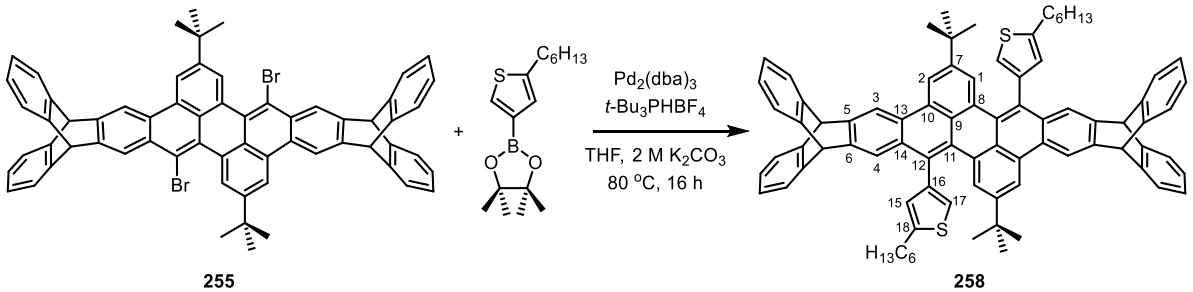

In a screw-capped glassy vial, a mixture of dibromide **255** (35 mg, 0.036 mmol) and 2-(5-hexylthiophen-3-yl)-4,4,5,5-tetramethyl-1,3,2-dioxaborolane (42 mg, 0.144 mmol) was suspended in argon-degassed THF (0.24 mL) and 2M aq. K_2CO_3 (0.06 mL). A mixture of $Pd_2(dba)_3$ (3.3 mg, 3.6 μmol) and *t*-Bu_3PHBF_4 (3.3 mg, 11.4 μmol) was then added. The mixture was stirred at 80 °C for 16 hours. After cooling down to room temperature, the mixture was diluted with dichloromethane (50 mL). The organic phase was washed with sat. aq. NH_4Cl (3 × 40 mL) and dried over anhydrous Na_2SO_4. After removal of the solvent by rotary evaporation, the crude product was purified by silica gel column chromatography (petroleum ether/ethyl acetate 50:1 to 30:1) to give the product **258** as a yellow solid (18 mg, 44 %).

m.p.: 262 °C. ^{1}H NMR (600 MHz, $CDCl_3$) δ (ppm) = 8.64 (s, 2H, H-3), 8.41 (d, J = 1.4 Hz, 2H, H-2), 7.80 (s, 2H, H-4), 7.71 (d, J = 1.2 Hz, 2H, H-1), 7.50 - 7.46 (m, 4H, H-triptycene), 7.44 - 7.37 (m, 4H, H-triptycene), 7.05 - 6.99 (m, 8H, H-triptycene), 6.94 (br, 2H, H-17), 6.77 (br, 2H, H-15), 5.69 (s, 2H, H-bridgehead), 5.46 (s, 2H, H-bridgehead), 2.85 (t, J = 7.5 Hz, 4H), 1.80 - 1.69 (m, 4H), 1.49 - 1.42 (m, 4H), 1.39 - 1.34 (m, 8H), 1.24 (s, 18H), 0.93 (t, J = 6.6 Hz, 6H). ^{13}C NMR (151 MHz, $CDCl_3$) δ (ppm) = 147.96 (C-7), 146.58 (C-18), 144.89 (C-triptycene), 144.81 (C-triptycene), 142.84 (C-5), 142.71 (C-6), 140.99 (C-16), 131.22 (C-11), 131.18 (C-14), 129.34 (C-12), 128.80 (C-10), 128.37 (C-15), 127.99 (C-9), 127.52 (C-13), 127.17 (C-1), 125.35 (C-triptycene), 125.31 (C-triptycene), 123.75 (C-triptycene), 123.68 (C-triptycene), 122.24 (C-17), 121.62 (C-4), 116.94 (C-3), 116.70 (C-2), 54.08 (C-bridgehead), 53.87 (C-bridgehead), 34.78, 31.63, 31.43, 31.35, 30.18, 29.05, 24.81, 22.68, 14.16. FT-IR (ATR) $\tilde{\nu}$ (cm^{-1}) = 3067 (w), 3019 (w), 2954 (m), 2927 (m), 2855 (w), 1604 (w), 1545 (w), 1500 (w), 1459 (m), 1430 (m), 1405 (w), 1362 (w), 1307 (w), 1274 (w), 1230 (w), 1204 (w), 1184 (w), 1159 (w), 1141 (w), 1105 (w), 1081 (w), 1023 (w), 967 (w), 934 (w), 888 (w), 868 (m), 816 (w), 803 (w), 744 (s), 702 (w), 684 (w), 654 (w), 628 (m). UV/Vis ($CHCl_3$): λ_{max} (nm) (log ε) = 259 (4.98), 297 (4.53), 308 (4.64), 322 (4.67), 346 (4.14), 430 (4.46), 447 (4.46). Fluorescence ($CHCl_3$): λ_{em} (λ_{ex}) (nm) = 492, 527 (322). Φ = 19±0.5%. τ = 1.5 ns. MALDI HRMS (DCTB) (*m*/*z*): $[M]^+$ calcd. for $C_{84}H_{76}S_2$, 1148.5388; found, 1148.5393.

Compound 173

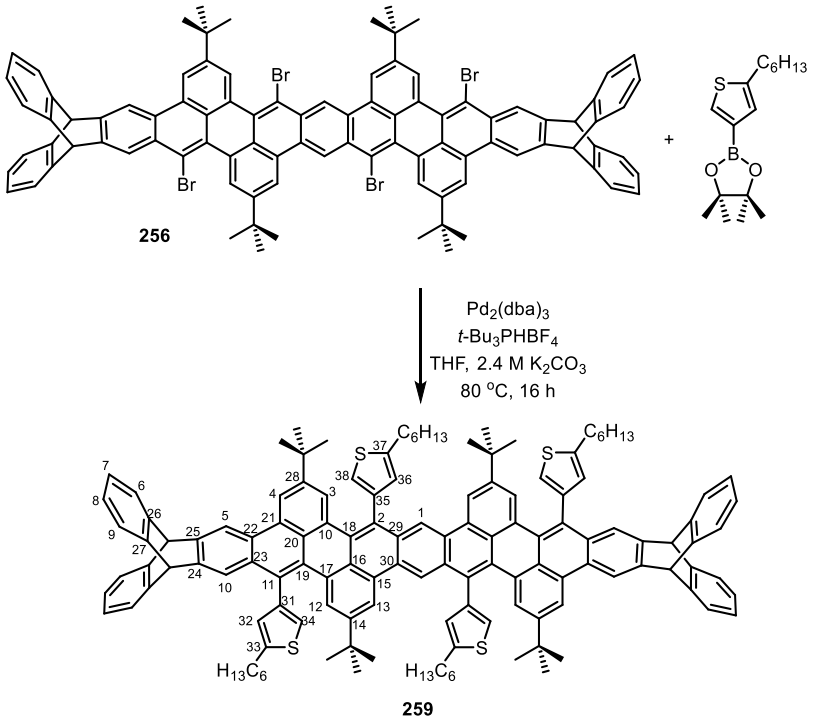

In a screw-capped glassy vial, a mixture of tetrabromide **256** (27 mg, 0.018 mmol) and 2-(5-hexylthiophen-3-yl)-4,4,5,5-tetramethyl-1,3,2-dioxaborolane (159 mg, 0.54 mmol, 30 equiv.) was suspended in argon-degassed THF (0.3 mL) and 2.4 M aq. K_2CO_3 (0.1 mL). A mixture of $Pd_2(dba)_3$ (2.5 mg, 2.7 µmol) and *t*-Bu_3PHBF_4 (2.5 mg, 8.5 µmol) was then added. The mixture was stirred at 80 °C for 16 hours. After cooling down to room temperature, the mixture was diluted with dichloromethane (50 mL). The organic phase was washed with sat. aq. NH_4Cl (3 × 40 mL) and dried over anhydrous Na_2SO_4. After removal of the solvent by rotary evaporation, the crude product was purified by silica gel column chromatography (hexane/ethyl acetate 40:1 to 35:1) to give the product **259** as an orange solid (6 mg, 18 %).

m.p.: 234 °C. ^{1}H NMR (600 MHz, $CDCl_3$) δ (ppm) = 9.06 (s, 2H , H-1), 8.67 (s, 2H , H-5), 8.48 (d, J = 1.4 Hz, 2H, H-4), 8.30 (s, 2H, H-13), 7.99 (s, 2H, H-3), 7.79 (s, 2H, H-12), 7.76 (s, 2H, H-10), 7.52 - 7.40 (m, 8H, H-6, 9), 7.03 (br, 16H, H-7, 8, 32, 34, 36, 38), 5.71 (s, 2H, H-bridgehead), 5.47 (s, 2H, H-bridgehead), 2.92 (br, 8H), 1.80 (br, 8H), 1.50 - 1.32 (m, 24H), 1.28 (s, 18H), 1.20 (s, 18H), 0.97 - 0.93 (m, 6H), 0.90 - 0.87 (m, 6H). ^{13}C NMR (151 MHz, $CDCl_3$) δ (ppm) = 148.17 (C-14), 147.96 (C-28), 147.04 (C-37), 146.74 (C-33), 144.91 (C-26,27), 144.83 (C-26,27), 142.91 (C-24), 142.72 (C-25), 141.14 (C-35), 141.12 (C-31), 132.02 (C-18), 131.49 (C-19), 131.39 (C-29), 131.16 (C-23), 129.61 (C-35), 129.58 (C-11), 129.04 (C-15), 128.99 (C-21), 128.62, 128.41 (C-36), 128.31 (C-32), 128.24 (C-16), 128.07 (C-20), 127.64 (C-3), 127.57 (C-30,22), 127.33 (C-12), 125.37 (C-7,8), 125.33 (C-7,8), 123.78 (C-6,9), 123.71 (C-6,9), 121.77 (C-10), 121.00 (C-1), 117.27 (C-13), 117.03 (C-4), 116.95 (C-5), 54.11 (C-bridgehead), 53.90 (C-bridgehead), 34.84, 34.73, 31.73, 31.65, 31.61, 31.46, 31.35, 31.21, 30.38, 30.23, 29.70, 29.27, 29.05, 22.70, 22.59, 14.16, 14.09. FT-IR (ATR) $\tilde{\nu}$ (cm^{-1}) = 2953 (m), 2926 (m), 2855 (m), 1605 (w), 1575 (w), 1547 (w), 1532 (w), 1497 (w), 1459 (m), 1434 (m), 1362 (w), 1274 (w), 1229 (w), 1202 (w), 1185 (w), 1159

(w), 1133 (w), 1085 (w), 1023 (w), 931 (w), 887 (m), 870 (m), 849 (w), 836 (w), 816 (w), 788 (w), 763 (w), 743 (s), 723 (m), 676 (w), 655 (w), 626 (m). UV/Vis ($CHCl_3$): λ_{max} (nm) (log ε) = 274 (5.22), 338 (4.94), 391 (4.44), 448 (4.68), 474 (4.92), 506 (4.97). Fluorescence ($CHCl_3$): λ_{em} (λ_{ex}) (nm) = 536 (338). Φ = 69±1%. τ = 1.7 ns. HRMS-MALDI (DCTB) (*m*/*z*): $[M]^+$ calcd. for $C_{134}H_{130}S_4$, 1867.9088; found, 1867.9135.

Compound 261

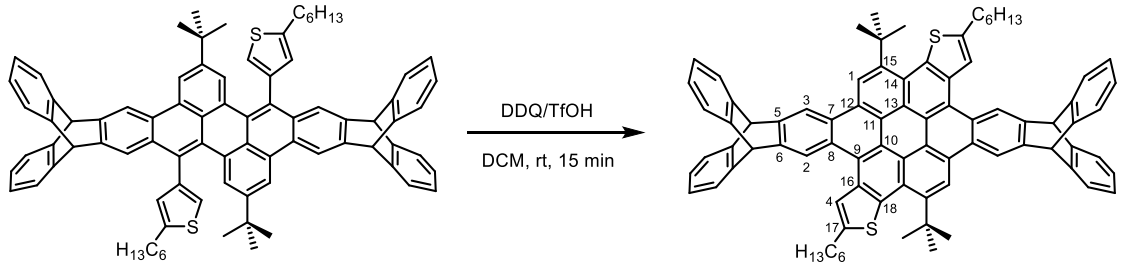

258 **261**

In a 25 mL Schlenk flask, a solution of **258** (14 mg, 12 µmol) in dry dichloromethane (7.2 mL) was purged with argon for 10 min. 2,3-Dichloro-5,6-dicyano-1,4-benzoquinone (DDQ, 8.2 mg, 36 µmol) was added in one portion at room temperature. Trifluoromethanesulfonic acid (TfOH, 0.24 mL) was then added dropwise. The mixture was stirred at room temperature for 15 minutes. The reaction was quenched by pouring into saturated aq. $NaHCO_3$ (10 mL). After stirring vigorously for 15 minutes, the mixture was extracted with dichloromethane (3 × 10 mL) and the organic layers combined. The organic phase was washed with aq. NH_4Cl (30 mL), water (30 mL) and dried over anhydrous Na_2SO_4. After removal of the solvent by rotary evaporation, the crude product mixture was purified by silica gel column chromatography (petroleum ether/chloroform/ethyl acetate 50:5:0 to 50:5:1). The product was obtained after precipitation from dichloromethane/methanol and drying in vacuum as a pale-yellow solid (7 mg, 51 %).

m.p.: >400 °C. ^{1}H NMR (600 MHz, $CDCl_3$) δ (ppm) = 9.50 (s, 2H, H-1), 9.31 (s, 2H, H-2), 9.10 (s, 2H, H-3), 8.25 (s, 2H, H-4), 7.62 - 7.53 (m, 8H, H-triptycene), 7.10 - 7.05 (m, 8H, H-triptycene), 5.92 (s, 2H, H-bridgehead), 5.83 (s, 2H, H-bridgehead), 3.16 (t, *J* = 7.5 Hz, 4H), 2.08 (s, 18H), 1.92 - 1.86 (m, 4H), 1.53 - 1.48 (m, 4H), 1.42 - 1.35 (m, 8H), 0.93 (t, *J* = 7.0 Hz, 6H). ^{13}C NMR (151 MHz, $CDCl_3$) δ (ppm) = 145.31 (C-17), 145.07 (C-triptycene), 145.01 (C-triptycene), 143.09 (C-15), 142.99 (C-5), 142.46 (C-6), 135.50 (C-18), 134.61 (C-16), 127.69 (C-7), 126.41 (C-8), 125.51 (C-triptycene), 125.47 (C-triptycene), 125.13 (C-14), 125.00 (C-10), 123.95 (C-triptycene), 123.92 (C-triptycene), 123.84 (C-triptycene), 123.18 (C-4), 122.71 (C-2), 122.62 (C-9), 122.29 (C-1), 122.01 (C-11), 121.57 (C-12), 118.43 (C-3), 54.32 (C-bridgehead), 54.27 (C-bridgehead), 37.28, 33.94, 31.65, 31.51, 30.48, 28.92, 22.64, 14.14. FT-IR (ATR) $\tilde{\nu}$ (cm^{-1}) = 3068 (w), 3019 (w), 2947 (w), 2925 (m), 2854 (w), 1590 (w), 1544 (w), 1455 (m), 1397 (w), 1365 (w), 1327 (w), 1298 (w), 1249 (w), 1211 (w), 1188 (w), 1166 (w), 1141 (w), 1108 (w), 1051 (w), 1023 (w), 936 (w), 917 (w), 898 (w), 873 (m), 841 (w), 821 (w), 790 (ms), 745 (s), 691 (w), 671 (w), 629 (m). UV/Vis ($CHCl_3$): λ_{max} (nm) (log ε) = 259 (5.05), 297 (4.35), 315 (4.29), 357 (4.93), 371 (5.22), 410 (4.40), 434 (4.40). Fluorescence ($CHCl_3$): λ_{em} (λ_{ex}) (nm) = 487, 516, 550 (371). Φ = 7.3±0.1%. τ = 1.4 ns. MALDI HRMS (DCTB) (*m*/*z*): $[M]^+$ calcd. for $C_{84}H_{72}S_2$, 1144.5075; found, 1144.5090.

Compound 262

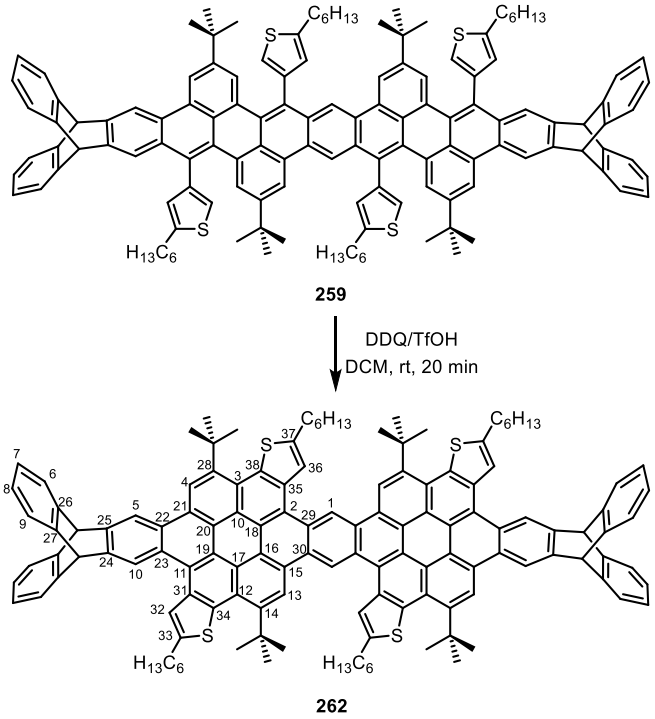

A 6 mL glassy vial charged with compound **259** (5 mg, 2.7 µmol) was purged with argon for 10 min. Dry dichloromethane (3 mL) was added to dissolve the substrate. DDQ (3 mg, 13.5 µmol, 5 eq.) was added in one portion at room temperature. TfOH (0.1 mL) was then added dropwise. The mixture was stirred at room temperature for 20 minutes. The reaction was quenched by pouring into saturated aq. $NaHCO_3$ (10 mL). After stirring vigorously for 15 minutes, the mixture was extracted with dichloromethane (3 × 10 mL) and the organic layers combined. The organic phase was washed with aq. NH_4Cl (30 mL), water (30 mL) and dried over anhydrous Na_2SO_4. After removal of the solvent by rotary evaporation, the crude product mixture was purified by silica gel column chromatography (hexane/chloroform/ethyl acetate 40:4:0 to 40:4:1). The product was obtained after precipitation from dichloromethane/methanol and drying in vacuum as a pale-yellow solid (2.5 mg, 50 %).

m.p.: >400 °C. ^{1}H NMR (600 MHz, $CDCl_3$) δ (ppm) = 11.07 (s, 2H, H-1), 10.04 (s, 2H, H-13), 9.57 (s, 2H, H-4), 9.35 (s, 2H, H-10), 9.15 (s, 2H, H-5), 8.90 (s, 2H, H-36), 8.27 (s, 2H, H-32), 7.63 - 7.56 (m, 8H, H-6,9), 7.12 - 7.07 (m, 8H, H-7,8), 5.96 (s, 2H, H-bridgehead), 5.87 (s, 2H, H-bridgehead), 3.29 (t, J = 7.5 Hz, 4H), 3.18 (t, J = 7.5 Hz, 4H), 2.23 (s, 18H), 2.20 (s, 18H), 2.06 - 2.00 (m, 4H), 1.93 - 1.88 (m, 4H), 1.54 - 1.49 (m, 8H), 1.43 - 1.35 (m, 16H), 0.92 (t, J = 6.9 Hz, 6H), 0.89 (t, J= 7.2 Hz, 6H). ^{13}C NMR (151 MHz, $CDCl_3$) δ (ppm) = 146.63 (C-37), 145.64 (C-33), 145.07 (C-26), 145.01 (C-27), 143.69 (C-14), 143.41 (C-28), 143.14 (C-24), 142.62 (C-25), 136.04 (C-35), 135.61 (C-38), 135.56 (C-31), 134.95 (C-34), 127.93 (C-29), 127.75 (C-30), 127.69 (C-22), 126.39 (C-12), 125.88 (C-23), 125.77 (C-3), 125.56 (C-7,8), 125.52 (C-7,8), 125.31 (C-2), 124.67 (C-17), 124.36 (C-18), 123.97 (C-6,9,19), 123.88 (C-6,9,19), 123.36 (C-32), 123.13 (C-1), 123.08 (C-36), 122.93 (C-4,13), 122.74 (C-16), 122.69 (C-10), 122.34 (C-11), 122.27 (C-20), 121.82 (C-15), 118.48 (C-5), 54.36 (C-bridgehead), 54.31 (C-bridgehead), 37.44, 37.37, 34.11, 33.95, 32.06,

31.68, 31.65, 31.53, 30.95, 30.49, 29.20, 28.92, 22.64, 22.62, 14.14, 14.10. FT-IR (ATR) $\tilde{\nu}$ (cm^{-1}) = 3068 (w), 3019 (w), 2953 (m), 2925 (m), 2854 (m), 1939 (w), 1900 (w), 1745 (w), 1588 (w), 1546 (w), 1454 (s), 1398 (w), 1365 (m), 1323 (w), 1288 (w), 1248 (w), 1186 (m), 1163 (m), 1139 (w), 1110 (w), 1084 (w), 1061 (w), 1023 (w), 917 (w), 899 (w), 873 (m), 838 (m), 789 (m), 739 (s), 689 (w), 627 (m), 607 (w). UV/Vis ($CHCl_3$): λ_{max} (nm) (log ε) = 261 (5.19), 280 (5.17), 320 (5.01), 355 (5.10), 372 (5.23), 399 (5.17), 422 (5.46), 465 (4.78), 495 (4.66). Fluorescence ($CHCl_3$): λ_{em} (λ_{ex}) (nm) = 514, 548 (422). Φ = 13±0.5%. τ = 1.1 ns. MALDI HRMS (DCTB) (*m*/*z*): $[M]^+$ calcd. for $C_{134}H_{122}S_4$, 1859.8462; found, 1859.8520.

6. References

[1] a) K. S. Novoselov, A. K. Geim, S. V. Morozov, D. Jiang, Y. Zhang, S. V. Dubonos, I. V. Grigorieva, A. A. Firsov, *Science* **2004**, *306*, 666-669; b) A. K. Geim, K. S. Novoselov, *Nat. Mater.* **2007**, *6*, 183-191; c) A. K. Geim, *Angew. Chem. Int. Ed.* **2011**, *50*, 6966-6985; *Angew. Chem.* **2011**, *123*, 7100-7122; d) K. S. Novoselov, *Angew. Chem. Int. Ed.* **2011**, *50*, 6986-7002; *Angew. Chem.* **2011**, *123*, 7123-7141.

[2] S. V. Morozov, K. S. Novoselov, M. I. Katsnelson, F. Schedin, D. C. Elias, J. A. Jaszczak, A. K. Geim, *Phys. Rev. Lett.* **2008**, *100*, 016602.

[3] C. Lee, X. Wei, J. W. Kysar, J. Hone, *Science* **2008**, *321*, 385-388.

[4] A. A. Balandin, S. Ghosh, W. Bao, I. Calizo, D. Teweldebrhan, F. Miao, C. N. Lau, *Nano Lett.* **2008**, *8*, 902-907.

[5] a) K. S. Novoselov, A. K. Geim, S. V. Morozov, D. Jiang, M. I. Katsnelson, I. V. Grigorieva, S. V. Dubonos, A. A. Firsov, *Nature* **2005**, *438*, 197-200; b) R. M. Westervelt, *Science* **2008**, *320*, 324-325.

[6] a) F. Schedin, A. K. Geim, S. V. Morozov, E. W. Hill, P. Blake, M. I. Katsnelson, K. S. Novoselov, *Nat. Mater.* **2007**, *6*, 652-655; b) V. Dua, S. P. Surwade, S. Ammu, S. R. Agnihotra, S. Jain, K. E. Roberts, S. Park, R. S. Ruoff, S. K. Manohar, *Angew. Chem. Int. Ed.* **2010**, *49*, 2154-2157; *Angew. Chem.* **2010**, *122*, 2200-2203.

[7] a) G. M. Scheuermann, L. Rumi, P. Steurer, W. Bannwarth, R. Mülhaupt, *J. Am. Chem. Soc.* **2009**, *131*, 8262-8270; b) D. R. Dreyer, C. W. Bielawski, *Chem. Sci.* **2011**, *2*, 1233-1240.

[8] a) M. Pumera, *Energy Environ. Sci.* **2011**, *4*, 668-674; b) Y. Sun, Q. Wu, G. Shi, *Energy Environ. Sci.* **2011**, *4*, 1113-1132.

[9] M. D. Stoller, S. Park, Y. Zhu, J. An, R. S. Ruoff, *Nano Lett.* **2008**, *8*, 3498-3502.

[10] T. Kuila, S. Bose, P. Khanra, A. K. Mishra, N. H. Kim, J. H. Lee, *Biosens. Bioelectron.* **2011**, *26*, 4637-4648.

[11] a) A. C. Ferrari, F. Bonaccorso, V. Fal'ko, K. S. Novoselov, S. Roche, P. Bøggild, S. Borini, F. H. L. Koppens, V. Palermo, N. Pugno, J. A. Garrido, R. Sordan, A. Bianco, L. Ballerini, M. Prato, E. Lidorikis, J. Kivioja, C. Marinelli, T. Ryhänen, A. Morpurgo, J. N. Coleman, V. Nicolosi, L. Colombo, A. Fert, M. Garcia-Hernandez, A. Bachtold, G. F. Schneider, F. Guinea, C. Dekker, M. Barbone, Z. Sun, C. Galiotis, A. N. Grigorenko, G. Konstantatos, A. Kis, M. Katsnelson, L. Vandersypen, A. Loiseau, V. Morandi, D. Neumaier, E. Treossi, V. Pellegrini, M. Polini, A. Tredicucci, G. M. Williams, B. Hee Hong, J.-H. Ahn, J. Min Kim, H. Zirath, B. J. van Wees, H. van der Zant, L. Occhipinti, A. Di Matteo, I. A. Kinloch, T. Seyller, E. Quesnel, X. Feng, K. Teo, N. Rupesinghe, P. Hakonen, S. R. T. Neil, Q. Tannock, T. Löfwander, J. Kinaret, *Nanoscale* **2015**, *7*, 4598-4810; b) K. S. Novoselov, V. I. Fal′ko, L. Colombo, P. R. Gellert, M. G. Schwab, K. Kim, *Nature* **2012**, *490*, 192-200; c) A. K. Geim, *Science* **2009**, *324*, 1530-1534.

[12] F. Schwierz, *Nat. Nanotechnol.* **2010**, *5*, 487-496.

[13] X. Y. Wang, A. Narita, K. Mullen, *Nat. Rev. Chem.* **2018**, *2*, 0100.

[14] a) W. Han, R. K. Kawakami, M. Gmitra, J. Fabian, *Nat. Nanotechnol.* **2014**, *9*, 794-807; b) T. Cao, F. Zhao, S. G. Louie, *Phys. Rev. Lett.* **2017**, *119*, 076401; c) J. Shen, Y. Zhu, X. Yang, C. Li, *Chem. Commun.* **2012**, *48*, 3686-3699; d) Z. Zhang, J. Zhang, N. Chen, L. Qu,

Energy Environ. Sci. **2012**, *5*, 8869-8890; e) G. Z. Magda, X. Jin, I. Hagymasi, P. Vancso, Z. Osvath, P. Nemes-Incze, C. Hwang, L. P. Biro, L. Tapaszto, *Nature* **2014**, *514*, 608-611.

[15] a) L. Chen, Y. Hernandez, X. L. Feng, K. Müllen, *Angew. Chem. Int. Ed.* **2012**, *51*, 7640-7654; *Angew. Chem.* **2012**, *124*, 7758-7773; b) X. Li, X. Wang, L. Zhang, S. Lee, H. Dai, *Science* **2008**, *319*, 1229-1232; c) L. A. Ponomarenko, F. Schedin, M. I. Katsnelson, R. Yang, E. W. Hill, K. S. Novoselov, A. K. Geim, *Science* **2008**, *320*, 356-358; d) X.-Y. Wang, X. Yao, A. Narita, K. Müllen, *Acc. Chem. Res.* **2019**, *52*, 2491-2505; e) Z. Sun, Q. Ye, C. Chi, J. Wu, *Chem. Soc. Rev.* **2012**, *41*, 7857-7889.

[16] a) X. Y. Wang, X. L. Yao, K. Müllen, *Sci. Chin. Chem.* **2019**, *62*, 1099-1144; b) K. Müllen, G. Wegner, *Electronic Materials: the Oligomer Approach*, John Wiley & Sons, Weinheim, **2008**; c) M. D. Watson, A. Fechtenkötter, K. Müllen, *Chem. Rev.* **2001**, *101*, 1267-1300.

[17] a) R. G. Harvey, *Polycyclic Aromatic Hydrocarbons*, Wiley-VCH, Weinheim, **1997**; b) Q. Miao, *Polycyclic Arenes and Heteroarenes: Synthesis, Properties, and Applications*, Wiley-VCH, Weinheim, **2015**.

[18] a) J. Wu, W. Pisula, K. Müllen, *Chem. Rev.* **2007**, *107*, 718-747; b) J. E. Anthony, *Chem. Rev.* **2006**, *106*, 5028-5048; c) A. R. Murphy, J. M. J. Fréchet, *Chem. Rev.* **2007**, *107*, 1066-1096; d) L. Dou, Y. Liu, Z. Hong, G. Li, Y. Yang, *Chem. Rev.* **2015**, *115*, 12633-12665.

[19] a) J. Fabian, H. Nakazumi, M. Matsuoka, *Chem. Rev.* **1992**, *92*, 1197-1226; b) L. Chen, C. Li, K. Müllen, *J. Mater. Chem. C* **2014**, *2*, 1938-1956; c) F. Würthner, C. R. Saha-Möller, B. Fimmel, S. Ogi, P. Leowanawat, D. Schmidt, *Chem. Rev.* **2016**, *116*, 962-1052.

[20] a) U. H. F. Bunz, *Acc. Chem. Res.* **2015**, *48*, 1676-1686; b) Q. Miao, *Adv. Mater.* **2014**, *26*, 5541-5549.

[21] H. I. Abdel-Shafy, M. S. M. Mansour, *Egyptian J. Pet.* **2016**, *25*, 107-123.

[22] a) G. Chen, Z. Zhuo, K. Ni, N. Y. Kim, Y. Zhao, Z. Chen, B. Xiang, L. Yang, Q. Zhang, Z. Lee, X. Wu, R. S. Ruoff, Y. Zhu, *Small* **2015**, *11*, 5296-5304; b) C. K. Chua, Z. Sofer, P. Šimek, O. Jankovský, K. Klímová, S. Bakardjieva, Š. Hrdličková Kučková, M. Pumera, *ACS Nano* **2015**, *9*, 2548-2555.

[23] F. Li, L. Kou, W. Chen, C. Wu, T. Guo, *NPG Asia Mater.* **2013**, *5*, e60-e60.

[24] D. V. Kosynkin, A. L. Higginbotham, A. Sinitskii, J. R. Lomeda, A. Dimiev, B. K. Price, J. M. Tour, *Nature* **2009**, *458*, 872-876.

[25] L. Jiao, L. Zhang, X. Wang, G. Diankov, H. Dai, *Nature* **2009**, *458*, 877-880.

[26] a) S. Eigler, M. Enzelberger-Heim, S. Grimm, P. Hofmann, W. Kroener, A. Geworski, C. Dotzer, M. Röckert, J. Xiao, C. Papp, O. Lytken, H.-P. Steinrück, P. Müller, A. Hirsch, *Adv. Mater.* **2013**, *25*, 3583-3587; b) S. Yang, S. Brüller, Z.-S. Wu, Z. Liu, K. Parvez, R. Dong, F. Richard, P. Samorì, X. Feng, K. Müllen, *J. Am. Chem. Soc.* **2015**, *137*, 13927-13932.

[27] M. C. Lemme, D. C. Bell, J. R. Williams, L. A. Stern, B. W. H. Baugher, P. Jarillo-Herrero, C. M. Marcus, *ACS Nano* **2009**, *3*, 2674-2676.

[28] D. Voiry, J. Yang, J. Kupferberg, R. Fullon, C. Lee, H. Y. Jeong, H. S. Shin, M. Chhowalla, *Science* **2016**, *353*, 1413-1416.

[29] R. Rieger, K. Müllen, *J. Phys. Org. Chem.* **2010**, *23*, 315-325.

[30] a) X. Yan, B. Li, L.-s. Li, *Acc. Chem. Res.* **2013**, *46*, 2254-2262; b) Y. Zhu, X. Guo, Y. Li, J. Wang, *J. Am. Chem. Soc.* **2019**, *141*, 5511–5517.

[31] E. H. Fort, P. M. Donovan, L. T. Scott, *J. Am. Chem. Soc.* **2009**, *131*, 16006-16007.

[32] E. Clar, M. Zander, *J. Chem. Soc.* **1957**, 4616-4619.

[33] E. H. Fort, L. T. Scott, *Angew. Chem. Int. Ed.* **2010**, *49*, 6626-6628; *Angew. Chem.* **2010**, *122*, 6776-6778.

[34] J. Lee, H. B. Li, A. J. Kalin, T. Y. Yuan, C. X. Wang, T. Olson, H. Y. Li, L. Fang, *Angew. Chem. Int. Ed.* **2017**, *56*, 13727-13731; *Angew. Chem.* **2017**, *129*, 13915-13919.

[35] a) A. Iuliano, P. Piccioli, D. Fabbri, *Org. Lett.* **2004**, *6*, 3711-3714; b) M. C. Bonifacio, C. R. Robertson, J.-Y. Jung, B. T. King, *J. Org. Chem.* **2005**, *70*, 8522-8526.

[36] J. Lee, B. B. Rajeeva, T. Yuan, Z.-H. Guo, Y.-H. Lin, M. Al-Hashimi, Y. Zheng, L. Fang, *Chem. Sci.* **2016**, *7*, 881-889.

[37] a) M. B. Goldfinger, K. B. Crawford, T. M. Swager, *J. Am. Chem. Soc.* **1997**, *119*, 4578-4593; b) T. Yao, M. A. Campo, R. C. Larock, *Org. Lett.* **2004**, *6*, 2677-2680; c) V. Mamane, P. Hannen, A. Fürstner, *Chem. Eur. J.* **2004**, *10*, 4556-4575; d) T.-A. Chen, R.-S. Liu, *Chem. Eur. J.* **2011**, *17*, 8023-8027; e) T.-A. Chen, T.-J. Lee, M.-Y. Lin, S. M. A. Sohel, E. W.-G. Diau, S.-F. Lush, R.-S. Liu, *Chem. Eur. J.* **2010**, *16*, 1826-1833.

[38] M. B. Goldfinger, T. M. Swager, *J. Am. Chem. Soc.* **1994**, *116*, 7895-7896.

[39] X. Zhang, M. A. Campo, T. Yao, R. C. Larock, *Org. Lett.* **2005**, *7*, 763-766.

[40] T. Jin, J. Zhao, N. Asao, Y. Yamamoto, *Chem. Eur. J.* **2014**, *20*, 3554-3576.

[41] J. Liu, B.-W. Li, Y.-Z. Tan, A. Giannakopoulos, C. Sanchez-Sanchez, D. Beljonne, P. Ruffieux, R. Fasel, X. Feng, K. Müllen, *J. Am. Chem. Soc.* **2015**, *137*, 6097-6103.

[42] a) B. Schuler, S. Collazos, L. Gross, G. Meyer, D. Pérez, E. Guitián, D. Peña, *Angew. Chem. Int. Ed.* **2014**, *53*, 9004-9006; *Angew. Chem.* **2014**, *126*, 9150-9152; b) E. C. Rüdiger, M. Porz, M. Schaffroth, F. Rominger, U. H. F. Bunz, *Chem. Eur. J.* **2014**, *20*, 12725-12728.

[43] a) I. Pozo, E. Guitián, D. Pérez, D. Peña, *Acc. Chem. Res.* **2019**, *52*, 2472-2481; b) D. Peña, S. Escudero, D. Pérez, E. Guitián, L. Castedo, *Angew. Chem. Int. Ed.* **1998**, *37*, 2659-2661; *Angew. Chem.* **1998**, *110*, 2804-2806.

[44] a) E. C. Rüdiger, F. Rominger, L. Steuer, U. H. F. Bunz, *J. Org. Chem.* **2016**, *81*, 193-196; b) E. C. Rüdiger, S. Koser, F. Rominger, J. Freudenberg, U. H. F. Bunz, *Chem. Eur. J.* **2018**, *24*, 9919-9927.

[45] K. Ozaki, K. Kawasumi, M. Shibata, H. Ito, K. Itami, *Nat. Commun.* **2015**, *6*, 6251.

[46] H. Ito, K. Ozaki, K. Itami, *Angew. Chem. Int. Ed.* **2017**, *56*, 11144-11164; *Angew. Chem.* **2017**, *129*, 11296-11317.

[47] a) X. L. Feng, W. Pisula, K. Müllen, *Pure Appl. Chem.* **2009**, *81*, 2203-2224; b) A. Narita, X.-Y. Wang, X. Feng, K. Müllen, *Chem. Soc. Rev.* **2015**, *44*, 6616-6643.

[48] a) K. P. C. Vollhardt, *Acc. Chem. Res.* **1977**, *10*, 1-8; b) J. A. Hyatt, *Org. Prep. Proced. Int.* **1991**, *23*, 460-463; c) A. Stabel, P. Herwig, K. Müllen, J. P. Rabe, *Angew. Chem. Int. Ed.* **1995**, *34*, 1609-1611; *Angew. Chem.* **1995**, *107*, 1768-1770; d) P. Herwig, C. W. Kayser, K. Müllen, H. W. Spiess, *Adv. Mater.* **1996**, *8*, 510-513; e) V. S. Iyer, M. Wehmeier, J. D. Brand, M. A. Keegstra, K. Müllen, *Angew. Chem. Int. Ed.* **1997**, *36*, 1604-1607; *Angew. Chem.* **1997**, *109*, 1675-1679; f) A. Fechtenkötter, K. Saalwächter, M. A. Harbison, K. Müllen, H. W. Spiess, *Angew. Chem. Int. Ed.* **1999**, *38*, 3039-3042; *Angew. Chem.* **1999**, *111*, 3224-3228; g) C. Kübel, K. Eckhardt, V. Enkelmann, G. Wegner, K. Müllen, *J. Mater. Chem.* **2000**, *10*, 879-886.

[49] X. Yang, X. Dou, K. Müllen, *Chem. Asian J.* **2008**, *3*, 759-766.

[50] a) W. Ried, K. H. Bönnighausen, *Chem. Ber.* **1960**, *93*, 1769-1773; b) M. A. Ogliaruso, L. A. Shadoff, E. I. Becker, *J. Org. Chem.* **1963**, *28*, 2725-2728; c) W. Ried, D. Freitag, *Angew.*

Chem. Int. Ed. **1968**, *7*, 835-844; *Angew. Chem.* **1968**, *80*, 932-942; d) M. Müller, V. S. Iyer, C. Kübel, V. Enkelmann, K. Müllen, *Angew. Chem. Int. Ed.* **1997**, *36*, 1607-1610; *Angew. Chem.* **1997**, *109*, 1679-1682; e) F. Dötz, J. D. Brand, S. Ito, L. Gherghel, K. Müllen, *J. Am. Chem. Soc.* **2000**, *122*, 7707-7717; f) S. Ito, M. Wehmeier, J. D. Brand, C. Kübel, R. Epsch, J. P. Rabe, K. Müllen, *Chem. Eur. J.* **2000**, *6*, 4327-4342.

[51] A. Halleux, R. H. Martin, G. S. D. King, *Helv. Chim. Acta* **1958**, *41*, 1177-1183.

[52] Y. Koga, T. Kaneda, Y. Saito, K. Murakami, K. Itami, *Science* **2018**, *359*, 435-439.

[53] H. Ito, Y. Segawa, K. Murakami, K. Itami, *J. Am. Chem. Soc.* **2019**, *141*, 3-10.

[54] a) M. Grzybowski, K. Skonieczny, H. Butenschön, D. T. Gryko, *Angew. Chem. Int. Ed.* **2013**, *52*, 9900-9930; *Angew. Chem.* **2013**, *125*, 10084-10115; b) M. Grzybowski, B. Sadowski, H. Butenschön, D. T. Gryko, *Angew. Chem. Int. Ed.* **2020**, *59*, 2998-3027; *Angew. Chem.* **2020**, *132*, 3020-3050; c) A. Yagi, Y. Segawa, K. Itami, *Chem* **2019**, *5*, 746-748.

[55] R. Scholl, J. Mansfeld, *Ber. Dtsch. Chem. Ges.* **1910**, *43*, 1734-1746.

[56] R. Scholl, C. Seer, R. Weitzenböck, *Ber. Dtsch. Chem. Ges.* **1910**, *43*, 2202-2209.

[57] a) R. Scholl, C. Seer, *Monatsh. Chem. Verw. Tl.* **1912**, *33*, 1-8; b) R. Scholl, C. Seer, *Justus Liebigs Ann. Chem.* **1912**, *394*, 111-177; c) R. Scholl, H. Neumann, *Ber. Dtsch. Chem. Ges. B* **1922**, *55*, 118-126; d) R. Scholl, G. Schwarzer, *Ber. Dtsch. Chem. Ges. B* **1922**, *55*, 324-330; e) C. Seer, O. Dischendorfer, *Monatsh. Chem. Verw. Tl.* **1913**, *34*, 1493-1502; f) R. Scholl, O. Dischendorfer, *Ber. Dtsch. Chem. Ges.* **1918**, *51*, 452-453.

[58] L. Zhai, R. Shukla, S. H. Wadumethrige, R. Rathore, *J. Org. Chem.* **2010**, *75*, 4748-4760.

[59] A. A. O. Sarhan, C. Bolm, *Chem. Soc. Rev.* **2009**, *38*, 2730-2744.

[60] S. R. Waldvogel, S. Trosien, *Chem. Commun.* **2012**, *48*, 9109-9119.

[61] L. Zhai, R. Shukla, R. Rathore, *Org. Lett.* **2009**, *11*, 3474-3477.

[62] C. D. Simpson, J. D. Brand, A. J. Berresheim, L. Przybilla, H. J. Räder, K. Müllen, *Chem. Eur. J.* **2002**, *8*, 1424-1429.

[63] B. T. King, J. Kroulík, C. R. Robertson, P. Rempala, C. L. Hilton, J. D. Korinek, L. M. Gortari, *J. Org. Chem.* **2007**, *72*, 2279-2288.

[64] a) J. Kenner, *J. Soc. Chem. Ind.* **1933**, *42*, 470; b) J. J. Ronney, R. C. Pink, *Proc. Chem. Soc.* **1961**, 142-143; c) G. A. Clowes, *J. Chem. Soc. C* **1968**, 2519-2526.

[65] a) G. Baddeley, J. Kenner, *J. Chem. Soc.* **1935**, 303-309; b) G. Baddeley, *J. Chem. Soc.* **1950**, 994-997; c) C. D. Nenitzescu, A. Balaban, *Chem. Ber.* **1958**, *91*, 2109-2116.

[66] a) P. Rempala, J. Kroulík, B. T. King, *J. Am. Chem. Soc.* **2004**, *126*, 15002-15003; b) P. Rempala, J. Kroulík, B. T. King, *J. Org. Chem.* **2006**, *71*, 5067-5081.

[67] J. Simons, R. McArthur, *Industrial & Engineering Chemistry* **1947**, *39*, 364-367.

[68] E. Clar, C. T. Ironside, *Proc. Chem. Soc.* **1958**, 150.

[69] M. Müller, C. Kübel, K. Müllen, *Chem. Eur. J.* **1998**, *4*, 2099-2109.

[70] a) H. Arslan, F. J. Uribe-Romo, B. J. Smith, W. R. Dichtel, *Chem. Sci.* **2013**, *4*, 3973-3978; b) T. S. Navale, M. V. Ivanov, M. M. Hossain, R. Rathore, *Angew. Chem. Int. Ed.* **2018**, *57*, 790-794; *Angew. Chem.* **2018**, *130*, 798-802; c) Q. Zhang, H. Peng, G. Zhang, Q. Lu, J. Chang, Y. Dong, X. Shi, J. Wei, *J. Am. Chem. Soc.* **2014**, *136*, 5057-5064.

[71] Y. Yang, K. Cheng, Y. Lu, D. Ma, D. Shi, Y. Sun, M. Yang, J. Li, J. Wei, *Org. Lett.* **2018**, *20*, 2138-2142.

[72] Y. Avlasevich, C. Kohl, K. Müllen, *J. Mater. Chem.* **2006**, *16*, 1053-1057.

[73] Chaolumen, M. Murata, A. Wakamiya, Y. Murata, *Angew. Chem. Int. Ed.* **2017**, *56*, 5082-5086; *Angew. Chem.* **2017**, *129*, 5164-5168.

[74] J. Z. Liu, A. Narita, S. Osella, W. Zhang, D. Schollmeyer, D. Beljonne, X. L. Feng, K. Müllen, *J. Am. Chem. Soc.* **2016**, *138*, 2602-2608.

[75] S. Nobusue, K. Fujita, Y. Tobe, *Org. Lett.* **2017**, *19*, 3227-3230.

[76] F. Morgenroth, C. Kübel, M. Müller, U. M. Wiesler, A. J. Berresheim, M. Wagner, K. Müllen, *Carbon* **1998**, *36*, 833-837.

[77] M. Kawamura, E. Tsurumaki, S. Toyota, *Synthesis* **2018**, *50*, 134-138.

[78] a) J. Z. Liu, S. Osella, J. Ma, R. Berger, D. Beljonne, D. Schollmeyer, X. L. Feng, K. Müllen, *J. Am. Chem. Soc.* **2016**, *138*, 8364-8367; b) J. He, S. Mathew, Z. J. Kinney, R. M. Warrell, J. S. Molina, C. S. Hartley, *Chem. Commun.* **2015**, *51*, 7245-7248.

[79] a) J. L. Ormsby, T. D. Black, C. L. Hilton, Bharat, B. T. King, *Tetrahedron* **2008**, *64*, 11370-11378; b) X. Dou, X. Yang, G. J. Bodwell, M. Wagner, V. Enkelmann, K. Müllen, *Org. Lett.* **2007**, *9*, 2485-2488; c) A. Pradhan, P. Dechambenoit, H. Bock, F. Durola, *J. Org. Chem.* **2013**, *78*, 2266-2274; d) S. L. Skraba-Joiner, E. C. McLaughlin, A. Ajaz, R. Thamatam, R. P. Johnson, *J. Org. Chem.* **2015**, *80*, 9578-9583.

[80] a) F. B. Mallory, C. W. Mallory, *Org, React.* **1984**, *30*, 1-456; b) W. H. Laarhoven, *Recl. Trav. Chim. Pays-Bas* **1983**, *102*, 185-204; c) H. Meier, *Angew. Chem. Int. Ed.* **1992**, *31*, 1399-1420; *Angew. Chem.* **1992**, *104*, 1425-1446.

[81] a) S. Xiao, M. Myers, Q. Miao, S. Sanaur, K. Pang, M. L. Steigerwald, C. Nuckolls, *Angew. Chem. Int. Ed.* **2005**, *44*, 7390-7394; *Angew. Chem.* **2005**, *117*, 7556-7560; b) C.-Y. Chiu, B. Kim, A. A. Gorodetsky, W. Sattler, S. Wei, A. Sattler, M. Steigerwald, C. Nuckolls, *Chem. Sci.* **2011**, *2*, 1480-1486.

[82] a) M. Daigle, A. Picard-Lafond, E. Soligo, J.-F. Morin, *Angew. Chem. Int. Ed.* **2016**, *55*, 2042-2047; *Angew. Chem.* **2016**, *128*, 2082-2087; b) L. Dössel, L. Gherghel, X. Feng, K. Müllen, *Angew. Chem. Int. Ed.* **2011**, *50*, 2540-2543; *Angew. Chem.* **2011**, *123*, 2588-2591.

[83] a) T. Sato, S. Shimada, K. Hata, *J. Chem. Soc. D* **1970**, 766-767; b) S. Takeo, S. Shigeru, H. Kazuo, *Bull. Chem. Soc. Jpn.* **1971**, *44*, 2484-2490.

[84] J. He, D. M. Agra-Kooijman, G. Singh, C. Wang, C. Dugger, J. Zeng, L. Zang, S. Kumar, C. S. Hartley, *J. Mater. Chem. C* **2013**, *1*, 5833-5836.

[85] I. Schnapperelle, T. Bach, *Chem. Eur. J.* **2014**, *20*, 9725-9732.

[86] a) D. Miao, M. Daigle, A. Lucotti, J. Boismenu-Lavoie, M. Tommasini, J.-F. Morin, *Angew. Chem. Int. Ed.* **2018**, *57*, 3588-3592; *Angew. Chem.* **2018**, *130*, 3650-3654; b) A. Jolly, D. Miao, M. Daigle, J.-F. Morin, *Angew. Chem. Int. Ed.* **2020**, *59*, 4624-4633; *Angew. Chem.* **2020**, *132*, 4652-4661.

[87] A. L. Mackay, H. Terrones, *Nature* **1991**, *352*, 762-762.

[88] A. Konishi, K. Horii, D. Shiomi, K. Sato, T. Takui, M. Yasuda, *J. Am. Chem. Soc.* **2019**, *141*, 10165-10170.

[89] a) M. A. Majewski, M. Stępień, *Angew. Chem. Int. Ed.* **2019**, *58*, 86-116; *Angew. Chem.* **2019**, *131*, 90-122; b) Y. Segawa, D. R. Levine, K. Itami, *Acc. Chem. Res.* **2019**, *52*, 2760-2767.

[90] J. C. Fetzer, *Large (C> = 24) Polycyclic Aromatic Hydrocarbons: Chemistry and Analysis*, Wiley & Sons, New York, **2000**.

[91] E. Clar, J. F. Stephen, *Tetrahedron* **1965**, *21*, 467-470.

[92] a) X. Guo, M. Myers, S. Xiao, M. Lefenfeld, R. Steiner, G. S. Tulevski, J. Tang, J. Baumert, F. Leibfarth, J. T. Yardley, M. L. Steigerwald, P. Kim, C. Nuckolls, *Proc. Natl. Acad. Sci.* **2006**, *103*, 11452-11456; b) M. Ball, Y. Zhong, Y. Wu, C. Schenck, F. Ng, M. Steigerwald, S. Xiao, C. Nuckolls, *Acc. Chem. Res.* **2015**, *48*, 267-276; c) A. A. Gorodetsky, C.-Y. Chiu, T. Schiros, M. Palma, M. Cox, Z. Jia, W. Sattler, I. Kymissis, M. Steigerwald, C. Nuckolls, *Angew. Chem. Int. Ed.* **2010**, *49*, 7909-7912; *Angew. Chem.* **2010**, *122*, 8081-8084; d) S. J. Kang, J. B. Kim, C.-Y. Chiu, S. Ahn, T. Schiros, S. S. Lee, K. G. Yager, M. F. Toney, Y.-L. Loo, C. Nuckolls, *Angew. Chem. Int. Ed.* **2012**, *51*, 8594-8597; *Angew. Chem.* **2012**, *124*, 8722-8725.

[93] a) L. Chen, S. R. Puniredd, Y.-Z. Tan, M. Baumgarten, U. Zschieschang, V. Enkelmann, W. Pisula, X. Feng, H. Klauk, K. Müllen, *J. Am. Chem. Soc.* **2012**, *134*, 17869-17872; b) L. Chen, K. S. Mali, S. R. Puniredd, M. Baumgarten, K. Parvez, W. Pisula, S. De Feyter, K. Müllen, *J. Am. Chem. Soc.* **2013**, *135*, 13531-13537.

[94] A. M. Hiszpanski, R. M. Baur, B. Kim, N. J. Tremblay, C. Nuckolls, A. R. Woll, Y.-L. Loo, *J. Am. Chem. Soc.* **2014**, *136*, 15749-15756.

[95] X. Guo, S. Xiao, M. Myers, Q. Miao, M. L. Steigerwald, C. Nuckolls, *Proc. Natl. Acad. Sci.* **2009**, *106*, 691-696.

[96] K. Baumgärtner, A. L. Meza Chincha, A. Dreuw, F. Rominger, M. Mastalerz, *Angew. Chem. Int. Ed.* **2016**, *55*, 15594-15598; *Angew. Chem.* **2016**, *128*, 15823-15827.

[97] K. Baumgärtner, F. Rominger, M. Mastalerz, *Chem. Eur. J.* **2018**, *24*, 8751-8755.

[98] E. Fresta, K. Baumgärtner, J. Cabanillas-Gonzalez, M. Mastalerz, R. D. Costa, *Nanoscale Horiz.* **2020**, *5*, 473-480.

[99] a) S. Grimme, J. Harren, A. Sobanski, F. Vögtle, *Eur. J. Org. Chem.* **1998**, *1998*, 1491-1509; b) M. Gingras, *Chem. Soc. Rev.* **2013**, *42*, 968-1006; c) M. Gingras, G. Félix, R. Peresutti, *Chem. Soc. Rev.* **2013**, *42*, 1007-1050; d) M. Gingras, *Chem. Soc. Rev.* **2013**, *42*, 1051-1095; e) M. Rickhaus, M. Mayor, M. Juríček, *Chem. Soc. Rev.* **2016**, *45*, 1542-1556.

[100] a) A. O. McIntosh, J. M. Robertson, V. Vand, *Nature* **1952**, *169*, 322-323; b) K. Mori, T. Murase, M. Fujita, *Angew. Chem. Int. Ed.* **2015**, *54*, 6847-6851; *Angew. Chem.* **2015**, *127*, 6951-6955; c) L. Barnett, D. M. Ho, K. K. Baldridge, R. A. Pascal, *J. Am. Chem. Soc.* **1999**, *121*, 727-733.

[101] a) R. Weitzenböck, A. Klingler, *Monatsh. Chem. Verw. Tl.* **1918**, *39*, 315-323; b) J. W. Cook, *J. Chem. Soc.* **1933**, 1592-1597.

[102] a) V. Berezhnaia, M. Roy, N. Vanthuyne, M. Villa, J.-V. Naubron, J. Rodriguez, Y. Coquerel, M. Gingras, *J. Am. Chem. Soc.* **2017**, *139*, 18508-18511; b) T. Hosokawa, Y. Takahashi, T. Matsushima, S. Watanabe, S. Kikkawa, I. Azumaya, A. Tsurusaki, K. Kamikawa, *J. Am. Chem. Soc.* **2017**, *139*, 18512-18521.

[103] M. A. Bennett, M. R. Kopp, E. Wenger, A. C. Willis, *J. Organomet. Chem.* **2003**, *667*, 8-15.

[104] N. Berova, L. D. Bari, G. Pescitelli, *Chem. Soc. Rev.* **2007**, *36*, 914-931.

[105] D. Dini, M. J. F. Calvete, M. Hanack, *Chem. Rev.* **2016**, *116*, 13043-13233.

[106] R. Naaman, D. H. Waldeck, *J. Phys. Chem. Lett.* **2012**, *3*, 2178-2187.

[107] F. Banhart, J. Kotakoski, A. V. Krasheninnikov, *ACS Nano* **2011**, *5*, 26-41.

[108] H. Christoph, J. Grunenberg, H. Hopf, I. Dix, P. G. Jones, M. Scholtissek, G. Maier, *Chem. Eur. J.* **2008**, *14*, 5604-5616.

[109] M. Rickhaus, M. Mayor, M. Juríček, *Chem. Soc. Rev.* **2017**, *46*, 1643-1660.

[110] J. Michl, E. W. Thulstrup, *Tetrahedron* **1976**, *32*, 205-209.

[111] a) V. M. Tsefrikas, L. T. Scott, *Chem. Rev.* **2006**, *106*, 4868-4884; b) V. M. Tsefrikas, S. Arns, P. M. Merner, C. C. Warford, B. L. Merner, L. T. Scott, G. J. Bodwell, *Org. Lett.* **2006**, *8*, 5195-5198; c) D. Eisenberg, A. S. Filatov, E. A. Jackson, M. Rabinovitz, M. A. Petrukhina, L. T. Scott, R. Shenhar, *J. Org. Chem.* **2008**, *73*, 6073-6078; d) M. Yanney, F. R. Fronczek, W. P. Henry, D. J. Beard, A. Sygula, *Eur. J. Org. Chem.* **2011**, *2011*, 6636-6639; e) T. Fujikawa, D. V. Preda, Y. Segawa, K. Itami, L. T. Scott, *Org. Lett.* **2016**, *18*, 3992-3995.

[112] a) I. R. Márquez, S. Castro-Fernández, A. Millán, A. G. Campaña, *Chem. Commun.* **2018**, *54*, 6705-6718; b) Q. Miao, *Chem. Rec.* **2015**, *15*, 1156-1159.

[113] a) T. Lenosky, X. Gonze, M. Teter, V. Elser, *Nature* **1992**, *355*, 333-335; b) V. Kapko, D. A. Drabold, M. F. Thorpe, *physica status solidi (b)* **2010**, *247*, 1197-1200.

[114] S. lijima, T. Ichihashi, Y. Ando, *Nature* **1992**, *356*, 776-778.

[115] J. Luo, X. Xu, R. Mao, Q. Miao, *J. Am. Chem. Soc.* **2012**, *134*, 13796-13803.

[116] a) K. Y. Cheung, X. Xu, Q. Miao, *J. Am. Chem. Soc.* **2015**, *137*, 3910-3914; b) X. Gu, H. Li, B. Shan, Z. Liu, Q. Miao, *Org. Lett.* **2017**, *19*, 2246-2249.

[117] a) K. Yamamoto, T. Harada, M. Nakazaki, T. Naka, Y. Kai, S. Harada, N. Kasai, *J. Am. Chem. Soc.* **1983**, *105*, 7171-7172; b) K. Yamamoto, Y. Saitho, D. Iwaki, T. Ooka, *Angew. Chem. Int. Ed.* **1991**, *30*, 1173-1174; *Angew. Chem.* **1991**, *103*, 1202-1203; c) K. Yamamoto, T. Harada, Y. Okamoto, H. Chikamatsu, M. Nakazaki, Y. Kai, T. Nakao, M. Tanaka, S. Harada, N. Kasai, *J. Am. Chem. Soc.* **1988**, *110*, 3578-3584; d) E. U. Mughal, D. Kuck, *Chem. Commun.* **2012**, *48*, 8880-8882; e) K. Kawasumi, Q. Zhang, Y. Segawa, L. T. Scott, K. Itami, *Nat. Chem.* **2013**, *5*, 739; f) H.-W. Ip, C.-F. Ng, H.-F. Chow, D. Kuck, *J. Am. Chem. Soc.* **2016**, *138*, 13778-13781.

[118] S. H. Pun, C. K. Chan, J. Luo, Z. Liu, Q. Miao, *Angew. Chem. Int. Ed.* **2018**, *57*, 1581-1586; *Angew. Chem.* **2018**, *130*, 1597-1602.

[119] I. R. Márquez, N. Fuentes, C. M. Cruz, V. Puente-Muñoz, L. Sotorrios, M. L. Marcos, D. Choquesillo-Lazarte, B. Biel, L. Crovetto, E. Gómez-Bengoa, M. T. González, R. Martin, J. M. Cuerva, A. G. Campaña, *Chem. Sci.* **2017**, *8*, 1068-1074.

[120] a) S. H. Pun, Q. Miao, *Acc. Chem. Res.* **2018**; b) Y. Yang, L. Y. Yuan, B. W. Shan, Z. F. Liu, Q. Miao, *Chem. Eur. J.* **2016**, *22*, 18620-18627; c) K. Y. Cheung, C. K. Chan, Z. Liu, Q. Miao, *Angew. Chem. Int. Ed.* **2017**, *56*, 9003-9007; *Angew. Chem.* **2017**, *129*, 9131-9135; d) H. Chen, Q. Miao, *ChemPlusChem* **2019**, *84*, 627-629; e) K. Y. Cheung, Q. Miao, *Chin. Chem. Lett.* **2019**, *30*, 1506-1508; f) S. H. Pun, Y. Wang, M. Chu, C. K. Chan, Y. Li, Z. Liu, Q. Miao, *J. Am. Chem. Soc.* **2019**, *141*, 9680-9686.

[121] W. I. F. David, R. M. Ibberson, J. C. Matthewman, K. Prassides, T. J. S. Dennis, J. P. Hare, H. W. Kroto, R. Taylor, D. R. M. Walton, *Nature* **1991**, *353*, 147-149.

[122] P. Jessup, J. Reiss, *Aust. J. Chem.* **1976**, *29*, 173-178.

[123] T. Kirschbaum, F. Rominger, M. Mastalerz, *Angew. Chem. Int. Ed.* **2020**, *59*, 270-274; *Angew. Chem.* **2020**, *132*, 9680-9686.

[124] Y. Sakamoto, T. Suzuki, *J. Am. Chem. Soc.* **2013**, *135*, 14074-14077.

[125] a) R. W. Miller, S. E. Averill, S. J. Van Wyck, A. C. Whalley, *J. Org. Chem.* **2016**, *81*, 12001-12005; b) R. W. Miller, A. K. Duncan, S. T. Schneebeli, D. L. Gray, A. C. Whalley, *Chem. Eur. J.* **2014**, *20*, 3705-3711.

[126] a) S. Nobusue, Y. Tobe, *Synlett* **2016**, *27*, 2140-2144; b) U. Simmross, K. Müllen, *Chem. Ber.* **1993**, *126*, 969-973; c) S. Nobusue, A. Shimizu, K. Hori, I. Hisaki, M. Miyata, Y. Tobe, *Angew. Chem. Int. Ed.* **2013**, *52*, 4184-4188; *Angew. Chem.* **2013**, *123*, 4278-4282.

[127] C.-N. Feng, M.-Y. Kuo, Y.-T. Wu, *Angew. Chem. Int. Ed.* **2013**, *52*, 7791-7794; *Angew. Chem.* **2013**, *125*, 7945-7948.

[128] a) G. Zhang, F. Rominger, M. Mastalerz, *Chem. Eur. J.* **2016**, *22*, 3084-3093; b) G. Zhang, F. Rominger, U. Zschieschang, H. Klauk, M. Mastalerz, *Chem. Eur. J.* **2016**, *22*, 14840-14845.

[129] a) S. Piesse, *Compt. Rend. Acad. Sci.* **1864**, *57*, 1016; b) A. E. Sherndal, *J. Am. Chem. Soc.* **1915**, *37*, 167-171.

[130] a) H. S. Xin, X. K. Gao, *Chempluschem* **2017**, *82*, 945-956; b) J.-X. Dong, H.-L. Zhang, *Chin. Chem. Lett.* **2016**, *27*, 1097-1104.

[131] a) S. Ito, N. Morita, *Eur. J. Org. Chem.* **2009**, *2009*, 4567-4579; b) T. Shoji, E. Shimomura, M. Maruyama, A. Maruyama, S. Ito, T. Okujima, K. Toyota, N. Morita, *Eur. J. Org. Chem.* **2013**, *2013*, 7785-7799; c) S. Ito, T. Kubo, N. Morita, T. Ikoma, S. Tero-Kubota, J. Kawakami, A. Tajiri, *J. Org. Chem.* **2005**, *70*, 2285-2293.

[132] a) X. Wang, J. K.-P. Ng, P. Jia, T. Lin, C. M. Cho, J. Xu, X. Lu, C. He, *Macromolecules* **2009**, *42*, 5534-5544; b) M. Murai, S.-Y. Ku, N. D. Treat, M. J. Robb, M. L. Chabinyc, C. J. Hawker, *Chem. Sci.* **2014**, *5*, 3753-3760.

[133] K. Kurotobi, K. S. Kim, S. B. Noh, D. Kim, A. Osuka, *Angew. Chem. Int. Ed.* **2006**, *45*, 3944-3947; *Angew. Chem.* **2006**, *118*, 4048-4051.

[134] a) P. G. Lacroix, I. Malfant, G. Iftime, A. C. Razus, K. Nakatani, J. A. Delaire, *Chem. Eur. J.* **2000**, *6*, 2599-2608; b) L. Cristian, I. Sasaki, P. G. Lacroix, B. Donnadieu, I. Asselberghs, K. Clays, A. C. Razus, *Chem. Mater.* **2004**, *16*, 3543-3551; c) A. Migalska-Zalas, Y. El kouari, S. Touhtouh, *Opt. Mater.* **2012**, *34*, 1639-1643.

[135] a) J. Xia, B. Capozzi, S. Wei, M. Strange, A. Batra, J. R. Moreno, R. J. Amir, E. Amir, G. C. Solomon, L. Venkataraman, L. M. Campos, *Nano Lett.* **2014**, *14*, 2941-2945; b) F. Schwarz, M. Koch, G. Kastlunger, H. Berke, R. Stadler, K. Venkatesan, E. Lörtscher, *Angew. Chem. Int. Ed.* **2016**, *55*, 11781-11786; *Angew. Chem.* **2016**, *128*, 11956-11961.

[136] a) M. T. Lusk, L. D. Carr, *Phys. Rev. Lett.* **2008**, *100*, 175503; b) M. T. Lusk, D. T. Wu, L. D. Carr, *Phys. Rev. B* **2010**, *81*, 155444.

[137] a) P. T. Araujo, M. Terrones, M. S. Dresselhaus, *Mater. Today* **2012**, *15*, 98-109; b) L. Liu, M. Qing, Y. Wang, S. Chen, *J. Mater. Sci. Technol.* **2015**, *31*, 599-606; c) B. Mortazavi, S. Ahzi, *Carbon* **2013**, *63*, 460-470; d) N. Jing, Q. Xue, C. Ling, M. Shan, T. Zhang, X. Zhou, Z. Jiao, *RSC Adv.* **2012**, *2*, 9124-9129.

[138] a) A. Konishi, A. Morinaga, M. Yasuda, *Chem. Eur. J.* **2018**, *24*, 8548-8552; b) J. Ma, Y. Fu, E. Dmitrieva, F. Liu, H. Komber, F. Hennersdorf, A. A. Popov, J. J. Weigand, J. Liu, X. Feng, *Angew. Chem. Int. Ed.* **2020**, *59*, 5637-5642; *Angew. Chem.* **2020**, *132*, 5686-5691.

[139] P. Baumgartner, E. Weltin, G. Wagnière, E. Heilbronner, *Helv. Chim. Acta* **1965**, *48*, 751-764.

[140] a) J. Hieulle, E. Carbonell-Sanromà, M. Vilas-Varela, A. Garcia-Lekue, E. Guitián, D. Peña, J. I. Pascual, *Nano Lett.* **2018**, *18*, 418-423; b) S. Mishra, T. G. Lohr, C. A. Pignedoli, J. Liu, R. Berger, J. I. Urgel, K. Müllen, X. Feng, P. Ruffieux, R. Fasel, *ACS Nano* **2018**, *12*, 11917-11927; c) D. Skidin, F. Eisenhut, M. Richter, S. Nikipar, J. Krüger, D. A. Ryndyk, R. Berger, G. Cuniberti, X. Feng, F. Moresco, *Chem. Commun.* **2019**, *55*, 4731-4734; d) J. Liu, S. Mishra, C. A. Pignedoli, D. Passerone, J. I. Urgel, A. Fabrizio, T. G. Lohr, J. Ma, H. Komber, M. Baumgarten, C. Corminboeuf, R. Berger, P. Ruffieux, K. Müllen, R. Fasel, X. Feng, *J. Am. Chem. Soc.* **2019**, *141*, 12011-12020.

[141] a) Y. Sasaki, M. Takase, T. Okujima, S. Mori, H. Uno, *Org. Lett.* **2019**, *21*, 1900-1903; b) K. Yamamoto, Y. Ie, N. Tohnai, F. Kakiuchi, Y. Aso, *Sci. Rep.* **2018**, *8*, 17663; c) X.-S. Zhang, Y.-Y. Huang, J. Zhang, W. Meng, Q. Peng, R. Kong, Z. Xiao, J. Liu, M. Huang, Y. Yi, L. Chen, Q. Fan, G. Lin, Z. Liu, G. Zhang, L. Jiang, D. Zhang, *Angew. Chem. Int. Ed.* **2020**, *59*, 3529-3533; *Angew. Chem.* **2020**, *132*, 3557-3561.

[142] J. T. Markiewicz, F. Wudl, *ACS Appl. Mater. Inter.* **2015**, *7*, 28063-28085.

[143] J. T. M. van Dijk, A. Hartwijk, A. C. Bleeker, J. Lugtenburg, J. Cornelisse, *J. Org. Chem.* **1996**, *61*, 1136-1139.

[144] J. Merz, A. Steffen, J. Nitsch, J. Fink, C. B. Schürger, A. Friedrich, I. Krummenacher, H. Braunschweig, M. Moos, D. Mims, C. Lambert, T. B. Marder, *Chem. Sci.* **2019**, *10*, 7516-7534.

[145] A. C. Ferrari, J. Robertson, G. R. Loppnow, L. Shoute, K. J. Schmidt, A. Savage, R. H. Hall, J. T. Bulmer, *Philos. Trans. R. Soc., A* **2004**, *362*, 2461-2476.

[146] G. Malloci, G. Cappellini, G. Mulas, A. Mattoni, *Chem. Phys.* **2011**, *384*, 19-27.

[147] a) T. Jiro, *Bull. Chem. Soc. Jpn.* **1963**, *36*, 1237-1249; b) Y. Tanizaki, T. Yoshinaga, H. Hiratsuka, *Spectrochim. Acta, Part A* **1978**, *34*, 205-210; c) J. R. Lakowicz, *Principles of Fluorescence Spectroscopy*, Springer, Boston, MA, **2010**.

[148] a) K. K. Ong, J. O. Jensen, H. F. Hameka, *J. Mol. Struct.: THEOCHEM* **1999**, *459*, 131-144; b) T. M. Halasinski, J. L. Weisman, R. Ruiterkamp, T. J. Lee, F. Salama, M. Head-Gordon, *J. Phys. Chem. A* **2003**, *107*, 3660-3669.

[149] D. N. Coventry, A. S. Batsanov, A. E. Goeta, J. A. K. Howard, T. B. Marder, R. N. Perutz, *Chem. Commun.* **2005**, 2172-2174.

[150] a) E. Clar, *Chem. Ber.* **1948**, *81*, 52-63; b) A. Bohnen, K.-H. Koch, W. Lüttke, K. Müllen, *Angew. Chem. Int. Ed.* **1990**, *29*, 525-527; *Angew. Chem.* **1990**, *102*, 548-550; c) R. Thamatam, S. L. Skraba, R. P. Johnson, *Chem. Commun.* **2013**, *49*, 9122-9124.

[151] a) S. Toffanin, V. Benfenati, A. Pistone, S. Bonetti, W. Koopman, T. Posati, A. Sagnella, M. Natali, R. Zamboni, G. Ruani, M. Muccini, *J. Mater. Chem. B* **2013**, *1*, 3850-3859; b) X. Zhan, J. Zhang, S. Tang, Y. Lin, M. Zhao, J. Yang, H.-L. Zhang, Q. Peng, G. Yu, Z. Li, *Chem. Commun.* **2015**, *51*, 7156-7159; c) G. Li, Y. Zhao, J. Li, J. Cao, J. Zhu, X. W. Sun, Q. Zhang, *J. Org. Chem.* **2015**, *80*, 196-203; d) J. t. Schiphorst, A. M. Kendhale, M. G. Debije, C. Menelaou, L. M. Herz, A. P. H. J. Schenning, *Chem. Mater.* **2014**, *26*, 3876-3878; e) M. Zhang, Z. Yao, C. Yan, Y. Cai, Y. Ren, J. Zhang, P. Wang, *ACS Photon.* **2014**, *1*, 710-717; f) H. Imahori, T. Umeyama, S. Ito, *Acc. Chem. Res.* **2009**, *42*, 1809-1818.

[152] E. Clar, *Ber. Dtsch. Chem. Ges. B* **1932**, *65*, 846-859.

[153] W. N. Lipscomb, J. M. Robertson, M. G. Rossmann, *J. Chem. Soc.* **1959**, 2601-2607.

[154] E. Clar, C. T. Ironside, M. Zander, *Tetrahedron* **1966**, *22*, 3527-3533.

[155] a) S. M. Draper, D. J. Gregg, R. Madathil, *J. Am. Chem. Soc.* **2002**, *124*, 3486-3487; b) M. Takase, V. Enkelmann, D. Sebastiani, M. Baumgarten, K. Müllen, *Angew. Chem. Int. Ed.* **2007**, *46*, 5524-5527; *Angew. Chem.* **2007**, *119*, 5620-5623; c) E. Gońka, P. J. Chmielewski, T. Lis, M. Stępień, *J. Am. Chem. Soc.* **2014**, *136*, 16399-16410; d) B. Liu, D. H. Shi, Y. H. Yang, D. Y. Liu, M. Li, E. N. Liu, X. G. Wang, Q. Zhang, M. Y. Yang, J. Li, X. Y. Shi, W. L. Wang, J. F. Wei, *Eur. J. Org. Chem.* **2018**, 869-873; e) K. Oki, M. Takase, S. Mori, H. Uno, *J. Am. Chem. Soc.* **2019**, *141*, 16255-16259.

[156] a) K. Y. Chernichenko, V. V. Sumerin, R. V. Shpanchenko, E. S. Balenkova, V. G. Nenajdenko, *Angew. Chem. Int. Ed.* **2006**, *45*, 7367-7370; *Angew. Chem.* **2006**, *119*, 7527-7530; b) Y. Sun, L. Tan, S. Jiang, H. Qian, Z. Wang, D. Yan, C. Di, Y. Wang, W. Wu, G. Yu, S. Yan, C. Wang, W. Hu, Y. Liu, D. Zhu, *J. Am. Chem. Soc.* **2007**, *129*, 1882-1883; c) W. Jiang, Y. Zhou, H. Geng, S. Jiang, S. Yan, W. Hu, Z. Wang, Z. Shuai, J. Pei, *J. Am. Chem. Soc.* **2011**, *133*, 1-3; d) R. Dong, M. Pfeffermann, D. Skidin, F. Wang, Y. Fu, A. Narita, M. Tommasini, F. Moresco, G. Cuniberti, R. Berger, K. Müllen, X. Feng, *J. Am. Chem. Soc.* **2017**, *139*, 2168-2171.

[157] D. Wu, W. Pisula, M. C. Haberecht, X. Feng, K. Müllen, *Org. Lett.* **2009**, *11*, 5686-5689.

[158] W. Jiang, Y. Li, W. Yue, Y. Zhen, J. Qu, Z. Wang, *Org. Lett.* **2010**, *12*, 228-231.

[159] a) K. Müllen, J. P. Rabe, *Acc. Chem. Res.* **2008**, *41*, 511-520; b) W. Pisula, X. Feng, K. Müllen, *Chem. Mater.* **2011**, *23*, 554-567.

[160] A. H. Endres, M. Schaffroth, F. Paulus, H. Reiss, H. Wadepohl, F. Rominger, R. Krämer, U. H. F. Bunz, *J. Am. Chem. Soc.* **2016**, *138*, 1792-1795.

[161] E. Clar, *The Aromatic Sextet*, John Wiley and Sons, London, **1972**.

[162] a) N. Miyaura, A. Suzuki, *Chem. Rev.* **1995**, *95*, 2457-2483; b) T. Hatakeyama, S. Hashimoto, K. Ishizuka, M. Nakamura, *J. Am. Chem. Soc.* **2009**, *131*, 11949-11963; c) A. Suzuki, *Angew. Chem. Int. Ed.* **2011**, *50*, 6722-6737; *Angew. Chem.* **2011**, *123*, 6854-6869; d) C. C. C. Johansson Seechurn, M. O. Kitching, T. J. Colacot, V. Snieckus, *Angew. Chem. Int. Ed.* **2012**, *51*, 5062-5085; *Angew. Chem.* **2012**, *124*, 5150-5174; e) A. Brennführer, H. Neumann, M. Beller, *Angew. Chem. Int. Ed.* **2009**, *48*, 4114-4133; *Angew. Chem.* **2009**, *121*, 4176-4196; f) A. J. J. Lennox, G. C. Lloyd-Jones, *Chem. Soc. Rev.* **2014**, *43*, 412-443.

[163] M. R. Netherton, G. C. Fu, *Org. Lett.* **2001**, *3*, 4295-4298.

[164] L. Liu, B. Yang, T. J. Katz, M. K. Poindexter, *J. Org. Chem.* **1991**, *56*, 3769-3775.

[165] A. Zinke, R. Dengg, *Monatsh. Chem. Verw. Tl.* **1922**, *43*, 125-128.

[166] a) S. Kumar, B. Lakshmi, *Tetrahedron Lett.* **2005**, *46*, 2603-2605; b) S. Kumar, S. K. Varshney, *Synthesis* **2001**, *2001*, 0305-0311.

[167] D. Firmansyah, M. Banasiewicz, I. Deperasińska, A. Makarewicz, B. Kozankiewicz, D. T. Gryko, *Chem. Asian J.* **2014**, *9*, 2483-2493.

[168] R. B. King, *J. Phys. Chem.* **1996**, *100*, 15096-15104.

[169] Y. Shao, L. F. Molnar, Y. Jung, J. Kussmann, C. Ochsenfeld, S. T. Brown, A. T. B. Gilbert, L. V. Slipchenko, S. V. Levchenko, D. P. O'Neill, R. A. DiStasio Jr, R. C. Lochan, T. Wang, G. J. O. Beran, N. A. Besley, J. M. Herbert, C. Yeh Lin, T. Van Voorhis, S. Hung Chien, A. Sodt, R. P. Steele, V. A. Rassolov, P. E. Maslen, P. P. Korambath, R. D. Adamson, B. Austin, J. Baker, E. F. C. Byrd, H. Dachsel, R. J. Doerksen, A. Dreuw, B. D. Dunietz, A. D. Dutoi, T. R. Furlani, S. R. Gwaltney, A. Heyden, S. Hirata, C.-P. Hsu, G. Kedziora, R. Z. Khalliulin, P. Klunzinger, A. M. Lee, M. S. Lee, W. Liang, I. Lotan, N. Nair, B. Peters,

E. I. Proynov, P. A. Pieniazek, Y. Min Rhee, J. Ritchie, E. Rosta, C. David Sherrill, A. C. Simmonett, J. E. Subotnik, H. Lee Woodcock Iii, W. Zhang, A. T. Bell, A. K. Chakraborty, D. M. Chipman, F. J. Keil, A. Warshel, W. J. Hehre, H. F. Schaefer Iii, J. Kong, A. I. Krylov, P. M. W. Gill, M. Head-Gordon, *Phys. Chem. Chem. Phys.* **2006**, *8*, 3172-3191.

[170] a) E. Clar, *J. Chem. Phys.* **1949**, *17*, 741-742; b) E. Clar, *Spectrochim. Acta* **1950**, *4*, 116-121; c) E. Clar, *Polycyclic Hydrocarbons, Vol. 1*, Springer-Verlag, Berlin Heidelberg, **1964**.

[171] N. C. Davy, G. Man, R. A. Kerner, M. A. Fusella, G. E. Purdum, M. Sezen, B. P. Rand, A. Kahn, Y.-L. Loo, *Chem. Mater.* **2016**, *28*, 673-681.

[172] a) K. Ota, T. Tanaka, A. Osuka, *Org. Lett.* **2014**, *16*, 2974-2977; b) A. Naibi Lakshminarayana, J. Chang, J. Luo, B. Zheng, K.-W. Huang, C. Chi, *Chem. Commun.* **2015**, *51*, 3604-3607; c) S. Kumar, M.-T. Ho, Y.-T. Tao, *Org. Lett.* **2016**, *18*, 200-203; d) Chaolumen, M. Murata, Y. Sugano, A. Wakamiya, Y. Murata, *Angew. Chem. Int. Ed.* **2015**, *54*, 9308-9312; *Angew. Chem.* **2015**, *127*, 9440-9444; e) L. J. Purvis, X. Gu, S. Ghosh, Z. Zhang, C. J. Cramer, C. J. Douglas, *J. Org. Chem.* **2018**, *83*, 1828-1841.

[173] J. M. Fernández-García, P. J. Evans, S. Medina Rivero, I. Fernández, D. García-Fresnadillo, J. Perles, J. Casado, N. Martín, *J. Am. Chem. Soc.* **2018**, *140*, 17188-17196.

[174] a) M. S. Little, S. G. Yeates, A. A. Alwattar, K. W. J. Heard, J. Raftery, A. C. Edwards, A. V. S. Parry, P. Quayle, *Eur. J. Org. Chem.* **2017**, *2017*, 1694-1703; b) Y. Yang, L. Yuan, B. Shan, Z. Liu, Q. Miao, *Chem. Eur. J.* **2016**, *22*, 18620-18627.

[175] a) R. Yamaguchi, S. Hiroto, H. Shinokubo, *Org. Lett.* **2012**, *14*, 2472-2475; b) H. Shinokubo, *Proc. Jpn. Acad. Ser. B* **2014**, *90*, 1-11; c) G. Li, H. Phan, T. S. Herng, T. Y. Gopalakrishna, C. Liu, W. Zeng, J. Ding, J. Wu, *Angew. Chem. Int. Ed.* **2017**, *56*, 5012-5016; *Angew. Chem.* **2017**, *129*, 5094-5098; d) Q. Chen, D. Wang, M. Baumgarten, D. Schollmeyer, K. Müllen, A. Narita, *Chem. Asian J.* **2019**, *14*, 1703-1707; e) Q. Chen, D. Schollmeyer, K. Müllen, A. Narita, *J. Am. Chem. Soc.* **2019**, *141*, 19994-19999.

[176] a) E. A. Bliss, R. J. Griffin, M. F. G. Stevens, *J. Chem. Soc., Perkin Trans. 1* **1987**, 2217-2228; b) R. A. Abramovitch, P. Chinnasamy, K. Evertz, G. Huttner, *J. Chem. Soc., Chem. Commun.* **1989**, 3-5; c) M. A. Castro, M. F. G. Stevens, *J. Chem. Soc., Chem. Commun.* **1992**, 869-870; d) A. Pradhan, P. Dechambenoit, H. Bock, F. Durola, *Angew. Chem. Int. Ed.* **2011**, *50*, 12582-12585; *Angew. Chem.* **2011**, *123*, 12790-12793.

[177] T. Ohe, N. Miyaura, A. Suzuki, *J. Org. Chem.* **1993**, *58*, 2201-2208.

[178] a) H. Quante, K. Müllen, *Angew. Chem. Int. Ed.* **1995**, *34*, 1323-1325; *Angew. Chem.* **1995**, *107*, 1487-1489; b) F. O. Holtrup, G. R. J. Müller, H. Quante, S. De Feyter, F. C. De Schryver, K. Müllen, *Chem. Eur. J.* **1997**, *3*, 219-225.

[179] E. A. Jackson, B. D. Steinberg, M. Bancu, A. Wakamiya, L. T. Scott, *J. Am. Chem. Soc.* **2007**, *129*, 484-485.

[180] a) B. Panda, T. K. Sarkar, *Tetrahedron Lett.* **2010**, *51*, 301-305; b) J. Cao, M. Miao, W. Chen, L. Wu, X. Huang, *J. Org. Chem.* **2011**, *76*, 9329-9337.

[181] W. Dilthey, G. Hurtig, *Ber. Dtsch. Chem. Ges. B* **1934**, *67*, 495-496.

[182] B. Dittrich, F. P. A. Fabbiani, J. Henn, M. U. Schmidt, P. Macchi, K. Meindl, M. A. Spackman, *Acta Crystallogr. Sect. B* **2018**, *74*, 416-426.

[183] a) R. J. Fox, F. W. Evans, M. Szwarc, *Trans. Faraday Soc.* **1961**, *57*, 1915-1927; b) J. P. Simons, A. J. Yarwood, *Trans. Faraday Soc.* **1961**, *57*, 2167-2175; c) J. P. Simons, A. J. Yarwood, *Trans. Faraday Soc.* **1963**, *59*, 90-100; d) Y. A. Mikheev, V. P. Pustoshnyi, D.

Y. Toptygin, *Bull. Acad. Sci. USSR, Div. Chem. Sci.* **1976**, *25*, 1962-1964; e) I. I. Levina, O. N. Klimovich, D. S. Vinogradov, T. A. Podrugina, D. S. Bormotov, A. S. Kononikhin, O. V. Dement'eva, I. N. Senchikhin, E. N. Nikolaev, V. A. Kuzmin, T. D. Nekipelova, *J. Phys. Org. Chem.* **2018**, *31*, e3844.

[184] a) S. A. Saleh, H. I. Tashtoush, *Tetrahedron* **1998**, *54*, 14157-14177; b) M. Tashiro, G. Fukata, T. Yamato, H. Watanabe, K. Oe, O. Tsuge, *Org. Prep. Proced. Int.* **1976**, *8*, 249-262; c) G. Fukata, T. Itoh, M. Tashiro, *J. Org. Chem.* **1981**, *46*, 4454-4458.

[185] a) R. Herges, D. Geuenich, *J. Phys. Chem. A* **2001**, *105*, 3214-3220; b) D. Geuenich, K. Hess, F. Köhler, R. Herges, *Chem. Rev.* **2005**, *105*, 3758-3772.

[186] a) P. Lazzeretti, E. Rossi, R. Zanasi, *J. Chem. Phys.* **1982**, *77*, 3129-3139; b) U. Fleischer, W. Kutzelnigg, P. Lazzeretti, V. Muehlenkamp, *J. Am. Chem. Soc.* **1994**, *116*, 5298-5306.

[187] E. L. Eliel, S. H. Wilen, *Stereochemistry of Organic Compounds*, Wiley, **1994**.

[188] H. Tanaka, Y. Inoue, T. Mori, *ChemPhotoChem* **2018**, *2*, 386-402.

[189] a) P. Tian, L. Tang, K. S. Teng, S. P. Lau, *Mater. Today Chem.* **2018**, *10*, 221-258; b) K. Nekoueian, M. Amiri, M. Sillanpää, F. Marken, R. Boukherroub, S. Szunerits, *Chem. Soc. Rev.* **2019**, *48*, 4281-4316.

[190] a) M. Bendikov, F. Wudl, D. F. Perepichka, *Chem. Rev.* **2004**, *104*, 4891-4946; b) A. C. Grimsdale, K. Müllen, *Angew. Chem. Int. Ed.* **2005**, *44*, 5592-5629; *Angew. Chem.* **2005**, *117*, 5732-5772; c) J. E. Anthony, *Angew. Chem. Int. Ed.* **2008**, *47*, 452-483; *Angew. Chem.* **2008**, *120*, 460-492.

[191] a) S. S. Zade, M. Bendikov, *Angew. Chem. Int. Ed.* **2010**, *49*, 4012-4015; *Angew. Chem.* **2010**, *122*, 4104-4107; b) M. Watanabe, K.-Y. Chen, Y. J. Chang, T. J. Chow, *Acc. Chem. Res.* **2013**, *46*, 1606-1615; c) Q. Ye, C. Chi, *Chem. Mater.* **2014**, *26*, 4046-4056; d) K. J. Thorley, J. E. Anthony, *Isr. J. Chem.* **2014**, *54*, 642-649.

[192] M. Bendikov, H. M. Duong, K. Starkey, K. N. Houk, E. A. Carter, F. Wudl, *J. Am. Chem. Soc.* **2004**, *126*, 7416-7417.

[193] a) R. A. Pascal, *Chem. Rev.* **2006**, *106*, 4809-4819; b) Y. Xiao, J. T. Mague, R. H. Schmehl, F. M. Haque, R. A. Pascal Jr., *Angew. Chem. Int. Ed.* **2019**, *58*, 2831-2833; *Angew. Chem.* **2019**, *131*, 2857-2859; c) B. Purushothaman, M. Bruzek, S. R. Parkin, A.-F. Miller, J. E. Anthony, *Angew. Chem. Int. Ed.* **2011**, *50*, 7013-7017; *Angew. Chem.* **2011**, *123*, 7151-7155; d) I. Kaur, M. Jazdzyk, N. N. Stein, P. Prusevich, G. P. Miller, *J. Am. Chem. Soc.* **2010**, *132*, 1261-1263; e) M. Müller, L. Ahrens, V. Brosius, J. Freudenberg, U. H. F. Bunz, *J. Mater. Chem. C* **2019**, *7*, 14011-14034.

[194] a) M. Stępień, E. Gońka, M. Żyła, N. Sprutta, *Chem. Rev.* **2017**, *117*, 3479-3716; b) U. H. F. Bunz, *Chem. Eur. J.* **2009**, *15*, 6780-6789; c) H. F. Bunz Uwe, in *Pure Appl. Chem., Vol. 82*, **2010**, p. 953; d) U. H. F. Bunz, J. U. Engelhart, B. D. Lindner, M. Schaffroth, *Angew. Chem. Int. Ed.* **2013**, *52*, 3810-3821; *Angew. Chem.* **2013**, *125*, 3898-3910; e) U. H. F. Bunz, J. Freudenberg, *Acc. Chem. Res.* **2019**, *52*, 1575-1587; f) Z. Cai, M. A. Awais, N. Zhang, L. Yu, *Chem* **2018**, *4*, 1-33.

[195] D. Cortizo-Lacalle, J. P. Mora-Fuentes, K. Strutyński, A. Saeki, M. Melle-Franco, A. Mateo-Alonso, *Angew. Chem. Int. Ed.* **2018**, *57*, 703-708; *Angew. Chem.* **2018**, *130*, 711-716.

[196] B.-L. Hu, C. An, M. Wagner, G. Ivanova, A. Ivanova, M. Baumgarten, *J. Am. Chem. Soc.* **2019**, *141*, 5130-5134.

[197] a) C. Wang, J. Zhang, G. Long, N. Aratani, H. Yamada, Y. Zhao, Q. Zhang, *Angew. Chem. Int. Ed.* **2015**, *54*, 6292-6296; *Angew. Chem.* **2015**, *127*, 6390-6394; b) P.-Y. Gu, Z. Wang, G. Liu, H. Yao, Z. Wang, Y. Li, J. Zhu, S. Li, Q. Zhang, *Chem. Mater.* **2017**, *29*, 4172-4175; c) Z. Wang, P. Gu, G. Liu, H. Yao, Y. Wu, Y. Li, G. Rakesh, J. Zhu, H. Fu, Q. Zhang, *Chem. Commun.* **2017**, *53*, 7772-7775; d) B. Kohl, F. Rominger, M. Mastalerz, *Angew. Chem. Int. Ed.* **2015**, *54*, 6051-6056; *Angew. Chem.* **2015**, *127*, 6149-6154; e) B. Kohl, M. V. Bohnwagner, F. Rominger, H. Wadepohl, A. Dreuw, M. Mastalerz, *Chem. Eur. J.* **2016**, *22*, 646-655; f) L. Ueberricke, D. Holub, J. Kranz, F. Rominger, M. Elstner, M. Mastalerz, *Chem. Eur. J.* **2019**, *25*, 11121-11134; g) L. Ueberricke, S. Wieland, F. Rominger, M. Mastalerz, *Org. Mater.* **2019**, *01*, 050-062.

[198] J. U. Engelhart, O. Tverskoy, U. H. F. Bunz, *J. Am. Chem. Soc.* **2014**, *136*, 15166-15169.

[199] a) R. Mondal, B. K. Shah, D. C. Neckers, *J. Am. Chem. Soc.* **2006**, *128*, 9612-9613; b) R. Einholz, H. F. Bettinger, *Angew. Chem. Int. Ed.* **2013**, *52*, 9818-9820; *Angew. Chem.* **2013**, *125*, 10000-10003; c) R. Mondal, C. Tönshoff, D. Khon, D. C. Neckers, H. F. Bettinger, *J. Am. Chem. Soc.* **2009**, *131*, 14281-14289; d) C. Tönshoff, H. F. Bettinger, *Angew. Chem. Int. Ed.* **2010**, *49*, 4125-4128; *Angew. Chem.* **2010**, *122*, 4219-4222.

[200] R. Einholz, T. Fang, R. Berger, P. Grüninger, A. Früh, T. Chassé, R. F. Fink, H. F. Bettinger, *J. Am. Chem. Soc.* **2017**, *139*, 4435-4442.

[201] a) J. Krüger, F. García, F. Eisenhut, D. Skidin, J. M. Alonso, E. Guitián, D. Pérez, G. Cuniberti, F. Moresco, D. Peña, *Angew. Chem. Int. Ed.* **2017**, *56*, 11945-11948; *Angew. Chem.* **2017**, *129*, 12107-12110; b) R. Zuzak, R. Dorel, M. Krawiec, B. Such, M. Kolmer, M. Szymonski, A. M. Echavarren, S. Godlewski, *ACS Nano* **2017**, *11*, 9321-9329.

[202] a) L. Zhang, Y. Cao, N. S. Colella, Y. Liang, J.-L. Brédas, K. N. Houk, A. L. Briseno, *Acc. Chem. Res.* **2015**, *48*, 500-509; b) L. Zhang, A. Fonari, Y. Liu, A.-L. M. Hoyt, H. Lee, D. Granger, S. Parkin, T. P. Russell, J. E. Anthony, J.-L. Brédas, V. Coropceanu, A. L. Briseno, *J. Am. Chem. Soc.* **2014**, *136*, 9248-9251; c) J. Xiao, H. M. Duong, Y. Liu, W. Shi, L. Ji, G. Li, S. Li, X.-W. Liu, J. Ma, F. Wudl, Q. Zhang, *Angew. Chem. Int. Ed.* **2012**, *51*, 6094-6098; *Angew. Chem.* **2012**, *124*, 6198-6202; d) W. Chen, X. Li, G. Long, Y. Li, R. Ganguly, M. Zhang, N. Aratani, H. Yamada, M. Liu, Q. Zhang, *Angew. Chem. Int. Ed.* **2018**, *57*, 13555-13559; *Angew. Chem.* **2018**, *130*, 13743-13747.

[203] Q. Ai, K. Jarolimek, S. Mazza, J. E. Anthony, C. Risko, *Chem. Mater.* **2018**, *30*, 947-957.

[204] a) D. Reinhard, F. Rominger, M. Mastalerz, *J. Org. Chem.* **2015**, *80*, 9342-9348; b) E. H. Menke, D. Leibold, A. P. Ullrich, Y. Vaynzof, M. Mastalerz, *Org. Chem. Front.* **2017**, *4*, 834-838; c) B. Kohl, K. Baumgärtner, F. Rominger, M. Mastalerz, *Eur. J. Org. Chem.* **2019**, *2019*, 4891-4896.

[205] F. Bertani, N. Riboni, F. Bianchi, G. Brancatelli, E. S. Sterner, R. Pinalli, S. Geremia, T. M. Swager, E. Dalcanale, *Chem. Eur. J.* **2016**, *22*, 3312-3319.

[206] a) C. Adamo, C. Amatore, I. Ciofini, A. Jutand, H. Lakmini, *J. Am. Chem. Soc.* **2006**, *128*, 6829-6836; b) V. A. Kallepalli, K. A. Gore, F. Shi, L. Sanchez, G. A. Chotana, S. L. Miller, R. E. Maleczka, M. R. Smith, *J. Org. Chem.* **2015**, *80*, 8341-8353; c) L. Metzler, T. Reichenbach, O. Brügner, H. Komber, F. Lombeck, S. Müllers, R. Hanselmann, H. Hillebrecht, M. Walter, M. Sommer, *Poly. Chem.* **2015**, *6*, 3694-3707.

[207] R. Viruela-Martín, P. M. Viruela-Martín, E. Ortí, *J. Chem. Phys.* **1992**, *97*, 8470-8480.

[208] a) C. G. Swain, A. L. Powell, W. A. Sheppard, C. R. Morgan, *J. Am. Chem. Soc.* **1979**, *101*, 3576-3583; b) in *Name Reactions: A Collection of Detailed Reaction Mechanisms*, Springer Berlin Heidelberg, **2006**, 107-108; c) Z. Wang, in *Comprehensive Organic Name Reactions and Reagents*, John Wiley & Sons, Inc., **2010**, 602-605.

[209] M. J. Frisch, G. W. Trucks, H. B. Schlegel, G. E. Scuseria, M. A. Robb, J. R. Cheeseman, G. Scalmani, V. Barone, B. Mennucci, G. A. Petersson, H. Nakatsuji, M. Caricato, X. Li, H. P. Hratchian, A. F. Izmaylov, J. Bloino, G. Zheng, J. L. Sonnenberg, M. Hada, M. Ehara, K. Toyota, R. Fukuda, J. Hasegawa, M. Ishida, T. Nakajima, Y. Honda, O. Kitao, H. Nakai, T. Vreven, J. A. Montgomery Jr., J. E. Peralta, F. Ogliaro, M. Bearpark, J. J. Heyd, E. Brothers, K. N. Kudin, V. N. Staroverov, K. T., R. Kobayashi, J. Normand, K. Raghavachari, A. Rendell, J. C. Burant, S. S. Iyengar, J. Tomasi, M. Cossi, N. Rega, J. M. Millam, M. Klene, J. E. Knox, J. B. Cross, V. Bakken, C. Adamo, J. Jaramillo, R. Gomperts, R. E. Stratmann, O. Yazyev, A. J. Austin, R. Cammi, C. Pomelli, J. W. Ochterski, R. L. Martin, K. Morokuma, V. G. Zakrzewski, G. A. Voth, P. Salvador, J. J. Dannenberg, S. Dapprich, A. D. Daniels, Ö. Farkas, J. B. Foresman, J. V. Ortiz, J. Cioslowski, D. J. Fox, *Gaussian 09, Revision D.01*, Gaussian, Inc., Wallingford CT, **2016**.

[210] H. Meier, U. Stalmach, H. Kolshorn, *Acta Polym.* **1997**, *48*, 379-384.

[211] I. B. Berlman, in *Handbook of Fluorescence Spectra of Aromatic Molecules (Second Edition)*, Elsevier Inc., **1971**, 67-95.

[212] W. C. Still, M. Kahn, A. Mitra, *J. Org. Chem.* **1978**, *43*, 2923-2925.

[213] G. M. Sheldrick, *SADABS 2012/1: Program for Absorption Correction; Bruker Analytical X-ray Division*, Madison (USA), **2012**.

[214] G. M. Sheldrick, *Acta Crystallogr. A* **2008**, *64*, 112-122.

[215] C. Würth, M. Grabolle, J. Pauli, M. Spieles, U. Resch-Genger, *Nat. Protoc.* **2013**, *8*, 1535-1550.

[216] a) P. Hohenberg, W. Kohn, *Phys. Rev.* **1964**, *136*, B864-B871; b) W. Kohn, L. J. Sham, *Phys. Rev.* **1965**, *140*, A1133-A1138; c) R. G. Parr, W. Yang, *Density-functional theory of atoms and molecules, 1. ed.*, Oxford Univ. Press, New York, NY, **1994**; d) W. Koch, *Chemist's Guide to Density Functional Theory, 2. ed.*, Wiley-VCH, Weinheim, **2001**.

[217] a) J. R. Cheeseman, G. W. Trucks, T. A. Keith, M. J. Frisch, *J. Chem. Phys.* **1996**, *104*, 5497-5509; b) R. Ditchfield, *Mol. Phys.* **1974**, *27*, 789-807; c) F. London, *J. Phys. Radium* **1937**, *8*, 397-409; d) R. McWeeny, *Phys. Rev.* **1962**, *126*, 1028-1034; e) K. Wolinski, J. F. Hinton, P. Pulay, *J. Am. Chem. Soc.* **1990**, *112*, 8251-8260.

[218] Q. Sun, B. Aguila, J. Perman, L. D. Earl, C. W. Abney, Y. Cheng, H. Wei, N. Nguyen, L. Wojtas, S. Ma, *J. Am. Chem. Soc.* **2017**, *139*, 2786-2793.

[219] a) X. Yang, F. Rominger, M. Mastalerz, *Org. Lett.* **2018**, *20*, 7270-7273; b) X. Yang, M. Hoffmann, F. Rominger, T. Kirschbaum, A. Dreuw, M. Mastalerz, *Angew. Chem. Int. Ed.* **2019**, *58*, 10650-10654; *Angew. Chem.* **2019**, *131*, 10760-10764; c) X. Yang, F. Rominger, M. Mastalerz, *Angew. Chem. Int. Ed.* **2019**, *58*, 17577-17582; *Angew. Chem.* **2019**, *131*, 17741-17746.

7. Appendix

The following sections only include the unpublished experimental data. The figures already published in this thesis can be found in the references.[219] All the spectra were recorded at room temperature unless otherwise noted.

7.1 NMR spectra

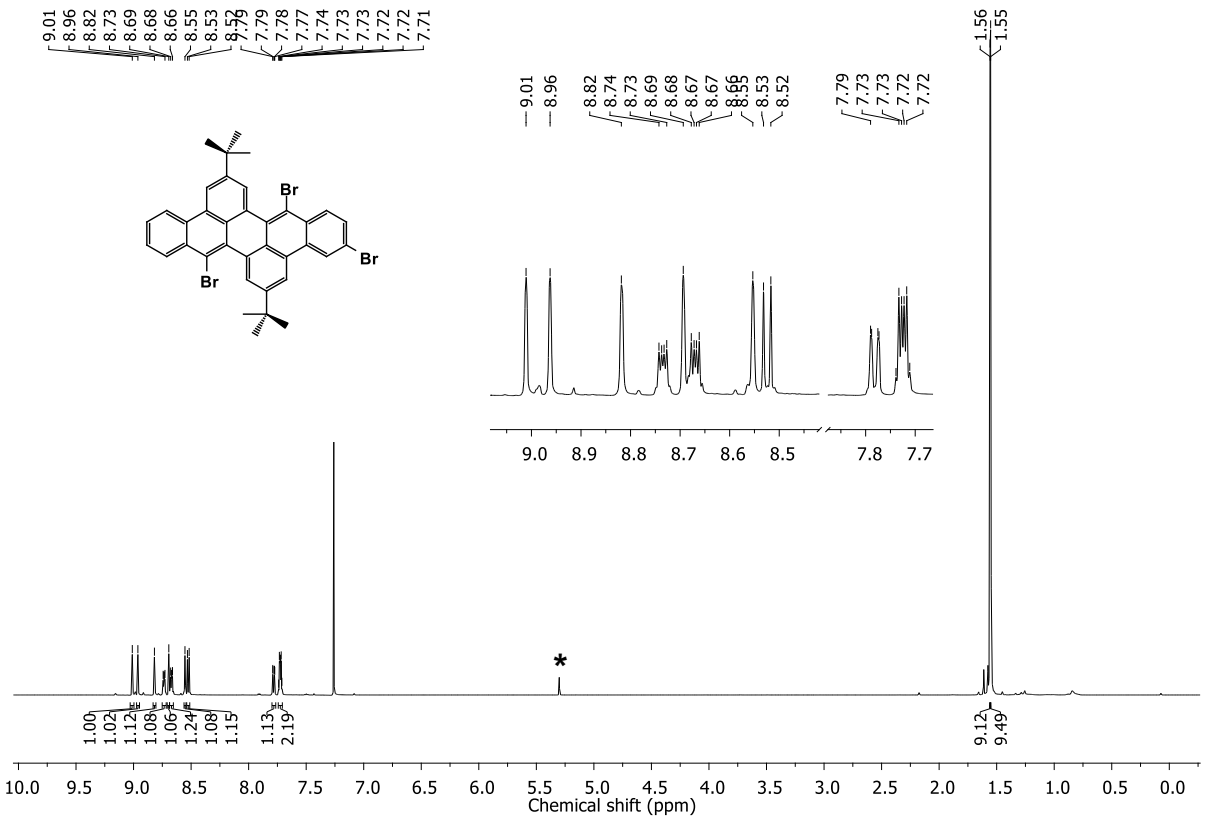

Figure 7.1 ^{1}H NMR spectrum (600 MHz, $CDCl_3$) of **134**. *CH_2Cl_2.

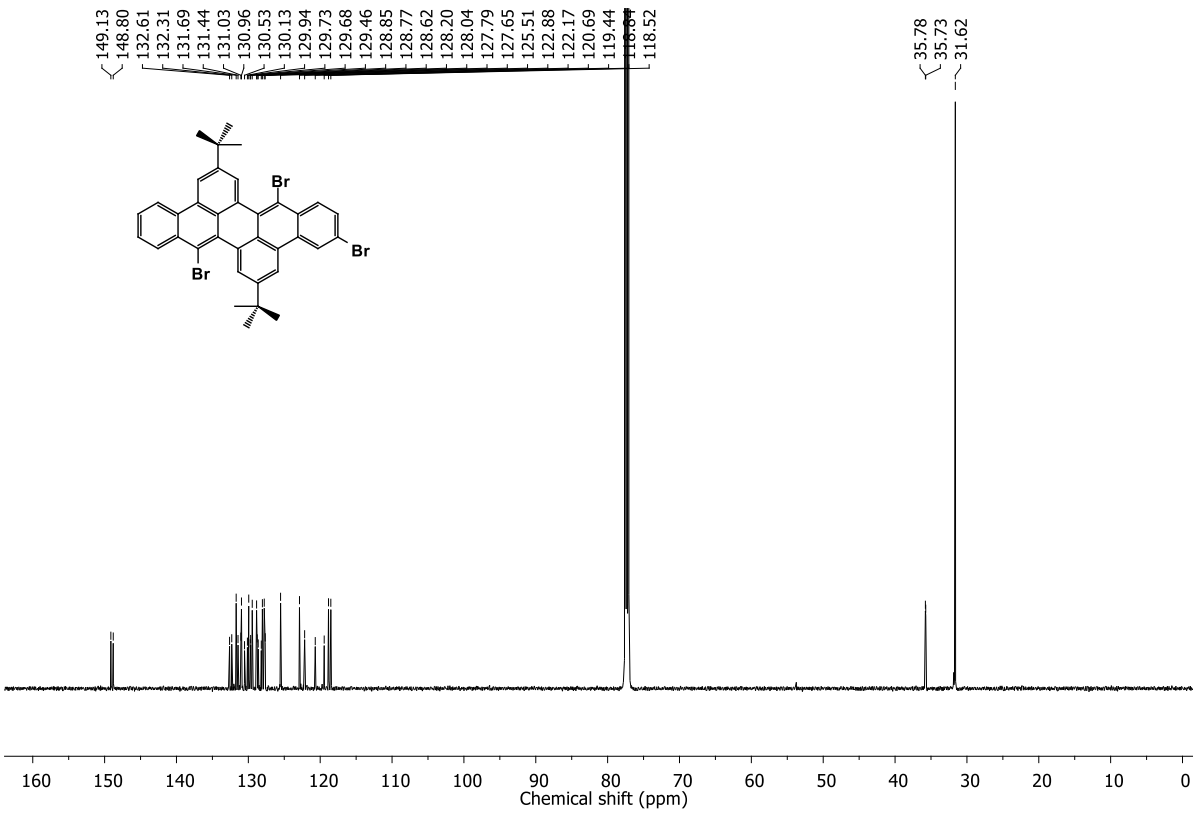

Figure 7.2 ^{13}C NMR spectrum (151 MHz, $CDCl_3$) of **134**.

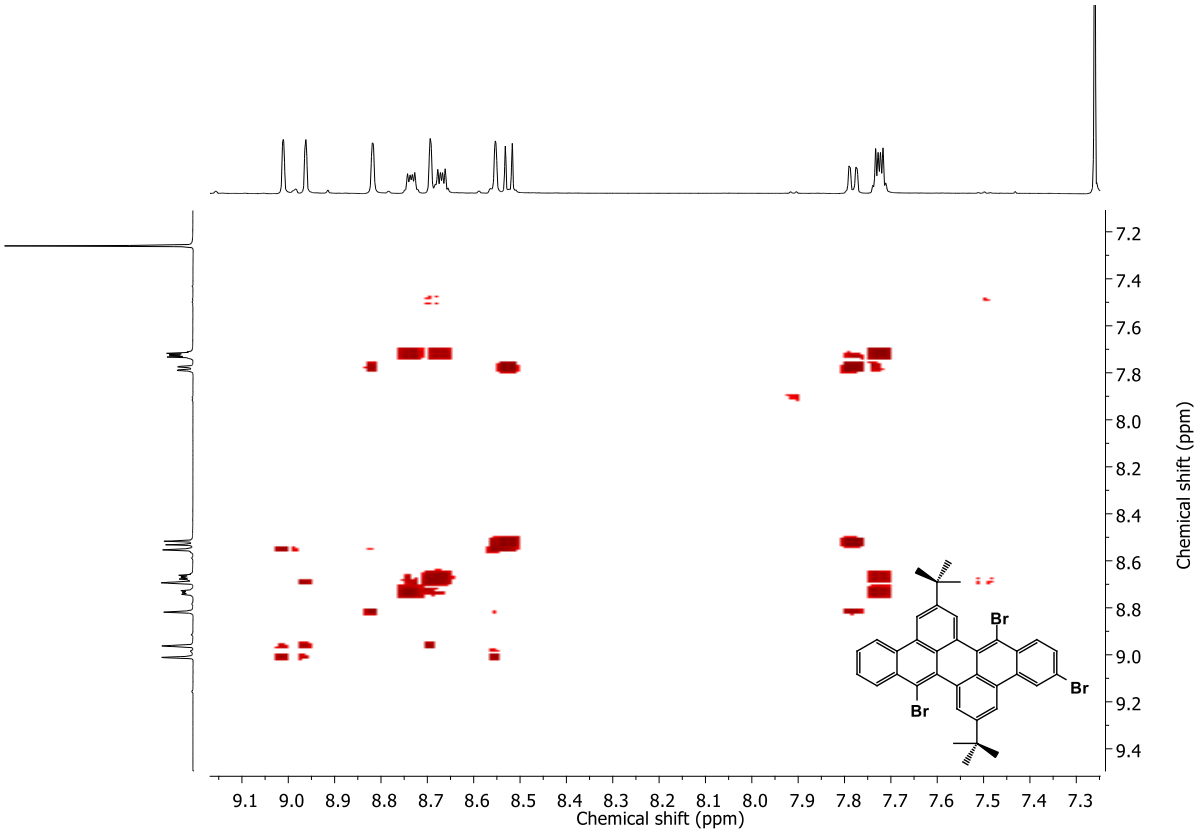

Figure 7.3 ^{1}H-^{1}H COSY NMR spectrum (600/600 MHz, $CDCl_3$) of **134**.

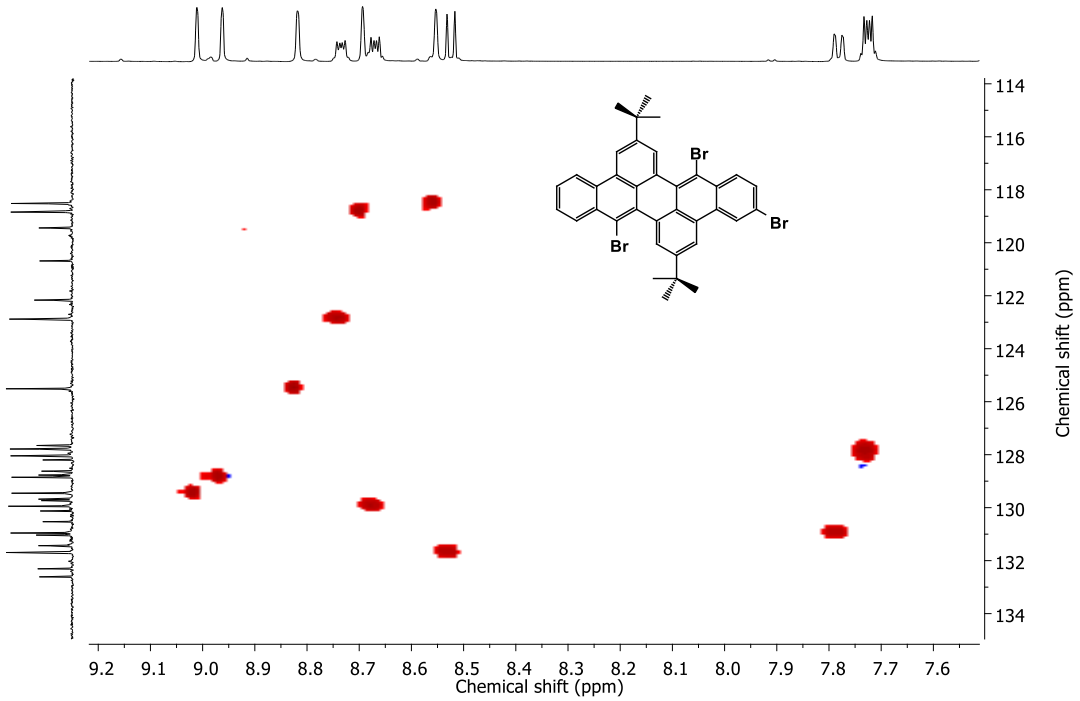

Figure 7.4 ^{1}H-^{13}C HSQC NMR spectrum (600/151 MHz, $CDCl_3$) of **134**.

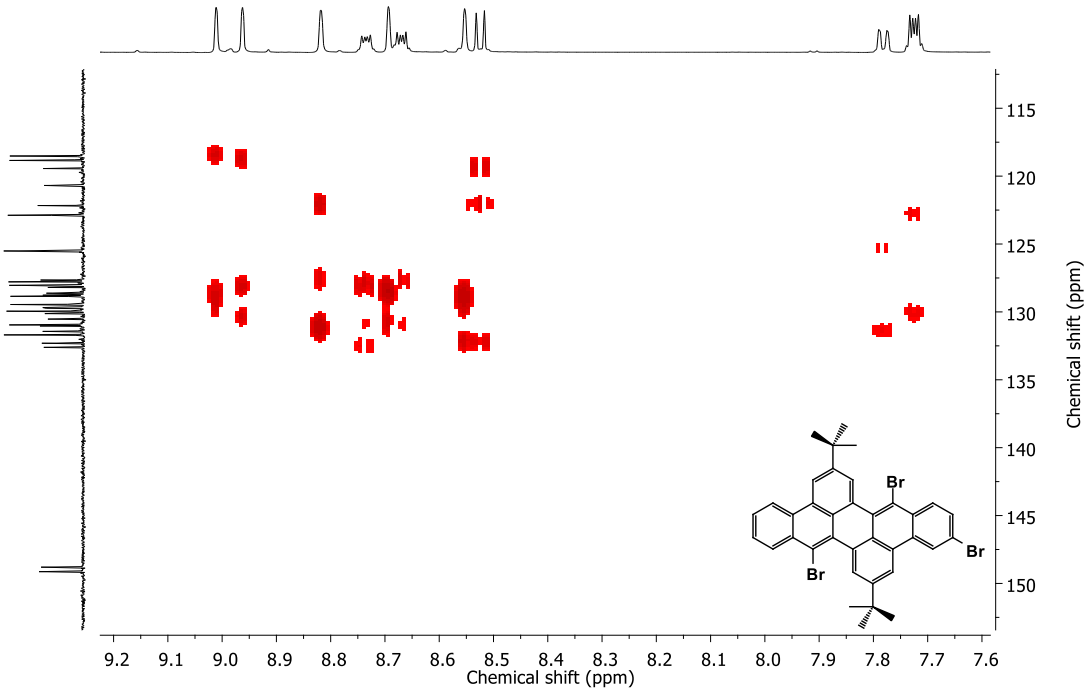

Figure 7.5 ^{1}H-^{13}C HMBC NMR spectrum (600/151 MHz, $CDCl_3$) of **134**.

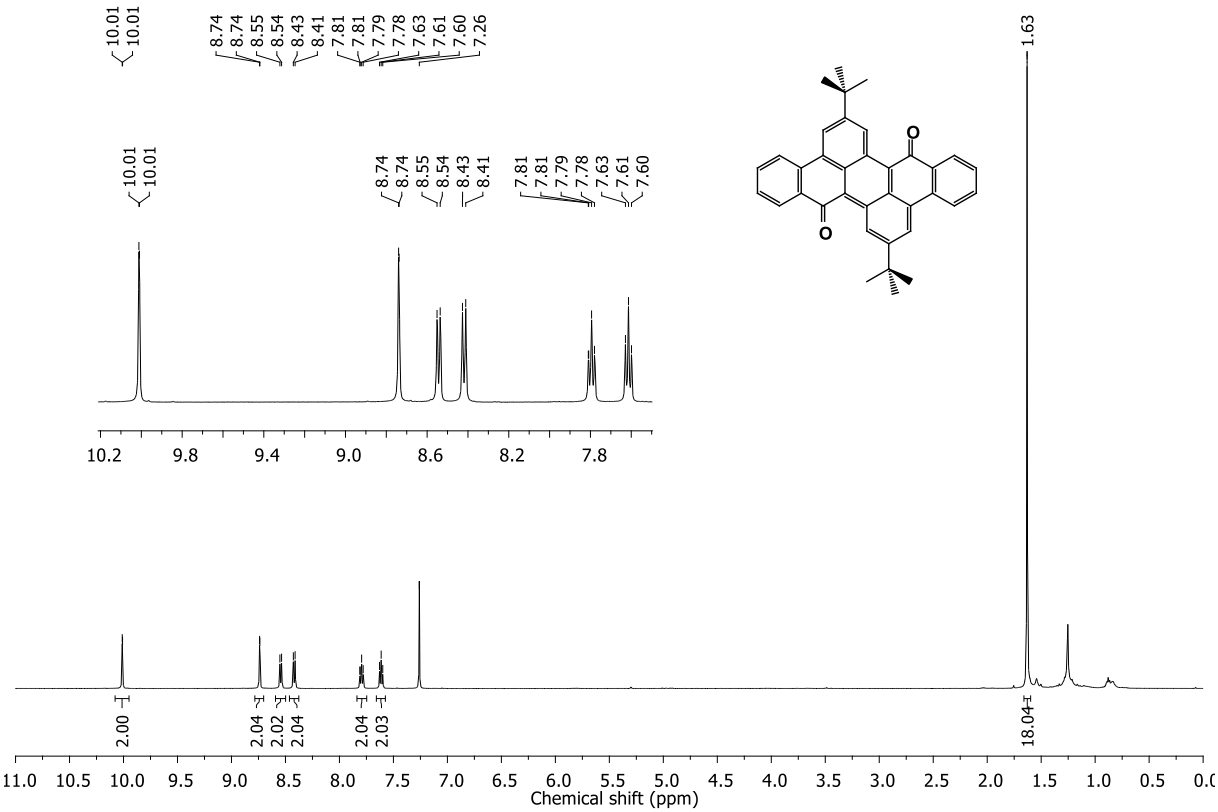

Figure 7.6 ^{1}H NMR spectrum (500 MHz, $CDCl_3$) of **136**.

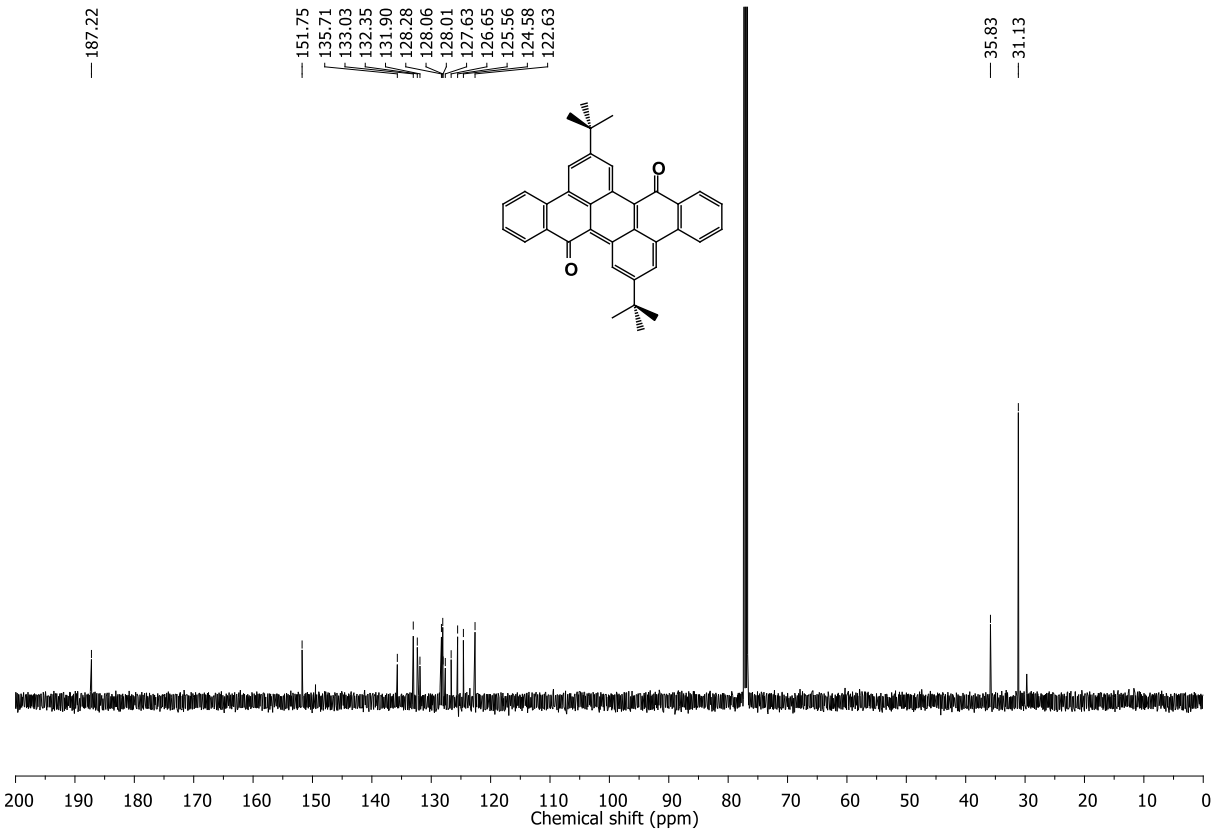

Figure 7.7 ^{13}C NMR spectrum (125 MHz, $CDCl_3$) of **136**.

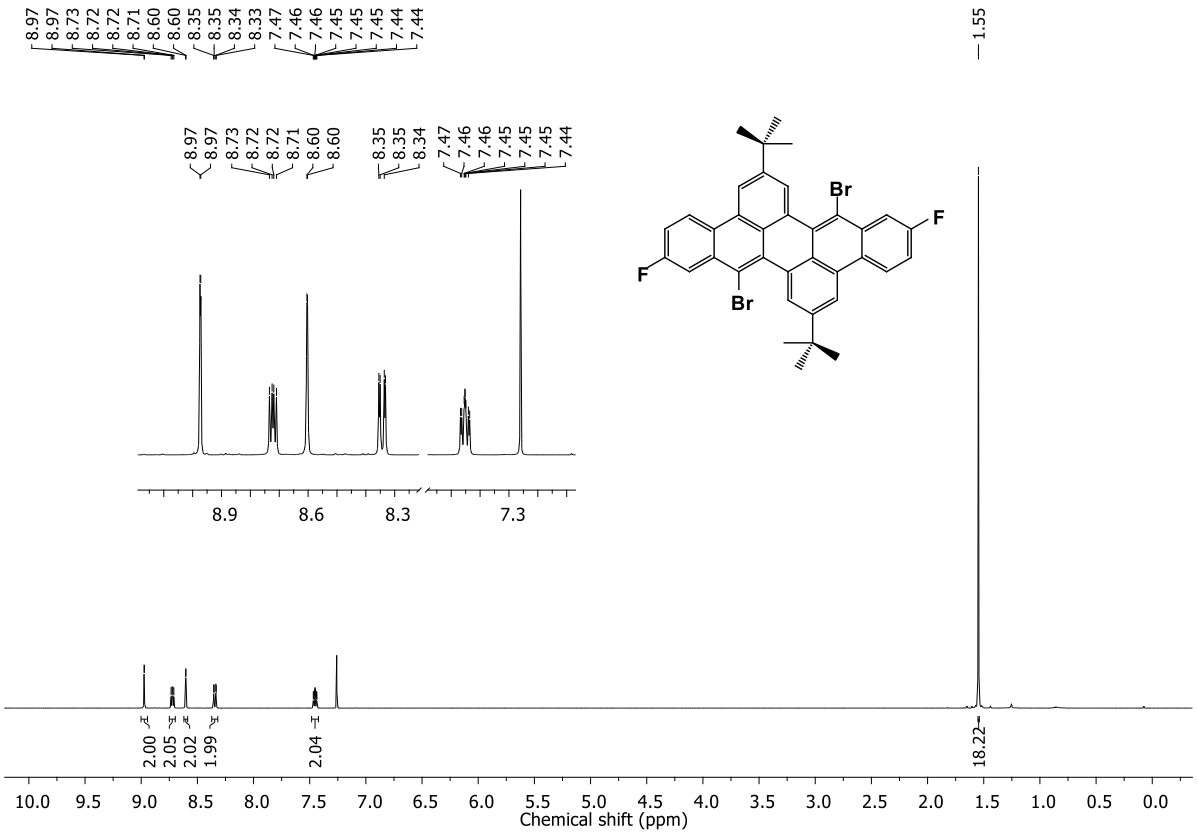

Figure 7.8 ^{1}H NMR spectrum (600 MHz, $CDCl_3$) of **138**.

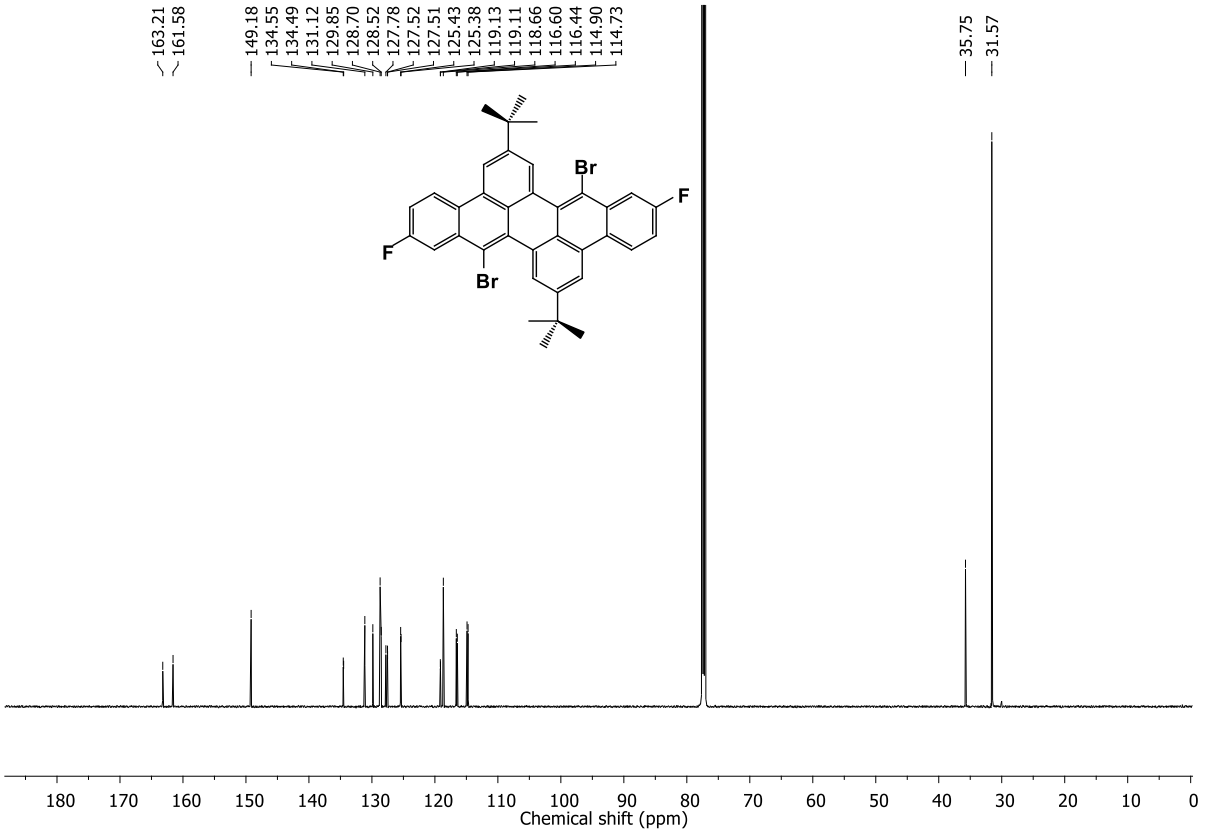

Figure 7.9 ^{13}C NMR spectrum (151 MHz, $CDCl_3$) of **138**.

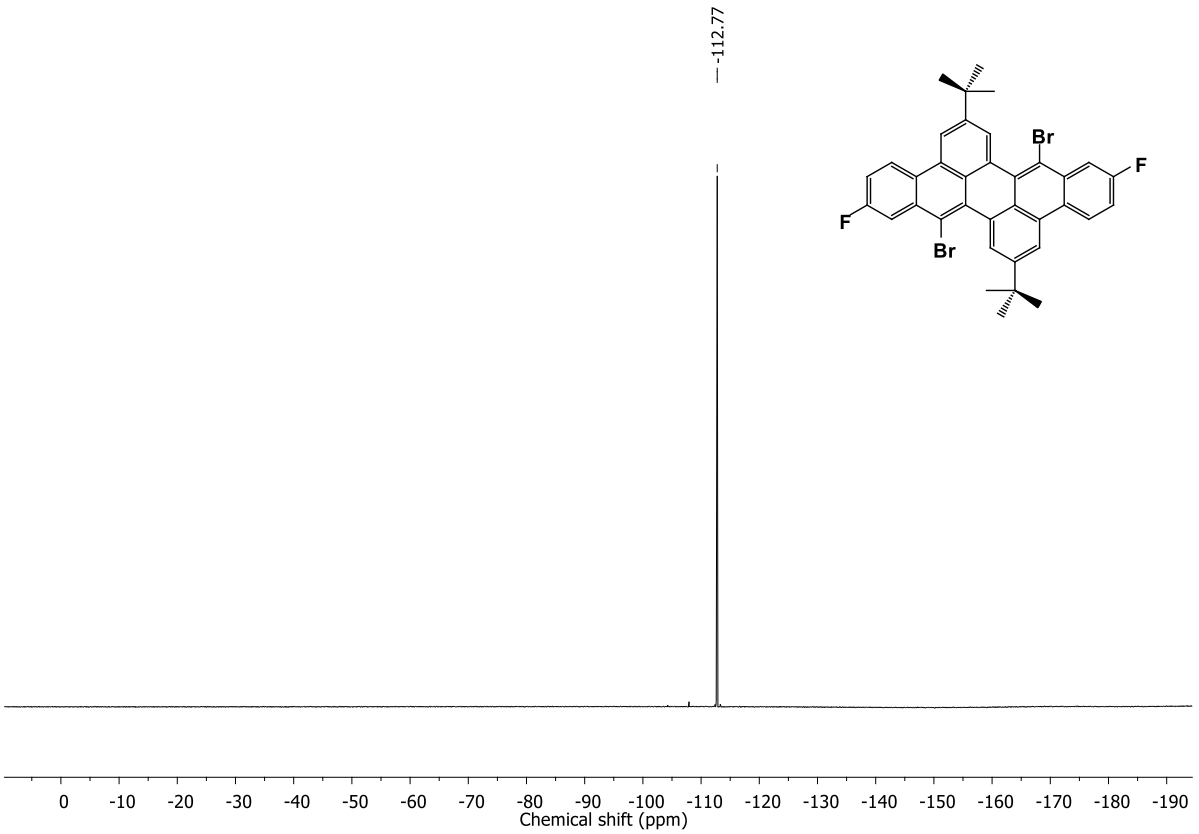

Figure 7.10 ^{19}F NMR spectrum (283 MHz, $CDCl_3$) of **138**.

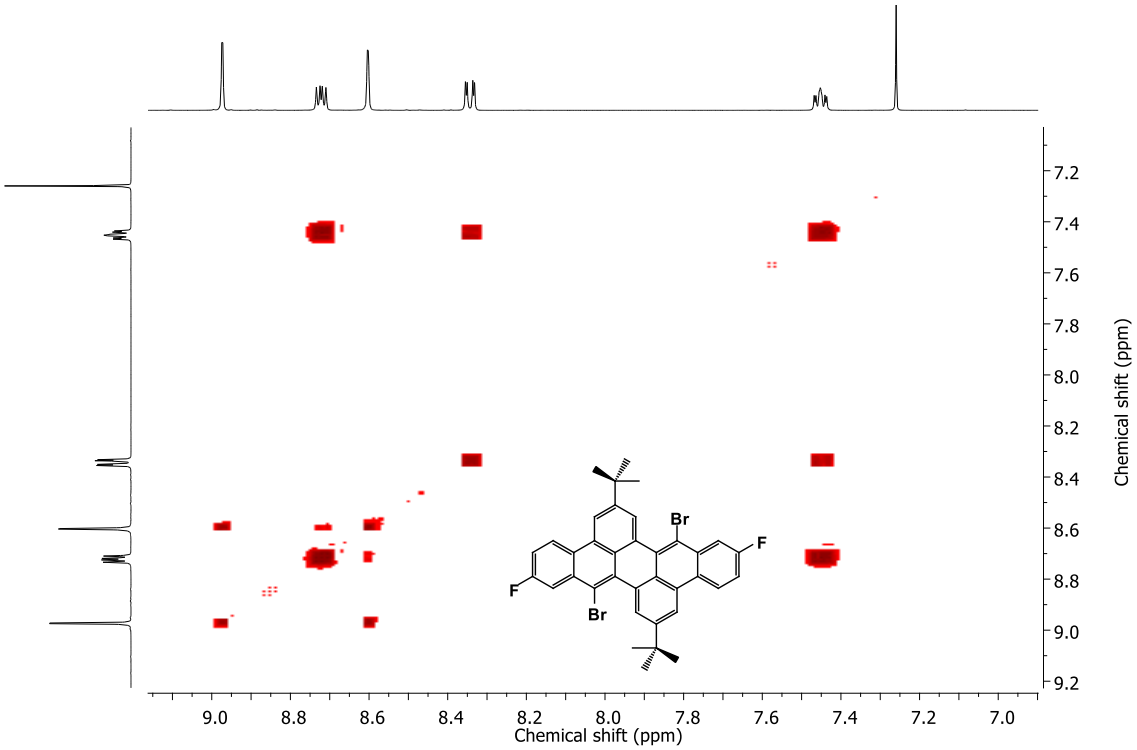

Figure 7.11 ^{1}H-^{1}H COSY NMR spectrum (600/600 MHz, $CDCl_3$) of **138**.

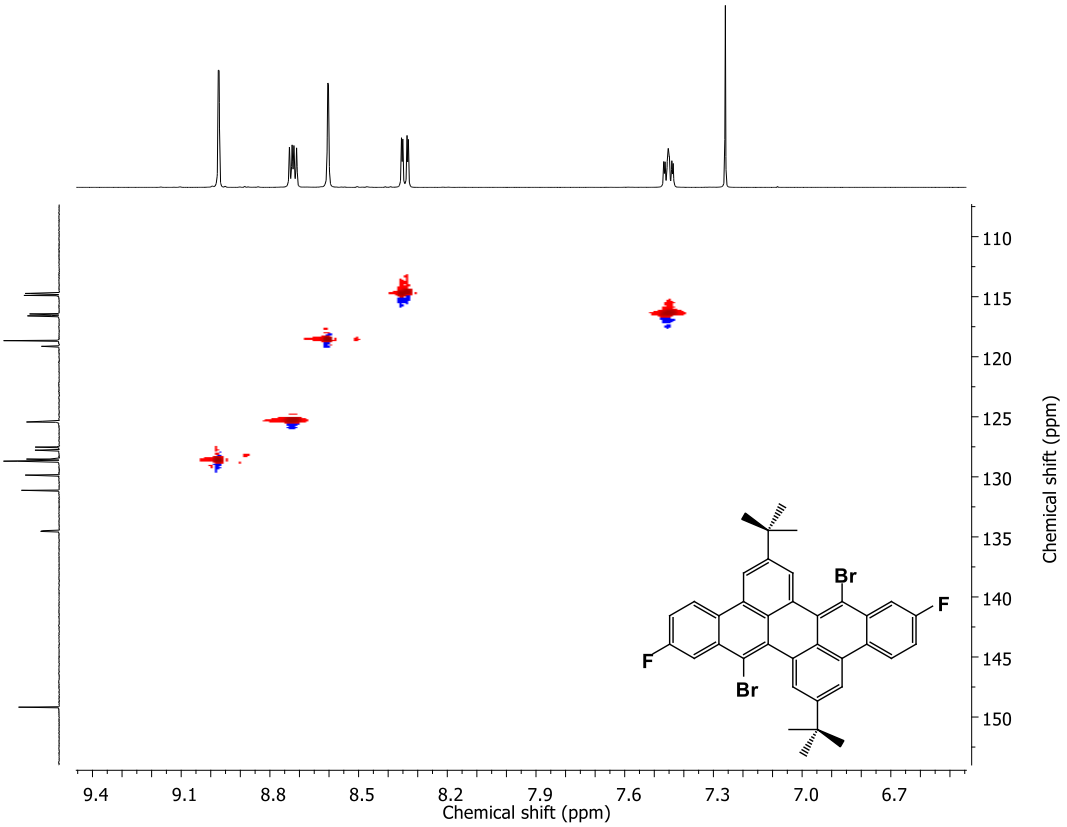

Figure 7.12 ^{1}H-^{13}C HSQC NMR spectrum (600/151 MHz, $CDCl_3$) of **138**.

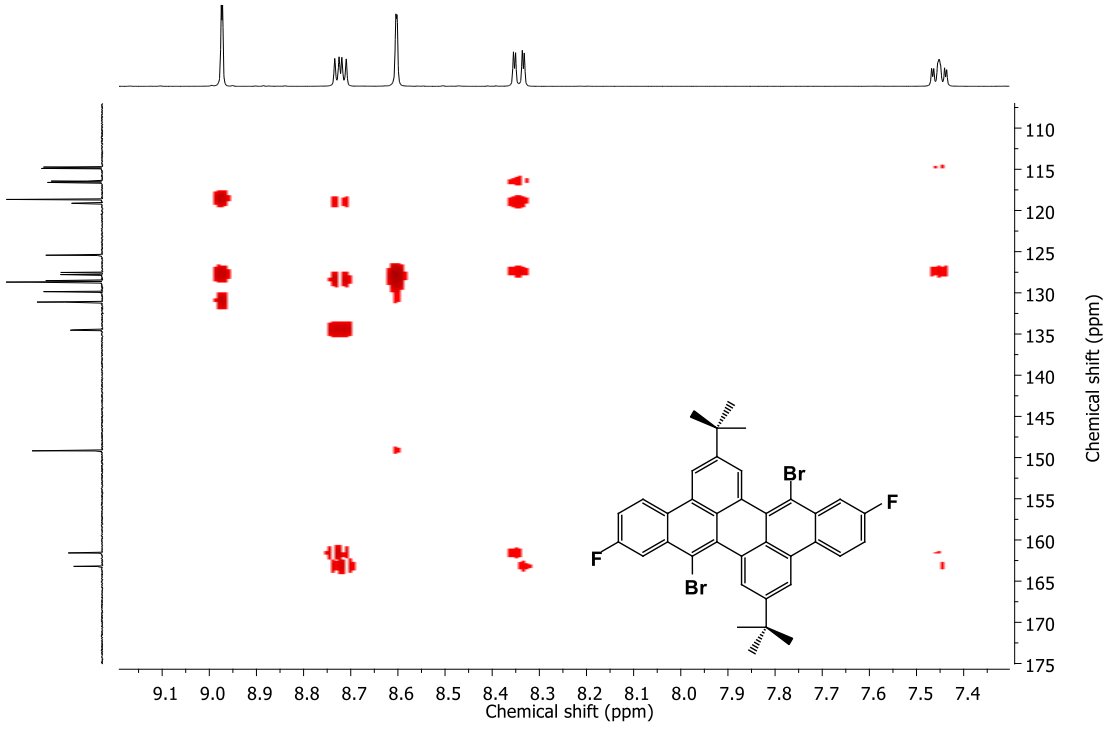

Figure 7.13 ^{1}H-^{13}C HMBC NMR spectrum (600/151 MHz, $CDCl_3$) of **138**.

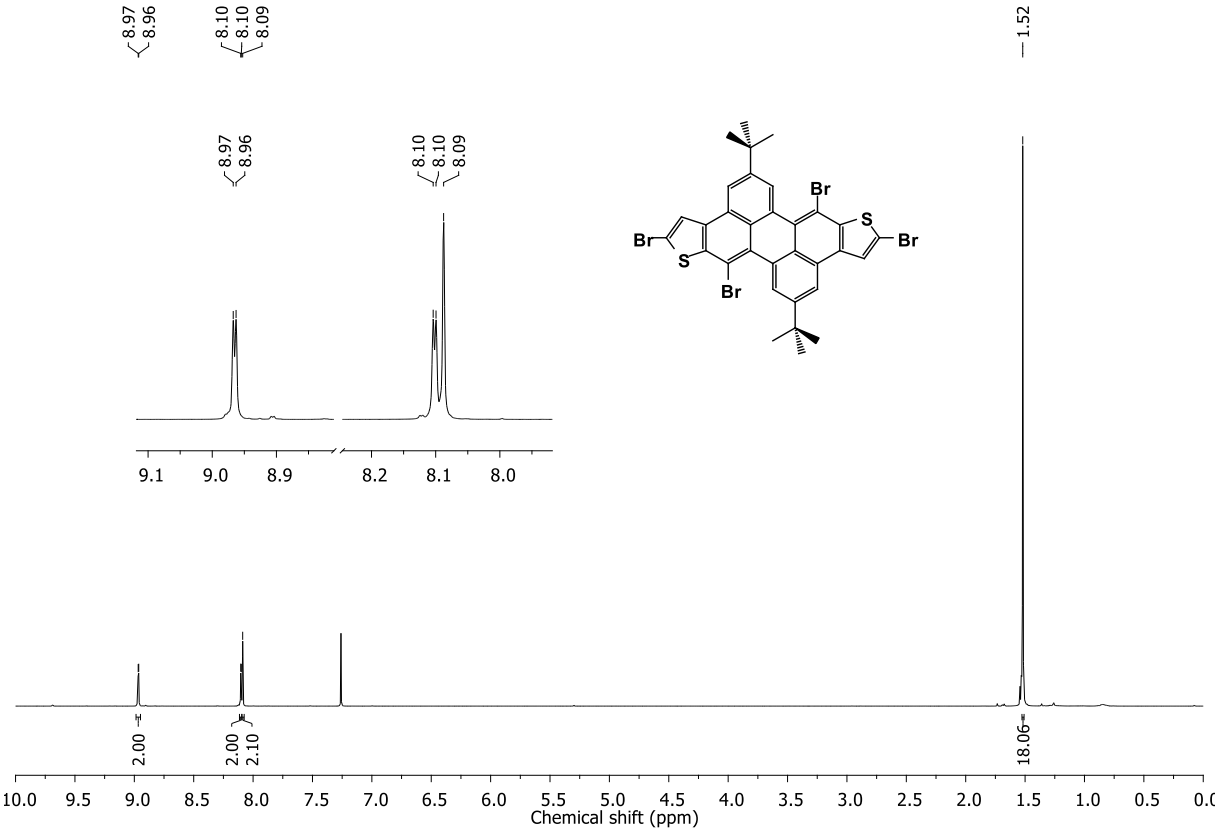

Figure 7.14 ^{1}H NMR spectrum (400 MHz, $CDCl_3$) of **139**.

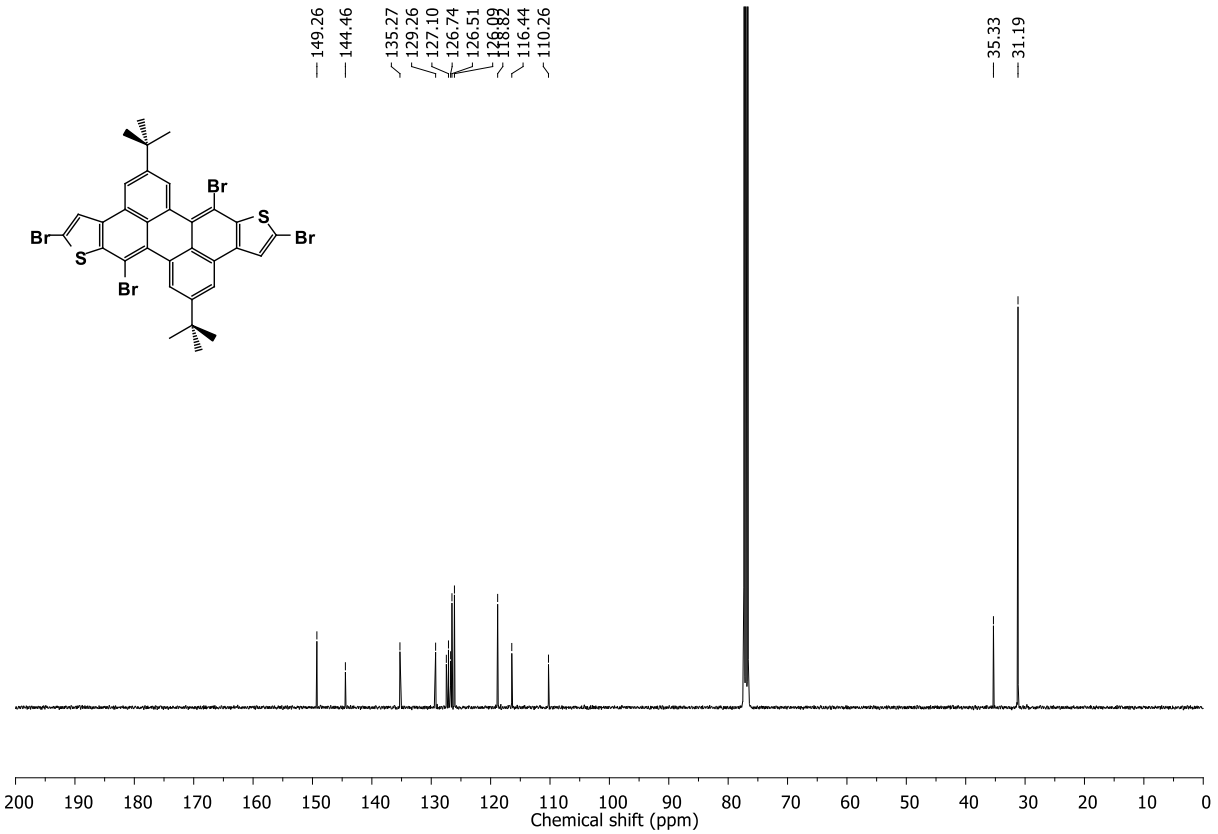

Figure 7.15 ^{13}C NMR spectrum (101 MHz, $CDCl_3$) of **139**.

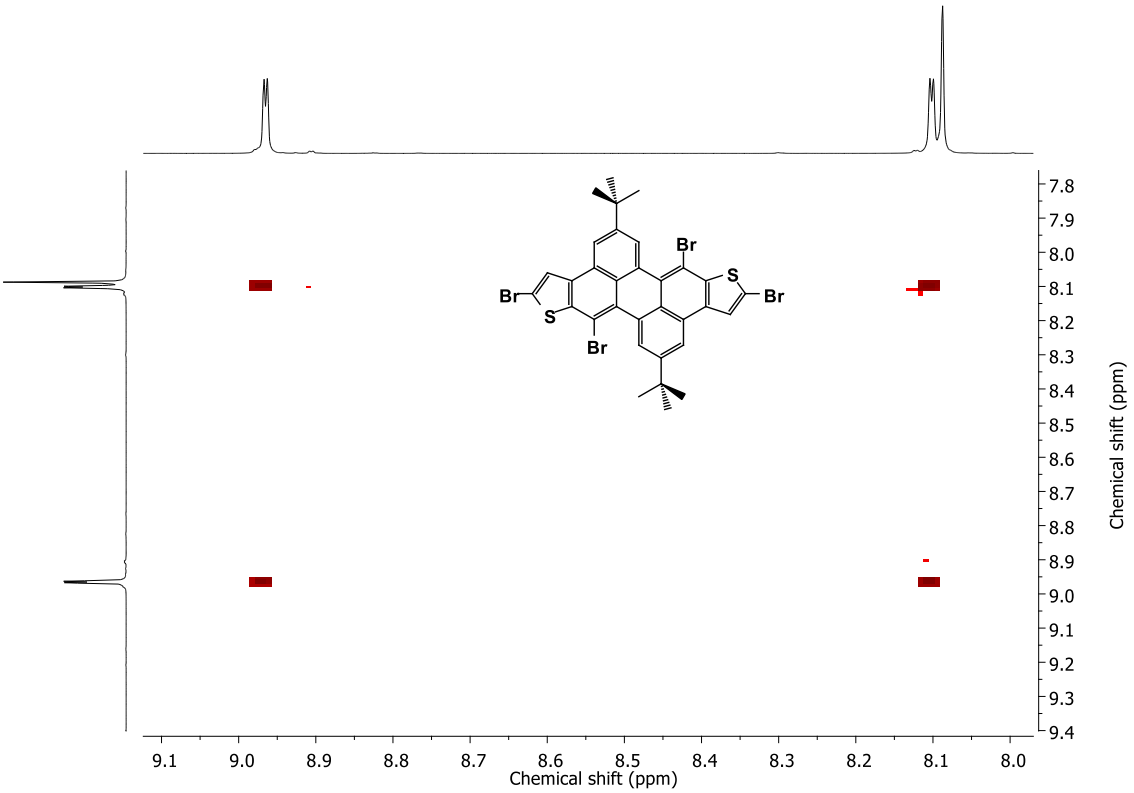

Figure 7.16 ^{1}H-^{1}H COSY NMR spectrum (400/400 MHz, $CDCl_3$) of **139**.

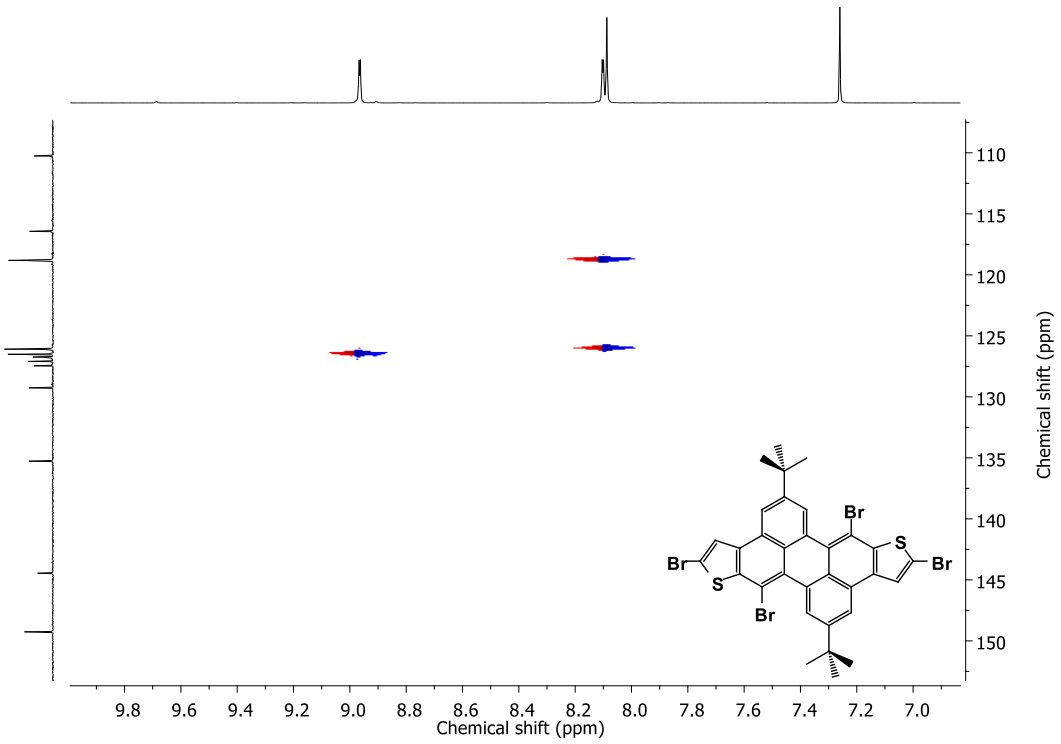

Figure 7.17 ^{1}H-^{13}C HSQC NMR spectrum (400/101 MHz, $CDCl_3$) of **139**.

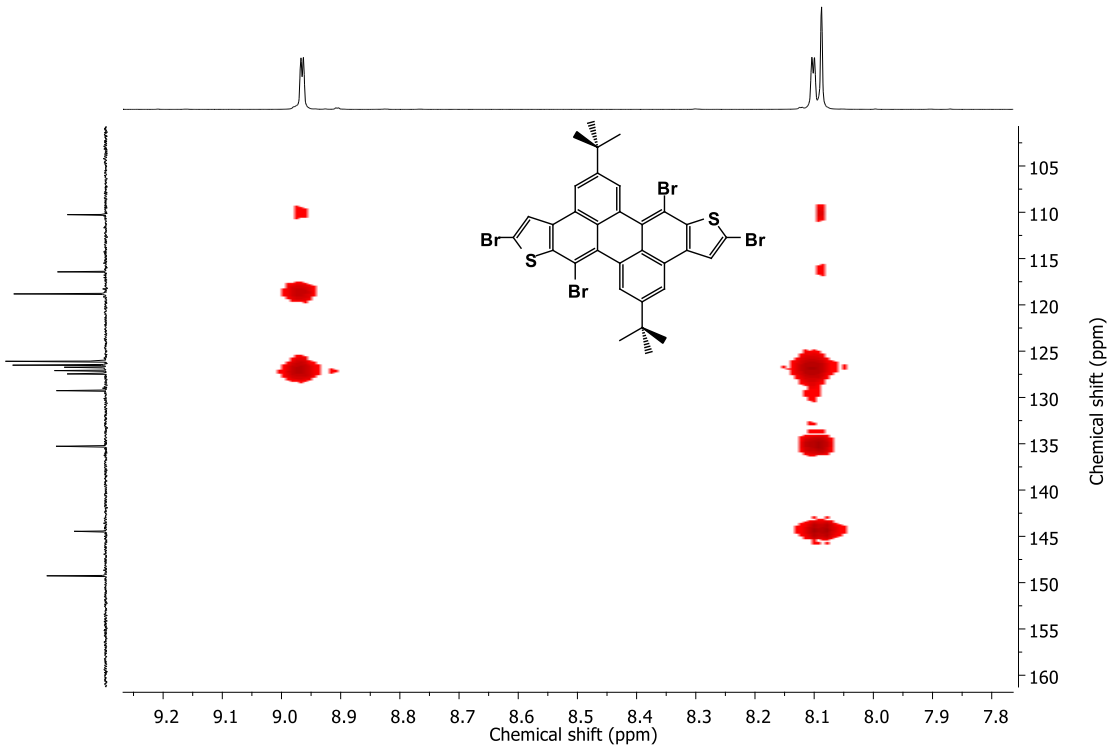

Figure 7.18 ^{1}H-^{13}C HMBC NMR spectrum (400/101 MHz, $CDCl_3$) of **139**.

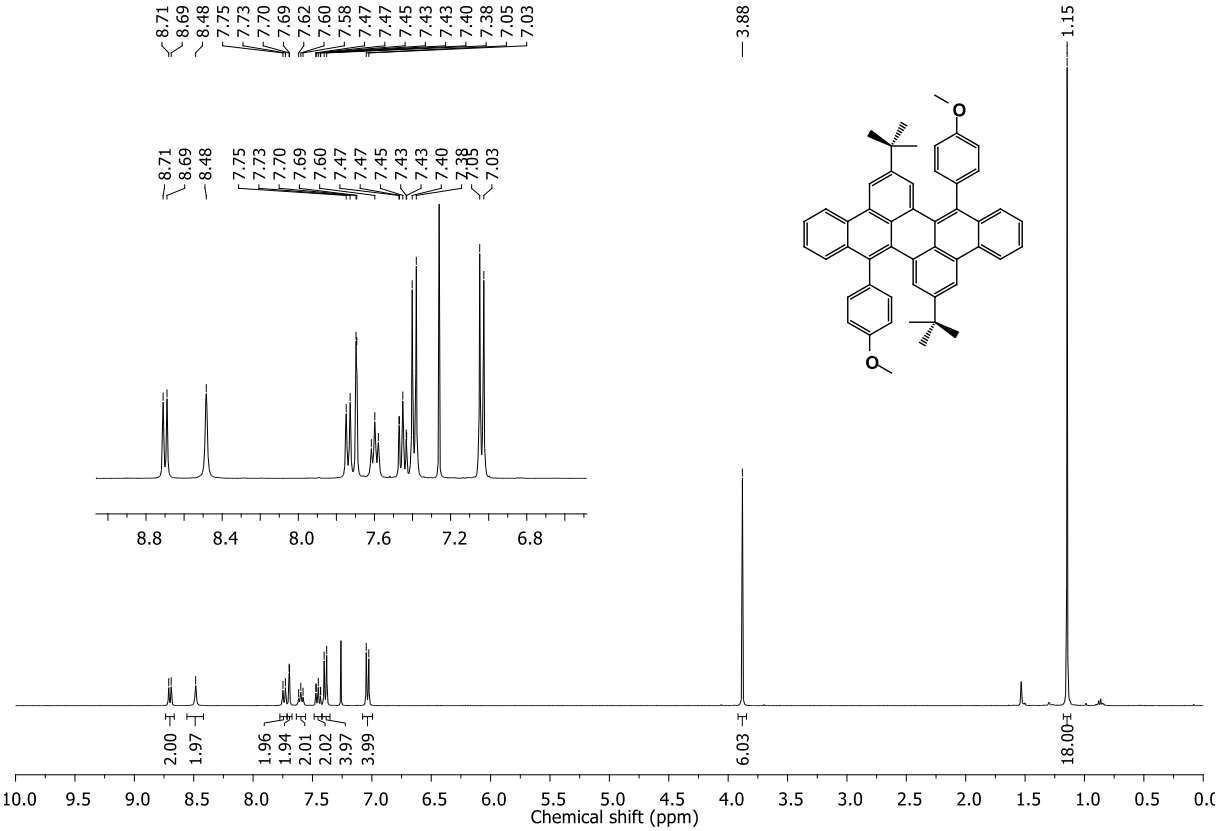

Figure 7.19 ^{1}H NMR spectrum (400 MHz, $CDCl_3$) of **144**.

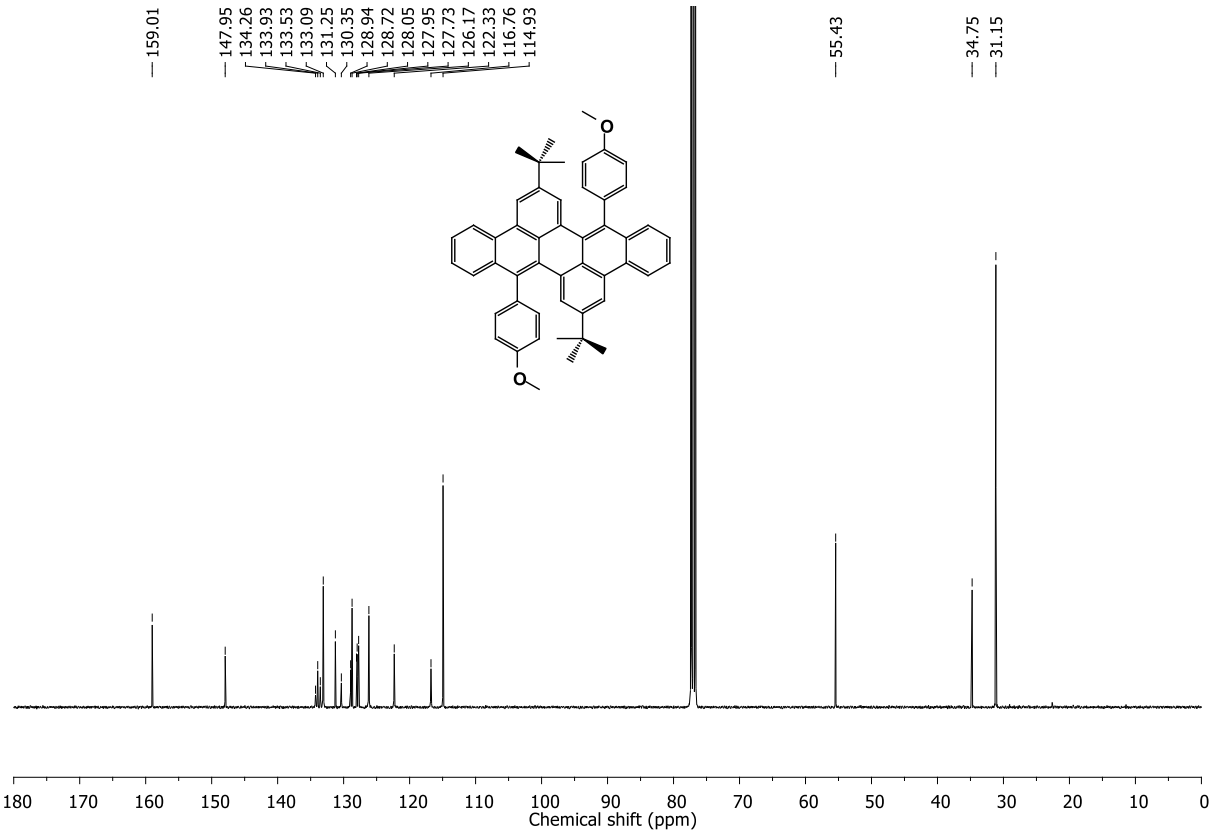

Figure 7.20 ^{13}C NMR spectrum (101 MHz, $CDCl_3$) of **144**.

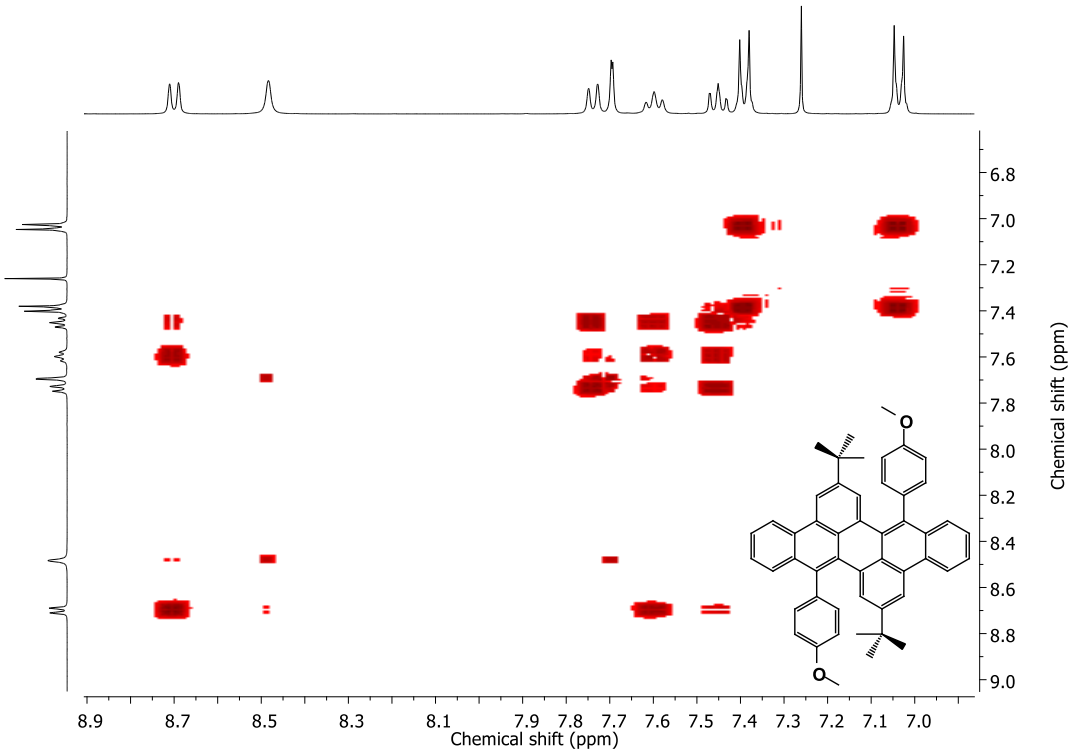

Figure 7.21 ^{1}H-^{1}H COSY NMR spectrum (400/400 MHz, $CDCl_3$) of **144**.

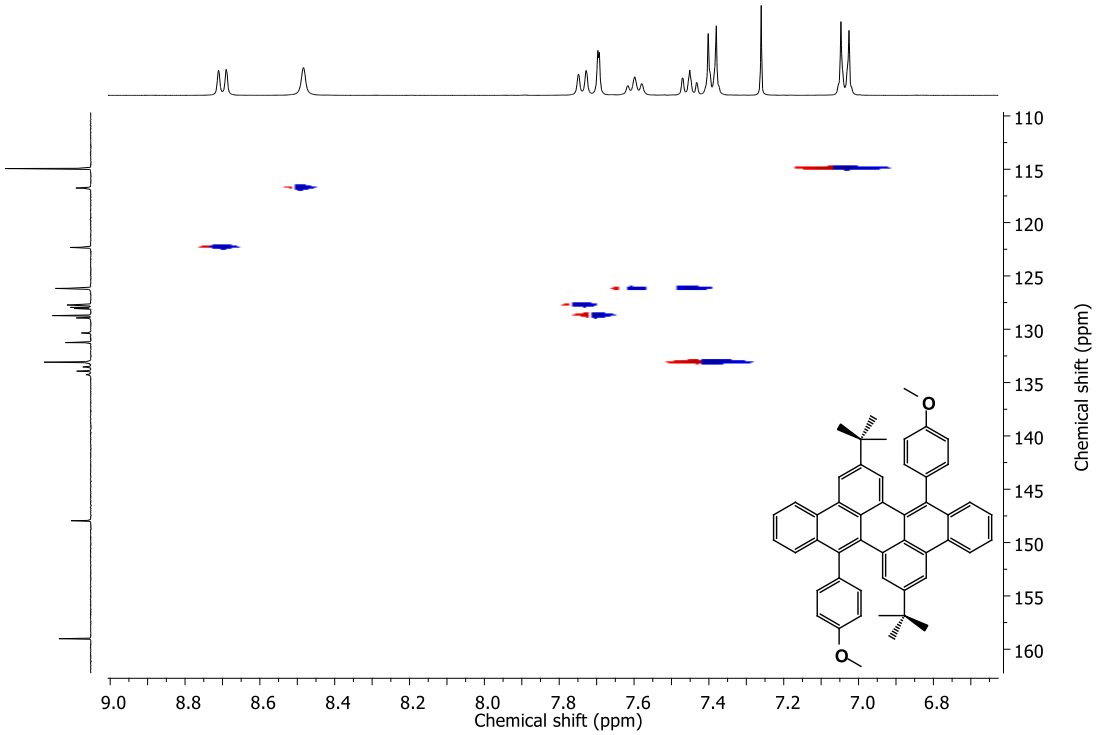

Figure 7.22 ^{1}H-^{13}C HSQC NMR spectrum (400/101 MHz, $CDCl_3$) of **144**.

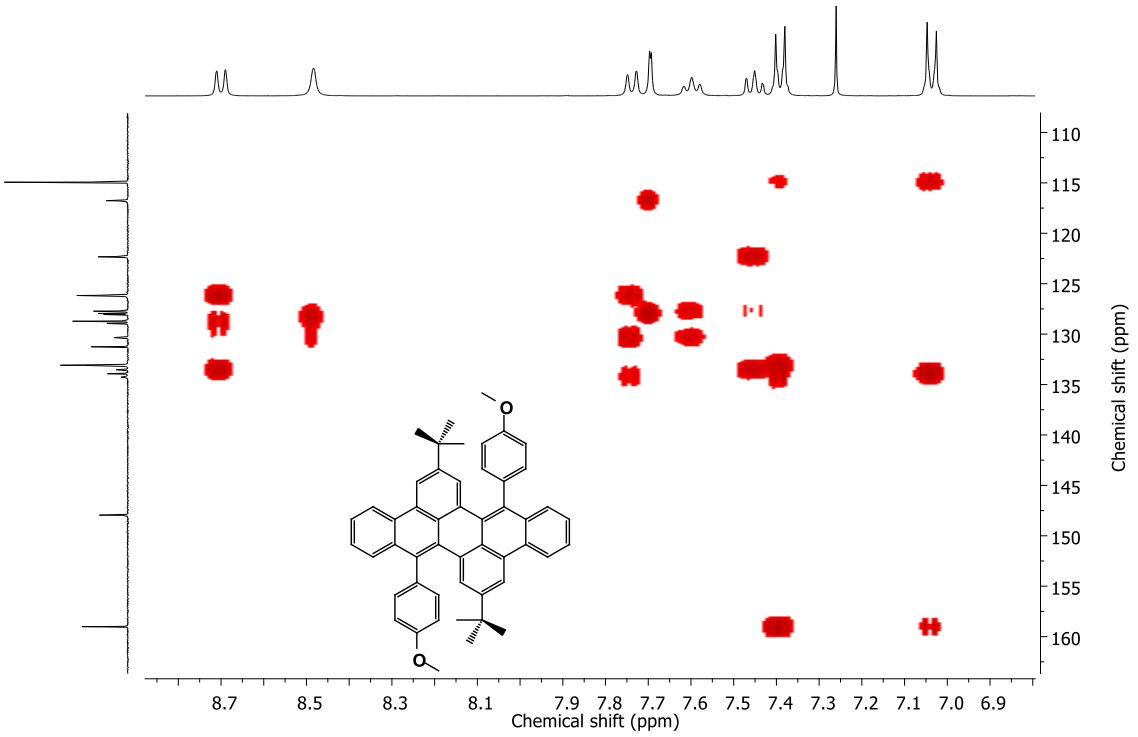

Figure 7.23 ^{1}H-^{13}C HMBC NMR spectrum (400/101 MHz, $CDCl_3$) of **144**.

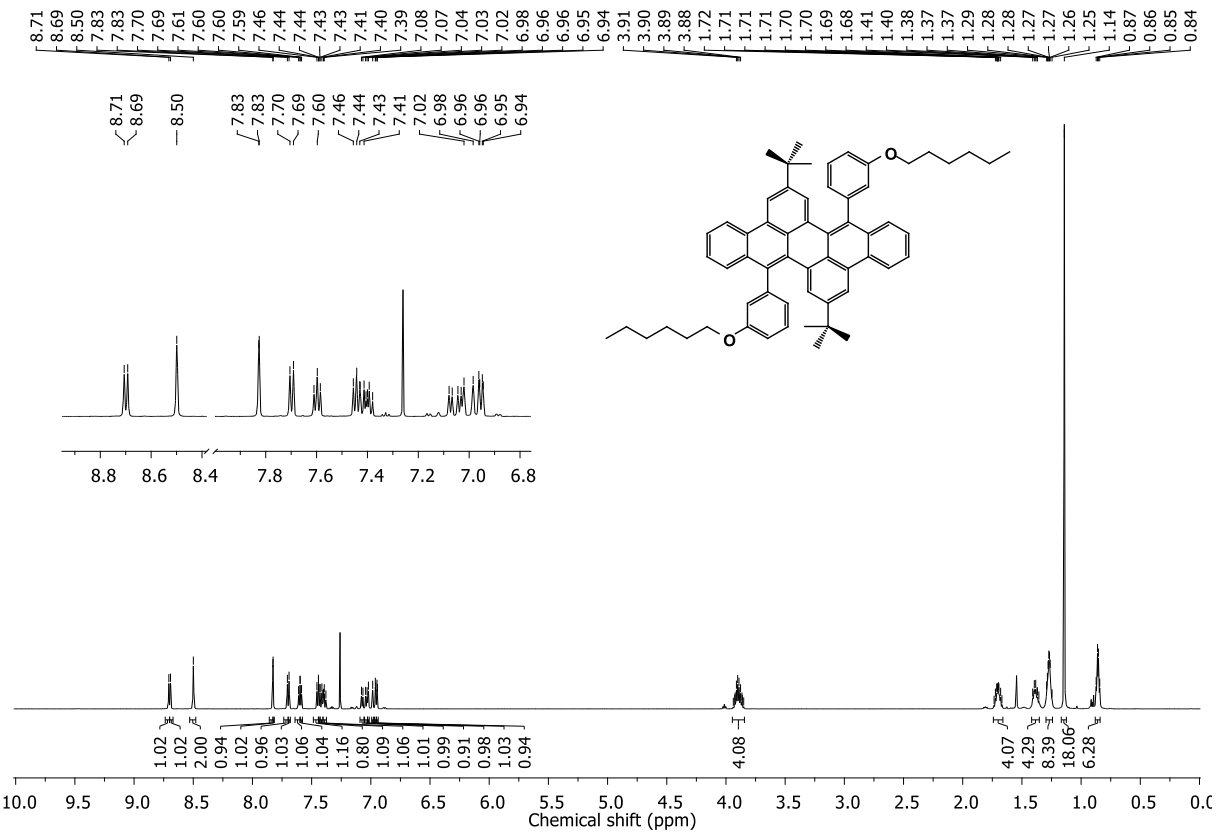

Figure 7.24 ^{1}H NMR spectrum (600 MHz, $CDCl_3$) of **145**.

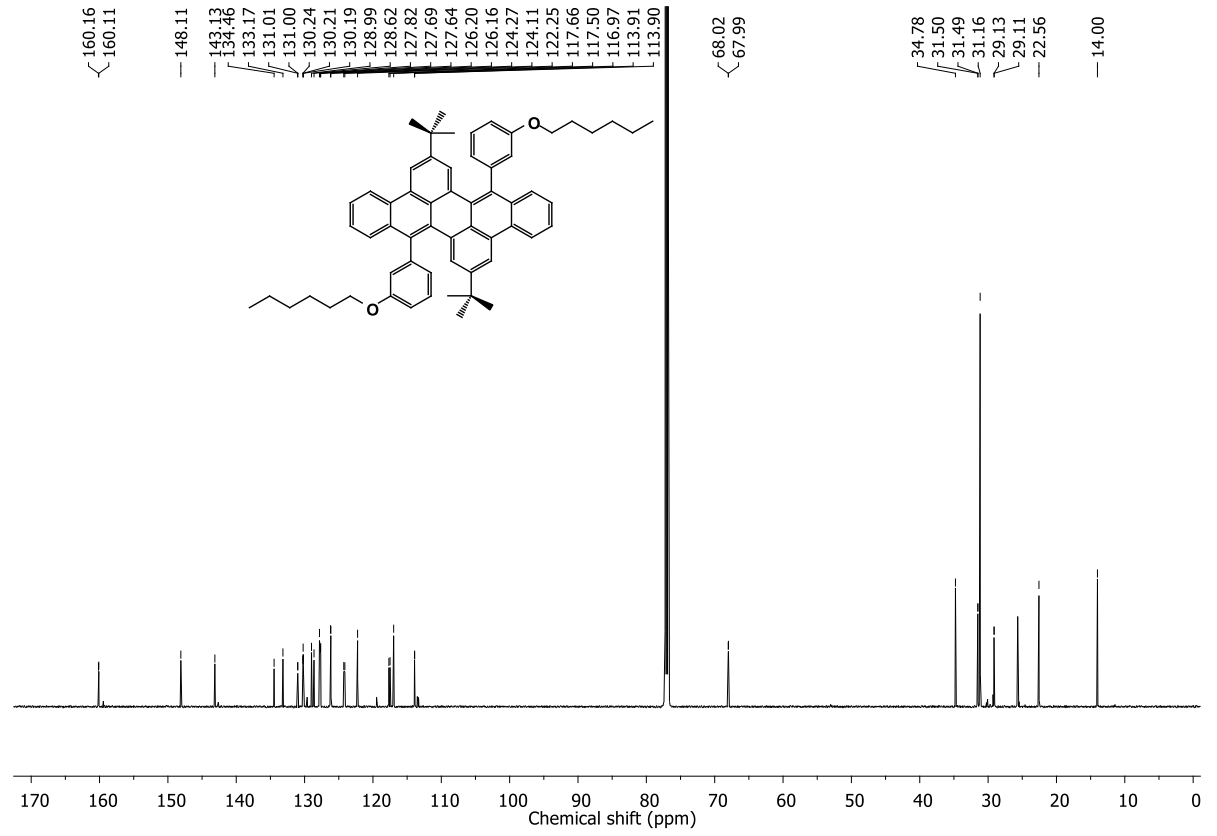

Figure 7.25 ^{13}C NMR spectrum (151 MHz, $CDCl_3$) of **145**.

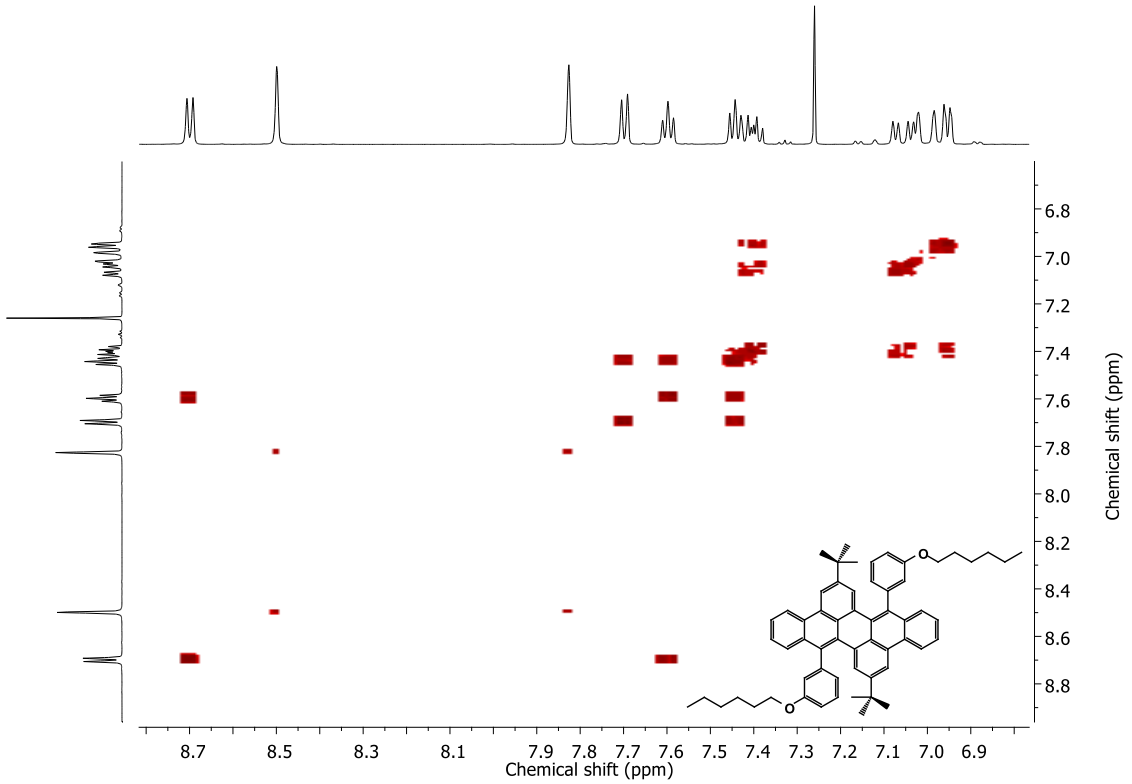

Figure 7.26 ^{1}H-^{1}H COSY NMR spectrum (600/600 MHz, $CDCl_3$) of **145**.

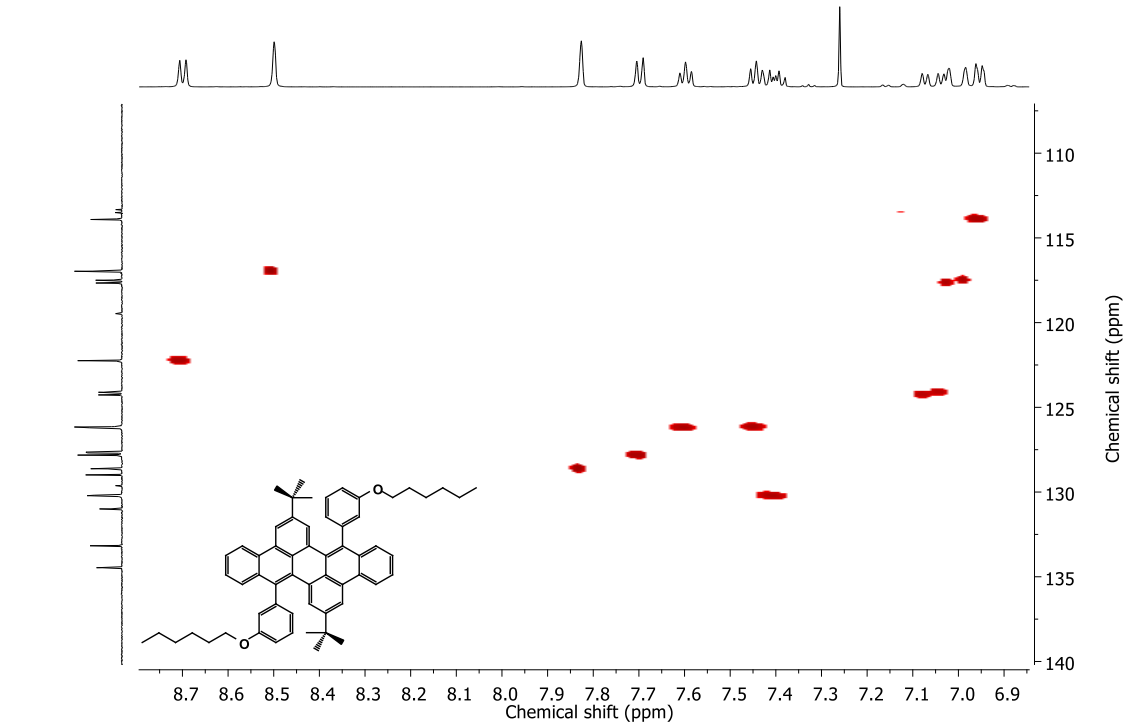

Figure 7.27 ^{1}H-^{13}C HSQC NMR spectrum (600/151 MHz, $CDCl_3$) of **145**.

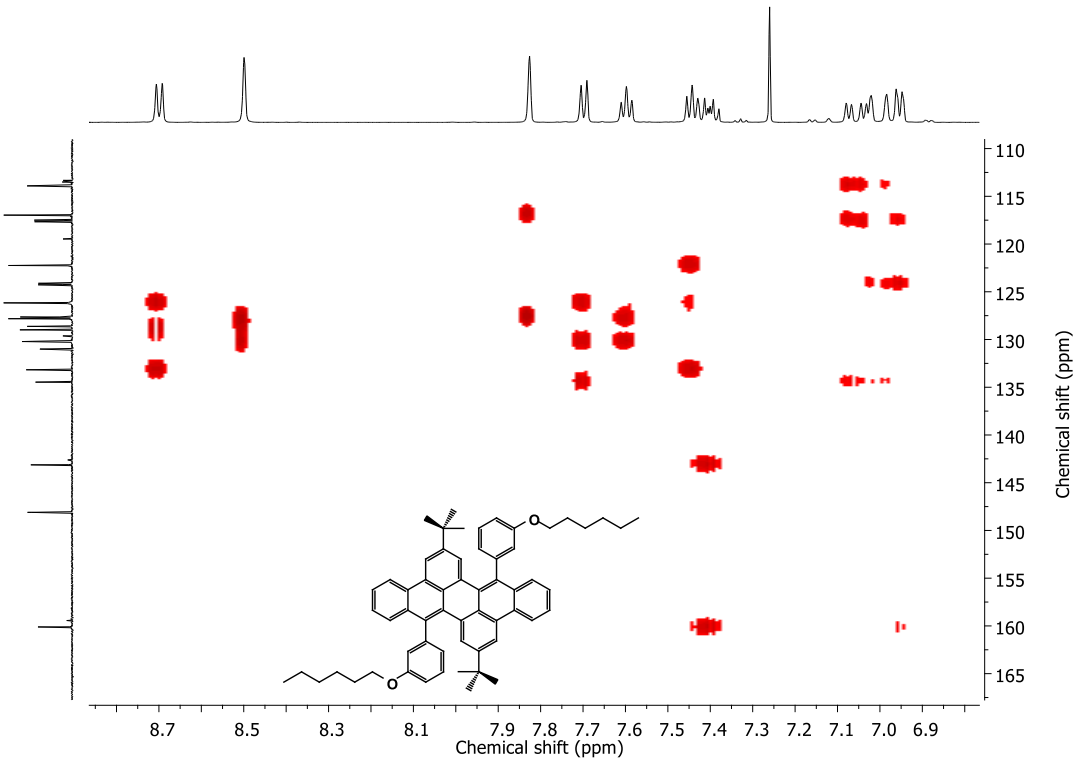

Figure 7.28 ^{1}H-^{13}C HMBC NMR spectrum (600/151 MHz, $CDCl_3$) of **145**.

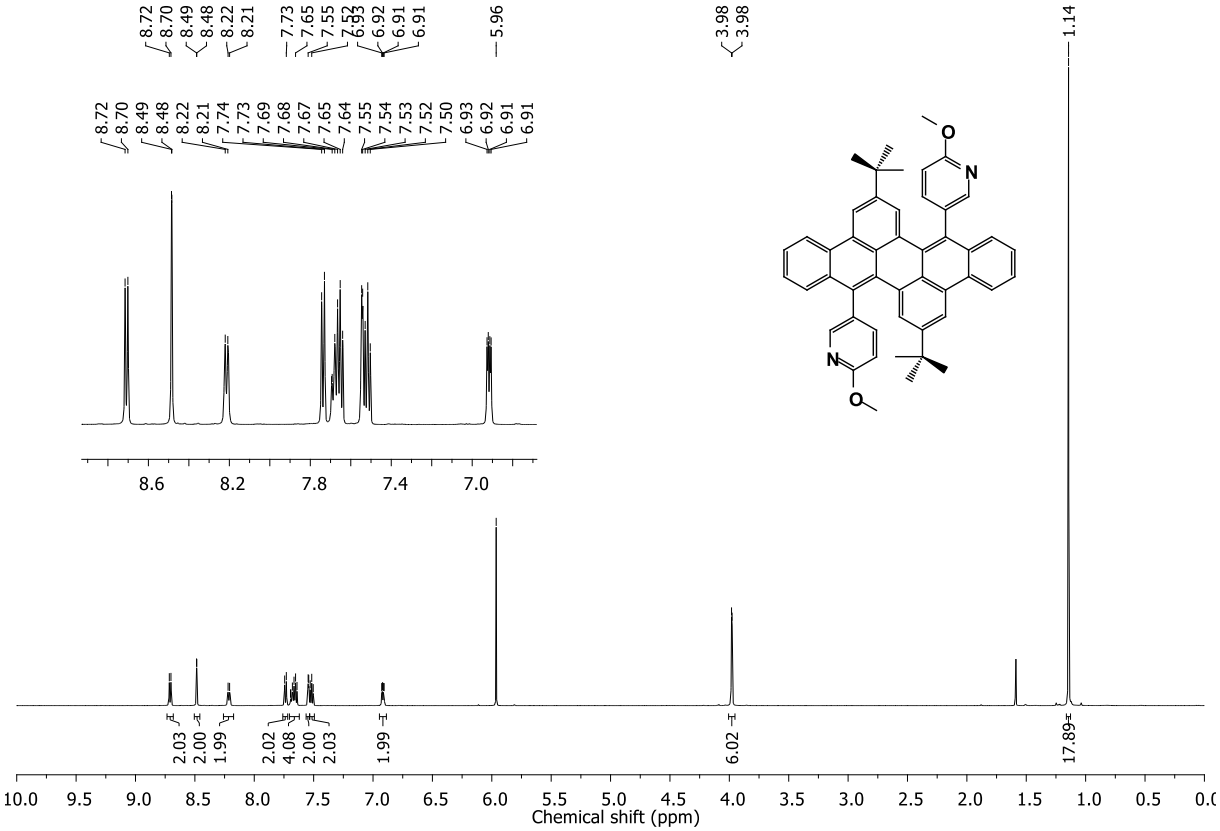

Figure 7.29 ^{1}H NMR spectrum (600 MHz, $Cl_2CDCDCl_2$) of **147**.

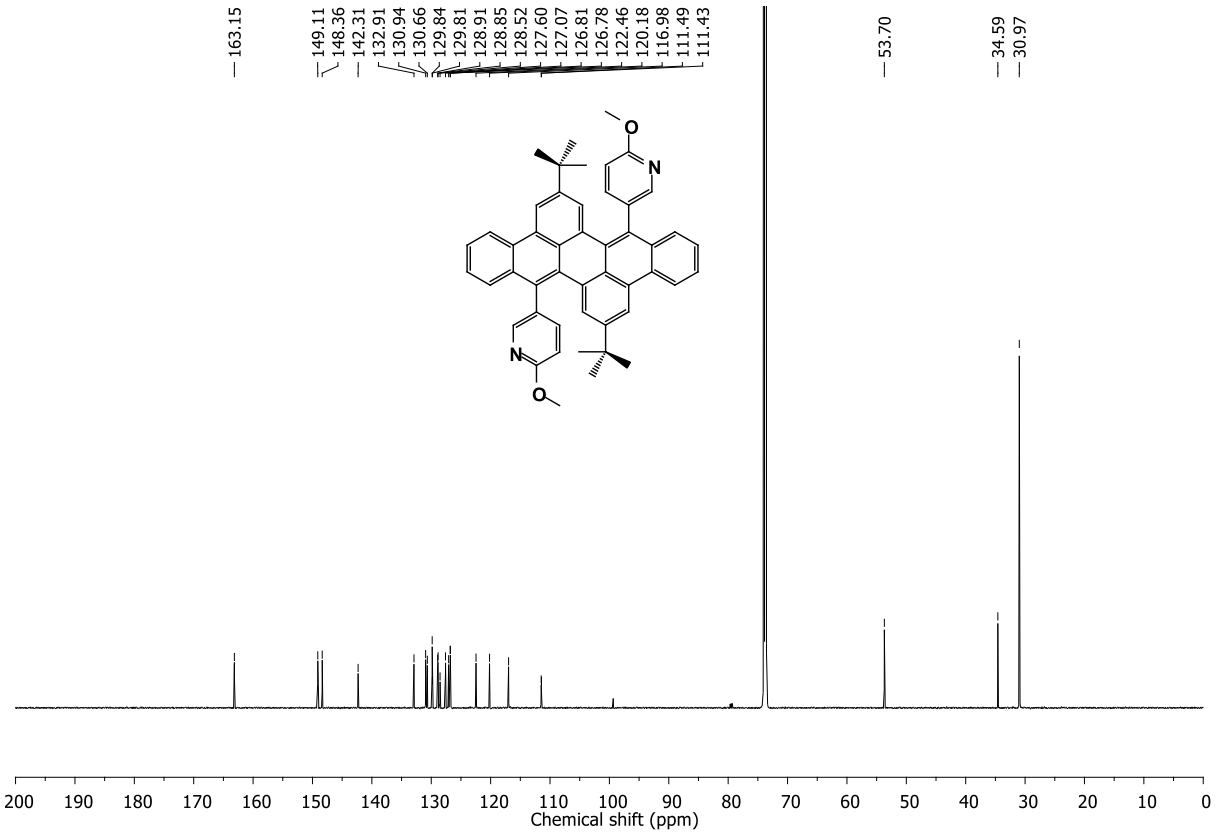

Figure 7.30 ^{13}C NMR spectrum (151 MHz, $Cl_2CDCDCl_2$) of **147**.

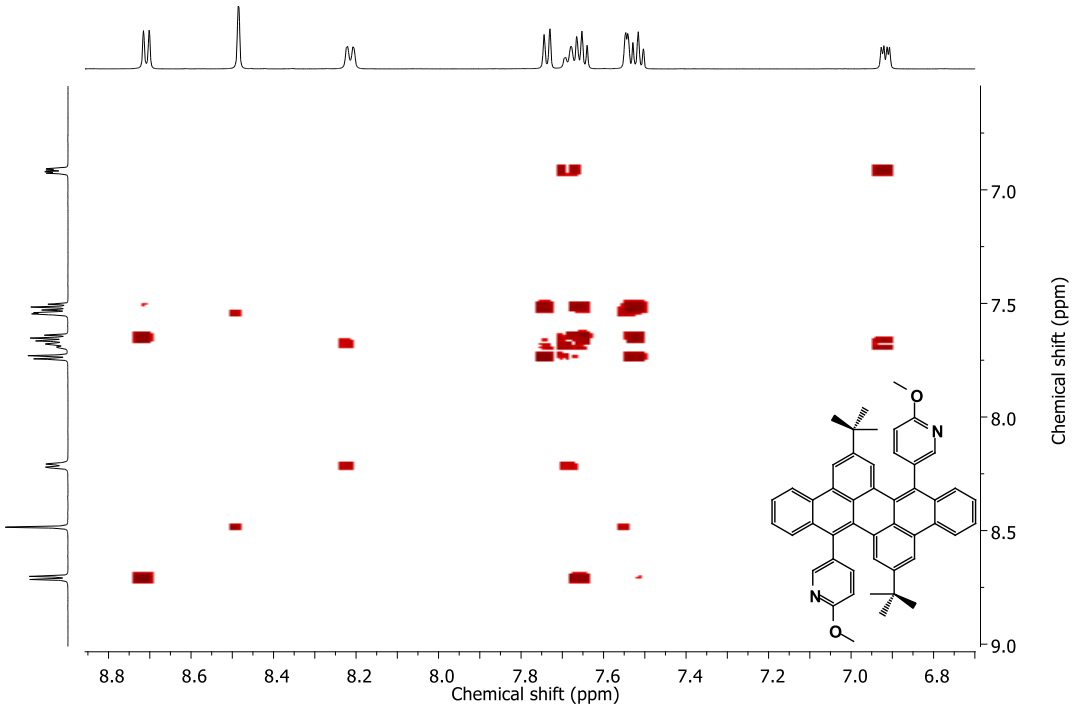

Figure 7.31 ^{1}H-^{1}H COSY NMR spectrum (600/600 MHz, $Cl_2CDCDCl_2$) of **147**.

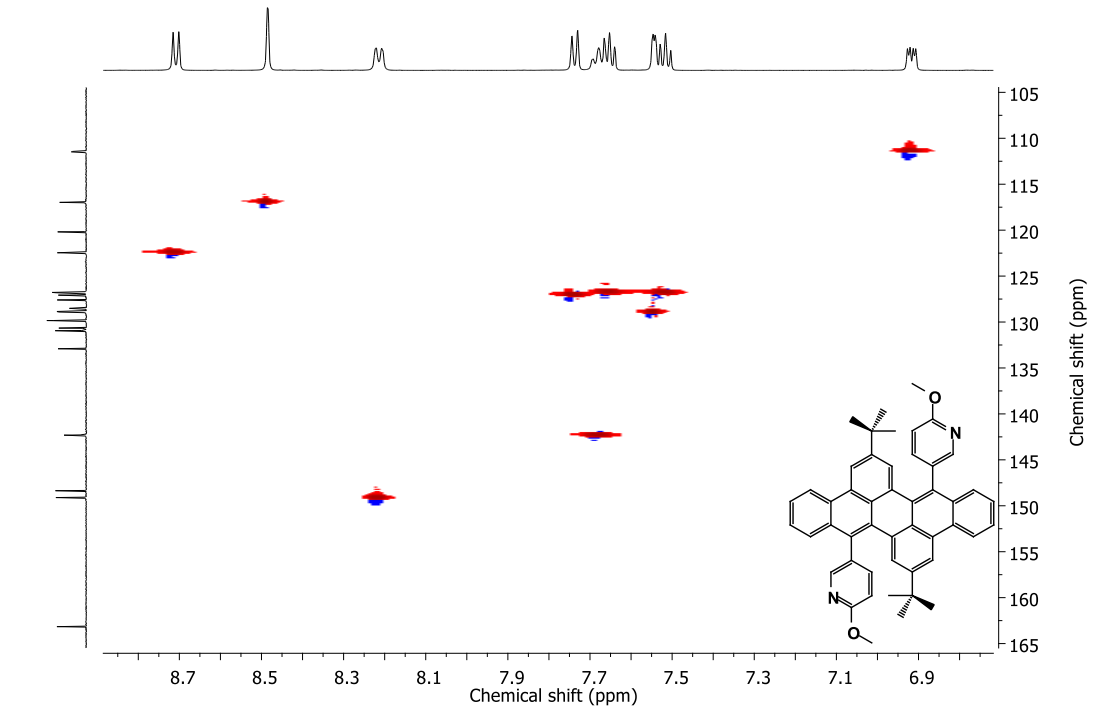

Figure 7.32 ^{1}H-^{13}C HSQC NMR spectrum (600/151 MHz, $Cl_2CDCDCl_2$) of **147**.

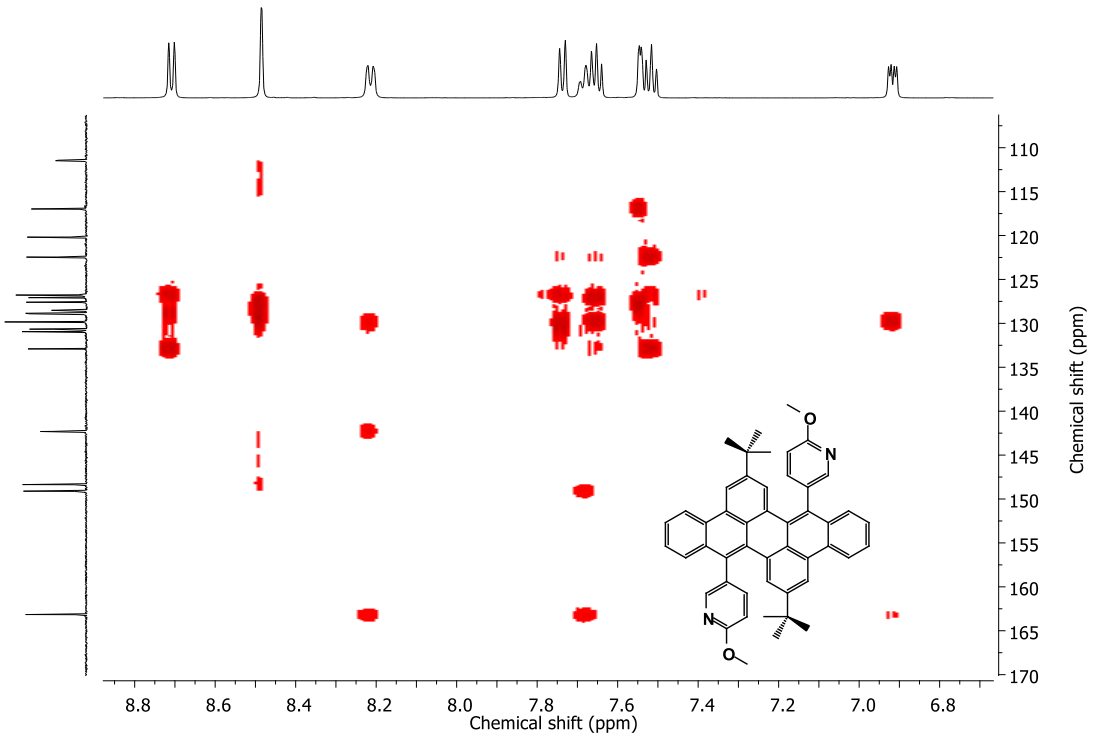

Figure 7.33 ^{1}H-^{13}C HMBC NMR spectrum (600/151 MHz, $Cl_2CDCDCl_2$) of **147**.

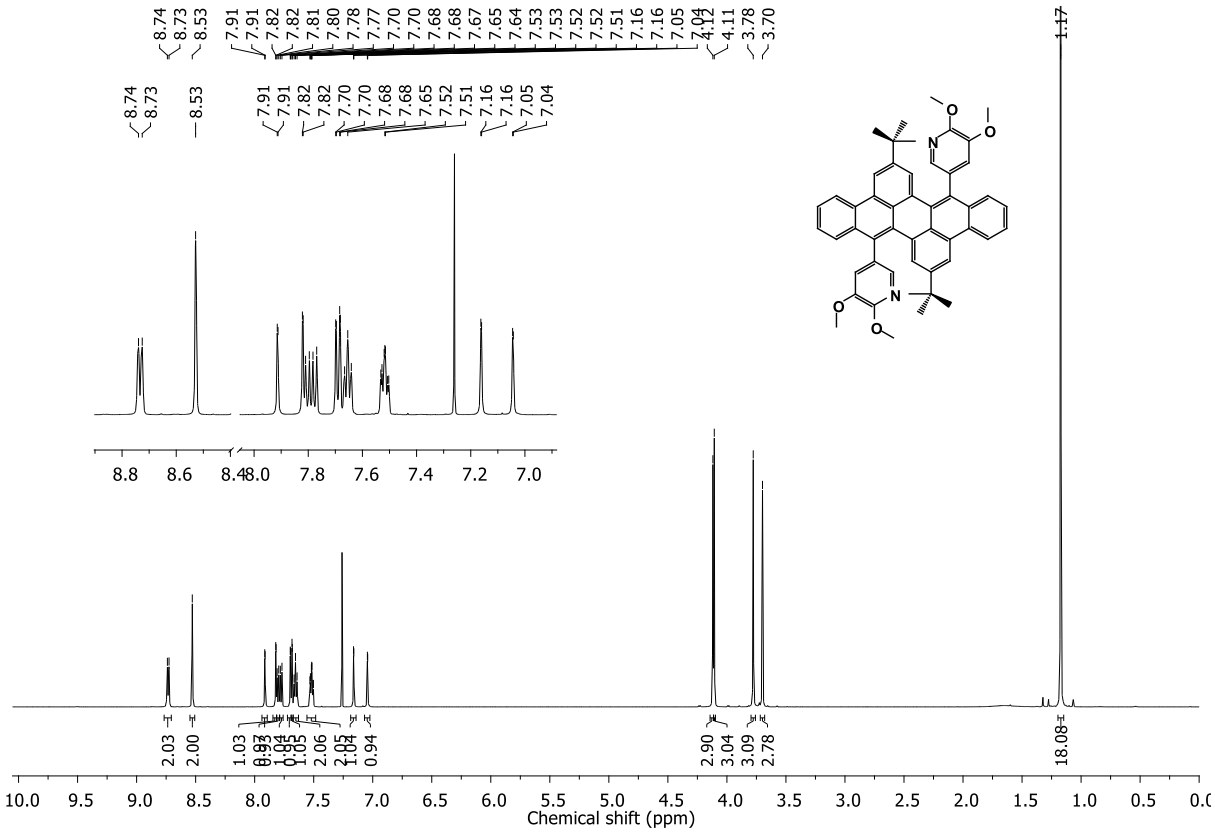

Figure 7.34 ^{1}H NMR spectrum (600 MHz, $CDCl_3$) of **148**.

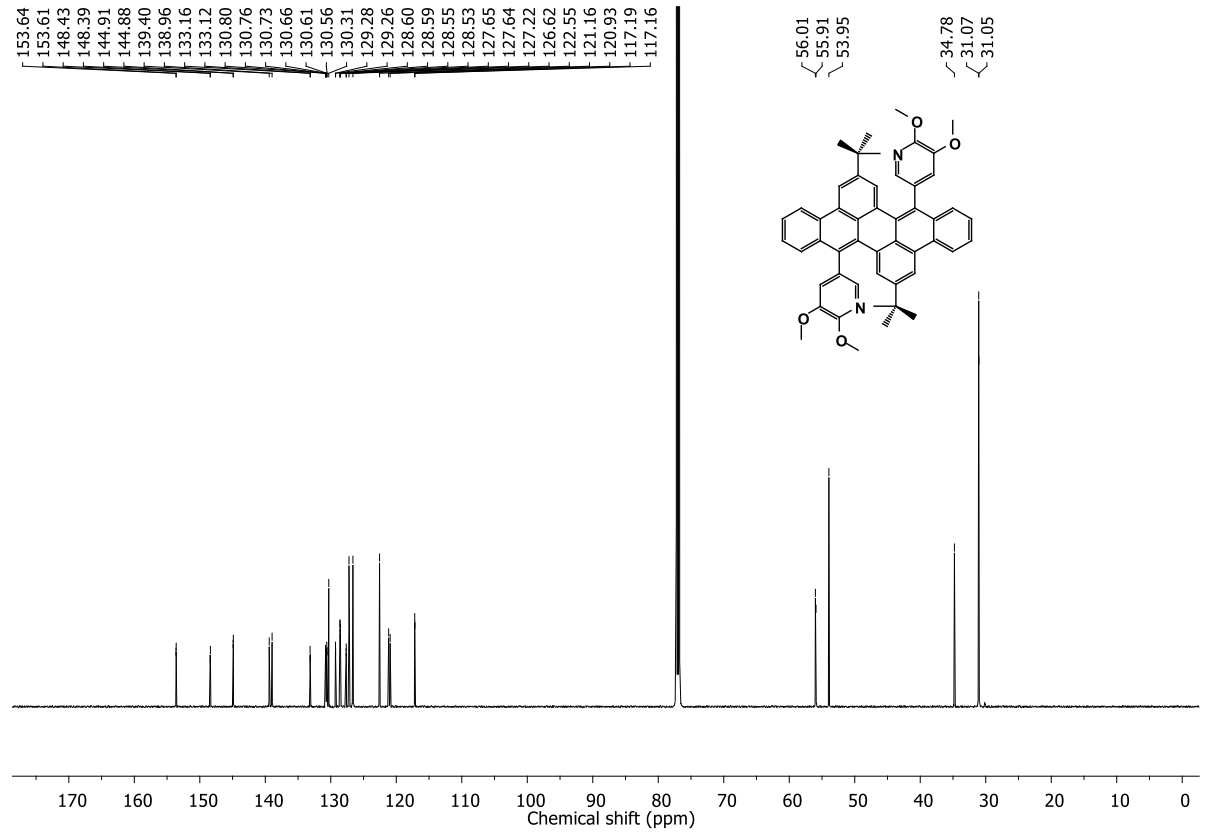

Figure 7.35 ^{13}C NMR spectrum (151 MHz, $CDCl_3$) of **148**.

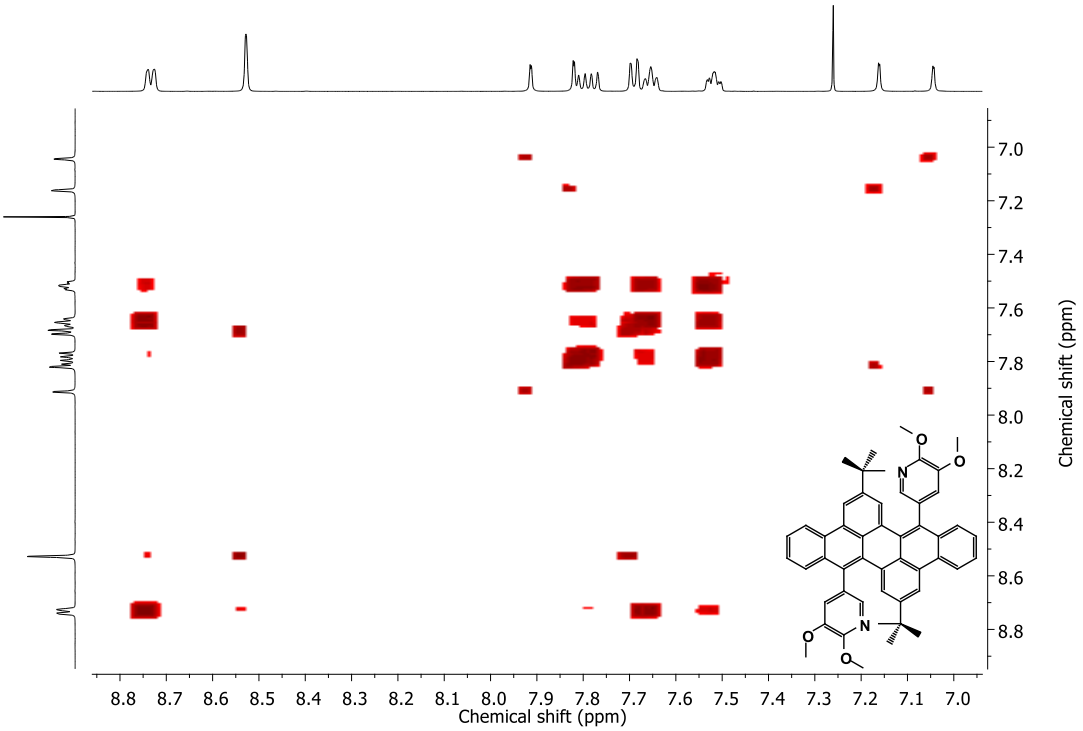

Figure 7.36 ^{1}H-^{1}H COSY NMR spectrum (600/600 MHz, $CDCl_3$) of **148**.

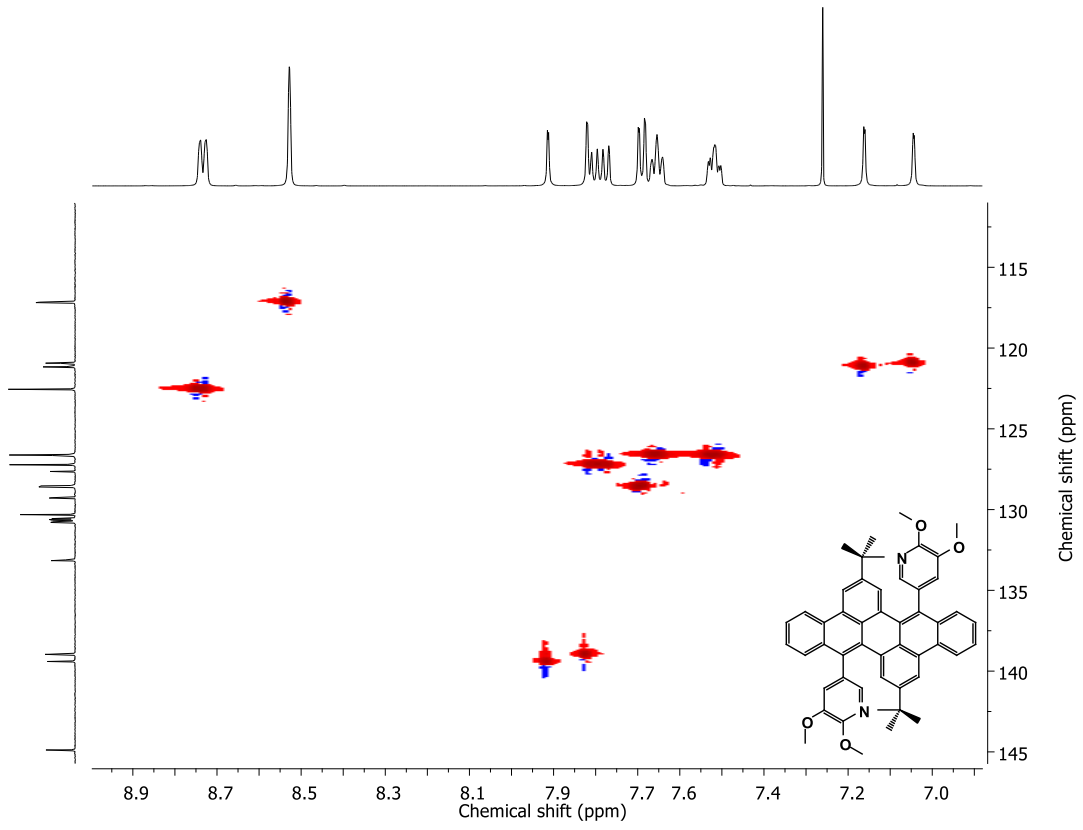

Figure 7.37 ^{1}H-^{13}C HSQC NMR spectrum (600/151 MHz, $CDCl_3$) of **148**.

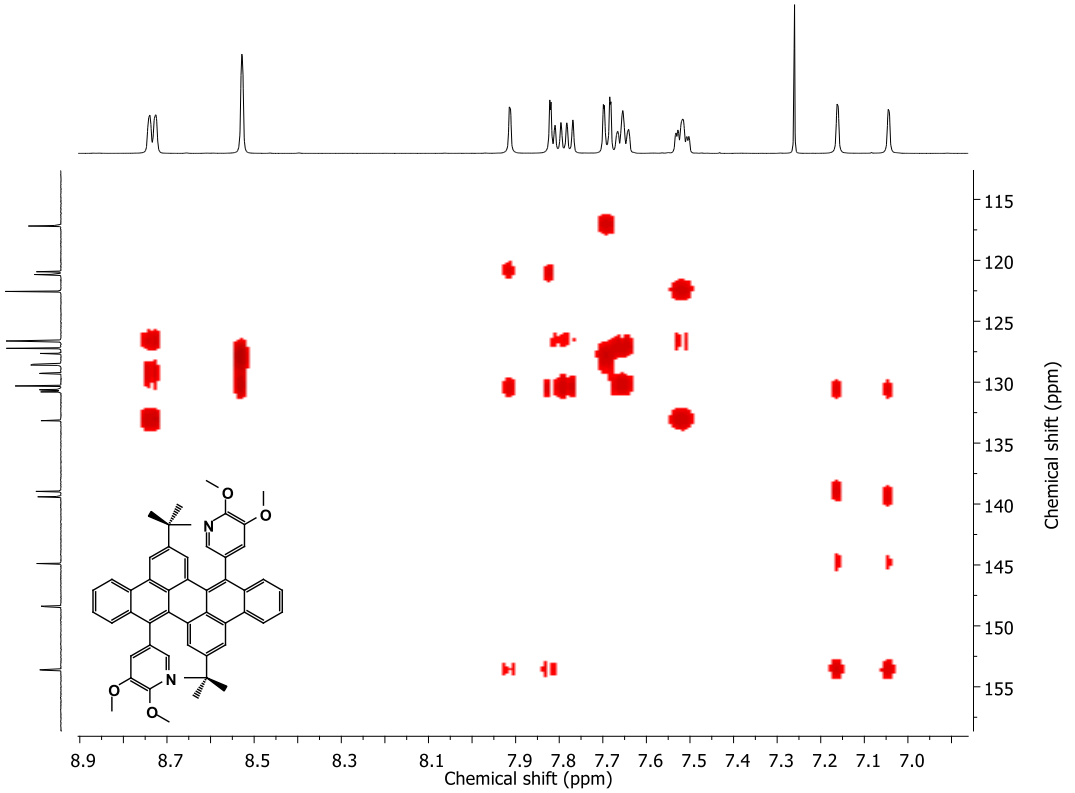

Figure 7.38 ^{1}H-^{13}C HMBC NMR spectrum (600/151 MHz, $CDCl_3$) of **148**.

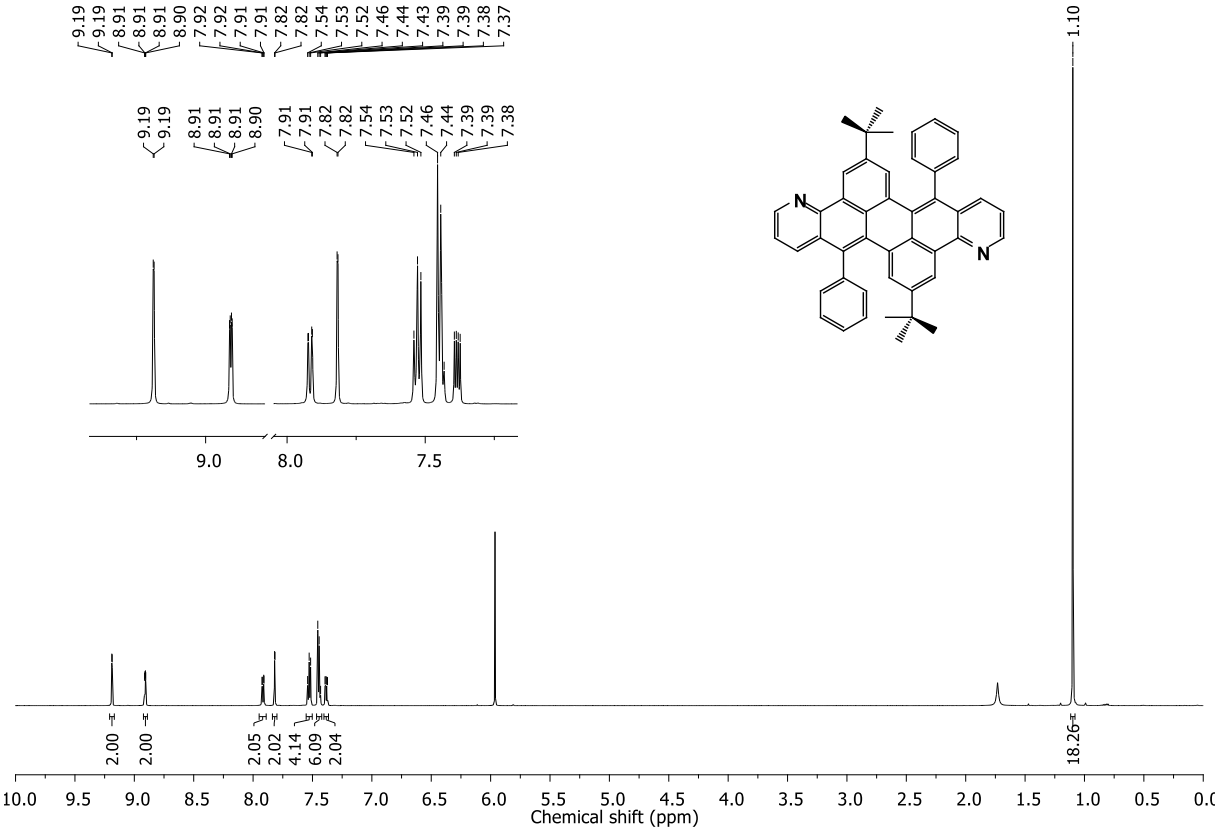

Figure 7.39 ^{1}H NMR spectrum (600 MHz, $Cl_2CDCDCl_2$) of **149**.

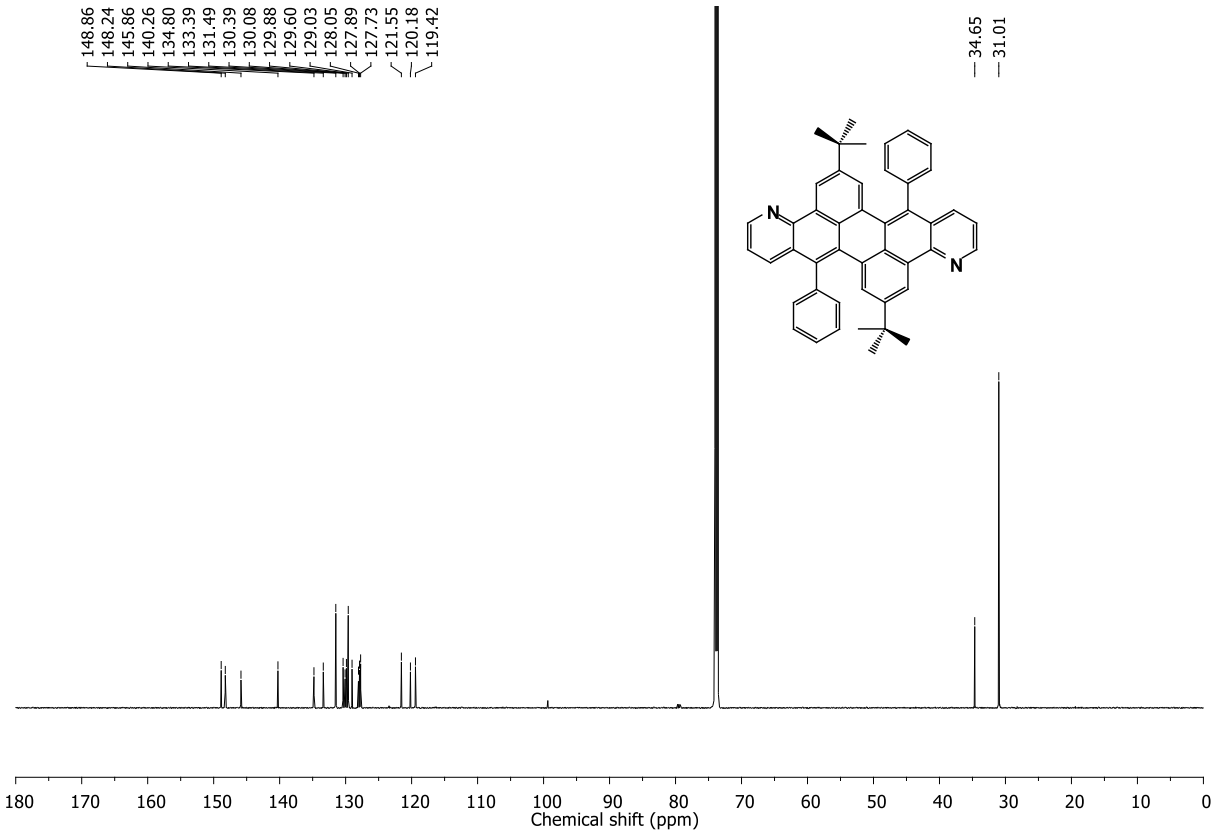

Figure 7.40 ^{13}C NMR spectrum (151 MHz, $Cl_2CDCDCl_2$) of **149**.

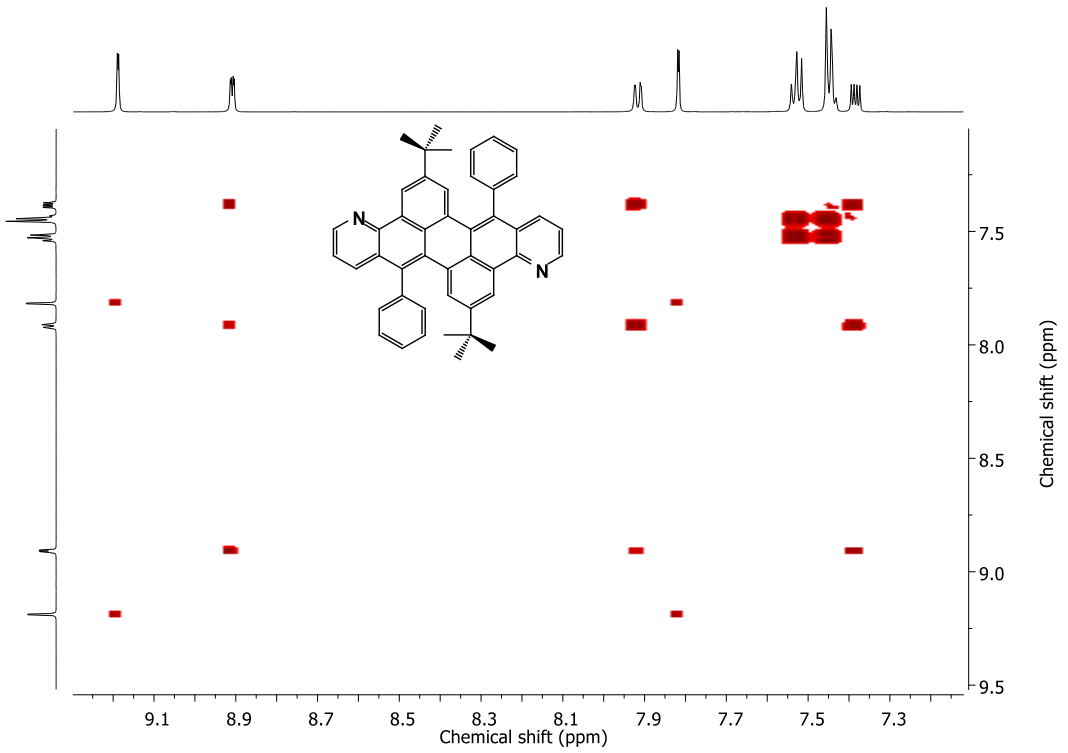

Figure 7.41 ^{1}H-^{1}H COSY NMR spectrum (600/600 MHz, $Cl_2CDCDCl_2$) of **149**.

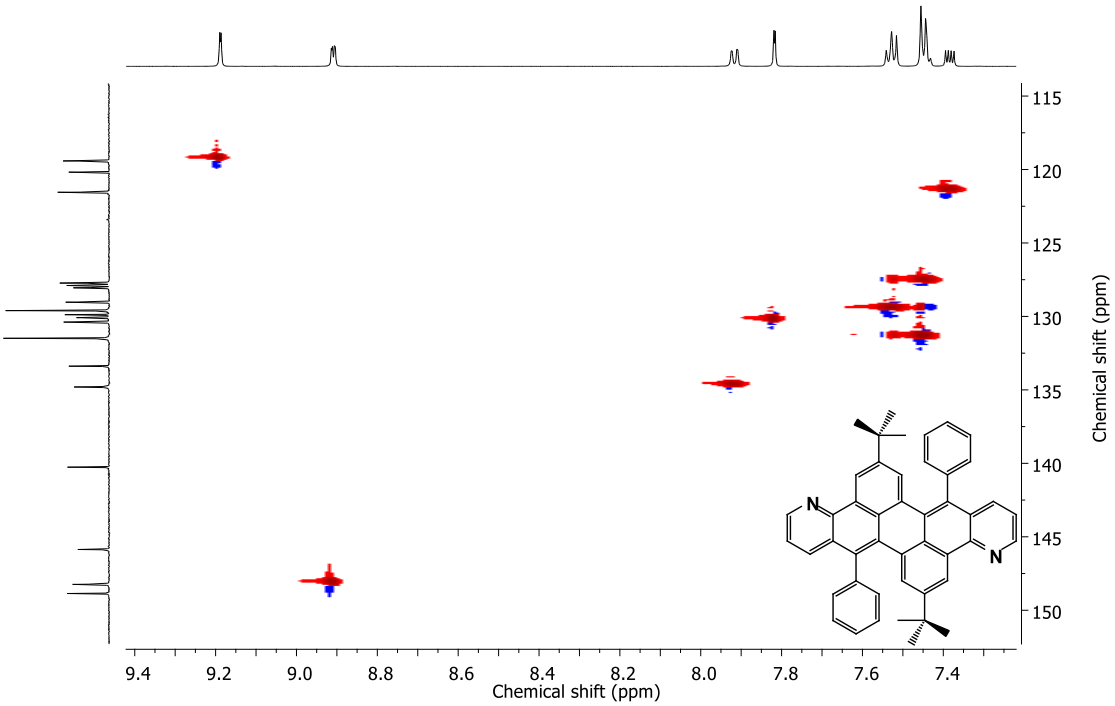

Figure 7.42 ^{1}H-^{13}C HSQC NMR spectrum (600/151 MHz, $Cl_2CDCDCl_2$) of **149**.

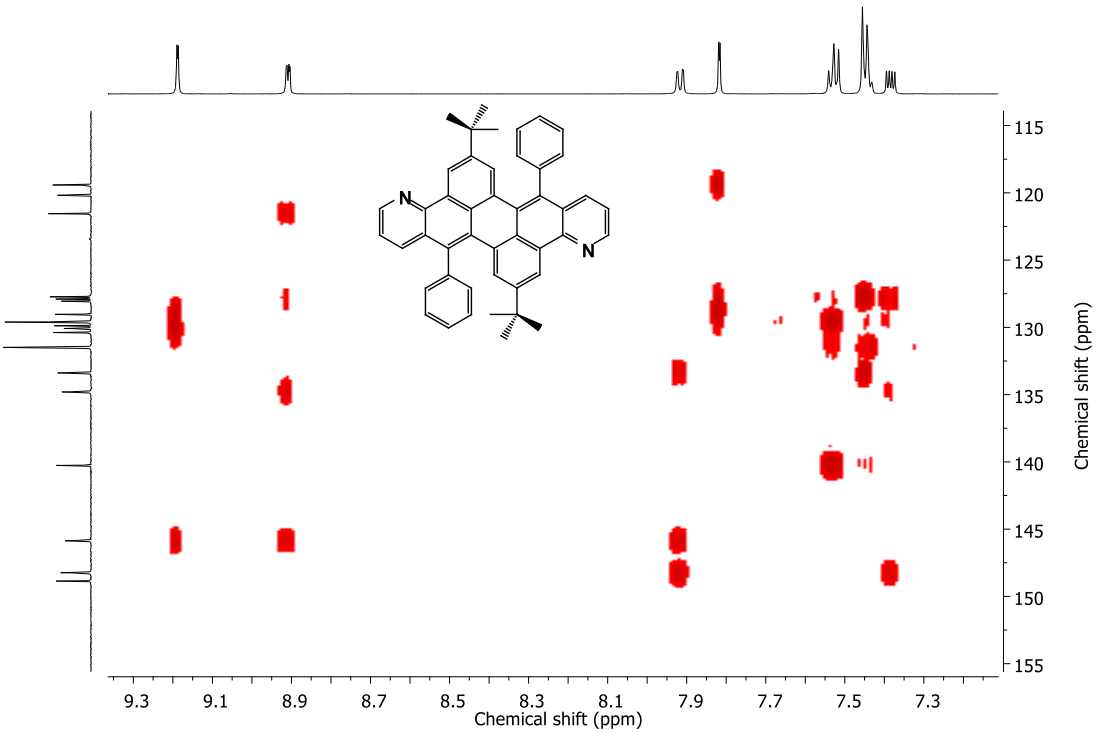

Figure 7.43 ^{1}H-^{13}C HMBC NMR spectrum (600/151 MHz, $Cl_2CDCDCl_2$) of **149**.

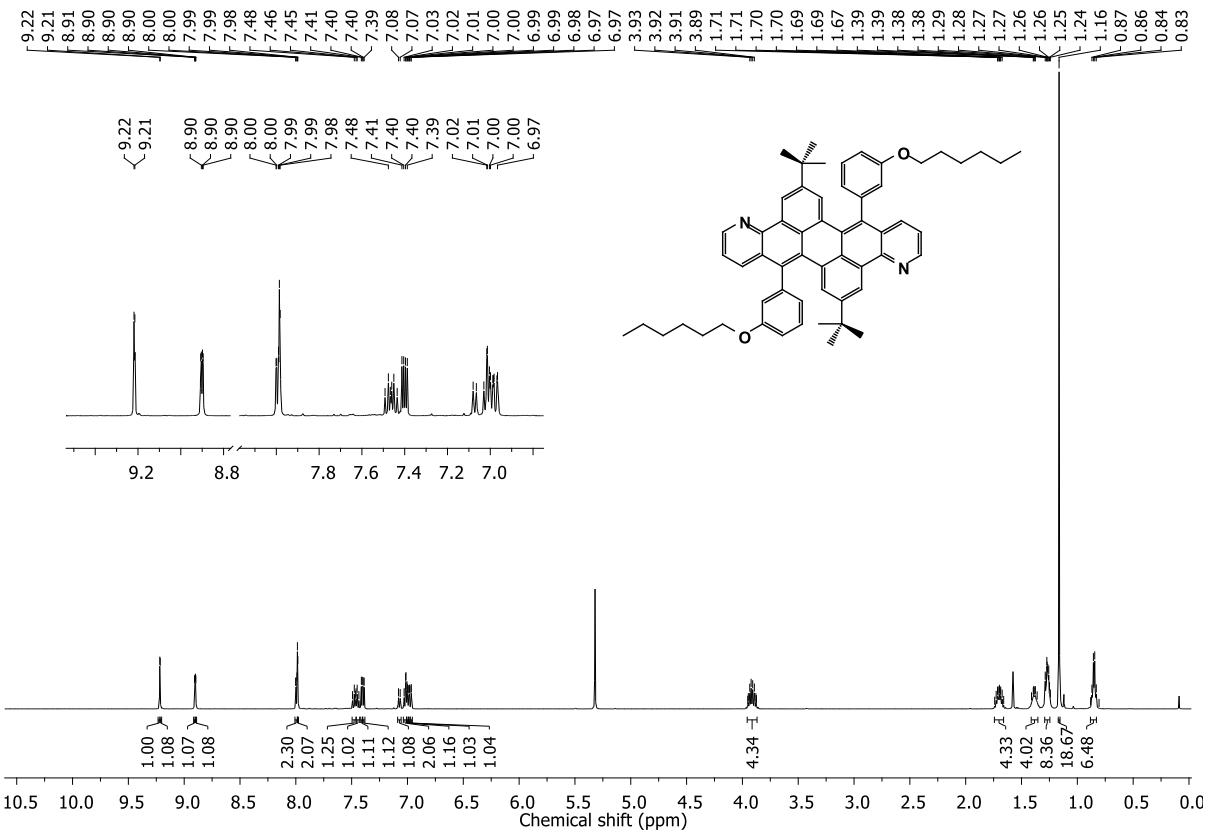

Figure 7.44 ^{1}H NMR spectrum (500 MHz, CD_2Cl_2) of **150**.

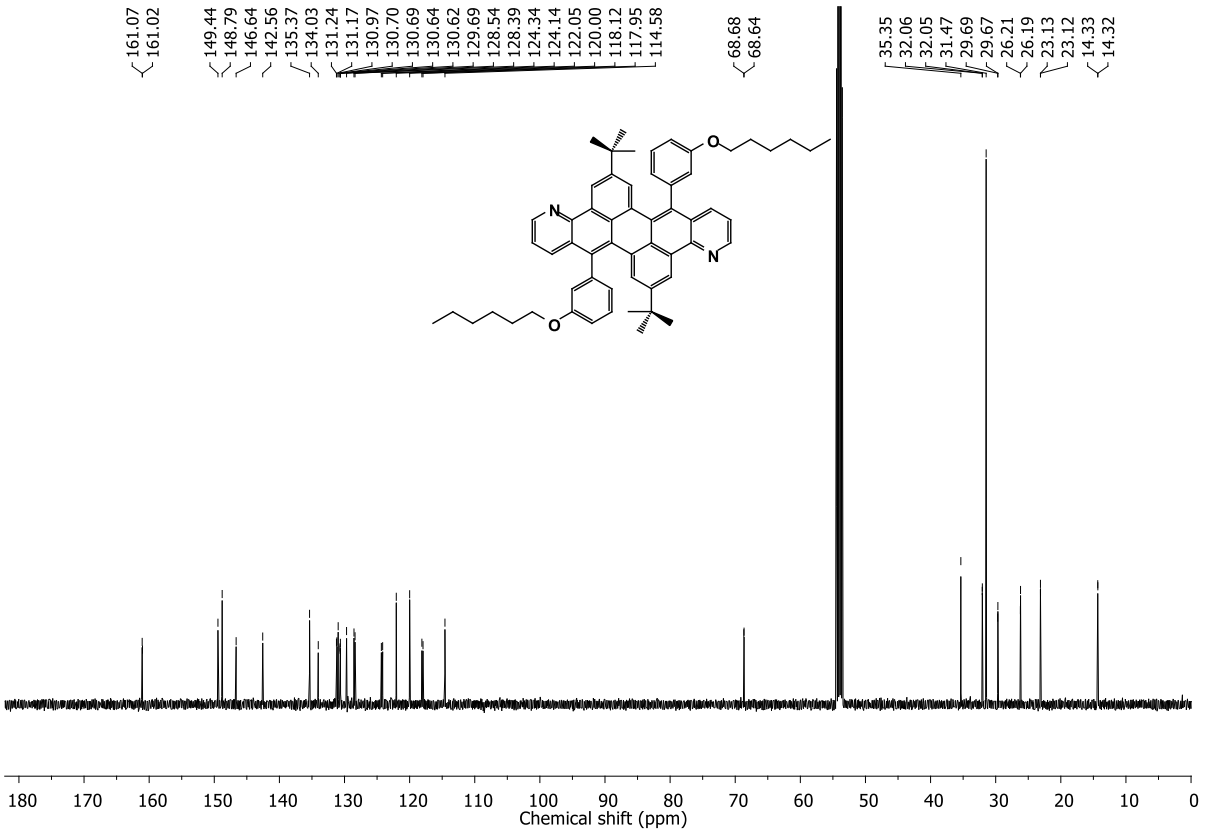

Figure 7.45 ^{13}C NMR spectrum (126 MHz, CD_2Cl_2) of **150**.

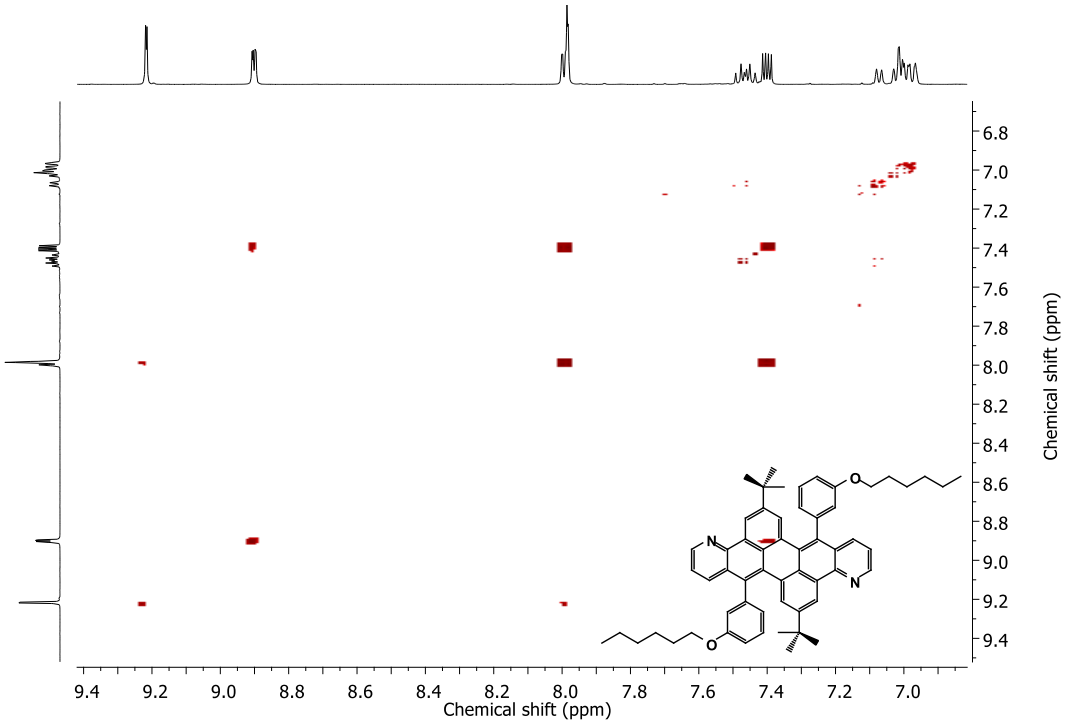

Figure 7.46 ^{1}H-^{1}H COSY NMR spectrum (500/500 MHz, CD_2Cl_2) of **150**.

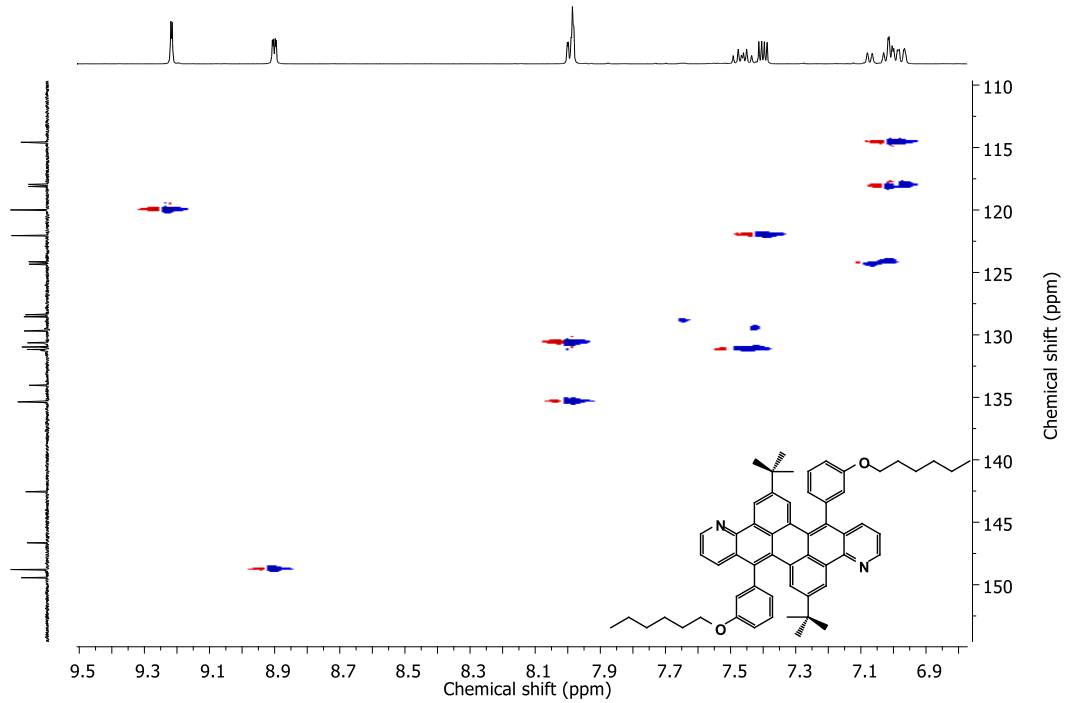

Figure 7.47 ^{1}H-^{13}C HSQC NMR spectrum (500/126 MHz, CD_2Cl_2) of **150**.

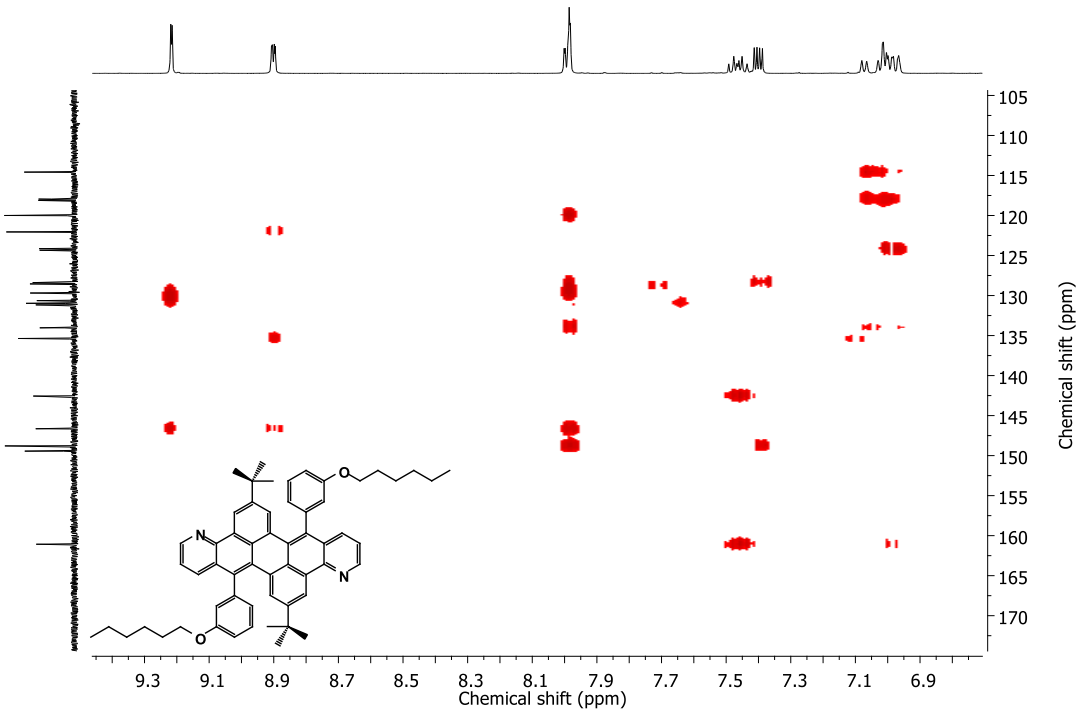

Figure 7.48 ^{1}H-^{13}C HMBC NMR spectrum (500/126 MHz, CD_2Cl_2) of **150**.

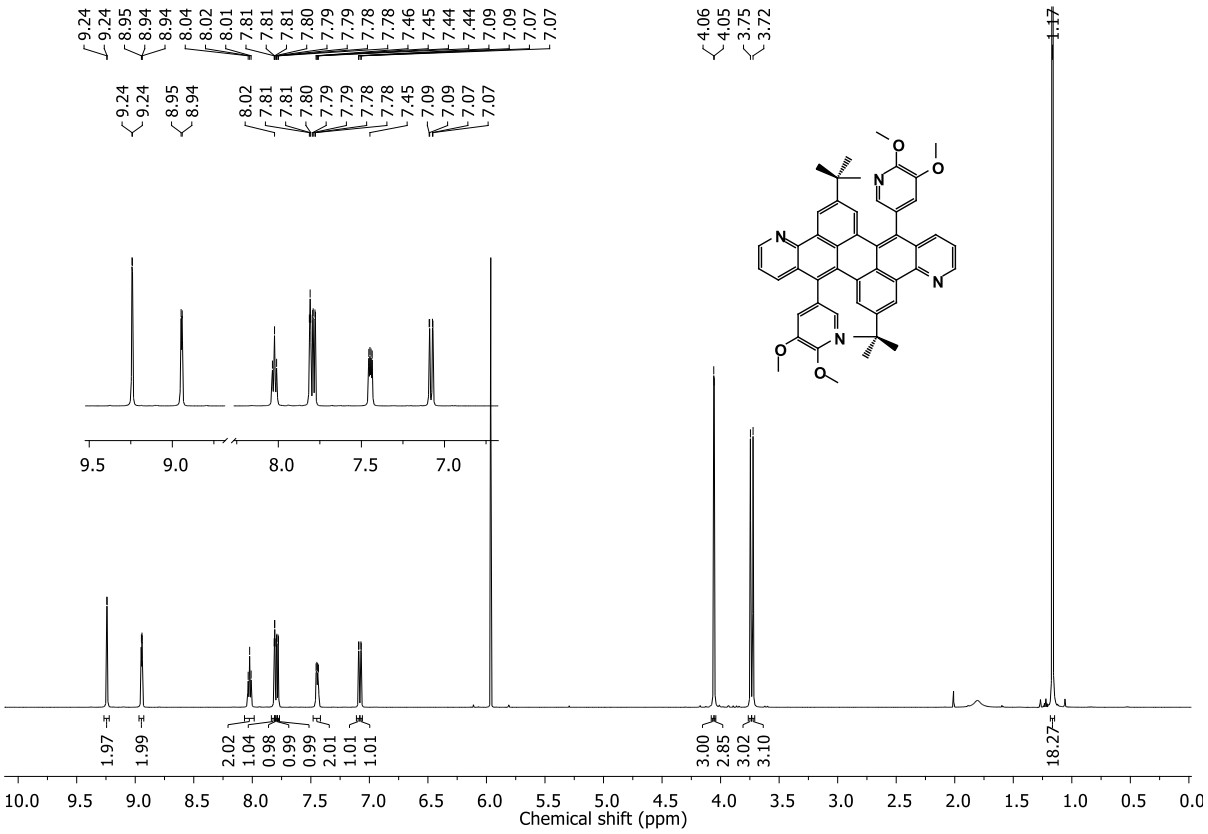

Figure 7.49 ^{1}H NMR spectrum (600 MHz, $Cl_2CDCDCl_2$) of **151**.

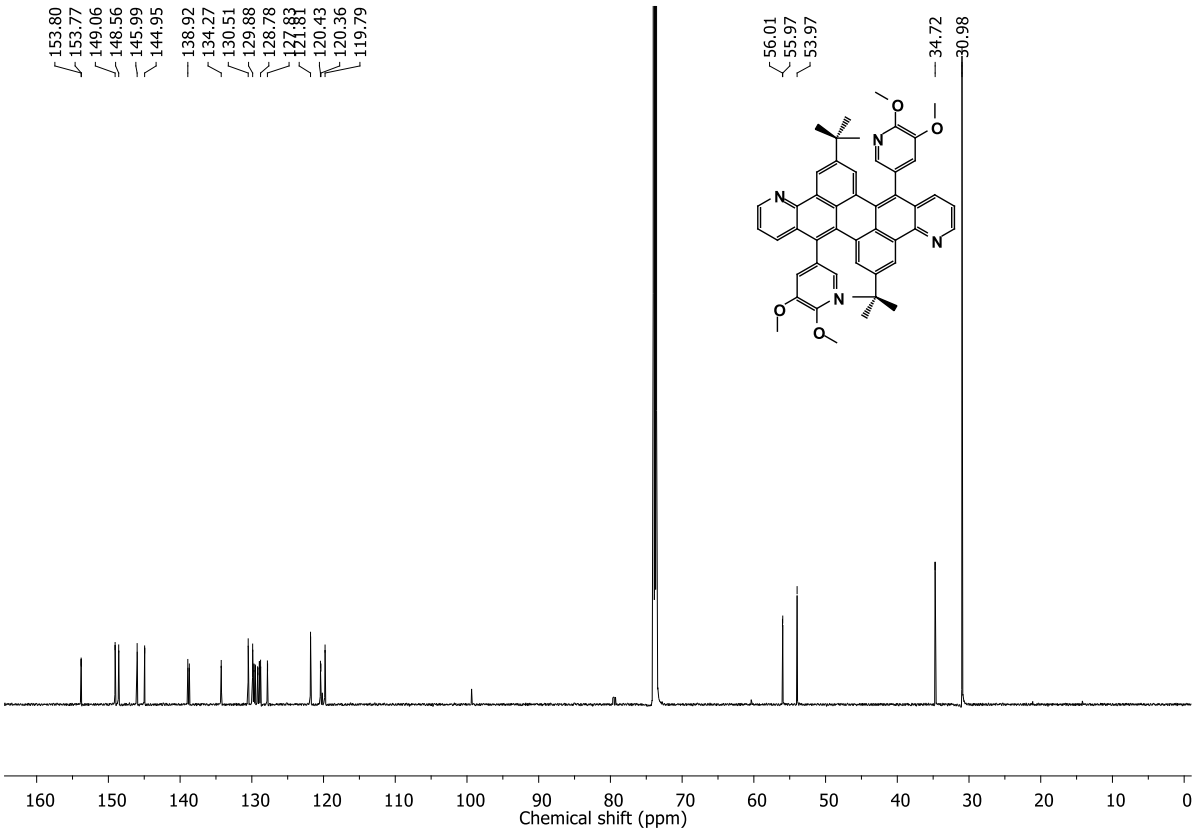

Figure 7.50 ^{13}C NMR spectrum (151 MHz, $Cl_2CDCDCl_2$) of **151**.

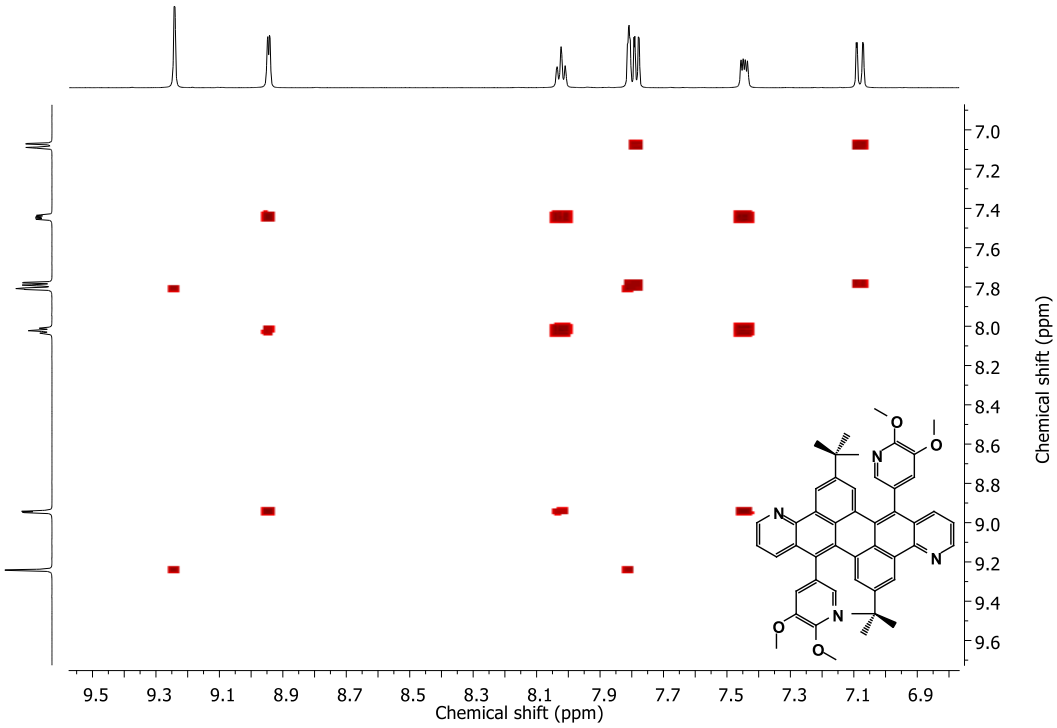

Figure 7.51 ^{1}H-^{1}H COSY NMR spectrum (600/600 MHz, $Cl_2CDCDCl_2$) of **151**.

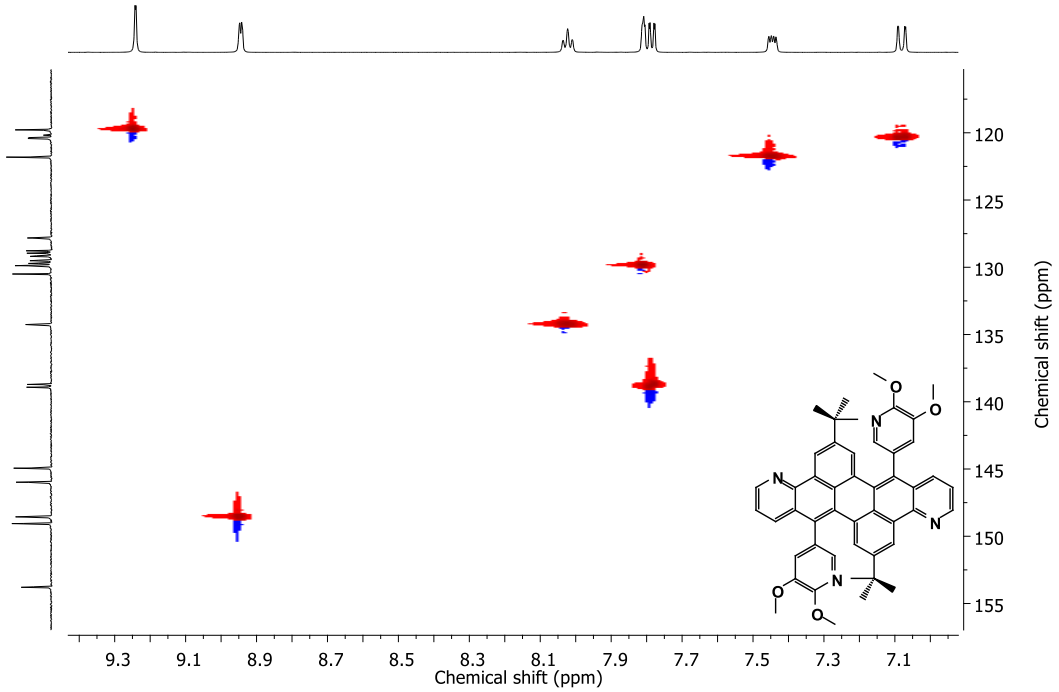

Figure 7.52 ^{1}H-^{13}C HSQC NMR spectrum (600/151 MHz, $Cl_2CDCDCl_2$) of **151**.

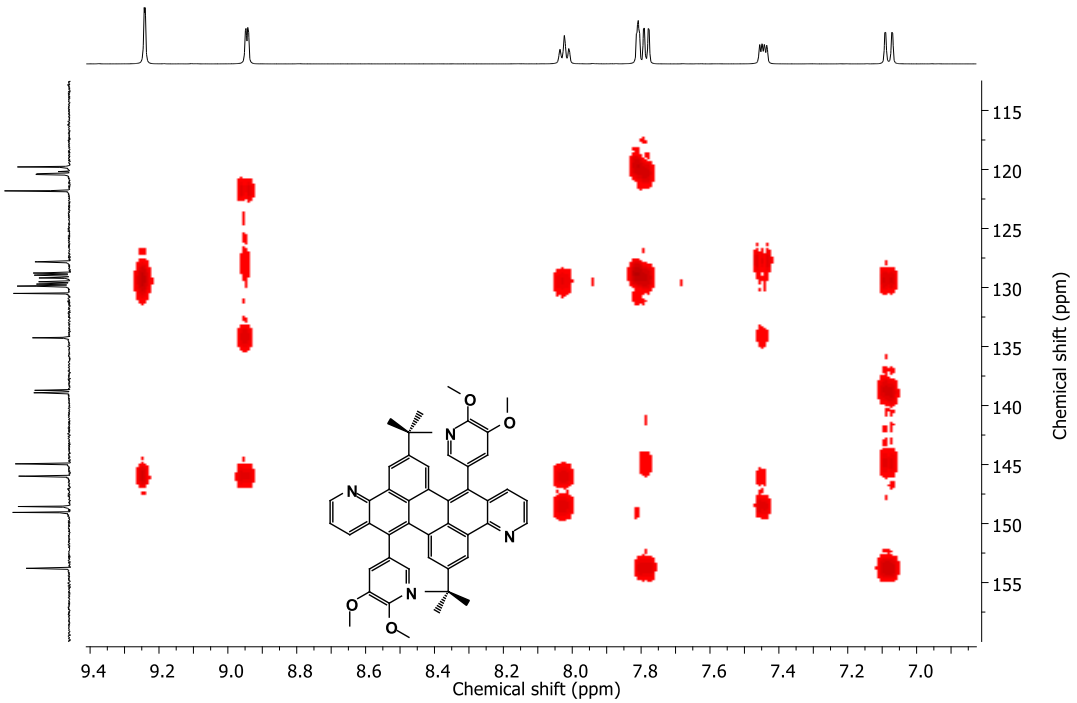

Figure 7.53 ^{1}H-^{13}C HMBC NMR spectrum (600/151 MHz, $Cl_2CDCDCl_2$) of **151**.

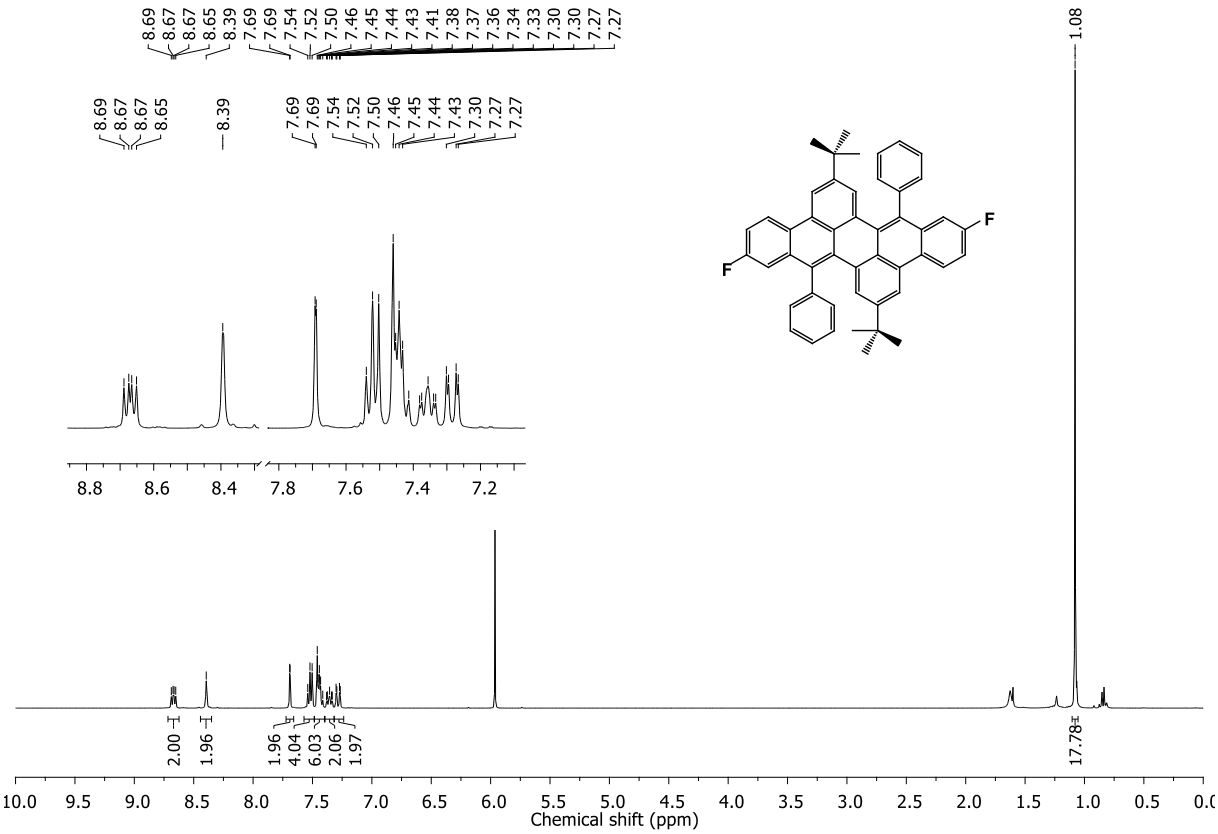

Figure 7.54 ^{1}H NMR spectrum (400 MHz, $Cl_2CDCDCl_2$) of **156**.

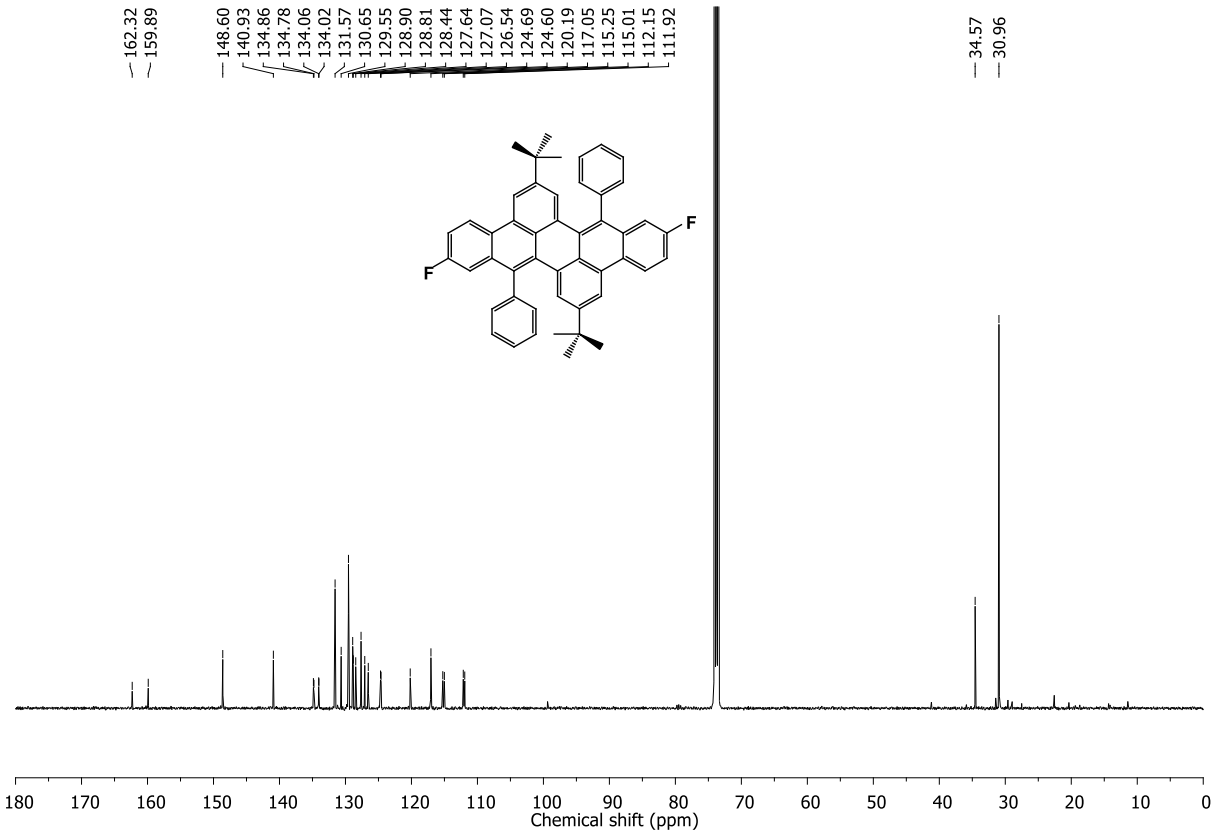

Figure 7.55 ^{13}C NMR spectrum (101 MHz, $Cl_2CDCDCl_2$) of **156**.

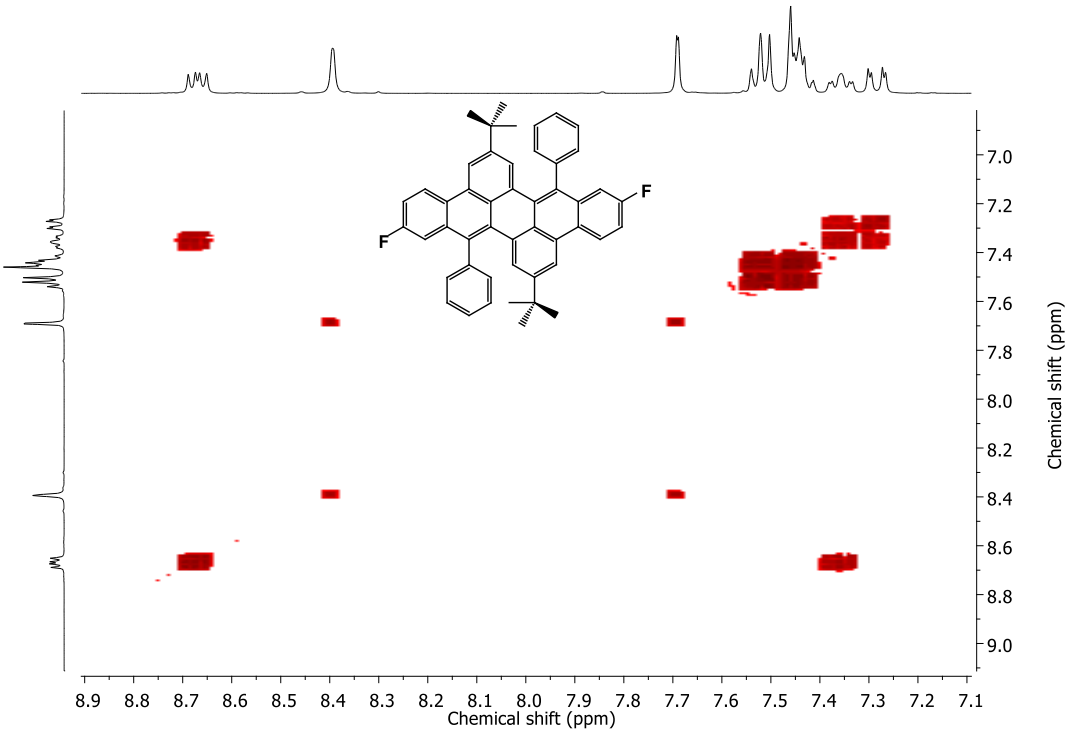

Figure 7.56 ^{1}H-^{1}H COSY NMR spectrum (400/400 MHz, $Cl_2CDCDCl_2$) of **156**.

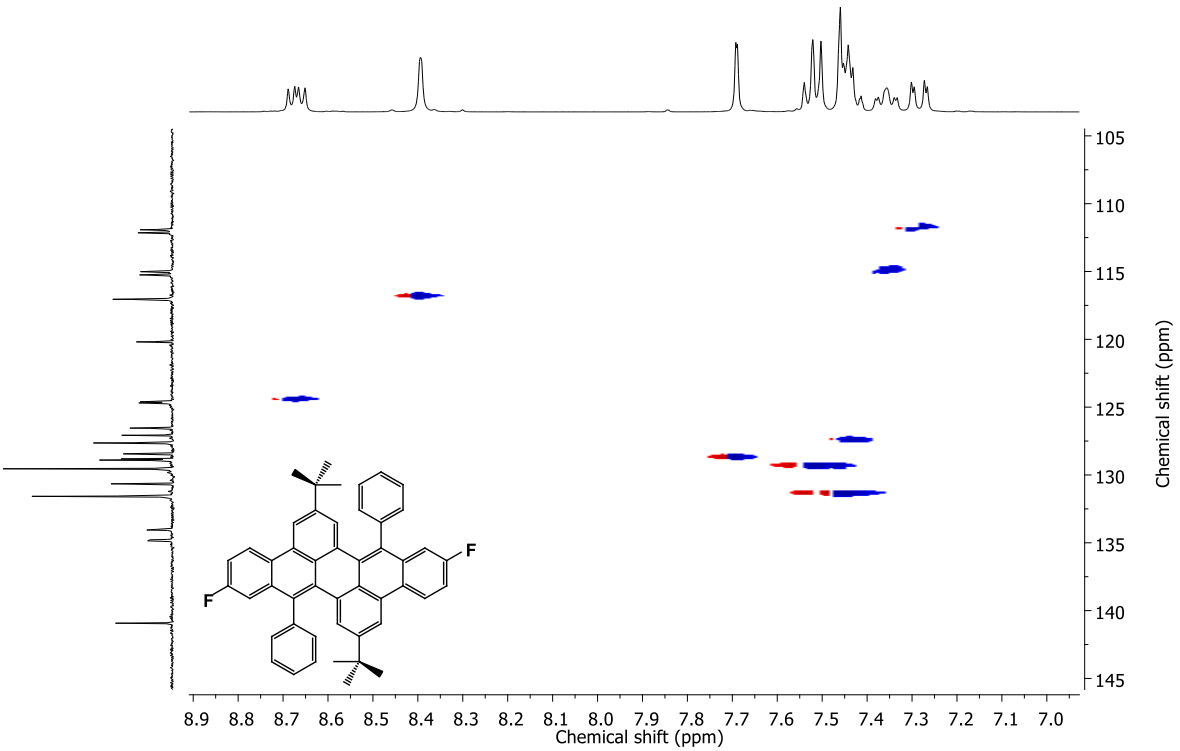

Figure 7.57 ^{1}H-^{13}C HSQC NMR spectrum (400/101 MHz, $Cl_2CDCDCl_2$) of **156**.

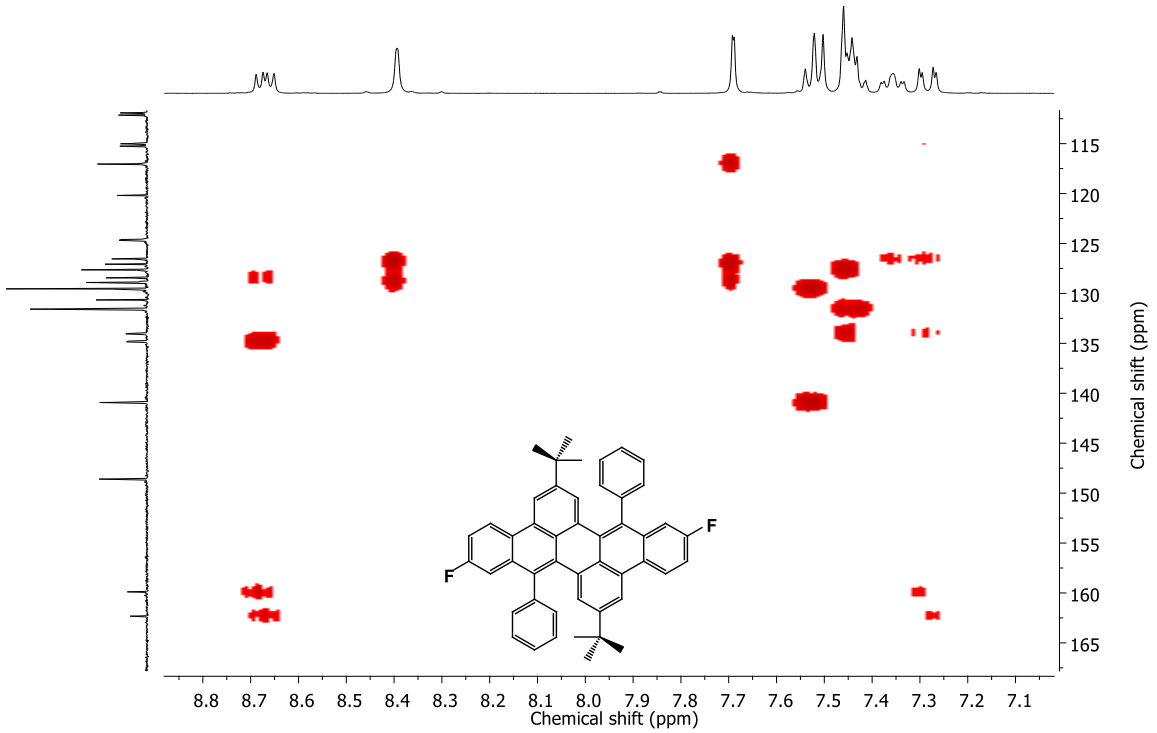

Figure 7.58 ^{1}H-^{13}C HMBC NMR spectrum (400/101 MHz, $Cl_2CDCDCl_2$) of **156**.

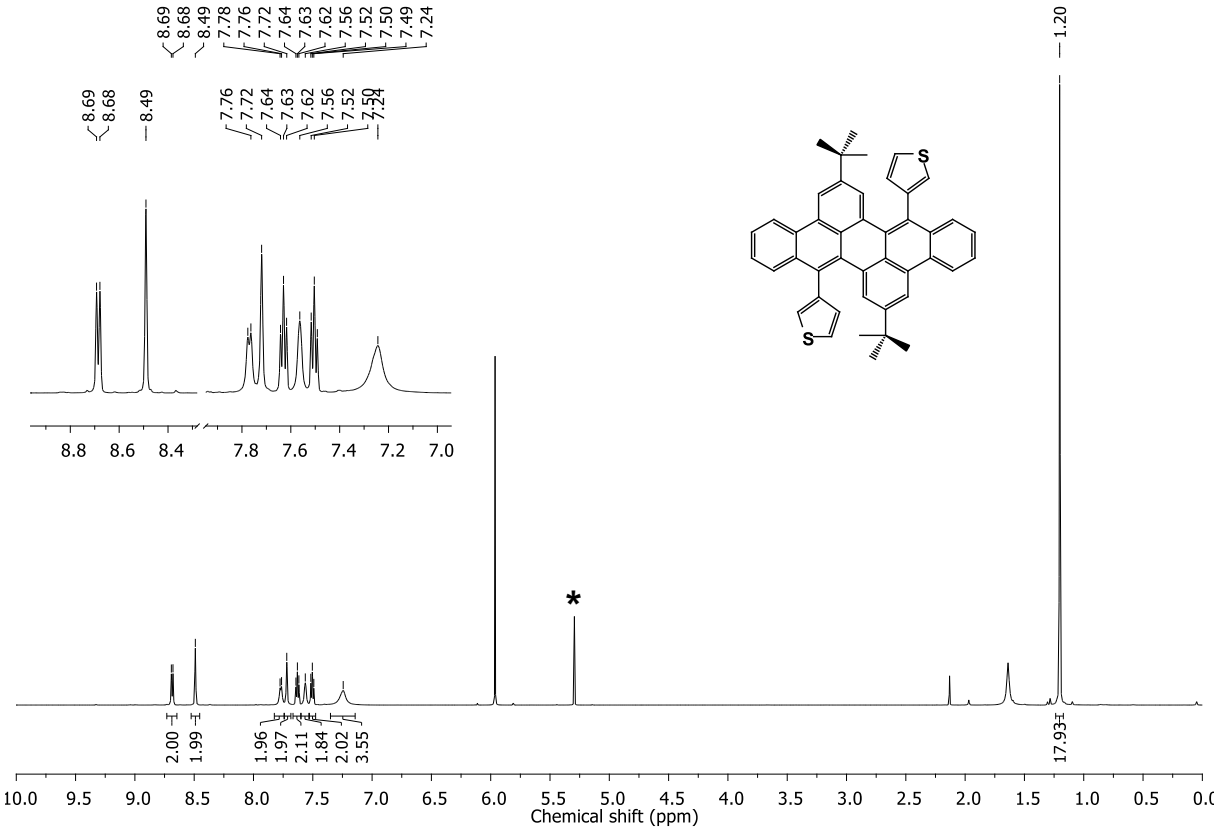

Figure 7.59 ^{1}H NMR spectrum (600 MHz, $Cl_2CDCDCl_2$) of **152**. *CH_2Cl_2.

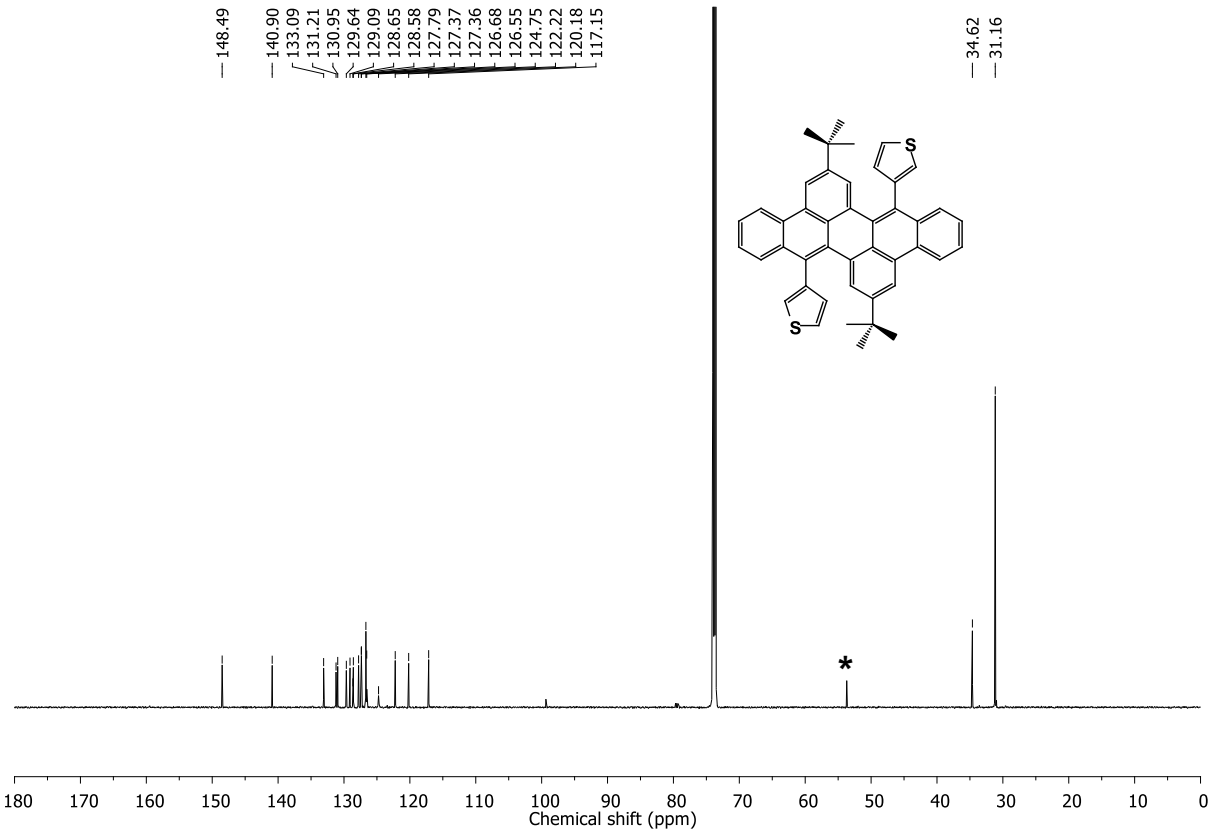

Figure 7.60 ^{13}C NMR spectrum (151 MHz, $Cl_2CDCDCl_2$) of **152**. *CH_2Cl_2.

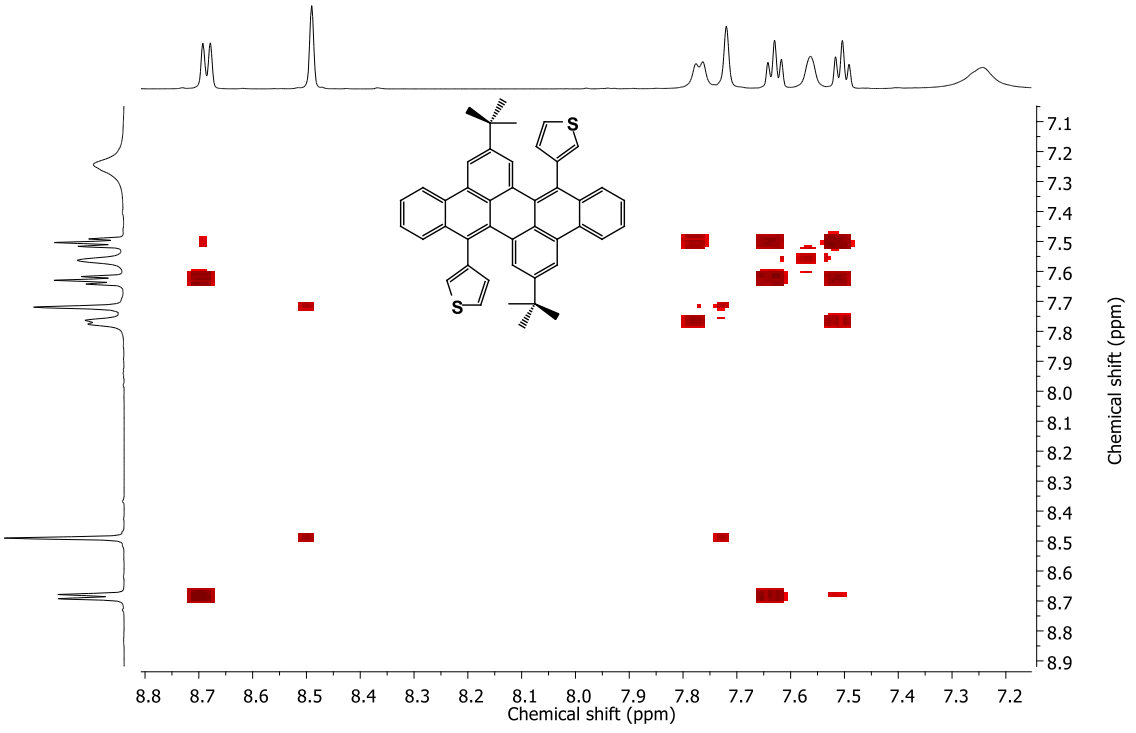

Figure 7.61 ^{1}H-^{1}H COSY NMR spectrum (600/600 MHz, $Cl_2CDCDCl_2$) of **152**.

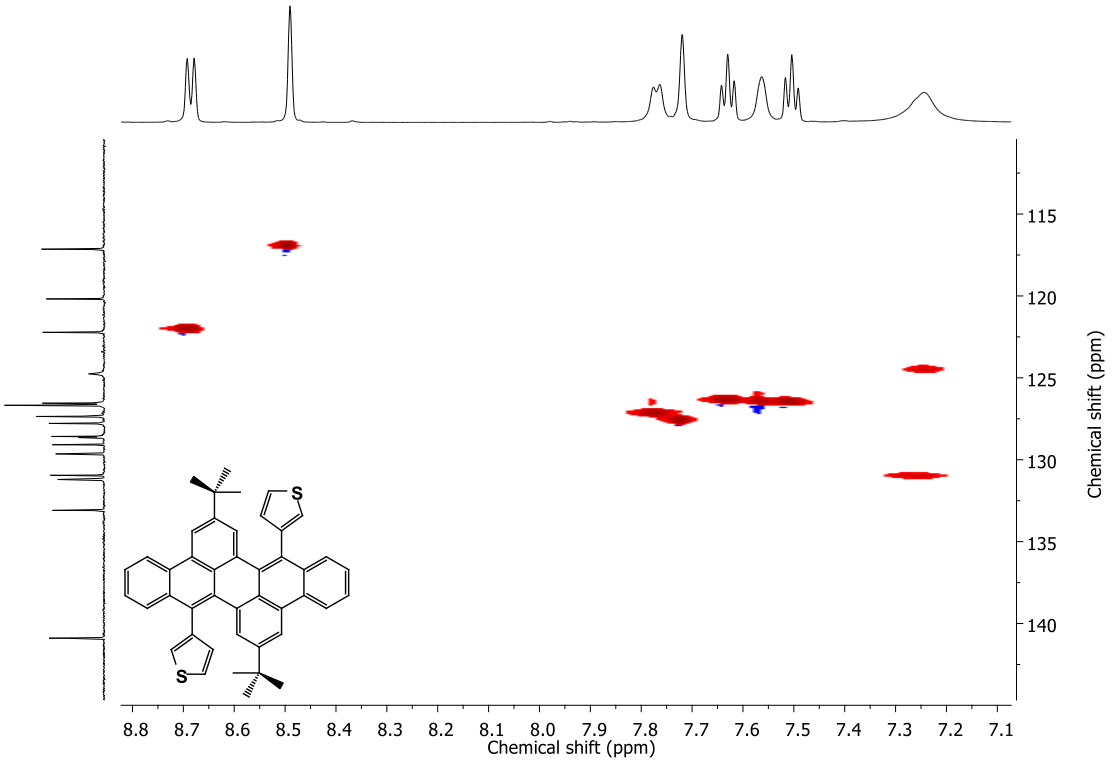

Figure 7.62 ^{1}H-^{13}C HSQC NMR spectrum (600/151 MHz, $Cl_2CDCDCl_2$) of **152**.

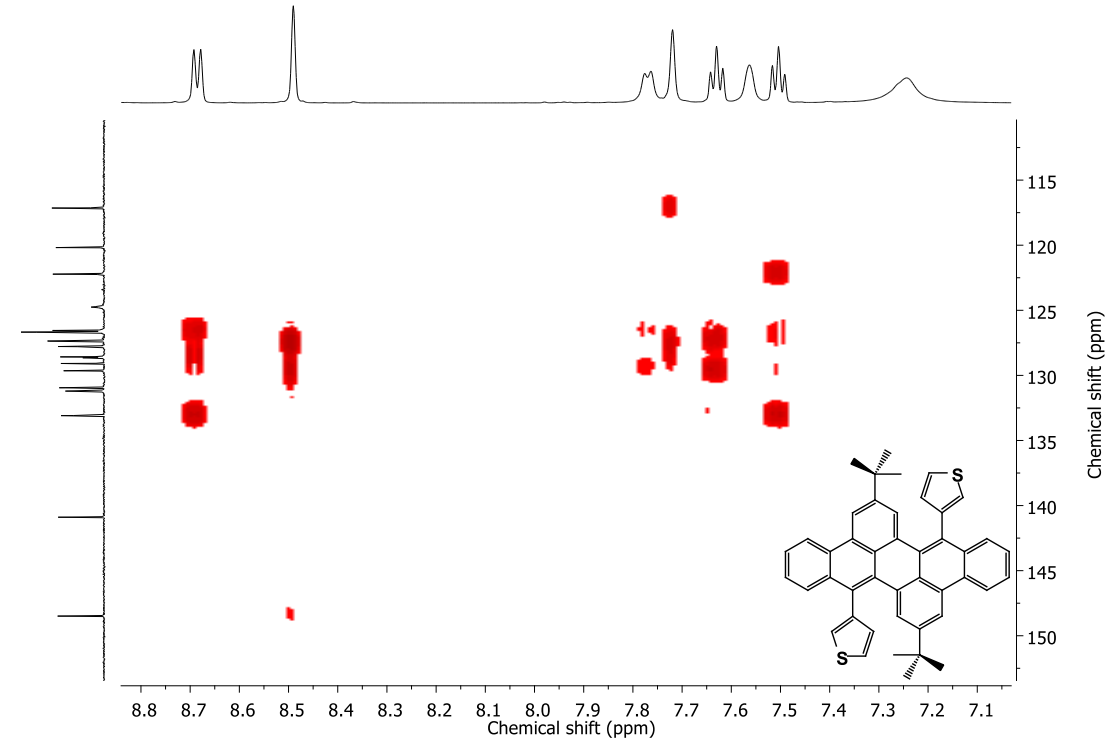

Figure 7.63 ^{1}H-^{13}C HMBC NMR spectrum (600/151 MHz, $Cl_2CDCDCl_2$) of **92**.

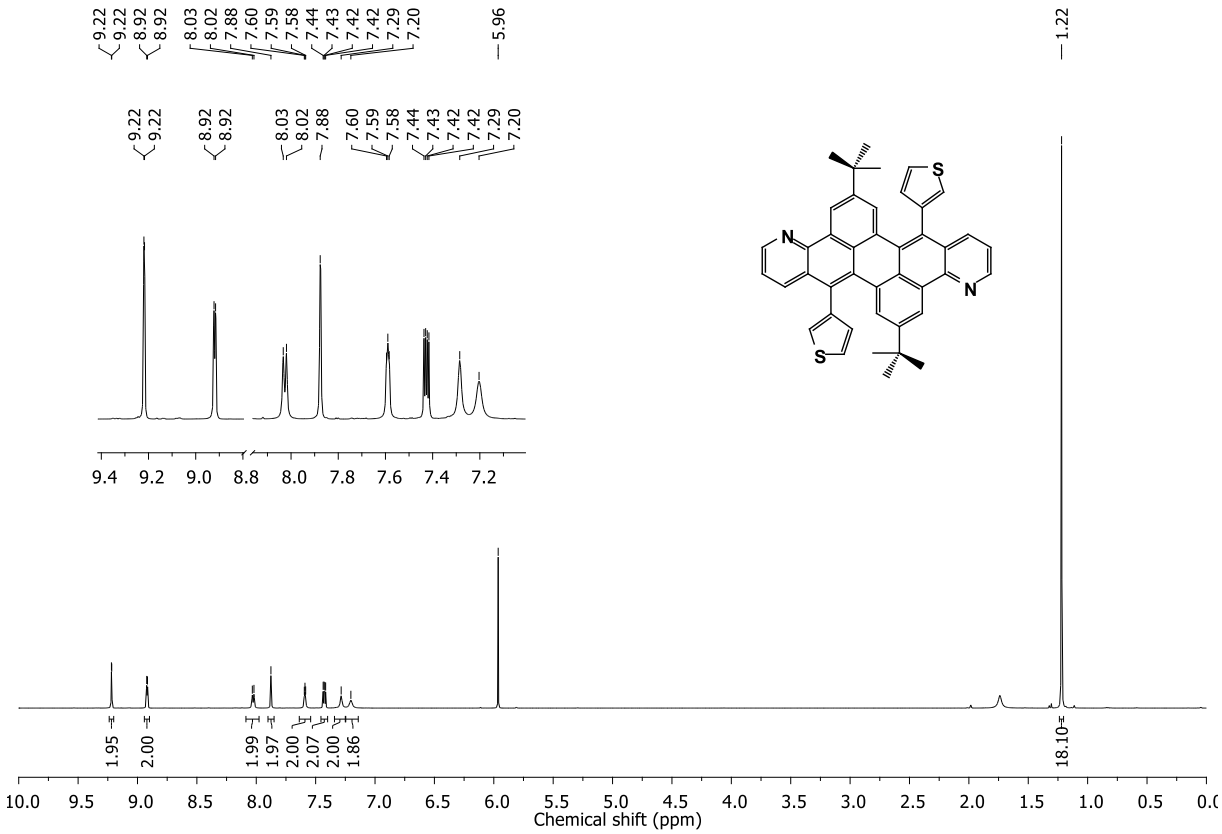

Figure 7.64 ^{1}H NMR spectrum (600 MHz, $Cl_2CDCDCl_2$) of **154**.

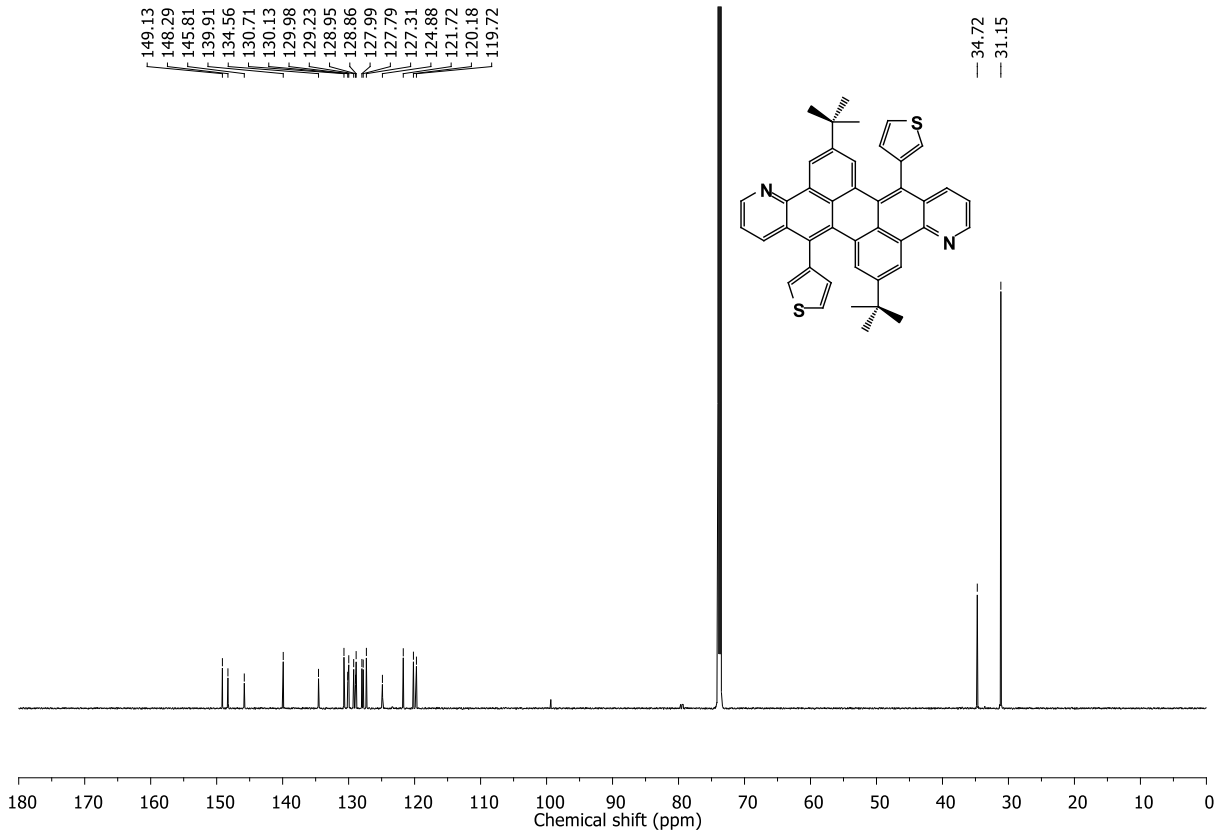

Figure 7.65 ^{13}C NMR spectrum (151 MHz, $Cl_2CDCDCl_2$) of **154**.

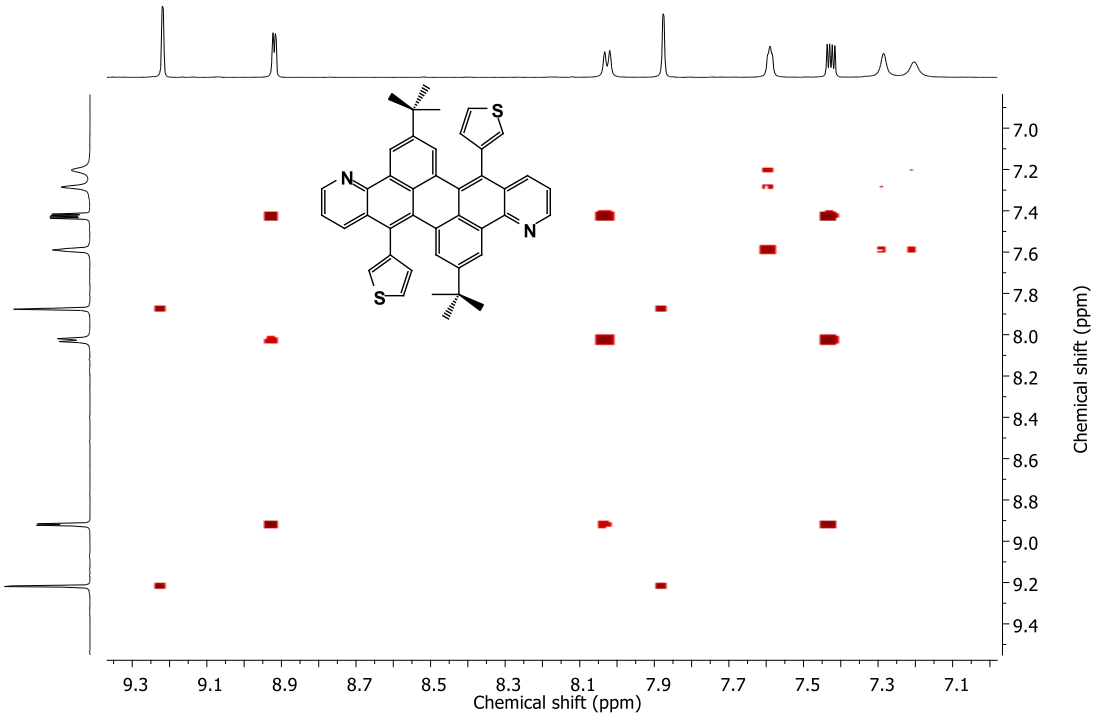

Figure 7.66 ^{1}H-^{1}H COSY NMR spectrum (600/600 MHz, $Cl_2CDCDCl_2$) of **154**.

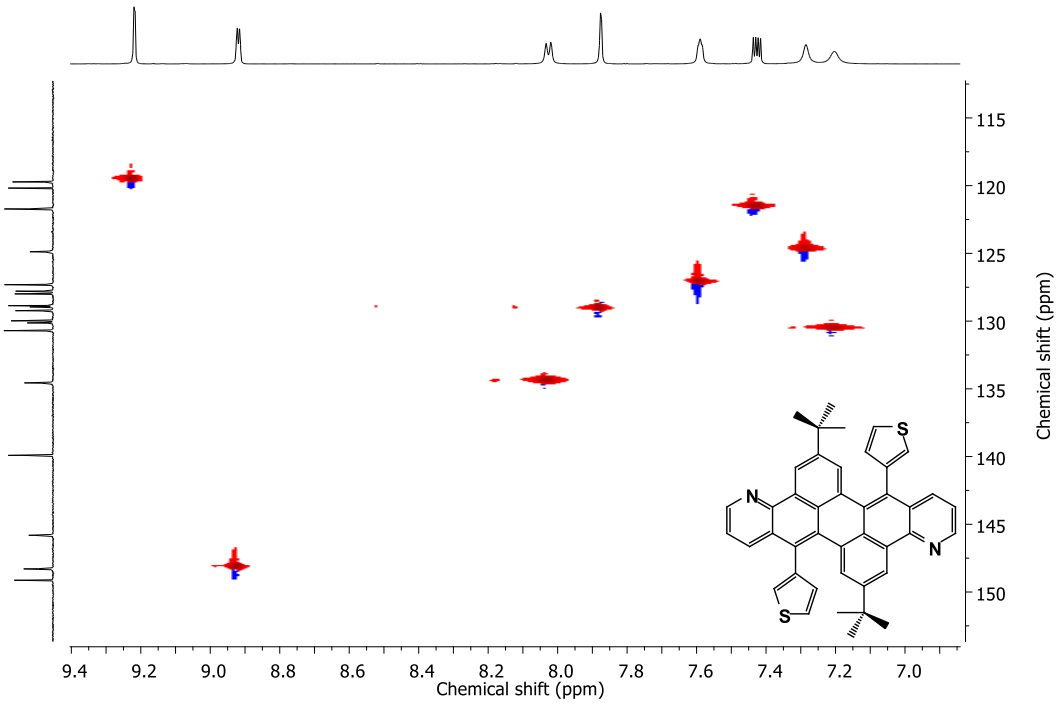

Figure 7.67 ^{1}H-^{13}C HSQC NMR spectrum (600/151 MHz, $Cl_2CDCDCl_2$) of **154**.

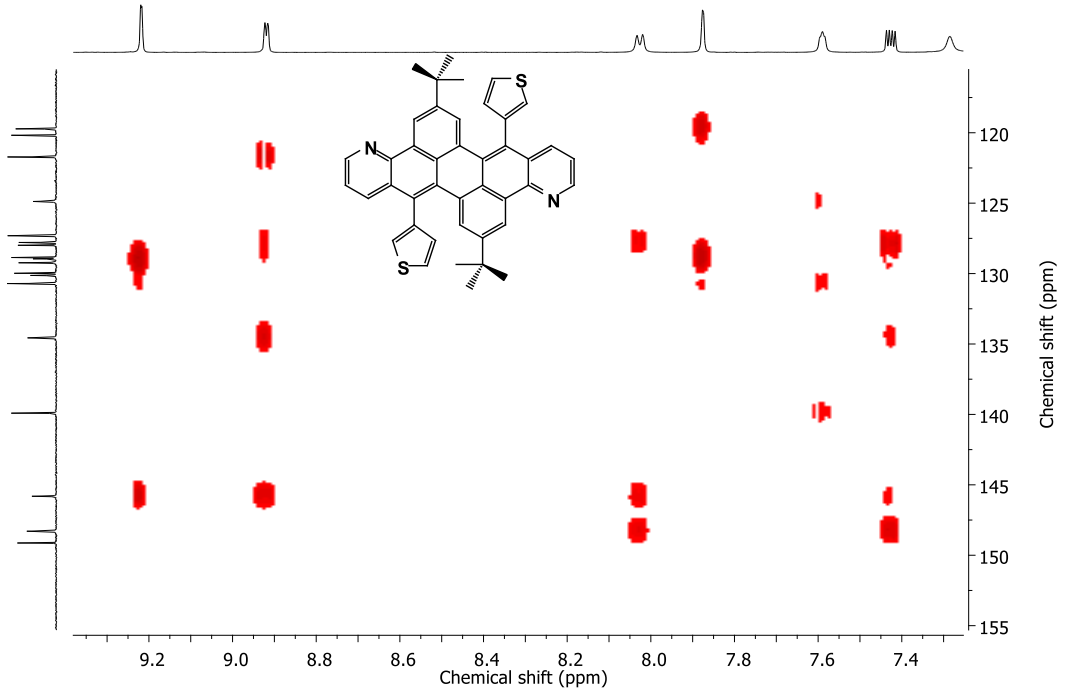

Figure 7.68 ^{1}H-^{13}C HMBC NMR spectrum (600/151 MHz, $Cl_2CDCDCl_2$) of **154**.

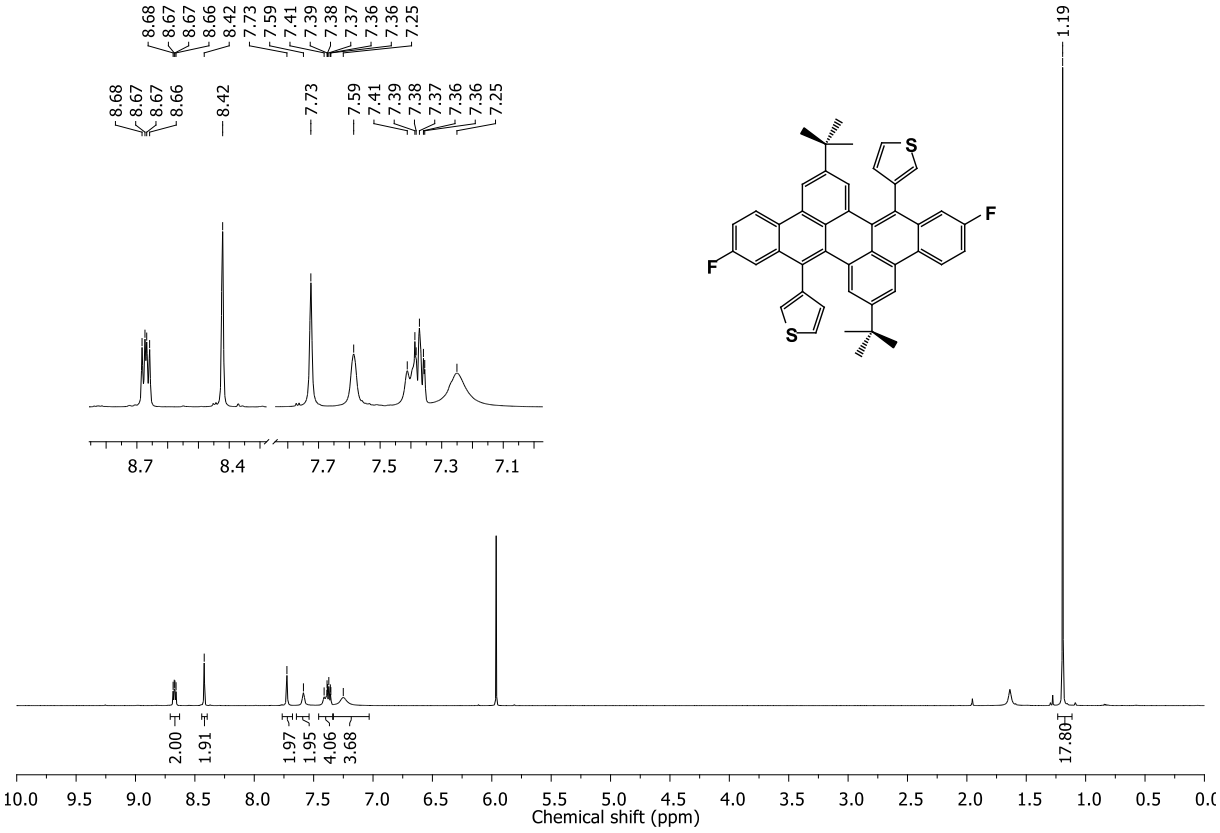

Figure 7.69 ^{1}H NMR spectrum (600 MHz, $Cl_2CDCDCl_2$) of **157**.

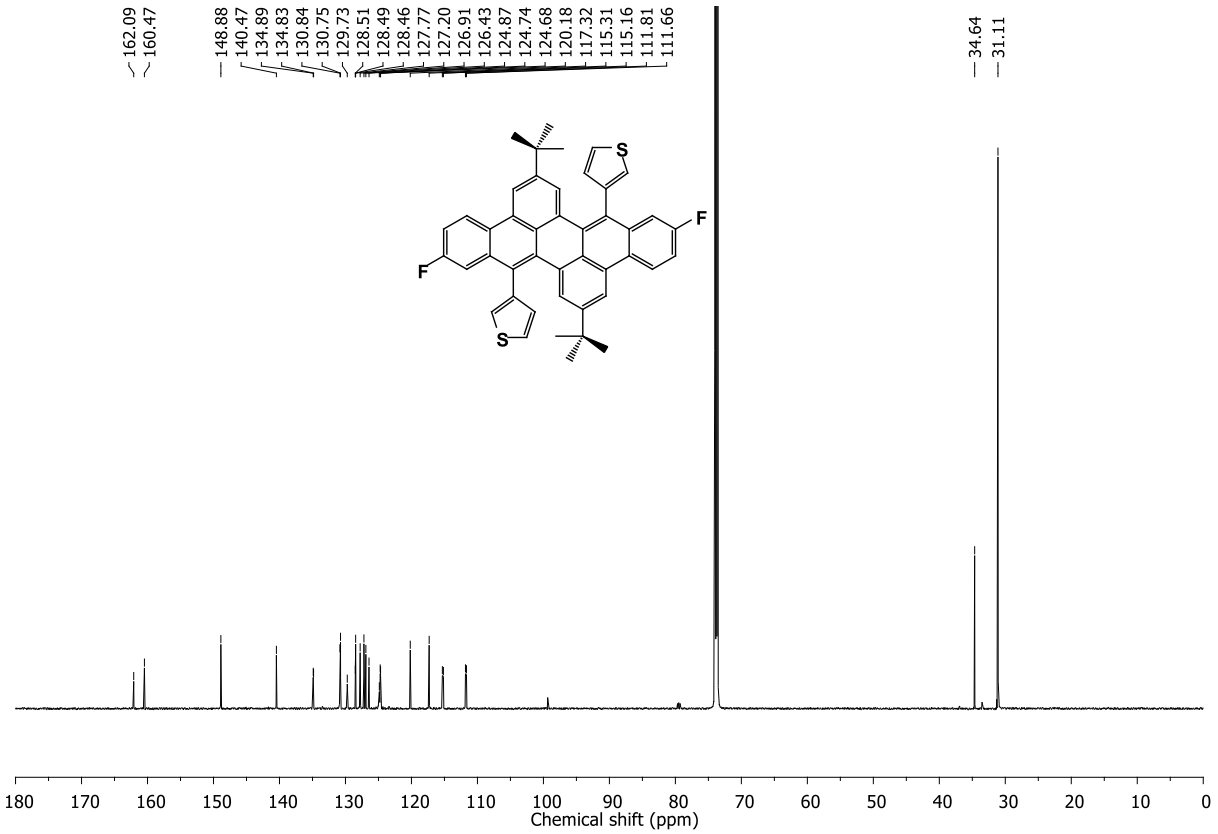

Figure 7.70 ^{13}C NMR spectrum (151 MHz, $Cl_2CDCDCl_2$) of **157**.

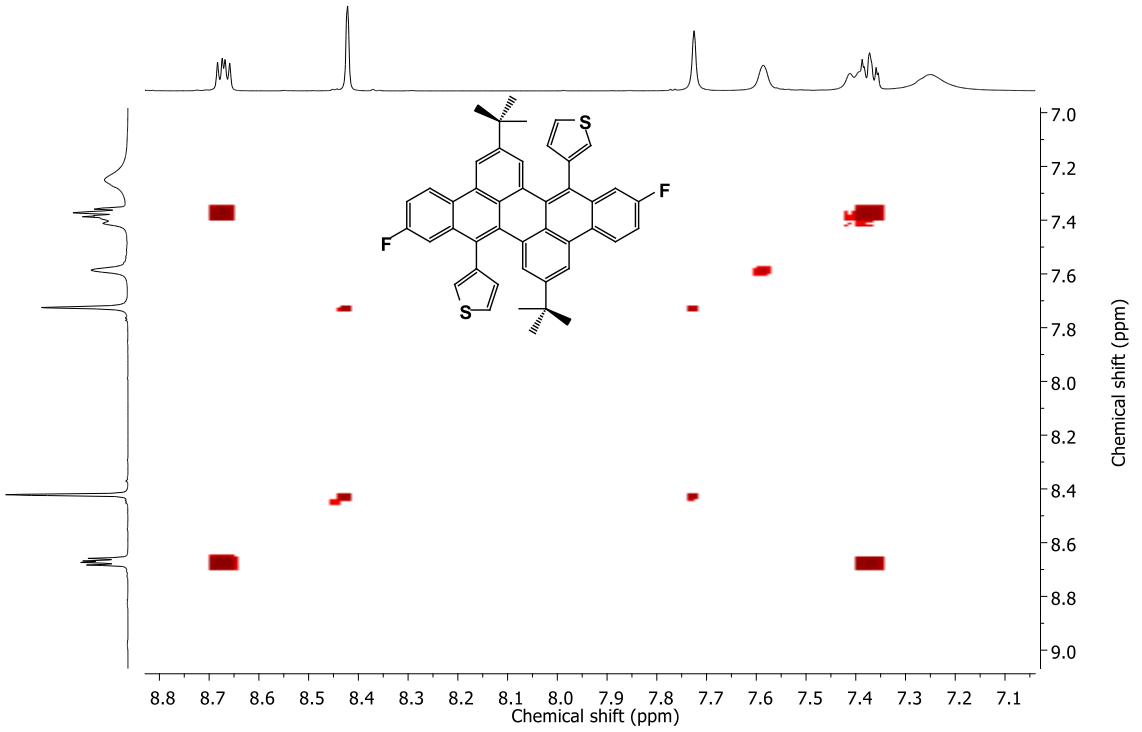

Figure 7.71 ^{1}H-^{1}H COSY NMR spectrum (600/600 MHz, $Cl_2CDCDCl_2$) of **157**.

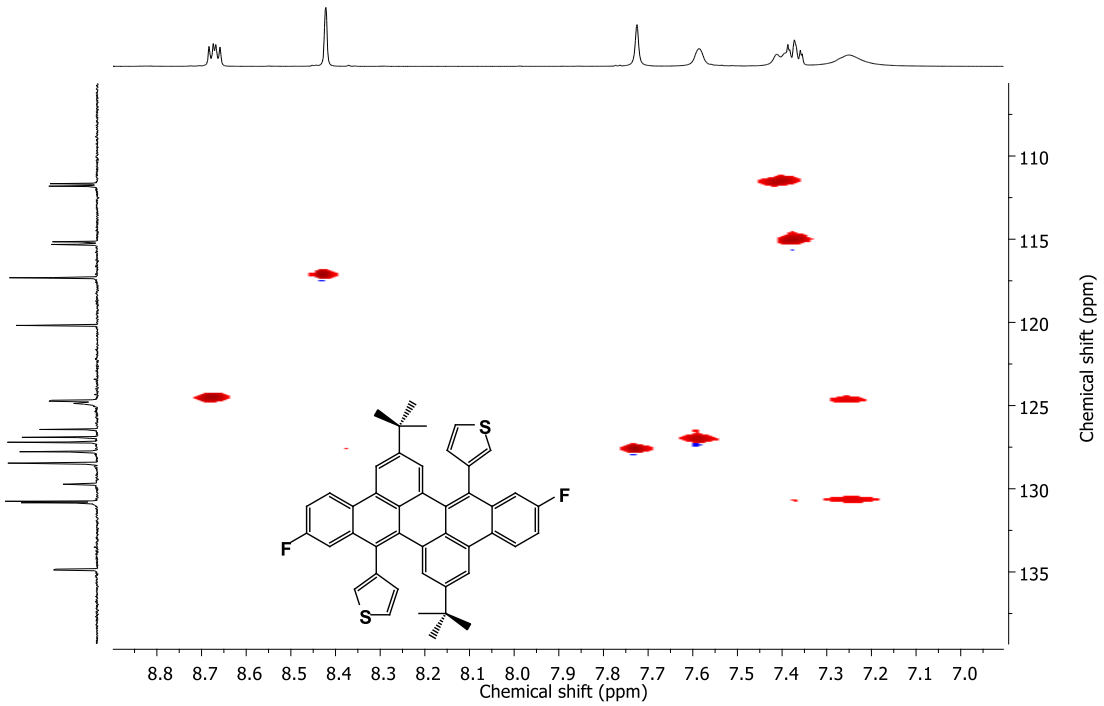

Figure 7.72 ^{1}H-^{13}C HSQC NMR spectrum (600/151 MHz, $Cl_2CDCDCl_2$) of **157**.

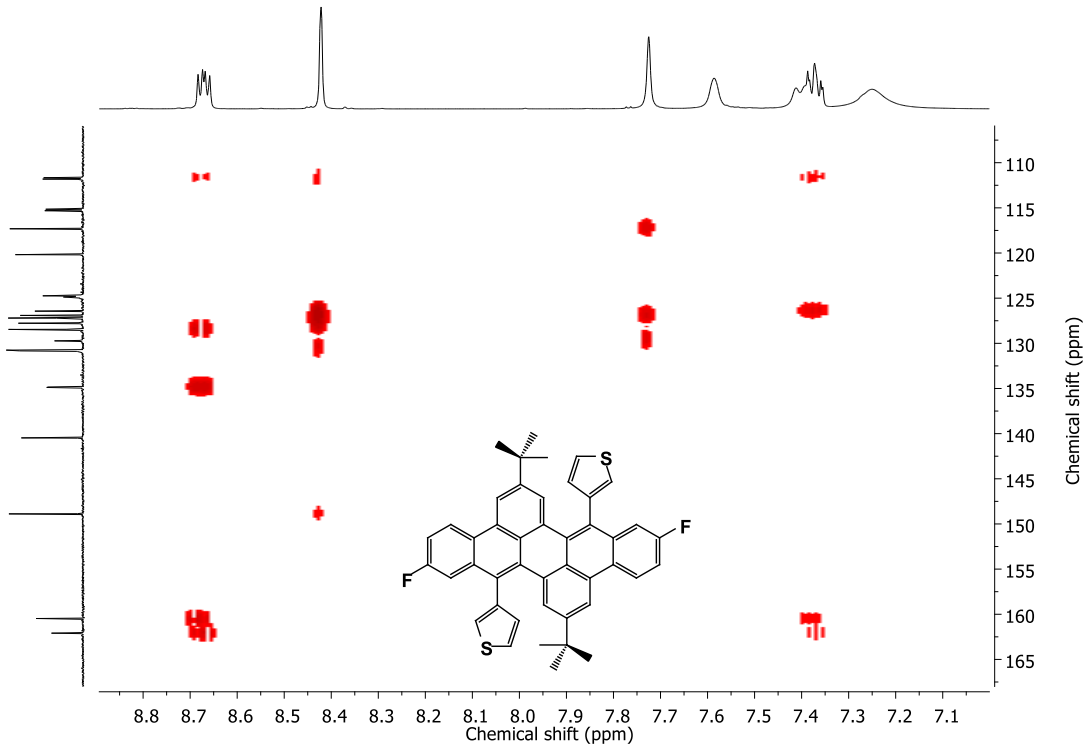

Figure 7.73 ^{1}H-^{13}C HMBC NMR spectrum (600/151 MHz, $Cl_2CDCDCl_2$) of **157**.

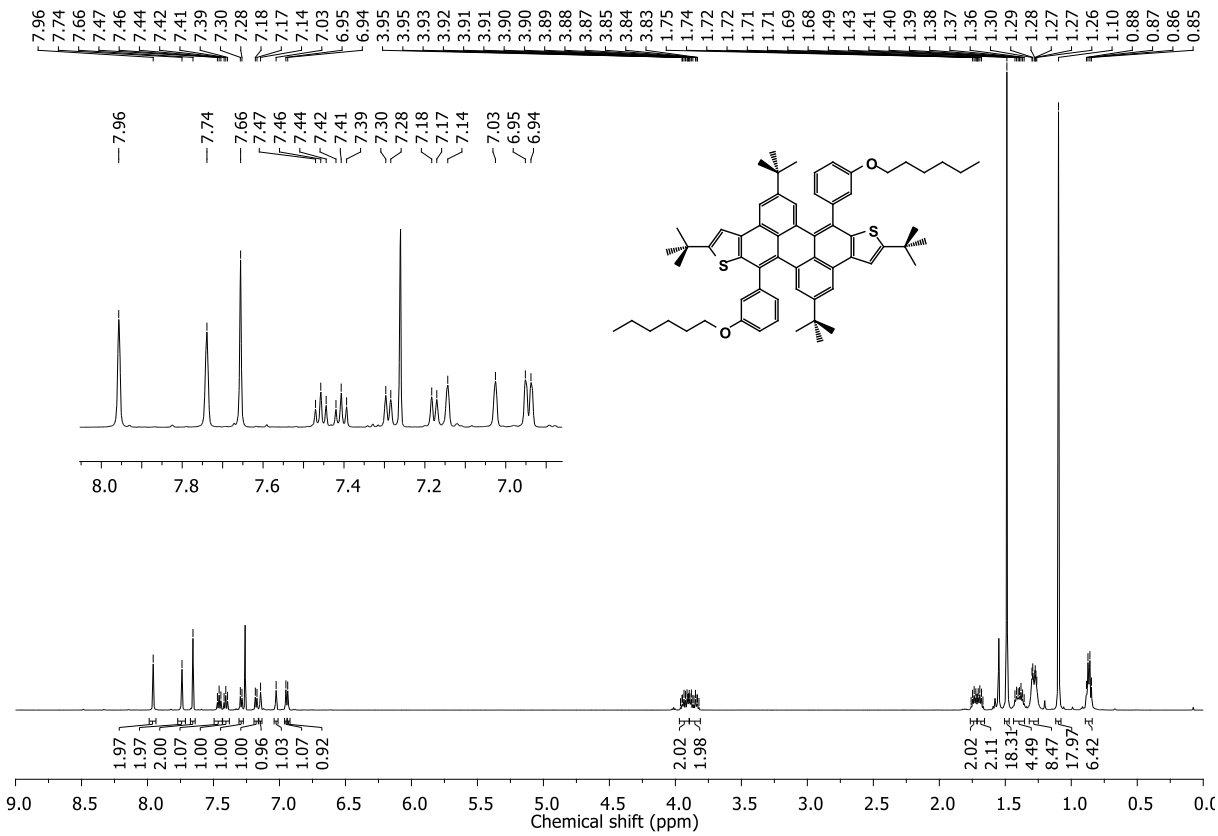

Figure 7.74 ^{1}H NMR spectrum (600 MHz, $CDCl_3$) of **158**.

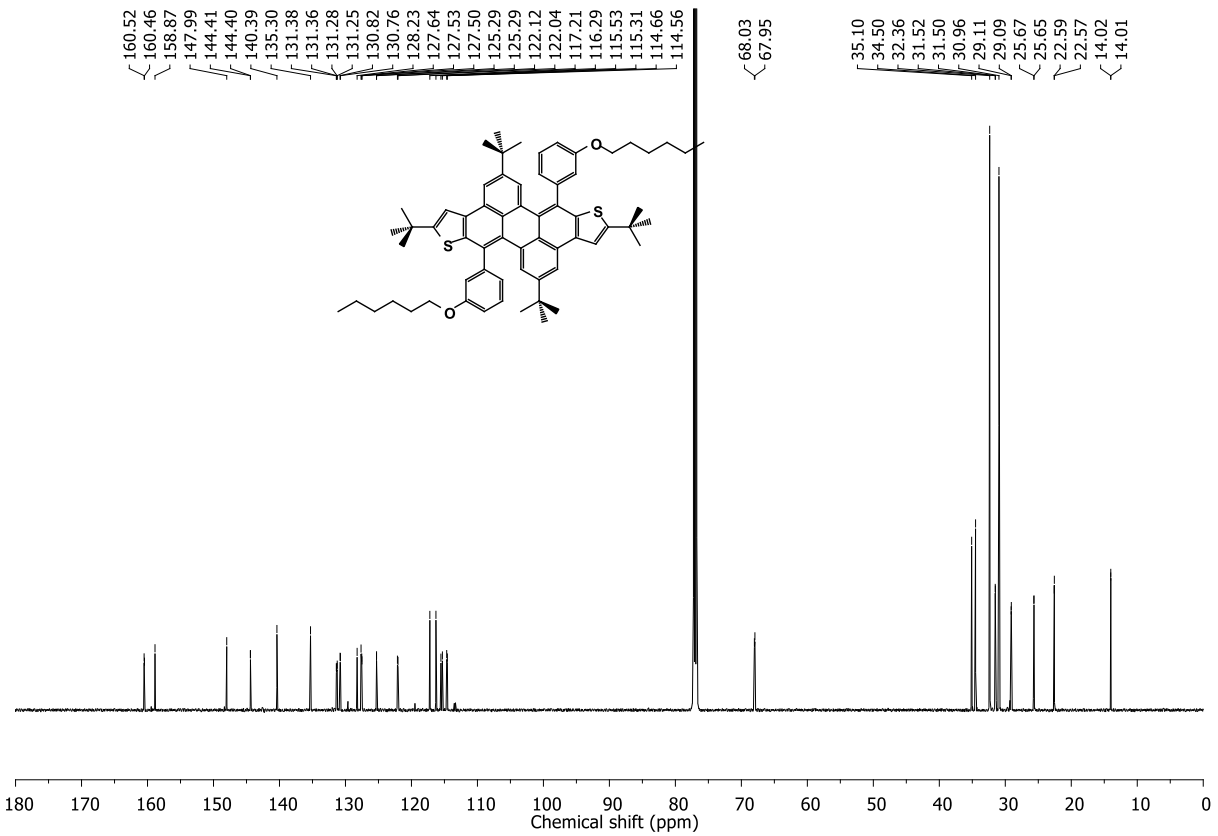

Figure 7.75 ^{13}C NMR spectrum (151 MHz, $CDCl_3$) of **158**.

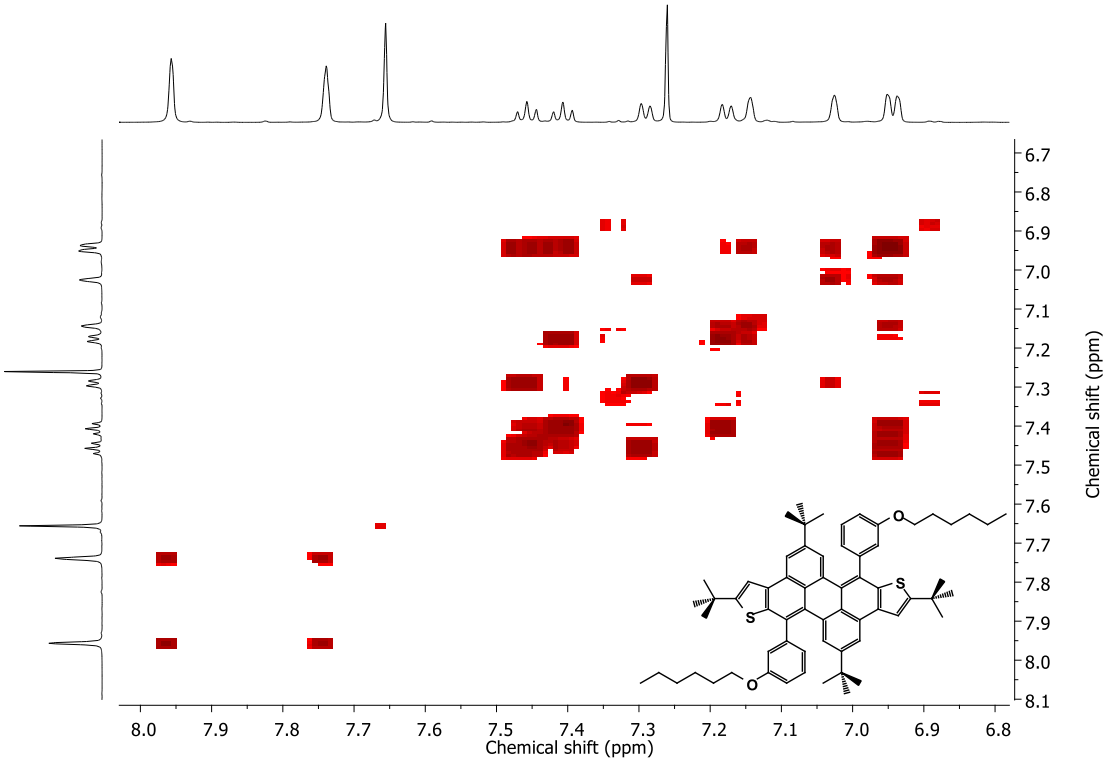

Figure 7.76 ^{1}H-^{1}H COSY NMR spectrum (600/600 MHz, $CDCl_3$) of **158**.

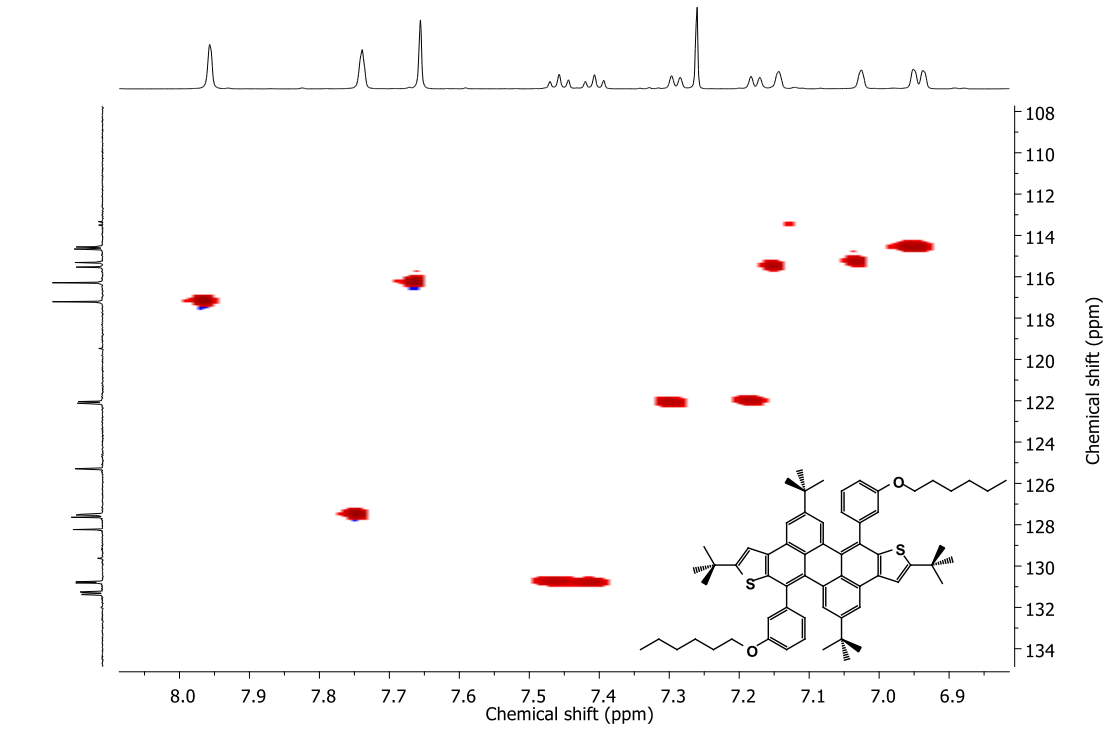

Figure 7.77 ^{1}H-^{13}C HSQC NMR spectrum (600/151 MHz, $CDCl_3$) of **158**.

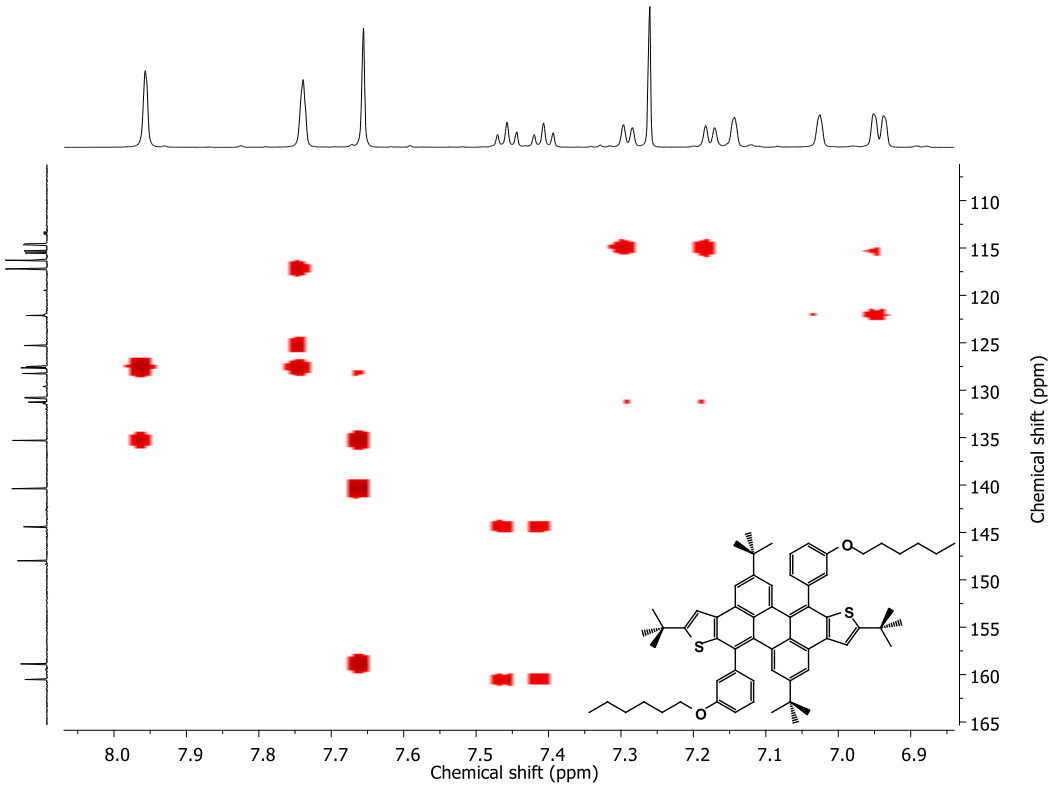

Figure 7.78 ^{1}H-^{13}C HMBC NMR spectrum (600/151 MHz, $CDCl_3$) of **158**.

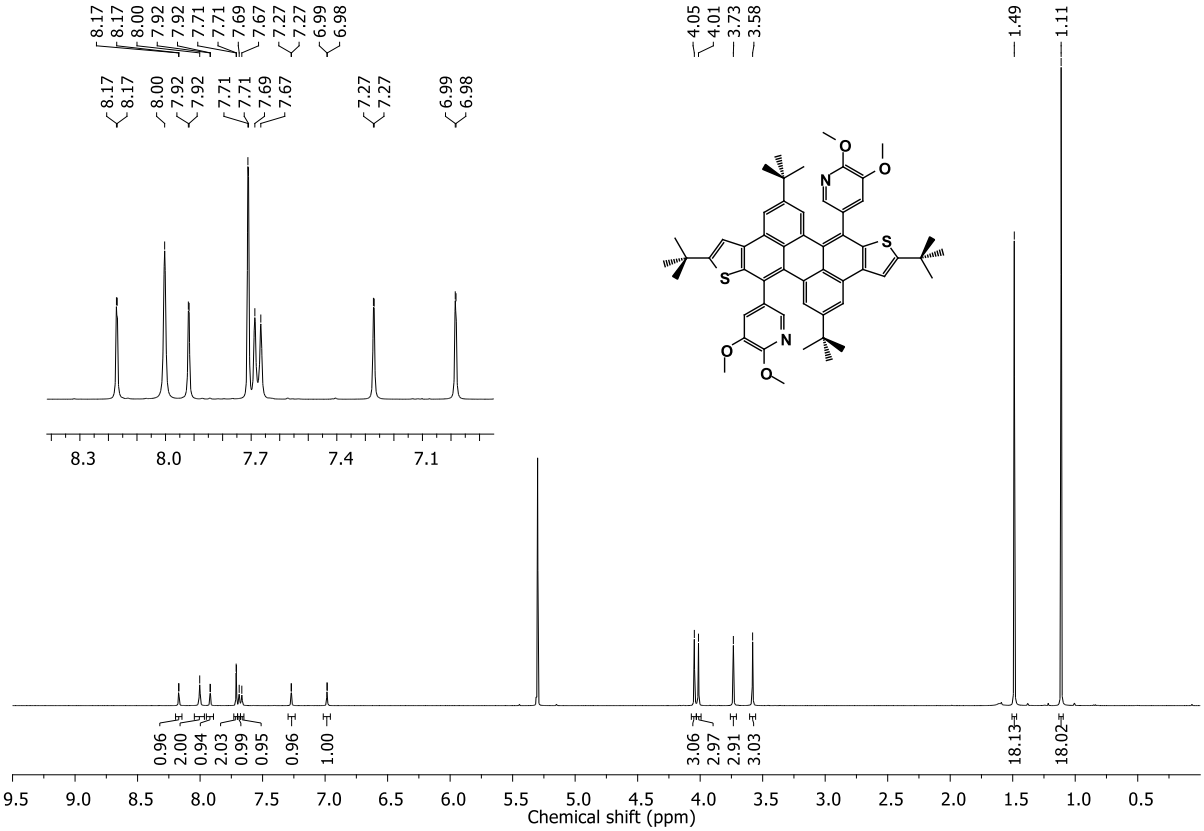

Figure 7.79 ^{1}H NMR spectrum (600 MHz, CD_2Cl_2) of **159**.

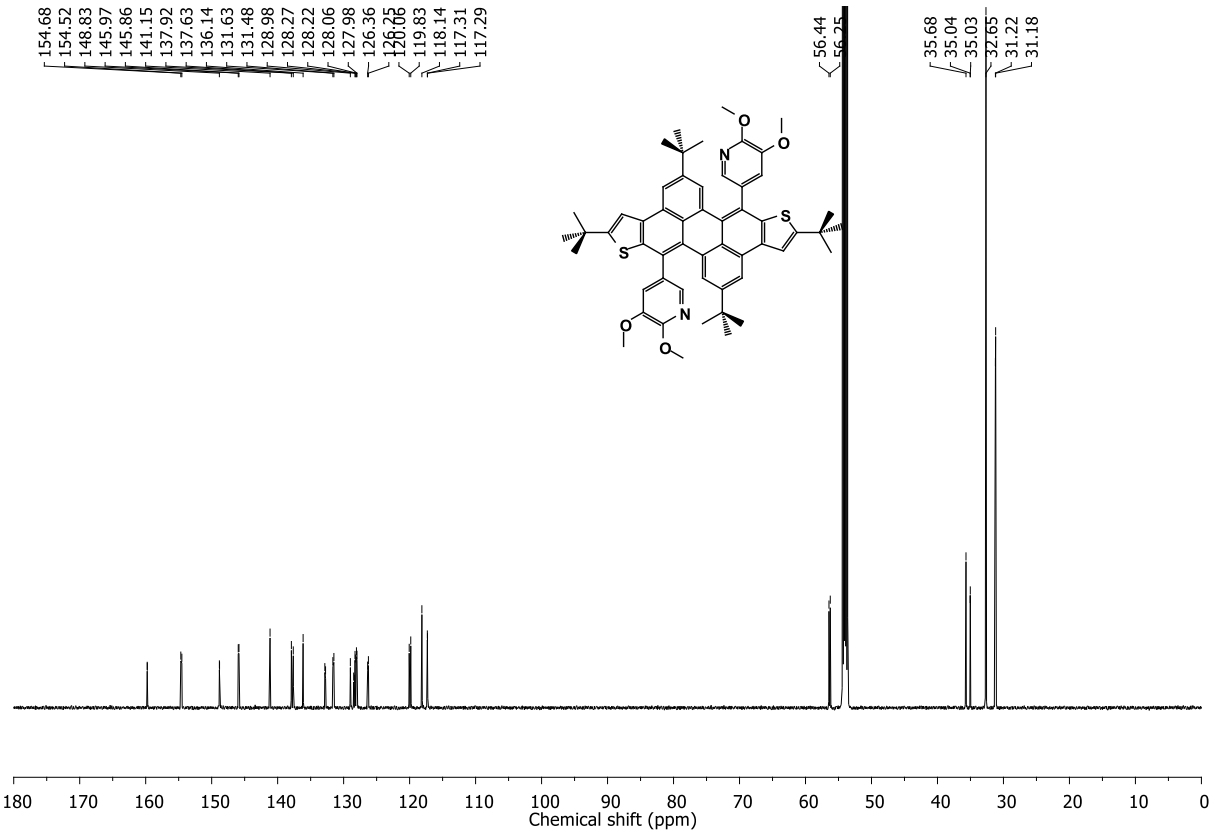

Figure 7.80 ^{13}C NMR spectrum (151 MHz, CD_2Cl_2) of **159**.

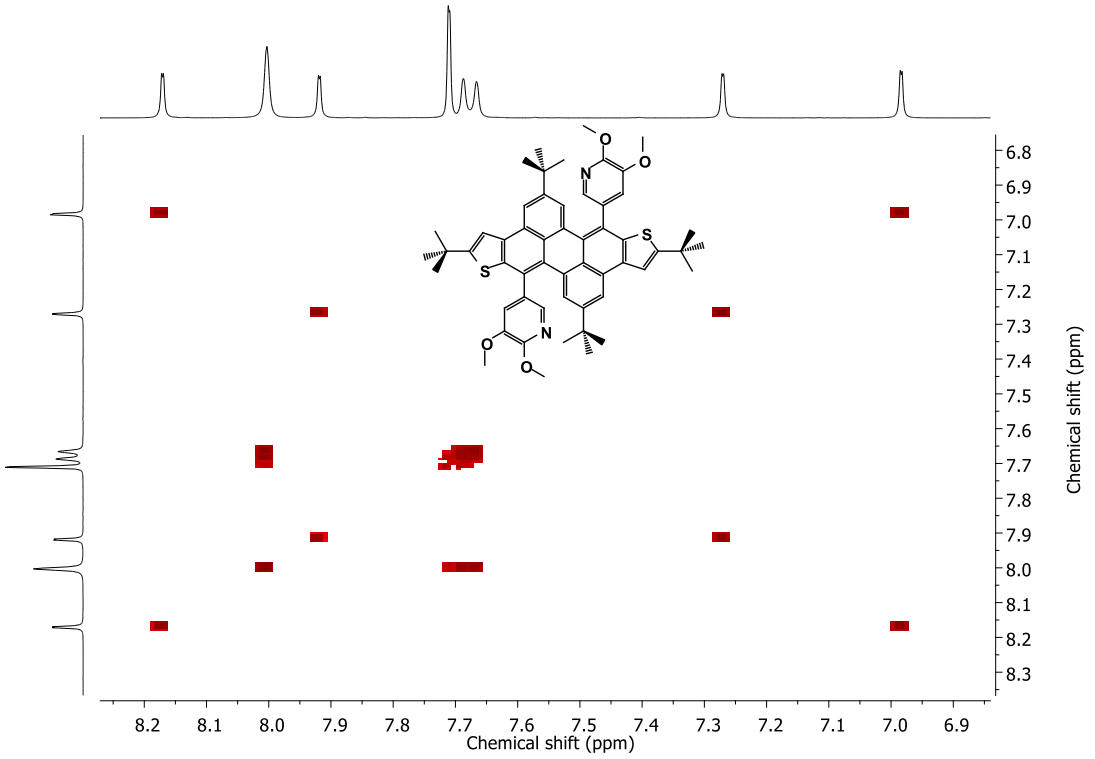

Figure 7.81 ^{1}H-^{1}H COSY NMR spectrum (600/600 MHz, CD_2Cl_2) of **159**.

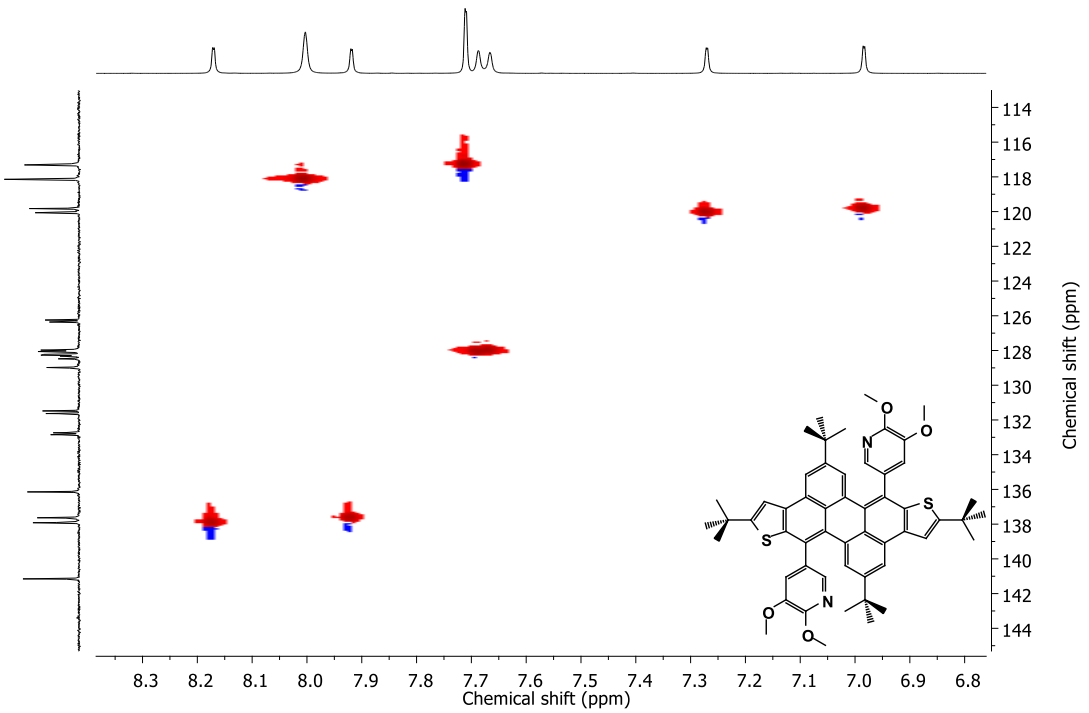

Figure 7.82 ^{1}H-^{13}C HSQC NMR spectrum (600/151 MHz, CD_2Cl_2) of **159**.

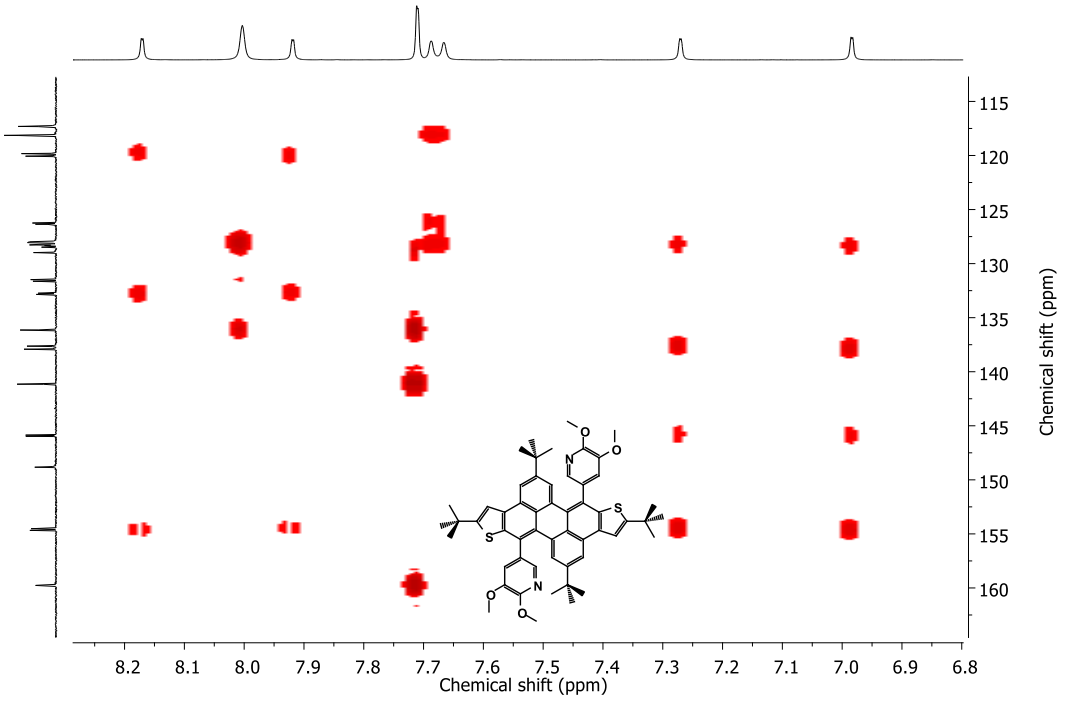

Figure 7.83 ^{1}H-^{13}C HMBC NMR spectrum (600/151 MHz, CD_2Cl_2) of **159**.

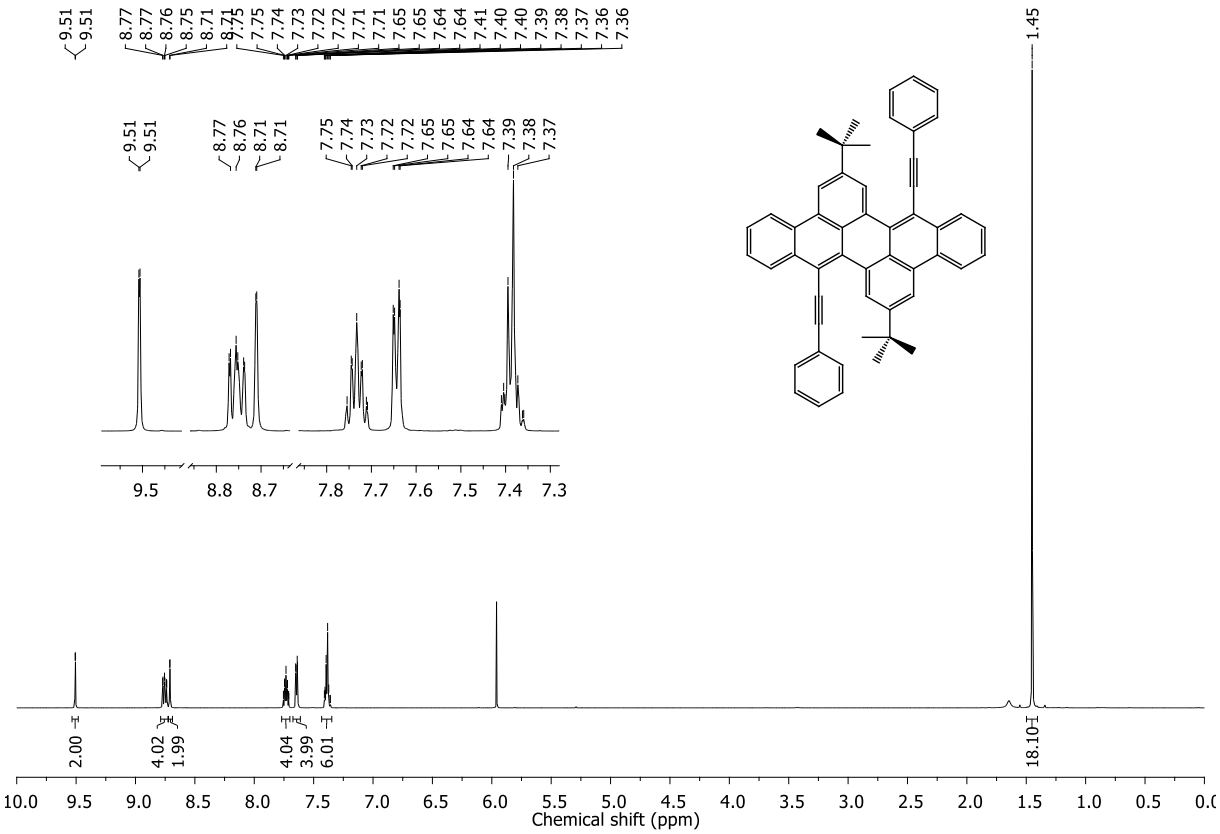

Figure 7.84 ^{1}H NMR spectrum (600 MHz, $Cl_2CDCDCl_2$) of **161**.

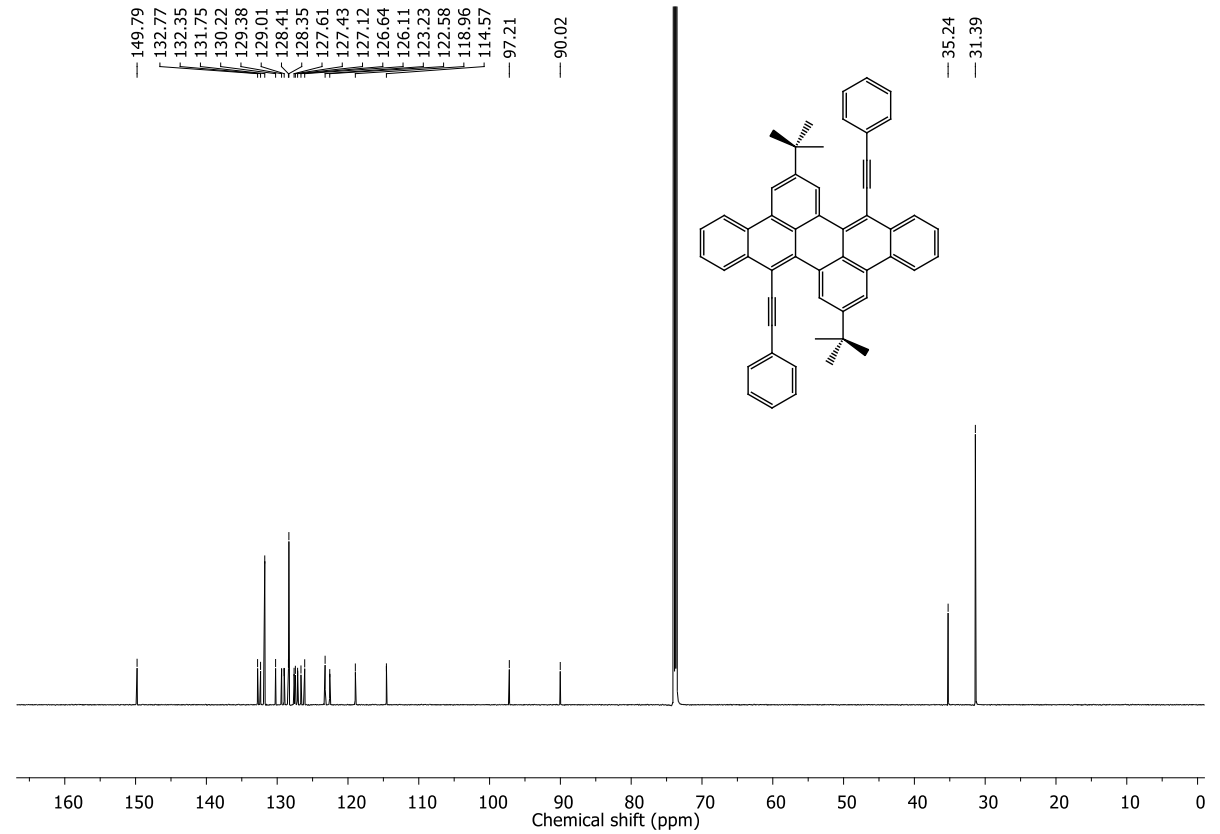

Figure 7.85 ^{13}C NMR spectrum (151 MHz, $Cl_2CDCDCl_2$) of **161**.

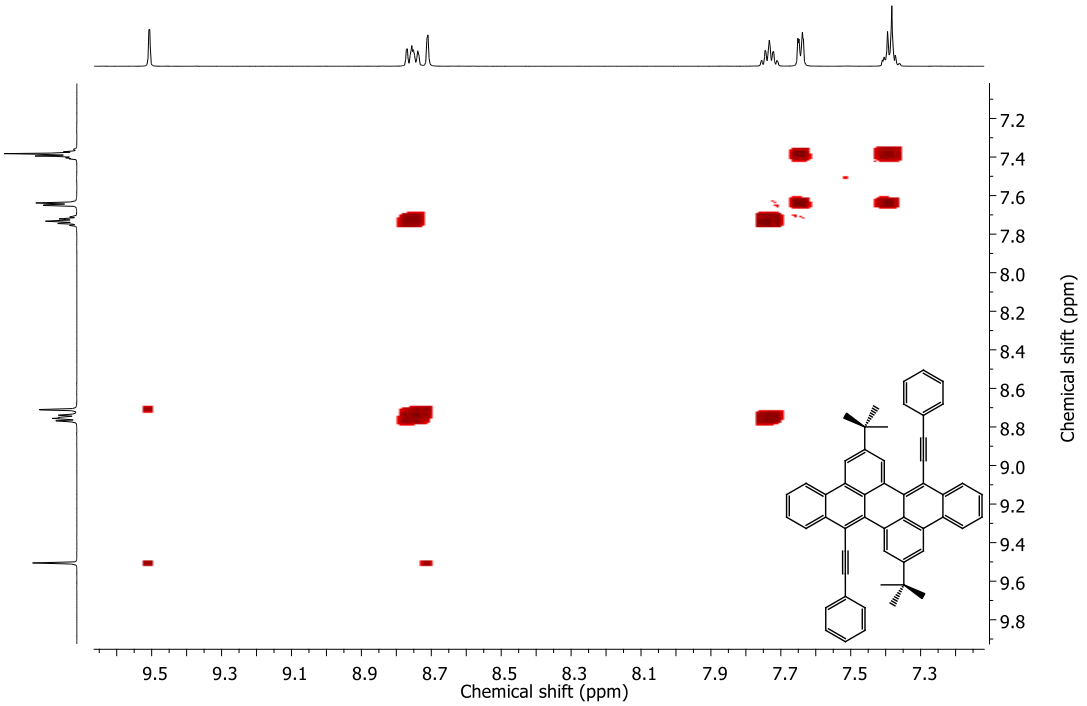

Figure 7.86 ^{1}H-^{1}H COSY NMR spectrum (600/600 MHz, $Cl_2CDCDCl_2$) of **161**.

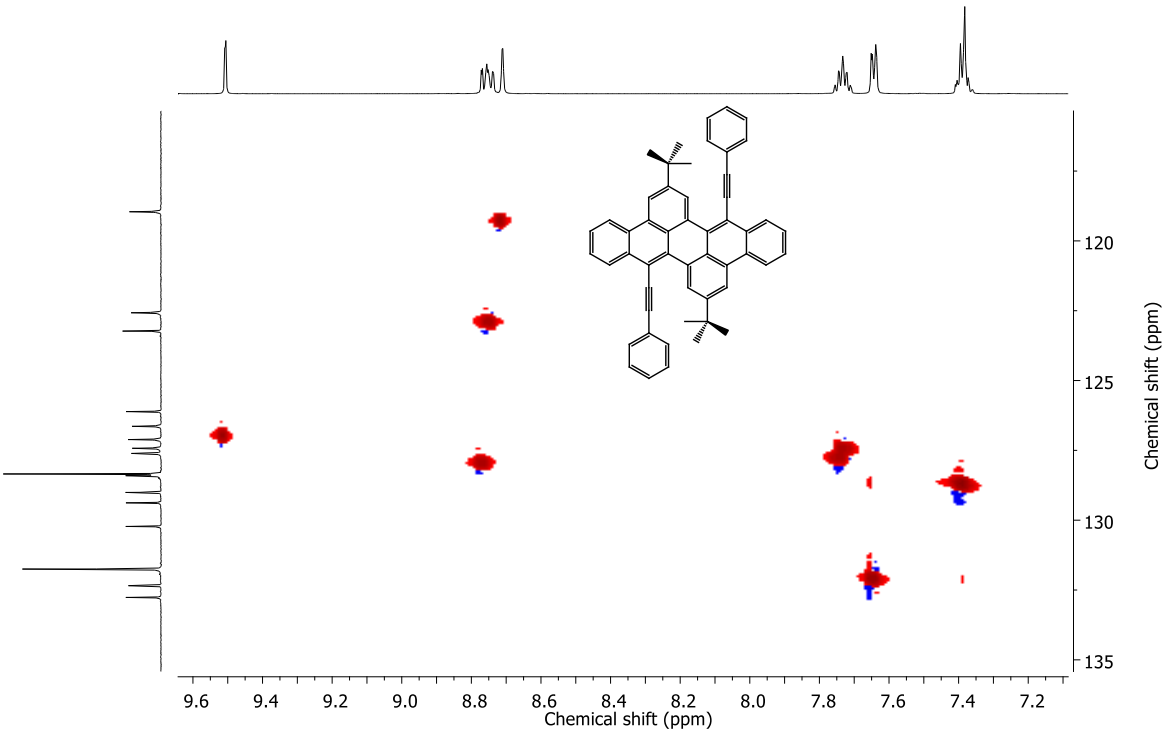

Figure 7.87 ^{1}H-^{13}C HSQC NMR spectrum (600/151 MHz, $Cl_2CDCDCl_2$) of **161**.

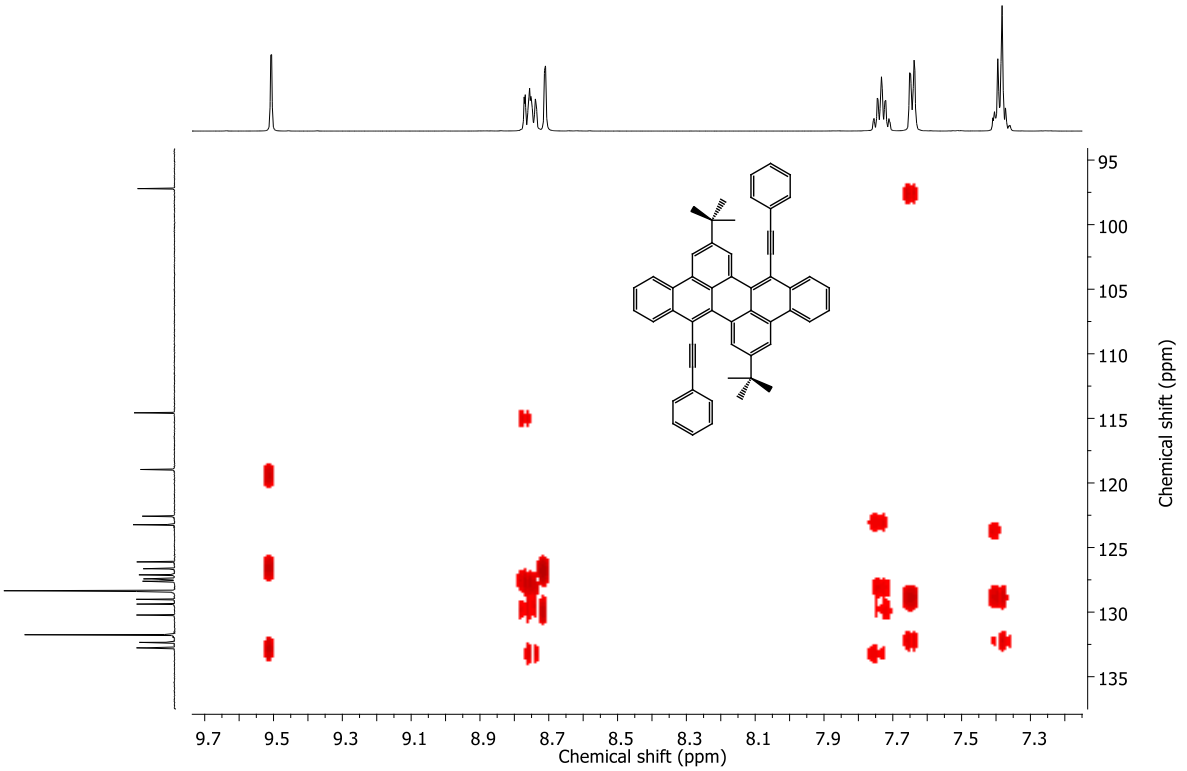

Figure 7.88 ^{1}H-^{13}C HMBC NMR spectrum (600/151 MHz, $Cl_2CDCDCl_2$) of **161**.

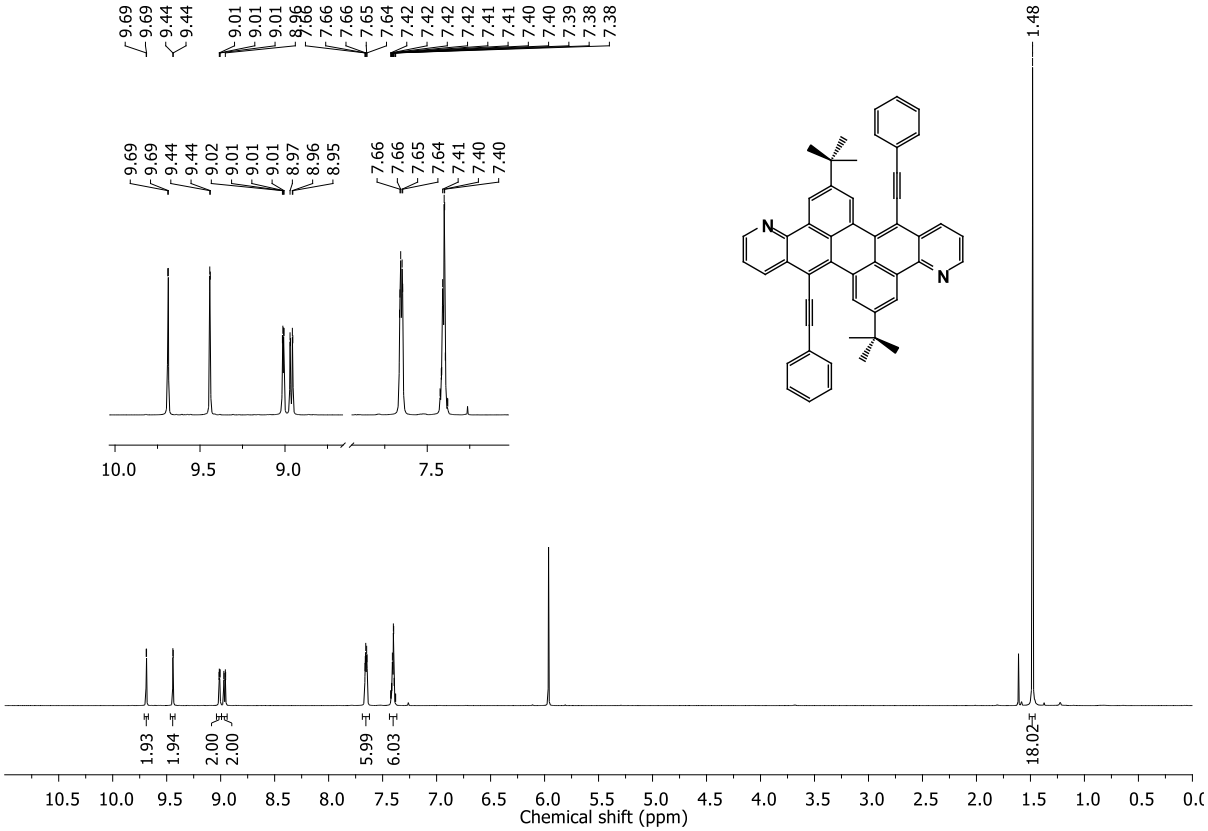

Figure 7.89 ^{1}H NMR spectrum (600 MHz, $Cl_2CDCDCl_2$) of **162**.

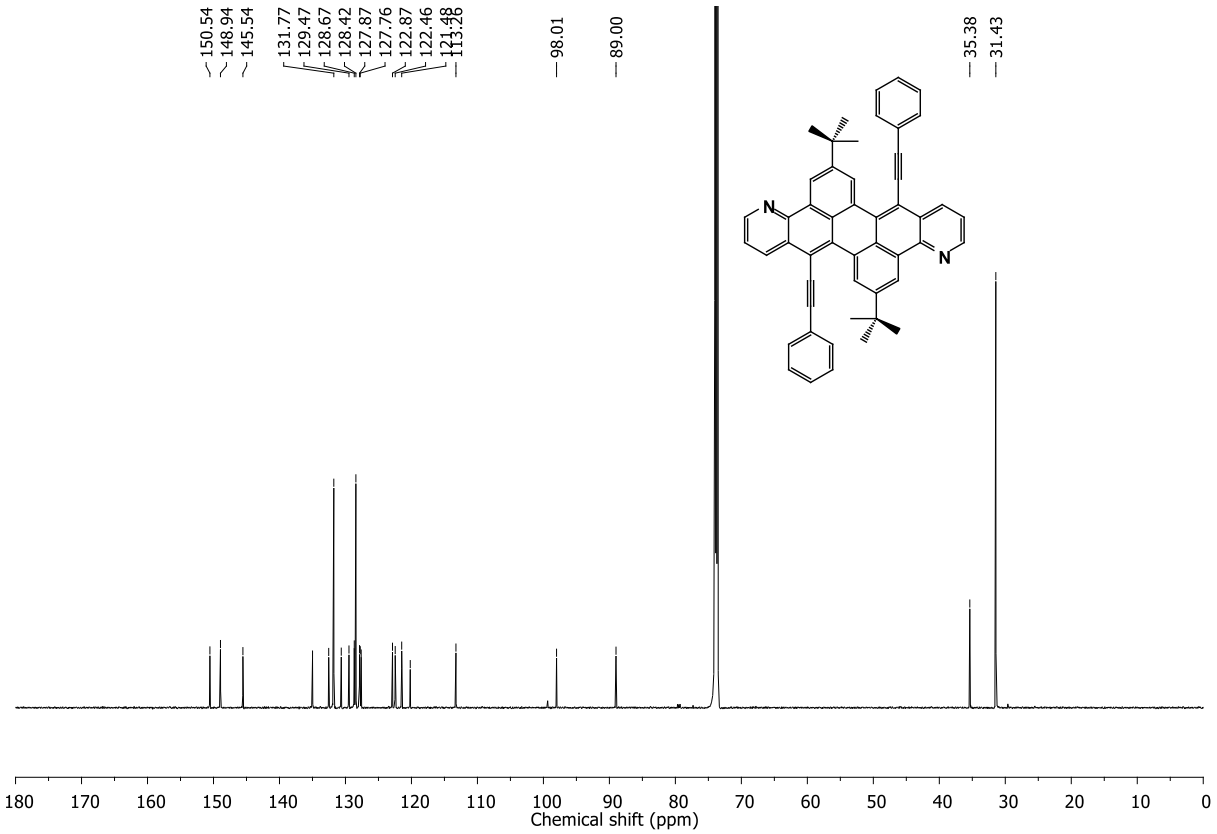

Figure 7.90 ^{13}C NMR spectrum (151 MHz, $Cl_2CDCDCl_2$) of **162**.

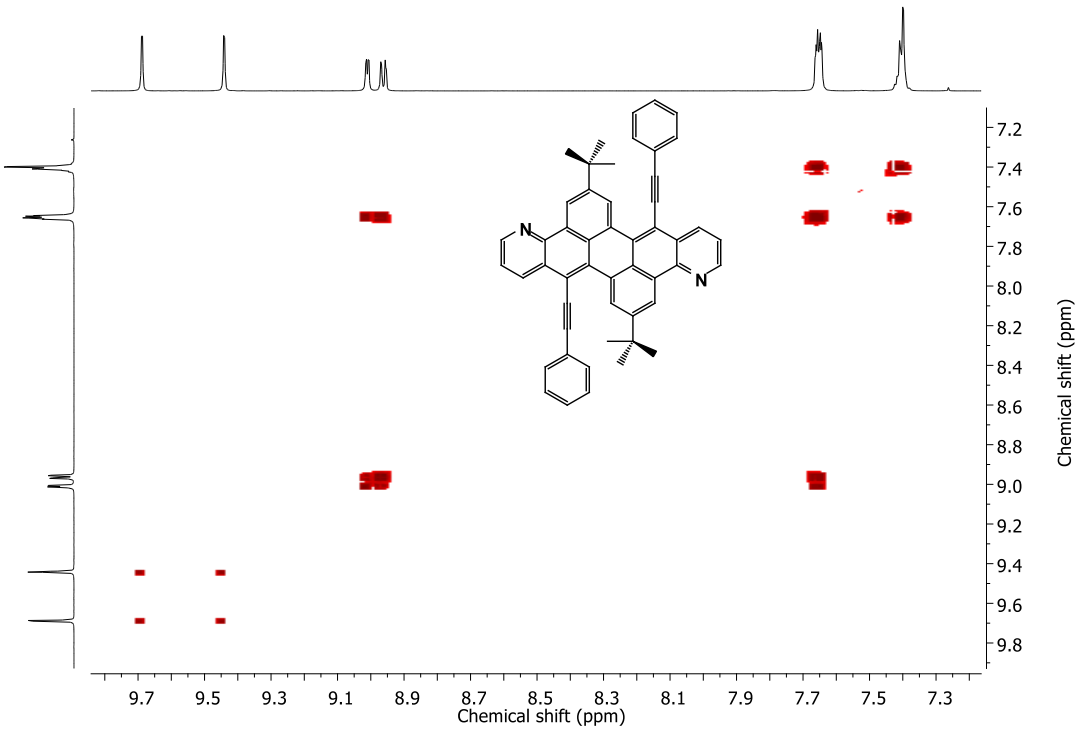

Figure 7.91 ^{1}H-^{1}H COSY NMR spectrum (600/600 MHz, $Cl_2CDCDCl_2$) of **162**.

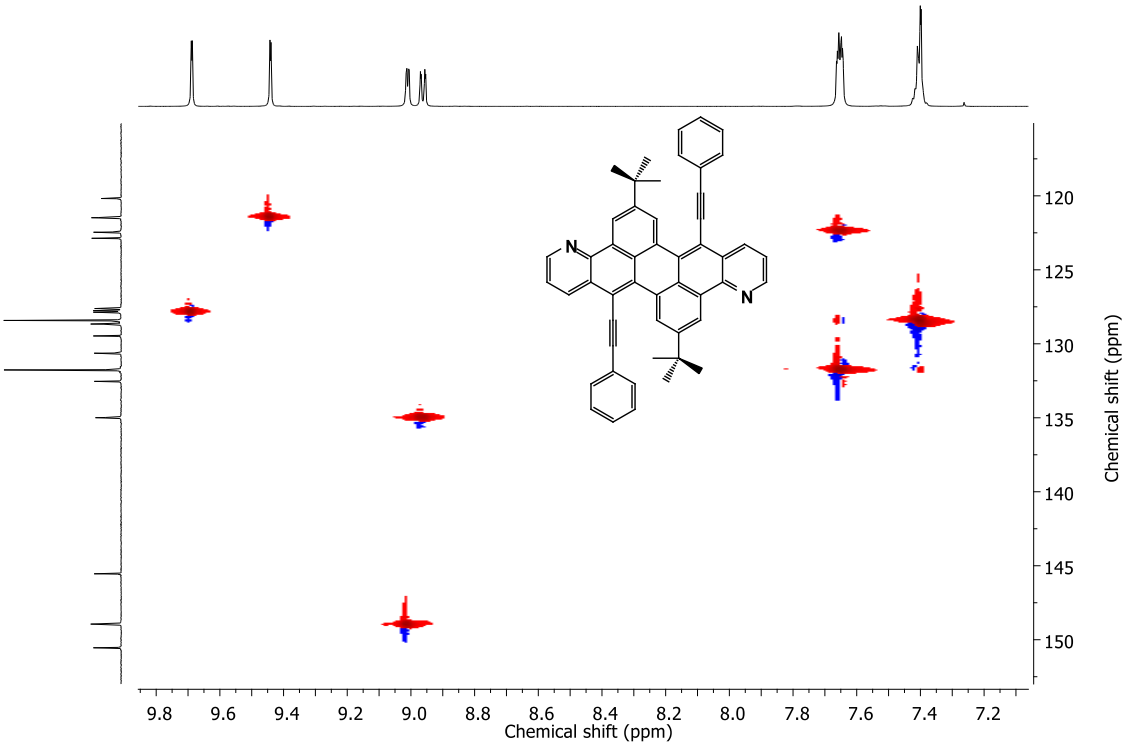

Figure 7.92 ^{1}H-^{13}C HSQC NMR spectrum (600/151 MHz, $Cl_2CDCDCl_2$) of **162**.

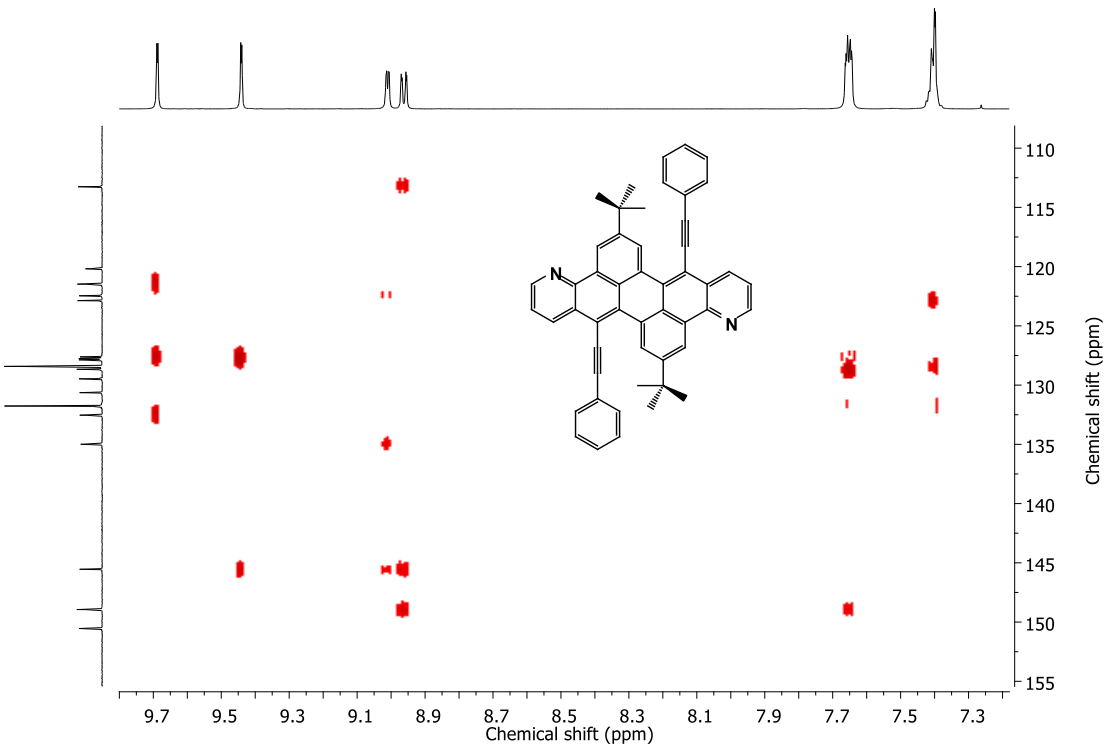

Figure 7.93 ^{1}H-^{13}C HMBC NMR spectrum (600/151 MHz, $Cl_2CDCDCl_2$) of **162**.

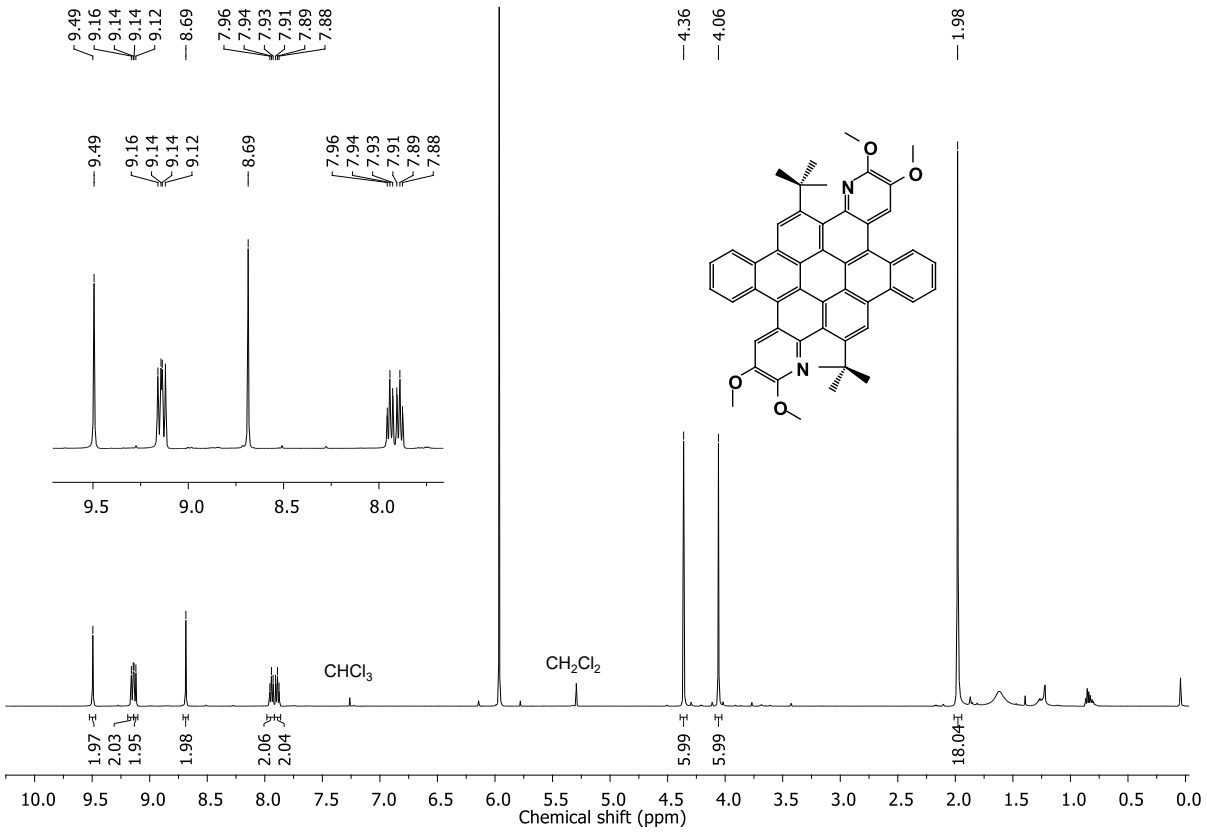

Figure 7.94 ^{1}H NMR spectrum (500 MHz, $Cl_2CDCDCl_2$) of **167**.

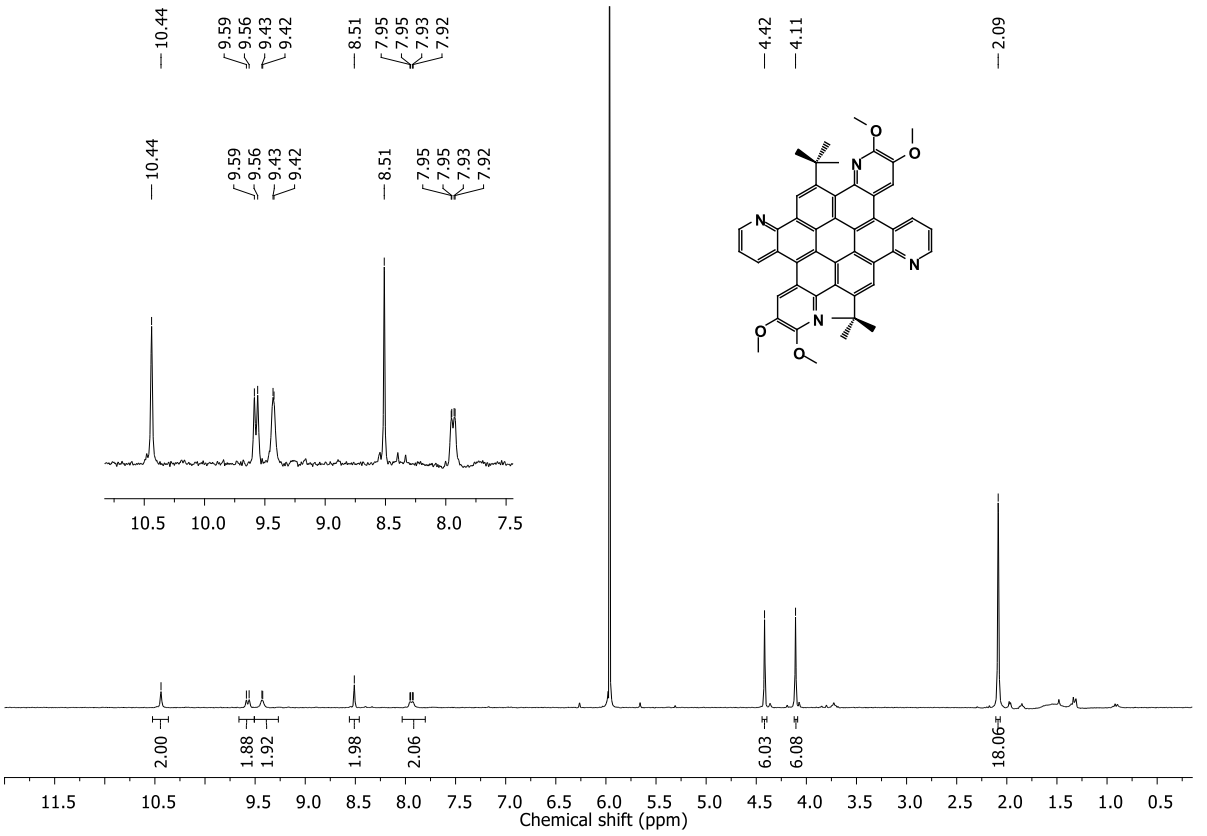

Figure 7.95 ^{1}H NMR spectrum (300 MHz, $Cl_2CDCDCl_2$, 373 K) of **168**.

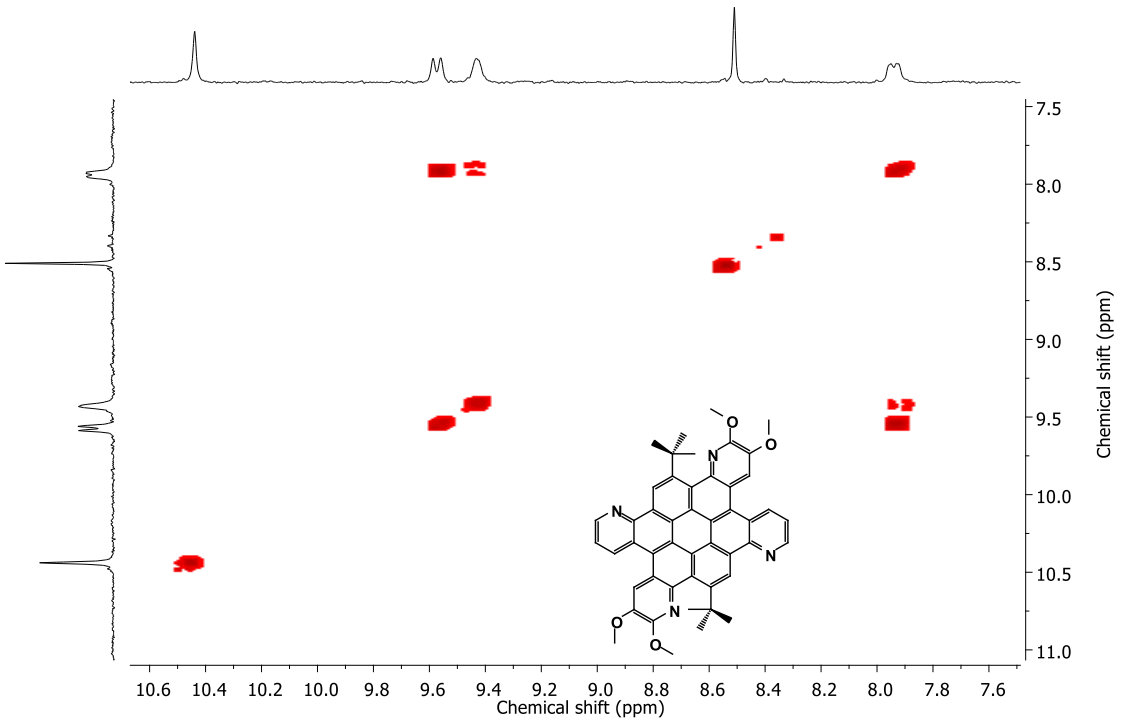

Figure 7.96 ^{1}H-^{1}H COSY NMR spectrum (300/300 MHz, $Cl_2CDCDCl_2$, 373 K) of **168**.

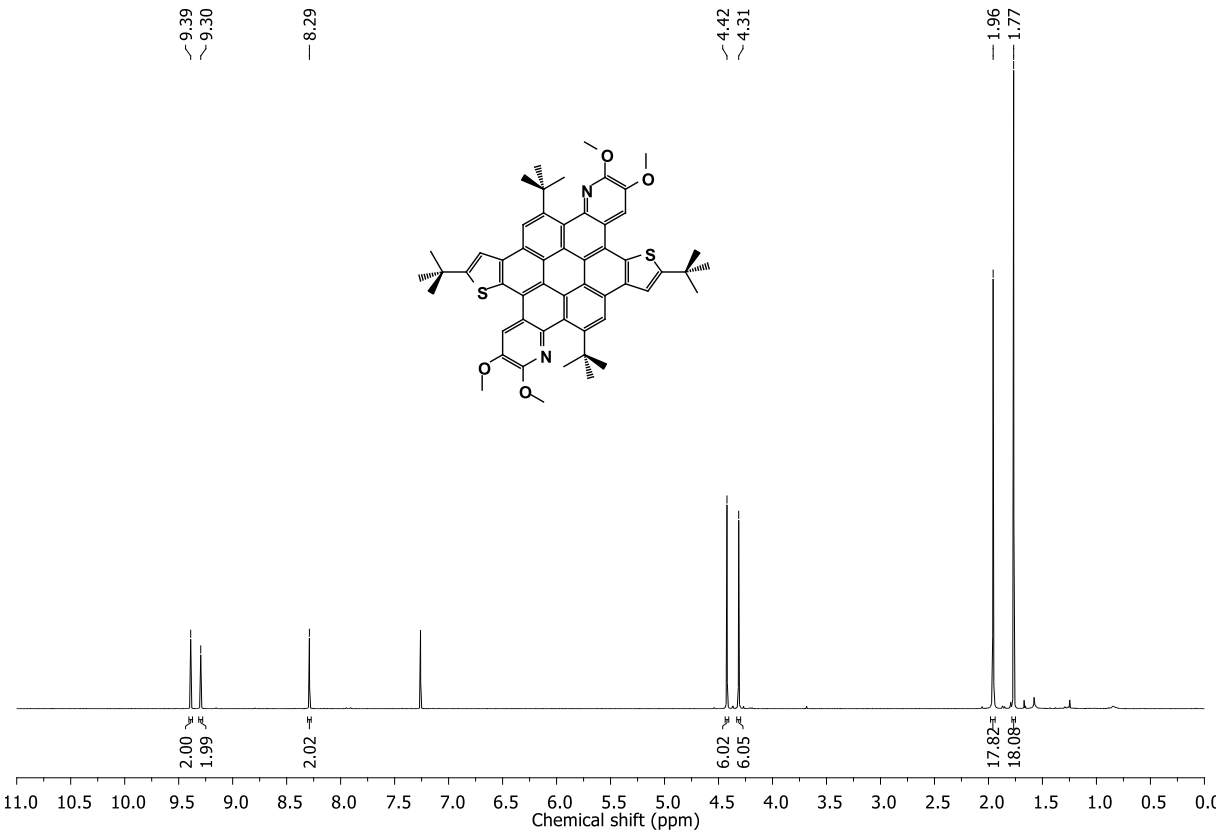

Figure 7.97 ^{1}H NMR spectrum (600 MHz, $CDCl_3$) of **169**.

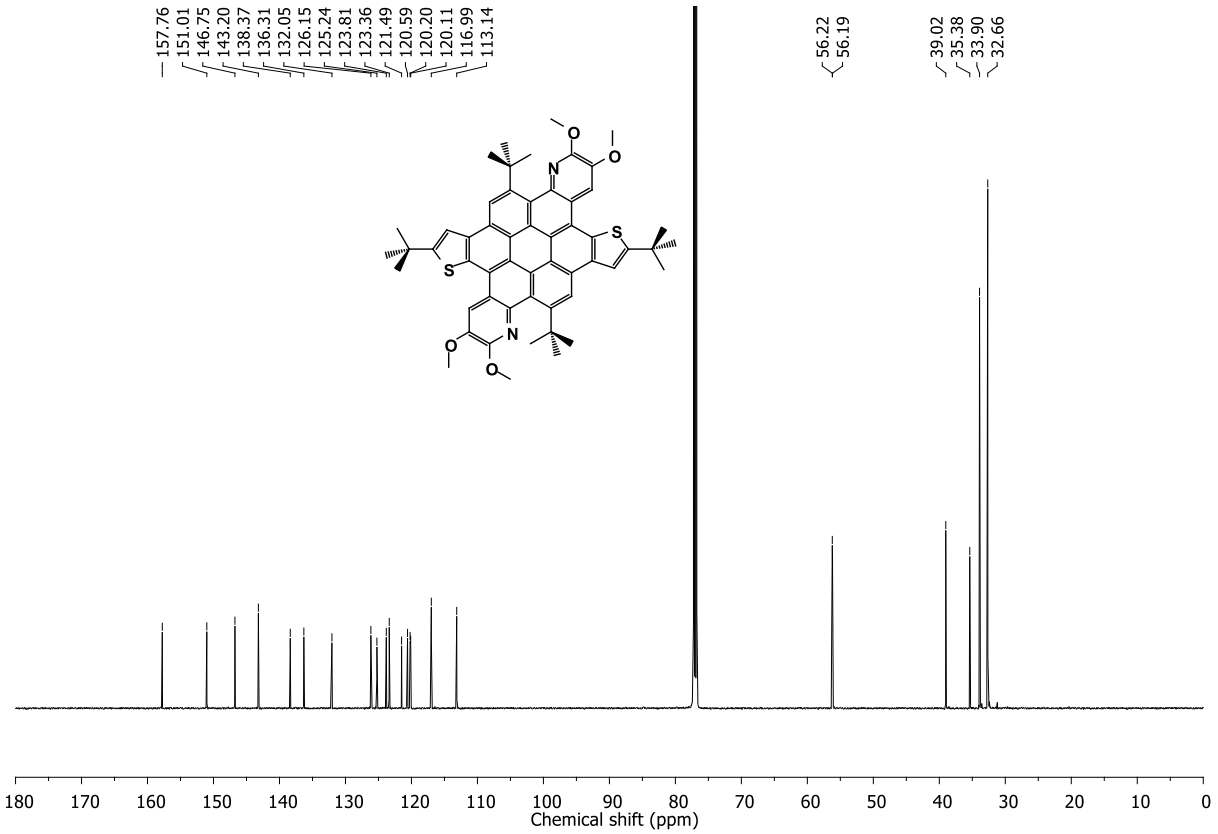

Figure 7.98 ^{13}C NMR spectrum (151 MHz, $CDCl_3$) of **169**.

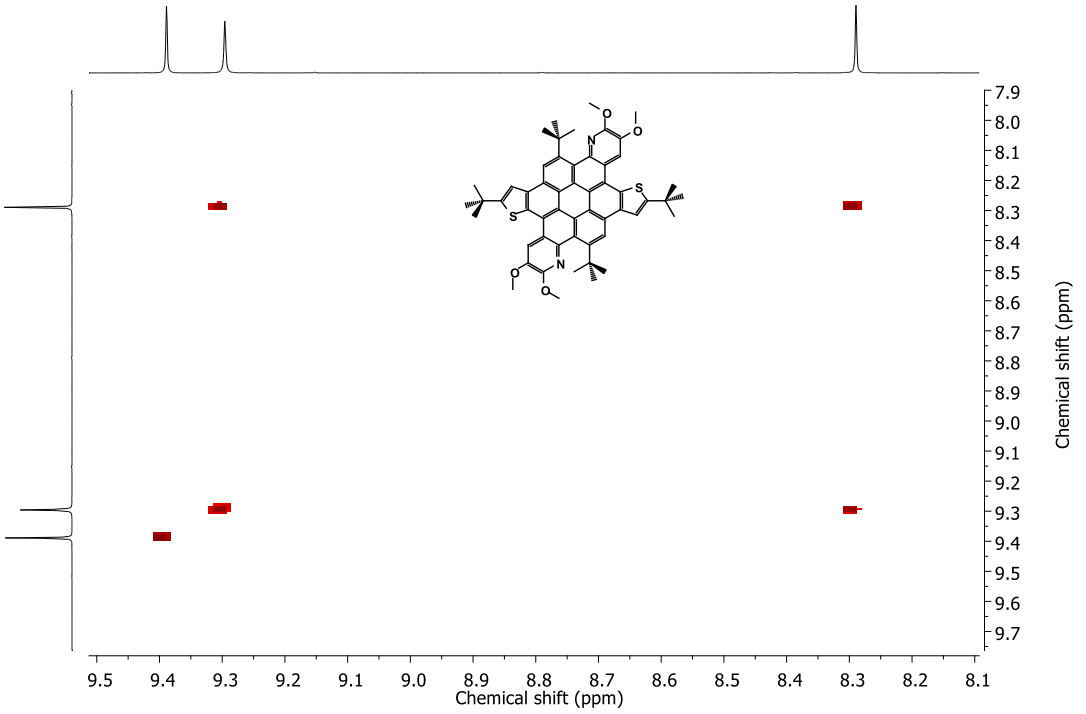

Figure 7.99 ^{1}H-^{1}H COSY NMR spectrum (600/600 MHz, $CDCl_3$) of **169**.

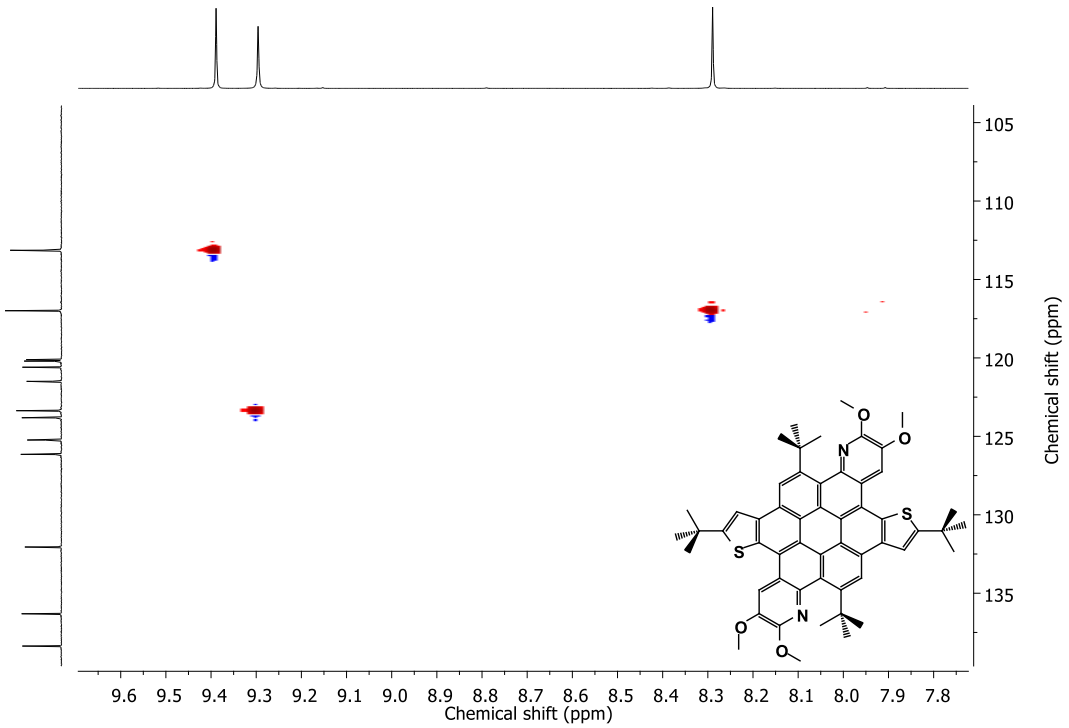

Figure 7.100 ^{1}H-^{13}C HSQC NMR spectrum (600/151 MHz, $CDCl_3$) of **169**.

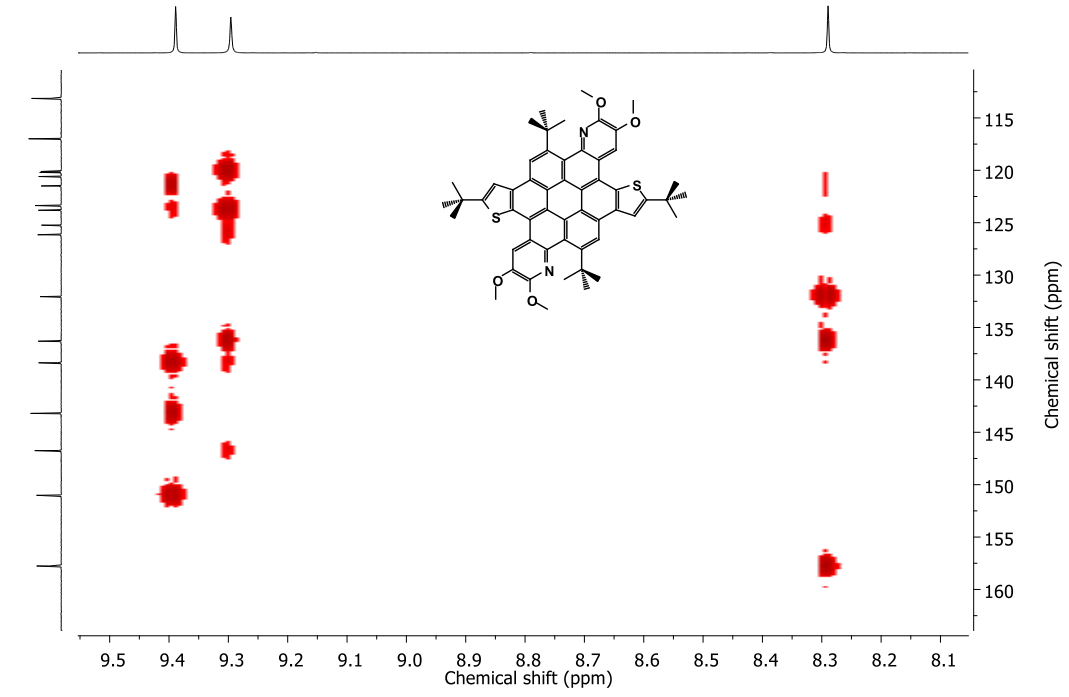

Figure 7.101 ^{1}H-^{13}C HMBC NMR spectrum (600/151 MHz, $CDCl_3$) of **169**.

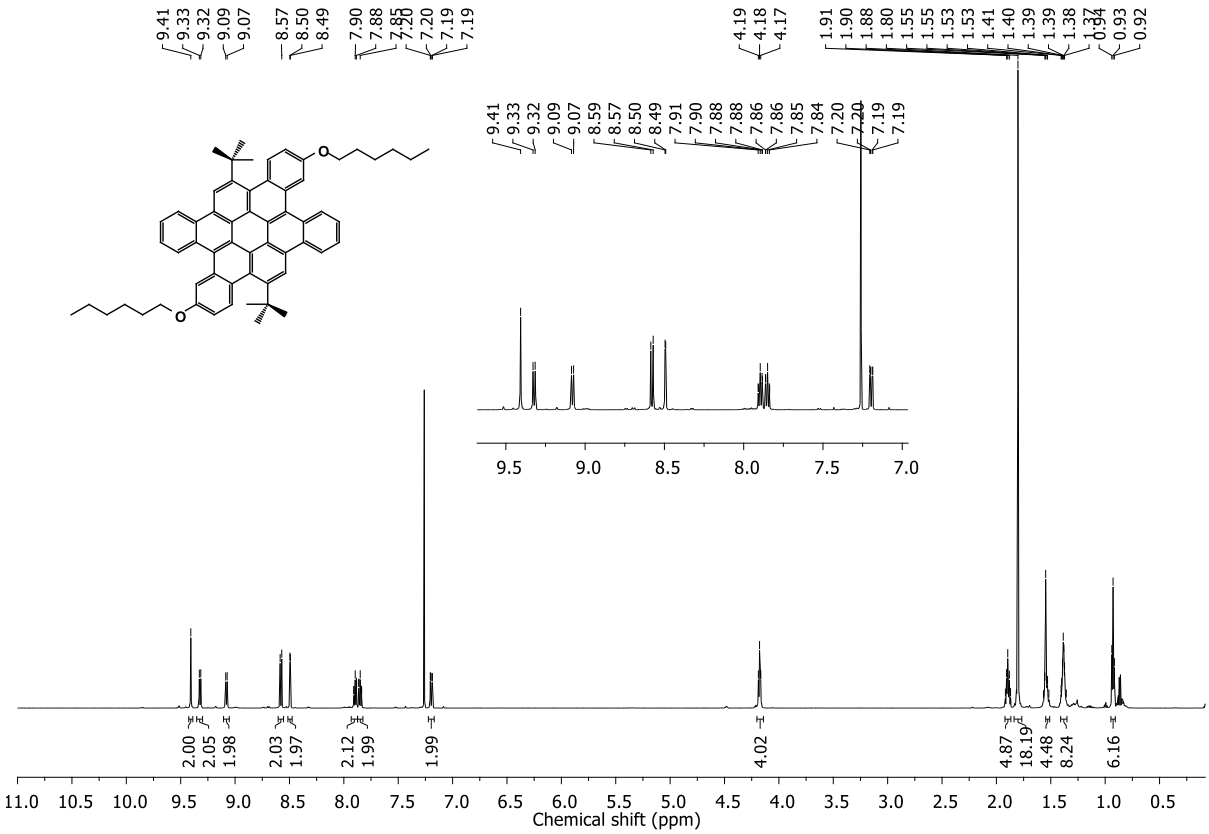

Figure 7.102 ^{1}H NMR spectrum (600 MHz, $CDCl_3$) of **170**.

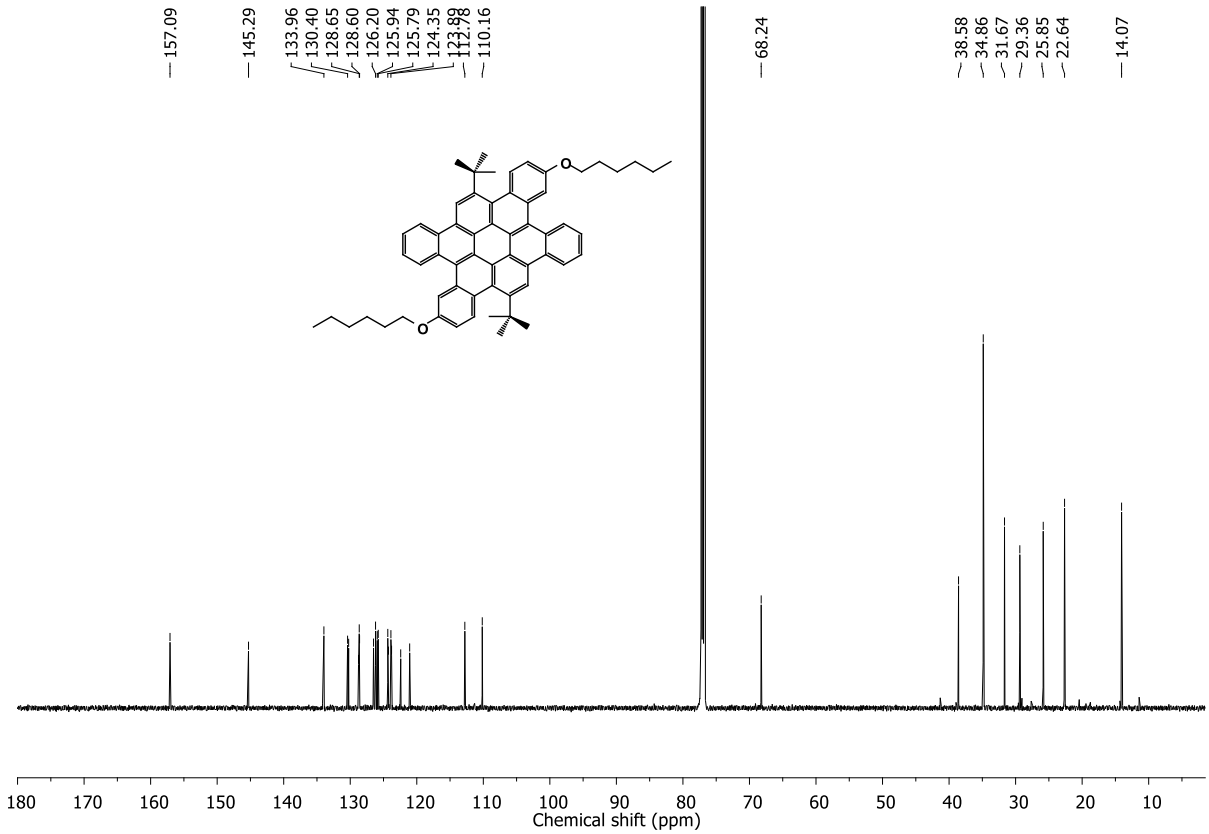

Figure 7.103 ^{13}C NMR spectrum (151 MHz, $CDCl_3$) of **170**.

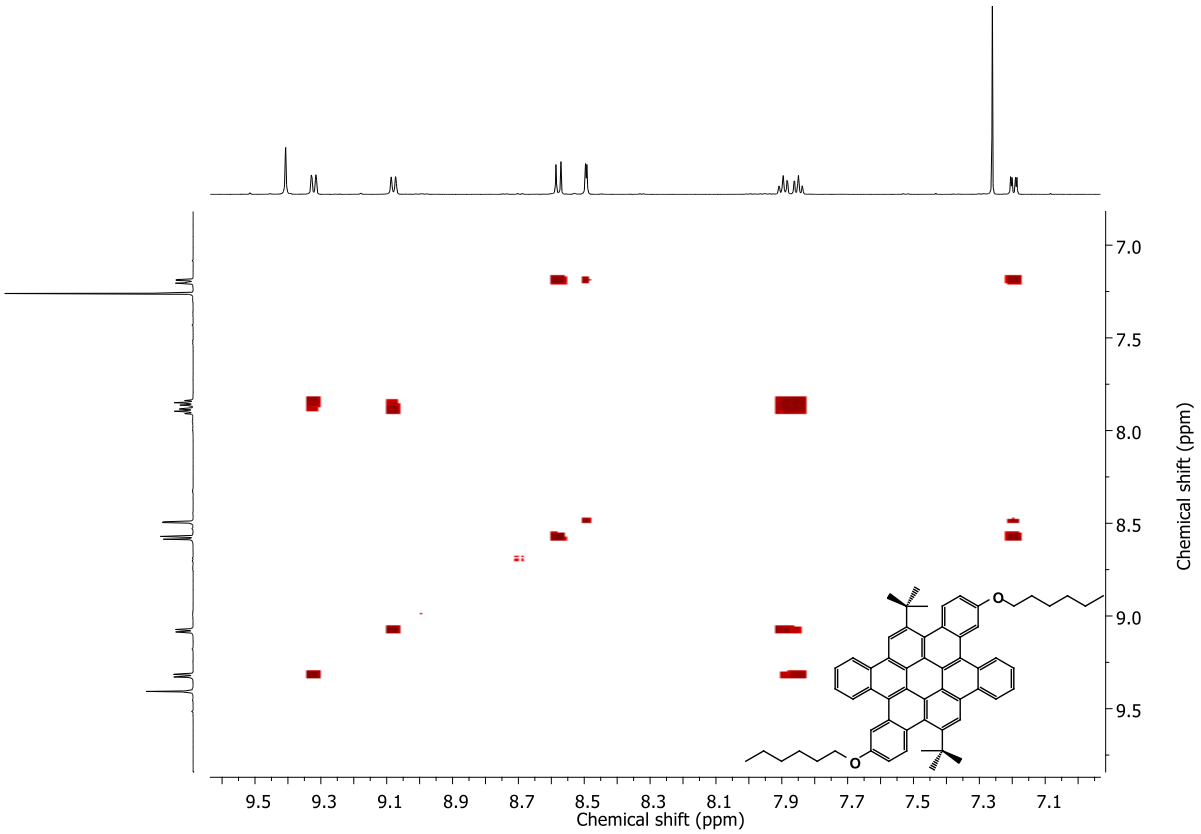

Figure 7.104 ^{1}H-^{1}H COSY NMR spectrum (600/600 MHz, $CDCl_3$) of **170**.

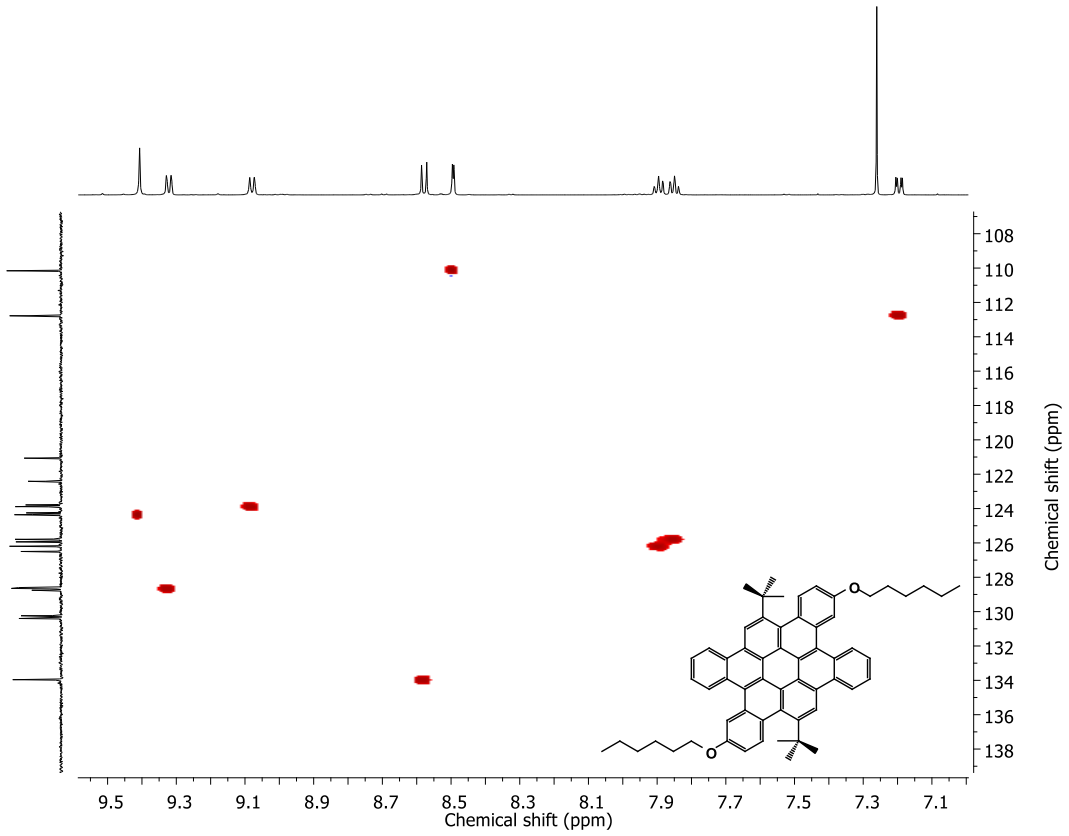

Figure 7.105 ^{1}H-^{13}C HSQC NMR spectrum (600/151 MHz, $CDCl_3$) of **170**.

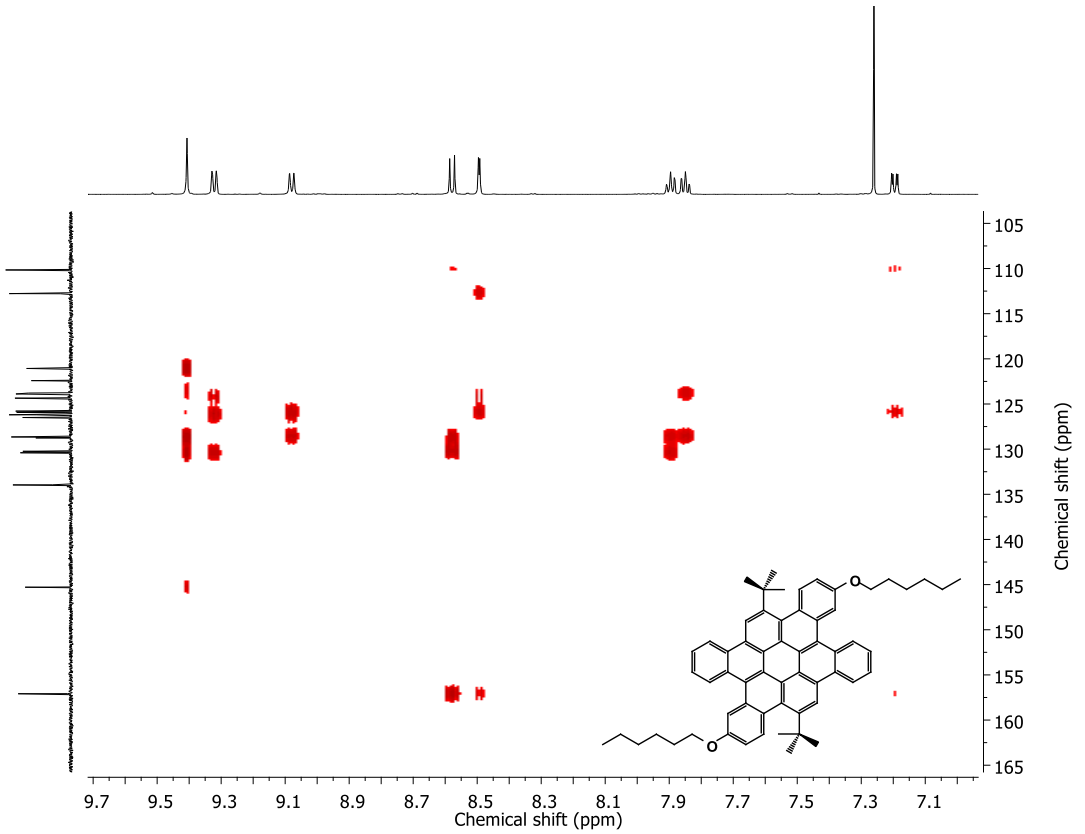

Figure 7.106 ^{1}H-^{13}C HMBC NMR spectrum (600/151 MHz, $CDCl_3$) of **170**.

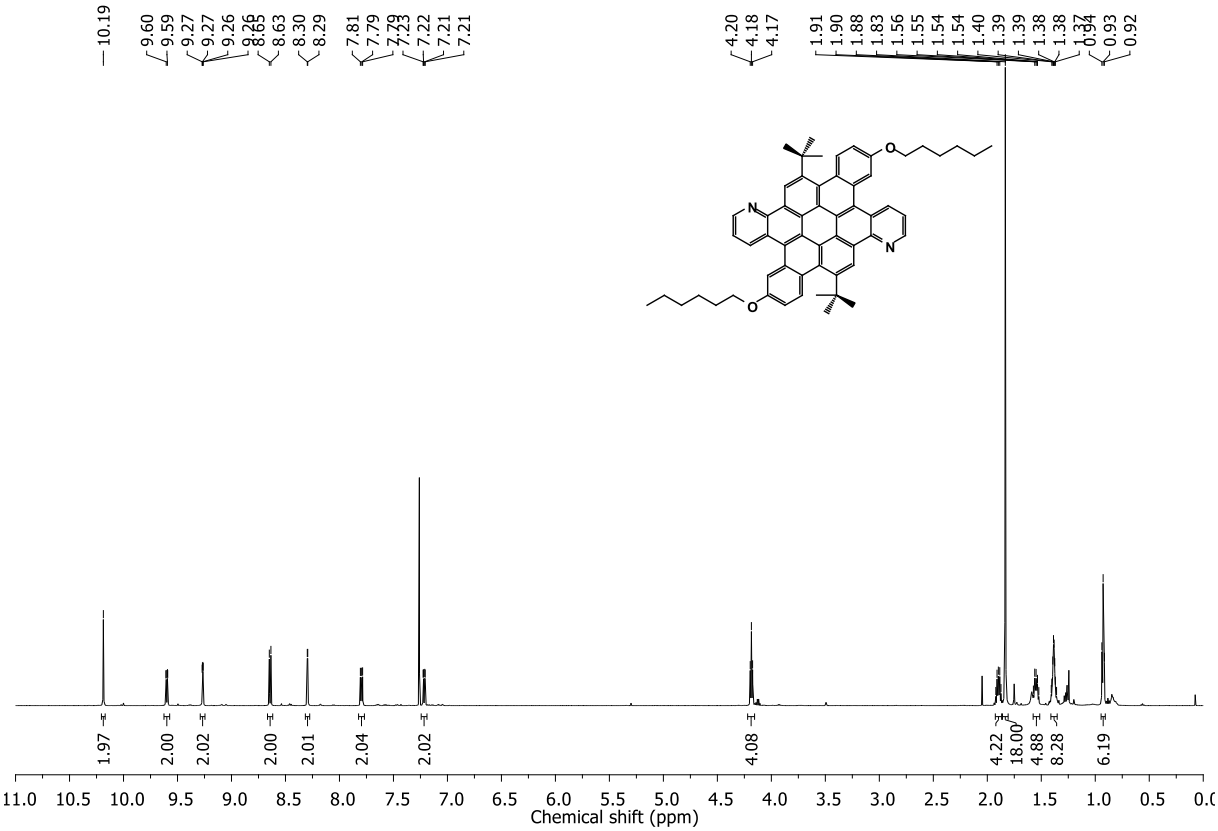

Figure 7.107 ^{1}H NMR spectrum (600 MHz, $CDCl_3$) of **171**.

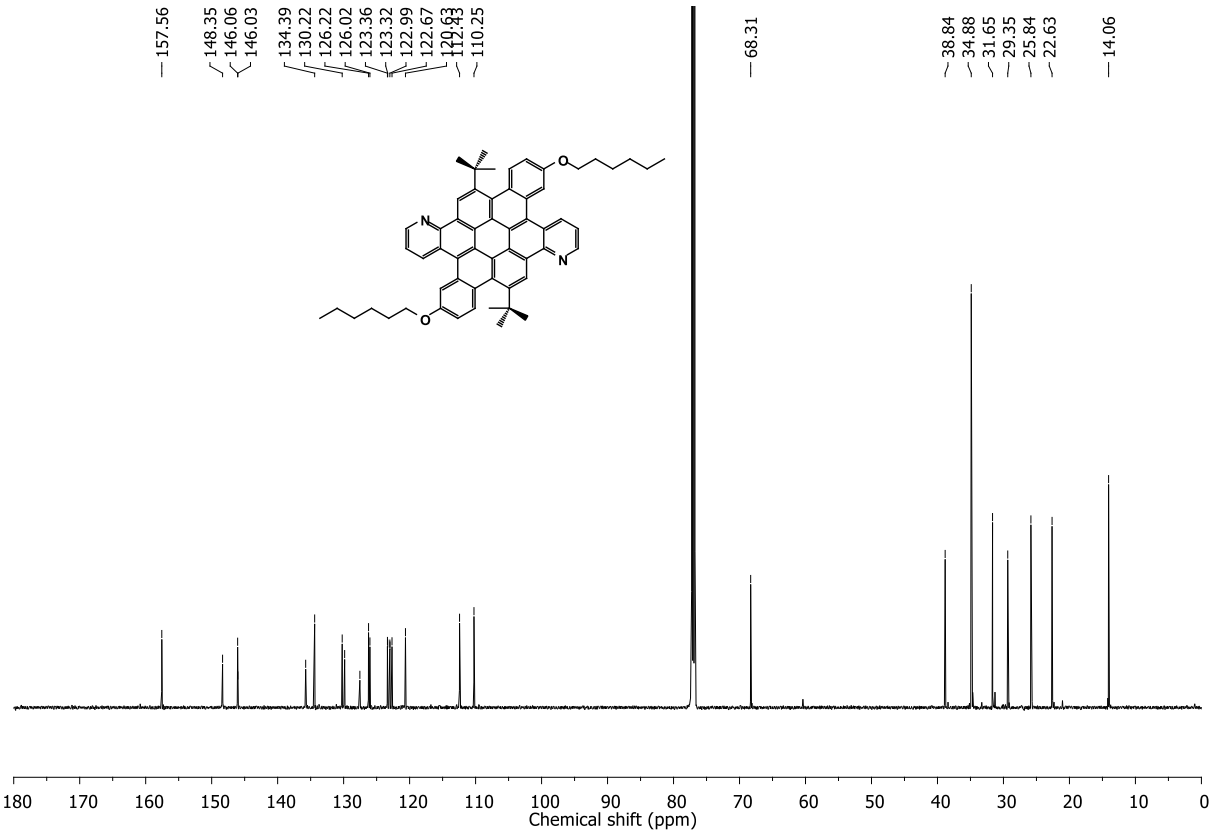

Figure 7.108 ^{13}C NMR spectrum (151 MHz, $CDCl_3$) of **171**.

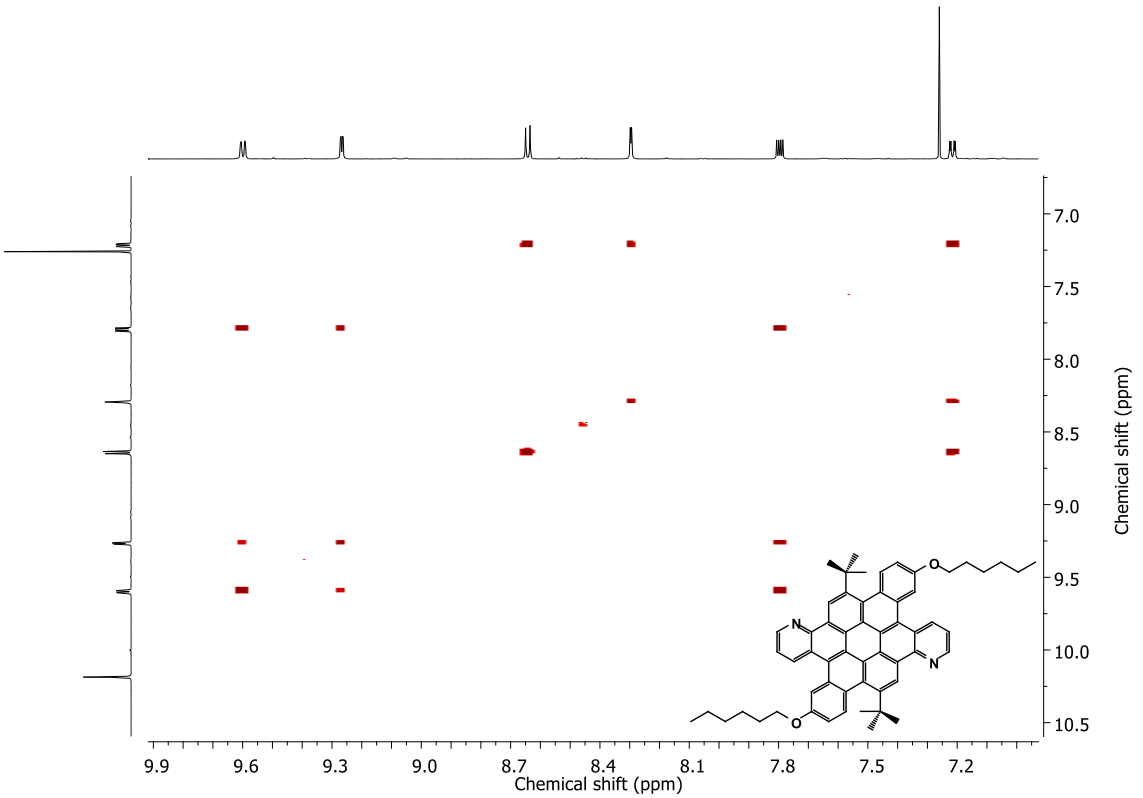

Figure 7.109 ^{1}H-^{1}H COSY NMR spectrum (600/600 MHz, $CDCl_3$) of **171**.

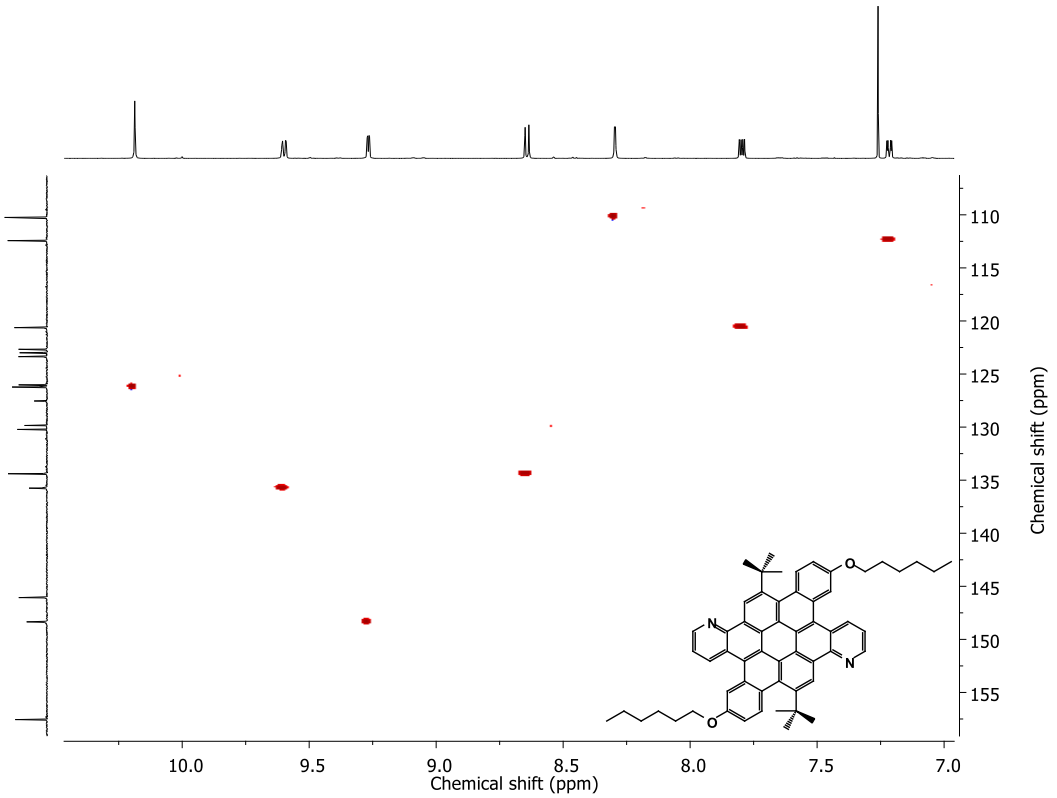

Figure 7.110 ^{1}H-^{13}C HSQC NMR spectrum (600/151 MHz, $CDCl_3$) of **171**.

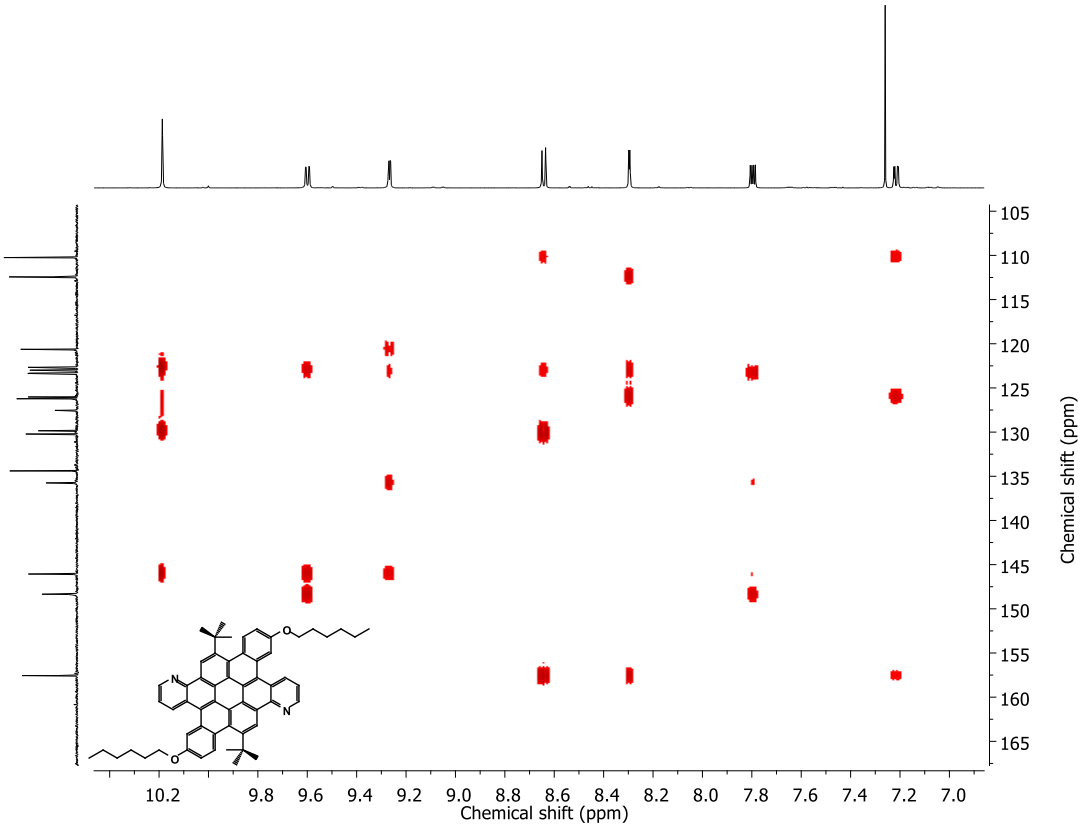

Figure 7.111 ^{1}H-^{13}C HMBC NMR spectrum (600/151 MHz, $CDCl_3$) of **171**.

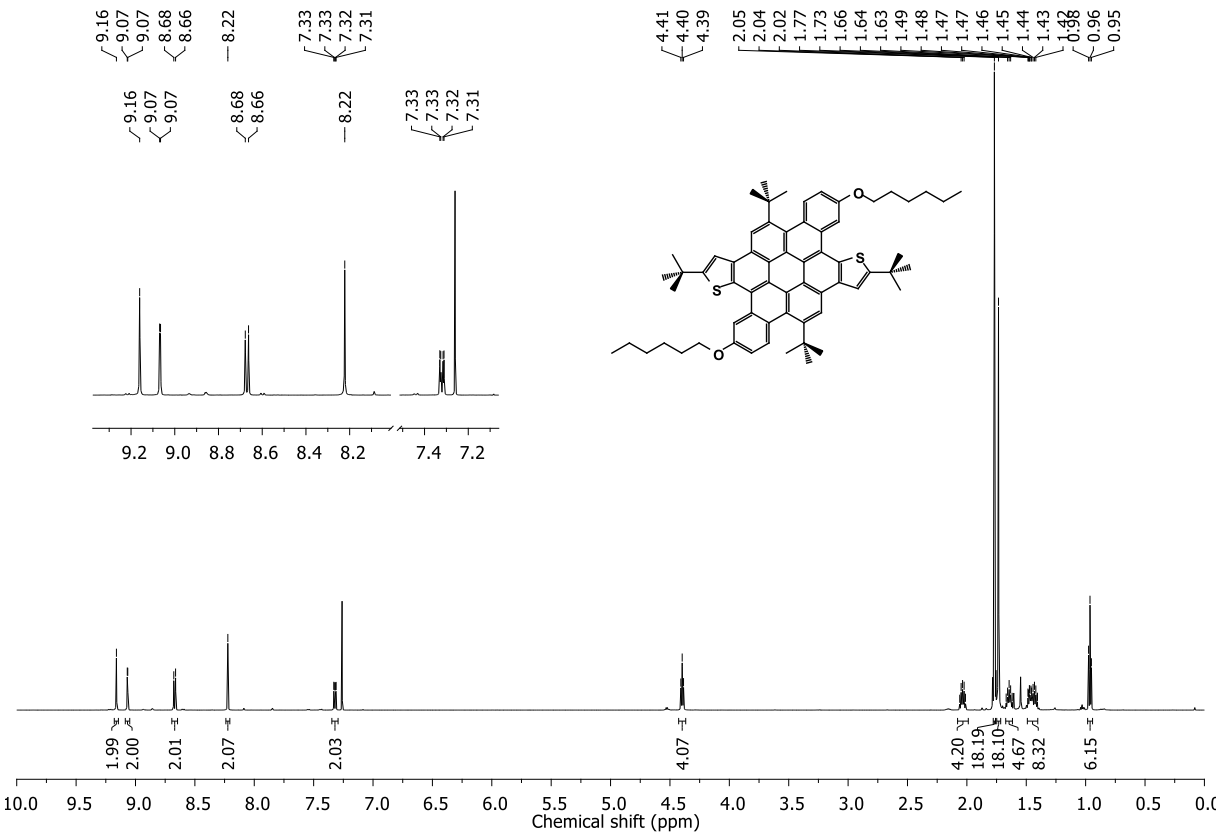

Figure 7.112 ^{1}H NMR spectrum (600 MHz, $CDCl_3$) of **172**.

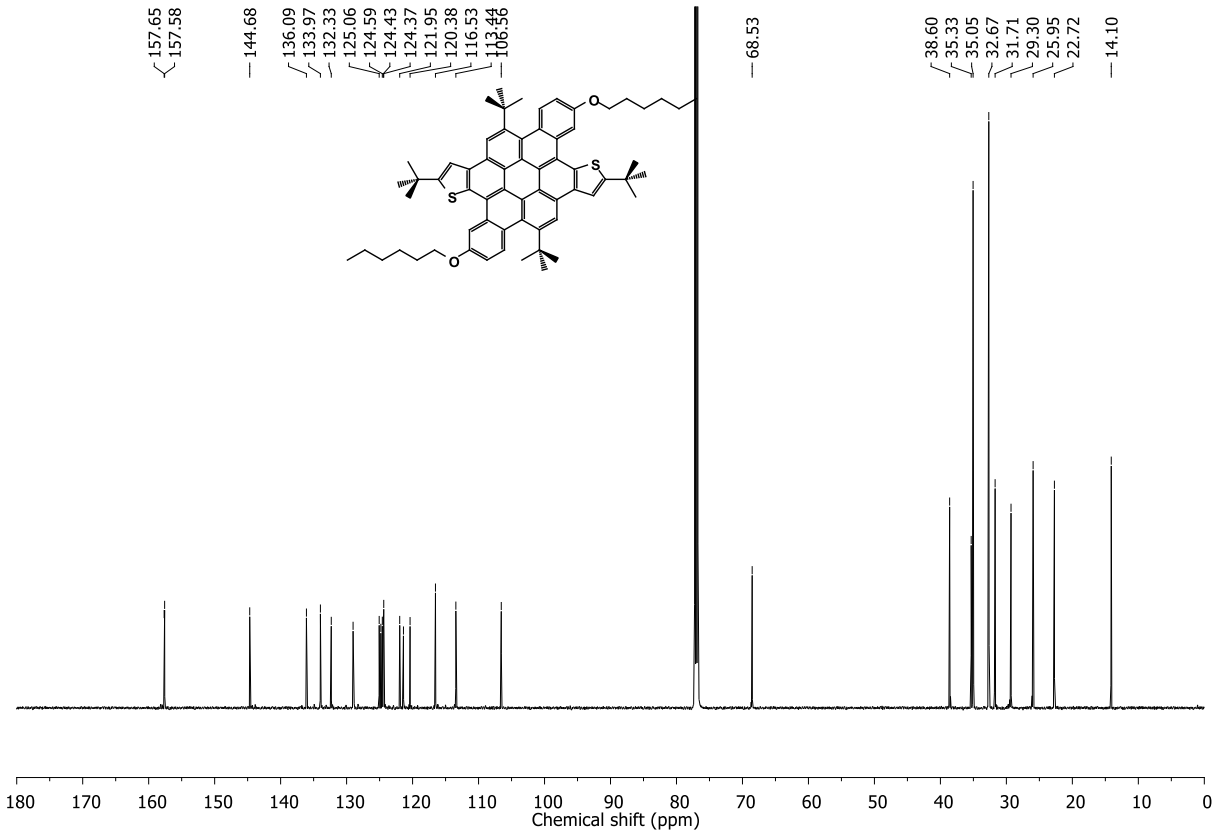

Figure 7.113 ^{13}C NMR spectrum (151 MHz, $CDCl_3$) of **172**.

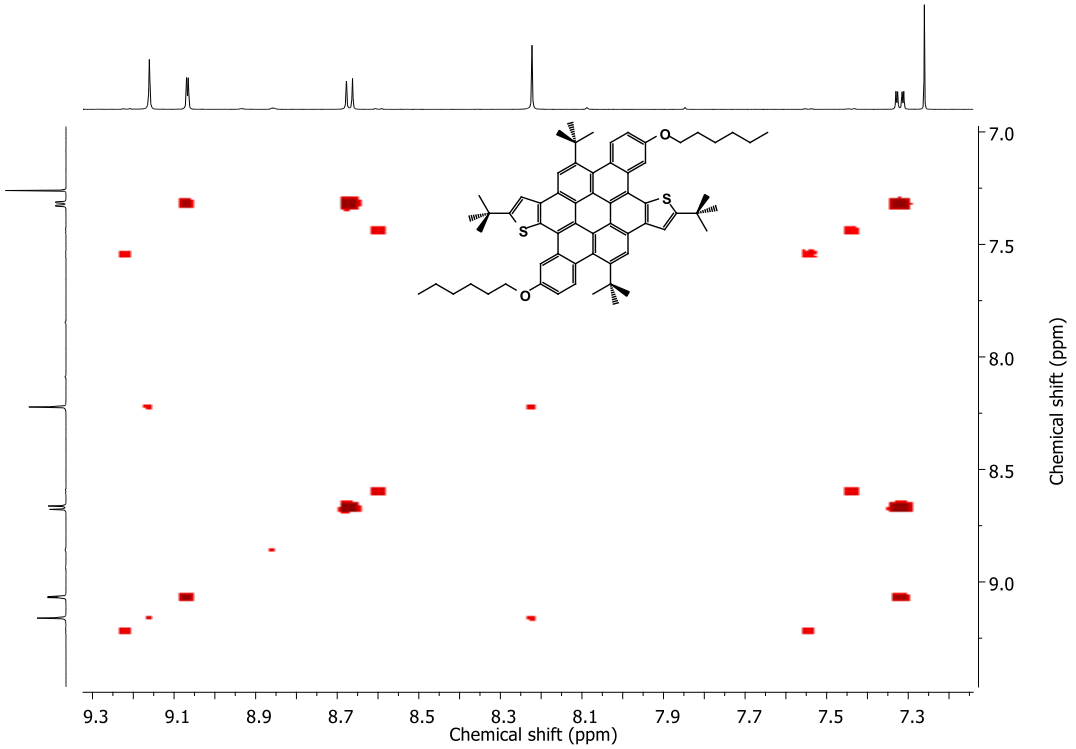

Figure 7.114 ^{1}H-^{1}H COSY NMR spectrum (600/600 MHz, $CDCl_3$) of **172**.

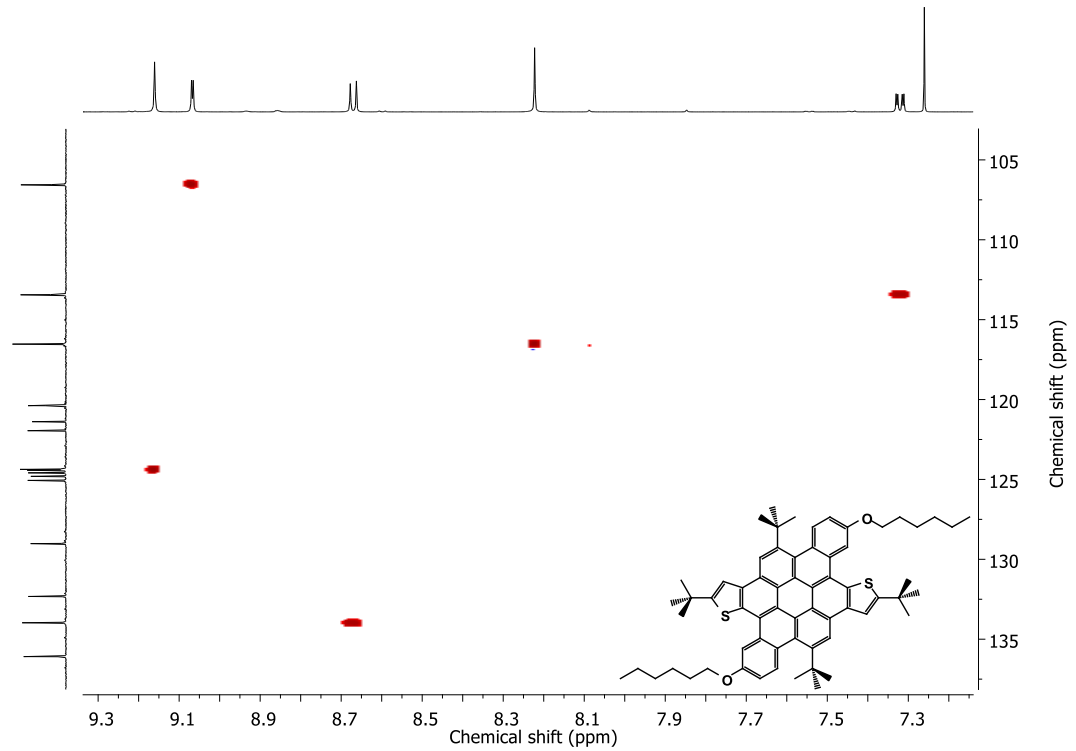

Figure 7.115 ^{1}H-^{13}C HSQC NMR spectrum (600/151 MHz, $CDCl_3$) of **172**.

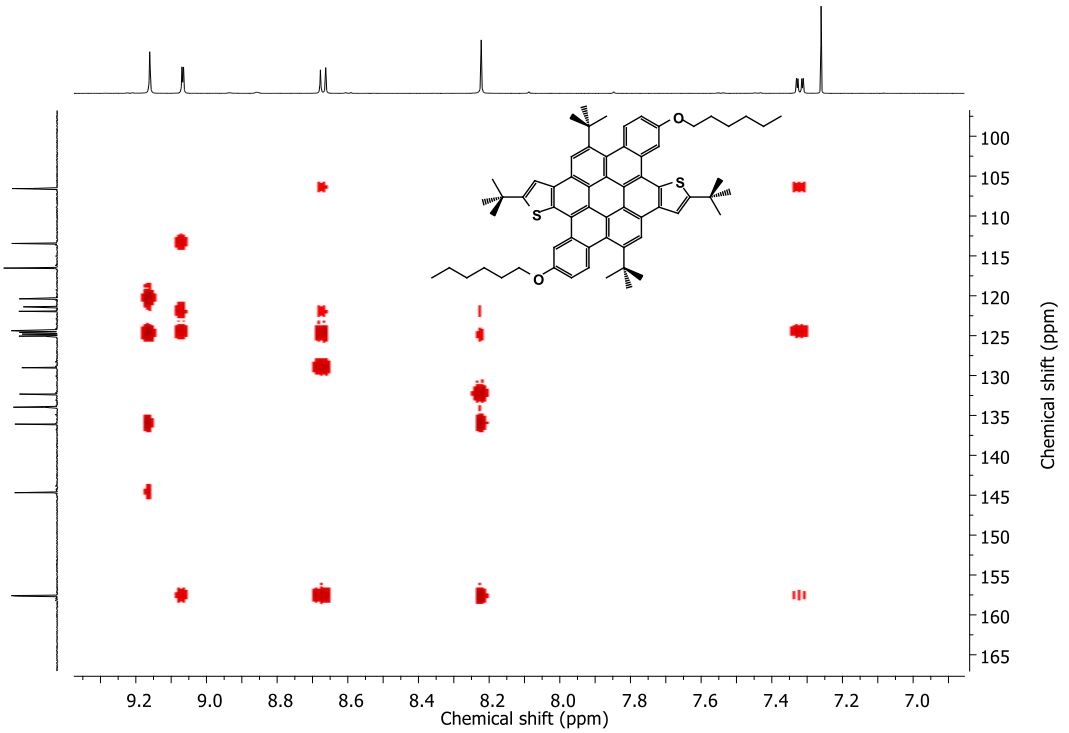

Figure 7.116 ^{1}H-^{13}C HMBC NMR spectrum (600/151 MHz, $CDCl_3$) of **172**.

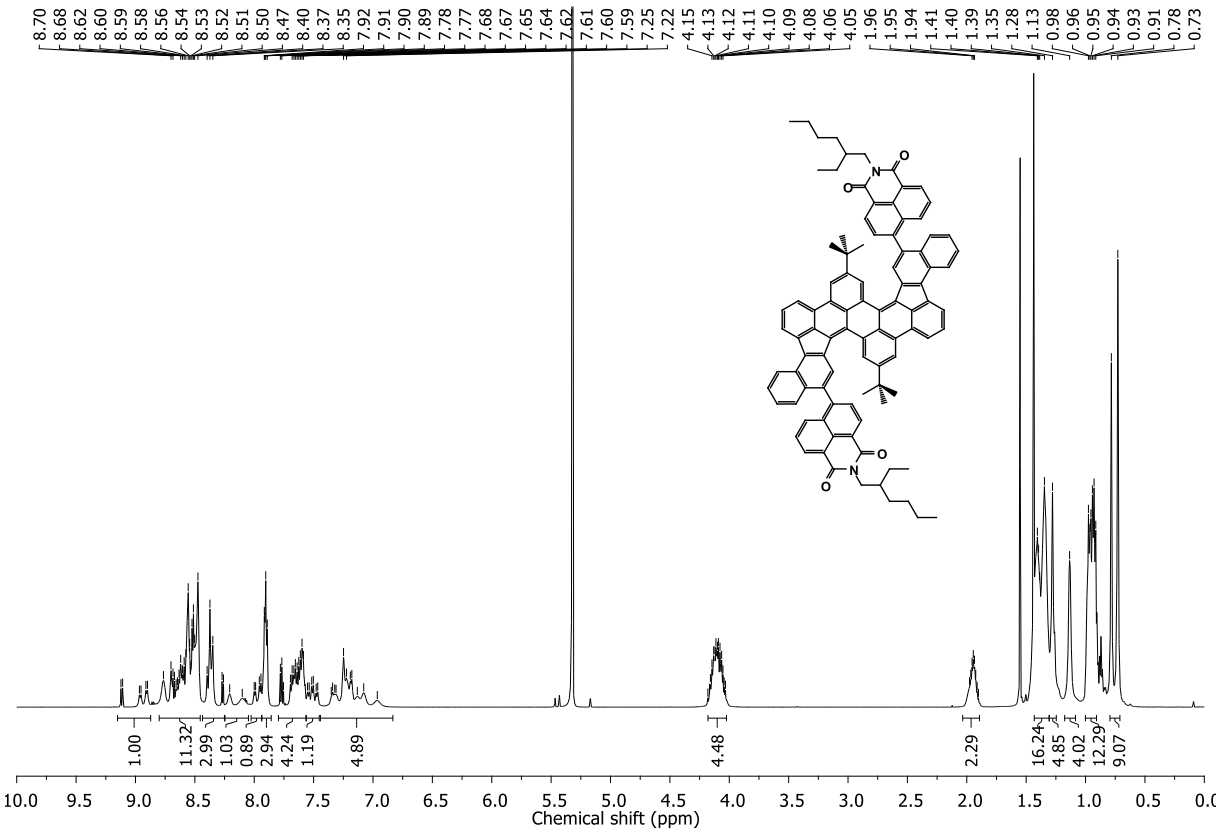

Figure 7.117 ^{1}H NMR spectrum (600 MHz, CD_2Cl_2) of **190**.

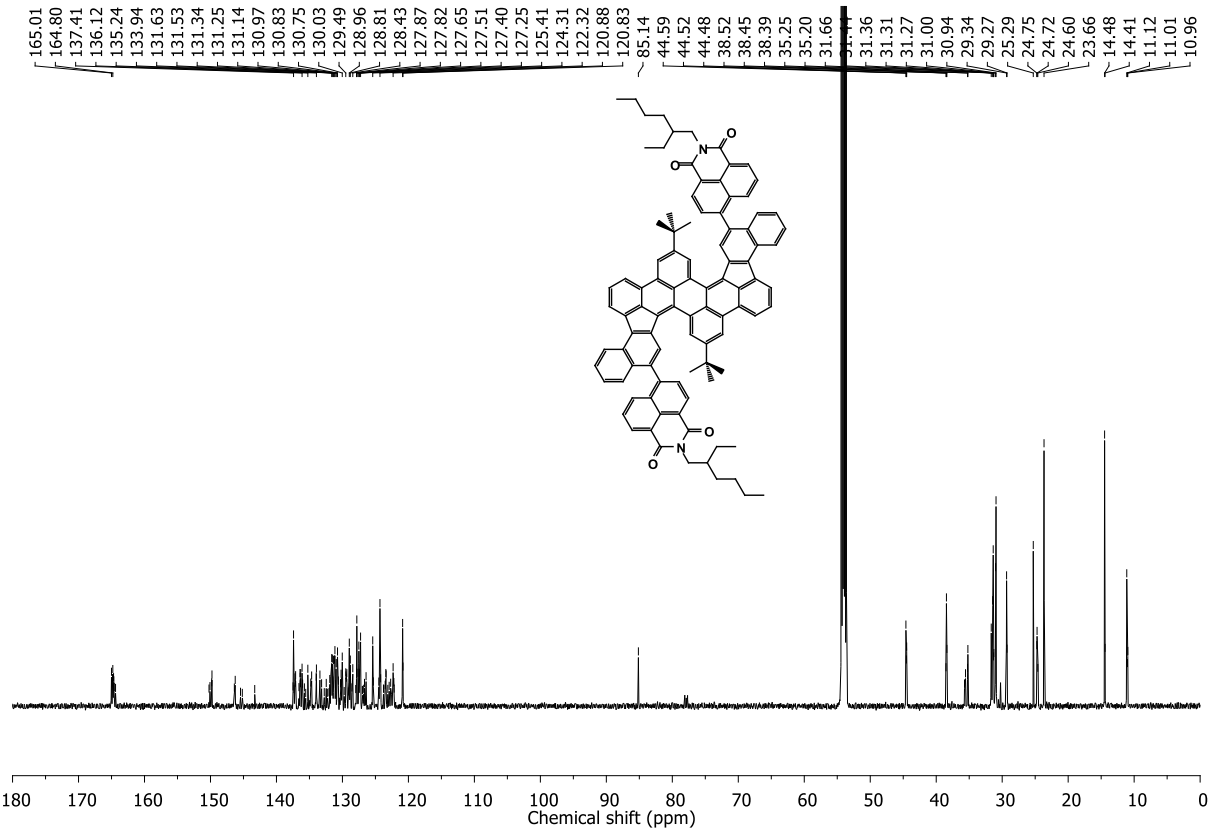

Figure 7.118 ^{13}C NMR spectrum (151 MHz, CD_2Cl_2) of **190**.

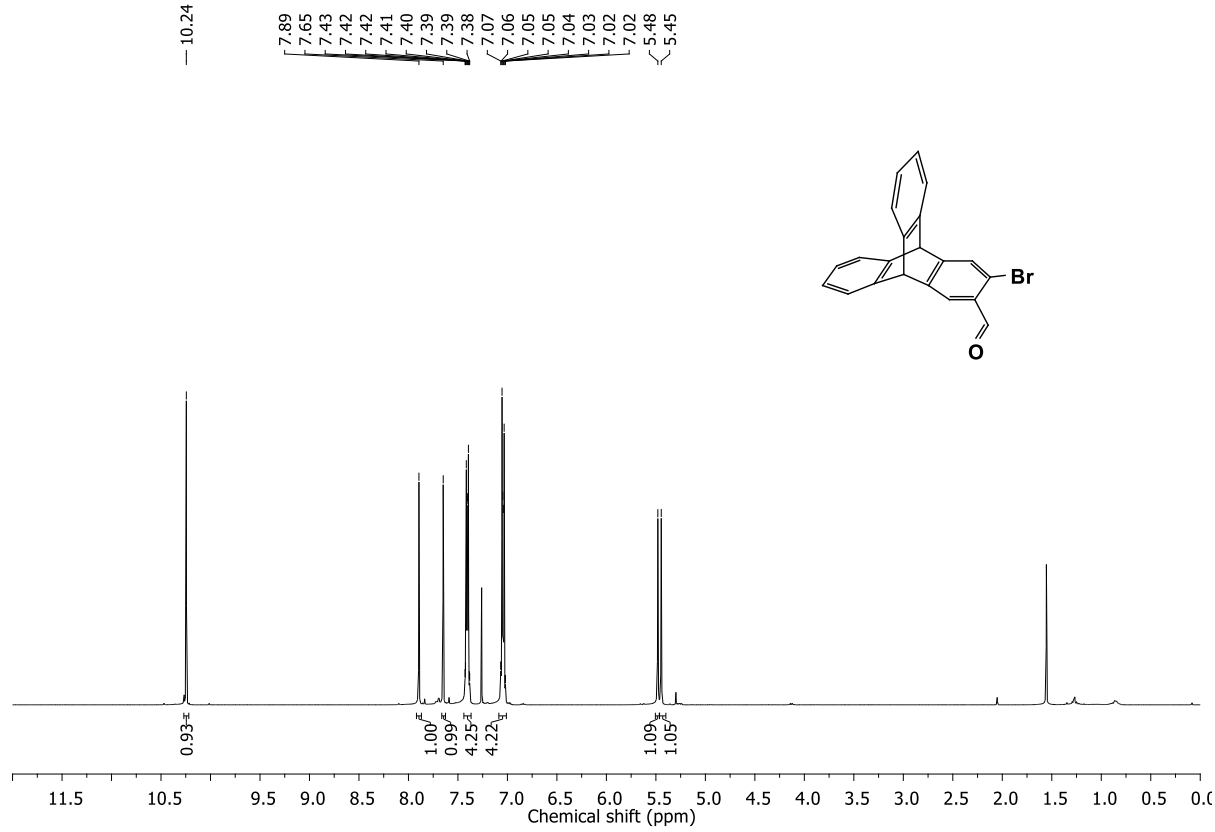

Figure 7.119 ^{1}H NMR spectrum (400 MHz, $CDCl_3$) of **233**.

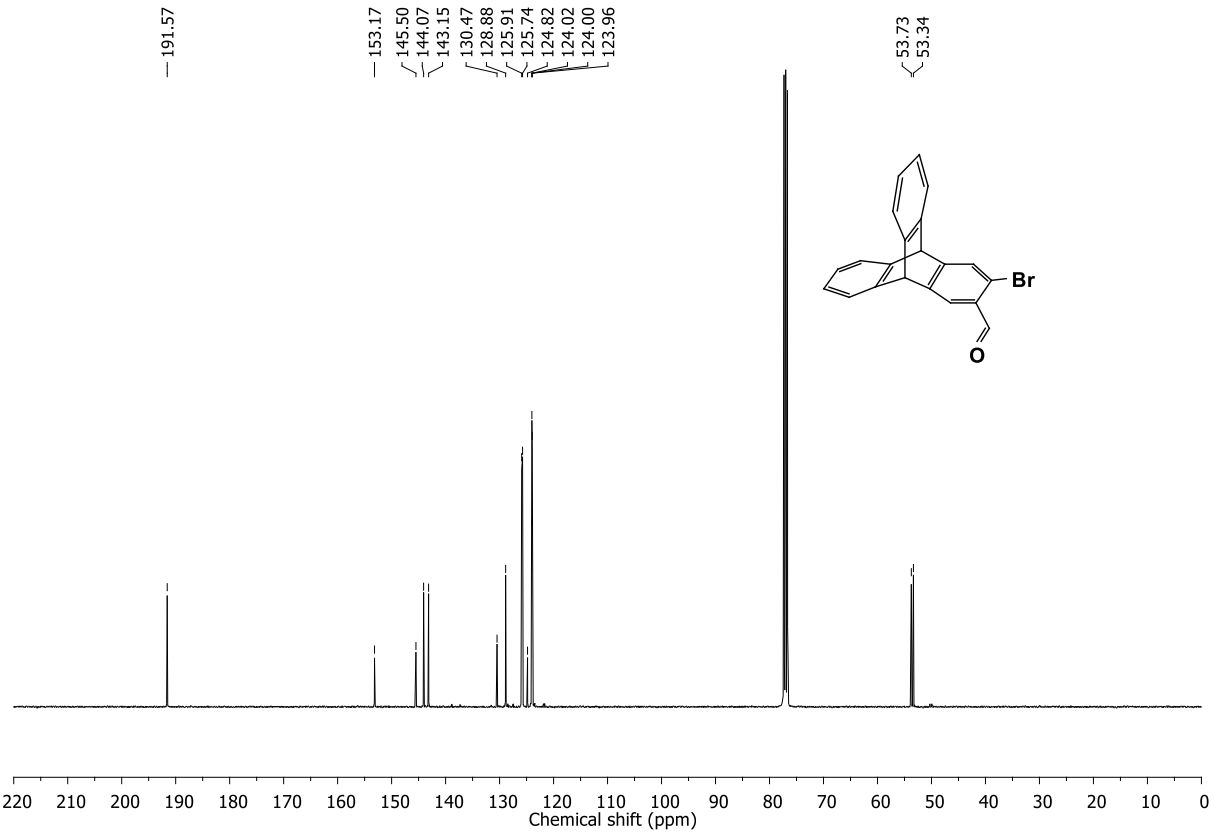

Figure 7.120 ^{13}C NMR spectrum (101 MHz, $CDCl_3$) of **233**.

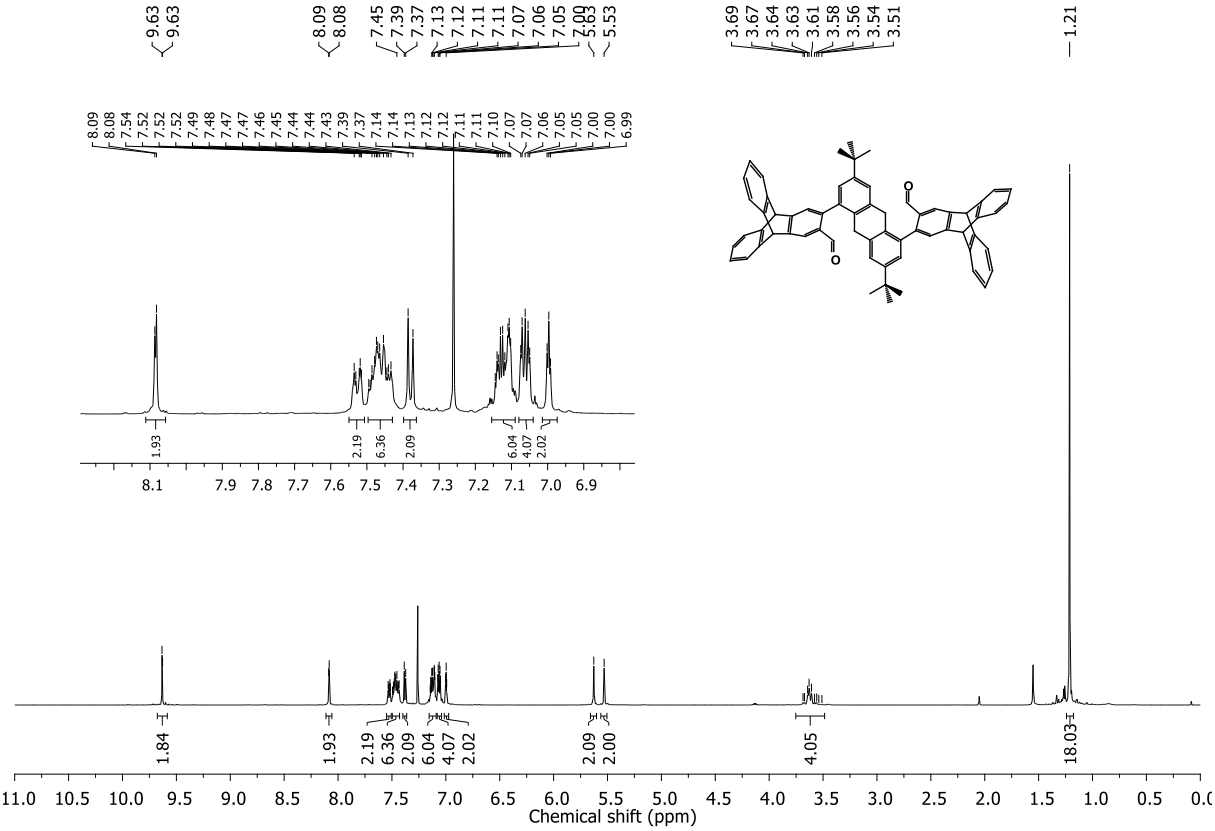

Figure 7.121 ^{1}H NMR spectrum (400 MHz, $CDCl_3$) of **234**.

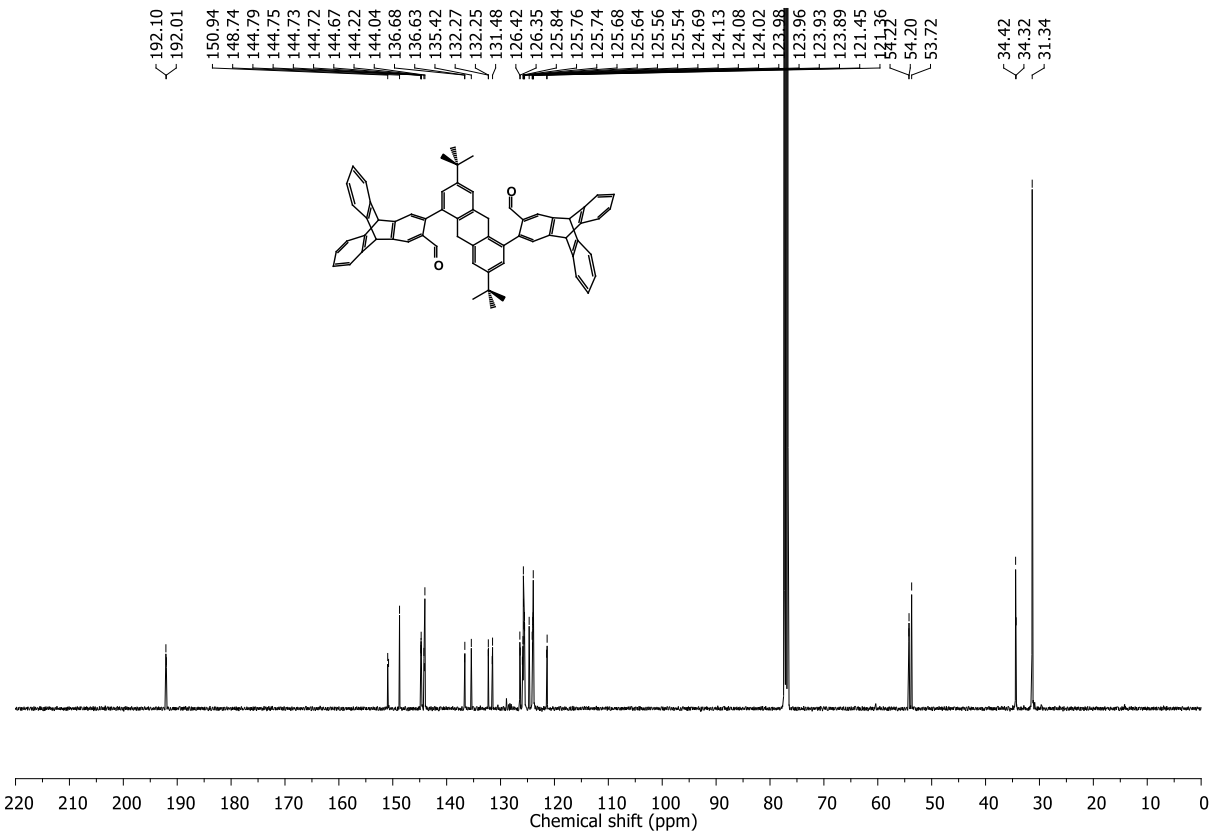

Figure 7.122 ^{13}C NMR spectrum (101 MHz, $CDCl_3$) of **234**.

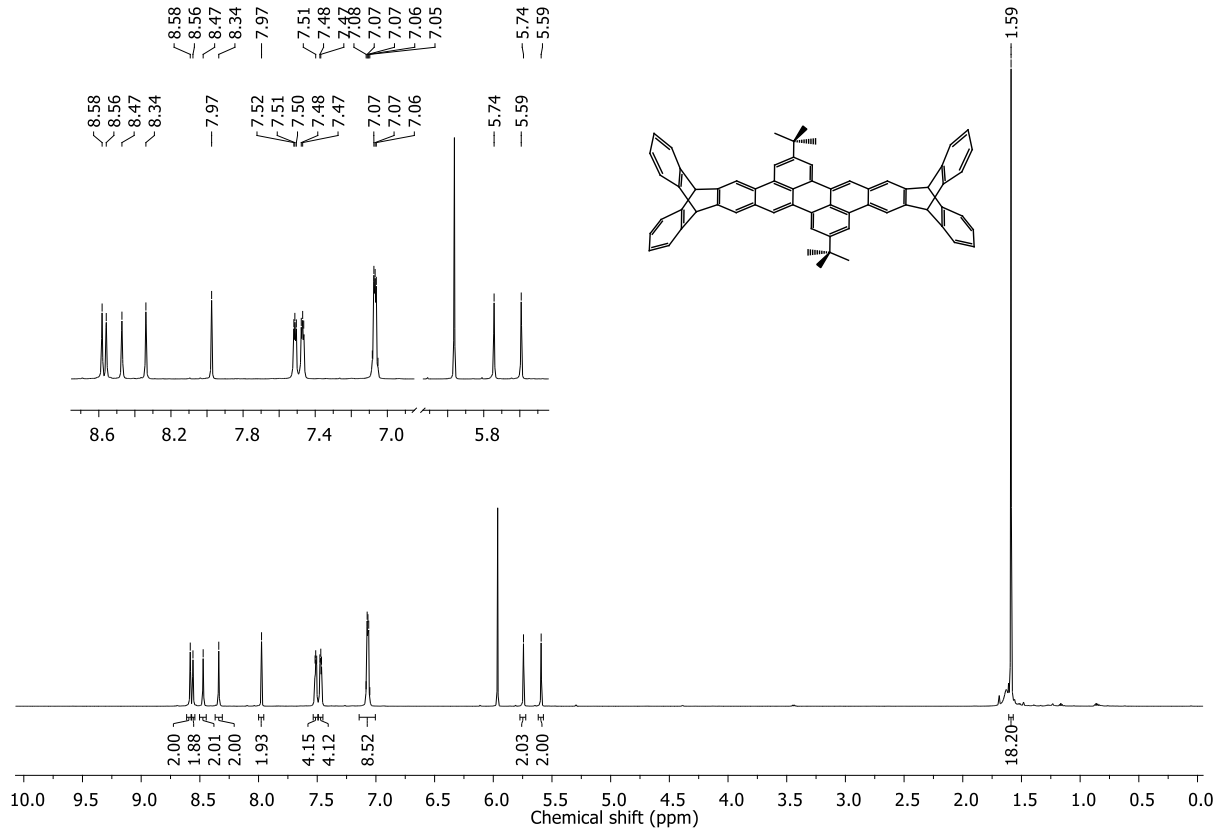

Figure 7.123 ^{1}H NMR spectrum (600 MHz, $Cl_2CDCDCl_2$) of PO-5 (**228**).

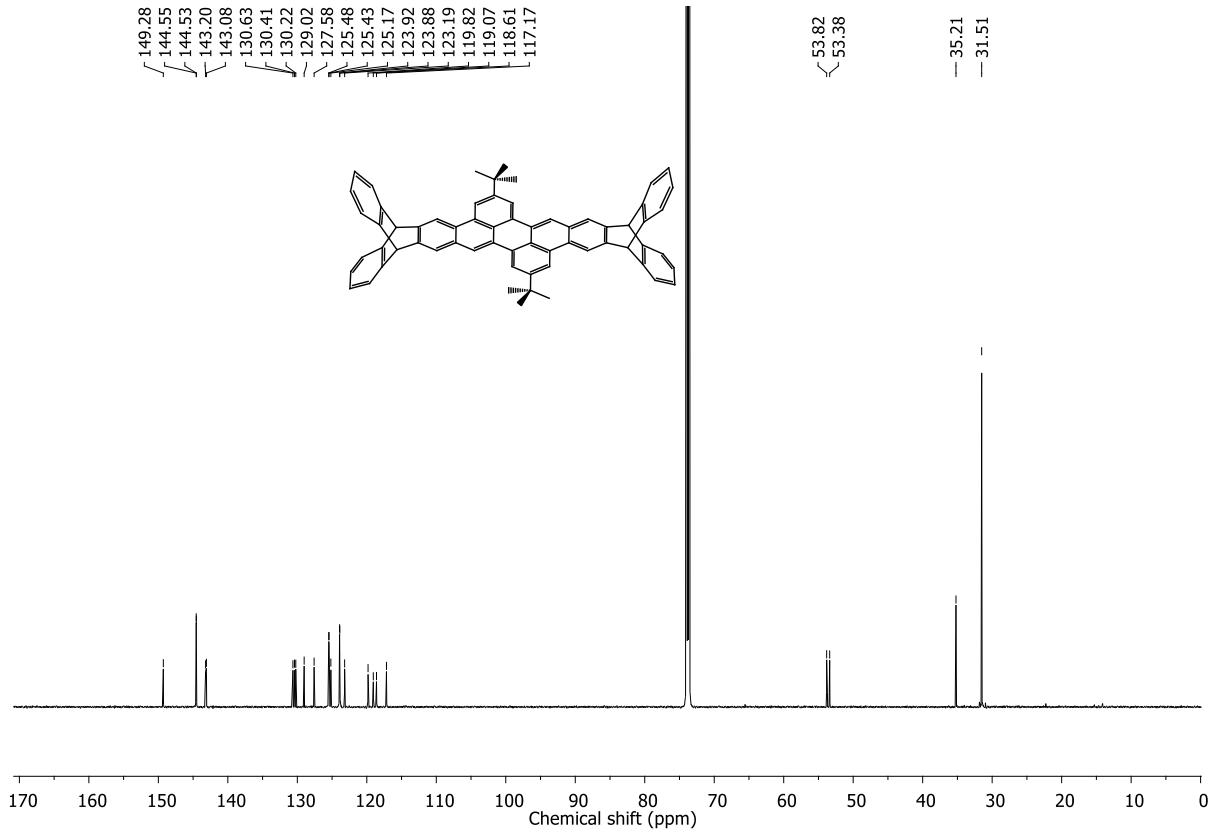

Figure 7.124 ^{13}C NMR spectrum (151 MHz, $Cl_2CDCDCl_2$) of PO-5 (**228**).

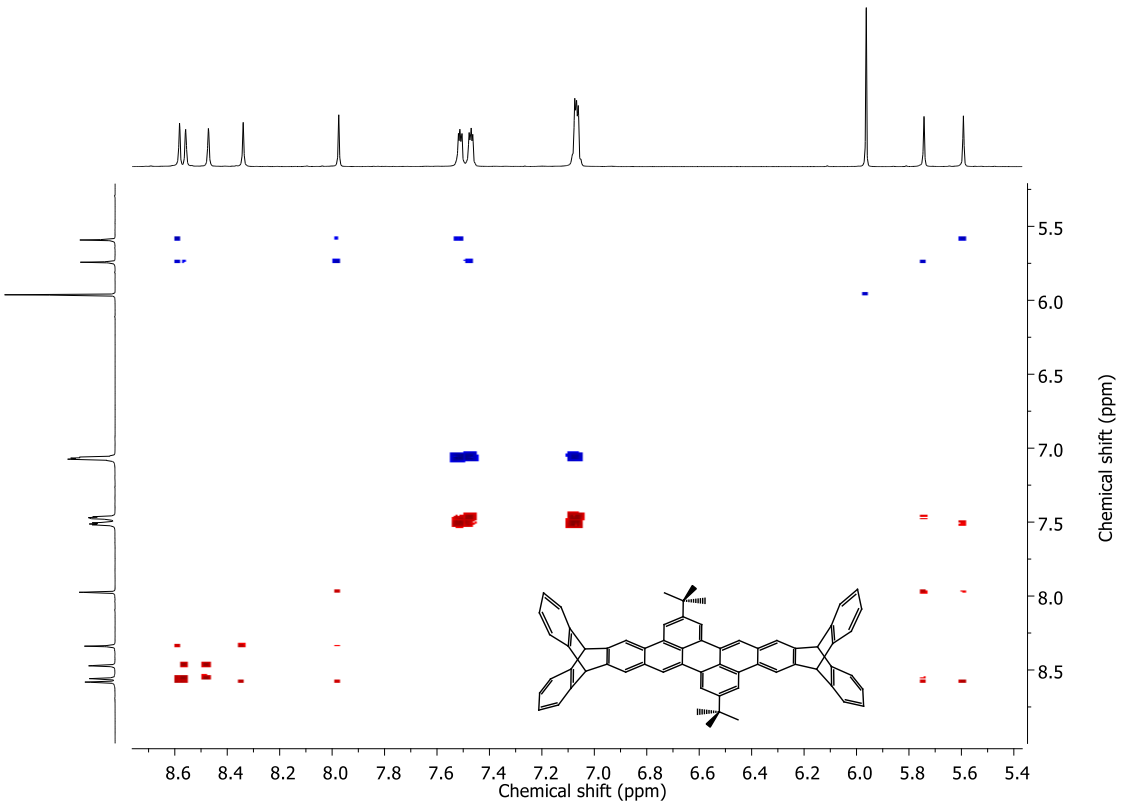

Figure 7.125 ^{1}H-^{1}H COSY NMR spectrum (600/600 MHz, $Cl_2CDCDCl_2$) of PO-5 (**228**).

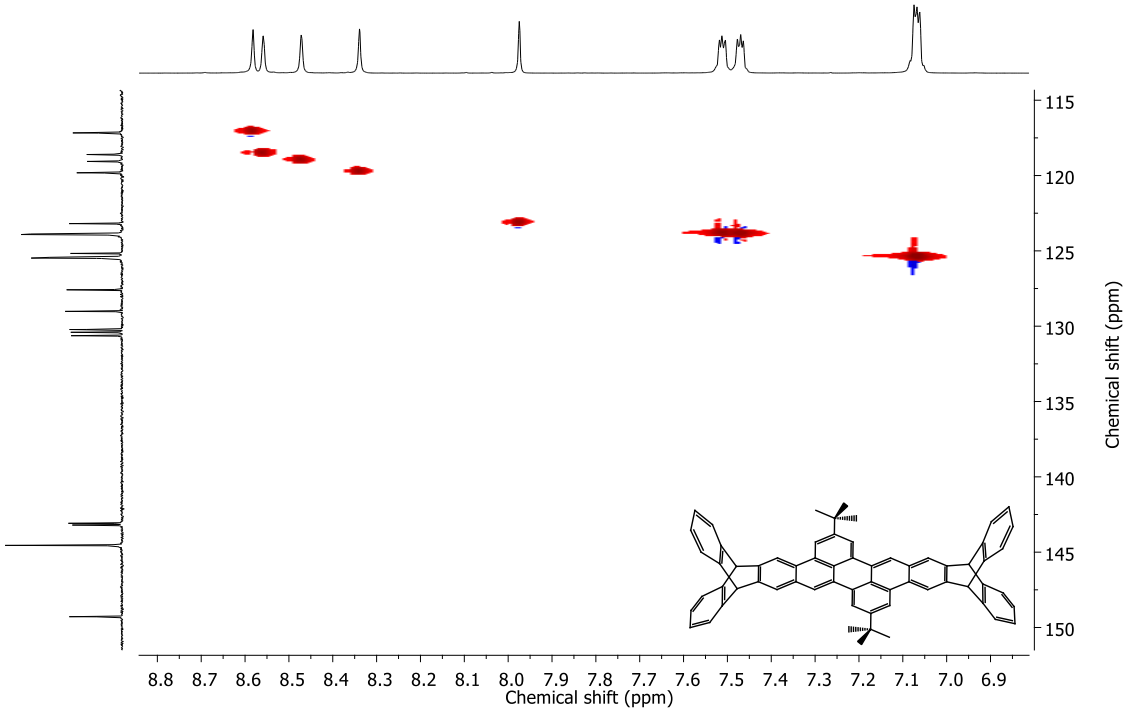

Figure 7.126 ^{1}H-^{13}C HSQC NMR spectrum (600/151 MHz, $Cl_2CDCDCl_2$) of PO-5 (**228**).

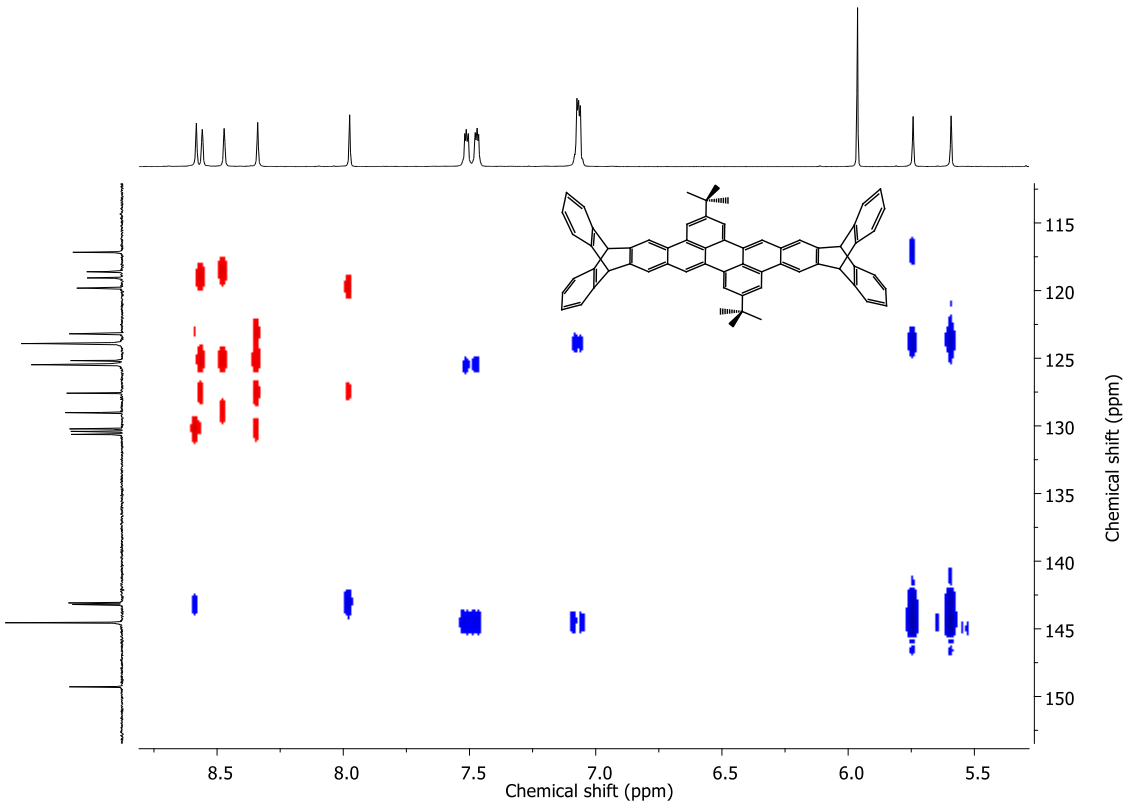

Figure 7.127 ^{1}H-^{13}C HMBC NMR spectrum (600/151 MHz, $Cl_2CDCDCl_2$) of PO-5 (**228**).

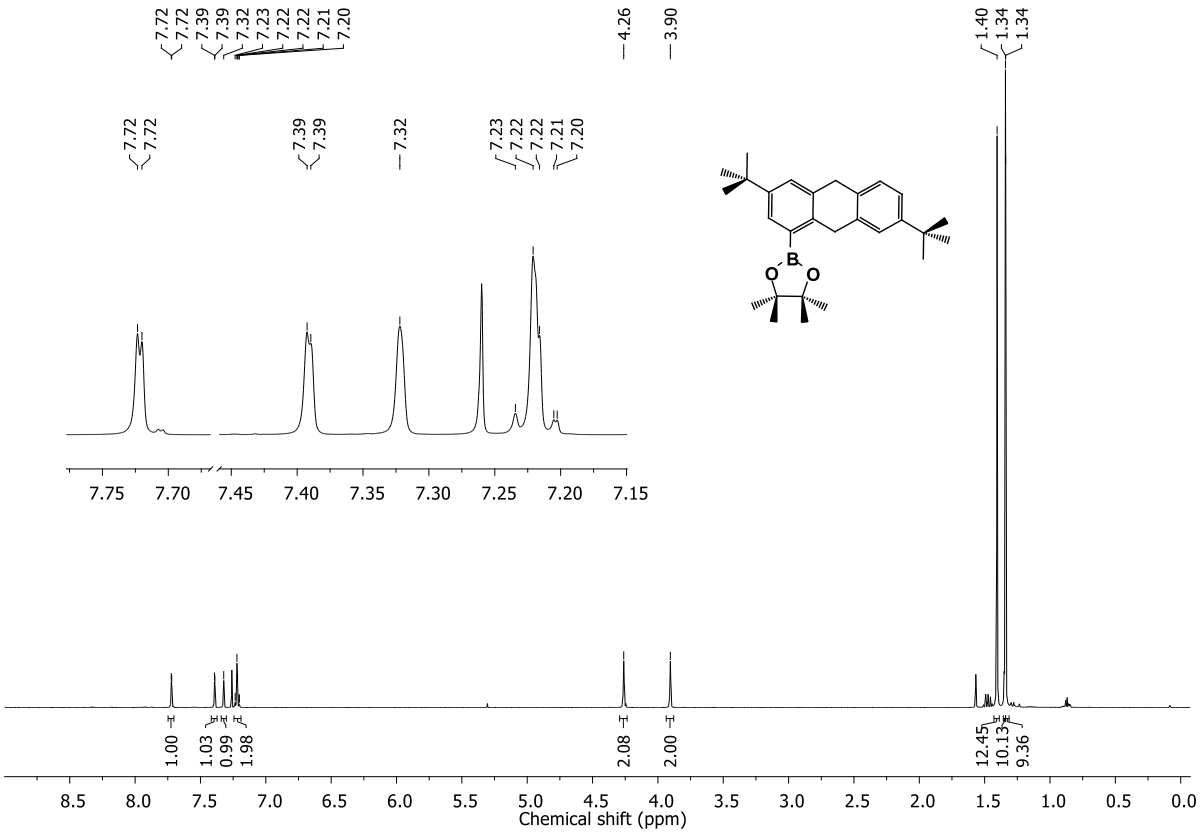

Figure 7.128 ^{1}H NMR spectrum (600 MHz, $CDCl_3$) of **238**.

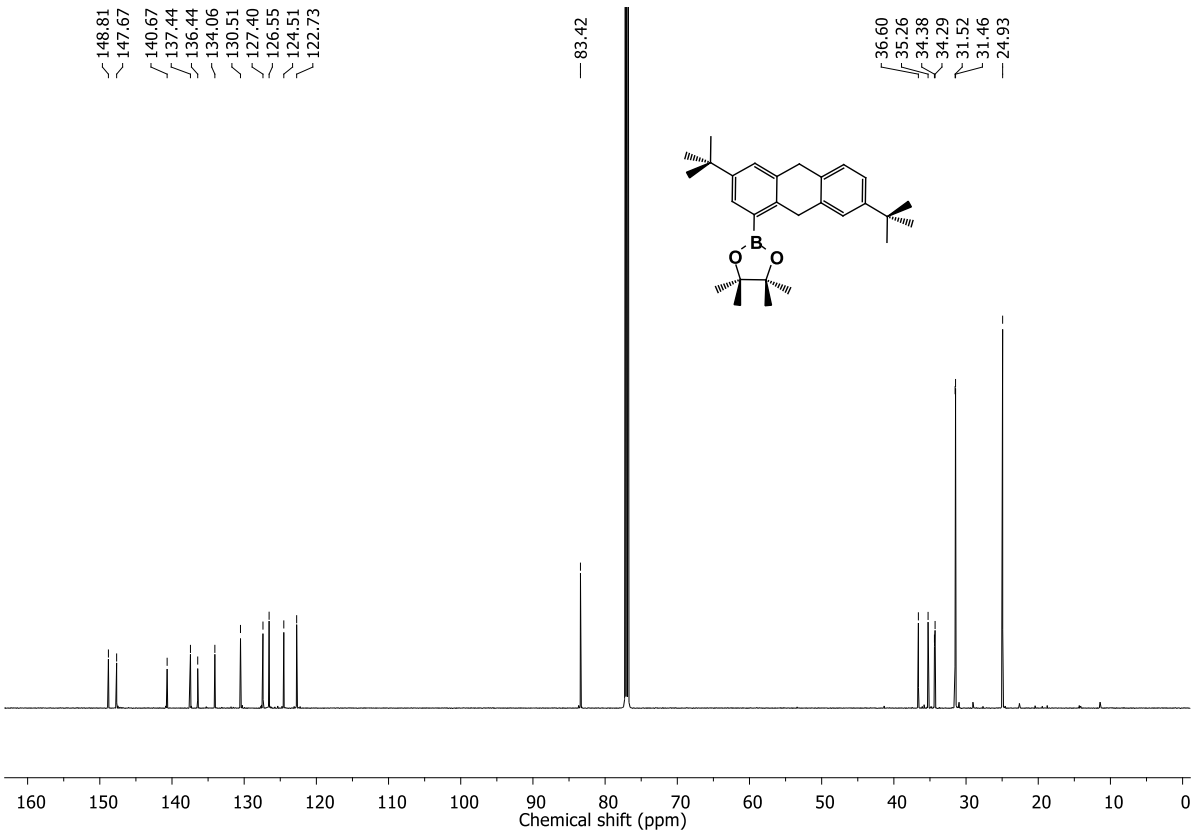

Figure 7.129 ^{13}C NMR spectrum (151 MHz, $CDCl_3$) of **238**.

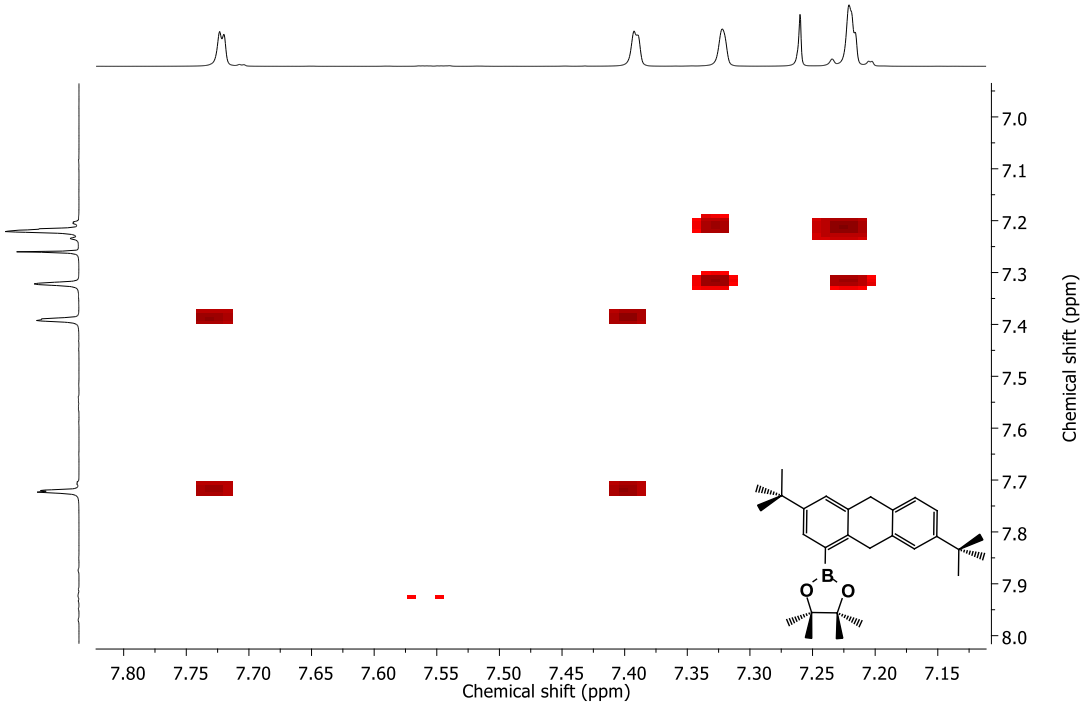

Figure 7.130 ^{1}H-^{1}H COSY NMR spectrum (600/600 MHz, $CDCl_3$) of **238**.

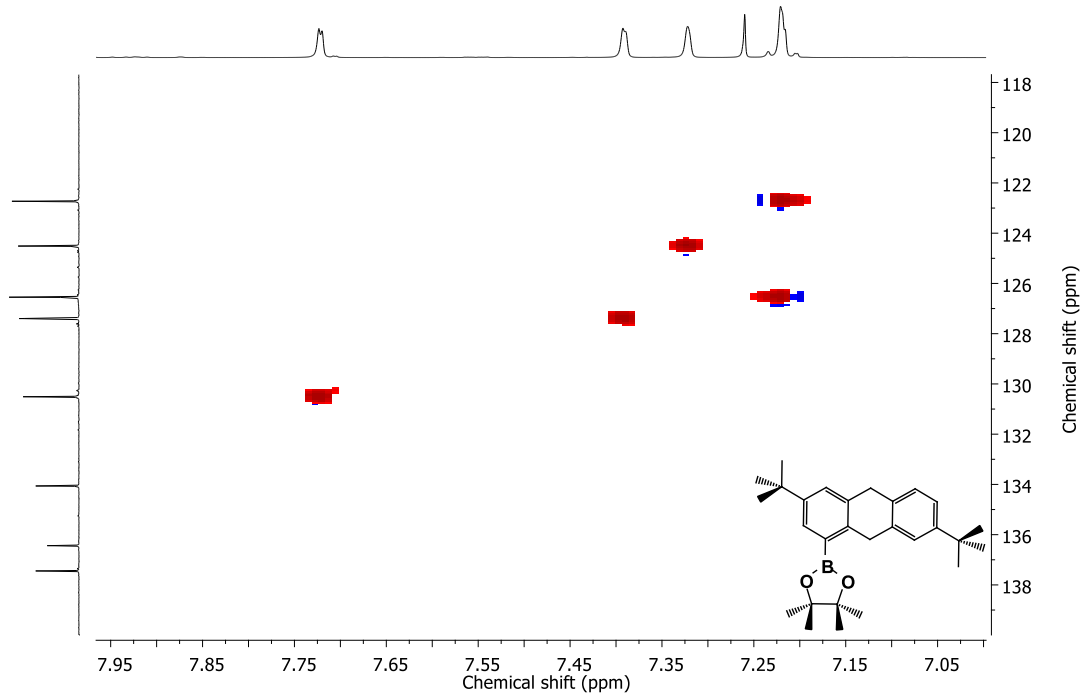

Figure 7.131 ^{1}H-^{13}C HSQC NMR spectrum (600/151 MHz, $CDCl_3$) of **238**.

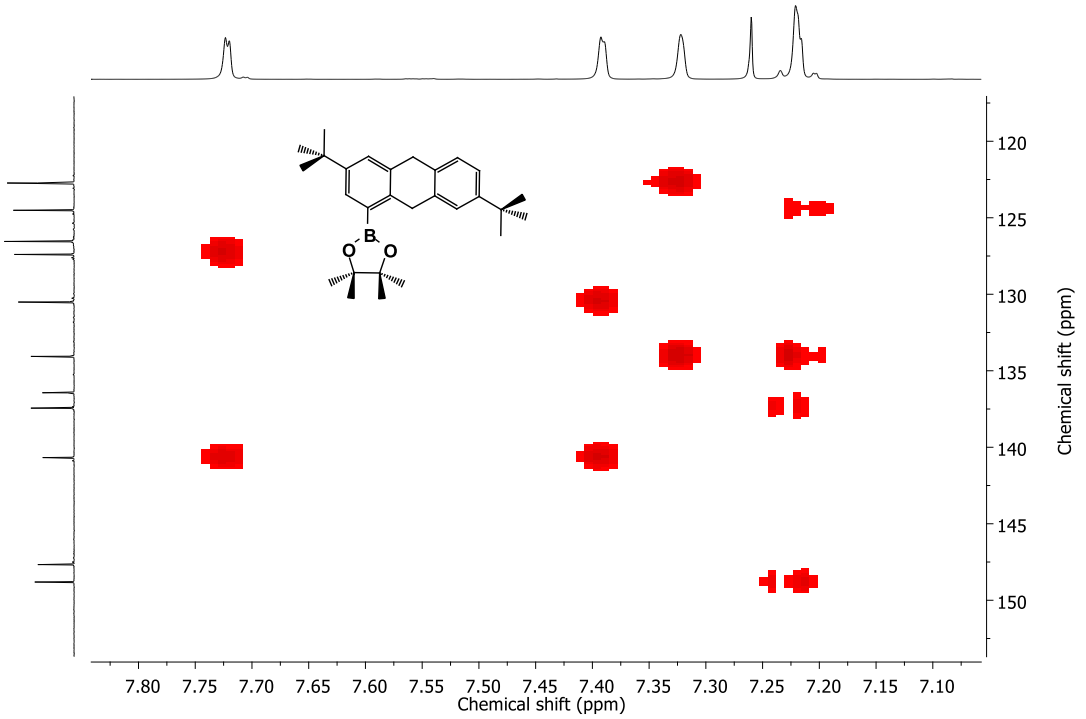

Figure 7.132 ^{1}H-^{13}C HMBC NMR spectrum (600/151 MHz, $CDCl_3$) of **238**.

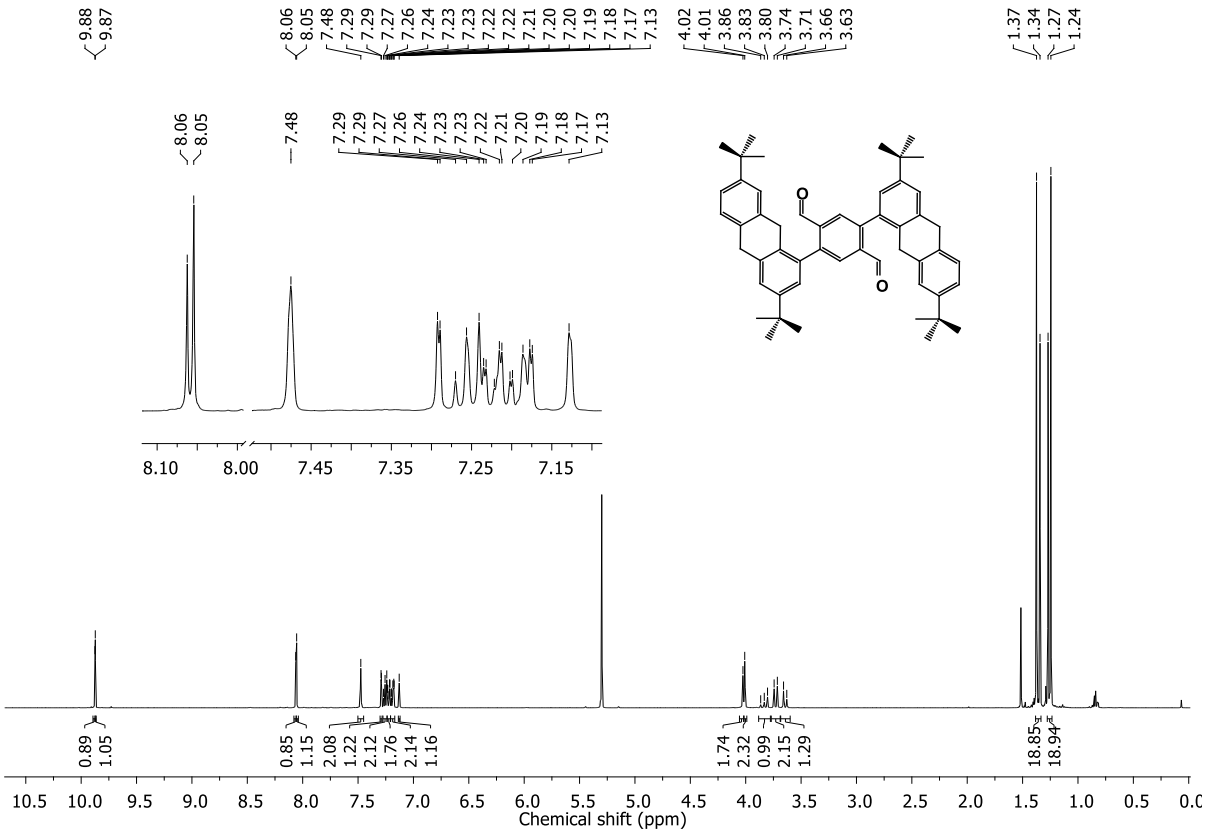

Figure 7.133 ^{1}H NMR spectrum (600 MHz, CD_2Cl_2) of **239**.

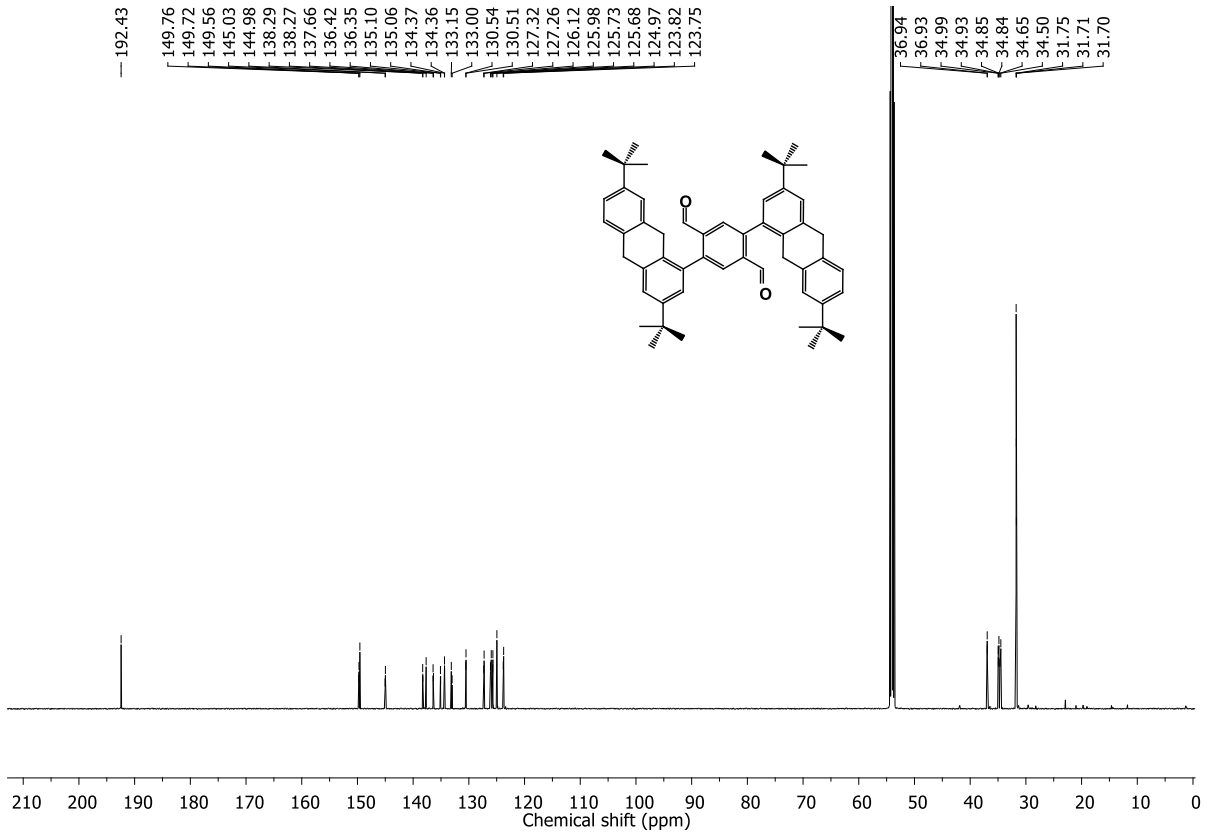

Figure 7.134 ^{13}C NMR spectrum (151 MHz, CD_2Cl_2) of **239**.

Figure 7.135 ^{1}H NMR spectrum (500 MHz, $Cl_2CDCDCl_2$) of **240**. *Ethanol. #THF.

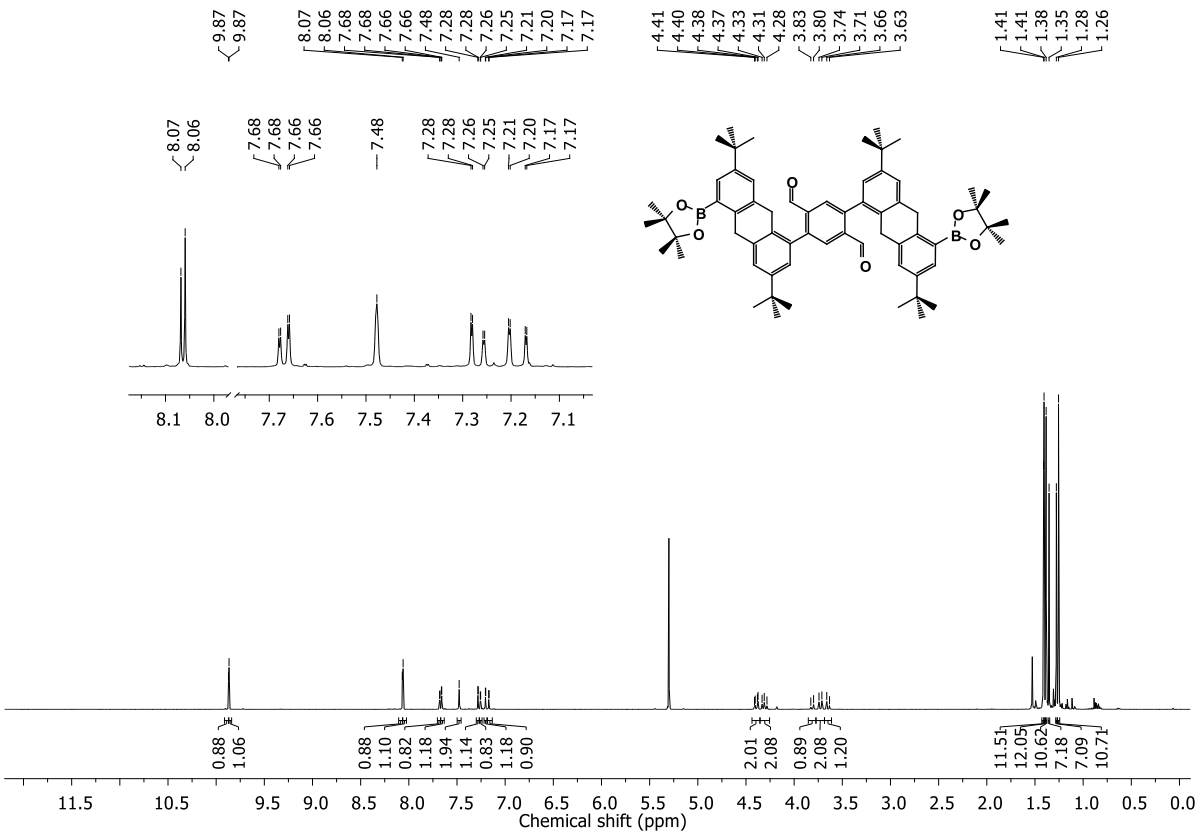

Figure 7.136 ^{1}H NMR spectrum (600 MHz, CD_2Cl_2) of **241**.

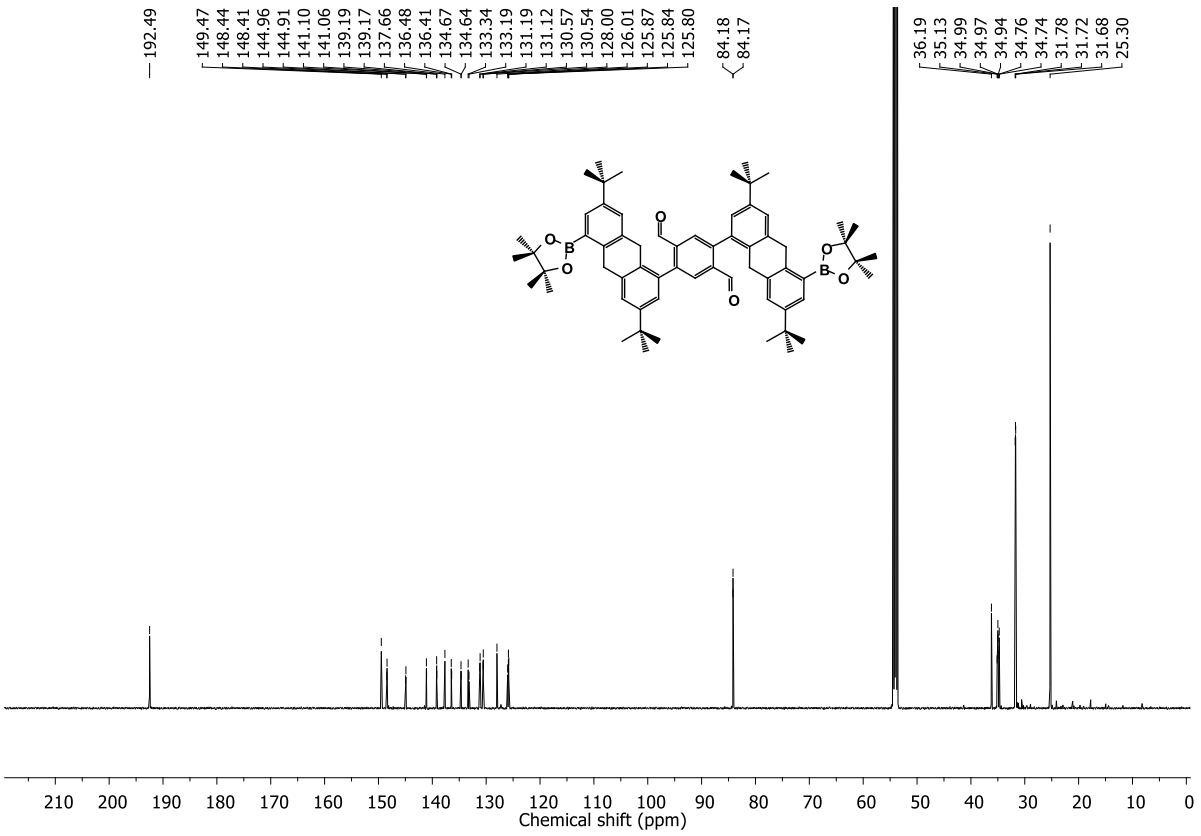

Figure 7.137 ^{13}C NMR spectrum (151 MHz, CD_2Cl_2) of **241**.

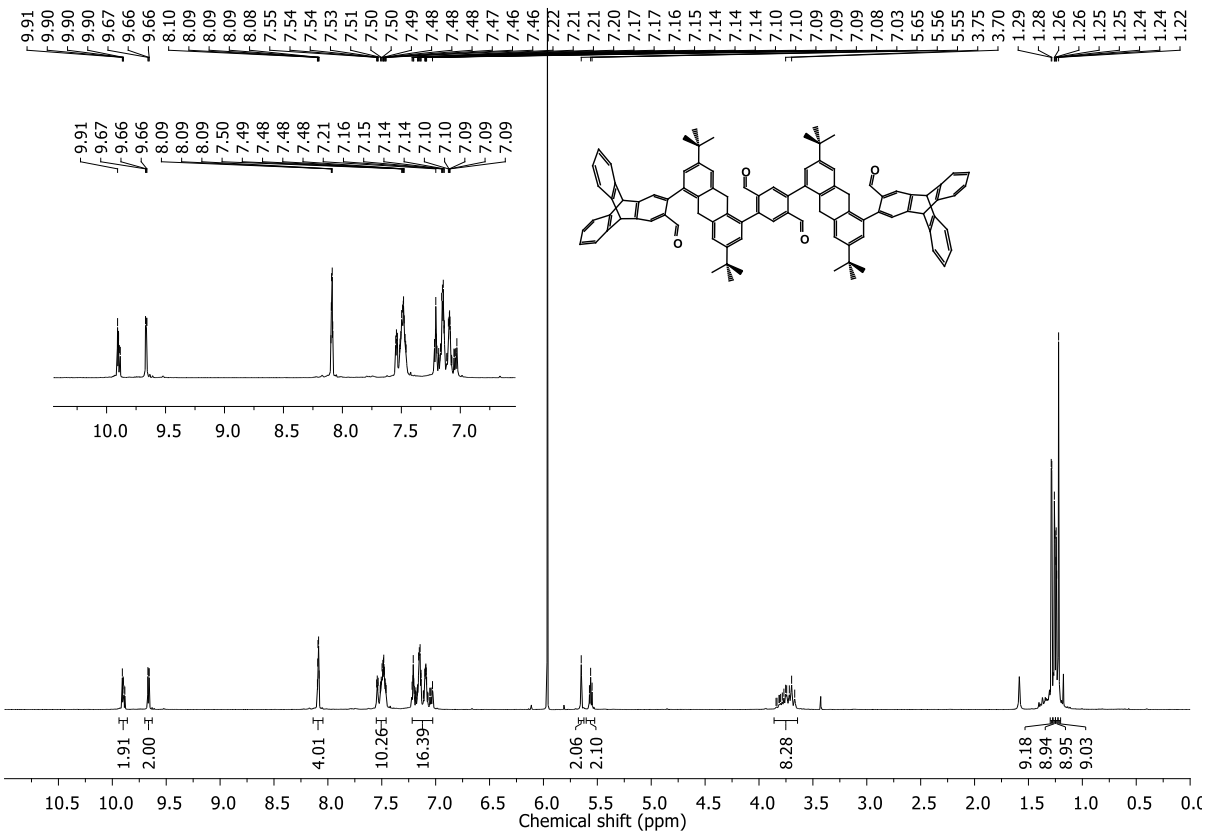

Figure 7.138 ^{1}H NMR spectrum (600 MHz, $Cl_2CDCDCl_2$) of **243**.

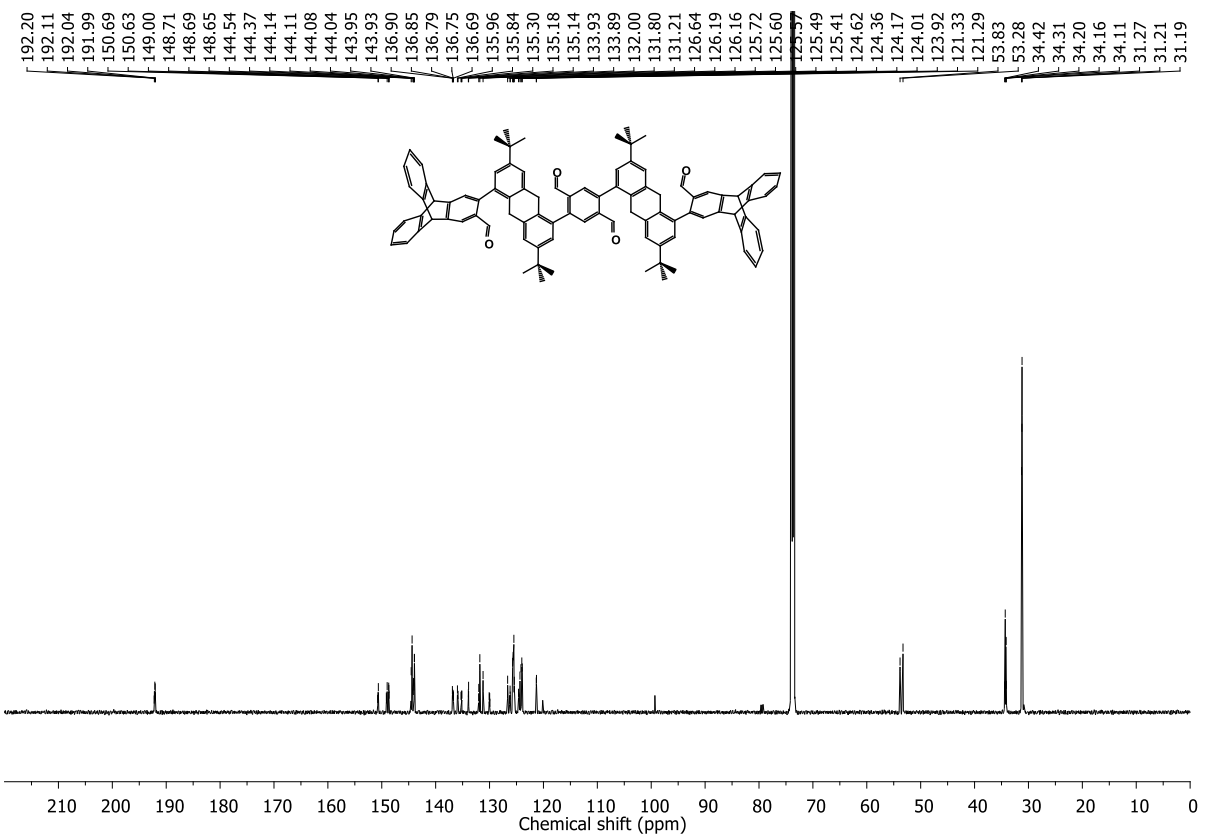

Figure 7.139 ^{13}C NMR spectrum (151 MHz, $Cl_2CDCDCl_2$) of **243**.

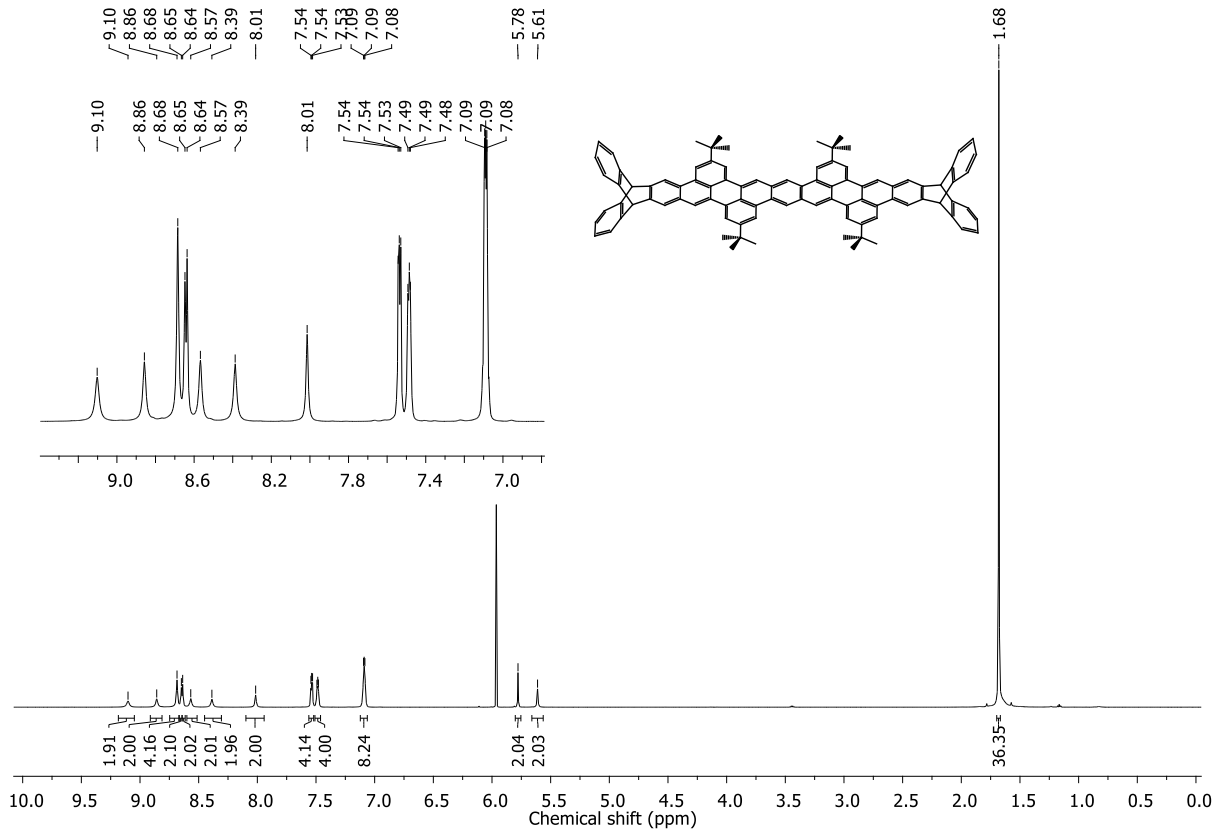

Figure 7.140 ^{1}H NMR spectrum (600 MHz, $Cl_2CDCDCl_2$) of PO-9 (**229**).

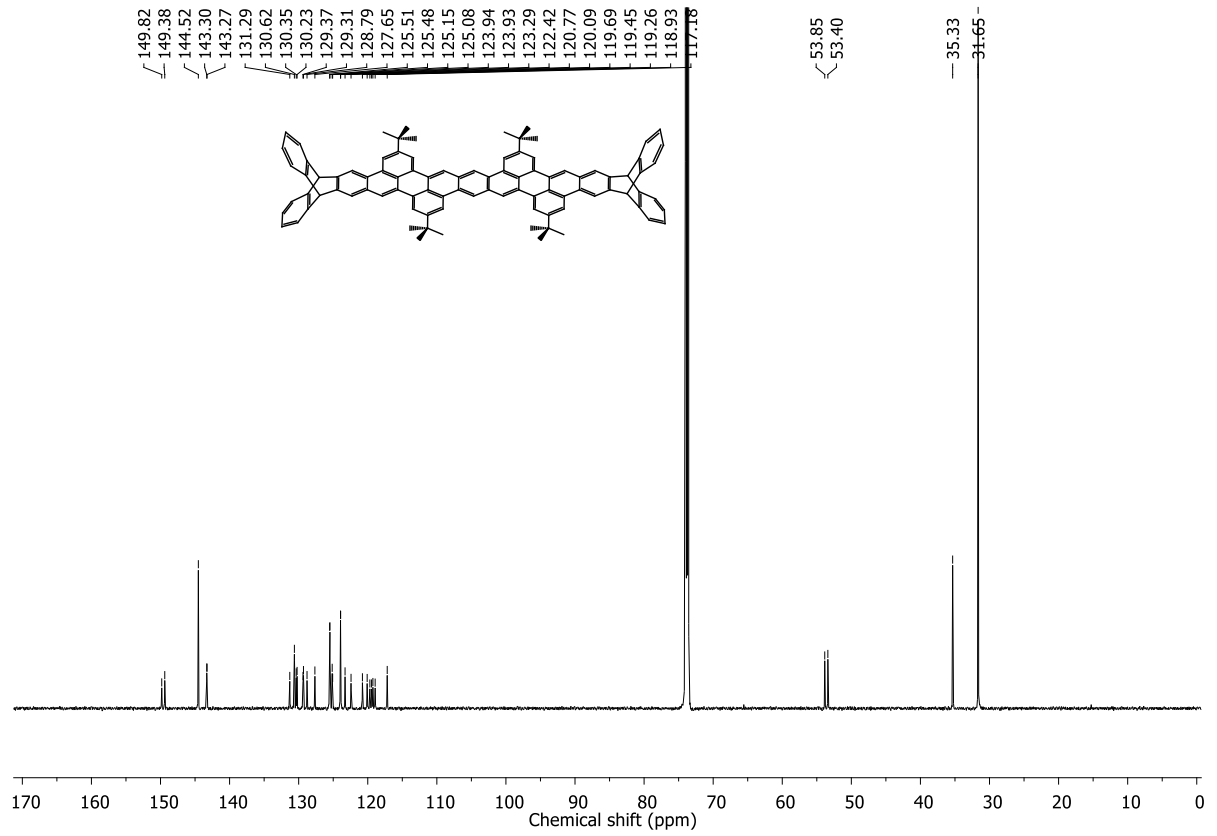

Figure 7.141 ^{13}C NMR spectrum (151 MHz, $Cl_2CDCDCl_2$) of PO-9 (**229**).

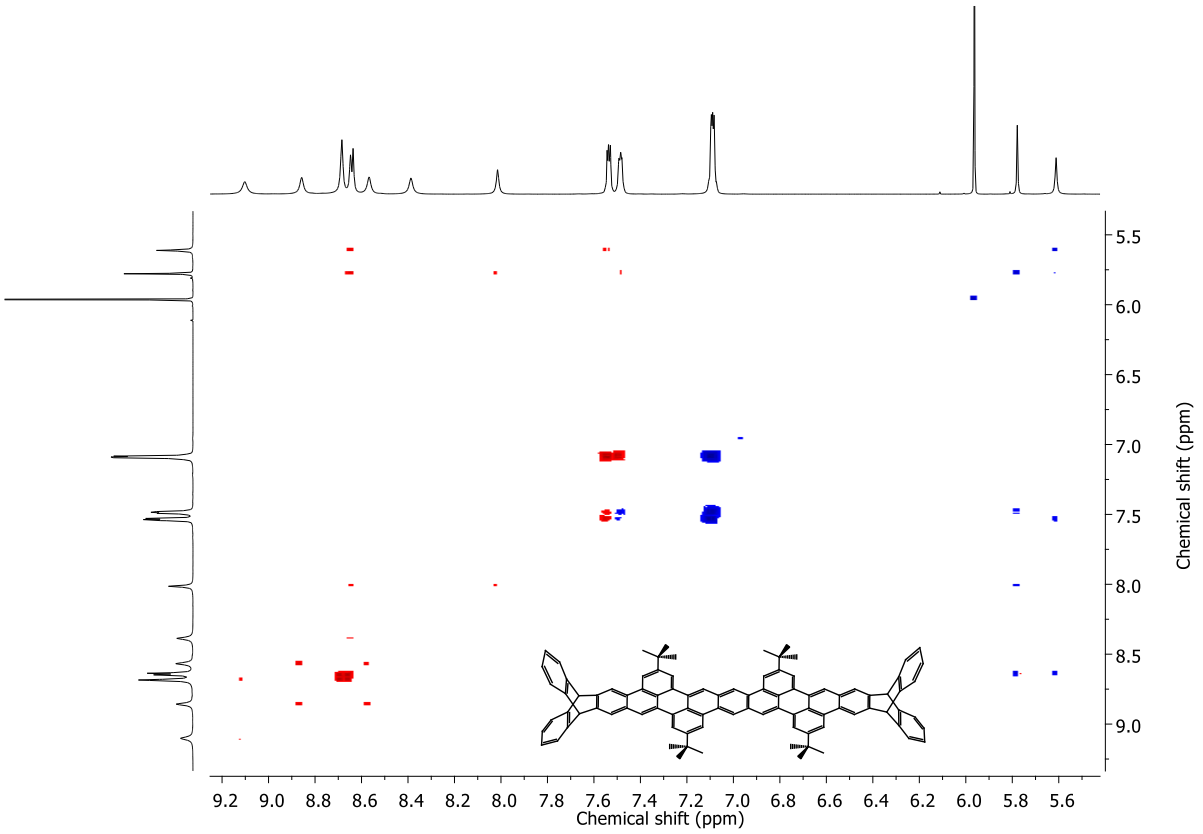

Figure 7.142 ^{1}H-^{1}H COSY NMR spectrum (600/600 MHz, $Cl_2CDCDCl_2$) of PO-9 (**229**).

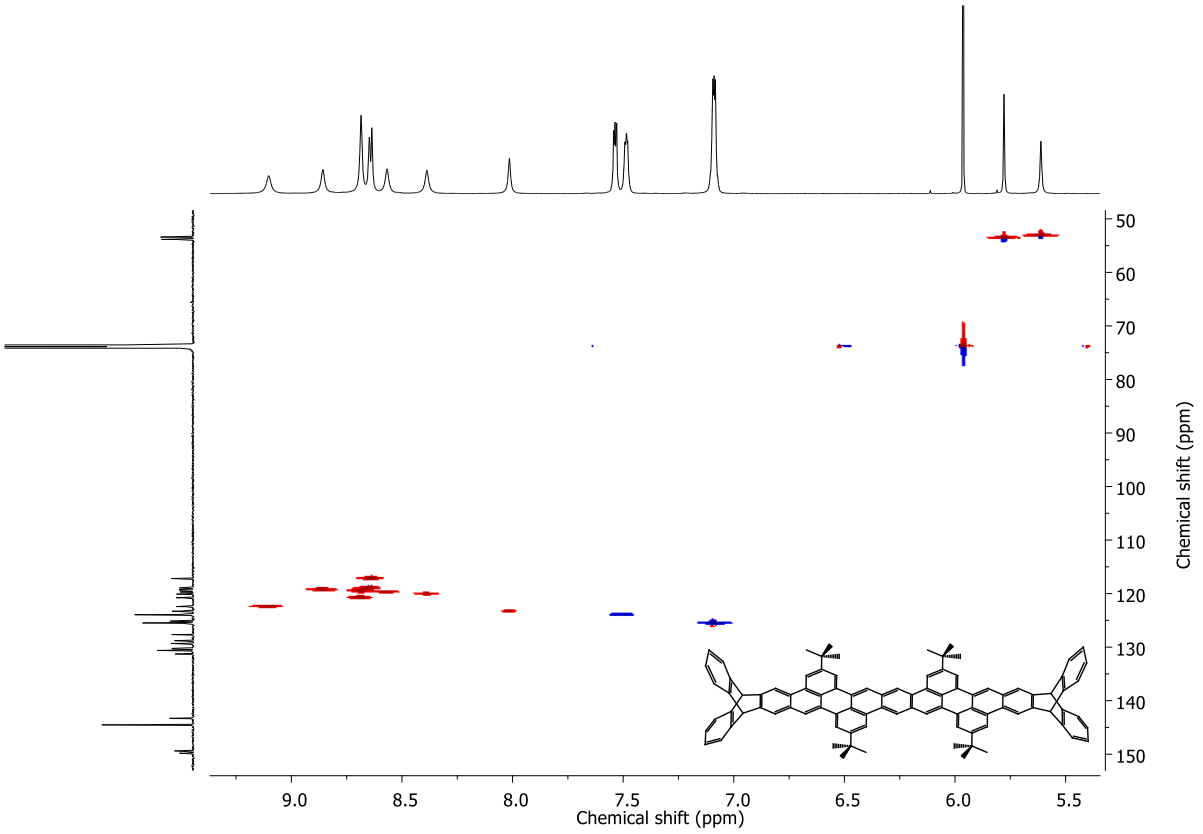

Figure 7.143 ^{1}H-^{13}C HSQC NMR spectrum (600/151 MHz, $Cl_2CDCDCl_2$) of PO-9 (**229**).

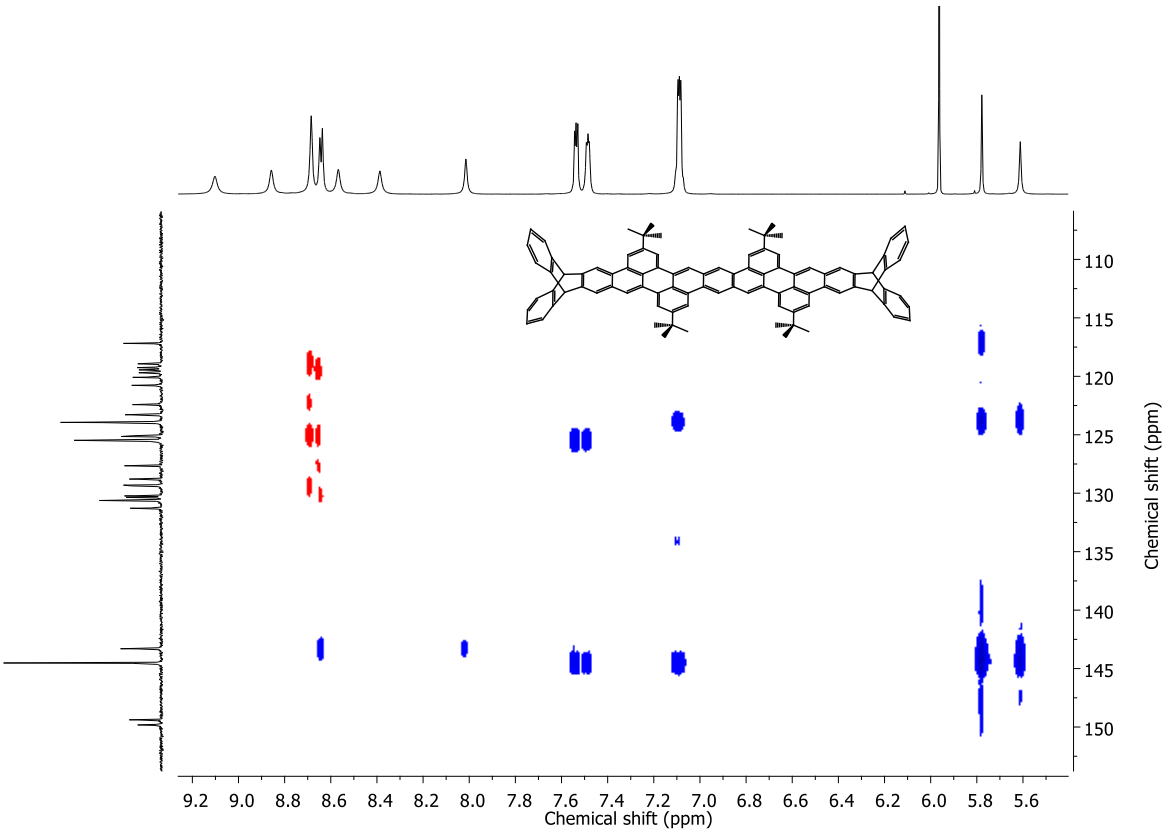

Figure 7.144 ^{1}H-^{13}C HMBC NMR spectrum (600/151 MHz, $Cl_2CDCDCl_2$) of PO-9 (**229**).

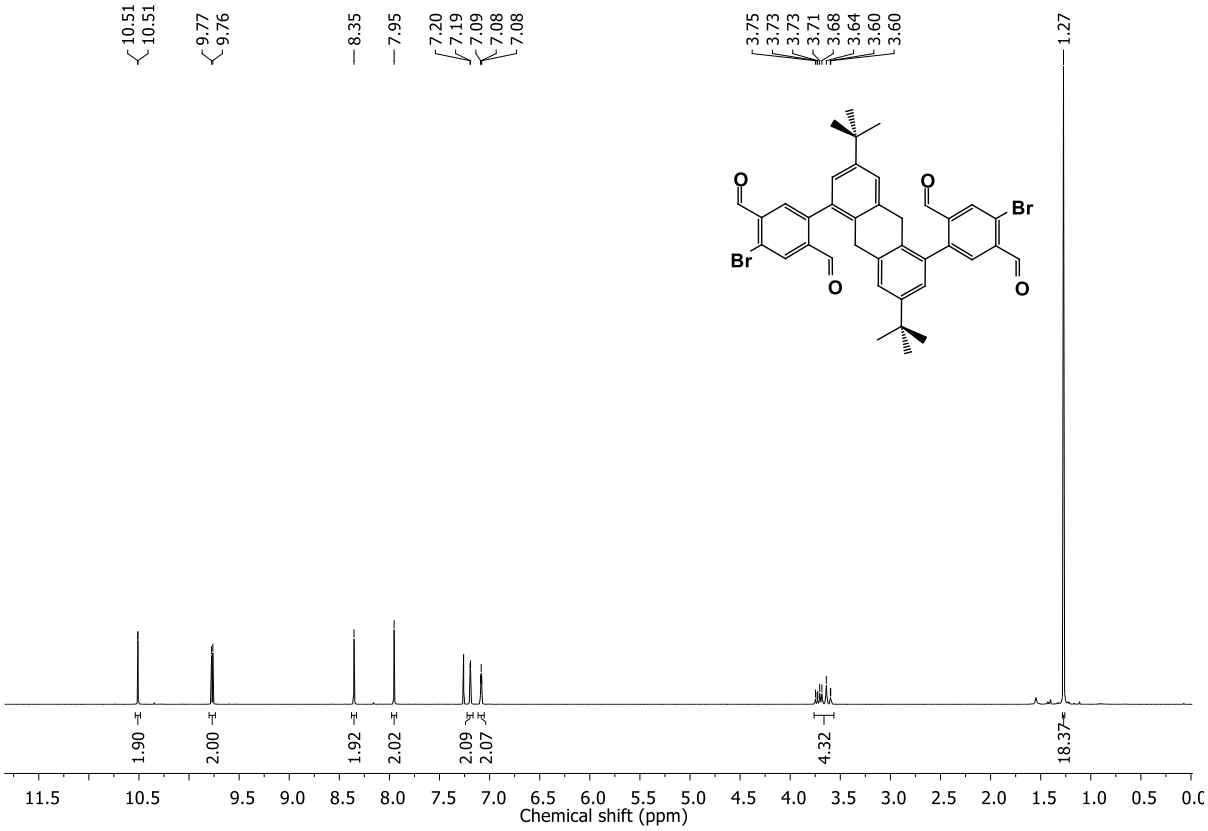

Figure 7.145 ^{1}H NMR spectrum (400 MHz, $CDCl_3$) of **244**.

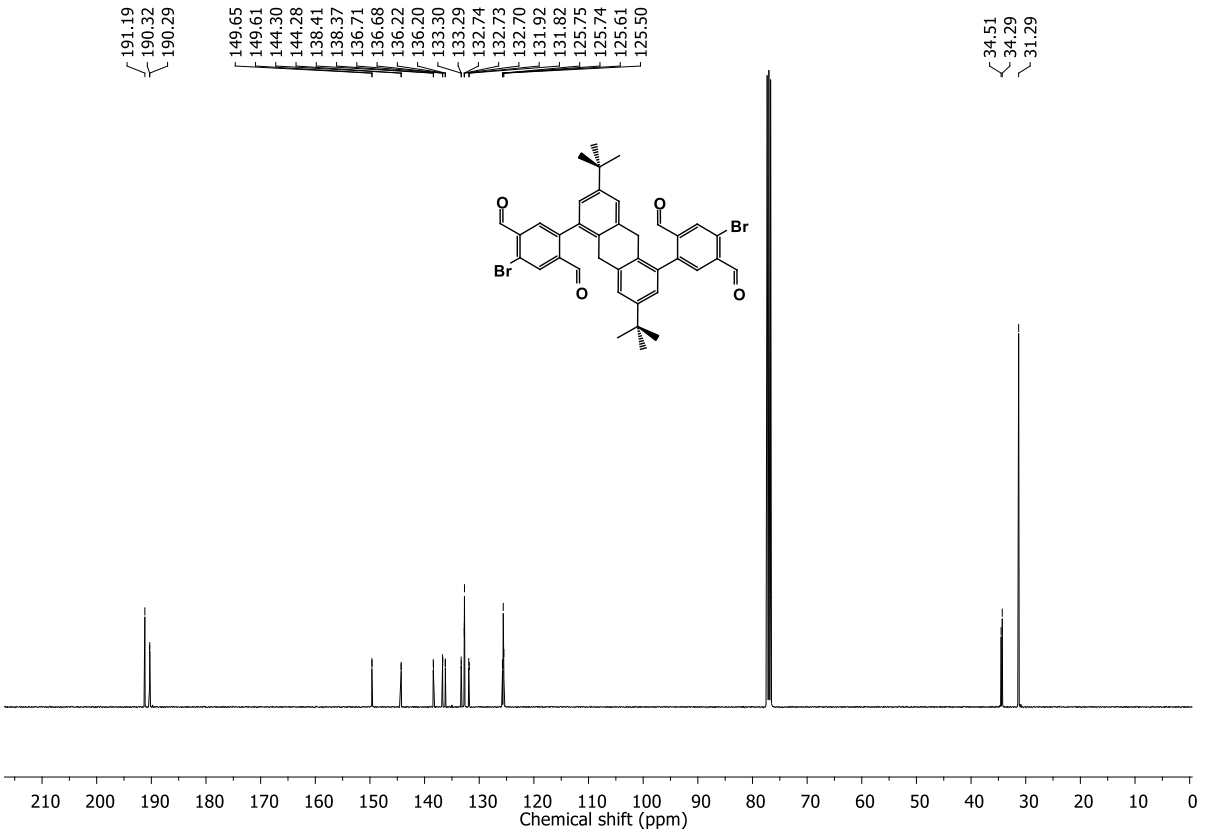

Figure 7.146 ^{13}C NMR spectrum (101 MHz, $CDCl_3$) of **244**.

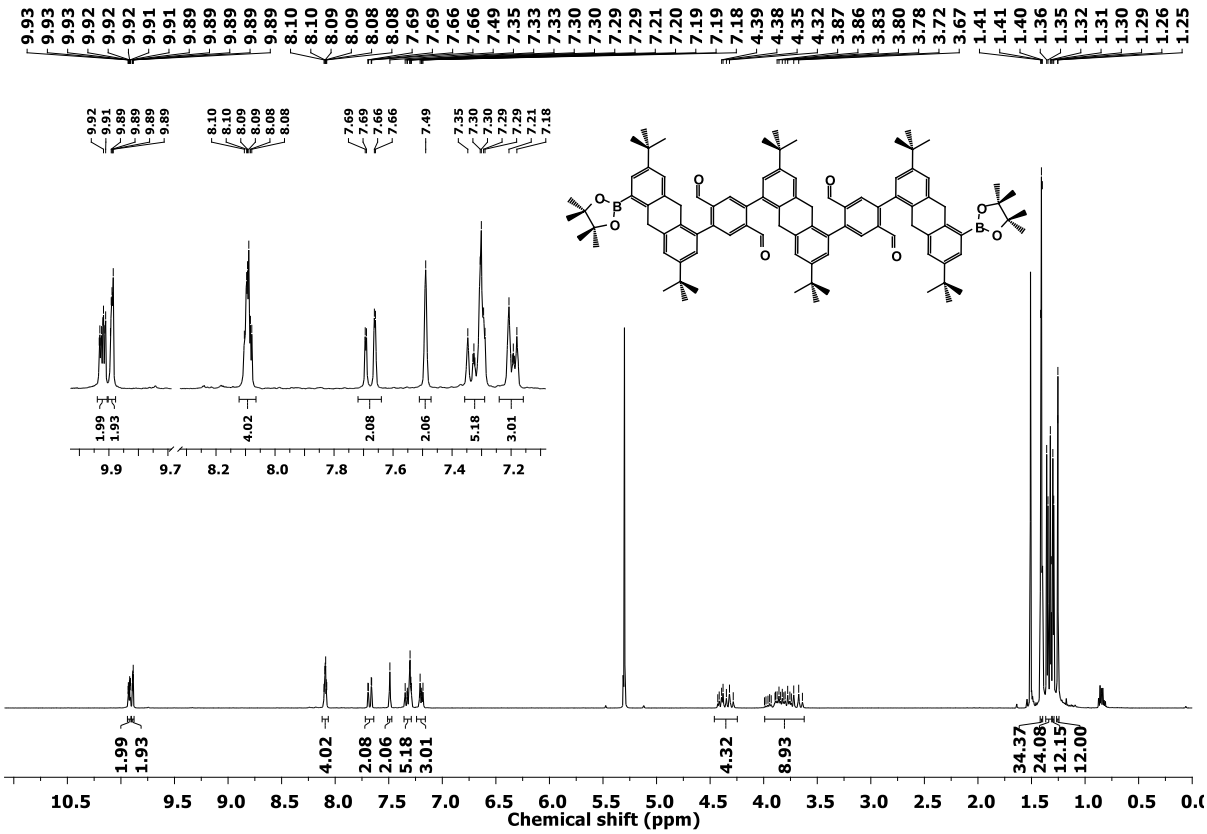

Figure 7.147 ^{1}H NMR spectrum (500 MHz, CD_2Cl_2) of **245**.

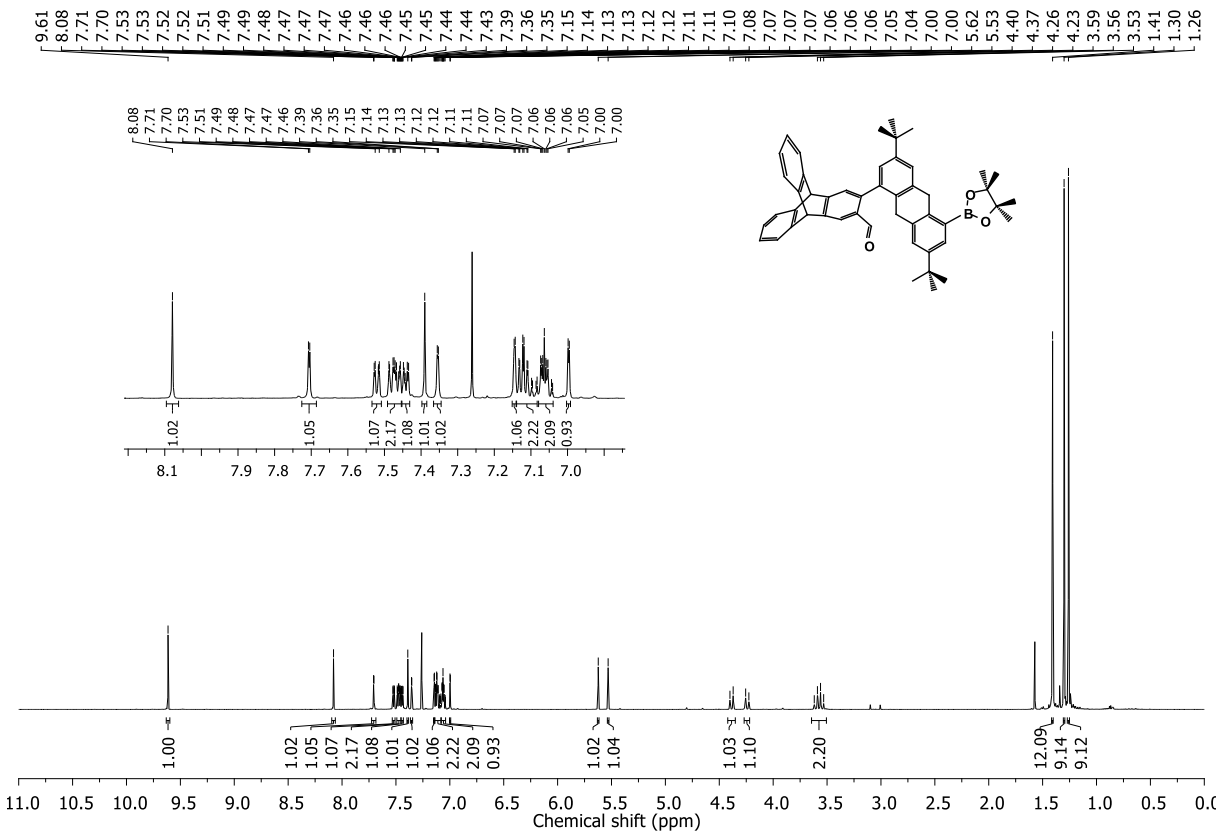

Figure 7.148 ^{1}H NMR spectrum (600 MHz, $CDCl_3$) of **247**.

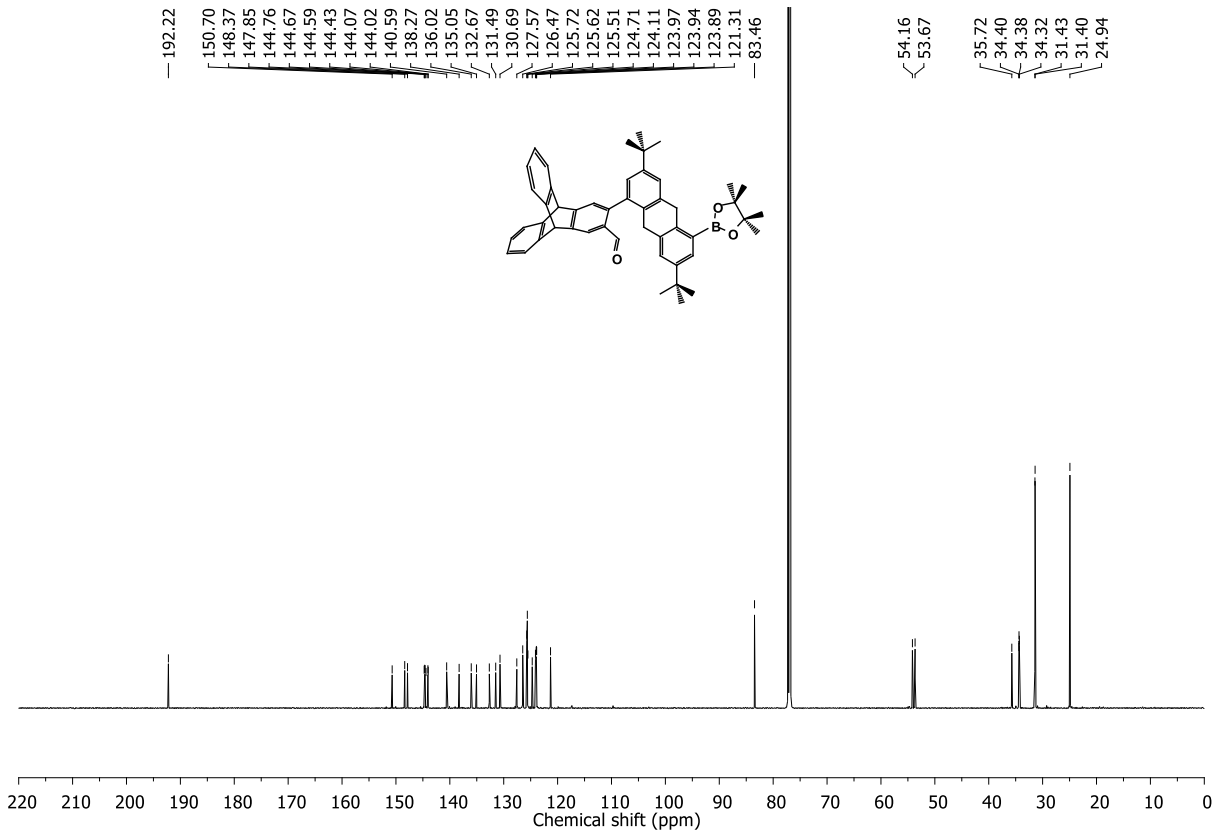

Figure 7.149 ^{13}C NMR spectrum (151 MHz, $CDCl_3$) of **247**.

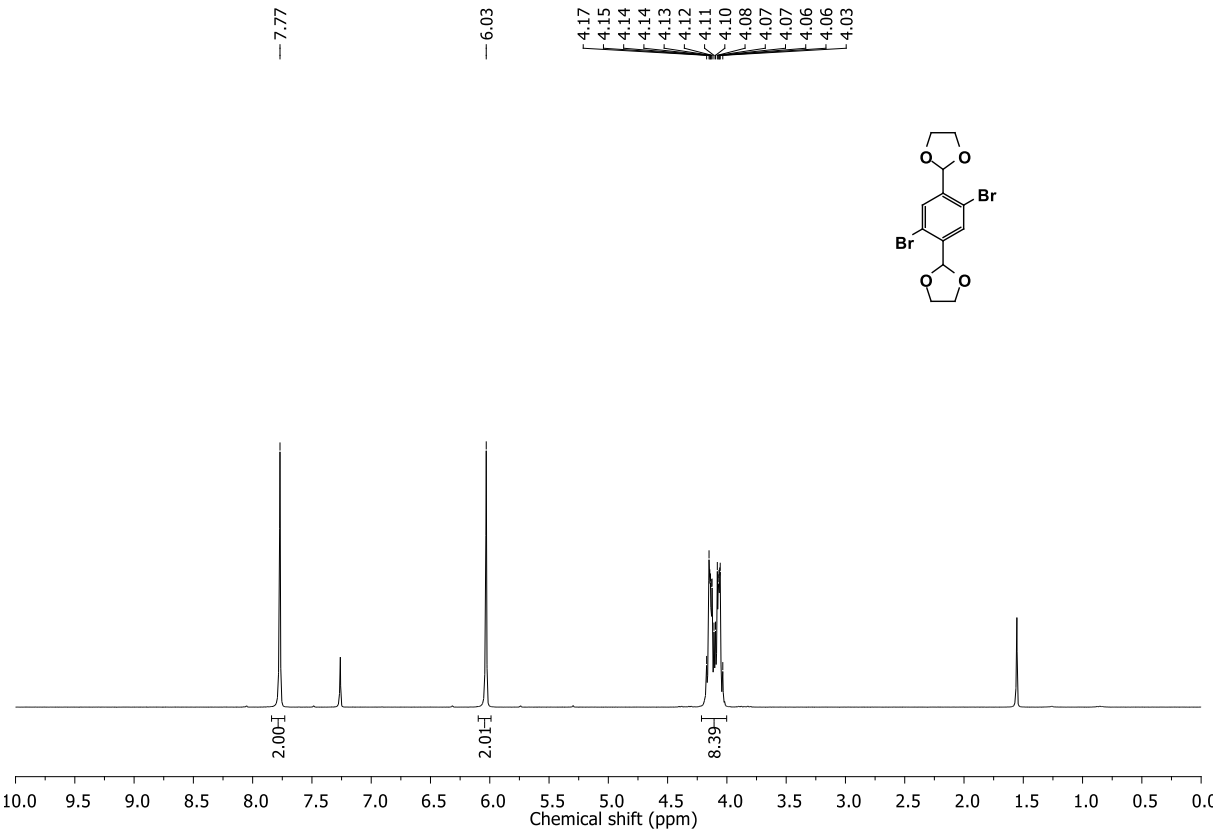

Figure 7.150 ^{1}H NMR spectrum (300 MHz, $CDCl_3$) of **248**.

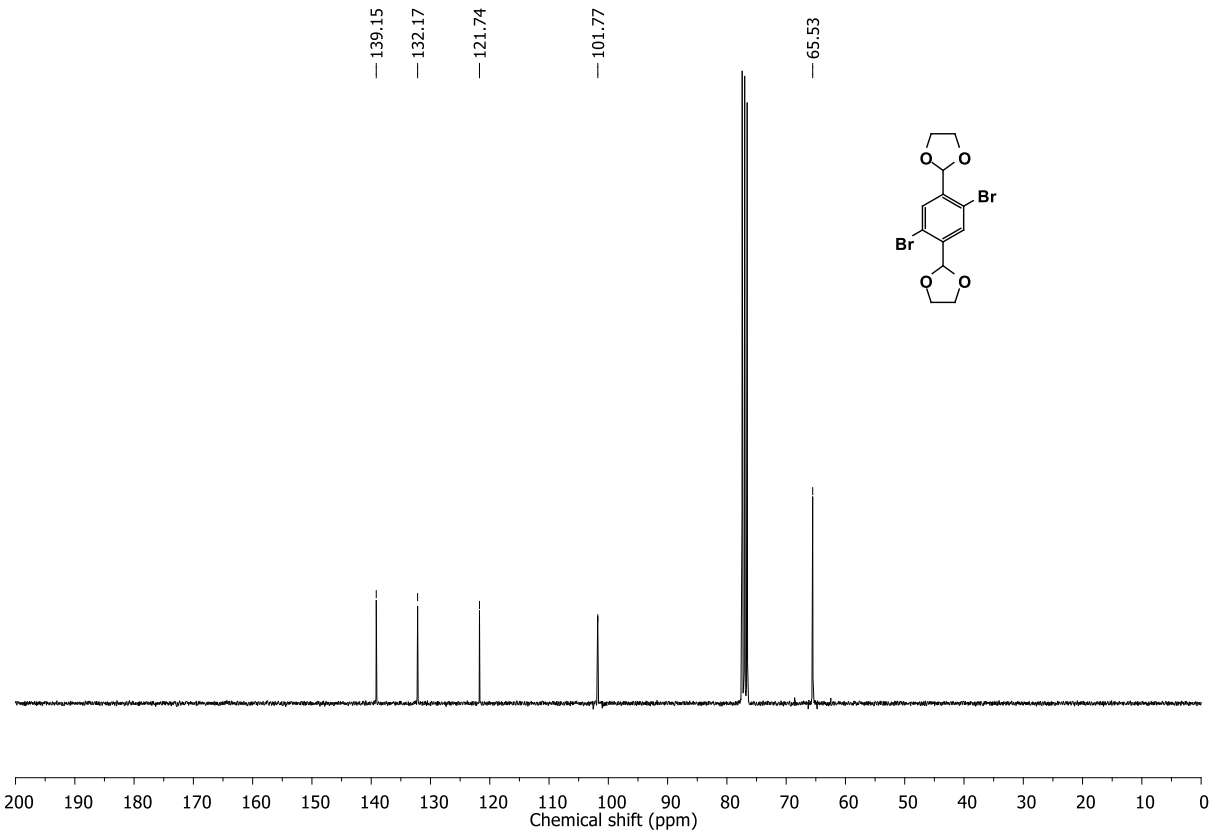

Figure 7.151 ^{13}C NMR spectrum (75 MHz, $CDCl_3$) of **248**.

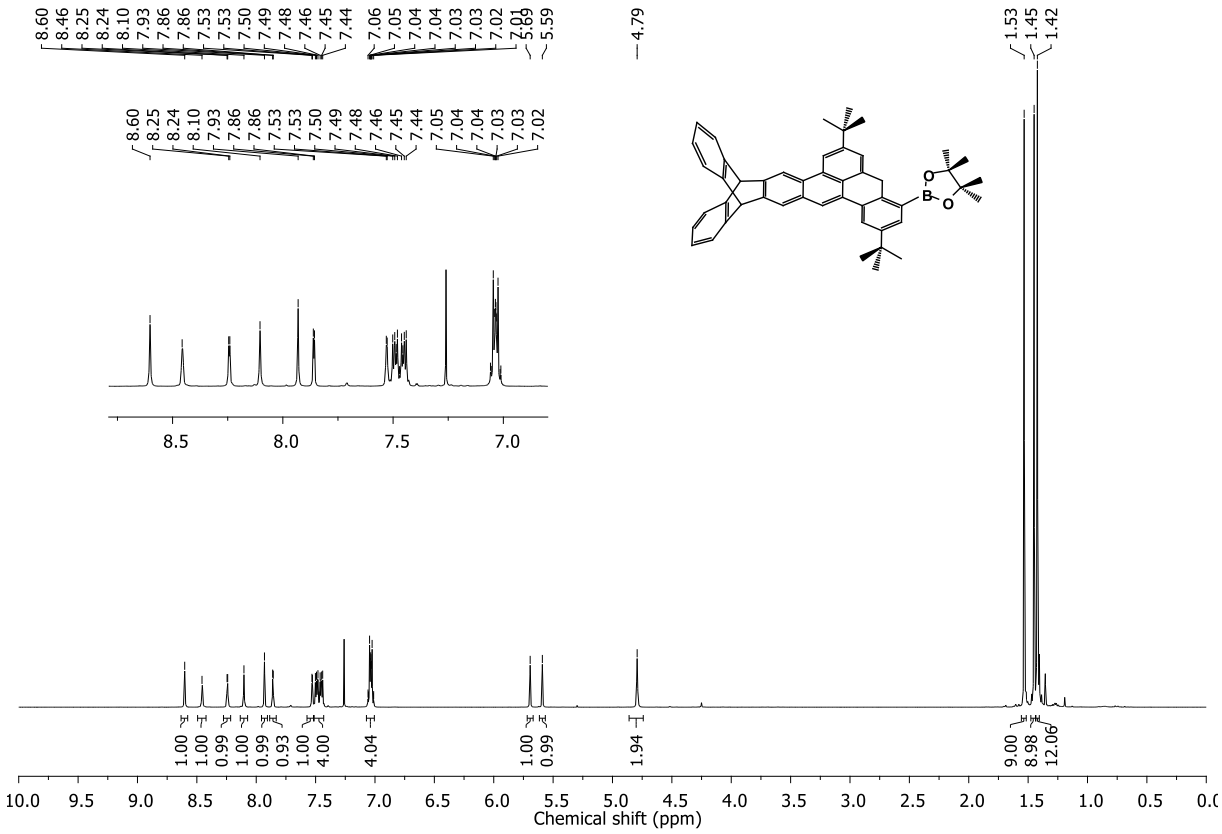

Figure 7.152 ^{1}H NMR spectrum (400 MHz, $CDCl_3$) of **250**.

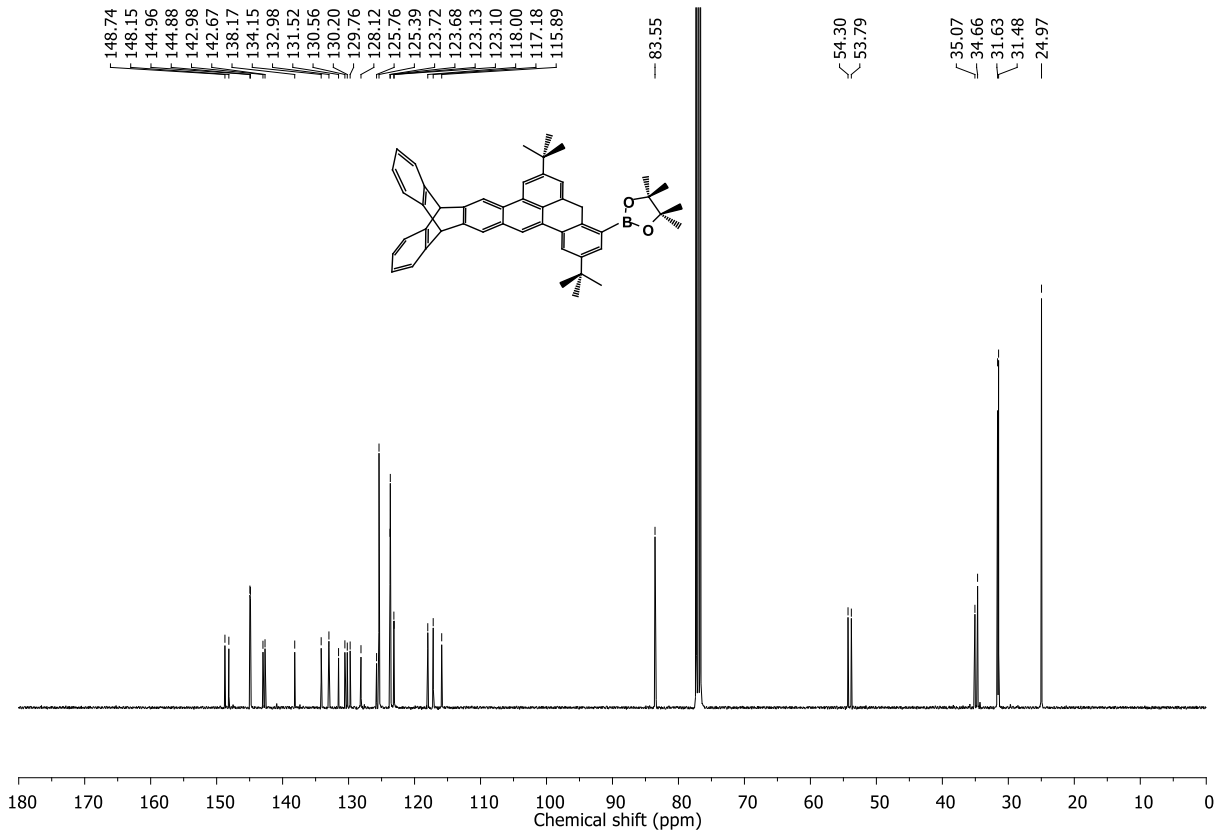

Figure 7.153 ^{13}C NMR spectrum (101 MHz, $CDCl_3$) of **250**.

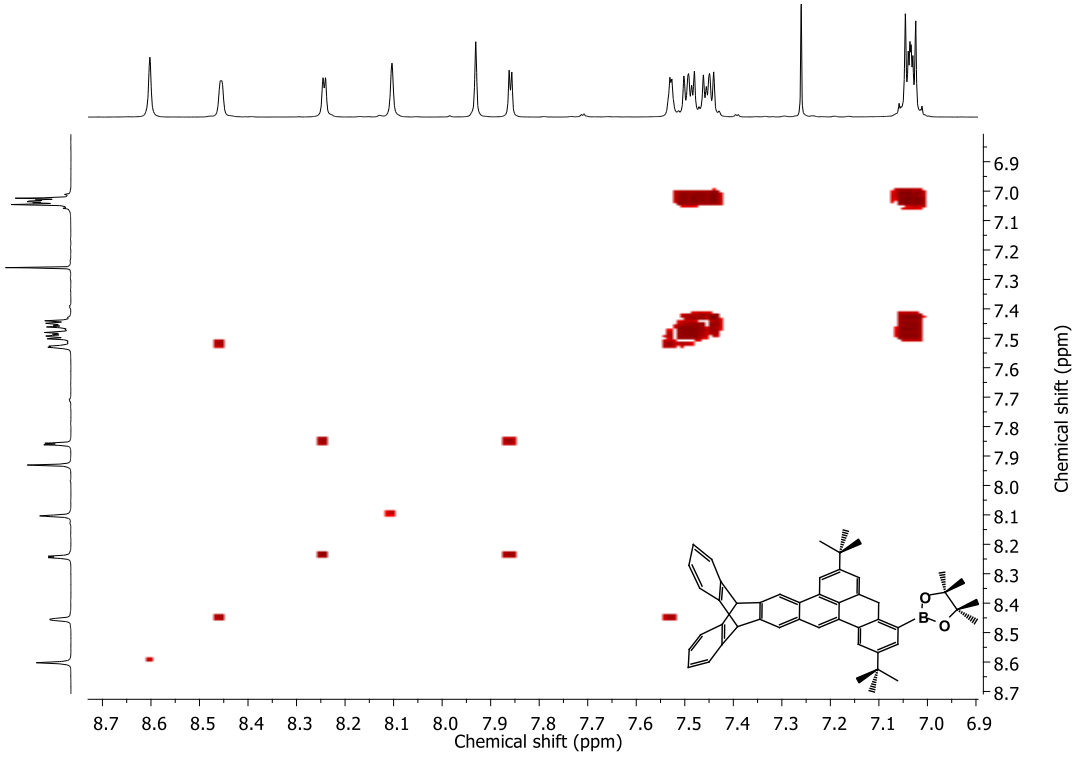

Figure 7.154 ^{1}H-^{1}H COSY NMR spectrum (400/400 MHz, $CDCl_3$) of **250**.

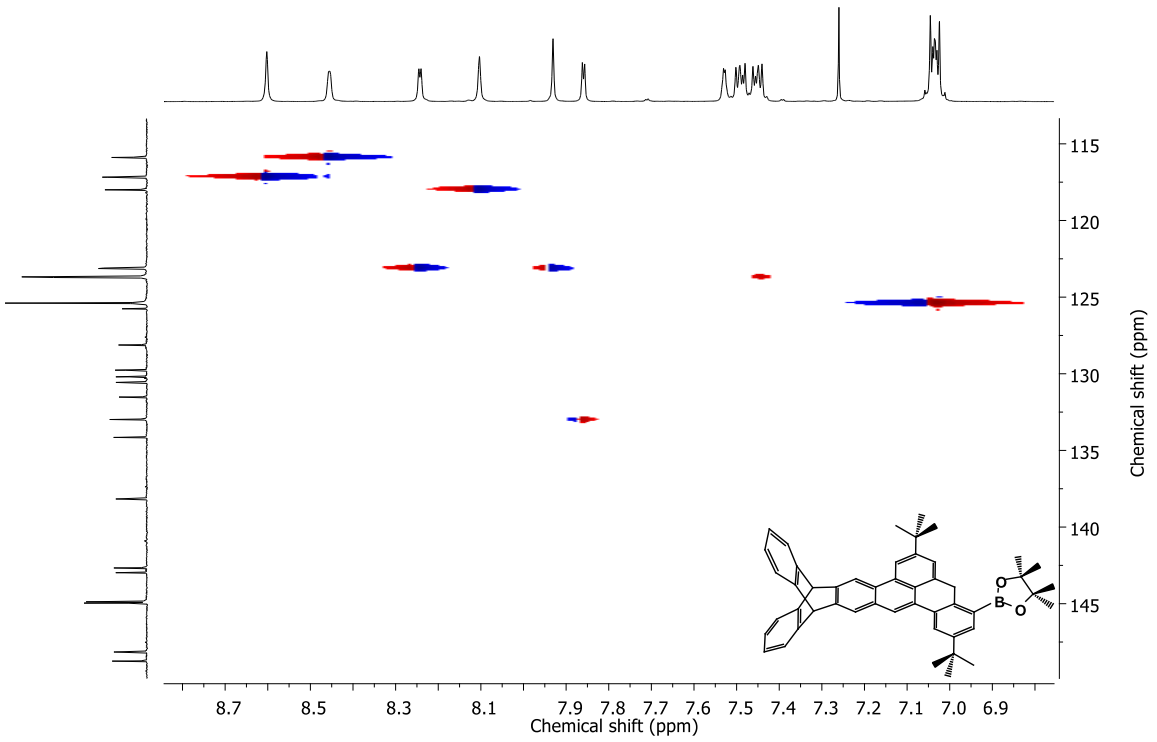

Figure 7.155 ^{1}H-^{13}C HSQC NMR spectrum (400/101 MHz, $CDCl_3$) of **250**.

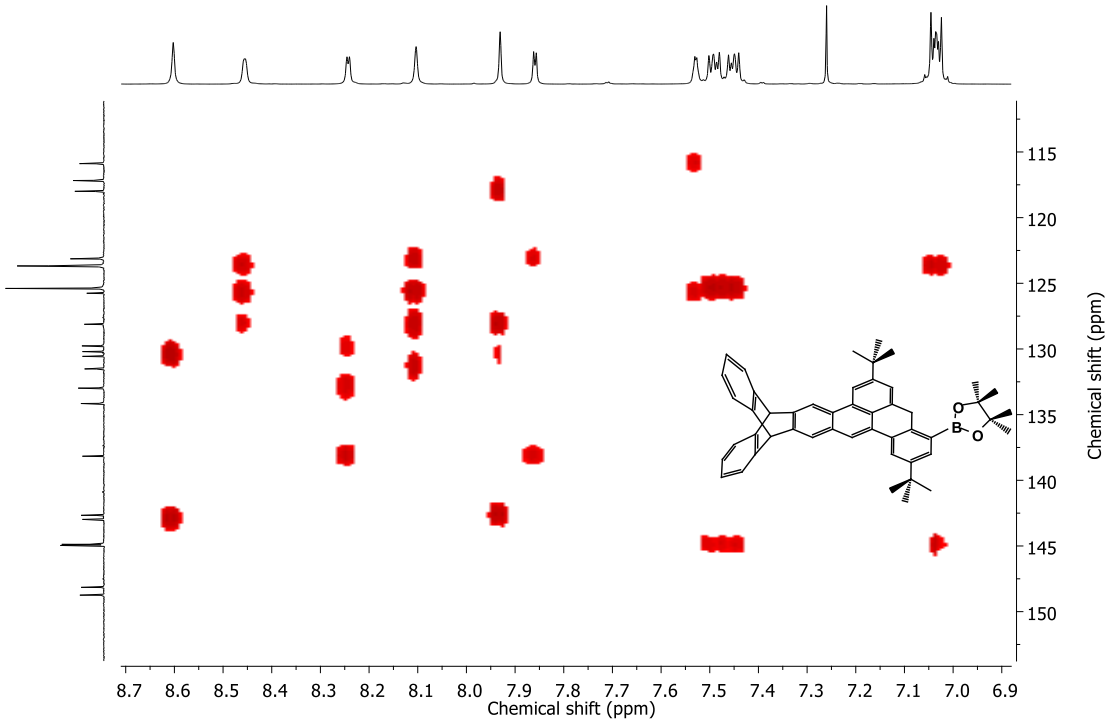

Figure 7.156 ^{1}H-^{13}C HMBC NMR spectrum (400/101 MHz, $CDCl_3$) of **250**.

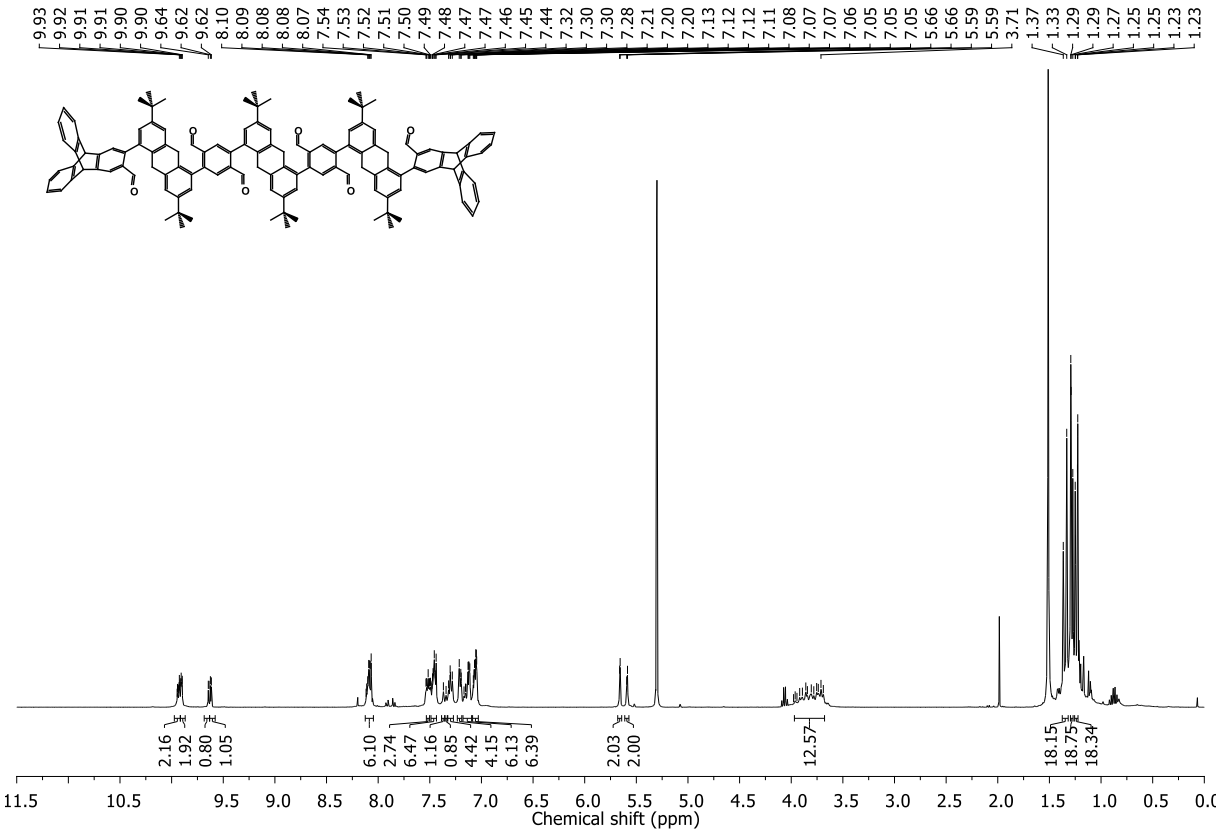

Figure 7.157 ^{1}H NMR spectrum (400 MHz, $Cl_2CDCDCl_2$) of **246**.

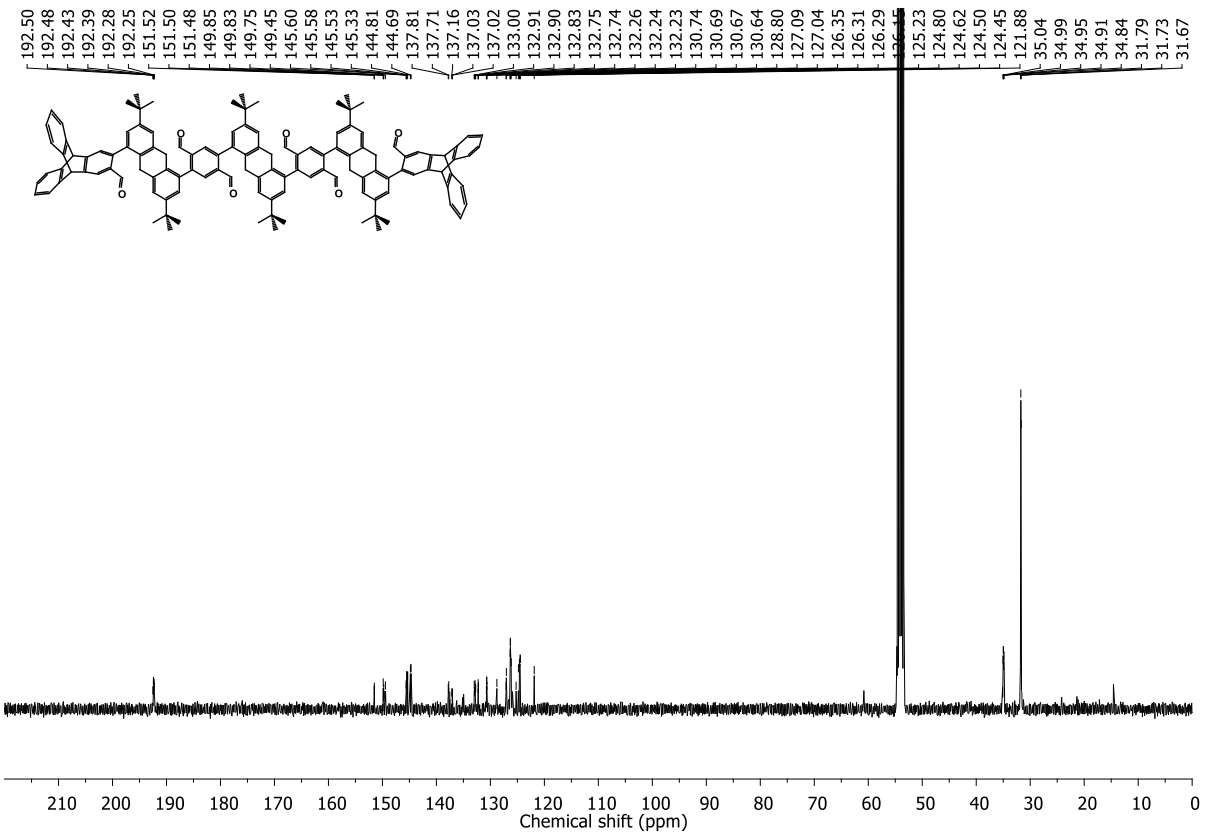

Figure 7.158 ^{13}C NMR spectrum (101 MHz, $Cl_2CDCDCl_2$) of **246**.

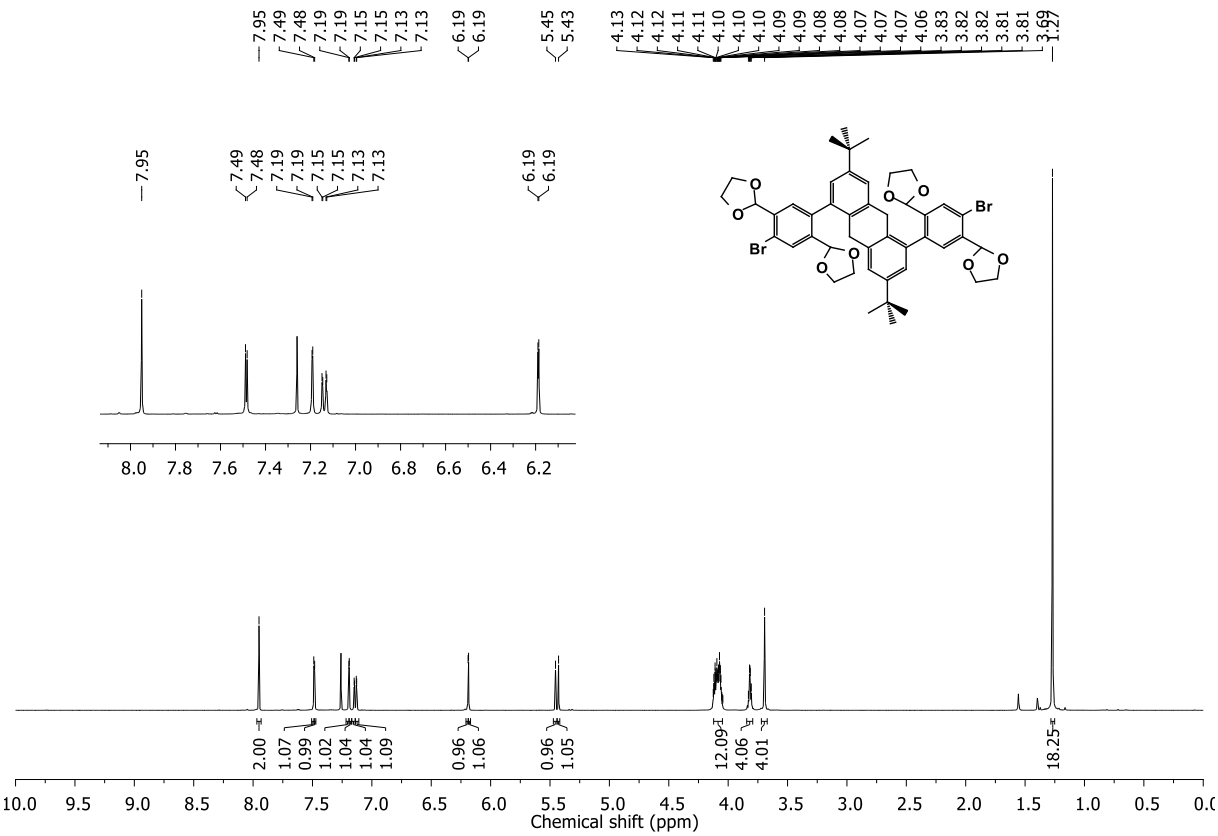

Figure 7.159 ^{1}H NMR spectrum (600 MHz, $CDCl_3$) of **249**.

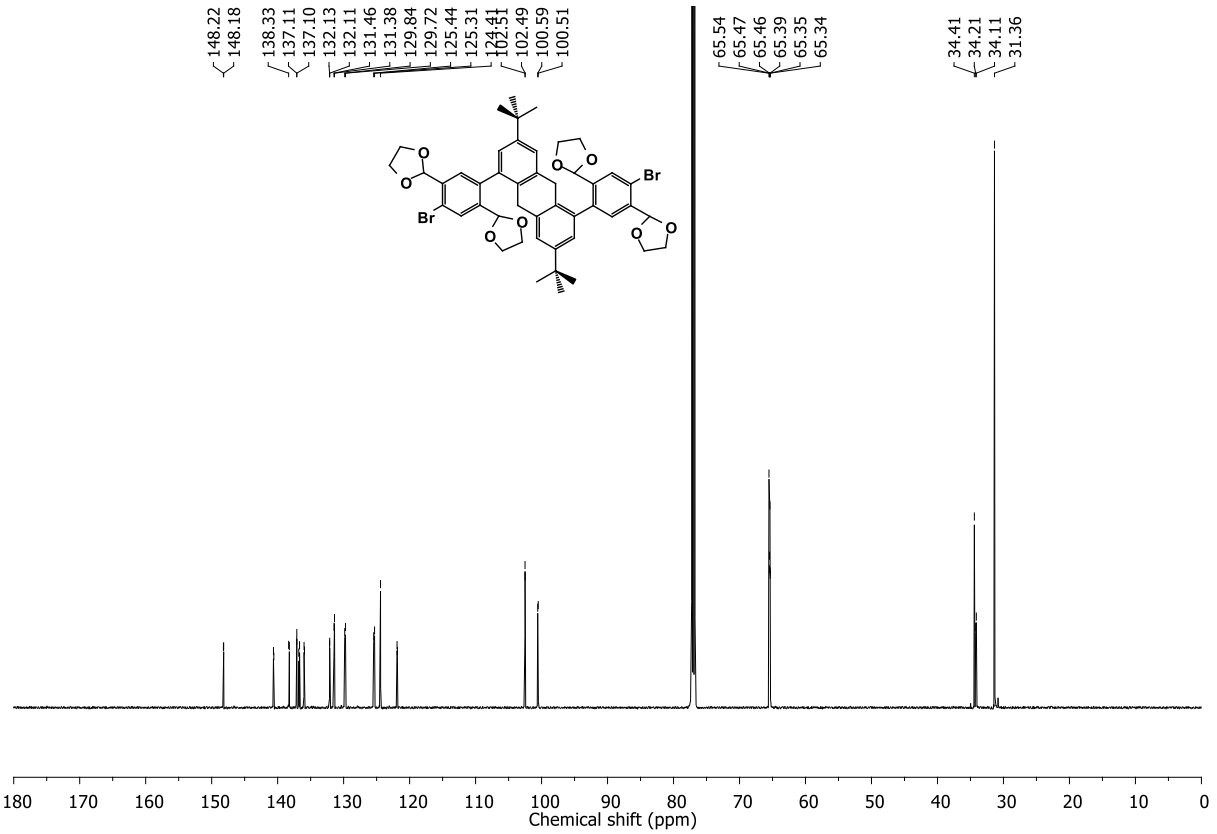

Figure 7.160 ^{13}C NMR spectrum (151 MHz, $CDCl_3$) of **249**.

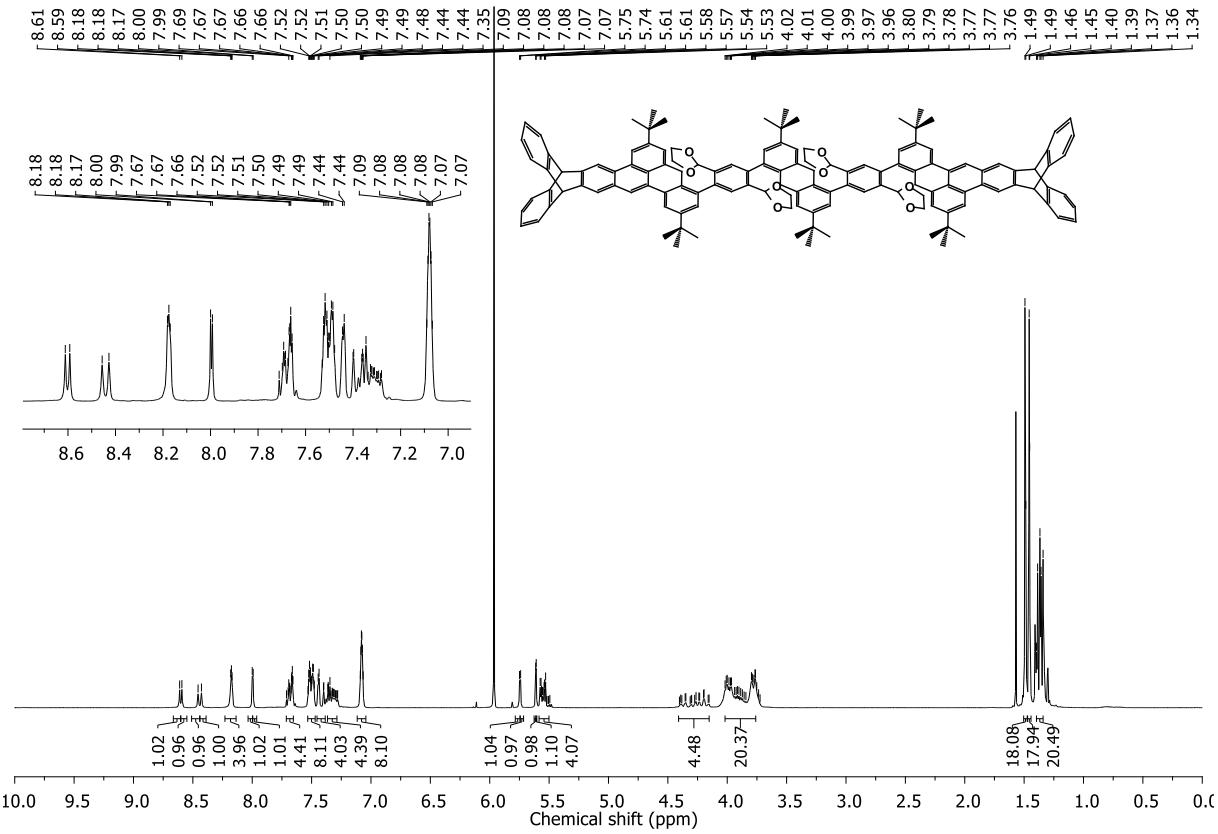

Figure 7.161 ^{1}H NMR spectrum (600 MHz, $Cl_2CDCDCl_2$) of **251**.

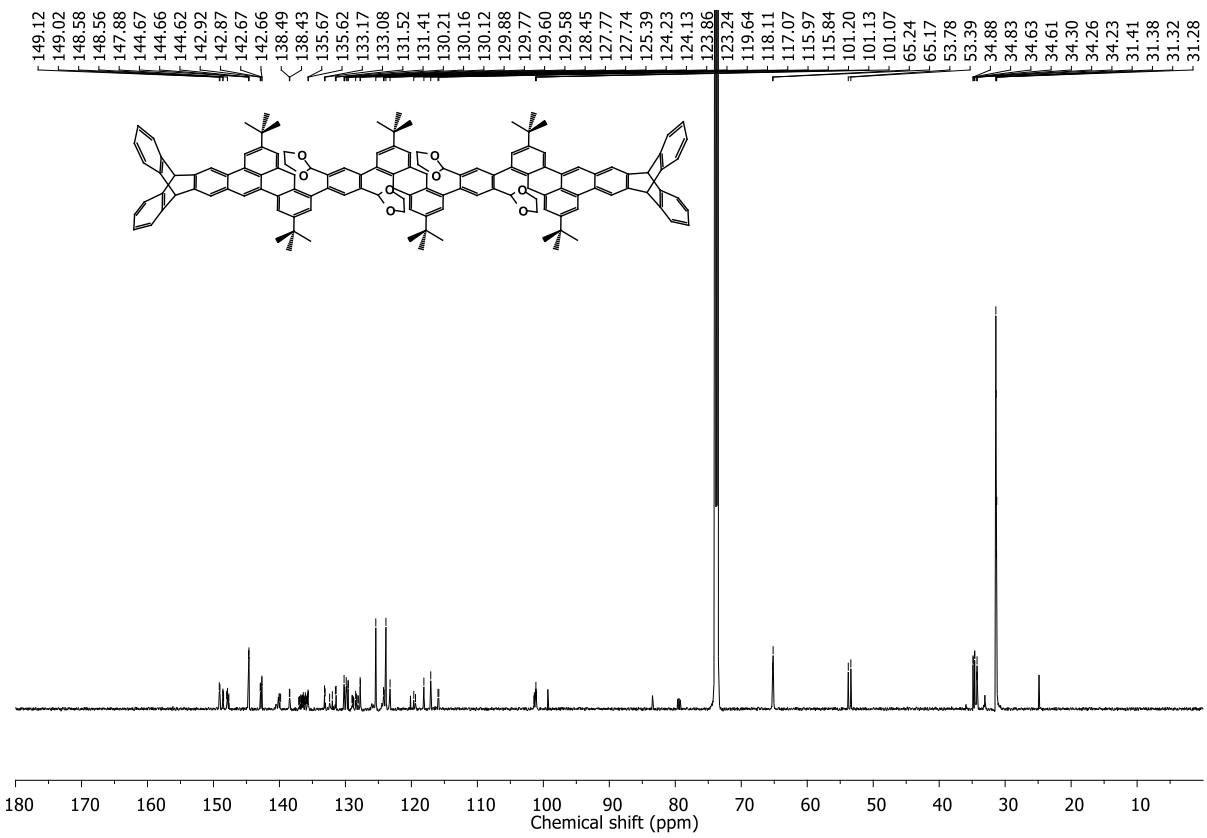

Figure 7.162 ^{13}C NMR spectrum (151 MHz, $Cl_2CDCDCl_2$) of **251**.

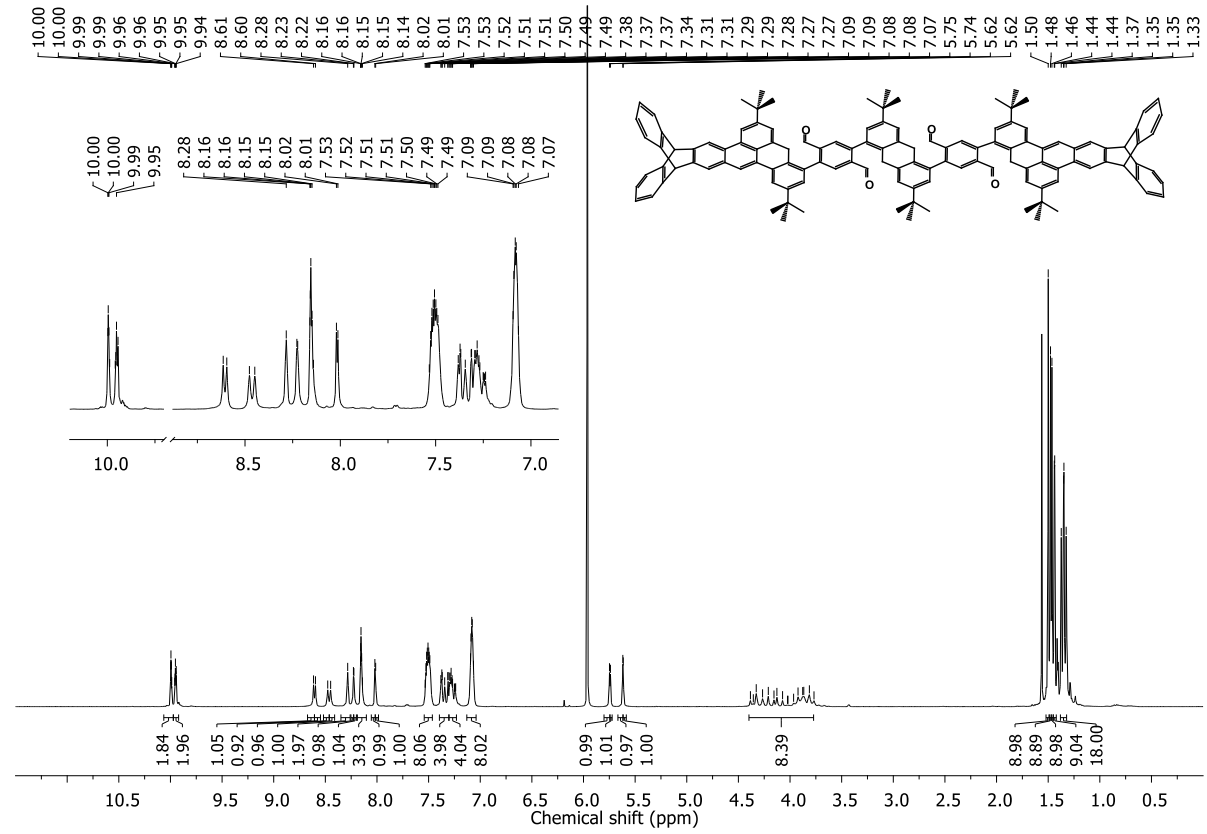

Figure 7.163 ^{1}H NMR spectrum (400 MHz, $Cl_2CDCDCl_2$) of **252**.

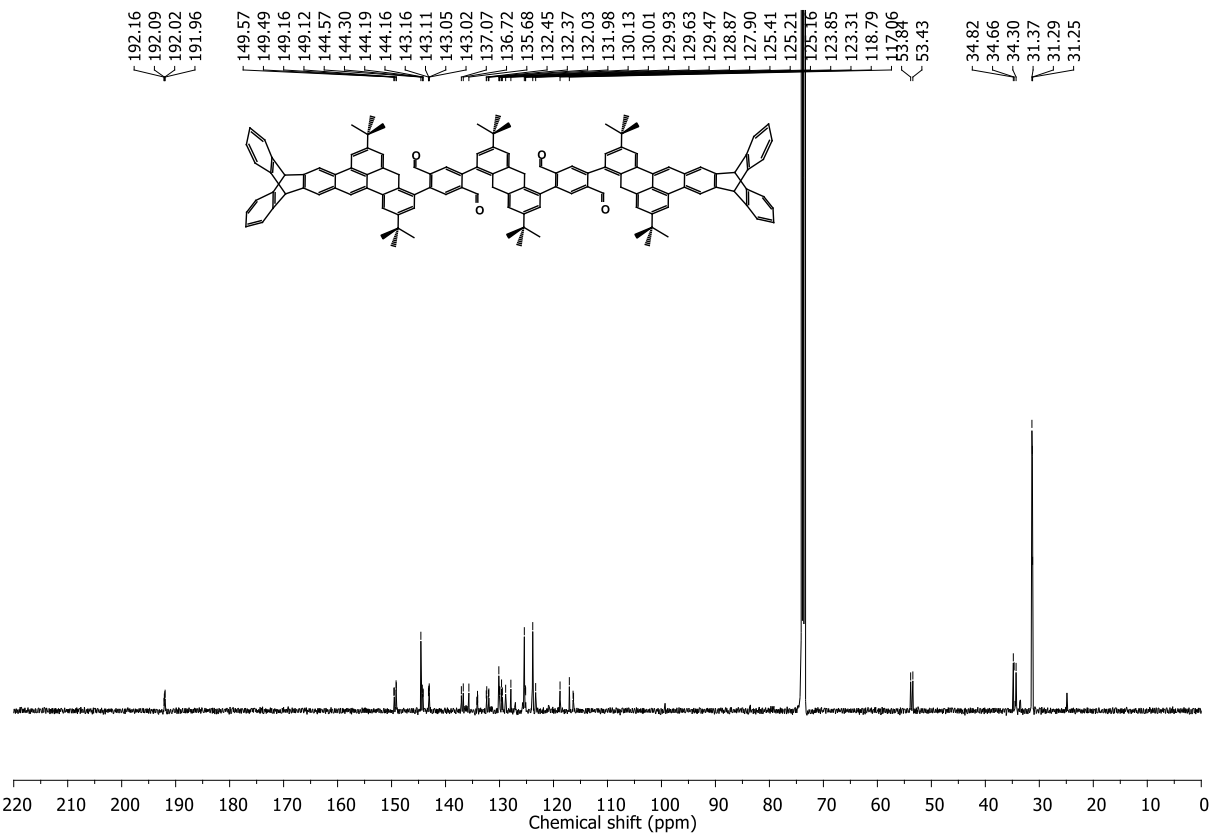

Figure 7.164 ^{13}C NMR spectrum (101 MHz, $Cl_2CDCDCl_2$) of **252**.

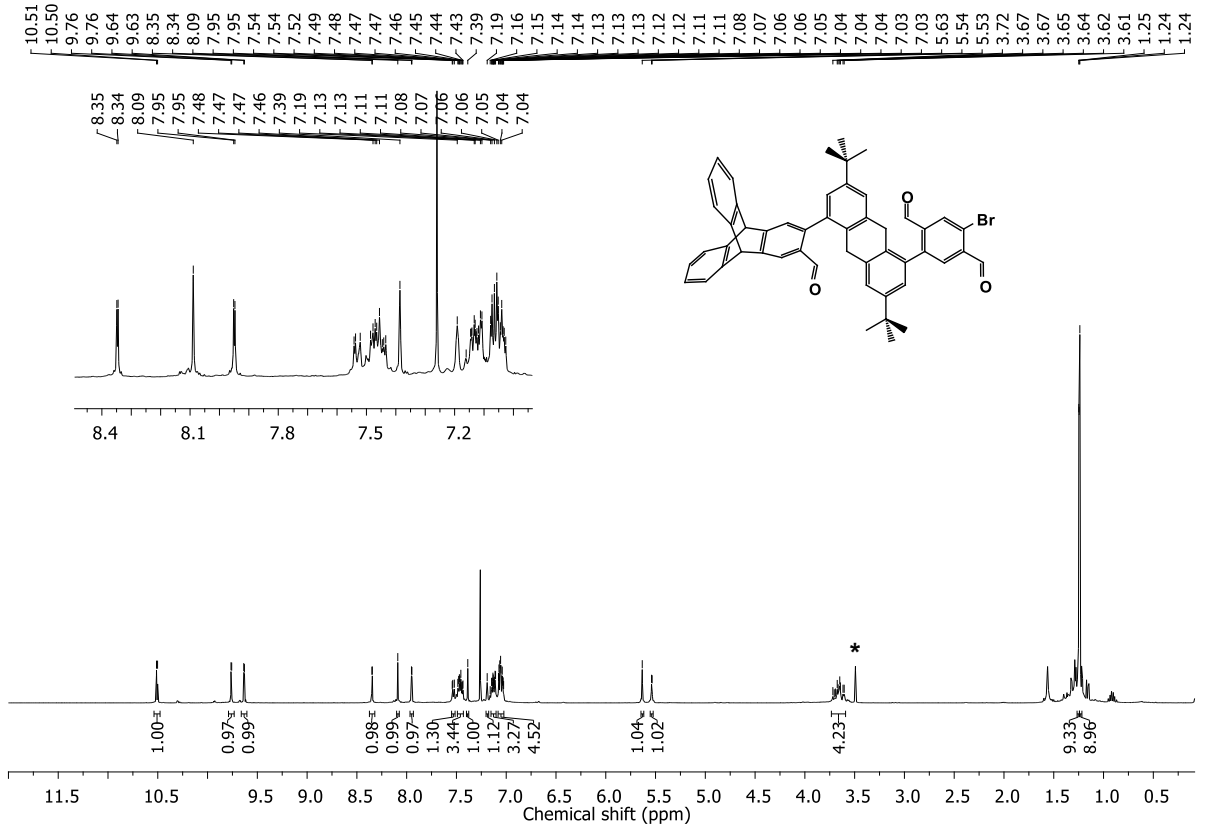

Figure 7.165 ^{1}H NMR spectrum (400 MHz, $CDCl_3$) of **253**. *MeOH.

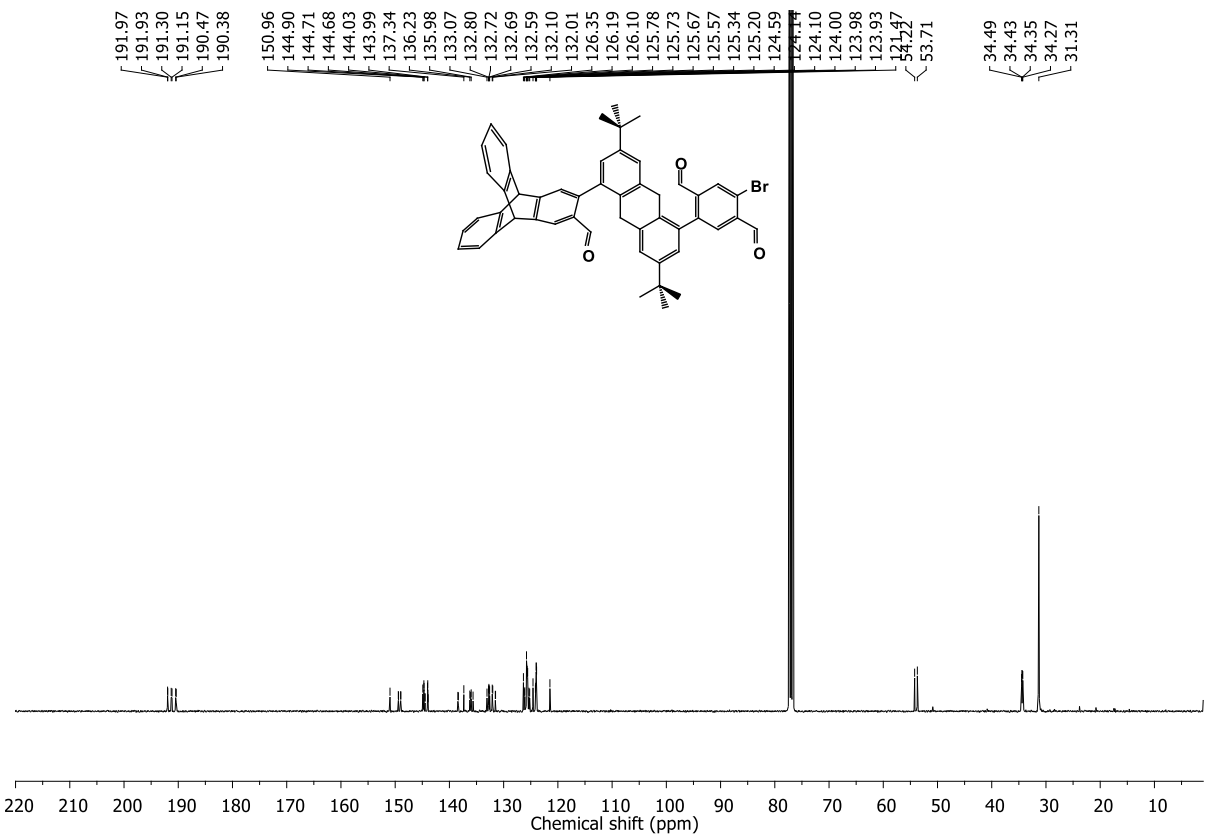

Figure 7.166 ^{13}C NMR spectrum (101 MHz, $CDCl_3$) of **253**.

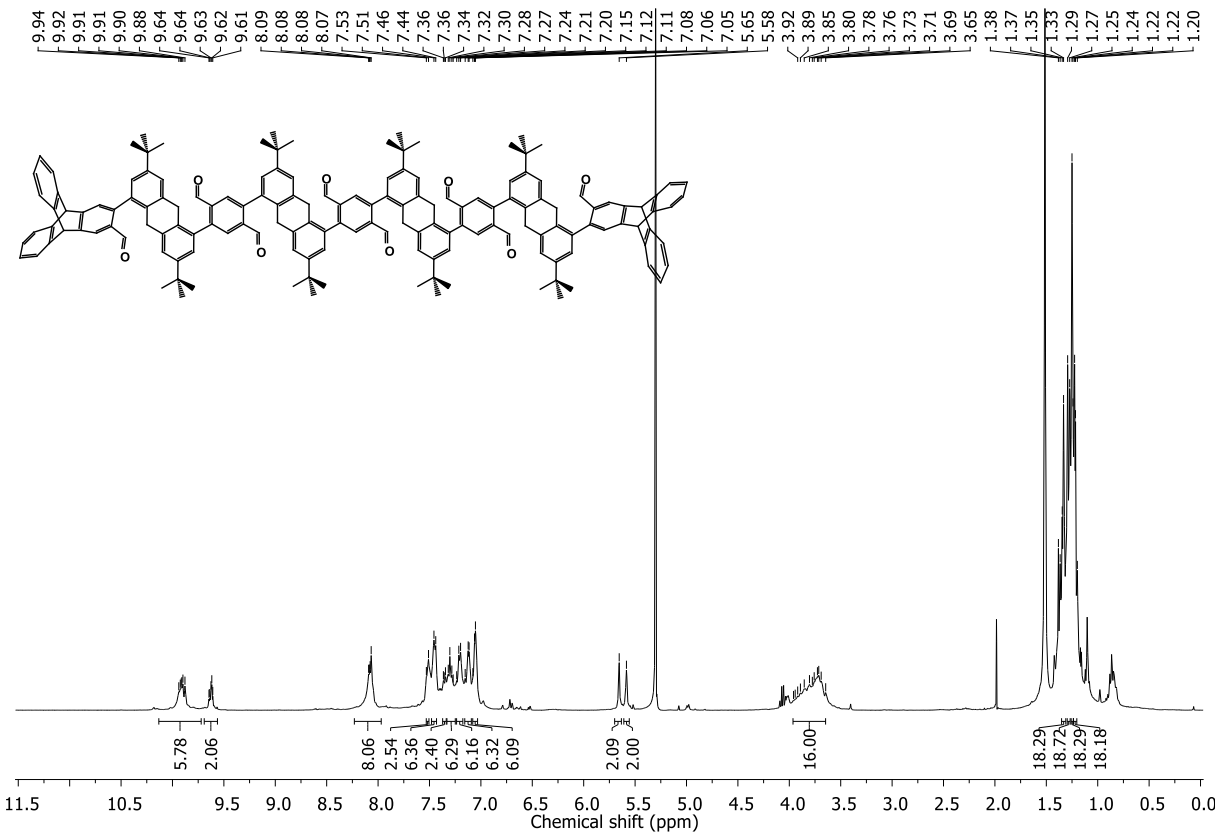

Figure 7.167 ^{1}H NMR spectrum (400 MHz, CD_2Cl_2) of **254**.

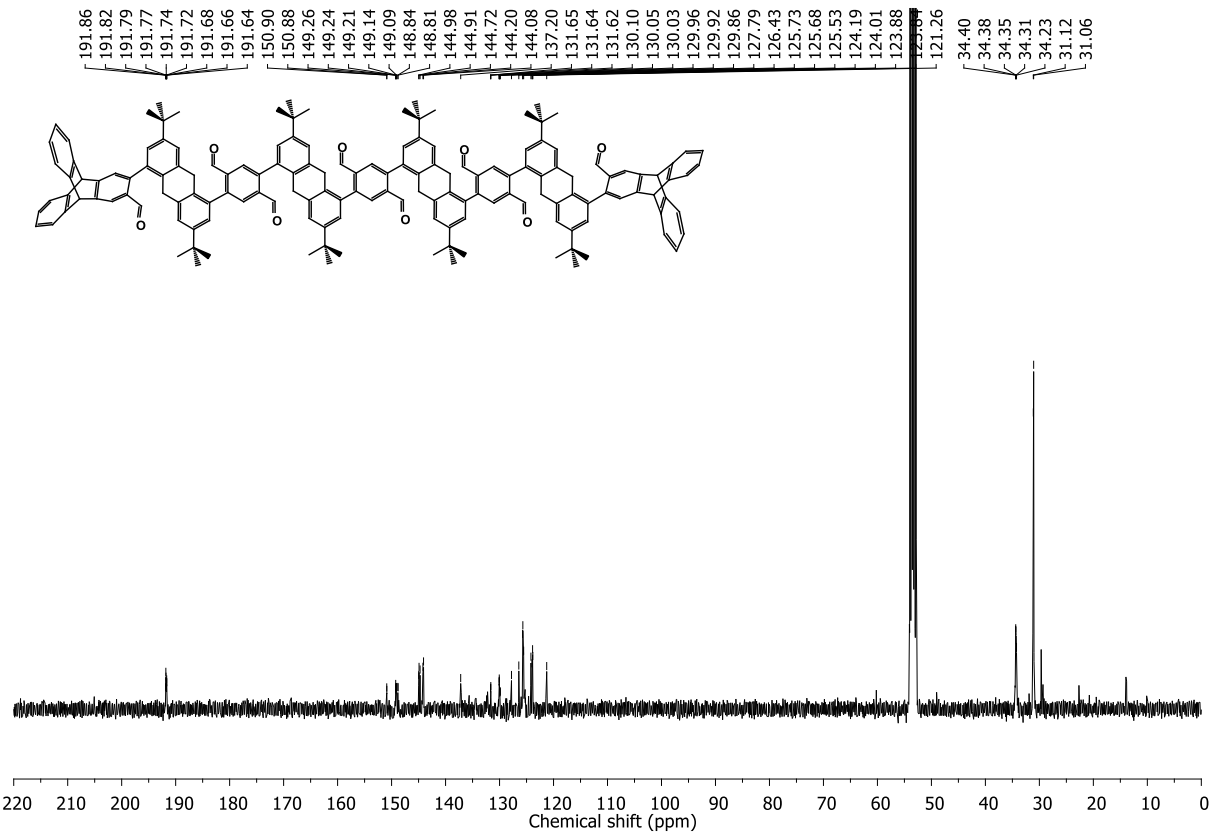

Figure 7.168 ^{13}C NMR spectrum (101 MHz, CD_2Cl_2) of **254**.

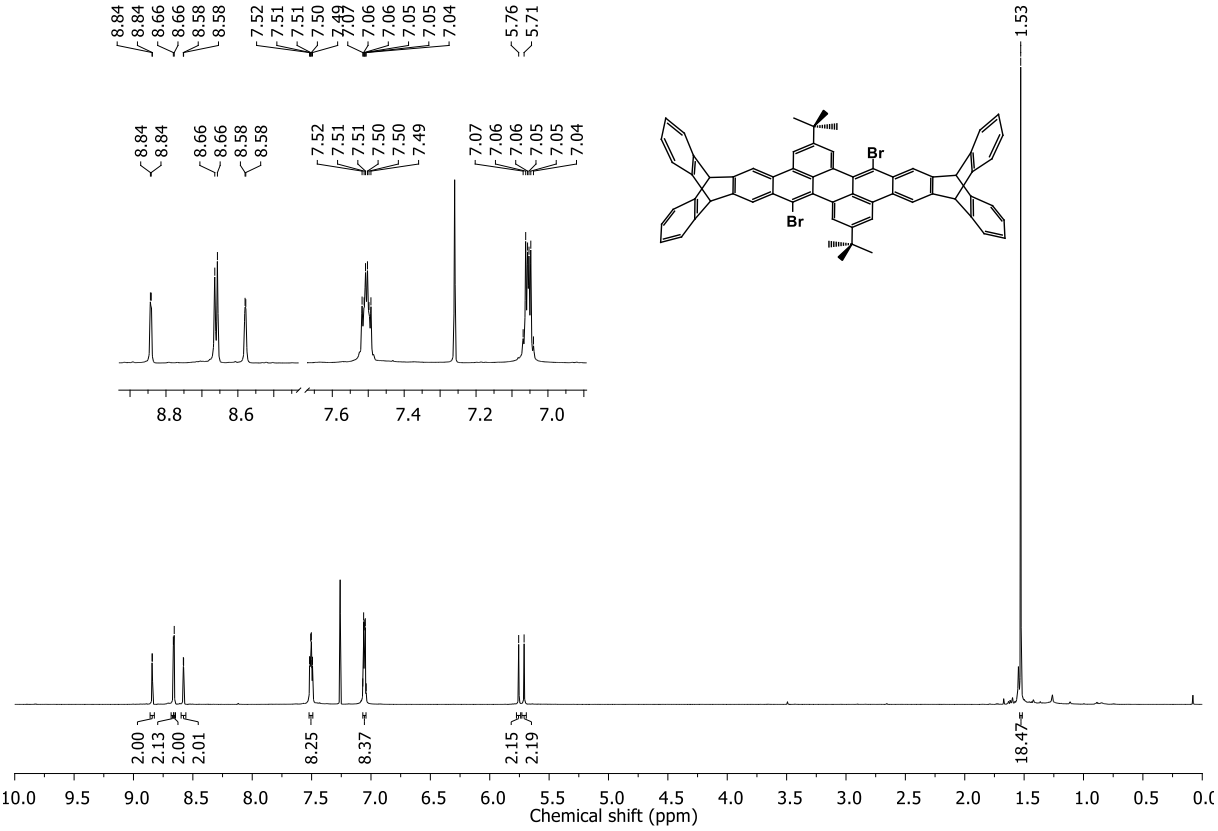

Figure 7.169 ^{1}H NMR spectrum (600 MHz, $CDCl_3$) of **255**.

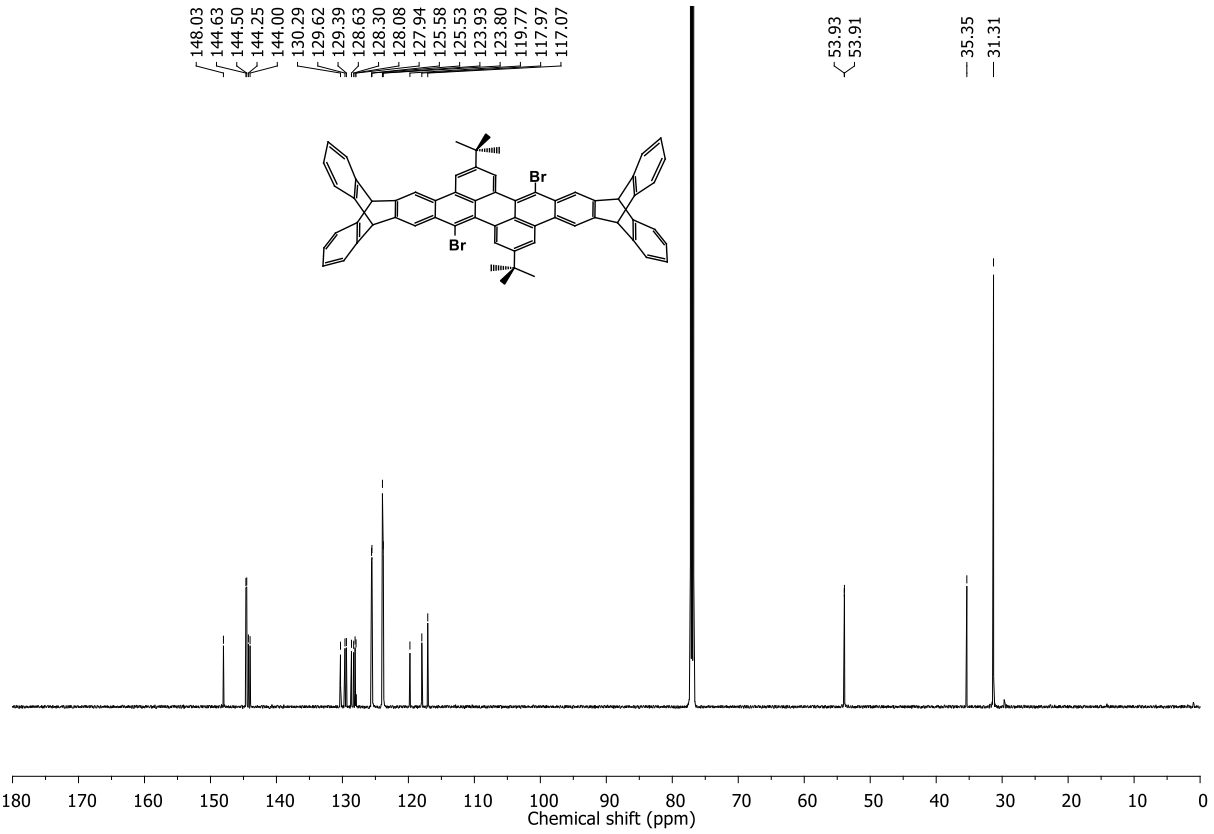

Figure 7.170 ^{13}C NMR spectrum (151 MHz, $CDCl_3$) of **255**.

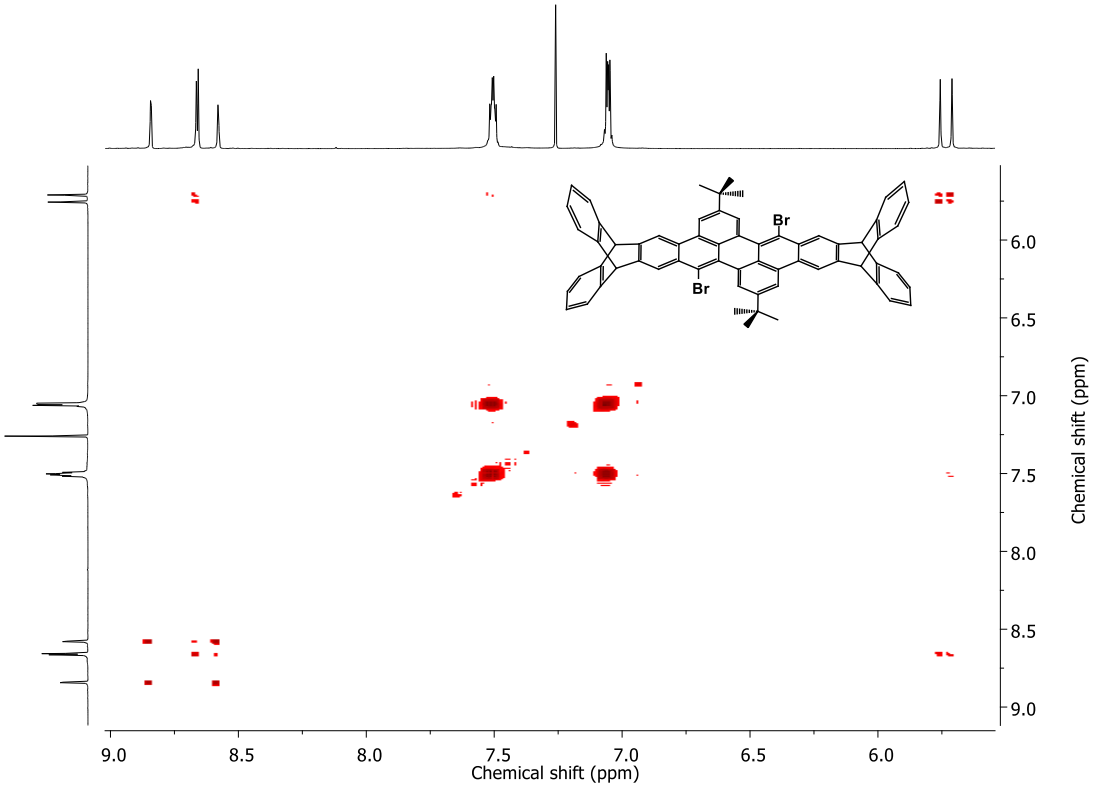

Figure 7.171 ^{1}H-^{1}H COSY NMR spectrum (600/600 MHz, $CDCl_3$) of **255**.

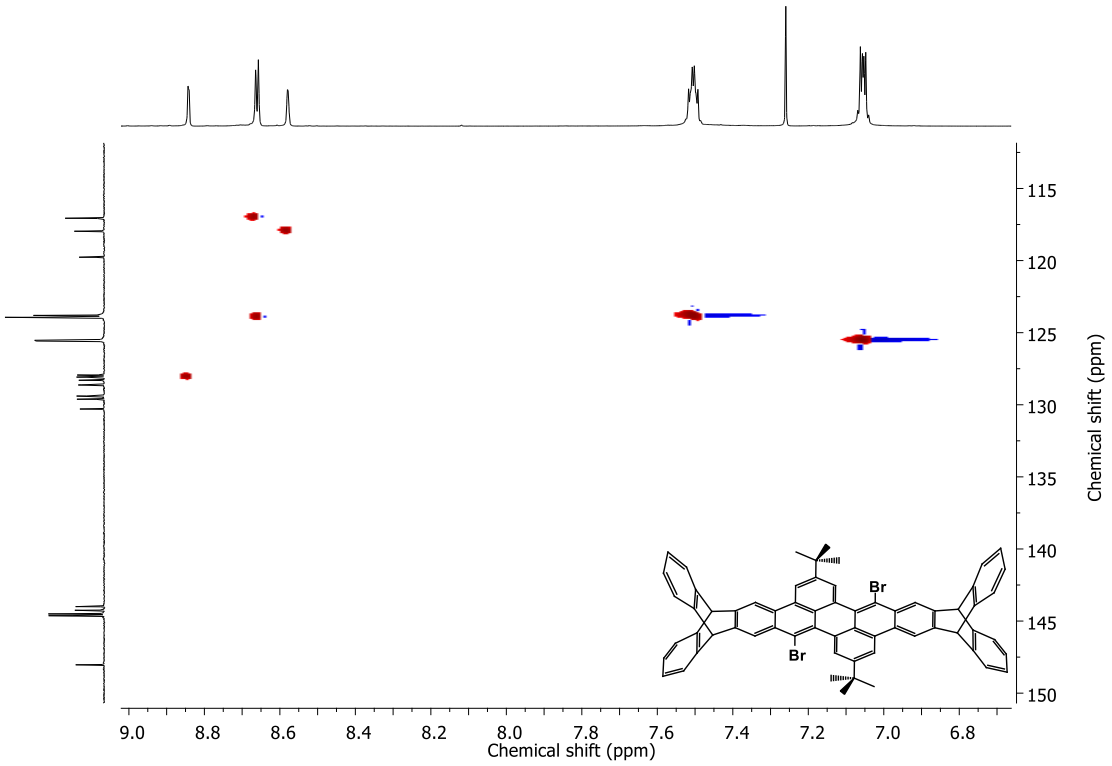

Figure 7.172 ^{1}H-^{13}C HSQC NMR spectrum (600/151 MHz, $CDCl_3$) of **255**.

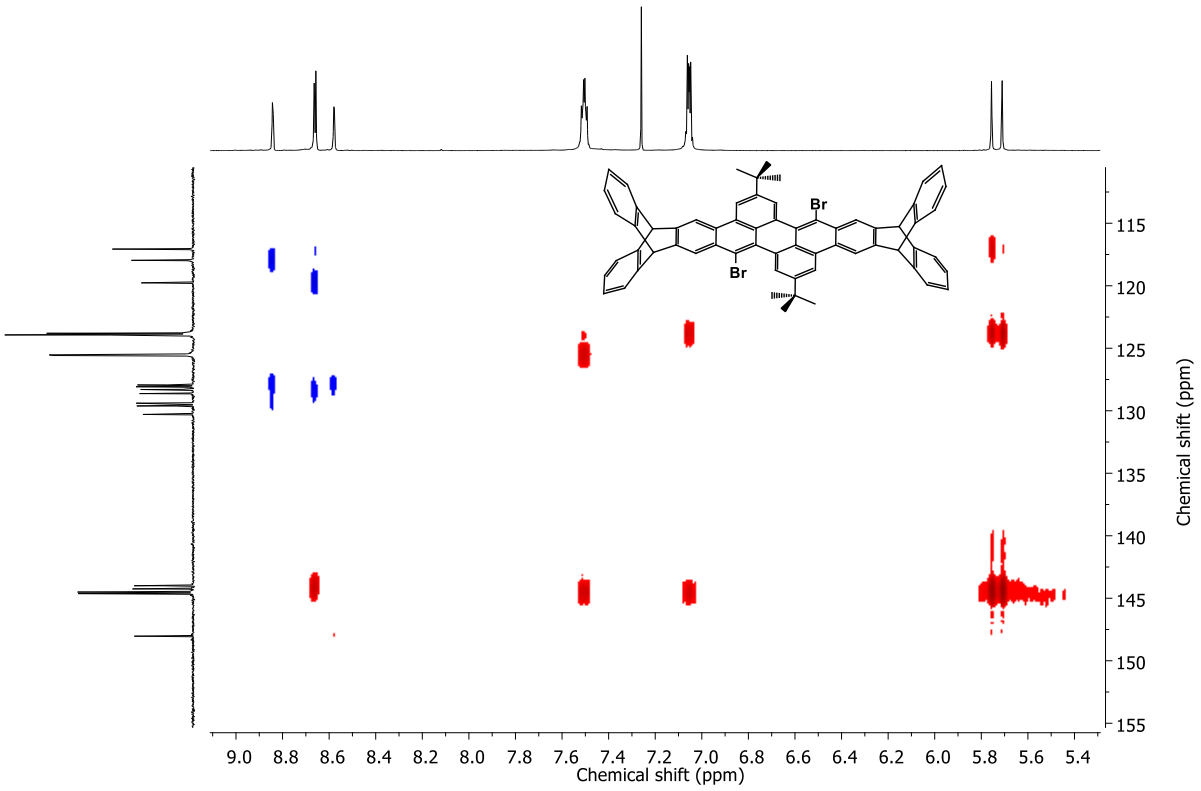

Figure 7.173 ^{1}H-^{13}C HMBC NMR spectrum (600/151 MHz, $CDCl_3$) of **255**.

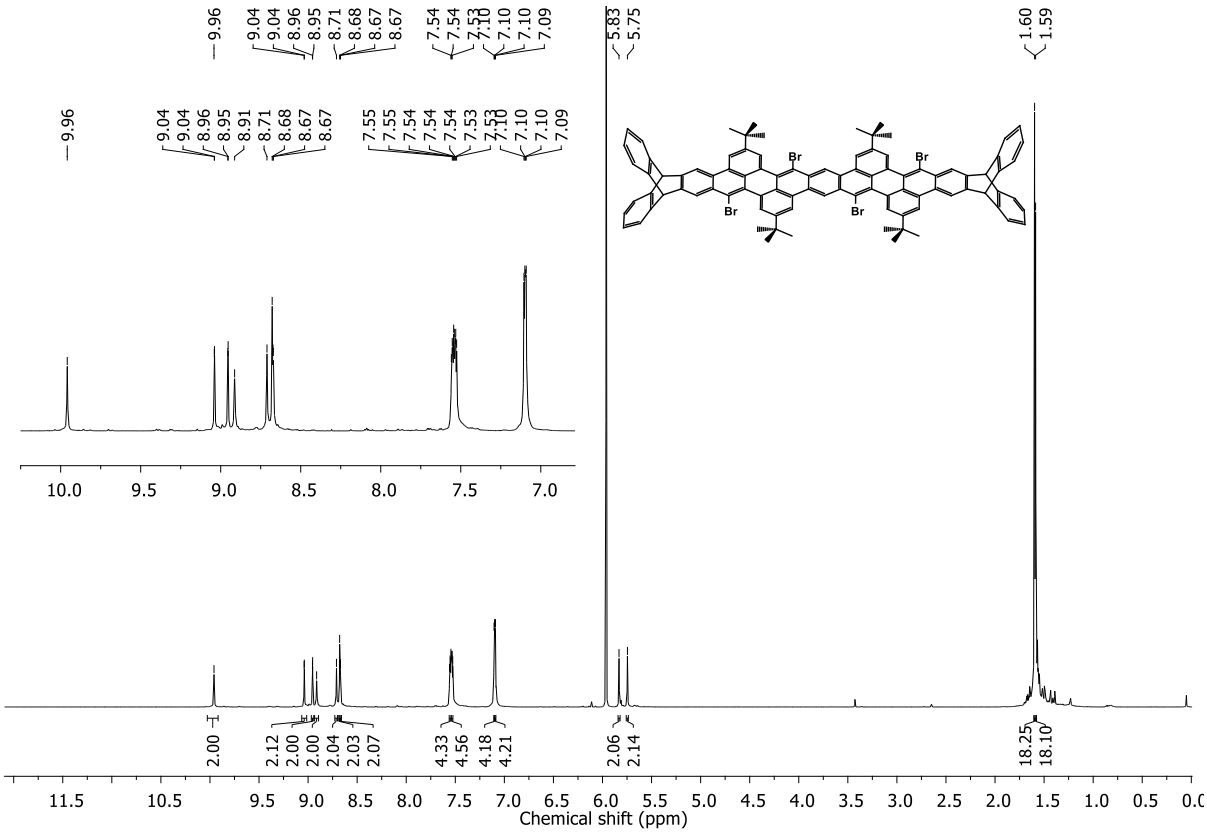

Figure 7.174 ^{1}H NMR spectrum (600 MHz, $Cl_2CDCDCl_2$) of **256**.

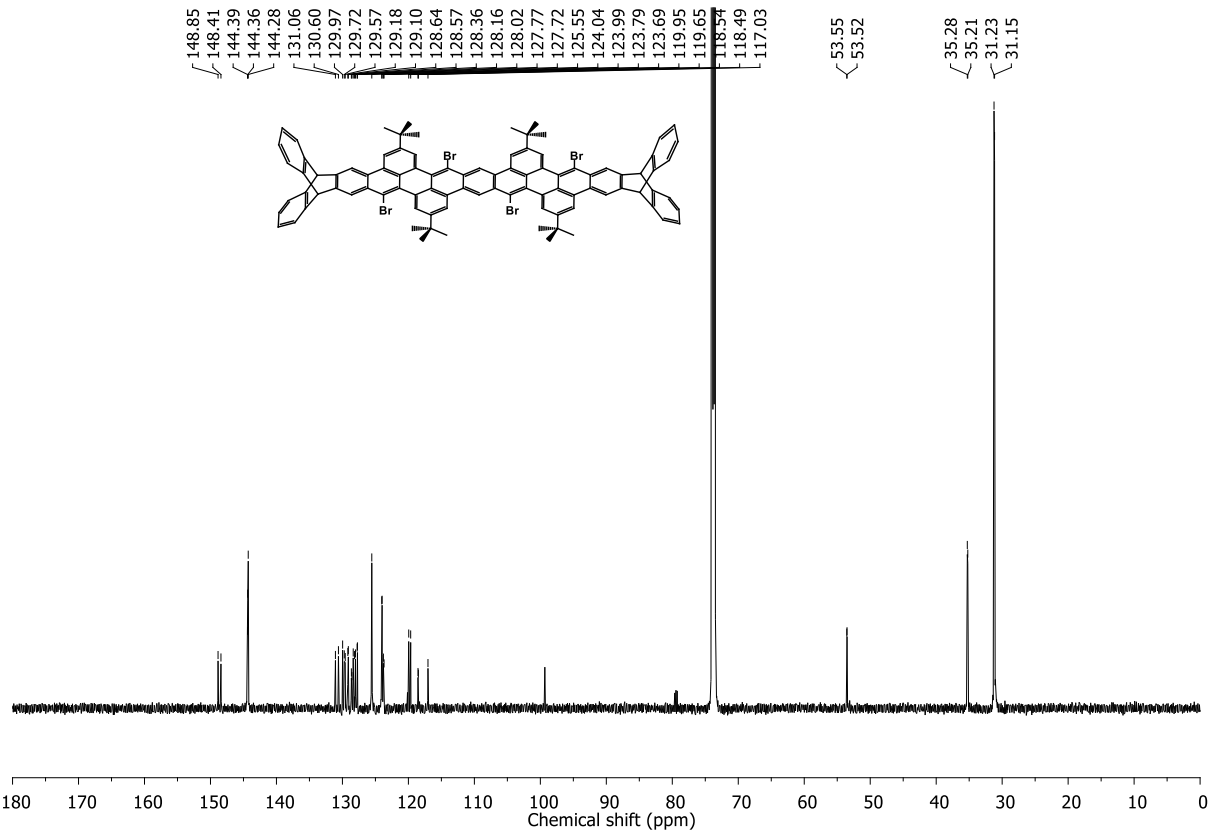

Figure 7.175 ^{13}C NMR spectrum (151 MHz, $Cl_2CDCDCl_2$) of **256**.

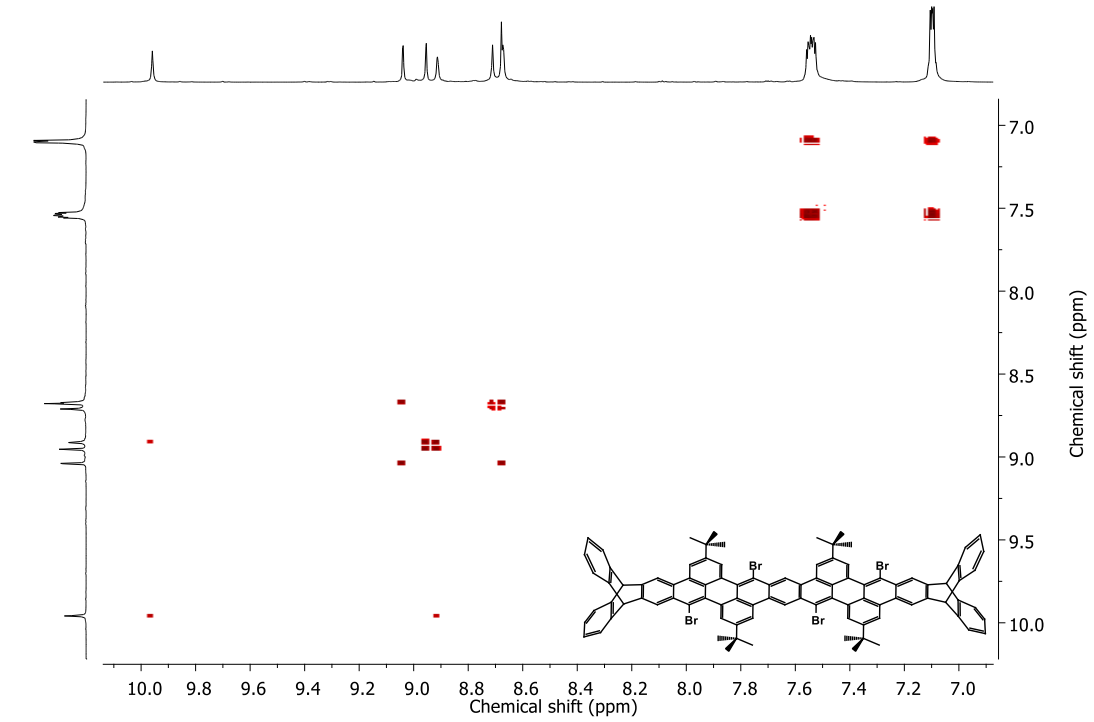

Figure 7.176 ^{1}H-^{1}H COSY NMR spectrum (600/600 MHz, $Cl_2CDCDCl_2$) of **256**.

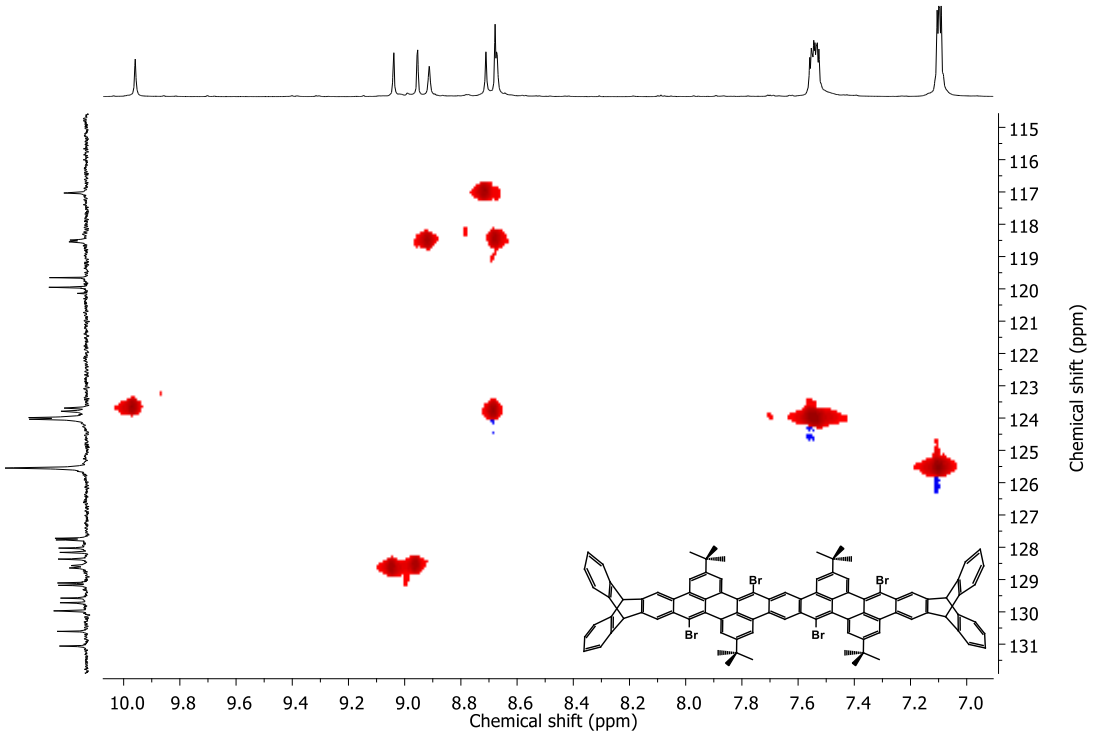

Figure 7.177 ^{1}H-^{13}C HSQC NMR spectrum (600/151 MHz, $Cl_2CDCDCl_2$) of **256**.

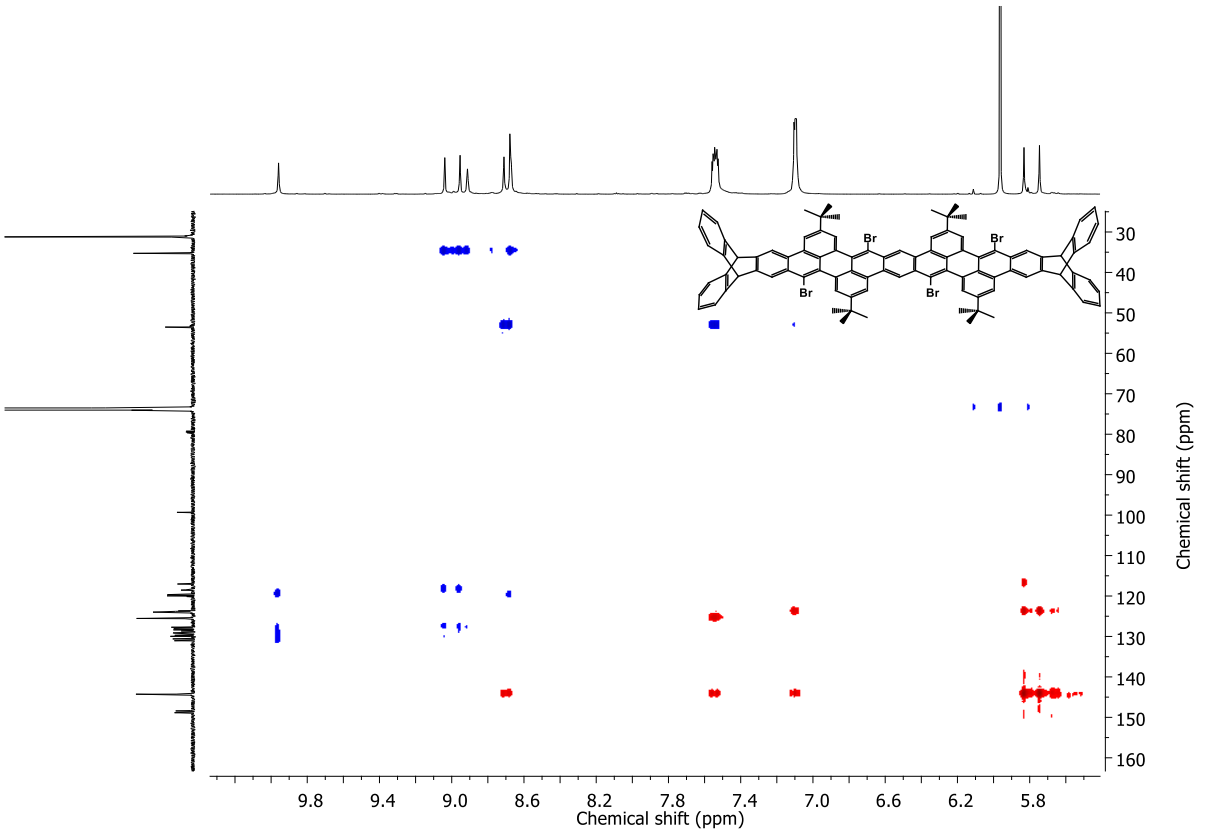

Figure 7.178 ^{1}H-^{13}C HMBC NMR spectrum (600/151 MHz, $Cl_2CDCDCl_2$) of **256**.

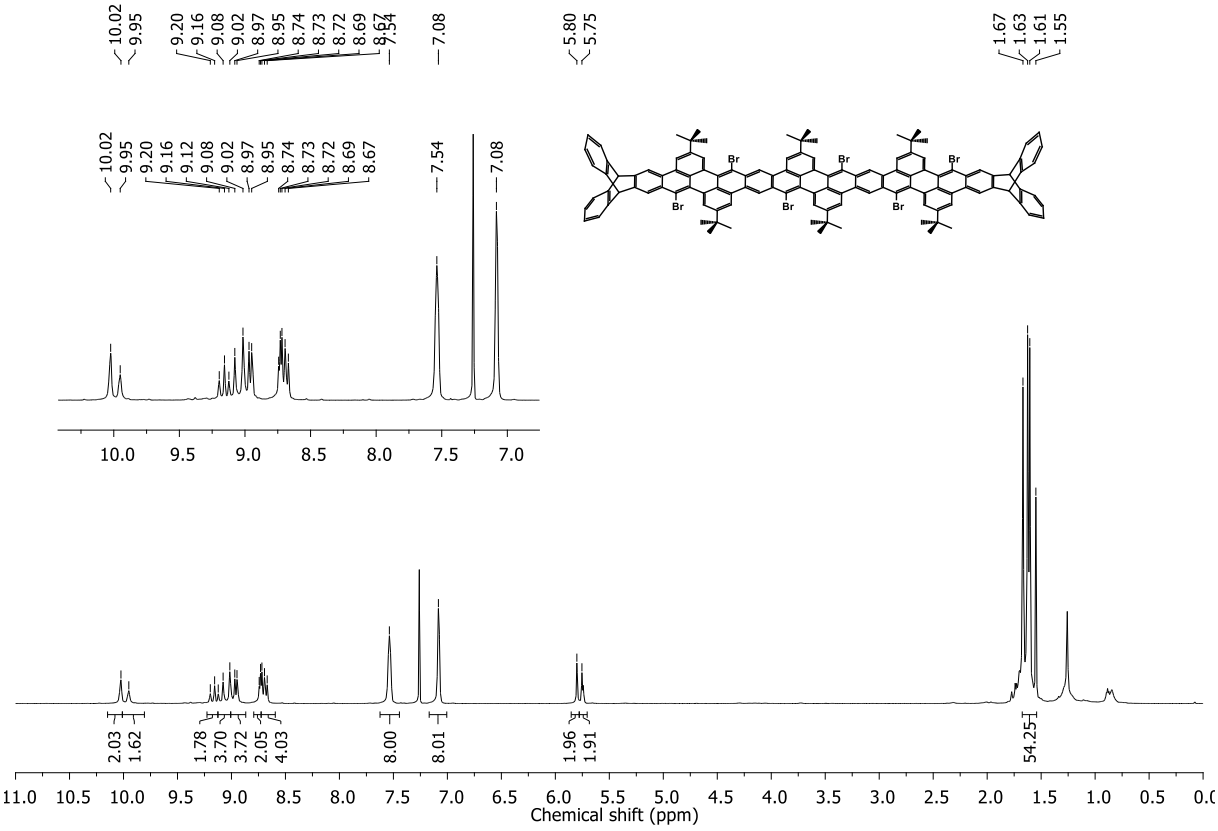

Figure 7.179 ^{1}H NMR spectrum (600 MHz, $CDCl_3$) of **257**.

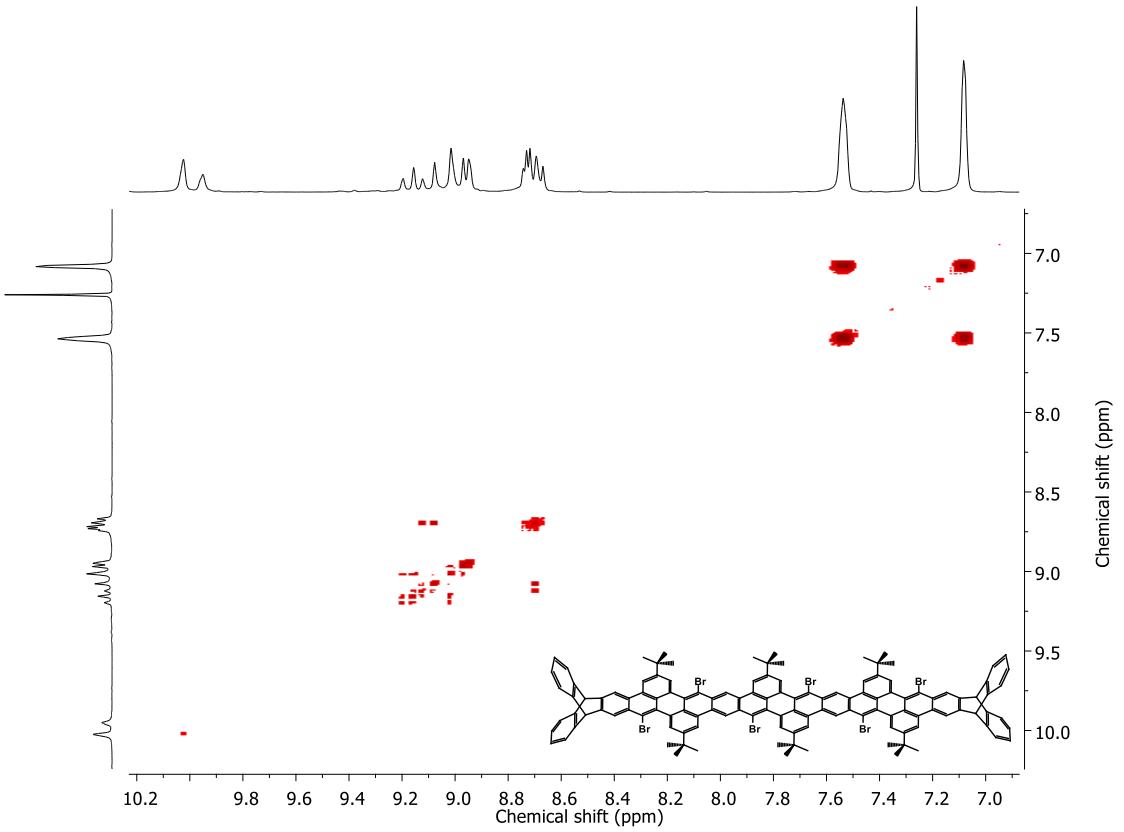

Figure 7.180 ^{1}H-^{1}H COSY NMR spectrum (600/600 MHz, $CDCl_3$) of **257**.

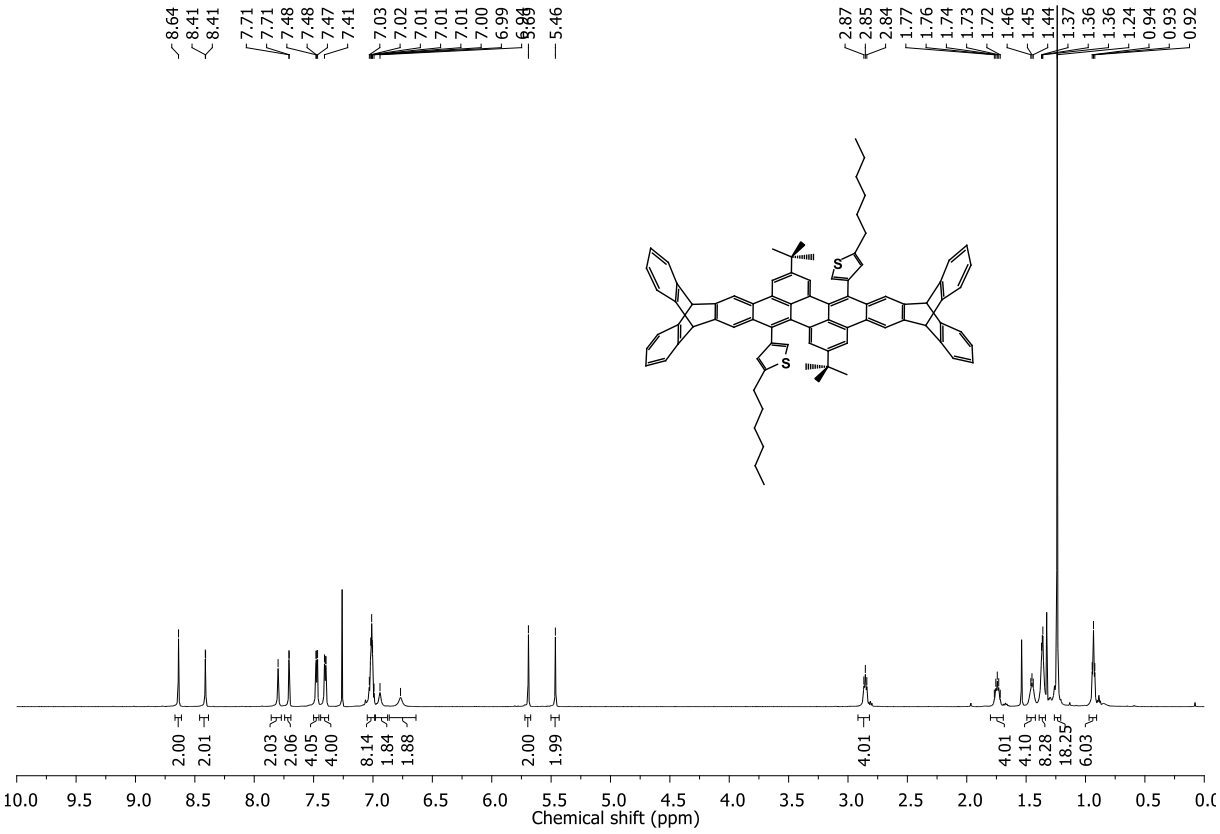

Figure 7.181 ^{1}H NMR spectrum (600 MHz, $CDCl_3$) of **258**.

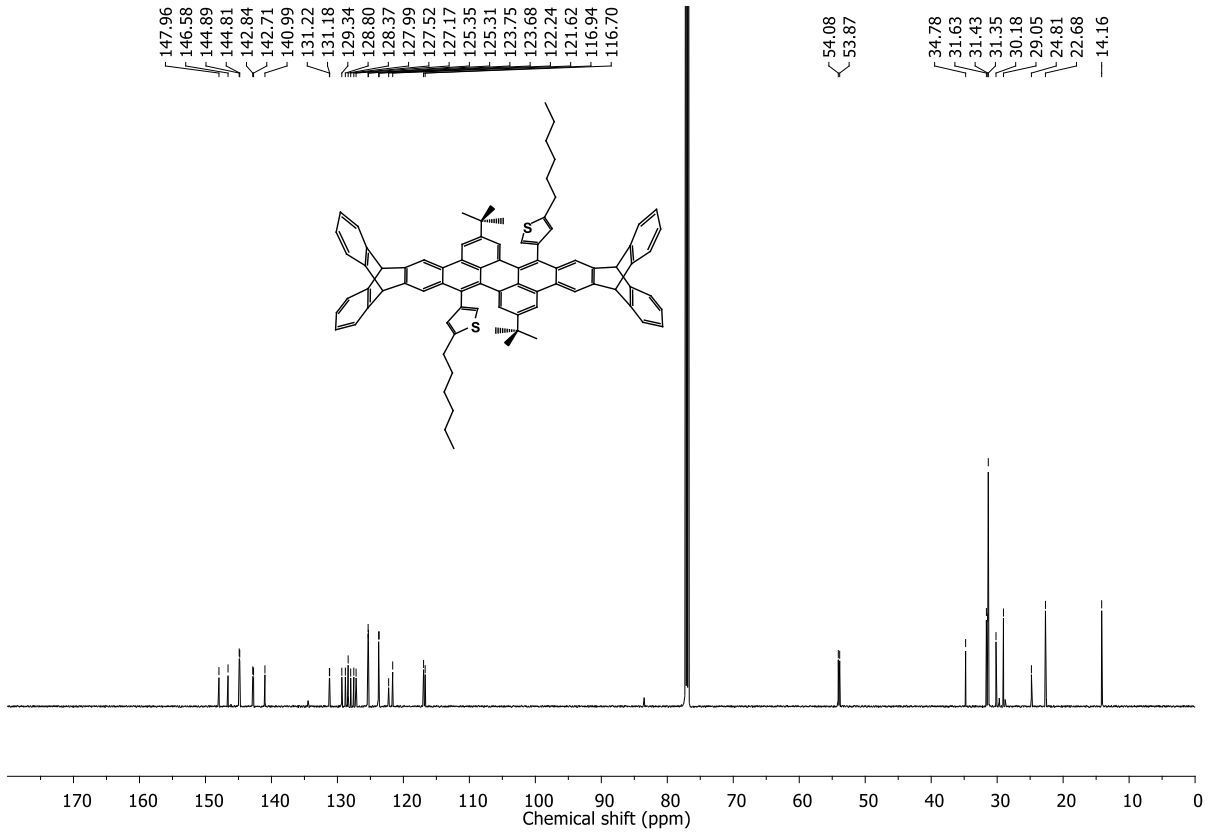

Figure 7.182 ^{13}C NMR spectrum (151 MHz, $CDCl_3$) of **258**.

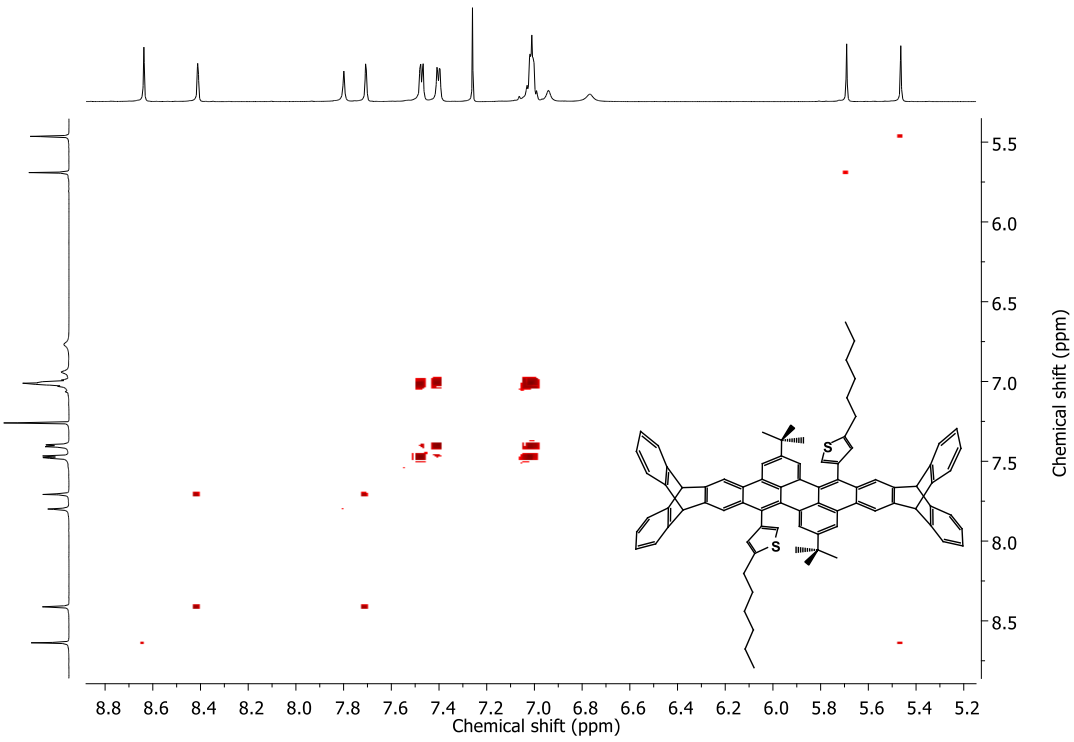

Figure 7.183 ^{1}H-^{1}H COSY NMR spectrum (600/600 MHz, $CDCl_3$) of **258**.

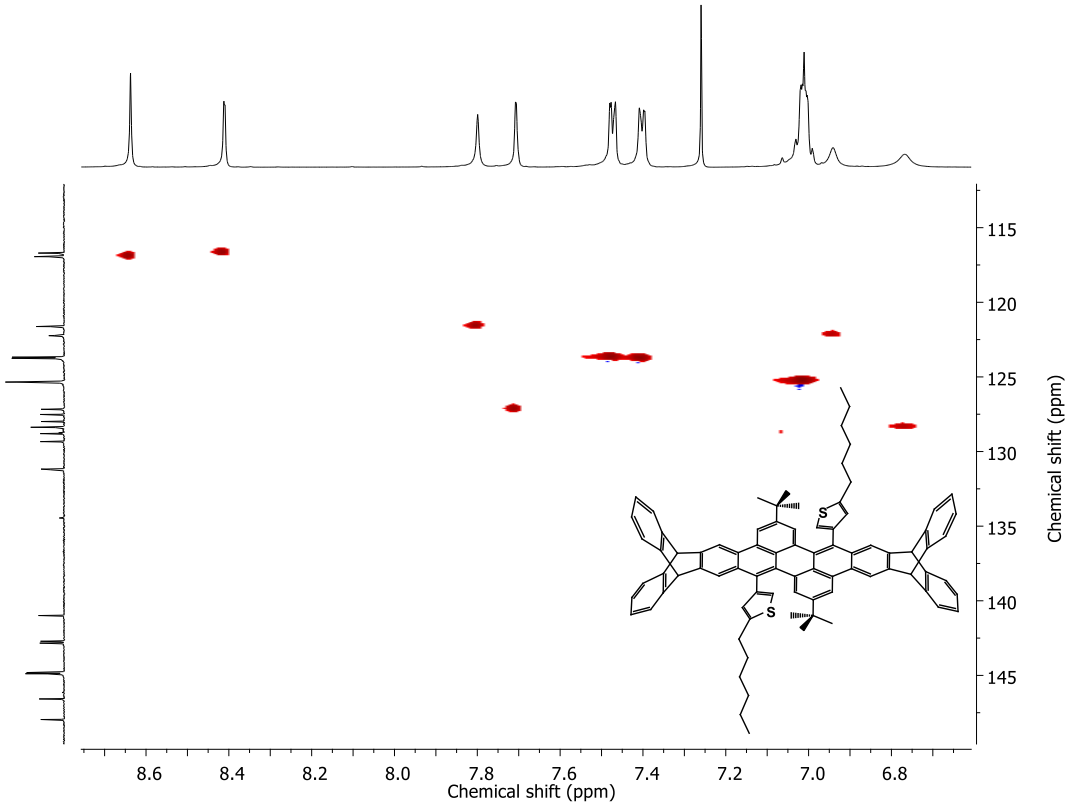

Figure 7.184 ^{1}H-^{13}C HSQC NMR spectrum (600/151 MHz, $CDCl_3$) of **258**.

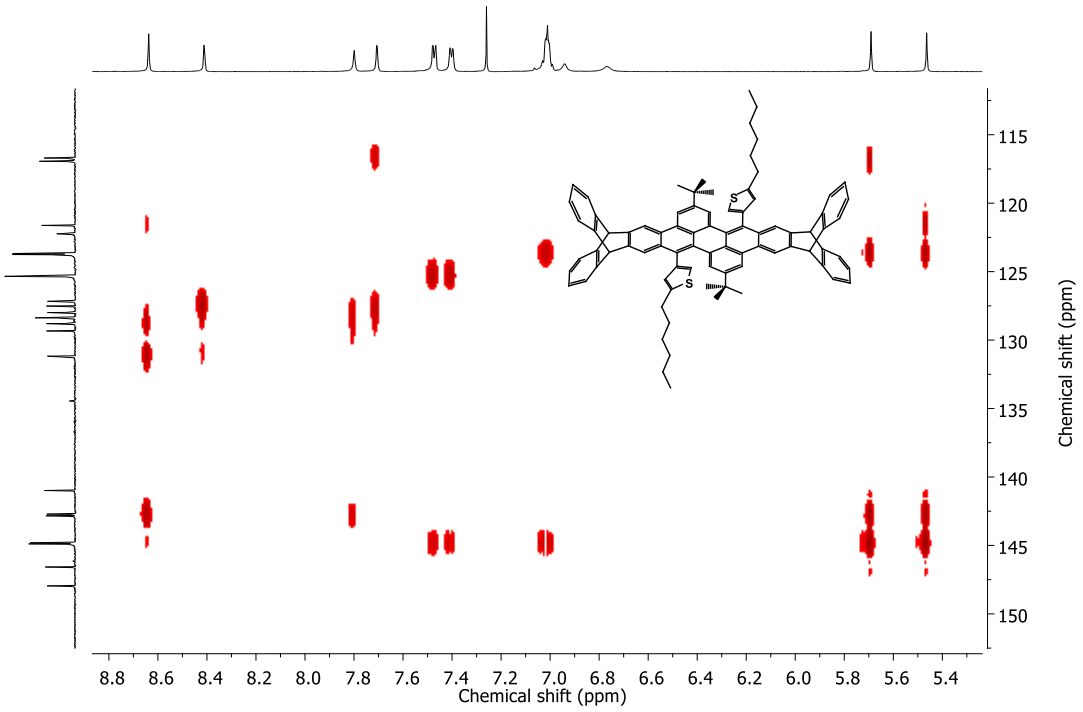

Figure 7.185 ^{1}H-^{13}C HMBC NMR spectrum (600/151 MHz, $CDCl_3$) of **258**.

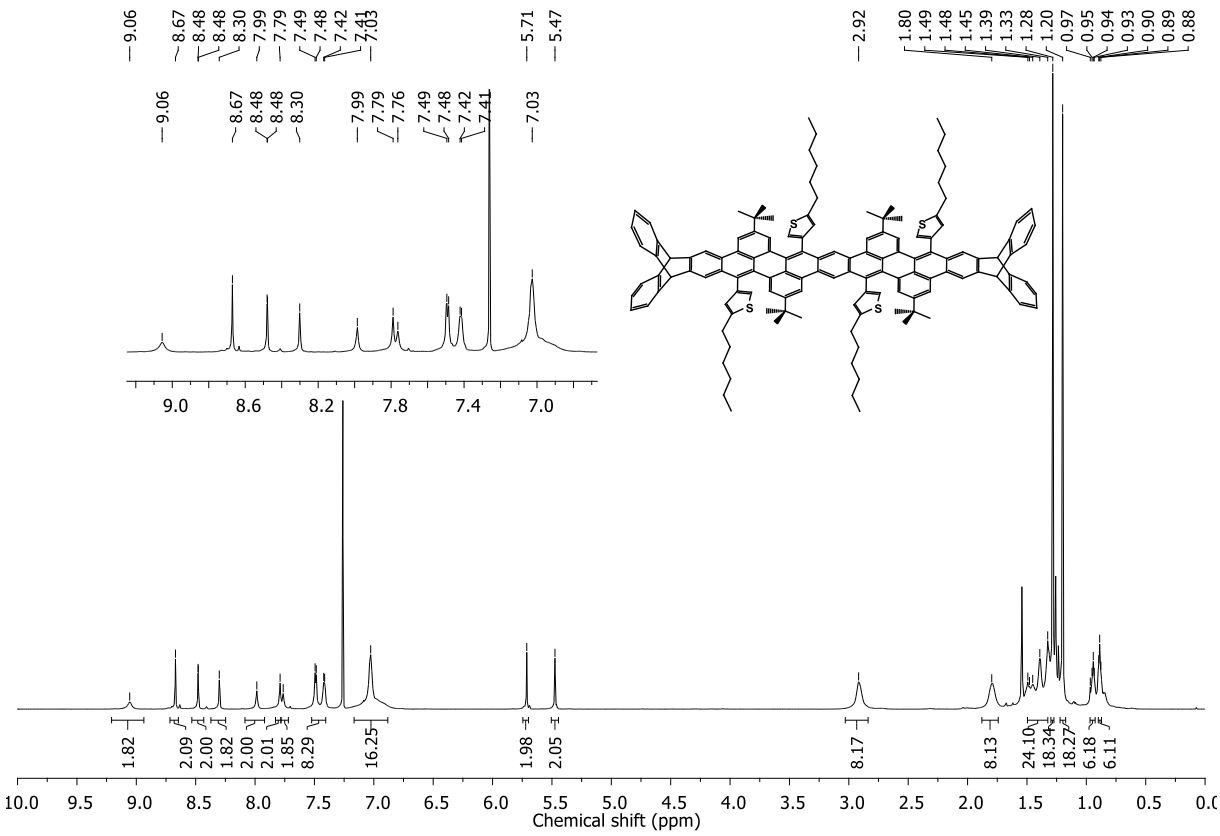

Figure 7.186 ^{1}H NMR spectrum (600 MHz, $CDCl_3$) of **259**.

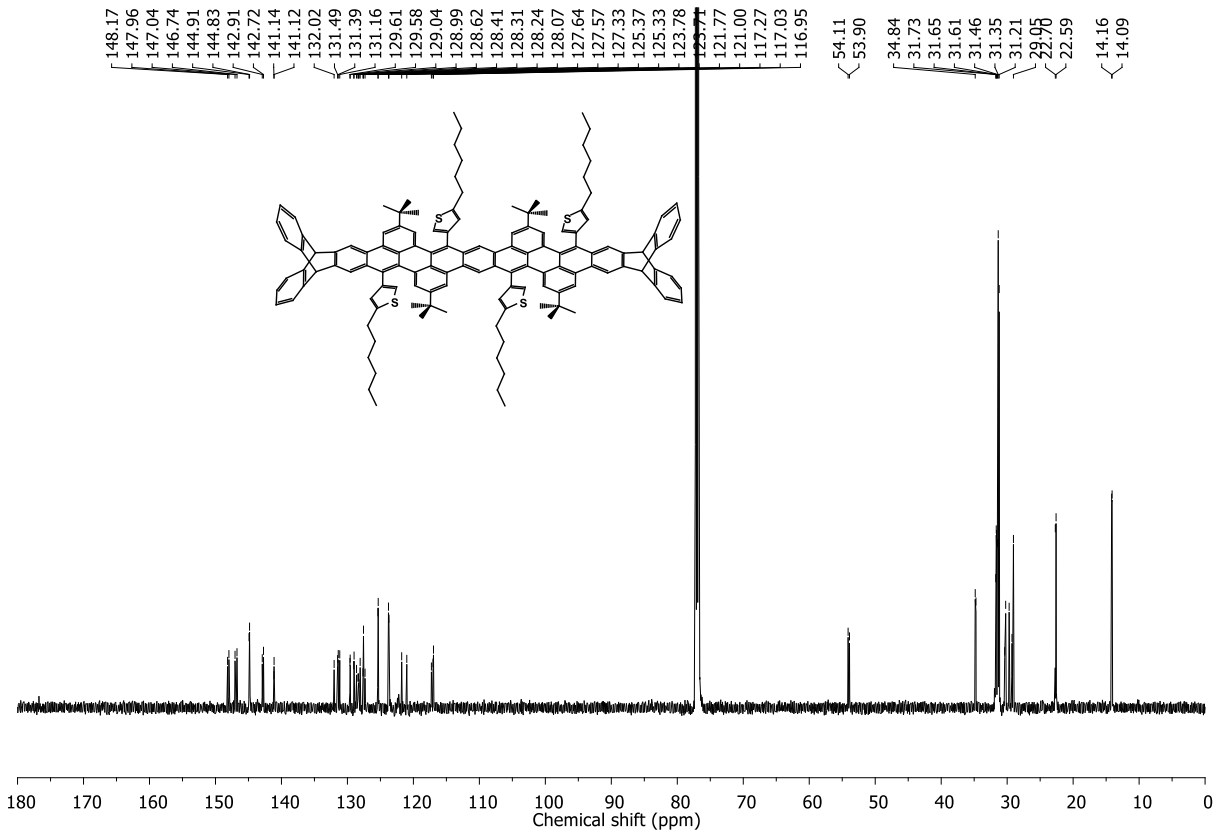

Figure 7.187 ^{13}C NMR spectrum (151 MHz, $CDCl_3$) of **259**.

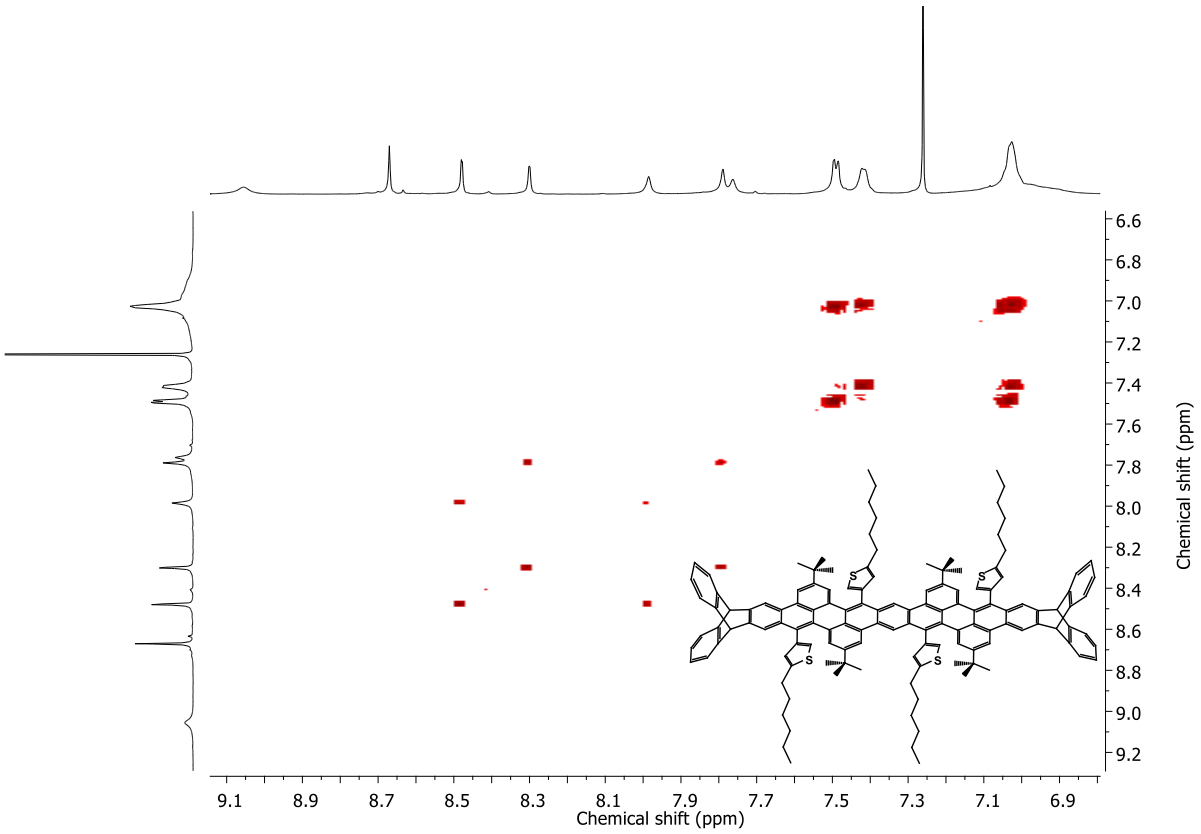

Figure 7.188 ^{1}H-^{1}H COSY NMR spectrum (600/600 MHz, $CDCl_3$) of **259**.

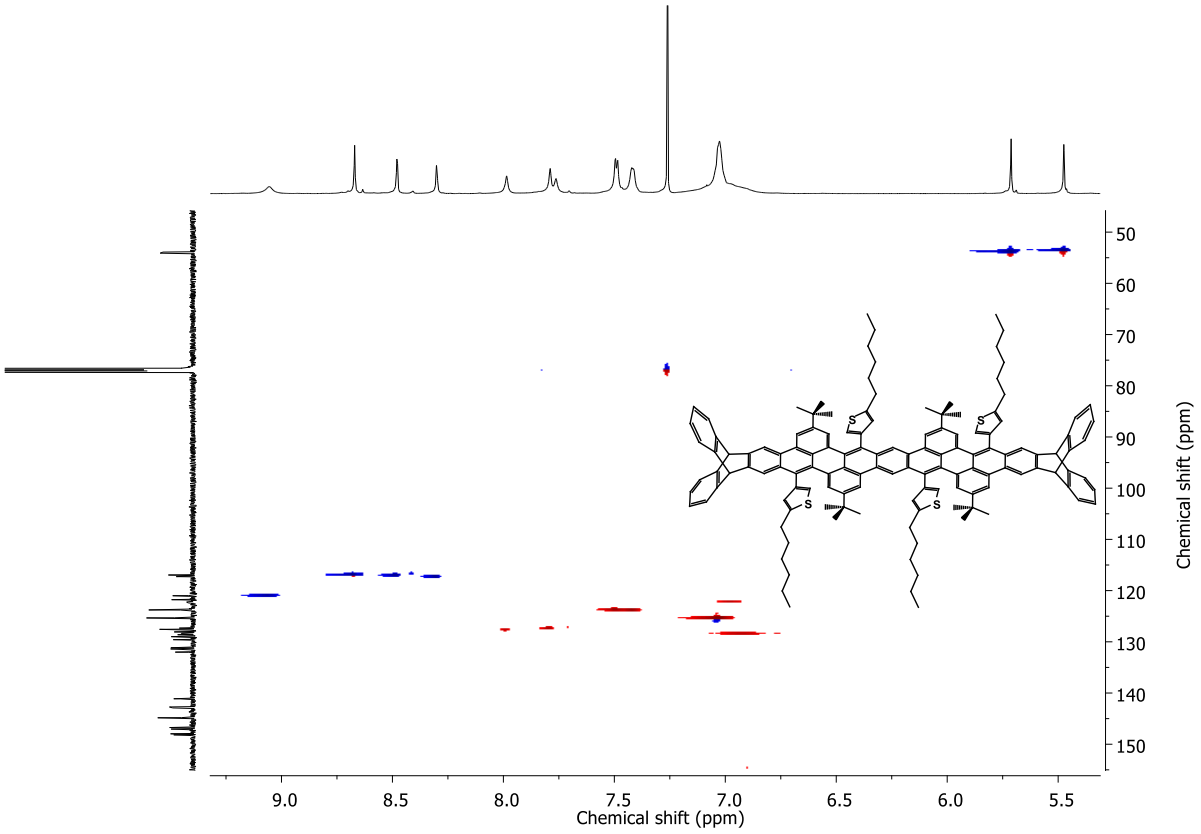

Figure 7.189 ^{1}H-^{13}C HSQC NMR spectrum (600/151 MHz, $CDCl_3$) of **259**.

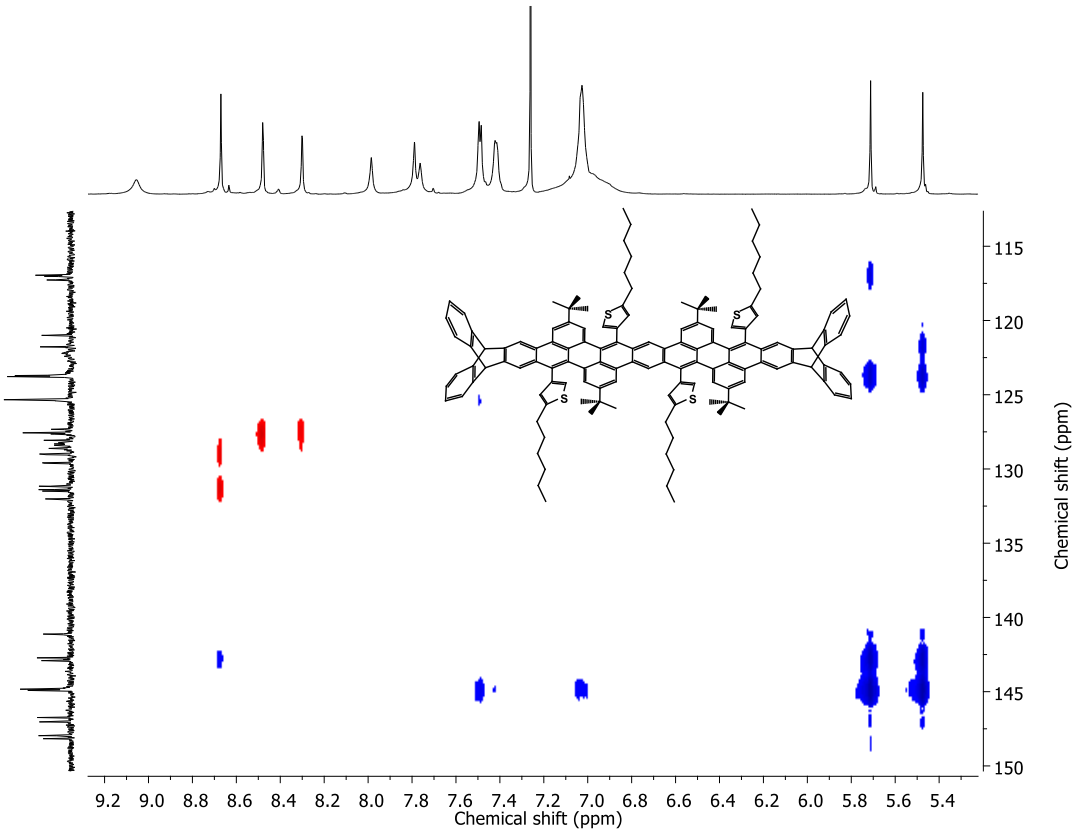

Figure 7.190 ^{1}H-^{13}C HMBC NMR spectrum (600/151 MHz, $CDCl_3$) of **259**.

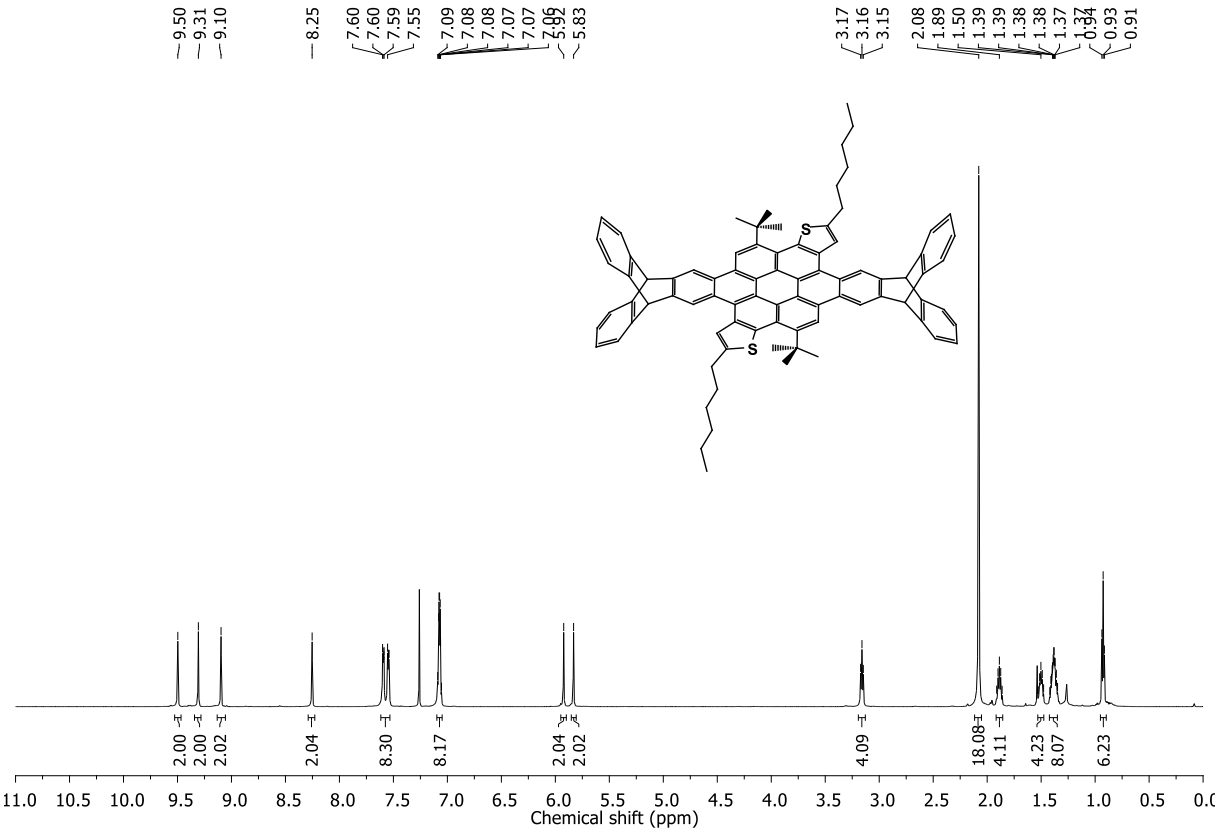

Figure 7.191 ^{1}H NMR spectrum (600 MHz, $CDCl_3$) of **261**.

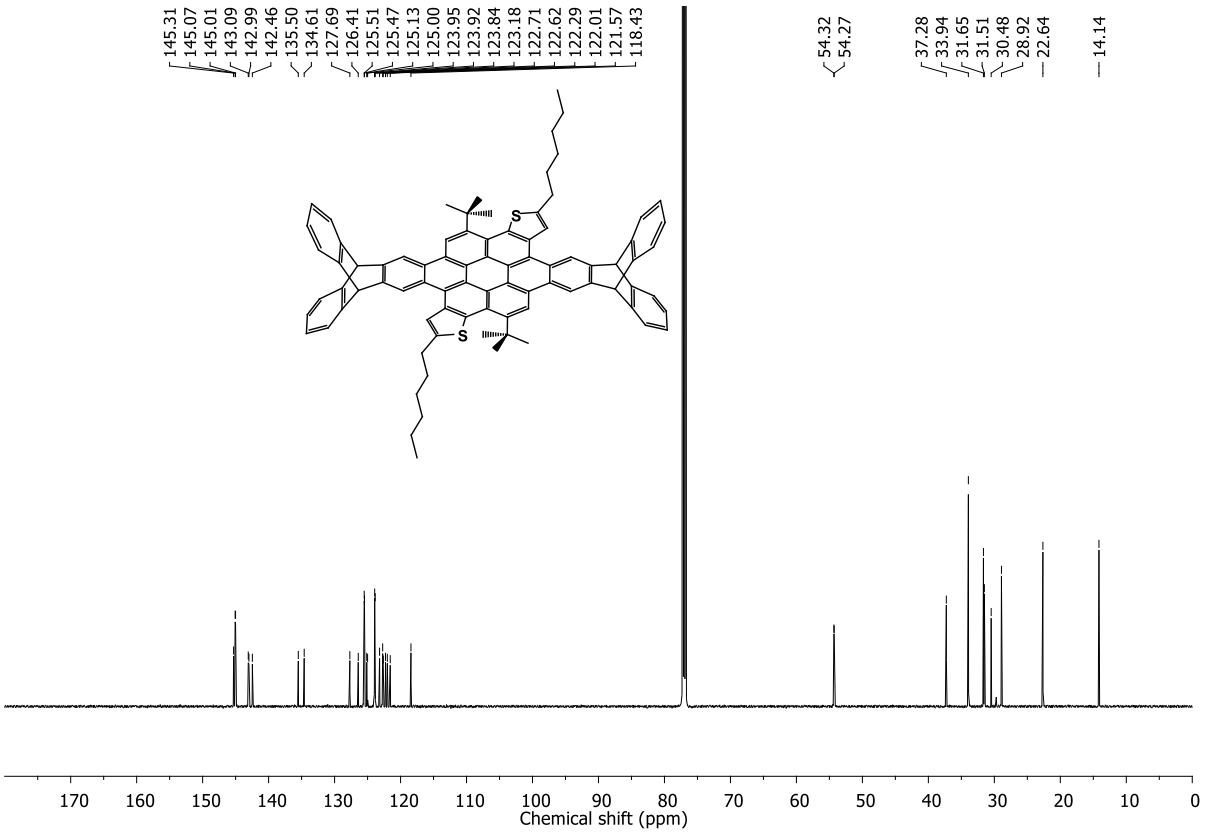

Figure 7.192 ^{13}C NMR spectrum (151 MHz, $CDCl_3$) of **261**.

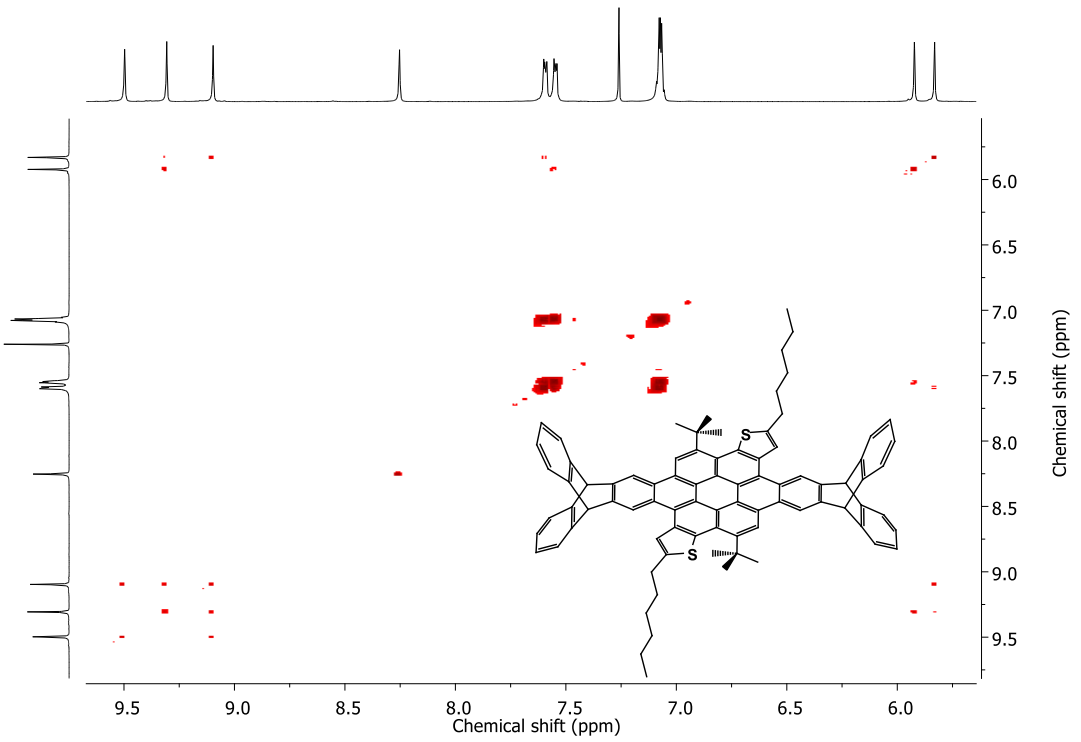

Figure 7.193 ^{1}H-^{1}H COSY NMR spectrum (600/600 MHz, $CDCl_3$) of **261**.

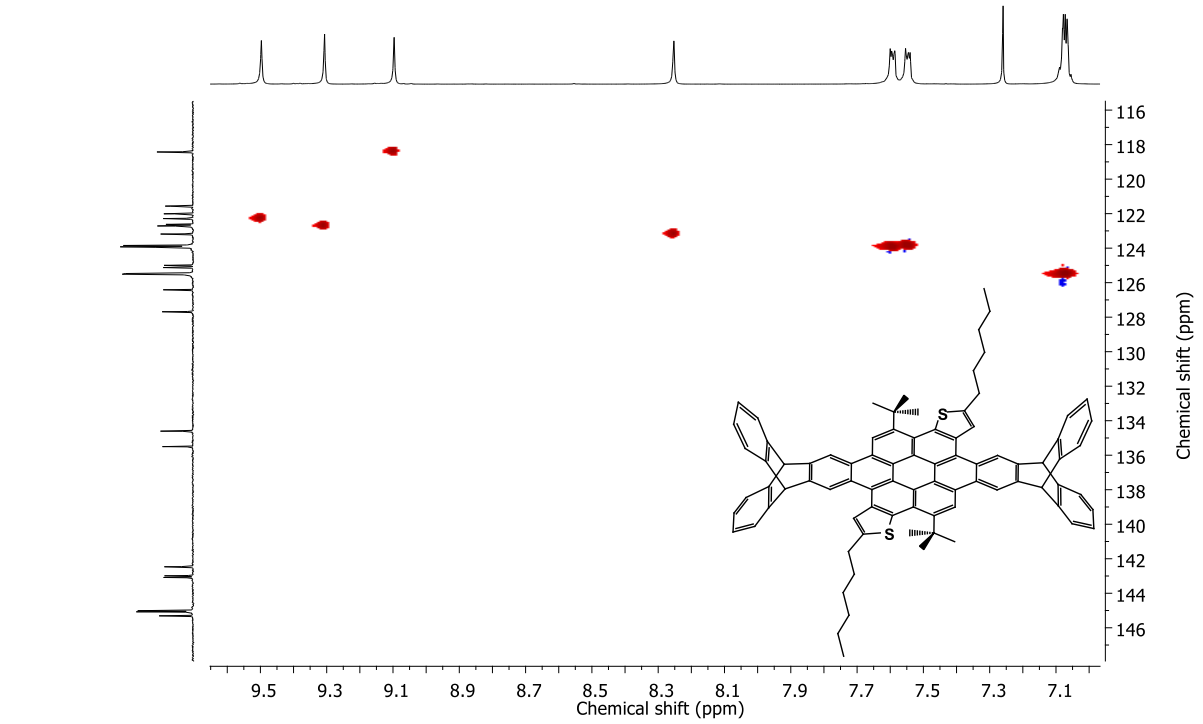

Figure 7.194 ^{1}H-^{13}C HSQC NMR spectrum (600/151 MHz, $CDCl_3$) of **261**.

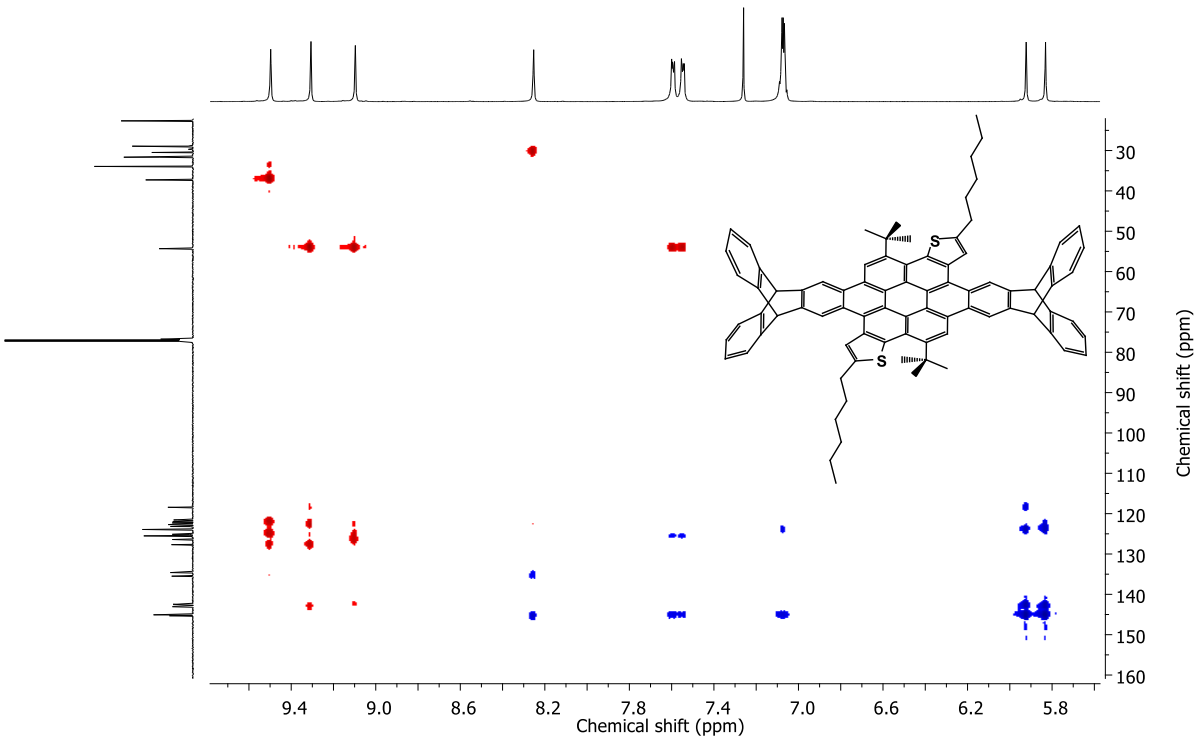

Figure 7.195 ^{1}H-^{13}C HMBC NMR spectrum (600/151 MHz, $CDCl_3$) of **261**.

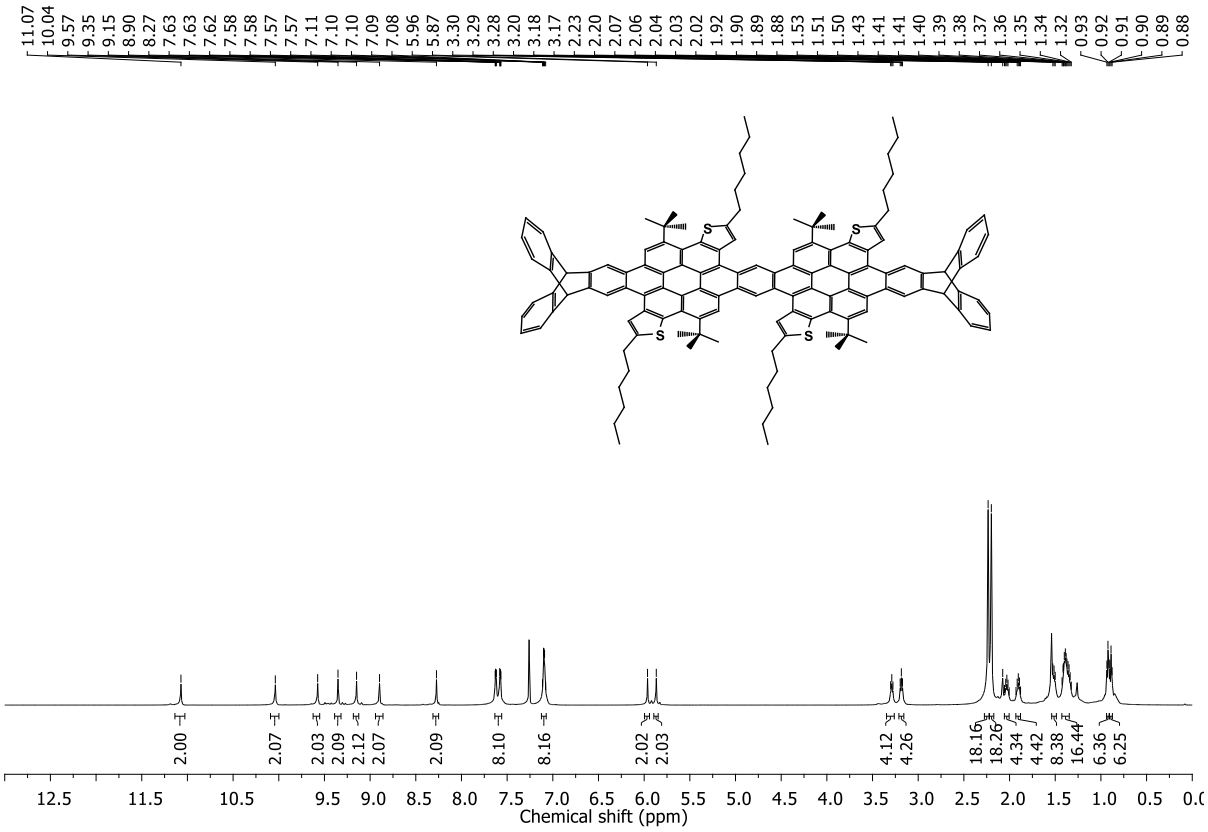

Figure 7.196 ^{1}H NMR spectrum (600 MHz, $CDCl_3$) of **262**.

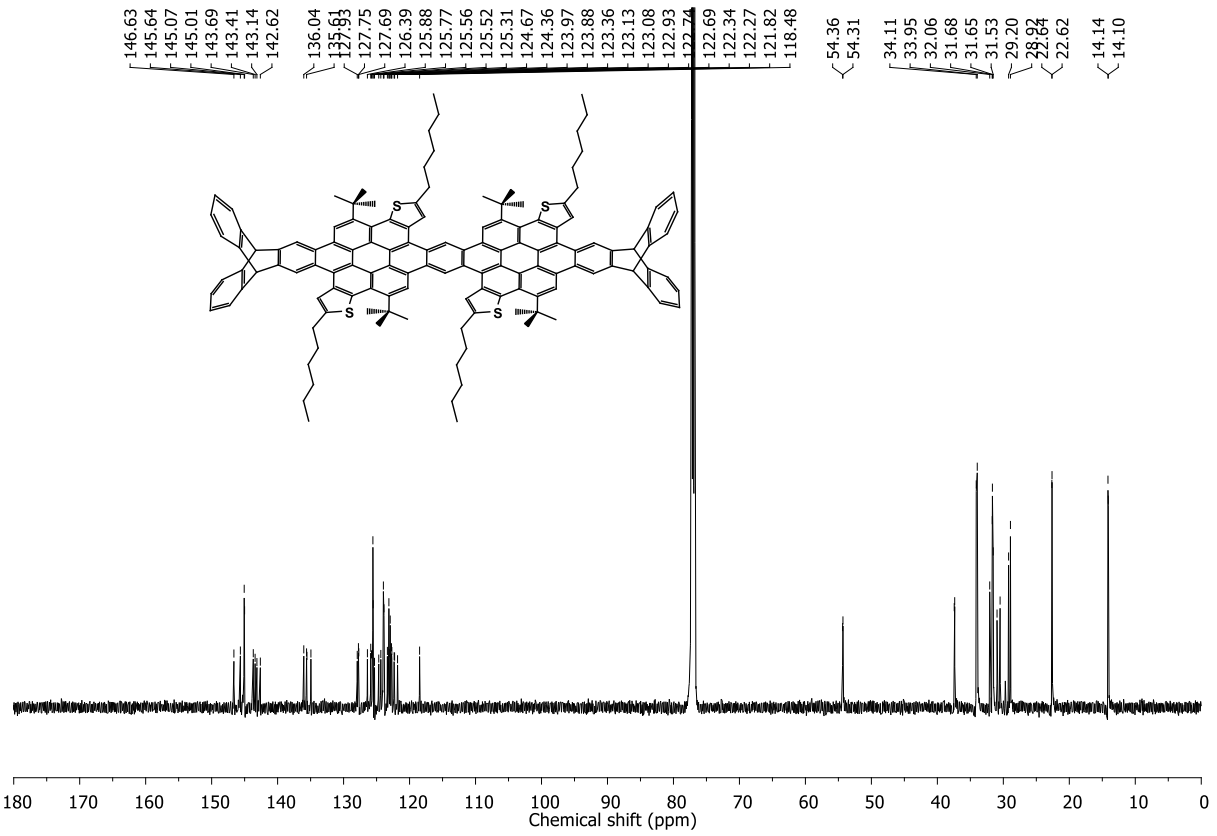

Figure 7.197 ^{13}C NMR spectrum (151 MHz, $CDCl_3$) of **262**.

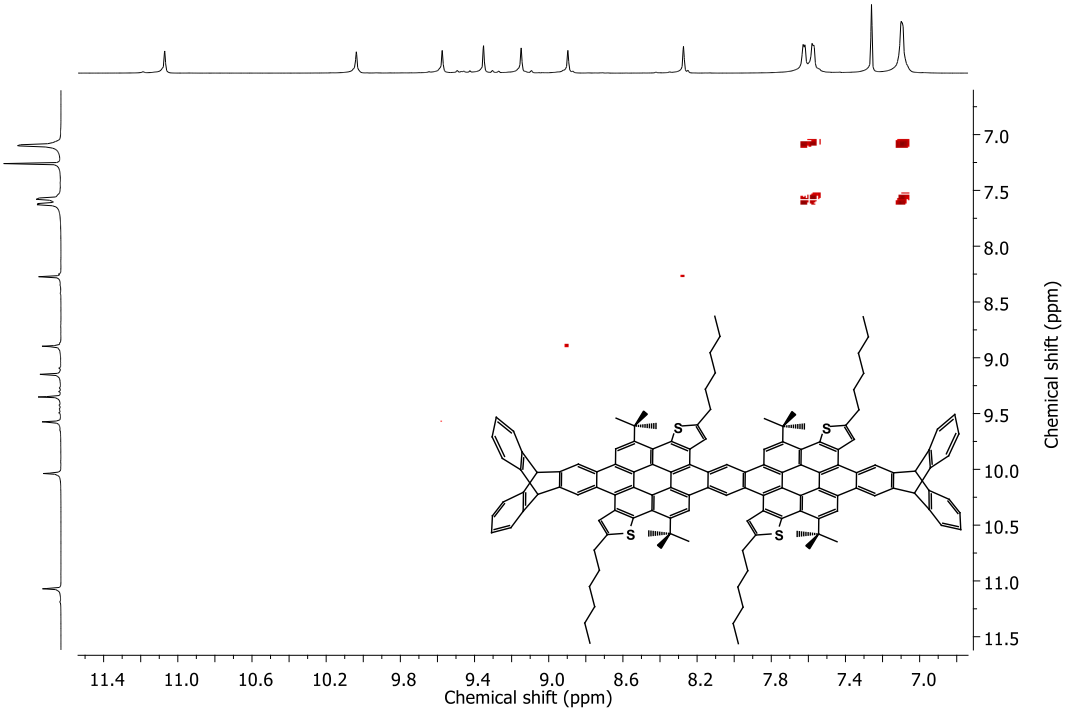

Figure 7.198 ^{1}H-^{1}H COSY NMR spectrum (600/600 MHz, $CDCl_3$) of **262**.

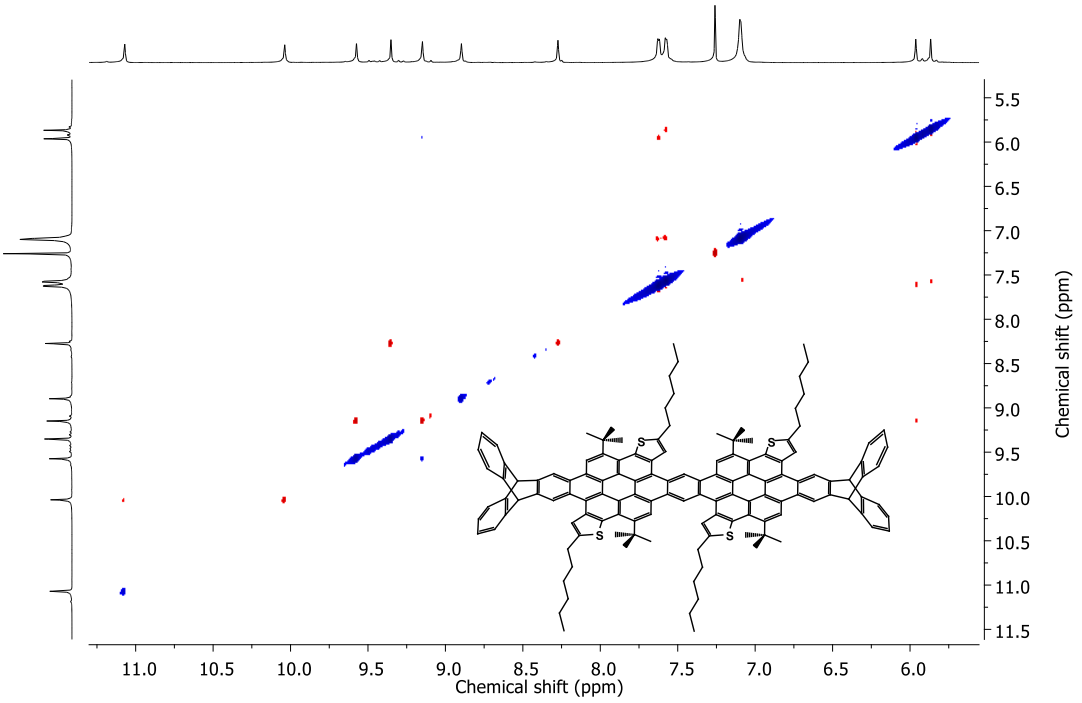

Figure 7.199 ^{1}H-^{1}H ROESY NMR spectrum (600/600 MHz, $CDCl_3$) of **262**.

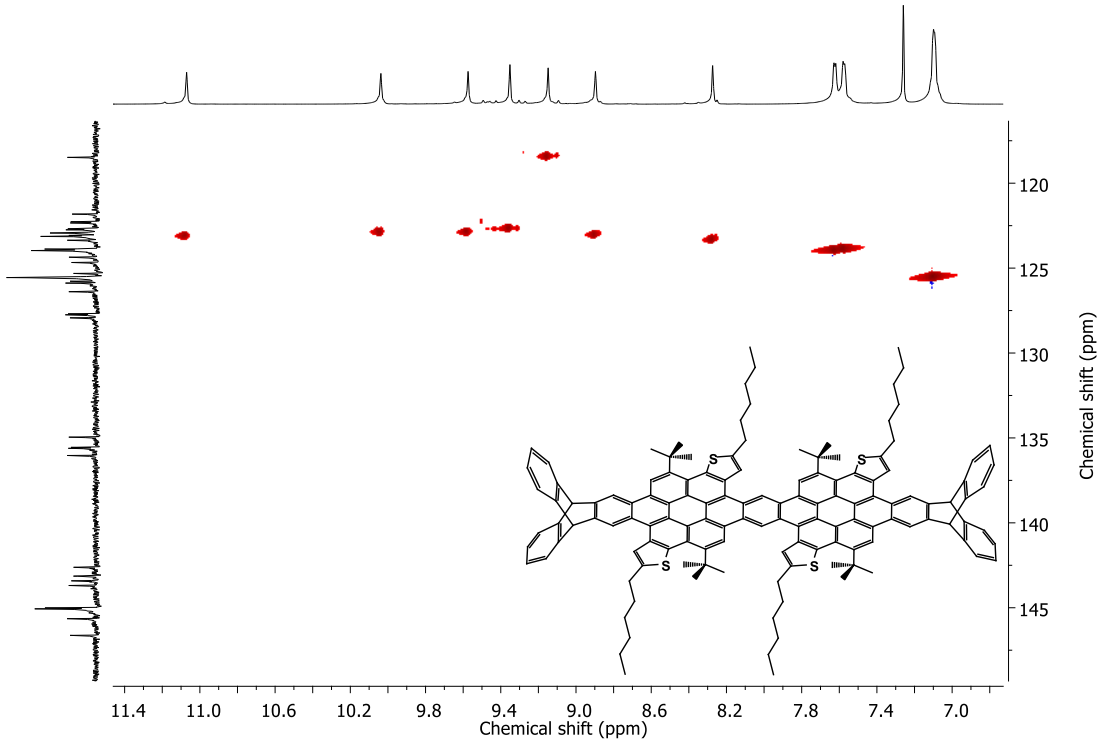

Figure 7.200 ^{1}H-^{13}C HSQC NMR spectrum (600/151 MHz, $CDCl_3$) of **262**.

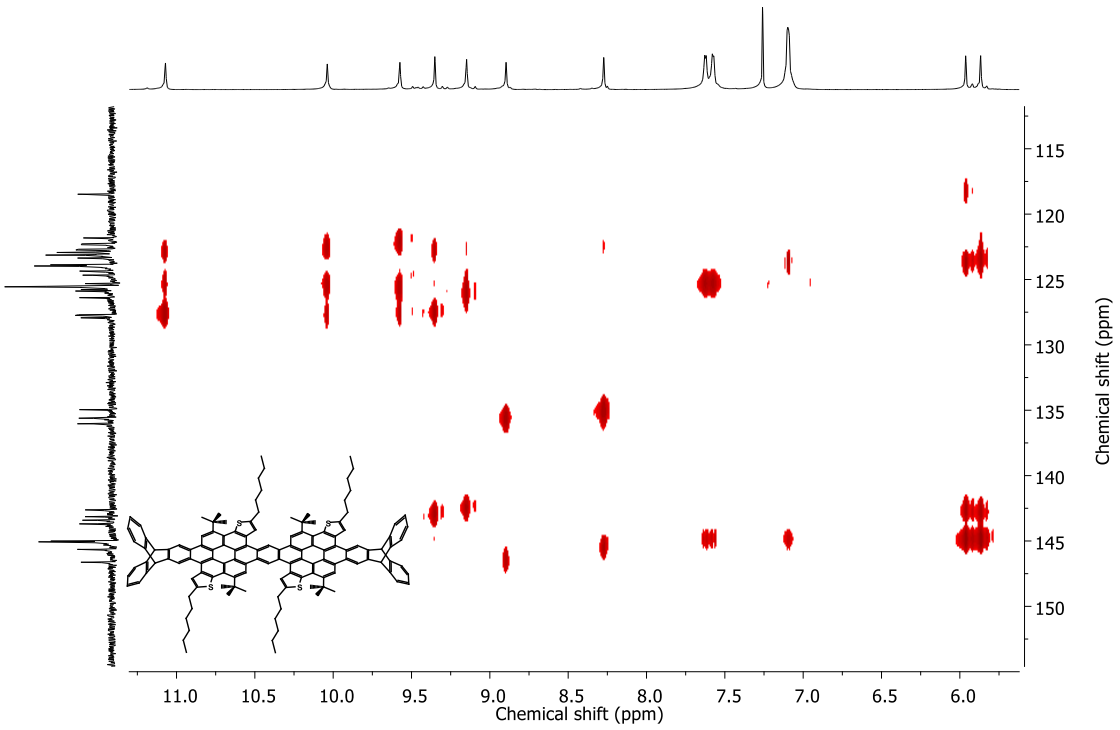

Figure 7.201 ^{1}H-^{13}C HMBC NMR spectrum (600/151 MHz, $CDCl_3$) of **262**.

7.2 Mass Spectra

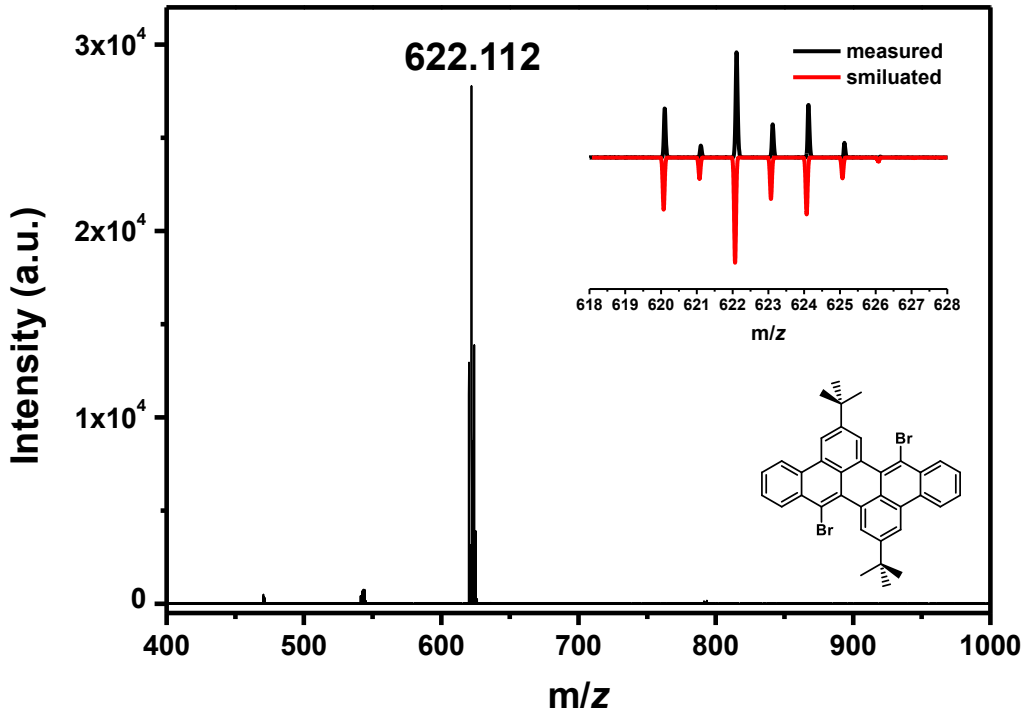

Figure 7.202 MALDI-TOF mass spectrum (DCTB) of **133**.

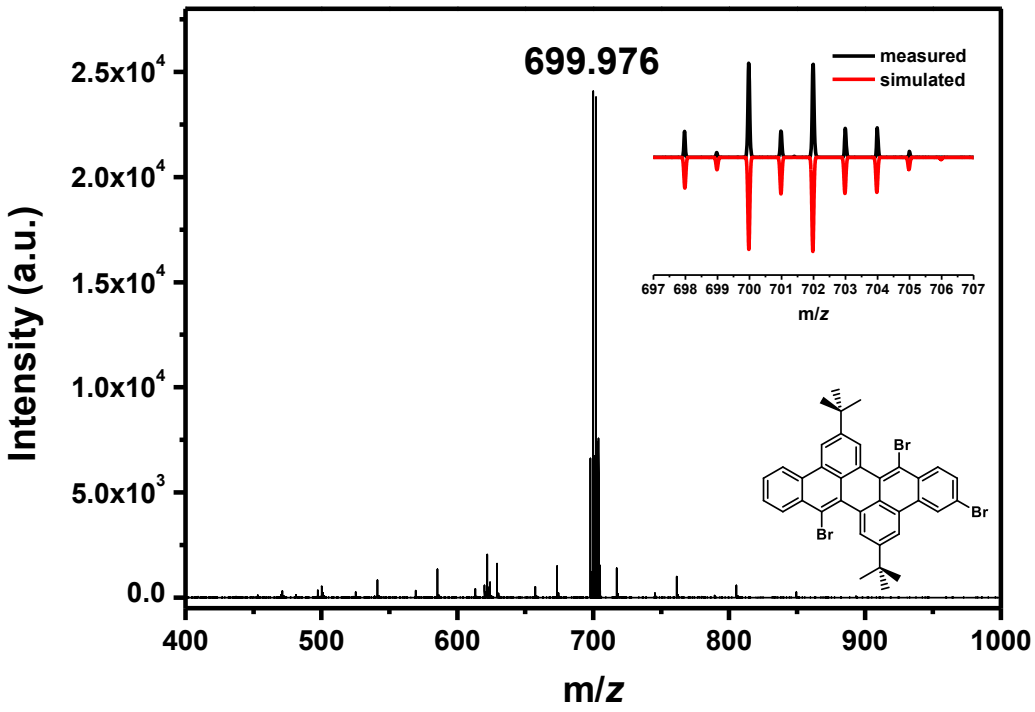

Figure 7.203 MALDI-TOF mass spectrum (DCTB, Kalib PEG600) of **134**.

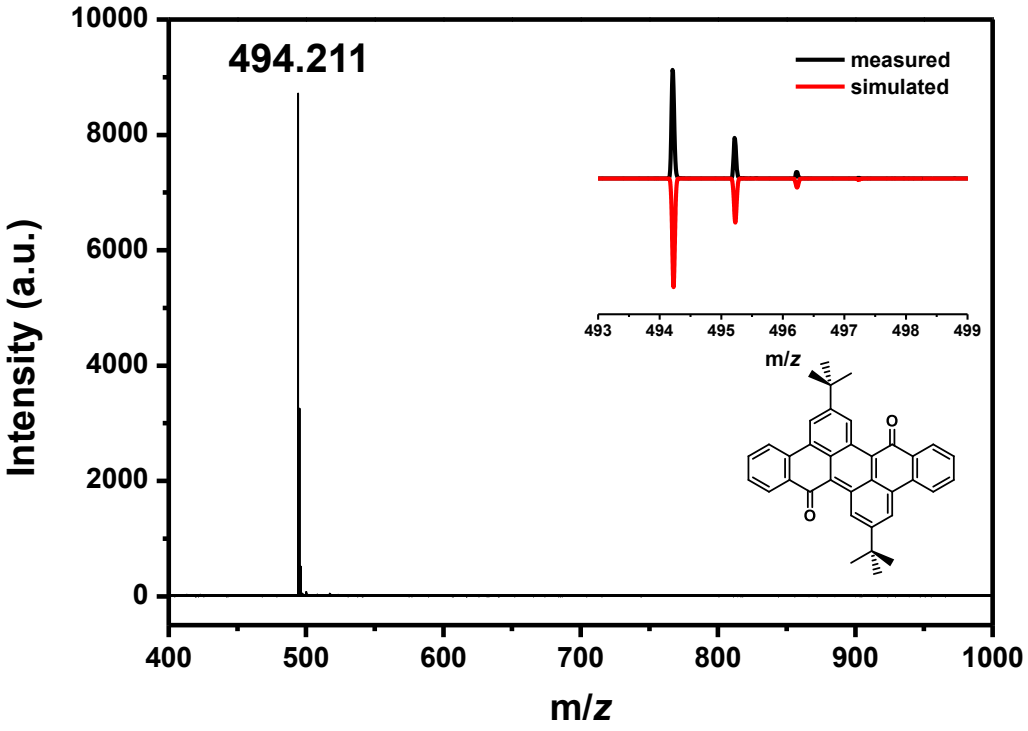

Figure 7.204 MALDI-TOF mass spectrum (DCTB) of **136**.

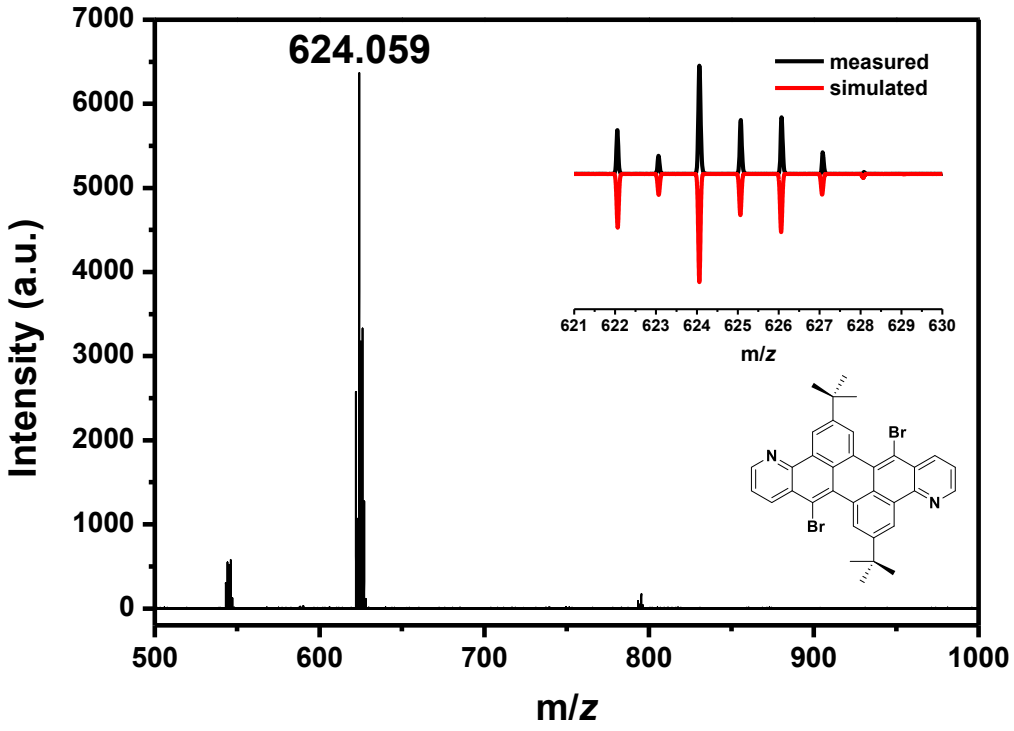

Figure 7.205 MALDI-TOF mass spectrum (DCTB) of **137**.

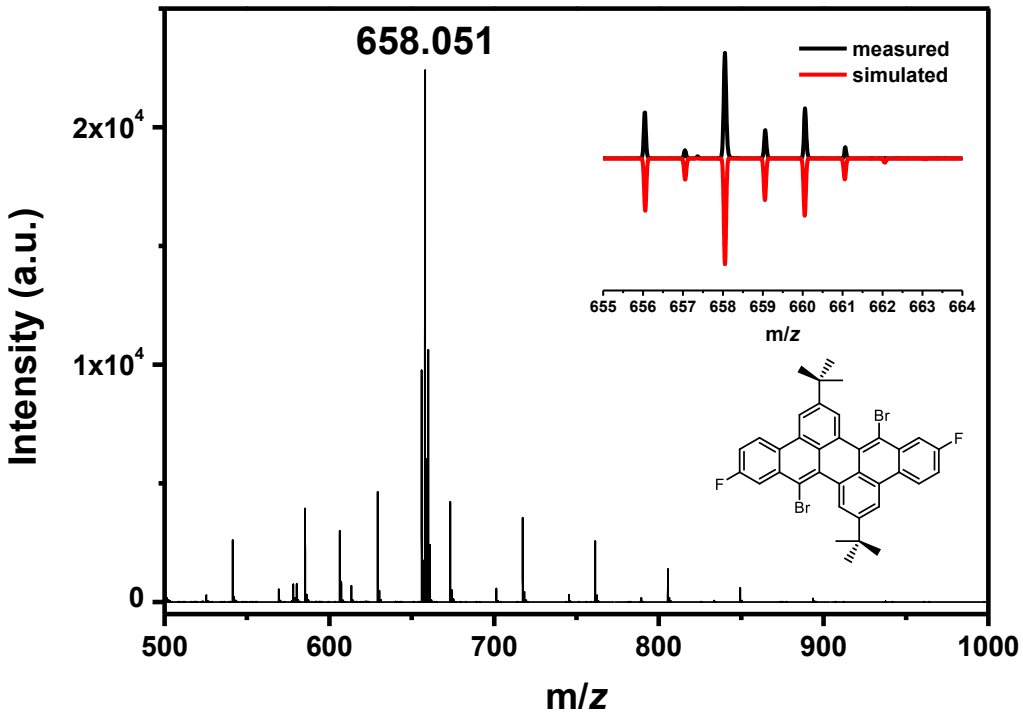

Figure 7.206 MALDI-TOF mass spectrum (DCTB, Kalib PEG600) of **138**.

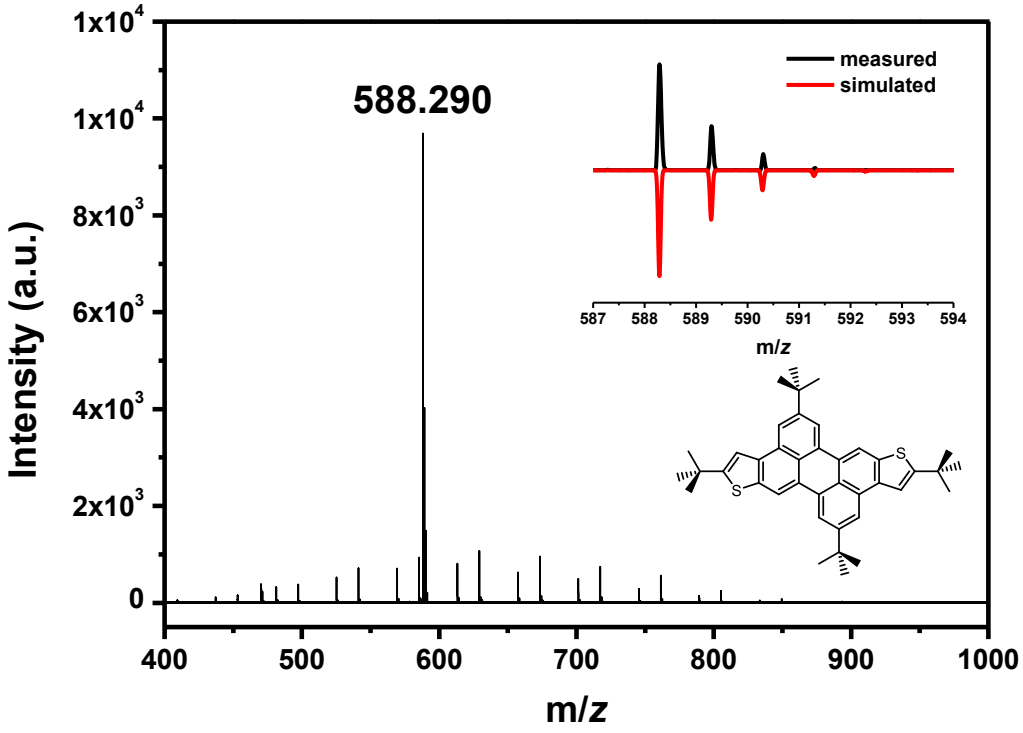

Figure 7.207 MALDI-TOF mass spectrum (DCTB, Kalib PEG600) of **141**.

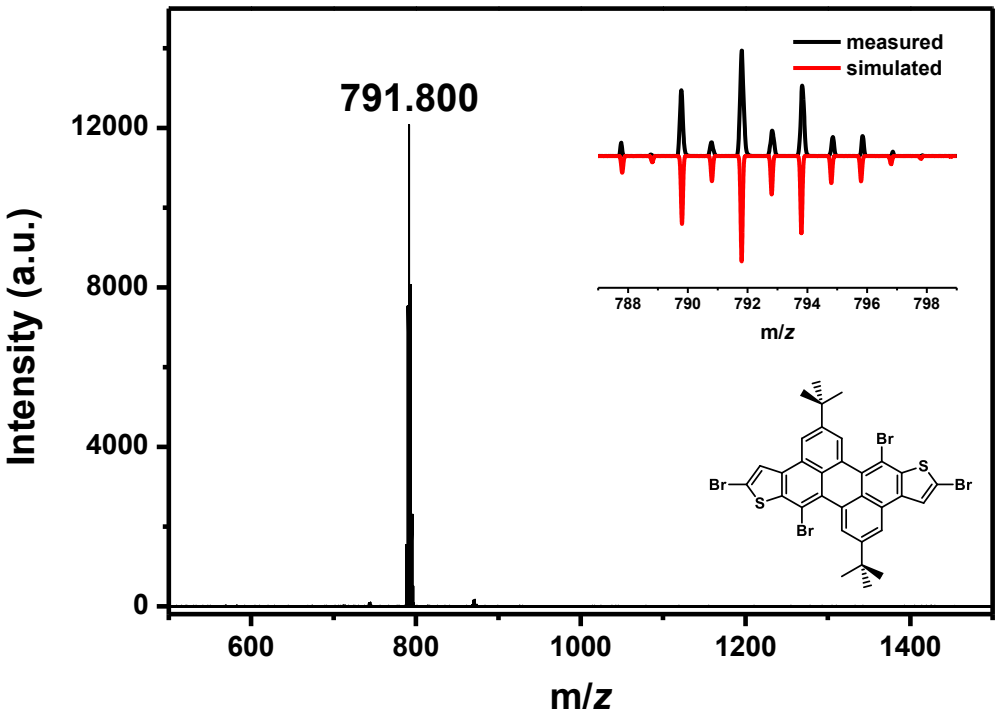

Figure 7.208 MALDI-TOF mass spectrum (DCTB) of **139**.

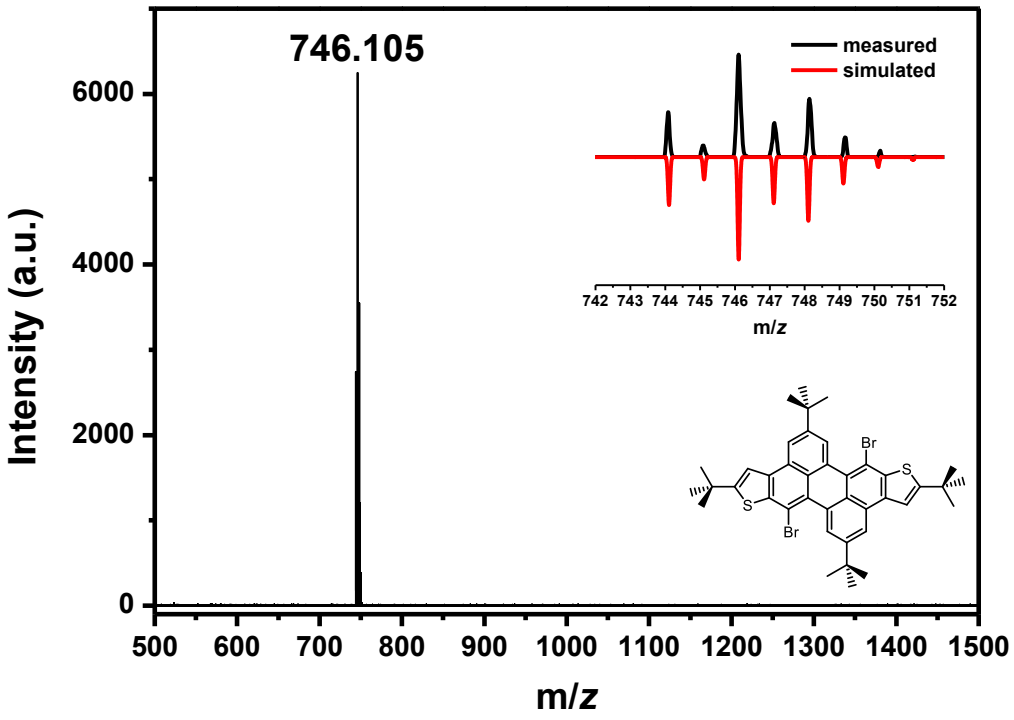

Figure 7.209 MALDI-TOF mass spectrum (DCTB) of **142**.

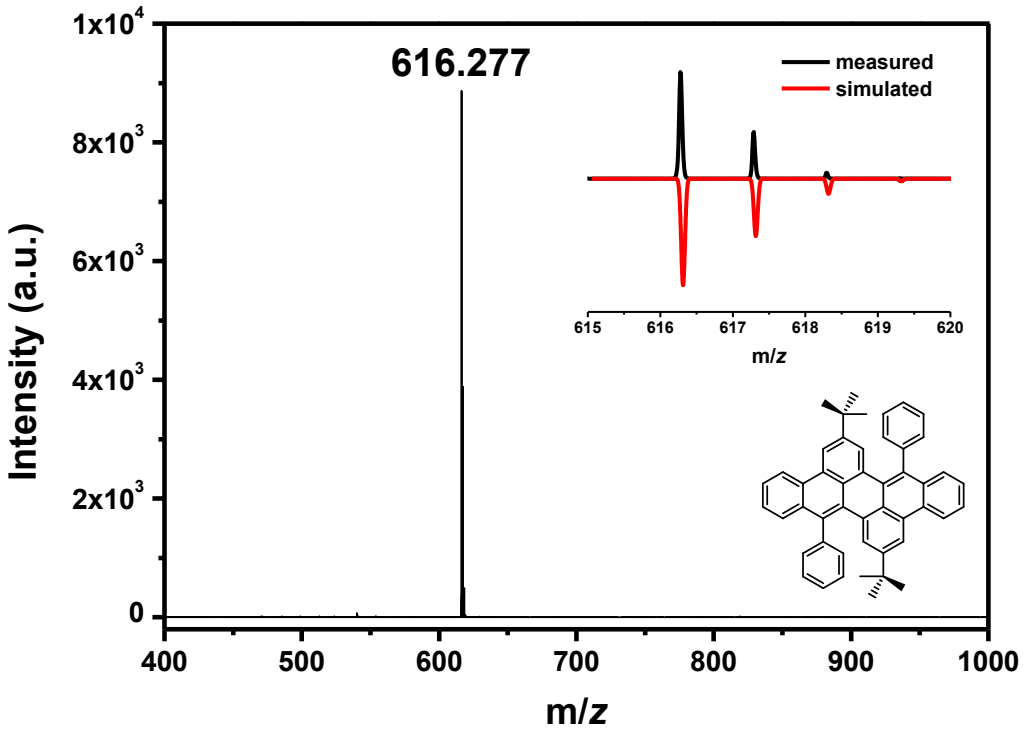

Figure 7.210 MALDI-TOF mass spectrum (DCTB) of **143**.

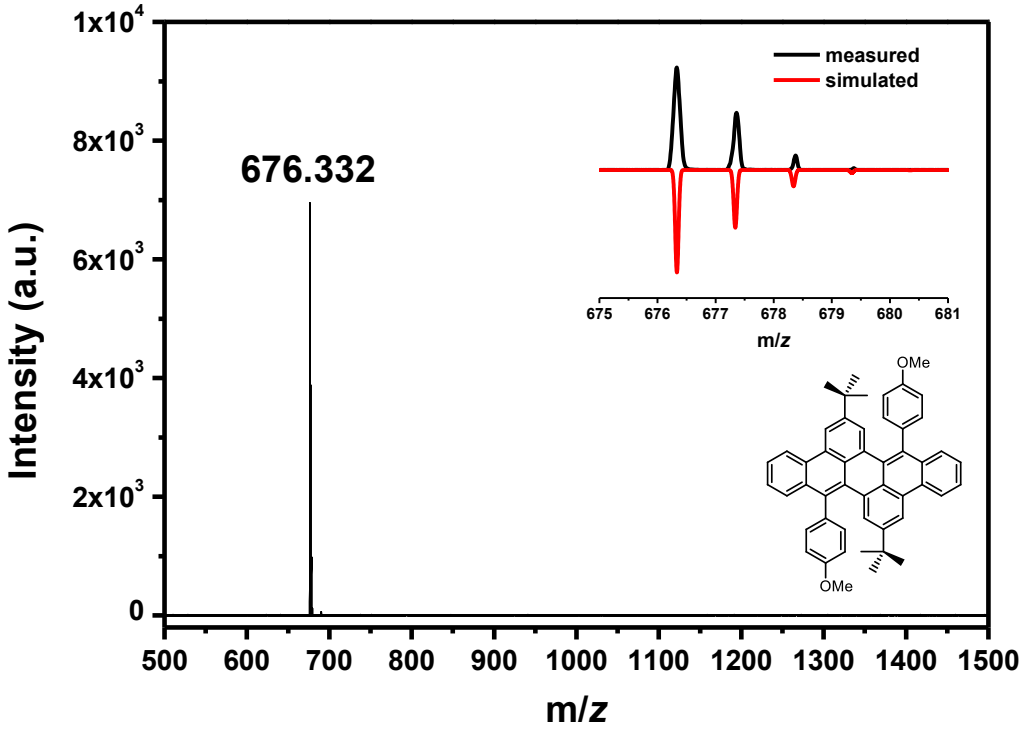

Figure 7.211 MALDI-TOF mass spectrum (DCTB) of **144**.

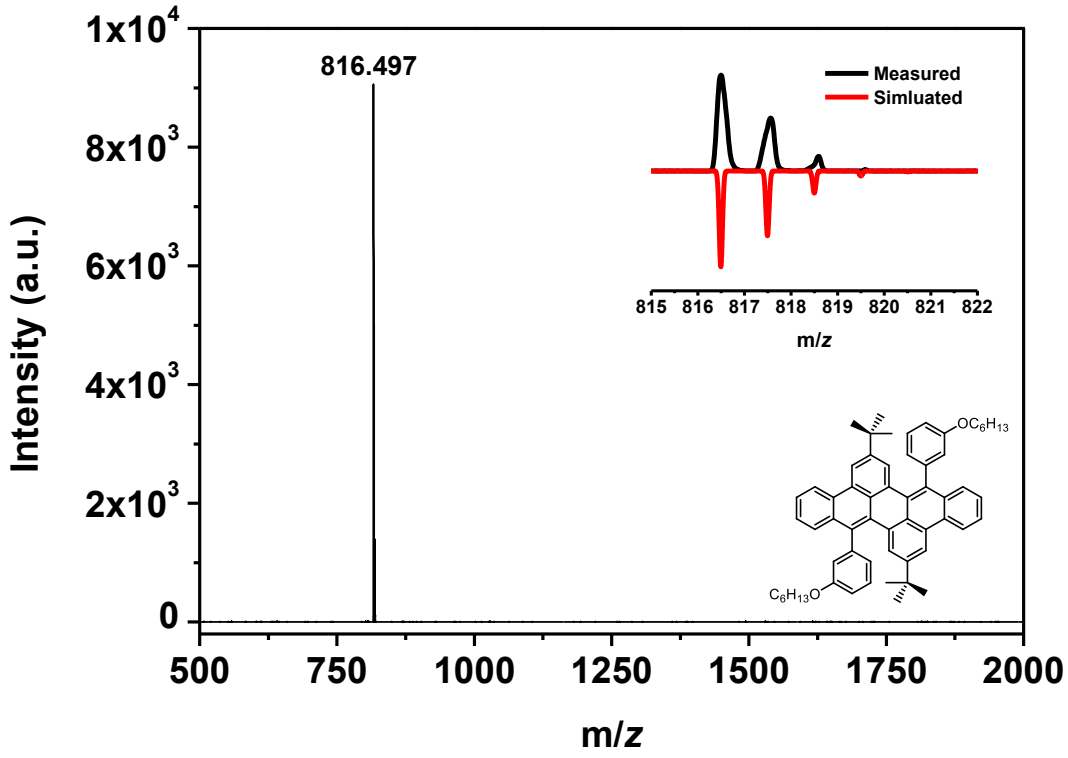

Figure 7.212 MALDI-TOF mass spectrum (DCTB) of **145**.

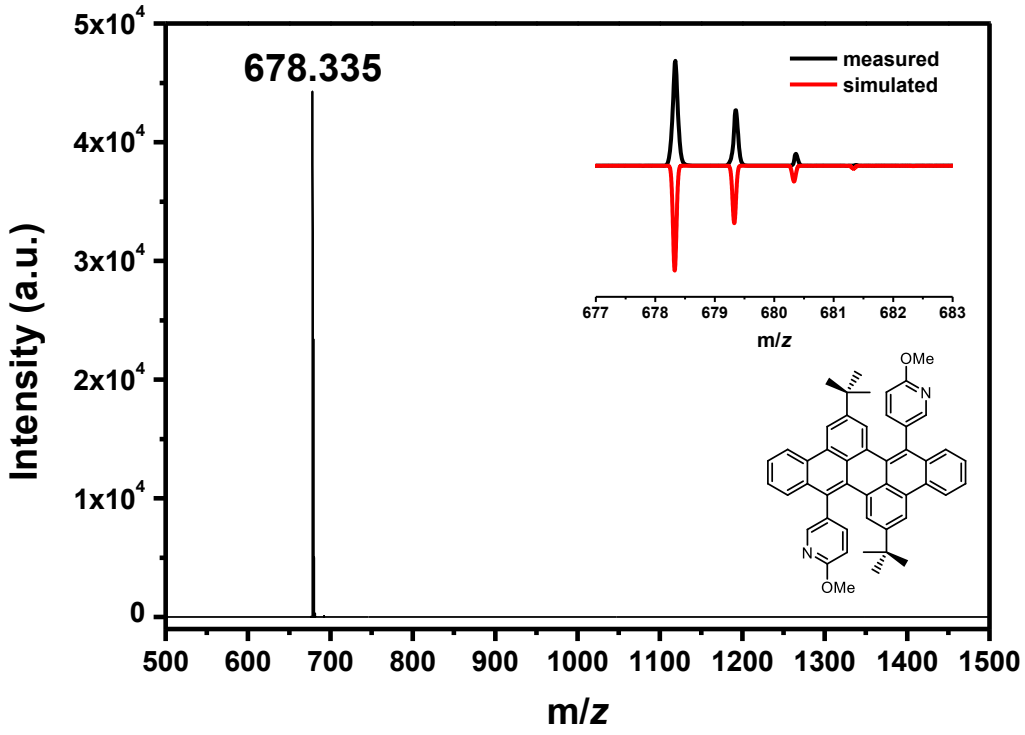

Figure 7.213 MALDI-TOF mass spectrum (DCTB) of **147**.

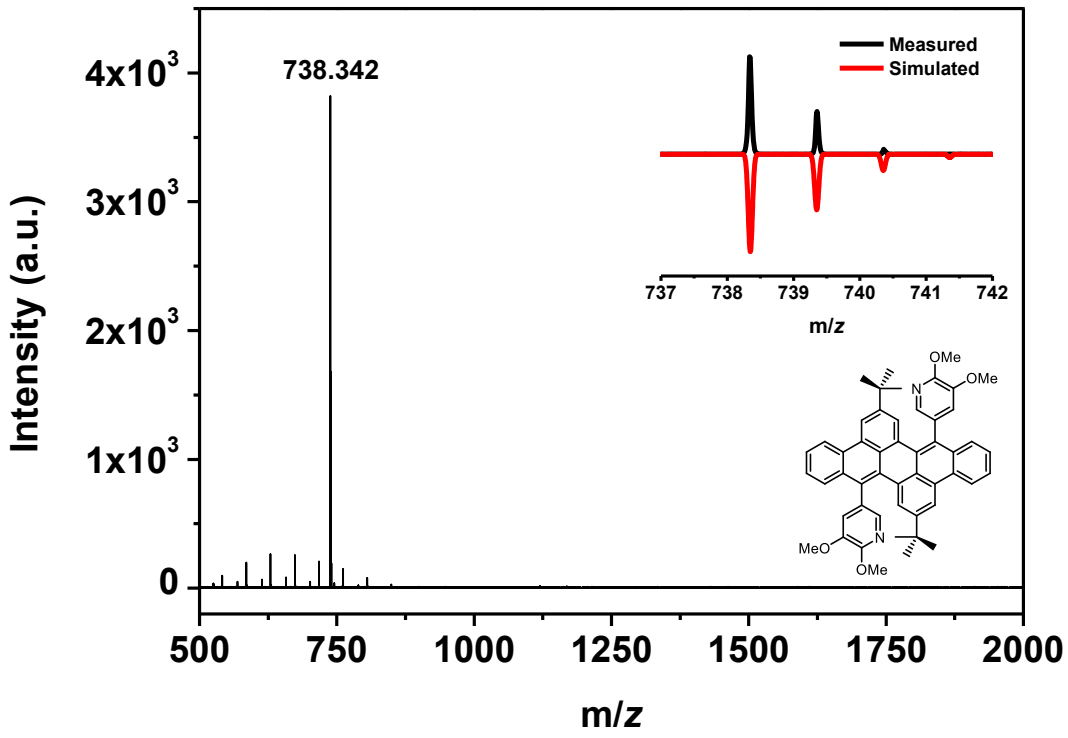

Figure 7.214 MALDI-TOF mass spectrum (DCTB, Kalib PEG 600) of **148**.

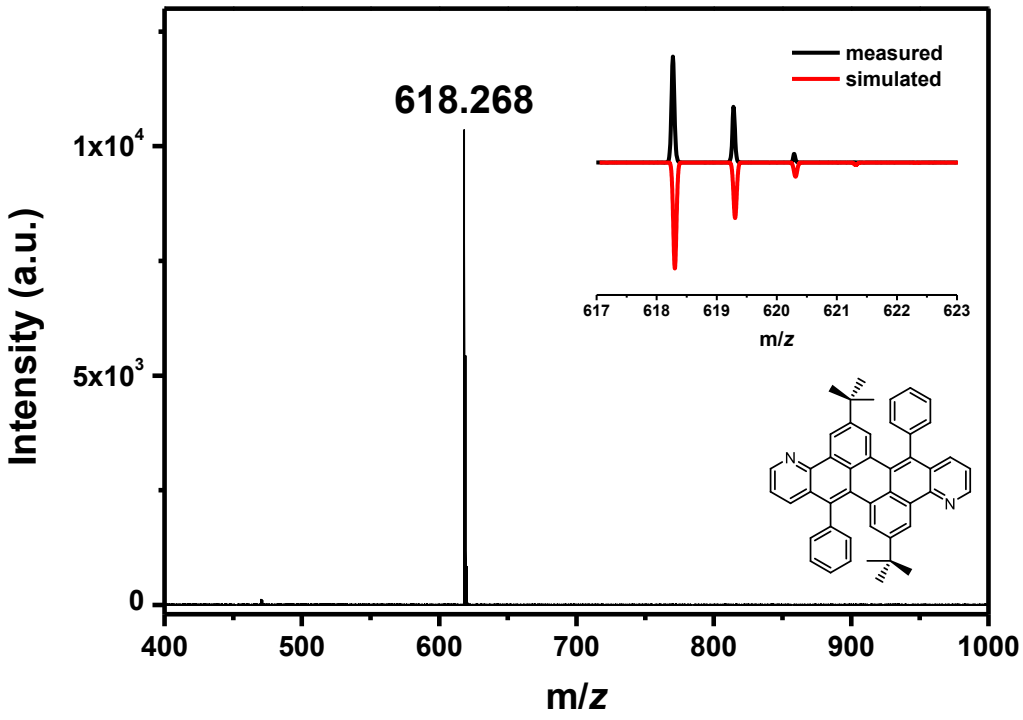

Figure 7.215 MALDI-TOF mass spectrum (DCTB) of **149**.

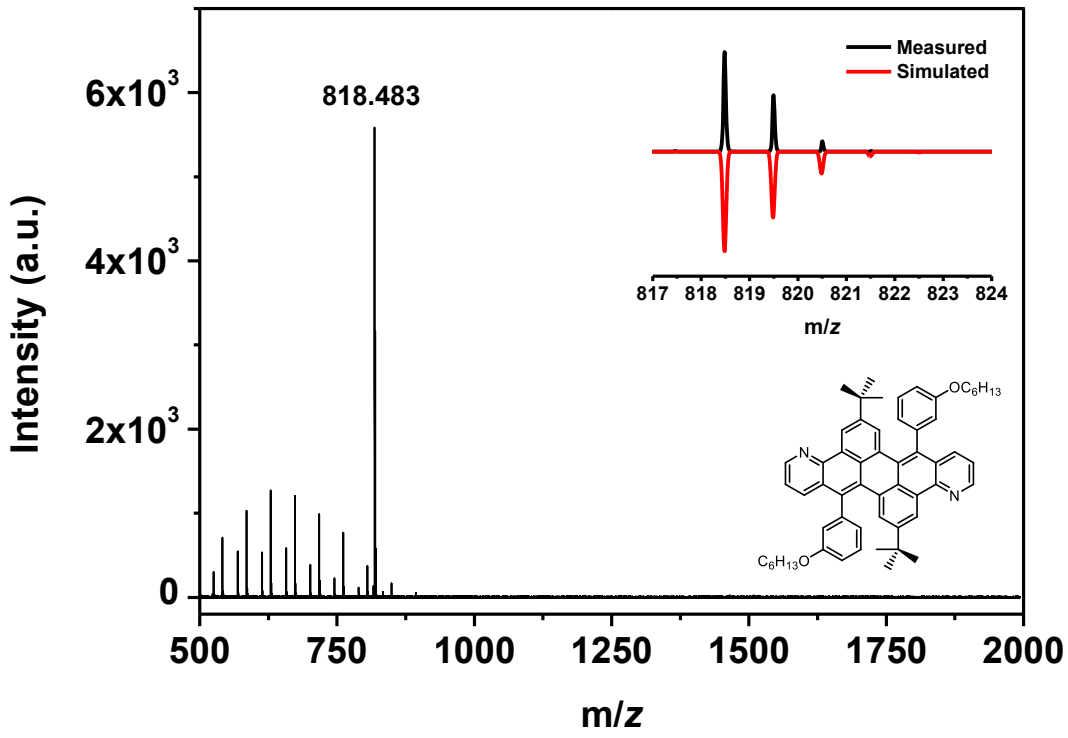

Figure 7.216 MALDI-TOF mass spectrum (DCTB, Kalib PEG 600) of **150**.

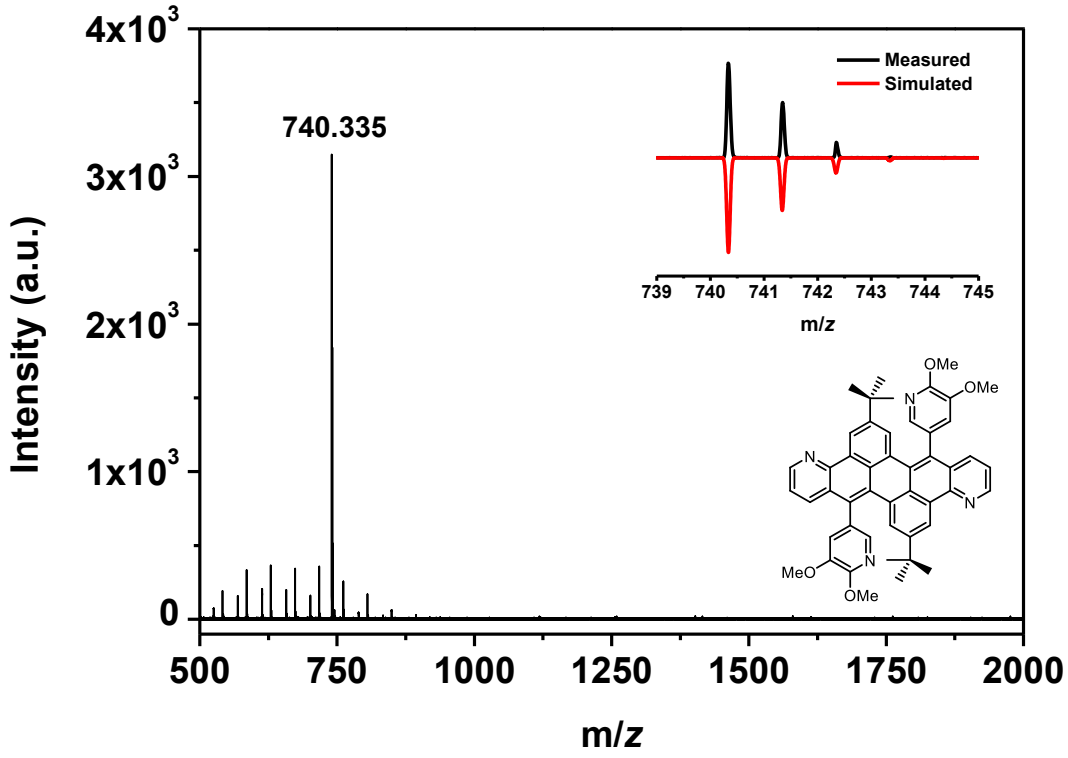

Figure 7.217 MALDI-TOF mass spectrum (DCTB, Kalib PEG 600) of **151**.

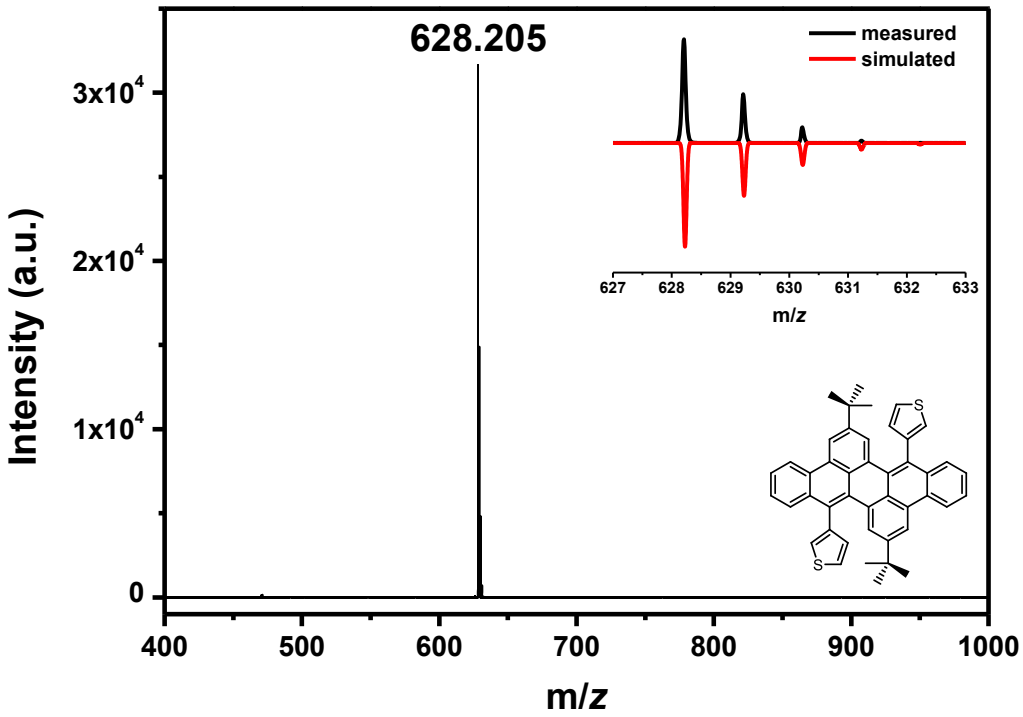

Figure 7.218 MALDI-TOF mass spectrum (DCTB) of **152**.

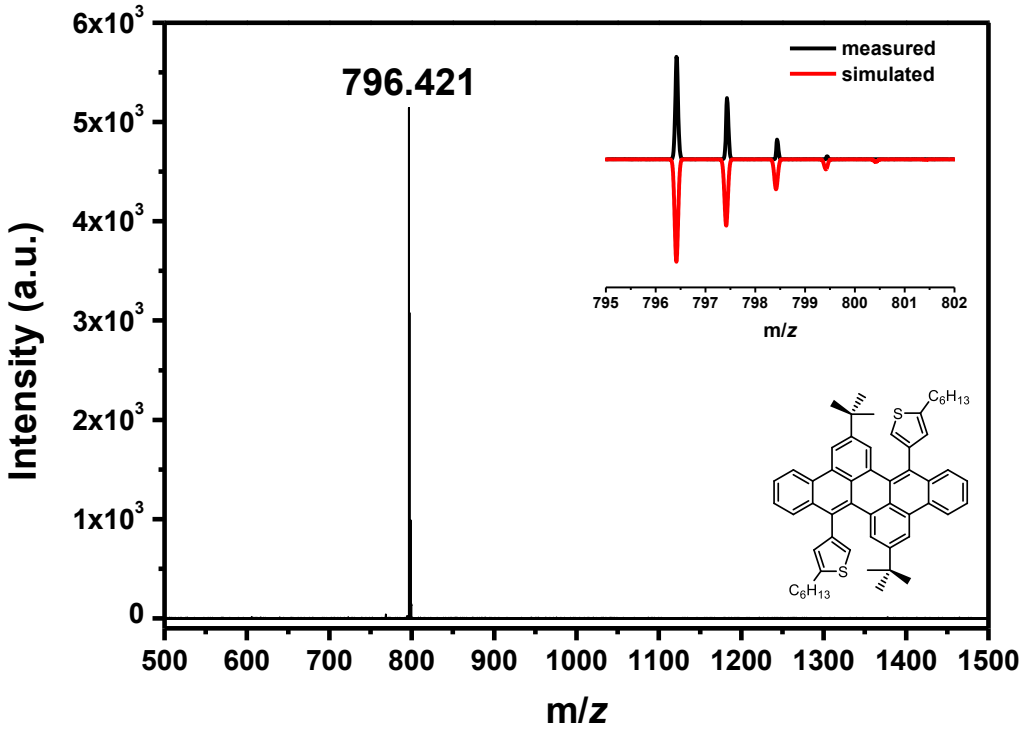

Figure 7.219 MALDI-TOF mass spectrum (DCTB) of **153**.

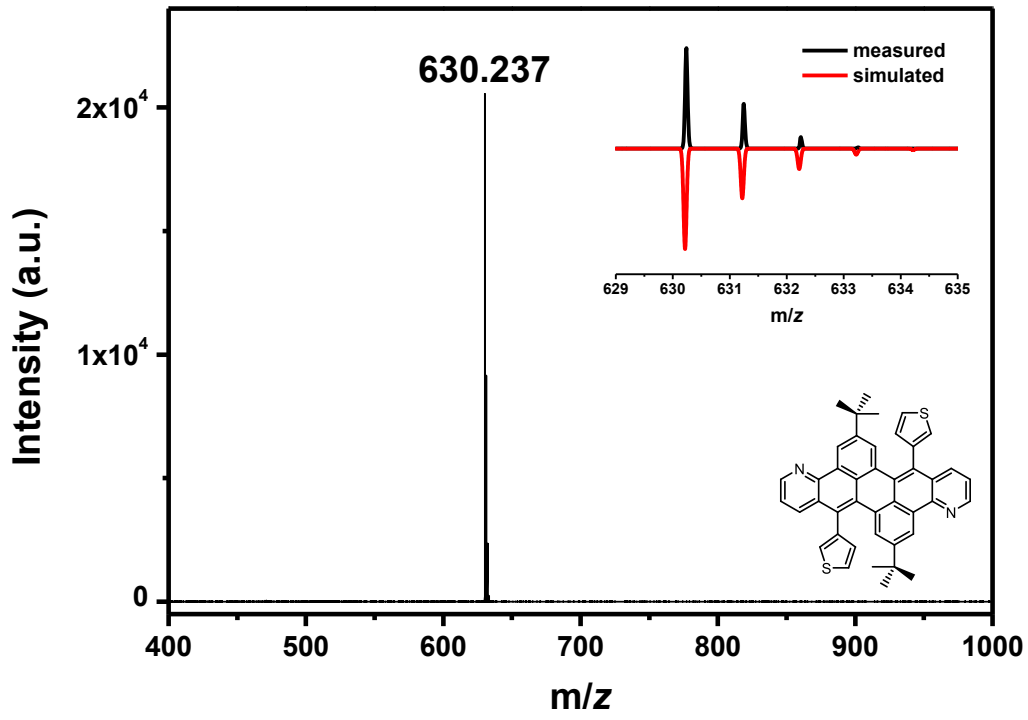

Figure 7.220 MALDI-TOF mass spectrum (DCTB) of **154**.

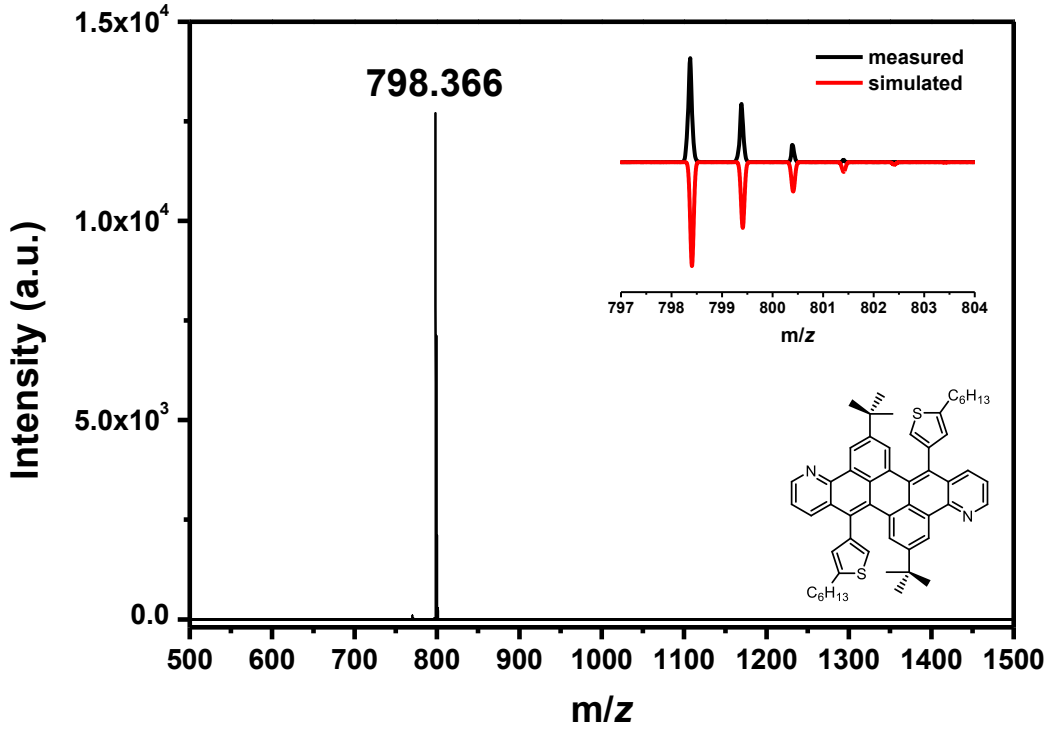

Figure 7.221 MALDI-TOF mass spectrum (DCTB) of **155**.

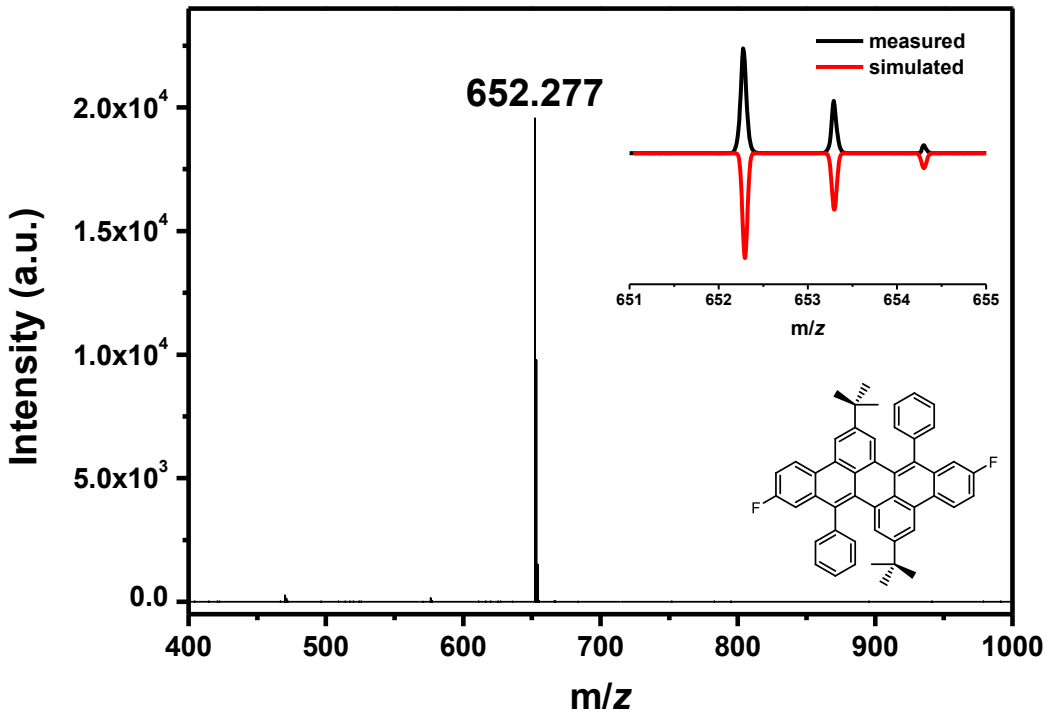

Figure 7.222 MALDI-TOF mass spectrum (DCTB) of **156**.

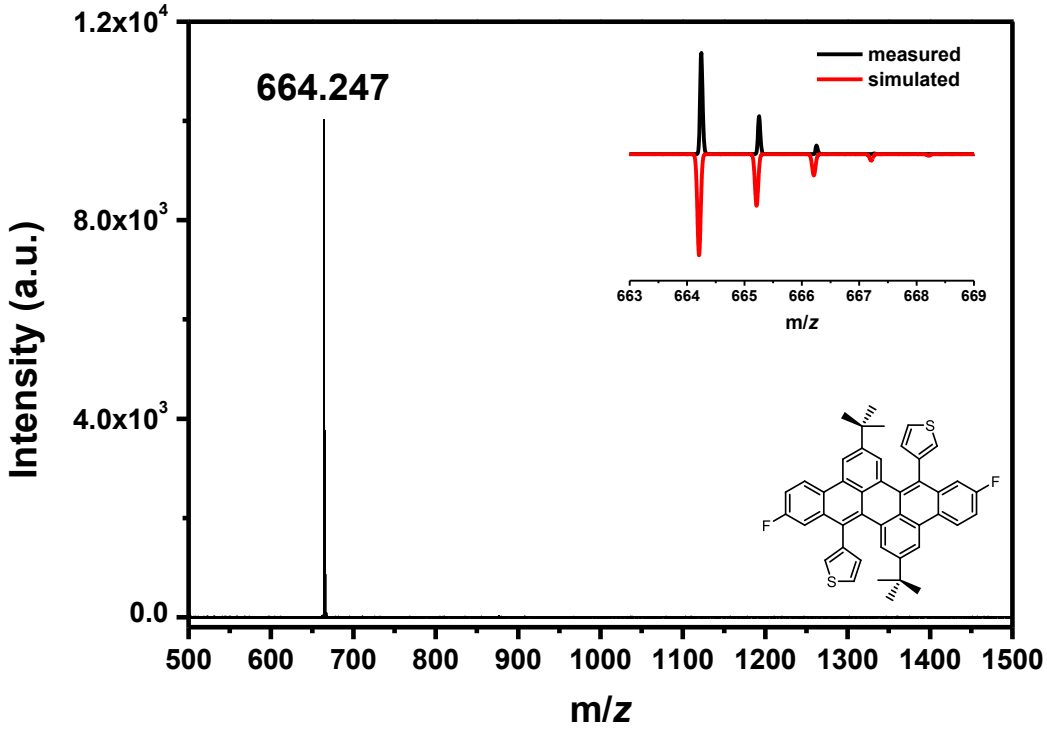

Figure 7.223 MALDI-TOF mass spectrum (DCTB) of **157**.

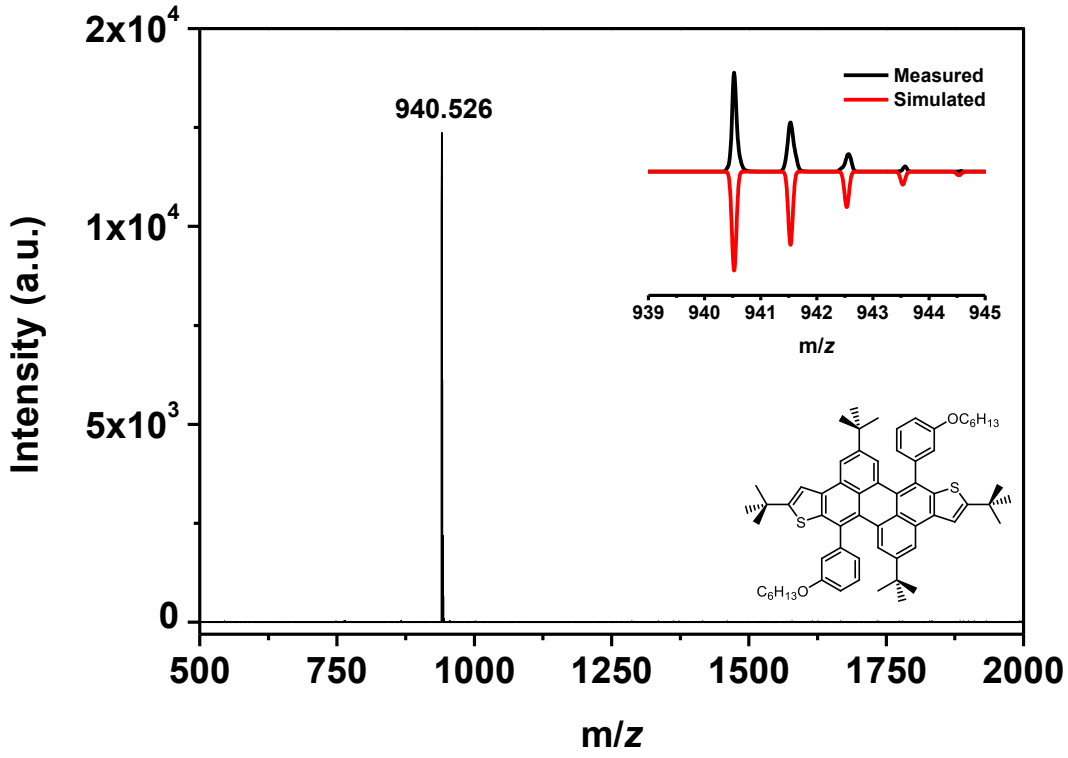

Figure 7.224 MALDI-TOF mass spectrum (DCTB) of **158**.

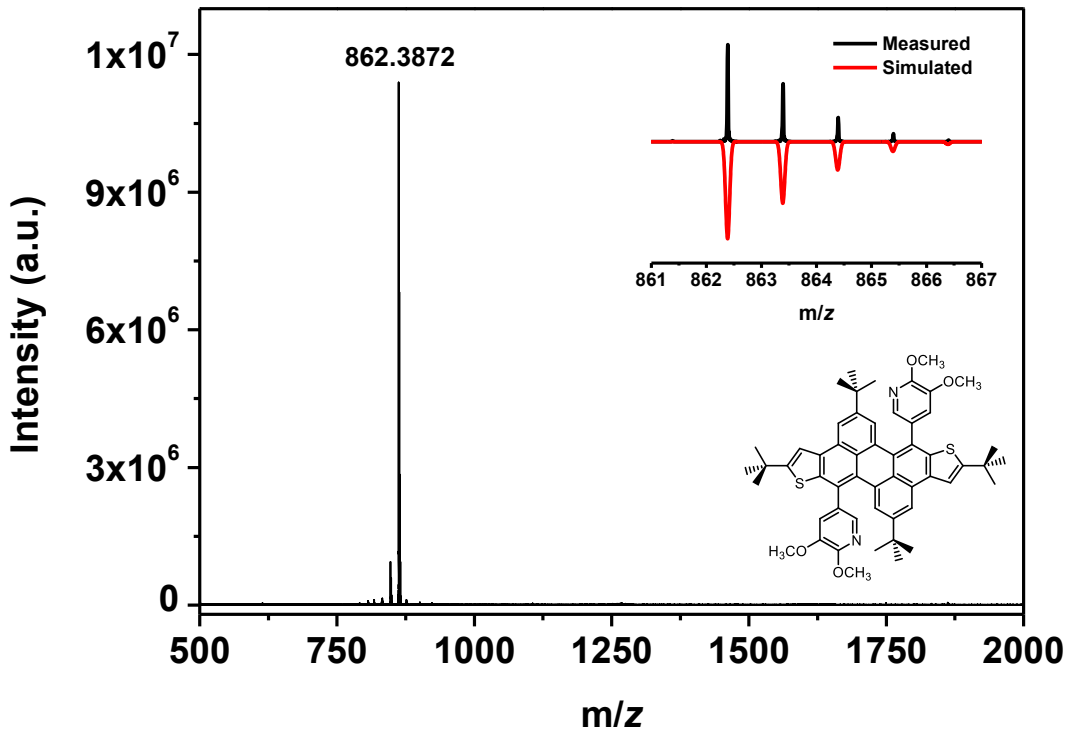

Figure 7.225 MALDI high resolution mass spectrum (DCTB) of **159**.

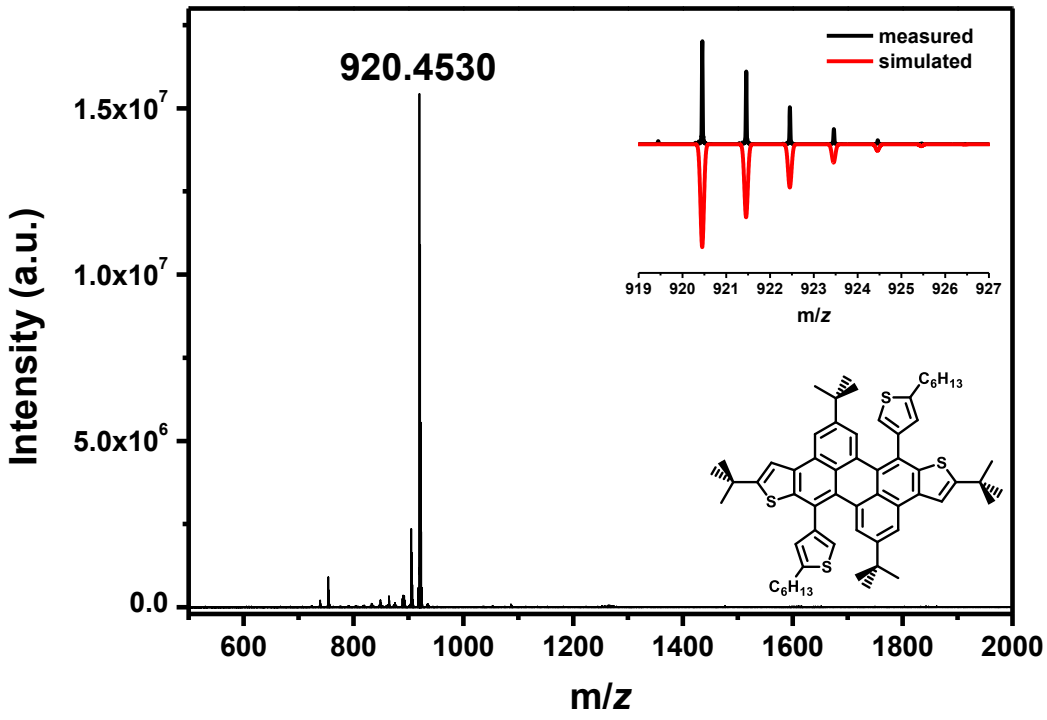

Figure 7.226 MALDI high resolution mass spectrum (DCTB) of **160**.

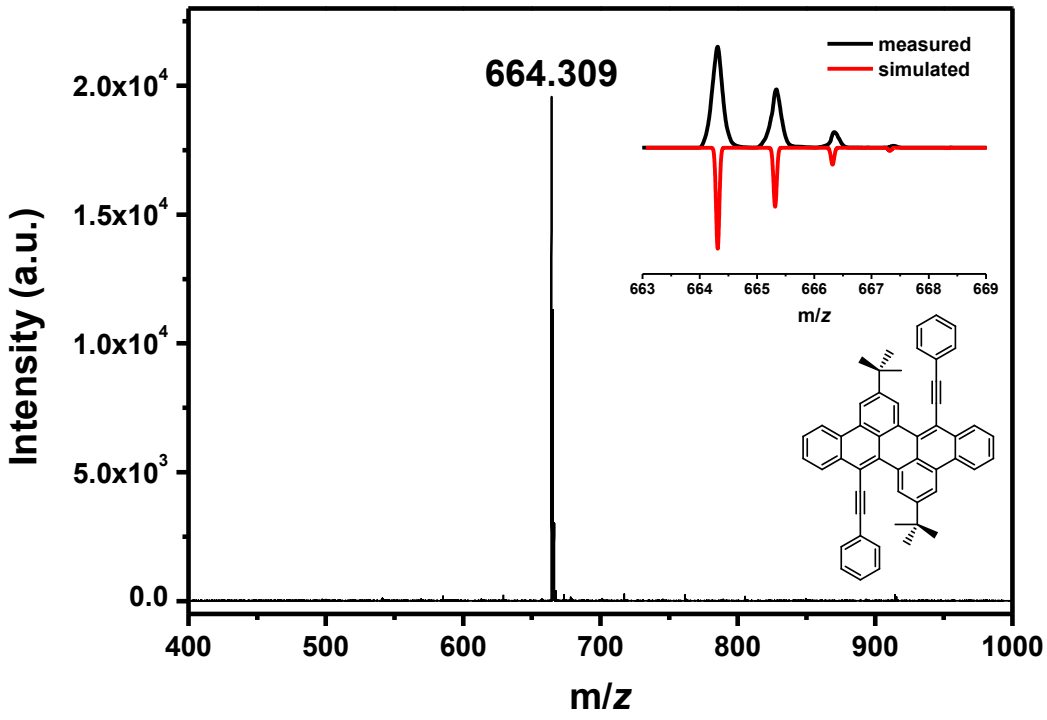

Figure 7.227 MALDI-TOF mass spectrum (DCTB, Kalib PEG600) of **161**.

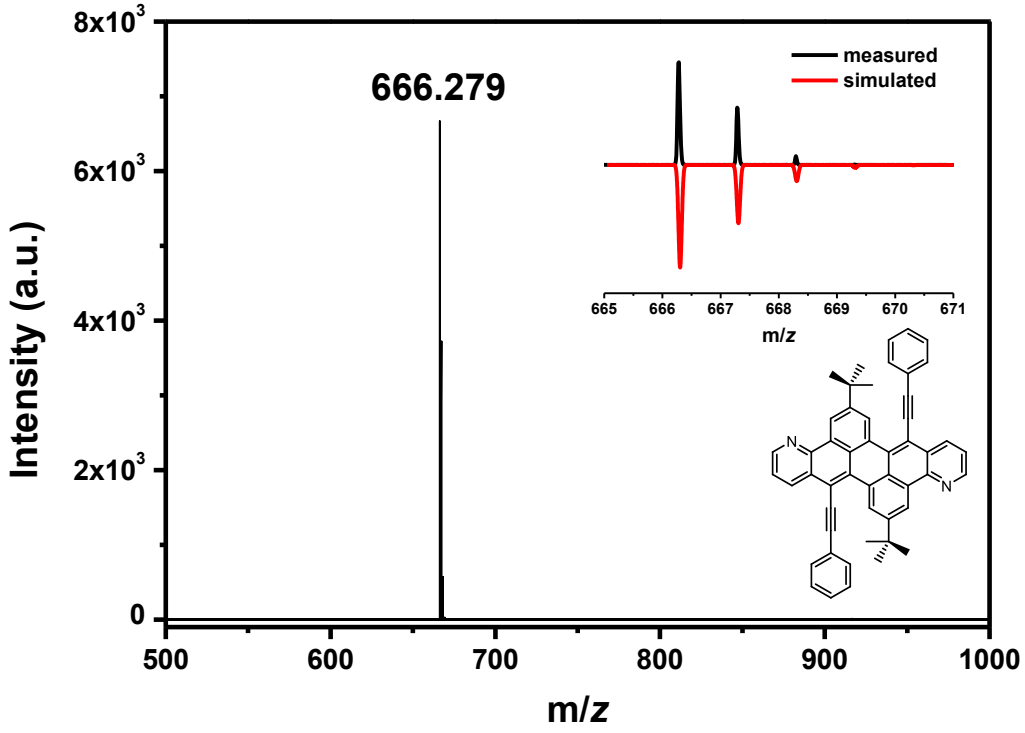

Figure 7.228 MALDI-TOF mass spectrum (DCTB) of **162**.

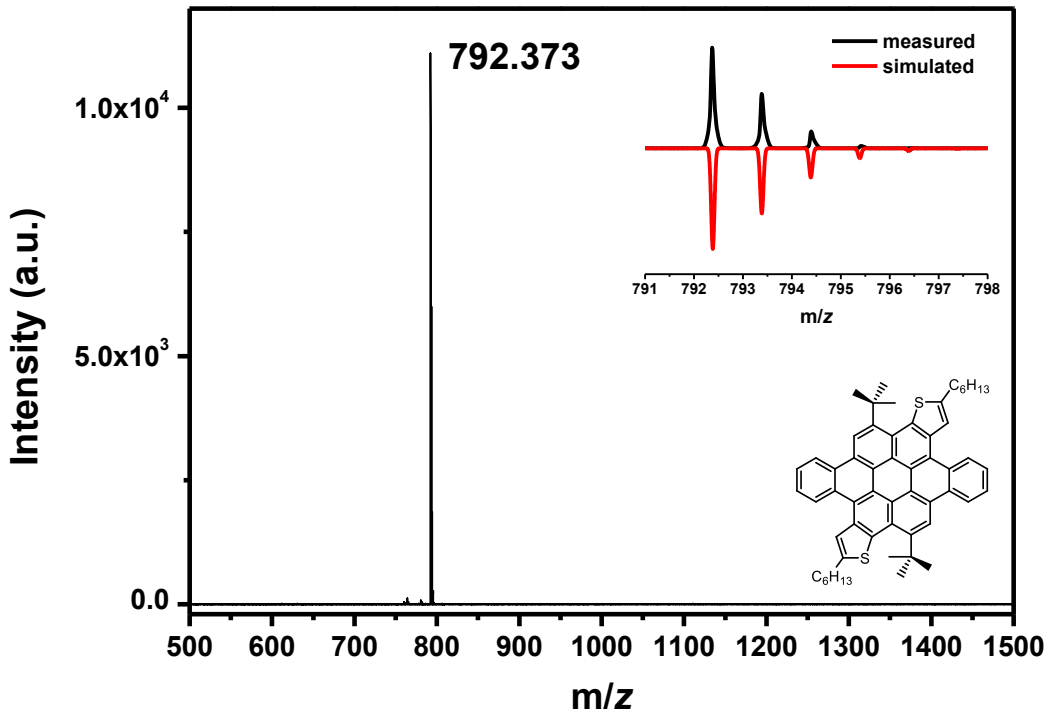

Figure 7.229 MALDI-TOF mass spectrum (DCTB) of **164**.

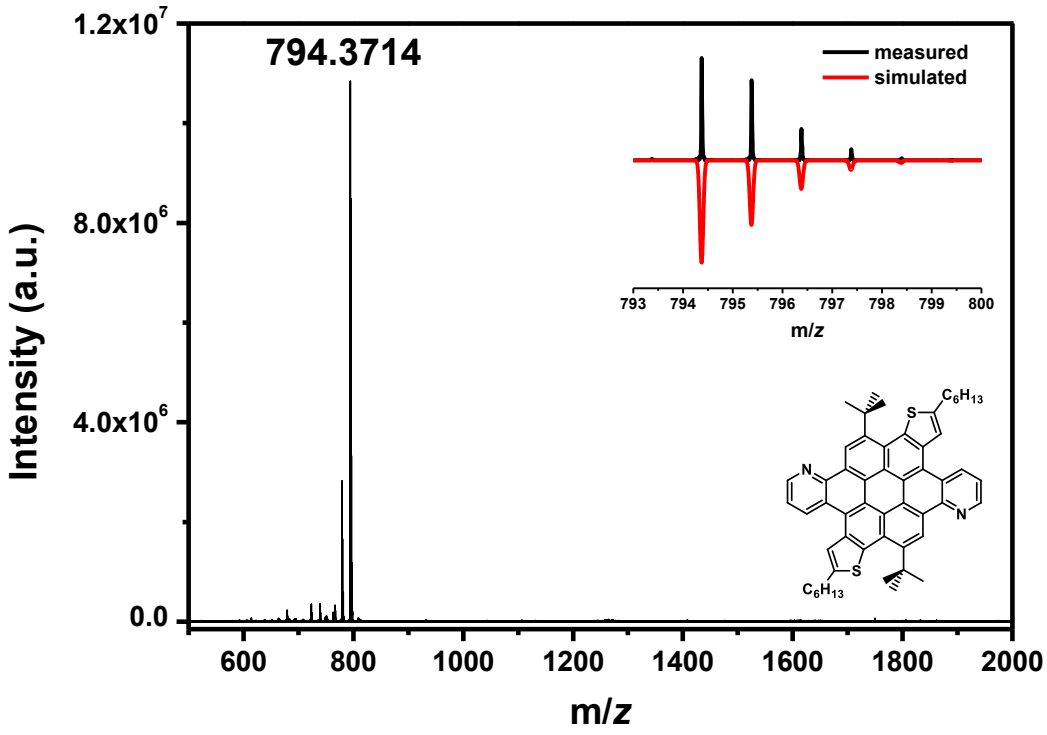

Figure 7.230 MALDI high resolution mass spectrum (DCTB) of **165**.

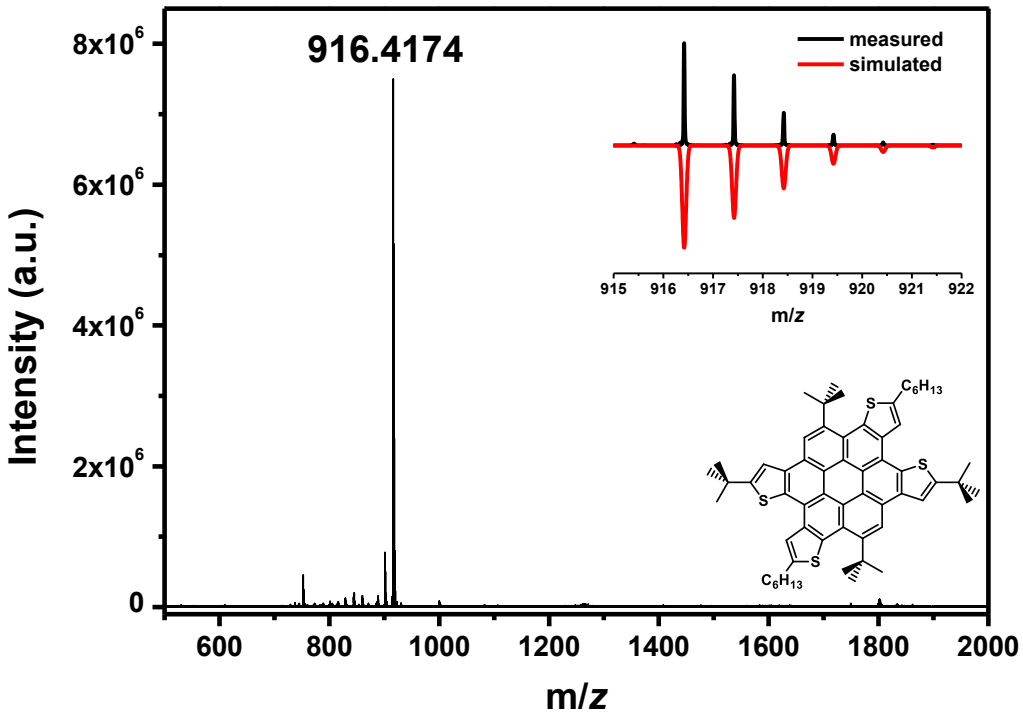

Figure 7.231 MALDI high resolution mass spectrum (DCTB) of **166**.

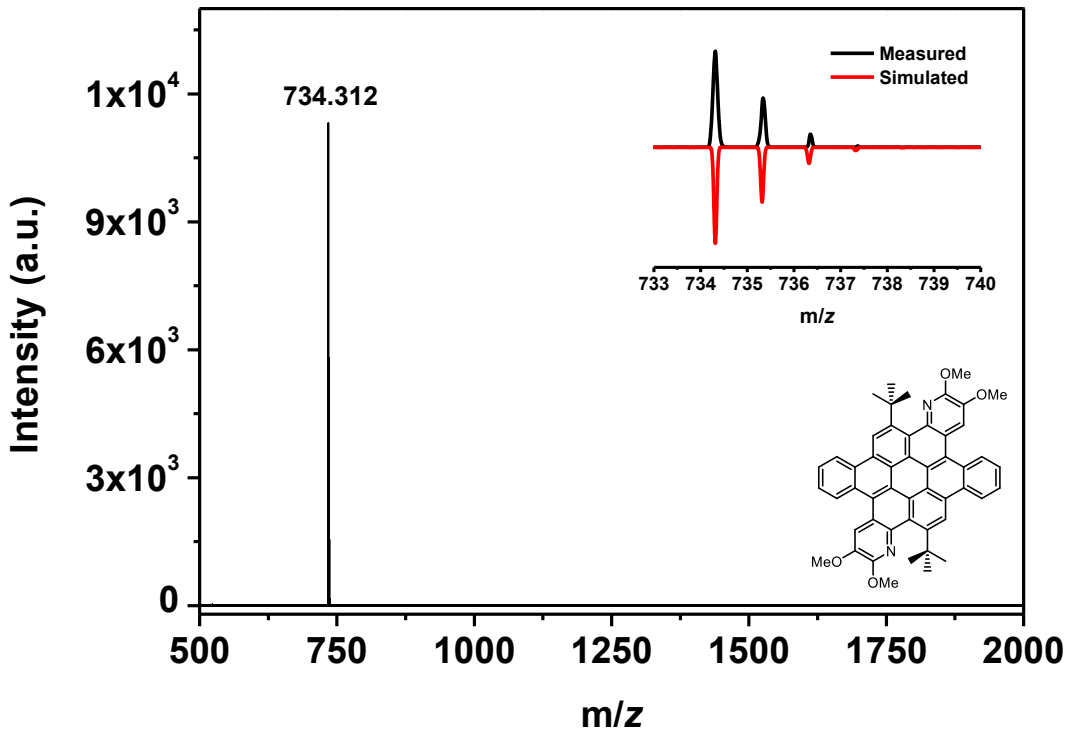

Figure 7.232 MALDI-TOF mass spectrum (DCTB) of **167**.

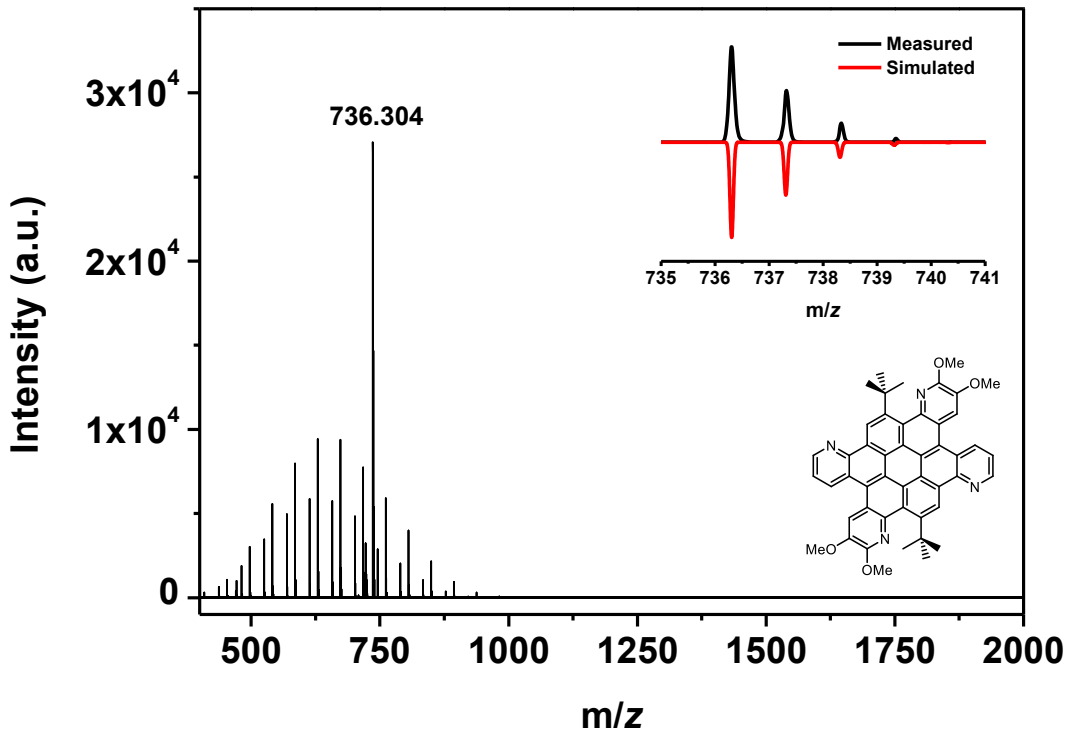

Figure 7.233 MALDI-TOF mass spectrum (DCTB, Kalib PEG 600) of **168**.

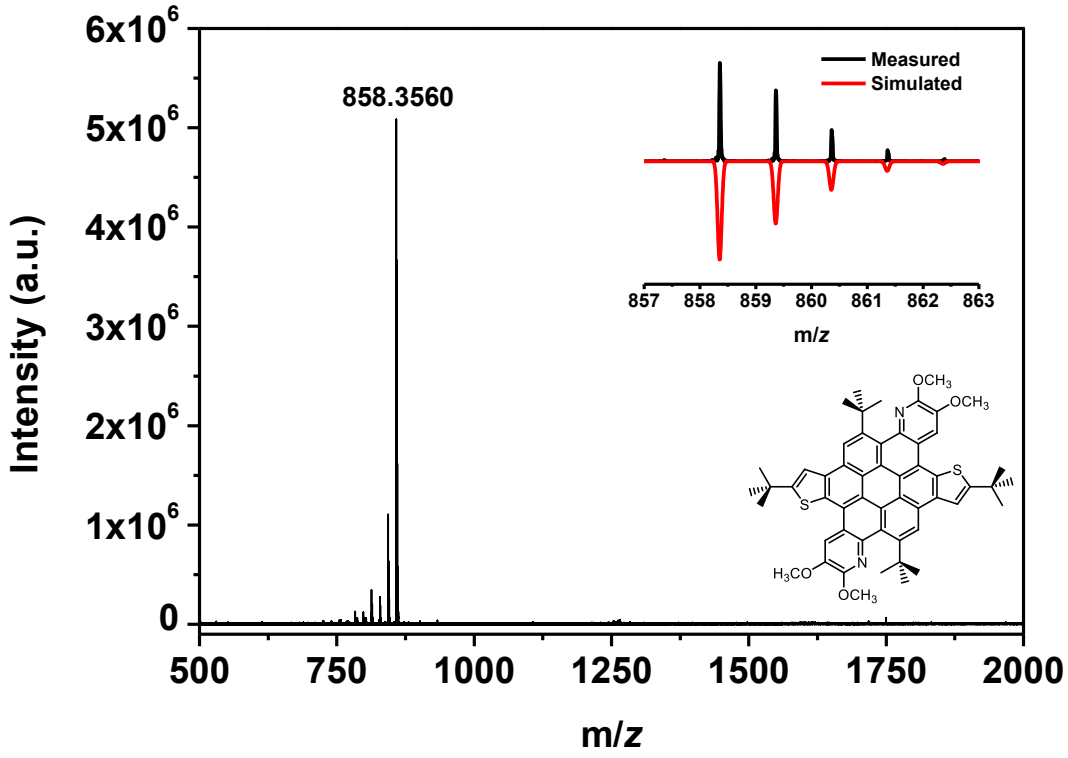

Figure 7.234 MALDI high resolution mass spectrum (DCTB) of **169**.

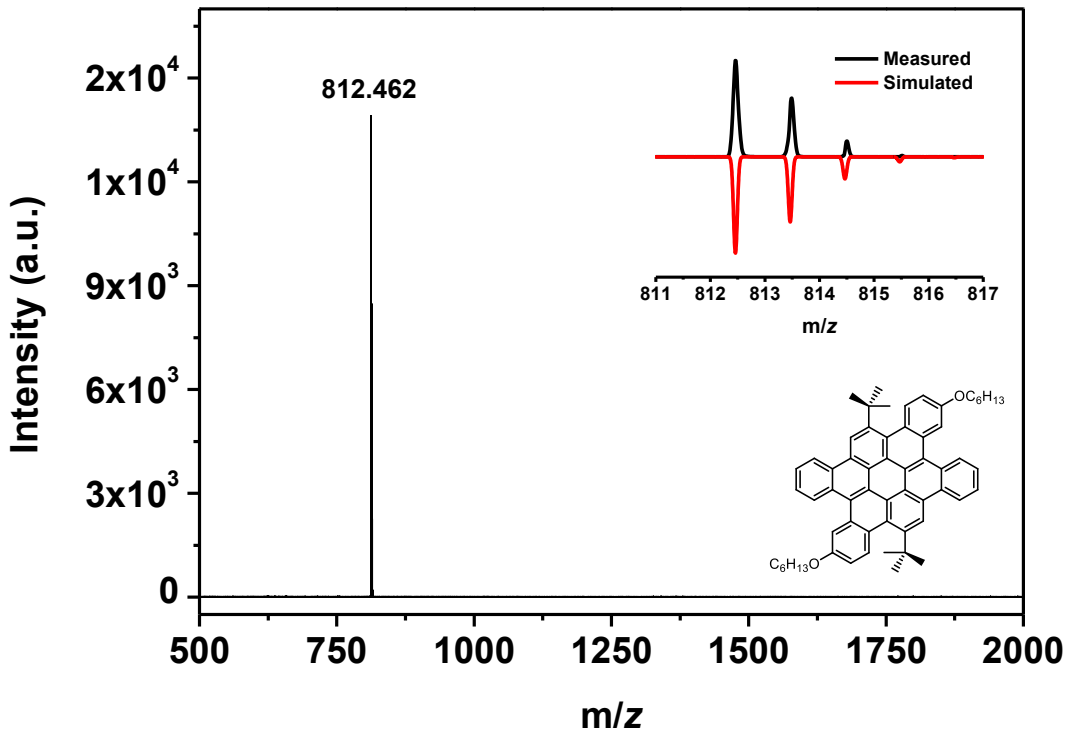

Figure 7.235 MALDI-TOF mass spectrum (DCTB) of **170**.

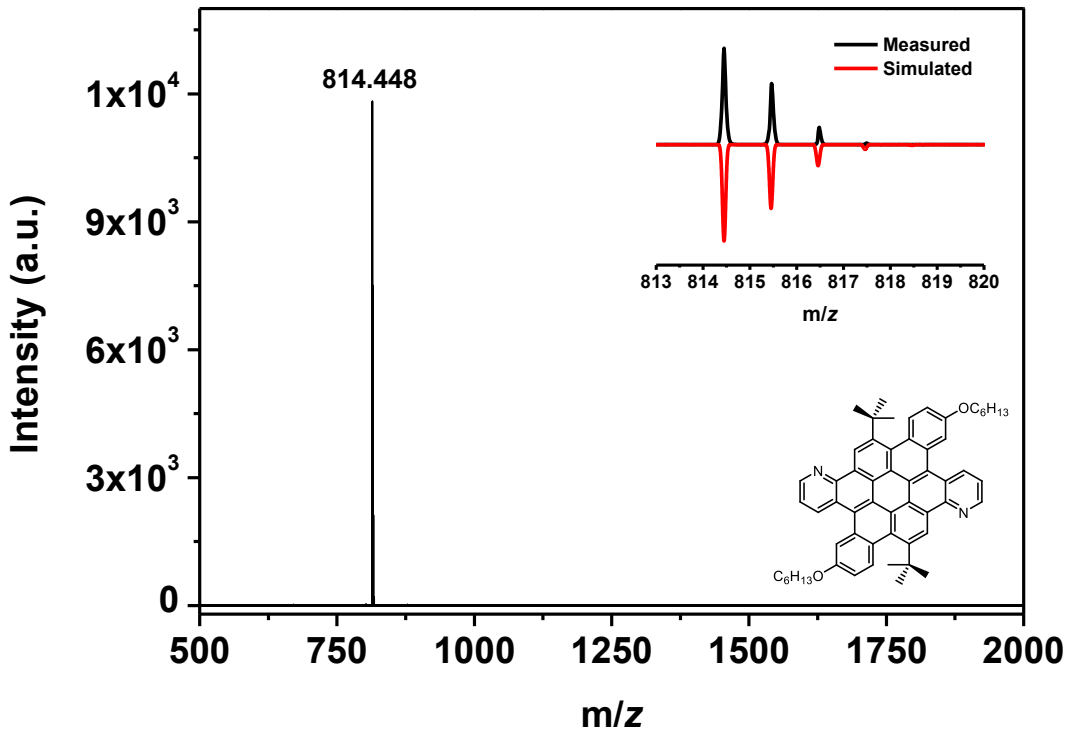

Figure 7.236 MALDI-TOF mass spectrum (DCTB) of **171**.

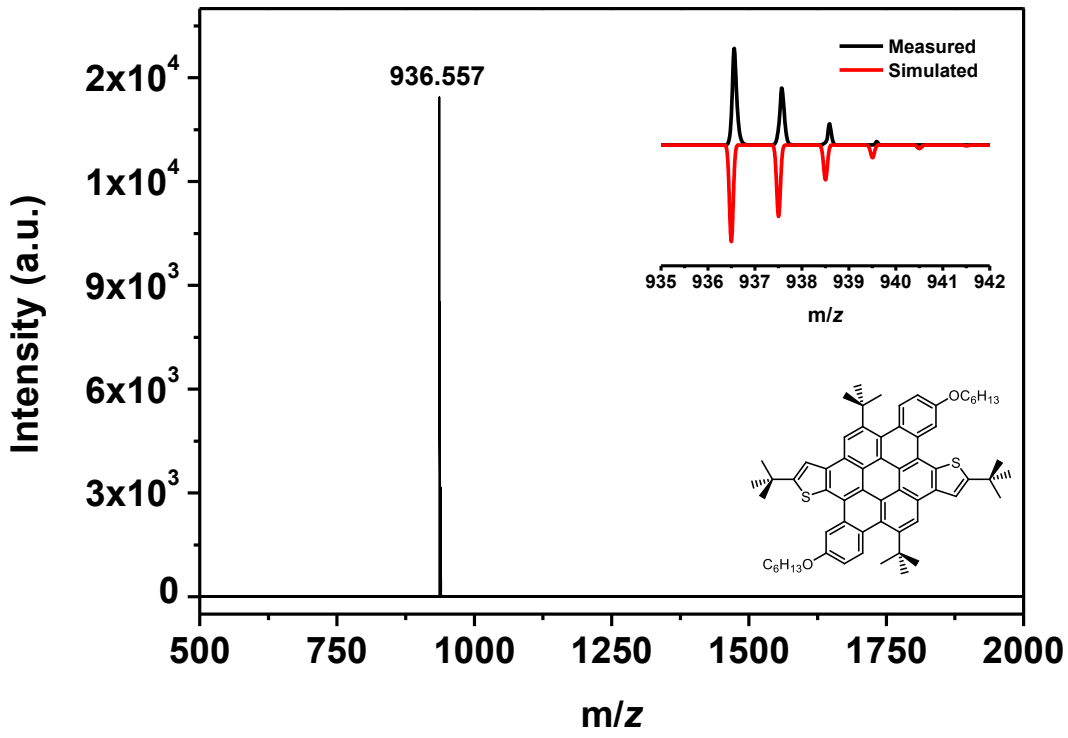

Figure 7.237 MALDI-TOF mass spectrum (DCTB) of **172**.

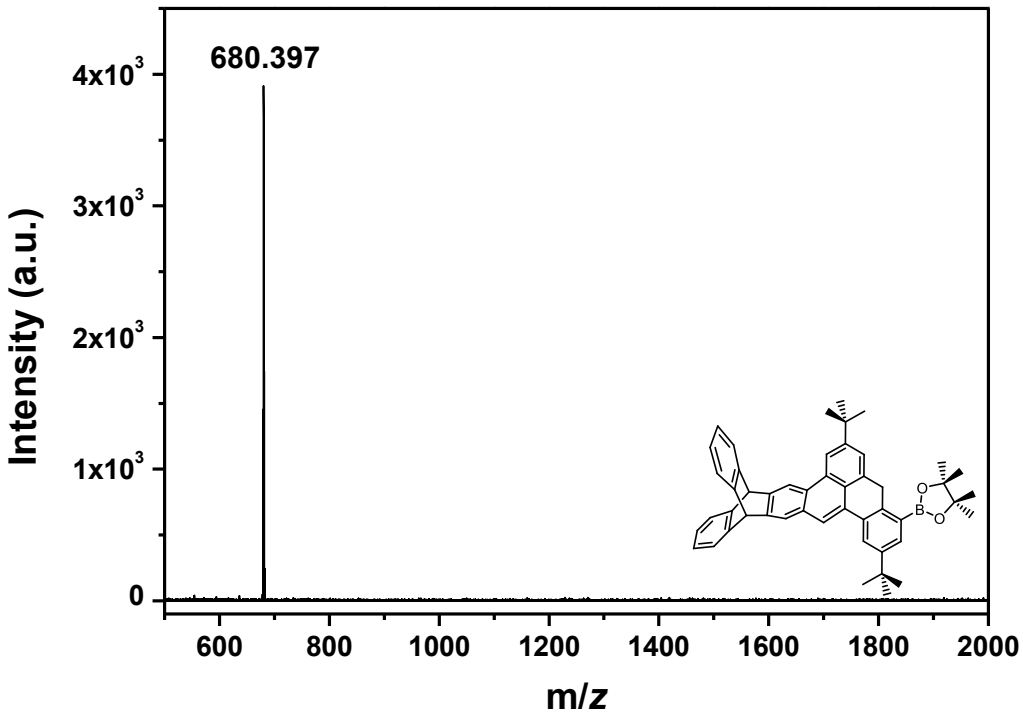

Figure 7.238 MALDI-TOF mass spectrum (DCTB) of **250**.

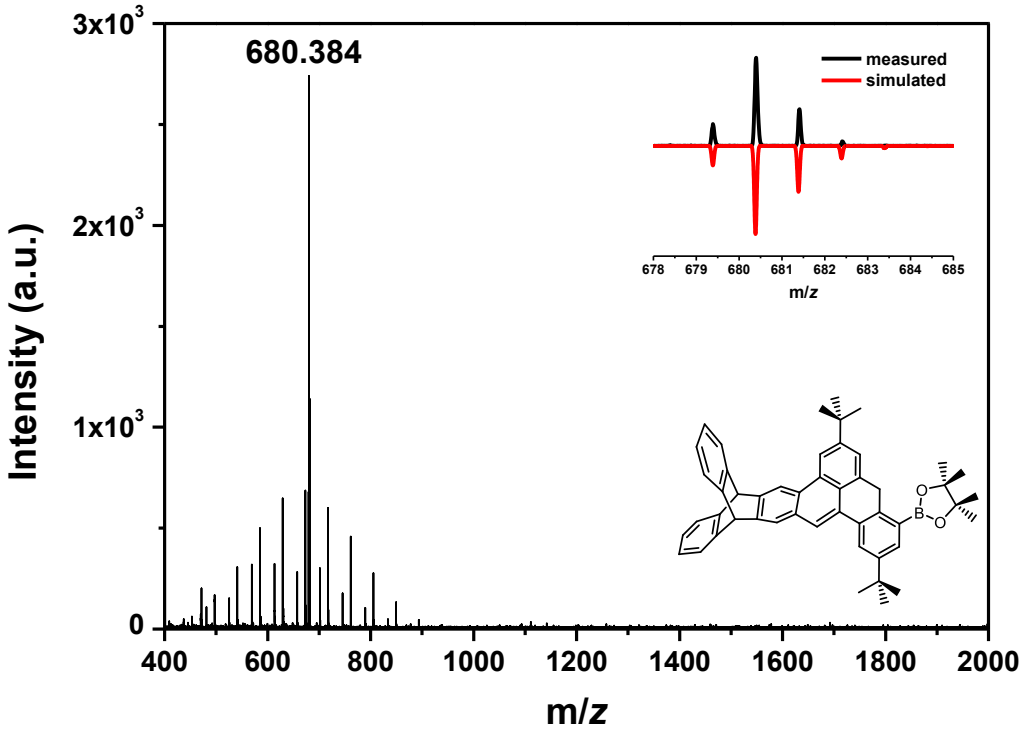

Figure 7.239 MALDI-TOF mass spectrum (DCTB, Kalib PEG600) (DCTB) of **162**.

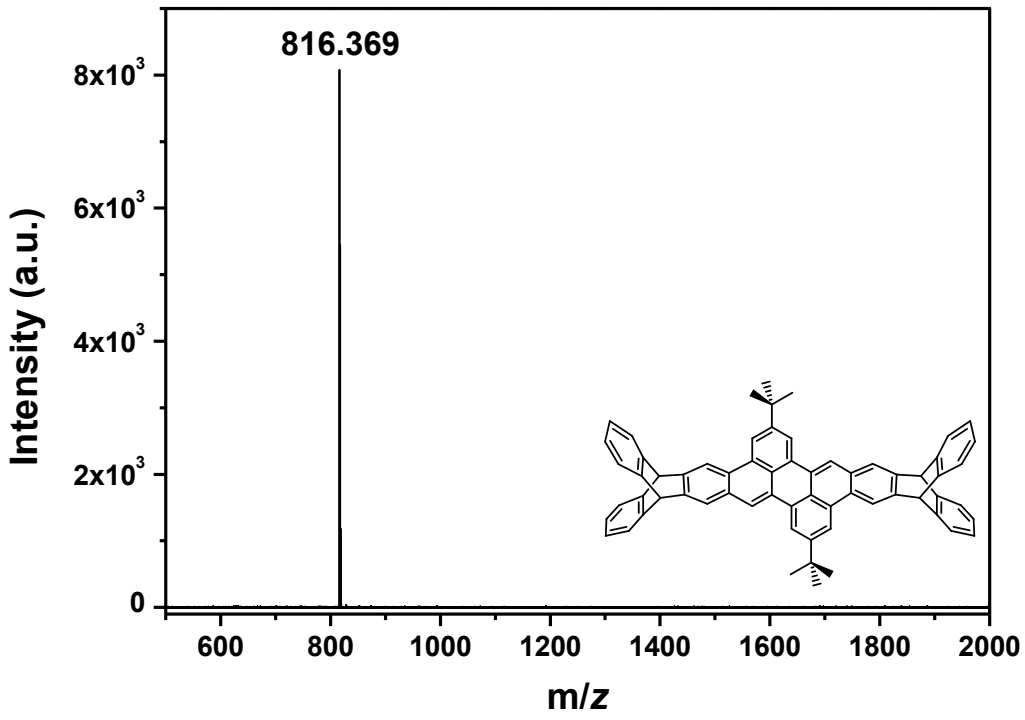

Figure 7.240 MALDI-TOF mass spectrum (DCTB) of PO-5 (**228**).

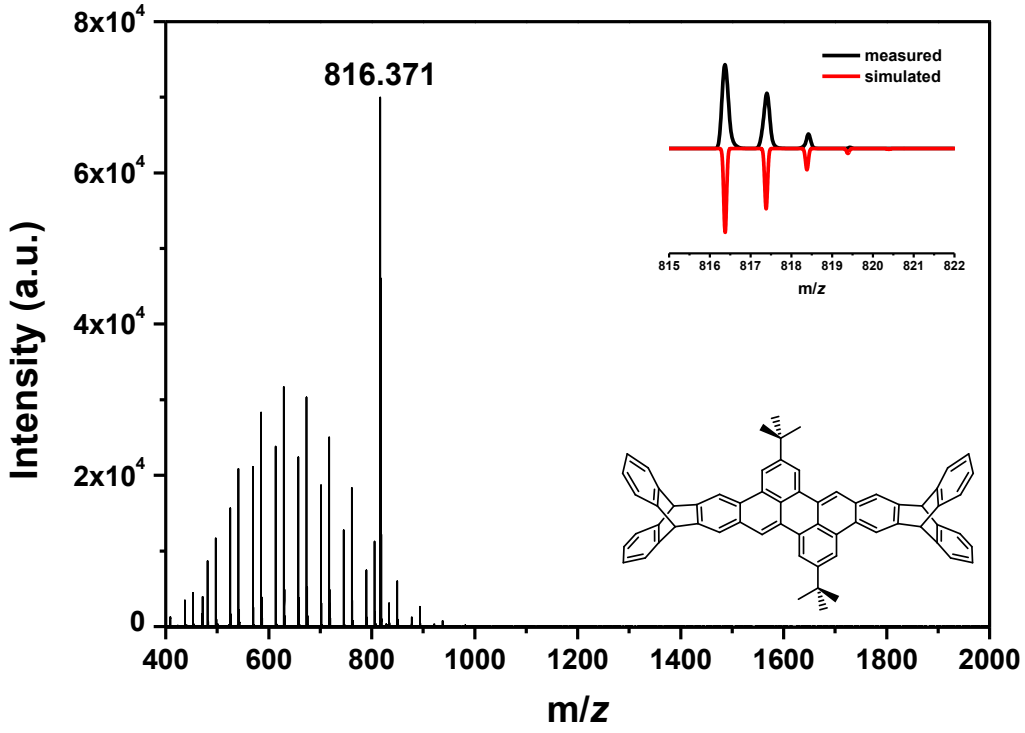

Figure 7.241 MALDI-TOF mass spectrum (DCTB, Kalib PEG600) of PO-5 (**228**).

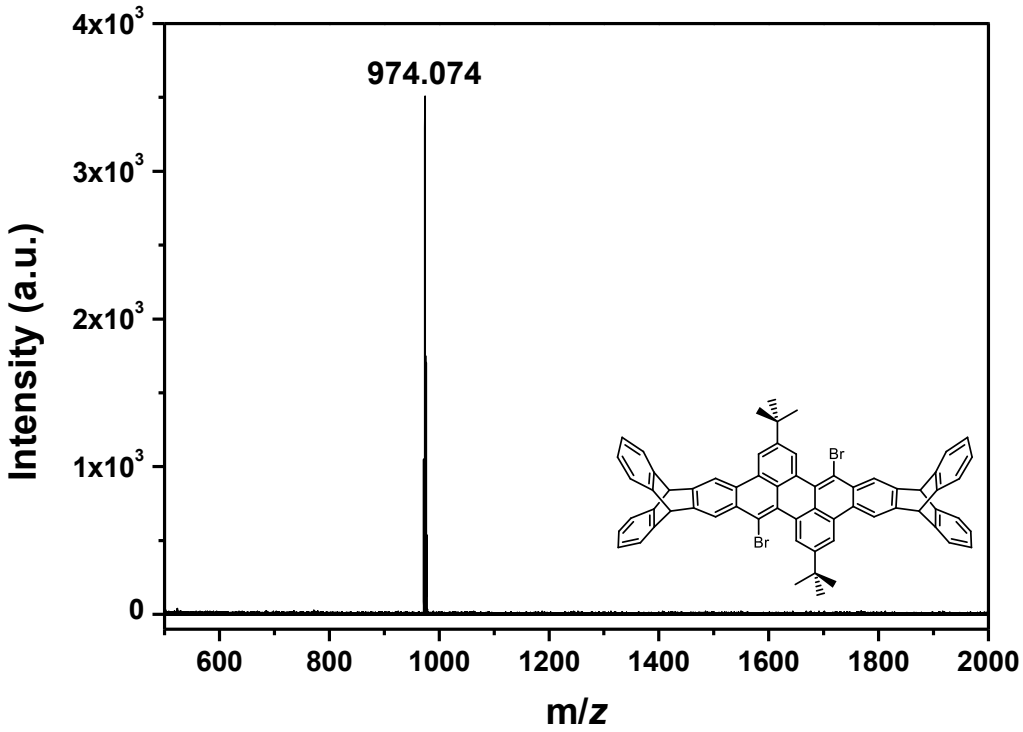

Figure 7.242 MALDI-TOF mass spectrum (DCTB) of **255**.

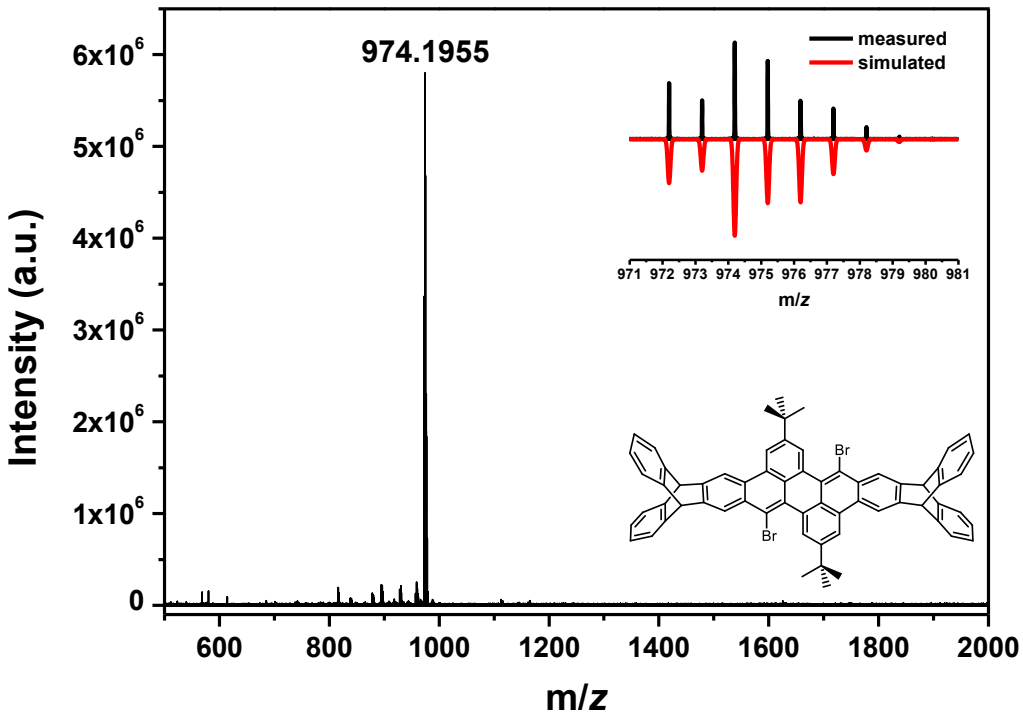

Figure 7.243 MALDI high resolution mass spectrum (DCTB) of **255**.

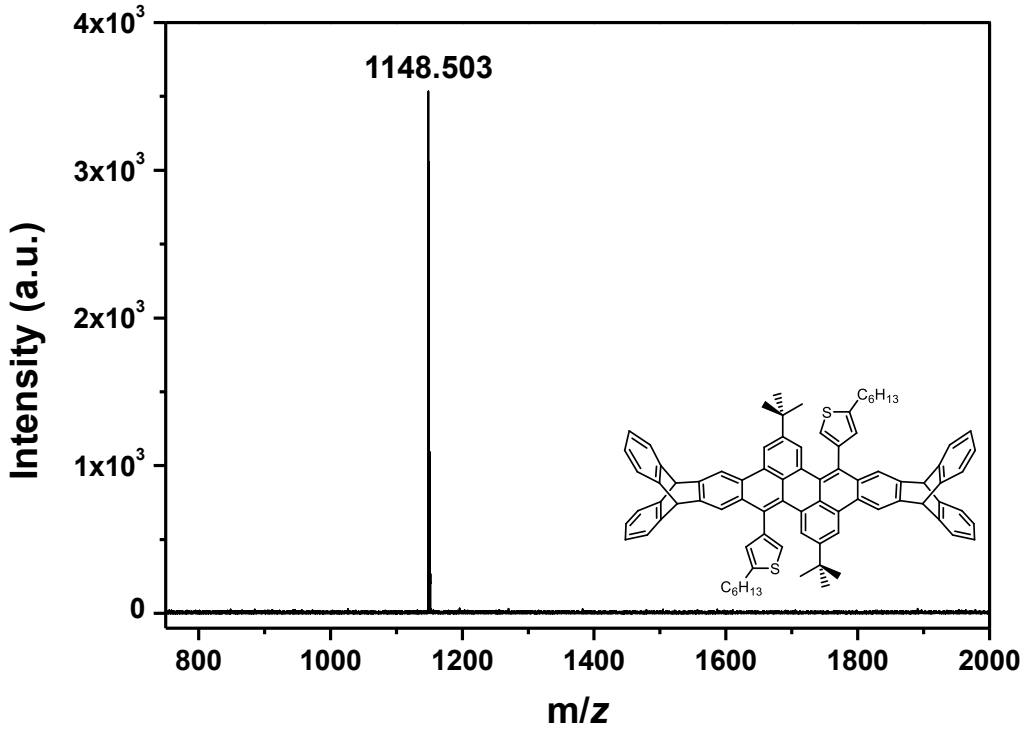

Figure 7.244 MALDI-TOF mass spectrum (DCTB) of **258**.

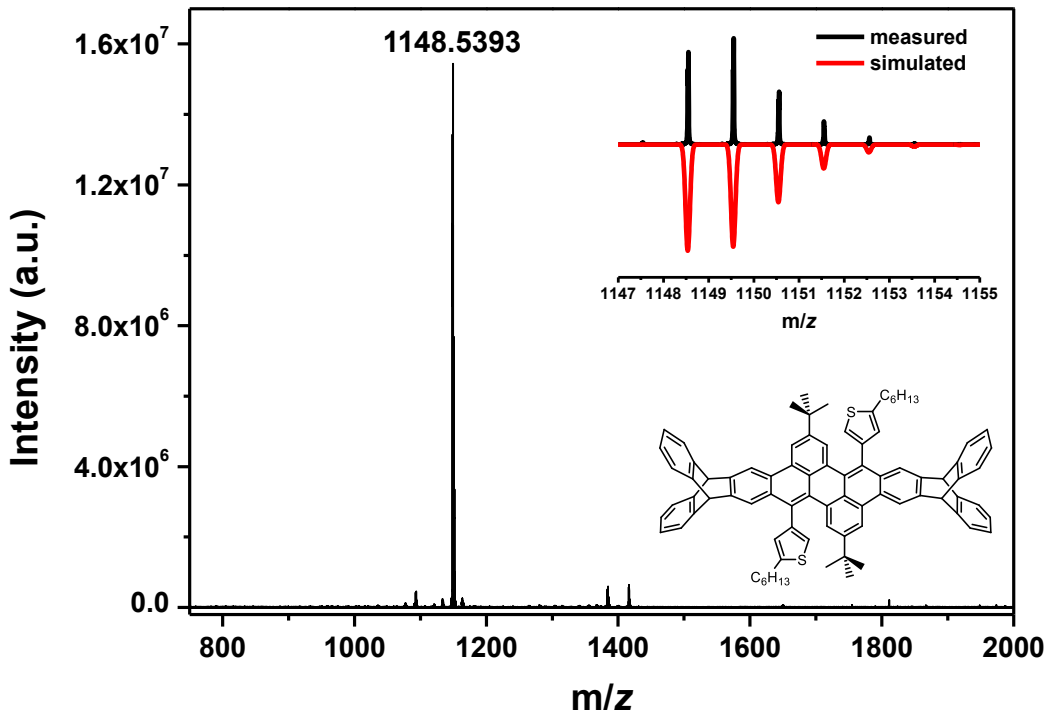

Figure 7.245 MALDI high resolution mass spectrum (DCTB) of **258**.

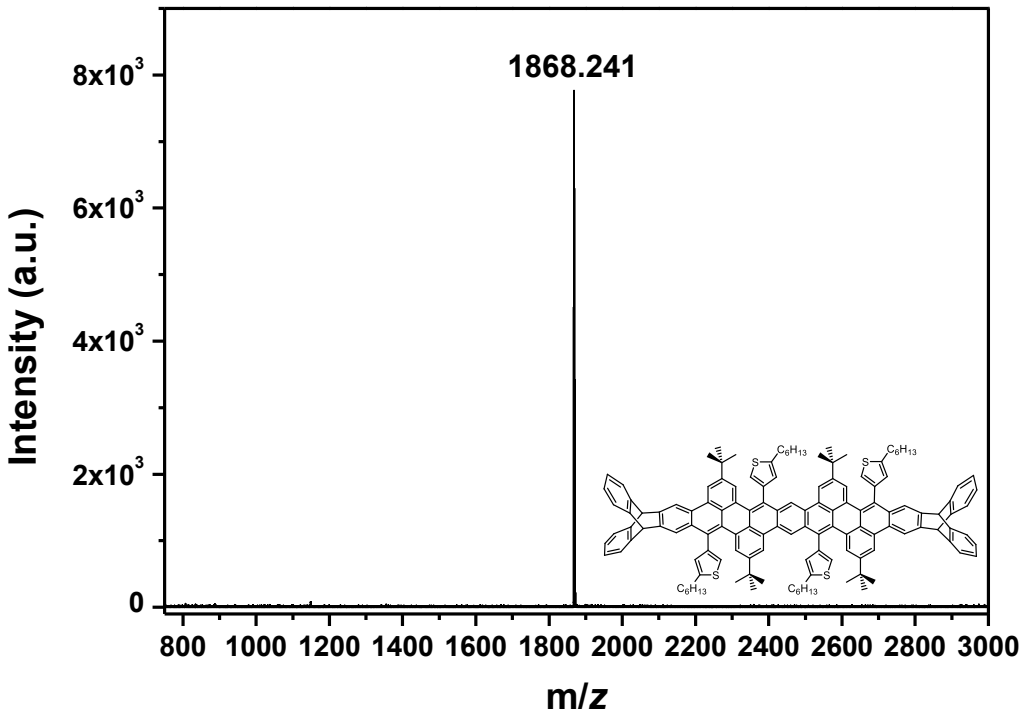

Figure 7.246 MALDI-TOF mass spectrum (DCTB) of **259**.

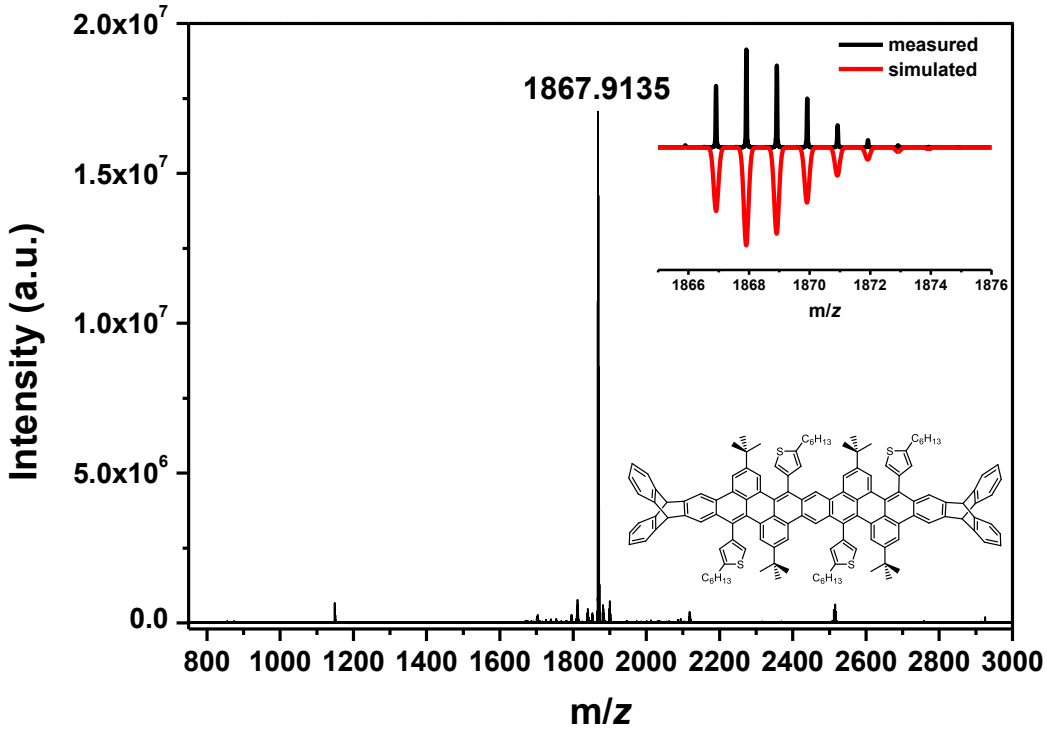

Figure 7.247 MALDI high resolution mass spectrum (DCTB) of **259**.

7.3 X-ray Crystallographic Structure Determination

The already published single crystal structures discussed in chapter 3 can be found in the Cambridge Structural Database (CSD). The CCDC numbers and corresponding references are given in Table 7.1.

Table 7.1 CCDC numbers and corresponding references of the published crystals.

compound	CCDC number	reference
133	1871082	[219a]
137	1871083	[219a]
142	1871084	[219a]
164	1871085	[219a]
165	1871086	[219a]
166	1871087	[219a]
179	1914188	[219b]
184	1914189	[219b]
197	1914190	[219b]
202	1922726	[219c]
208	1922727	[219c]
213	1922728	[219c]

Table 7.2 Crystal data and structure refinement for **134**.

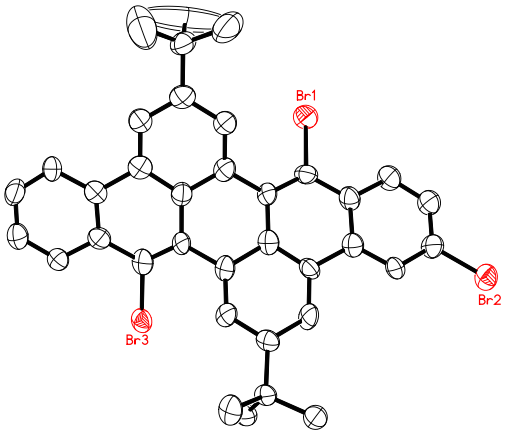

Empirical formula	$C_{40}H_{37}Br_3O$
Formula weight	773.42
Temperature	100(2) K
Wavelength	1.54178 Å
Crystal system	monoclinic
Space group	$P2_1/c$
Z	4
Unit cell dimensions	a = 10.8376(6) Å α =90 deg.
	b = 33.7009(16) Å β = 110.095(4) deg.
	c =9.6033(5) Å γ = 90 deg.
Volume	3294.0(3) $Å^3$
Density (calculated)	1.56 g/cm^3
Absorption coefficient	4.78 mm^{-1}
Crystal shape	needle
Crystal size	0.620 x 0.100 x 0.040 mm^3
Crystal colour	yellow
Theta range for data collection	6.8 to 52.7 deg.
Index ranges	$-11 \le h \le 8$, $-34 \le k \le 34$, $-8 \le l \le 9$
Reflections collected	43217
Independent reflections	3758 (R(int) = 0.0961)
Observed reflections	2021 ($I > 2\sigma(I)$)
Absorption correction	Semi-empirical from equivalents
Max. and min. transmission	1.58 and 0.47
Refinement method	Full-matrix least-squares on F^2
Data/restraints/parameters	43217 / 397 / 408
Goodness-of-fit on F^2	1.03
Final R indices (I>2sigma(I))	R1 = 0.102, wR2 = 0.264
Largest diff. peak and hole	1.00 and -0.75 $eÅ^{-3}$

Table 7.3 Crystal data and structure refinement for **136**.

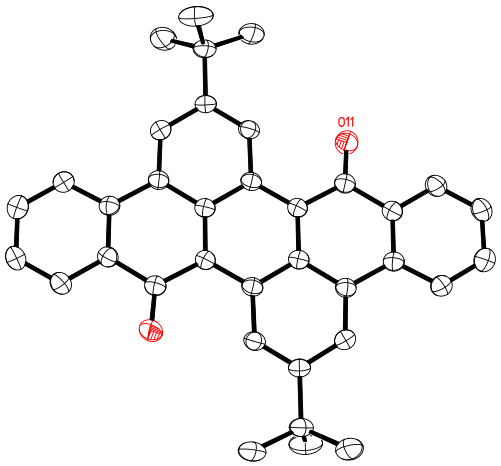

Summenformel	$C_{36}H_{30}O_2$	
Molmasse	494.60	
Temperatur	200(2) K	
Wellenlänge	0.71073 Å	
Kristallsystem	monoklin	
Raumgruppe	C2/c	
Z	4	
Gitterkonstanten	a = 27.451(4) Å	α =90 °
	b =6.1694(9) Å	β =132.005(3) °
	c = 20.419(3) Å	γ = 90 °
Zellvolumen	2569.7(6) $Å^3$	
Dichte (berechnet)	1.278 g/cm^3	
Absorptionskoeffizient µ	0.077 mm^{-1}	
Kristallform	needle	
Kristallgröße	0.380 x 0.040 x 0.021 mm^3	
Kristallfarbe	red	
Gemessener Theta-Bereich	1.997 bis 25.030 °	
Indexgrenzen	$-32 \le h \le 32$, $-7 \le k \le 7$, $-24 \le l \le 24$	
Gemessene Reflexe	11563	
Unabhängige Reflexe	2276 (R(int) = 0.0542)	
Beobachtete Reflexe	1601 ($I > 2\sigma(I)$)	
Absorptionskorrektur	Semi-empirical from equivalents	
Max/min Transmission	0.96 and 0.85	
Strukturverfeinerung	Full-matrix least-squares an F^2	
Daten/Restraints/Parameter	2276 / 0 / 175	
Goodness-of-fit an F^2	1.08	
R-Werte (I>2sigma(I))	R1 = 0.057, wR2 = 0.154	
Extinktionskoeffizient	n/a	
Max/min Restelektronendichte	0.33 und -0.20 $eÅ^{-3}$	

Table 7.4 Crystal data and structure refinement for **149**.

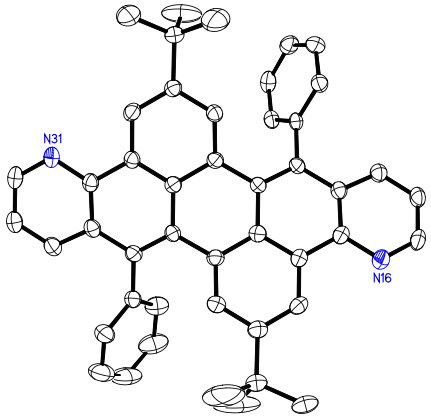

Empirical formula	$C_{46}H_{38}N_2$
Formula weight	618.78
Temperature	200(2) K
Wavelength	0.71073 Å
Crystal system	monoclinic
Space group	$P2_1/c$
Z	4
Unit cell dimensions	a = 15.5806(16) Å α =90 deg. b = 12.1555(12) Å β =91.4664(19) deg. c = 19.1108(19) Å γ = 90 deg.
Volume	3618.2(6) $Å^3$
Density (calculated)	1.14 g/cm^3
Absorption coefficient	0.06 mm^{-1}
Crystal shape	plate
Crystal size	0.301 x 0.173 x 0.119 mm^3
Crystal colour	yellow
Theta range for data collection	2.0 to 26.4 deg.
Index ranges	$-19\leq h\leq 19$, $-14\leq k\leq 15$, $-23\leq l\leq 23$
Reflections collected	24519
Independent reflections	7404 (R(int) = 0.0731)
Observed reflections	4065 ($I > 2\sigma(I)$)
Absorption correction	Semi-empirical from equivalents
Max. and min. transmission	0.96 and 0.90
Refinement method	Full-matrix least-squares on F^2
Data/restraints/parameters	7404 / 45 / 449
Goodness-of-fit on F^2	1.02
Final R indices (I>2sigma(I))	R1 = 0.062, wR2 = 0.138
Largest diff. peak and hole	0.23 and -0.25 $eÅ^{-3}$

Table 7.5 Crystal data and structure refinement for **152**.

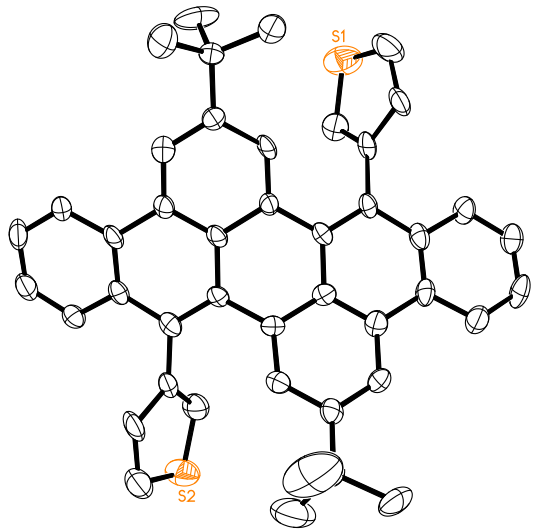

Empirical formula	$C_{44}H_{36}O_2S_2$
Formula weight	660.85
Temperature	200(2) K
Wavelength	0.71073 Å
Crystal system	triclinic
Space group	$P\bar{1}$
Z	2
Unit cell dimensions	a = 10.035(4) Å α =86.977(9) deg.
	b = 13.684(5) Å β =86.376(9) deg.
	c = 14.455(5) Å γ =87.082(8) deg.
Volume	1976.1(13) $Å^3$
Density (calculated)	1.11 g/cm^3
Absorption coefficient	0.17 mm^{-1}
Crystal shape	plate
Crystal size	0.201 x 0.116 x 0.042 mm^3
Crystal colour	yellow
Theta range for data collection	1.4 to 20.8 deg.
Index ranges	$-10\leq h\leq 10$, $-13\leq k\leq 13$, $-14\leq l\leq 14$
Reflections collected	10858
Independent reflections	4133 (R(int) = 0.1227)
Observed reflections	1759 ($I > 2\sigma(I)$)
Absorption correction	Semi-empirical from equivalents
Max. and min. transmission	0.96 and 0.80
Refinement method	Full-matrix least-squares on F^2
Data/restraints/parameters	4133 / 570 / 423
Goodness-of-fit on F^2	0.93
Final R indices (I>2sigma(I))	R1 = 0.076, wR2 = 0.159
Largest diff. peak and hole	0.28 and -0.30 $eÅ^{-3}$

Table 7.6 Crystal data and structure refinement for **154**.

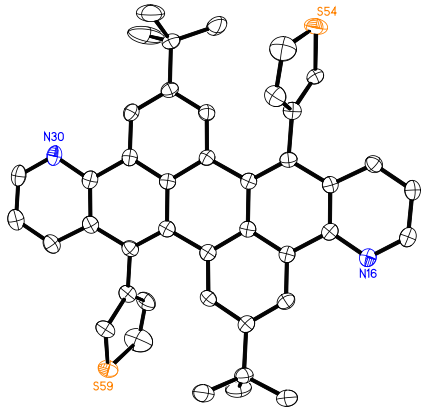

Empirical formula	$C_{42}H_{34}N_2S_2$
Formula weight	630.83
Temperature	100(2) K
Wavelength	1.54178 Å
Crystal system	monoclinic
Space group	$P2_1/c$
Z	4
Unit cell dimensions	a =6.2228(2) Å α =90 deg. b = 17.6163(6) Å β =90.890(2) deg. c = 28.0848(8) Å γ = 90 deg.
Volume	3078.36(17) $Å^3$
Density (calculated)	1.36 g/cm^3
Absorption coefficient	1.83 mm^{-1}
Crystal shape	needle
Crystal size	0.165 x 0.125 x 0.055 mm^3
Crystal colour	yellow
Theta range for data collection	3.0 to 68.3 deg.
Index ranges	$-7 \le h \le 4$, $-20 \le k \le 19$, $-33 \le l \le 30$
Reflections collected	19882
Independent reflections	5481 (R(int) = 0.0658)
Observed reflections	3826 ($I > 2\sigma(I)$)
Absorption correction	Semi-empirical from equivalents
Max. and min. transmission	1.63 and 0.44
Refinement method	Full-matrix least-squares on F^2
Data/restraints/parameters	5481 / 1055 / 513
Goodness-of-fit on F^2	1.10
Final R indices (I>2sigma(I))	R1 = 0.066, wR2 = 0.126
Largest diff. peak and hole	0.26 and -0.24 $eÅ^{-3}$

Table 7.7 Crystal data and structure refinement for **156**.

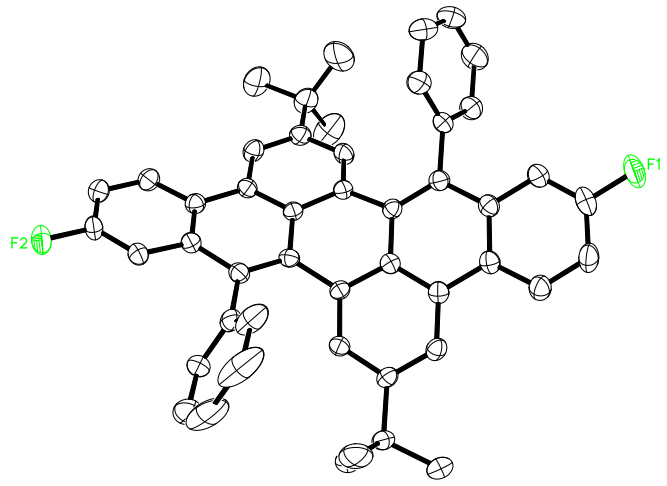

Empirical formula	$C_{54}H_{50}F_2O_{1.50}$
Formula weight	760.94
Temperature	200(2) K
Wavelength	0.71073 Å
Crystal system	monoclinic
Space group	C2/c
Z	8
Unit cell dimensions	a = 24.2308(11) Å α =90 deg. b = 14.4147(6) Å β =100.1361(15) deg. c = 24.2573(12) Å γ = 90 deg.
Volume	8340.3(7) $Å^3$
Density (calculated)	1.21 g/cm^3
Absorption coefficient	0.08 mm^{-1}
Crystal shape	big
Crystal size	0.355 x 0.213 x 0.131 mm^3
Crystal colour	yellow
Theta range for data collection	1.8 to 23.8 deg.
Index ranges	$-27 \le h \le 27$, $-16 \le k \le 16$, $-27 \le l \le 24$
Reflections collected	23726
Independent reflections	6385 (R(int) = 0.0680)
Observed reflections	3725 ($I > 2\sigma(I)$)
Absorption correction	Semi-empirical from equivalents
Max. and min. transmission	0.96 and 0.87
Refinement method	Full-matrix least-squares on F^2
Data/restraints/parameters	6385 / 731 / 547
Goodness-of-fit on F^2	1.02
Final R indices (I>2sigma(I))	R1 = 0.063, wR2 = 0.156
Largest diff. peak and hole	0.32 and -0.40 $eÅ^{-3}$

Table 7.8 Crystal data and structure refinement for **161**.

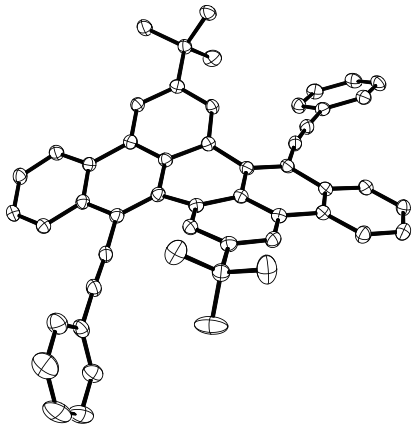

Empirical formula	$C_{52}H_{40}$
Formula weight	664.84
Temperature	100(2) K
Wavelength	1.54178 Å
Crystal system	monoclinic
Space group	$P2_1/n$
Z	4
Unit cell dimensions	a = 10.7067(2) Å α =90 deg.
	b = 19.5134(6) Å β =105.284(2) deg.
	c = 17.7978(4) Å γ = 90 deg.
Volume	3586.87(16) $Å^3$
Density (calculated)	1.23 g/cm^3
Absorption coefficient	0.52 mm^{-1}
Crystal shape	plate
Crystal size	0.200 x 0.190 x 0.030 mm^3
Crystal colour	yellow
Theta range for data collection	3.4 to 71.6 deg.
Index ranges	$-13 \le h \le 12$, $-23 \le k \le 21$, $-21 \le l \le 16$
Reflections collected	25995
Independent reflections	6860 (R(int) = 0.0280)
Observed reflections	5843 ($I > 2\sigma(I)$)
Absorption correction	Semi-empirical from equivalents
Max. and min. transmission	1.64 and 0.56
Refinement method	Full-matrix least-squares on F^2
Data/restraints/parameters	6860 / 0 / 475
Goodness-of-fit on F^2	1.03
Final R indices (I>2sigma(I))	R1 = 0.040, wR2 = 0.098
Largest diff. peak and hole	0.41 and -0.25 $eÅ^{-3}$

Table 7.9 Crystal data and structure refinement for **169**.

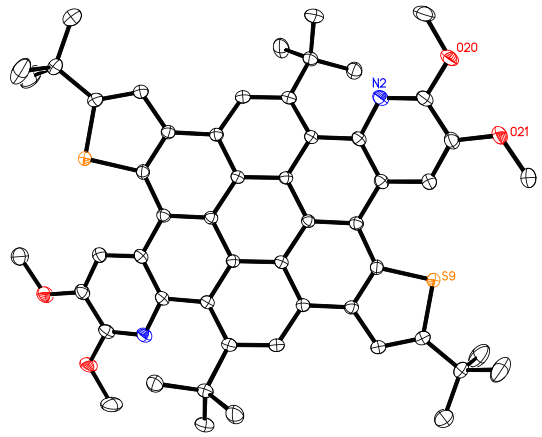

Empirical formula	$C_{54}H_{54}N_2O_4S_2 \cdot 2CHCl_3$	
Formula weight	1097.84	
Temperature	100(2) K	
Wavelength	1.54178 Å	
Crystal system	monoclinic	
Space group	$P2_1/n$	
Z	2	
Unit cell dimensions	a = 11.100(3) Å	α =90 deg.
	b = 17.121(5) Å	β =106.537(18) deg.
	c = 14.669(4) Å	γ = 90 deg.
Volume	2672.5(13) $Å^3$	
Density (calculated)	1.36 g/cm^3	
Absorption coefficient	4.04 mm^{-1}	
Crystal shape	plate	
Crystal size	0.194 x 0.154 x 0.062 mm^3	
Crystal colour	orange	
Theta range for data collection	4.1 to 76.7 deg.	
Index ranges	$-13 \le h \le 8$, $-21 \le k \le 18$, $-18 \le l \le 17$	
Reflections collected	13827	
Independent reflections	5389 (R(int) = 0.0188)	
Observed reflections	4871 ($I > 2\sigma(I)$)	
Absorption correction	Semi-empirical from equivalents	
Max. and min. transmission	1.99 and 0.57	
Refinement method	Full-matrix least-squares on F^2	
Data/restraints/parameters	5389 / 126 / 361	
Goodness-of-fit on F^2	1.05	
Final R indices (I>2sigma(I))	R1 = 0.050, wR2 = 0.137	
Largest diff. peak and hole	0.65 and -0.48 $eÅ^{-3}$	

Table 7.10 Crystal data and structure refinement for **170**.

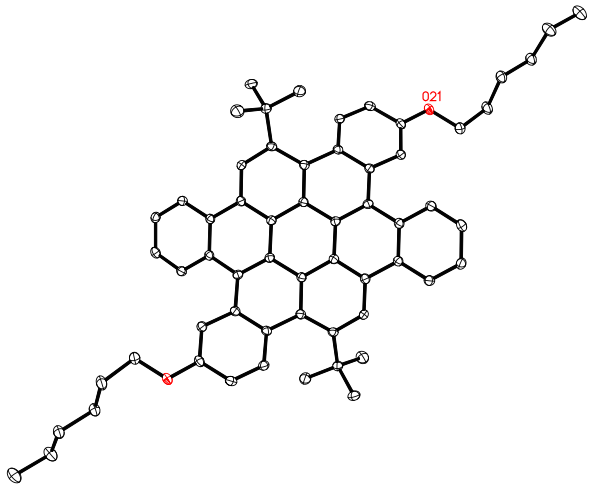

Empirical formula	$C_{60}H_{60}O_2$	
Formula weight	813.08	
Temperature	100(2) K	
Wavelength	1.54178 Å	
Crystal system	triclinic	
Space group	$P\bar{1}$	
Z	1	
Unit cell dimensions	a =9.0467(4) Å	α =96.790(4) deg.
	b = 10.4098(5) Å	β =109.532(4) deg.
	c = 12.4858(6) Å	γ =98.542(4) deg.
Volume	1077.96(9) $Å^3$	
Density (calculated)	1.25 g/cm^3	
Absorption coefficient	0.56 mm^{-1}	
Crystal shape	plate	
Crystal size	0.161 x 0.107 x 0.046 mm^3	
Crystal colour	brightyellow	
Theta range for data collection	3.8 to 71.7 deg.	
Index ranges	$-11 \le h \le 10$, $-11 \le k \le 12$, $-15 \le l \le 10$	
Reflections collected	13240	
Independent reflections	4083 (R(int) = 0.0265)	
Observed reflections	3518 ($I > 2\sigma(I)$)	
Absorption correction	Semi-empirical from equivalents	
Max. and min. transmission	1.86 and 0.57	
Refinement method	Full-matrix least-squares on F^2	
Data/restraints/parameters	4083 / 0 / 284	
Goodness-of-fit on F^2	1.07	
Final R indices (I>2sigma(I))	R1 = 0.042, wR2 = 0.106	
Largest diff. peak and hole	0.30 and -0.22 $eÅ^{-3}$	

Table 7.11 Crystal data and structure refinement for **171**.

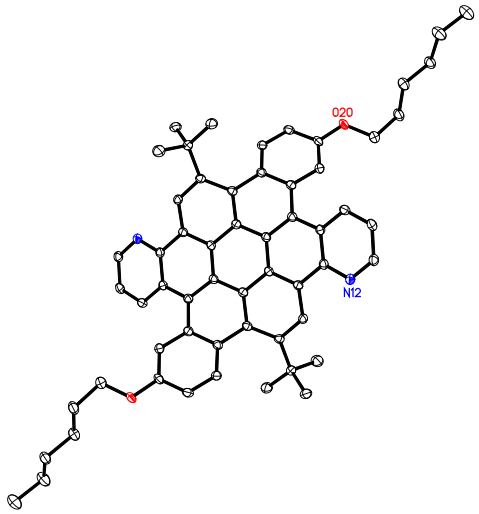

Empirical formula	$C_{58}H_{58}N_2O_2$	
Formula weight	815.06	
Temperature	100(2) K	
Wavelength	1.54178 Å	
Crystal system	triclinic	
Space group	$P\bar{1}$	
Z	1	
Unit cell dimensions	a =9.0089(5) Å	α =96.826(5) deg.
	b = 10.3683(6) Å	β =110.301(4) deg.
	c = 12.4729(7) Å	γ =97.674(4) deg.
Volume	1065.66(11) $Å^3$	
Density (calculated)	1.27 g/cm^3	
Absorption coefficient	0.58 mm^{-1}	
Crystal shape	plate	
Crystal size	0.151 x 0.090 x 0.021 mm^3	
Crystal colour	yellow	
Theta range for data collection	3.8 to 68.3 deg.	
Index ranges	-10≤h≤4, -12≤k≤12, -13≤l≤14	
Reflections collected	13448	
Independent reflections	3810 (R(int) = 0.0265)	
Observed reflections	2936 (I > 2σ(I))	
Absorption correction	Semi-empirical from equivalents	
Max. and min. transmission	1.69 and 0.58	
Refinement method	Full-matrix least-squares on F^2	
Data/restraints/parameters	3810 / 0 / 284	
Goodness-of-fit on F^2	1.03	
Final R indices (I>2sigma(I))	R1 = 0.038, wR2 = 0.099	
Largest diff. peak and hole	0.33 and -0.23 $eÅ^{-3}$	

Table 7.12 Crystal data and structure refinement for **172**.

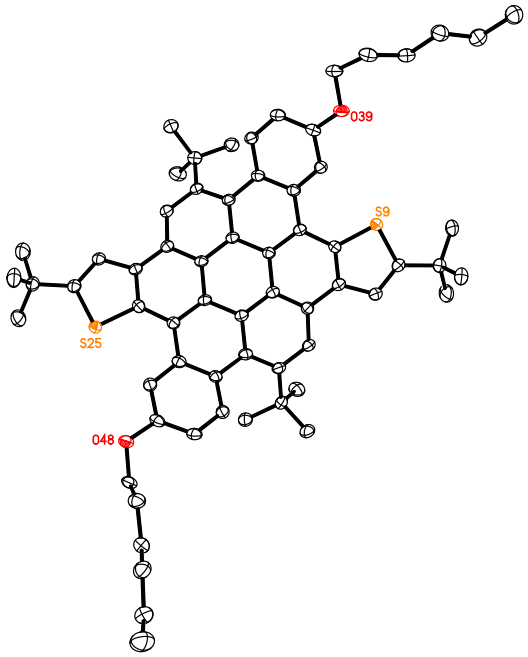

Empirical formula	$C_{64}H_{72}O_2S_2$
Formula weight	937.33
Temperature	100(2) K
Wavelength	1.54178 Å
Crystal system	orthorhombic
Space group	Fdd2
Z	16
Unit cell dimensions	a = 25.6943(6) Å α = 90 deg.
	b = 34.3666(9) Å β = 90 deg.
	c = 23.0756(4) Å γ = 90 deg.
Volume	20376.3(8) $Å^3$
Density (calculated)	1.22 g/cm^3
Absorption coefficient	1.28 mm^{-1}
Crystal shape	brick
Crystal size	0.177 x 0.107 x 0.102 mm^3
Crystal colour	yellow
Theta range for data collection	2.9 to 68.2 deg.
Index ranges	$-30 \le h \le 24$, $-37 \le k \le 41$, $-18 \le l \le 27$
Reflections collected	19709
Independent reflections	6498 (R(int) = 0.0183)
Observed reflections	6109 ($I > 2\sigma(I)$)
Absorption correction	Semi-empirical from equivalents
Max. and min. transmission	1.67 and 0.66
Refinement method	Full-matrix least-squares on F^2
Data/restraints/parameters	6498 / 1 / 628
Goodness-of-fit on F^2	1.04
Final R indices (I>2sigma(I))	R1 = 0.029, wR2 = 0.074
Absolute structure parameter	0.155(16)
Largest diff. peak and hole	0.28 and -0.17 $eÅ^{-3}$

Table 7.13 Crystal data and structure refinement for PO-9 (**229**).

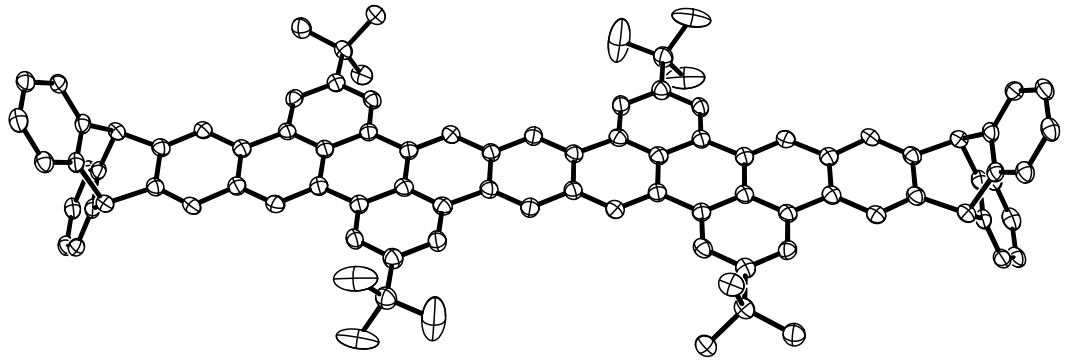

Empirical formula	$C_{94}H_{74}\cdot 6CH_2Cl_2$
Formula weight	1713.08
Temperature	100(2) K
Wavelength	1.54178 Å
Crystal system	triclinic
Space group	$P\bar{1}$
Z	1
Unit cell dimensions	a =8.1918(5) Å α =93.409(5) deg.
	b =9.2120(5) Å β =97.209(5) deg.
	c = 29.0059(17) Å γ = 104.436(4) deg.
Volume	2093.6(2) $Å^3$
Density (calculated)	1.36 g/cm^3
Absorption coefficient	4.01 mm^{-1}
Crystal shape	plate
Crystal size	0.147 x 0.073 x 0.023 mm^3
Crystal colour	orange
Theta range for data collection	3.1 to 68.3 deg.
Index ranges	$-9\leq h\leq 8$, $-10\leq k\leq 9$, $-34\leq l\leq 34$
Reflections collected	25646
Independent reflections	7399 (R(int) = 0.0780)
Observed reflections	5142 ($I > 2\sigma(I)$)
Absorption correction	Semi-empirical from equivalents
Max. and min. transmission	1.99 and 0.38
Refinement method	Full-matrix least-squares on F^2
Data/restraints/parameters	7399 / 594 / 544
Goodness-of-fit on F^2	1.03
Final R indices (I>2sigma(I))	R1 = 0.081, wR2 = 0.204
Largest diff. peak and hole	0.62 and -0.56 $eÅ^{-3}$

8. Abbreviations

°C	degree centigrade
°	degree
1D	one-dimensional
2D	two-dimensional
3D	three-dimensional
Å	angstrom
ACID	anisotropy of the induced current density
Ad	1-adamantyl
ATR	attenuated total reflection
B_2pin_2	bis(pinacolato)diboron
B3LYP	Becke, 3-parameter, Lee-Yang-Parr
BHT	butylated hydroxytoluene
Bpin	boronic acid pinacol ester
bpy	2,2'-bipyridine
Bu	*n*-butyl
Calcd.	calculated
CCDC	Cambrigde Crystallographic Data Centre
CD	circular dichroism
CDHC	cyclodehydrochlorination
cata-HBC	hexa-*cata*-hexabenzocoronene
cm	centimeter
CNTs	carbon nanotubes
COD	1,5-cyclooctadiene
Compd	compound
conc.	concentrated
COSY	correlation spectroscopy
CPME	cyclopentyl methyl ether
CV	cyclovoltammetry
dba	dibenzylideneacetone
DCM	dichloromethane
DCTB	*trans*-2-[3-(4-*tert*-Butylphenyl)-2-methyl-2-propenylidene]malononitrile
DCV	dichlorovinylidene
DDQ	2,3-dichloro-5,6-dicyano-1,4-benzoquinone
dec.	decomposition
DFT	density functional theory

DMF	*N*,*N*-dimethylformamide
DNA	deoxyribonucleic acid
dtbpy	4,4'-di-*tert*-butyl-2,2'-dipyridine
EA	elemental analysis
equiv.	equivalent
Et	ethyl
eV	electronvolt
Fc	ferrocene
Fc^+	ferrocenium
FETs	field-effect transistors
FMOs	frontier molecular orbitals
FT-IR	Fourier transform-infrared
g	gram
g_{abs}	absorptive dissymmetry factor
GIAO	gauge-independent atomic orbital
GNRs	graphene nanoribbons
GP	general procedure
h	hour
HMBC	heteronuclear multiple-bond correlation spectroscopy
HOMO	highest occupied molecular orbital
HPLC	high-performance liquid chromatography
HRMS	high resolution mass spectrometry
HSQC	heteronuclear single-quantum correlation spectroscopy
hv	light irradiation
i-Pr	*iso*-propyl
K	Kelvin
kcal	kilocalorie
kJ	kilojoule
LUMO	lowest unoccupied molecular orbital
M	mol per liter
MALDI	matrix-assisted laser desorption
max	maximal
Me	methyl
Mes	mesityl
MHz	megahertz
min	minute
mM	millimol per liter

MS	mass spectrometry
mV	millivolt
m.p.	melting point
NBS	*N*-bromosuccinimide
NICS	nuclear independent chemical shifts
NIR	near-infrared
nm	nanometer
NMR	nuclear magnetic resonance
NOESY	nuclear Overhauser effect spectroscopy
ns	nanosecond
o-	*ortho*-
o-DCB	*ortho*-dichlorobenzene
OFETs	organic field-effect transistors
ORTEP	oak ridge thermal ellipsoid plot
OTf	trifluoromethanesulfonate
PAHs	polycyclic aromatic hydrocarbons
PBE	Perdew-Burke-Ernzerhof
PCM	polarized continuum model
PDIs	perylene diimides
PEG	polyethylene glycol
Ph	phenyl
peri-HBC	hexa-*peri*-hexabenzocoronene
PIFA	phenyliodine bis(trifluoroacetate)
PMIs	perylene monoimides
PMMA	polymethylmethacrylate
PO	propylene oxide (in chapter 3.1); perylene oligomer (in chapter 3.3)
ppm	parts per million
psi	pound-force per square inch
PTCDA	perylene-3,4,9,10-tetracarboxylic dianhydride
r.t.	room temperature
RCM	ring-closing olefin metathesis
Ref.	reference
R_f	retention factor
r-GPC	recycling gel permeation chromatography
ROESY	rotating frame nuclear overhauser effect spectroscopy
s	second
SADABS	Bruker/Siemens area detector absorption

sat.	saturated
SCE	saturated calomel electrode
SEC	size exclusion chromatography
STM	scanning tunneling microscope
t-Bu	*tert*-butyl
TCE	tetrachloroethane
TCNQ	tetracyano-*p*-quinodimethane
TDDFT	time-dependent density functional theory
TEA (or Et_3N)	triethylamine
TFA	trifluoroacetic acid
TfOH	trifluoromethanesulfonic acid
TFTs	thin-film transistors
THF	tetrahydrofuran
TIPS	triisopropylsilyl
TLC	thin layer chromatography
TMPhen	3,4,7,8-tetramethyl-9,10-phenanthroline
TMS	trimethylsilyl
TOF	time of flight
TS	transition state
UV/Vis	ultraviolet-visible spectroscopy
W	watt
XRD	X-ray diffraction
δ	chemical shift
ε	molar extinction coefficient
μ_h	hole mobility
μm	micrometer
Φ	fluorescence quantum yield
τ	fluorescence lifetime

9. Acknowledgements

The four-year time period I spent in Heidelberg, a beautiful college town, is a precious reminiscence in my life. When I recall this experience someday in China after a few decades, I will be confident that I did not regret making the choice to study in Germany. Here I should say thanks sincerely to all of the people who supported me in my doctoral thesis.

First, I would like to express my sincere appreciation to my PhD supervisor Prof. Dr. Michael Mastalerz for his generous support and guidance during the time of my research. His valuable ideas, suggestions and discussions are indispensable to the progress of my projects. His enthusiastic speciality attitude and emphasis on safety in laboratories are helpful to my future career. Furthermore, I would like to thank Prof. Dr. Milan Kivala as the second reviewer of my thesis.

I am thankful for a three-year PhD scholarship of the Chinese Scholarship Council (CSC), which helped me to fulfill my dream to study overseas.

I would like to thank my collaborators, Prof. Dr. Andreas Dreuw and Marvin Hoffmann for their theoretical calculation and mechanism analysis for the cyclopentannulation project. Support by the state of Baden-Württemberg through bwHPC and the Deutsche Forschungsgemeinschaft (DFG) through grant no INST 40/467-1 FUGG (JUSTUS cluster) is acknowledged.

I would like to thank Dr. Frank Rominger, Dr. Thomas Oeser, the technicians Sarah Götz and Margit Brückner for their hard work on single crystal structure analysis, which played a big role in all my publications during the time period of doctoral study. I would like to thank the MS and NMR teams of University of Heidelberg, including Dr. Jürgen H. Gross, Doris Lang and Iris Mitsch for the MS-MALDI measurements and Dr. Jürgen Graf for the nice NMR spectra.

Great appreciation should be given to all of my colleagues in the research group of Prof. Dr. Michael Mastalerz and those from other groups of organic chemistry institute (OCI) of University of Heidelberg. I especially acknowledge Dr. Sven M. Elbert for the discussions and careful revisions for my thesis, Tobias Kirschbaum for the abstract translation, discussions of the DFT calculations and very careful proofreading of the thesis and Dr. Xubin Wang for the second-time proofreading. Acknowledgement should also be given to Dr. Tobias Schaub for the discussion of the mechanism of the formation of azulene PAHs. I would like to say thanks to my colleagues Xinyue Hu, Prof. Dr. Gang Zhang, Dr. Bahiru Punja Benke, Jochen Lauer, Lucas Ueberricke, Philippe Wagner, Dennis Reinhard, Ke Tian and Gangxiang Zhou for their kind help and scientific discussions during my research, Ute Gärtner for her assistance of ordering chemicals and equipments and elemental analysis measurements, Janine Tornow-Gaisbauer and Eva-Maria Waldherr for their help in administrative documentations. Many thanks are given to my chinese colleagues in the OCI, in

particular Wei Huang, Gaozhan Xie, Hao Zhang, Yangyang Yang, Yufeng Wu, Xianhai Tian. I wish a bright future for you all.

Appreciation should also be given to my colleagues from my previous research group in Nankai University and all of my friends both in China and Germany, who have been contacting me throughout my doctoral study. You are always the indispensable part of my career and my life. In particular, I would like to say thanks to Ru Zhao, who appeared in my life and serves as one of my goals to strive for.

Last but not least, I am sincerely grateful for the consistent support from my parents and family. You are the inexhaustible driving force of my progress forever.

Xuan YANG

杨宣

08.05.2020

Heidelberg

NATURWISSENSCHAFTLICH-MATHEMATISCHE GESAMTFAKULTÄT

COMBINED FACULTY OF NATURAL SCIENCES AND MATHEMATICS

RUPRECHT-KARLS-
UNIVERSITÄT
HEIDELBERG

Eidesstattliche Versicherung gemäß § 8 der Promotionsordnung für die Naturwissenschaftlich-Mathematische Gesamtfakultät der Universität Heidelberg / Sworn Affidavit according to § 8 of the doctoral degree regulations of the Combined Faculty of Natural Sciences and Mathematics

1. Bei der eingereichten Dissertation zu dem Thema / The thesis I have submitted entitled

   ….**Extended Polycyclic Aromatic Hydrocarbons based on Diarenoperylenes**……..……..

   ……

   handelt es sich um meine eigenständig erbrachte Leistung / is my own work.

2. Ich habe nur die angegebenen Quellen und Hilfsmittel benutzt und mich keiner unzulässigen Hilfe Dritter bedient. Insbesondere habe ich wörtlich oder sinngemäß aus anderen Werken übernommene Inhalte als solche kenntlich gemacht. / I have only used the sources indicated and have not made unauthorised use of services of a third party. Where the work of others has been quoted or reproduced, the source is always given.

3. Die Arbeit oder Teile davon habe ich ~~wie folgt/~~bislang nicht[1)] an einer Hochschule des In- oder Auslands als Bestandteil einer Prüfungs- oder Qualifikationsleistung vorgelegt. / I have not yet ~~/ have already~~[1)] presented this thesis or parts thereof to a university as part of an examination or degree.

   Titel der Arbeit / Title of the thesis: ……..

   Hochschule und Jahr / University and year: ……..…….....

   Art der Prüfungs- oder Qualifikationsleistung / Type of examination or degree: ……..

4. Die Richtigkeit der vorstehenden Erklärungen bestätige ich. / I confirm that the declarations made above are correct.

5. Die Bedeutung der eidesstattlichen Versicherung und die strafrechtlichen Folgen einer unrichtigen oder unvollständigen eidesstattlichen Versicherung sind mir bekannt. / I am aware of the importance of a sworn affidavit and the criminal prosecution in case of a false or incomplete affidavit.

Ich versichere an Eides statt, dass ich nach bestem Wissen die reine Wahrheit erklärt und nichts verschwiegen habe. / I affirm that the above is the absolute truth to the best of my knowledge and that I have not concealed anything.

…….. ……..…….

Ort und Datum / Place and date — Unterschrift / Signature

[1)] Nicht Zutreffendes streichen. Bei Bejahung sind anzugeben: der Titel der andernorts vorgelegten Arbeit, die Hochschule, das Jahr der Vorlage und die Art der Prüfungs- oder Qualifikationsleistung. / Please cross out what is not applicable. If applicable, please provide: the title of the thesis that was presented elsewhere, the name of the university, the year of presentation and the type of examination or degree.

The German text is legally binding.